Mitigation and remediation of CO_2 leakage from geological storage

Handbook of corrective measures

Project no.	608608
Start date of project	2014-03-01
Duration	3 years

Contents

Contents

Introduction

Filip Neele[1], Alv-Arne Grimstad[2], Marc Fleury[3], Cornelia Schmidt-Hattenberger[4], Anna Korre[5]
[1] TNO, The Netherlands
[2] SINTEF PR, Norway
[3] IFPEN, France
[4] GFZ, Germany
[5] Imperial College, UK

Background

ABSTRACT

CO_2 storage projects must develop a corrective measures plan (CMP), as part of the application for a storage license. This plan describes the measures that can be taken if the behaviour of the CO_2 in the subsurface does not conform expectations. For non-conformance due to problems related to wells, or when the CO_2 from the storage complex reaches the (near) surface, current CMPs list a range of deployable technologies. In case non-conformance relates to the reservoir (e.g., faults, spill points) only few options for in-situ measures appear to be available to the operator. In such cases current CMPs propose to stop injection and, if necessary, back-production to release pressure.

The MiReCOL project (2014-2017) has investigated a wide range of potentially useful methods to correct, or mitigate the effects of, non-conformance, focusing on application in the deep subsurface, within or close to the storage formation. The point of view was that correction or mitigation close to the origin of the cause could be more effective than near the surface, where the CO_2 is likely to have become dispersed and difficult to detect.

This handbook contains all public reports from the MiReCOL project. The reports show key results and explain the approach taken to produce results that are ready to use by both site operators and regulators.

STARTING POINT FOR MIRECOL

The starting point for all MiReCOL studies was a storage complex (containing the storage formation, a sealing formation, at least one injection well and a quantity of CO_2 already injected) in which CO_2 behaves unexpectedly. This could be due to, for example, an open fault or an undetected spill point.

CORRECTIVE MEASURES

Three classes of causes for the non-conformance were considered, each with a range of corrective measures.

1. Loss of conformance in the reservoir due to reservoir compartmentalisation / discontinuity (leading to unexpected increase of injection well pressure), spread of the CO_2 plume beyond the desired region (e.g. spread beyond the spill point).

   Corrective measures in this case can be characterized as operational migration management. Unexpected fluid flow within the reservoir can represent a threat to safe and secure storage, if e.g. the CO_2 plume is migrating towards a spill point or a fault zone. Corrective measures considered include localized reduction in permeability by injecting gels or foams, by immobilizing the CO_2 in solid reaction products, a change of injection strategy, or localized injection of brine creating a competitive fluid movement. CO_2 migration management in the reservoir can also be achieved by either brine withdrawal or CO_2 back-production. Both measures create pressure gradients towards the withdrawal point and enforce a specific flow direction. Data from back-production projects at K12-B and Ketzin were used to complement the model simulations.

   These studies are covered in the following sections:
   - Section I – CO_2 flow diversion and mobility control within the reservoir;
   - Section II – Reservoir pressure management as CO_2 migration and remediation measure.

2. Natural barrier breach, referring to migration of CO_2 or displaced brine through seals, faults or fractures.

   The feasibility of reducing or interrupting leakages through faults and fracture networks was considered by assessing the efficacy of reducing pressure to lower the leakage rate, or of using sealants (gels, foams) to close the leak. In addition, several other possibilities were explored, like transferring CO_2 through a fault in a compartment originally unconnected to the main reservoir, improving the sealing capacity of a cap rock by injecting nitrogen before or during CO_2 injection or generating a flow barrier above the cap rock by creating a reverse pressure gradient.

These results can be found in the following sections:
- Section III – Remediation linked to transport properties of faults and fracture networks;
- Section IV – Remediation and mitigration methods using sealants in fault and fractures;
- Section V – Remediation and preventative measures using hydraulic gas barriers.

3. Well-related non-conformance.

The oil and gas industry has a best-practice portfolio of remediation technologies in place, which is also applicable to CO_2 injection wells. New developments and emerging technologies were considered in the project. Laboratory tests were performed to examine the merits of CO_2-reactive suspensions, of polymer-based gels, of smart cements with a latex-based component and of polymer resins for squeezing. A field test was held at the Serbian Bečej natural CO_2 field, where the effectiveness of a CO_2-reactive suspension to seal the well was demonstrated.

Well-related results can be found in these sections:
- Section VI – O&G industry best practice for remediation of well leakage;
- Section VII – Novel materials and technologies for remediation of well leakage.

NEAR-SURFACE REMEDIATION

While strenuous efforts will be made to minimise the risk of the leakage of CO_2 from engineered storage sites, there will always remain a residual risk that CO_2 could migrate from the storage site into the shallow subsurface along permeable pathways such as faults or wells.

A comprehensive review was made of the available techniques for CO_2 leakage remediation in the near surface environment considering relevant experience and expertise from pilot scale CCS projects and natural analogues, CO_2-EOR operations, natural gas storage, and other industries as well as consider the cost and effectiveness of the techniques; special attention was given to the applicability of each available method to remediate CO_2 leakage in the near surface environment, the ease of implementation of the method and the associated costs.

This work is presented in
- Section VIII – Near-surface environmental remediation, methods and plans.

DELIVERING THE RESULTS: SUPPORTING THE CO_2 STORAGE SITE OPERATOR

For the results from MiReCOL to be operationally useful, the overall results must be presented in a ready-to-use way. Remediation technologies considered in this project were described 1) in terms of leakage prevention (technical efficiency), 2) impact on the overall risk level of a storage project, and 3) impact on the environment and cost-effectiveness. To this end, a number of key performance indicators (KPIs) were defined for each corrective measure: timescale to effective cessation of leakage, longevity of remediation, likelihood of success, economic cost, environmental impact at the surface, location of retention of the CO_2 (i.e. within reservoir, within storage complex etc.).

To improve the applicability of the project results and help clarify options open to site operators, a web-based tool was developed that evaluates these KPIs for each corrective measure, for a non-conformance case defined by the user. This provides insight in the applicability or relevance of corrective measures for the user-defined cases. In this way, the tool supports site operators to create a corrective measures plan for their site, and supports competent authorities to understand the options that are open to site operators in case of non-conformance.

This is described in
- Section IX – Assessment of remediation consequences and corrective measures handbook.

CONCLUSION

The results from the MiReCOL project support the development of corrective measures plans and help build confidence in the safety of deep subsurface CO_2 storage by providing a toolbox of techniques to mitigate and/or remediate undesired migration of CO_2. The MiReCOL reports, as well as the corrective measures web tool, can be accessed through www.mirecol-CO_2.eu and tool.mirecol-CO_2.eu.

ACKNOWLEDGEMENT

Part of the research reported in this document has been conducted with funding from the European Commission FP7 project MIRECOL (www.mirecol-CO_2.eu), Grant Agreement no. 608608, and additional funding from Shell, Statoil and ENGIE.

Public Introduction

CO_2 capture and storage (CCS) has the potential to reduce significantly the carbon emission that follows from the use of fossil fuels in power production and industry. Integrated demo-scale projects are currently being developed to demonstrate the feasibility of CCS and the first such projects are expected to start operating in Europe under the Storage Directive in the period 2015 – 2020. For the license applications of these projects, a corrective measures plan is mandatory, describing the measures to be taken in the unlikely event of CO_2 leakage.

The reports collected here are part of the research project MiReCOL (Mitigation and Remediation of CO_2 leakage) funded by the EU FP7 program. This project supports the creation of such corrective measures plans and helps to build confidence in the safety of deep subsurface CO_2 storage, by laying out a toolbox of techniques available to mitigate and/or remediate undesired migration or leakage of CO_2. The project was particularly aimed at (new) operators and relevant authorities.

Research activities were aimed at developing this handbook of corrective measures that can be considered in the event of undesired migration of CO_2 in the deep subsurface reservoirs. The MiReCOL project investigates various techniques for control of CO_2 migration including: i) injection strategy, ii) gel or foam injection, iii) water or brine injection and iv) injection of chemicals which react with CO_2 and precipitate it as a solid. MiReCOL results support CO_2 storage project operators in assessing the value of specific corrective measures if the CO_2 in the storage reservoir does not behave as expected. The general scenarios considered in MiReCOL are 1) loss of conformance in the reservoir (undesired migration of CO_2 within the reservoir), 2) natural barrier breach (CO_2 migration through faults or fractures), and 3) well barrier breach (CO_2 migration along the well bore).

Section I

CO_2 FLOW DIVERSION AND MOBILITY CONTROL WITHIN THE RESERVOIR

Chapter I

Current flow diversion techniques in the petroleum industry relevant to CO_2 leakage remediation

Laura Wasch[1], Robert Drysdale[2], Marc Fleury[3], Bernd Wiese[4], Anna Korre[5], Sevket Durucan[5]
[1]TNO, The Netherlands
[2]SINTEF PR, Norway
[3]IFPEN, France
[4]GFZ, Germany
[5]Imperial College, UK

SUMMARY

This chapter sets out to investigate the possibilities for flow diversion and mobility control of an unwanted migration of CO_2 within the storage reservoir. Other elements will consider mitigation of leakage through the caprock, faults or fractures, and the control of unwanted migration beyond the reservoir seals. More specifically, this work will investigate techniques for controlling CO_2 migration by means of the following techniques: a revised injection strategy, injection of gel or foam to form a barrier, injection of water or brine, and injection of reactant chemicals which cause the CO_2 to precipitate as a solid. This deliverable considers any current practices and theoretical techniques in the petroleum industry which are similar, or which might be applied to the CO_2 mitigation techniques to be investigated in this work.

1 INTRODUCTION

CO_2 capture and storage (CCS) has the potential to reduce significantly the carbon emission that follows from the use of fossil fuels in power production and industry. Integrated demo-scale projects are currently being developed to demonstrate the feasibility of CCS and the first such projects are expected to start operating in Europe under the Storage Directive in the period 2015 – 2020. For the license applications of these projects a corrective measures plan is mandatory, describing the measures to be taken in the unlikely event of CO_2 leakage. This project will support the creation of such corrective measures plans and help to build confidence in the safety of deep subsurface CO_2 storage, by laying out a toolbox of techniques available to mitigate and/or remediate undesired migration or leakage of CO_2. The project is particularly aimed at (new) operators and relevant authorities.

One of the main objectives of MiReCOL project is to investigate the possibilities for flow diversion and mobility control of an unwanted migration of CO_2 within the storage reservoir. This is distinguished from mitigation of leakage through the caprock and other seals, and the investigation of specific techniques for control of unwanted migration beyond the seals, which are the objectives of other elements of the MiReCOL project.

This report reviews current flow diversion techniques in the petroleum industry which are similar, or which might be applied to mitigating against non-conformal behaviour of CO_2 within the storage reservoir. These include: i) injection strategy, ii) gel or foam injection, iii) water or brine injection and iv) injection of chemicals which react with CO_2 and precipitate it as a solid. The first of these techniques is only introduced briefly since it is covered in detail in Deliverable D4.1 "Report on current reservoir pressure management measures in the petroleum industry".

Many concepts for flow diversion have been considered by industry, mainly for increasing the recovery of oil or gas, but several of these have remained theoretical and have not been widely applied in practice. Both applied and theoretical techniques are potentially interesting candidates for this investigation.

The results of this work will contribute to later activities in the project, which will assess the effectiveness and consequences of all measures taken against non-conformal behaviour, leading to the production of a Corrective Measures Handbook.

2 BACKGROUND AND REVIEW OF THE VARIOUS FLOW DIVERSION TECHNIQUES CONSIDERED

2.1 Injection strategies

The position of a CO_2 plume is crucial in determining the leakage risk. It is desired to keep the plume away from geologically weak zones, such as faults, spill points, old abandoned wells or weak regions of the cap rock. Therefore, MiReCOL will investigate whether possibilities exist to affect the plume's position by reservoir management methods.

In the hydrocarbons industry context, the concept of plume control is mainly applied to oil fields, where the presence of numerous wells allows a comparatively accurate spatial determination and allows the choice of optimal production and injection from/into wells as a control device. In CO_2 storage the number of wells may be limited primarily due to cost, but also due to the wish to minimise the number of potential leakage sites. Therefore, new strategies for CO_2 flow diversion shall be investigated within this part of MiReCOL.

Flow diversion and pressure management are physically closely connected to the same processes in the reservoir. During injection and plume expansion water is replaced by CO_2 and the resulting pressure gradient is a direct consequence of this replacement. Despite the fact that the same physical process underlies both phenomena, the position and shape of the plume are much more difficult to predict or monitor compared with pressure. The pressure is rather similar at different reservoir positions, regardless of whether CO_2 or brine is present, but multiphase flow phenomena such as fingering, channelling and hysteresis allow many different saturation states for the same reservoir pressure (Lu and Lichtner, 2007, Wang et al., 2013). Heterogeneities can significantly alter flowrate and the flow field, while the pressure may be less affected. Furthermore, pressure is typically monitored at a limited number of wells, while the spatial distribution of a CO_2 plume contains many more degrees of freedom and can be determined by seismic or geoelectrical methods.

These techniques are covered in detail in Deliverable D4.1 "Report on current reservoir pressure management measures in the petroleum industry".

2.2 Gel and foam injection

2.2.1 Gel injection

Cross-linked hydrolysed polymer-gel injection is used in petroleum industry to improve conformity of fluid flow in the reservoir, remediate leakage around wells and also used in conjunction with the prospect of enhanced oil recovery under various temperature and pressure conditions (Sydansk, 1988; Hunter et al., 1992; Gao et al., 1993; Whitney et al., 1996; Hutchins et al., 1996; Bryant et al., 1996; Kantzas et al., 1999; Ricks and Portwood, 2000; Sydansk and Southwell, 2000; Wouterlood et al., 2002; Herbas et al., 2004; Sydansk et al., 2004; Sydansk et al., 2005; Norman et al., 2006; Zhao et al., 2006; Turner and Zahner, 2009; Al-Muntasheri et al., 2010) and to improve miscible CO_2 floods (Hild and Wackowski, 1999; Saez et al., 2012).

The majority of field practice in applying gel treatments aimed to reduce channelling in high-pressure gas floods and to reduce water production from gas wells (Seright, 1995; Raje et al., 1999; Grattoni et al., 2001; Sydansk and Seright, 2007). Often referred to as relative permeability modification (RPM) or disproportionate permeability reduction (DPR) and water shut off (WSO) treatments, there are many examples of production performance modelling data for gel treated wells in the literature (Wassmuth et al., 2004; Herbas et al., 2004). In the early days of the technology, RPM treatment was mainly used in controlling flow in matrix-rock porous media. More recent research have reported successful treatment of fractured rock where relatively strong gels impart RPM/DPR to fluid flow within gel filled fractures and achieve total shutoff (Sydansk et al., 2005).

Hydrolysed polyacrylamide (Figure 1a), in various proportions, is one of the widely used polymers within the petroleum industry (Flew and Sellin, 1993; Rodriguez et al., 1993). The polymer exists as loose molecular chains in the aqueous solution. When appropriate cross-linker is added, these polymer chains are aligned and this polymer solution is turned into a solid gel which resembles the structure illustrated in Figure 1b. Metal ions such as Cr^{3+} (Prud'homme and Uhl, 1984; Sydansk, 1990; Albonico and Lockhart, 1993; Lu et al., 2010) and Aluminium (Dovan, 1987; Smith, 1995) have been used as a crosslinkers, although occasional use of organic cross-linkers such as formaldehyde (Albonico et al., 1995) was also observed. Polyacrylamide based-gel solutions are used in the industry to selectively shut off undesired gas influx in production fields (Sanders et al., 1994; Sydansk et al., 2004; Simjoo et al., 2009; Reddy et al., 2012) and sometimes in combination with other surfactants (Woo et al., 1999). Application of polyacrylamide-gel solution for modifying injectant flow profile are also noted (Chan, 1989) in addition to remediating non-conformal flow within the reservoir (Mebratu et al., 2004).

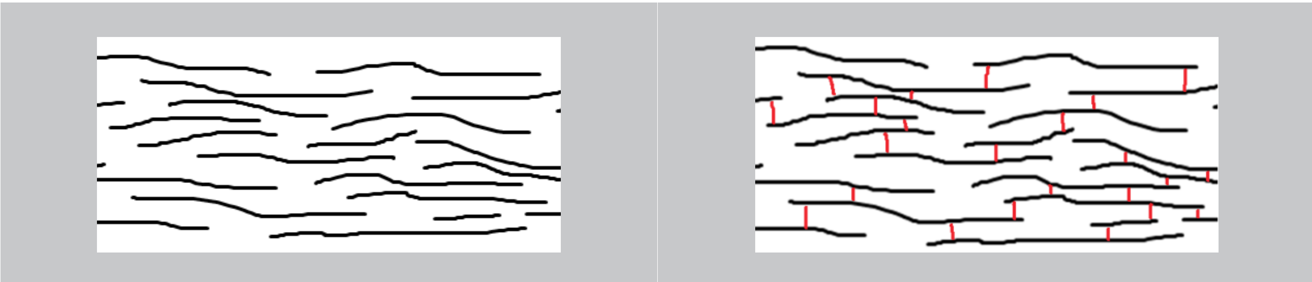

Figure 1 Artistic representation of polymer chains in carrier fluid and (b) effect of cross-linker on the arrangement of polymer molecules in the solution.

The rheological characteristics of polymers injected into the subsurface reservoir are modified in time either by adding an additive, or just by interaction with the environment such as variation in temperature, pressure or surrounding fluids. These changes are observed to be accomplished either through the injection of individual components i.e., monomer, cross-linker and other additives or through injection of cross-linked polymer directly into the reservoir (Hubbard et al., 1988).

The time taken for hydrolysed polymer to be converted into polymer gel upon the addition of cross linker is generally termed as gelation time, which is also an indicator of the possible penetration of the injected polymer gel solution into the reservoir before it solidifies. Gelation time is also defined as the time when the elastic and viscous moduli of the gel are equal (Tung and Dynes, 1982). This time is dependent on the characteristics such as chemical composition, molecular weight and concentration of the polymer, temperature and cross-linker type. Hence, the temperature and salinity of the reservoir are important factors in the selection of appropriate concentration of a polymer and the cross-linker. Addition of organic ligands and pre formed Cr^{3+} complexes with suitable ligands added to the polymer solution were found to control the gelation time over the temperature range of 60-135°C (Albonico et al., 1993). Furthermore, aqueous solution of dilute polyacrylamide was reported to be reasonably stable under shear (Bruce and Schwarz, 1969). The stability of a polymer-gel system was reported to be dependent on the stability of polymer molecules themselves (Albonico and Lockhart, 1993; Moradi-Araghi et al., 1993).

Preliminary laboratory characterisation and assessment for field application of one polyacrylamide based polymer gel system was carried out as part of the EU funded CO_2CARE project. The important conclusions of the work are summarised here:

1. The gelation time decreases with increase in polyacrylamide concentration; furthermore, for identical combination of polyacrylamide and a cross-linker, the gelation time was found to decrease with increase in temperature.
2. CO_2 permeability reduction of more than 99% can be achieved in high permeability sandstones
3. It was found that an increase in brine salinity generally leads to the destruction of the polymer chains and a notable reduction in effectiveness of the gel. However, almost 90% reduction in permeability was still achieved in higher salinity (12 to 25%) environments.
4. Water slug injection experiments in the laboratory have confirmed that the negative impact of high salinity can be reduced by this technique.
5. In summary, high molecular weight, anionic and hydrolysed polymer chains such as polyacrylamide along with cross-linker such as Cr^{+3} can be used to remediate leakage of CO_2 if the area of influence is carefully evaluated and the injection process designed accordingly.

The design of an efficient remediation strategy using polymer gel for possible CO_2 leakage would depend on engineering the gelation time of the polymer and cross-linker combination for the targeted subsurface reservoir conditions, which would be investigated though the current research.

2.2.2 Foam injection

Foams have been used in EOR as a very promising and cost effective means to alleviate the drawbacks associated with gas-based processes leading to early gas breakthrough. Foams can be used for in-depth gas mobility control, as blocking agents in thief zones and for conformance control in fractures or layered reservoirs. Thus, besides their use for EOR purposes, they can be also used to secure gas storage operations through gas confinement and gas leakage remediation.

A foam system consists of a continuous water phase with dispersed gas bubbles at a given volumetric fraction. Gas bubble formation requires a certain amount of energy provided by shear, and is stabilized by surfactant foaming agents dissolved in the water phase, or the gas phase in the case of CO_2.

Among the properties of foams, stability is of most importance. Foams are dispersed systems and as such they are intrinsically unstable with time. However for gas mobility control in EOR, foam should be stable and propagate within the reservoir, while for conformance and blocking purposes they should remain stable in place for a given time to ensure the economic viability of the process.

For CO_2, the mobility reduction factor is usually much lower than with hydrocarbon gas and the maximum attainable effect decreases rapidly with CO_2 density (Chabert et al., 2012; Solbakken et al., 2013). With supercritical CO_2 it was inferred from a laboratory study using a classical foaming agent that probably only coarse foam-emulsions could be formed. However, more recent results have shown that using dedicated surfactant formulations, high gas mobility reduction factors could be obtained, even with dense- phase CO_2, indicating the formation of strong foams (Chabert et al., 2014).

Currently, large uncertainties still remain regarding the actual physics underlying foam flow in porous media. Though previous studies have not proposed a satisfactory physical model for foam flow and propagation, they have generated a general, though useful, phenomenological description of the rheological behaviour of foams in porous media (Gauglitz et al., 2002; Skauge et al., 2002; Tanzil et al., 2002; Farajzadeh et al., 2009; Enick et al., 2012; Chabert et al., 2013).

2.2.2.1 Foam use

Foams have been widely used during EOR operations both for conformance improvement and in-depth gas mobility control, with varying success. The main successes have been for conformance purposes while disappointing results have been obtained for in-depth gas mobility control. A detailed literature review, including pilot trial analyses, can be found here (Enick et al., 2012)

The use of foams to improve underground gas storage has been investigated by several authors (Bernrad et al., 1964; Persoff et al., 1990; Smith et al., 1993). The use of foam for leak remediation in such operations could benefit greatly from the experience gained from the oil industry, especially in conformance remediation and limitation of gas coning from the gas cap (Albrecht and Marsden, 1970; Wong et al., 1997).

For the use of foams as gas flow blocking agents, the foam emplacement, its resistance to gas flow and its durability and stability are of the outmost importance for the efficiency and economics of the process. Though the use of "classical" foams has been considered as a promising technology for controlling excessive GOR, it was shown that these foams have limited lifetime (weeks to months) and the treatment needs to be repeated often (Albrecht and Marsden et al., 1970; Wong et al., 1997; Wassmuth et al., 2001; Cubillos et al., 2012)

These aspects are even more crucial in the case of the use of CO_2-foams for gas leakage prevention/remediation during CO_2 storage operations. Indeed, compared to others foam systems such as N_2-foams or natural gas-foams, CO_2-foams usually generate much lower Mobility Reduction Factors due to the impact of CO_2 on the interfacial tension (Gauglitz et al., 2002; Chabert et al., 2012; Solbakken et al., 2013; Chabert et al., 2014).

In addition, CO_2-foam-induced mobility reduction is very sensitive to the CO_2 density and thus to injection and reservoir conditions of pressure and temperature (Solbakken et al., 2013). Chabert et al. (2014) inferred from a laboratory study that (supercritical) $scCO_2$-dedicated surfactant could improve foam resistance to flow and showed that better mobility reduction could be obtained even with high CO_2 density, but not enough to block gas leakage.

2.2.2.2 Gel Foams

Alternatively, several improvements have been proposed with the objective of increasing the foam-system strength, its resistance to gas flow and its durability once emplaced in the targeted area. This includes mainly polymer enhanced foams and gel foams (Dalland and Hanssen., 1997; Friedmann et al., 1999; Hughes et al., 1999; Wassmuth et al., 2001). From these previous studies, gel-foam appeared to be the more promising technology for gas flow blockage, but it requires a careful design together with an optimization of the strategy of injection and emplacement.

Gel foams consist of gas bubbles in a liquid solution that is able to undergo gelation. They are formed using a surfactant foaming agent usually consisting of a high molecular weight polymer with reactive ends distributed along the molecular chains. Gelation is invoked by a specific cross-linker that is able to react with the polymer reactive ends to form intermolecular bridges and polymer gel. This reaction is controlled using a delaying chemical agent. However, gel-foam application is a very complex process that requires careful investigation to identify an effective solution for a given reservoir application.

One of the most interesting applications of gel foams is to increase well productivity by blocking gas influx. Similarly, they can be used also for confinement purposes to prevent CO_2 leakage across the cap-rock in CO_2 storage.

2.3 Brine/water injection

Brine or water injection has a long history of use for secondary oil recovery worldwide, either to support reservoir pressure or to displace oil towards producing wells. There is a correspondingly wide range of techniques and theories about how water injection can be used to increase oil recovery. Volumetric sweep management and realignment of production in contiguous layers are the nearest analogues in the oil industry to the use of water injection to stop migration of CO_2 (Omorgie et al., 1995).

In CO_2 geological storage there are several mechanisms by which water injection can be used to reduce CO_2 migration. The first and most obvious of these is to form a zone of high pressure in front of the migrating CO_2, sufficient to resist the buoyancy and pressure forces driving the CO_2 forward. This mechanism has been described in general terms by Kuuskraa and Gedec. (2007) as attempting to create an over-pressure in the formation above a leaking caprock and by Réveillère and Rohmer. (2011) with a numerical simulation analysis.

Within MiReCOL this mitigation technique will be addressed both in the context of an overall reservoir management approach to mitigation, and by investigating the local pressure effects of water injection.

The second mechanism is to inject relatively dense brine to form a curtain in front of the advancing CO_2. The aim in this case is to generate sufficient gravitational force on the brine together with local over-pressure from injection to overcome the buoyancy and pressure forces advancing the CO_2, thereby preventing the CO_2 from entering the brine curtain.

This work will concentrate on CO_2 moving in a general lateral direction, under the caprock. Control of vertical migration of CO_2 representing leakage from a fracture in the caprock or a leaking fault will be studied in another part of the project.

The nearest analogue of such a gravity technique in the oil industry is a variant of Water Alternating Gas injection (WAG), namely Simultaneous Water and Gas injection (SWAG) with the aim of increasing secondary oil production. In this case the water and gas are injected at the same time but in separate horizontal wells, with the water being injected higher in the reservoir than the gas in order to restrain the buoyancy effect of the gas by the higher density of the water. Thus the gas sweep in the reservoir is prolonged resulting in additional oil recovery. This technique has been studied first by Stone (2004) and by many later authors such as Jamshidnezhad et al. (2010).

The third mechanism to be considered is that of injecting water directly into the advancing CO_2 plume. This will promote contact between the CO_2 and virgin water, thereby enhancing dissolution of the CO_2 into the water and by reducing the saturation of CO_2 will cause capillary trapping. These mechanisms are normally associated with the tail-end of the CO_2 plume, where the bulk of the CO_2 has moved away and the concentration is dropping. Thus directed water injection is intended to accelerate these processes.
This technique has been studied before e.g. by Esposito and Benson (2010) with respect to leakage mitigation and Anchliya et al. (2012) with the aim of accelerating immobilization of injected CO_2 thus decreasing the storage volume required in a reservoir and the overall risk of leakage. Esposito and Benson (2010) also point out that water injection into the plume spreads the remaining CO_2, making extraction more difficult.

It is intended to investigate the three mitigation techniques outlined above in this part of the project.

2.4 Solid reactants

Limited literature is available on actively changing the permeability of a reservoir to prevent or remediate leakage. More is available on unplanned precipitation by a variety of causes which can clog the reservoir pore space. Injection (and production) of water could induce chemical reactions during oil and gas production (EOR) or geothermal energy. According to Headlee (1945), mineral precipitates formed during oil and gas production are mostly chlorides, sulphates, and bicarbonates of sodium, calcium, magnesium, potassium, strontium and barium. Especially water injection may cause precipitation issues such as the formation of calcium carbonate during re-injection of production water (Rocha et al., 2001; Moghadasi et al., 2004; Birkle et al., 2008) and strontium, barium and calcium sulphates for seawater injection (Delshad and Pope, 2003; Mota et al., 2004; Bedrikovetsky et al., 2006). Mineral clogging in the reservoir is reported to occur in geothermal systems under a wide range of temperature and chemical conditions and may involve precipitation of carbonates, silica (polymorphs), metal compounds (oxides, hydroxides, sulphides, sulphate) and clays (e.g. Kühn et al., 1997; Tarcan, 2005; Izgec et al., 2005; Regensprug et al., 2010). In addition to fluid-fluid reactions, evaporation reactions could also yield mineral precipitation. Salt precipitation and induced clogging of the reservoir porosity is commonly regarded as a potential issue in natural gas and oil production (e.g. Kleinitz et al., 2001) and CO_2 storage in saline aquifers (e.g. Pruess and Müller, 2009; Zeidouni et al., 2009) and depleted gas fields (Giorgis et al., 2007 and Tambach et al., 2014). CO_2 interaction with the host reservoir rock and the pore fluid can also lead to mineral precipitation in the pore space. Much research has been done on this topic since these reactions trap and immobilize the CO_2 which increases the storage safety (e.g. Gaus, 2010). Concerning intentional precipitation within the reservoir, all the mentioned minerals are potential candidates, since there formation has proven to occur 'naturally'.

A couple of studies report on controlled precipitation and permeability decrease (Wasch et al., 2013) proposed salt precipitation around the wellbore as a method for leakage prevention. To precipitate salt in the reservoir, the process of water evaporation into dry gas and subsequent salting-out of the dissolved halite was used. TOUGH2 simulations of multiple cycles of brine and CO_2 injection in the reservoir showed that alternating brine-CO_2 injection could be a promising method for intentional salt-clogging of the near-wellbore area. Intentional salt clogging appears to be particularly suitable for application in depleted gas fields with relatively immobile water and accordingly little chance of re-dissolution of the salt seal by the back-flow of displaced water (Tambach et al., 2014). Selective plugging of well perforations is already practiced in the context of water shut-off during oil production. Plugging reduces water production and enhances oil production from low permeable layers. Plugging agents such as foams and polymers are usually used to clog parts of the reservoir. Selective plugging has also been reported by chemical reactions due to injection of a fluid that is chemically incompatible to the reservoir brine, causing mineral precipitation (Nasr-El-Din et al., 2004). This process is similar to the studies on unplanned precipitation during water injection described above. Looking into specific leakage remediation, bio-mineralization has been proposed (Mitchell et al., 2009, Cunningham et al., 2011). This technique involves engineered biofilms covering grains which will subsequently result in carbonate precipitation by the process of ureolysis. The work of Ito et al. (2014) relates closely to the work planned within MiReCOL. This work reports experiments and modelling of a chemical substance that will react with CO_2 to form a barrier for further CO_2 leakage. They injected both silica and calcium grouts into synthetic porous medium of glass beads. The experimental and modelling work indicates that especially silica has potential as a leakage remediating reactive substance.

3 CONCLUSIONS

This report reviewed flow diversion techniques currently used within the hydrocarbons industry and focused mainly on three processes, namely:

- Injection of gel or foam,
- Injection of water or brine, and
- Injection of reactant substances.

A fourth technique, that of injection strategies, has been introduced briefly and is covered in more detail in Deliverable D4.1 "Report on current reservoir pressure management measures in the petroleum industry".

The petroleum industry uses cross-linked hydrolysed polymer-gel injection to improve conformity of fluid flow in the reservoir and to remediate leakage around wells. Polymer-gel solutions are injected to reduce channelling in high-pressure gas floods and to reduce water production from gas wells. More recently, the same process has been suggested for the treatment of fractured rock where relatively strong gels achieve total shutoff due to gel filled fractures. Preliminary laboratory characterisation and assessment for field application of one polyacrylamide based polymer gel system carried out by one of the MiReCOL partners have shown that CO_2 permeability reduction of more than 99% can be achieved in high permeability sandstones. This will form the basis for the characterisation and assessment of a number of polymer gel solutions for the purposes of MiReCOL, which will be used in numerical evaluation of the use of these solutions in diverting flow within the storage reservoir.

The hydrocarbons industry also used foams for gas mobility control, as blocking agents in thief zones and for conformance control in fractures or layered reservoirs. Therefore, besides their use for EOR purposes, they can also be used to secure gas storage operations through gas confinement and gas leakage remediation. However, foams are dispersed systems and are intrinsically unstable with time, yet for conformance and blocking purposes they should remain stable for a given time. It is believed that, in order to increase the foam-system strength, and its resistance to gas flow, polymer enhanced foams and gel foams can be considered. This potential use for flow diversion purposes will be explored by the researchers within MiReCOL.

In CO_2 geological storage there are several mechanisms by which water injection can be used to reduce CO_2 migration. The options to be considered in MiReCOL include: i) forming a zone of high pressure in front of the migrating CO_2 which will be sufficient to resist the buoyancy and pressure forces driving the CO_2 forward; ii) injecting relatively dense brine to form a curtain in front of the advancing CO_2; iii) injecting water directly into the advancing CO_2 plume to enhance dissolution of the CO_2 into the water and achieve capillary trapping.

MiReCOL researchers have, in the past, studied controlled precipitation and permeability reduction by salt precipitation around the wellbore as a method for leakage prevention. In this project, researchers will consider experiments and modelling of chemical grouts, which will react with CO_2 to form a barrier for further CO_2 migration.

References

Albrecht, R.A. and Marsden, S.S. 1970. Foams as Blocking Agents in Porous Media. SPE J. 10 (1): 51–55. SPE-2357-PA.

Albonico, P., Burrafato, G., Di Lullo, A. and Lockhart, T.P., 1993. Effective gelation delaying additives for Cr^{3+}/ polymer gels. In SPE International Symposium on Oilfield Chemistry, New Orleans, 2-5 March.

Albonico, P., and Lockhart, T., 1993. Divalent ion-resistant polymer gels for high-temperature applications: Syneresis inhibiting additives, in SPE International Symposium on Oilfield Chemistry, Society of Petroleum Engineers, Inc., New Orleans, Louisiana.

Albonico, P., Bartosek, M., Malandrino, A., Bryant, S. and Lockhart, T., 1995. Studies on phenol-formaldehyde crosslinked polymer gels in bulk and in porous media, in SPE International Symposium on Oilfield Chemistry, Society of Petroleum Engineers, Inc., San Antonio, Texas.

Al-Muntasheri, Sierra, G. A., L., Garzon, F. O., Lynn, J. D. and Izquierdo, G. A., 2010. Water shut-off with polymer gels in a high temperature horizontal gas well: A success story, in SPE Improved Oil Recovery Symposium, Society of Petroleum Engineers, Tulsa, Oklahoma, USA.

Anchliya, A. and Ehlig-Economides, C., 2009, Aquifer management to accelerate CO_2 dissolution and trapping, SPE International Conference on CO_2 Capture, Storage, and Utilization, 219-235.

Anchliya A., Ehlig-Economides C. and Jafarpour B., 2012,Aquifer management to accelerate CO_2 dissolution and trapping, SPE 126688.

Bedrikovetsky, P.G., Mackay, E., Montelro, R.P., Gladstone and P.M., Rosário, F.F., 2006. Laboratory and field prediction of sulfate scaling damage. SPE Eighth International Symposium on Oilfield Scale 2006 2006, 309-326.

Bernrad G.G.,and Holm, L.W, Model study of foam as a sealant for leak in gas storage reservoir, Soc.Petrol.Eng. J., 1964, 4, 9-16

Birkle, P., Pruess, K., Xu, T., Hernández Figueroa, R.A., Díaz López, M. and Contreras López, E., 2008. Using laboratory flow experiments and reactive chemical transport modeling for designing waterflooding of the Agua Fría Reservoir, Poza Rica-Altamira Field, Mexico. SPE Reserv. Eval. Eng. 11, 1029-1045.

Bruce, C. and Schwarz, W. H., 1969. Rheological properties of ionic and non ionic polyacrylamide solutions, Journal of Polymer Science Part A-2: Polymer Physics, 7(5), 909-927.

Bryant, S. L., Rabaioli, M. and Lockhart, T. P., 1996. Influence of syneresis on permeability reduction by polymer gels, SPE Production & Operations, 11(4), 209-215.

Chabert, M., Morvan, M. and Nabzar, L., Advanced Screening Technologies for the Selection of Dense CO_2 Foaming Surfactants, 33rd IEA EOR Symp. August 26-30, 2012.

Chabert M., Nabzar L., Rohaida, S., Hamid P., Sedaralit M.F. and Darman N., An integrated laboratory workflow for the design of a foam pilot in Malaysia, IOR 2013 – 17th European Symposium on IOR. St. Petersburg, Russia, 16-18 April 2013

Chabert, M., Nabzar, L., Beunat, V., Lacombe E. and Cuenca, A., Impact of Surfactant Structure and Oil Saturation on the Behavior of Dense CO_2 Foams in Porous Media , SPE 169176, SPE Improved Oil Recovery Symposium held in Tulsa, Oklahoma, USA, 12–16 April 2014.

Chan, K. S., 1989. Injection profile modification with a new non-polymer gelling system, in Annual Technical Meeting, Petroleum Society of Canada, Banff.

Cubillos, H., Montes, J. Prieto, C. and Romero, P., Assessment of foam for GOR control to optimize miscible gas injection recovery, SPE 152113, SPE IOR symposium, Tulsa, Oklahoma, 14-18 April 2012

Cunningham, A.B., Gerlach, R., Spangler, L., Mitchell, A.C., Parks, S. and Phillips, A., 2011. Reducing the risk of well bore leakage of CO_2 using engineered biomineralization barriers. Energy Procedia 4, 5178-5185.

Dalland, M. and Hanssen, J.E.: "Enhanced Foams for Efficient Gas Influx Control," paper SPE 37217 presented at the 1997 SPE International Symposium on Oilfield Chemistry, Houston, 18–21 February.1997

Delshad, M. and Pope, G.A., 2003. Effect of Dispersion on Transport and Precipitation of Barium and Sulfate in Oil Reservoirs. SPE Int. Symp. Oilfield Chem. , 393-400.

Dovan, H.T., 1987. Development of a new Aluminium/polymer gel system for permeability adjustment, SPE Reservoir Engineering, 2(2), 177-183.

Enick, R.M, Olsen, D., Ammer, J. and Schuller, W., Mobility and Conformance Control for CO_2-EOR via Thickeners, Foams, and Gels - A Literature Review of 40 Years of Research and Pilot Tests, SPE 154122, SPE IOR symposium, Tulsa, Oklahoma, 14-18 April 2012

Esposito A. and Benson S.M. (2010), Optimization of remediation of possible leakage from geologic CO_2 storage reservoirs, SPE 133604

Farajzadeh, R., Andrianov, A., and Zitha, P. L. J., 2009,. Investigation of Immiscible and Miscible Foam for Enhancing Oil Recovery, Industrial & Engineering Chemistry Research 49:1910-1919.

Flew, S. and Sellin, R. H. J., 1993. Non-newtonian flow in porous media-a laboratory study of polyacrylamide solutions, Journal of Non-Newtonian Fluid Mechanics, 47(0), 169-210.

Friedmann, F., Hughes, T.L., Smith, M.E., Hild, G.P., Wilson, A., and Davies, S.N., Development and testing of a foam-gel technology to

improve conformance of Rangely CO_2 flood, SPE Reservoir Eval & Eng 2 (1), February 1999
Gao, H. W., Chang, M.-M., Burchfield, T. E. and Tham, M. K., 1993. Permeability modification simulator studies of polymer-gel-treatment initiation time and crossflow effects on waterflood oil recovery, SPE Reservoir Engineering, 8(3), 221-227.
Gauglitz, A., Friedmann, F., Kam, I., and Rossen, R., 2002, Foam generation in homogeneous porous media. Chemical Engineering Science, 57, 4037-4052
Gaus, I., 2010, Role and impact of CO_2-rock interactions during CO_2 storage in sedimentary rocks. International Journal of Greenhouse Gas Control 4, 73-89.
Giorgis, T., Carpita, M. and Battistelli, A., 2007. 2D modeling of salt precipitation during the injection of dry CO_2 in a depleted gas reservoir. Energy Convers. Manage. 48, 1816-1826.
Grattoni, C.A., Jing, X.D. and Zimmerman, R.W, 2001. "DisproportionatePermeability Reduction When a Silicate Gel is Formed in-Situ to Control Water Production". Paper SPE 69534 presented at the SPE Latin American and Caribbean Petroleum Engineering Conference, Buenos Aires, 25-28 March.
Headlee, A.J.W., 1945, Interactions Between Interstitial And Injected Water-A Review, Drilling and Production Practice Conference, 1 January, New York, API-45-059.
Herbas, J., Kumar, S., Moreno, R., Romero, M.F and Avendano, H., 2004. "Reservoir Simulations of Gel Treatments to Control Water Production, Improve the Sweep Efficiency and the Conformance Factor in Eastern Venezuelan HPHT Fractured Reservoirs" Paper Presented at the SPE Int. Petroleum Conf., Mexico, SPE 92003.
Herbas, J., Moreno, R., Romero, M. F. and Coombe, D., 2004. Reservoir simulation of non selective placement of a polymer gel treatment to improve water injection profiles and sweep efficiency in the Lagomar field Western Venezuela, in SPE International Petroleum Conference in Mexico, Society of Petroleum Engineers, Puebla Pue., Mexico.
Hild, G., and Wackowski, R., 1999. Reservoir polymer gel treatments to improve miscible CO_2 flood, SPE Reservoir Evaluation & Engineering, 2(2), 196-204.
Hubbard, S., Roberts, L.J. and Sorbie, K.S., 1998. Experimental and theoretical investigation of time setting polymer gels in porous media, SPE Reservoir Engineering, 3 (4), 1257-1267.
Hughes, T.L., Friedmann, F., Johnson, D., Hild, G.P., Wilson, A., and Davies, S.N., Large-volume foam-gel treatment to improve conformance of the Rangely CO_2 flood, SPE Reservoir Eval. & Eng., 2 (1), February 1999
Hunter, B., Buell, R. and Abate, T., 1992. Application of a polymer gel system to control steam breakthrough and channeling, in SPE Western Regional Meeting, Society of Petroleum Engineers Inc., Bakersfield, California.
Hutchins, R., Dovan, H. and Sandiford, B., 1996. Field applications of high temperature organic gels for water control, in SPE/DOE Improved Oil Recovery Symposium, Society of Petroleum Engineers, Inc., Tulsa, Oklahoma.
Ito T., Xu T., Tanaka H., Taniuchi Y. and Okamoto A. 2014. Possibility to remedy CO_2 leakage from geological reservoir using CO_2 reactive grout. International Journal of Greenhouse Gas Control, 310–323.
Izgec O., Demiral B., Bertin H, Akin S., 2005. Calcite precipitation in low temperature geothermal systems: An experimental approach, Proceedings of the Thirtieth Workshop on Geothermal Reservoir Engineering, Stanford University, California, January 31-February 2, 2005, SGP-TR-176
Jamshidnezhad M., v.d. Bol L. and Rossen W.R., (2010) Injection of water above gas for improved sweep in gas EOR: nonuniform injection and sweep in 3D, SPE 138443.
Kantzas, A., Marentette, D. F. and Allsopp, K., 1999. Utilization of polymer gels, polymer enhanced foams, and foamed gels for improving reservoir conformance, Journal of Canadian Petroleum Technology, 38(13).
Kleinitz, W., Koehler and M., Dietzsch, G., 2001, The Precipitation of Salt in Gas Producing Wells, SPE European Formation Damage Conference, 21-22 May, The Hague, Netherlands, SPE-68953
Kuuskraa V., and Gedec M., 2007, Remediation of leakage from CO_2 storage reservoirs, IEA GHG report 2997/11.
Kühn M., Vernoux J.F., Kellner T., Isenbeck-Schröter M. and Schulz H.D., 1997. Onsite experimental simulation of brine injection into a clastic reservoir as applied to geothermal exploitation in Germany, Applied Geochemistry, 13(4), 477-490
Lockhart, T. P., and Albonico, P., 1994. New chemistry for the placement of chromium(lli)/polymer gels in high-temperature reservoirs, SPE Production & Operations, 9(4), 273-279.
Lu, C. and Lichtner, P., 2007, High resolution numerical investigation on the effect of convective instability on long term CO_2 storage in saline aquifers, Journal of Physics: Conference Series, 78 (1).
Lu, X., Wang, W., Wang, R., Liu, Y. and Shan, J., 2010. The performance characteristics of Cr^{3+} polymer gel and its application analysis in Bohai oilfield, in International Oil and Gas Conference and Exhibition in China, Society of Petroleum Engineers, Beijing, China.
Mebratu, A., Nerland, B. and Kleppan, T., 2004. Annular barrier re-establishment using a long-life, high-strength polymer gel system, in SPE International Symposium and Exhibition on Formation Damage Control, Society of Petroleum Engineers, Lafayette, Louisiana.
Mitchell, A.C., Phillips, A.J., Hiebert, T., Gelrach, R., Spangler, L.H. and, Cunningham, A.B., 2009. Biofilm enhanced geologic sequestration of supercritical CO_2. International Journal of Greenhouse Gas Control 3 (1), 90–99.
Moghadasi J., Jamialahmadi M., Müller-Steinhagen H. and Sharif A.. 2004. Formation Damage Due to Scale Formation in Porous Media Resulting From Water Injection. SPE-86524-MS. SPE International Symposium and Exhibition on Formation Damage Control, 18-20 February, Lafayette, Louisiana.
Moradi-Araghi, A., Bjornson, G. and Doe, P., 1993. Thermally stable gels for near-wellbore permeability contrast corrections, SPE Advanced Technology Series, 1(1), 140-145.
Mota, R.O., Bezerra, M.C.M., Rosario, F.F. and Prais, F., 2004. Forecasts and alternative analysis for sulphate removal or chemical treatments for barium and strontium scale deposition - Offshore Brazil. Proceedings - SPE Sixth International Symposium on

Oilfield Scale; Exploring the Boundaries of Scale Control , 393-402.

Nasr-El-Din, H.A., Raju, K.U., Hilab, V.V. and Esmail, O.J., 2004. Injection of incompatible water as a means of water shut-off. Proc. SPE Int. Symp. Oilfield Scale Exploring Boundaries Control , 291-303.

Norman, C., Turner, B. O., Romero, J. L., Centeno, G. A. and Muruaga, E., 2006. A review of over 100 polymer gel injection well conformance treatments in Argentina and Venezuela: Design, field implementation, and evaluation, in First International Oil Conference and Exhibition in Mexico, Society of Petroleum Engineers, Cancun, Mexico.

Omorgie Z.S., King G.R., Strang C., Hodgson P. and Pressney R.A, 1995, Reservoir management in the Ninian field – a case history, SPE 30443.

Persoff, P., Preuss, K., Benson, S.M. and Wu, Y.S, "Aqueous Foams for Control of Gas Migration and Water Coning in Aquifier Gas Storage", Energy Sources, Vol. 12, 479-497, 1990

Prud'homme, R., and Uhl, J., 1984. Kinetics of polymer/metalion gelation, in SPE Enhanced Oil Recovery Symposium, Tulsa, Oklahoma.

Pruess, K. and Müller, N., 2009. Formation dry-out from CO_2 injection into saline aquifers: 1. Effects of solids precipitation and their mitigation. Water Resour. Res. 45.

Raje, M., Asghari, K., Vassoughi, S., Green, D.W. and Willhite, G.P., 1999. "Gel Systems for Controlling CO_2 Mobility in Carbon Dioxide Miscible Flooding" SPE Reservoir Eval. & Eng., 2(2), pp. 205-210. SPE 55965, Paper presented at the SPE/DOE Symp. on Improved Oil Recovery, Tulsa.

Reddy, B. R. R., Crespo, F. and Eoff, L. S., 2012. Water shut off at ultralow temperatures using organically cross-linked polymer gels, in SPE Improved Oil Recovery Symposium, Society of Petroleum Engineers, Tulsa, Oklahoma, USA.

Regenspurg S., Wiersberg T., Brandt W., Huenges E., Saadat A., Schmidt K. and Zimmermann G., 2010. Geochemical properties of saline geothermal fluids from the in-situ geothermal laboratory Groß Schöonebeck (Germany), Chemie der Erde, 70(3), 3-12

Réveillère A and Rohmer J, 2011, Managing the risk of CO_2 leakage from deep saline aquifer reservoirs through the creation of a hydraulic barrier, Energy Procedia, 4, 2011, 3187-3194.

Ricks, G., and Portwood, J. T., 2000. Injection-side application of marcit polymer gel improves waterflood sweep efficiency, decreases water-oil ratio, and enhances oil recovery in the Mcelroy field, Upton county, Texas, in SPE Permian Basin Oil and Gas Recovery Conference, Society of Petroleum Engineers Inc., Midland, Texas.

Rocha, A.A., Frydman, M., da Fontoura, S.A.B., Rosario, F.F. and Bezerra, M.C.M., 2001. Numerical Modeling of Salt Precipitation During Produced Water Reinjection.

Rodriguez, S., Romero, C., Sargenti, M. L., Mueller, A. J., Saez, A. E. and Odell, J. A., 1993. Flow of polymer solutions through porous media, Journal of Non-Newtonian Fluid Mechanics, 49(1), 63{85.

Saez, M., Paponi, H. M., Cabrera, F. A., Muniz, G., Romero, J. L. and Norman, C., 2012. Improving volumetric efficiency in an unconsolidated sandstone reservoir with sequential injection of polymer gels, in SPE Improved Oil Recovery Symposium, Society of Petroleum Engineers, Tulsa, Oklahoma, USA.

Sanders, G., Chambers, M. and Lane, R., 1994. Successful gas shut off with polymer gel using temperature modeling and selective placement in the Prudhoe bay field, in SPE Annual Technical Conference and Exhibition, 1994 Society of Petroleum Engineers, New Orleans, Louisiana.

Seright, R. S., 1995. "Reduction of Gas and Water Permeabilities using Gels" SPE Production & Facilities pp.103-108.

Simjoo, M., Koohi, A. D., Seftie, M. V. and Zitha, P. L. J., 2009. Water shut-off in a fractured system using a robust polymer gel, In 8th European Formation Damage Conference, Society of Petroleum Engineers, Scheveningen, The Netherlands.

Skauge, A., Aarra, M. G., Surguchev, L., Martinsen, H. A. and Rasmussen, L., 2002, Foam-Assisted WAG: Experience from the Snorre Field. SPE 75157.

Smith, D.H, and Jikich, S.A, "Foams and Surfactants for Improved Underground Storage of Natural Gas by Blockage of water Coning", SPE 26908, SPE Eastern Regional Meeting, 2-4 Nov. Pittsbourg, 1993

Smith, J., 1995. Performance of 18 polymers in Aluminum citrate colloidal dispersion gels, in SPE International Symposium on Oilfield Chemistry, Society of Petroleum Engineers, Inc., San Antonio, Texas.

Solbakken, J.S., Skauge A. and Aarra, M.G., Supercritical CO_2 foam- The importance of CO_2 density on Foam Performance, SPE 165296, SPE EOR Conference, Kuala Lumpur, Malaysia, 2-4 July 2013

Stone, 2004, A simultaneous water and gas flood design with extraordinary vertical gas sweep, SPE 91724.

Sydansk, R. D., 1988. A new conformance improvement treatment Chromium(III) gel technology, in SPE Enhanced Oil Recovery Symposium, Tulsa, Oklahoma.

Sydansk, R. D., 1990. A newly developed Chromium(III) gel technology, SPE Reservoir Engineering, 5(3), 346-352.

Sydansk, R. D., and Southwell, G. P. 2000. More than 12 years experience with a successful conformance-control polymer-gel technology, SPE Production & Operations, 15(4), 270-278.

Sydansk, R., Al-Dhafeeri, A., Xiong, Y. and Seright, R., 2004a. Polymer gels formulated with a combination of high- and low molecular weight polymers provide improved performance for water-shut off treatments of fractured production wells, SPE Production & Operations, 19(4), 229-236.

Sydansk R.D., Xiong, Y., Al-Dhafeeri, A.M., Schrader, R.J. and. Seright, R.S., 2005. "Characterisation of Partially Formed Polymer Gels for Application to Fractured Production Wells for Water-Shutoff Purposes" SPE Production & Facilities, 20(3), pp.240-249, SPE 89401.

Sydansk R.D. and Seright, R.S., 2007. "When and Where Relative Permeability Modification Water-Shutoff Treatments Can be Successfully Applied" SPE Production and Operations, pp.236-247. SPE 99371, Paper presented at the SPE/DOE Symp. on Improved Oil Recovery, Tulsa.

Tambach, T.J., Loeve, D., Hofstee, C., Plug, W.J. and Maas, J.G., 2014. Effect of CO_2 Injection on Brine Flow and Salt Precipitation After

Gas Field Production. Transport in Porous Media.
Tanzil,D., Hirasaki G. and Miller C.A., Conditions of foam generation in Homogeneous Porous Media, SPE/DOE IOR Symp., Tulsa, Oklahoma, 13-17 April 2002
Tarcan G., 2005. Mineral saturation and scaling tendencies of waters discharged from wells (>150ºC) in geothermal areas of Turkey, Journal of Volcanology and Geothermal Research, 142, 263-283
Tung, C.-Y. M., and Dynes, P. J., 1982. Relationship between viscoelastic properties and gelation in thermosetting systems, Journal of Applied Polymer Science, 27(2), 569-574.
Turner, B. O., and Zahner, R. L., 2009. Polymer gel water-shut off applications combined with stimulation increase oil production and life of wells in the Monterey formation offshore California, in SPE Western Regional Meeting, Society of Petroleum Engineers, San Jose, California.
Wang, Y., Bryan, C., Dewers, T., Heath, J. and Jove-Colon, C., 2013, Ganglion dynamics and its implications to geologic carbon dioxide storage, Environmental Science and Technology, 47 (1), 219-226.
Wasch L.J., Wollenweber J. and Tambach T.J., A novel concept for long-term CO_2 sealing by intentional salt clogging, GHG:S&T, Vol 3 (6), p. 491-502, 2013.
Wassmuth, F.R., Hodgins, L.A., Schramm, L.L., and Kutay, S.M., Screening and coreflood testing of gel foams to control excessive gas production in oil wells, SPE Reservoir Evaluation & Engineering, June 2001
Wassmuth, F.R., Green, K, and Hodgins, L., 2004. "Water Shutoff in Gas Wells: Proper Gel Placement is the Key to Success" SPE Production & Facilities, pp.217-227. SPE 89403, Paper presented at the SPE/DOE Symp. on Improved Oil Recovery, Tulsa.
Whitney, D., Montgomery, D. and Hutchins, R., 1996. Water shutoff in the North Sea: Testing a new polymer gel system in the Heather field, UKCS block 2/5, SPE Production & Operations, 11(2), 108-112.
Wong, F.Y., Fong, D.K., McIntyre, F.J. and Kuehne, D.L., 1997 Design and field trial application of foam in production wells to improve conformance, J. Cdn. Pet. Tech. 36(2), 21-32.
Woo, G., Lopez, H., Metcalf, A. and Boles, J., 1999. A new microemulsion polymer gelling agent with an external surfactant gellant activator improves acid fracturing, in Latin American and Caribbean Petroleum Engineering Conference, Society of Petroleum Engineers, Caracas, Venezuela.
Wouterlood, C., Falcigno, E., Gazzera, C. and Norman, C., 2002. Conformance improvement with low concentration polymer gels in a heterogeneous, multilayer reservoir, in SPE/DOE Improved Oil Recovery Symposium, Society of Petroleum Engineers Inc., Tulsa, Oklahoma.
Zeidouni, M., Pooladi-Darvish, M. and Keith, D., 2009. Analytical solution to evaluate salt precipitation during CO_2 injection in saline aquifers. Int. J. Greenh. Gas Control, 3, 600-611.
Zhao, H., Zhao, P., Bai, B., Xiao, L. and Liu, L. 2006. Using associated polymer gels to control conformance for high temperature and high salinity reservoirs, Journal of Canadian Petroleum Technology, 45(5).
Zhao, D.W. and Gates, I.D., 2013. Stochastic Optimisation of Hot Water Flooding Strategy in Thin Heavy Oil Reservoirs. SPE paper 165541, presented at the SPE Heavy Oil Conference, Calgary, Canada, June 11-13, 2013.

Chapter II

Adaption of injection strategy as flow diversion option

Bernd Wiese[1], Daniel Loeve[2], Cor Hofstee[2]
[1] GFZ, Germany
[2] TNO, The Netherlands

SUMMARY

This report is part of the research project MiReCOL (Mitigation and Remediation of CO_2 leakage) funded by the EU FP7 program. Research activities aim at developing a handbook of corrective measures that can be considered in the event of undesired migration of CO_2 in the deep subsurface reservoirs. MiReCOL results support CO_2 storage project operators in assessing the value of specific corrective measures if the CO_2 in the storage reservoir does not behave as expected. MiReCOL focuses on corrective measures that can be taken while the CO_2 is in the deep subsurface. The general scenarios considered in MiReCOL are 1) loss of conformance in the reservoir (undesired migration of CO_2 within the reservoir), 2) natural barrier breach (CO_2 migration through faults or fractures), and 3) well barrier breach (CO_2 migration along the well bore).

The aim of this report is to model the effects of different injection scenarios to control the CO_2 movement in the reservoir and to prevent CO_2 from arriving at and passing through pre-defined undesired migration paths, which may be faults, fracture zones or spill points. Based on the outcome of the different model scenarios, the response time of remediation, longevity of the remediation measure, spatial extension of the remediation and remediation costs are assessed.

Different reservoir management scenarios are carried out based on the Ketzin test site for geological storage and the Johansen geological model.

The most efficient management strategies are those that include a variation of the injection position. Lateral movements may induce minor variations that occur due to slight differences in the distance of the fracture zone and varying dip gradients. Alternation of the injection position is cost efficient, although local surface conditions might induce minor differences, the order of magnitude remains constant as long as the number of wells is not increased.

Reservoir management strategies that are based on temporal changes of the injection regime do not result in high costs, but the longevity of remediation is very low, there is no significant impact on the arrival time. The injection through multiple wells produces high costs of drilling and installation, but the longevity of this measure is also not significant.

Three different scenarios are found for the Johansen model which will serve as a base case for further work in the MiReCOL project, for which flow diversion can be a potential a diversion option.

1 INTRODUCTION

The selection of appropriate CO_2 injection strategies offers potential for increasing safety and longevity of the containment. An appropriate strategy can potentially prevent or at least retard CO_2 from arriving at and passing through pre-defined undesired migration paths, which may be faults, fracture zones or spill points. By this it may decrease the risk that active remediation becomes necessary, such as gel and foam injection, brine injection or chemical immobilization of CO_2 itself at a later stage of the storage cycle. Therefore an appropriate injection strategy as proactive measure maybe quite cost efficient compared to active remediation.

The potentials and limitations of an adapted injection strategy are investigated at two sites. The impact of different management techniques such as variation of injection location and injection rate also considering different geological conditions are investigated at the Ketzin site for CO_2 storage, Germany. As a result, the choice of the injection location is probably the most effective management technique. This is investigated in the second part of the report. At the Johansen field site for CO_2 storage, Norway, a detailed case study is carried out to optimise the injection location.

This is the second report on CO_2 plume diversion by adapting the injection strategy in the MiReCOL project. Deliverable D 3.1 named "Current flow diversion techniques in the petroleum industry relevant to CO_2 leakage remediation" summarizes the state of the art for flow diversion with a wider scope; forming the base for work on flow diversion that includes injection of other fluids and materials into the reservoir.

2 MANGEMENT TECHNIQUES - KETZIN MODEL

2.1 Site description

The Ketzin site for CO_2 storage is located in the sedimentary Northeast German Basin about 25 km west of Berlin, Germany, at the south-eastern flank of the Roskow-Ketzin double anticline. The CO_2 is injected into the Upper Triassic Stuttgart Formation. The injection well Ktzi 201 is located at the southern flank of the anticline, penetrating the Stuttgart formation approximately between 630 and 710 m below ground level, with the main reservoir facies between 633 and 651 m below ground level. A total amount of about 67,000 tons of CO_2 have been injected between June 2008 and August 2013. All simulations are carried out with Eclipse 300. Dissolution of CO_2 in reservoir brine is included.

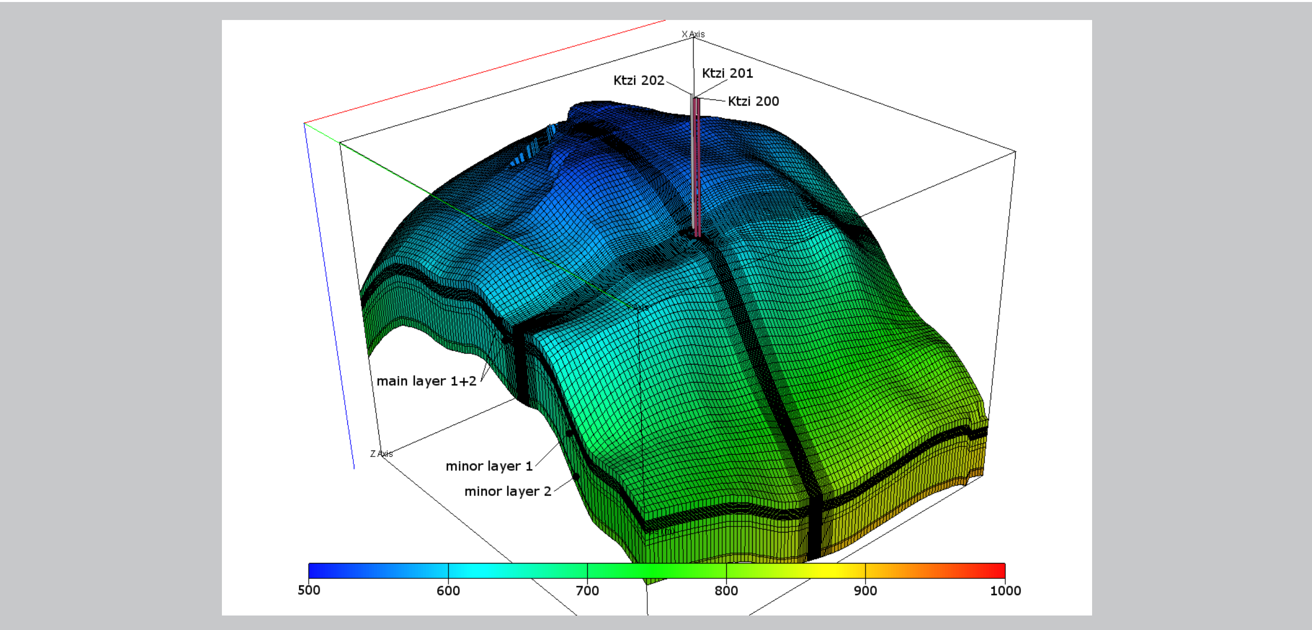

Figure 1 South West view of the Ketzin storage site geological model. The colours indicate the depth of the cells, the black lines indicate cell outlines. The model has an extent of 5x5 km. The three vertical lines indicate the injection well Ktzi 201 and the two observation wells Ktzi 200 and Ktzi 202. The main layers in the upper part of the reservoir have a model thickness of 6 m each.

2.2 Method

2.2.1 Geology

The geological model is constructed based on the lithostratigraphy observed in the wells Ktzi 200, Ktzi 201 and Ktzi 202. The sandstone facies found in these wells is introduced to the entire model, with the layer structure following the topology of the anticline. The main reservoir horizons have a vertical discretization of 1 m, appearing as dark layer in Figure 1. The horizontal discretization is 10 m close to the wells, appearing as dark cross, and increases to 50 m for the far field.

Two minor reservoir layers below are represented with a single model layer each. The reservoir permeability follows single wellbore pumping tests (Wiese et al., 2010) in each of the three wells with a value of 100 mD. The main reservoir consists of two sandstone

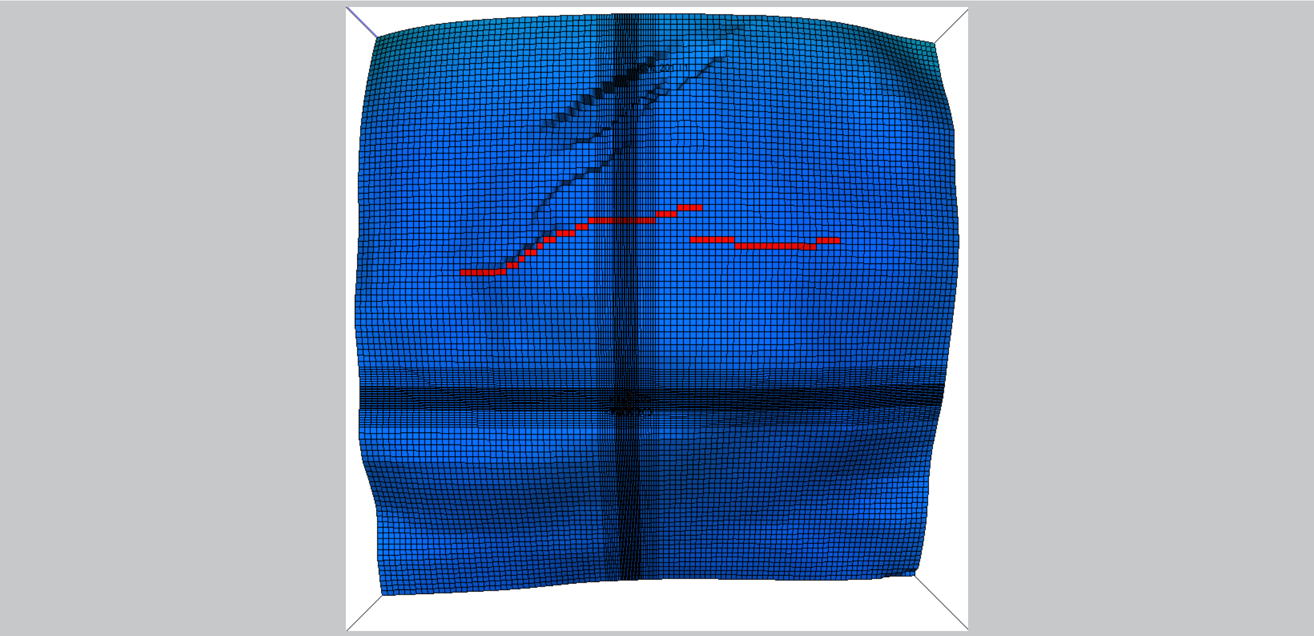

Figure 2 Top view on the Ketzin anticline model. The injection well Ktzi 201 is located in the lower part of the model. Faults exist in the upper part of the model, some of them show vertical displacements. The red lines indicate the southern faults. These represent the undesired migration paths that should not be reached by the CO_2 plume.

layers that are horizontally divided by an anhydrite layer. Upstream of the injection point, at observation well Ktzi 202 one of these sandstone layers disappears. Although it is not evident which of both sandstone layers is continuous, the upper layer is considered as continuous in this study while the permeability of the lower layer is reduced to 1 mD close to Ktzi 202.

Several faults exist at the top of the anticline. These faults (Figure 2) represent the pre-defined undesired migration pathways because CO_2 might percolate to overlying strata. For practical reasons simulations are carried out such that these faults should not get in contact with CO_2 and the simulations are interrupted when CO_2 arrives at the faults. Arrival at the faults and arrival times are therefore prime criteria to assess effectiveness of the different model scenarios and reservoir managements studied. The faults are introduced as permeable.

2.2.2 Relative permeability

Relative permeability values follow core experiments (Scherpenisse and Maas, 2009, Figure 3). Hysteresis is not considered. For computational efficiency capillary pressure is not included in regular simulations. The outer boundary conditions mimic time constant hydraulic potential.

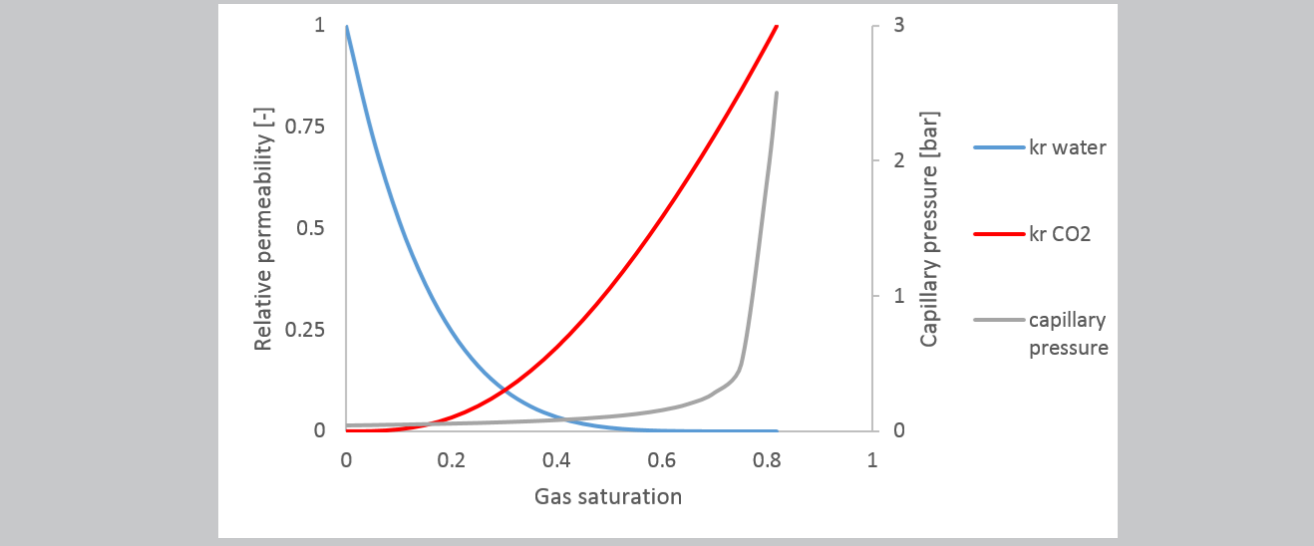

Figure 3 Relative permeability functions applied to the reservoir facies (following Scherpenisse and Maas 2009).

2.2.3 Temporal discretisation

The temporal discretisation follows changes in the injection rate. Changes of the injection rate are introduced with the real time and an average injection rate for the respective period. On average, the periods of constant injection rate have duration of three weeks.

2.2.4 Main reference Model

The above described model is set up with parameters similar to the Ketzin test site. It is the main reference model for the following investigation and therefore named "scenario 0". In variations on scenario 0 different operational scenarios are simulated. These scenarios imply a modification of the Ketzin field conditions and evaluate the consequences with respect to the predefined undesired migration path represented by faults at the top of the anticline. Operational scenarios investigate the impact of different injection well positions and different temporal injection scenarios. Furthermore, geological scenarios are calculated to rank the potential impact of geological conditions with respect to operational potential.

2.3 Results

2.3.1 Variation of the injection location

A variation of the injection location is probably the most basic method to change the plume shape and spreading of CO_2. Eight scenarios of injection locations are simulated, with a shift of 400 and 800 m, respectively to each cardinal direction (Table 1). The west/east shifting follows approximately the iso-depth of the anticline, while the north/south shift follows the largest gradient (Figure 4).

Table 1 Spatial variation of the injection positions and resulting arrival times at the critical faults zones.

	Direction	Distance [m]	Arrival time [years]	Difference to Case 0 [days]
Scenario 0	-	-	14	0
Scenario E400	East	400	13	-135
Scenario E800	East	800	16	554
Scenario W400	West	400	10	-1050
Scenario W800	West	800	8	-1591
Scenario N400	North	400	7	-1818
Scenario N800	North	800	3	-2867
Scenario S400	South	400	19	1350
Scenario S800	South	800	21	1859

In all simulated scenarios the CO_2 arrives at the fault. The most effective way of increasing the duration is to move the injection point further from the faults in southern direction. This increases the horizontal distance and also the difference in elevation. The arrival time is less affected by variation in east-west direction, and the duration decreases for most variations. These occur due to local depth gradients of the reservoir. For some injection points the plume can spread into two minor plumes, however with little impact on the arrival time (scenario W400, Figure 4b).

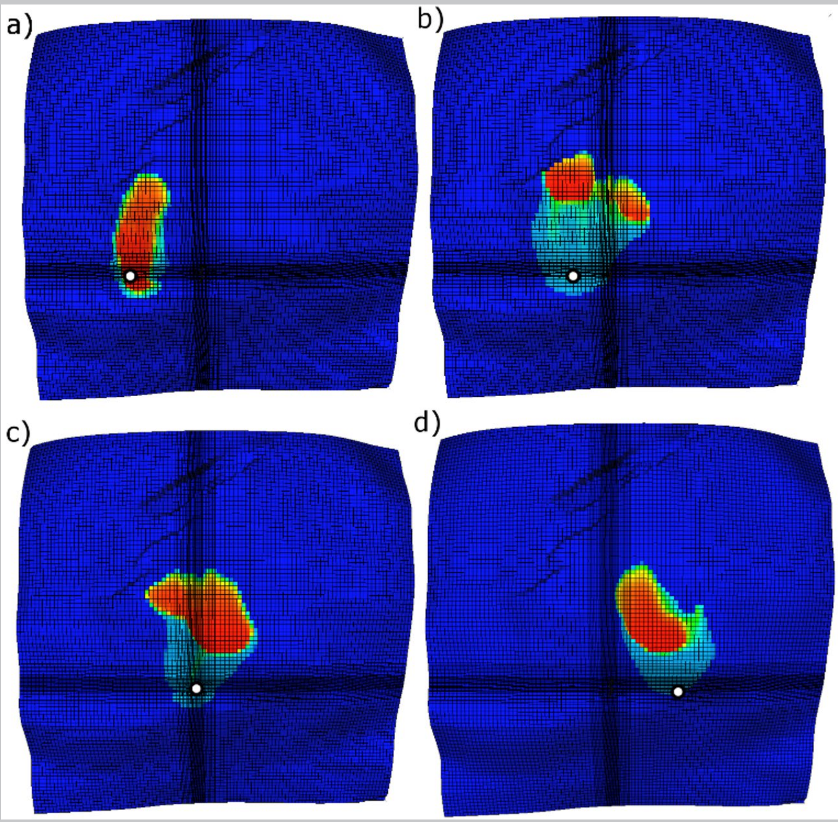

Figure 4 Plume shape at the time of arrival at the faults, with different well positions. a) Scenario W800, b) scenario W400, c) scenario 0, d) scenario E800. The plume shape differs due to the different anticline shape, in scenario W400 the plume splits up at a saddle point.

2.3.2 Variation of injection rate

The variation of the injection rate is an inexpensive reservoir management option, albeit with large implications on site design or contractual implications. It is investigated whether a temporal change of the injection rate results in a different plume behavior. For comparison it is ensured that the injected mass is identical for all scenarios.

For a constant injection rate different durations are simulated. Scenario const has the duration of the real injection but applying constant rate, the scenarios const2 and const4 have a duration that is the fraction of the real injection with accordingly higher injection rate (Table 2, Figure 5).

Table 2 Arrival times for the scenarios involving a modified injection rate. The number behind the constant scenarios refers to the ratio of injection duration. The number behind the alternation scenarios refers to the duration of each alternation cycle in days. The injected mass is identical for all scenarios.

	Type	Injection duration [days]	Arrival time [years]	Difference to Case 0 [days]
Scenario 0	Real injection rate and duration	1886	14	0
Scenario const	Constant rate	1886	13	-132
Scenario const2	Constant rate	943	14	126
Scenario const4	Constant rate	471.5	15	333
Scenario alt1	Alternation duration 1 day	1886	13	-103
Scenario alt10	Alternation duration 10 days	1886	13	-78
Scenario alt100	Alternation duration 100 days	1886	14	-11
Scenario 3w	Three injection wells with the positions of Case W400, Case 0, Case E400	1886	11	-581

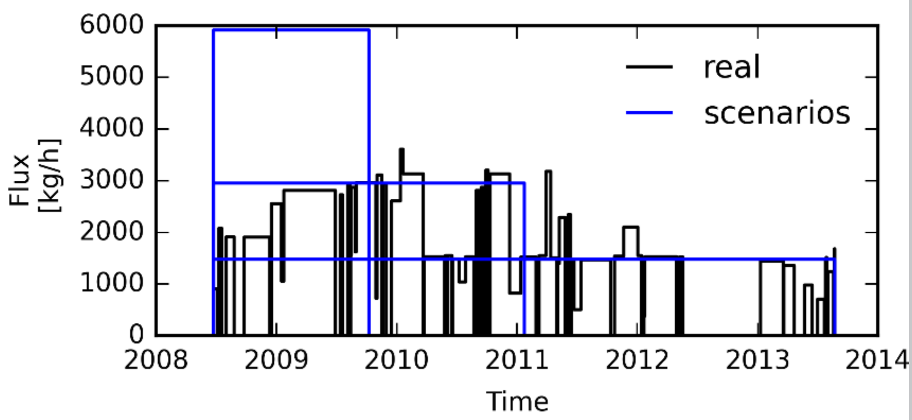

Figure 5 Injection rates for scenario 0 and the constant rate scenarios. The black curve represents the real injection rate of the Ketzin site, the blue curves represent constant injection rates with different duration. The injected mass is identical for all curves.

The impact of alternating injection is tested by three scenarios in which 50% of the time injection occurs and 50% is shut-in time. The duration of the intervals is 1, 10 and 100 days, indicated by the names scenario alt1, scenario alt10 and scenario alt100.
The impact of multiple injection wells is tested by an additional scenario (scenario 3w). In this scenario the real injection rate is equally distributed to three wells. In addition to the injection well Ktzi 201 two hypothetical injection wells are introduced to the model with the position 400 m east and west of Ktzi 201, respectively (Figure 6).

Generally, the arrival time of all scenarios does not show large differences. The largest difference occurs for the scenario with multiple injection wells, where the arrival time decreases by 581 days. The subplume generated by the eastern well reaches the fractures first. The arrival time of 11 years is comparable to scenario W400, which has the same well positions but only one third of the injection rate and leads to an arrival time of 10 years. This means that the impact of the injection rate is significantly lower compared to the impact of the well position. This is confirmed by the scenarios with constant injection rate and different duration. Constant rate injection shows a very similar arrival time of only 132 days earlier compared to real injection rate, which is characterized by interruptions and discontinuities. The arrival time does not show a substantial variation for the higher rate and shorter time rates (scenario const 2 and const 4). Nevertheless, the arrival time shows a slight increase of 126 and 333 days, respectively. This is surprising, since the CO_2 is injected effectively earlier compared to scenario const. The behaviour occurs because the Ketzin model is a multilayer system. Higher injection pressure has a larger gravity override effect and therefore causes a larger fraction of the CO_2 to be injected in the minor layers

(Figure 7). Although some of the CO_2 from the lower layers flows through the open well after injection stop, there is a smaller amount of CO_2 present in the main layer 1 where the arrival at the faults occurs.

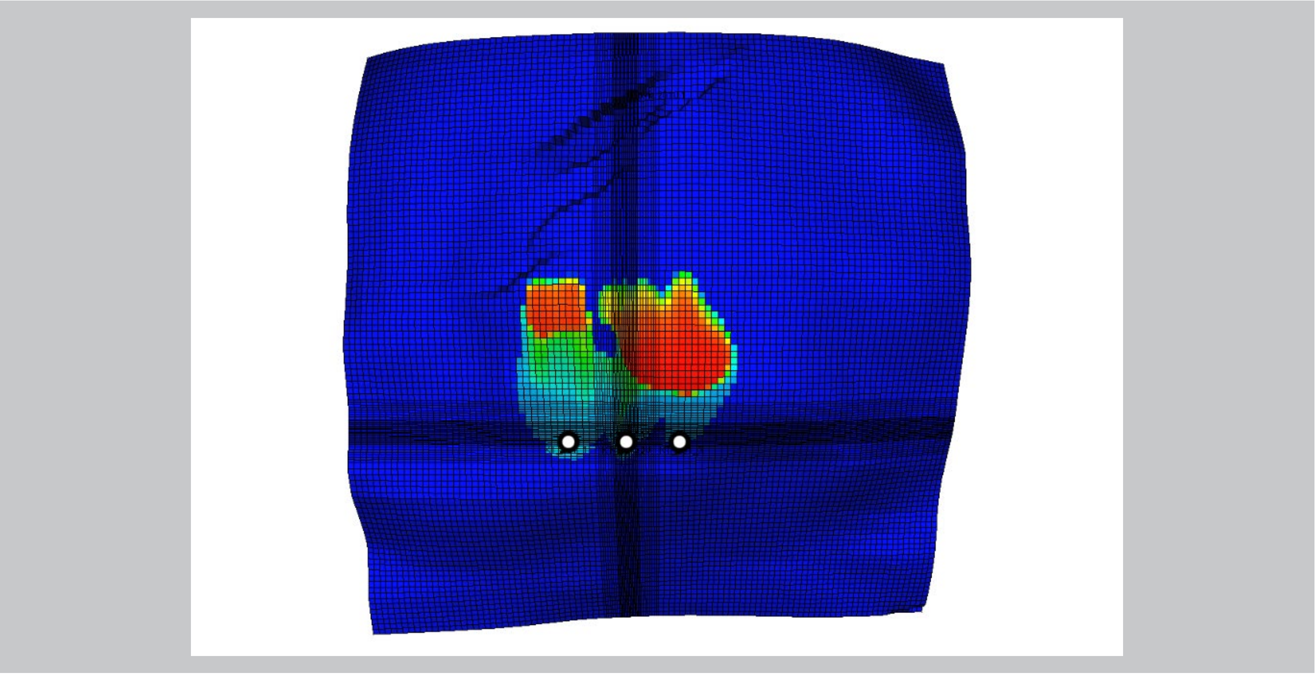

Figure 6 Gas saturation of scenario 3w. The dots indicate the well positions.

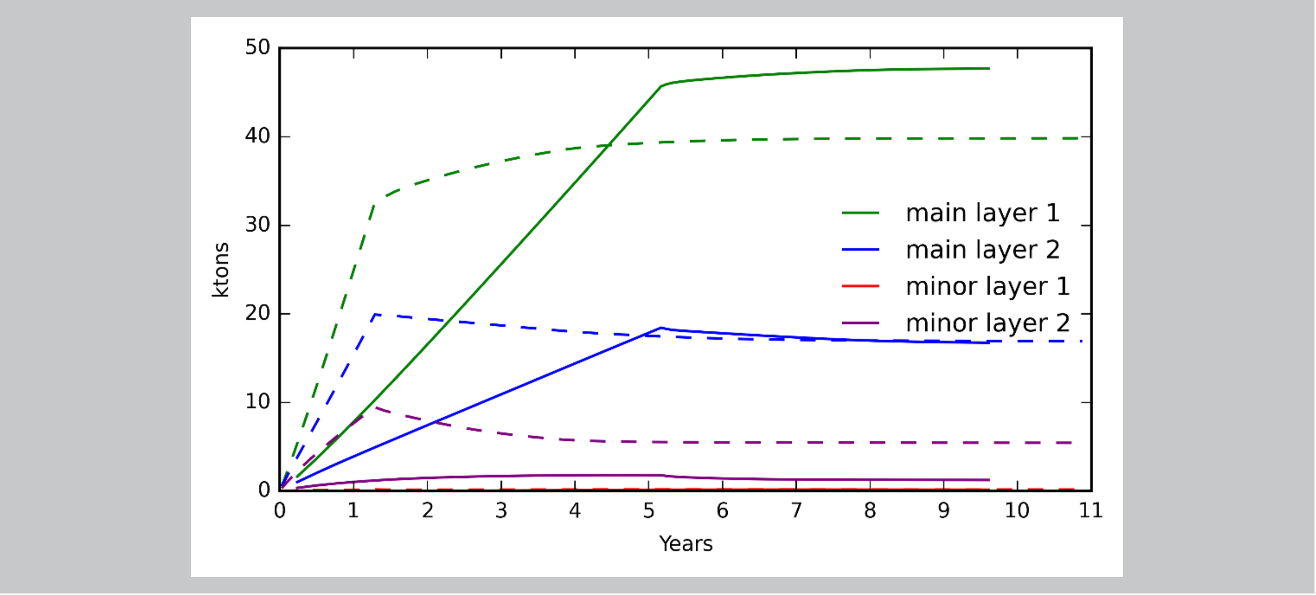

Figure 7 Distribution of CO_2 in the reservoir layers with different injection rate. The continuous lines show the base scenario (scenario 0), the dashed lines show scenario const4, where the fourfold rate is injected during a quarter of the injection time.

2.3.3 Variation of the geological model

The geologic setting of the reservoir itself may have a dominating impact on the arrival time. Although geology cannot be the subject of reservoir management, it determines the movement and spreading of the CO_2 plume. The shape of the anticline is well known from seismic surveys, wherefore the geologic structures follows Norden and Frykman (2013). The horizontal distribution of the reservoir facies is subject to higher uncertainty. This uncertainty of the reservoir characteristics is reflected in different scenarios (Table 3).

For scenario 0, the reservoir layers are generally assumed as homogenous (Figure 8). This is a reasonable approximation to unknown geology and represents an average permeability for the Ketzin reservoir. A heterogeneous field imposes strong prior constraints on the management scenarios e.g. since the permeability in the near wellbore area depends on the well position. This would induce discontinuities and secondary effects on the variation of single parameters. The vertical representation of well permeable reservoir facies follows the wellbore profiles in the three wells Ktzi 200, Ktzi 201, Ktzi 202. The main reservoir layers are represented with a thickness of 6 m each (discretisation 1m). To these layers generally a permeability of 100 mD is assigned, with exception for the northern part of the upper sandstone layer, since only one layer is present in the well Ktzi 202 (Figure 3).

The scenario pcap includes the capillary pressure function in multiphase simulation. Nevertheless, the impact of capillary pressure is similar for all scenarios, therefore this is neglected in the other simulations for computational efficiency. The capillary pressure function follows Lengler (2012). The application of capillary pressure increases the arrival time by 555 days. The shape of the plume is not significantly affected.

Table 3 Arrival time for scenarios involving a modification of the geological model.

	Geology	Arrival time [years]	Difference to Case 0 [days]
Scenario 0	Mainly homogenous model, 100 mD	14	0
Scenario pcap	With capillary pressure	16	555
Scenario 50	Mainly homogenous model, 50 mD	28	3794
Scenario 200	Mainly homogenous model, 200 mD	7	-1822
Scenario swap	upper and lower sandstone layer swapped	15	480
Scenario invers	Permeability calibrated on pressure and arrival time	22	2219
Scenario stoch	Stochastic permeability and porosity	46	8565

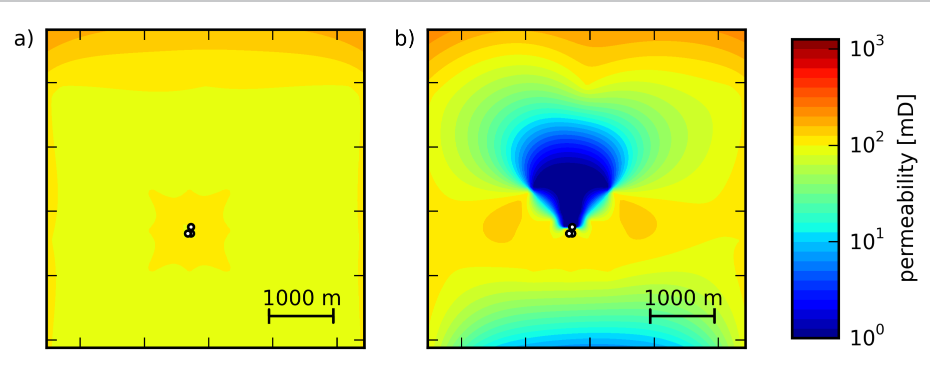

Figure 8 Hydraulic permeability for "Scenario 0", plot a) corresponds to the upper sandstone layer, plot b) corresponds to the lower sandstone layer. The wells are represented by points.

"Scenario 50" and "Scenario 200" have the same geologic structure with variation of the reservoir facies permeability by factor 2, to 50 and 200 mD, respectively. The arrival time follows proportionally to this property. Having in mind the permeability may vary over several orders of magnitude, it has a dominating impact on potential remediation.

Further scenarios should provide an overview of the impact of horizontal variability. Considering the enormous bandwidth of potential geological structures, the approach intends to capture some realistic magnitude. However, the full range cannot be captured here.

The "Scenario swap" reflects that the reservoir layer found in Ktzi 202 may be part of the lower sandstone layer. The latter is continuous up to the fault region wherefore arrival occurs there. The arrival time is increased by 480 days. Gravity segregation between CO_2 and brine induces preferred flux in more shallow layers under otherwise identical geological conditions. Therefore the arrival is delayed when the lower reservoir layer is continuous.

The "Scenario invers" is based on a pressure data constrained permeability field. It is generated to match the pressure data of pre-injection hydraulic tests, pressure data of the first 30 days of injection, and the arrival time in observation well Ktzi 200 (Figure 9). Strong heterogeneities occur in the vicinity of the near wellbore area (Figure 9 c, d), while the far field is comparatively homogenous. The arrival time increases by 7 years since the permeability around the injection well screen reduced the flux into the upper layer, where the arrival occurs, is significantly reduced (Figure 9c) and therefore the injected amount of CO_2 is decreased. Furthermore, the permeability is slightly lower compared to "Scenario 0".

The "Scenario stoch" is based on a stochastic permeability and porosity field (Norden and Frykman, 2013). The permeability varies over 6 orders of magnitude, with an arithmetic mean value of 100 mD and a geometric mean value of 4 mD. The high permeability structures do not form a continuous network, the CO_2 has to pass through several low permeable regions. As consequence the arrival time of 46 years is longest for all considered scenarios.

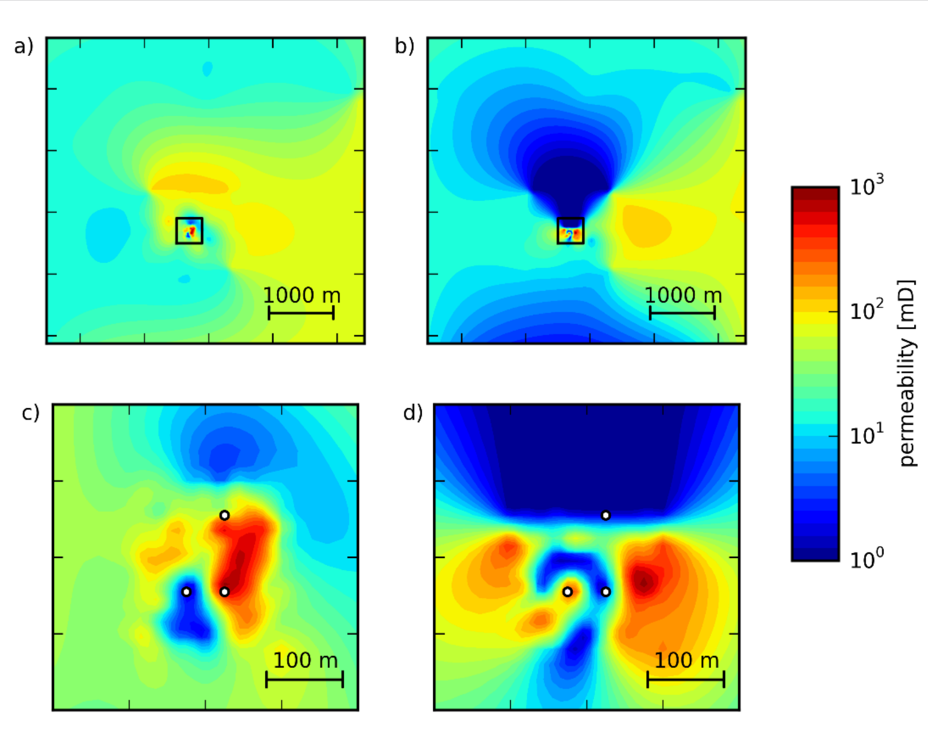

Figure 9 Calibrated permeability field matching hydraulic tests, CO_2 injection pressure and arrival time. Plots a) and b) show the main sandstone layers 1 and 2, the fault positon follows Figure 2, plots c) and d) show the insets from the above plots. The wells are represented by points.

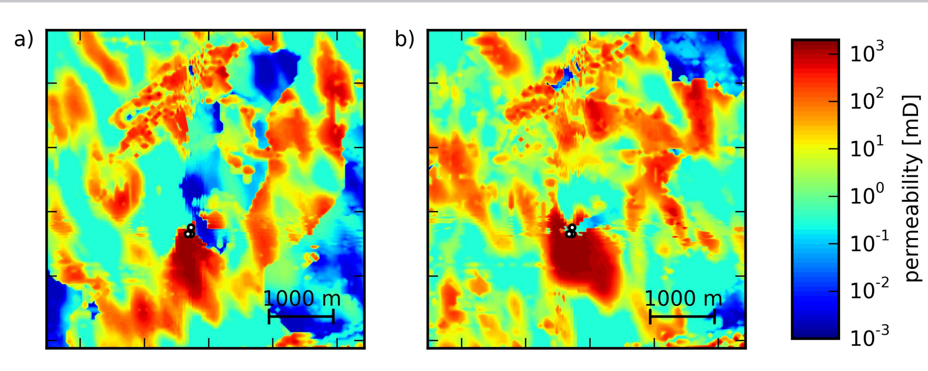

Figure 10 Stochastic permeability heterogeneity field following Norden and Frykman (2013). The plot a) shows a cross section of the upper sandstone layer, plot b) a cross section of the lower sandstone layer. The wells are represented by points.

2.4 Conclusions on Ketzin

Based on the Ketzin test site for geological storage, different reservoir management scenarios are carried out. In all scenarios the CO_2 reached the pre-defined undesired migration paths, represented by faults. An equilibrium state where the CO_2 does not reach the fault zone was not obtained. The most efficient management strategies are those that include a variation of the injection position. A downdip shift may increase the arrival time by 7 years, but an updip shift by the same distance can severely decrease the arrival time by 11 years. Lateral movements may induce minor variations that occur due to slight differences in the distance of the fracture zone and varying dip gradients. Reservoir management strategies that are based on temporal changes of the injection regime do not provide high cost, but the longevity of remediation is very low, there is no significant impact on the arrival time. The injection through multiple wells produces high costs of drilling and installation, but the longevity of this measure is also not significant.

Different geologic structures are simulated. Although geology cannot be subject of reservoir management, its variability should be considered for further management strategies. The effective permeability has a dominating impact on the plume behaviour and induces an arrival time variation proportional to the variation in permeability. This is generally also valid for heterogeneous permeability fields, the heterogeneity based on Ketzin data has been found to increase arrival time the most, by a time of 32 years since it implies a significant lower effective permeability on the reservoir scale. The distribution of the injected CO_2 to the different layers in a multilayer reservoir can induce significant variations in the arrival time. Due to gravity segregation CO_2 flows preferably into more shallow parts of the reservoir. For containment, however, it would be desirable to focus injection to layers where geologic structures reduce the connectivity to the fault region.

3 CASE STUDY - JOHANSEN MODEL

3.1 Site description

The field under consideration for this study is the Johansen formation, located off the coast of Norway (Figure 11). The aquifer is located at a depth of 2100-2400 m with an average thickness of roughly 100m (Eigestad et al, 2009, Christiansen et al, 2009). The lateral extent is about 100 km in the North-South direction and 60 km in the east-west direction. The average porosity is approximately 20-25 percent and permeability ranging from 64 to 1660 mDarcy. A theoretical storage capacity of >1Gton is estimated by Eigestad et al. (2009).

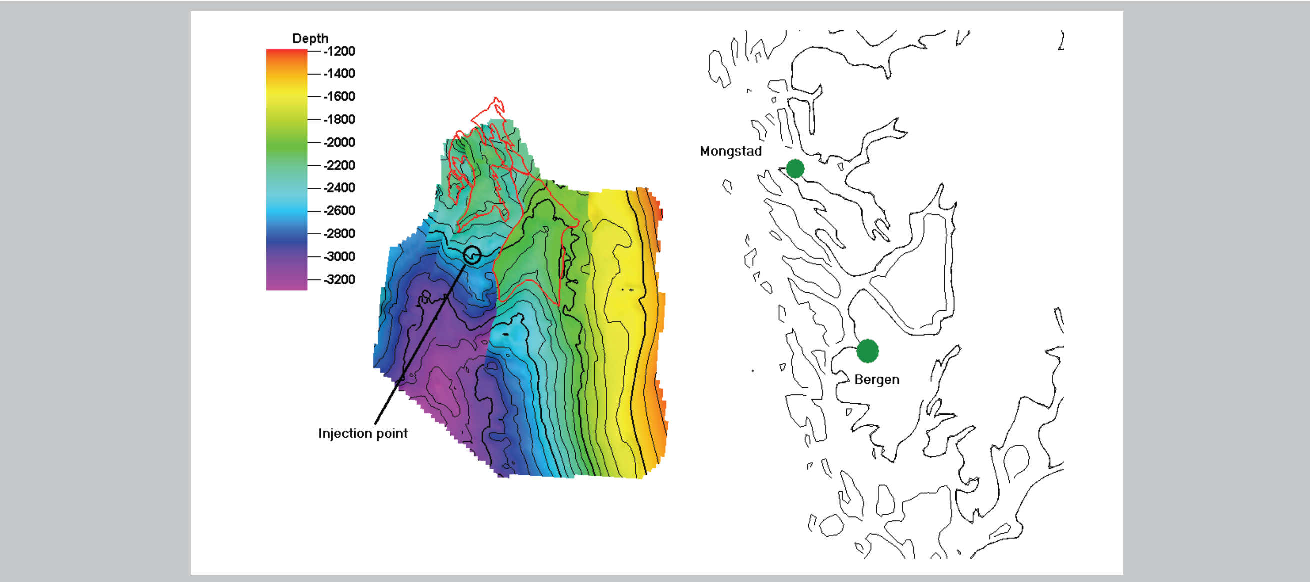

Figure 11 Depth map of the top of the Johansen formation and its location, with respect to the coast of Norway. Also indicated is a proposed injection site (from Bergmo et al, 2009).

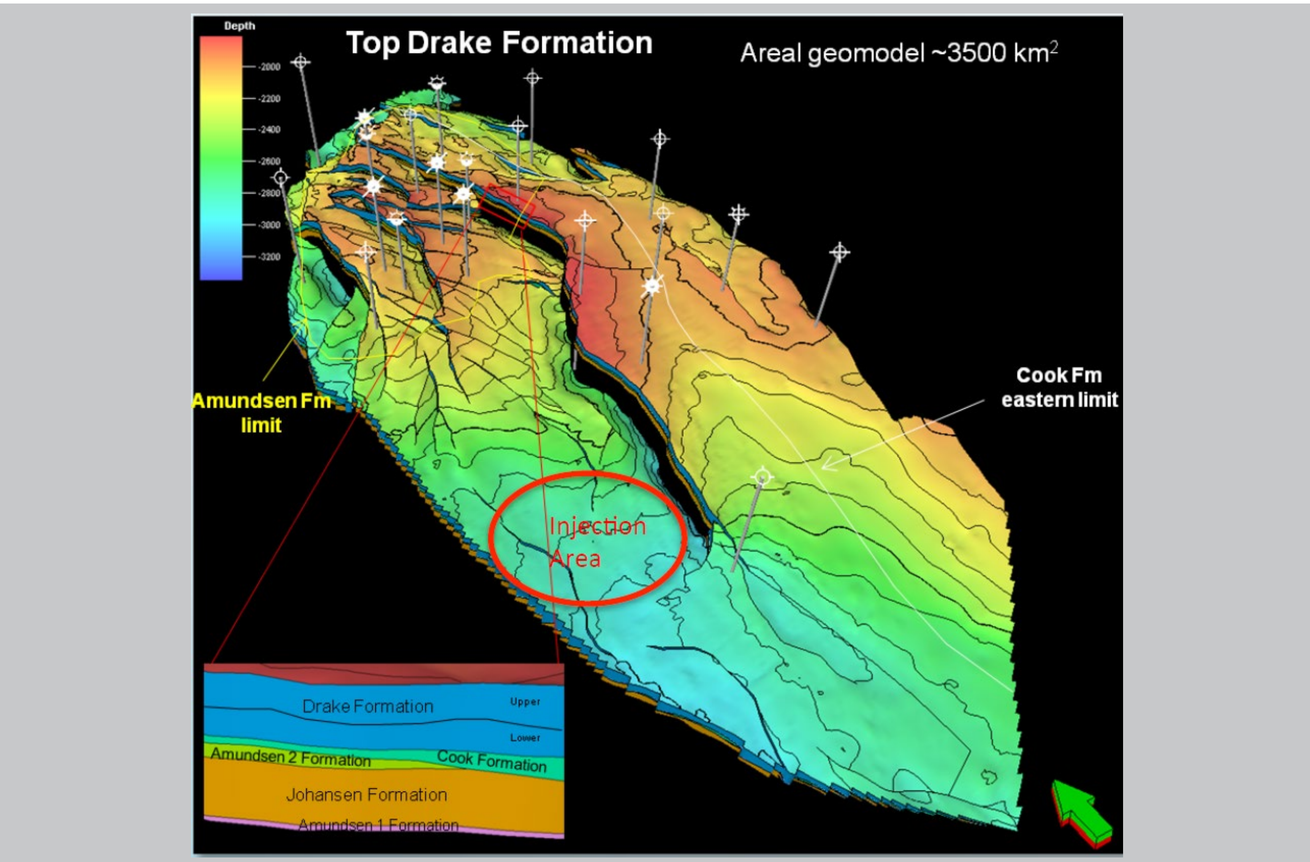

Figure 12 Overview of geological model with Drake formation (seal) and two aquifer formations (Johansen and Amundsen). The image is courtesy of Gassnova.

The area of most interest is around the Troll hydrocarbon field (red lines in Figure 11), which is located in the upper part of the aquifer. In this way the storage project can benefit the most of the existing infrastructure and is also close to the CO_2 source in Mongstad.

This aquifer has been subject of a feasibility study into the possible underground storage of CO_2 coming from industrial companies on-shore Norway. The robust storage capacity was estimated to be 330 Mton of CO_2 (Bergmo et al, 2009), which takes into account the main uncertainties as the size of the communicating pore volume, fault properties and properties of the primary sealing formation. Reservoir simulations on this storage compartment were also reported by Wei and Saaf (2009).

The Johansen formation is bounded by faults in the north and east. In the northern part of the Johansen formation many faults are identified with possible spill-points. The main seal of the aquifer is formed by the Drake formation (Figure 12).

3.2 Method

3.2.1 Simulator used Schlumberger's Eclipse 100 black-oil simulator

For the dynamic modeling of the Johansen field we have used Schlumberger's Eclipse black-oil simulator (also known as Eclipse 100). The Eclipse black-oil reservoir simulation software is a fully implicit, three-phase, three-dimensional, general purpose black-oil simulator. The black-oil model assumes that the reservoir fluids consist of three phases namely oil, water, and gas, with gas dissolving in oil. In our model we only enabled the water and the gas phases, representing water and CO_2 respectively. Dissolution of CO_2 is not considered.

The geological grid used in this study is described by Bergmo et al (2008) In this report we focus on a smaller area of the Johansen field and a section was made inactive, which can be seen in the number of grid blocks used in the final dynamic model.

Table 4 Overview of grid dimensions in the simulation model.

	Number grid blocks x-direction NX	Number grid blocks y-direction NY	Number grid blocks z-direction NZ	Total number of grid blocks	Number of activegrid blocks
Dynamic grid	55	281	83	995,170	526,272

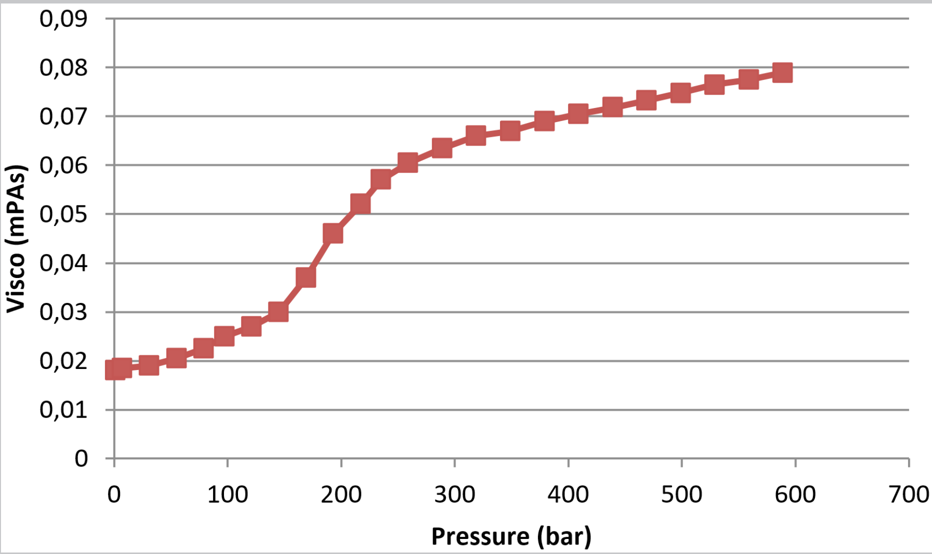

Figure 13 Viscosity of pure CO_2 as function of pressure, at a temperature of 94 °C.

3.2.2 Pressure, Volume, Temperature (PVT) data

3.2.2.1 Gas PVT

For the Gas PVT we applied NIST data to generate tables based on an aquifer temperature of 94 °C (Bergmo et al, 2008).
The gas viscosity and the formation volume factor as function of pressure of the pure CO_2 are shown in Figure 13 and Figure 14, respectively.

3.2.2.2 Water PVT

The water formation volume factor is 1.0132 rm^3/sm^3 at reservoir conditions at a reference pressure of 215 bar. The water compressibility at reservoir conditions is 3.97954 x 10^{-5}/bar. The water viscosity is 0.39851 (mPas) at reservoir conditions at a reference pressure of 215 bar.

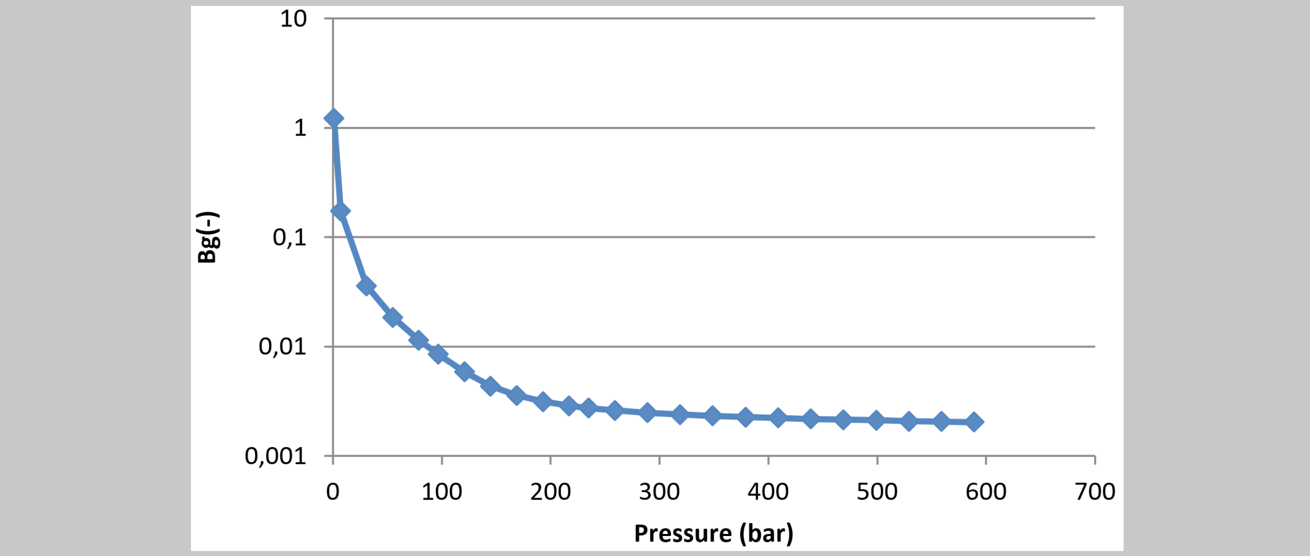

Figure 14 Reservoir volume factor (BG) versus pressure, at a temperature of 94 °C.

3.2.3 Saturation functions and pressure dependent rock properties

3.2.3.1 Relative permeability

The relative permeability-saturation curves for the carbon dioxide were made hysteretic, while those of the wetting fluid (brine) were left non-hysteretic (see Figure 15).

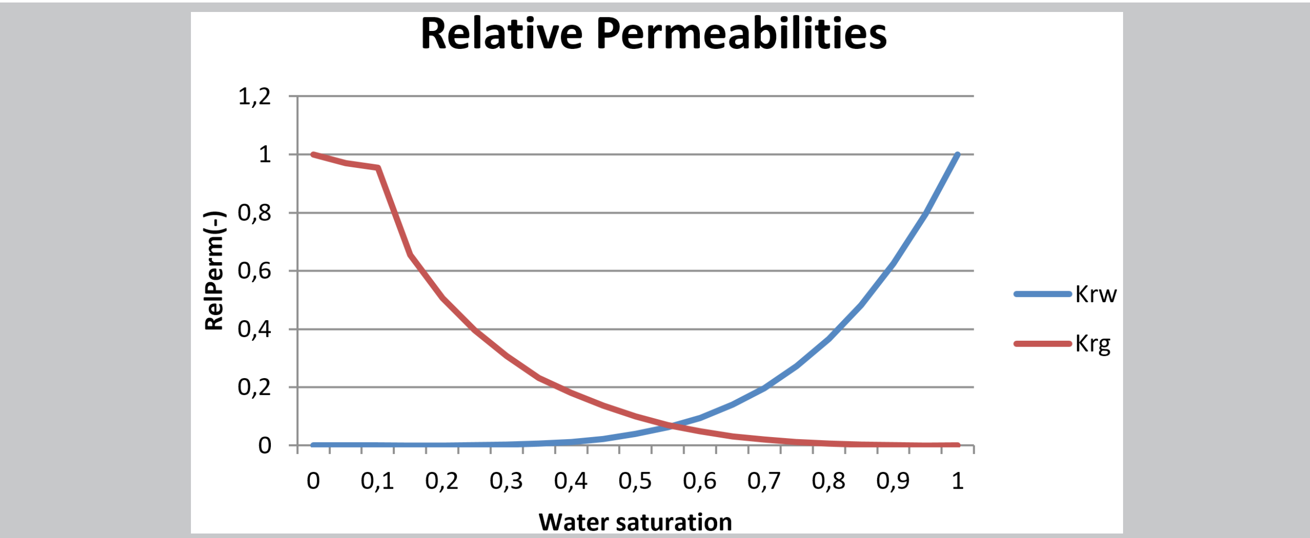

Figure 15 Relative permeability (based on a similar Dutch aquifer).

3.2.3.2 Capillary pressure

In our modelling we assumed the capillary pressure does not play an important role and was set to 0.

3.2.3.3 Rock Compressibility

The rock compressibility is set to standard value of 5.0e-5 1/bar at a reference pressure of 200 bar.

3.2.4 Initial conditions

The starting point was a static geological model of the Johansen aquifer, as supplied by Bergmo et al, 2008). From the complete model the western section (63*183*36 grid cells, Figure 12) with most measured properties was selected for the reservoir modelling. The reservoir is initially assumed to be in hydrodynamic equilibrium with a reservoir pressure of 220 bar at a depth of 2200 m and a reservoir temperature of 94 °C. We used an isothermal model, hence all temperature dependent fluid and rock properties are specified at reservoir temperature.

3.2.5 Well Locations

For all simulations 1.1 Mton CO_2 per year were injected for 113 years in layer 15-18 (Johansen formation) of the model. Various injection locations were chosen and the resulting migration paths investigated for critical issues concerning the storage compartment integrity. To allow enough time for the migration the modelling was continued until the year 9000. The various injection locations are displayed in Figure 16.

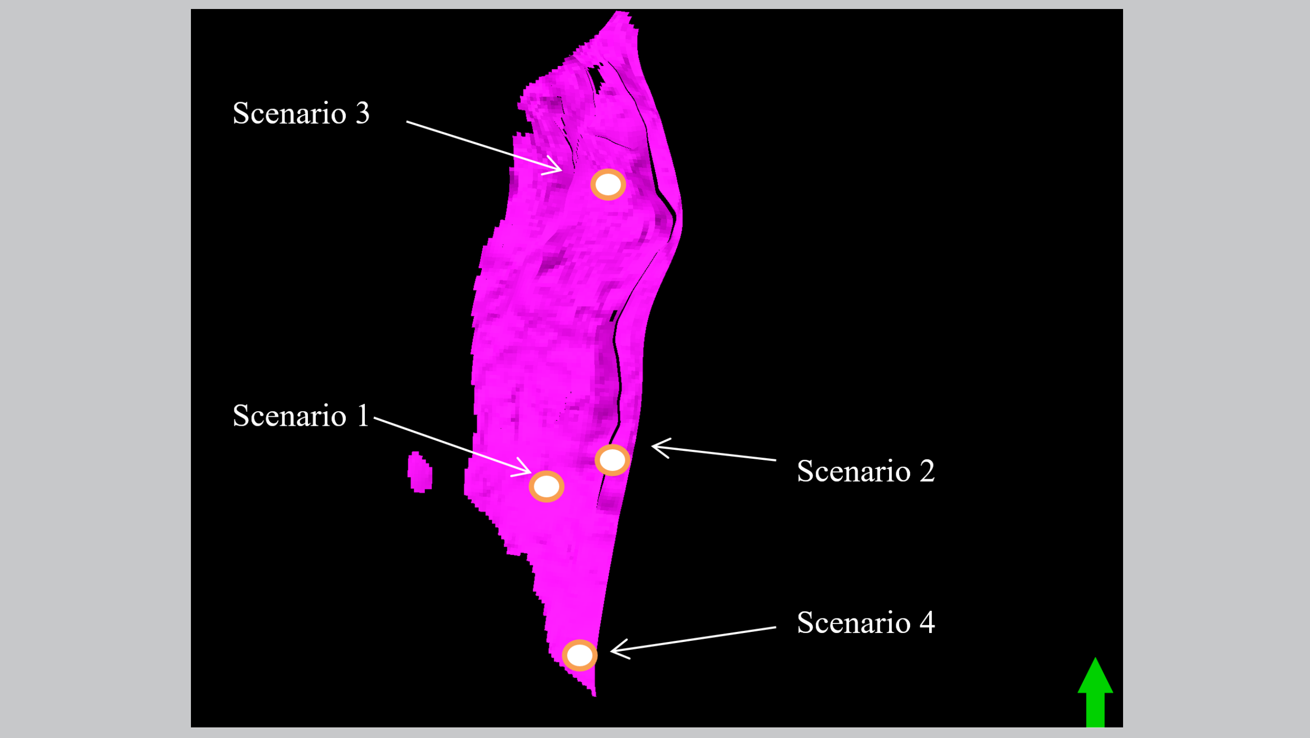

Figure 16 Plane view of layer 18 in the static model with the four hypothetical injector locations as used in this study.

3.3 Results

We present four scenarios in this report, from which one – Scenario 1 - appeared to be not critical (in the sense no diversion is needed) and three are critical and diversion is needed. These critical scenarios will serve as base cases for further work in this area, where brine/ water injection will serve as CO_2 flow diversion option and can serve as a corrective measure.

3.3.1 Non-critical scenario

3.3.1.1 Scenario 1

In total 124.3 Mton of CO_2 were injected in the South West area of the Johansen formation. We observe that directly after injection and even after 9000 years the CO_2 is close to the well area and does not migrate to the fault area close to the injection site (see Figure 17) and no corrective measure are necessary in this scenario.

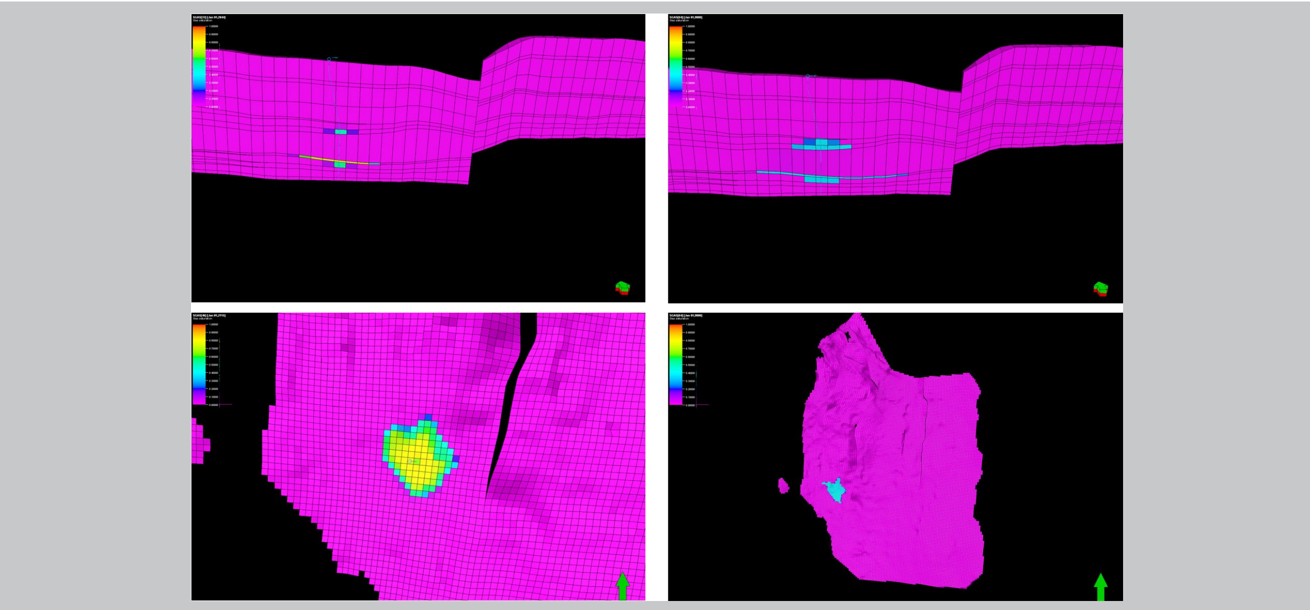

Figure 17 Gas saturation in scenario 1. Sideview directly after injection (top left) and after 9000 years (top right). Topview directly after injection (bottom left) and after 9000 years (bottom right).

3.3.2 Critical scenarios

3.3.2.1 Scenario 2

In the first critical scenario the injection well is placed in the eastern part of the model, close to a major fault. During injection the plume migrates from injector to the north along the fault with a large offset. These faults are usually sealing due to clay smearing. In our simulation we considered the migration along a fault not as a risk and no corrective measure is necessary. In Figure 18 we observed that the Johansen formation varies in thickness laterally and becomes very thin just north of the injection well (Figure 18).

We identified this as a spillpoint and the anticipated storage location is before the thin zone, where a pinch out almost occurs. Immediately after the injection period the CO_2 migrated within the intended storage zone (Figure 19). However after a longer period (now 9000 years is shown) the CO_2 migrated further to the north beyond the spill point. An unwanted migration and a corrective measure is needed here.

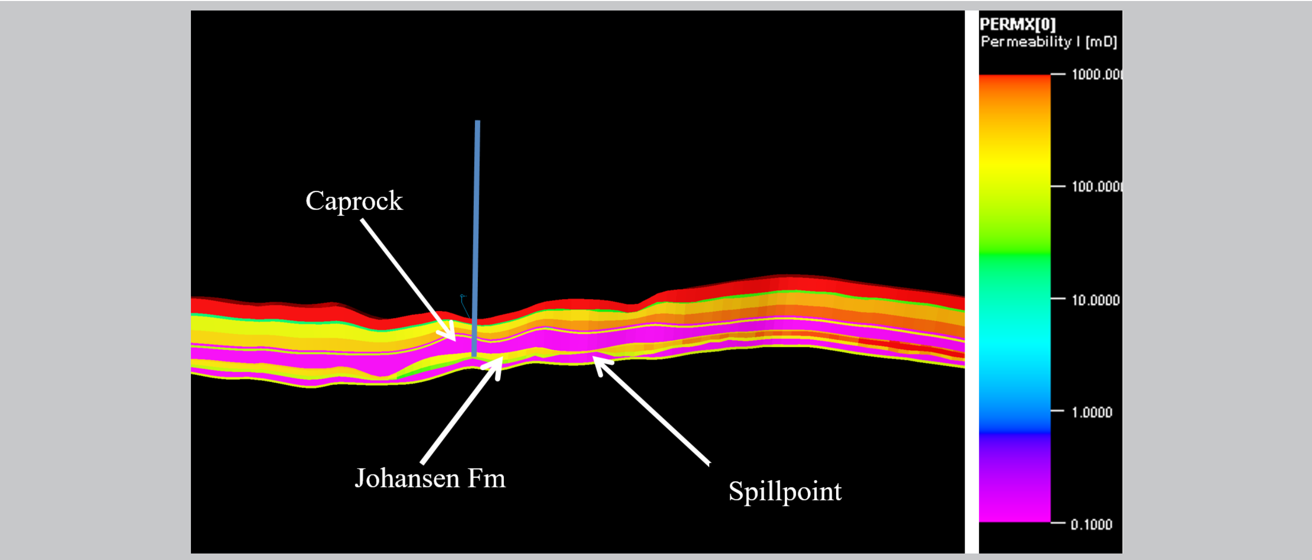

Figure 18 Permeability of scenario 2.

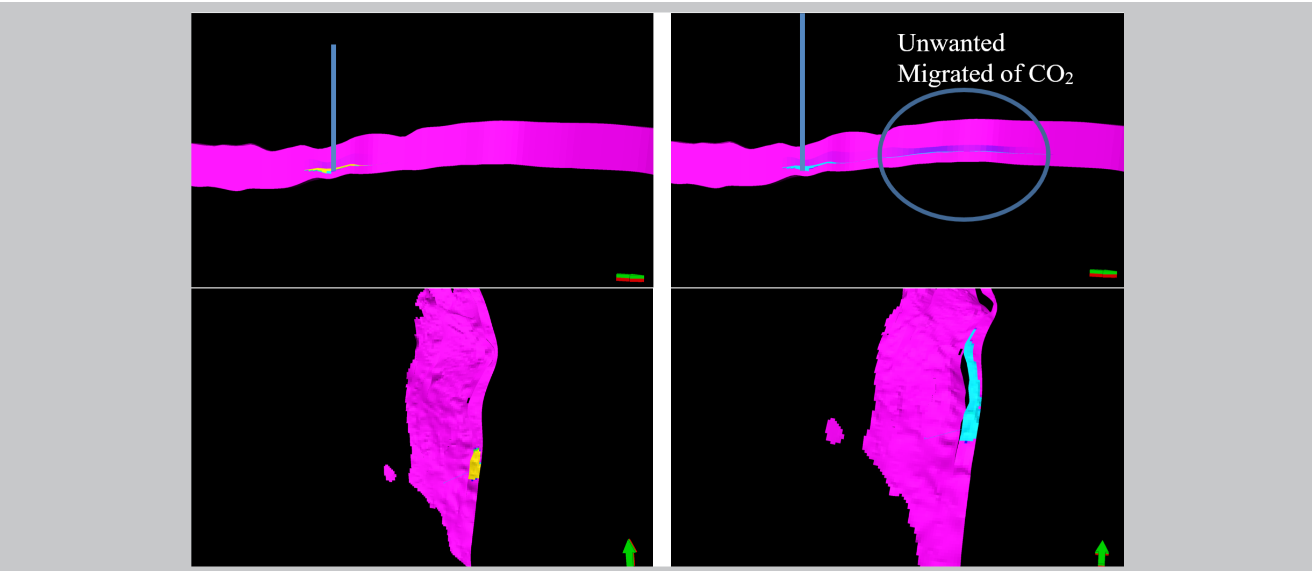

Figure 19 Gas saturation in scenario 2. Sideview directly after injection (top left) and after 9000 years (top right). Topview directly after injection (bottom left) and after 9000 years (bottom right).

3.3.2.2 Scenario 3

In scenario 3 a well is placed down dip from a fault and the CO_2 starts migrating to the fault (Figure 20). We assume in this scenario the fault appears to be not sealing or safe and therefore corrective measures are needed.

3.3.2.3 Scenario 4

In Scenario 4 the CO_2 is flowing towards a fault of the model, during the injection period. In this scenario the risk of fault reactivation and flow into fractures is increased.

Due to the CO_2 storage operations the pressure along the fault changed and the related stress changes around the fault as well. This is a potential leakage scenario and intervention is needed, which will be described in a future report.

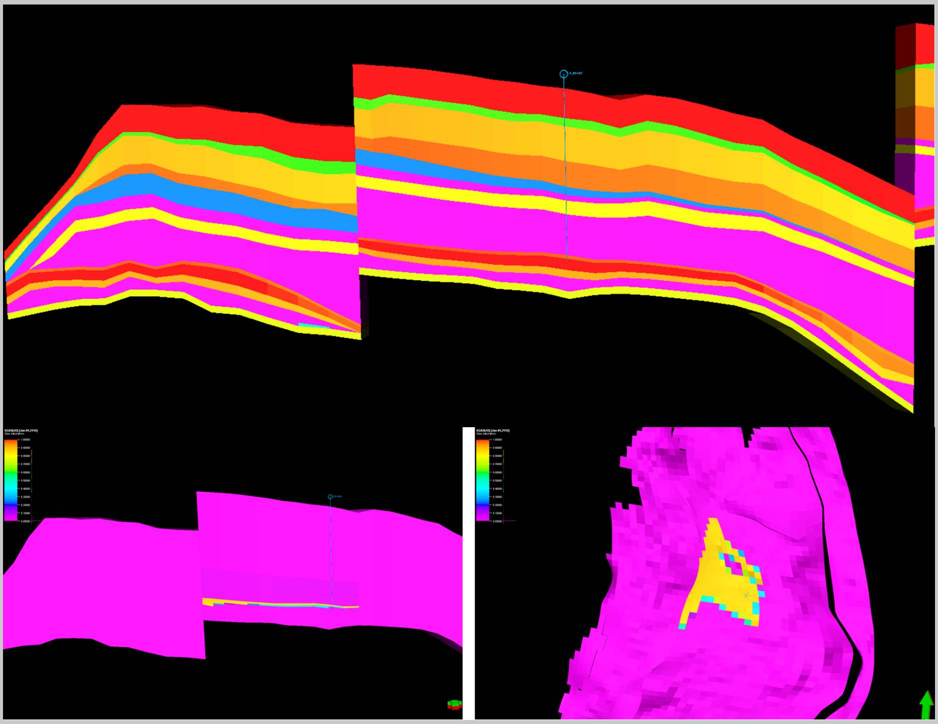

Figure 20 (top) Permeability (scale see Figure 18) (lower left) Sideview CO_2 migration after injection and (lower right) CO_2 migration topview after injection.

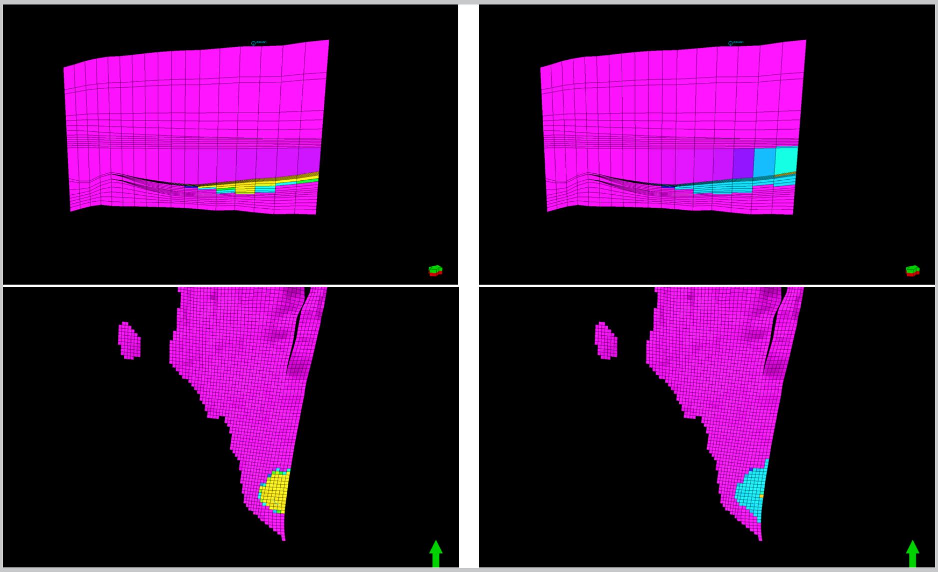

Figure 21 Gas saturation in scenario 4. Sideview directly after injection (top left) and after 9000 years (top right). Topview directly after injection (bottom left) and after 9000 years (bottom right).

3.4 Discussion on Johansen

- We defined 3 different scenarios which will serve as base cases for further work on flow diversion techniques, for which flow diversion can be a potential corrective measure.
- We defined 2 different type of scenarios:
  - Unwanted migration happens during the monitoring period (or after the injection period) to a spill point, and
  - Unwanted migration happens during the injection period itself to a fault.

4 FINAL CONCLUSIONS

Based on the Ketzin test site for geological storage and the Johansen geological model different reservoir management scenarios are carried out. All Ketzin scenarios imply the arrival of the CO_2 at the fracture zone. In most of the Johansen scenarios the CO_2 arrives at fault zones. In both cases, these structures were assumed to represent potential leakage paths.

The most efficient management strategies are those that include a variation of the injection position. Lateral movements may induce minor variations that occur due to slight differences in the distance of the fracture zone and varying dip gradients. Reservoir management strategies that are based on temporal changes of the injection regime do not incur high cost, but the longevity of remediation is very low and there is no significant impact on the arrival time at the location of potential leakage. The injection through multiple wells produces high costs of drilling and installation and the longevity of this measure is also not significant.

Three different scenarios are found for the Johansen model which will serve as a base case for further work on flow diversion techniques.

References

Bergmo, P.E.S., Lindeberg, E., Riis, F and J.T. Johansen (2009). Exploring geological storage sites for CO_2 from Norwegian gas power plants: Johansen formation. Energy Procedia 1 2945–2952.

Bergmo, P.E.S., Lindeberg, E., Riisb F., Johansen W.T. (2008). Exploring geological storage sites for CO_2 from Norwegian gas power plants: Johansen formation, GHGT-9.

Christiansen H.P, Hansen, E.H. and H. HØydaksvik (2009). How to develop saline aquifer storage –oportunities and solutions. Powerpoint Gasnova.

Eigestad, G.T., Dahle, H.K., Hellevang, B., Riis F., Johansen, W.T. and E. Øian (2009). Geological modeling and simulation of CO_2 injection in the Johansen formation. Comput Geosci. 13:435-450.

Lengler, U. (2012), Einfluss von heterogenen Permeabilitätsfeldern auf die CO_2-Speicherung in salinen Aquiferen am Beispiel vom Pilotstandort Ketzin, PhD thesis, Technische Universität Hamburg-Harburg.

Norden, B. & Frykman, P. (2013), Geological modelling of the Triassic Stuttgart Formation at the Ketzin CO_2 storage site, Germany, International Journal of Greenhouse Gas Control 19, 756-774.

Scherpenisse, W. & Maas, J. (2009), Ketzin relative permeabilities and capillary pressures, Technical report, Shell.

Wei, L., Saaf, F., (2009) Estimate of CO_2 storage capacity of the Johansen formation: numerical investigations beyond the benchmarking exercise, Comput Geosci 13:451-467.

Wiese, B.; Böhner, J.; Enachescu, C.; Würdemann, H. & Zimmermann, G. (2010), Hydraulic characterisation of the Stuttgart formation at the pilot test site for CO_2 storage, Ketzin, Germany, International Journal of Greenhouse Gas Control 4, 960-971.

Chapter III

Gel and foam injection as flow diversion option in CO_2 storage operations

Mojgan Hadi Mosleh[1], Rajesh Govindan[1], Ji-Quan Shi[1], Anna Korre[1],
Sevket Durucan[1], Dag Wessel-Berg[2], Robert Drysdale[2]
[1] Imperial College, UK
[2] SINTEF PR, Norway

SUMMARY

A foam system consists of a continuous water phase with dispersed gas bubbles at a given volumetric fraction. Gas bubble formation requires a certain amount of energy which is provided by shear, and is stabilized by surfactant foaming agents dissolved in the water phase, or the gas phase in the case of CO_2. For the use of foams as gas blocking agents, the placement of the foam, its resistance to gas flow and its durability are of the outmost importance for the efficiency and economics of the process. Though the use of "classical" foams has been considered as a promising technology for controlling excessive gas movement, it was shown that these foams have limited lifetime (weeks to months) and the treatment needs to be repeated often (Albrecht and Marsden et al., 1970; Wong et al., 1997; Wassmuth et al., 2001; Cubillos et al., 2012).

Compared with other foam systems such as N_2-foams or natural gas-foams, CO_2-foams usually generate much lower Mobility Reduction Factors due to the impact of CO_2 on the interfacial tension. For CO_2, the mobility reduction factor is usually much lower than with hydrocarbon gas and the maximum attainable effect decreases rapidly with CO_2 density (Chabert et al., 2012; Solbakken et al., 2013). With supercritical CO_2 it was inferred from a laboratory study using a classical foaming agent that probably only coarse foam-emulsions could be formed. However, recent results have shown that with dedicated surfactant formulations, high gas mobility reduction factors could be obtained even with dense- phase CO_2, indicating the formation of strong foams (Chabert et al., 2014).

Currently, large uncertainties remain regarding the actual physics underlying foam flow in porous media. Although previous studies have not proposed a satisfactory physical model for foam flow and propagation, they have generated a general though useful, phenomenological description of the rheological behaviour of foams in porous media (Gauglitz et al., 2002; Skauge et al., 2002; Tanzil et al., 2002; Farajzadeh et al., 2009; Enick et al., 2012; Chabert et al., 2013).

As part of the MiReCOL project, this chapter presents the results of numerical modelling work carried out to investigate the application of polymer-gels and foams for flow diversion of the CO_2 plume within the storage reservoir. The objective of the polymer-gel barrier simulations was: i) to perform reservoir simulations for different remediation layouts after CO_2 leakage has been detected, ii) to perform sensitivity analyses in order to assess the effectiveness of the polymer-gel barriers in diverting the flow of CO_2 plume. The results of laboratory investigations on polymer-gel characterisation and core flooding experiments carried out in the project were used to define a range of permeabilities of the polymer-gel barriers.

Two scenarios were defined based on different layouts of polymer-gel barriers within the reservoir. Sensitivity analyses were carried out to assess the effectiveness of the barrier in diverting the flow of CO_2 plume from the leaky fault.

The second part of the report describes a model for the creation of foam from injected surfactant and water that was developed within the Eclipse simulator, which was used to test the effects of various injection parameters on leakage in a generic reservoir model. The most effective parameters in reducing CO_2 migration were found to be the duration of surfactant solution injection and the location of the injection well, to prevent early by-passing of the foam plug. Generally the most effective leakage mitigation was achieved by injecting over a long time, i.e. using the highest amounts of surfactant.

The results of this work will support further work with regards to polymer-gel barrier remediation implementation and eventually the comparison of various remediation methods in a later part of the MiReCOL project.

1 INTRODUCTION

A number of risks of varying degree are associated with underground storage of CO_2. Contingency planning and analysis of possible future remediation actions are a requirement for realizing a permit for geological CO_2 storage.

In comparison with other likely storage sites, such as the depleted hydrocarbon fields, knowledge of the geological and petrophysical properties of saline aquifers is usually rather limited. Hence, a considerable degree of uncertainty in the conformance of CO_2 flow in the subsurface in comparison to that estimated by theoretical/numerical computations is expected. This uncertainty may lead to undesired and unpredicted preferential flow of CO_2 into parts of the host reservoir, or leakage into shallower formations.

Mechanisms that could lead to migration or leakage of CO_2 into shallower formations and ultimately leakage to the atmosphere could include: unwarranted intrusion, equipment failure e.g. abandoned wells, faults reactivation due to over-pressurisation, or geochemical reactions between the CO_2 and the cap rock, and sub-seismic faults undetected during the site characterisation phase prior to CO_2 injection (IEAGHG Report, 2007).

In order to mitigate undesired migration of the CO_2 plume and its leakage into shallower formations, flow diversion measures may be implemented, such as: i) localised injection of brine creating a competitive fluid movement, ii) change of injection strategy, or iii) localised reduction in permeability by the injection of various types of sealant.

The aim of the work reported here was to test the effectiveness of foam and gel injection as two distinct means of mitigating unwanted CO_2 migration within a storage reservoir. This was be done by means of characterizing typical examples of both foam and gel, then performing simulations in a numerical simulator of CO_2 migration and the flow diversion effect of the injected media. The results will be used later in the MiReCOL project to compare the effectiveness of various methods to counteract unwanted migration of CO_2.

2 POLYMER GEL REMEDIATION AS FLOW DIVERSION OPTION

In comparison to other likely storage sites, such as the depleted hydrocarbon fields, knowledge on the geological and petrophysical properties of saline aquifers is usually more limited. Hence, a considerable degree of uncertainty in the conformance of CO_2 flow in the subsurface in comparison to that estimated by theoretical/numerical computations is expected. This uncertainty may lead to undesired and unpredicted preferential flow of CO_2 into parts of the host reservoir, or leakage into shallower formations. Mechanisms that could lead to migration or leakage of CO_2 into shallower formation and ultimately leakage to the atmosphere could include: unwarranted intrusion, equipment failure e.g. abandoned wells, faults reactivation due to over-pressurisation, or geochemical reactions between the CO_2 and the cap rock, and sub-seismic faults undetected during the site characterisation phase prior to CO_2 injection (IEAGHG Report, 2007).

In order to mitigate undesired CO_2 plume migration and its leakage into shallower formations, flow diversion measures may be implemented, such as: i) localised injection of brine creating a competitive fluid movement, ii) change of injection strategy, or iii) localised reduction in permeability by the injection of gels or foams, or by immobilising the CO_2 in the pore space.

Crosslinked hydrolysed polymer-gel injection is used in petroleum industry to improve conformity of fluid flow in the reservoir, remediate leakage around wells, and also used in conjunction with enhanced oil recovery at various temperature and pressure conditions (Sydansk, 1998; Hild and Wackowski, 1999; Sydansk and Southwell, 2000; Sydansk, et al., 2004; Turner and Zahner, 2009; Al-Muntasheri et al., 2010; Saez et al., 2012). Water-based gels are highly elastic semi-solids with high water content, trapped in the three-dimensional polymer structure of the gel (Vossoughi, 2000). Polyacrylamide (PAM) is the main crosslinked polymer used mostly by the industry (Flew and Sellin, 1993; Rodriguez et al., 1993). The use of biopolymers is more challenging as compared to the synthetic polymers due to chemical degradation at higher temperatures, causing the loss of mechanical strength (Sheng, 2011). Most of polymer-gel systems are based on crosslinking of polymers with a heavy metal ion. The most common heavy metal ion used is chromium III. However, in view of its toxicity and related environmental concerns (Stavland and Jonsbraten, 1996; Vossoughi, 2000), its application in reservoir conformance and CO_2 leakage remediation is considered to be limited. Therefore, more environmental friendly crosslinkers such as boron (Sun and Qu, 2011; Legemah et al., 2014), aluminium (Smith, 1995; Stavland and Jonsbraten, 1996) and zirconium (Lei and Clark, 2004) have been proposed and used in recent years.

Several commercial and research-purpose simulators have been used to simulate chemical/polymer injection into deep geological formations, most of which was developed for the purpose of Enhanced Oil Recovery (EOR) from hydrocarbon reservoirs. For instance, a two phase, four component polymer EOR model was developed by Wegner and Ganzer (2012) using COMSOL to simulate the displacement of oil by aqueous polymer solutions. Gharbi et al. (2012) performed history-matching to assess the potential of surfactant/polymer flooding in a Middle Eastern reservoir, using the chemical flood reservoir simulator (UTCHEM) developed at The University of Texas at Austin. In addition, Schlumberger's simulator, Eclipse, has also been used for polymer flooding and EOR in the Norne Field E-Segment, e.g. by Sarkar (2012) and Amirbayov (2014).

As part of the MiReCOL project, this report presents the results of the numerical modelling carried out to investigate the application of polymer-gel barriers for flow diversion of a CO_2 plume within the storage reservoir. The objective of this work was: i) to perform reservoir simulations for different remediation layouts after CO_2 leakage has been detected, ii) to perform sensitivity analyses in order to assess the effectiveness of the polymer-gel barriers in diverting the flow of CO_2 plume. The results of laboratory investigations on polymer-gel characterisation and core flooding experiments, provided in Deliverable 6.2 of the project, were used to define a range of permeabilities of the polymer-gel barriers.

2.1 Reservoir model description

2.1.1 Structural and geological model

A numerical reservoir model was set up to study the mobility control of CO_2 plume using polymer-gel injection within a heterogeneous saline aquifer. The structural model used in this study represents a saline aquifer with a broad and considerably dipping anticlinal structure (Figure 1), where the containment of CO_2 is envisaged. The model grid spans an area of 36km×10km and includes five major sealing faults. The grid broadly comprises of three layers, namely: (1) a reservoir layer with an average thickness of 240m and resolution of 200m×200m×4m; (2) a caprock (seal) layer with an average thickness of 225m and resolution of 200m×200m×225m; and (3) a shallow aquifer layer with an average thickness of 175m and resolution of 200m×200m×175m. The depth of the model ranges between 1,087m and 3,471m.

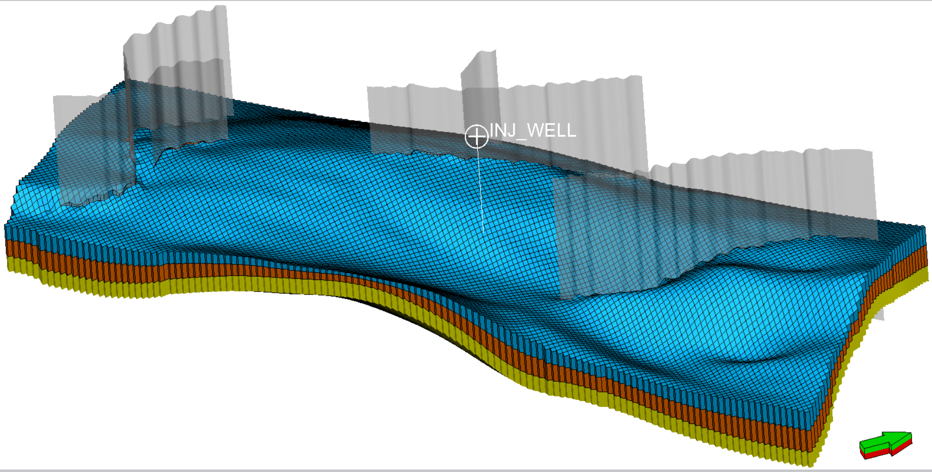

Figure 1 The structural model of the numerical saline aquifer (36km×10km) containing five major faults and three stratigraphic layers: reservoir layer, caprock (seal) layer and shallow aquifer layer.

The geological model of the reservoir layer is represented by a fluvial-channel system, typically containing braided sandstone channels and interbedded floodplain deposits (the inter-channel region) of mudstone or siltstone. These generally represent the fluviodeltaic progradation and floodplain deposition formations found in the Triassic of the Barents Sea. The channel layout

Table 1 Channel layout parameters used in the reservoir layer of the geological model.

	Min	Mean	Max
Amplitude [m]	400	500	600
Wavelength [m]	14,000	15,000	16,000
Width [m]	1,400	1,500	1,600
Thickness [m]	4	8	12

Table 2 Petrophysical properties used in the geological model.

Petrophysical properties		Channels	Inter-channel region	Caprock	Shallow aquifer
Porosity	Min, Mean, Max	0.1, 0.18, 0.25	0, 0.1, 0.25	0.01	0.05, 0.15, 0.25
	Standard deviation	0.05	0.05	0	0.05
Horizontal Permeability [mD] *	Min, Mean, Max	125, 3000, 7000	0.1, 10, 100	0.0001	100, 3000, 5000
	Standard deviation	2000	40	0	1000
NTG	Min, Mean, Max	0.6, 0.9, 1	0, 0.2, 0.5	0.01	0.6, 0.9, 1
	Standard deviation	0.05	0.05	0	0.05

*vertical permeability = 0.1 × horizontal permeability parameters implemented in the model to represent the fluvial-channel system are given in Table 1. The range of the petrophysical properties used in the static geological model attribution (Table 2) are based on the Late Triassic Fruholmen Formation in the Hammerfest Basin (NPD, 2013), which is located at depths similar to those considered in this model. The petrophysical attributions of the geological model were generated using Sequential Gaussian Simulation (SGS) in order to represent the variability in the distribution of these values. Example realisations of the porosity and horizontal permeability distributions for the top reservoir layer are illustrated in Figure 2.

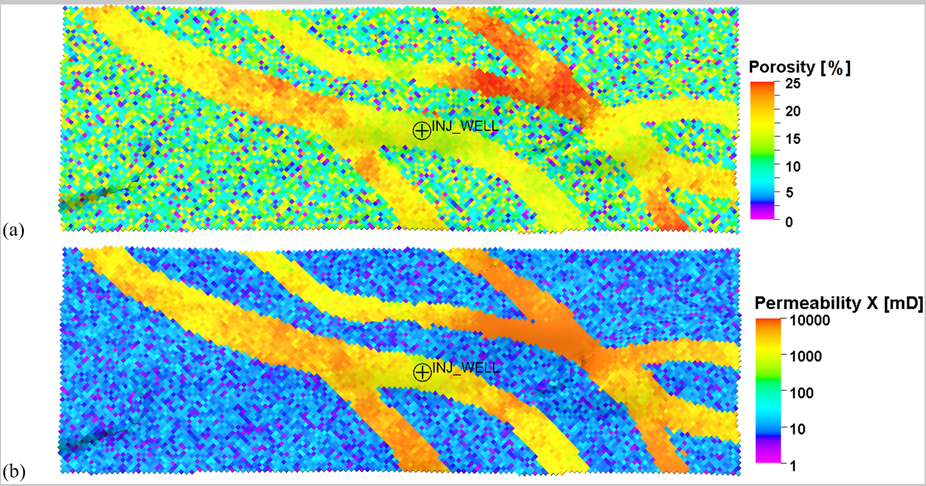

Figure 2 Example realisations of petrophysical properties distribution for the top layer of the reservoir: (a) Porosity; (b) Horizontal permeability covering the area of the reservoir model (36km×10km).

2.1.2 Dynamic properties of the reservoir model

Similar to the petrophysical properties of the geological model attribution, the dynamic properties of the reservoir model have been selected based on the values reported for the reservoir conditions found in the corresponding or neighbouring Barents Sea formations. The salinity of the formation water was chosen to be 14% based on the values reported for the Tubåen formation of the Snøhvit field (Benson, 2006), which is also part of the Realgrunnen Subgroup overlying the Fruholmen. The reservoir temperature was set at 93°C and the initial pressure of the reservoir model was assumed to be at hydrostatic pressure.

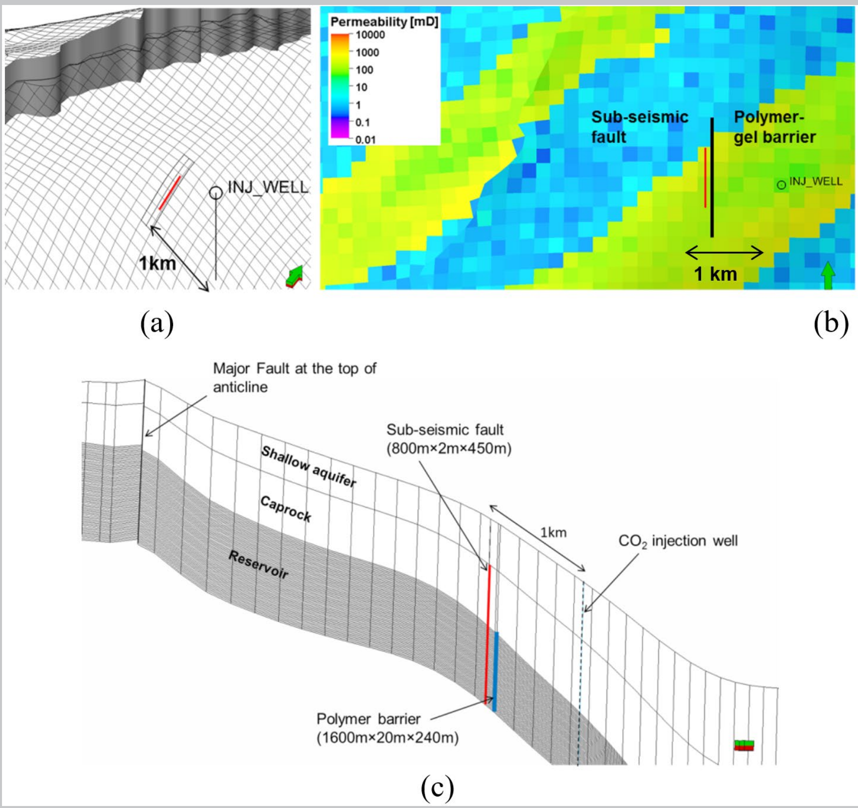

Figure 3 (a) The grid refinement representing the sub-seismic fault feature (800m×2m) and polymer-gel barrier (1600m×20m), located 1km away from the injection well; (b) permeability attribution and position of the polymer-gel barrier between the injection well and the sub-seismic fault at the top of the storage reservoir; (c) cross-sectional view showing the local grid refinement representing the sub-seismic fault feature in red, and the vertical polymer-gel barrier in blue.

2.2 Dynamic modelling of CO_2 flow diversion

The dynamic model was set up in Schlumberger's Eclipse 300 (E300) software using the static geological model and the dynamic reservoir parameters described in the previous sections. The compositional flow simulation of CO_2 storage in the saline aquifer model was carried out by implementing a quasi-isothermal, multi-phase, and multi-component algorithm, enabled by the CO2STORE option, wherein mutual solubilities of CO_2 and brine are considered. Simulations were carried out for 30 years, comprising of the CO_2 injection, leakage detection, remediation, and post-remediation CO_2 injection periods.

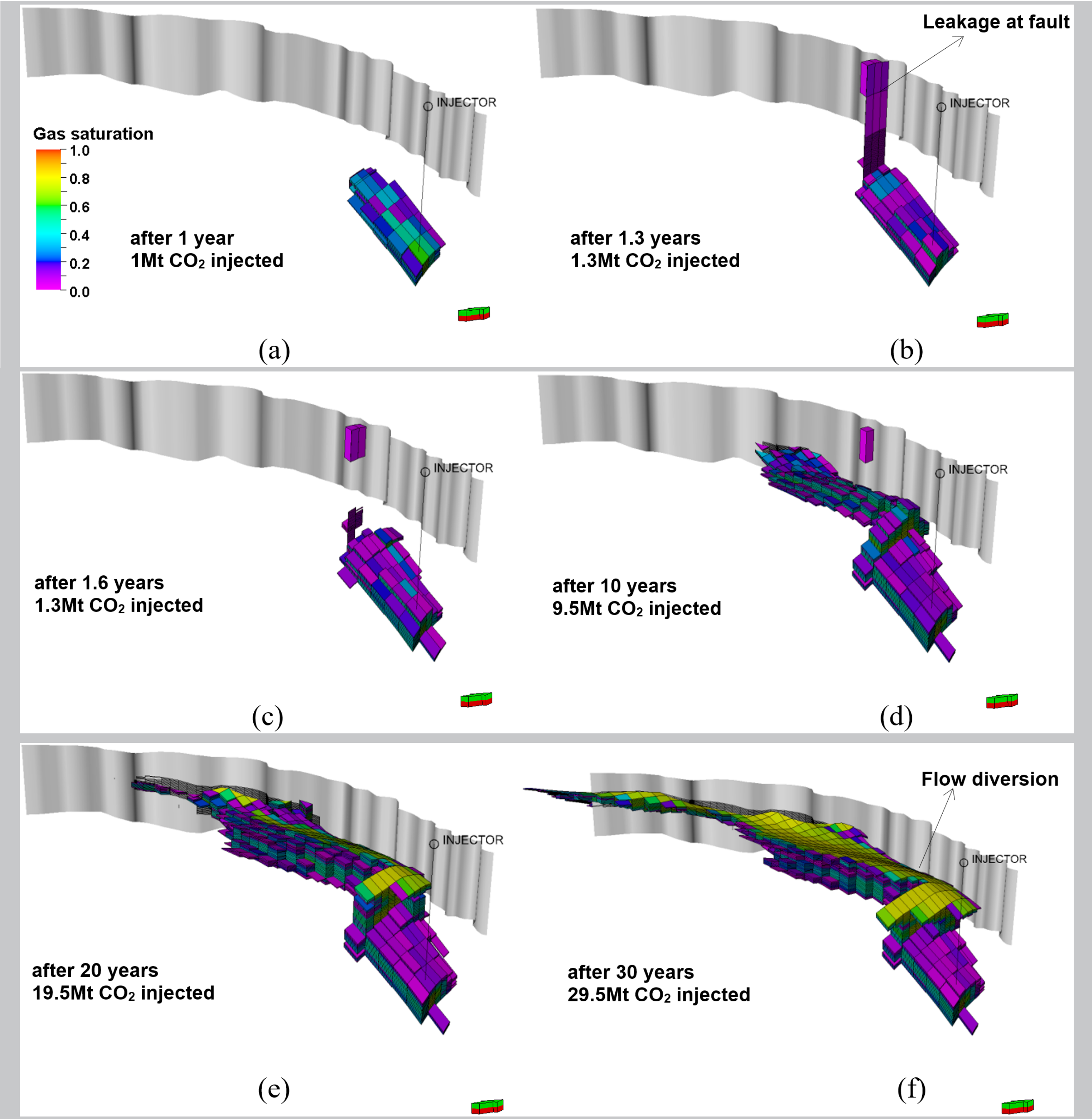

Figure 4 Distribution of free CO_2 after: (a) 1 year of simulation (January 2016); (b) 1.3 years of simulation when leakage was detected and CO_2 injection was stopped (April 2016); (c) 1.6 years of simulation when remediation was completed (October 2016); (d) 10 years of simulation (January 2025); (e) 20 years of simulation (January 2035); and (f) after 30 years of simulation (January 2045).

For the purpose of this study, it was assumed that a sub-seismic fault is present in the formation as a pre-defined undesired migration pathway. This is represented by a local grid refinement additionally introduced in the structural model by means of the CARFIN option in Eclipse. Two scenarios were considered based on different layouts of the polymer-gel barriers for leakage remediation and flow diversion within the reservoir formation.

2.2.1 Scenario 1: Vertical polymer-gel remediation barrier layout

In order to setup the first scenario, a sub-seismic vertical fault was introduced in the model at a distance of 1km away from the injection well (INJ_WELL), located at the flank of the anticline (Figure 3). The fault has a lateral dimension of 800m×2m and is assumed to be non-sealing, with a uniform vertical permeability of 10,000mD and spanning the reservoir and the caprock thickness (approximately 450m) without appreciable formation displacement between the two sides of the fault.

The simulation of CO_2 injection in the saline aquifer was carried out at a rate of 1Mt/year, for a total period of thirty years comprising three stages: initial CO_2 injection until leakage detection, polymer-gel injection (remediation) in the reservoir, and post-remediation CO_2 injection. The leakage detection threshold assumed was 5,000 tonnes of free CO_2 in the shallow aquifer (Benson, 2006).

Once the leakage through the sub-seismic fault was detected, CO_2 injection was stopped for a period of six months, at the end of which permeability reduction in the reservoir due to polymer-gel injection is implemented. The polymer-gel barrier was assumed to span the reservoir thickness and have an effective region of influence much longer than the subseismic fault. The dimensions of the effective remediation barrier implemented were 1,600m×20m×240m, at a distance of approximately 100m away from the fault towards the injection well, as illustrated in Figure 3.

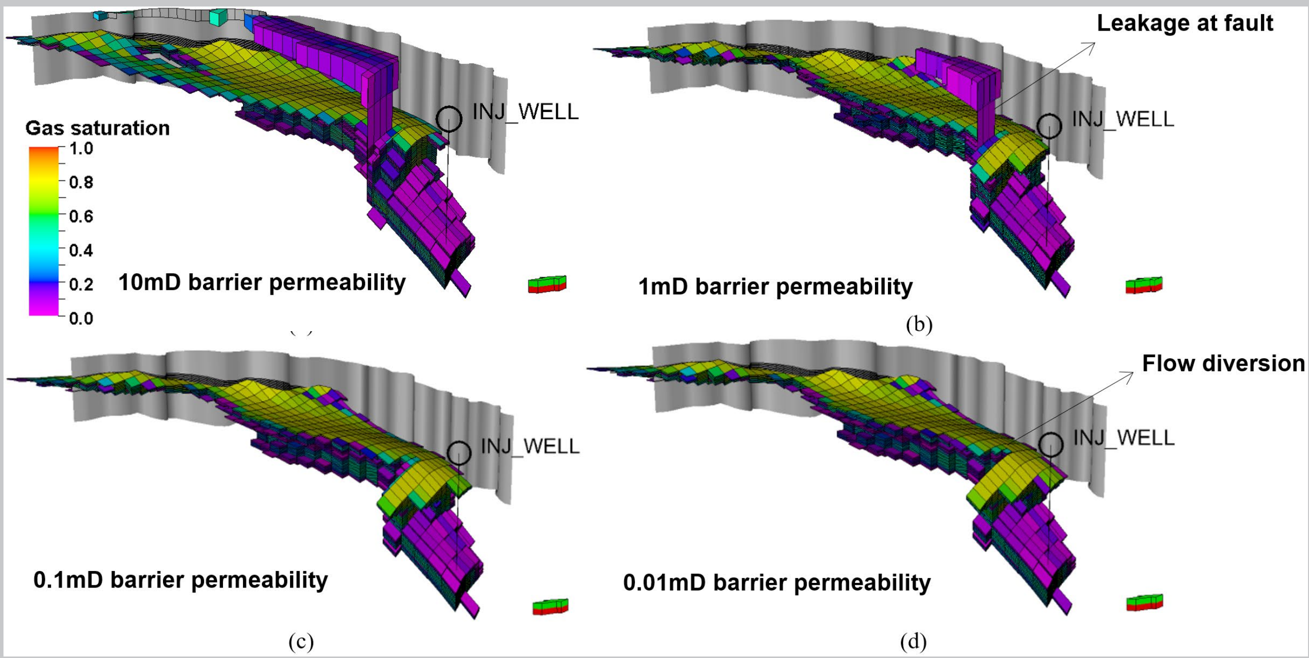

Figure 5 Plume distribution at the end of the 30 year simulation period when the permeability of the polymer–gel barrier is: (a) 10mD; (b) 1mD; (c) 0.1 mD; (d) 0.01mD.

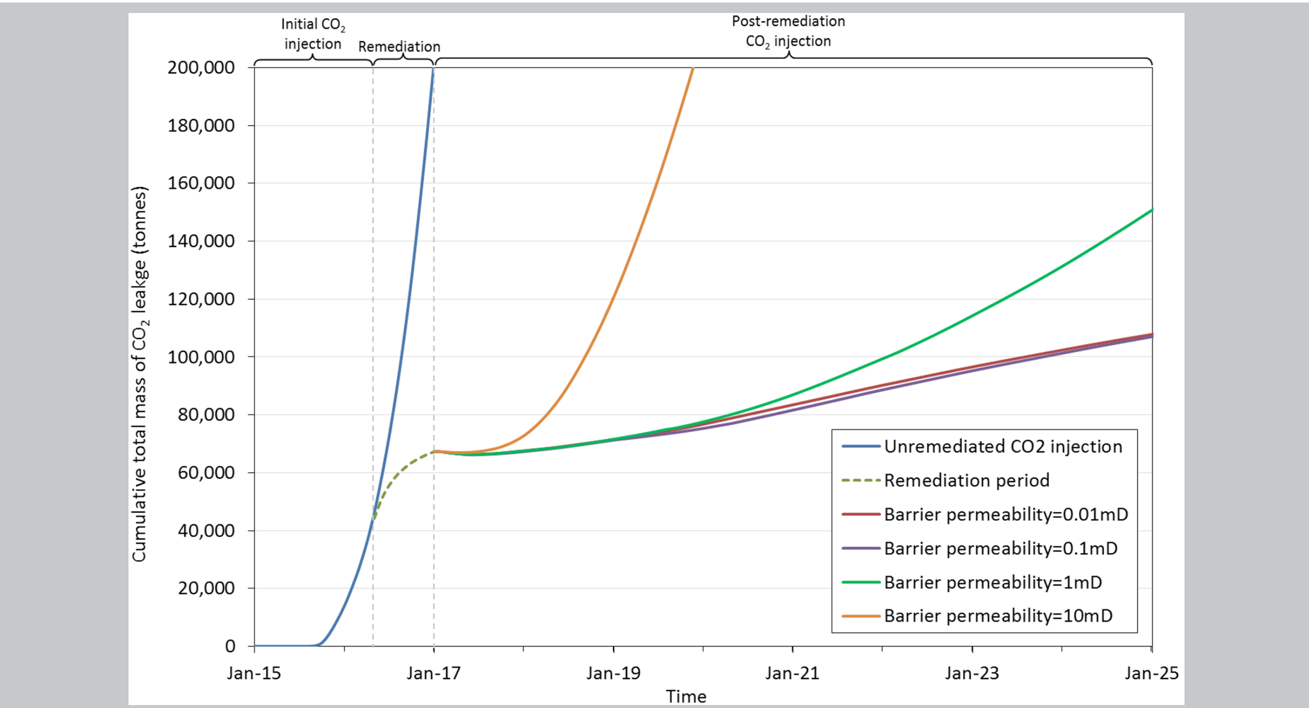

Figure 6 Cumulative mass of total CO_2 (which includes free, dissolved and trapped components) that could leak in to the shallow aquifer for different cases of polymer-gel barrier permeabilities.

2.2.1.1 CO_2 plume migration results

With the remediation barrier in place, CO_2 injection was then re-started for the remaining simulation period, representing the post-remediation period.

The CO_2 injection was assumed to start in January 2015. Figure 4 illustrates the simulation results indicating the free CO_2 plume distribution after: (a) 1 year of simulation (January 2016); (b) 1.3 years of simulation when leakage was detected and CO_2 injection was stopped (April 2016); (c) 1.6 years of simulation when remediation was completed (October 2016); (d) 10 years of simulation (January 2025); (e) 20 years of simulation (January 2035); and (f) 30 years of simulation (January 2045). The results illustrate that polymer-gel

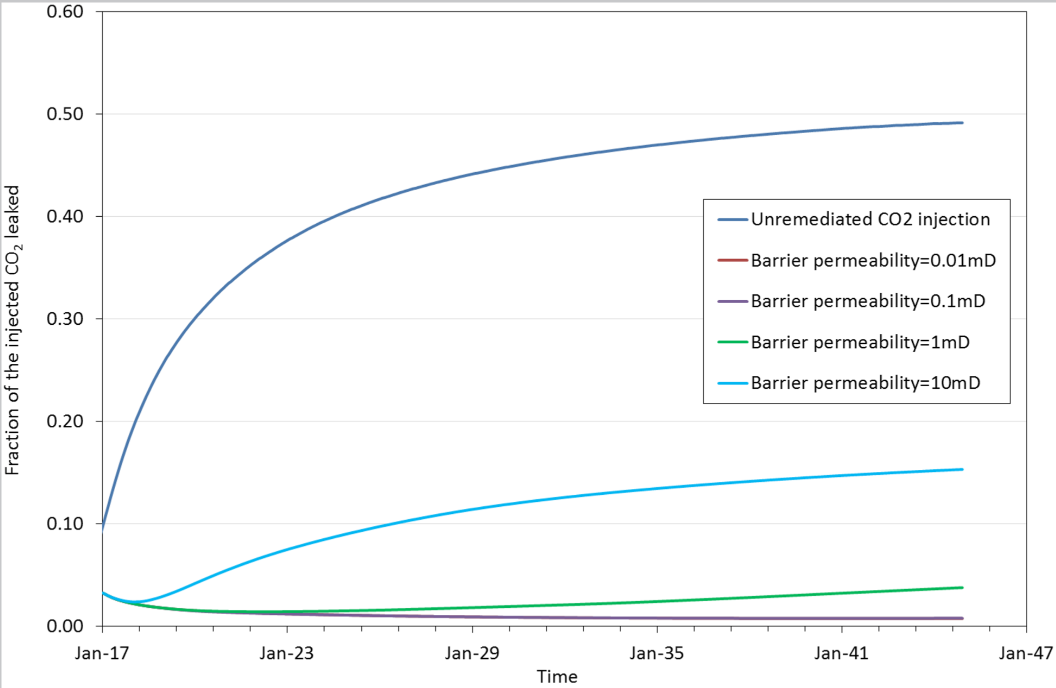

Figure 7 Fraction of the injected CO_2 that could have leaked into the shallow aquifer for different cases of polymer-gel barrier permeabilities during the post-remediation period.

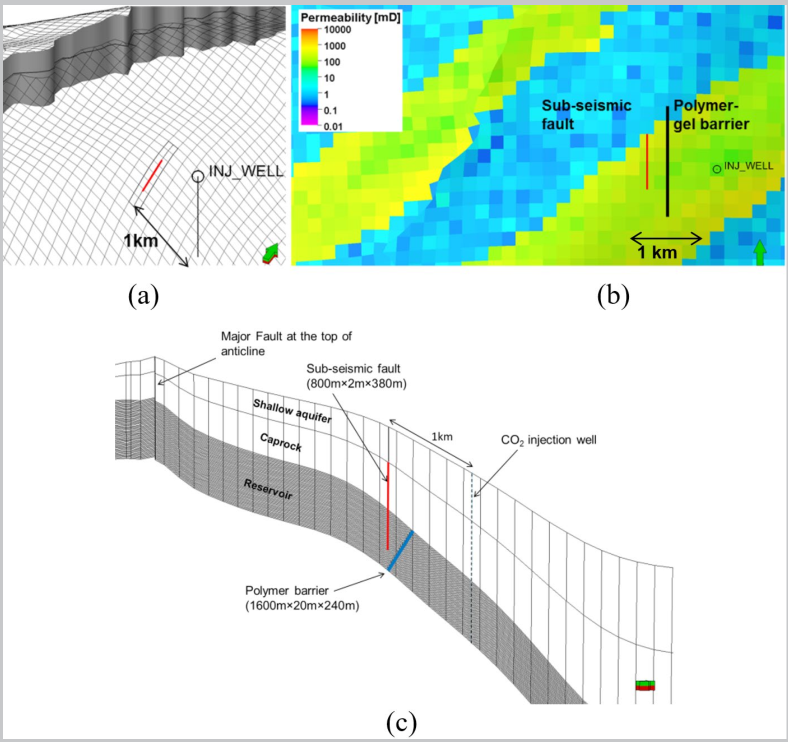

Figure 8 (a) The grid refinement representing the sub-seismic fault feature (800m×2m), located 1km away from the injection well, and the polymer-gel barrier (1600m×20m); (b) permeability attribution and position of the polymer-gel barrier between the injection well and the sub-seismic fault at the top of the storage reservoir; (c) cross-sectional view showing the local grid refinement representing the sub-seismic fault feature in red, and the vertical polymer-gel barrier in blue.

barrier remediation induces flow diversion and consequently reduces the cumulative amount of CO_2 leakage into the shallow aquifer from 6 Mt, if no remediation is implemented, to approximately 0.2 Mt by the end of thirty years (shown Figure 6).

2.2.1.2 Sensitivity analysis for the effect of polymer-gel barrier permeability on flow diversion

Different permeability values at the location of the polymer-gel barrier were tested in the model, ranging from 0.01-10mD. This considers 2-5 orders of magnitude of permeability reduction for the channel region (with an average horizontal permeability of 3000mD), and 0-3 orders of magnitude of permeability reduction for the inter-channel region (with an average horizontal permeability of 10mD). The free CO_2 plume distributions at the end of the thirty years injection period, as illustrated in Figure 5, suggest that leakage through the fault continues during the post-remediation period when the barrier permeability is >0.1mD. For permeabilities below this value, the plume is more effectively diverted away from the fault.

Figure 6 illustrates the mass of cumulative CO_2 leakage in the shallow aquifer for the first ten years of the simulation period. The model estimates that, for example, leakage reduction achieved after five years of simulation lies in the range of 84% to 96% (i.e. reduced by ~1.6Mt to ~1.9Mt) for this scenario. Hence, leakage through the fault continues at a lesser rate during the post-remediation period for all the barrier permeabilities considered. In this the cumulative total mass of CO_2 leakage indicated in Figure 6, the free CO_2 accounts only for one fraction of the total CO_2 leakage. In fact, the detection limit of 5,000tonnes of free CO_2 corresponds to 86.3kt of the cumulative mass of total CO_2.

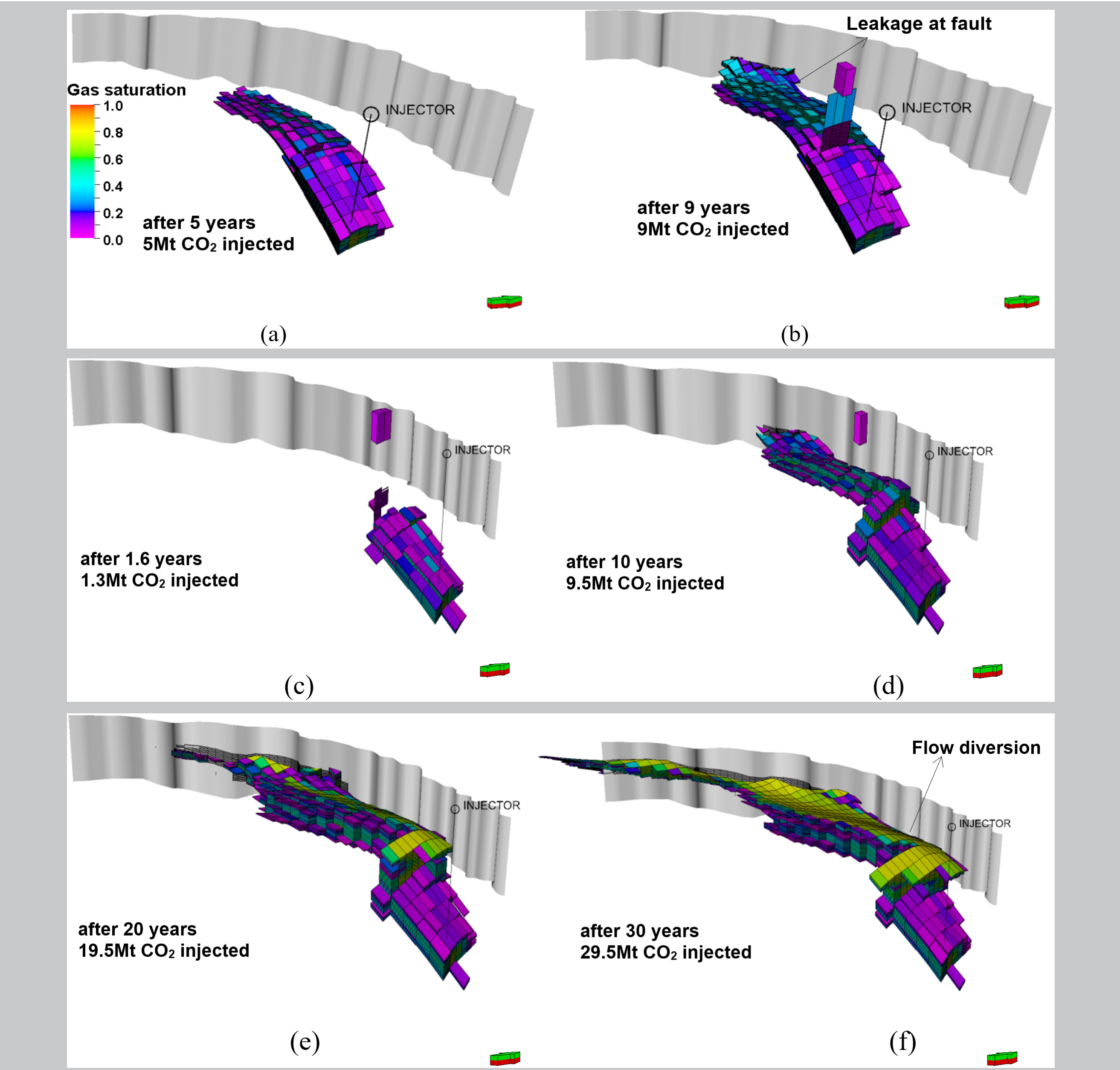

Figure 9 Distribution of free CO_2 after: (a) 5 years of simulation (January 2020); (b) 9 years of simulation when leakage was detected and CO_2 injection was stopped (February 2024); (c) 9.5 years of simulation when remediation was completed (August 2024); (d) 15 years of simulation (January 2030); (e) 20 years of simulation (January 2035); and (f) 30 years of simulation (January 2045).

Figure 7 illustrates fraction of the injected CO_2 leaked into the shallow aquifer during post-remediation period. The results show that for case of un-remediated CO_2 injection, up to 49% of the injected CO_2 can be expected to leak; whereas for the remediated cases, the amount of CO_2 leakage is reduced to 0.7-15% of the injected CO_2, depending on the range of barrier permeabilities considered.

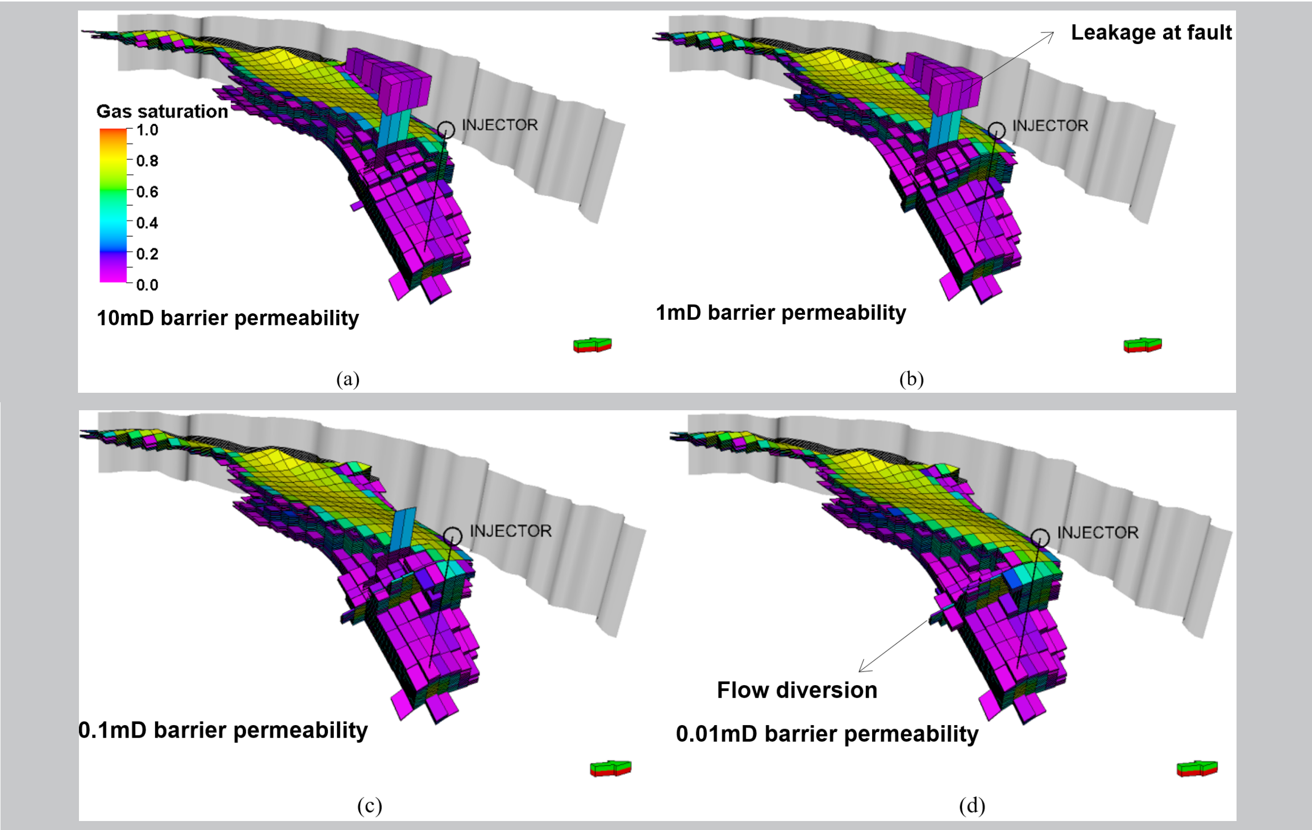

Figure 10 Plume distribution at the end of the 30 year simulation period when the permeability of the polymer–gel barrier is: (a) 10mD; (b) 1mD; (c) 0.1mD; (d) 0.01mD.

2.2.2 Scenario 2: Inclined polymer-gel remediation barrier layout

Similar to the previous scenario, a sub-seismic vertical fault was introduced in the model at a distance of 1km away from the injection well (INJECTOR), located at the flank of the anticline (Figure 8). The fault has a lateral dimension of 800m×2m and assumed to be non-sealing, with a uniform vertical permeability of 10,000mD. In this scenario, however, it was assumed that the sub-seismic fault has a shorter vertical span (approximately 380m) such that it does not cut through the entire reservoir formation. Similar to Scenario 1, no appreciable formation displacement between the two sides of the fault is assumed.

The simulation of CO_2 injection in the saline aquifer was similarly carried out at a rate of 1Mt/year, for a total period of thirty years comprising three stages: initial CO_2 injection until leakage detection, polymer-gel injection (remediation), and post-remediation CO_2 injection. The leakage detection threshold assumed was 5,000 tonnes of free CO_2 in the shallow aquifer (Benson, 2006).

Once the leakage through the sub-seismic fault was detected, CO_2 injection was stopped for a period of six months, at the end of which permeability reduction in the reservoir due to polymer-gel injection is implemented. The polymer-gel barrier was assumed to have a region of influence with a dimension of 1,600m×20m×240m and with the closest distance to the fault being approximately 100m, as illustrated in Figure 8. This scenario was considered in order to test a different layout of polymer-gel injection and resulting barrier in terms of its orientation with respect to the leaky fault.

2.2.2.1 CO_2 plume migration results

With the barrier in place, CO_2 injection was then re-started for the remaining period of the injection simulation at a rate of 1Mt/year, representing the post-remediation period. Figure 9 illustrates the distribution of free CO_2 after: (a) 5 years of simulation (January2020); (b) 9 years of simulation when leakage was detected and CO_2 injection was stopped (February 2024); (c) 9.5 years of simulation when remediation was completed (August 2024); (d) 15 years of simulation (January 2030); (e) 20 years of simulation (January 2035); and (f) 30 years of simulation (January 2045).

The results suggest that the leakage has been effectively remediated and flow diversion of the CO_2 plume is achieved. Considering the much slower leakage rate, and that a fixed detection threshold is used for this scenario, leakage is detected much later as compared to Scenario 1.

2.2.2.2 Sensitivity analysis for the effect of permeability reduction on flow diversion

Different permeability values at the location of the polymer-gel barrier were tested in the model, ranging from 0.01-10mD. This considers 2-5 orders of magnitude of permeability reduction for the channel region (with an average horizontal permeability of 3000mD), and 0-3 orders of magnitude of permeability reduction for the inter-channel region (with an average horizontal permeability of 10mD). The free CO_2 plume distributions at the end of the thirty years injection period, as illustrated in Figure 10, suggest that leakage through the fault continues during the post-remediation period at a small rate when the barrier permeability is >0.1mD. For permeabilities below this value, the plume is effectively diverted away from the fault.

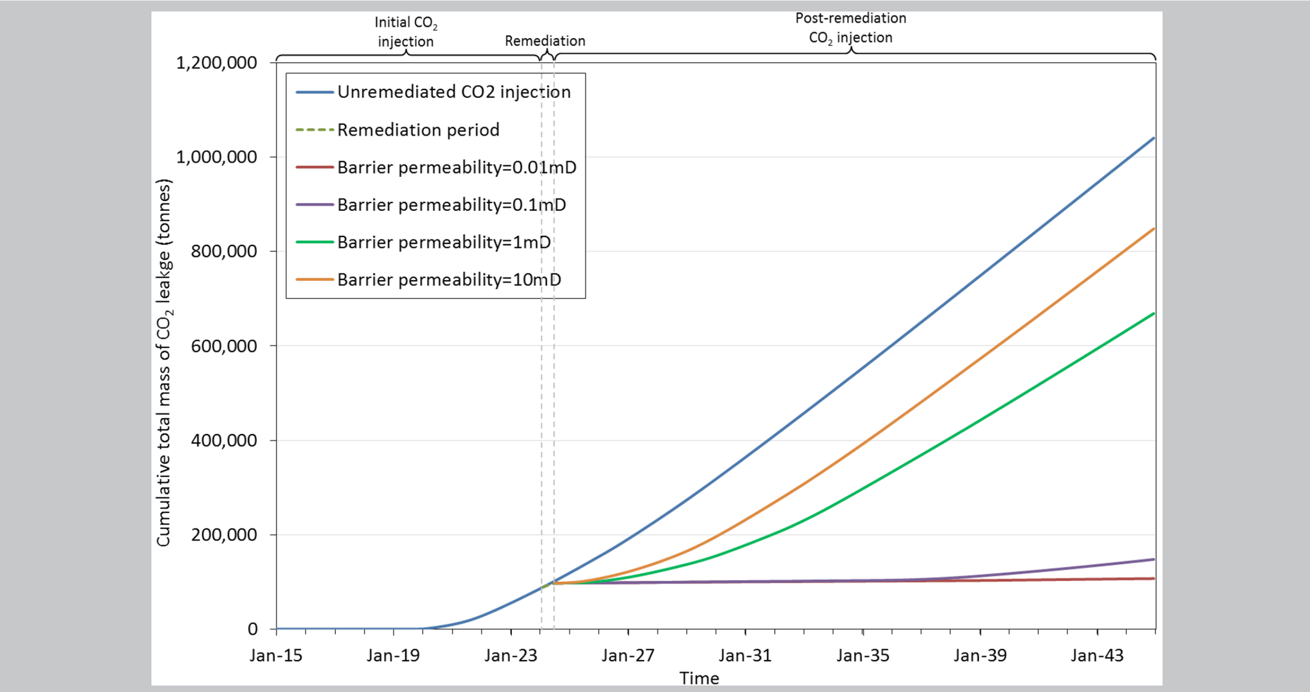

Figure 11 Cumulative mass of total CO_2 (which includes free, dissolved and trapped components) that could leak in to the shallow aquifer for different cases of polymer-gel barrier permeabilities.

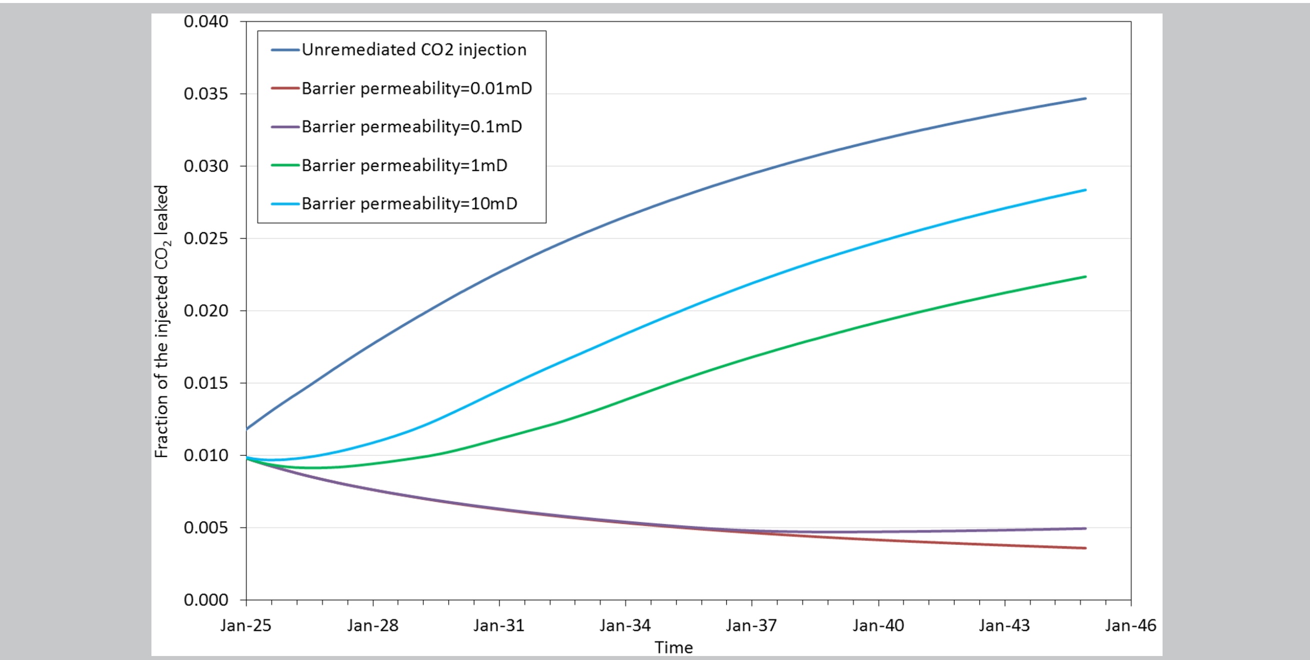

Figure 12 Fraction of the injected CO_2 leaked into shallow aquifer during post-remediation period.

Figure 11 illustrates the mass of cumulative CO_2 that could leak into the shallow aquifer for the thirty years of the simulation period. The simulation indicates that, for example, leakage reduction achieved after thirty years of simulation lies in the range of 18% to 90% (i.e. is reduced by ~0.1Mt to ~0.9Mt) for this scenario. Hence, leakage through the fault continues at a lesser rate during the post-remediation period for all the barrier permeabilities considered. As in Scenario 1, in the cumulative total mass of CO_2 leakage indicated in Figure 11, the free CO_2 accounts only for one fraction of the total CO_2 leakage. The detection limit of 5,000 tonnes of free CO_2 corresponds to 86.3kt of the cumulative mass of total CO_2.

Figure 12 illustrates the fraction of the injected CO_2 that could leak in to the shallow aquifer during post-remediation period for different barrier permeabilities. The results show that for the case of un-remediated CO_2 injection, up to 3.5% of the injected CO_2 can be expected to leak; whereas for the remediated cases, the amount of CO_2 leakage is reduced to 0.4-2.7% of the injected CO_2, depending on the range of barrier permeabilities considered.

2.3 Remarks on polymer-gel remediation

Based on polymer-gel characterisation and permeability reduction results obtained from the laboratory experiments carried out in MiReCOL, a numerical model of a fluviatile saline aquifer was set up to assess the effectiveness of polymer-gel injection in diverting the flow of CO_2 plume away from a leaking sub-seismic fault within the storage reservoir. Two scenarios were defined based on different vertical extent of the sub-seismic fault as well as different layouts of the polymer-gel injection and eventual barrier position.

The modelling results obtained for a thirty-year simulation period in this study suggest that undesired CO_2 plume migration can be potentially prevented using polymer-gel solutions for flow diversion. Sensitivity analyses carried out suggest that the polymer-gel barrier is likely to be more effective if the resultant barrier permeability is less than 1mD.

Currently, the polymer injection modelling is being progressed further within the MiReCOL project towards remediation of leakage through faults and the caprock. Well layouts, volume of gel needed, the spatial extension of remediation, response time and longevity of remediation will be further investigated and reported in a future report (see Chapter XVI).

3 FOAM INJECTION AS FLOW DIVERSION OPTION

In order to apply foam to reduce leakage of CO_2 in a underground reservoir, a well is drilled near the leakage site and a solution of surfactant and brine is injected. The presence of CO_2 will then cause the formation of foam, which will reduce the mobility of the CO_2 phase thereby minimizing further leakage.

The plugging effect of foam treatment depends on geology, position and type of leakage, injected surfactant volumes, surfactant concentration, adsorption, foam strength and foam stability. The main purpose of the study is to explore ranges of some of these factors and to quantify their impact on continued leakage.

In this study we consider containment of a possible leakage of CO_2 under a structural spill point.

3.1 Foam modelling

The background explanation of the use of foam is given in earlier MiReCOL reports (Nabzar et al., 2015; Wasch et al., 2015). Foam is used in the oil & gas industry for mobility control of gas sweep during enhanced oil recovery. In this case surfactant is injected together with the water phase, and foam is generated when gas contacts the surfactant/brine solution. The desired effect is to reduce the mobility of the gas, forcing the injected gas to take alternative paths thus contacting more oil as well as delaying gas breakthrough in the production wells. Foam can also be used to reduce gas coning/cresting at producing wells. However due to various difficulties, foam has not yet been widely implemented on a field scale for enhanced oil recovery, with the possible exception of the Foam-Assisted Water Alternating Gas project on the Snorre field.

The present piece of work investigated an example of the use of foam as a plugging agent for leaking CO_2.

3.1.1 Modelling foam and prediction of its behaviour

In order to perform an assessment of the effectiveness of foam as a plugging medium it was decided to model scenarios in a numeric simulator. This is challenging due to several reasons, as follows:

- The interpretation of laboratory measurements can be challenging,
- Field data used is uncertain, not least because of the effects of reservoir heterogeneity,
- Up-scaling to field scale is not well understood,
- The macroscopic numerical model is complicated and approximate in itself.

As a result the prediction of field-scale foam behaviour is indeed challenging and quite uncertain, in particular for assessment of the plugging properties of foam.

The factors affecting the behaviour of foam in a reservoir include:

- The surfactant type,
- Temperature,
- Salinity,
- The lithology and rock surface properties,
- Liquid properties,
- Flow rates,
- Wettability,

- The surfactant concentrations achieved,
- The rates of component exchange.

In turn all of the above can affect:

- Adsorption of the surfactant onto the formation,
- The foam strength achieved,
- The stability/durability of the foam.

Foam decay is obviously an important issue. Within the reservoir foam does not form a solid material, but ideally should retain its plugging effect for a relatively long time. Ideally the stability of foam should compete with the time scales for CO_2 dissolution and CO_2 capillary trapping. Its stability is affected by non-equilibrium processes such as component exchange, viscous forces and saturation changes, which lead to degradation of the foam. This area is far from understood and it is difficult to find data in literature on the durability of foam.

AOS14 foam was adopted for this analysis, which has moderate foam strength at CO_2 storage conditions. For this work a numerical model was developed using the foam model in Eclipse 100 (Schlumberger). The following functional form was used:-

Gas relative permeability	$k_{rg\_foam} = k_{rg} / (1 + (M_r F_s(c) F_w (S_w))$
(note that rate and oil dependencies are also possible)	
Reference gas mobility reduction factor	M_r , values of 6 and 20 were used.
Surfactant dependence	$F_s(c) = (c / c_{ref})^{\alpha_s}$, where c is surfactant concentration.
Reference surfactant concentration for strong or weak foam	$c_{ref}=0.1\%$
Exponent	$\alpha_s = 1$
Water saturation dependence	$F_w (S_w) = 1/2 + (1/\pi) \arctan(\alpha (S_w - S_w^*))$
Dry out weighting factor	$\alpha = 8$
Dry out water saturation	$S_w^* = 0.4$

Adsorption and desorption of surfactant is a function of foam concentration, with alternative maximum values of 0.1 mg/g and 0.5 mg/g being used.

Decay of foam is given by specifying a half-time (not well documented in the literature), and values of 1 day, 45 days, and 365 days were used.

Note that since the injection point is assumed to be deeper than 800m, the CO_2 is in the dense phase and the foam strength is significantly reduced compared with foam strength for gaseous CO_2 (Aarra et al., 2014). Also, the water mobility was seen to be significantly reduced for this foam system.

3.1.2 Generic simulation model

A generic numeric model was prepared to simulate CO_2 leakage under a spill point, as shown in Figure 13. The active model measured 3.35 km x 0.6km x 300m with block dimensions of 23.7m x 20m x 6m. The reservoir properties were homogeneous throughout the model, with porosity = 0.3 and permeability = 500mD. The generic relative permeabilities used are shown in Figure 14 and no capillary pressure was applied. Water and gas were the only components modelled.

The depth of the top of the reservoir was defined as 1000m and open boundary conditions were implemented at the ends of the model by means of passive pressure relief wells W1 and W2.

The simulation was composed of 3 stages. Firstly 1Mt/y of CO_2 was injected at 4,000 sm^3/d into the top of the anticline for 7.5 years (via injector G1), resulting in the onset of leakage under the spill point at the right-hand side as shown in Figure 13 (note – sm^3 denotes standard conditions).

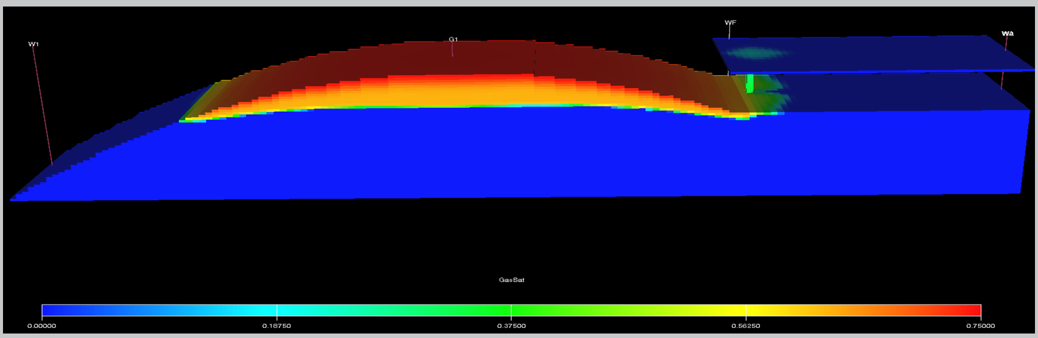

Figure 13 Generic simulation model of CO_2 spill-over.

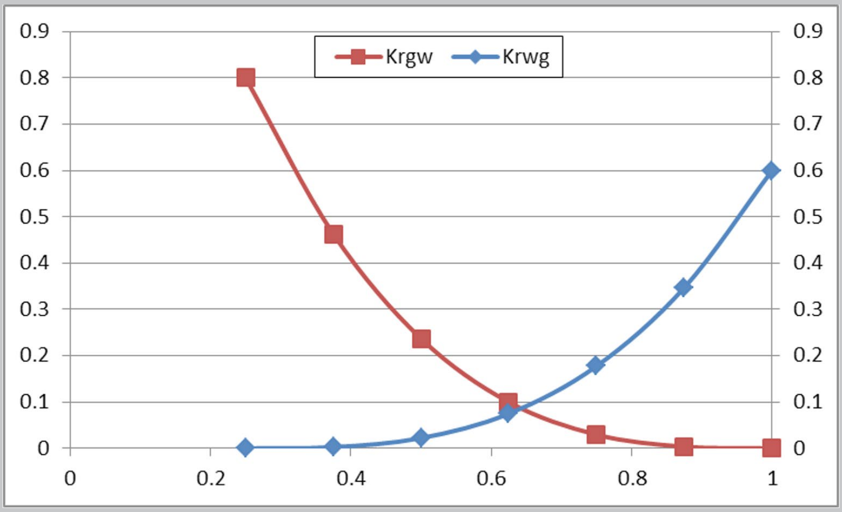

Figure 14 Relative permeabilities.

In stage 2 surfactant was introduced via a horizontal well WF located at the spill-point as shown in Figure 15. A 0.5% wt. solution of surfactant and brine was injected at 1,000 rm³/d for 0.25 year (rm³ denotes reservoir conditions), amounting to 450,000 kg of surfactant in total. (In this preliminary model a conduit up to small shallower aquifer was included to assist leakage measurement, but this was subsequently removed).

In the third stage, CO_2 injection into the anticline was continued for another 12 years at the same injection rate as before, without further injection of surfactant. The final state of CO_2 saturation in the model reservoir is shown in Figure 16, which indicates that the foam created provides resistance, if not a complete block, to the migration of CO_2.

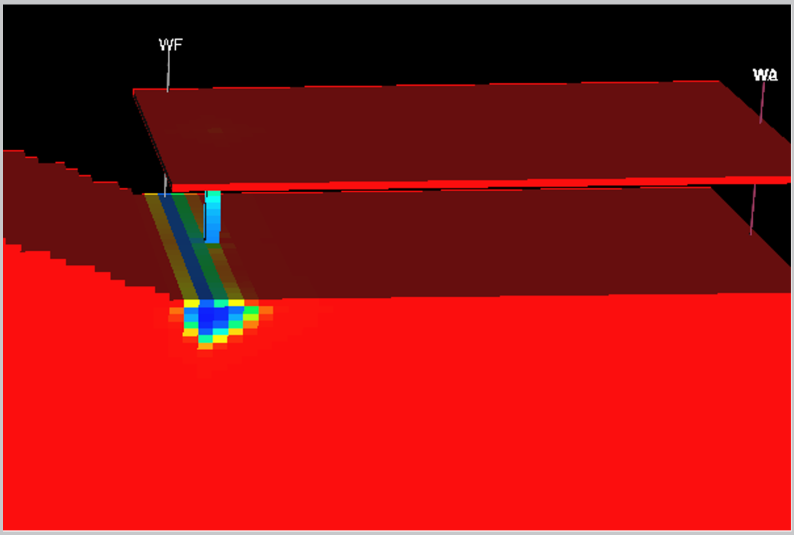

Figure 15 Preliminary arrangement at the spill point showing the surfactant injection well and a temporary secondary aquifer (the colours show the gas mobility factor, dark blue= 0, red = 1.0)

Several additional simulations were run in which the maximum adsorption factor, the reference gas mobility reduction factor and the foam decay half-life were varied individually. The results in Figure 17 and Figure 18 show that the maximum adsorption factor and the reference gas mobility factor had significant effects on the leakage rate, while the results were insensitive to the foam decay half-life. This foam model was used hereafter in further simulations to assess the practical application of foam to mitigation of CO_2 leakage.

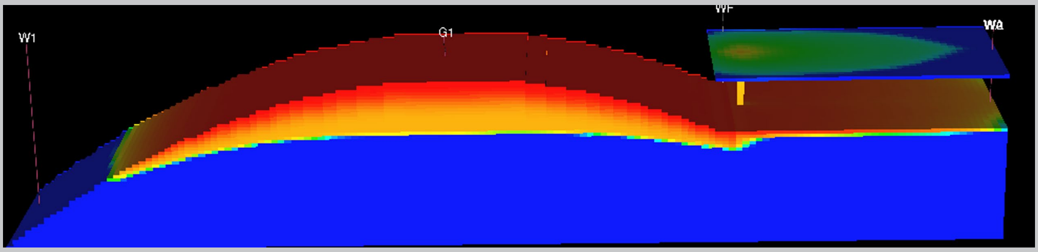

Figure 16 Final state of the generic reservoir showing gas (CO_2 saturation blue=0, red=1).

3.2 Assessment of capability of foam to mitigate CO_2 migration

The same generic model was used to support a series of flow simulations in Eclipse to assess the efficacy of injected foam to reduce the unwanted migration of injected CO_2 underground. This forms input to relative comparison of mitigation measures that will be conducted in WP11.

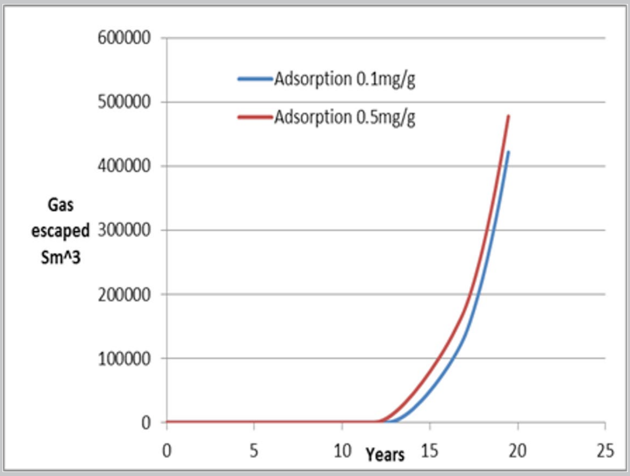

Figure 17 Constant reference mobility reduction factor M=6

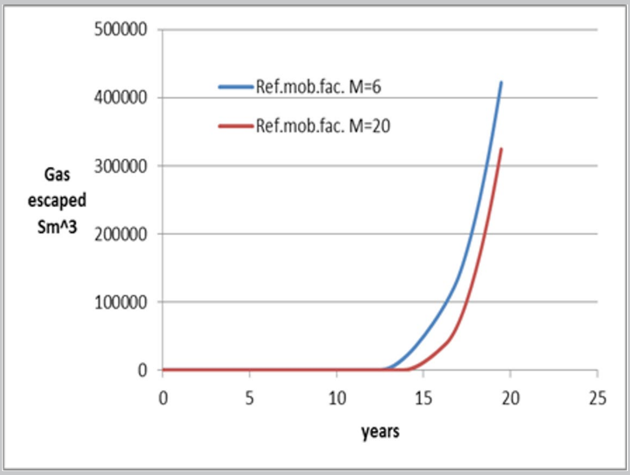

Figure 18 Constant adsorption factor=0.5mg/g

3.2.1 Simulation model

The same model was used as in Section 3.1.2 on modelling foam, i.e. a 2-dimensional anticline with a spill-point, and largely the same injection and production strategy was used, i.e. injection of 4000 rm^3/d CO_2 for 7.5 years, then injection of the surfactant solution, then continued injection of CO_2 for the remainder of 19.75 years.

Note that it was decided not to stop CO_2 injection when surfactant injection was begun, as continued CO_2 injection is a more demanding scenario and is expected to be the Operator's preferred choice (note that the alternative of re-routing the CO_2 to another storage reservoir, or other contractual options are likely to be much more expensive than a comprehensive mitigation programme). In order to derive quantitative data on leakage and reduction thereof, it was necessary to divide the model into regions for which volumetric data can be extracted from the numerical simulator. In order to make this as straightforward as possible, the secondary reservoir and upward conduit in the previous model were removed. In addition the main part of the reservoir was divided onto two Fluid-in-Place Regions, using the line of the horizontal injection well WF as the boundary, as shown in Figure 19. The quantities of CO_2 (gas) flowing from Region 1 to Region 2, i.e. the leakage past the surfactant injection well, could be found in each periodic report and are the most important data source. Note that the current volumes of the regions are of no interest because they are affected by the injection and production volumes of CO_2 and water.

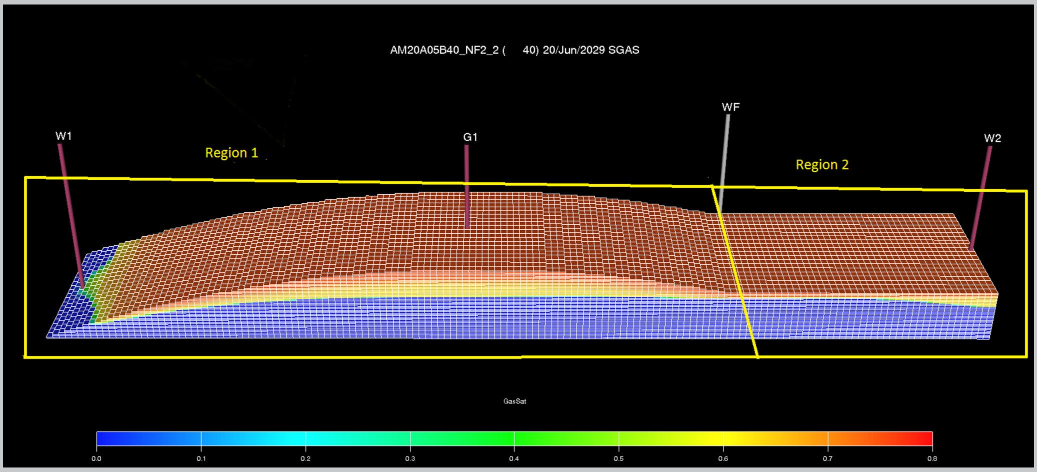

Figure 19 Regions applied to quantify leakage volumes.

A Base Case simulation was run 4000 rm^3/d CO_2 injection at the top of the anticline (via well G1) and zero surfactant injection. This gave the uncontrolled amount of leakage over the 19.75 years considered, against which the various mitigation measures were measured.

The build-up of uncontrolled "leakage" or migration into Region 2 is shown in Figure 20.

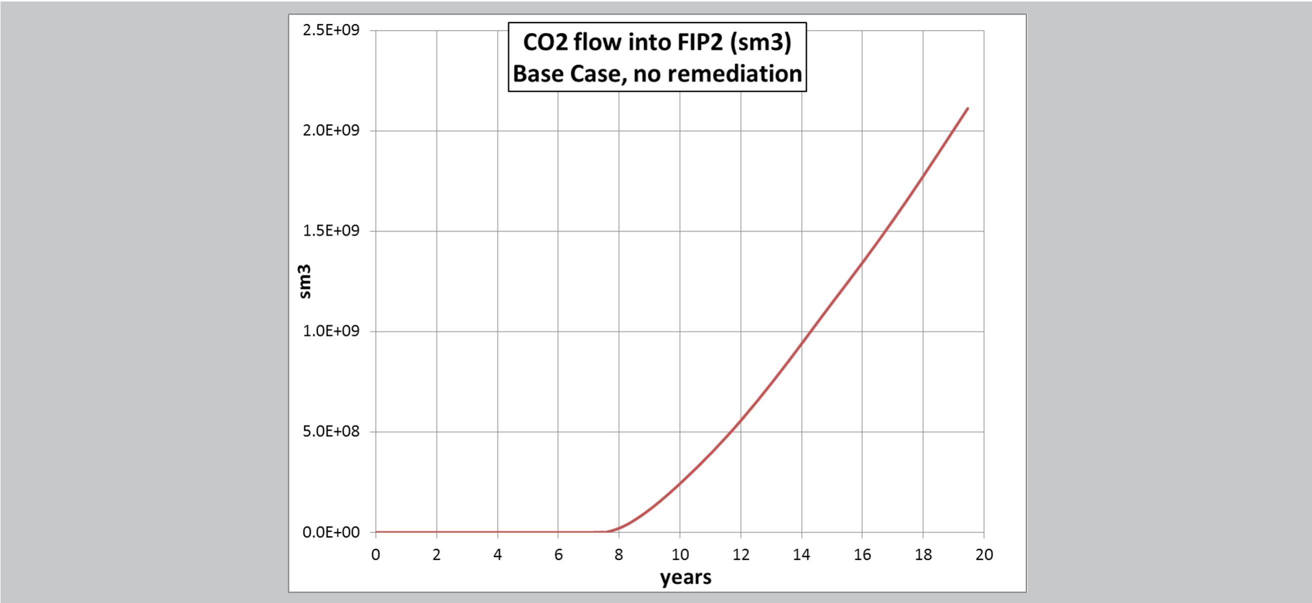

Figure 20 Uncontrolled leakage in Base Case.

A Reference Case mitigation scenario was chosen, utilising a middle set of foam parameters from the foam modelling work described in Section 3.1.2, with the following parameters:

- Reference CO_2 mobility reduction factor = 20,
- CO_2 adsorption = 5 mg/g,
- Foam half-life = 40 days,
- Operational parameters:
  - Injected surfactant concentration = 5 kg/sm^3 water,
  - Duration of surfactant injection = 90 days,
  - Surfactant solution injection rate = 1000 rm^3/d,
  - CO_2 injection rate = 4000 rm^3/d.

Variations on the operational parameters were simulated in order to investigate what could be achieved in a leakage-control situation, on the basis of the adopted foam characteristics.

Two measures of mitigation were used for comparison, namely:

- The reduction of leakage as a percentage of the Base Case leakage and
- The percentage reduction of leakage per million kg of surfactant injected, which gives a measure of unit (cost-) effectiveness.

3.2.2 Cases investigated

The main cases simulated plus their results are given in Appendix.1.

3.2.2.1 Surfactant injector orientation

Three initial variations of the surfactant injection well configuration were run, namely a vertical well perforated only in the top layer of the reservoir z=17, a horizontal well in layer z=18 (as in Section 3.1.2) and a horizontal well at the top of the reservoir in layer z=17. The horizontal wells were perforated on all blocks across the reservoir.

The results showed 98% leakage with the vertical well, 93% with the z=18 horizontal well and 91% with the z=17 horizontal well. The differences were easily explained by the lack of horizontal foam coverage provided by the vertical well and CO_2 over-run (i.e. CO_2 passing above) the horizontal well at z=18. These effects can be seen in the pictures of gas CO_2 saturation in Figure 21, Figure 22 and Figure 23.

It was decided that all further simulations would be based on a horizontal surfactant injection well located primarily at z=17, but with an alternative well at z=18 as a sensitivity.

3.2.2.2 Surfactant concentration

In addition to the original simulations using 5kg/sm^3 surfactant concentration, additional cases were run with 50 kg/sm^3 and 100 kg/sm^3 and all other parameters unchanged.

Pictures of the foam and CO_2 saturations in Figure 24 and Figure 25 show that the cross-sectional area containing the foam is quite small in all cases considered, with the result that the CO_2 is blocked only for a short period, but soon under-runs the foam plug.

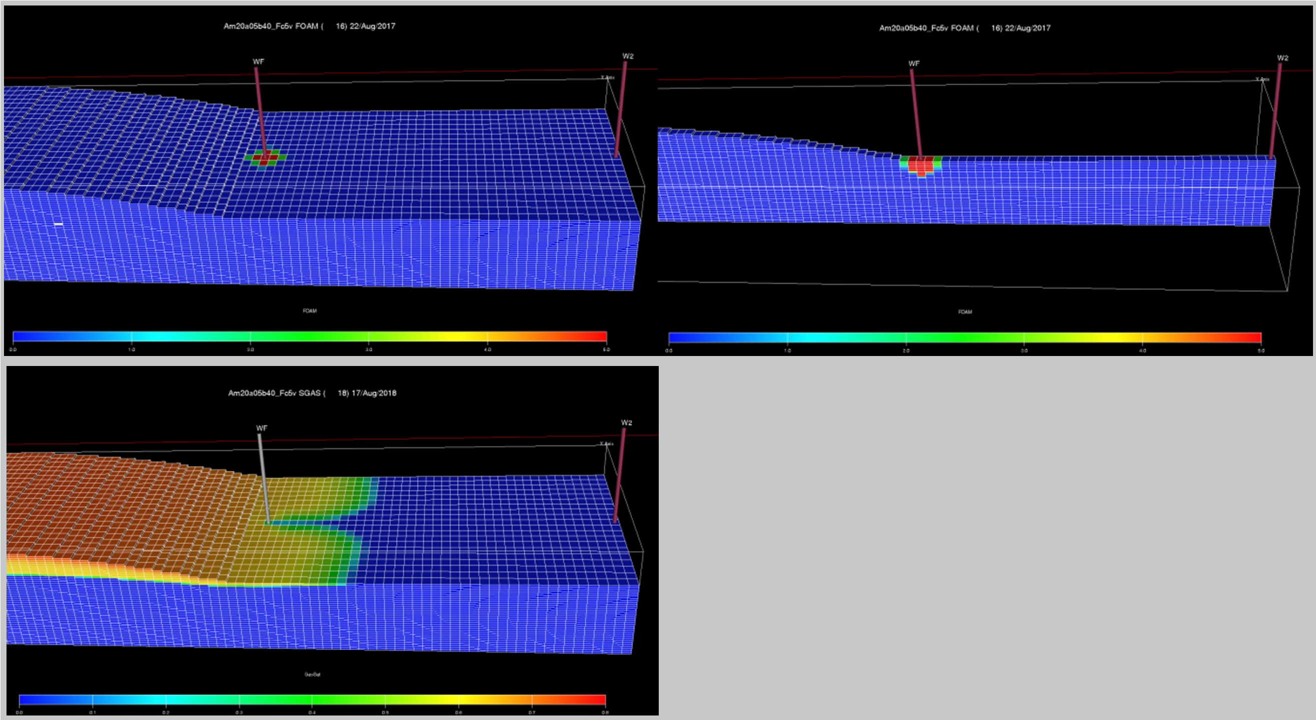

Figure 21 Vertical well, a) and b) foam concentration and c) CO_2 saturation all at 7.6 years.

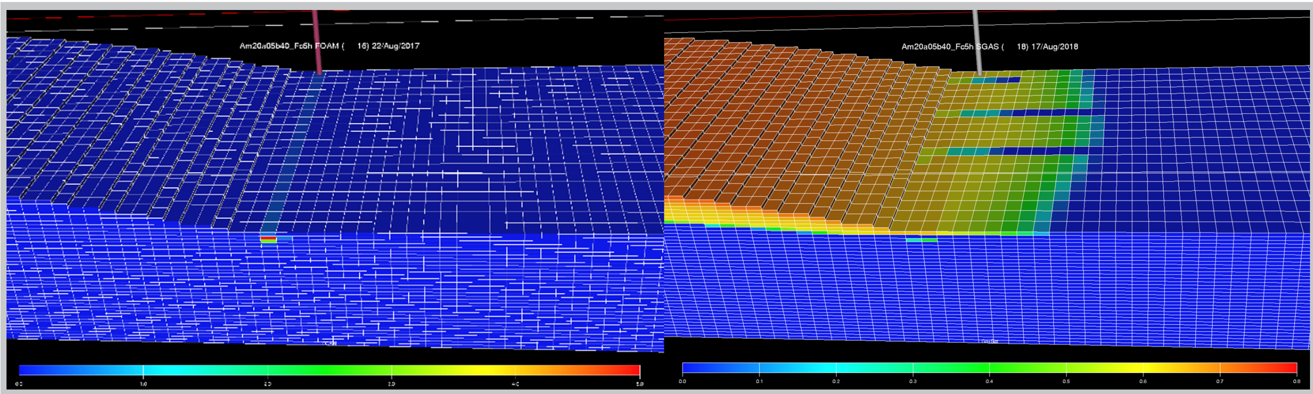

Figure 22 Horizontal well at z=18, a) foam concentration at 7.6 years and b) CO_2 saturation at 8.6 years.

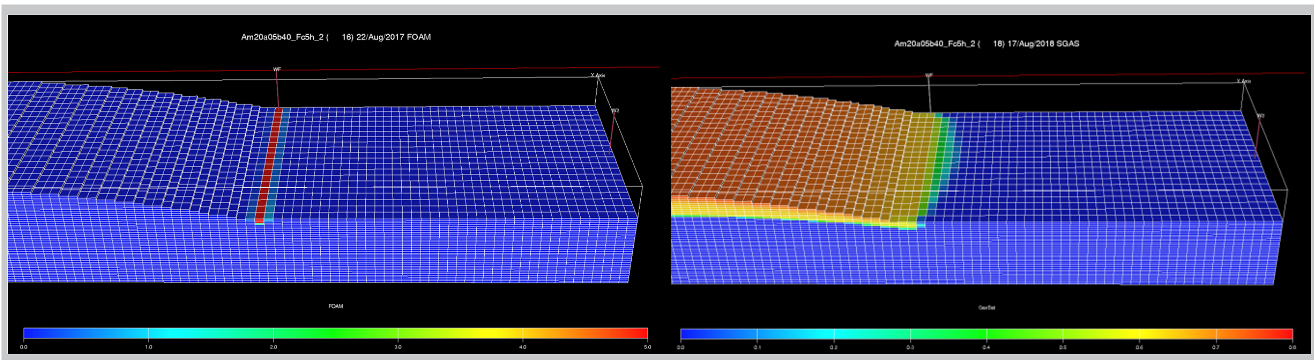

Figure 23 Horizontal well at z=17, a) foam concentration at 7.6 years and b) CO_2 saturation at 8.6 years

3.2.2.3 Surfactant injection duration

From the results of Section 3.2.2.2 it appeared that a foam "plug" of greater volume would be beneficial, instead of greater concentration. Therefore variations on the duration of surfactant injection were tried, starting from 0.25 year in the Reference Case, to 1 year, 5 years and 12.25 years.

It can be seen from Figure 24 and Figure 26 to Figure 28 that with long injection durations (i.e. greater injected volume) the foam plug is much larger and the total leakage is reduced. Obviously the amount of surfactant injected increases proportionally with the duration of injection, i.e. 50 times after 12.25 years injection.

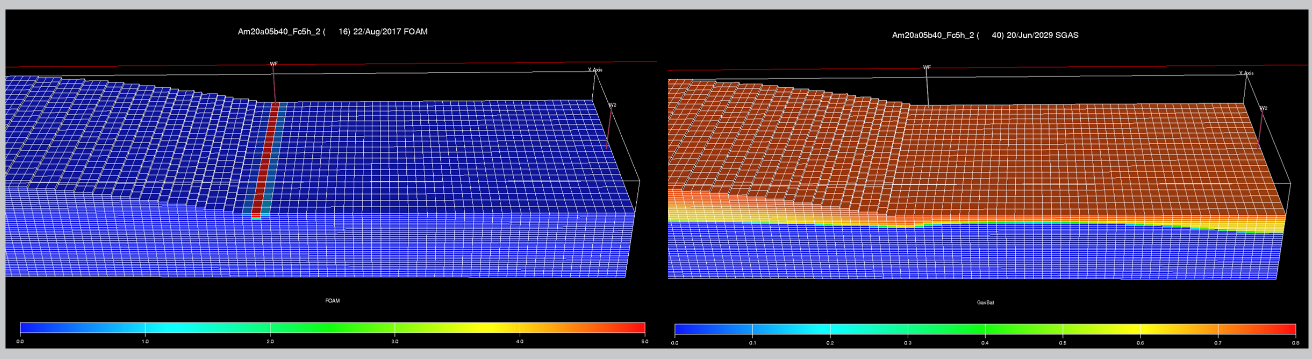

Figure 24 5kg/sm³ surfactant, foam concentration at 7.6 years and CO_2 saturation at 19.7 years (Reference Case).

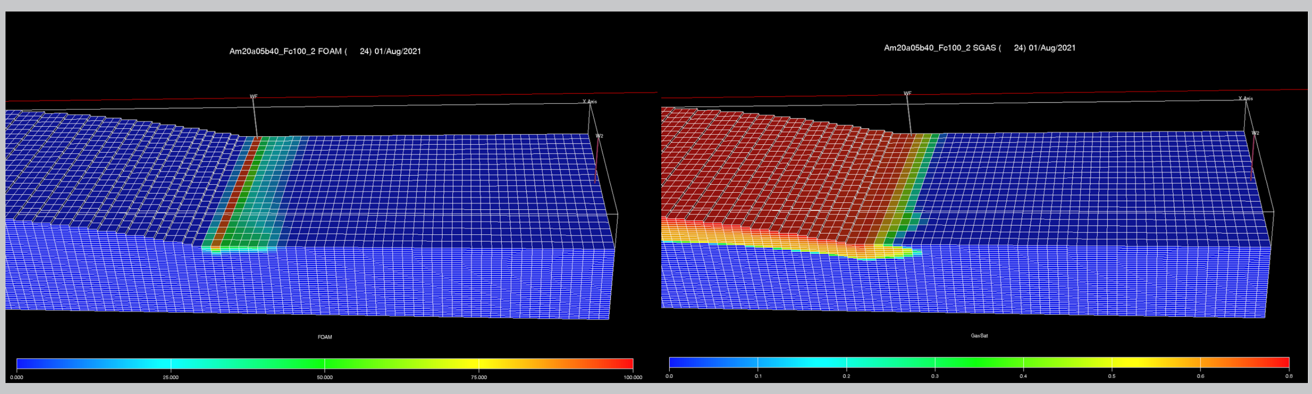

Figure 25 100 kg/sm³ surfactant, foam concentration and CO_2 saturation at 11.5 years. This is the point of under-run occurring and the CO_2 continues to occupy all of the topmost layers.

Figure 28 shows clearly that under-run is the main mechanism for CO_2 to pass the foam plug.

3.2.2.4 Surfactant injection rate

As an alternative to injecting for a longer period is to inject surfactant at a higher rate, in order to build a large plug more quickly. In addition to the Reference Case rate of 1,000 rm³/d, two other rates were tried, namely 5,000 rm³/d and 10,000 rm³/d, all with 0.25 year injection.

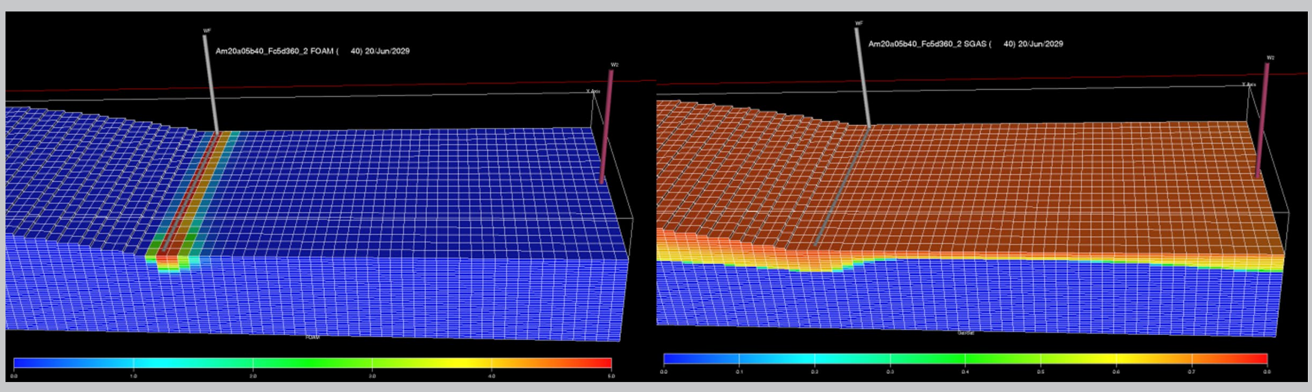

Figure 26 Surfactant injection for 1 year, showing a) foam concentration and b) CO_2 saturation at 19.7 years.

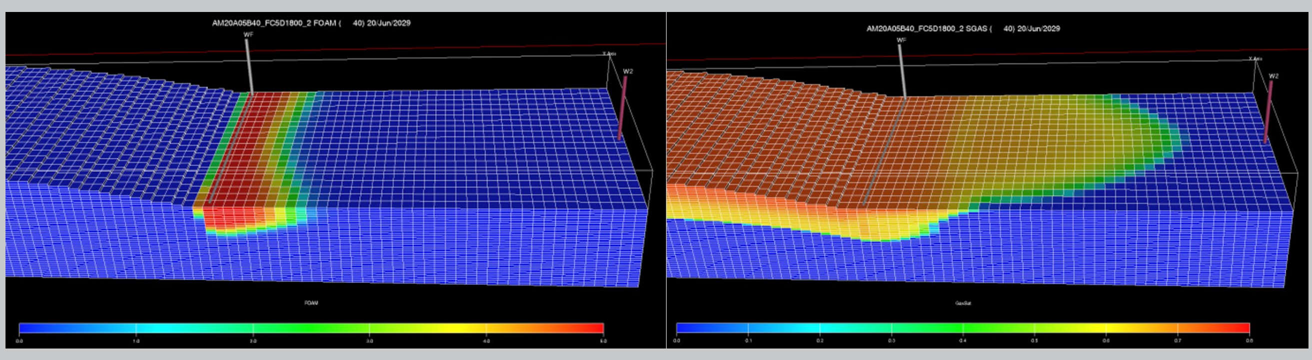

Figure 27 Surfactant injection for 5 years, showing a) foam concentration and b) CO_2 saturation at 19.7 years.

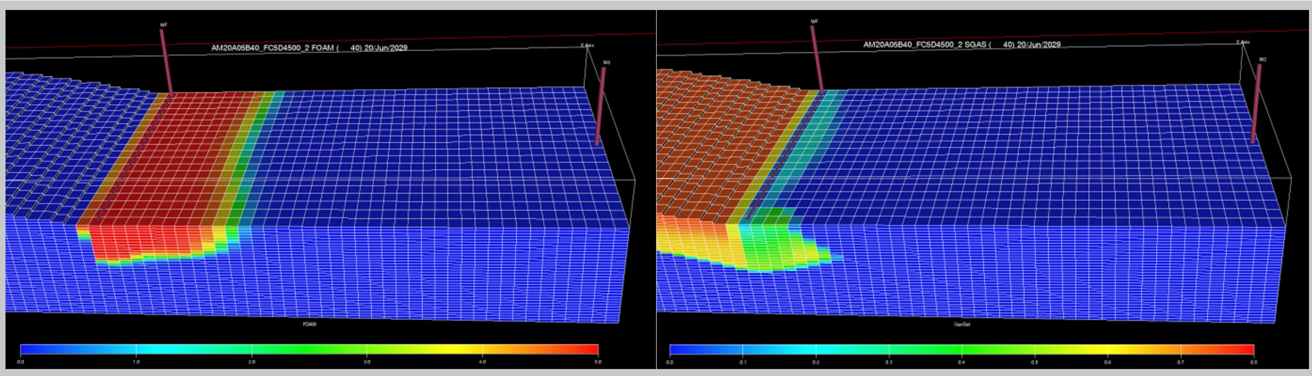

Figure 28 Surfactant injection for 12.25 years, showing a) foam concentration and b) CO_2 saturation at 19.7 years.

The pictures in Figure 29 show that the increased injection rate forms a more substantial plug which holds back the CO_2 for four years, when large-scale under-run occurs. It can be seen that the effect is similar to injecting for a longer period.

3.2.2.5 CO_2 injection rate.

A few alternatives for the CO_2 injection rate were simulated in order to demonstrate its effect on the leakage rate. The Reference Case used a value of 4,000 rm^3/d and in subsequent simulations values of 6,000 and 8,000 rm^3/d were tried.

3.2.3 Simulation results

The results of the simulations described above were depicted graphically, as shown in Figure 30 to Figure 33.

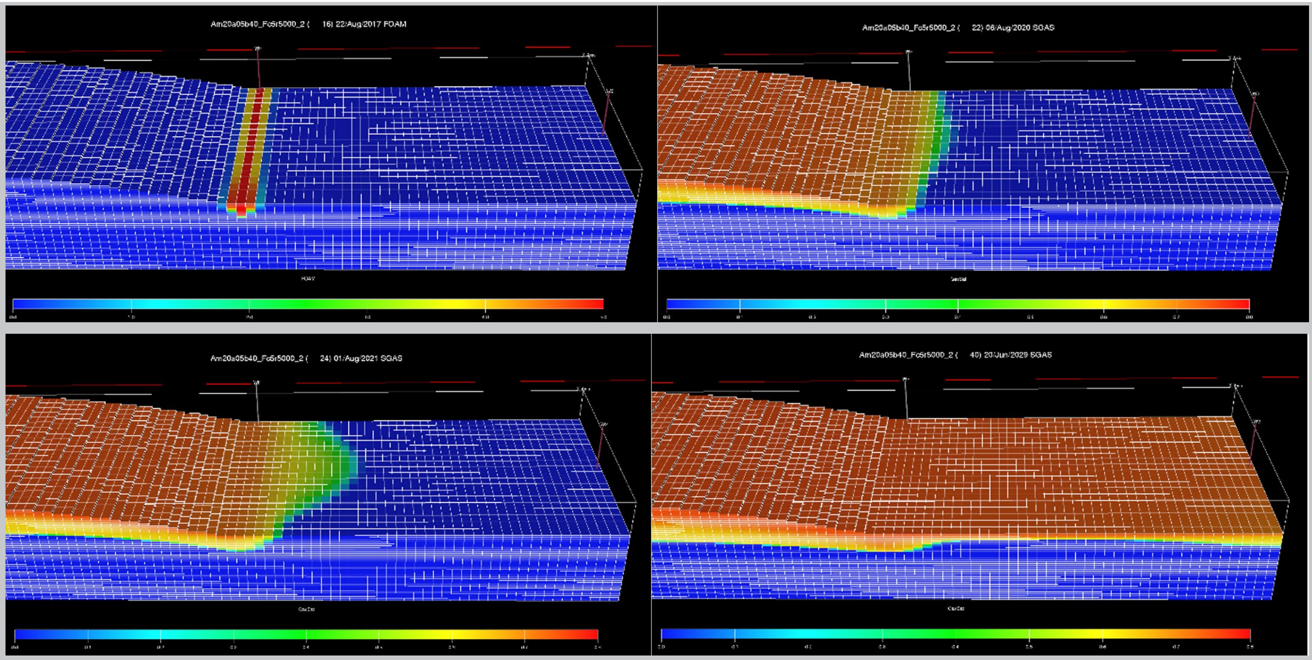

Figure 29 Surfactant injection rate at 5,000 rm^3/d for 0.25 year, a) initial foam concentration achieved, b) CO_2 restrained at 3 years after surfactant injection, b) under-run and break-through occurring 1 year later and d) final CO_2 saturation at 19.7 years.

In Figure 30 it can be seen that very little improvement in blocking occurs with increased surfactant concentrations above 60 kg/sm^3. On the contrary Figure 31 and Figure 32 show that migration keeps falling with increasing surfactant injection duration and injection rate. This might be explained by the limited size of plug generated by increased surfactant concentration alone, without a larger volume of water to carry and spread the surfactant.

Considering unit effectiveness (migration reduction per million kg of surfactant injected) it can be seen that CO_2 migration is reduced rapidly with the initial increase of all the parameters tested. However while this measure tends to level out with increasing injection concentration and injection duration (Figure 30 and Figure 31), it keeps decreasing with increasing injection rate (Figure 32).

From the two observations above it might be suggested that injection duration has the greatest single potential for increased leakage mitigation, since leakage can be reduced with longer injection without reducing its unit effectiveness.

Note also that since no effect was observed for the foam half-life in Eclipse simulations (Section 3.1.2), injecting surfactant over a longer period of time would help to counteract the assumed effects of foam degradation in a real reservoir.

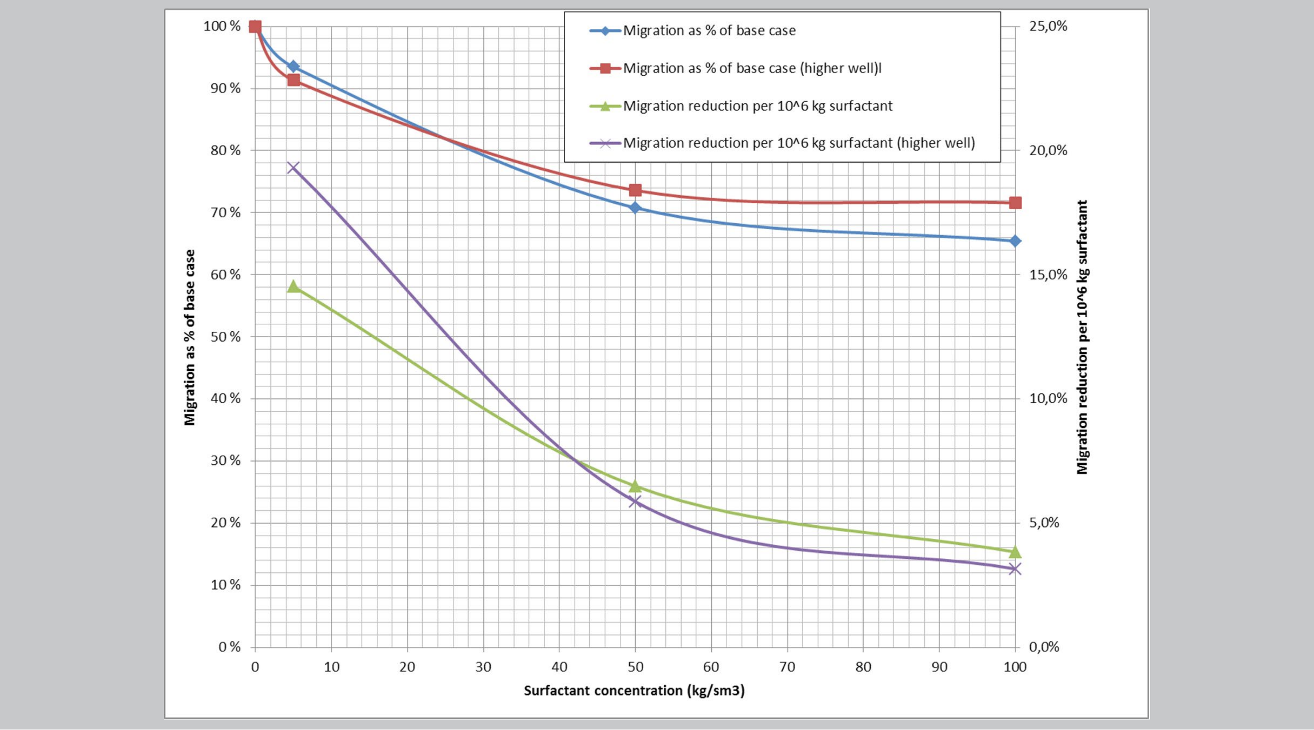

Figure 30 Mitigation measures versus surfactant concentration.

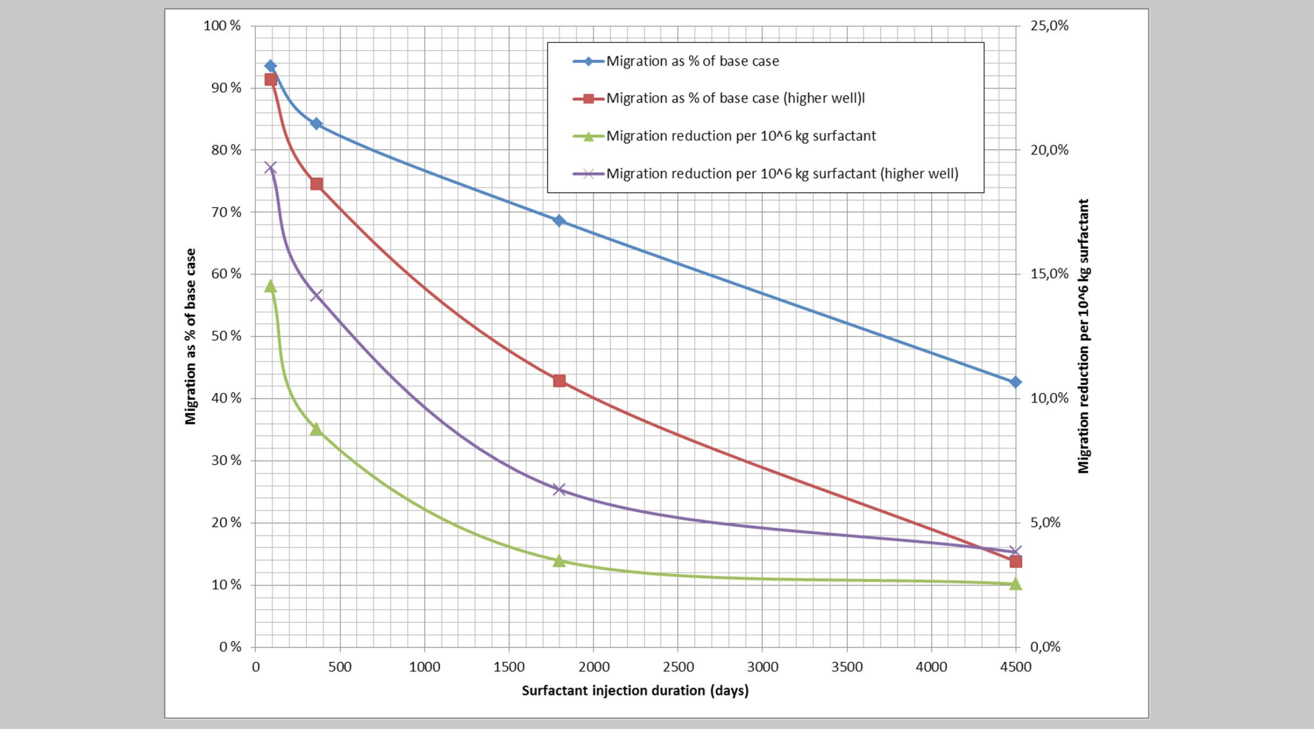

Figure 31 Mitigation measures versus surfactant injection duration.

Figure 33 shows the results for increased CO_2 injection rates where an almost linear increase in leakage is evident with a corresponding near-linear reduction in unit effectiveness. This was as expected.

In all cases, the mitigation of leakage is limited by under-run of the CO_2. This suggests that there might be potential improvement from additional injection of surfactant at lower depths in the reservoir to increase the vertical size of the foam plug.

3.2.4 Limited optimisation

A very limited exercise was performed to gauge the potential for optimising the reduction of leakage by simultaneously varying several of the parameters used.

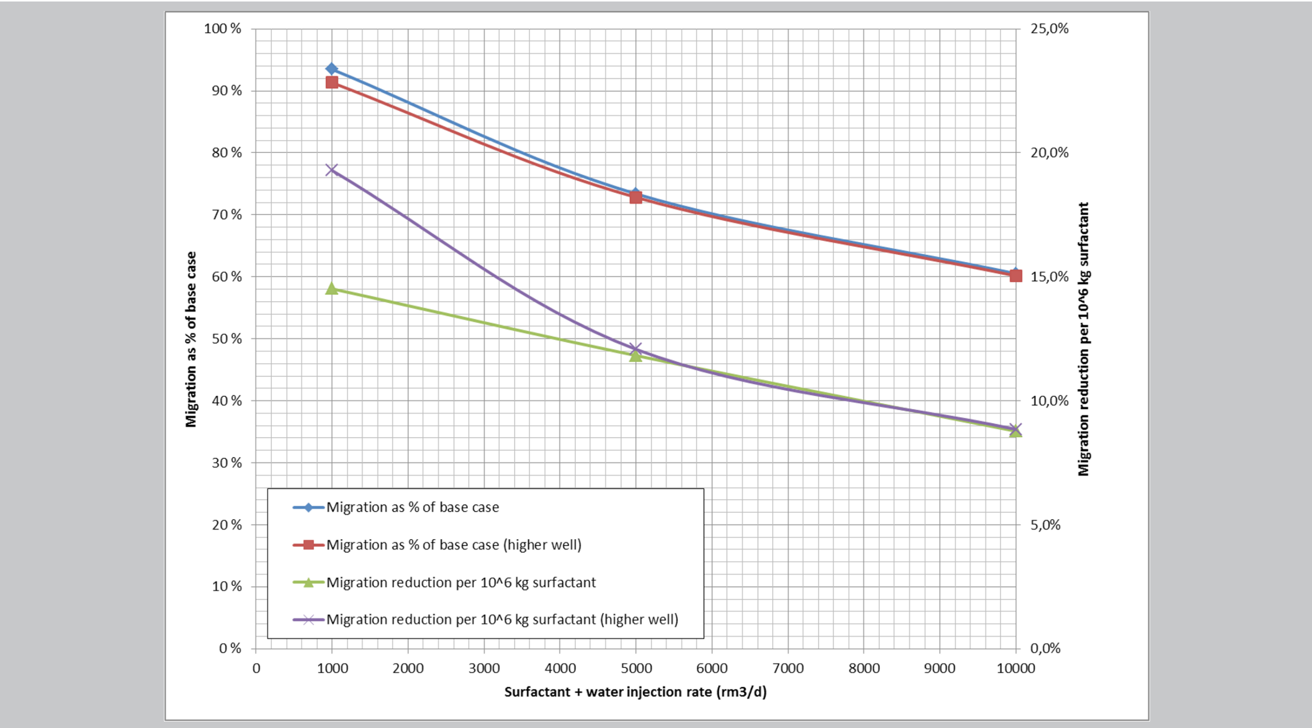

Figure 32 Mitigation measures versus surfactant injection rate

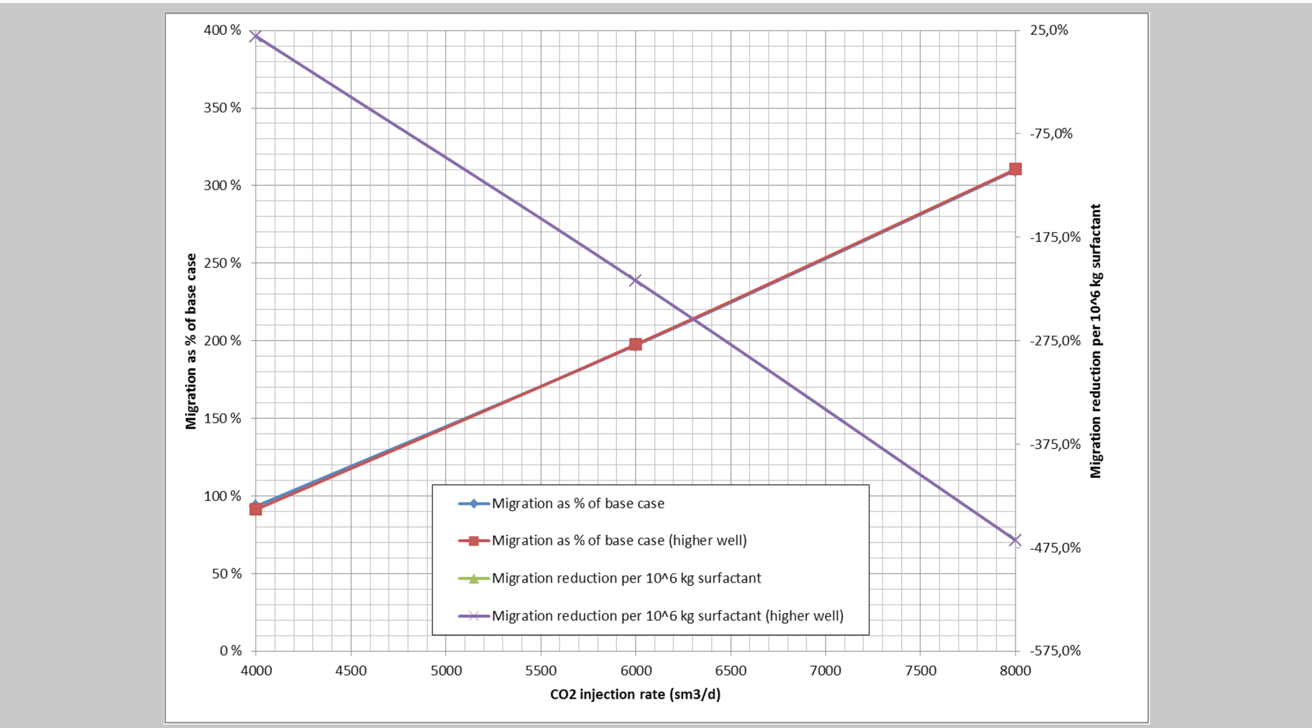

Figure 33 Mitigation measures versus CO_2 injection rate

1. The starting point is the Reference Case shown in Figure 24 which to repeat, utilised a surfactant concentration of 5 kg/sm³, an injection rate of 1,000 rm³/d and an injection duration of 0.25 year starting at 7.5 years into the simulation. Note the very small foam plug formed.
2. The next step was to increase the injection rate to 5,000 rm³/d, as already described and shown in Figure 29. This generated a slightly larger foam plug, which delayed CO_2 breakthrough for three years.

3. In order to extend the duration of blockage an additional 0.25 year of surfactant injection at the same rate was implemented, commencing at 3 years after the start of the first injection period, i.e. at t=10.5 years. The results in Figure 34 show that an even larger foam plug was generated, which delayed the leakage, but was eventually under-ridden by the CO_2. Note also that the foam plug has a significant CO_2 saturation, i.e. is not impermeable.
4. As an alternative to two discrete periods of surfactant injection, a continuous process was implemented. After the first 0.25 year injection period at 5,000 rm^3/d, injection continued for the remainder of the simulation at a reduced rate of 1,000 rm^3/d. The aim of this was to maintain the effectiveness of the foam plug and possibly extend its depth. The pictures in Figure 35 show that a somewhat massive foam plug was developed by the end of the simulation which succeeded to a large degree in preventing leakage of CO_2. The numerical results showed that the leakage had been reduced to 14% of the Base Case, but with a very low unit effectiveness of 3.6%. This result was the same as achieved earlier with 12.25 years injection at a constant 1,000 rm^3/d, suggesting that constant surfactant injection is more important than a high initial injection rate.
5. In the final optimization trial the initial 0.25 year injection period was maintained at 5000 sm^3/d, but during the remainder of the simulation this was reduced further to 500 sm^3/d. The results in Figure 36 show that foam plug is not as deep as in the previous simulation with the result that CO_2 under-run occurs to a significant degree. The final leakage increased to 28% of the Base Case at 5.5% unit effectiveness.

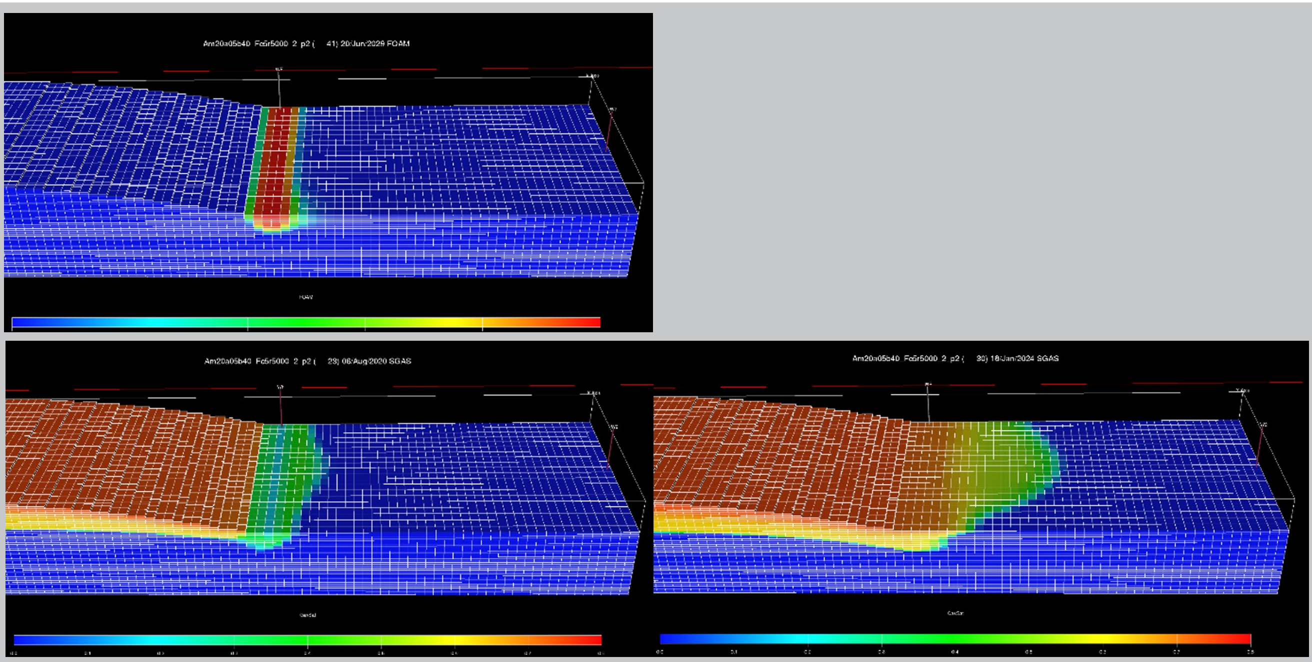

Figure 34 Surfactant injection at 5,000 rm^3/d for 2x0.25 years, a) foam concentration at the end of 19.75 years, b) CO_2 concentration after the second surfactant injection period showing migration through the foam plug, c) CO_2 concentration 3.5 years later, showing under-run.

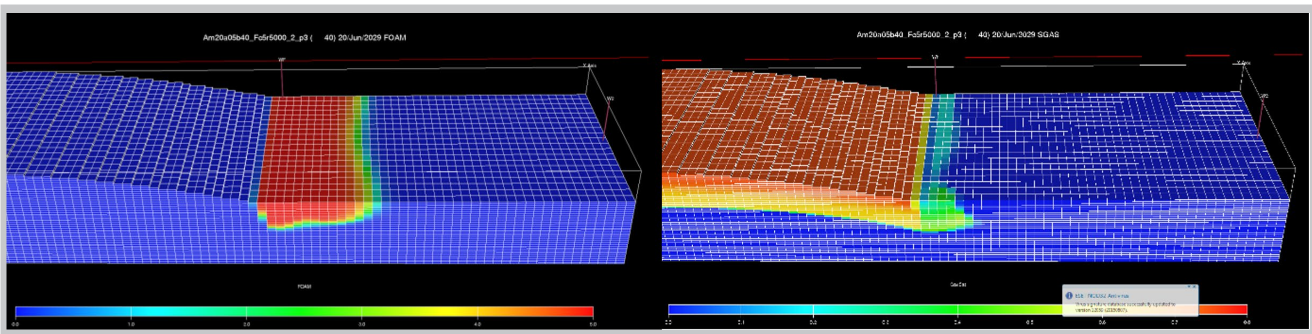

Figure 35 Surfactant injection at 5,000 rm^3/d for 0.25 year followed by 12 years at 1,000 rm^3/d, a) foam concentration at the end of 19.75 years, b) CO_2 concentration at the end of 19.75 years showing almost complete blockage.

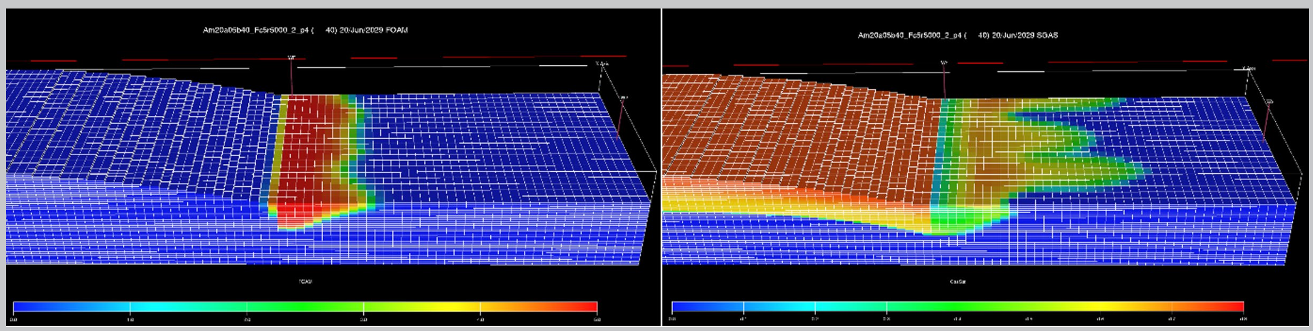

Figure 36 Surfactant injection at 5,000 rm^3/d for 0.25 year followed by 12 years at 500 rm^3/d, a) foam concentration at the end of 19.75 years, b) CO_2 concentration at the end of 19.75 years.

3.3 Remarks on foam injection remediation

Based on the numerical investigations performed, the following conclusions can be drawn on CO_2 leakage mitigation by means of foam:

- Foam behaviour in porous media is complicated and depends on a large number of parameters. It is challenging to model numerically, in particular at the field scale, even ignoring the heterogeneities occurring in a real reservoir.
- An acceptable model for foam as a plugging agent was created within the Eclipse simulator, although the initial results suggest that the simulations are insensitive to variations in the foam decay half-life parameter.
- Data have been generated to illustrate the effect of a foam plug on CO_2 leakage in a conceptual reservoir model. The effects of surfactant concentration, injection rate and injection duration, have been studied. Data are presented in terms of percentage reduction of leakage and percentage reduction of leakage per million kg of surfactant used (unit effectiveness). The effect of well location and orientation and CO_2 injection rates have been tested to a very limited extent.
- An inverse relationship was found between the leakage reduction and the unit effectiveness (leakage reduction % per million kg surfactant used)
- The greatest reduction in leakage volume achieved was down to 14% of the unimpeded leakage, but this requires a lot of surfactant giving a unit effectiveness of 3.6% reduction per million kg surfactant.
- High surfactant concentration alone is insufficient to create an effective foam plug; sufficient water must be injected to form a large enough plug to prevent by-passing by CO_2.
- A foam plug is not very durable and needs to be maintained by continuous or frequent intermittent surfactant injection.
- The foam plug should form a continuous wall towards the approaching CO_2, wide enough and reaching from the top layer (to prevent over-run) down to a deep enough level to prevent under-run by the accumulating CO_2.
- The injection well configuration has not been investigated thoroughly, but in view of the previous point, the use of several well branches (vertical or horizontal) may give a large enough plug cross-section with less surfactant injection than used in this study. This depends heavily on the actual topography of the leakage area in the reservoir.

References

Aarra M.G., Skauge A., Solbakken J., Ormehaug P.A., (2014) Properties of N_2- and CO_2-foams as function of pressure. J.Pet. Sci. Eng. 116:72-80.

Albrecht, R.A. and Marsden, S.S. 1970. Foams as Blocking Agents in Porous Media. SPE J. 10 (1): 51–55. SPE-2357-PA.

Al-Muntasheri, G.A., Sierra, L., Garzon, F.O., Lynn, J.D. and Izquierdo, G.A., 2010. Water shut-off with polymer gels in a high temperature horizontal gas well: A success story. Society of Petroleum Engineers, SPE 129848.

Amirbayov, T., 2014. Simulation study of the polymer flooding applied to the Norne Field E-Segment. MSc Thesis, Norwegian University of Science and Technology.

Benson, S.M., 2006. Monitoring carbon dioxide sequestration in deep geological formations for inventory verification and carbon credits. Society of Petroleum Engineers, SPE 102833.

Chabert, M., Morvan, M. and Nabzar, L., Advanced Screening Technologies for the Selection of Dense CO_2 Foaming Surfactants, 33rd IEA EOR Symp. August 26-30, 2012.

Chabert M., Nabzar L., Rohaida, S., Hamid P., Sedaralit M.F. and Darman N., An integrated laboratory workflow for the design of a foam pilot in Malaysia, IOR 2013 – 17th European Symposium on IOR. St. Petersburg, Russia, 16-18 April 2013

Chabert, M., Nabzar, L., Beunat, V., Lacombe E. and Cuenca, A., Impact of Surfactant Structure and Oil Saturation on the Behavior of Dense CO_2 Foams in Porous Media , SPE 169176, SPE Improved Oil Recovery Symposium held in Tulsa, Oklahoma, USA, 12–16 April 2014.

Cubillos, H., Montes, J. Prieto, C. and Romero, P., Assessment of foam for GOR control to optimize miscible gas injection recovery, SPE 152113, SPE IOR symposium, Tulsa, Oklahoma, 14-18 April 2012

Enick, R.M, Olsen, D., Ammer, J. and Schuller, W., Mobility and Conformance Control for CO_2-EOR via Thickeners, Foams, and Gels - A Literature Review of 40 Years of Research and Pilot Tests, SPE 154122, SPE IOR symposium, Tulsa, Oklahoma, 14-18 April 2012

Farajzadeh, R., Andrianov, A., and Zitha, P. L. J., 2009,. Investigation of Immiscible and Miscible Foam for Enhancing Oil Recovery, Industrial & Engineering Chemistry Research 49:1910-1919.

Flew, S., Sellin, R.H.J., 1993. Non-Newtonian flow in porous media-a laboratory study of polyacrylamide solutions. Journal of Non-Newtonian Fluid Mechanics, (47) 169-210.

Gauglitz, A., Friedmann, F., Kam, I., and Rossen, R., 2002, Foam generation in homogeneous porous media. Chemical Engineering Science, 57, 4037-4052

Gharbi, R., Alajmi, A., and Algharaib, M., 2012. The potential of a surfactant/polymer flood in a Middle Eastern Reservoir. Energies, (5) 58-70.

Hild, G.P., Wackowski, R.K., 1999. Reservoir polymer gel treatments to improve miscible CO_2 flood. Society of Petroleum Engineers, SPE 56008.

IEAGHG Report, 2007. Remediation of leakage from CO_2 storage reservoirs. IEA Greenhouse Gas R&D Programme, Report No. 2007/11.
IEAGHG Report, 2007. Remediation of leakage from CO_2 storage reservoirs. IEA Greenhouse Gas R&D Programme, Report No. 2007/11.
Nabzar, L., Fleury, M., Durucan, S., Pizzocolo, F., ter Heege, J., and Peters, L., 2015. Report to partners summarizing the choice of models (use of sealant as a corrective measure to stop CO_2 flow through fault: review and work-plan), MiReCOL report D6.1 (www.mirecol-CO_2.eu).

Legemah, M., Guerin, M., Sun, H., and Qu, Q., 2014. Novel high-efficiency boron crosslinkers for low-polymer-loading fracturing fluids. Society of Petroleum Engineers, SPE 164118.

Lei, C., and Clark, P.E., 2004. Crosslinking of guar and guar derivatives. Society of Petroleum Engineers, SPE 90840.

NPD, 2013. Norwegian Petroleum Directorate CO_2 Storage Atlas: The Barents Sea. Norwegian Continental Shelf. pp. 107-145.

Rodriguez, S., Romero, C., Sargenti, M.L., Müller, A.J., Sáez, A.E., Odell, J.A., 1993. Flow of polymer solutions through porous media. Journal of Non-Newtonian Fluid Mechanics, (49) 63-85.

Saez, M., Paponi, H.M., Cabrera, F.A., Muniz, G., Romero, J.L., Norman, C., 2012. Improving volumetric efficiency in an unconsolidated sandstone reservoir with sequential injection of polymer gels. Society of Petroleum Engineers, SPE 150492.

Sarkar, S., 2012. Evaluation of alkaline, surfactant and polymer flooding for enhanced oil recovery in the Norne E-segment based on applied reservoir simulation. MSc Thesis, Norwegian University of Science and Technology.

Schlumberger (2011) ECLIPSE Simulation software manuals.

Sheng, J.J., 2011. Chapter 6 - Polymer viscoelastic behaviour and its effect on field facilities and operations, in: Sheng J.J. (Ed.) Modern chemical enhanced oil recovery, Gulf Professional Publishing, Boston, pp 207-238.

Skauge, A., Aarra, M. G., Surguchev, L., Martinsen, H. A. and Rasmussen, L., 2002, Foam-Assisted WAG: Experience from the Snorre Field. SPE 75157.

Smith, J.E., 1995. Performance of 18 polymers in aluminium citrate colloidal dispersion gels. Society of Petroleum Engineers, SPE

28989.
Solbakken, J.S., Skauge A. and Aarra, M.G., Supercritical CO_2 foam- The importance of CO_2 density on Foam Performance, SPE 165296, SPE EOR Conference, Kuala Lumpur, Malaysia, 2-4 July 2013.
Stavland, A., and Jonsbraten, H.C., 1996. New insight into aluminium citrate/ polyacrylamide gels for fluid control. Society of Petroleum Engineers, SPE 35381.
Sun, H., and Qu, Q., 2011. High-efficiency boron crosslinkers for low-polymer fracturing fluids. Society of Petroleum Engineers, SPE 140817.
Sydansk, R.D., 1998. A new conformance-improvement-treatment chromium(III) gel technology. Society of Petroleum Engineers, SPE 17329.
Sydansk, R.D., Al-Dhafeeri, A.M., Xiong, Y., Seright, R.S., 2004. Polymer gels formulated with a combination of high- and low-molecular-weight polymers provide improved performance for water-shutoff treatments of fractured production wells. Society of Petroleum Engineers, SPE 89402.
Sydansk, R.D., Southwell, G.P., 2000. More than 12 years' experience with a successful conformance-control polymer-gel technology. Society of Petroleum Engineers, SPE 66558.
Tanzil,D., Hirasaki G. and Miller C.A., Conditions of foam generation in Homogeneous Porous Media, SPE/DOE IOR Symp., Tulsa, Oklahoma, 13-17 April 2002
Turner, B.O., Zahner, R.L., 2009. Polymer gel water-shutoff applications combined with stimulation increase oil production and life of wells in the Monterey Formation offshore California. Society of Petroleum Engineers, SPE 121194.
Vossoughi, S., 2000. Profile modification using in situ gelation technology-a review. Journal of Petroleum Science and Engineering, (26) 199-209.
Wasch, L., Drysdale, R., Fleury, M., Wiese, B., Korre, A., and Durucan, S., 2015. D3.1 "Current flow diversion techniques in the petroleum industry relevant to CO_2 leakage remediation", MiReCOL report D3.1 (www.mirecol-CO_2.eu).
Wassmuth, F.R., Hodgins, L.A., Schramm, L.L., and Kutay, S.M., 2001. Screening and coreflood testing of gel foams to control excessive gas production in oil wells, SPE Reservoir Evaluation & Engineering, June 2001
Wegner, J., Ganzer, L., 2012. Numerical Simulation of Oil Recovery by Polymer Injection using COMSOL. in, Proceedings of the 2012 COMCOL Conference, Milan, Italy.
Wong, F.Y., Fong, D.K., McIntyre, F.J. and Kuehne, D.L., 1997. Design and field trial application of foam in production wells to improve conformance, J. Cdn. Pet. Tech. 36(2), 21-32.

APPENDIX A

	Case	Description	Results	surf conc kg/sm3	surf inj duration days (1)	w+surf inj rate (1) rm3/d=sm3/d	surf inj duration days (2)	w+surf inj rate (2) rm3/d=sm3/d	CO2 inj rate sm3/d	CPU sec	CO2 flow into FIP2 (sm3) - *from last report in -PRT files*	leakage % of base case (z=18)	leakage % of base case (z=17)	Surfactant used (kg)	%reduction / 10^6 kg surfactant
	Am20a05b40_NF2_2	As _NF2 but with surf conc in WFOAM set to 0. Water injection for 90 days. (Horiz injector, z=18.)	This shows that _NF, _NF2 & _NF3 still carried the action of surfactant., i.e. FOAMDCYW was not sufficient to stop this. The effect of surfactant in _NF2 etc was significant. **This is now used as the new baseline.**	**0**	**90**	**1000**			**4000**	**396**	**2,112,024,395**		100%	0	0.0%
	Am20a05b40_NF2_2nw	As _NF2_2 but WI cut out. (Well WF horiz)	Relatively little effect cf NF2_2. Shows that the effect of WI is minimal (at the present rate) cf the effect of surfactant.	0	0	1000			4000	391	2,120,916,401		100%	0	0.0%
	Am20a05b40_Fc5v (previously Am20a05b40_Fc5)	Re-introduce surfactant concentration (0.005% wt) but with injection well G1 now vertical, perforated at (110, 10, 17). Surfactant injection for 90 days only.	Higher leakage (flow into region2) due to vertical well unstead of horizontal. Same water inj rate plus surfactant. Will revert to horiz well plus water for future sensitivities. Injection must be in the top layer (17) otherwise the CO2 bypasses it above.	5	90	1000			4000	391	2,065,657,232		98%	450,000	4.9%
Surf. Concentration	Am20a05b40_Fc5h	As _NF-2_2 with surfactant restored at 0.5%wt. Decay half-life = 40 days. (Well WF horiz) z=18	Difference compared with NF2_2 shows effect of surfactant. Floviz FOAM shows quite a small plug and under-run by the CO2 - check.	**5**	90	1000			4000	423	1,974,050,548	93%		450,000	14.5%
	Am20a05b40_Fc5h_2	As Am20a05b40_Fc5h but with injector WF raised to z=17.	**Reference case for variations in parameters.**	**5**	90	1000			4000	403	1,928,714,422		91%	450,000	19.3%
	Am20a05b40_Fc50	As Am20a05b40_Fc5h but with surf conc increased to 5% wt. Half-life restored to 40 days.(Well WF horiz)	Significant reduction in leakage.	**50**	90	1000			4000	500	1,495,197,858	71%		4,500,000	6.5%
	Am20a05b40_Fc50_2	As Am20a05b40_Fc50 but with injector WF raised to z=17.	Higher leakage than with injection in z=18.	**50**	90	1000			4000	404	1,554,379,354		74%	4,500,000	5.9%
	Am20a05b40_Fc100	As Am20a05b40_Fc50 but with surf conc increased to 10% wt.	Further reduction.	**100**	90	1000			4000	487	1,381,969,883	65%		9,000,000	3.8%
	Am20a05b40_Fc100_2	As Am20a05b40_Fc100 but with injector WF raised to z=17.	Higher leakage than with injection in z=18. The CO2 appears to be diluted and spread downstream, and covers little depth. The result is that the CO2 undercuts the foam.	**100**	90	1000			4000	396	1,511,842,082		72%	9,000,000	3.2%
Surf.Injn. duration	Am20a05b40_Fc5d360	As -Fc5h but surf injection duration increased to 1 year		5	**360**	1000			4000	449	1,778,151,545	84%		1,800,000	8.8%
	Am20a05b40_Fc5d360_2	As Am20a05b40_Fc5d360 but with injector WF raised to z=17.	Improved with raised injector	5	**360**	1000			4000	478	1,573,769,892		75%	1,800,000	14.2%
	Am20a05b40_Fc5d1800	As -Fc5d360 but surf injection duration increased to 5 years		5	**1800**	1000			4000	670	1,449,650,764	69%		9,000,000	3.5%
	Am20a05b40_Fc5d1800_2	As Am20a05b40_Fc5d1800 but with injector WF raised to z=17.	Large improvement with raised injector	5	**1800**	1000			4000	423	906,244,331		43%	9,000,000	6.3%
	Am20a05b40_Fc5d4500	As -Fc5d360 but surf injection duration increased to 12.50 years (end of run)	FOAM variable in Floviz shows significant extent of foam at the end of the simulation period. This appears to present a deep enough barrier to the CO2 in Region 1, while continued penetration of injected CO2 suggests significant remaining permeability for CO2 in the plug. Note that the surfactant sinks nicely.	5	**4500**	1000			4000	719	899,388,811	43%		22,500,000	2.6%
	Am20a05b40_Fc5d4500_2	As Am20a05b40_Fc5d4500 but with injector WF raised to z=17.	Very large improvement with raised injector. This gives the lowest leakage of all cases tested, joint with _Fc5r5000_2_p3	5	**4500**	1000			4000	561	292,329,343		14%	22,500,000	3.8%

	Case	Description	Results	surf conc kg/sm3	surf inj duration days (1)	w+surf inj rate (1) rm3/d=sm3/d	surf inj duration days (2)	w+surf inj rate (2) rm3/d=sm3/d	CO2 inj rate sm3/d	CPU sec	CO2 flow into FIP2 (sm3) - *from last report in -PRT files*	leakage % of base case (z=18)	leakage % of base case (z=17)	Surfactant used (kg)	%reduction / 10^6 kg surfactant
Surf + water injn rate	Am20a05b40_Fc5r5000	As -Fc5h with water+surfactant injection rate increased from 1000 to 5000 rm3/d. 90 days injn at 0.5% conc.	Quite a good reduction for a short injection period. However the foam plug is small and dilutes quickly.	5	90	**5000**			4000	554	1,550,049,489	73%		2,250,000	11.8%
	Am20a05b40_Fc5r5000_2	As Am20a05b40_Fc5r5000 but with injector WF raised to z=17.	insignificant reduction	5	90	**5000**			4000	485	1,538,038,246		73%	2,250,000	12.1%
	Am20a05b40_Fc5r10000	As -Fc5r5000 with water+surfactant injection rate increased from 5000 to 10,000 rm3/d. 90 days injn at 0.5% conc.		5	90	**10000**			4000	597	1,278,175,392	61%		4,500,000	8.8%
	Am20a05b40_Fc5r10000_2	As Am20a05b40_Fc5r10000 but with injector WF raised to z=17.	insignificant reduction	5	90	**10000**			4000	579 (9min)	1,270,779,352		60%	4,500,000	8.9%
CO2 injn rate	Am20a05b40_Fc5i6000	As Am20a05b40_Fc5h with CO2 injection rate increased from 4000 rm3/d (1Mt/d?) to 6000 sm3/d. Horizontal injector at z=18.		5	90	1000			**6000**	773	4,165,065,766	197%		450,000	-216.0%
	Am20a05b40_Fc5i6000_2	As Am20a05b40_Fc5i6000 but with injector WF raised to z=17.	no effect	5	90	1000			**6000**	750	4,172,986,826		198%	450,000	-216.8%
	Am20a05b40_Fc5i8000	As Am20a05b40_Fc5i6000 but with CO2 injection rate increased to 8000 rm3/d	3x leakage rate for 2x injection rate!	5	90	1000			**8000**	1052	6,544,759,925	310%		450,000	-466.4%
	Am20a05b40_Fc5i8000_2	As Am20a05b40_Fc5i8000 but with injector WF raised to z=17.	No effect	5	90	1000			**8000**	1054	6,557,079,355		310%	450,000	-467.7%
Leakage minimisation	Am20a05b40_Fc5h_2 as above	5 kg/sm3 surf conc, 1000 rm3/d surf+water injection for 90 days	A very small foam plug is formed, which largely remains until the end of the simulation. However the CO2 manages to under-ride and perforate the plug relatively quickly.	5	90	1,000	90		4,000		1,928,714,422		91%	450,000	19%
	Am20a05b40_Fc5r5000_2 as above	Low conc is OK, inject more early on to establish a bigger plug. 5 kg/sm3 surf conc, 5000 rm3/d surf+water injection for 90 days	Stops significant break-through for 4 years until 2021, by which time the foam has degraded and spread out somewhat. Try a repeat injection in August 2020.	5	90	5,000	90		4,000		1,538,038,246		73%	2,250,000	12%
	Am20a05b40_Fc5r5000_2_p2	Now extend the duration - try a second batch later instead of continuous injection. As -Fc5r5000_2 above, with a second 90 day 5000 rm3/d injection period 3 years later, beginning in May 2020 (occurs in timestep 23)	The refill is achieved by report #23 (Aug 2023) and the plug remains largely intact for the remainder of the simulation. However although the CO2 flow is restrained it is not stopped and a significant leakage occurs by the end of the simulation. This is due to under-run as well as remaining permeability.	5	180	5,000	180	5,000	4,000	586	1,183,789,368		56%	4,500,000	9.8%
	Am20a05b40_Fc5r5000_2_p3	Try an initial 5000 rm3/d injection for 90 days (as -Fc5r5000_2) followed by continuous injection at 1000 sm3/d. More long-lasting but modest maintenance of the plug.	This gives a very powerful block to CO2 migration, limiting it to the region of the plug right to the end of the simulation. However the resulting foam plug is very long and might be reduced in size. Nearly the lowest leakage total obtained.	5	90	5000	4320	1000	4,000	463	295,096,314		14%	23,850,000	3.6%
	Am20a05b40_Fc5r5000_2_p4	As -Fc5r5000_2_p3 but with second stage surfactant injection reduced to 500 rm3/d. Try to economise on the maintenace of the plug.	Good blocking until 2025, when the well of CO2 upstream begins to under-run the plug and begins to by-pass it significantly. The critical aspect seems to be maintaining a deep enough plug, plus enough concentration within the plug to restrict gas transmissibility. Double so much leakage as in r500_2_p3	5	90	5000	4320	500	0	433	588,948,057		28%	13,050,000	5.5%

Chapter IV

Brine/water injection as flow diversion option in CO_2 storage operations

Robert Drysdale[1], Sevket Durucan[2], Anna Korre[2], Bernd Wiese[3], Daniel Loeve[4]
[1]SINTEF PR, Norway
[2] Imperial College, UK
[3] GFZ, Germany
[4]TNO, The Netherlands

SUMMARY

This chapter concentrates on the assessing water injection as a remediation measure for unwanted migration of CO_2 within an underground storage reservoir. Four different investigations of water injection remediation have been performed by different partners, mostly by numerical simulation: i) SINTEF have modelled migration in a portion of the Johansen formation model, three key reservoir to represent 20 sensitivities to the base case; ii) Using a generic model, Imperial College have studied reduction of CO_2 leakage through a sub-seismic fault by means of water injection; iii) GFZ have modelled and analysed a water injection experiment on the Ketzin CO_2 storage field to gain a better understanding of the drainage and imbibition processes, and iv) TNO have modelled 10 alternative scenarios of water injection and CO_2 back-production also using the Johansen model.

1 INTRODUCTION

Carbon capture and storage (CCS) technology involves capturing climate change inducing carbon dioxide emissions from industrial sources (e.g. cement, steel, ammonia production) and fossil fuel based power generation. The separated CO_2 stream is typically transported via a network of pipelines, injected in the subsurface and trapped within the pores of rocks located kilometres underground. The IPCC report on CCS, published in 2005, suggests that CCS could store up to 10 Gt of CO_2 per year when applied globally by 2050.

Many of the sites which are selected for CO_2 storage have held hydrocarbons for millions of years. This suggests that, because of the proven integrity of oil/gas storage, when CO_2 is injected into these formations it will also remain secure for geological timescales. Saline aquifers are also considered as potential CO_2 storage formations. These are not considered as proven storage sites and are likely to be less understood as relevant data may not have been collected. As a result, the possibility that CO_2 could migrate out of these formations needs to be studied carefully and potential leakage mitigation and remediation is an important element of a storage site licensing process according to the EU CCS Directive (2009).

The MiReCOL project provides analysis of a wide range of possible mitigation and remediation measures for leakage from underground CO_2 storage reservoirs. Both existing and new remediation and mitigation techniques are investigated, by means of numerical analysis, laboratory experiments and a field test.

One of the leakage categories considered in MiReCOL is the possibility of unwanted migration of CO_2 within the storage reservoir, i.e. within the storage formation, but escaping due to unforeseen circumstances such as:- a) a local high permeability channel or fractured region, b) an unseen feature in the structural geology, such as an unexpectedly high spill-point, c) an inclined CO_2-water interface due to lateral water flow through the reservoir.

Several remedial measures were identified for this type of migration including:- i) adjustment of the injection strategy, ii) gel or foam injection, iii) water injection and iv) injection of chemicals that react with CO_2 and precipitate it as a solid. This report concentrates on the assessing water injection as a remediation measure.

Four different examples of water injection remediation have been examined by different partners as follows.

- SINTEF have used a portion of the Johansen formation as the basic model with water injection in front of the CO_2 migration plume. The model was then modified to represent the key characteristics of 20 other possible CO_2 storage aquifers.
- Using a generic model, Imperial College have studied reduction of CO_2 leakage through a sub-seismic fault by means of water injection via the well previously used for CO_2 injection.
- GFZ have analysed and modelled a water injection experiment on the Ketzin CO_2 storage field to gain a better understanding of the drainage and imbibition processes.
- TNO also used the Johansen model to simulate 10 alternative scenarios of water injection and CO_2 back-production as remediation measures

The results of the MiReCOL project will be published both as handbook and as an interactive web-based tool, directed at storage project operators and competent authorities, to provide initial advice on the options available for remediation and mitigation.

2 MITIGATION BY WATER INJECTION IN JOHANSEN (SINTEF)

2.1 The model used

The reservoir selected for this study was a segment of the Johansen formation in the Norwegian North Sea, in the vicinity of the Troll field. This is part of a large aquifer which has been used several times as the subject for studies on CO_2 Geological Storage. The model was kindly made available to the project by Gassnova.

The Johansen formation is in the Jurassic Dunlin Group and consists of east to west dipping sandstone layers, from approximately 1600m to 2400m. The formation is bounded to the north and west by bounding faults and the sandstone layers pinch out to the eastern side, leaving the southern boundary potentially open. There are also several large vertical faults running north – south within the formation, which are considered to be sealing.

Only the extreme north-western corner of the formation is used for this study, with the open boundary conditions only to the south (see Figure 1). The overall dimensions of the model are 68km west-east, 250km north-south with thickness varying between approximately 100 to 500m. The formation is modelled by 7 layers of alternating sandstone and shale, the latter being sealing, but the shale layers pinches out towards the eastern and northern end of the reservoir. Grid blocks were used of approximate dimensions Δx=500m, Δy= 500m, Δz=12m in the sandstone layers.

The porosity and permeability distributions for the top of the formation are shown in Figure 2 and Figure 3. In the area used for leakage testing the average porosity is 0.24, permeability is 1125 mD and the depth varied from 2100 to 2200 m.

A dynamic model was developed in Eclipse 100, using oil and gas fluid representations for pure water and CO_2 respectively. This provides a simple method to represent the dissolution of the CO_2 in water.

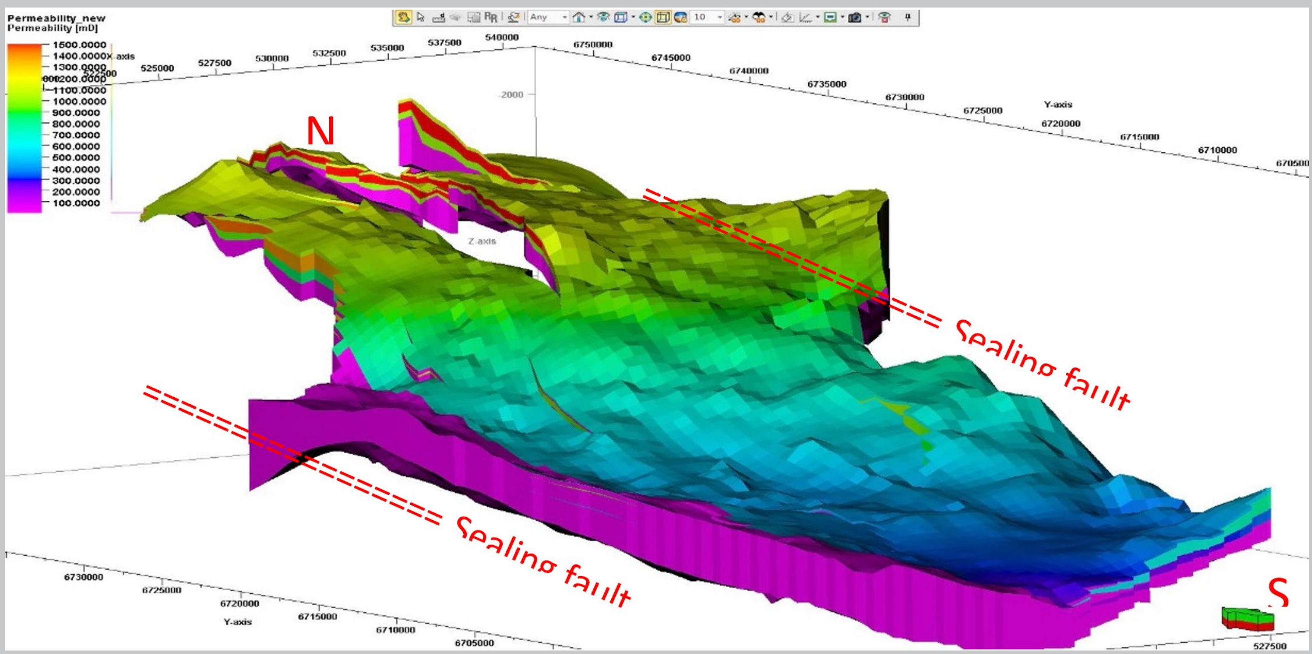

Figure 1 The part of the Johansen aquifer modelled.

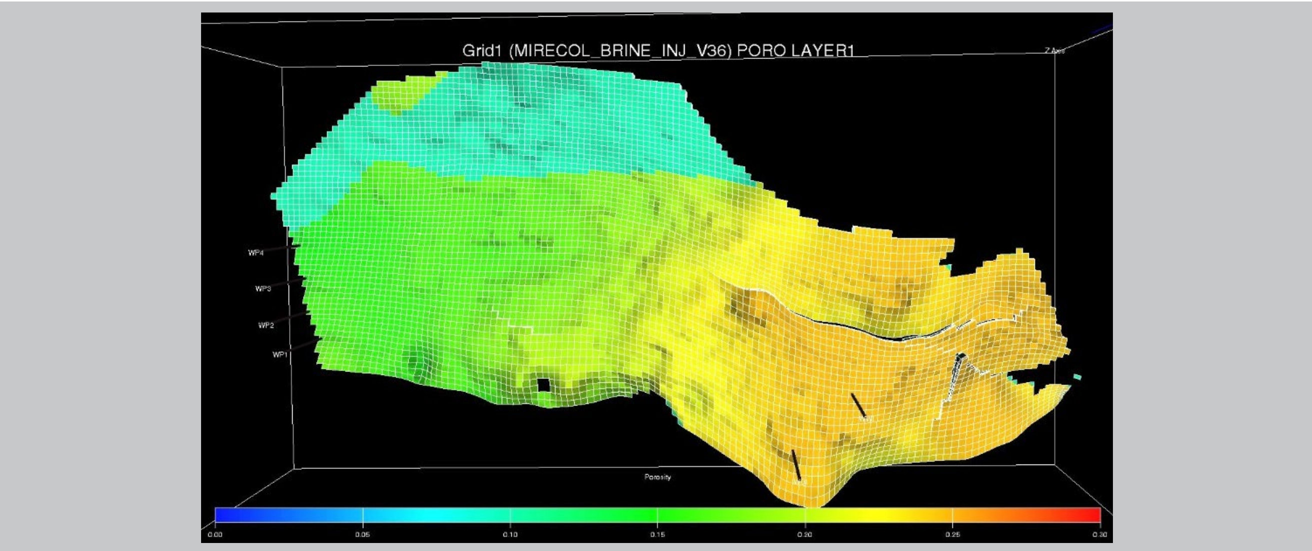

Figure 2 Porosity distribution in top layer of model.

The dynamic properties were largely drawn from those previously developed for the MatMoRA project Ref http://www.sintef.no/projectweb/matmora/downloads//johansen

The open boundary at the south of the model was represented by 4 water production wells, which were operated only during periods of injection, at a total equivalent rate to the injection rate (at reservoir conditions).

A bottom-hole pressure upper limit was imposed on all injectors, representative of the fracture safety limit. This was set at 75% of the lithostatic pressure, which was never reached.

All layers in the model were used initially for injection and production, but it was evident that all the injected CO_2 floated up to the top layer very quickly inside a small radius. Therefore the procedure was adjusted to inject into and produce from only the top layer to improve speed and ease of monitoring.

2.2 The leakage site

First the model was explored to find a good site to simulate leakage. Rather than looking for a possibly non-existent spill-point, effort was concentrated on finding a location offering good controlled migration. An imaginary CO_2 injection well would mimic the instigation of leakage and thereafter the leaking CO_2 would migrate by gravity along a shallow ridge structure trending upwards in a known direction. The mitigating effect of water injection could be studied by introducing an injection well at a suitable place along the leakage path.

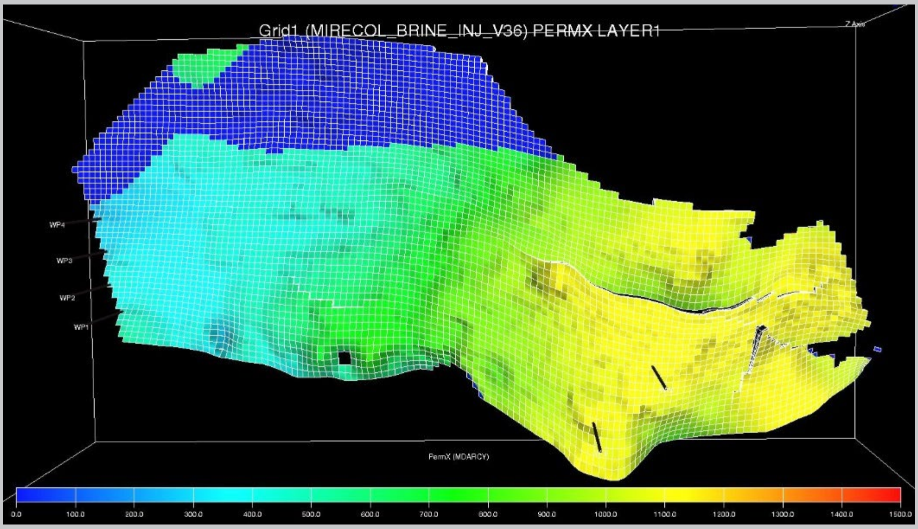

Figure 3 Permeability distribution in the top layer of the model.

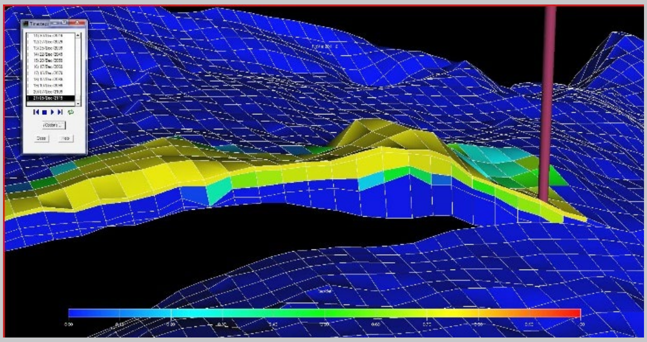

Figure 4 Location (a) looking eastward.

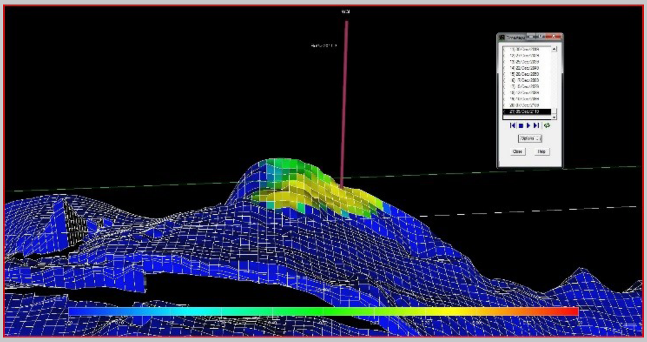

Figure 5 Location (b) looking eastward.

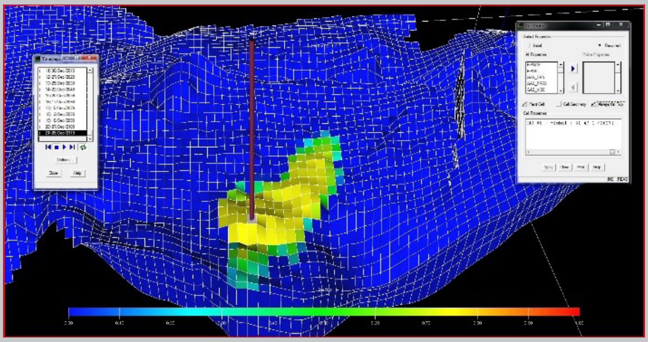

Figure 6 Location (c) looking westward.

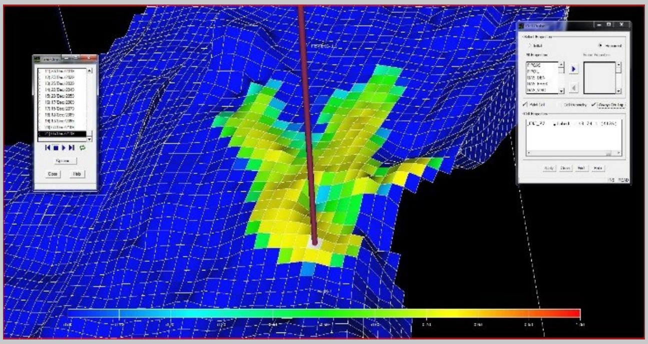

Figure 7 Location (d) looking northward.

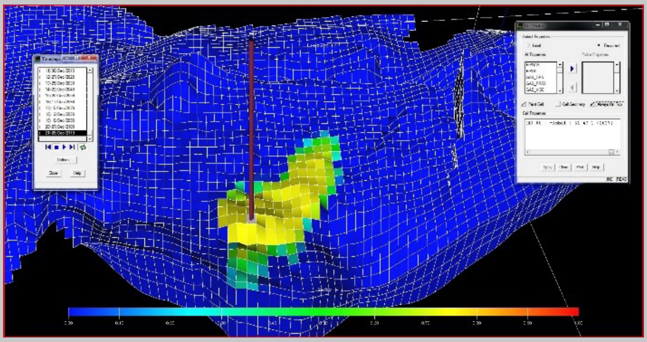

Figure 8 Location (e) looking northward.

CO_2 was injected into several different locations in the reservoir to look for the most suitable site, as illustrated in Figure 4 to Figure 8. Location (c) in Figure 6 was chosen as the best, offering a reasonably concentrated migration path, a good upward trend to encourage migration and a "collection area" limited by faults.

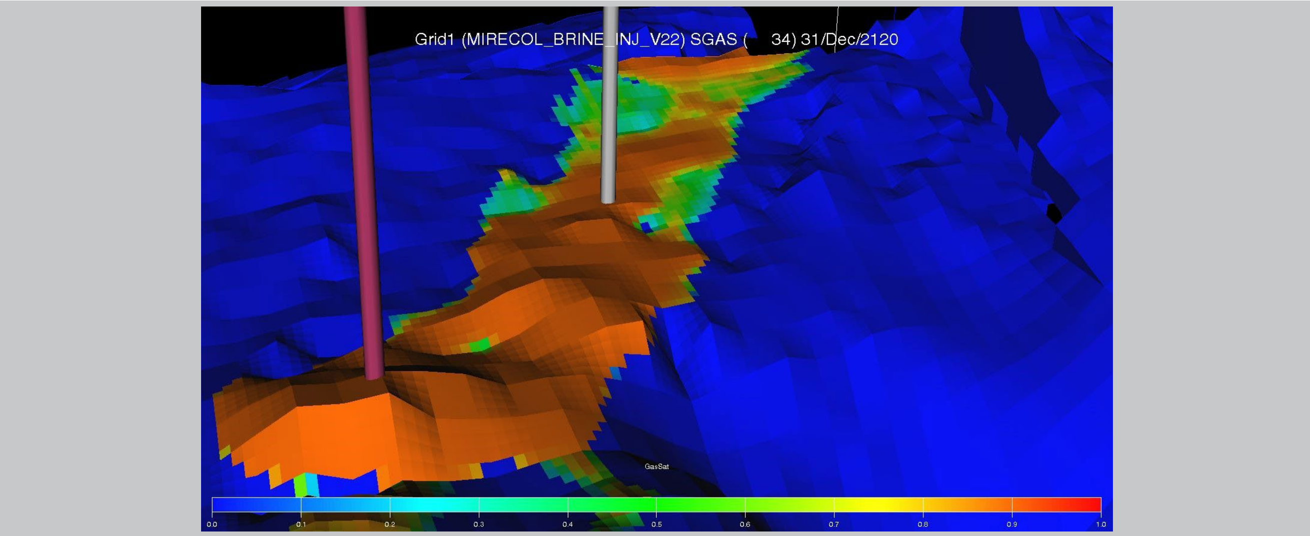

Figure 9 Leakage path along selected location.

In order to measure the leakage occurring, a "fluids in place numerical region" or FIPNUM was defined in the Eclipse model downstream of the water injection well, from a boundary perpendicular to the direction of migration and passing through the injection well. This is illustrated in Figure 10 . It was possible to obtain the total volume of CO_2 both free and dissolved, within this numerical region, thus quantifying the total leakage.

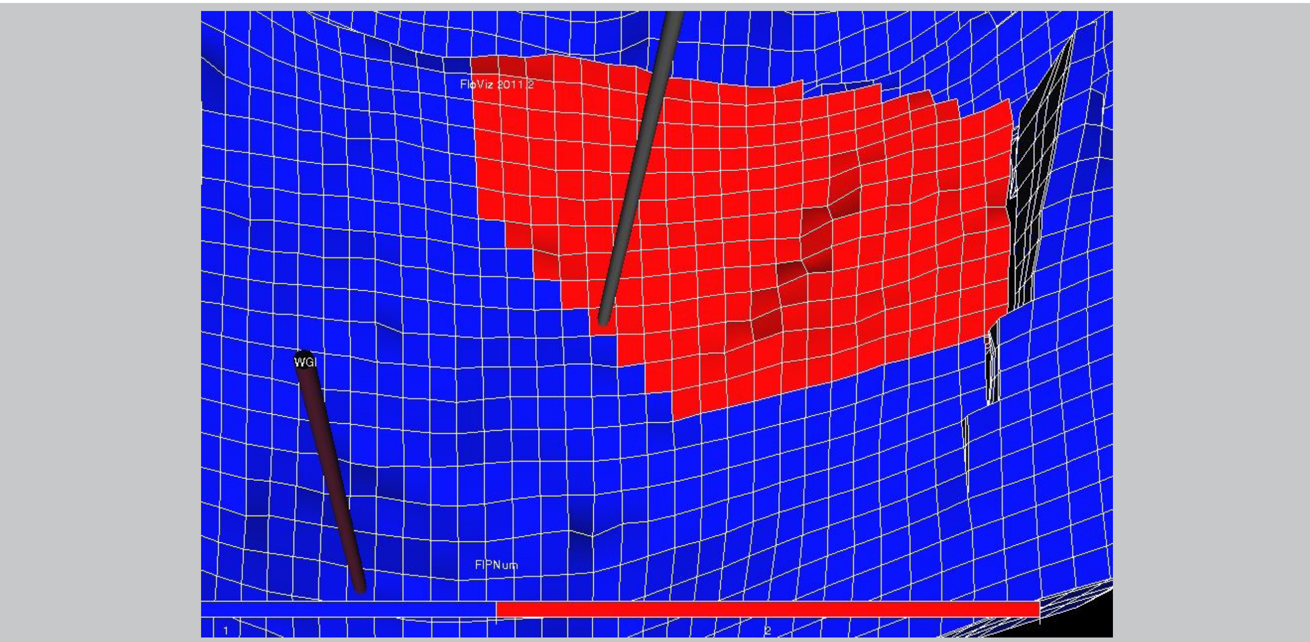

Figure 10 Location of FIPNUM (in red).

2.3 Requirements for data

The summary deliverable from the MiReCOL Project will be a web-tool to allow comparison of different remediation methods for a user's specific underground CO_2 leakage problem. The researchers working on each remediation method will generate data for this tool and will select the most relevant parameters against which they will generate performance data. For brine injection, SINTEF considered the following parameters to be the most important:

1. CO_2 injection rate. Actually the CO_2 leakage rate is the most interesting parameter, but this is difficult to estimate in the case of real leakage, so injection rate is taken as the next-best approximation.
2. Average permeability, which controls the migration of CO_2 and water. This is also considered to be related to porosity.
3. Reservoir depth (reflecting reservoir pressure, but more obtainable), which affects the fluid properties.

In order to generate a representative range for these parameters the NPD's "CO_2 Storage Atlas of the Norwegian Continental Shelf" was used as a source (Norwegian Petroleum Directorate, 2014). In this the main aquifers with potential for CO_2 storage on the NCS are identified, together with their basic data. These data were grouped to provide a smaller number of cases for the present work (Table 1).

Table 1 List of reservoir cases considered.

CO2Inj rate (t/yr)	K (mD)	Depth (m)	Case
5.0E+05	200	1800	v52
		2200	v49
	500	1700	v46
		2400	v43
	1000	1050	v40
		1650	v37
	1125	2200	v35
1.0E+06	200	1800	v53
		2200	v50
	500	1700	v47
		2400	v44
	1000	1050	v41
		1650	v38
	1125	2200	v34
3.0E+06	200	1800	v54
		2200	v51
	500	1700	v48
		2400	v45
	1000	1050	v42
		1650	v39
	1125	2200	v36

2.4 Results generated

2.4.1 Output required

The outputs required for the web-tool for each leakage case are listed below:

1. Likelihood of success – such a probability could not be estimated from the numerical simulations performed, but instead data was generated on the total reduction of leakage achieved by the water injection.
2. Economic cost of implementing the remediation process. Typically this would include the total cost of planning, designing, drilling and completing a water injection well, including the water injection system and a rig or vessel to support these operations. Since SINTEF has no access to such cost data, typical costs will have to be suggested by the partner Operating Companies within the project.
3. Response time – this is the time needed to implement a new water injection well once leakage has been detected. Lacking any practical data, this assumed to be one year in all cases.
4. Longevity – how long the injected water restrains or significantly reduces the migration of the CO_2 plume.
5. Spatial extent – this was taken to be the width of the cross-section of the CO_2 plume which is blocked by the injected water.

2.4.2 Standard injection and remediation procedure

It proved to be impossible to define a standard procedure for the leakage and remediation scenario which would satisfy all requirements, so the best compromise had to be used. The main alternatives identified were as follows:-

1. To inject CO_2 at a fixed location for a constant 50 years, then to start injecting water one year later, for one year at a second fixed location along the migration path. This has the major disadvantage that the CO_2 plume extends to varying degrees depending on the parameters used and therefore is in a different position relative to the fixed water injector for each case.
2. As (1), but the water injection well would be placed just ahead of the CO_2 plume at a fixed date. The disadvantages here were that the volume of the FIPNUM would vary, the topography around the water injector would vary and not least considerable effort would be required to redefine the FIPNUM for each case.

Table 2 Total CO_2 leakage, delay and extent values obtained from simulations.

Simulation	CO2 inj rate (te/yr)	K (mD)	Depth (m)	Water inj. Rate (sm3/d)	Total leakage (sm3)	Final leakage reduction (sm3)	Final Reductn (%)	Delay in leakage breakthrough (yrs)	Cross section extent (m)
v35e2	5.00E+05	1125	2200	0	8,871,106,610				
v35d2	5.00E+05	1125	2200	5000	8,850,286,082	-20,820,528	-0.23 %	1.8	700
v34d2	1.00E+06	1125	2200	0	12,265,447,757				
v34e2	1.00E+06	1125	2200	5000	12,219,293,672	-46,154,085	-0.38 %	1.4	1400
v36f2	3.00E+06	1125	2200	0	20,475,826,347				
v36g2	3.00E+06	1125	2200	5000	20,413,727,195	-62,099,152	-0.30 %	1.7	1400
v37e3	5.00E+05	1000	1650	0	7,559,248,729				
v37f3	5.00E+05	1000	1650	5000	7,531,059,577	-28,189,152	-0.37 %	1.6	1400
v38c2	1.00E+06	1000	1650	0	10,331,227,696				
v38d2	1.00E+06	1000	1650	5000	10,296,207,585	-35,020,111	-0.34 %	1.7	1400
v39c2	3.00E+06	1000	1650	0	18,353,103,572				
v39d2	3.00E+06	1000	1650	5000	18,289,216,449	-63,887,123	-0.35 %	1.6	1400
v40e2	5.00E+05	1000	1050	0	5,402,622,347				
v40f2	5.00E+05	1000	1050	5000	5,376,643,715	-25,978,632	-0.48 %	1.5	1400
v41c2	1.00E+06	1000	1050	0	7,555,634,286				
v41d2	1.00E+06	1000	1050	5000	7,522,112,842	-33,521,444	-0.44 %	1.6	1400
v42c2	3.00E+06	1000	1050	0	15,339,159,925				
v42d2	3.00E+06	1000	1050	5000	15,270,430,672	-68,729,253	-0.45 %	1.7	1400
v43c	5.00E+05	500	2400	0	11,562,423,630				
v43d	5.00E+05	500	2400	5000	11,482,916,024	-79,507,606	-0.69 %	2.7	1400
v44c2	1.00E+06	500	2400	0	16,226,764,770				
v44d2	1.00E+06	500	2400	5000	16,145,694,808	-81,069,962	-0.50 %	3.0	1400
v45c	3.00E+06	500	2400	0	30,685,062,619				
v45d	3.00E+06	500	2400	5000	30,565,233,760	-119,828,859	-0.39 %	3.5	1400
v46c2	5.00E+05	500	1700	0	9,892,909,045				
v46d2	5.00E+05	500	1700	5000	9,840,545,383	-52,363,662	-0.53 %	3	1400
v47c2	1.00E+06	500	1700	0	13,716,805,787				
v47d2	1.00E+06	500	1700	5000	13,646,235,482	-70,570,305	-0.51 %	2.3	1400
v48c2	3.00E+06	500	1700	0	28,461,666,370				
v48d2	3.00E+06	500	1700	5000	28,356,464,388	-105,201,982	-0.37 %	2.4	1400
v49c	5.00E+05	200	2200	0	7,463,343,829				
v49d	5.00E+05	200	2200	5000	7,336,503,515	-126,840,314	-1.70 %	6	1400
v50c	1.00E+06	200	2200	0	9,857,764,315				
v50d	1.00E+06	200	2200	5000	9,759,059,295	-98,705,020	-1.00 %	6	1400
v51c	3.00E+06	200	2200	0	11,366,574,297				
v51d	3.00E+06	200	2200	5000	11,388,303,241	**21,728,944**	**0.19 %**	5	1400
v52c2	5.00E+05	200	1800	0	8,556,323,198				
v52d2	5.00E+05	200	1800	5000	8,435,416,211	-120,906,987	-1.41 %	6	1400
v53c	1.00E+06	200	1800	0	10,912,528,220				
v53d	1.00E+06	200	1800	5000	10,781,550,516	-130,977,704	-1.20 %	7	1400
v54c	3.00E+06	200	1800	0	12,049,920,874				
v54d	3.00E+06	200	1800	5000	12,072,781,480	**22,860,606**	**0.19 %**	5	1400

3. As (1), but the duration of CO_2 injection would be varied to stop one year before the CO_2 plume reaches the water injection well. In this case the total amount of CO_2 injected would vary between cases, but since it was intended to use percentage total leakage reduction as the measure of effectiveness of remediation, this was considered to be best alternative.

Therefore the standard procedure used for generating all results was as follows:-
1. Inject CO_2 for up to 250 years without any water injection, in order to determine when the CO_2 plume reaches the location of the water injection well, i.e. at x years.
2. Repeat the no-water injection simulation with initial CO_2 injection for x-1 years, i.e. allowing 1 year implementation time before starting water injection.
3. Water injection for 1 year, which is then stopped permanently. A standard water injection rate of 5000 sm^3/d is used. A water injection period of only 1 year was adopted since it was clear that this remediation method has only a very short-term effect on migration of the CO_2.
4. The injected CO_2 is allowed to migrate further for the remainder of 510 years.

2.4.3 Results

For each of the 21 cases (Table 2) two main simulations were run for each case of reservoir properties, the first without any water injection, the second with water injection according to the standard procedure in Section 2.4.2.

The final volume of CO_2 in the FIPNUM was used as a measure of the leakage. The difference in these leakage values for the "no water injection" and the "water injection" sub-cases quantifies the effect of water injection in reducing CO_2 leakage. The resulting values obtained for all cases are given in Table 2, as absolute figures and as a percentage of the no water injection result.

In addition the estimated delay in leakage breakthrough obtained by water injection and the estimated lateral extent of the blockage to CO_2 flow are given for each case.

In order to assist analysis, the simulation results in Table 2 were summarised and re-ordered in three ways, according to each of the main parameters, as shown in Table 3, Table 4 and Table 5.

For each main parameter, the cases are ordered into a number of scenarios for comparison.

Table 3 Results arranged according to CO_2 injection rate.

CO2Inj rate (t/yr)	K (mD)	Depth (m)	Case	Final leakage reductn (%)	Delay in leakage break-through (yrs)	Scen-arios
5.0E+05	200	1800	v52	-1.41%	6.0	1
5.0E+05	200	2200	v49	-1.70%	6.0	2
5.0E+05	500	1700	v46	-0.53%	3.0	3
5.0E+05	500	2400	v43	-0.69%	2.7	4
5.0E+05	1000	1050	v40	-0.48%	1.5	5
5.0E+05	1000	1650	v37	-0.37%	1.6	6
5.0E+05	1125	2200	v35	-0.23%	1.8	7
1.0E+06	200	1800	v53	-1.20%	7.0	1
1.0E+06	200	2200	v50	-1.00%	6.0	2
1.0E+06	500	1700	v47	-0.51%	2.3	3
1.0E+06	500	2400	v44	-0.50%	3.0	4
1.0E+06	1000	1050	v41	-0.44%	1.6	5
1.0E+06	1000	1650	v38	-0.34%	1.7	6
1.0E+06	1125	2200	v34	-0.38%	1.4	7
3.0E+06	200	1800	v54	0.19%	5.0	1
3.0E+06	200	2200	v51	0.19%	5.0	2
3.0E+06	500	1700	v48	-0.37%	2.4	3
3.0E+06	500	2400	v45	-0.39%	3.5	4
3.0E+06	1000	1050	v42	-0.45%	1.7	5
3.0E+06	1000	1650	v39	-0.35%	1.6	6
3.0E+06	1125	2200	v36	-0.30%	1.7	7

Table 4 Results arranged according to permeability.

CO2Inj rate (t/yr)	K (mD)	Depth (m)	Case	Final leakage reductn (%)	Delay in leakage break-through (yrs)	Scen-arios
5.0E+05	200	1800	v52	-1.41%	6.0	1
5.0E+05	200	2200	v49	-1.70%	6.0	2
1.0E+06	200	1800	v53	-1.20%	7.0	3
1.0E+06	200	2200	v50	-1.00%	6.0	4
3.0E+06	200	1800	v54	0.19%	5.0	5
3.0E+06	200	2200	v51	0.19%	5.0	6
5.0E+05	500	1700	v46	-0.53%	3.0	1
5.0E+05	500	2400	v43	-0.69%	2.7	2
1.0E+06	500	1700	v47	-0.51%	2.3	3
1.0E+06	500	2400	v44	-0.50%	3.0	4
3.0E+06	500	1700	v48	-0.37%	2.4	5
3.0E+06	500	2400	v45	-0.39%	3.5	6
5.0E+05	1000	1050	v40	-0.48%	1.5	
5.0E+05	1000	1650	v37	-0.37%	1.6	1
1.0E+06	1000	1050	v41	-0.44%	1.6	
1.0E+06	1000	1650	v38	-0.34%	1.7	3
3.0E+06	1000	1050	v42	-0.45%	1.7	
3.0E+06	1000	1650	v39	-0.35%	1.6	5
5.0E+05	1125	2200	v35	-0.23%	1.8	2
1.0E+06	1125	2200	v34	-0.38%	1.4	4
3.0E+06	1125	2200	v36	-0.30%	1.7	6

Table 5 Results arranged according to reservoir depth.

CO2Inj rate (t/yr)	K (mD)	Depth (m)	Case	Final leakage reductn (%)	Delay in leakage break-through (yrs)	Scen-arios
5.0E+05	1000	1050	v40	-0.48%	1.5	1
1.0E+06	1000	1050	v41	-0.44%	1.6	2
3.0E+06	1000	1050	v42	-0.45%	1.7	3
5.0E+05	200	1800	v52	-1.41%	6.0	4
5.0E+05	500	1700	v46	-0.53%	3.0	5
5.0E+05	1000	1650	v37	-0.37%	1.6	1
1.0E+06	200	1800	v53	-1.20%	7.0	6
1.0E+06	500	1700	v47	-0.51%	2.3	7
1.0E+06	1000	1650	v38	-0.34%	1.7	2
3.0E+06	200	1800	v54	0.19%	5.0	8
3.0E+06	500	1700	v48	-0.37%	2.4	9
3.0E+06	1000	1650	v39	-0.35%	1.6	3
5.0E+05	200	2200	v49	-1.70%	6.0	4
5.0E+05	1125	2200	v35	-0.23%	1.8	1
1.0E+06	200	2200	v50	-1.00%	6.0	6
1.0E+06	1125	2200	v34	-0.38%	1.4	2
3.0E+06	200	2200	v51	0.19%	5.0	8
3.0E+06	1125	2200	v36	-0.30%	1.7	3
5.0E+05	500	2400	v43	-0.69%	2.7	5
1.0E+06	500	2400	v44	-0.50%	3.0	7
3.0E+06	500	2400	v45	-0.39%	3.5	9

2.5 Discussion

2.5.1 Migration pattern

As an initial insight it is interesting to consider the variation in the overall migration pattern in terms of the reservoir parameters studied. The final CO_2 distributions for several cases are shown in Figure 11. It can be seen that:-

- At higher permeabilities (1125mD & 1000 mD) the injection rate has only a slight effect on the final saturation distribution after 510 years. At 3.0E6 t/y the narrowest part of the migration path is approximately twice as wide and there is a slight development of the secondary route to the west. Both of these features suggest that the capacity of the ridge structure is being exceeded at the highest injection rate.
- At 500mD permeability a wider migration path plus a secondary path are evident from 1.0E6 t/ r injection upwards. At 3.0E6 t/y injection the width of the migration path is nearly double that for 1125mD permeability.
- At 200mD the broadening of the migration path is even more pronounced for all CO_2 injection rates, with much more development of the secondary migration path.
- Variations in the reservoir depth were not found to give large changes in the migration pattern. Shallower reservoirs showed slightly more free gas, but this was less evident with higher permeability.

These observations are largely explained by the changing balance between the viscous and gravitational forces on the fluids. At high permeabilities it is easy for the CO_2 to flow therefore the viscous forces are less and the relative effect of gravity (buoyancy) is more.

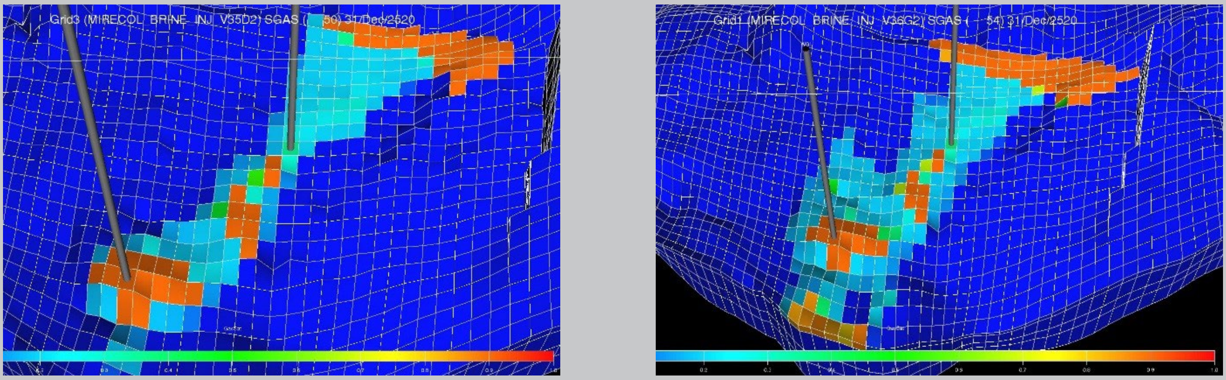

Final CO_2 saturations, 1125mD, 2200m deep, 0.5E6 t/y (left) & 3.0E6 t/y (right)

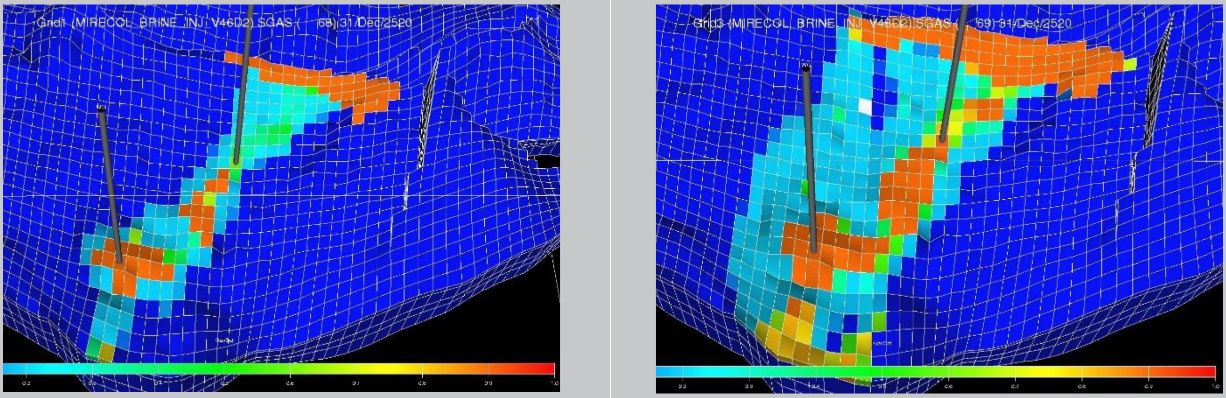

Final CO_2 saturations, 500mD, 1700m deep, 0.5E6 t/y (left) & 3.0E6 t/y (right)

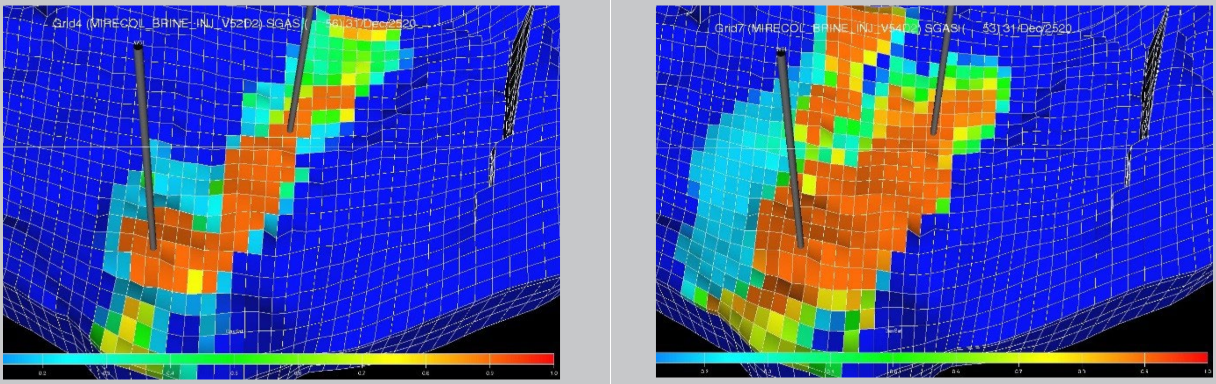

Final CO_2 saturations, 200mD, 1800m deep, 0.5E6 t/y (left) & 3.0E6 t/y (right)

Figure 11 Examples of migration pattern at the end of the simulations (510 years).

Hence the effect of the topography is more pronounced and CO_2 tends to follow the top of the ridge structure. At low permeabilities and at higher injection rates it is much more difficult for the CO_2 to press forward, i.e. the viscous forces dominate and the CO_2 now spreads out over a greater area in a diffuse flow pattern.

Note that the wider migration paths visible at the end of the simulation are developed long after the year of water injection and so do not refute the conclusions in Section 2.5.4 about the physical extent of remediation.

2.5.2 Total leakage reduction

The results for leakage reduction as a percentage of the cases without water injection are given graphically in Figure 12, Figure 13 & Figure 14.

Firstly it should be re-iterated that the leakage reduction values obtained were very small (less than 0.2%), due to the fact that water injection was applied for only 1 year out of a total of 510 years of the simulation. However this is sufficient to see the relative effects in the different scenarios.

Figure 12 shows the effect of varying the CO_2 injection rate. Most of the scenarios show slightly less reduction in leakage with increasing injection rate, which might simply reflect the greater volume of CO_2 injected into the reservoir and the very brief effect of water injection. However the 200 mD scenarios exhibit a very strong decrease in the leakage reduction with increased CO_2 injection rate. This is attributed to the much broader migration occurring with low permeability, allowing much of the CO_2 to avoid the blockage caused by water injection.

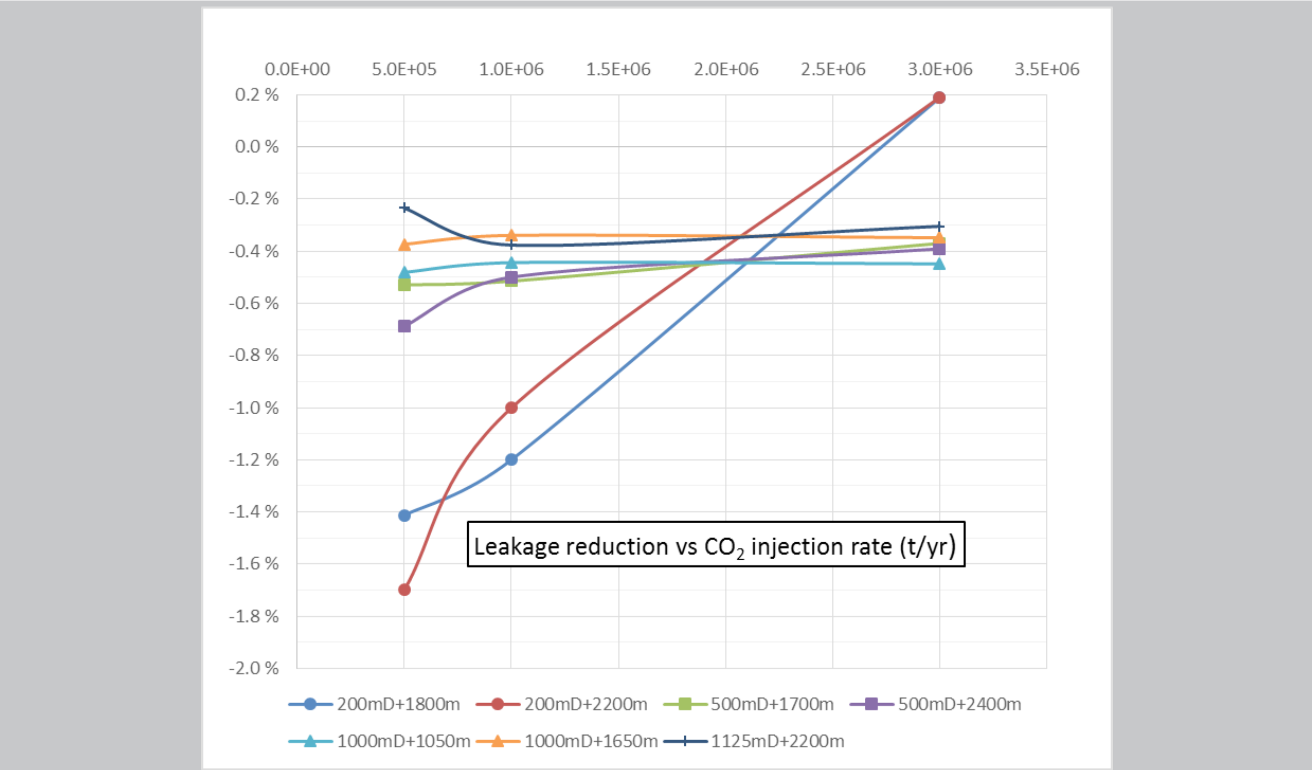

Figure 12 Leakage reduction vs CO_2 injection rate.

Figure 13 shows the effect of permeability on leakage reduction. For most scenarios increased permeability gives significantly less reduction in leakage, especially at the lower values of permeability. This might be explained by greater flowing capacity reducing the net effect of a short blockage by water injection.

The two scenarios with high CO_2 injection rates at very low permeability differ again from the rest, giving slightly increased leakage under water injection, as explained above for Figure 12.

Figure 14 shows the effect of reservoir depth on leakage reduction. In general no consistent trend can be seen, suggesting that this is not a significant parameter in the effectiveness of water injection as a migration mitigation measure.

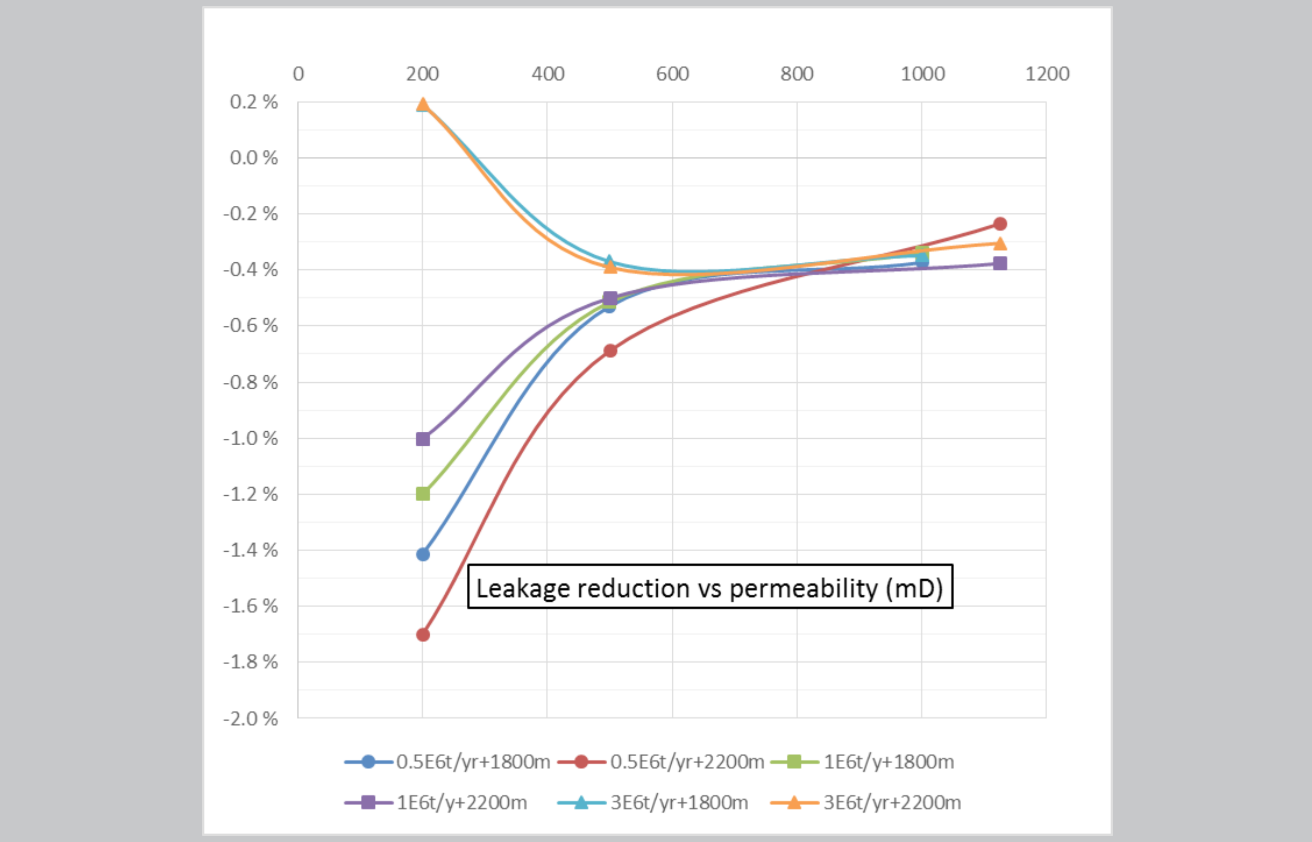

Figure 13 Leakage reduction versus permeability.

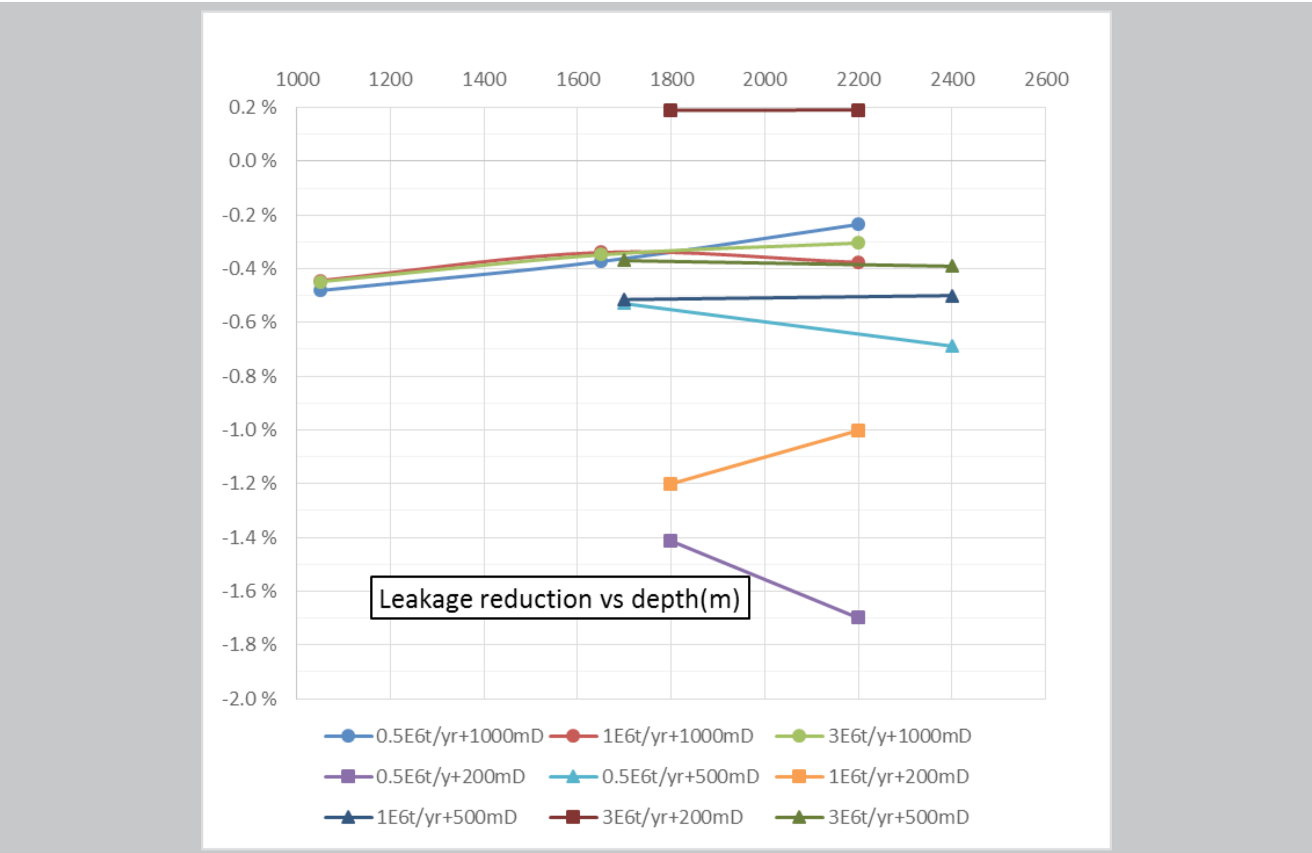

Figure 14 Leakage reduction vs reservoir depth.

2.5.3 Longevity of remediation

This characteristic was estimated by the delay to CO_2 leakage caused by water injection and it this was measured from the commencement of water injection. The average value for delay obtained from all the cases listed was 3.2 years.

Two means of measurement were tried: i) by comparing graphically the reported figures of the volume of gas in the FIPNUM for the water injection and no water injection cases, and ii) monitoring the onset of gas saturation in the grid block (43,38,1) containing the water injection well (on the boundary of the FIPNUM, in the centre of the main migration path) for both water injection and no water injection cases.

The first method is the most logical, being based on the definition of leakage in this study, and was tried first. Unfortunately it proved to be very difficult to extract a consistent delay period from the graphs of FIPNUM volume, due to the differing curvature of the two lines (see Figure 15 for an example).

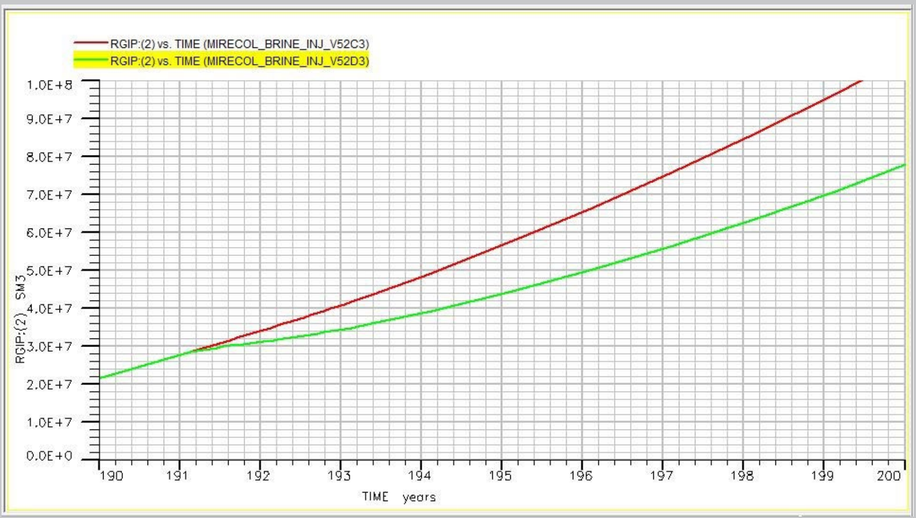

Figure 15 Gas leakage volume for 0.5E6 t/yr CO_2 injection, 200 mD permeability and 1800m reservoir depth, without and with water injection.

The second method offered a much more precise, albeit somewhat arbitrary measure, but gave easily measureable period for the delay in leakage, as shown in Figure 16. In a few cases a small preliminary leakage was observed, due to the start of water injection being slightly late, but this was judged to be insignificant.

It was noted that sometimes grid block (43,38,1) was found to be not the point of first leakage into the FIPNUM. The adjacent grid block to the southwest occasionally showed leakage before the reference grid block, but this was not important since a fixed common location was the main requirement. This is a reason for slightly different gas break-through dates being obtained sometimes from the two methods.

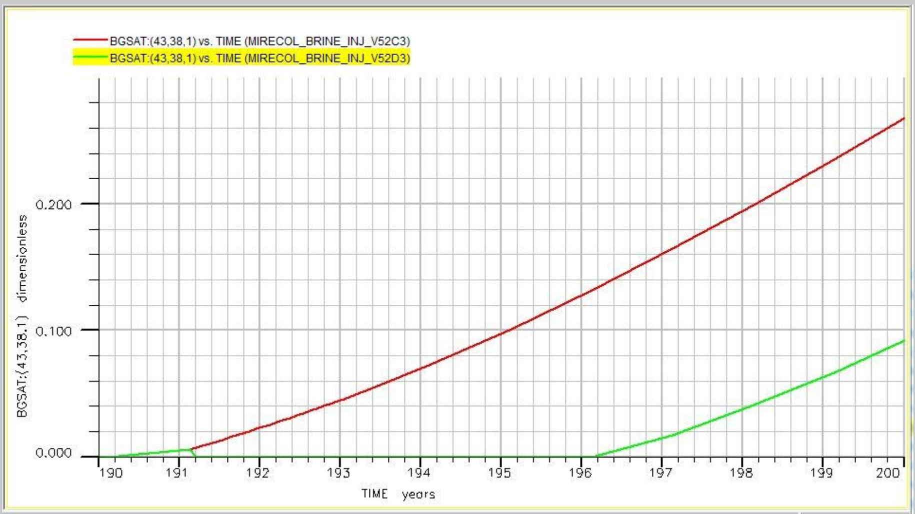

Figure 16 Onset of non-zero gas saturation in grid block (43, 38,1), for 0.5E5 t/yr CO_2 injection, 200 mD permeability and 1800 m reservoir depth, with and without water injection.

Figure 17 shows the effect of the different CO_2 injection rates on the delay in leakage, i.e. the longevity of the water injection remediation. It can be seen that in general the injection rate itself has relatively little effect on the delay. However significant differences can be seen between the scenarios, especially for the 200mD cases, which also exhibit a clear effect from varying CO_2 injection rate. These data show some similarity to Figure 12.

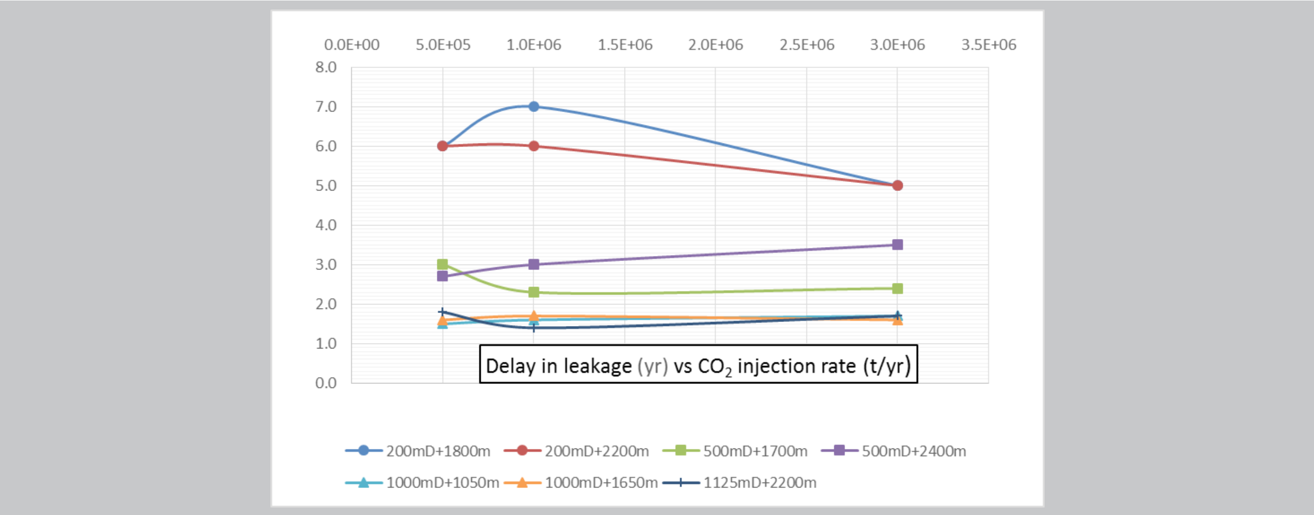

Figure 17 Delay in leakage vs CO_2 injection rate.

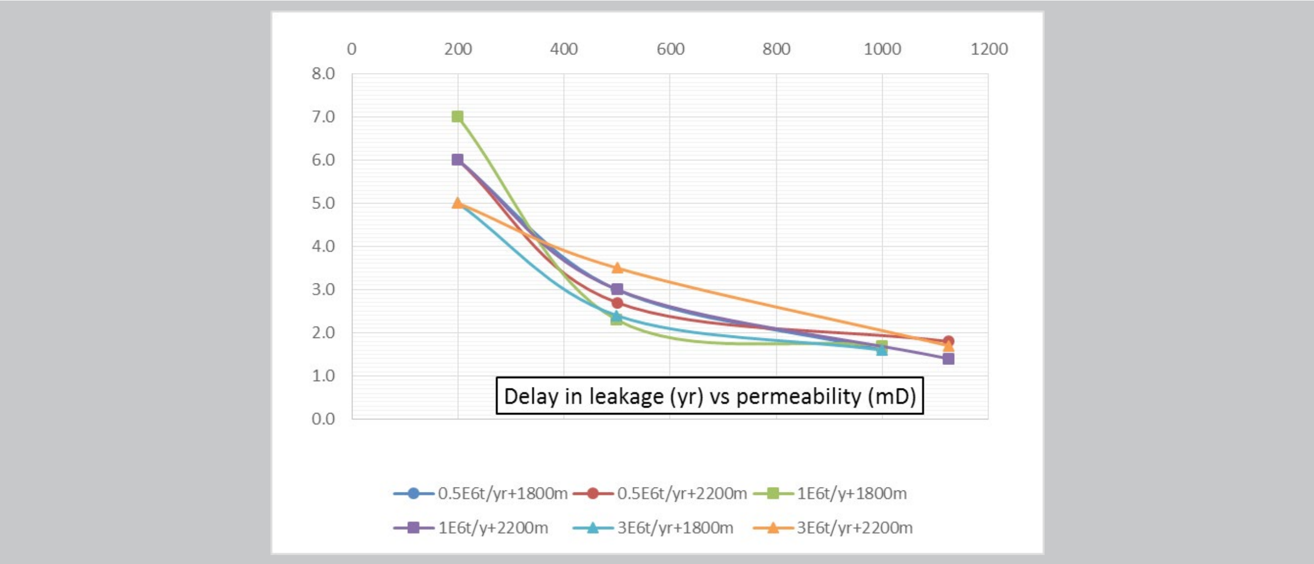

Figure 18 Delay in leakage vs permeability.

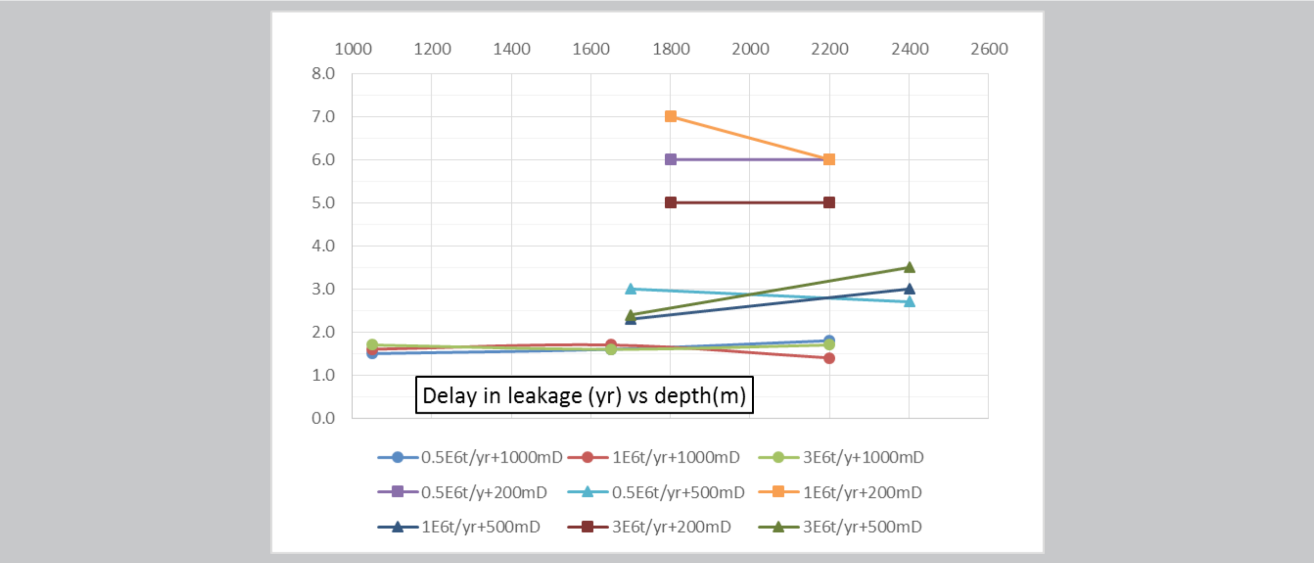

Figure 19 Delay in leakage vs reservoir depth.

Figure 18 shows a clear reduction in leakage delay at higher permeability for all scenarios. This suggests that the higher local pressure and water concentration caused by water injection are more rapidly dissipated with higher permeability, hence shortening the migration effect. Note from Figure 16 that water injection appears to stop CO_2 migration very effectively for the delay period, at least near the injection well and within the simulation accuracy of the grid used.

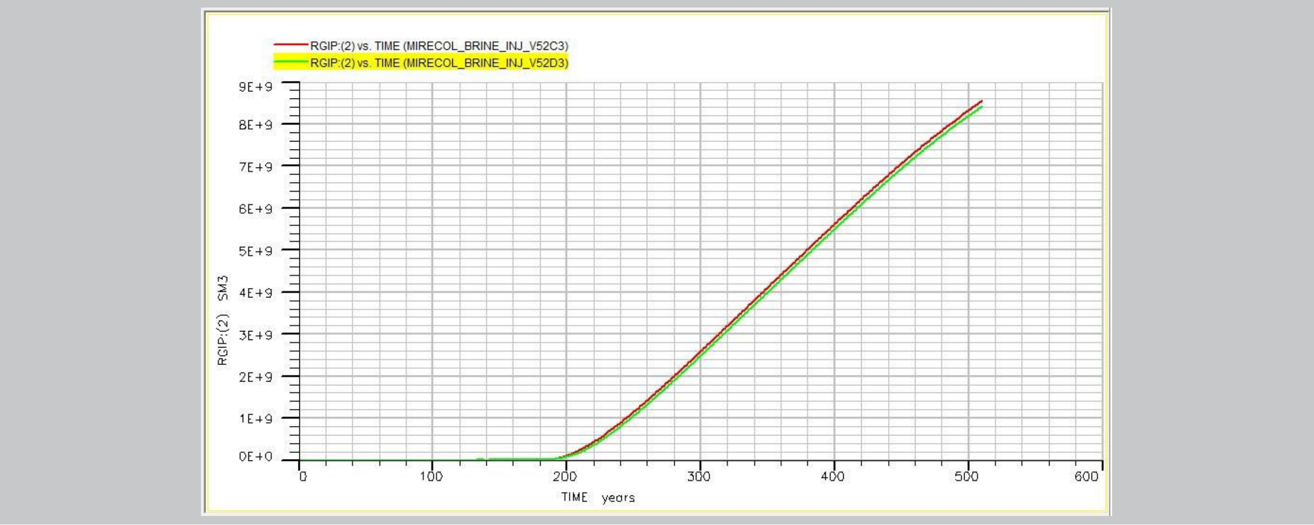

Figure 20 Complete leakage volume profiles over the entire simulation period for the 0.5E5 t/yr CO_2 injection, 200 mD permeability and 1800 m reservoir depth case, with and without water injection.

Figure 19 shows very little overall effect of the reservoir depth on the delay in leakage derived from simulations.

In Figure 16 above the period of total blockage was 6 years, one of the longest measured. Looking at the total leakage curves for the same case with and without water injection in Figure 20 shows that there is no further effect on the leakage. This demonstrates that the mitigation effect of water injection is short-term if the water injection is not continued.

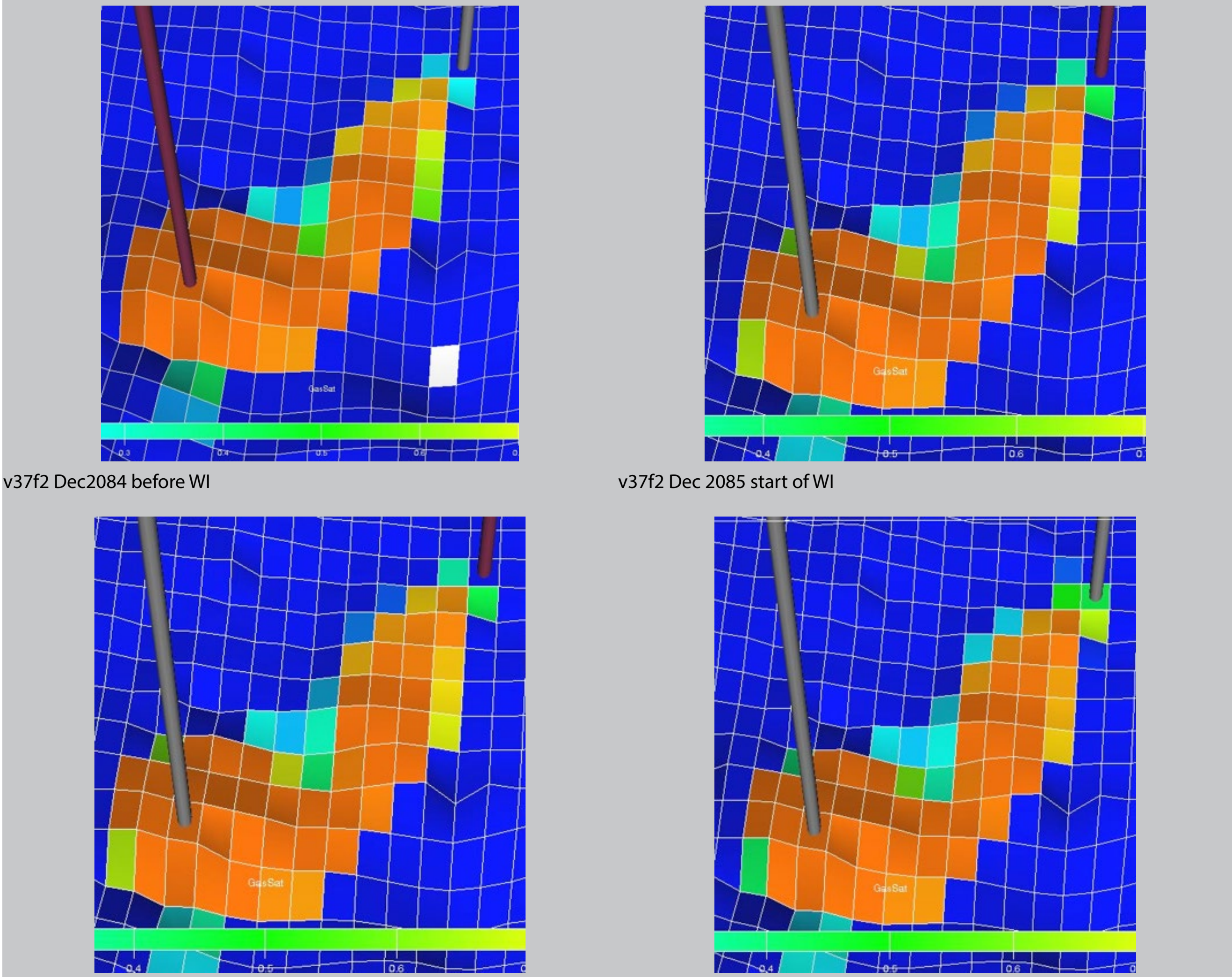

v37f2 Dec2084 before WI

v37f2 Dec 2085 start of WI

v37f3 Dec 2086 end WI

v37f3 Dec2089 after WI

Figure 21 Examples of estimating mitigation extent by monitoring CO_2 saturation (the leakage boundary is shown as a red line).

2.5.4 Spatial extent of remediation

Estimating the spatial extent of remediation proved to be a difficult objective. Initially the gridblock pressures along the entry boundary of the leakage numerical area were investigated, but lacking a clear criterion for the pressure increase required to block the migration of CO_2, this approach was of no use.

Instead the gas saturations were monitored in the cells surrounding the water injector (block 43, 38, 1) during and immediately following water injection. This was performed graphically using the FloViz utility. From the detected flow of gas it was possible to determine how many grid-blocks at the boundary experienced the break-though of CO_2, as illustrated in Figure 21. In this example it can be seen that the CO_2 reaches the leakage area diagonal boundary at two grid-blocks in year 73, is halted for two years (the CO_2 concentration builds up) and in year 75 it begins to migrate upwards from both grid-blocks. It was clear from spot-checks of saturation that the CO_2 did not enter the leakage region via any other grid-blocks.

Each grid-block measures 500 m in the x & y directions, so since the leakage boundary is diagonal across the grid-blocks at this location, the linear width of the CO_2 migration after water injection was 1410, say 1400m. This quantifies the spatial extent of remediation.

This method was applied to all cases and the results are shown in the last column of Table 2. From this table it can be seen that in all cases considered the observed spatial extent was the same, 1400m, except for the first case with 0.5 E6 t/yr CO_2 injection, 1125 mD permeability and 2200m depth, which showed a spatial extent of 700m. Thus the results from the model used show minimal variation between the cases considered.
The main reasons for so little difference in the spatial extent of mitigation are believed to be:-

1. The CO_2 migration appears to be controlled primarily by the topography of the top layer of the model. The gas moves along the top of a ridge which is relatively narrow at the location of the water injection well.
2. There appears to be a relatively weak pressure gradient acting on the CO_2, which is then largely controlled by buoyancy.
3. Thus when the injected water blocks the migration of CO_2, there is little accumulated force to move the CO_2 further sideways than the two grid-blocks observed.
4. The use of smaller grid-blocks might have helped to differentiate between the cases, but because a local grid refinement could not be set-up in the same location as a FIPNUM, this could not be implemented so late in the study.

2.5.5 Effect of reservoir depth on free gas

The main reason that reservoir depth was considered as a varied parameter in these simulations was that the lower ambient pressure in shallower reservoirs will give rise to more free CO_2 at lower density, which might affect the relative flow conditions for gaseous CO_2 versus water. The final amounts of both free CO_2 and dissolved CO_2 within the leakage reference area (FIPNUM) are given in the reports for each simulation and the fraction of free CO_2 in the total leakage volumes are summarised against reservoir depth for each case in Figure 22.

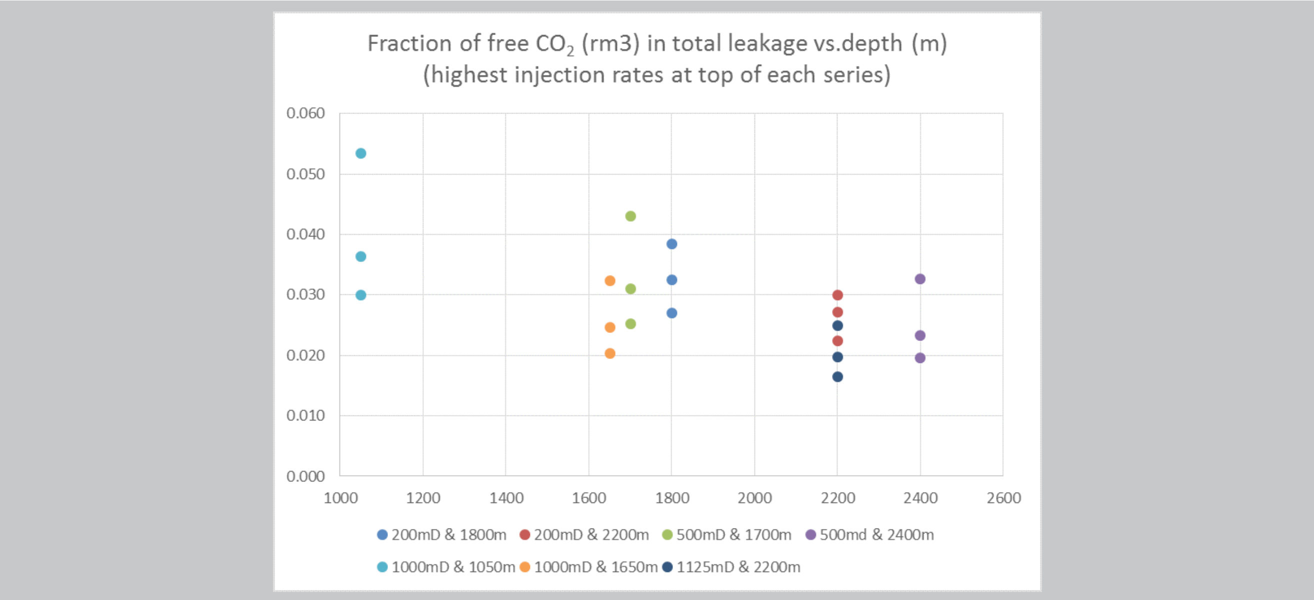

Figure 22 Fraction of free CO_2 in total leakage volume vs reservoir depth, for 0.5 E6, 1.0 E6 & 3.0 E6 t/yr injection rates.

Figure 22 confirms that at reduced reservoir depth, more free CO_2 occurs in the final leakage volume, presumably due to the lower ambient pressures releasing more free CO_2 and the resulting increased relative permeability of the gas. Higher injection rates also result in more free gas in the reservoir, offset somewhat by the higher pressure caused. The net result for higher injection rates also appears to be higher free CO_2 fractions in the final leakage volume.

2.6 Conclusions

- Simulations were performed of CO_2 migration along a ridge structure in the Johansen aquifer, in order to extract data on the effectiveness of water injection as a mitigation measure. Twenty-one combinations of CO_2 injection rate, permeability and reservoir depth, representing possible Norwegian CO_2 storage sites were simulated.
- The effect of one year of water injection, just ahead of the CO_2 plume, was studied. Data on the percentage reduction in leakage after 510 years migration were collected.
- In general it was seen that in high permeability reservoirs the CO_2 is able to migrate rapidly along a narrow path, since the viscous forces are low and buoyancy keeps the gas in the ridge structure. However at low permeabilities, especially with high CO_2 injection rates, high viscous forces cause the flow to become much more diffuse, thereby by-passing the water injector and potentially reducing its mitigating effect.
- In most cases CO_2 injection rate has little effect on the leakage reduction achieved by one year of water injection. However in very low permeability reservoirs the leakage reduction is reduced greatly by high CO_2 injection rates, due to the very broad migration path largely avoiding area affected by water injection.
- For most reservoirs very low permeability results in large reductions in leakage, although at high CO_2 injection rates and low permeability the reductions are very small. These two extremes represent the difference between gravity and viscous forces controlling the flow pattern.
- No consistent trend in leakage reduction was observed due to variations in reservoir depth.
- The delay in CO_2 migration (i.e. the longevity of mitigation) resulting from water injection was generally found to be unaffected by variations in CO_2 injection rate or reservoir depth. However decreasing permeability has a strong increasing effect on the duration of mitigation, especially at lower permeabilities.
- The spatial effect of mitigation by water injection showed almost no variation between twenty of the cases studied. This is believed to be due to the topography of the location in the model used, namely that the ridge is relatively narrow. This, combined with the weak forces moving the CO_2, was enough to block the tip of the CO_2 plume in all cases.
- Shallower reservoir depth was found to create more CO_2 as free gas at lower density, due to the corresponding lower pressures. This effect and also higher CO_2 injection rates resulted in more free CO_2 in the leakage area.
- It is clear that water injection does not provide a long-lasting blockage to CO_2 migration, with its effect lasting only from 1.4 to 7 years from the beginning of water injection. Since migration of injected CO_2 will continue over many hundred years, water injection cannot be considered a long-term remediation measure. This suggests that it might well be better to drill a CO_2 producer instead of a water injector and concentrate on removing the CO_2 plume, possibly with a water injector or other remediation as a temporary measure.

3 BRINE INJECTION AS A FLOW DIVERSION OPTION (IMPERIAL COLLEGE)

In secondary oil recovery, brine or water injection has a long history either to support reservoir pressure or to displace oil towards producing wells. There is a range of techniques and theories (e.g. Buckley Leverett analysis) about how water injection can be used to increase oil recovery. Volumetric sweep management and realignment of production in contiguous layers are the nearest analogues in the oil industry to the use water injection in order to stop the migration of CO_2 (Omorgie et al., 1995). Industry has studied several mechanisms by which water injection can be used to reduce CO_2 migration like creating a high pressure barrier in front of the migrating CO_2 plume (Kuuskraa and Gedec, 2007) or by chasing CO_2 with brine ensuring storage security (Qi et al., 2008) and injecting water directly into the advancing CO_2 plume (Esposito and Benson, 2010; Anchliya et al., 2012).

This section presents the results of the numerical modelling carried out by Imperial College, which investigated the application of brine injection for flow diversion of CO_2 plume within the storage reservoir. In the scenarios set up, it was assumed that a sub-seismic fault is present in the formation as a pre-defined undesired migration pathway. Three separate scenarios were considered by varying the fault location along the anticlinal structure if the model at distances of 1km, 2km and 3km from the CO_2 injection well, and the effectiveness of brine injection as a remediation technique assessed.

3.1 Reservoir model description

3.1.1 Structural and geological model

A numerical reservoir model was set up to study the flow diversion of CO_2 plume using brine water injection within a heterogeneous saline aquifer. The structural model used in this study represents a saline aquifer with a broad and considerably dipping anticlinal structure (Figure 23), where the containment of CO_2 is envisaged. The model grid spans an area of 36km×10km and includes five major sealing faults. The grid broadly comprises of three layers, namely: (1) a reservoir layer with an average thickness of 240m and resolution of 200m×200m×4m; (2) a caprock (seal) layer with an average thickness of 225m and resolution of 200m×200m×225m; and (3) a shallow aquifer layer with an average thickness of 175m and resolution of 200m×200m×175m. The depth of the model ranges between 1,087m and 3,471m.

The geological features of the reservoir layer represent a fluvial-channel system, typically containing braided sandstone channels and interbedded floodplain deposits (the inter-channel region) of mudstone or siltstone. These generally represent the fluviodeltaic progradation and floodplain deposition formations found in the Triassic of the Barents Sea. The channel layout parameters implemented in the model to represent the fluvial-channel system are given in Table 6. The range of the petrophysical properties

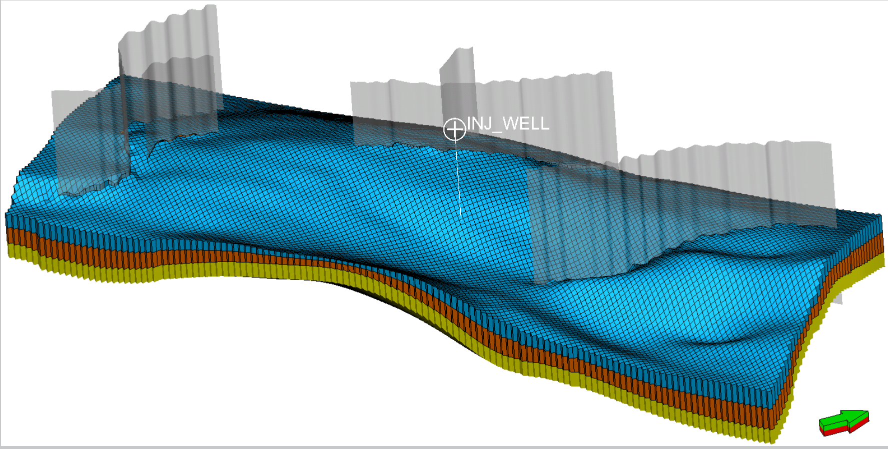

Figure 23 The structural model of the numerical saline aquifer (36km×10km) containing five major faults and three stratigraphic layers: reservoir layer, caprock (seal) layer and shallow aquifer layer.

used in the static geological model attribution (Table 7) are based on the Late Triassic Fruholmen Formation in the Hammerfest Basin (NPD, 2013), which is located at depths similar to those considered in this model. The petrophysical attributions of the geological model were generated using Sequential Gaussian Simulation (SGS) in order to represent the variability in the distribution of these values. Example realisations of the porosity and horizontal permeability distributions for the top reservoir layer are illustrated in Figure 2.

Table 6 Channel layout parameters used in the reservoir layer of the geological model.

	Min	Mean	Max
Amplitude [m]	400	500	600
Wavelength [m]	14,000	15,000	16,000
Width [m]	1,400	1,500	1,600
Thickness [m]	4	8	12

Table 7 Petrophysical properties used in the geological model.

Petrophysical properties		Channels	Inter-channel region	Caprock	Shallow aquifer
Porosity	Min, Mean, Max	0.1, 0.18,0.25	0, 0.1, 0.25	0.01	0.05,0.15,0.25
	Standard deviation	0.05	0.05	0	0.05
Horizontal Permeability [mD] *	Min, Mean, Max	125, 3,000, 7,000	0.1, 10, 100	0.0001	100, 3,000, 5,000
	Standard deviation	2,000	40	0	1,000
NTG	Min, Mean, Max	0.6, 0.9, 1	0, 0.2, 0.5	0.01	0.6, 0.9, 1
	Standard deviation	0.05	0.05	0	0.05

*vertical permeability = 0.1 × horizontal permeability

3.1.2 Dynamic properties of the reservoir model

Similar to the petrophysical properties of the geological model attribution, the dynamic properties of the reservoir model have been selected based on the values reported for the reservoir conditions found in the corresponding or neighbouring Barents Sea formations. The salinity of the formation water was chosen to be 14% based on the values reported for the Tubåen formation of the Snøhvit field (Benson, 2006), which is also part of the Realgrunnen Subgroup overlying the Fruholmen. The reservoir temperature was set at 93°C and the initial pressure of the reservoir model was assumed to be at hydrostatic pressure.

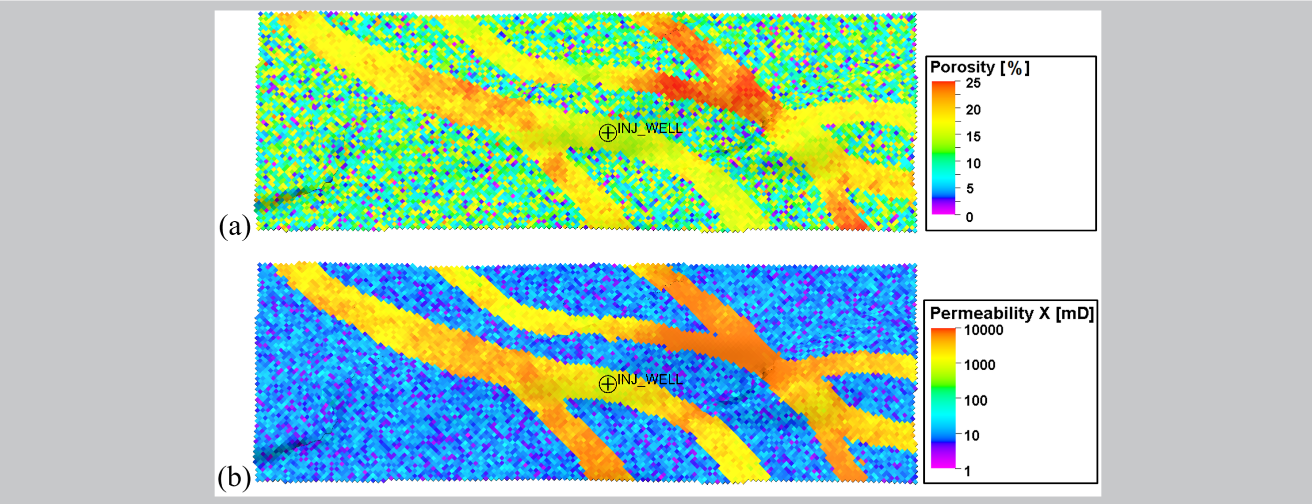

Figure 24 Example realisations of petrophysical properties distribution for the top layer of the reservoir: (a) Porosity; (b) Horizontal permeability covering the area of the reservoir model (36km×10km).

3.1.3 Modelling of CO_2 flow diversion with brine injection

The dynamic model was set up in Schlumberger's Eclipse 300 (E300) software using the static geological model and the dynamic reservoir parameters described in the previous sections. The compositional flow simulation of CO_2 storage in the saline aquifer model was carried out by implementing a quasi-isothermal, multi-phase, and multi-component algorithm, enabled by the CO2STORE option, wherein mutual solubilities of CO_2 and brine are considered. Simulations were carried out for 30 years, comprising of the CO_2 injection, leakage detection, remediation and observation phases.

For the purposes of this study, it was assumed that a sub-seismic fault is present in the formation as a pre-defined undesired migration pathway. This is represented by a local grid refinement introduced in the structural model by means of the CARFIN option in Eclipse. Three separate scenarios were considered by varying the fault locations along the anticlinal structure at distances of 1km, 2km and 3km with respect to the CO_2 injection well. The amount of leakage into the shallow aquifer and the time it takes to remediate the leakage were assessed.

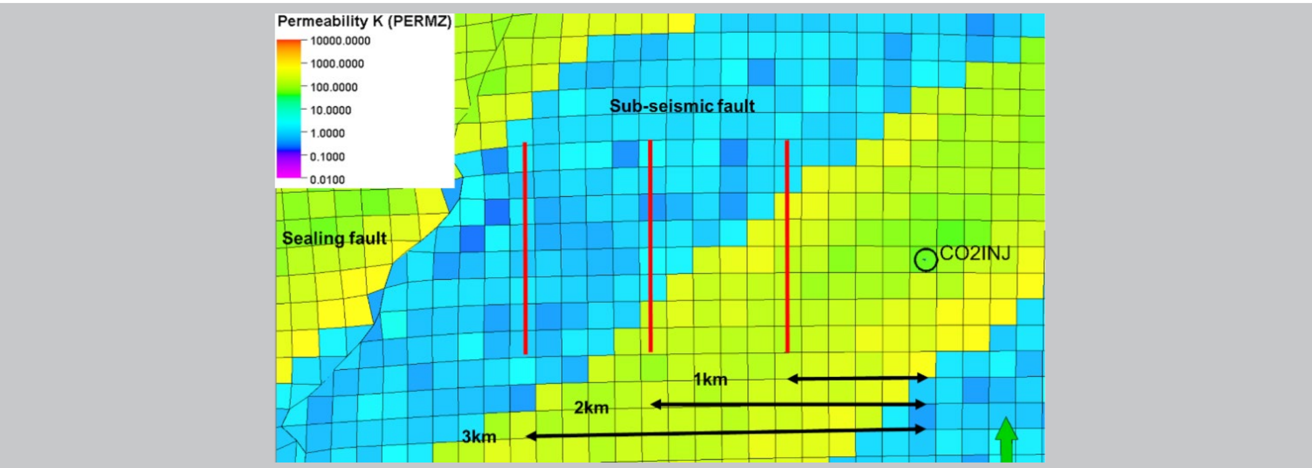

Figure 25 Permeability attribution and position of sub-seismic fault at 1km from the CO_2 injection well.

The fault has a lateral dimension of 800m×2m and is assumed to be non-sealing, with a uniform vertical permeability of 10,000mD and spanning the reservoir and the caprock thickness (approximately 450m), and without appreciable formation displacement between the two sides of the fault.

The simulation of CO_2 injection in the saline aquifer was carried out at a rate of 1Mt/year until leakage through the sub-seismic fault into the shallow aquifer is detected. The leakage detection is based on a threshold which was assumed as 5,000 tonnes of mobile CO_2 (Benson, 2006). Once the leakage is detected, CO_2 injection was stopped and brine was injected for a maximum period of 12 months to investigate the effectiveness of flow diversion.

3.2 CO_2 Injection and leakage detection

3.2.1 Scenario 1: Fault at 1km away from the CO_2 injection well

When the sub-seismic fault was assumed at 1km away from the CO_2injection well, leakage in the shallow aquifer was detected after 8 months from the start of injection. Figure 26 illustrates the simulation results indicating the free CO_2 plume distribution after: (a)

3 months of simulation; (b) when the leakage was detected and CO_2 injection was stopped (after 8 months); and (c) after 30 years of simulation (un-remediated).

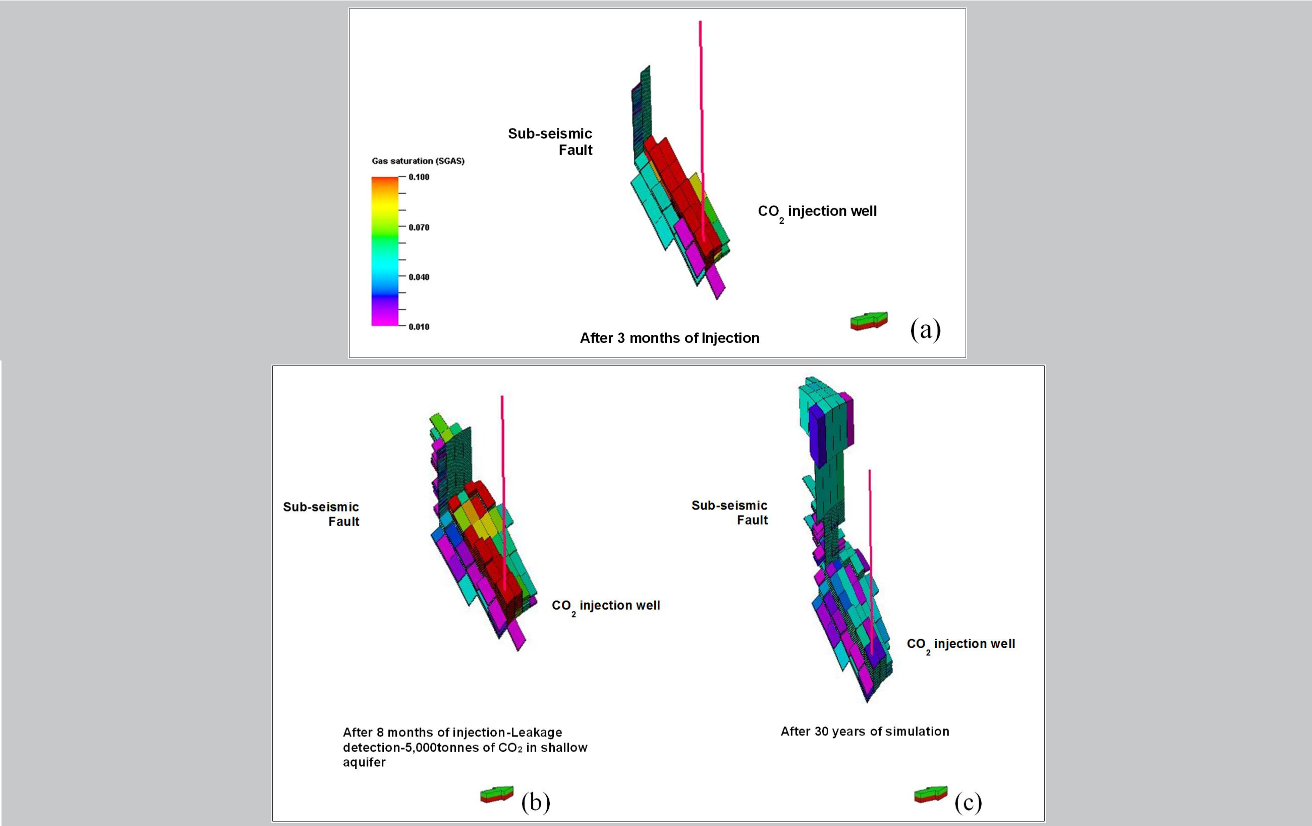

Figure 26 Plume distribution at different time steps in shallow aquifer for 1km fault scenario: (a) after 3 months; (b) after 8 months (when leakage is detected); (c) after 30 years of simulation (un-remediated).

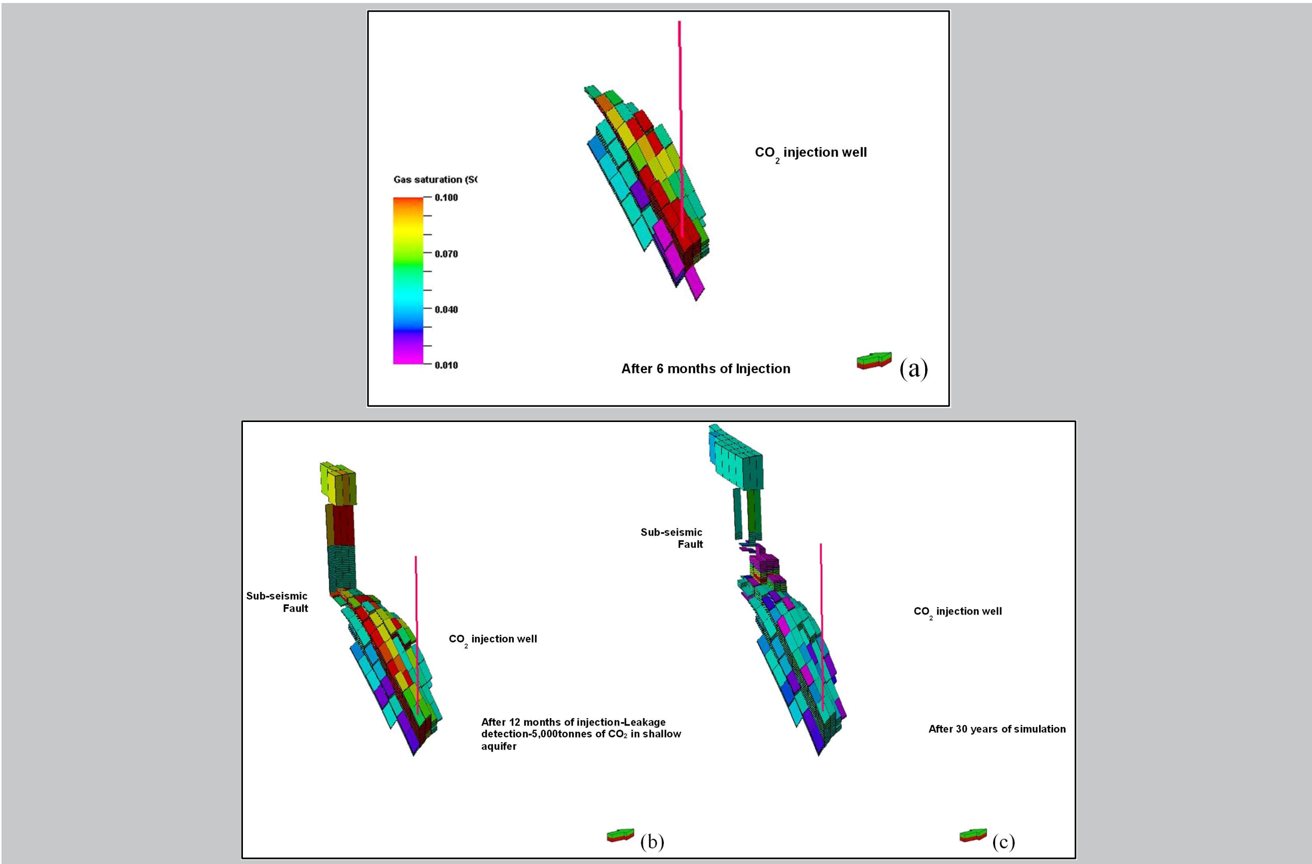

Figure 27 Plume distribution at different time steps in shallow aquifer for 2km fault scenario: (a) after 6 months; (b) after 12 months (when leakage is detected); (c) after 30 years of simulation (un-remediated).

The plume migration results for this case shows that, soon after the start of CO_2 injection the plume hits the sub-seismic leaky fault because of its proximity to the CO_2 injector well, and because it is in the high permeability channel. Due to the buoyancy effects, the CO_2 reaches the top of anticline and breaks into shallow the aquifer, and thus 5,000 tonnes of free CO_2 is detected just after 8 months of injection. After that, CO_2 injection was stopped and brine injection was started to stop further migration of the CO_2.

3.2.2 Scenario 2: Fault at 2km from the CO_2 injection well

When the sub-seismic fault was assumed at 2km away from the CO_2 injection well, leakage in shallow aquifer was detected after 12 months from the start of CO_2 injection. Figure 27 illustrates the simulation results indicating the free CO_2 plume distribution after: (a) 6 months of simulation; (b) when leakage was detected and CO_2 injection was stopped (after 12 months); and (c) after 30 years of simulation (un-remediated).

The plume migration results for this case show that, the CO_2 plume does not hit the sub-seismic leaky fault immediately as compared to the fault at 1km. After 12 months of CO_2 injection, leakage in the sub-seismic leaky fault has been detected. After that CO_2 injection was stopped and brine injection was started to stop further migration of the CO_2.

3.2.3 Scenario 3: Fault at 3km from the CO_2 injection well

When the sub-seismic fault was assumed at 3km away from the CO_2 injection well, and relatively closer to the top of the anticlinal structure, leakage was detected in the shallow aquifer after 18 months from the start of CO_2 injection. Figure 28 illustrates the simulation results indicating the free CO_2 plume distribution after: (a) 6 months of simulation; (b) when leakage was detected and CO_2 injection was stopped (after 18 months); (c) after 30 years of simulation (un-remediated).

The plume migration results for this case show that a significantly larger amount of CO_2 is injected before it reaches the sub-seismic leaky fault as compared to the scenarios when the fault was at 1km and 2km distance because 75% of the full extent of this fault is not in the high permeability channel (Figure 25).

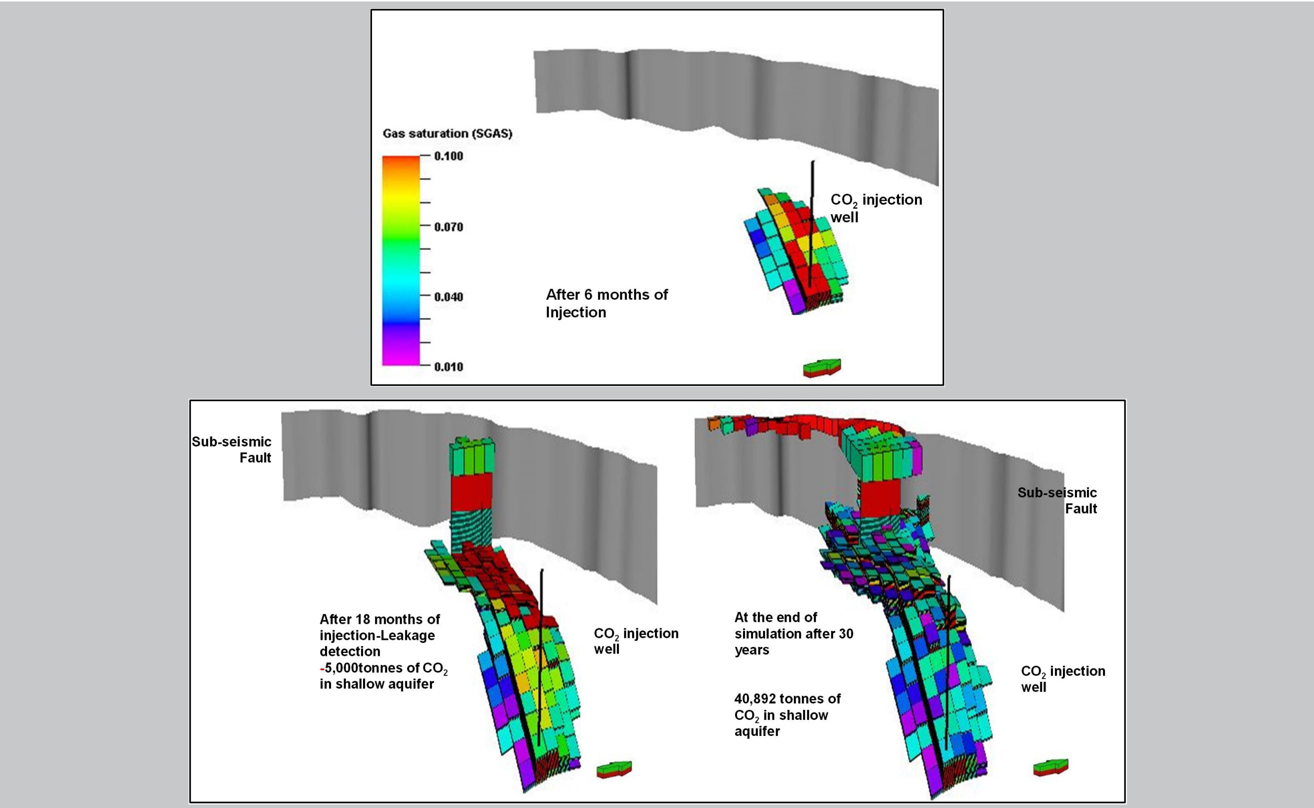

Figure 28 Plume distribution at different time steps in shallow aquifer for 3km fault scenario: (a) after 6 months; (b) after 18 months (when leakage is detected); (c) after 30 years of simulation (un-remediated).

3.3 CO_2 leakage remediation using brine injection

When injected in deep saline aquifers, CO_2 moves radially away from the injection well and progressively higher in the formation because of buoyancy forces. Once 5,000 tonnes of CO_2 has been detected in the shallow aquifer, CO_2 injection was stopped and the injection well was used for brine injection to investigate its effectiveness for flow diversion, thus remediate the leakage. Brine was injected at a rate of 1Mt/year and for a maximum period of 12 months. Secondary mode of control for brine injection was implemented in the model by setting an upper bottom hole pressure limit of 300 bars in order to maintain reservoir pressure below the fracture pressure limit.

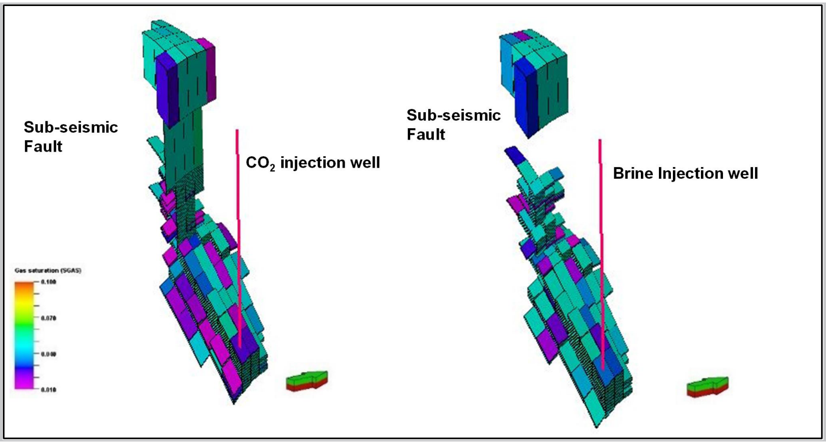

Figure 29 Plume distribution at the end of 30 years' simulation: (a) without remediation; (b) with brine injection.

3.3.1 Scenario 1: Fault at 1km from the CO_2 injection well

In the first scenario, wherein the sub-seismic fault is considered along the anticline at 1km from the CO_2 injector well, brine injection induces flow diversion because of the dissolution in the reservoir and consequently reduces the cumulative amount of CO_2 leakage into the shallow aquifer within 30 days of injection as compared to the non-remediated case where the leakage will continue up to 2 years (29 & 30).

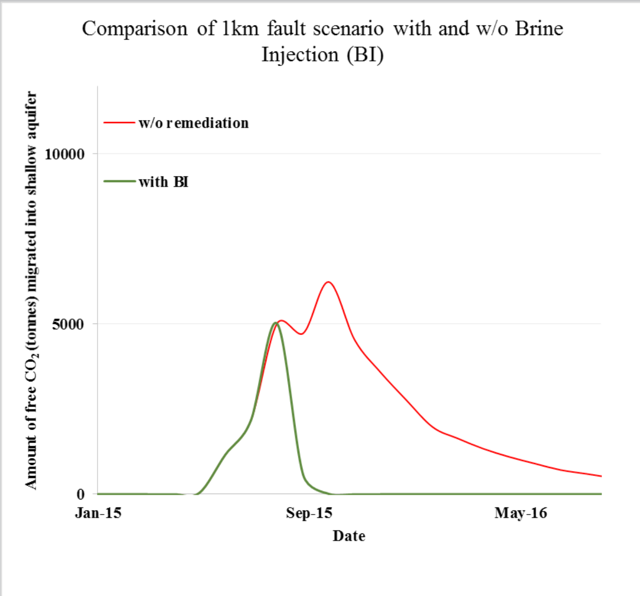

Figure 30 Estimated amount of free CO_2 that could leak in to the shallow aquifer for the 1km fault scenario.

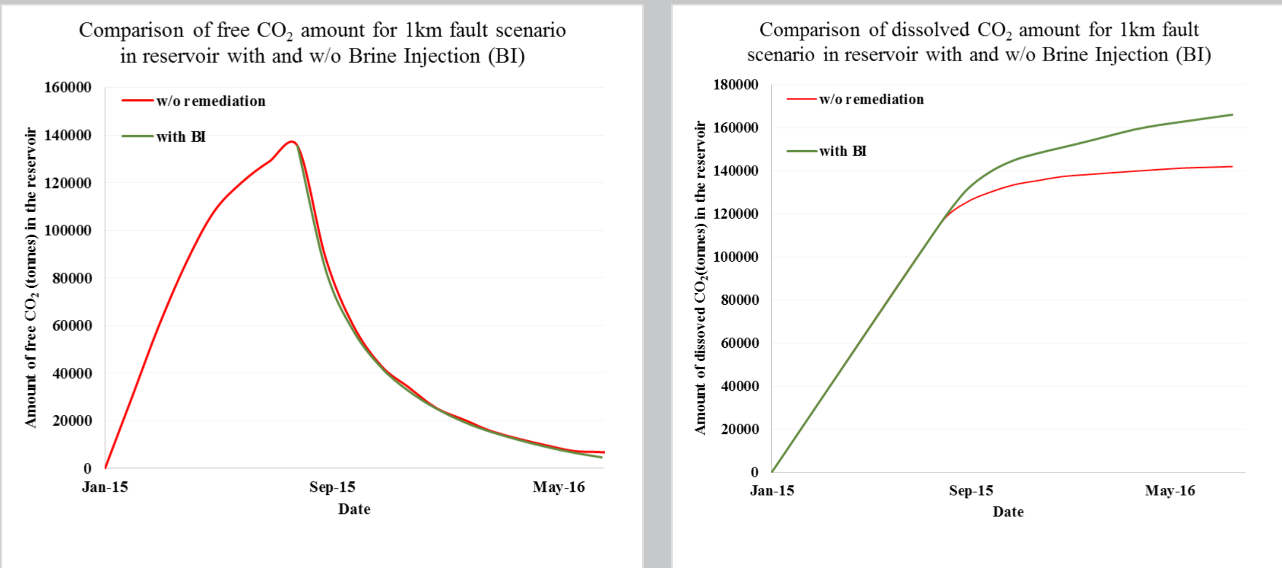

Figure 31 Estimated amount of free and dissolved CO_2 amount in reservoir with and without brine injection.

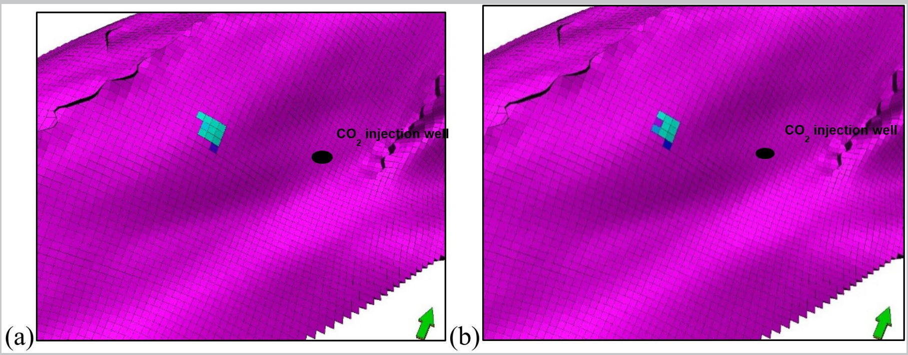

Figure 32 Top view of the reservoir for 1km scenario: (a) without remediation; (b) with brine injection.

The above plume migration results for with and without brine injection for 1km fault scenario clearly show that, with brine injection, the leakage of CO_2 from the sub-seismic fault has been stopped and no more leakage is taking place.
The storage mechanism, which has the largest role in brine injection in reducing the amount of free CO_2 present in shallow aquifer is dissolution, as illustrated by the summary plots for the dissolved and free CO_2 in the reservoir (Figure 31). Dissolution increase with brine injection, which results in less amount of CO_2 in the mobile phase for leakage. Hence, the amount of CO_2 present in the mobile phase in the shallow aquifer is less as compared to un-remediated case.

The top view of the reservoir for this scenario (Figure 32) clearly shows that less CO_2 has leaked when brine injection is implemented. This further strengthens the fact that, because of dissolution in the reservoir, less CO_2 free is available for leakage.

3.3.2 Scenario 2: Fault at 2km from the CO_2 injection well

In the second scenario, wherein the sub-seismic fault is considered along the anticline at 2km from the CO_2 injector well, brine

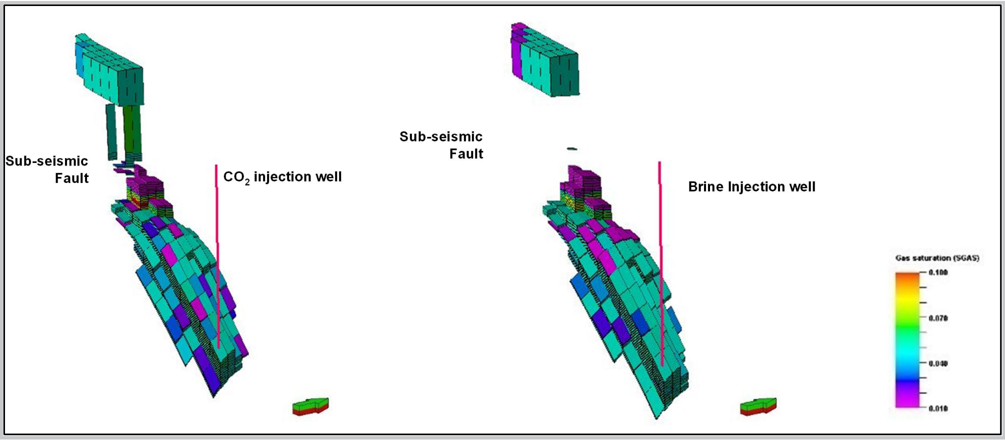

Figure 33 Plume distribution at the end of 30 years' simulation: (a) without remediation; (b) with brine injection.

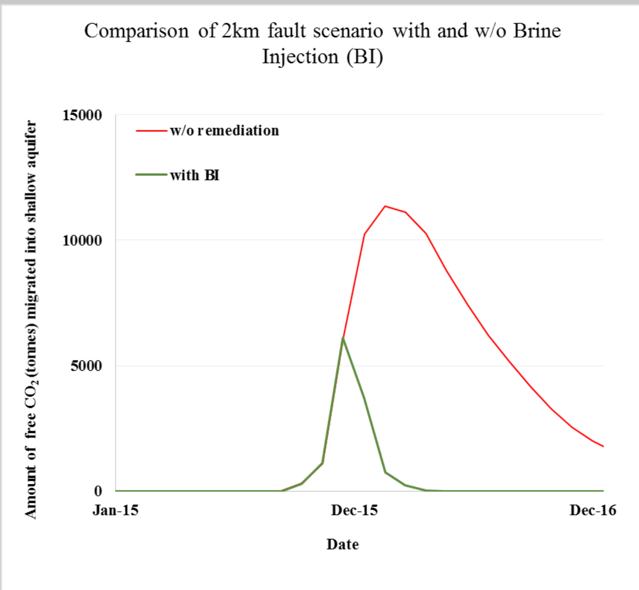

Figure 34 Estimated amount of free CO_2 that could leak into the shallow aquifer for the 2km fault scenario.

injection induces flow diversion because of dissolution in the reservoir and consequently reduces the cumulative amount of CO_2 leakage into the shallow aquifer within 2 months of brine injection as compared to the non-remediated case where the leakage will continue up to 2 years (Figure 33 & Figure 34).

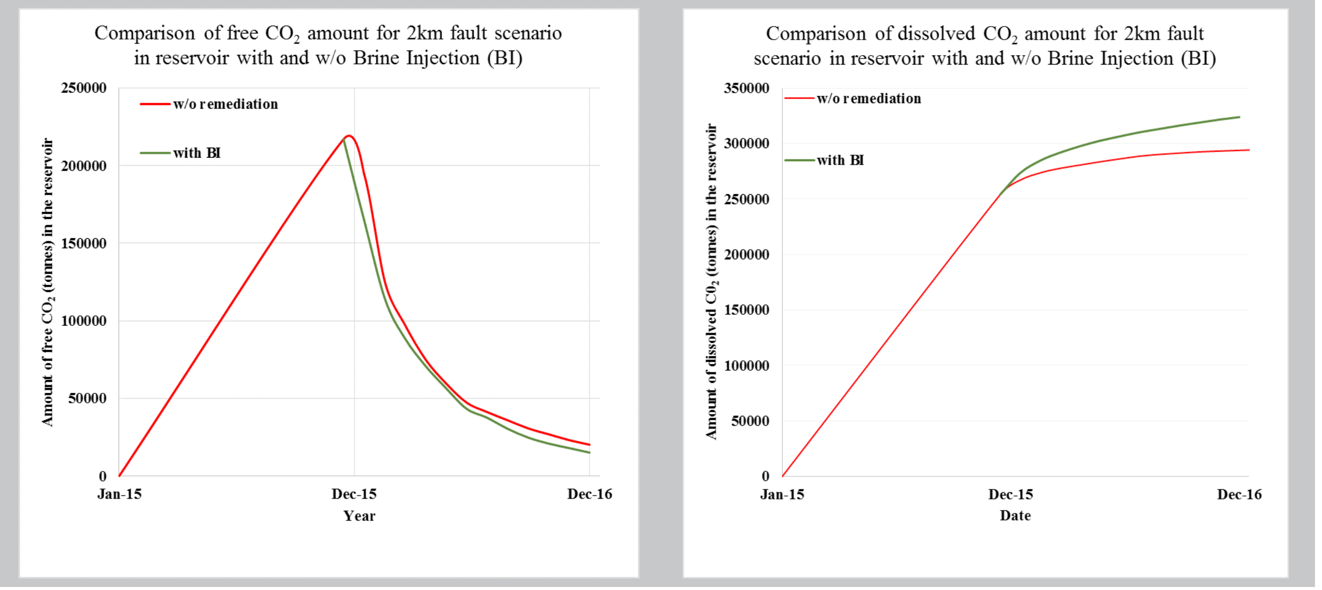

Figure 35 Estimated amount of free and dissolved CO_2 in the reservoir with and without brine injection.

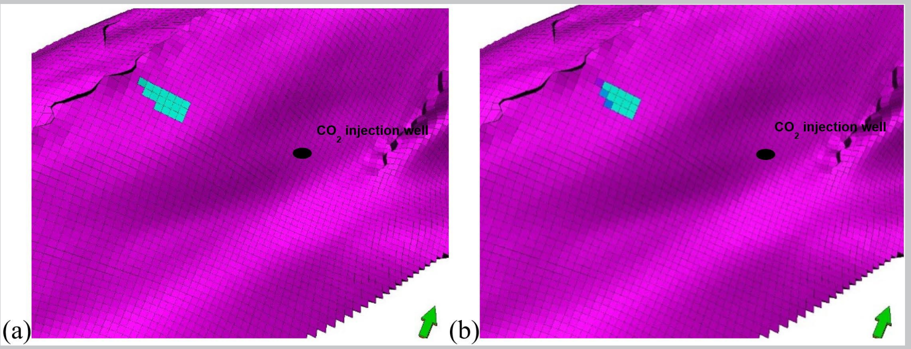

Figure 36 Top view of the reservoir for 2km scenario: (a) without remediation; (b) with brine injection.

The above plume migration results for with and without brine injection for the 2km fault scenario clearly show that, with brine injection, the leakage of CO_2 from the sub-seismic fault has been stopped and no more leakage is taking place.

The storage mechanism, which has the largest role in reducing the amount of free CO_2 present in the shallow aquifer is dissolution, as illustrated by the summary plots for the dissolved and free CO_2 in the reservoir (Figure 35). Dissolution increases with brine injection, which results in less amount of CO_2 in the mobile phase for leakage. Hence, the amount of CO_2 present in the mobile phase in the shallow aquifer is less as compared to the unremediated case.

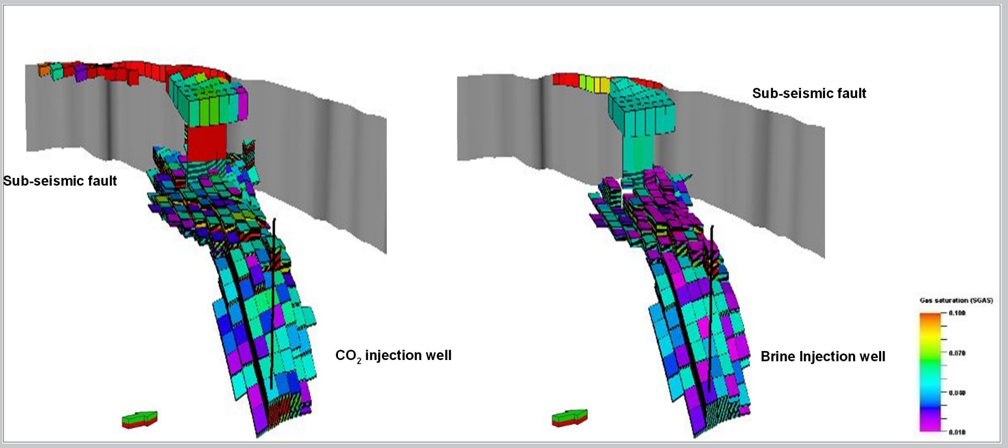

Figure 37 Plume distribution at the end of 30 years' simulation: (a) without remediation; (b) with brine injection.

The top view of the reservoir for this scenario (Figure 36) clearly shows that less CO_2 has leaked when brine injection is implemented. This further strengthens the fact that, because of dissolution in the reservoir, less free CO_2 is available for leakage.

3.3.3 Scenario 3: Fault at 3km from CO_2 Injection well

In the final scenario, wherein the sub-seismic fault is considered along the anticline at 3km from the CO_2 injector well, brine injection induces flow diversion and, it is estimated that the cumulative amount of CO_2 leakage into the shallow aquifer consequently reduces from 40,892 tonnes (for an un-remediated case) to 27,684 tonnes by the end of the thirty years simulation period (as shown in Figure 37 & Figure 38).

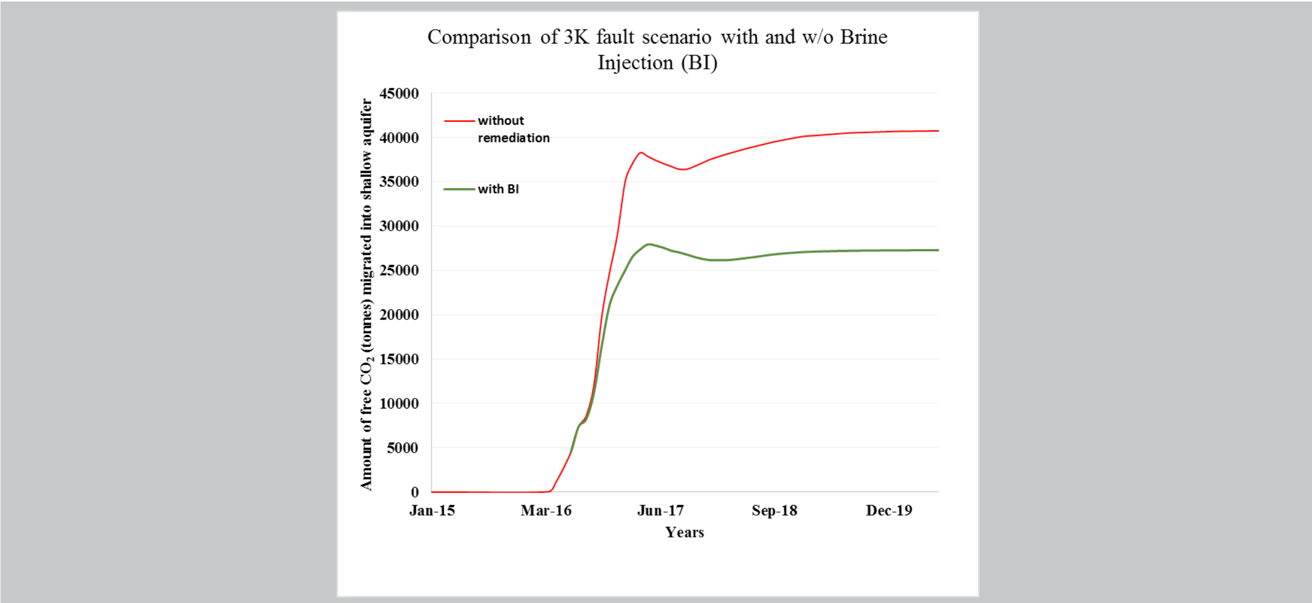

Figure 38 Estimated amount of free CO_2 that could leak for the 3km fault scenario.

The above plume migration results with brine injection clearly show that there is a reduction in the amount of leakage into shallow aquifer. In addition, the plume saturation results suggest that CO_2 dissolution enhancement owing to brine injection plays a significant role in leakage reduction.

The storage mechanism which has an impact in reducing the amount of free CO_2 present in shallow aquifer is CO_2 dissolution in the reservoir, as illustrated by the plots for the dissolved and mobile CO_2 in the reservoir (Figure 39). Dissolution increases with brine injection, which results in less amount of CO_2 in the mobile phase for leakage.

The top view of the reservoir for this scenario (Figure 40) clearly shows that less CO_2 has leaked when brine injection is implemented. This further strengthens the fact that, because of dissolution in the reservoir, less free CO_2 is available for leakage.

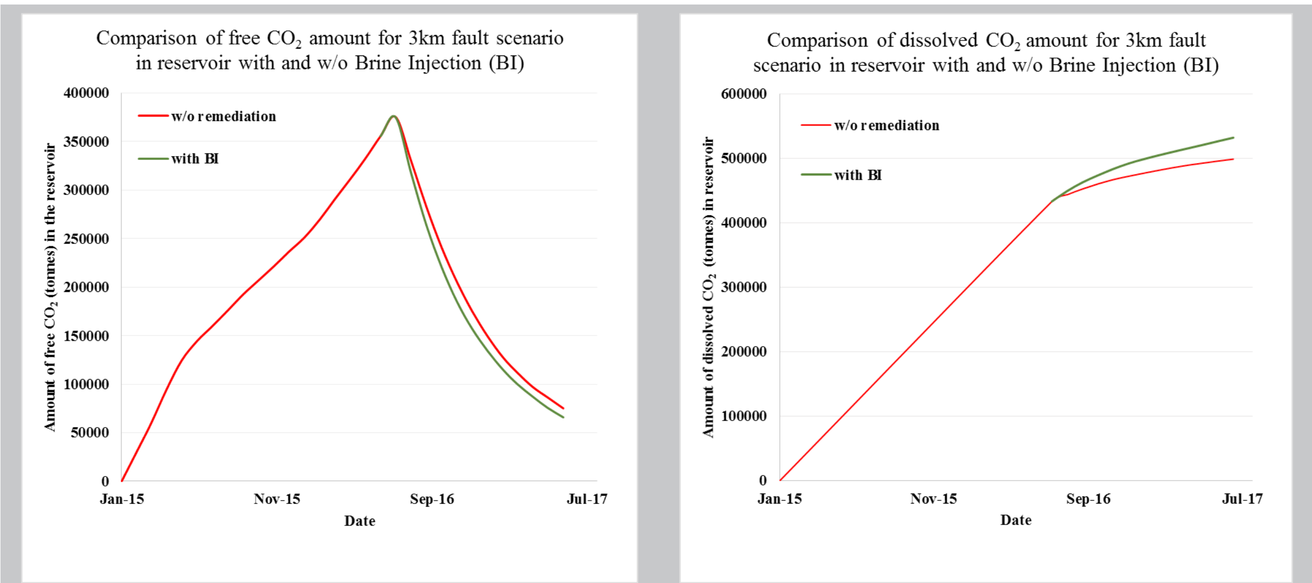

Figure 39 Estimated amount of dissolved and trapped CO_2 for the 3km fault scenario.

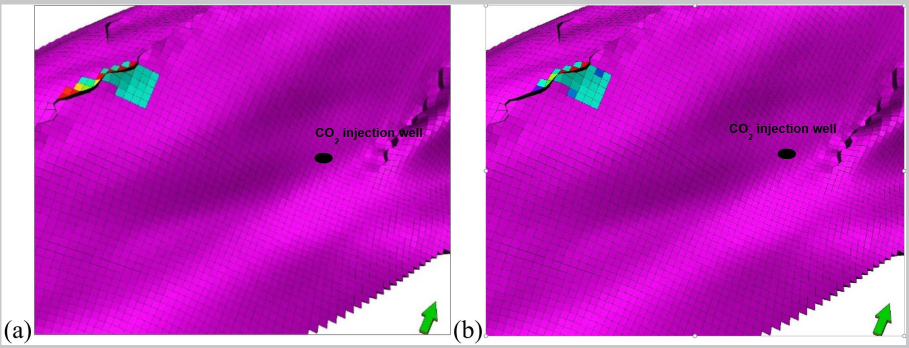

Figure 40 Top view of the reservoir for 1km scenario: (a) without remediation; (b) with brine injection.

In order to further investigate the flow diversion performance of brine injection for 3km scenario, brine injection rate as well as period of injection was varied. First brine injection rate was increased to 2Mt/year. The results show that there is a limit with which one can achieve remediation by using brine injection, as the difference in remediation achieved by using 1Mt/year and 2 Mt/year is not much. Table 8 illustrates the percentage of remediation achieved by using two different injection rates. Brine injection was continued up to 36 months and it was found that there is a very slight decrease in the amount of free CO_2 in shallow aquifer, which further illustrates this conclusion (Figure 41).

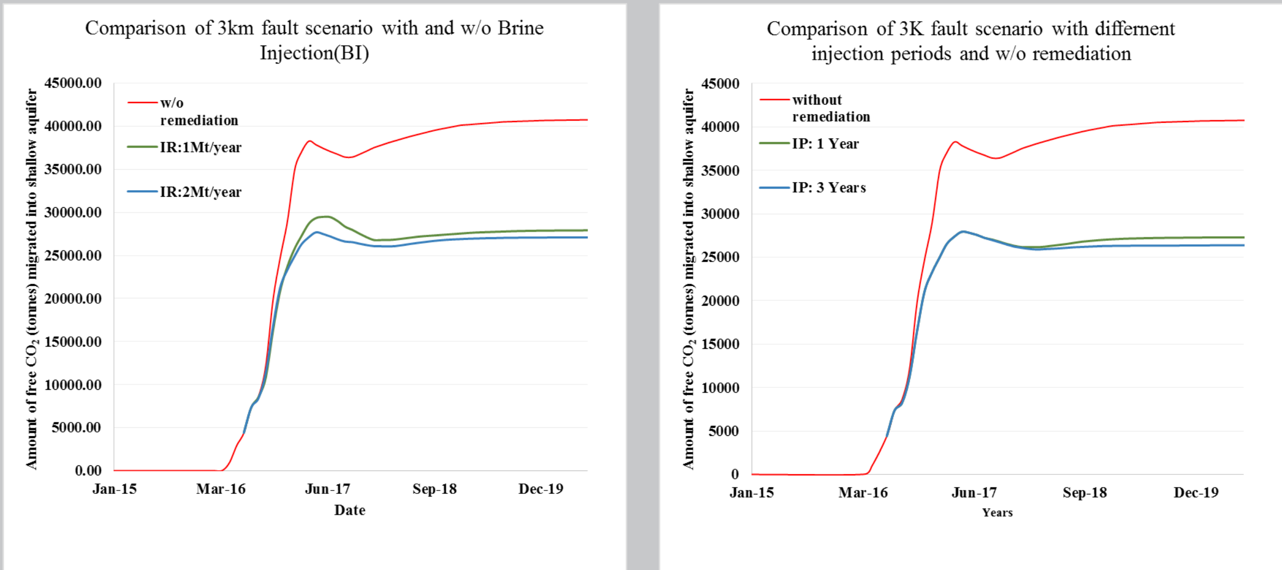

Figure 41 Estimated amount of free CO_2 that could leak for the 3km fault scenario with different injection rates and different injection periods.

The comparison between different injection rates and periods suggests that, by increasing the injection rate or injection period, the increase in the amount of remediation achieved is insignificant, which further confirms the fact that the amount of remediation achieved with brine injection will be limited beyond a certain threshold.

Table 8 Percentage remediation achieved for 3km fault scenarios at different injection rates.

Brine Injected for 12 months at a rate of	Remediation Achieved
1 Mt/year	27.9%
2 Mt/year	32.3%

Generally the storage mechanisms like capillary trapping and dissolution renders the CO_2 less mobile over a timescale of decades to hundreds of years. Overall, with brine injection, there is a decrease in the cumulative mass of CO_2 in the shallow aquifer (Figure 42).

3.4 Discussion and conclusions

In this part of the project, the brine injection scenarios were defined based on the distance of the sub-seismic fault from the CO_2 injector along the anticlinal structure. Simulations were performed in order to assess the migration of the CO_2 plume and the effectiveness of brine injection as a mitigation measure. Brine was injected at a rate of 1Mt/year and for a maximum period of 12 months. Secondary mode of control for brine injection was implemented in the model by setting an upper bottom hole pressure limit of 300 bars in order to maintain reservoir pressure below the fracture pressure limit. Three scenarios were considered by changing the sub-seismic fault location as 1km, 2km and 3km away from the CO_2 injection well.

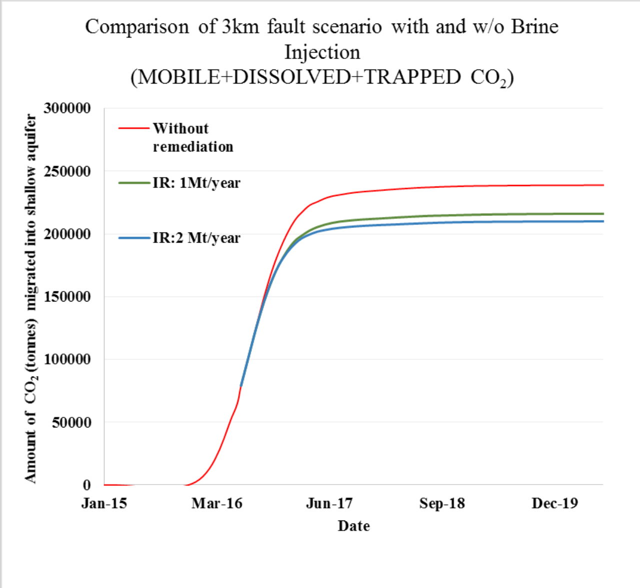

Figure 42 Estimated cumulative mass of CO_2 that could leak for the 3km fault scenario.

The comparison of fault scenarios without remediation (Figure 43) suggests that the fraction of the total amount of CO_2 that would migrate into the shallow aquifer depends on the injection period, and hence the cumulative amount of CO_2 injected until the time of leakage detection (Table 9). For a fault location along the anticline at distances greater than 2km from the CO_2 injector well, and particularly when it lies very close to the top of anticline, it is envisaged that CO_2 will continue to remain there because of buoyancy effects in the reservoir and shallow aquifer, and will not be dissolved or trapped significantly over a period of 30 years, which includes the post- CO_2 injection period.

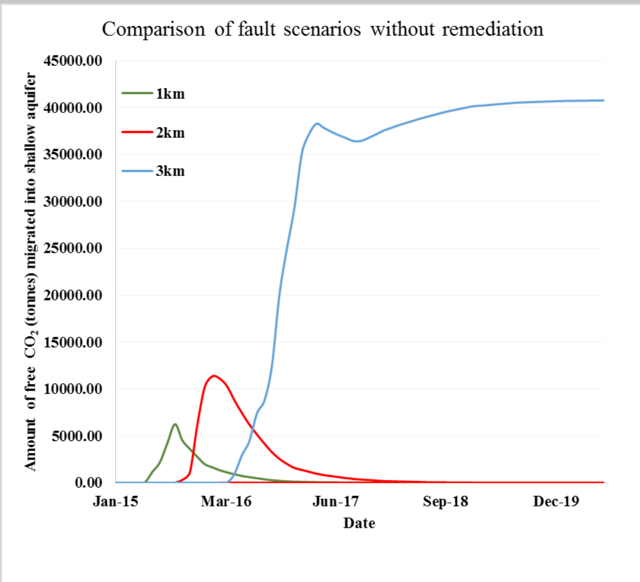

Figure 43 Estimated amount of free CO_2 that could leak for different fault scenarios without remediation.

The comparison between fault scenarios with brine injection (Figure 44) illustrates that, for a fault at 1km and 2km, brine injection very quickly stops the leakage and, in the long-term, the dissolution process in the reservoir/shallow aquifer plays an important role and the amount of mobile CO_2 decreases towards zero. Furthermore, the leakage is pressure driven and, where the fault is in

Table 9 Percentage of CO_2 that has migrated into the shallow aquifer for different fault location scenarios.

Distance of Fault from CO_2 Injection Well (km)	Time to detection (5,000 tonnes of CO_2 leaked) after injection	Total amount of CO_2 injected until leakage detection (Mt)	Percentage of CO_2 Injected that has migrated into shallow aquifer (%)
1	8 months	0.66	9
2	12 months	1.00	11
3	18 months	1.50	26

the transient region of the reservoir, the timescale when mobile CO_2 is available for leakage is limited. However, for the 3km fault scenario, injecting brine at a rate of 2Mt/year for 12 months can reduce the amount of free CO_2 in the shallow aquifer to 67.7% of that which would otherwise be there after 30 years if not remediated. This is because the fault in this scenario is closer to the top of the anticline, hence the leakage is more buoyancy driven and more cumulative amount of CO_2 is available for leakage. These findings are summarised in Table 10.

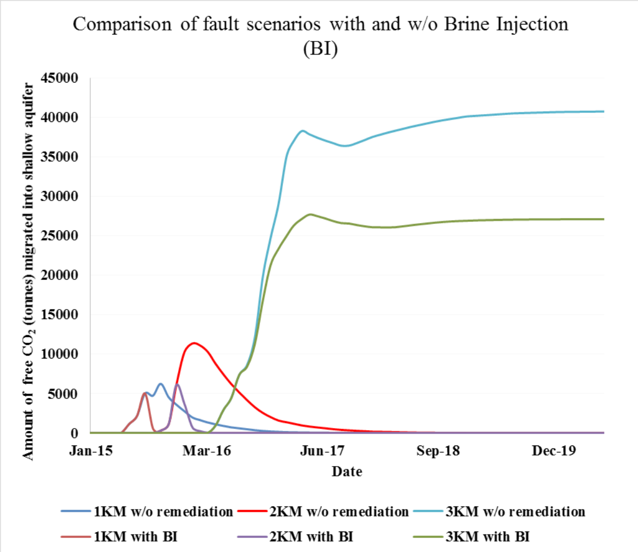

Figure 44 Estimated amount of free CO_2 that could leak for different fault scenario with brine injection.

As planned, the performance of brine injection as a remediation measure for CO_2 leakage was evaluated by estimating the cost of implementing the scenarios considered here (USEPA, 2010; IEAGHG, 2011; Element Energy, 2012). Furthermore, the response time, spatial extent and length of remediation process were also assessed. These findings are presented in Table 11.

Table 10 Percentage of Remediation achieved for different fault location scenarios.

Distance of Fault from CO_2 Injection Well (km)	Time to leakage detection after start of injection	Total amount of CO_2 injected until leakage detection (Mt)	Leakage into shallow aquifer without remediation (tonnes) (Leakage over total mass injected)	Leakage into shallow aquifer with remediation (tonnes) (Leakage over total mass injected)	Remediation achieved against leakage without remediation
1	8 months	0.66	6,240 (9.5%)	5,043 (7.6%)	19.2%
2	12 months	1.00	11,346 (11.3%)	6,096 (6.1%)	46.3%
3	18 months	1.50	40,892 (27.3%)	27,684 (18.5%)	32.3%

The results have shown that brine injection causes an increase in dissolution which consequently reduces the amount of mobile CO_2 available for leakage to the shallow aquifer. The comparison of CO_2 plume migration results between the un-remediated case (without brine injection) and remediated case (with brine injection) for 1km and 2km fault scenarios suggest that, with brine injection, the leakage of CO_2 from the sub-seismic fault has been effectively stopped. For the 3km fault scenario, however, CO_2 plume migration results suggest that, with brine injection, there is a reduction in the amount of CO_2 leakage to the shallow aquifer. Additionally, the gas saturation plots also show that without brine injection, more CO_2 migrates through the leaky fault and into the shallow aquifer.

Table 11 Key Performance Indicators for brine injection (1Mt brine injection).

Location of sub-seismic fault with respect to the Injection well	Amount of brine injected (Mt)	Length of remediation (days)	Response time to remediation* (days)	Estimated cost (€)	Spatial extend of remediation# (km²)
1km	1.0	360	30	640,000	2.80
2km	1.0	360	60		
3km	1.0	360	330		

* Response time: The time it takes for the leakage profile in the shallow aquifer to change through brine injection.
# Spatial extent of remediation: The area covered by the injected fluid at the top layer of the reservoir at the end of 12 months injection period.

On the other hand, with brine injection, a higher gas saturation is retained in the reservoir. Naturally, reservoir topography and the heterogeneity introduced in the model also played a role on the results obtained from the three scenarios.

Further investigation on the flow diversion performance of brine injection for the 3km fault scenario was carried out by changing the injection rate as well as injection period. The results suggest that there is a limited benefit from flow diversion that can be achieved with longer term brine injection. The results were evaluated using four key performance indicators (KPI), namely: response time to remediation, length of remediation, spatial extent of remediation and remediation cost.

4 BRINE/WATER INJECTION AS A FLOW DIVERSION OPTION IN A CO_2 STORAGE OPERATION (GFZ)

The GFZ carried out a brine injection experiment at the pilot site for CO_2 storage at Ketzin. Between 12. Oct. 2015 and 6. Jan. 2016 a total amount of 2884 tons of brine were injected into the CO_2 reservoir (Möller et al., 2016). The experiment aimed to evaluate the use of brine injection as remediation technique. It could be carried out with existing equipment from oil and gas industry and requires less preparation compared to other remediation methods. Therefore it allows rapid action in case of leakage. Brine injection does not achieve a durable remediation effect, wherefore it must be followed by a permanently acting technique.

Ketzin is the first CO_2 storage site where a large amount of liquid was injected into a CO_2 reservoir. Therefore the experiment was operationally and scientifically challenging and addresses four main objectives:

1. Development of a technical setup: The field operation has not been carried out before. A technical setup for safe and reliable brine injection had to be developed. This should prevent reservoir damage and ensure monitoring of all relevant physical and chemical parameters.
2. Assessment of remediation impact: The oil and gas industry inactivate gas-filled wells in a so called kill operation by injection of heavy liquids. This injection typically aims at the well itself and therefore has a limited duration. The current experiment does not only aim at the well but also at the reservoir. The effective remediation time shall be determined to provide a timeframe in which to prepare further remediation measures.
3. Multiphase flow simulation: Prior to injection of CO_2 the reservoir was filled with brine. This brine is partly replaced by the injected CO_2, but residual brine remains in the rock matrix. This process is called drainage. The injection of brine into a reservoir that was previously drained by CO_2 replaces only a ratio of the CO_2 with the newly injected brine while a residual concentration of CO_2 phase remains in the pores. This process is called imbibition. On a lab scale these processes are well described (Bachu and Bennion, 2008). The residual CO_2 phase in the pores is commonly referred to as capillary-trapped CO_2. It is very important to consider the residual CO_2 also on the field scale.
4. Evaluate the potential of geoelectric monitoring: The injection well is equipped with a downhole geoelectrical array (Schmidt-Hattenberger et al., 2011). The injection brine changes the reservoir resistivity by replacing the low conductive CO_2 with highly conductive brine. The natural reservoir brine has a slightly lower conductivity than the injection brine and is also replaced during the imbibition process. It is investigated to which extent these processes can be monitored with geoelectric methods.

4.1 Technical setup

The brine injection was carried out between 12 Oct. 2015 and 6 Jan. 2016 with a total amount of 2884 tons of brine being injected. The equipment was provided and the technical operation was carried out by UGS Geotechnologiesysteme (Mittenwalde, Germany). The brine was made oxygen free with sodium sulfite, delivered by trucks and pumped into the brine storage tanks on site (Figure 45). From these the brine was pumped by electric pumps through candle filters, electrical conductivity measurement and a coriolis flow meter to the wellhead of Ktzi 201 (Figure 46).

Figure 45 Installation of the storage tanks with 35 m^3 capacity each. The left tank acts as backup

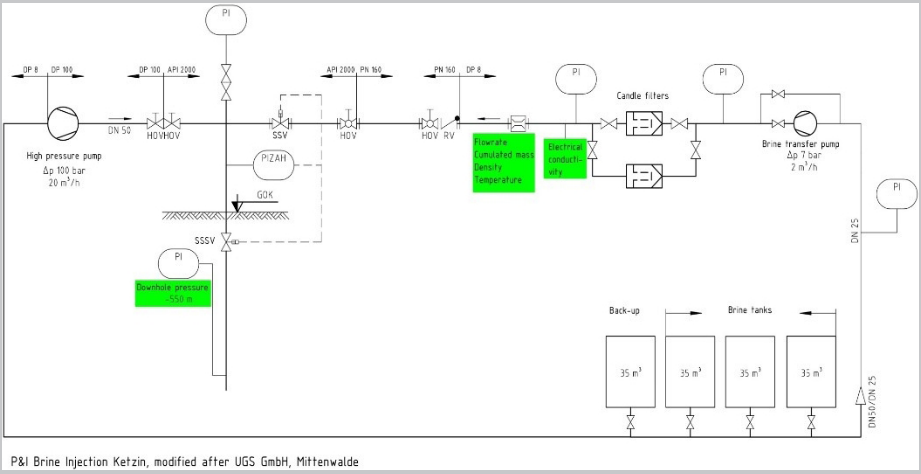

Figure 46 Flow chart of technical installations used for the brine injection. Green fields indicate gauges.

The maximum pressure was 81.15 bar at the reservoir reference level of 630 m, the maximum allowable reservoir pressure is 85 bar. During the test the following brine parameters were continuously recorded: mass flux, cumulated mass, density, temperature and electrical conductivity. Further, pressure was monitored at 550 m below ground level in the injection well. The average conductivity of the brine was 250 mS/cm, the mean density was 1.17 kg/dm³ with only minor temporal variations.

The most demanding point of the operation is the so-called well killing. The borehole is filled with CO_2 gas and the head pressure is about 50 bars. This pressure was to be exceeded with the amount of 4.7 tons of brine with a high injection rate, to fill the well with brine and entrain all gas bubbles with the brine into the reservoir. The operation was carried out with a high performance diesel-powered piston pump. After the successful operation the liquid column decreases below wellhead level and pumping was switched to the electrical centrifugal pump.

The target rate was 1400 kg/h until the 9th of November (Figure 47). From this time two pumps were cascaded to increase the injection rate. The rate shows higher variations due to interruptions for testing different pumps, pump failures and repairs. In the following period the rate was adjusted manually to maximize injection rate and simultaneously to ensure that the pressure does not exceed 81 bars at reservoir level.

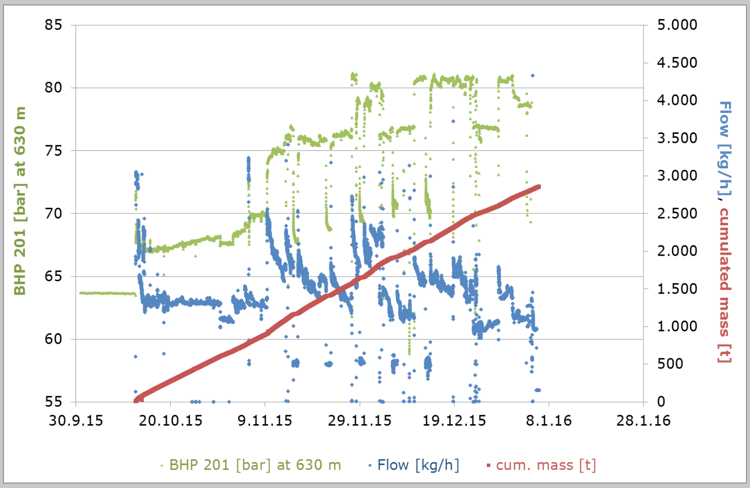

Figure 47 Overview on the operational parameters during the injection period.

4.2 Assessment of remediation impact

One of the key questions is the a priori estimation of the possible injection rate. As a first approximation the experiment is compared a pre-injection pumping (production) test (Wiese et al., 2010). This allows the application of characteristic numbers that provide a general overview to the operator. The injection test shows a larger differential pressure and longer duration compared with the pre-injection pumping test (Table 12). Nevertheless, the tests are comparable with respect to injectivity. The productivity index decreased from values slightly lower than 1 (m³/hr/bar) in the first minutes to a pseudostatic value of about 0.25 m³/hr/bar during the pumping test. Similarly, the values decreased from 0.77 in the first minutes to about 0.35 during the first week of brine injection (Figure 48). Within the next 5 weeks the productivity index decreases almost linearly to 0.1. Within the next 7 weeks the index decreases more slowly to 0.07. During a pumping test a productivity index is determined, during an injection test an injectivity index is determined. Both values are physically equivalent and therefore used synonymous in the following.

Table 12 Comparison of the key characteristics of the pre-injection pumping test in Ktzi 201 and the brine injection (injection test) 8 years later.

	Pumping Test	Injection Test
Date	Sep 2007	Oct 2015 - Jan 2016
Volume [m³]	71	2414
Duration [d]	2.7	85
Max. differential pressure [bar]	-4.5	+17
Mean rate [m³/d]	26.3	28.4

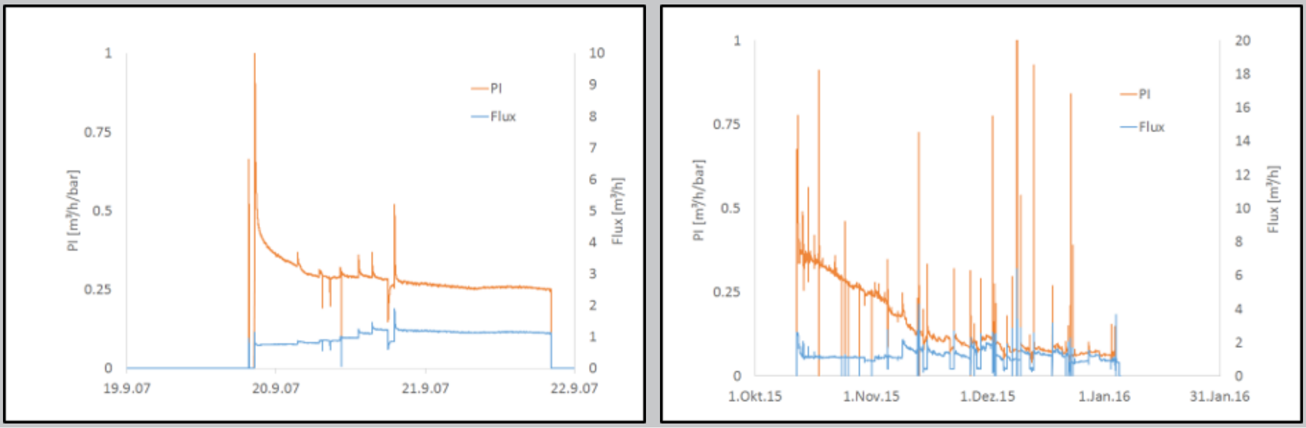

Figure 48 Productivity index PI (orange, left axis) and pumping rate (blue, right axis) for the pumping test (a) and the brine injection (b). Please note that the productivity index has the same y- scale on both figures, but can only be compared for the first days, since the brine injection had a much longer duration.

During injection, the brine replaced the CO_2 in the injection well until the 11. March 2016, in total slightly more than two months (Figure 49). During this time there is no mobile CO_2 present in the reservoir at the location of the injection well. From this point CO_2 starts trickling back into the well and it takes one month to fill the volume of 2.5 m³ between the wellhead and 550 m depth. Re-drainage opens only small preferential flow paths, therefore it is a slow process. It has to be taken into account that the center of mass of the CO_2 plume migrated away from the well Ktzi 201 in a north-western direction and the reservoir pressure was already again close to the pre-injection values.

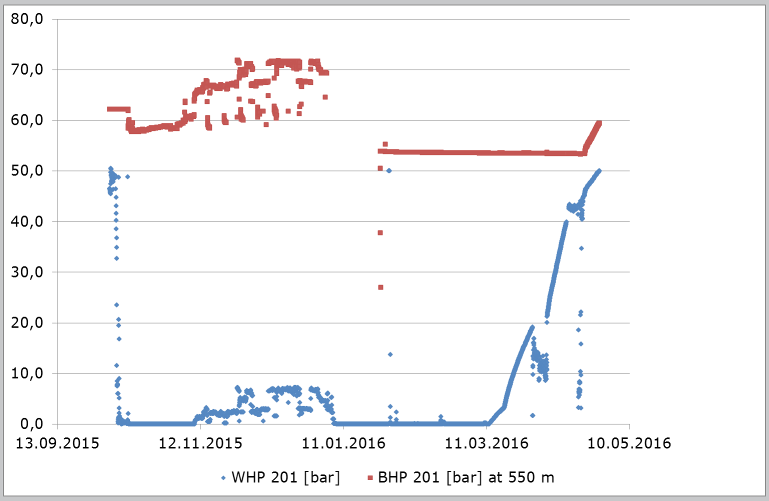

Figure 49 Wellhead (WHP) and bottomhole (BHP) pressure at the injection well Ktzi 201 between beginning of the brine injection and re-establishment of saturated CO_2 conditions.

4.3 Multiphase flow simulation

A multiphase flow model of the Ketzin reservoir has been set up. The model comprises an area of 5x5 km. The model comprises four permeable layers of which the two upper layers are the main reservoir layers and two minor layers located below (Figure 50). It is based on the hydrogeophysical model presented by Wiese et al., (in short), and follows its spatial extent and discretisation. The intrinsic permeability of the sandstone facies is calibrated and spatially distributed. The relative permeability curvature parameters of a Brooks-Corey parameterization are also calibrated.

Some modifications were introduced to the existing model in order to meet the requirements of the brine injection. The model of Wiese et al. (in short) comprises the first 270 days of Ketzin injection history until the arrival of CO_2 in all observation wells. To include the brine injection, it was necessary to include the entire reservoir injection history and the brine injection itself. The model represents the operation between June 2008 and October 2016.

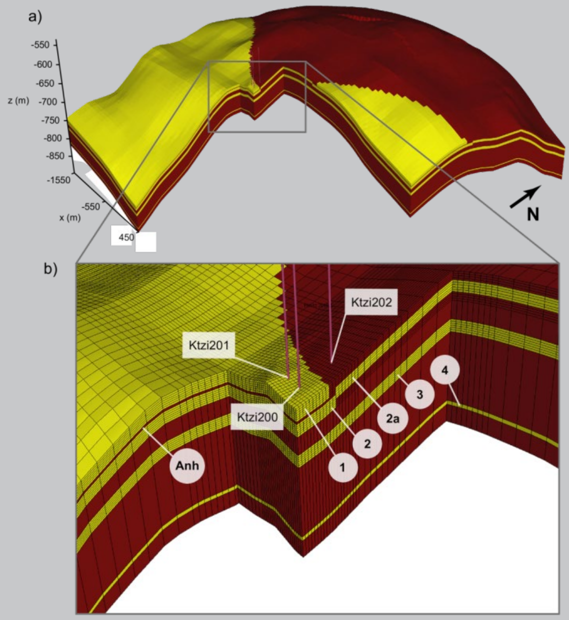

Figure 50 (a) Model domain of the Ketzin reservoir model. The yellow colour indicates sandstone facies with good reservoir quality, the brown colour indicates mudstone with poor reservoir quality. (b) The vertical distribution of reservoir facies in the vicinity of the wells.

The model is calibrated to the extended duration with the goal to match the pressure of three pre-injection cross-hole pumping tests (of which the injectivity of the injection well is calculated in the previous section, see Figure 48a) and reservoir pressure at the injection well Ktzi 201. The pressure match for the latter is shown in Figure 51. The pressure match shows a satisfying fit during the entire injection history. The trend of the pressure level is well matched for the entire injection history between 2008 until 2013. Also the short term pressure fluctuations that occur on variations of the injection rate have the same magnitude for observed and calibrated values.

The simulated pressure fluctuations during the brine injection test at the end of 2015/beginning of 2016, however, show a magnitude that is significantly smaller than observed fluctuations. The calibration model does not take into account the complex drainage and imbibition processes that are mathematically described with hysteresis. During brine injection residual CO_2 remains in the largest pores and therefore reduces the relative permeability compared with previous conditions. This effect is simulated with a further reservoir model. The resulting pressure curves are shown in Figure 52.

It can be seen that the hysteresis model shows a much stronger pressure response to the brine injection than the model without hysteresis. However, the response is still significantly too small to explain the high pressure dynamics in the reservoir.

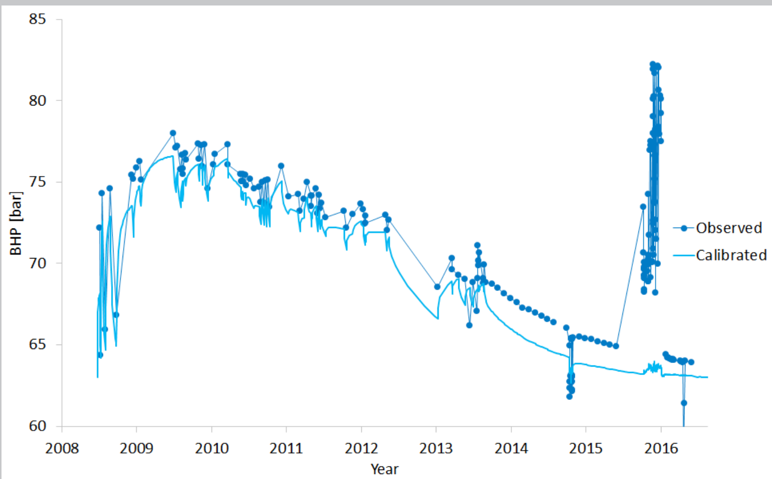

Figure 51 Observed and calibrated bottom-hole pressure of injection well Ktzi 201 for the entire injection history.

The significant mismatch between a calibrated reservoir model including hysteresis and the pressure response of the brine injection is remarkable. A possible reason for the mismatch is the model discretisation of 10 m grid size in the vicinity of the injection well Ktzi 201. A finer resolution may be required to capture fine scale saturation changes and therefore impact the pressure indirectly by the relative permeability. Another reason may be the presence of cemented fractures, as hypothesized by Wiese et al., 2010. For saturated conditions they have a smaller permeability compared to the dominating sandstone facies. Under alternating saturations, these cemented areas may trap residual CO_2 more efficiently due to the smaller pore size and therefore are transformed to a practically impermeable matrix. Further simulations are required to test these hypotheses.

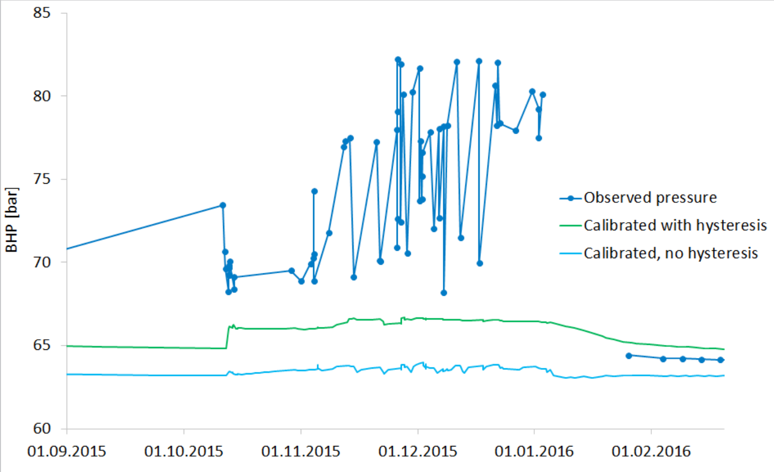

Figure 52 Observed and calibrated bottomhole pressure of injection well Ktzi 201 for the brine injection experiment. The calibration is carried out without and with hysteresis, the pressures are indicated by the light blue and green curve, respectively.

4.4 Geoelectrical Monitoring

The brine injection was monitored by geoelectric cross-hole measurements between wells Ktzi 200 and Ktzi 201 (Schmidt-Hattenberger et al., 2011). In addition to the 15 electrodes for each borehole, three newly installed permanent surface electrodes allows for surface-downhole measurements (Rippe et al., 2016).

A geoelectric baseline was measured directly before brine injection at the 5th Oct 2016. During the injection a combined dataset of cross-hole and surface-downhole measurements was obtained and allows a high temporal resolution. The measurement of such a combined dataset takes approximately 12 hours and passes all relevant AB-MN electrode configurations with a sufficient signal to noise ratio. This results in a dataset with daily resolution, which is inverted with respect to the baseline.

Furthermore, the contact resistances of each neighboured electrode pair are measured several times a day. This allows the coupling of the electrodes to the host rock and between each other to be quantified. Electrodes that are located in an open borehole annulus show a change of contact resistance on a change of the fluid. In the present situation a low contact resistance indicates that the electrodes are located in brine, and a high contact resistance indicates that the electrodes are located in CO_2. Electrodes that are located in concrete are not affected and show a constant contact resistance (Figure 53).

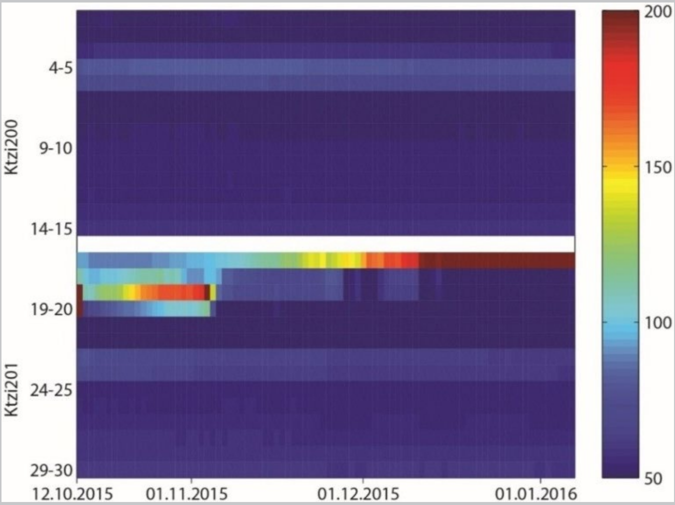

Figure 53 Contact resistances of well Ktzi 200 (upper graph) and Ktzi 201 (lower graph). Blue colour indicates low contact resistance, red colour indicates high contact resistance (Ohm). The largest changes occur for the upper four electrode configurations in well Ktzi 201.

Electrodes in Ktzi 201 are located in an open annulus. The configurations #18-#19 and #19-#20 show a significant drop from 2000 to 50-60 ohm, which is reasonable since the injected brine replaces the CO_2. The uppermost electrode configuration #15-#16, however, shows a constant increase of the contact resistance from 100 to 300 ohm. This is caused by xanthan gum that resides in the borehole annulus due to operations during well drilling and combined accumulation of CO_2, since the borehole annulus is a dead end in the upwards direction. Changes in the contact resistance show a good correlation to the corresponding changes in the injection rate.

The first tomographic time-lapse inversions of the cross-hole measurements carried out by Rippe et al., 2016, show decreasing resistivities in the reservoir compared to the baseline and therefore show the displacement (imbibition) of the reservoir CO_2 by the injected brine (Figure 54). Due to the open annulus the smallest resistivities are in the vicinity of the injection well, following the highest brine saturation there. However, the values for the baseline and the injection are comparable. Probably the lower borehole electrodes were filled with brine from the beginning. The inversion results show a lower resistivity between both wells at reservoir elevation. The temporal development is shown in the lower part of Figure 54. The decrease is not continuous but resembles a step function. These steps may be induced by rapid changes in the pumping rate that occurred during a pump failure. At changing pressure the steps may be induced by rapid mobilization of CO¬2 due to formation of preferential flow paths.

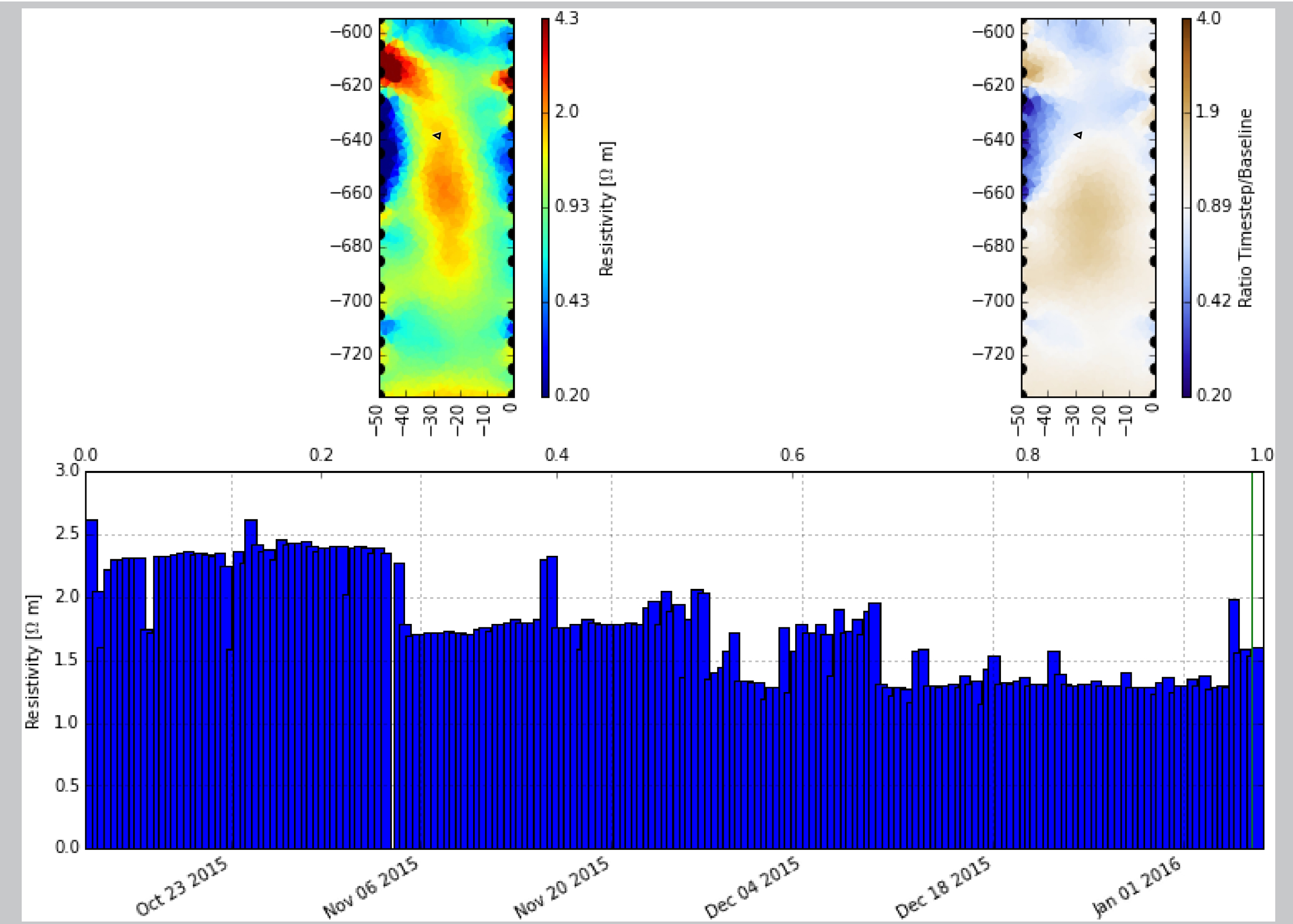

Figure 54 Tomographic time lapse inversion of the cross-hole measurements for the last day of brine injection (top left) compared to the baseline a few days before brine injection (top right). The lower bar chart shows the temporal resistivity development of a model cell between both wells. The cell is located in the reservoir, the position is indicated by a small black triangle in the cross sections.

4.5 Conclusions

The brine injection experiment was carried out successfully. The well was successfully killed with a high power diesel piston pump. The operational procedures were appropriate to inject 2884 t of brine between 12 Oct. 2015 and the 6 Jan. 2016. The well was maintained brine filled during the entire operation, also during short interruptions on the scale of several hours due to pump failures. The injectivity was similar to pre-injection values. This is somehow surprising, as pre-injection values have been determined with single phase a pumping test. The additional physical processes due to multiphase flow and hysteresis approximately cancel out each other.

First simulation attempts have been carried out. A reservoir model was calibrated to the CO_2 injection history. However, the model is not appropriate to reproduce the pressure response during the brine injection experiment. A slight improvement could be achieved by considering hysteresis. Geoelectrical monitoring can reproduce the general trend of higher electrical conductivity due to higher brine concentration and shows a close correlation to the injection dynamics. Temporally some discontinuities occur for which the underlying processes cannot be definitely identified. Further simulations aim to combining hydraulic and geoelectrical simulations to obtain a better constrained inverse problem and get an improved understanding of the drainage and imbibition processes.

5 MITIGATION BY WATER INJECTION AND CO_2 WITHDRAWAL (TNO)

5.1 Introduction

In Deliverable 3.2 "Adaptation of injection strategy as flow diversion option" two critical scenarios were created in which unwanted migration of CO_2 appeared. These scenarios serve as the base case for the mitigation simulations using brine/water injection and/or CO_2 withdrawal considered in this part of the report.

For completeness the setup and the description of the Johansen model described in Deliverable D3.2 is included in this report. In the next section the reservoir simulator is described including the critical scenarios.

5.1.1 Description of the Johansen formation

The field under consideration for this study is the Johansen formation, located off the coast of Norway (Figure 55). The aquifer is located at a depth of 2100-2400 m with an average thickness of roughly 100m (Eigestad et al, 2009, Christiansen et al, 2009). The lateral extent is about 100 km in the North-South direction and 60 km in the east-west direction. The average porosity is approximately 20-25 percent and permeability ranging from 64 to 1660 mDarcy. A theoretical storage capacity of >1Gton is estimated by Eigestad et al. (2009).

The area of most interest is around the Troll field (red lines in Figure 55), which is located in the upper part of the aquifer. In this way the storage project can benefit from most of the existing infrastructure and is also close to the CO_2 source in Mongstad.

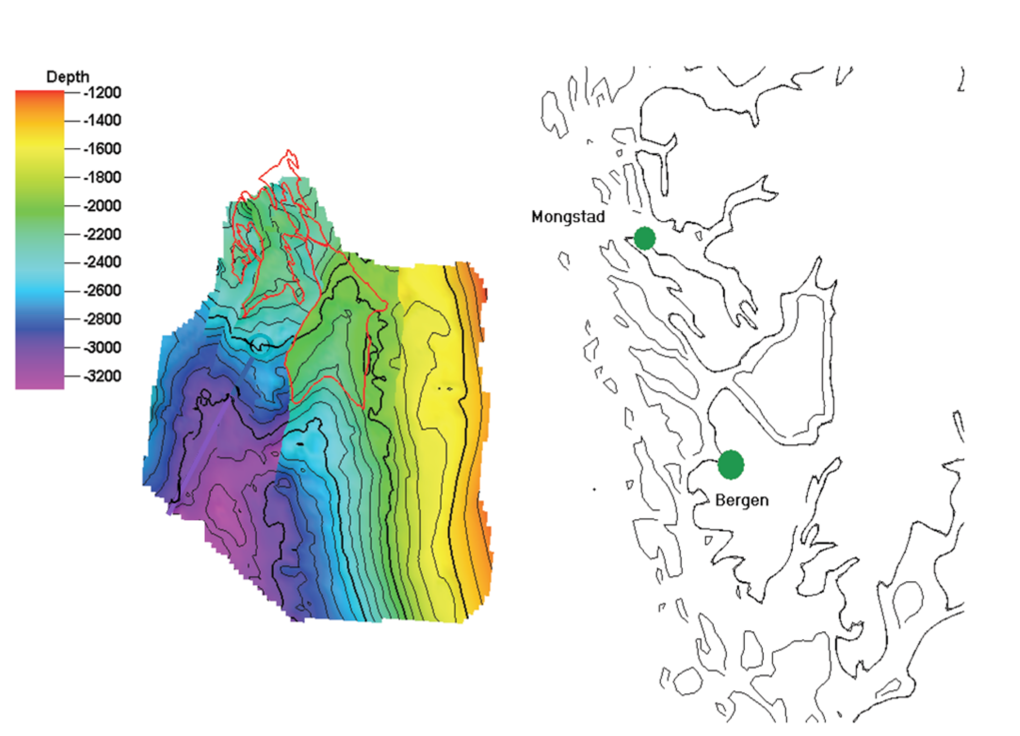

Figure 55 Depth map of the top of the Johansen formation and its location, with respect to the coast of Norway. (from Bergmo et al, 2009).

5.2 Method

In Deliverable 3.2 "Adaptation of injection strategy as flow diversion option" two critical scenarios were created in which unwanted migration of CO_2 appeared. These scenarios serve as a base case for the mitigation by brine/water injection as a flow diversion option.

5.2.1 Simulator used Schlumberger's Eclipse 100 black-oil simulator

For the dynamic modeling of the Johansen field we have used Schlumberger's Eclipse black-oil simulator (also known as Eclipse

Table 13: Overview of grid dimensions in the simulation model.

	Number grid blocks x-direction NX	Number grid blocks y-direction NY	Number grid blocks z-direction NZ	Total number of grid blocks	Number of activegrid blocks
Dynamic grid	55	281	83	995,170	526,272

100). The Eclipse black-oil reservoir simulation software is a fully implicit, three-phase, three-dimensional, general purpose black-oil simulator. The black-oil model assumes that the reservoir fluids consist of three phases namely oil, water, and gas, with gas dissolving in oil. In our model we only enabled the water and the gas phases, representing water and CO_2 respectively. Dissolution of CO_2 is not considered.

The geological grid used in this study is described by Bergmo et al (2008). In this report we focus on a smaller area of the Johansen field and a section was made inactive, which can be seen in the number of grid blocks used in the final dynamic model.

5.2.2 Pressure, Volume, Temperature (PVT) data

5.2.2.1 Gas PVT

For the Gas PVT we applied NIST data to generate tables based on an aquifer temperature of 94 oC (Bergmo et al, 2008).
The gas viscosity and the formation volume factor as function of pressure of the pure CO_2 are shown in Figure 56 and Figure 57, respectively.

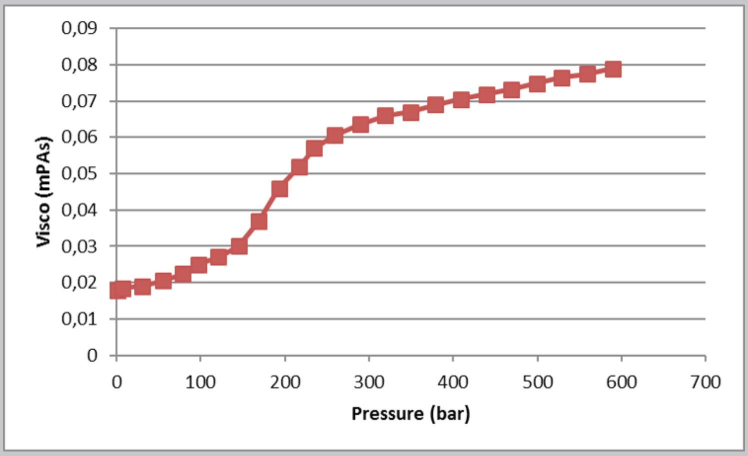

Figure 56 Viscosity of pure CO_2 as function of pressure, at a temperature of 94 °C.

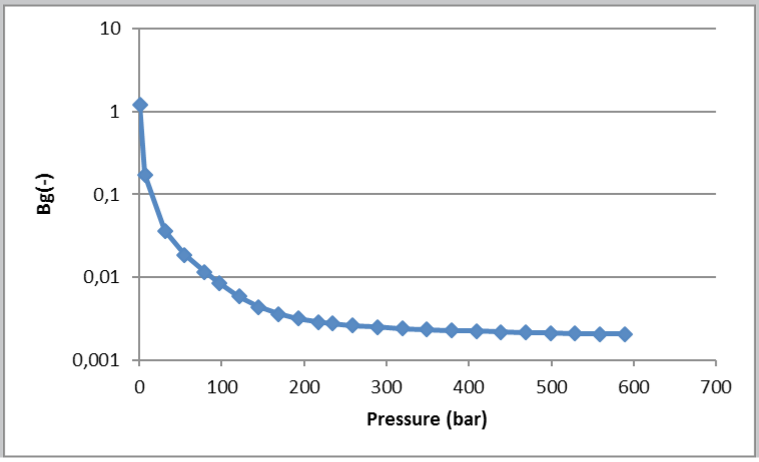

Figure 57 Reservoir volume factor (BG) versus pressure, at a temperature of 94 °C

5.2.2.2 Water PVT

The water formation volume factor is 1.0132 rm^3/sm^3 at reservoir conditions at a reference pressure of 215 bar. The water compressibility at reservoir conditions is $3.97954*10^{-5}$/bar. The water viscosity is 0.39851 (mPas) at a reference pressure of 215 bar.

5.2.3 Saturation functions and pressure dependent rock properties

5.2.3.1 Relative permeability

The relative permeability-saturation curves for the carbon dioxide were made hysteretic, by using the EHYSTER keyword in the Eclipse reservoir simulation software, with an entrapped non-wetting fluid saturation of 0.1 while those of the wetting fluid (brine) were left non-hysteretic (see Figure 58). This means that below a minimum CO_2 saturation (0.1 in this case), the gaseous phase is considered to be discontinuous and the relative permeability of the CO_2 phase goes to zero.

5.2.3.2 Capillary pressure

In our modelling we assumed the capillary pressure does not play an important role and was set to 0.

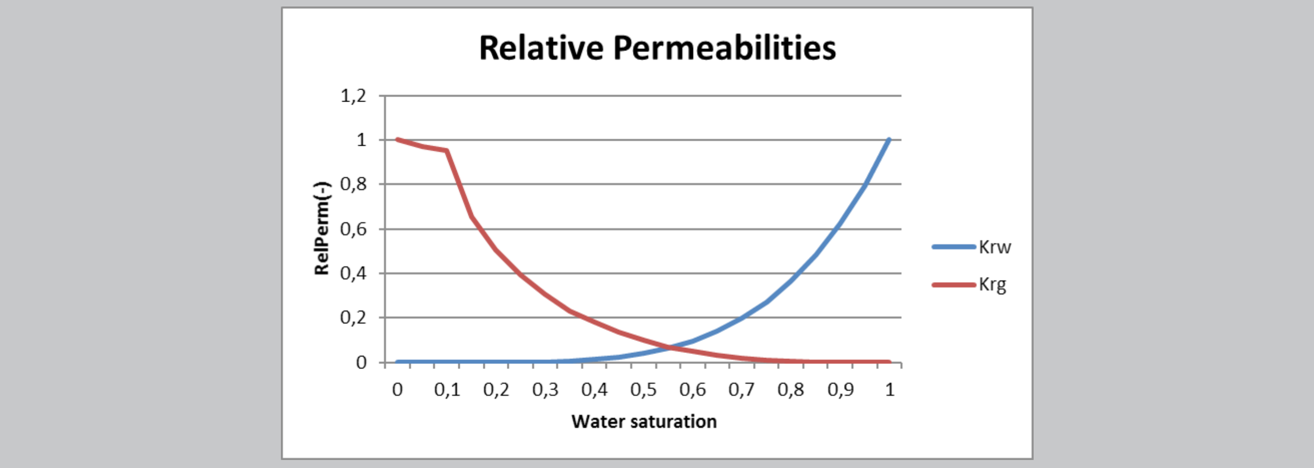

Figure 58 Original non-hysteretic relative permeability values, (based on a Dutch aquifer).

5.2.3.3 Rock Compressibility

The rock compressibility is set to standard value of 5.0e-5 1/bar at a reference pressure of 200 bar

5.2.4 Initial conditions

The starting point of the reservoir model was a static geological model of the Johansen aquifer, as supplied by Bergmo et al, 2008. From the complete model geological model only the western section was used with a total of 63x183x36 grid cells.

The reservoir is initially assumed to be in hydrodynamic equilibrium with a reservoir pressure of 220 bar at a depth of 2200 m and a reservoir temperature of 94 °C. We used an isothermal model, hence all temperature dependent fluid and rock properties are specified at reservoir temperature.

5.2.5 Well Locations

In all simulations 1.1 Mton CO_2 per year was injected for 113 years in layer 15-18 (which is the Johansen formation) of the model. Various injection locations were chosen and the resulting migration paths investigated for critical issues concerning the storage compartment integrity. To allow enough time for the migration the modelling was continued until the year 9000. The various injection locations are displayed in Figure 59.

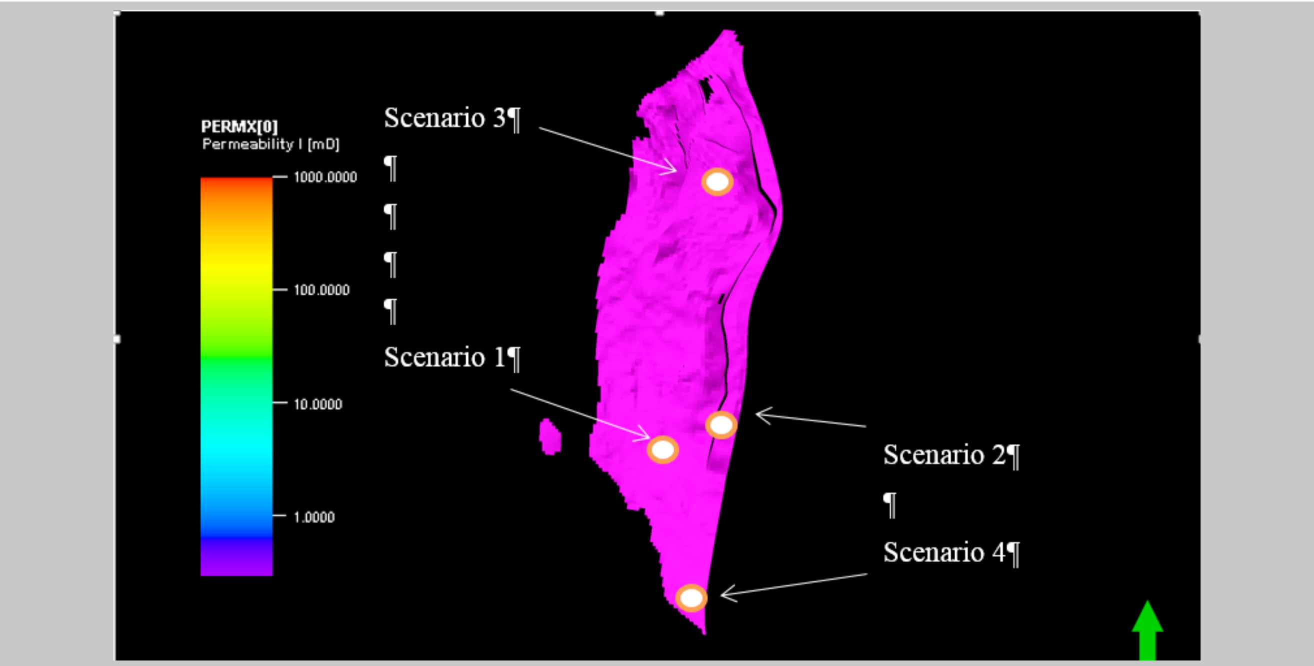

Figure 60 (top) Permeability (scale see Figure 61) (lower left) Sideview CO_2 migration after injection and (lower right) CO_2 migration top view after injection.

5.2.6 Critical scenarios

5.2.6.1 Critical Scenario 1

In scenario 1 a well is placed down dip from a fault and the CO_2 starts migrating to the fault (Figure 60). We assume in this scenario the fault appears to be not sealing or safe and therefore corrective measures are needed.

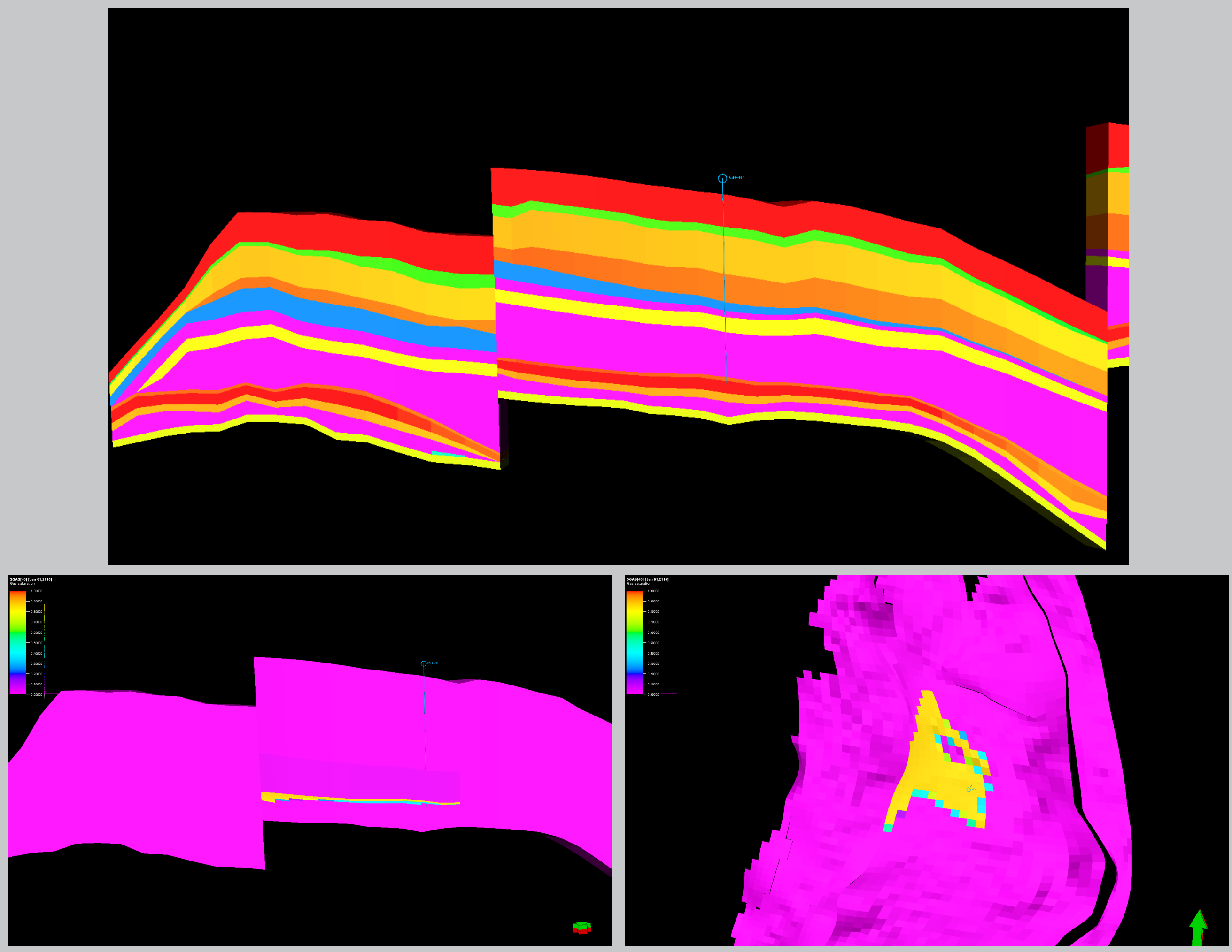

Figure 60 (top) Permeability (scale see Figure 61) (lower left) Sideview CO_2 migration after injection and (lower right) CO_2 migration top view after injection.

5.2.6.2 Critical Scenario 2

In the second critical scenario the injection well is placed in the eastern part of the model, close to a major fault. During injection the plume migrates from injector to the north along the fault with a large offset. These faults are usually sealing due to clay smearing.

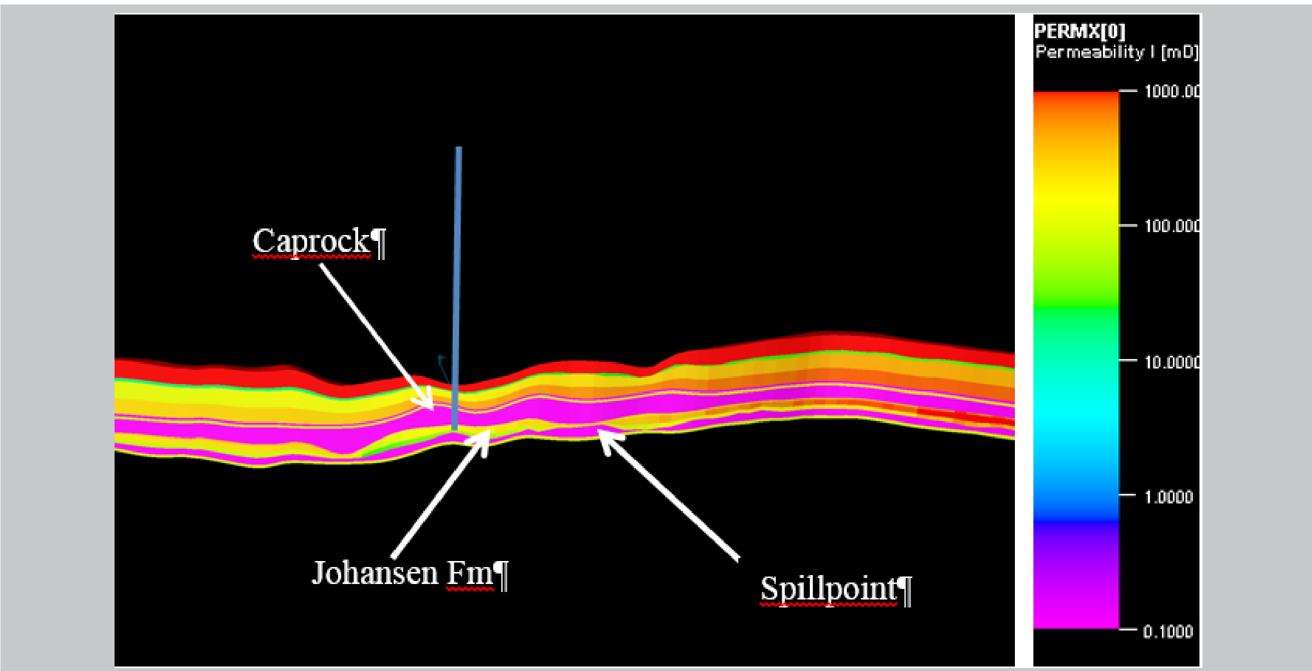

Figure 61 Permeability of scenario 2.

In our simulation we considered the migration along a fault not as a risk and no corrective measure is necessary. In Figure 61 we observed that the Johansen formation varies in thickness laterally and becomes very thin just north of the injection well (Figure 61). We identified this as a spill-point and the anticipated storage location is before the thin zone, where a pinch out almost occurs. Immediately after the injection period the CO_2 migrated within the intended storage zone (Figure 62). However after a longer period (now 9000 years is shown) the CO_2 migrated further to the north beyond the spill point. An unwanted migration and a corrective measure is needed here.

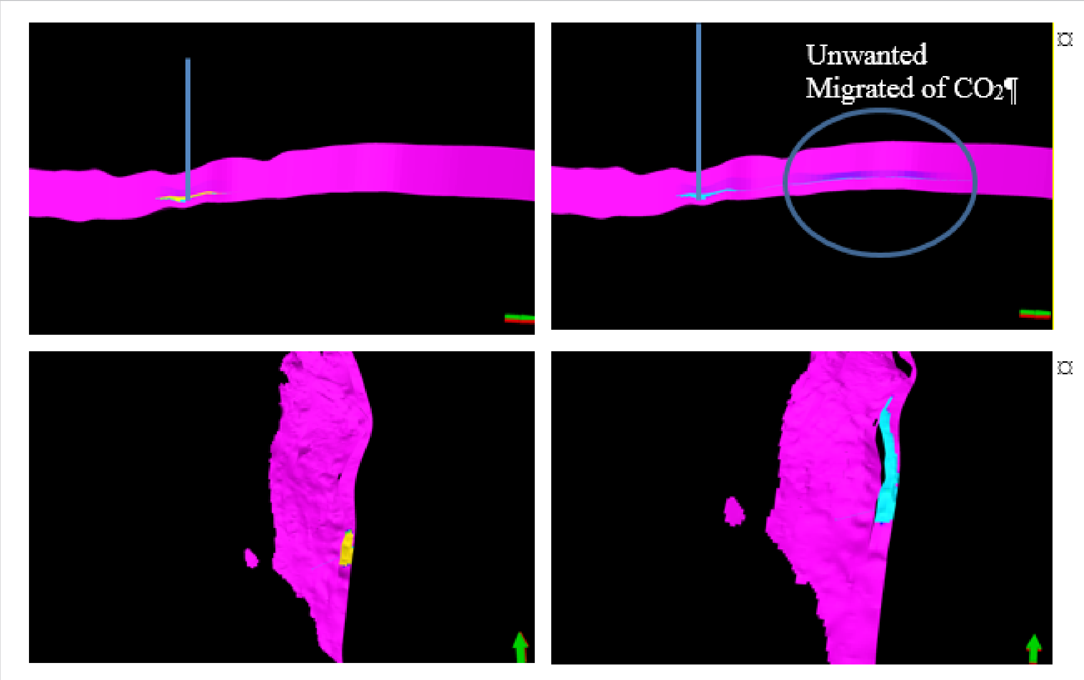

Figure 62 Gas saturation in scenario 2. Sideview directly after injection (top left) and after 9000 years (top right). Topview directly after injection (bottom left) and after 9000 years (bottom right).

5.3 Results

5.3.1 Critical scenario 1

In critical scenario 1 the CO_2 is migrating into the direction of the fault, since the fault appears to be not sealing, a safety area around the fault is defined which we consider as unwanted migration, as shown in Figure 63.

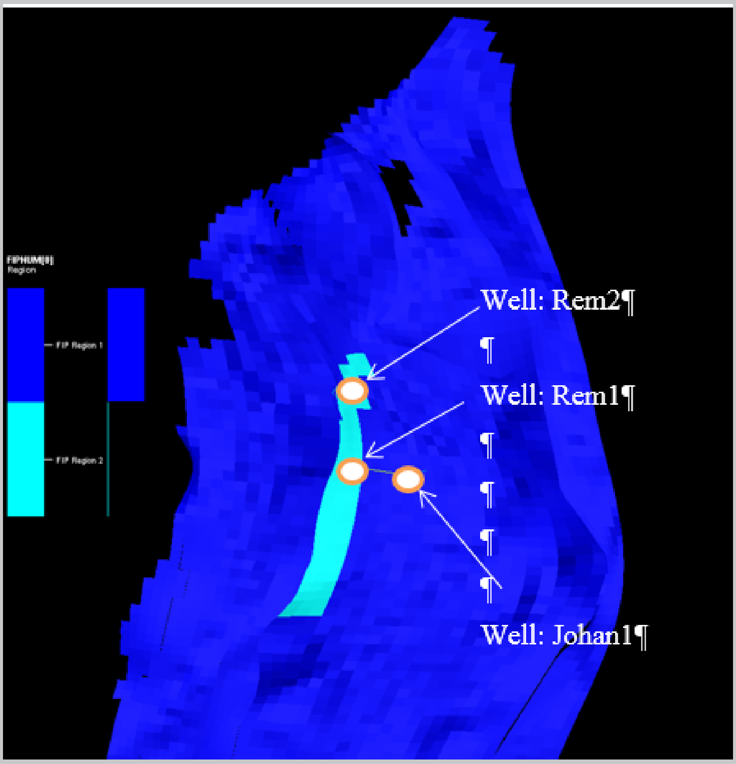

Figure 63 Safety area along the fault indicated in light blue and the CO_2 injection well Johan1 and the remediation wells Rem1, and Rem2.

An injection rate of 1Mton/yr was applied on the Johan1 well, after 17 years of injection unwanted migration was detected and the injection was stopped. The base case scenario is the "do nothing" scenario. No remediation is performed by water injection, but just monitoring of the CO_2 volumes migrating into the safety area defined in Figure 63. By comparing the mitigation scenarios to the base case scenario, it is possible to identify how efficient the mitigation strategy is. A short description of the mitigation scenarios is given in Table 14 and full results of the mitigation scenarios are given in Section 5.5 Appendix. The summary of the results is presented in the present section.

Table 14 Description of the mitigation scenarios.

Name scenario	Description	Injection control & production rate
Base Case	Injection of 1Mton/yr CO_2 for 17 years and no water injection by the remediation wells, CO_2 is monitored for the whole simulation period (91 years)	
Scenario 1	After detection of unwanted migration of CO_2, CO_2 injection stopped and injection of water by one remediation well for 64 years	BHP constraint (10% above initial pressure, approximately 20.000 m^3/day)
Scenario 2	After detection of unwanted migration of CO_2, CO_2 injection stopped and injection of water by two remediation wells for 64 years	BHP constraint (10% above initial pressure, approximately 40.000 m^3/day)
Scenario 3	After detection of unwanted migration of CO_2, CO_2 injection stopped and injection of water by two remediation wells for 64 years and the second remediation well after 30 years.	BHP constraint (10% above initial pressure, approximately 20.000 m^3/day)
Scenario 4	After detection of unwanted migration of CO_2, CO_2 injection stopped and injection of water for 5 years by one remediation well	BHP constraint (10% above initial pressure, approximately 20.000 m^3/day)
Scenario 5	After detection of unwanted migration of CO_2, CO_2 injection stopped and injection of water for 10 years by one remediation well	BHP constraint (10% above initial pressure, approximately 20.000 m^3/day)
Scenario 6	After detection of unwanted migration of CO_2, CO_2 injection stopped and injection of water for 18 years by one remediation well	BHP constraint (10% above initial pressure, approximately 20.000 m^3/day)
Scenario 7	After detection of unwanted migration of CO_2, CO_2 injection stopped and back production started for a period of 50 years (gas rate constraint of 1 Mton/yr). Injection of water for 18 years by one well.	BHP constraint (10% above initial pressure, approximately 20.000 - 90.000 m^3/day)
Scenario 8	After detection of unwanted migration of CO_2, CO_2 injection stopped and back production started for a period of 50 years (gas rate constraint of 0.5Mt/yr). Injection of water for 18 years by one well.	BHP constraint (10% above initial pressure, approximately 20.000 - 90.000 m^3/day)
Scenario 9	After detection of unwanted migration of CO_2, CO_2 injection stopped and back production started for a period of 50 years (gas rate constraint of 1 Mton/yr). Injection of water for 10 years by one well.	BHP constraint (10% above initial pressure, approximately 20.000 - 90.000 m^3/day)
Scenario 10	After detection of unwanted migration of CO_2, CO_2 injection stopped and back production started for a period of 50 years (gas rate constraint of 1 Mton/yr). Injection of water for 10 years by one well.	5000 m^3/day

The efficiency of the scenarios is defined as combination of the amount of water injected versus how much CO_2 has reached the safety zone around the fault (and is assumed to migrate to the fault). The safety zone is defined in Eclipse by the FIPNUM keyword and the CO_2 in this zone can be traced by the regional gas in place (RGIP) keyword. In Figure 63 the CO_2 volumes migrating into this safety zone is given for each individual scenario.

The base case scenario shows obviously the highest leakage rate. Scenarios 4, 5 & 6 also show relatively high leakage rates (see Figure 64) compared to the other scenarios (scenario 1- 3 and 7-10). The reason for this is that these 3 scenarios have only 5, 10 and 18 years of water injection during the remediation period, which is relatively short compared to scenario 1-3. Obviously in scenario 7-10 back production of the CO_2 gives a lower migration to the fault.

Table 15 Results of the mitigation scenarios.

	% of the total amount of CO_2 injected migrated to the safety zone	total CO_2 leakage (Mton)	Cum CO_2 back produced
Base_Case	15.42%	2.62	0.00%
Remediation_1	0.98%	0.17	0.00%
Remediation_2	0.28%	0.05	0.00%
Remediation_3	0.18%	0.03	0.00%
Remediation_4	12.06%	2.05	0.00%
Remediation_5	10.35%	1.76	0.00%
Remediation_6	8.00%	1.36	0.00%
Remediation_7	0.17%	0.03	66.79%
Remediation_8	0.17%	0.03	62.54%
Remediation_9	0.17%	0.03	68.34%
Remediation_10	0.40%	0.07	70.97%

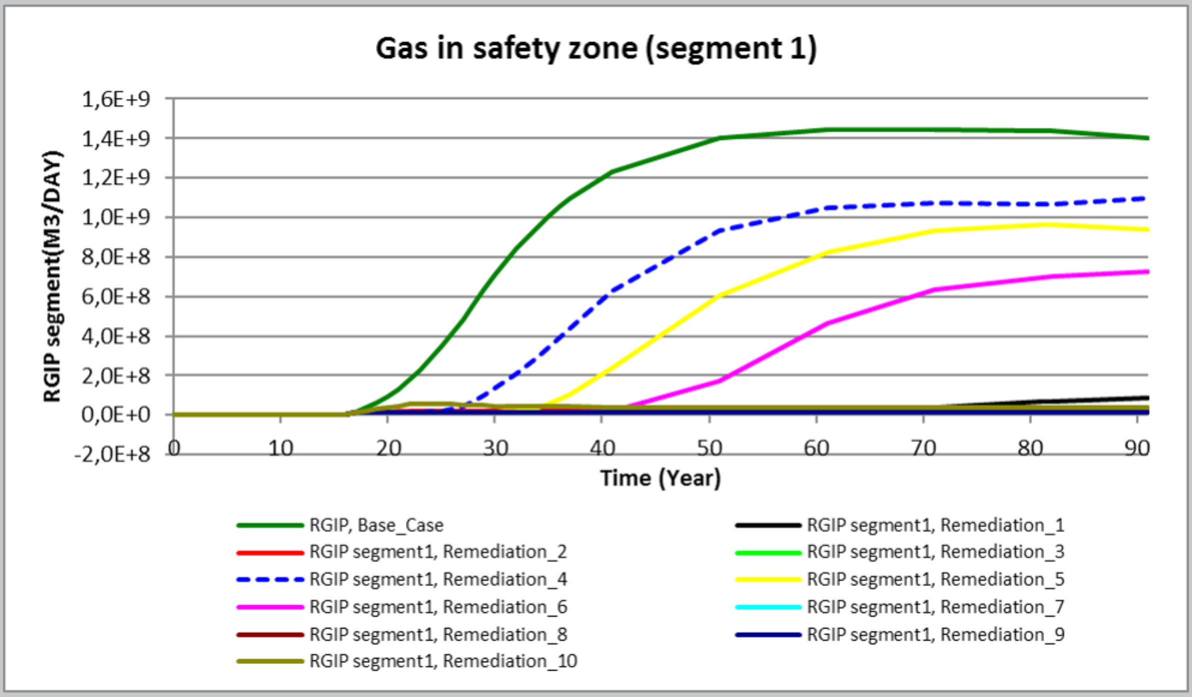

Figure 64 Gas in segment safety zone around the fault. Once the gas is in the safety area it is assumed to migrate to the fault.

The scenarios shows that injection of water for a short period is not a good remediation method for CO_2 leakage. It will only postpone the leakage and reduce the total amount of CO_2 migration for a few percent as can be seen in Table 15. The remediation method can be improved significantly by not only injecting water but also or back producing of the CO_2, which is performed in scenario 7-10.

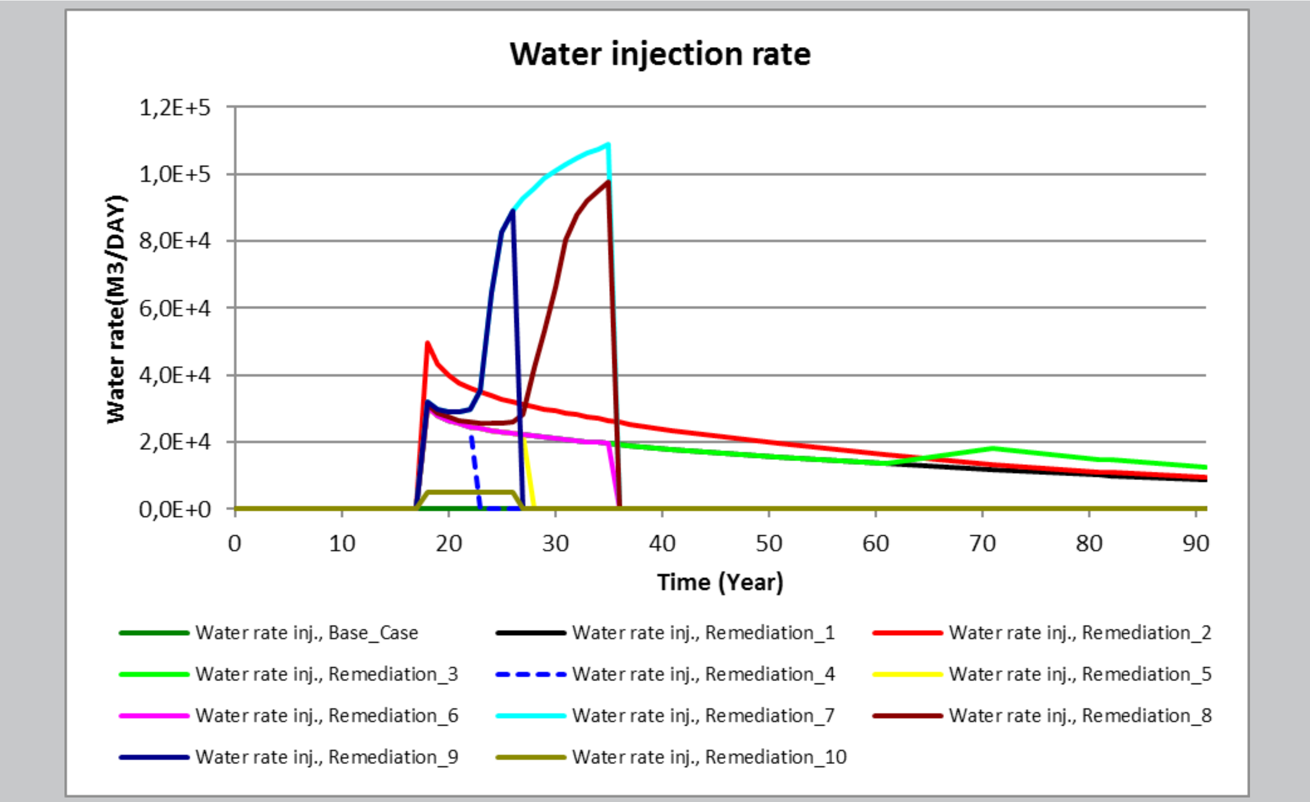

Figure 65 Water injection rate for the different mitigation scenarios.

The results of Table 17 shows that the amount of CO_2 remediation by water injection is not an efficient option and the combination of back production and water injection is the most optimal approach.

5.4 Conclusions

After CO_2 leakage is observed the remediation technique by water injection only is not efficient and back production in combination with water injection is the most efficient option to avoid further migration of the CO_2 present in the aquifer near the spill point or fault.

6 SUMMARY AND CONCLUSIONS

SINTEF

Simulations were performed of CO_2 migration along a ridge structure in the Johansen aquifer, with water injection as a mitigation measure. Twenty-one combinations of CO_2 injection rate, permeability and reservoir depth were simulated.
It was shown that water injection effectively stops CO_2 migration but does not provide a long-lasting effect, lasting only from 1.4 to 7 years. Since migration of injected CO_2 will continue over many hundred years, water injection cannot be considered a long-term solution.

Obviously lower permeability will reduce the migration rate, but in addition it was seen that low permeability, especially with high CO_2 injection rates cause the flow to become much more diffuse, thereby by-passing the water injector and potentially reducing its mitigating effect.

No consistent trend in leakage reduction was observed due to variations in reservoir depth.

Imperial College

Using a generic model, Imperial College have studied the reduction of CO_2 leakage through a sub-seismic fault by means of water injection via the well previously used for CO_2 injection.

The results have shown that brine injection causes an increase in CO_2 dissolution which consequently reduces the amount of mobile CO_2 available for leakage.

For distances of 1km and 2km between the injector and the fault it appears that brine injection effectively stops leakage of CO_2 via the sub-seismic fault. For the 3km fault scenario however, there is a reduction in the amount of CO_2 leakage but it is not stopped.

Brine injection has the effect of retaining higher CO_2 saturation in the reservoir.

Further investigation of the 3km fault scenario by changing the injection rate and the injection period suggested that there is only a limited benefit longer term brine injection.

GFZ

The results from an actual water injection test on a former injection well on the Ketzin field were modelled and analysed. Water injection for three months prevented CO_2 from re-entering the well for two months.

A numerical simulation was prepared and calibrated with the injection history, but while this matched the bottom-hole pressure response will during the previous CO_2 injection phase, it did not predict correctly the significant pressure increase and fluctuations during water injection. Further work on the model is required.

Geo-electrical monitoring was found to reproduce the general trend of higher electrical conductivity due to higher brine concentration and showed good correlation with the injection dynamics.

TNO

Four injection locations were chosen near a major fault or a spill point in the Johansen formation to investigate mitigation of CO_2 migration. Remedition wells were used to inject water for up to 64 years and back-production of CO_2 was also applied in some cases. A base case and 10 remediation scenarios were simulated.

It was concluded that after CO_2 leakage is observed, the remediation technique by water injection only is not efficient and the addition of back-production of CO_2 is the most effective option to avoid further migration of the CO_2 present in the aquifer near the spill point or fault.

References

Anchliya A., Ehlig-Economides C. and Jafarpour B., 2012. "Aquifer management to accelerate CO_2 dissolution and trapping",SPE 126688.

Bachu, S. & Bennion, B. (2008), 'Effects of in-situ conditions on relative permeability characteristics of CO_2-brine systems', Environmental Geology 54, 1707-1722.

Element Energy, 2012. Economic impacts of CO_2-enhanced oil recovery for Scotland - Final report, https://www.scottish-enterprise.com/knowledge-hub/articles/publication/co2-enhanced-oil-recovery.

IEAGHG, 2011. Global storage resources gap analysis for policy makers, Report 2011/10, September, 2011.

Kuuskraa V., Gedec M., 2007, Remediation of leakage from CO_2 storage reservoirs, IEA GHG report 2997/11.

Möller, F.; Liebscher, A. & Schmidt-Hattenberger, C. (2016), 'Report on the dataset of the Brine Injection at the CO_2 Storage Pilot Site Ketzin, Germany'(16/05), Technical report, GFZ German Research Centre for Geosciences.

Norwegian Petroleum Directorate, 2014, "CO_2 Storage Atlas, Norwegian Continental Shelf", ISBN 978-82-7257-134-3.

Omorgie Z.S., King G.R., Strang C., Hodgson P. & Pressney R.A, 1995, "Reservoir management in the Ninian field – a case history", SPE 30443.

Qi R., LaForce T.C. and J. Blunt M.J., 2009. "Design of carbon dioxide storage in aquifers." International Journal of Greenhouse Gas Control, 3.2: 195-205.

Rippe, D., Bergmann, P., Labitzke, T., Wagner, F. M., Schmidt-Hattenberger, C. (2016): Surface-downhole and crosshole geoelectrics for monitoring of brine injection at the Ketzin CO_2 storage site. Geophysical Research Abstracts, 18, EGU2016-15388, EGU General Assembly 2016.

Schmidt-Hattenberger, C.; Bergmann, P.; Kießling, D.; Krüger, K.; Rücker, C. & Schütt, H. (2011). Application of a Vertical Electrical Resistivity Array (VERA) for monitoring CO_2 migration at the Ketzin site: First performance evaluation Energy Procedia, 2011, 4, 3363-3370.

USEPA, 2010. Geologic CO_2 Sequestration Technology and Cost Analysis, technical support documents. https://www.epa.gov/sites/production/files/2015-07/documents/support_uic_co2_technologyandcostanalysis.pdf.

Wiese, B.; Böhner, J.; Enachescu, C.; Würdemann, H. & Zimmermann, G. (2010), Hydraulic characterisation of the Stuttgart formation at the pilot test site for CO_2 storage, Ketzin, Germany, International Journal of Greenhouse Gas Control 4, 960-971.

Wiese, B.; Wagner, F.; Norden, B. & Schmidt-Hattenberger, C. (in short), Fully coupled hydrogeophysical inversion of hydraulics, gas pressure and geoelectric, Energy Procedia, GHGT Lausanne.

APPENDIX

Table 16 Summary of the results of the mitigation scenarios.

	Total Water injected (SM3)	CO_2 in segment 1 (SM3)	CO_2 leaked to segment 2 (SM3)	total CO_2 leakage reduction (SM3)	total CO_2 in reservoir (SM3)	Cum water back produced (SM3)	Cum CO_2 back produced (SM3)
Base_Case	0.00E+00	7.69E+09	1.40E+09	0.00E+00	9.09E+09	0.00E+00	0.00E+00
Remediation_1	4.30E+08	9.00E+09	8.93E+07	1.31E+09	9.09E+09	0.00E+00	0.00E+00
Remediation_2	5.57E+08	9.06E+09	2.59E+07	1.38E+09	9.09E+09	0.00E+00	0.00E+00
Remediation_3	4.95E+08	9.07E+09	1.68E+07	1.38E+09	9.09E+09	0.00E+00	0.00E+00
Remediation_4	5.15E+07	7.99E+09	1.10E+09	3.05E+08	9.09E+09	0.00E+00	0.00E+00
Remediation_5	9.40E+07	8.15E+09	9.41E+08	4.60E+08	9.09E+09	0.00E+00	0.00E+00
Remediation_6	1.55E+08	8.36E+09	7.27E+08	6.74E+08	9.09E+09	0.00E+00	0.00E+00
Remediation_7	4.83E+08	3.00E+09	1.54E+07	1.39E+09	3.02E+09	1.74E+09	6.07E+09
Remediation_8	3.18E+08	3.39E+09	1.56E+07	1.39E+09	3.40E+09	1.46E+09	5.68E+09
Remediation_9	1.48E+08	2.86E+09	1.51E+07	1.39E+09	2.87E+09	1.60E+09	6.21E+09
Remediation_10	1.64E+07	2.60E+09	3.65E+07	1.37E+09	2.64E+09	1.53E+09	6.45E+09

A-1 REMEDIATION SCENARIO 1

Table 17 Scenario description.

Scenario	**Remediation 1**
Description	After detection of unwanted migration of CO_2, CO_2 injection stopped and injection of water by remediation well for 64 years (whole simulation period)

Table 18 Simulation settings.

General		Remarks
Begin simulation	0	(year)
End simulation	91	(year)
CO_2 Injection well	**JOHAN1**	
Constraints	Rate constraint: 1 Mton/yr BHP constraint 360*BAR	
Location	Vertical well in gridblock (x,y)→(45, 47)	
Perforation	Z-coordinates of gridblock (15-17)	
On stream	From 0 to 17 years	
Remediation well	REM 1	
Constraints	BHP constraint 234*BAR (10% above P initial)	
Location	Vertical well in gridblock (x,y)→(38, 47)	
Perforation	Z-coordinates of gridblock (15-17)	
On stream	From 18 to 91 years	

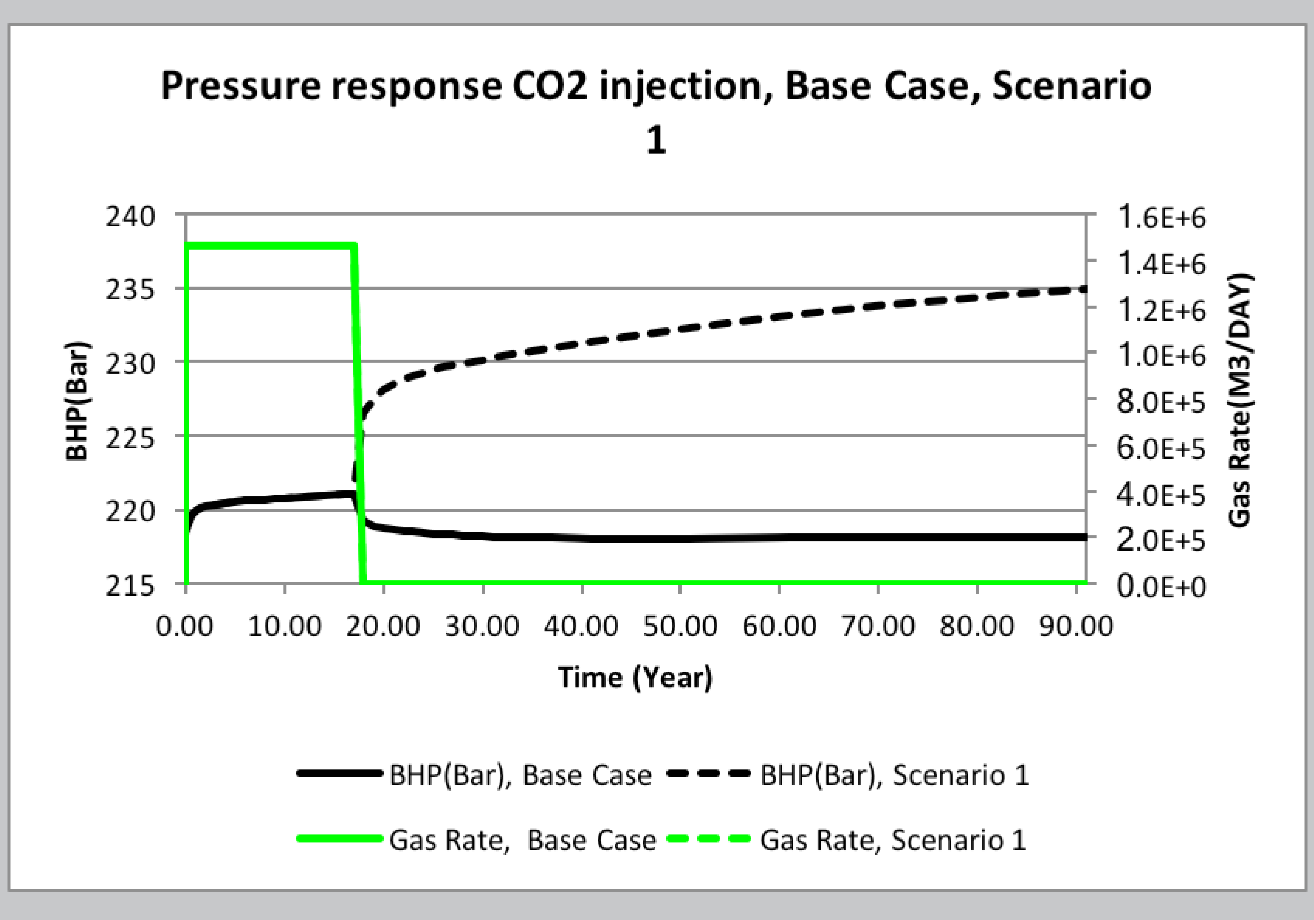

Figure 66 Gas injection rate and pressure response, compared to the base case (no remediation).

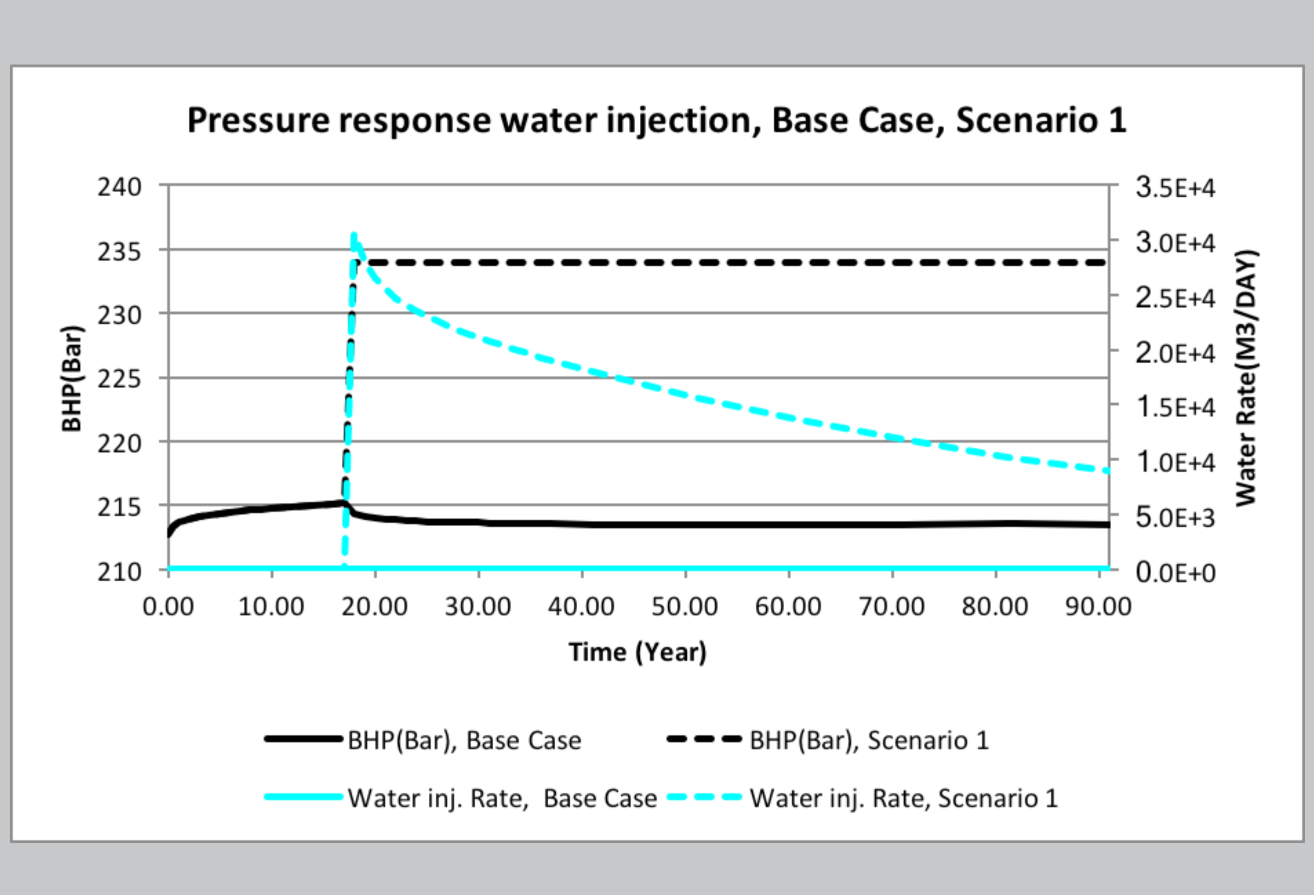

Figure 67 Water injection rates and cumulatives of well REM1, compared to the base case (no remediation) scenario.

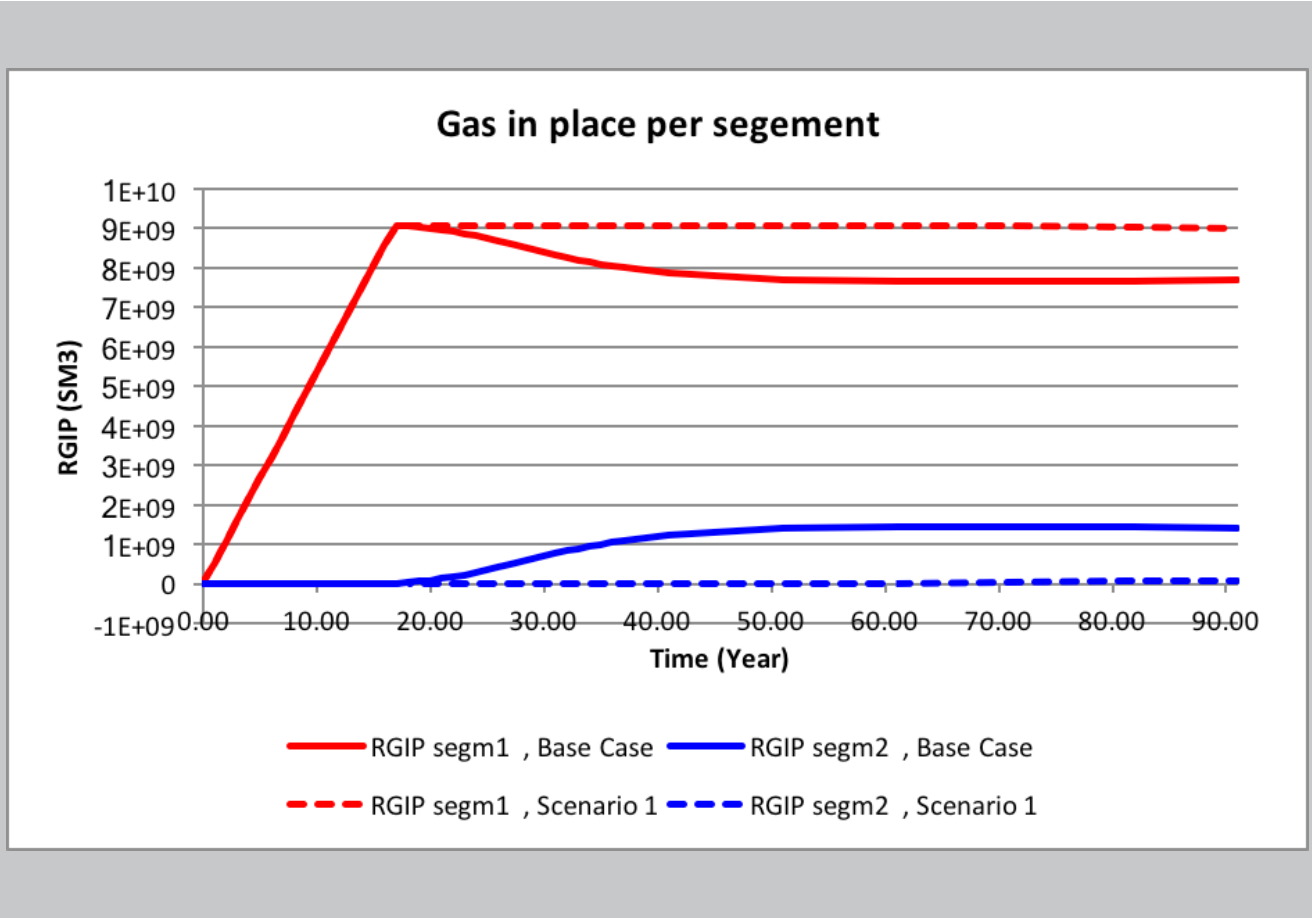

Figure 68 Unwanted migration to segment 2 compared to the base case (no remediation) scenario.

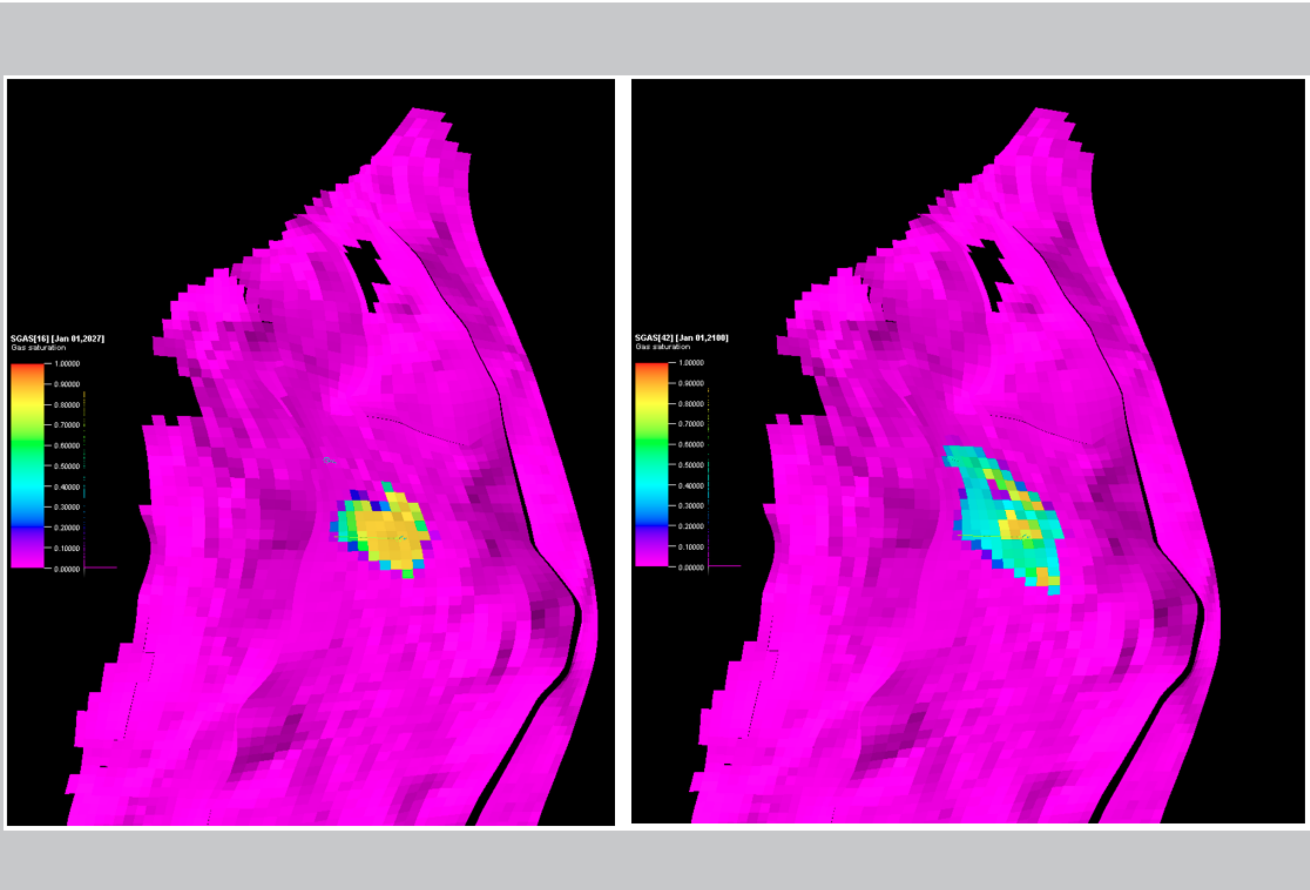

Figure 69 CO_2 plume after first detection of unwanted migration (right) CO_2 plume after 93 years

A-2 REMEDIATION SCENARIO 2

Table 19: Scenario description.

Scenario	Remediation 2
Description	After detection of unwanted migration of CO_2, CO_2 injection stopped and injection of water by two remediation wells for 64 years (whole simulation period)

Table 20 Simulation settings.

General		Remarks
Begin simulation	0	(year)
End simulation	91	(year)
CO_2 Injection well	**JOHAN1**	
Constraints	Rate constraint: 1 Mton/yr BHP constraint 360*BAR	
Location	Vertical well in gridblock (x,y)→(45, 47)	
Perforation	Z-coordinates of gridblock (15-17)	
On stream	From 0 to 17 years	
Remediation well	REM 1	
Constraints	BHP constraint 234*BAR (10% above P initial)	
Location	Vertical well in gridblock (x,y)→(38, 47)	
Perforation	Z-coordinates of gridblock (15-17)	
On stream	From 18 to 91 years	
Remediation well	REM 2	
Constraints	BHP constraint 234*BAR (10% above P initial)	
Location	Vertical well in gridblock (x,y)→(40, 40)	
Perforation	Z-coordinates of gridblock (15-17)	
On stream	From 18 to 91 years	

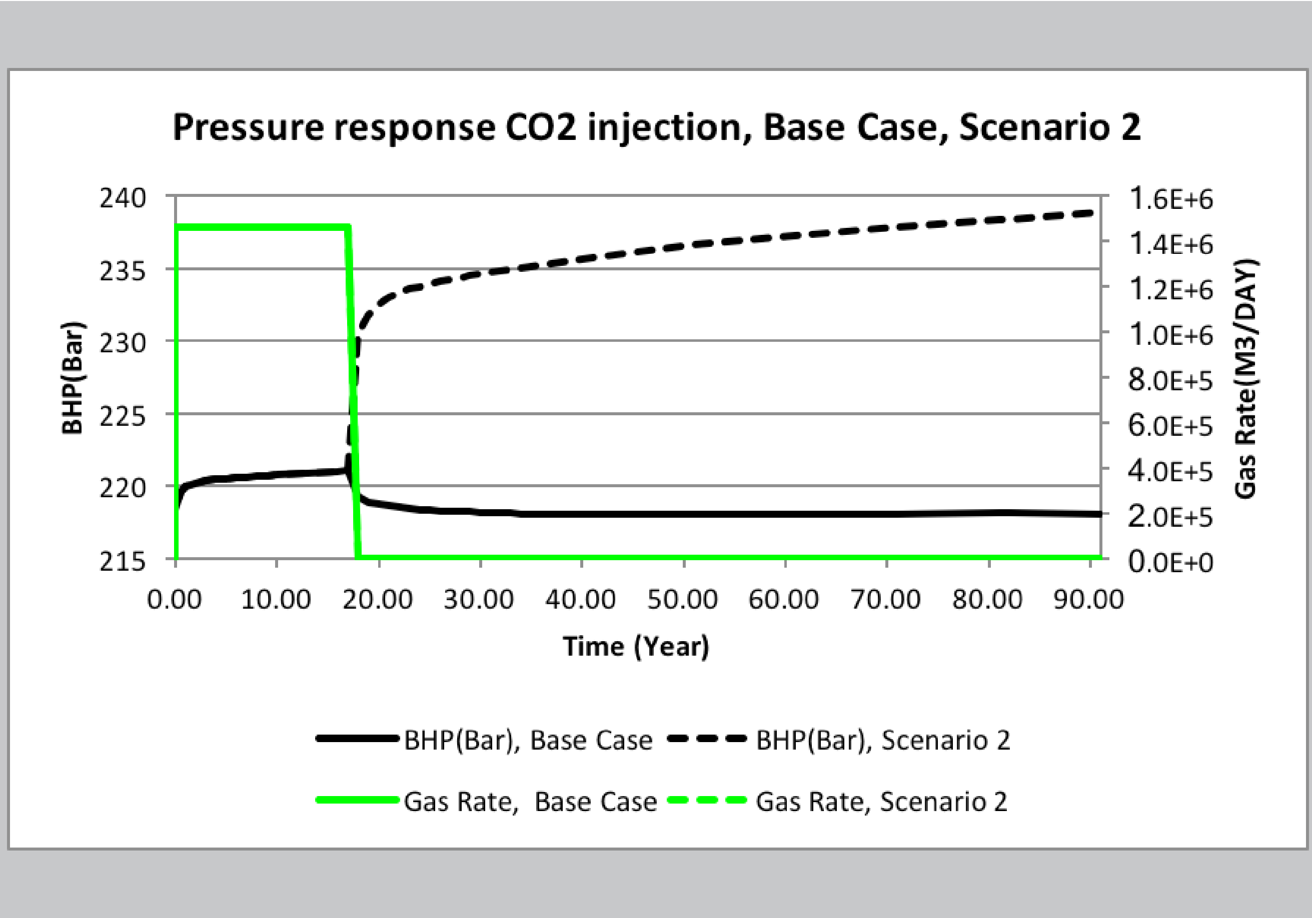

Figure 70 Gas injection rate and pressure response, compared to the base case (no remediation).

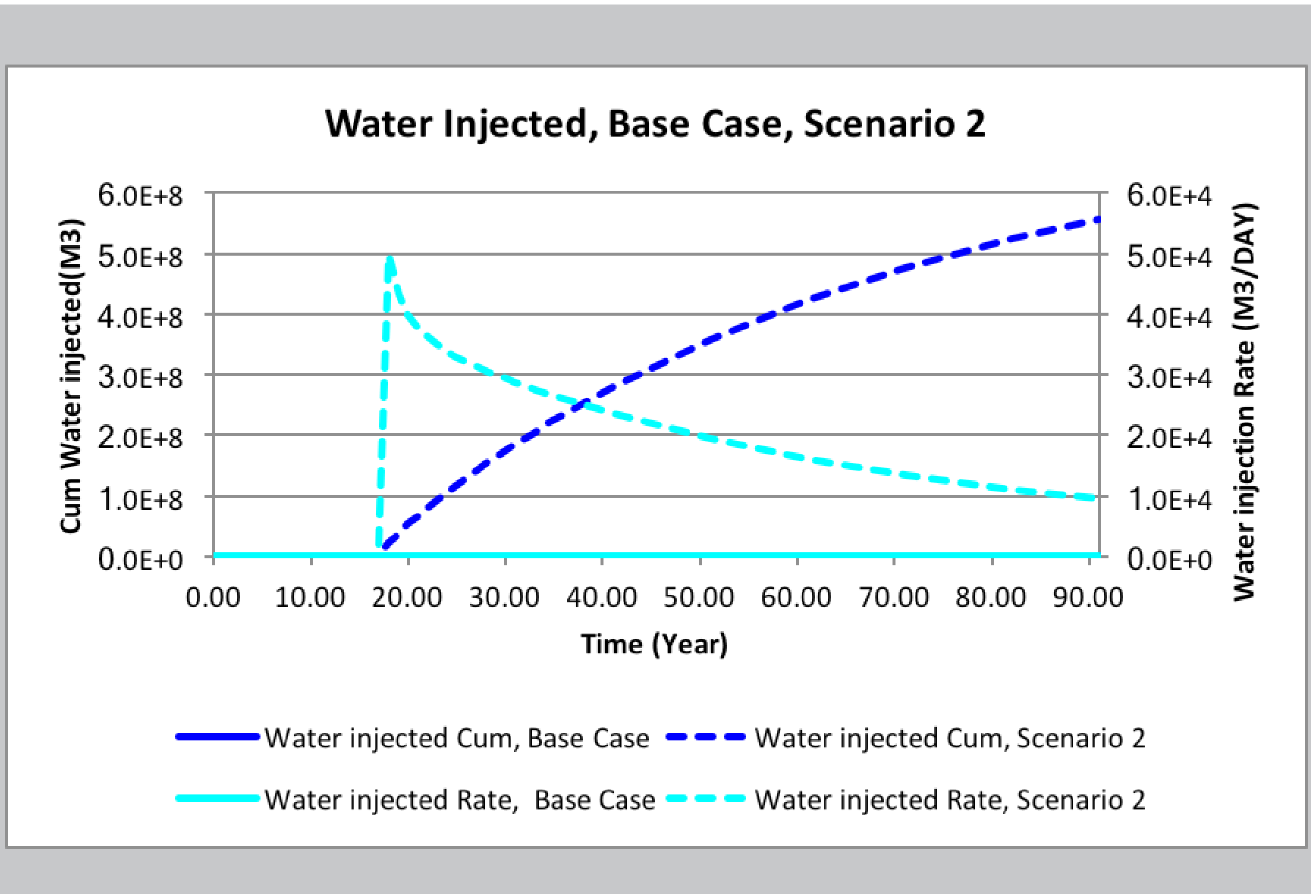

Figure 71 Water injection rates and cumulatives of well REM1, compared to the base case (no remediation) scenario.

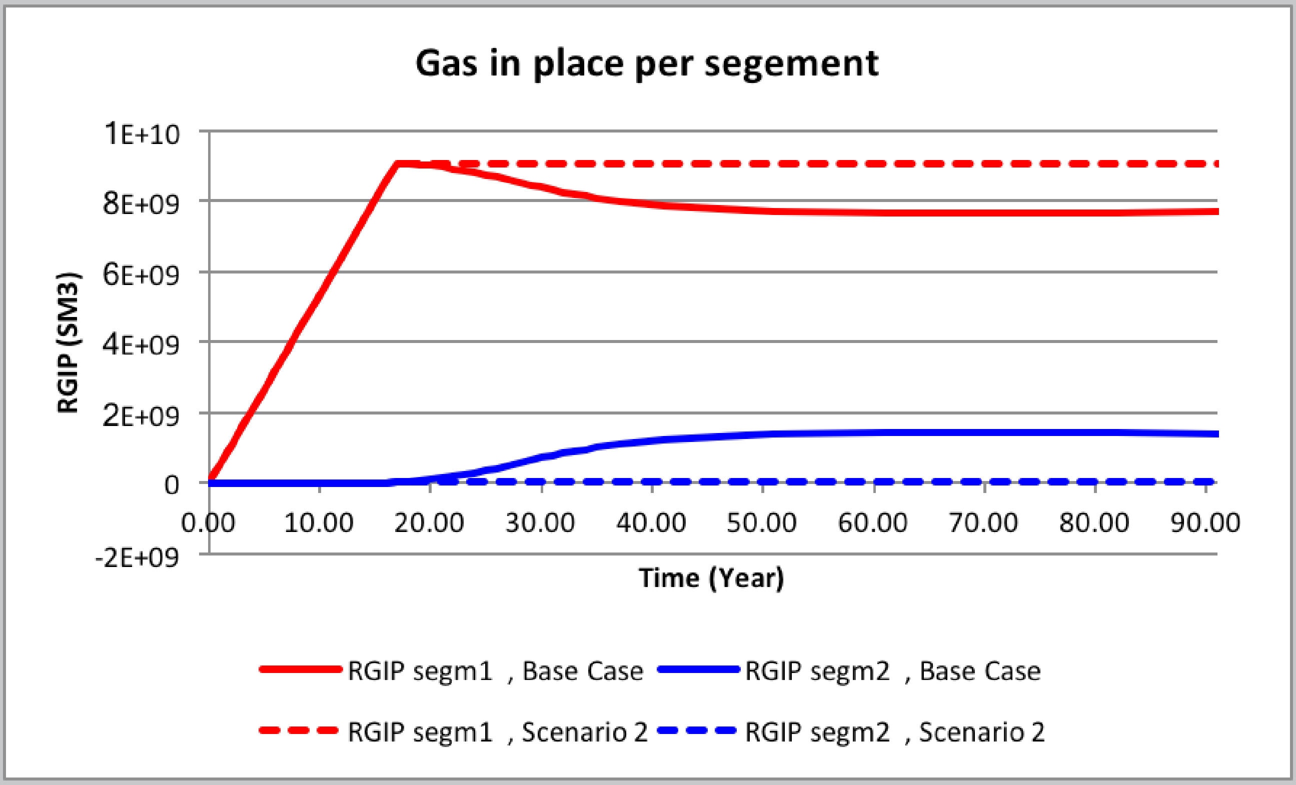

Figure 72 Unwanted migration to segment 2 compared to the base case (no remediation) scenario.

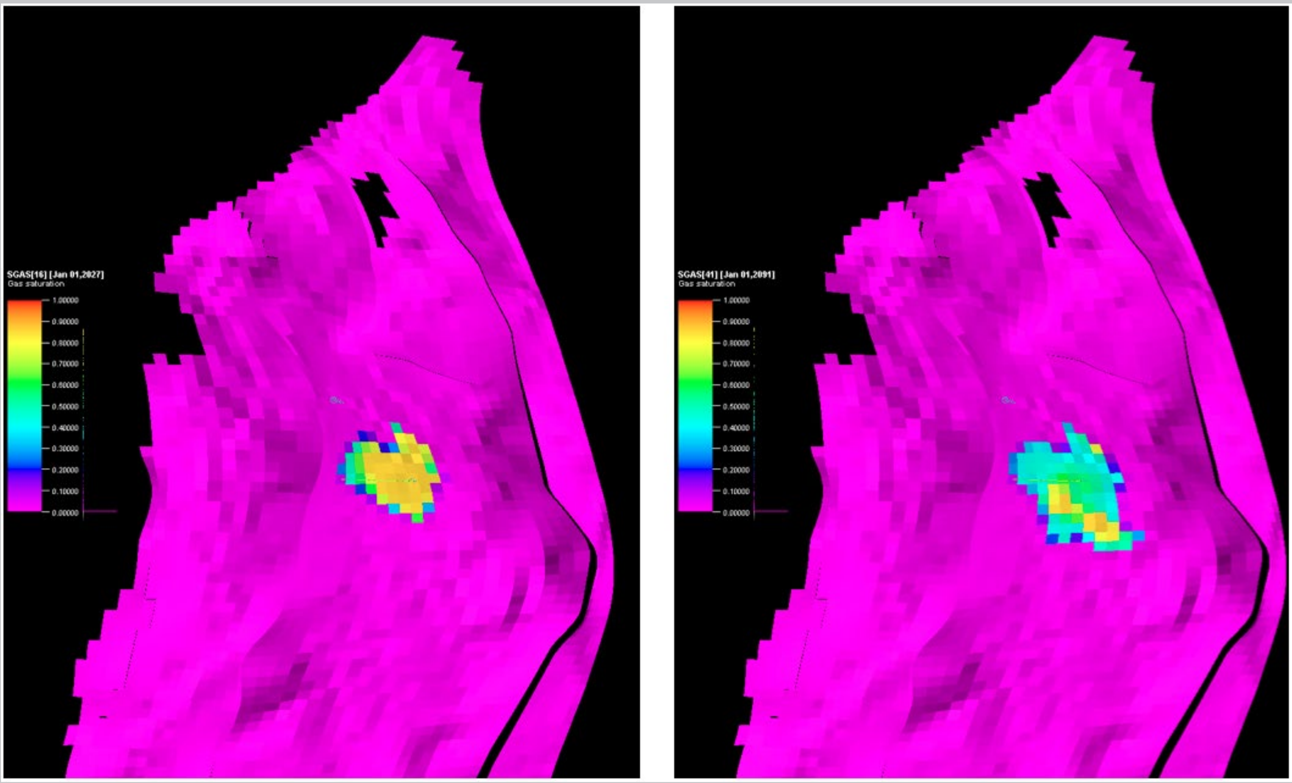

Figure 73 CO_2 plume after first detection of unwanted migration (left) and CO_2 plume after remediation at the end of simulation period of 93 years (right).

A-3 REMEDIATION SCENARIO 3

Table 21: Scenario description.

Scenario	**Remediation 3**
Description	After detection of unwanted migration of CO_2, CO_2 injection stopped and injection for 64 years (whole simulation period)

Table 22 Simulation settings.

General		Remarks
Begin simulation	0	(year)
End simulation	91	(year)
CO_2 Injection well	**JOHAN1**	
Constraints	Rate constraint: 1 Mton/yr BHP constraint 360*BAR	
Location	Vertical well in gridblock (x,y)→(45, 47)	
Perforation	Z-coordinates of gridblock (15-17)	
On stream	From 0 to 17 years	
Remediation well	REM 1	
Constraints	BHP constraint 234*BAR (10% above P initial)	
Location	Vertical well in gridblock (x,y)→(38, 47)	
Perforation	Z-coordinates of gridblock (15-17)	
On stream	From 18 to 91 years	
Remediation well	REM 2	
Constraints	BHP constraint 234*BAR (10% above P initial)	
Location	Vertical well in gridblock (x,y)→(40, 40)	
Perforation	Z-coordinates of gridblock (15-17)	
On stream	From 61 to 91 years	

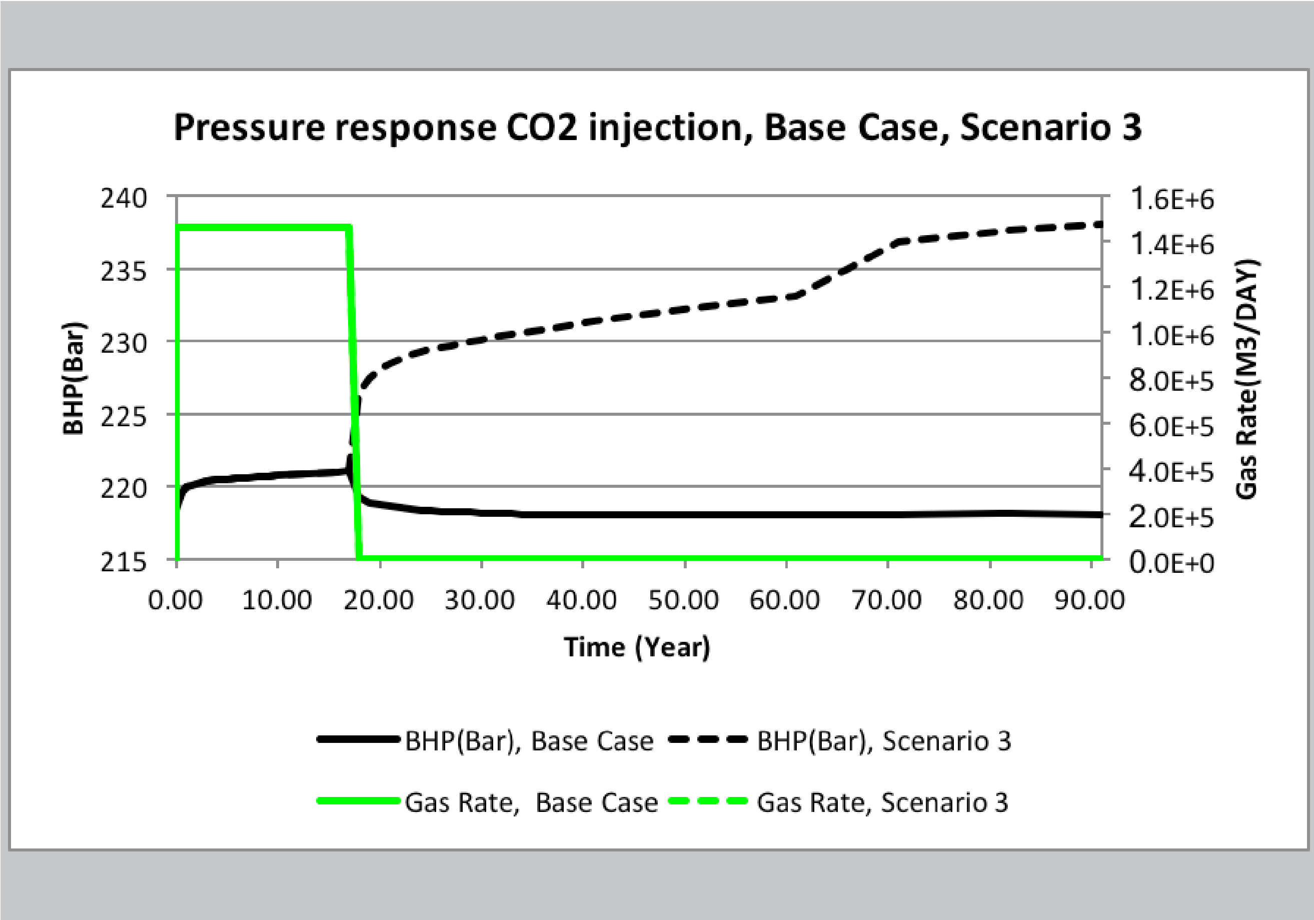

Figure 74 Gas injection rate and pressure response, compared to the base case (no remediation).

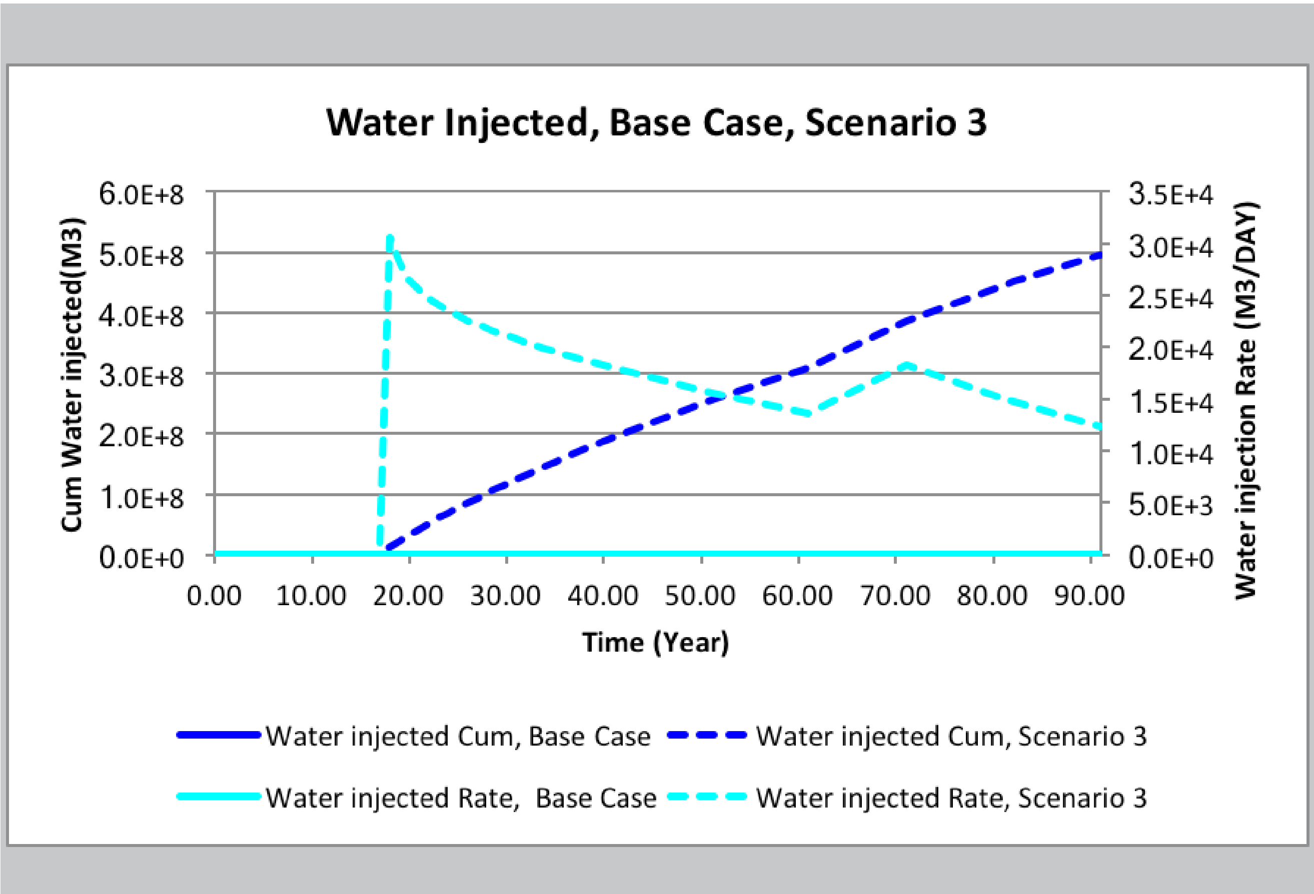

Figure 75 Water injection rates and cumulatives of well REM1, compared to the base case (no remediation) scenario.

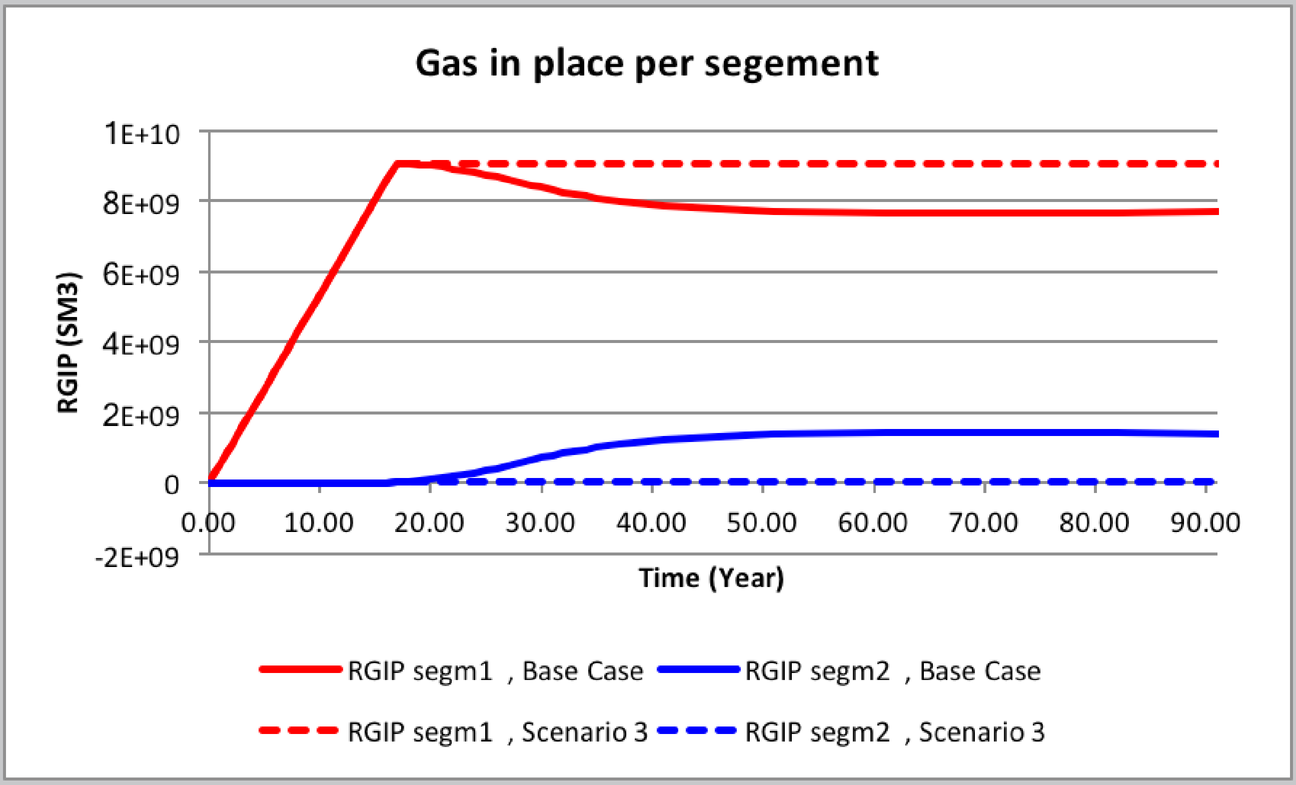

Figure 76 Unwanted migration to segment 2 compared to the base case (no remediation) scenario.

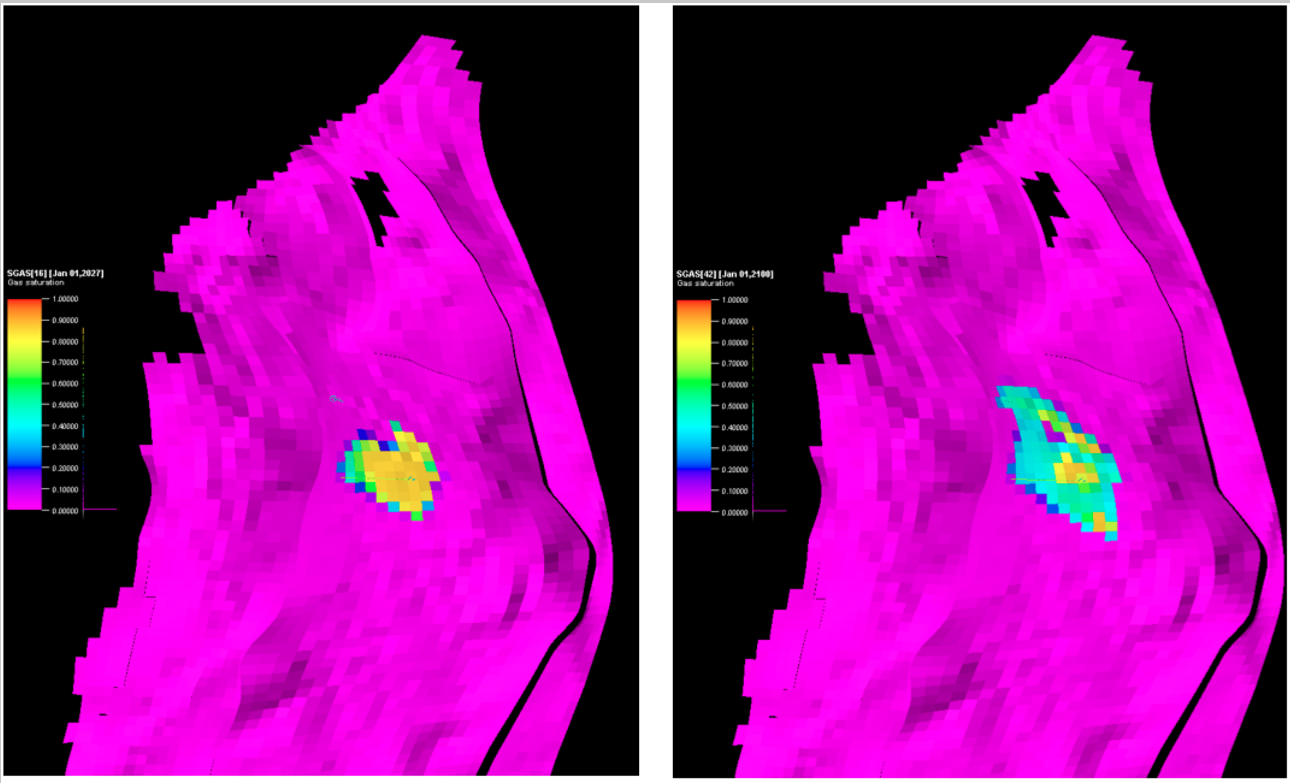

Figure 77 CO_2 plume after first detection of unwanted migration (left) and CO_2 plume after remediation at the end of simulation period of 93 years (right).

A-4 REMEDIATION SCENARIO 4

Table 23: Scenario description.

Scenario	**Remediation 4**
Description	After detection of unwanted migration of CO_2, CO_2 injection stopped and injection of water for 5 years by one well

Table 24 Simulation settings.

General		Remarks
Begin simulation	0	(year)
End simulation	91	(year)
CO_2 Injection well	**JOHAN1**	
Constraints	Rate constraint: 1 Mton/yr BHP constraint 360*BAR	
Location	Vertical well in gridblock (x,y)→(45, 47)	
Perforation	Z-coordinates of gridblock (15-17)	
On stream	From 0 to 17 years	
Remediation well	REM 1	
Constraints	BHP constraint 234*BAR (10% above P initial)	
Location	Vertical well in gridblock (x,y)→(38, 47)	
Perforation	Z-coordinates of gridblock (15-17)	
On stream	From year 18 to year 23	

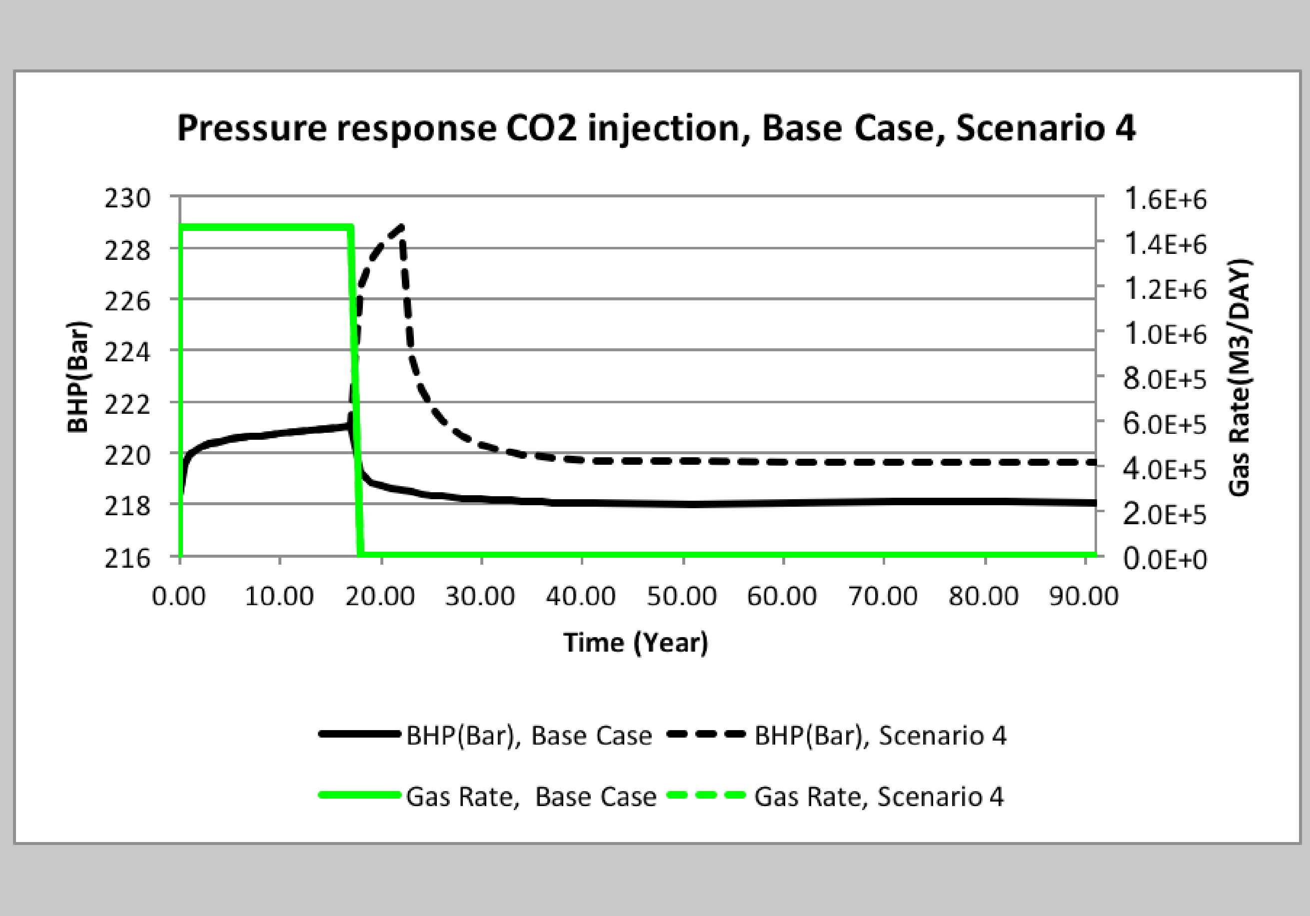

Figure 78 Gas injection rate and pressure response, compared to the base case (no remediation).

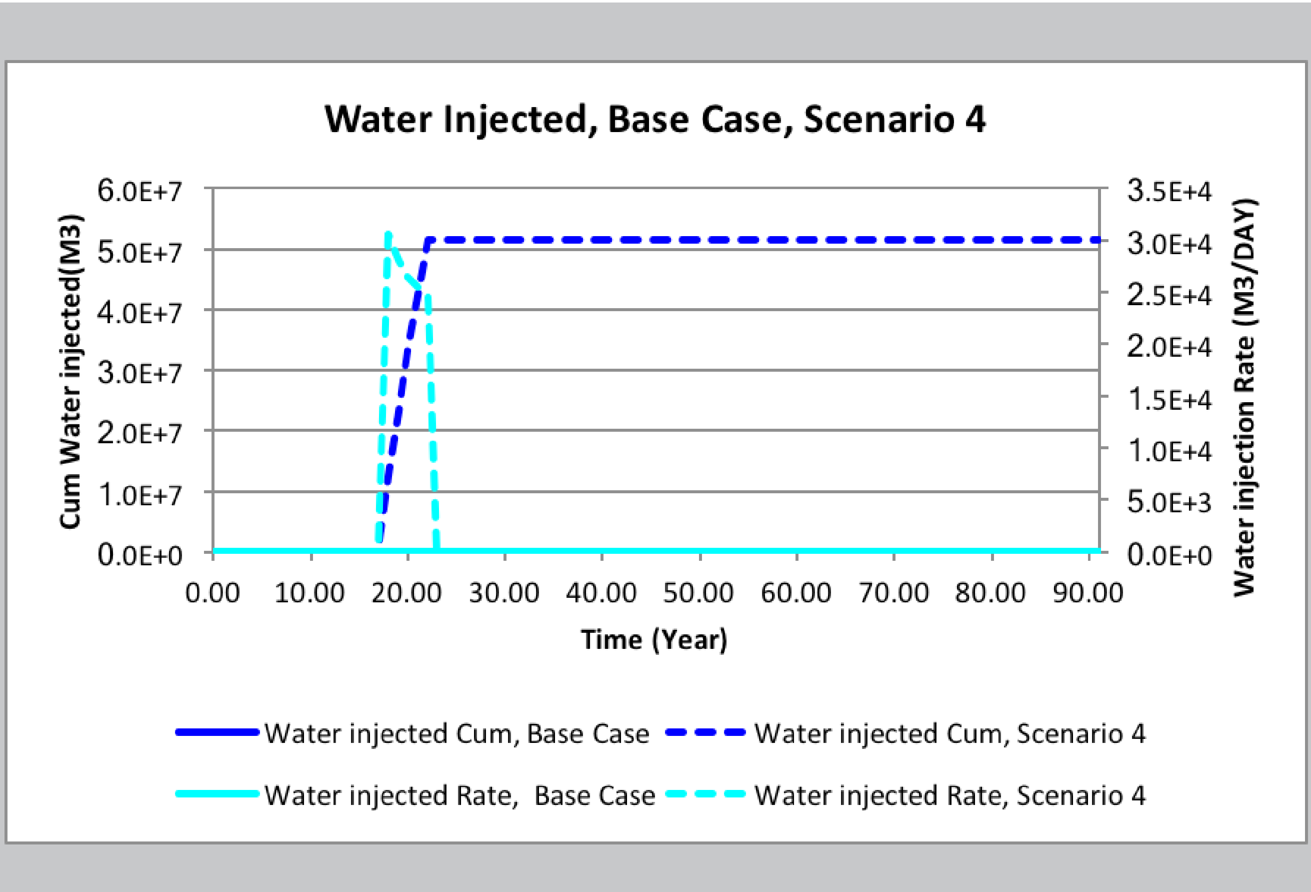

Figure 79 Water injection rates and cumulatives of well REM1, compared to the base case (no remediation) scenario.

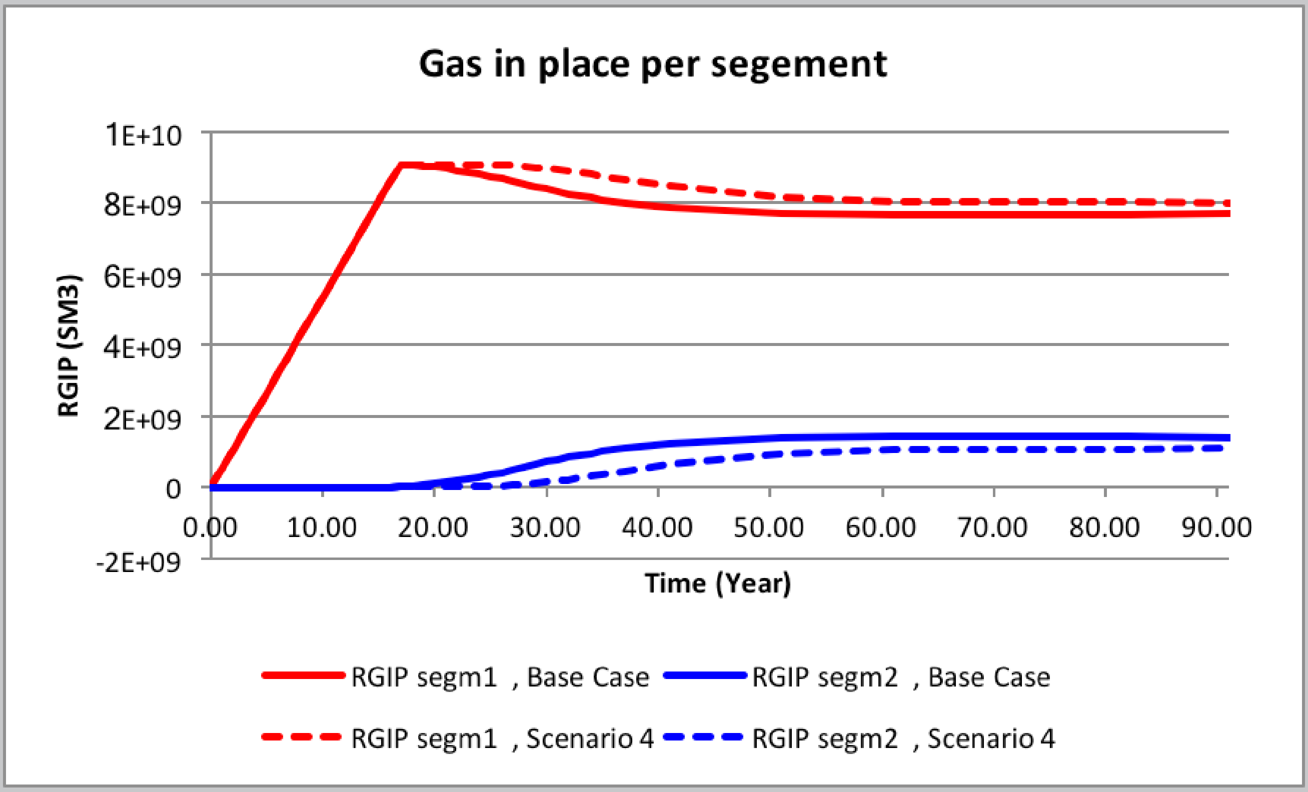

Figure 80 Unwanted migration to segment 2 compared to the base case (no remediation) scenario.

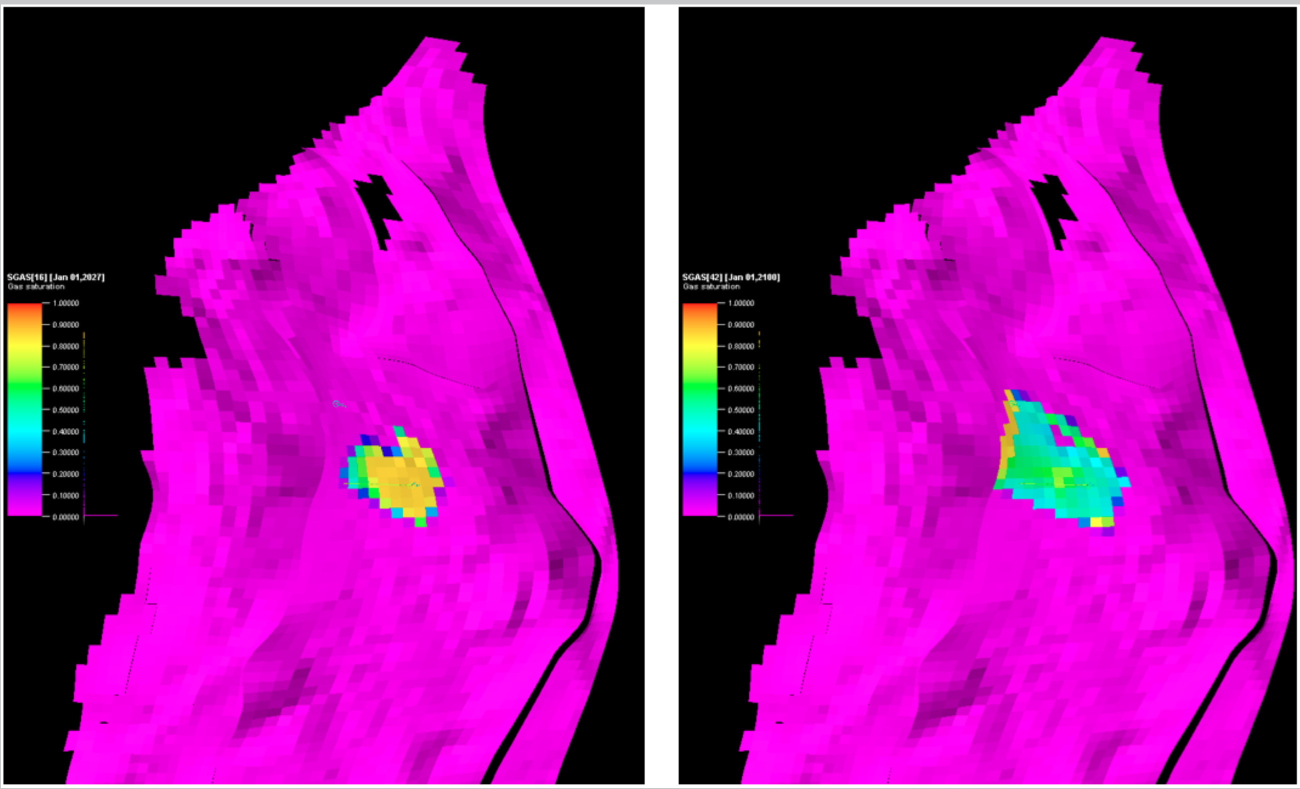

Figure 81 CO_2 plume after first detection of unwanted migration (left) and CO_2 plume after remediation at the end of simulation period of 93 years (right).

A-5 REMEDIATION SCENARIO 5

Table 25: Scenario description.

Scenario	**Remediation 5**
Description	After detection of unwanted migration of CO2, Co2 injection stopped and injection of water for 10 years by one well

Table 26 Simulation settings.

General		Remarks
Begin simulation	0	(year)
End simulation	91	(year)
CO_2 Injection well	**JOHAN1**	
Constraints	Rate constraint: 1 Mton/yr BHP constraint 360*BAR	
Location	Vertical well in gridblock (x,y)→(45, 47)	
Perforation	Z-coordinates of gridblock (15-17)	
On stream	From 0 to 17 years	
Remediation well	REM 1	
Constraints	BHP constraint 234*BAR (10% above P initial)	
Location	Vertical well in gridblock (x,y)→(38, 47)	
Perforation	Z-coordinates of gridblock (15-17)	
On stream	From year 18 to year 23	

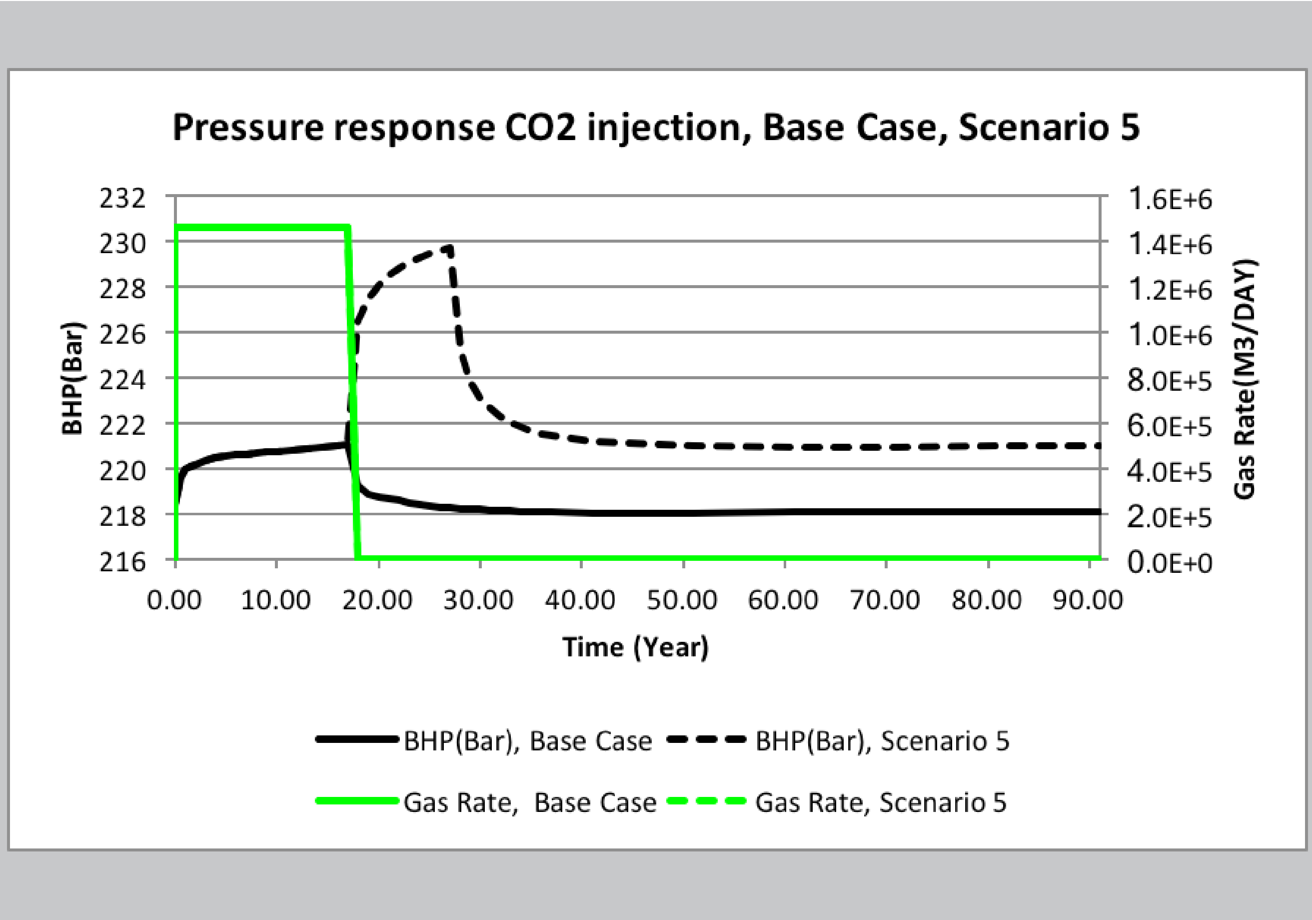

Figure 82 Gas injection rate and pressure response, compared to the base case (no remediation).

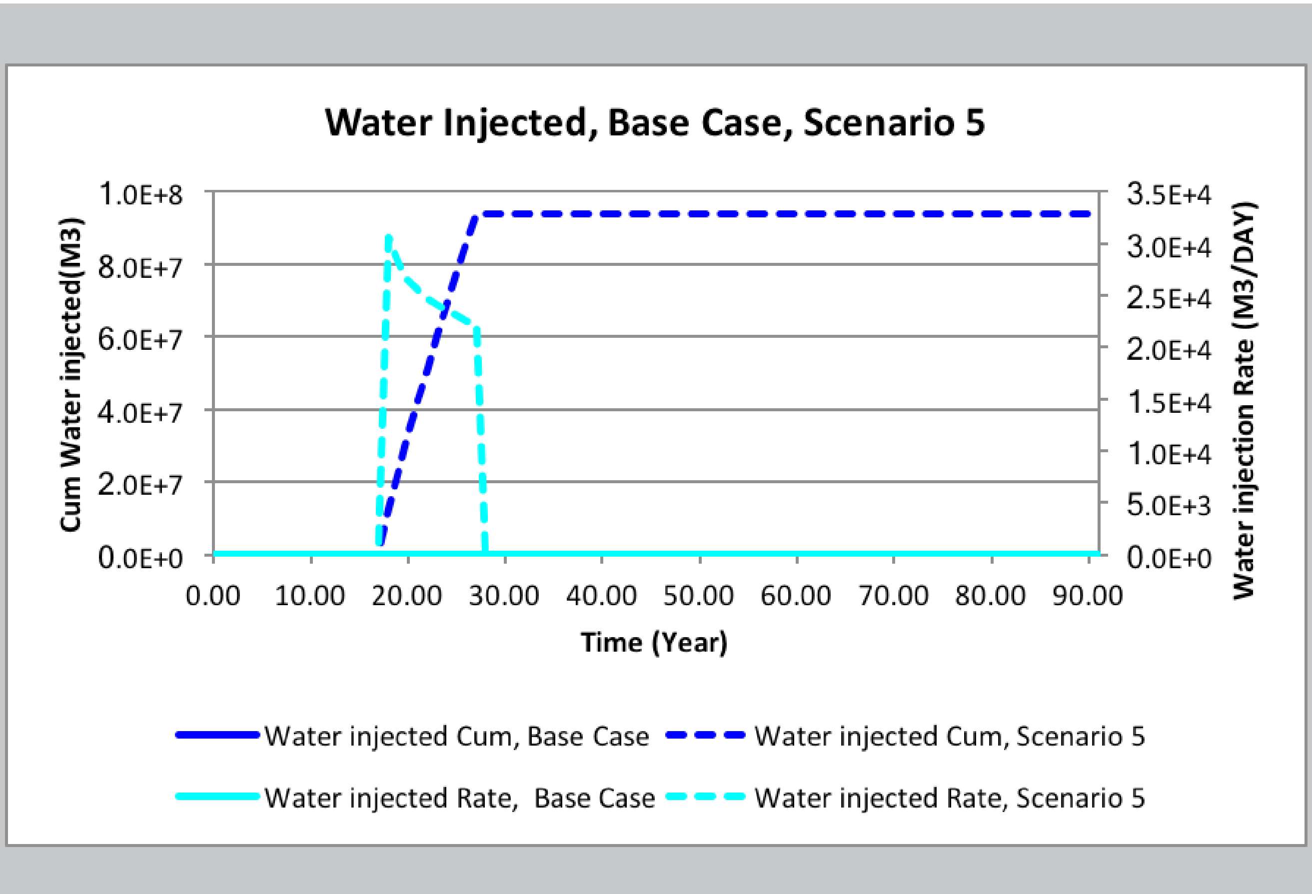

Figure 83 Water injection rates and cumulatives of well REM1, compared to the base case (no remediation) scenario.

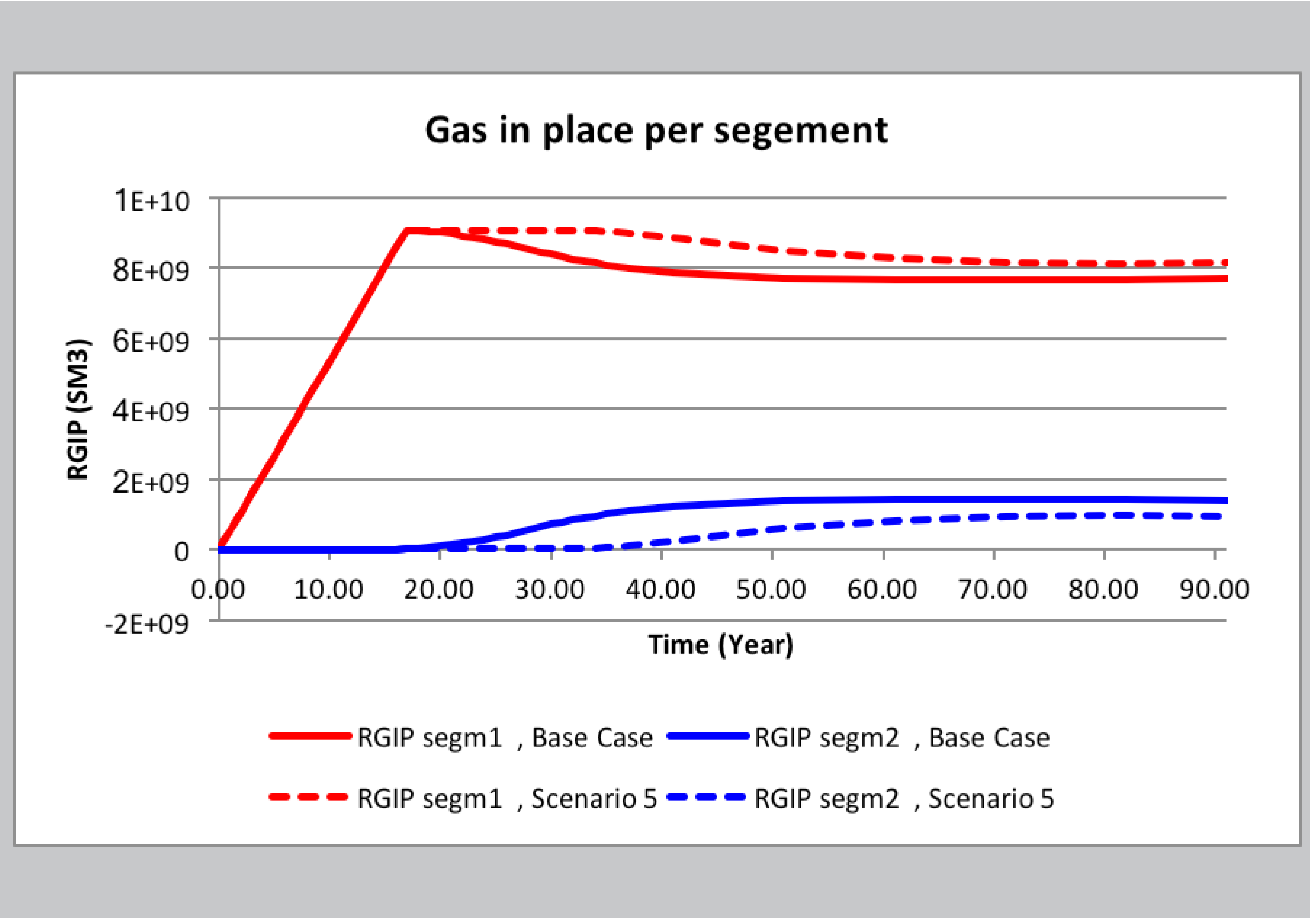

Figure 84 Unwanted migration to segment 2 compared to the base case (no remediation) scenario.

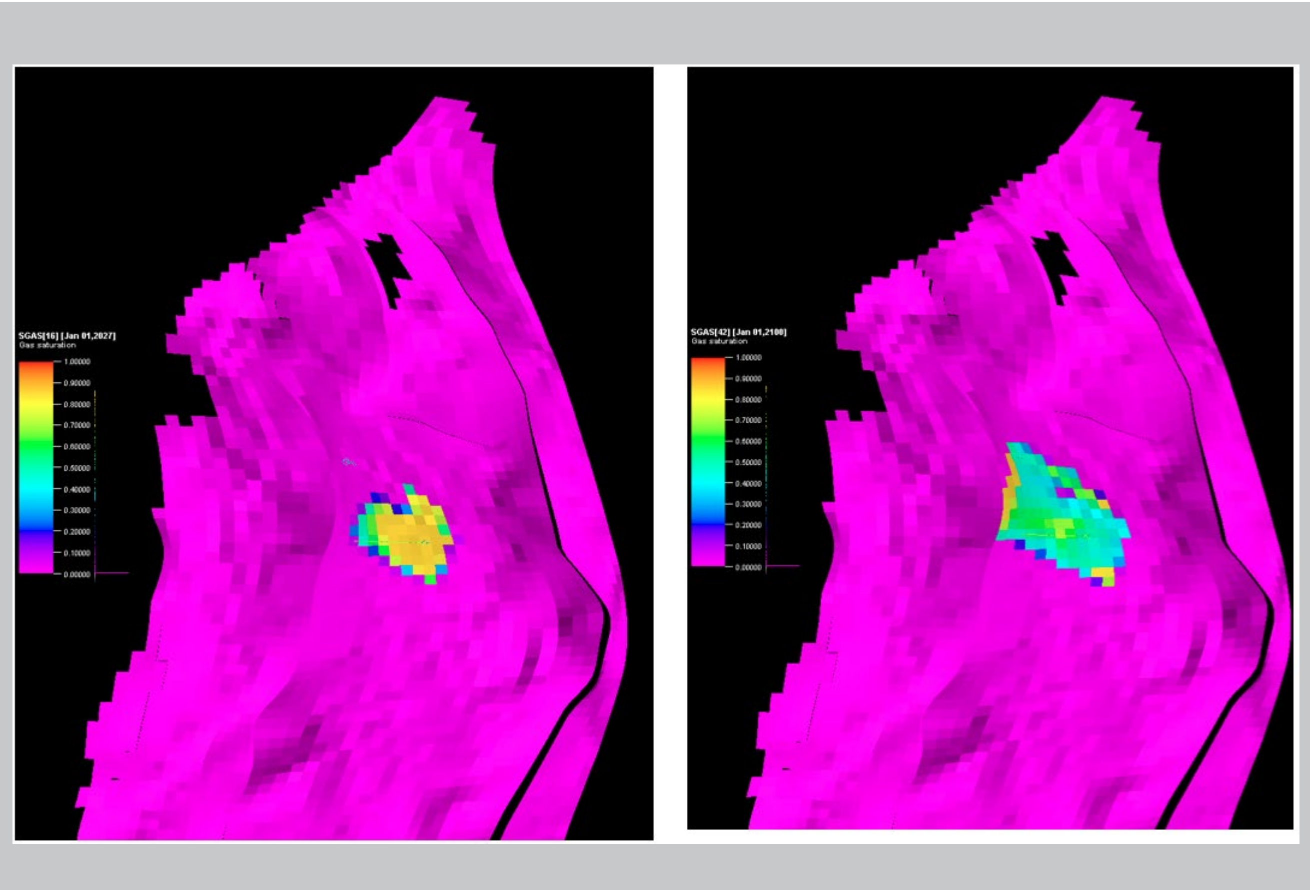

Figure 85 CO_2 plume after first detection of unwanted migration (left) and CO_2 plume after remediation at the end of simulation period of 93 years (right).

A-6 REMEDIATION SCENARIO 6

Table 27: Scenario description.

Scenario	Remediation 6
Description	After detection of unwanted migration of CO2, CO2 injection stopped and injection of water for 17 years by one well (whole simulation period)

Table 28 Simulation settings.

General		Remarks
Begin simulation	0	(year)
End simulation	91	(year)
CO_2 Injection well	**JOHAN1**	
Constraints	Rate constraint: 1 Mton/yr BHP constraint 360*BAR	
Location	Vertical well in gridblock (x,y)→(45, 47)	
Perforation	Z-coordinates of gridblock (15-17)	
On stream	From 0 to 17 years	
Remediation well	REM 1	
Constraints	BHP constraint 234*BAR (10% above P initial)	
Location	Vertical well in gridblock (x,y)→(38, 47)	
Perforation	Z-coordinates of gridblock (15-17)	
On stream	From year 18 to year 23	

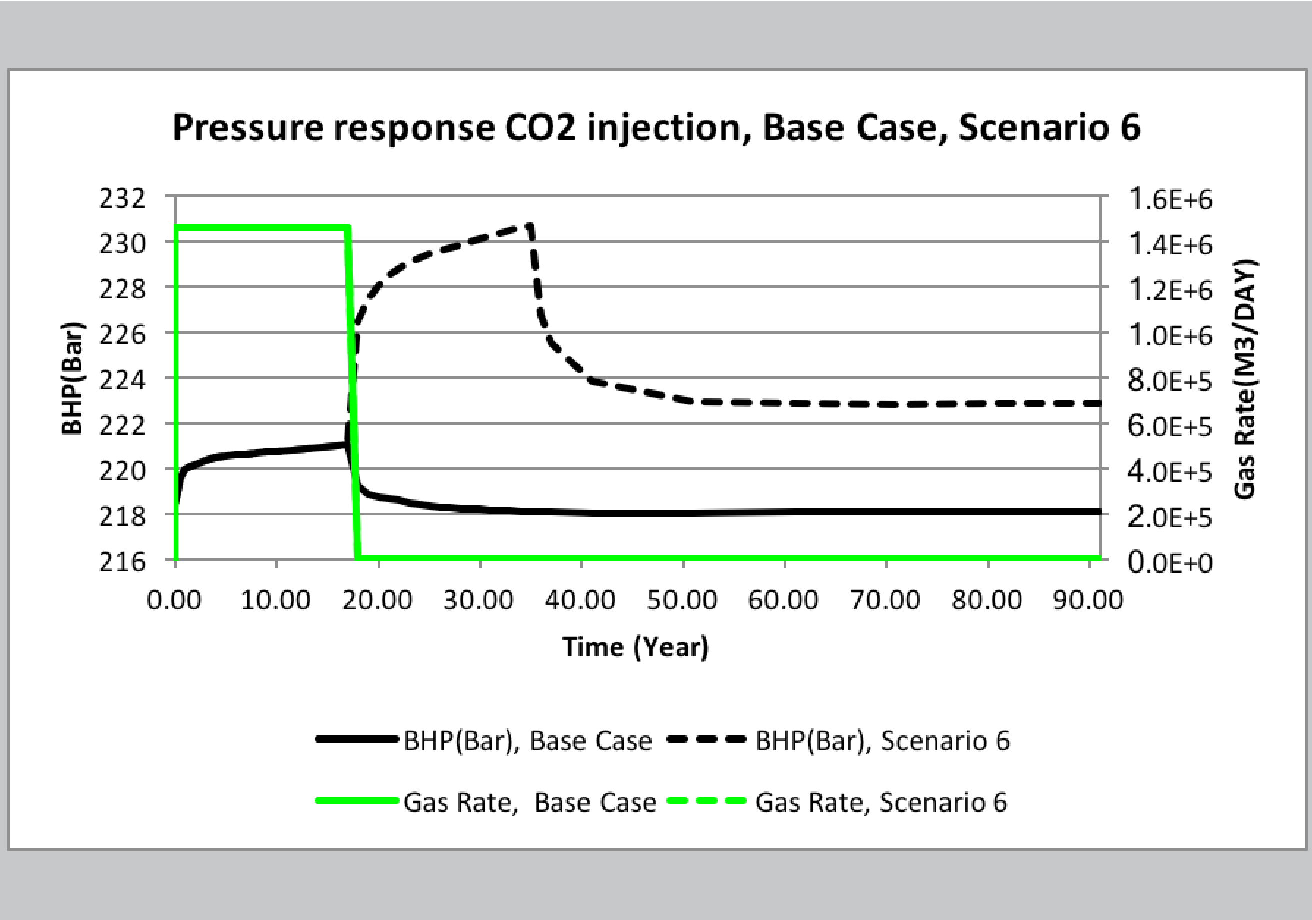

Figure 86 Gas injection rate and pressure response, compared to the base case (no remediation).

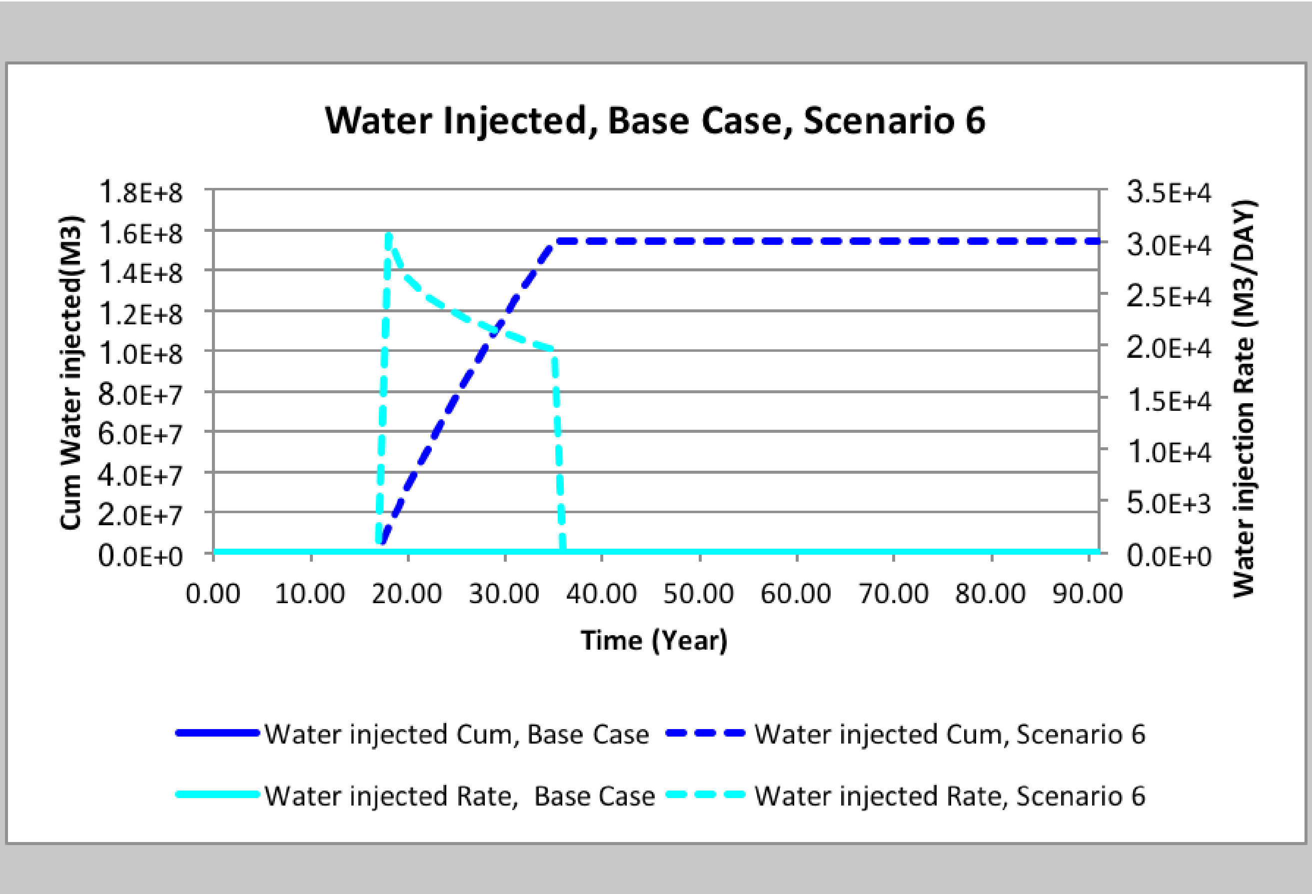

Figure 87 Water injection rates and cumulatives of well REM1, compared to the base case (no remediation) scenario.

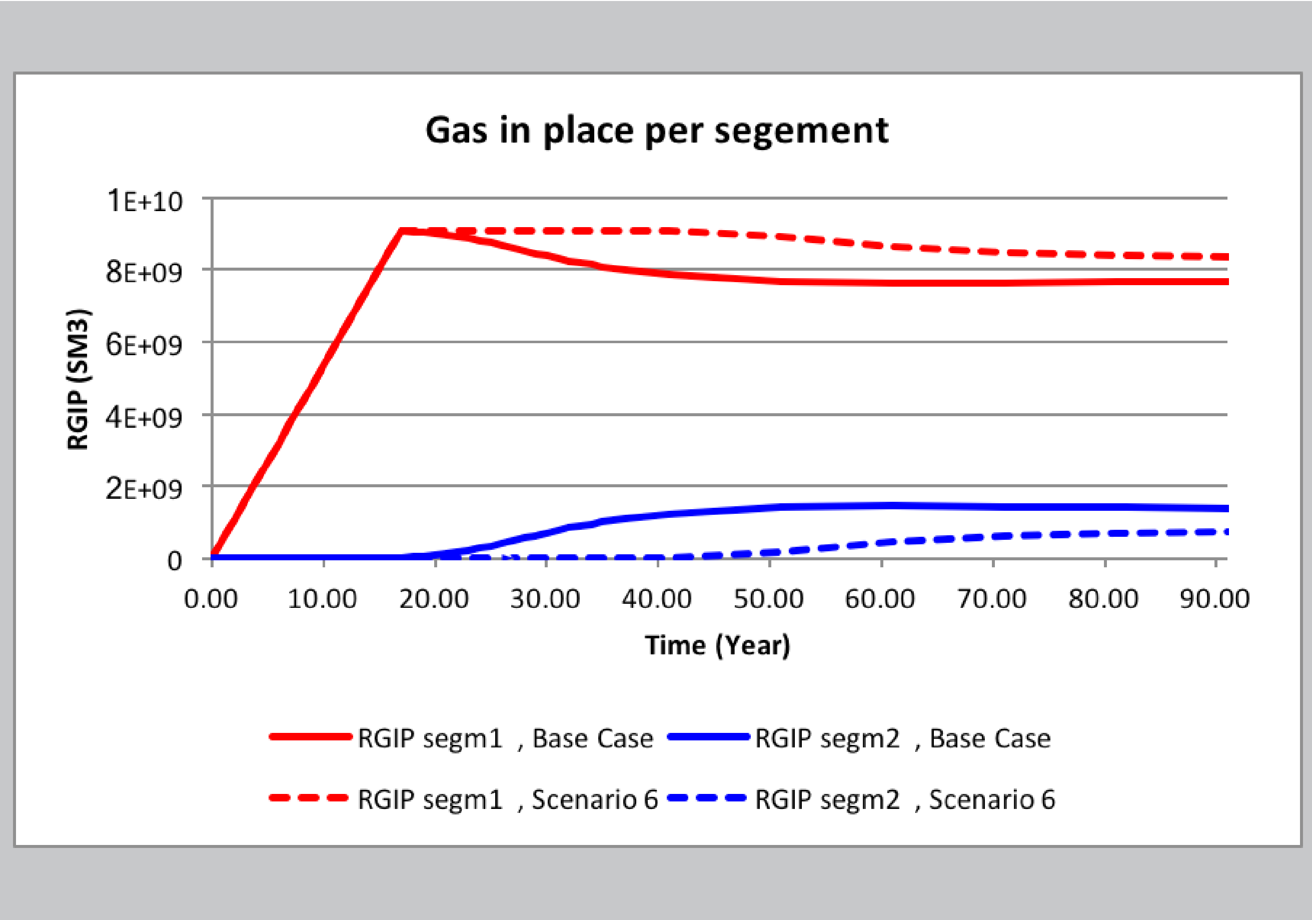

Figure 88 Unwanted migration to segment 2 compared to the base case (no remediation) scenario.

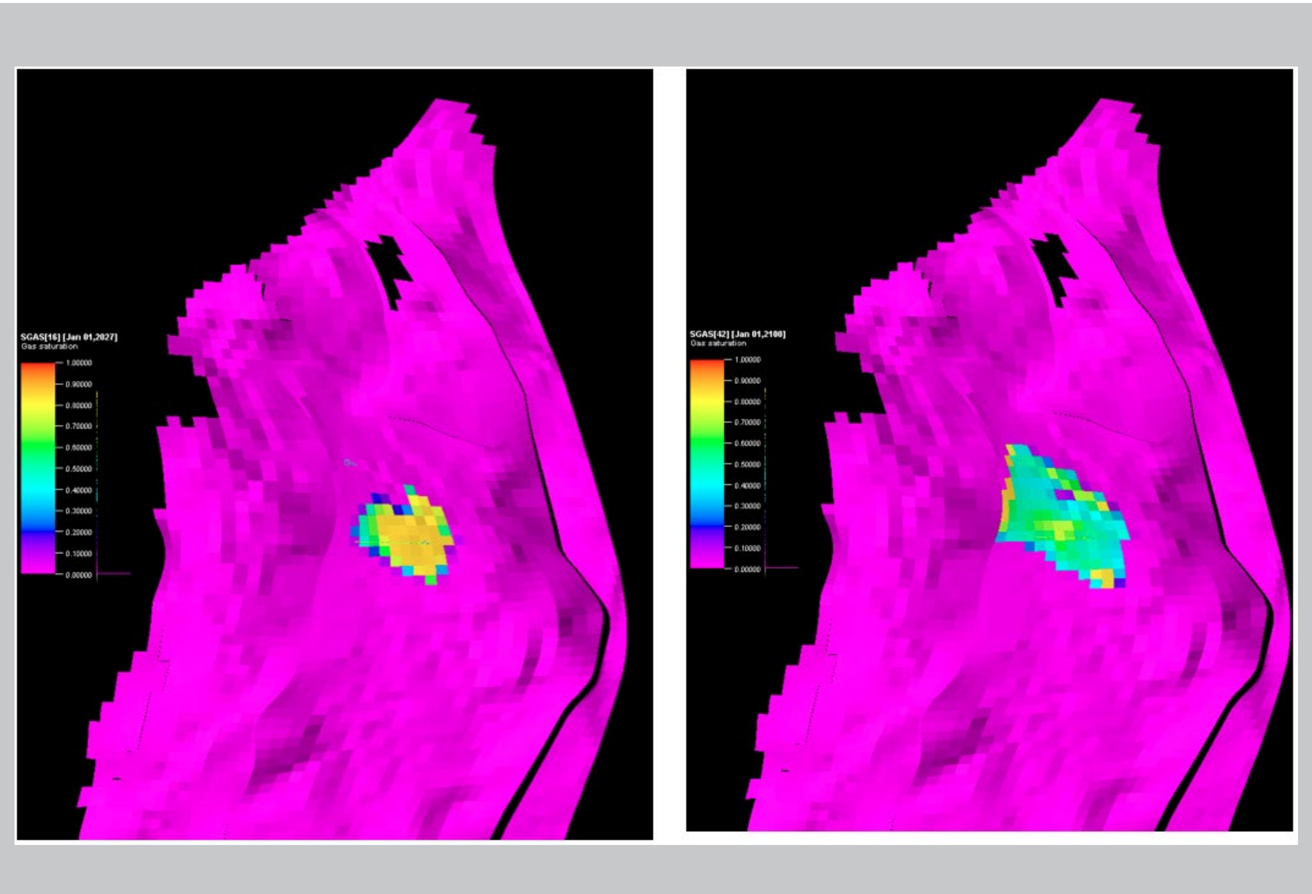

Figure 89 CO_2 plume after first detection of unwanted migration (left) and CO_2 plume after remediation at the end of simulation period of 93 years (right)

A-7 REMEDIATION SCENARIO 7

Table 29: Scenario description.

Scenario	Remediation 7
Description	After detection of unwanted migration of CO2, CO2 injection stopped and back production started for a period of 50 years (gas rate constraint of 1 Mton/yr). Injection of water for 18 years by one well.

Table 30 Simulation settings.

General		Remarks
Begin simulation	0	(year)
End simulation	91	(year)
CO_2 Injection well	**JOHAN1**	
Constraints	Rate constraint: 1 Mton/yr BHP constraint 360*BAR	
Location	Vertical well in gridblock (x,y)→(45, 47)	
Perforation	Z-coordinates of gridblock (15-17)	
On stream	From 0 to 17 years	
Remediation well	REM 1	
Constraints	BHP constraint 234*BAR (10% above P initial)	
Location	Vertical well in gridblock (x,y)→(38, 47)	
Perforation	Z-coordinates of gridblock (15-17)	
On stream	From year 18 to year 36	
Back production	JOHAN1	
Constraints	Gas Rate constraint: 1.4 e6 m3/day	
Location	Vertical well in gridblock (x,y)→(45, 47)	
Perforation	Z-coordinates of gridblock (15-17)	
On stream	From year 18 to year 69	

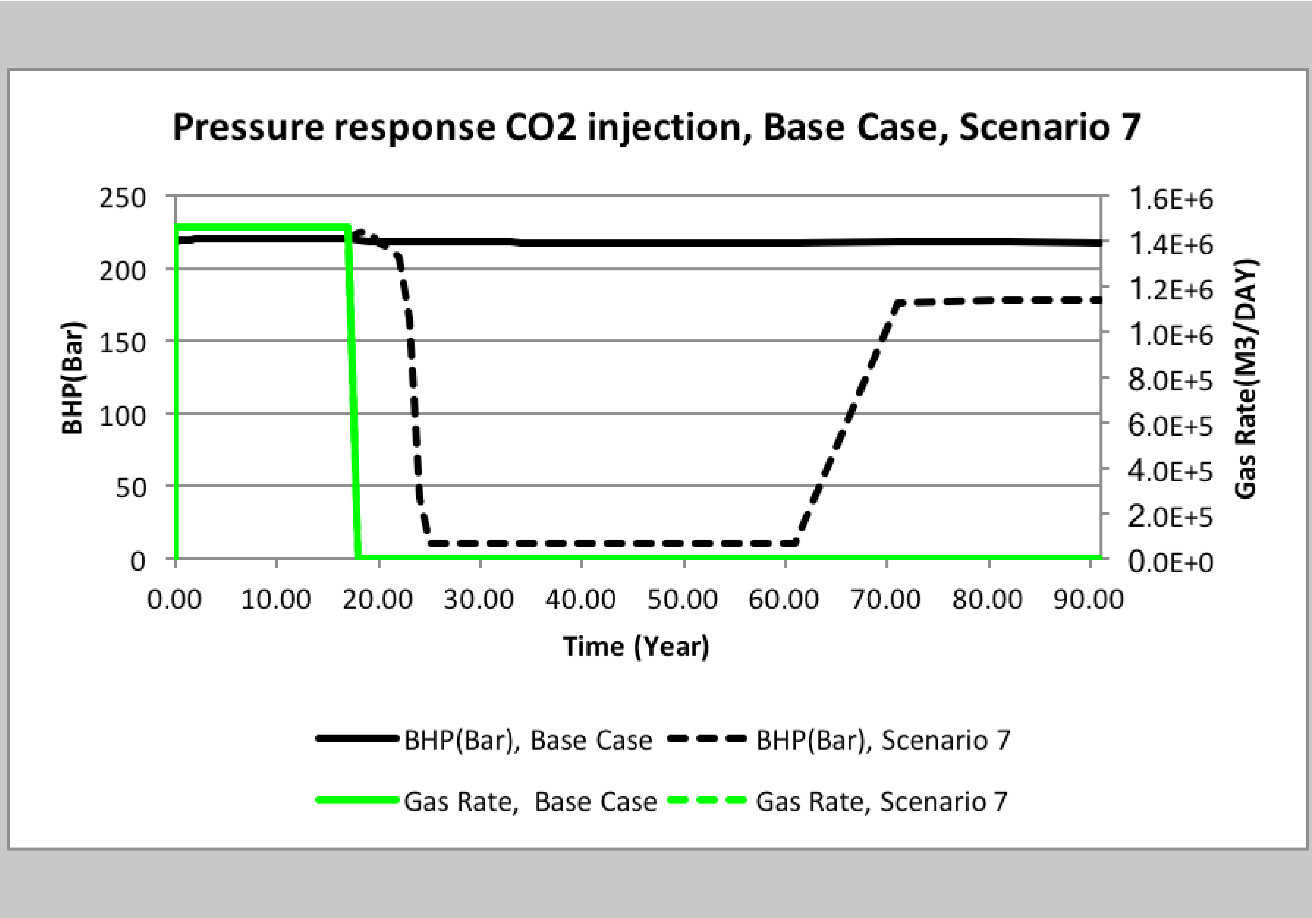

Figure 90 Gas injection rate and pressure response, compared to the base case (no remediation).

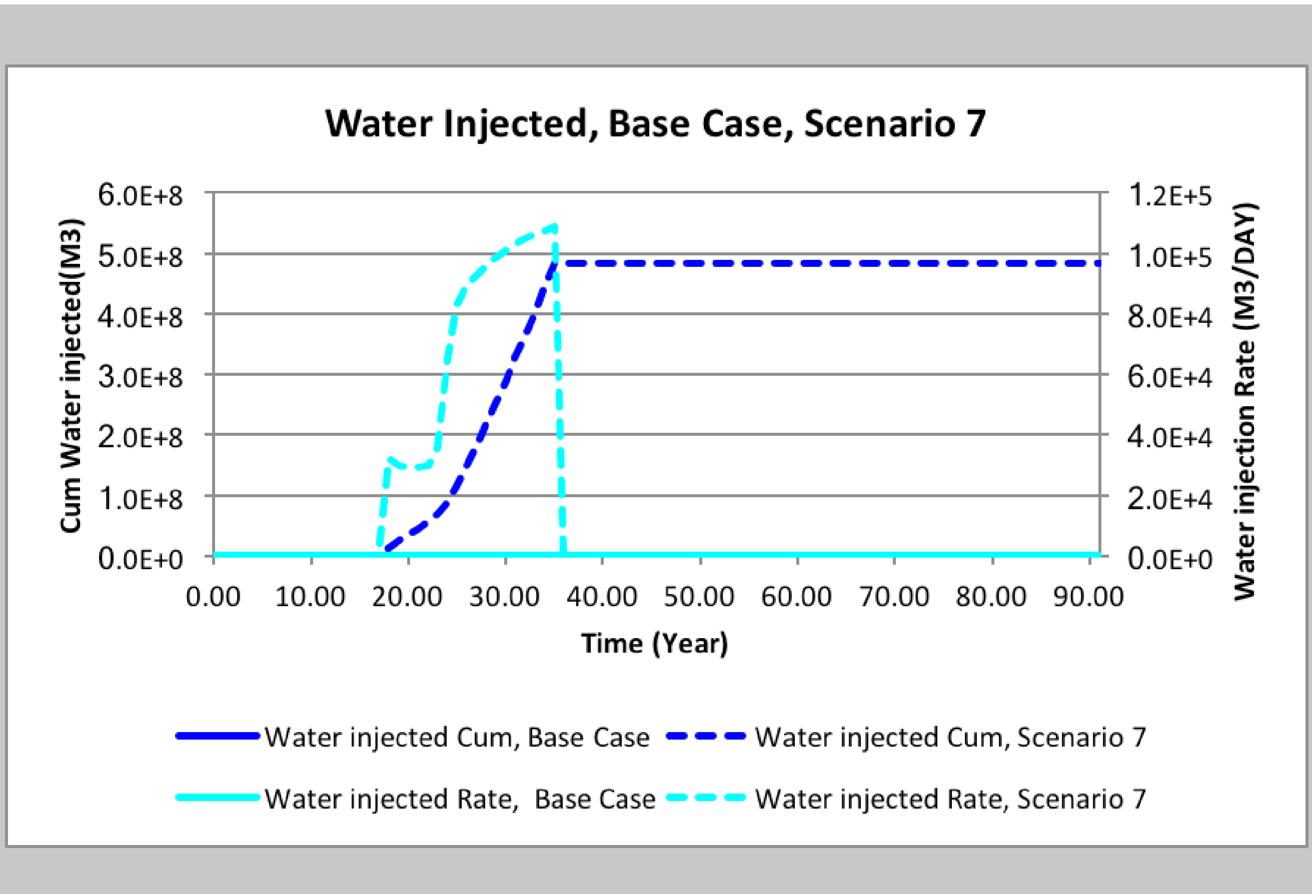

Figure 91 Water injection rates and cumulatives of well REM1, compared to the base case (no remediation) scenario.

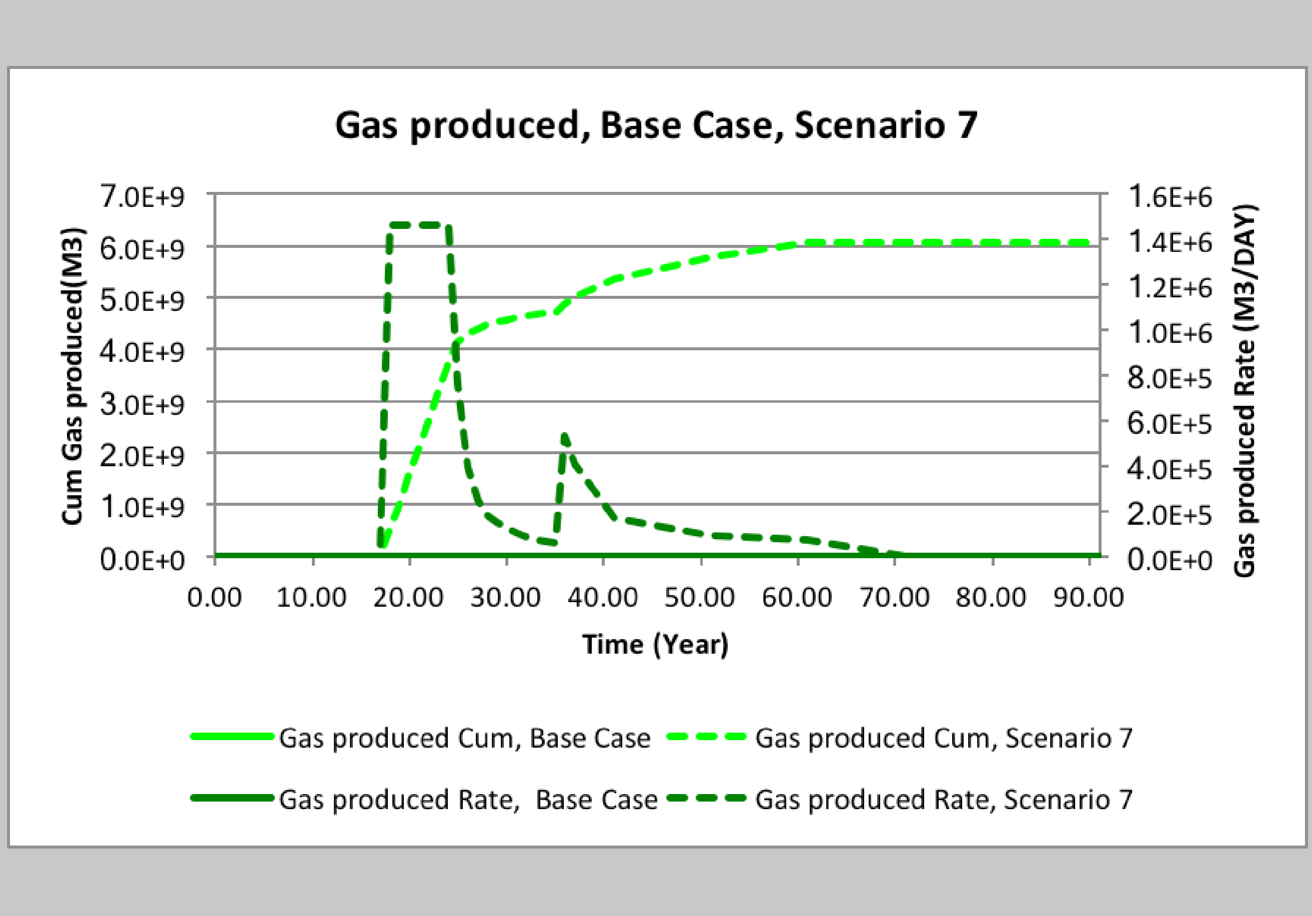

Figure 92 Gas back production rate and cumulatives of well JOHAN compared to the base case (no remediation) scenario.

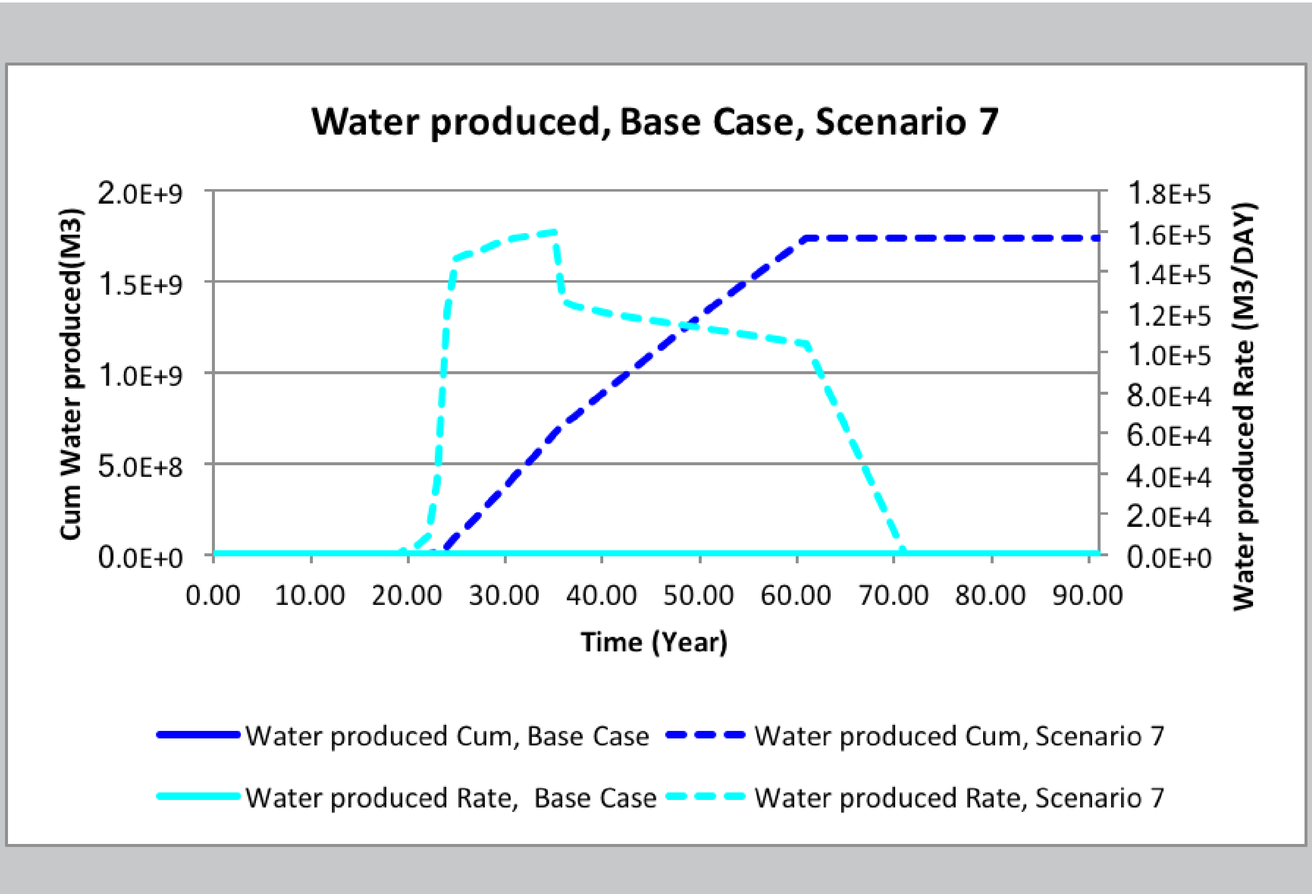

Figure 93 Water back production rate and cumulatives of well JOHAN compared to the base case (no remediation) scenario.

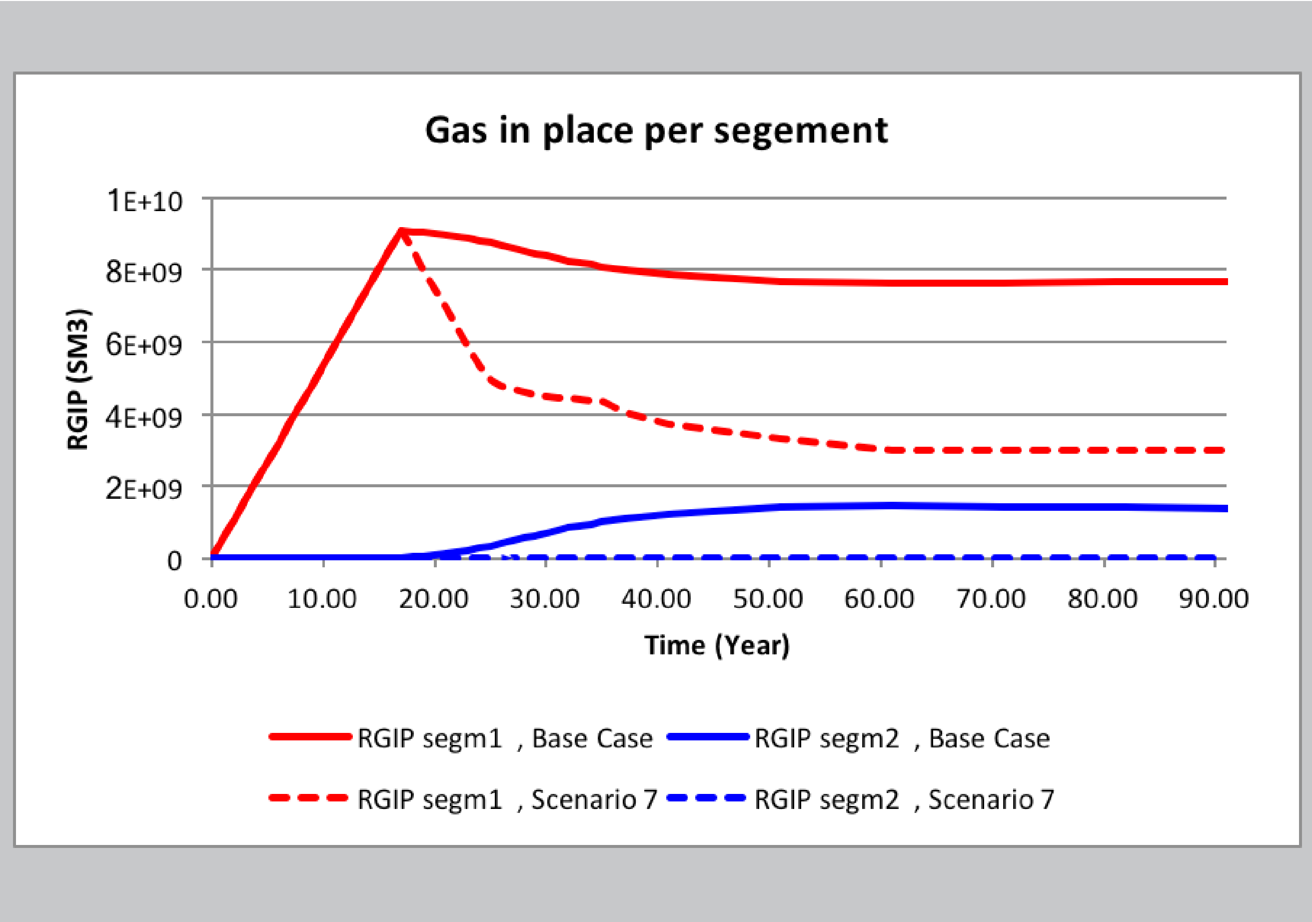

Figure 94 Unwanted migration to segment 2 compared to the base case (no remediation) scenario.

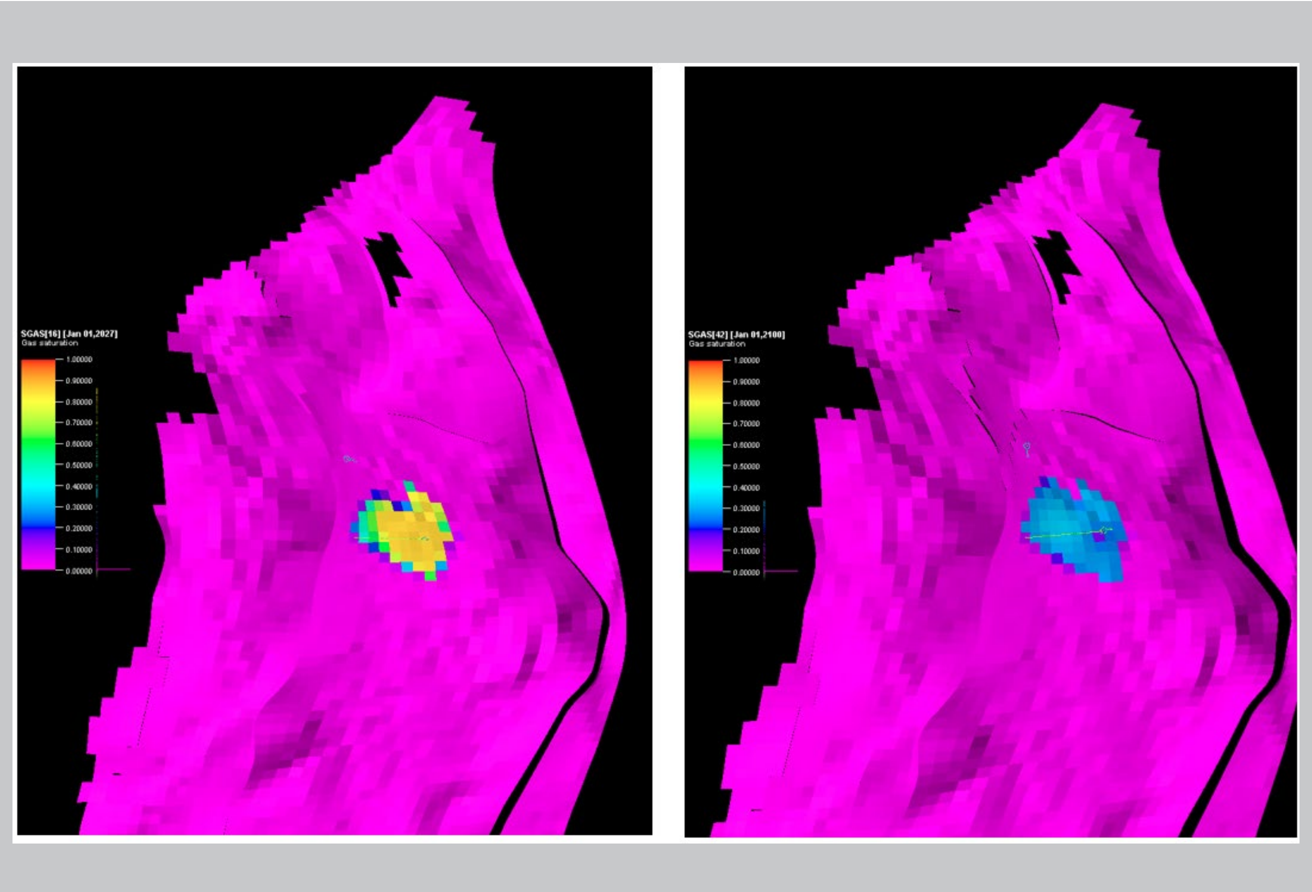

Figure 95 CO_2 plume after first detection of unwanted migration (left) and CO_2 plume after remediation at the end of simulation period of 93 years (right).

A-8 REMEDIATION SCENARIO 8

Table 31: Scenario description.

Scenario	Remediation 8
Description	After detection of unwanted migration of CO_2, CO_2 injection stopped and back production started for a period of 50 years (gas rate constraint of 0.5 Mton/yr). Injection of water for 18 years by one well.

Table 32 Simulation settings.

General		Remarks
Begin simulation	0	(year)
End simulation	91	(year)
CO_2 Injection well	**JOHAN1**	
Constraints	Rate constraint: 1 Mton/yr BHP constraint 360*BAR	
Location	Vertical well in gridblock (x,y)→(45, 47)	
Perforation	Z-coordinates of gridblock (15-17)	
On stream	From 0 to 17 years	
Remediation well	REM 1	
Constraints	BHP constraint 234*BAR (10% above P initial)	
Location	Vertical well in gridblock (x,y)→(38, 47)	
Perforation	Z-coordinates of gridblock (15-17)	
On stream	From year 18 to year 36	
Back production	JOHAN1	
Constraints	Gas Rate constraint 234: 0.7 e6 m3/day	
Location	Vertical well in gridblock (x,y)→(45, 47)	
Perforation	Z-coordinates of gridblock (15-17)	
On stream	From year 18 to year 69	

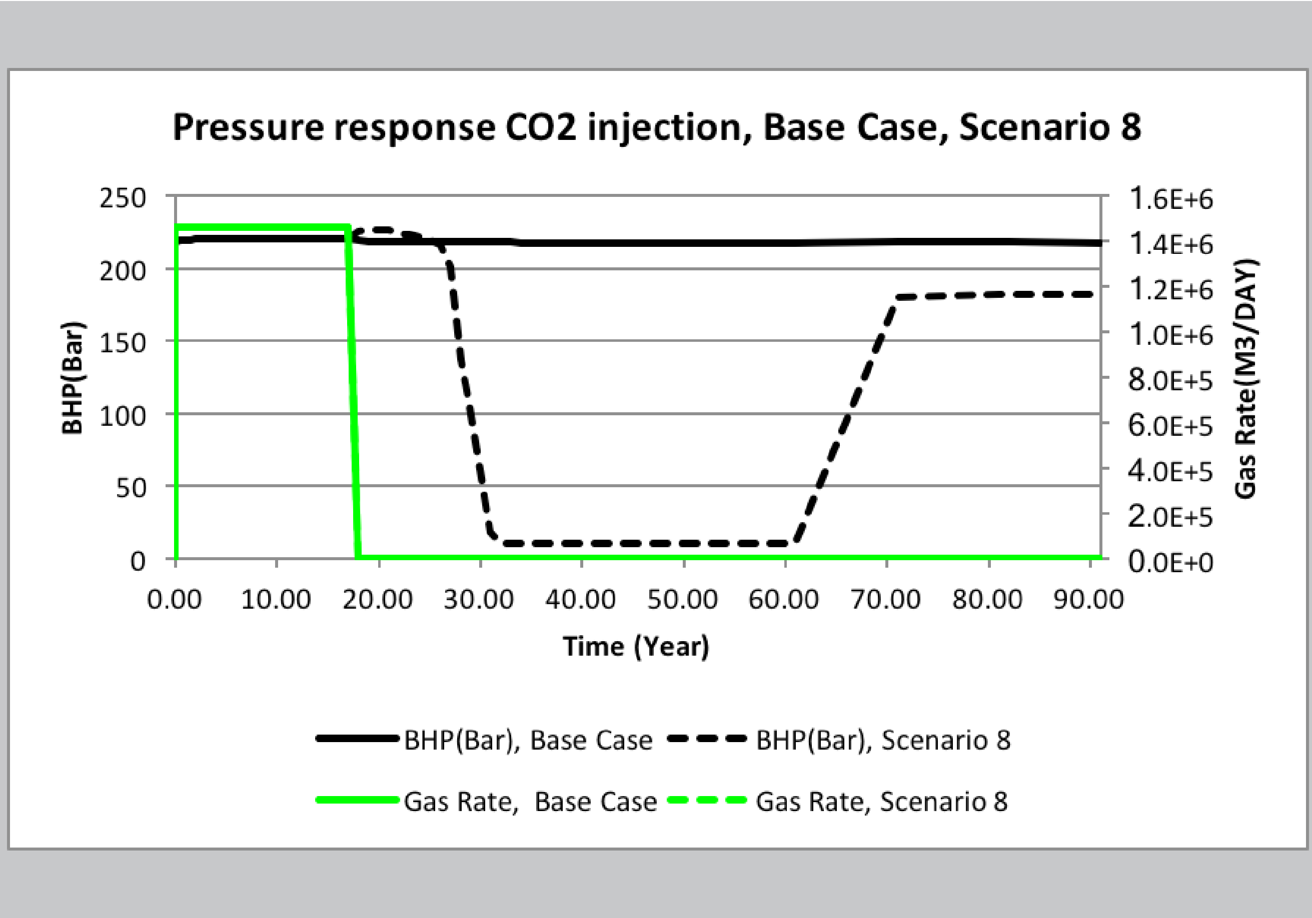

Figure 96 Gas injection rate and pressure response, compared to the base case (no remediation).

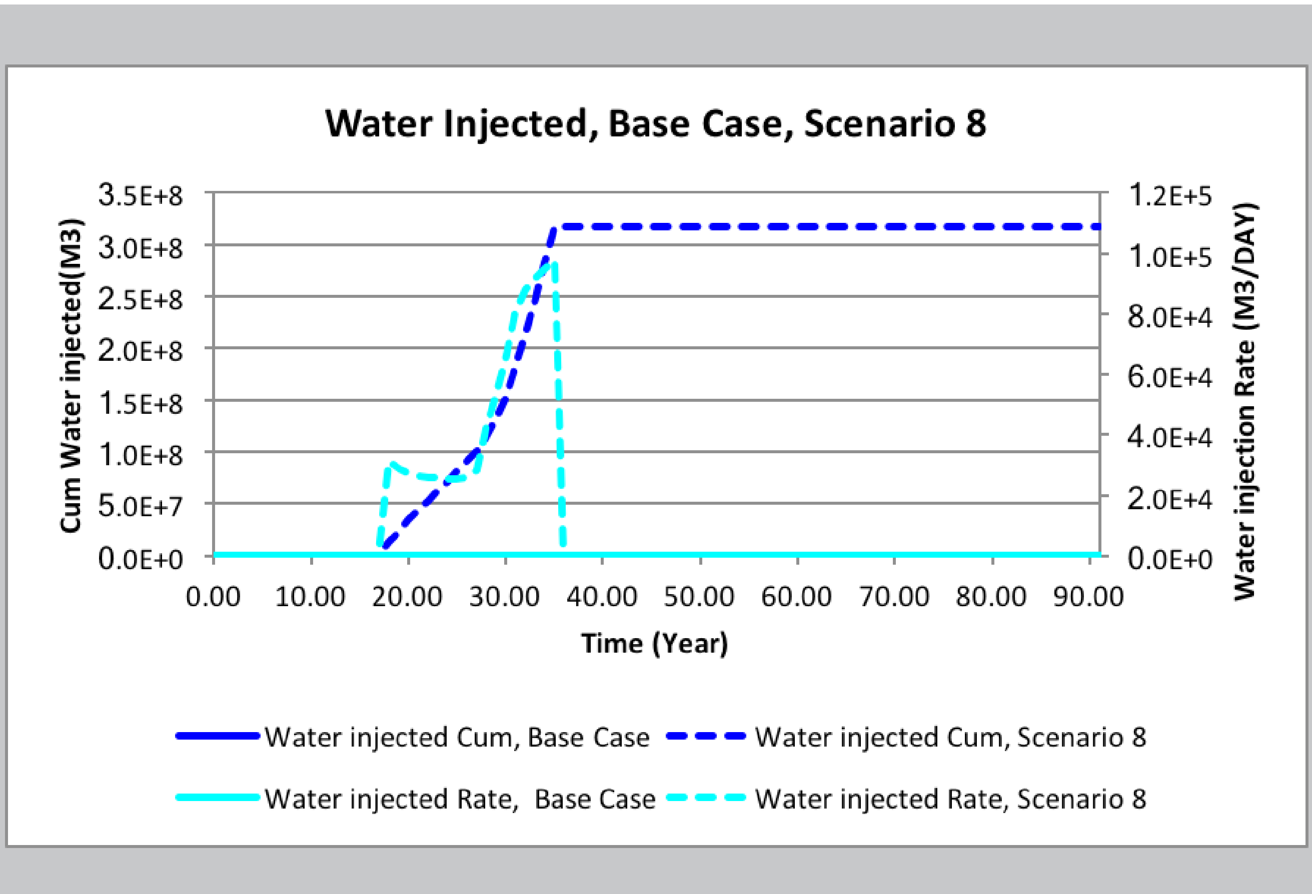

Figure 97 Water injection rates and cumulatives of well REM1, compared to the base case (no remediation) scenario.

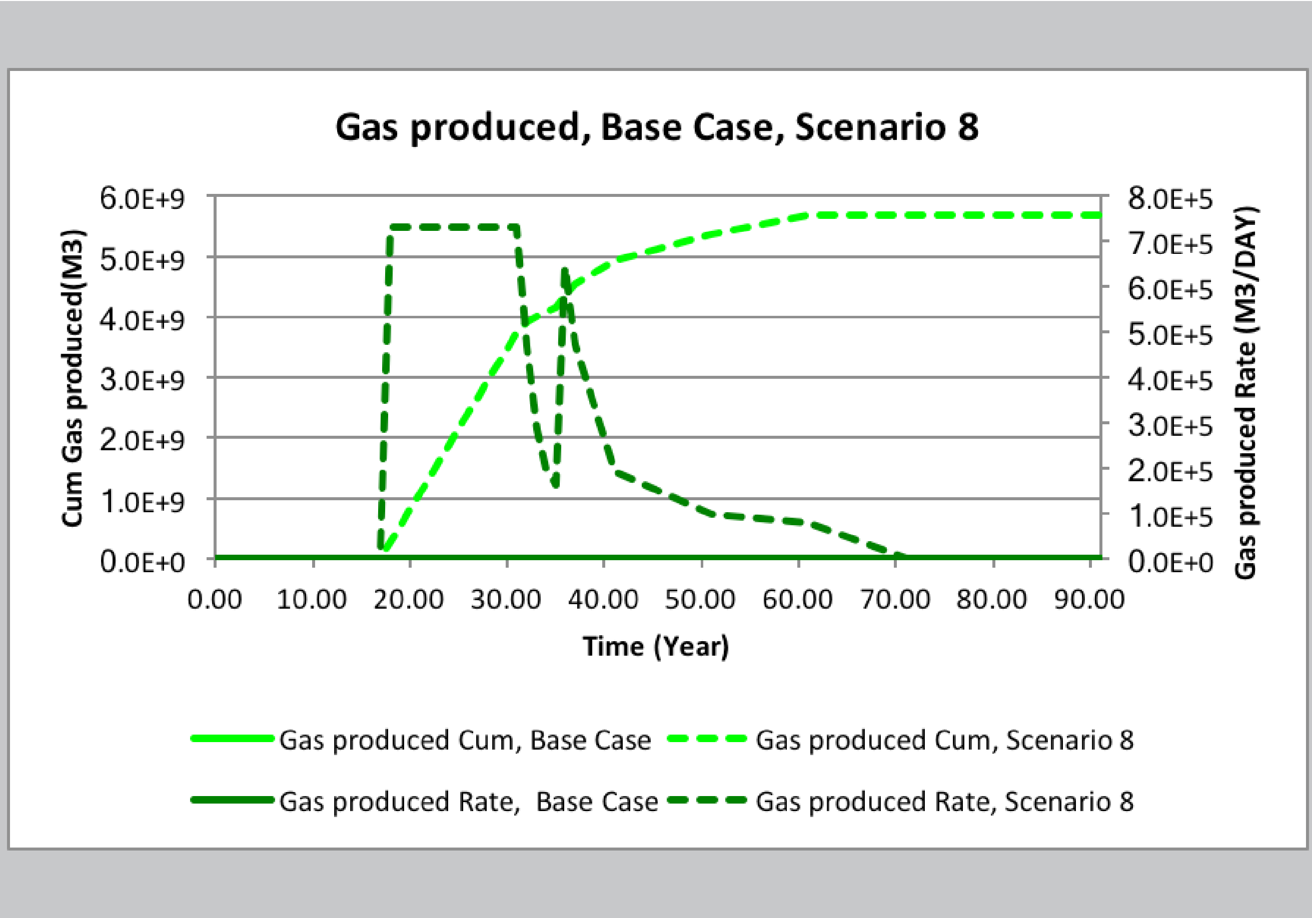

Figure 98 Gas back production rate and cumulatives of well JOHAN compared to the base case (no remediation) scenario.

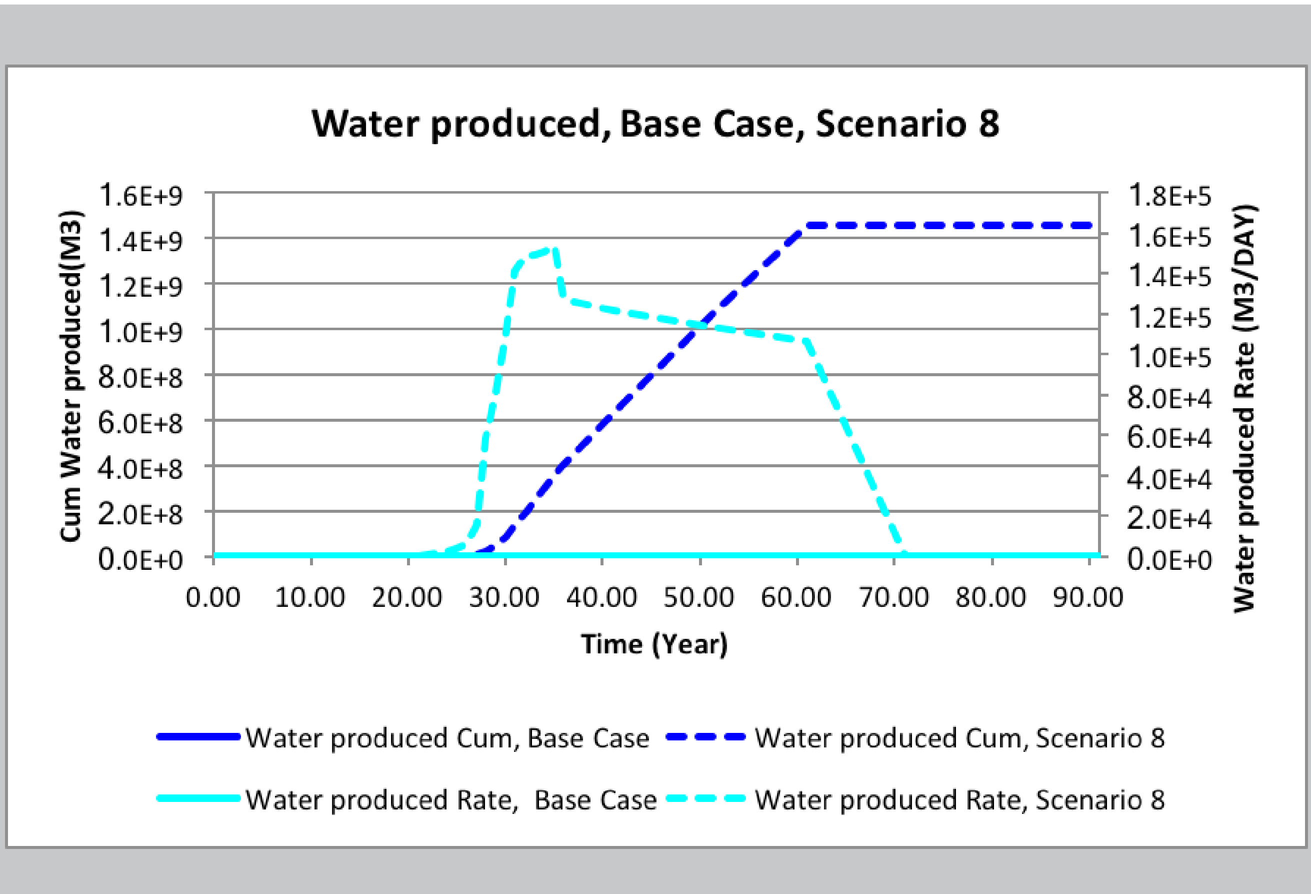

Figure 99 Water back production rate and cumulatives of well JOHAN compared to the base case (no remediation) scenario.

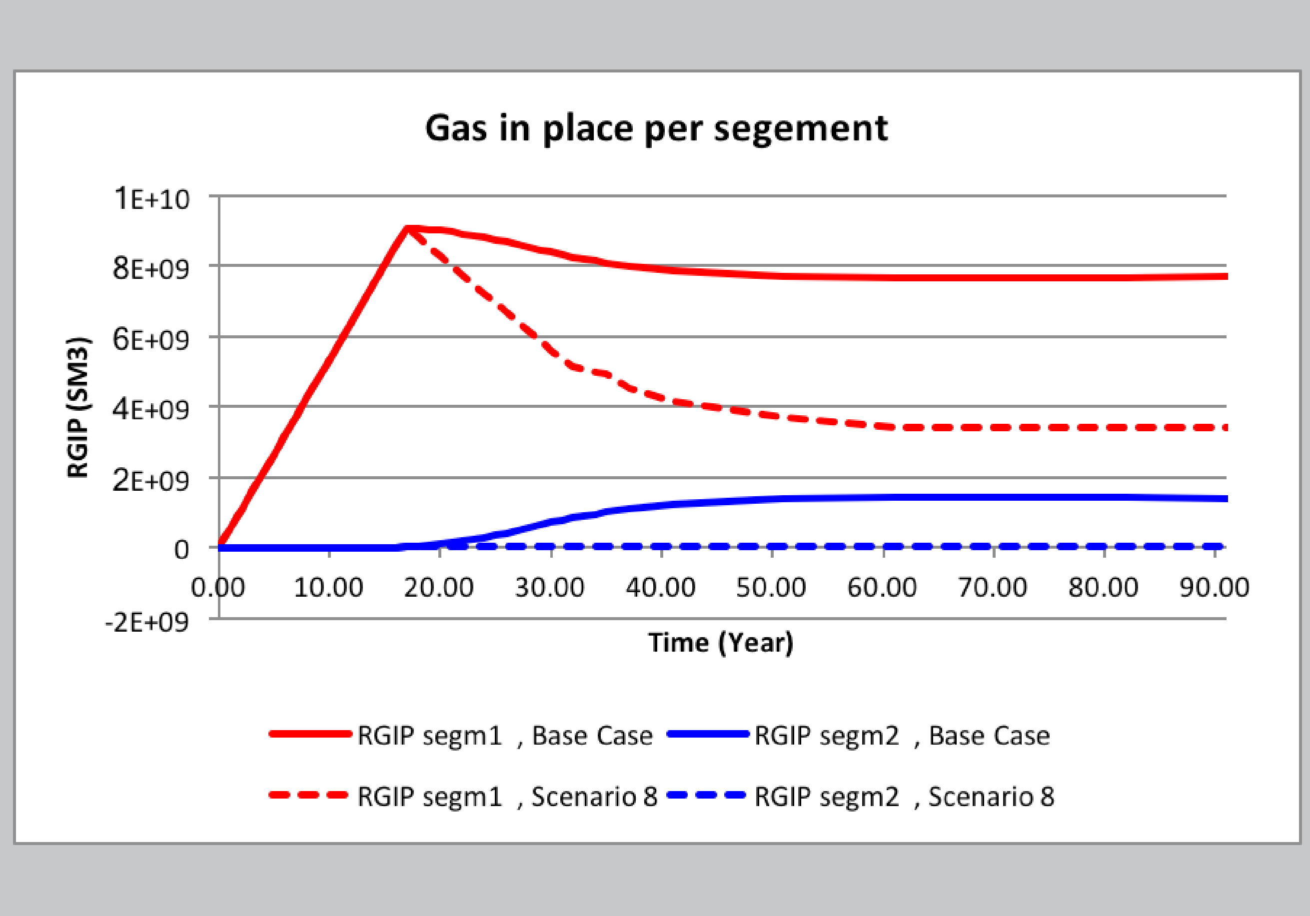

Figure 100 Unwanted migration to segment 2 compared to the base case (no remediation) scenario.

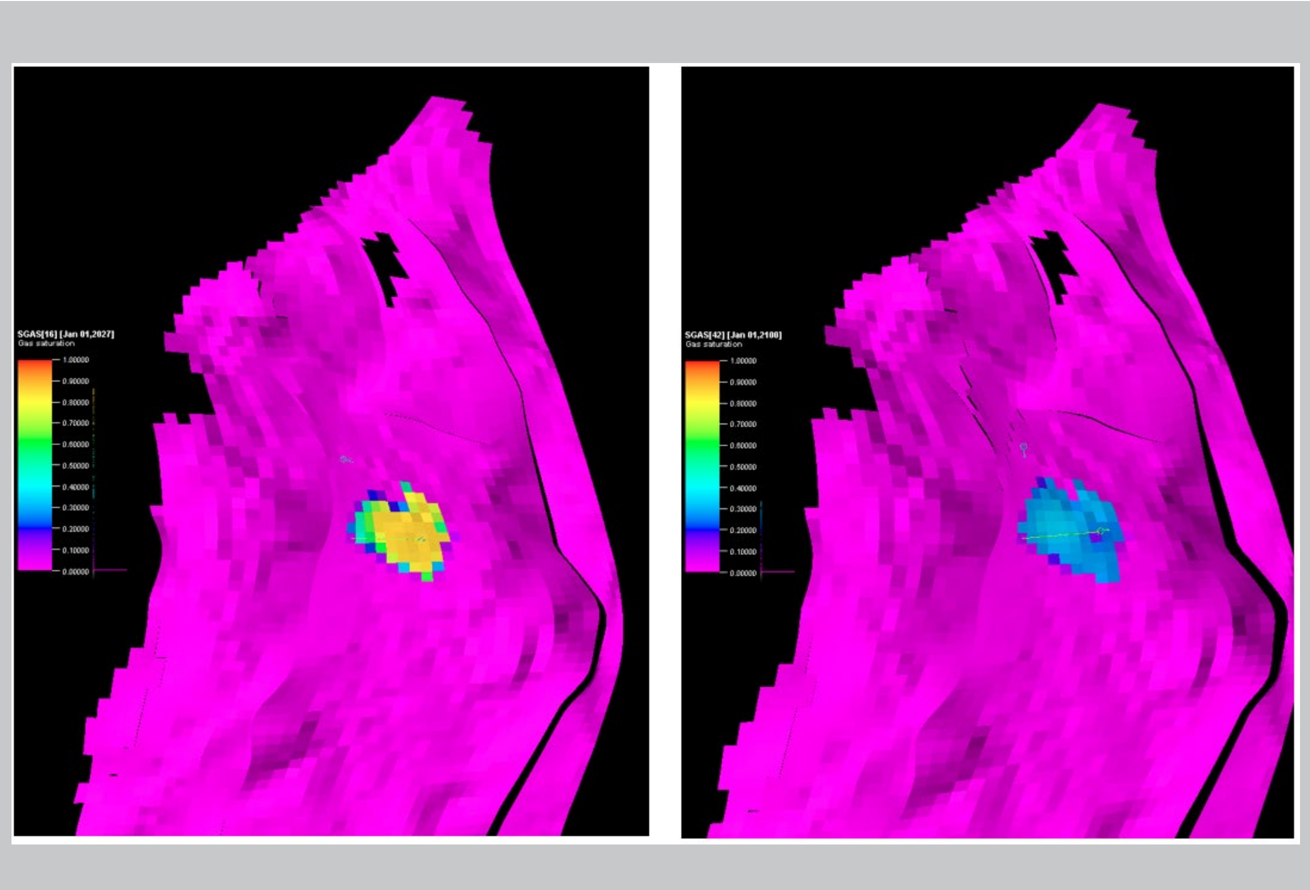

Figure 101 CO_2 plume after first detection of unwanted migration (left) and CO_2 plume after remediation at the end of simulation period of 93 years (right).

A-9 REMEDIATION SCENARIO 9

Table 33: Scenario description.

Scenario	**Remediation 9**
Description	After detection of unwanted migration of CO2, CO2 injection stopped and back production started for a period of 50 years (gas rate constraint of 1 Mton/yr). Injection of water for 10 years by one well.

Table 34 Simulation settings.

General		Remarks
Begin simulation	0	(year)
End simulation	91	(year)
CO_2 Injection well	**JOHAN1**	
Constraints	Rate constraint: 1 Mton/yr BHP constraint 360*BAR	
Location	Vertical well in gridblock (x,y)→(45, 47)	
Perforation	Z-coordinates of gridblock (15-17)	
On stream	From 0 to 17 years	
Remediation well	REM 1	
Constraints	BHP constraint 234*BAR (10% above P initial)	
Location	Vertical well in gridblock (x,y)→(38, 47)	
Perforation	Z-coordinates of gridblock (15-17)	
On stream	From year 18 to year 27	
Back production	JOHAN1	
Constraints	Gas Rate constraint 234: 0.7 e6 m3/day	
Location	Vertical well in gridblock (x,y)→(45, 47)	
Perforation	Z-coordinates of gridblock (15-17)	
On stream	From year 18 to year 69	

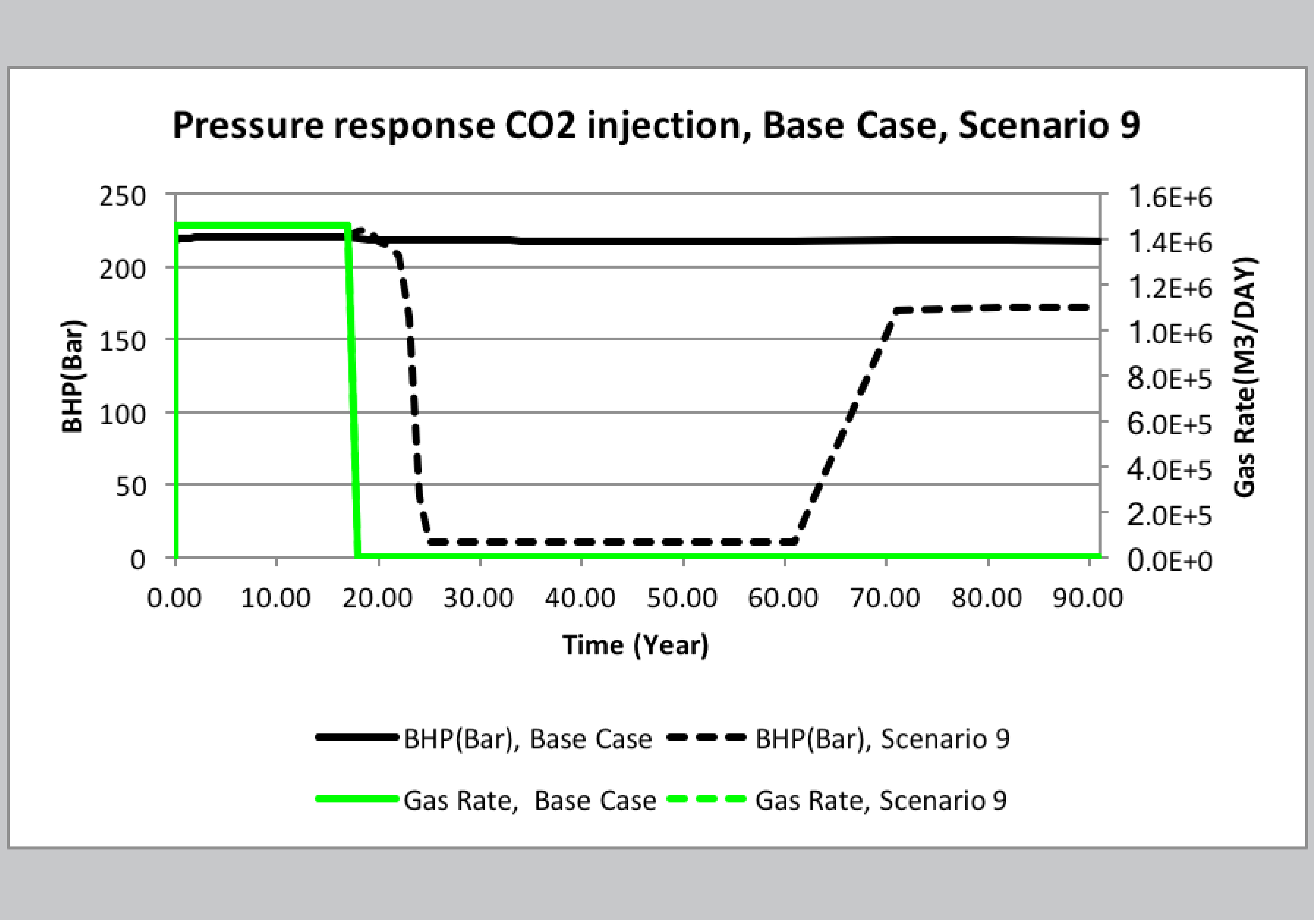

Figure 102 Gas injection rate and pressure response, compared to the base case (no remediation).

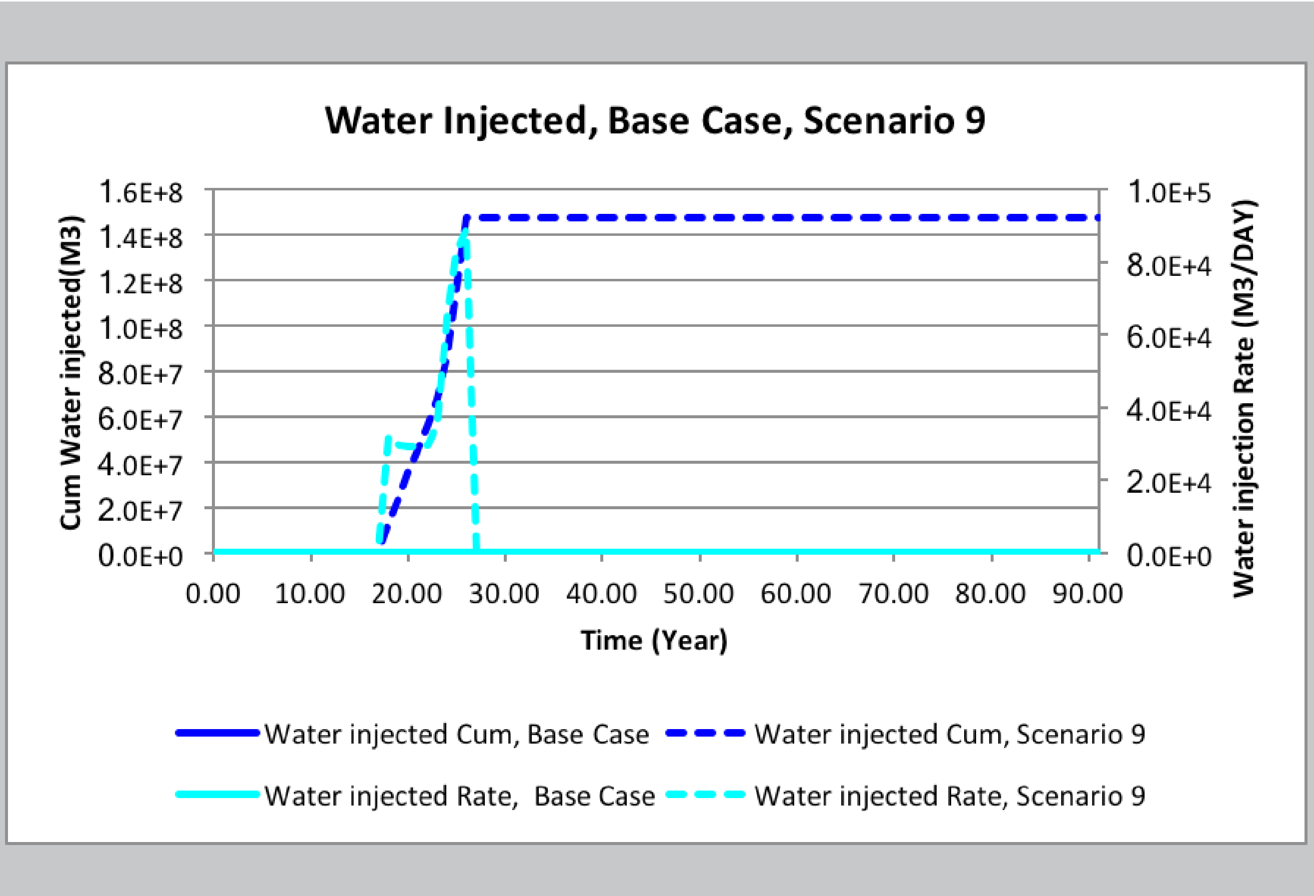

Figure 103 Water injection rates and cumulatives of well REM1, compared to the base case (no remediation) scenario.

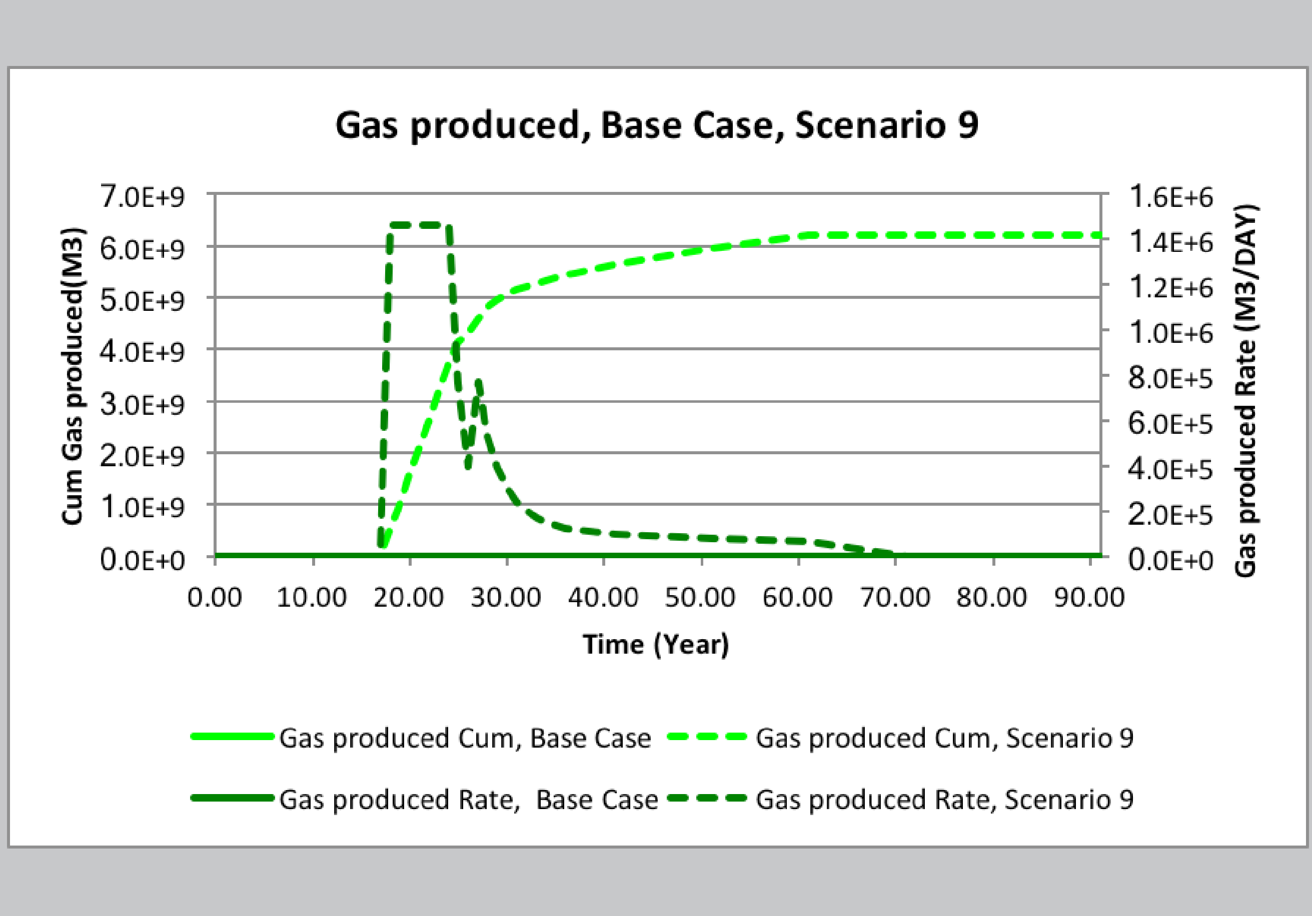

Figure 104 Gas back production rate and cumulatives of well JOHAN compared to the base case (no remediation) scenario.

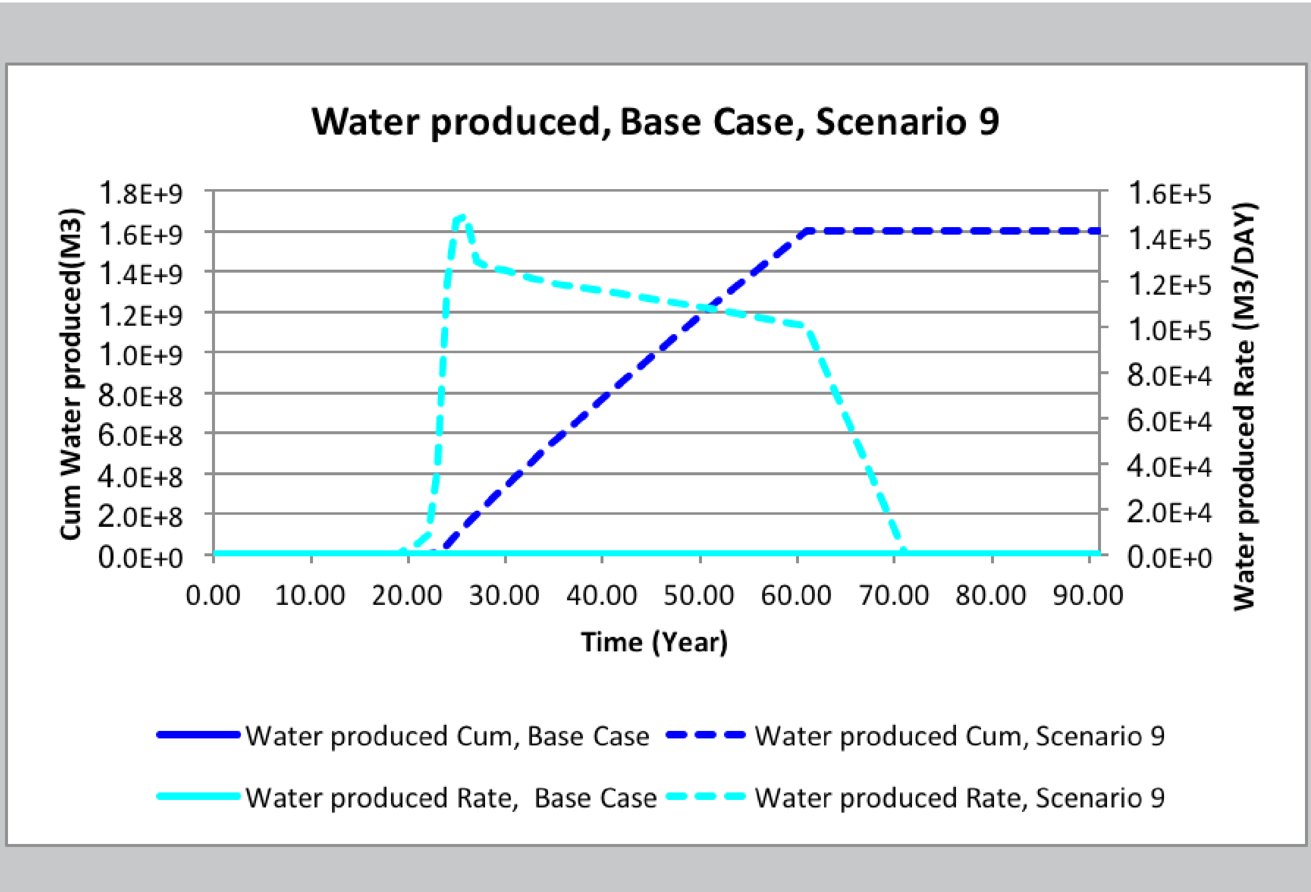

Figure 105 Water back production rate and cumulatives of well JOHAN compared to the base case (no remediation) scenario.

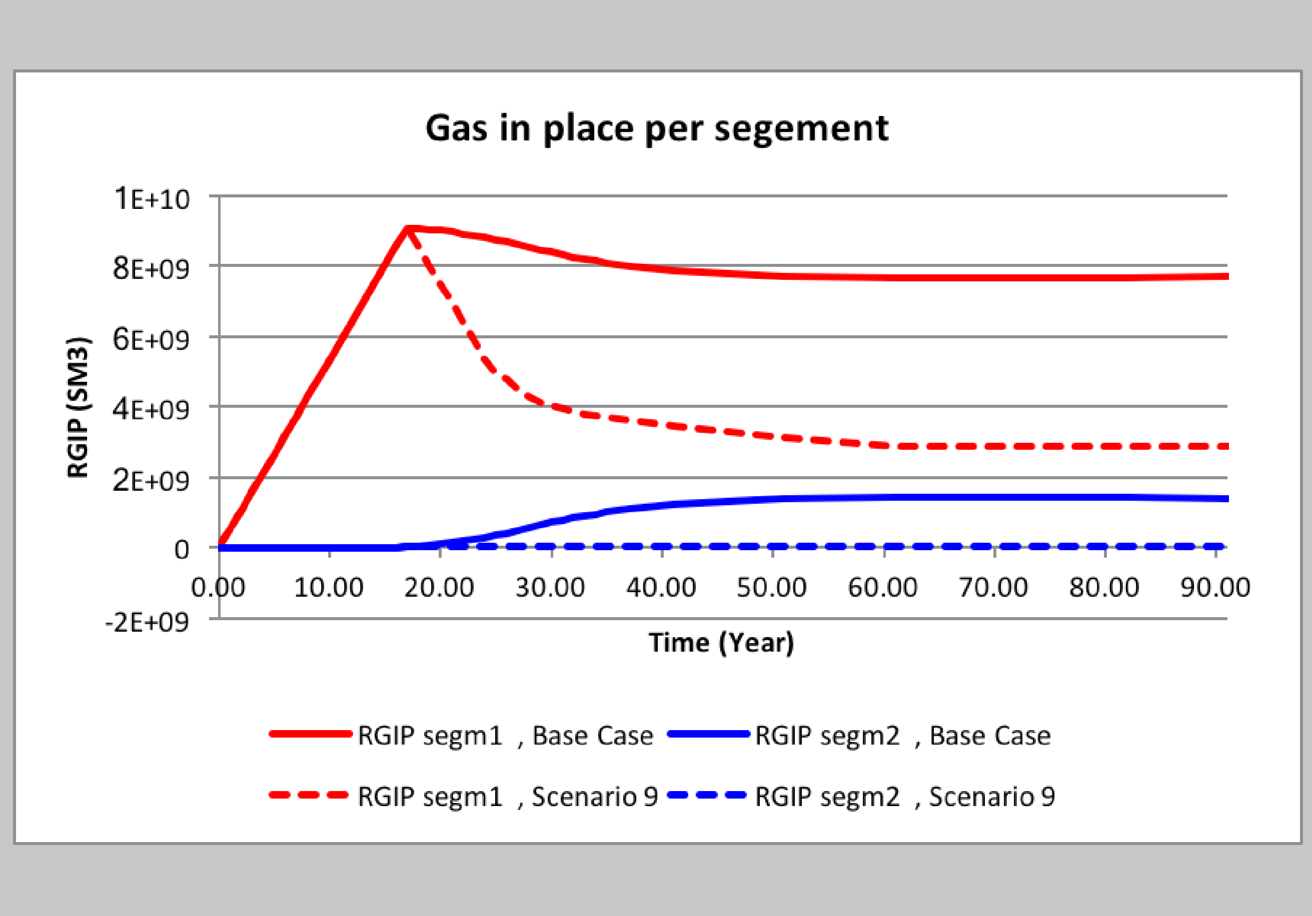

Figure 106 Unwanted migration to segment 2 compared to the base case (no remediation) scenario.

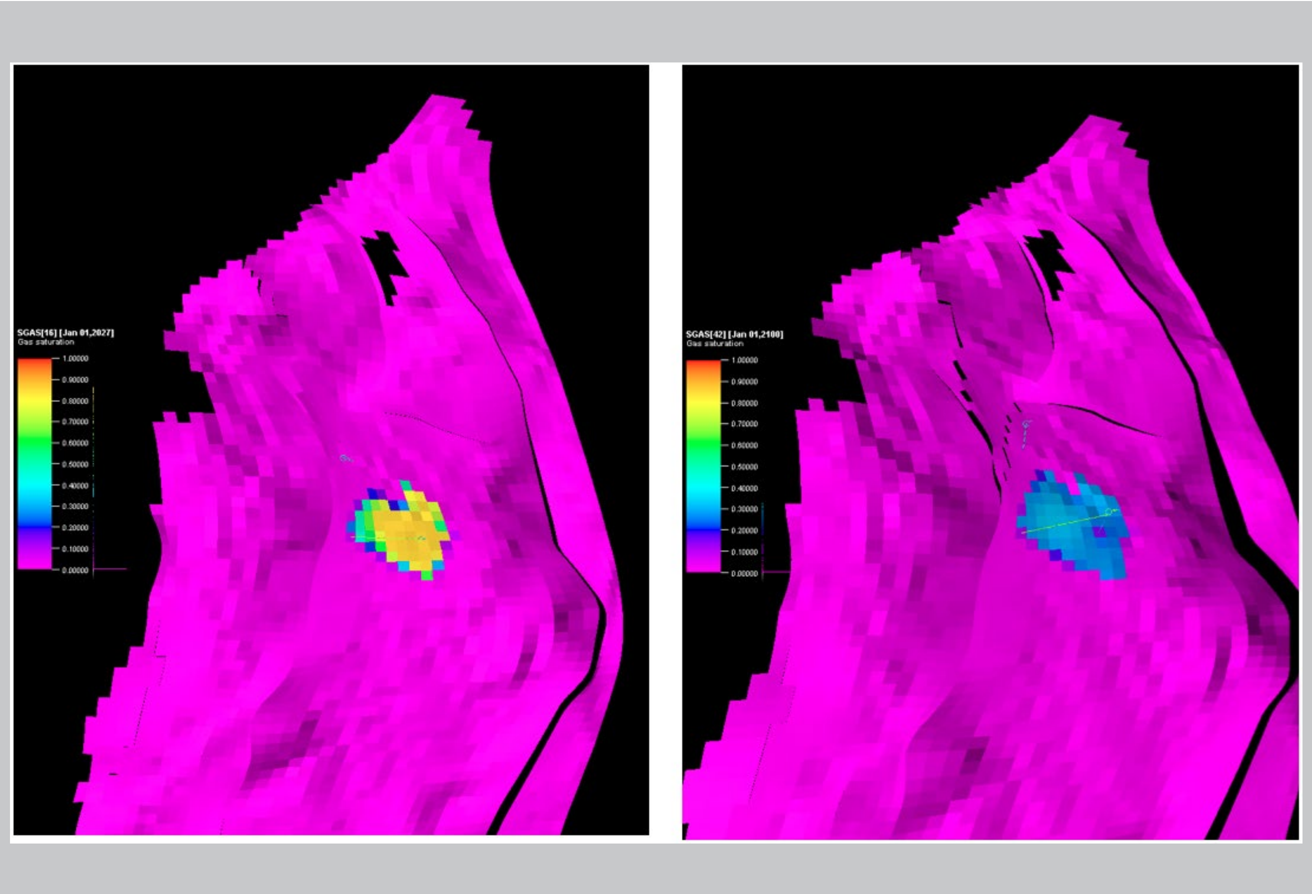

Figure 107 CO_2 plume after first detection of unwanted migration (left) and CO_2 plume after remediation at the end of simulation period of 93 years (right).

A-10 REMEDIATION SCENARIO 10

Table 35: Scenario description.

Scenario	Remediation 10
Description	After detection of unwanted migration of CO2, Co2 injection stopped and injection of water for 10 years by one well (whole simulation period)

Table 36 Simulation settings.

General		Remarks
Begin simulation	0	(year)
End simulation	91	(year)
CO_2 Injection well	**JOHAN1**	
Constraints	Rate constraint: 1 Mton/yr BHP constraint 360*BAR	
Location	Vertical well in gridblock (x,y)→(45, 47)	
Perforation	Z-coordinates of gridblock (15-17)	
On stream	From 0 to 17 years	
Remediation well	REM 1	
Constraints	BHP constraint 234*BAR (10% above P initial)	
Location	Vertical well in gridblock (x,y)→(38, 47)	
Perforation	Z-coordinates of gridblock (15-17)	
On stream	From year 18 to year 23	
Back production	JOHAN1	
Constraints	Gas Rate constraint 234: 0.7 e6 m3/day	
Location	Vertical well in gridblock (x,y)→(45, 47)	
Perforation	Z-coordinates of gridblock (15-17)	
On stream	From year 18 to year 69	

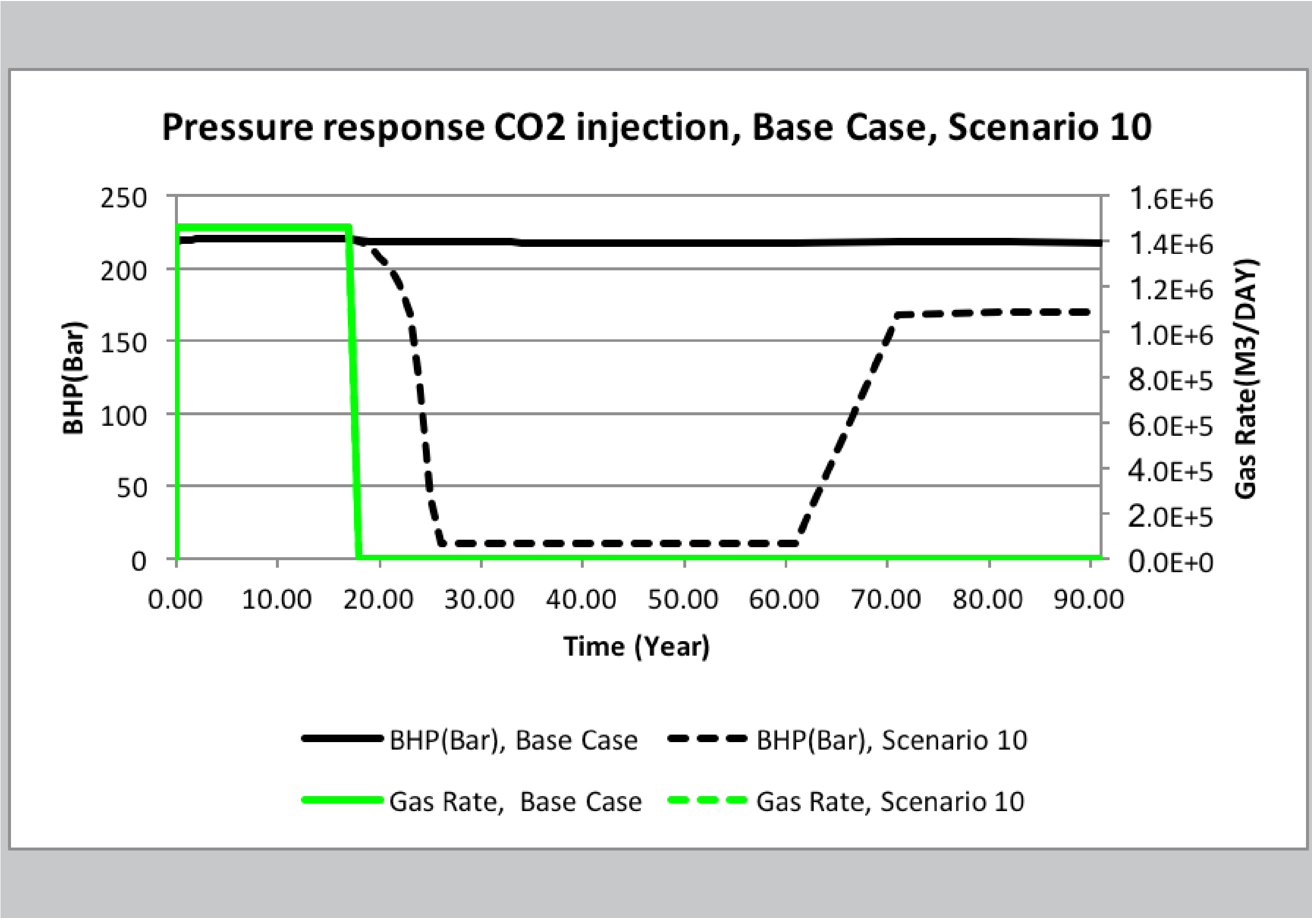

Figure 108 Gas injection rate and pressure response, compared to the base case (no remediation).

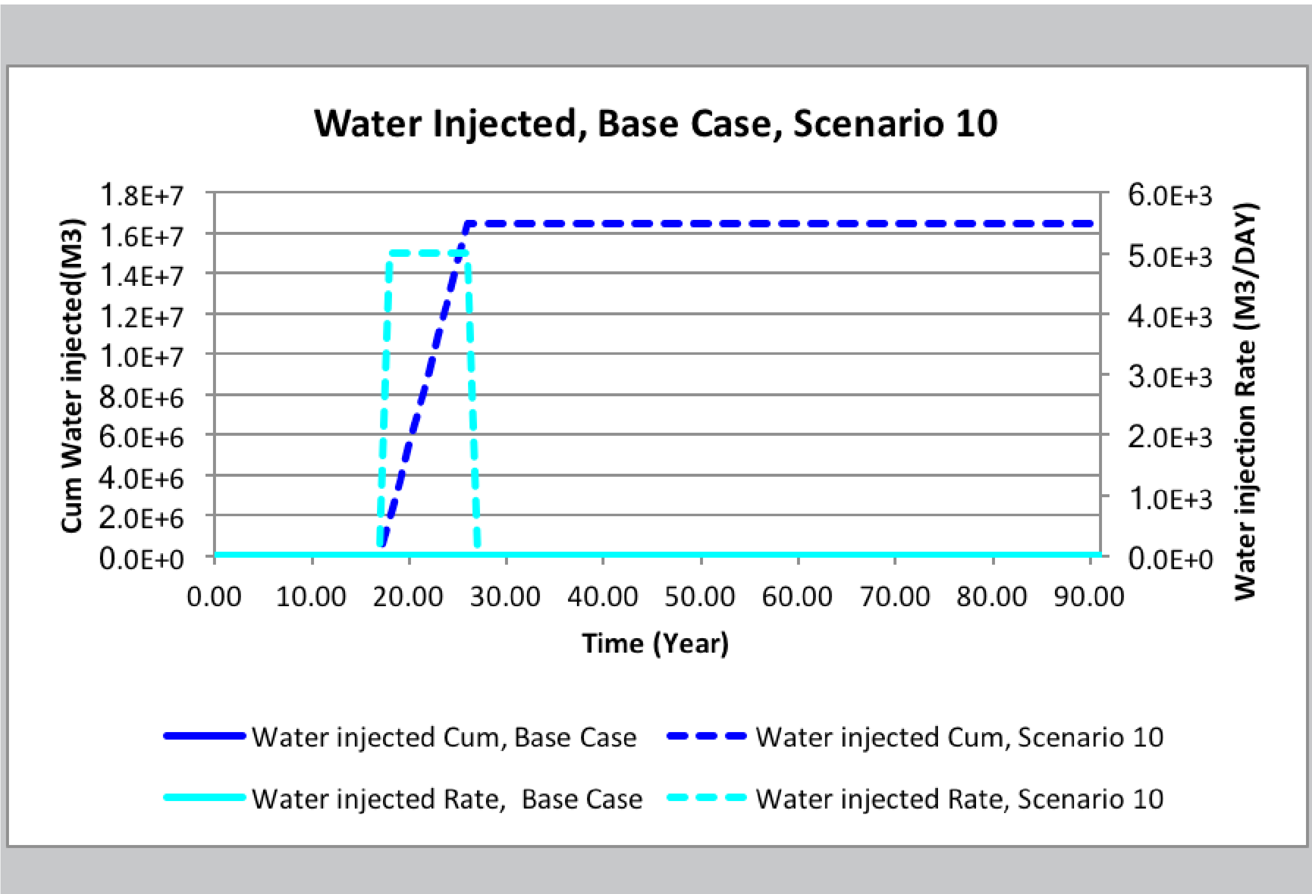

Figure 109 Water injection rates and cumulatives of well REM1, compared to the base case (no remediation) scenario.

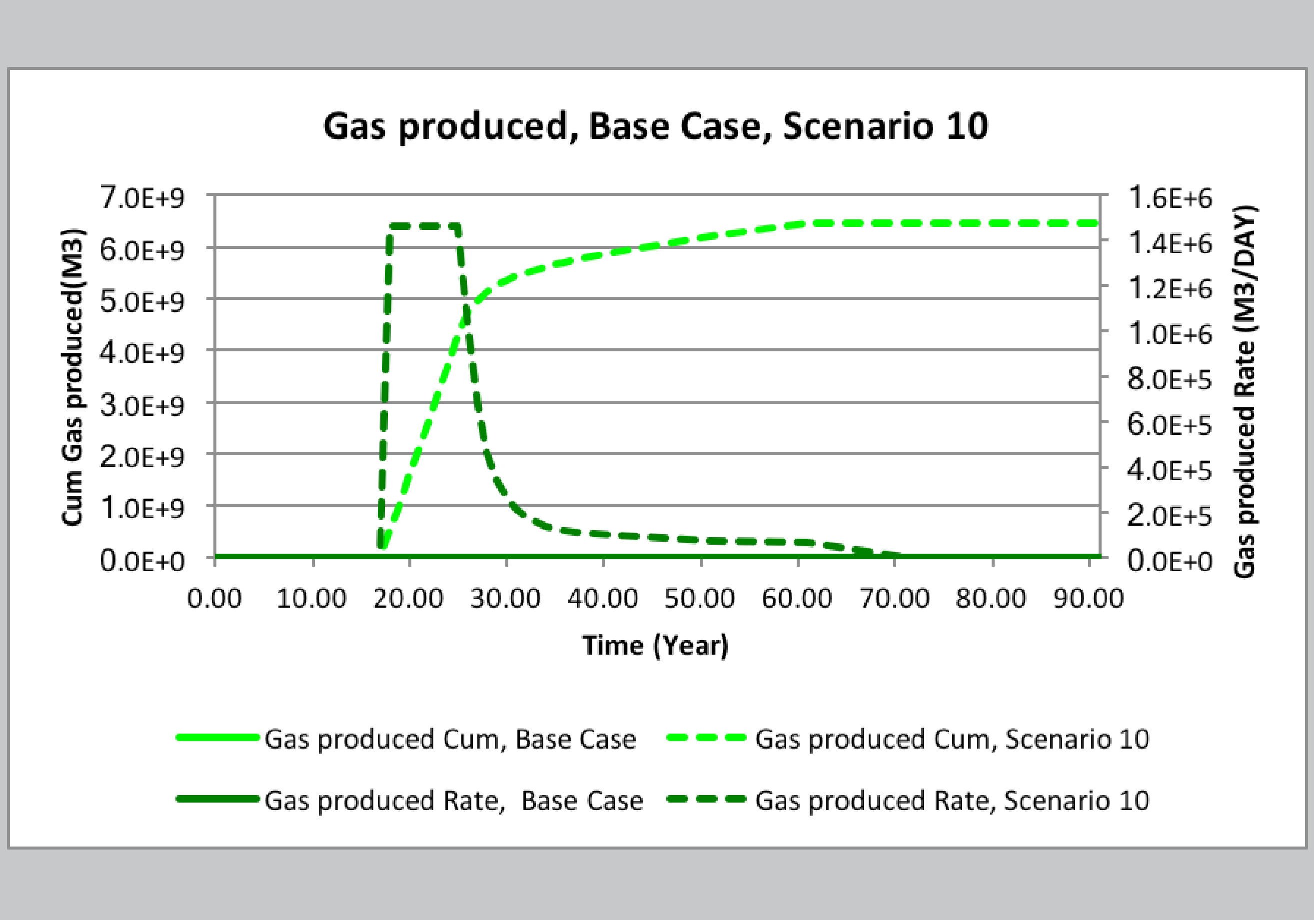

Figure 110 Gas back production rate and cumulatives of well JOHAN compared to the base case (no remediation) scenario.

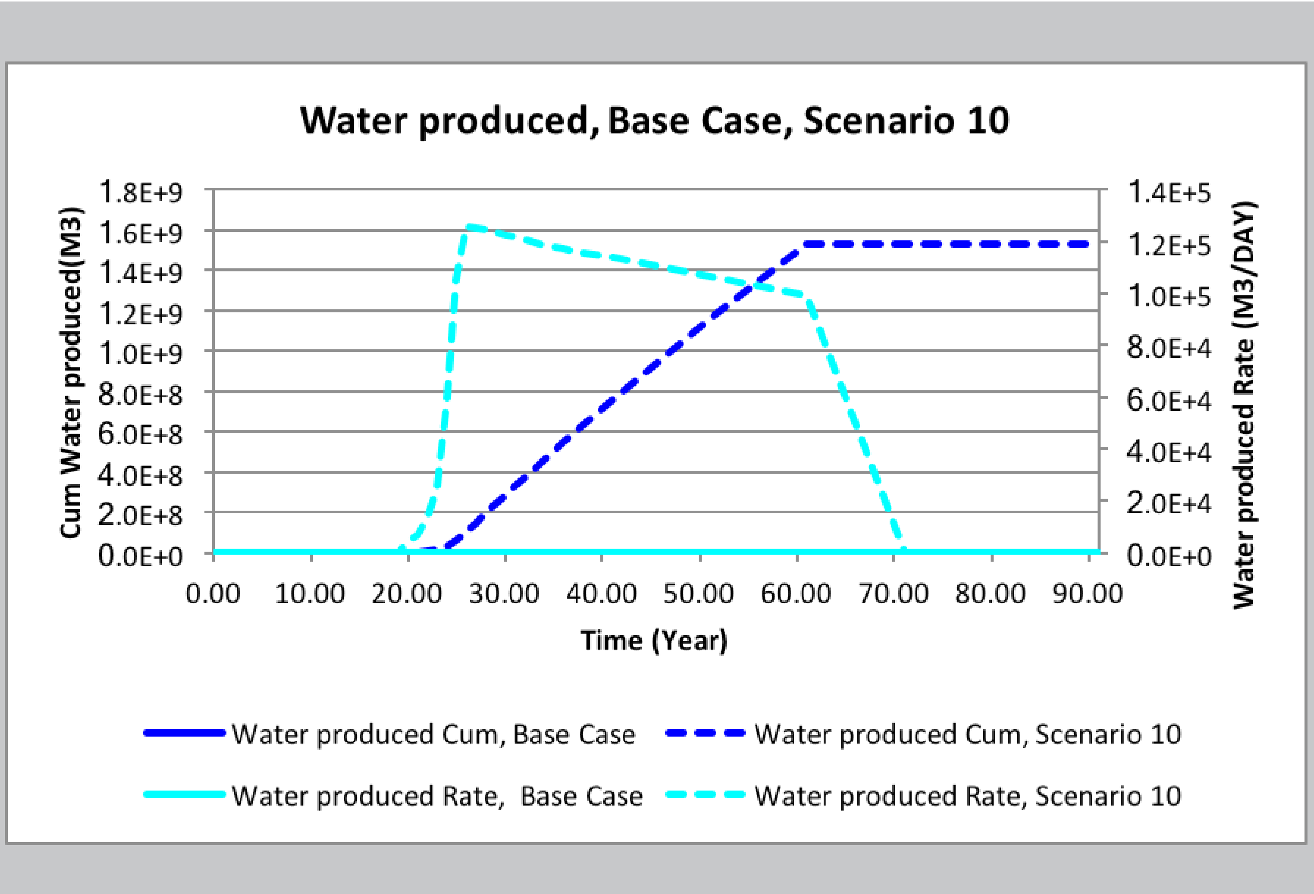

Figure 111 Water back production rate and cumulatives of well JOHAN compared to the base case (no remediation) scenario.

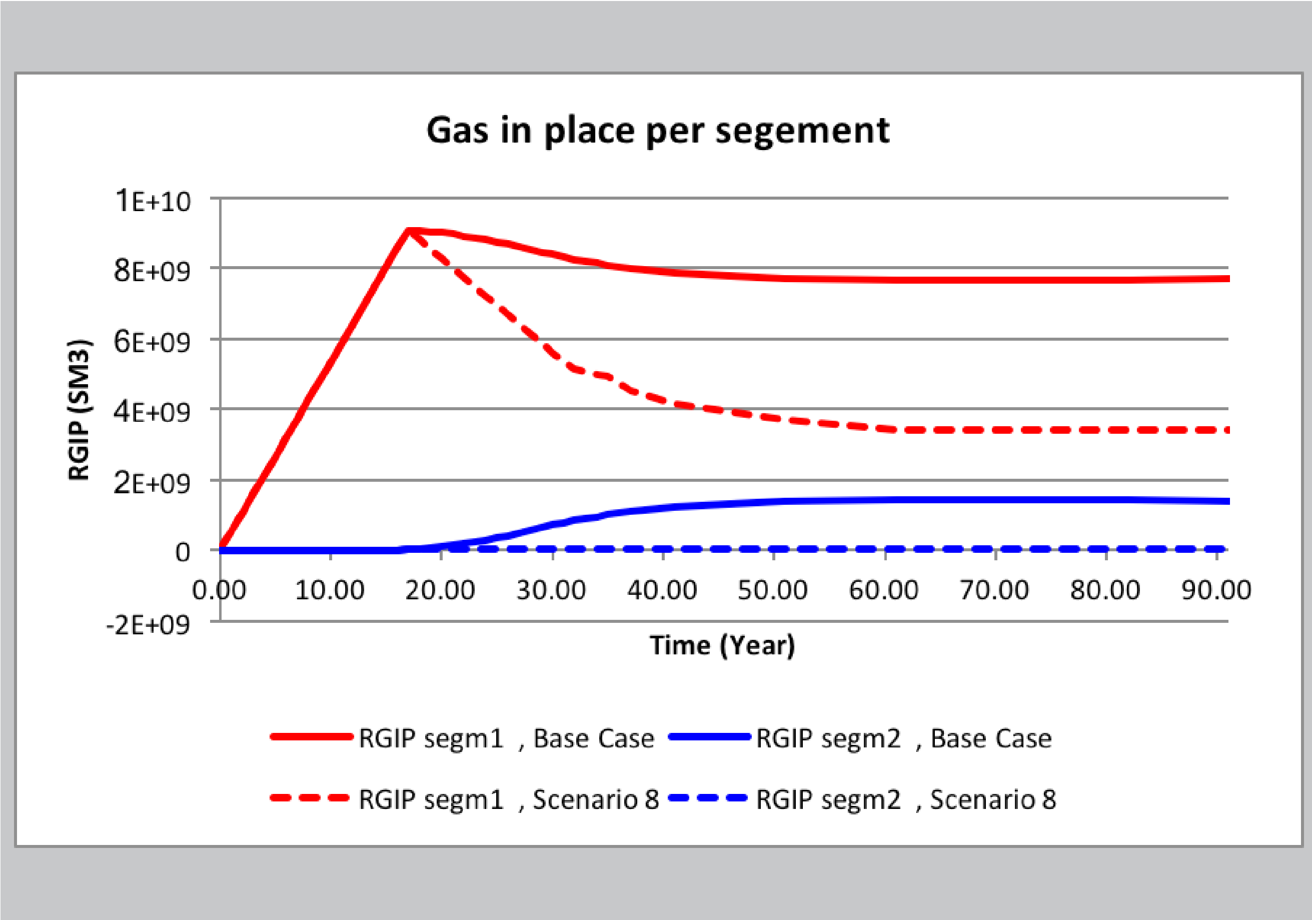

Figure 112 Unwanted migration to segment 2 compared to the base case (no remediation) scenario.

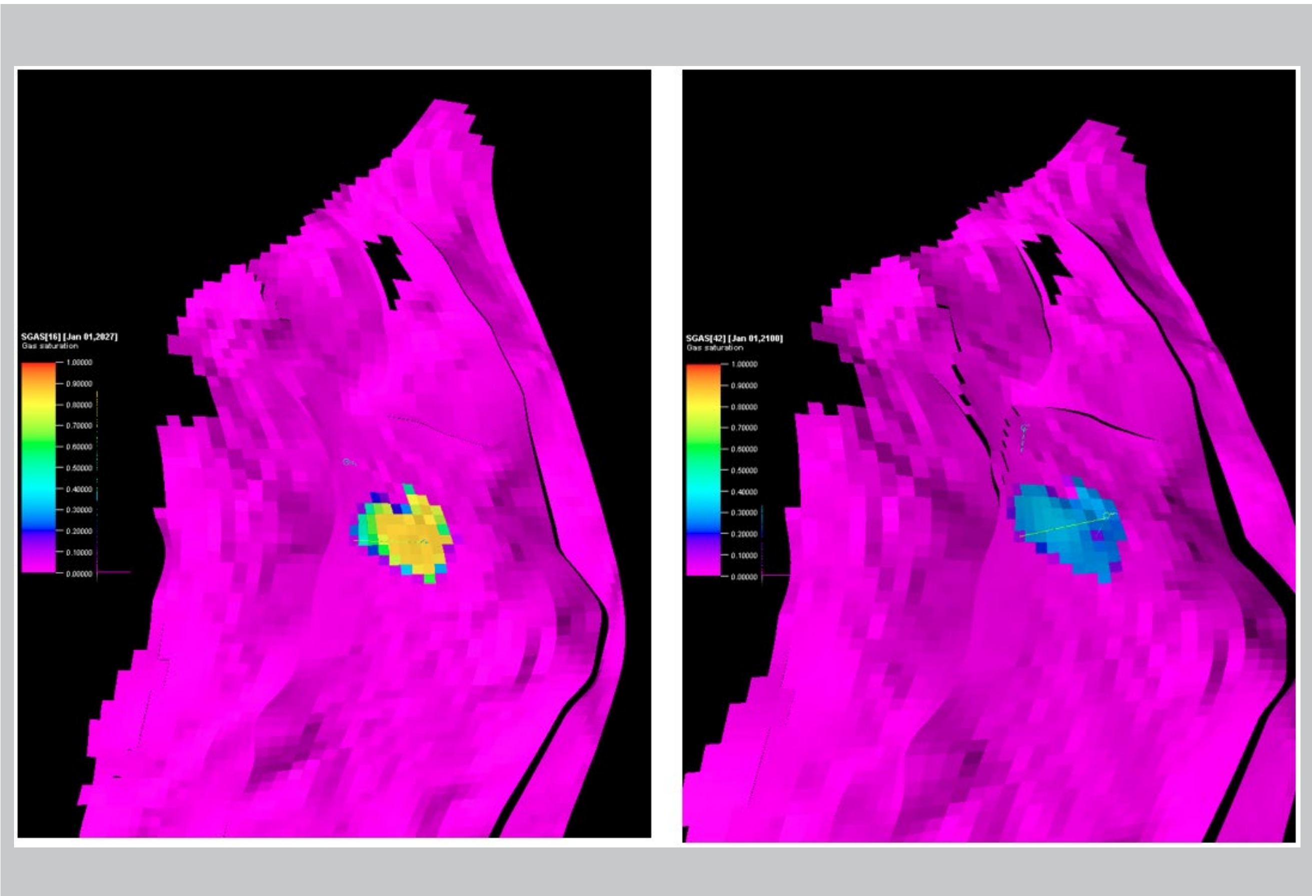

Figure 113 CO_2 plume after first detection of unwanted migration (left) and CO_2 plume after remediation at the end of simulation period of 93 years (right).

Chapter V

Blocking of CO_2 movement by immobilization of CO_2 in solid reaction products

Laura Wasch[1]
[1] TNO, The Netherlands

SUMMARY

In the unlikely case of localized CO_2 leakage from a storage reservoir, it is desirable to close the leak quickly, efficiently and permanently. This could be done by injection of material in the leak path, thereby blocking the flow. With regard to permanent closure, it is straightforward to look into materials that occur naturally in the subsurface, since they are stable in the long-term, ensuring permanent CO_2 containment in the storage site. This report describes a numerical modelling approach to assess the feasibility of injecting lime-saturated water as a CO_2-reactive solution to form calcite, block CO_2 flow and remediate leakage. We performed reactive transport simulations with the software TOUGHREACT. A 3D model was developed of a CO_2 reservoir at the bottom, an aquifer at the top and a cell connecting the two layers, representing a caprock leakage pathway (such as a permeable fault or along a wellbore). A CO_2 plume was developed in the top aquifer by defining a leak in the caprock. The initial state of a CO_2 plume present takes into account the time required for a plume to become large enough to be detected by monitoring techniques.

A scenario analysis was performed to assess the effectivity and efficiency of the remediation method and evaluate the uncertainty related to the key parameters. The scenarios represent a range of possible characteristics of the storage reservoir and the leak that could affect the leakage remediation method. The key parameters include: reservoir pressure, gas saturation below the leak, permeability, leakage rate, injection distance from the leak and injection rate. Results for leakage reduction were obtained during and after remediation. This showed that leakage is affected by the injection of water and pressure changes (hydraulic remediation) as well as clogging of the pore space (chemical remediation). Of the two, only the chemical part remains after injection is stopped. Modelling showed that injection of the reactive solution in a CO_2-containing rock does not yield enough calcite, while full porosity clogging requires additional supply of CO_2 by the leak itself. Hence the leak should be maintained to allow the build-up of calcite until full porosity clogging is achieved. This situation requires a balance of injection rate, leakage rate, injection rate and reaction rate. The scenarios analysed indicated certain combinations of conditions and parameters which promoted chemical clogging. Scenarios showed a success of leakage remediation varying between 0 and 95%. The degree of leakage reduction can be used to calculate the likelihood of success of remediation and provide input for the MiReCOL webtool. This tool will help site owners to find appropriate remediation methods in the unlikely case that CO_2 leakage occurs.

1 INTRODUCTION

To store CO_2 permanently in the subsurface, reservoirs are selected that provide physical and chemical containment of CO_2. However, future control on the movement of CO_2 is asked for in the unlikely case that CO_2 migrates out of its intended storage reservoir. Flow control measures are developed to demonstrate possibilities for preventing CO_2 leakage to overlying aquifers or to the surface, safeguarding the contribution of the stored CO_2 in reducing global warming. Immobilizing migrating CO_2 by consuming the gas and forming solid reactants is a relatively new field. Flow control by precipitating solids in the pore space has been practiced in the oil and gas industry in the context of 'water shut-off', blocking water production from high permeable layers and enhancing oil production from low permeable layers. Plugging agents such as foams and polymers are generally used, but for permanent CO_2 immobilization they lack the proven long-term stability in the subsurface. Forming mineral solid reactants will have the advantage of creating a naturally stable barrier against CO_2 flow.

Experience with unintentional precipitation or scaling and formation damage, as commonly encountered in the oil and gas or geothermal industries, sheds some light onto the possibilities for forming solid reactants. Minerals observed to form 'naturally' within the reservoir may all be potential candidates for controlled precipitation. Frequently occurring scales associated with oil and gas production are calcite, anhydrite, barite, celestite, gypsum, iron sulphide and halite (Cowan and Weintritt, 1976). Re-injection of production water is prone to scaling of calcium carbonate (Rocha et al., 2001, Moghadasi et al 2004, Birkle et al., 2008), while strontium, barium and calcium sulphates are more relevant for seawater injection (Delshad & Pope, 2003, Mota et al., 2004, Bedrikovetsky et al., 2006). Water injection in geothermal systems may involve precipitation of carbonates, silica (polymorphs), metal compounds (oxides hydroxides sulphides sulphate) and clays (e.g. Kuhn et al., 1997, Tarcan, 2005, Izgec et al. 2005, Regenspurg et al., 2010). The possibilities of precipitation due to water injection have been recognized by Nasr-El-Din et al. (2004), who aimed to achieve selective plugging by introducing fluid which is chemically incompatible with the reservoir brine, thereby causing mineral precipitation. In addition to fluid-fluid reactions, fluid-gas interaction may promote mineralization. Linked to well abandonment after CO_2 storage Wasch et al. (2013) proposed controlled intentional clogging with salt to prevent possible leakage of CO_2. Salt will precipitate when the solubility is exceeded due to evaporation into injected dry gas. This process is similar to salt scaling in natural gas and oil production (e.g. Kleinitz et al., 2001) and CO_2 injection in saline aquifers (e.g. Pruess and Müller, 2009, Zeidouni et al., 2009) and depleted gas fields (Giorgis et al., 2007 and Tambach et al., 2014). After injection, slower mineralization reactions between the stored CO_2 and the host rock may occur on the longer term. Much research has been done on this topic since these reactions provide permanent trapping and increased the storage safety (e.g. of Gaus, 2010).

Previous work on the induced formation of solid reactants for leakage remediation concerns calcite or silica. Bio-mineralization has been proposed for engineering biofilms covering grains subsequently forming carbonate by ureolysis (Mitchell et al., 2009, Cunningham et al., 2011). Carbonate can also be directly formed by injecting reactive suspensions or solutions into the CO_2 containing environment (Ito et al., 2014). Ito et al., (2014) report experiments and modelling of a chemical substance that will react with CO_2 to form a barrier for further CO_2 leakage. They injected both silica and calcium grouts into synthetic porous medium of glass beads. The experimental results support the feasibility of the method for reactive clogging of a high permeable leak path. Druhan et al. (2014) numerically investigated amorphous silica formation adapted for a higher molecular volume analogues to silica polymers. We investigated the feasibility of injecting a CO_2-reactive and CO_2-consuming reactive solution. Lime-saturated water is selected which reacts readily upon contact with CO_2. This approach has the advantage that reactions can be modelled with available software and databases without modifications. Furthermore a solution will have a low viscosity, which simplifies injection. The production and practical use of such a fluid is beyond the scope of this study. The results derived for the lime solution will provide general insight in leakage mitigation using non-swelling CO_2 reactive substances.

2 METHODS

2.1 Simulator

The simulations were performed with the TOUGHREACT reactive transport flow simulator, using the Petrasim interface. TOUGHREACT has been developed for coupled modeling of subsurface multiphase fluid and heat flow, solute transport, and chemical reactions by introducing reactive transport into the flow simulator TOUGH2 (Xu et al., 2006). TOUGH2 is a numerical simulation program for multi-dimensional fluid and heat flow of multiphase, multicomponent fluid mixtures in porous and fractured media (Pruess et al., 1999). We used the ECO2N fluid property module for CO_2 and brine mass transfer including the thermodynamics and thermophysical properties of H_2O-NaCl-CO_2 mixtures (Pruess, 2005). The mineral reaction kinetics are included for the solid reactant using reaction rates of Palandri and Kharaka (2004).

2.2 Workflow

2.2.1 Mesh making

The model was developed to represent a CO_2 storage site with a CO_2 storage reservoir, a caprock and an overlying aquifer (Figure 1, image 0). The dimensions are 200*200*140 meter and the model was arbitrarily located between 2000 and 2140 m depth. Vertical sub-layering was chosen to obtain more detail in the top aquifer where leakage remediation is required (Table 1). For the x,y direction a custom regular grid was defined (Table 2). Note that the grid is asymmetric and has finer gridding at the right side where injection is envisaged. We developed a model to find an optimum between model size and grid refinement within the maximum of 8000 active cells allowed by TOUGHREACT.

Table 1 Model layering (z direction).

	Total thickness (m)	*Number of layers*	*Layer thickness (m)*
Top aquifer	80	1	24
		3	13 1/3
		3	5 1/3
Caprock	20	1	20
Storage reservoir	40	3	13 1/3

Table 2 Cell sizes in the x and y direction.

number of cells	1	4	2	1	10	2	1	1
cell size (m)	30	15	4	2	4	15	30	30

The rock properties were based on the P18 field with a reservoir porosity of 15% and flow properties as listed in Table 3. Preliminary modelling showed that the permeability of the aquifer is the limiting factor for the leakage rate and a higher permeability for the leak path through the caprock does not increase the leakage rate significantly. Hence for simplicity the flow properties of the aquifer, caprock (leak) and reservoir were taken equal. Only for the leak the vertical permeability is not decreased by a factor of ten.

Table 3 Rock properties.

	Permeability	
	(mD)	(m^2)
Horizontal (kh)	20	2E-14
Vertical (kv)	2	2E-15
	Relative permeability	
	Slr	Sgr
Corey's Curves	0.18	0.121
	Capillary pressure	
	P0	Slr
Leverett's function	1.00E+06	0.18

2.2.2 Initialization of conditions prior to CO_2 storage

The initial conditions for model initialization are 200 bar pressure, 1E-10 gas saturation and a 0.06 salt mass fraction. Note that the gas saturation is close to zero and hence resembles an aquifer before CO_2 storage. The temperature is selected to be 80°C and non-isothermal behaviour is neglected. The model is run for 20,000 years for initialization, distributing the pressure, gas saturation and brine composition with depth according gravitational forces. The caprock was set to permeable to allow for pressure distribution. The resulting pressure with depth is shown in Figure 1.

Table 4 Mineralogy for calculating of the formation water.

Mineral	*Volume fraction*
Quartz(alpha)	0.7
Microcline	0.1
Illite(Al)	0.1
Albite(high)	0.1

Table 5 Formation water composition.

Formation water (mol/L)	
Cl	1
Na+	9.99E-01
H4SiO4	7.30E-04
K+	1.09E-03
Al	3.04E-07
pH	8.03

2.2.3 Initialization of chemistry and conditions after CO_2 storage

The initialized conditions of the previous step were used and chemical properties were included. The whole model was assigned the same formation water. The formation water composition was calculated in a separate batch model, equilibrating NaCl brine with a simple sandstone mineralogy (Table 4 and Table 5). Only the water is used for further modelling, reservoir rock – fluid/gas reactions are neglected given short time of interest for leakage remediation. To aid chemical convergence a mineralogy was defined with only (nearly inert) quartz.

The reservoir is subsequently filled with CO_2 by assigning the cells a gas saturation of 80%. Two situations were considered: a) hydrostatic pressure in the reservoir as for storage in a depleted gasfield and b) 20 bar overpressure to represent aquifer storage (Figure 1, images 2a/2b). The caprock was disabled and the leak pathway was assigned a zero permeability to obtain initial containment of CO_2 in the reservoir. The model was ran for 2 years to initialize pressure and gas saturation, furthermore the water chemistry in the reservoir was allowed to equilibrate with CO_2.

2.2.4 Initialization of the CO_2 Leak

The initialized conditions of the previous step were used and the caprock leak cell was enabled with a permeability equal to the horizontal permeability the aquifer. The lateral boundary conditions are open (i.e. given a 1E50 volume factor) to allow free flow away and towards the leak. Top and lower boundary conditions are closed, assuming impermeable bounding formations. The leakage rate is allowed to develop following the pressure and saturation conditions and the flow properties. Buoyancy drives CO_2 upwards forming a plume of CO_2 in the aquifer above the leak (Figure 1, image 3). Since MiReCOL aims to supply mitigation methods for the case of an existing leak, we allow a plume to develop for a period of 10 years. This period is arbitrarily chosen, but should allow for a leak to become substantially large enough to be detected by monitoring even though the flow rate is small.

2.2.5 Injection of the lime-saturated fluid

After the CO_2 plume is established, a CO_2 reactive fluid is injected (Figure 1, image 4). We study injection into an aquifer above the storage reservoir. This method would have several advantages over injection in the reservoir itself. The caprock does not have to be penetrated by a new well, and hence no additional leakage risk is created. Gravitational effects of the dense liquid help suppress the leaking gas. In contrast, injection below the caprock may cause the liquid to sink and move away from the leak as buoyant CO_2 flows upwards. A disadvantage of injection above the leak is that the characteristics of the top aquifer may be poorly known while – especially for a depleted gas field – flow properties and pressure response are far better understood for the reservoir itself.

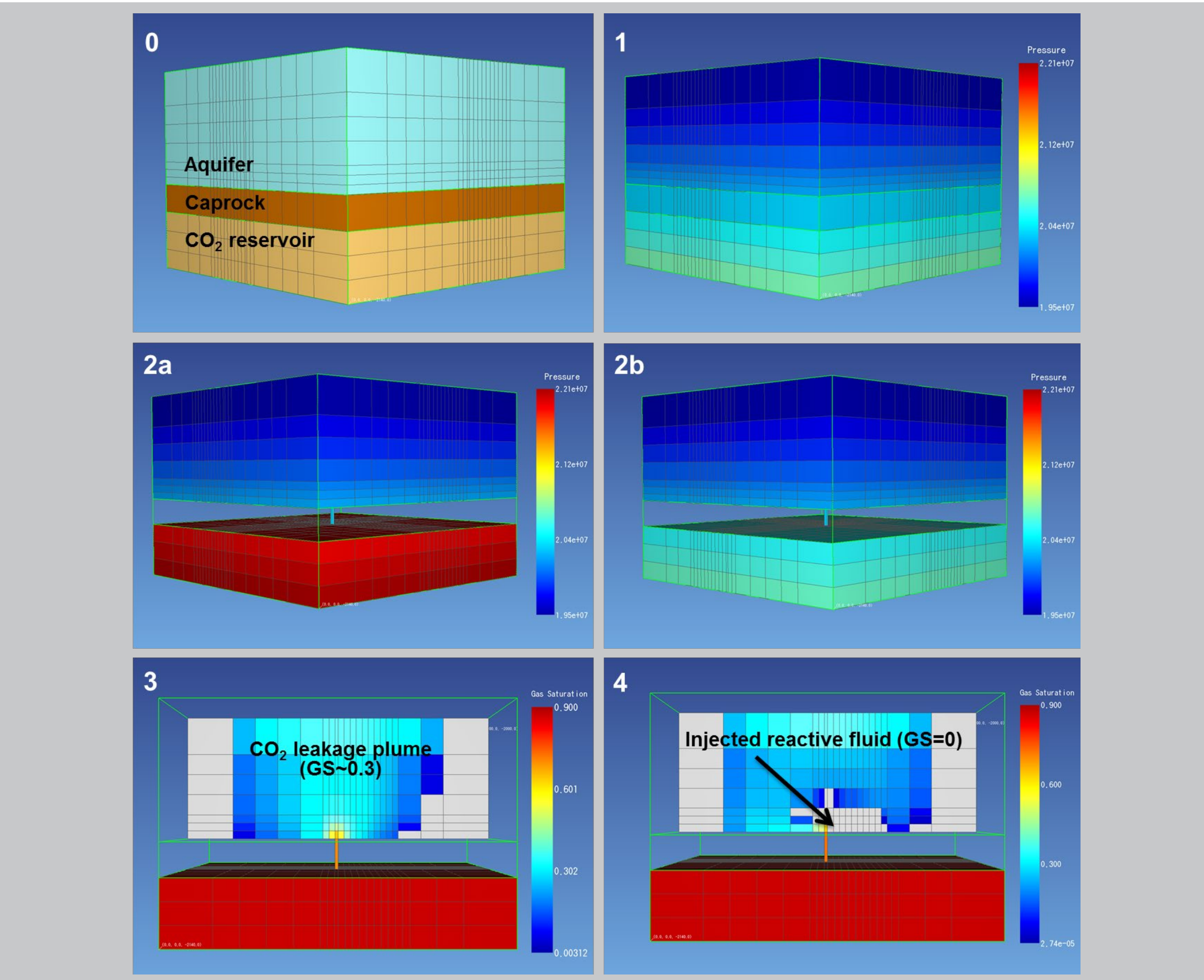

Figure 1 Step 1 to 4 of the workflow.

Injection of the solution is implemented by defining a source cell with a specific (lime-saturated) water flux. Note that the injection rate is constant and cannot be defined as being dependent on pressure with TOUGHREACT. As a result, pressure rises due to water injection. When the area above the leak is near complete clogging, injection becomes difficult and pressure may rise severely, while in reality the injection rate would be lowered and eventually stopped when reaching a certain pressure. Note that models are run until permeability and pressure changes hamper further injection, affecting the remediation time.

We used a calcium solution (lime-equilibrated) to stimulate calcite when reacted with dissolved CO_2 (Equation 1). The reactive solution has a calcium concentration of 0.68 mol/kg water and a pH of 12. All cells were assigned a porosity-permeability relationship to model the effect of precipitation on the CO_2 leakage. We used the porosity permeability relationship of Verma-Pruess as implemented in TOUGHREACT (Xu et al., 2006). The relation uses two parameters, a critical porosity (the porosity at which the permeability is reduced to zero) and a power law exponent (defining the rate at which the permeability decreases). We assumed a critical porosity of 12%, and a power law exponent of 8. These numbers are rock dependent and probably not known for many aquifers, hence the effect is studied in a sensitivity analyses.

$$Ca^{2+} + CO_3^{2-} \leftrightarrow CaCO_3 \qquad (1)$$

2.2.6 Equilibration stage

After injection of the reactive solution an equilibration stage is run to establish equilibrium after the remediation stage. After injection is stopped, flow occurs according to the pressure and saturation gradients created during injection of the reactive solution. This step will indicate if leakage will commence again or if further migration of CO_2 is prevented and is crucial to assess the success of remediation and the longevity of leakage reduction.

2.3 Scenarios

Several factors determine whether or not the solid reactant successfully remediates unwanted migration of CO_2. For successful clogging there should be a balance between the injection rate, leakage rate and reaction rate to ensure that sufficient solids form at the right location. The leakage rate is controlled by the pressure difference between the reservoir and the top aquifer, and by the flow properties of the leak. To consider a range in leakage rates, several simulations were run with varying key parameters.

2.3.1 Injection rate & distance

The injection rate and distance from the leak are parameters that are not site specific but can, to a certain degree, be controlled by the operator. We investigated a range to take into account the uncertainty linked to the seismic resolution or other monitoring techniques (not allowing for a precise determination of the location of the leak), and uncertainty in permeability and pressure response of the aquifer (causing injection not be executed as planned). The three selected injection locations are indicated in a cross-section of the model, also showing the CO_2 plume (Figure 2). The distance of injection to the leak point is 3, 11 and 19 meters (based on the cell centres). The selected injection rates range between 1 and 20 kg/s/cell and are considered to be achievable injection rates. Injection is specified for a column of three cells representing a perforation interval of 15 meters. Note that the total injection should be summed for the three injection cells, and hence for a rate of 10 kg/s/cell this is 30 kg/s in total, which is approximately 100 m^3/hr of fluid down the well.

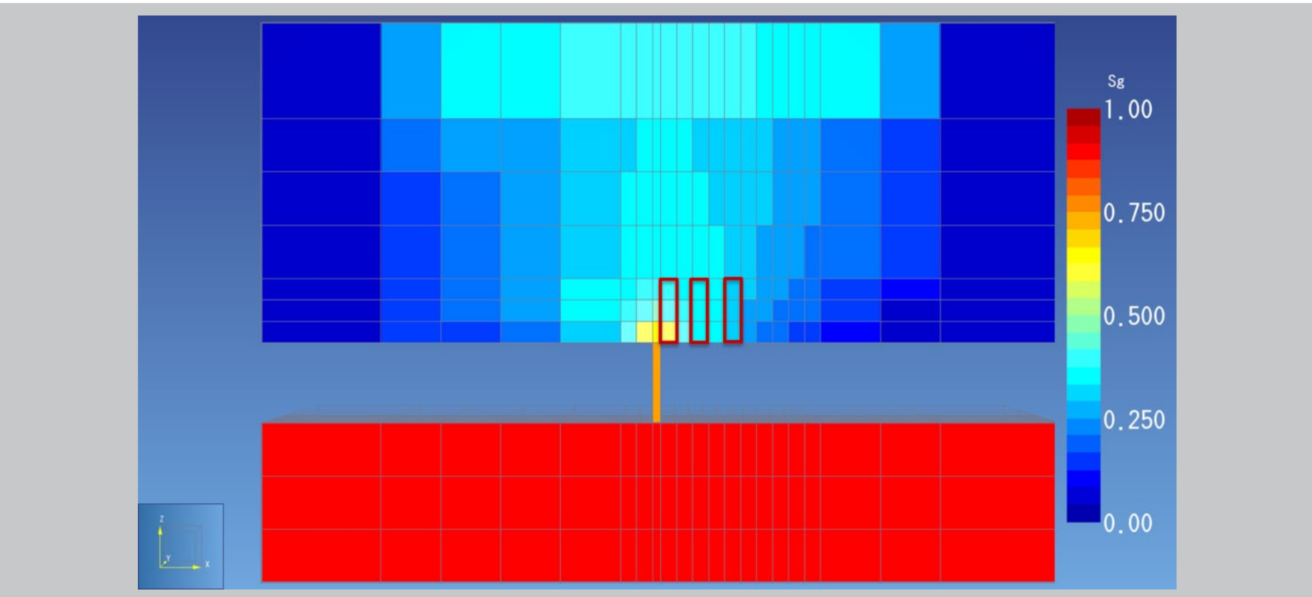

Figure 2 Cross section of the model with red squares indicating the three perforation intervals for injection of the reactive solution. The colour scale is for gas saturation, indicating the CO_2 plume above a leak path and the CO_2 reservoir below.

Table 6 Scenarios for permeability of the reservoir, aquifer and leak.

Permeability scenario	*Reservoir/ aquifer* Kh (mD)	Kv (mD)	*Leak* Kh (mD)
1	20	2	20
2	200	20	200
3	400	40	400
4	800	80	800

Table 7 Scenarios for CO_2 conditions in the reservoir.

Reservoir **scenario**	*Reservoir type* **Pressure**	**Gas saturation**
a	20 bar overpressure	Saturated (0.9)
b	hydrostatic	Saturated (0.9)
c	20 bar overpressure	Undersaturated (0.3)

2.3.2 Permeability, pressure & gas saturation

The range in permeability scenarios is assumed to represent relevant values, not too low that water injection becomes challenging and up to values of a reasonable reservoir rock (Table 6). Pressure conditions will be different for different types of storage sites. We distinguished between overpressurised and hydrostatic pressures. The first represents aquifer storage where the pressure increases during CO_2 injection. Hydrostatic pressure conditions are as would be expected for CO_2 storage in a depleted gas field where an

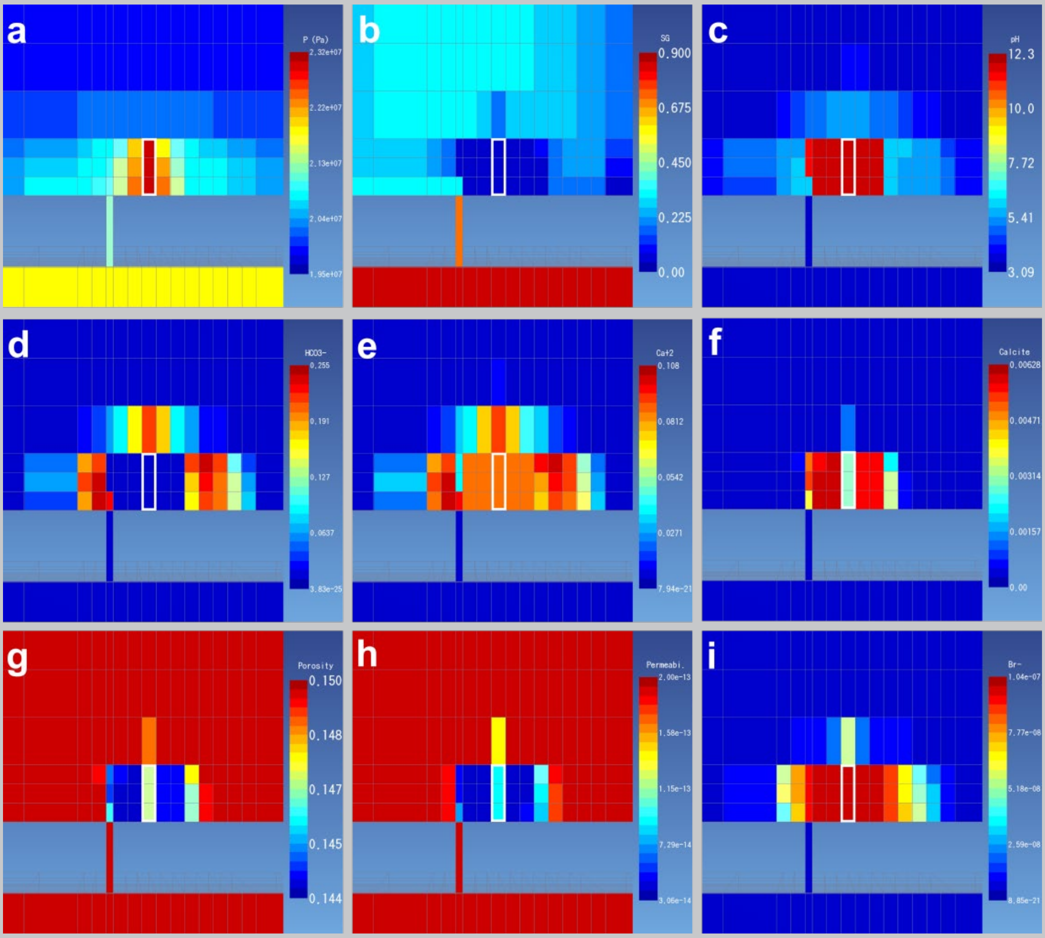

Figure 3 Results for several parameters in 80 by 90 m details of a y-axis cross section through the centre of the model. Injection of the CO_2 reactive solution is characterized by: a) pressure increase, b) gas saturation decrease, c) high pH zone within the low pH CO_2 plume, d/c) high HCO^{3-} and Ca^{+} concentrations at the front of the injected solution, e) calcite precipitation, g/h) porosity and permeability decrease due to calcite precipitation, i) co-injected Br^{-} tracer showing the extent of the injected fluid.

empty field is filled until hydrostatic pressure is regained. We used two saturations, close to fully saturated (Sg of 0.9) and 30% gas saturated. These values represent end members of gas saturation in a storage reservoir, high close the well and low further into the CO_2 plume. The selected pressure and saturation conditions yield three scenarios (Table 7). Although pressure boundary conditions also affect the leakage rate, open boundary conditions are used assuming an infinite aquifer and reservoir with respect to the 200 m cube model.

3 LEAKAGE REMEDIATION BY SOLID REACTANTS

3.1 The process of reactive clogging

The characteristics of clogging are discussed for a scenario of injection at 11 m distance from the leak with an injection rate of 5 kg/s/cell in an overpressurized reservoir of 200 mD permeability. Since gas in the pore space is pushed away by injection of the reactive solution, the pressure rises (Figure 3 a) and the gas saturation drops (Figure 3 b). The 10 bar pressure rise falls within the approximately 20% pressure increase allowable for water injection.

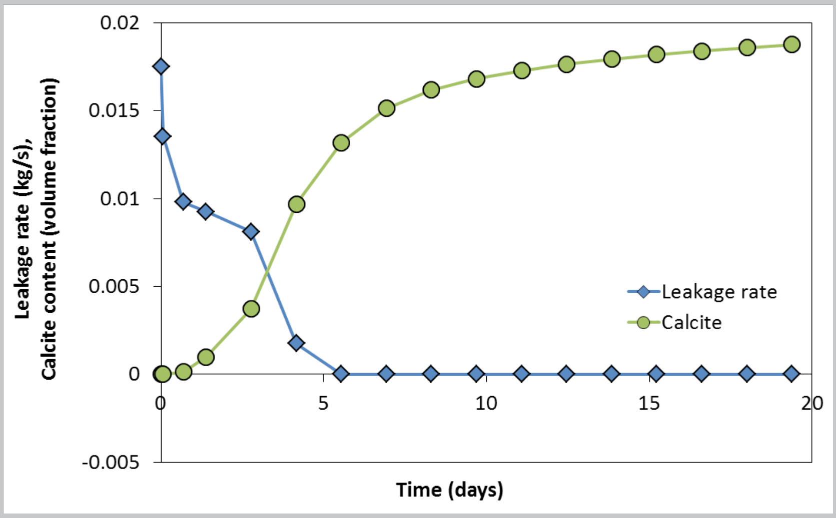

Figure 4 Graph of the leakage rate through the caprock (z direction) and the calcite content in the cell above the leak (same scale used). With time, more calcite precipitates and the leakage rate decreases.

The high pH calcium solution (Figure 3 c) is injected into the CO_2 plume where the dissolved CO_2 (Figure 3 d) combines with calcium (Figure 3 e) to form calcite (Figure 3 f). Since most dissolved CO_2 is consumed by the reaction, new calcite forms at the front of the injected solution where HCO^{3-} is still present. In addition, the leak itself provides CO_2 for the formation of calcium carbonate. This is favorable for the remediation process since this calcite forms right above the leak, clogging the pore space and decreasing porosity (Figure 3 g) and permeability (Figure 3 h).

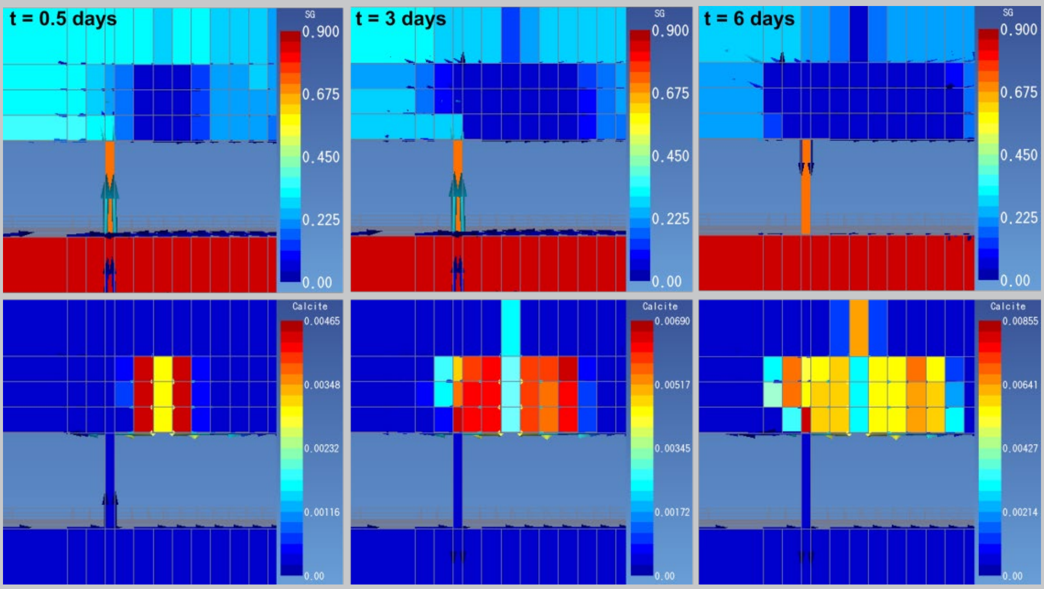

Figure 5 Gas saturation (in colour) and flow (vectors) for three time steps and associated calcite precipitation below. As more reactive solution is injected, it reaches the leak (t = 2 days) and overflows it (t = 6 days). Direct CO_2 leakage into the solution above, increases calcite forming until gas flow is inverted after 6 days of injection.

Successful remediation is defined as mitigation of unwanted migration of CO_2 by blocking the pore space. This is shown by the reduction in flow rate through the leak path and calcite precipitation above the leak (Figure 4 and Figure 5). The first drop in leakage rate is due to the injected water and the related pressure increase. At this stage, the reactive solution did not reach the leak yet (Figure 5, t = 0.5 day). The second reduction in flow occurs when the reactive fluid reaches the leak point and calcite starts to precipitate and clog the pore space (Figure 4 and Figure 5, t = 3 days). With continuous injection, the flow of CO_2 changes direction as it is pushed downwards (Figure 5, t = 6 days). The leakage rate is reduced to zero (Figure 4), suggesting successful remediation. The success of the remediation could be expressed as the degree of leakage reduction from the initial flow rate to the flow rate at the end of remediation. In this case that would be 100%.

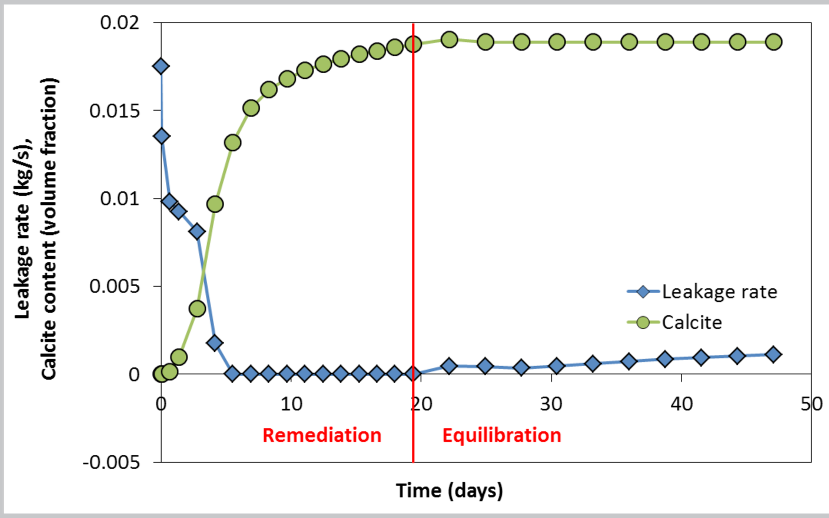

Figure 6 Graph of the leakage rate through the caprock (z direction) and the calcite content in the cell above the leak (same scale used). With time after remediation, calcite remains stable while leakage re-established to some degree.

To test whether the mitigation of unwanted CO_2 migration remains successful in time, the flow is studied after injection is stopped (when the permeability becomes too low for further injection). For this stage some leakage is re-established after the complete leakage reduction during remediation (Figure 6). This can be explained since the remediation during injection is a combined chemical and hydraulic process, meaning that flow through the leak is suppressed by a reduction in permeability and by the additional pressure of water injection. When no more water is injected, the chemical remediation remains, which yields in this case a leakage reduction of 95%. Hence the actual success of remediation is 95% instead of a 100%.

4 UNCERTAINTY ANALYSIS

4.1 Leakage scenarios

Scenarios for the initial leakage rate were based on the different pressure conditions and the geological variability as defined in section 2.3.2. For the 'overpressurized, high gas saturation reservoir' scenarios the leakage rates range from 0.27 to 10.93 mton for different permeabilities (1a to 4a, Table 8). Basically, double the permeability yields twice as fast leakage. This linear relation is shown for all three reservoir types, although the absolute leakage rates are far lower. The lower leakage rate is due to the smaller pressure gradient for the hydrostatic scenarios (1b to 4b, Table 8) and due to the lower gas content for the low saturation scenarios (1c to 4c, Table 8). The low saturation scenarios yield mobile water and hence leakage of water (and dissolved CO_2) as well as gaseous CO_2. Since

Table 8 Leakage scenarios and resulting leakage rates for the combinations of 4 permeability and 3 reservoir scenarios. SG is the CO_2 gas saturation.

Leakage scenario name	Permabillity Scenario	Aquifer Kh (mD)	Kv (mD)	Leak Kh (mD)	Reservoir scenario		Leakage rates Gas (mton/yr)	Water (mton/yr)
1a	*1*	20	2	20	*a*	0.9 SG, P + 20 bar	**0.27**	**0**
2a	*2*	200	20	200	*a*	0.9 SG, P + 20 bar	**2.71**	**0**
3a	*3*	400	40	400	*a*	0.9 SG, P + 20 bar	**5.39**	**0**
4a	*4*	800	80	800	*a*	0.9 SG, P + 20 bar	**10.93**	**0**
1b	*1*	20	2	20	*b*	0.9 SG, P hydrostatic	**0.02**	**0**
2b	*2*	200	20	200	*b*	0.9 SG, P hydrostatic	**0.18**	**0**
3b	*3*	400	40	400	*b*	0.9 SG, P hydrostatic	**0.36**	**0**
4b	*4*	800	80	800	*b*	0.9 SG, P hydrostatic	**0.72**	**0**
1c	*1*	20	2	20	*c*	0.3 SG, P+20 bar	**0.01**	**0.01**
2c	*2*	200	20	200	*c*	0.3 SG, P+20 bar	**0.12**	**0.13**
3c	*3*	400	40	400	*c*	0.3 SG, P+20 bar	**0.24**	**0.26**
4c	*4*	800	80	800	*c*	0.3 SG, P+20 bar	**0.47**	**0.52**

the overpressurized, high saturation scenarios 1a to 4a yield the most variation in leakage rates, these 4 scenarios were selected for the uncertainty assessment. Each scenario is applied to the three storage types (Table 8).

4.2 Remediation scenarios

4.2.1 Effect of permeability, injection rate and injection distance

The remediation scenarios were run for four of the leakage scenarios described above, thus considering four permeability's and corresponding leakage rates as starting points for remediation (1a to 4a, Table 8). The remediation scenarios are combinations of 4 injection rates and 3 injection locations, yielding 48 scenarios. The success of these scenarios at the end of the injection process, in terms of the change in leakage rate, is reported in Table 9. Note that the low permeability did not allow high injection rates, and hence these scenarios could not be run. Leakage can be reduced more than a 100 per cent if flow is inverted through the leak path. For all permeabilities and related leakage rates, a full decrease in leakage rate can be achieved given a right combination of injection distance and injection rate. For higher permeabilities, higher injection rates are required to achieve successful remediation. This is most pronounced for the highest permeability, yielding complete success only for injection at 3 meter distance. It appears that injection close to the leak point or faster injection will generally increase the likelihood of success for leakage reduction during the remediation procedure.

As mentioned before, stopping flow through the leak path is a combined effect of injection of water and clogging of the pore space by the solid reactant. Comparing the amount of calcite formed above the leak (Table 10) and the change in leakage rate (Table 9) clearly indicates that the two do not necessarily correlate. This will have an effect on the equilibration stage, as described in the section 4.3. Especially for injection far from the leak point (19 meter scenario), some scenarios were successful in leakage remediation but have a very small contribution of chemical remediation (i.e. calcite clogging). Since none of the scenarios reaches the critical

Table 9 Scenario overview for the change in leakage rate (%). The colours show a ranking from more (green) to less (red) successful scenarios. Scenarios that did not run are shown in grey.

Injection distance (m)	Permeability kh, kv (mD)	Injection rate 1 (kg/s/cell)	5 (kg/s/cell)	10 (kg/s/cell)	20 (kg/s/cell)
3	20, 2	-103			
3	200, 20	-100	-102	-101	-97
3	400, 40	-68	-100	-102	-101
3	800, 80	-41	-100	-100	-108
11	20, 2	-101	-113		
11	200, 20	-39	-100	-100	-107
11	400, 40	-22	-83	-97	-100
11	800, 80	-14	-47	-76	-85
19	20, 2	-64	-114		
19	200, 20	-28	-65	-72	-102
19	400, 40	-13	-43	-45	-72
19	800, 80	-3	-23	-19	-40

Table 10 Scenario overview for calcite precipitation (volume factor) above the leak. The colours show a ranking from more (green) to less (red) successful scenarios. Scenarios that did not run are shown in grey.

Injection distance (m)	Permeability kh, kv (mD)	Injection rate 1 (kg/s/cell)	5 (kg/s/cell)	10 (kg/s/cell)	20 (kg/s/cell)
3	20, 2	5.1E-03			
3	200, 20	1.8E-02	4.4E-03	3.9E-03	9.7E-04
3	400, 40	1.5E-02	1.3E-02	3.7E-03	4.2E-03
3	800, 80	1.3E-02	1.7E-02	1.3E-02	2.1E-03
11	20, 2	7.8E-03	5.5E-03		
11	200, 20	1.1E-02	1.9E-02	7.7E-03	3.9E-03
11	400, 40	9.2E-03	1.4E-02	1.1E-02	6.2E-03
11	800, 80	8.7E-03	1.2E-02	1.3E-02	9.9E-03
19	20, 2	1.8E-05	9.8E-06		
19	200, 20	4.8E-03	7.9E-03	7.9E-04	6.6E-05
19	400, 40	1.7E-03	7.5E-03	4.9E-04	5.2E-05
19	800, 80	3.4E-04	6.7E-03	3.5E-05	1.9E-05

volume of calcite of 3.0E-2 (which yields a porosity reduction of 15% to the critical value of 12% after which permeability is assumed to be zero) as we defined for complete permeability impairment, chemical remediation was always less than a 100% (Table 10). There is a sweet spot of high calcite precipitation for medium to high permeabilities (and initial corresponding leakage rate) with low to medium injection rates. It cannot be concluded that higher permeability or faster injection will necessarily be better, but the combination has to be right. However, injection at 19 m distance yields little calcite precipitation above the leak, indicating that the remediation method needs to be practiced close to the leak point at least < 20 m.

Since the combination of injection rate and location for the specific aquifer conditions is of such importance, Figure 7 shows the processes of successful or unsuccessful leakage reduction. We discuss 1) successful clogging with significant calcite precipitation above the leak, 2) partially successful clogging with calcite precipitation but also premature suppression of leakage, stopping further supply of CO_2 and 3) unsuccessful scenarios with calcite porosity clogging before the leak point was reached. The calcite volume fraction in Figure 7 shows the gradually increasing calcite formation for the effective scenario, whereas calcite precipitation stops for the partially successful scenario. This can be explained by the gas saturation, which is reduced to zero and hence no more CO_2 is available for calcite precipitation after all dissolved CO_2 is consumed (Figure 7, middle graph). This indicates that the hydraulic component of remediation should not be too large, as water suppressing the gas migration also stops new supply of CO_2. Since the leakage rate reduces to zero for both the successful and partially successful scenarios, both appear to be effective in remediation during injection. The figures on the right in Figure 7 clearly illustrate how scenarios can be unsuccessful (bottom figure) as calcite clogging simply occurs at the wrong location. The calcite distribution of the partially successful scenario shows less calcite in the cell above the leak compared to the successful one, but more calcite clogging at a larger distance around the leak. Looking at only the calcite above the leak will therefore not tell the whole story of leakage remediation. Another step of simulations is required to assess if the effectivity of the remediation after the procedure is stopped, which will be discussed in the next chapter.

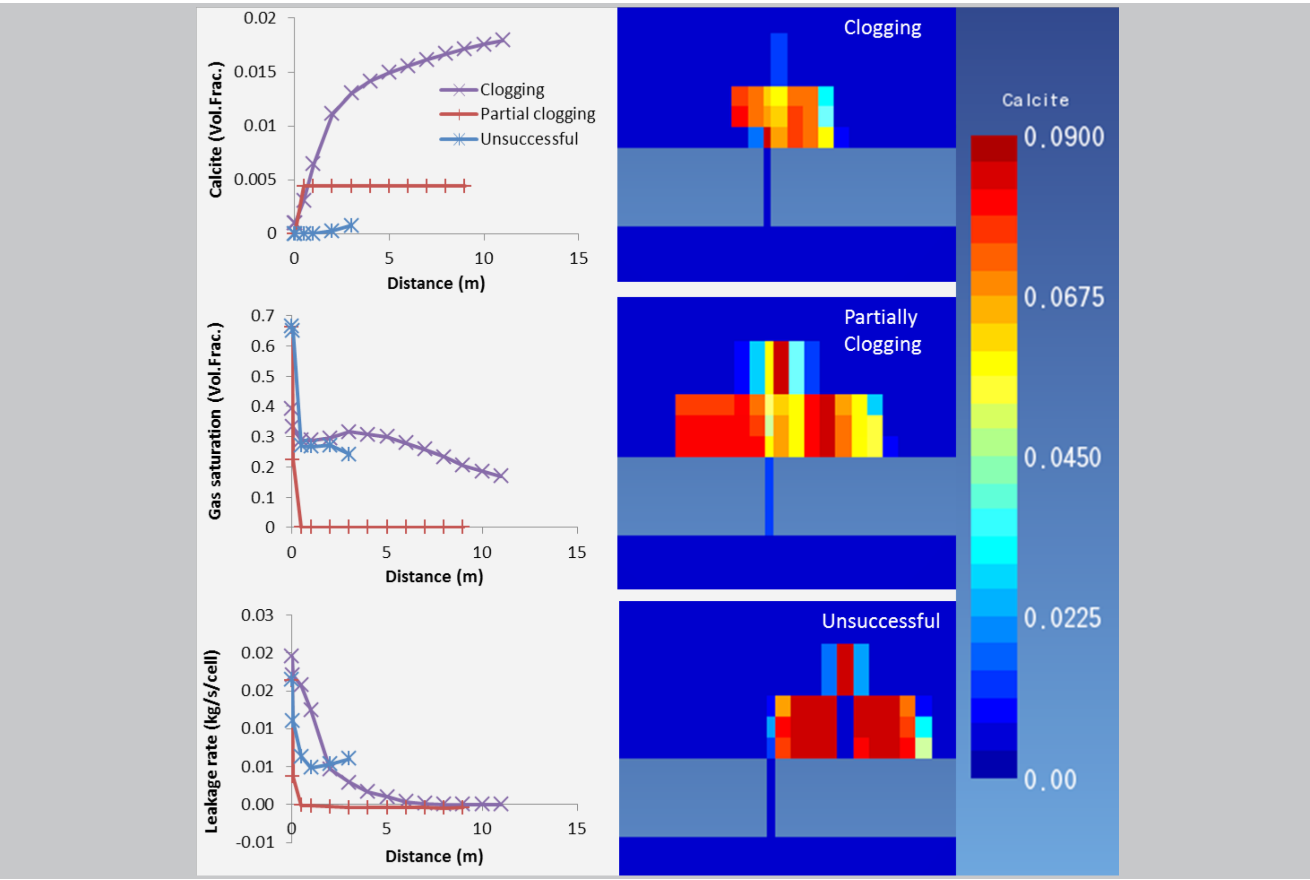

Figure 7 Three examples of scenarios yielding unsuccessful (2a-19m-10kgs), partially successful (2a-3m-5kgs) and unsuccessful (2a-3m-1kgs) leakage reduction. The graphs on the left show, from top to bottom, the calcite content and gas saturation above the leak and the leakage rate through the leak path. The figures on the right visualize the calcite precipitation in 80 m details of y-axis cross sections of the model.

4.2.2 Effect of reservoir pressure and gas saturation

The previous scenarios were all for the high pressure and gas saturation reservoir (a, Table 8). The hydrostatic (b) and low saturation conditions (c) were tested for the scenario of 200 mD permeability with 11 m distance 5 kg/s/cell injection. The change in leakage rate for the base case reservoir scenario a was 100%, for b this is -103.8% and for c -83.5% for gas and -95.6% for water leakage. Hence c is the least effective, but the calcite content shows that b and c are actually both less successful than a (Figure 8). These reservoir scenarios have a much lower initial leakage rate (Table 8) and hence CO_2 leakage is more easily suppressed by water injection, limiting the CO_2 supply and calcite precipitation. These scenarios require lower injection rates to achieve the balance between fast enough injection to reach the leak but slow enough to allow for CO_2 supply until clogging is complete.

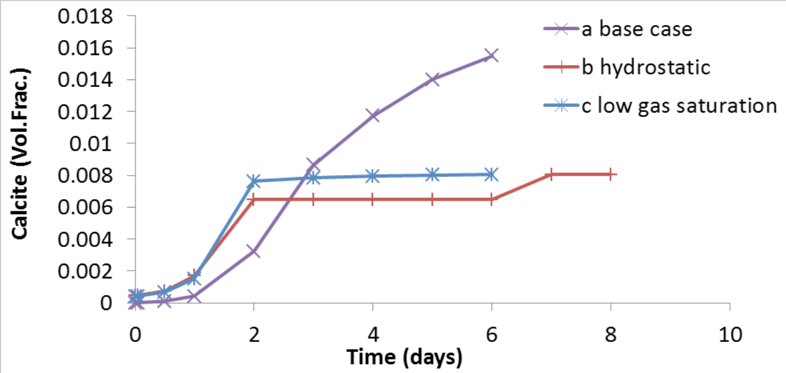

Figure 8 The calcite content in the cell above the leak for three reservoir scenarios. Scenario b and c first show an increase in calcite similar to scenario a, but calcite precipitation roughly stops after 2 days of injection

4.2.3 Sensitivity to the porosity-permeability relationship

The sensitivity of leakage reduction towards the porosity-permeability relationship was assessed by varying the Verma-Pruess relation input parameters, the critical porosity and the power law component. In addition, two other porosity-permeability relationships available for TOUGHREACT were checked, Cubic Law (CL) and Simplified Carmen-Kozeny (SCK). All porosity permeability relationships were tested for the scenario of 200 mD permeability with 3m distance and 1 kg/s/cell injection.

With a higher power law exponent, the permeability change is larger when porosity changes. This is illustrated by the similar calcite content but lower permeability for higher power law exponents (12-6 and 12-10 versus the base case 12-8, Table 11).

With a lower critical porosity, more calcite needs to precipitate in order to clog the pore space and hence the remediation method would be less effective although the calcite content is higher (11-8 and 13-8 versus the base case 12-8, Table 11). Interestingly, scenario 12-6 and 11-8 yield quite similar results, showing that a higher power law component can compensate the higher degree of clogging required. The Cubic Law (CL) and Simplified Carmen-Kozeny (SCK) yield comparable results. Both are characterized by high calcite precipitation but still a high permeability resulting in little leakage reduction and hence remediation success.

Table 11 Remediation results for different porosity-permeability relationships. The first number in the scenario name is the critical porosity for complete permeability reduction, the second the power law exponent.

Scenario	Change in leakage rate (%)	Calcite (Vol.Frac)	Permeability (m2)
12-8	-100.0	1.79E-02	1.38E-16
12-6	-79.1	1.86E-02	6.03E-16
12-10	-100.0	1.77E-02	2.61E-17
11-8	-76.0	2.02E-02	7.33E-16
13-8	-100.0	1.45E-02	6.42E-18
CL	-24.3	8.75E-02	1.45E-14
SKC	-24.8	8.73E-02	1.20E-14

4.3 Equilibration

For several scenarios the actual success of the remediation method is numerically assessed by running the equilibration phase after injection of the reactive fluid. Since the 19 m injection scenarios resulted in little to no calcite in the remediation stage these were not considered for equilibration. The 37 remaining remediation scenarios were used for subsequent equilibration. For all equilibration scenarios, the leakage re-establishes to a certain degree, as was expected from the injection stage which indicated a lack of complete clogging. Figure 9 shows examples for the development of the leakage rate. Two of the scenarios were able to stop leakage completely during injection, but the new leakage rate that develops during equilibration varies largely (2a 3m 5kgs and 2a 11m 1kgs, Figure 9). In fact the less successful scenario of the two yields the same final leakage rate as the scenario that never achieved full leakage reduction during remediation (2a 11m 1kgs, Figure 9). Note that due to the new leakage and supply of CO_2, the calcite content can even increase during the equilibration stage. It can be concluded that the success of leakage remediation during injection is very different from the actual success after equilibration.

The success of remediation after the equilibration phase for scenarios with different permeabilities, injection rates and injection distances are reported in Table 12. The fastest injection rate and the lowest permeability (initial leakage rate) yield little success in remediation. The most successful scenarios are characterised by a medium to high permeability and a low injection rate. The most successful scenarios after equilibration also have the highest calcite precipitation above the leak (Table 10 compared to Table 12).

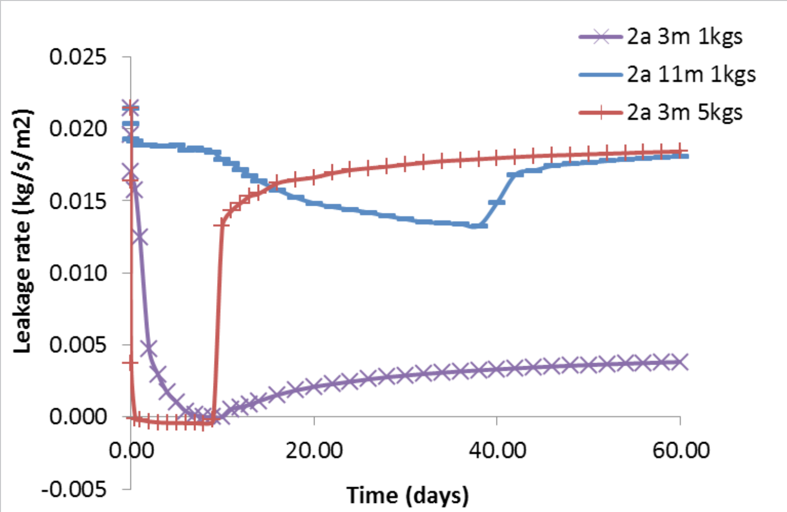

Figure 8 The calcite content in the cell above the leak for three reservoir scenarios. Scenario b and c first show an increase in calcite similar to scenario a, but calcite precipitation roughly stops after 2 days of injection

Table 12 Overview of the change in leakage rate for the different scenarios indicating the remediation success. Scenarios in grey failed to run. The colours show the relative ranking from the best (green) to the worst results (red).

Injection distance (m)	Permeability kh, kv (mD)	Injection rate 1 (kg/s/cell)	5 (kg/s/cell)	10 (kg/s/cell)	20 (kg/s/cell)
3	20, 2	-33			
3	200, 20	-80	-12	-37	
3	400, 40	-45	-47	-11	-0.1
3	800, 80	-24	-59	-47	-4
11	20, 2	-17	-14		
11	200, 20	-16	-95	-8	-6
11	400, 40	-7	-32	-10	-4
11	800, 80	-1	-14	-22	-0.2

4.4 Remediation efficiency

It takes increasingly more time for the reactive solution to reach the leak with injection at larger distance. Considering the radial distribution of injected solution, the method becomes less efficient with distance as more volume is required. Flow will not remain radial since it is affected by the clogging process. The extent of the clogging zone varies largely between scenarios (Figure 7), showing that besides the effectivity of clogging the efficiency of clogging may be very different from one scenario to another. The

Table 13 The volume of remediation solution injected for the different scenarios. The volume (kg) is calculated by multiplying the injection rate (kg/s/cell) with the injection time (s).

Injection distance (m)	Permeability kh, kv (mD)	Injection rate 1 (kg/s/cell)	5 (kg/s/cell)	10 (kg/s/cell)	20 (kg/s/cell)
3	20, 2	8.8E+06			
3	200, 20	**2.3E+06**	1.2E+07	1.6E+07	2.2E+05
3	400, 40	**1.6E+07**	**1.2E+07**	1.0E+07	2.6E+06
3	800, 80	1.9E+07	**2.6E+06**	**5.2E+06**	2.6E+06
11	20, 2	9.3E+06	7.8E+06		
11	200, 20	1.1E+07	**1.2E+07**	5.2E+06	1.6E+07
11	400, 40	9.8E+06	2.1E+07	5.2E+06	5.2E+06
11	800, 80	1.6E+07	2.3E+07	1.8E+07	5.2E+06
19	20, 2	3.4E+06	2.6E+06		
19	200, 20	1.1E+07	1.2E+07	1.6E+07	2.6E+06
19	400, 40	1.2E+07	3.9E+06	7.8E+06	2.6E+06
19	800, 80	8.8E+06	1.6E+07	5.2E+06	1.3E+06

efficiency of scenarios can be expressed as the total volume of reactive solution injected during the remediation procedure, i.e. until permeability and pressure hamper further injection.

Table 13 shows that the volume injected varies by three orders of magnitude. The most effective scenarios with 45% or more leakage reduction remaining after equilibration are indicated by bold numbers. The variation is significant, even for the best scenarios, indicating that efficiency and effectivity are not well correlated. The volume of the injected fluid and injection time will govern the cost of the remediation method and are therefore of utmost importance for feasibility of this technique.

5 DISCUSSION

This study shows that remediation of unwanted CO_2 flow to an overlying aquifer could be successful. Yet, large uncertainties in the success of remediation are related to the porosity-permeability relation of calcite precipitation, or formation of any other solid reactant. The actual volume of solid reactant required for full clogging depends heavily on the porosity-permeability relationship. As mentioned by Druhan et al. (2015) and Ito et al. (2014), the porosity-permeability relation is of utmost importance for predicting effective leakage remediation. The sensitivity presented in this paper showed a difference from hardly any remediation to a 100% leakage reduction during remediation depending on the chosen parameters. In the case of intentional salt clogging (Wasch et al., 2013), the same challenge was encountered. It remains a question of debate as to which degree precipitation in the pore space reduces the flow of gas and water. More insights in the porosity-permeability relations need to be obtained through well-designed experimental studies.

The simulation results also showed that the requirement of CO_2 supply from the leak for calcite formation – in addition to the CO_2 present in the plume – is the main disadvantage of the proposed technique. It requires a delicate balance between injection rate, leakage rate and location of injection in order to achieve sufficient pore blockage. The work of Druhan et al. (2015) also identified the balance between the flow rate through the leak and fluid injection rate as a major influence in the successful placement of the sealant. Delivering a reactive solution at the right location remains a challenge, regardless of the reactant used. The use of swelling silica polymers as used by Druhan et al. (2015) would benefit the method in the sense that less reactant is required to be put in place. However, the stability of such a polymer on the long term is currently not proven. Amorphous silica may become more crystalline over time, a process which is faster at higher temperatures, causing mineral shrinkage and possibly re-established leakage. Besides swelling, delayed precipitation of the solid reactant might take away some difficulties of the remediation method proposed in this report. Instead of the reactivity according to the equilibrium constant and kinetic parameters, engineered solutions with delaying additives could open opportunities for injection further from the leak point as the solid reactant will not precipitate directly upon contact with CO_2. This would reduce the level of detail of knowledge required of the flow properties of the aquifer and the leak characteristics, properties which are not easily measured. For this reason, the use of substances that increase in volume with some delay would benefit the method, since injection would not be restrained and the solution has time to reach the leak where it can subsequently react to form solids and clog the leakage pathway.

6 CONCLUSION

The use of calcite as a solid reactant is a promising method for leakage remediation due to the natural stability of calcite in the subsurface. This enables the formation of a strong and long-lived barrier against unwanted migration of CO_2. TOUGHREACT was successfully applied to inject a lime-saturated solution in the vicinity of a CO_2 leak. The reaction of the injected calcium solution with CO_2 caused calcite precipitation blocking the pore space and reducing CO_2 leakage. The method proved to have both a hydraulic and a chemical component, meaning that leakage was partially remediated by chemical precipitation and partially by the pressure of injected water. Since part of the remediation is attributed to water injection which is only a temporary process, stopping injection at the end of the remediation procedure leaves only the chemical clogging. As a result, leakage can partially be re-established. The scenario analyses showed a large variation in the resulting leakage reduction during remediation and afterwards during equilibration. The key parameters including leakage rate, permeability, injection rate and injection distance should be well attuned to achieve a high degree of leakage remediation. In general, fast leakage may contribute to clogging by supplying additional reactive CO_2. Fast injection of the solution on the other hand may push all the CO_2 away – even causing flow into the leak – thus limiting the reaction with CO_2 and hence clogging with the solid reactant.

References

Bedrikovetsky, P.G., Mackay, E., Montelro, R.P., Gladstone, P.M., Rosário, F.F., 2006. Laboratory and field prediction of sulfate scaling damage. SPE Eighth International Symposium on Oilfield Scale 2006 2006, 309-326.

Birkle, P., Pruess, K., Xu, T., Hernández Figueroa, R.A., Díaz López, M., Contreras López, E., 2008. Using laboratory flow experiments and reactive chemical transport modeling for designing waterflooding of the Agua Fría Reservoir, Poza Rica-Altamira Field, Mexico. SPE Reserv. Eval. Eng. 11, 1029-1045.

Cowan, J. and Weintritt, D. 1976. Water-Formed Scale Deposits, 187-188. Houston, Texas: Gulf Publishing Co.

Cunningham, A.B., Gerlach, R., Spangler, L., Mitchell, A.C., Parks, S., Phillips, A., 2011. Reducing the risk of well bore leakage of CO_2 using engineered biomineralization barriers. Energy Procedia 4, 5178-5185.

Delshad, M., Pope, G.A., 2003. Effect of Dispersion on Transport and Precipitation of Barium and Sulfate in Oil Reservoirs. SPE Int. Symp. Oilfield Chem. , 393-400.

Druhan J.L., Vialle S, Maher K., Benson S., 2015. Numerical simulation of reactive barrier emplacement to control CO_2 migration. In: Carbon Dioxide Capture for Storage in Deep Geologic Formations – Results from the CO_2 Capture Project. Chapter 45. Ed. K.F. Gerdes. CPL Press and BPCNAI.

Gaus, I., 2010. Role and impact of CO_2-rock interactions during CO_2 storage in sedimentary rocks. International Journal of Greenhouse Gas Control 4, 73-89.

Giorgis, T., Carpita, M., Battistelli, A., 2007. 2D modeling of salt precipitation during the injection of dry CO_2 in a depleted gas reservoir. Energy Convers. Manage. 48, 1816-1826.

Ito T., Xu T., Tanaka H., Taniuchi Y., Okamoto A., 2014. Possibility to remedy CO_2 leakage from geological reservoir using CO_2reactive grout. International Journal of Greenhouse Gas Control, 310–323.

Izgec O., Demiral B., Bertin H, Akin S., 2005. Calcite precipitation in low temperature geothermal systems: An experimental approach, Proceedings of the Thirtieth Workshop on Geothermal Reservoir Engineering, Stanford University, California, January 31-February 2, 2005, SGP-TR-176

Kleinitz, W., Koehler, M., Dietzsch, G., 2001. The Precipitation of Salt in Gas Producing Wells.

Kühn M., Vernoux J.F., Kellner T., Isenbeck-Schröter M., Schulz H.D., 1997. Onsite experimental simulation of brine injection into a clastic reservoir as applied to geothermal exploitation in Germany, Applied Geochemistry, 13(4), 477-490

Mitchell, A.C., Phillips, A.J., Hiebert, T., Gelrach, R., Spangler, L.H., Cunningham, A.B.,2009. Biofilm enhanced geologic sequestration of supercritical CO_2. International Journal of Greenhouse Gas Control 3 (1), 90–99.

Moghadasi J., Jamialahmadi M., Müller-Steinhagen H., Sharif A., 2004. Formation Damage Due to Scale Formation in Porous Media Resulting From Water Injection. SPE-86524-MS. SPE International Symposium and Exhibition on Formation Damage Control, 18-20 February, Lafayette, Louisiana.

Mota, R.O., Bezerra, M.C.M., Rosario, F.F., Prais, F., 2004. Forecasts and alternative analysis for sulphate removal or chemical treatments for barium and strontium scale deposition - Offshore Brazil. Proceedings - SPE Sixth International Symposium on Oilfield Scale; Exploring the Boundaries of Scale Control , 393-402.

Nasr-El-Din, H.A., Raju, K.U., Hilab, V.V., Esmail, O.J., 2004. Injection of incompatible water as a means of water shut-off. Proc. SPE Int. Symp. Oilfield Scale Exploring Boundaries Control , 291-303.

Palandri, J., Kharaka, Y.K., 2004. A compilation of rate parameters of water-mineral interaction kinetics for application to geochemical modeling. In: US Geological Survey Open File Report 2004-1068. USGS.

Parkhurst, D.L., Appelo, C.A.J., 1999. User's Guide to PHREEQC (Version 2) – A Computer Program for Speciation, Batch Reaction, One-Dimensional Transport, and Inverse Geochemical Calculations. Report 99-4259. US Geological Survey Water Resources Investigations.

Pruess, K., 2005. ECO_2N: A TOUGH2 Fluid Property Module for Mixtures of Water, NaCl, and CO_2. Earth Sciences Division, Lawrence Berkeley National Laboratory, University of California, Berkeley, CA.

Pruess K, Oldenburg C and Moridis G, TOUGH2 User's Guide, Version 2.0. Report LBNL-43134. Lawrence Berkeley National Laboratory, Berkeley, CA (1999)

Pruess, K., Müller, N., 2009. Formation dry-out from CO_2 injection into saline aquifers: 1. effects of solids precipitation and their mitigation. Water Resour. Res. 45.

Xu, T., Sonnenthal, E., Spycher, N., Pruess, K., 2006. TOUGHREACT – a simulation program for non-isothermal multiphase reactive geochemical transport in variably saturated geologic media: applications to geothermal injectivity and CO_2 geological sequestration. Comput. Geosci. 32, 145–165.

Regenspurg S., Wiersberg T., Brandt W., Huenges E., Saadat A., Schmidt K., Zimmermann G., 2010. Geochemical properties of saline geothermal fluids from the in-situ geothermal laboratory Groß Schöonebeck (Germany), Chemie der Erde, 70(3), 3-12

Rocha, A.A., Frydman, M., da Fontoura, S.A.B., Rosario, F.F., Bezerra, M.C.M., 2001. Numerical Modeling of Salt Precipitation During Produced Water Reinjection.

Tambach, T.J., Loeve, D., Hofstee, C., Plug, W.J., Maas, J.G., 2014. Effect of CO_2 Injection on Brine Flow and Salt Precipitation After Gas Field Production. Transport in Porous Media.

Tarcan G., 2005. Mineral saturation and scaling tendencies of waters discharged from wells (>150°C) in geothermal areas of Turkey, Journal of Volcanology and Geothermal Research, 142, 263-283

Zeidouni, M., Pooladi-Darvish, M., Keith, D., 2009. Analytical solution to evaluate salt precipitation during CO_2 injection in saline aquifers. Int. J. Greenh. Gas Control 3, 600-611.

Wasch L.J., Wollenweber J. and Tambach T.J., 2013, A novel concept for long-term CO_2 sealing by intentional salt clogging, GHG:S&T, Vol 3 (6), p. 491-502, 2013.

Section II

RESERVOIR PRESSURE MANAGEMENT AS CO_2 MIGRATION AND REMEDIATION MEASURE

Chapter VI

Report on current reservoir pressure management measures in petroleum industry

Bernd Wiese[1], Anna Korre[2], Cor Hofstee[3], Lies Peters[3], Dan Bossie-Cordreanu[4], Marc Fleury[4], Andrew Cavanagh[5]
[1] GFZ, Germany
[2]Imperial College, UK
[3] TNO, The Netherlands
[4]IFPEN, France
[5]Statoil, Norway

SUMMARY

This report summarizes the studies regarding the topic "Reservoir pressure management" as part of the overarching research task "Migration management", and is focused on three major fields: 1) Feasibility test and numerical modelling of CO_2 back-production as remediation measure to reduce reservoir pressure and induce inward directed flow in case of lateral leakage beyond spill point. 2) Feasibility test and numerical modelling of brine/water withdrawal as remediation measure to reduce reservoir pressure and create pressure gradients with directed flow in case of lateral leakage beyond a spill point. 3) Assessment and test of novel approaches and sensing technologies to manage reservoir pressure. This report represents a first step to investigate the conditions that require the deployment of pressure management techniques as corrective measures in case of undesired CO_2 migration in the subsurface.

1. INTRODUCTION

This report is part of the research project MiReCOL (Mitigation and Remediation of CO_2 leakage) funded by the EU FP7 programme. Research activities aim at developing a handbook of corrective measures that can be considered in the event of undesired migration of CO_2 in the deep subsurface reservoirs. MiReCOL results support CO_2 storage project operators in assessing the value of specific corrective measures if the CO_2 in the storage reservoir does not behave as expected. MiReCOL focuses on corrective measures that can be taken while the CO_2 is in the deep subsurface. The general scenarios considered in MiReCOL are 1) loss of conformance in the reservoir (undesired migration of CO_2 within the reservoir), 2) natural barrier breach (CO_2 migration through faults or fractures), and 3) well barrier breach (CO_2 migration along the well bore).Storing CO_2 geologically in saline reservoirs or depleted gas fields to reduce emissions into the atmosphere is one of the options to mitigate climate change. Storing CO_2 leads to an increase in formation pressure, which is with regard to saline reservoirs, the major risk to damage the storage complex and for CO_2 leakage. Therefore pressure management is an important part of day-to-day CO_2 storage operation. Pressure management can also be used to mitigate the effects of undesired migration of CO_2 in the subsurface. As part of the MiReCOL project's overall aim to develop guidelines on corrective measures to mitigate the effects of undesired CO_2 migration, this report represents a first step to investigating the conditions that require the deployment of pressure management techniques in case of undesired CO_2 migration in the subsurface.

Pressure management is closely connected to the individual configuration of geology and technical site development. There are numerous relevant geological parameters and technical configurations such that a universal solution does not exist. This is typical for highly nonlinear multi parameter systems (Moore and Doherty, 2006). To account for the almost infinite number of combining different technical actions in different geological conditions, the research in the MiReCOL project follows a top down approach. This report consists of 4 sections.

In the first section (chapter 2) the main geological settings and technical conditions will be assessed on a general level. The principal factors of influence will be named and identified such that operators can deduce guidelines for assessing a storage reservoir and estimate the reservoir behavior. This work is carried out in the research topic “Selection of scenarios” of MiReCOL.

In the second section (chapter 3) modeling studies are presented to show exemplarily procedures of pressure management. These studies are about existing field sites. For example, the back production of CO_2 is an important option to lower reservoir pressure and the first field experiment has been carried out at the pilot site Ketzin. An alternative approach is demonstrated by modelling of CO_2 injection scenarios at the P18 field in the Netherlands.

The third section (chapter 4) addresses individual processes related with the general pressure buildup. The reservoir behavior during back production is expected to differ considerably from injection operation. The difference is based on hysteresis effects on the pore scale and well effects. These investigations are closely connected with the back production test at the Ketzin pilot site and will be studied on the laboratory and the reservoir scale, respectively. In addition to more traditional methods that are described above, a novel method of reservoir pressure management is presented. Therein, the infiltration of nanoparticles in the subsurface is applied with the purpose of either increasing mixture of the phases or the dissolution of CO_2.

The fourth section (chapter 5) is a short overview on industry practice on pressure management and field measurement and instrumentation.

2. PRINCIPAL FACTORS RELEVANT FOR PRESSURE BUILD UP IN THE RESERVOIR AND COUNTER MEASURES

1. Reservoir boundaries: The type of boundary conditions is the most important criterion for type and management of pressure buildup. Brine extraction to counteract pressure buildup gains importance the more isolated a reservoir is from surrounding aquifers (Zhou et al., 2008). In case of closed boundary conditions the pressure increases rapidly. Only small amounts of CO_2 can be stored. Open systems are hydraulically connected over large areas wherefore the pressure buildup can dissipate laterally and larger amounts of CO_2 can be stored. The application of pressure relief wells that allow pressure dissipation by means of fluid discharge is therefore of essential relevance for closed systems. The volume of brine production required to reduce seismic and leakage risks to near zero was shown to be approximately equal to the volume of injected CO_2 (Buscheck et al., 2011). But also for semi-closed and open systems also beneficial effects may be obtained. For open systems Wiese et al. (2010) identified the principal factors affecting injection pressure.
2. Interaction of injection wells: The injection pressure decreases with the number of wells to which the CO_2 flux is partitioned. Large CO_2 projects may include a high number of injection wells which affect each other and have a similar effect as semi-closed or closed boundary conditions. As a first approximation their interaction can be described with the superposition theory, but also adapted analytical solutions for simulation of pressure build up with CO_2 injection and brine withdrawal already exist (Mijic et al., 2012). Generally, it has to be considered that the additional benefit decreases continuously with the number of injection wells.
3. Type of pressure buildup: The total pressure buildup consists of two parts: Dynamic and static pressure. The dynamic pressure is induced by the injection well and dissipates through migration of the over-pressured reservoir fluid to regions with a lower hydraulic potential. After this equilibration only the static pressure remains, which is induced by buoyancy of the injected CO_2.

Pressure management addresses primarily dynamic reservoir pressure (Zhou and Birkholzer, 2011) since it is typically higher than static reservoir pressure and can be counteracted more efficiently due to its transient nature.

4. Type of storage: Saline aquifers and former gas fields are the two most common storage options Saline aquifers are completely saturated with reservoir fluid prior to injection, during injection the brine is replaced by CO_2. The pore space in former gas fields typically is occupied with residual gas, while reservoir fluid may be present below the gas water contact and residual capillary water may occupy the lower pore spaces. Structural trapping of the caprock is inherent to both storage types, the caprock counteracts the buoyancy of the gas phase and ensures the containment of the stored CO_2. The other trapping mechanisms (capillary trapping, solubility trapping, mineral trapping) differ between the storage types. The Ketzin reservoir is an example for a saline aquifer storage (Task 4.3), while the P18 field is an example for a former gas field (Task 4.4)
5. Caprock integrity: For a former gas fields the caprock has proven to prevent gas migration within geologic time scales, and therefore is likely to form an effective barrier. However, changing pressure conditions during exploitation potentially may induce open fractures and migration paths. The caprock of a saline aquifer may comprise open fractures and weak zones which have to be identified with geophysical methods. The pressure management has to take into account position and type of the different potential leakage pathways. Lowering the reservoir pressure by removing water or other fluids from the storage structure is one of the remediation options suggested by Benson and Hepple (2005) for CO_2 storage projects within the scenario of leakage up faults, fractures and spill points. Birkholzer et al. (2012) demonstrated the use of brine extraction to minimise pressure build-up at specific locations, such as near a fault zone.
6. Reservoir fluid: The reservoir fluid increases storage safety through capillary forces and dissolution, wherefore both processes are mainly relevant for saline aquifers. This has consequences on potential remediation options. Brine extraction is always a management option for saline aquifers, while it may not be feasible for former gas fields. In contrast, the mobility of gas is higher for former gas fields, therefore, a rather faster release of CO_2 is possible. While the presence of reservoir fluid enhances the storage safety, corresponding effect of water coning may impair the controlled CO_2 release remediation (see also chapter 4, Figure 11).
7. Brine disposal: The practical feasibility of pressure management is closely related to the disposal of extracted reservoir fluid. The main environmental concern is the typically high salt concentration. In the absence of other contaminants, the discharge to the sea is a simple disposal option. Breunig et al. (2013) assessed whether recovered heat, water, and minerals from large volumes of extracted brine can turn the brine into a resource. Brine extraction was also shown to create economic value via beneficial use of treated brine and reduce other costs for CO_2 storage, thereby achieving higher dynamic storage capacity of large-scale CO_2 storage (Bourcier et al., 2011; Maulbetsch and DiFilippo, 2010). Some studies suggest the reinjection in different geological horizons. Depending on the local conditions the effort for brine disposal may preclude the application of pressure management through brine extraction.

The current state regarding the selection of models and scenarios from the data base has been drawn in another report of MiReCOL. The aim of the modelling work is to get a deeper understanding of physical and mechanical parameters which accompany a pressure reduction regime. The requirements to these models and their performance for the various pressure management applications are still under investigation.

3. NUMERICAL MODELLING OF PRESSURE MANAGEMENT

3.1 Numerical Modelling of the Ketzin pilot site

The potential of CO_2 back production and brine withdrawal to reduce the reservoir pressure and divert the CO_2 plume will be assessed. Hypothetical brine extraction wells will be implemented into the applied Ketzin model.

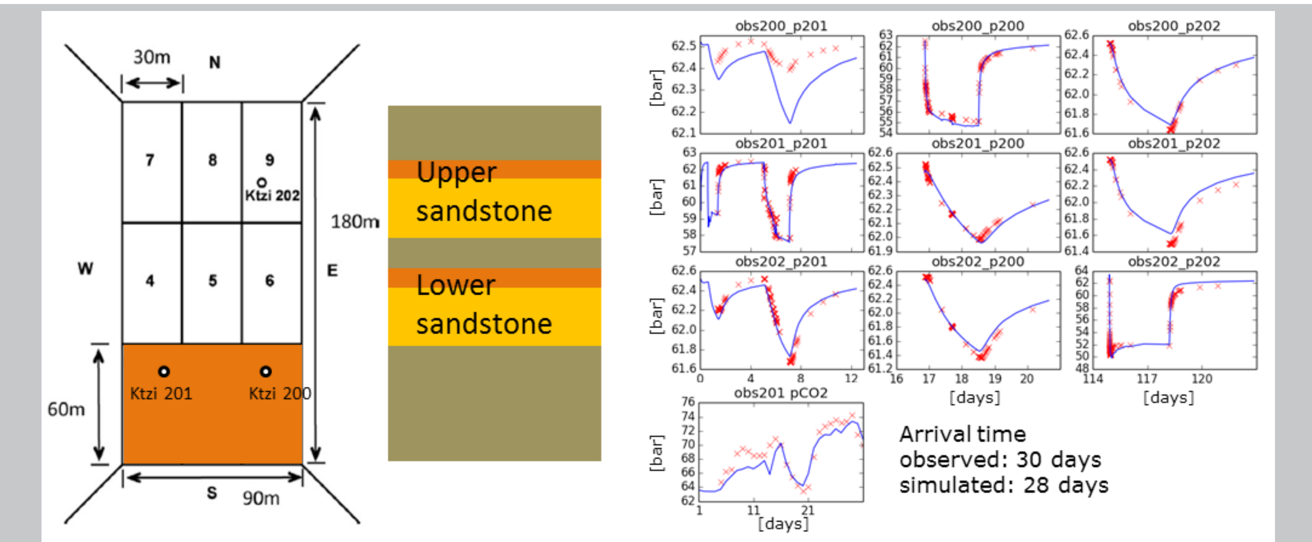

Figure 1 Simple inverse reservoir model including single phase hydraulic data, multiphase injection pressure and arrival time. The orange regions show sandstone areas with high permeability that act as channels for preferential CO_2 flow.

Description of the model selected

A simple inverse model exists for the Ketzin Pilot site. It integrates three hydraulic tests and the first thirty days of CO_2 injection. The model focuses on the joint inversion of the observed pressure during the hydraulic test, injection pressure in the CO_2 injection well and the arrival time of CO_2 arrival data. It contains 30 free parameters and is feasible to model channeling effects due to layered permeability (Figure 1). It is an advanced continuation of the hydraulic modelling work (Chen et al., 2014) and a necessary complement for description of near wellbore modelling effects and consistency with hydraulic testing. These aspects focus on the near wellbore area and are not captured by the former large scale Ketzin reservoir modelling work (Kempka and Kühn, 2013).

Modelling approaches that consider only single phase hydraulic tests indicate a region of low permeability between the injection well Ktzi 201 and observation well Ktzi 200. Multiphase simulations of CO_2 injection in contrast indicate a high permeability between both wells. Single phase simulations predict a higher effective permeability than constrained multiphase simulations. The problem is resolved by joint inversion of one single and one multiphase model. It is crucial for this calibration to develop a geological concept that contains the relevant features and allows to reproduce the different type of observations. In general, the large amounts of data that are recollected from the tests site represent different aspects of the same geological features. Joint inversion is the only promising approach to achieve a comprehensive interpretation to integrate pressure management in the context of other management objectives, e.g. flow diversion and back production (also called venting).

Hypothetical brine extraction wells will be implemented into the inverse Ketzin model. The potential of brine extraction to reduce the reservoir pressure and to divert the CO_2 plume will be assessed. Different spatial well configurations will be tested for the most effective application of the remediation measure. Due to the high content of dissolved minerals the proper disposal of extracted brine is expected to be expensive if discharge to the sea is not possible. In case that preliminary simulations show the withdrawal is far from economic viability, a change of the focus is suggested.

In 2015, a brine injection test is carried out at the pilot site in Ketzin. Brine injection enhances residual trapping and therefore increases the safety of CO_2 storage. Although this brine injection test is not directly in the scope of the research topic “Pressure management”, the safety of CO_2 storage is an elementary remediation measure and generally relevant for the MiReCOL project. It appears worthwhile to slightly shift the focus and consider performing dynamic flow simulations on the Ketzin brine injection field test. Moreover, collaboration with another research topic of MiReCOL, “CO_2 flow diversion”, appears to be advantageous.

3.2 Numerical Modelling of the P18 field

The rate of brine withdrawal required from the existing wells around a CO_2 injection well in a storage structure where pressure build up due to CO_2 injection is “higher than expected”. In order to relieve the pressure, various combinations of brine withdrawal through available wells in the gas reservoir will be examined.

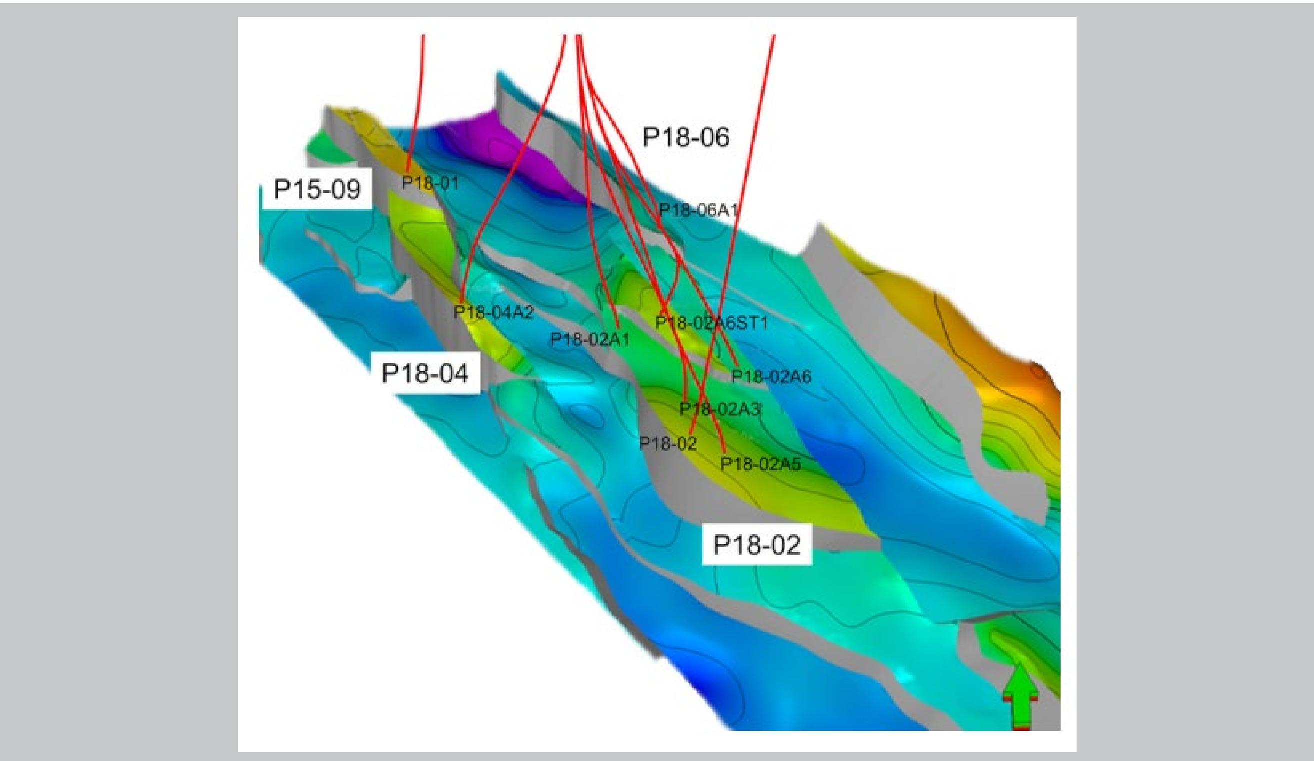

Figure 2 3D view on the top of the P18 gas fields. Faults are shown in grey; well traces are shown in red (Arts et al., 2012).

Description of the model selected

The storage complex must exhibit pressure build-up due to CO_2 injection. Therefore the model must be closed or have little pressure communication with the surrounding hydraulic systems. A closed/semi-closed partially depleted gas reservoir based on the P18-A gas fields (near the coast of Rotterdam) from the SP5 database is chosen to carry out brine/water withdrawal simulations in this scenario (Figure 2).

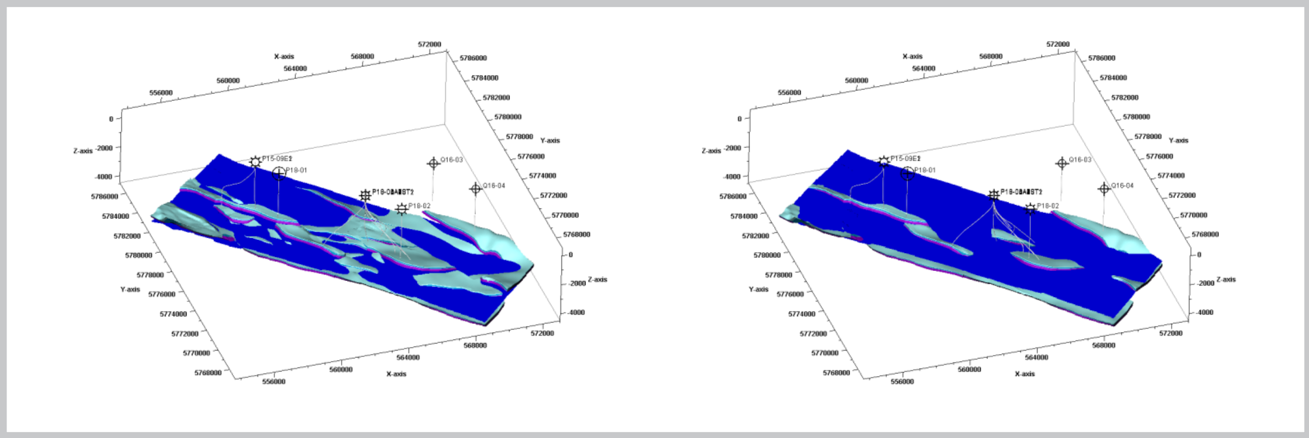

Figure 3 (a) the water-gas contact before gas production, (b) the water-gas contact after gas production.

According to Arts et al. (2012), natural gas production in the P18-4 field is projected to end just before the start of the CO_2 injection. The gas fields in block P18-A (P18-2, P18-4 and P18-6) are situated at approximately 3,500 m depth below sea level. The fields are located in a heavily faulted area and consist mainly of fault bounded compartments, which are (at least on production time scales) hydraulically isolated from their surroundings.

Pre- and post-gas production gas–water contact (Figure 3) and pressure distribution can be quantified for this reservoir. The isolation of the reservoir could be confirmed by the different compositions of gas produced from P15-9 and P-18-4, and different gas–water contacts in P15-9 and P18-4. Arts et al. (2012) demonstrated that based on the history matched model, they could inject 8 Mt of CO_2 to build-up the original reservoir pressure up to 350 bar. However uncertainty exists for the data regarding the gas production history, the chosen abandonment pressure and the total amount of gas produced. Therefore it is assumed the CO_2 is injected with a rate higher than permissible rate and as a consequence the pressure has exceedingly built-up for the reservoir.

Different strategies of brine production will be utilised to investigate:

- the brine extraction rates required;
- the number of brine extraction wells required;
- the interval of brine extraction required;
- the response time required to relieve the excessive pressure build-up

3.3 Numerical Modelling of a saline deep aquifer

Subject of investigation is a real saline aquifer, which cannot be specified at this stage of work due to non-disclosure agreements. This aquifer was once considered and evaluated as a potential storage site. Even after a thorough feasibility study, several uncertainties

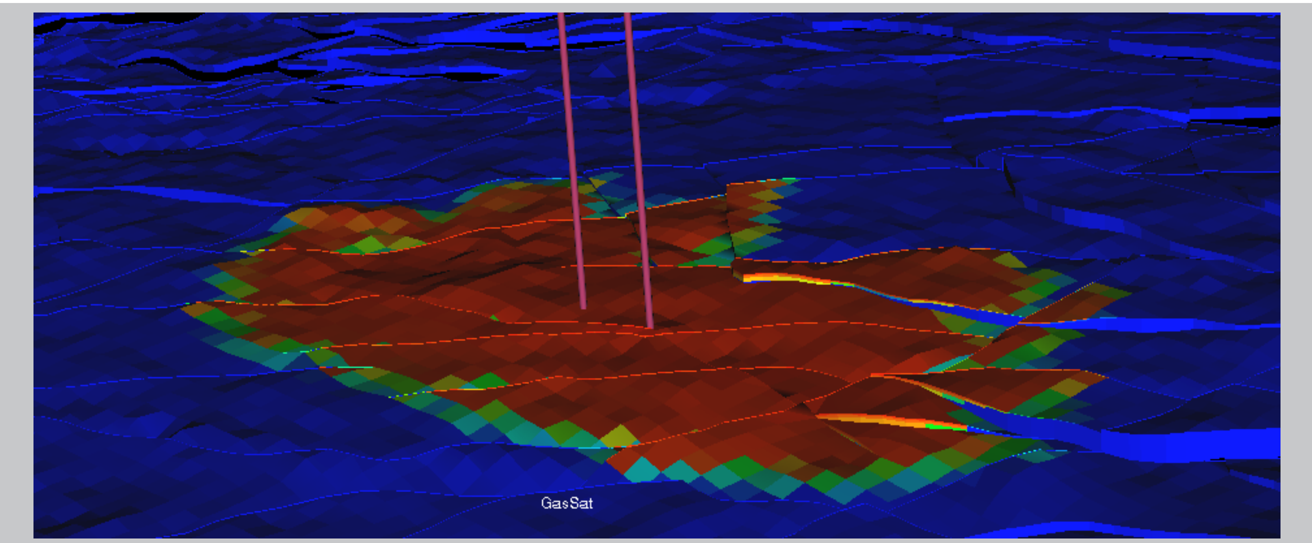

Figure 4 CO_2 saturation profile at the end of the injection.

concerning the safety of storage in this compartment remained. Like the P18 field, this aquifer is located in a highly faulted area. The seal of this compartment is also unproven. The total projected injection of CO_2 injection in this compartment was around 50 Mt. The fastest method to reduce the overpressure, once a problem occurs, is venting of the CO_2 although hysteresis and well effects might reduce the venting velocity. Both are subject of research in WP4.

4. INDIVIDUAL PROCESSES RELATED TO PRESSURE MANAGEMENT

4.1 Hysteresis and CO_2 storage

Relative permeabilities are essential concepts participating to the classical formulation of multiphase flow in porous media. For some time, experimental evidence and analysis of pore-scale physics demonstrate conclusively that relative permeabilities are not single functions of fluid saturations, displaying strong hysteresis effects. In the following subchapter, the relevance of relative permeability hysteresis is evaluated for modeling the geological CO_2 sequestration process, with a strong focus on saline aquifer reservoirs. Many authors have presented simulations of CO_2 injection and migration (Ennis-King and Paterson, 2002; Wellmann et al., 2003; Xu et al., 2003; Flett et al., 2004; Kumar et al., 2005; Obi and Blunt, 2006) using a variety of approaches. Because of the density difference between CO_2 and brine, the low-viscous CO_2 tends to migrate to the top of the geologic structure. This upward migration is sometimes delayed or suppressed by low permeability layers that impede the vertical flow of CO_2. Several trapping mechanisms are recognized as affecting the stored CO_2, these being:

- Hydrodynamic trapping; the buoyant CO_2 is mobile, blocked by an impermeable cap rock.
- Solution trapping; dissolution of the CO_2 in the brine (Pruess and Garcia, 2002), possibly enhanced by gravity instabilities due to the larger density of the brine–CO_2 liquid mixture (Riaz et al., 2006)
- Mineral trapping; geochemical binding to the rock due to mineral precipitation (Pruess et al., 2003)
- Capillary trapping, disconnection of the CO_2 phase into an immobile (trapped) fraction (Flett et al., 2004; Kumar et al., 2005)

During the injection period, the less wetting CO_2 displaces the more wetting brine in a drainage-like process. However, after injection, the buoyant CO_2 migrates laterally and upward, and water displaces CO_2 at the trailing edge of the plume in an imbibition-like process. This leads to disconnection of the once-continuous plume into blobs and ganglia, which are effectively immobile. The importance of the "residual" CO_2 saturation has been pointed out in Hovorka et al. (2004), referenced to laboratory and field data from the Frio brine pilot experiment. However, no distinction was made between critical saturation (during drainage) and residual saturation (during imbibition) in their simulations. A study of CO_2 storage in saline aquifers that accounted for dissolution and chemical reaction (Kumar et al., 2005) considered relative permeability hysteresis using a Land-type model (see next subchapter). They concluded that the majority of CO_2 is stored as residual phase and, therefore, the more dominant mechanism than solubility or mineral trapping.

4.1.1 Pore-scale study

Hysteresis refers to irreversibility or path dependence in multiphase flow, and it manifests itself through the dependence of the relative permeabilities and capillary pressures on the saturation path and the saturation history. From the point of view of pore-scale processes, hysteresis has at least two sources. The first one is the contact angle hysteresis: the advancing contact angle (of wetting phase displacing a non-wetting phase) is larger than the receding contact angle (of wetting phase retreating by non-wetting phase invasion) due to chemical heterogeneities or surface roughness. The second source is trapping of the non-wetting phase: during an imbibition process, a fraction of the non-wetting phase gets disconnected in the form of blobs or ganglia, becoming effectively immobile (trapped). Hysteresis effects are larger in processes with strong flow reversals. This is the case of cyclic water and gas injection in a porous medium, in which the gas phase is trapped during water injection after a gas flood. A detailed explanation of trapping and hysteresis at the pore scale can be found in Lenormand et al. (1983).

Hysteresis Models

The most important quantity determining the significance of hysteresis effects is the trapped gas saturation after a flow reversal (from drainage to imbibition). A trapping model attempts to relate the trapped (residual) gas saturation to the maximum gas saturation, that is, the actual gas saturation at flow reversal. Most relative permeability hysteresis models make use of the trapping model proposed in Killough (1976). In this model, the trapped gas saturation S_{gt} is computed as:

$$S_{gt} = \frac{S_{gi}}{1 + CS_{gi}} \tag{1}$$

where: S_{gi} = Initial gas saturation (gas saturation at flow reversal)
C = Land trapping coefficient

The Land trapping coefficient is computed from the bounding drainage and imbibition relative permeability curves as follows:

$$C = \frac{1}{S_{gt,\max}} - \frac{1}{S_{g,\max}} \tag{2}$$

where: $S_{g,max}$ = maximum gas saturation
$S_{gt,max}$ = maximum trapped saturation, associated with the bounding imbibition curve.

All these quantities are illustrated in Figure 5. The Land trapping model has been validated by comparison with experiments in Killough (1976). The bounding drainage and imbibition curves from the experimental data of Figure 5 result in a Land trapping coefficient $C \sim 1$.

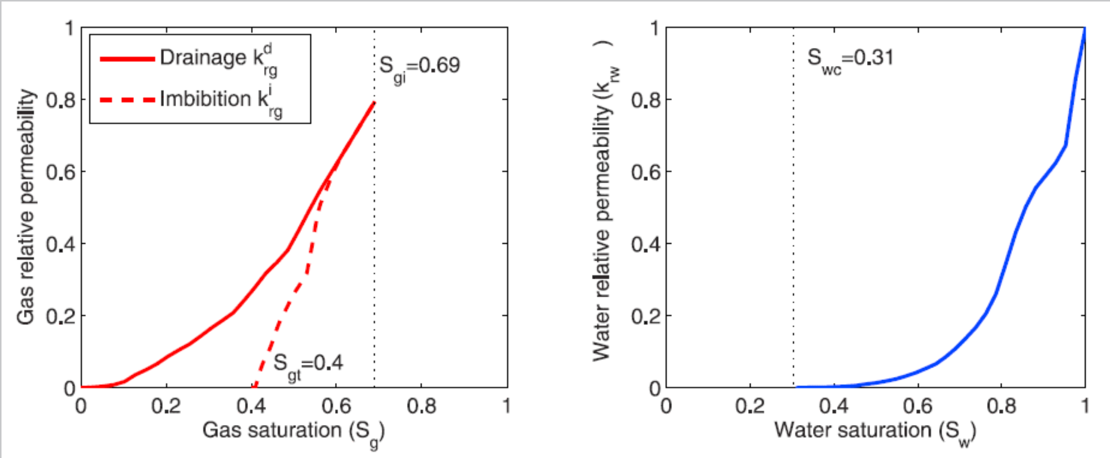

Figure 5 Relative permeability (water-wet Berea sandstone).

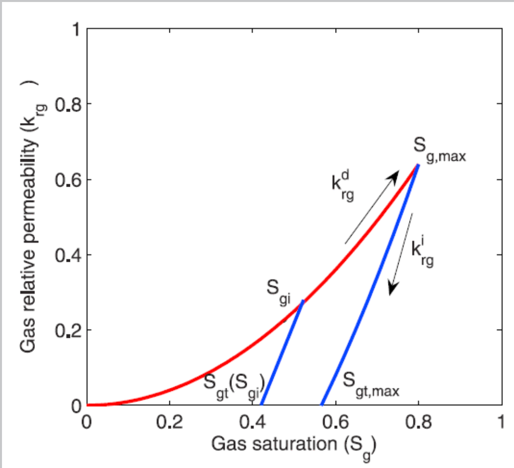

Figure 6 Parameters of Land model.

Another popular relative permeability (K_r) model is the Killough model (Killough, 1976). In Killough's method, the gas relative permeability along a scanning curve, such as the one depicted in Figure 6, is computed as:

$$K^{i}_{rg}\left(S_g\right) = K^{ib}_{rg}\left(S^*_g\right)\frac{K^{d}_{rg}\left(S_{gi}\right)}{K^{d}_{rg}\left(S_{gi,\max}\right)} \tag{3}$$

$$S^*_g = S_{gt,\max} + \frac{\left(S_g - S_{gt}\right)\left(S_{gi,\max} - S_{gt,\max}\right)}{S_{gi} - S_{gt}} \tag{4}$$

In the above equations, K_{rg}^{d} and K_{rg}^{ib} represent the bounding drainage and imbibition curves, respectively. The bounding imbibition curve is assumed to be available from experiments, or computed using Land's imbibition model. In Killough's model, scanning curves are assumed to be "reversible", so that the imbibition curve is representative of a subsequent drainage process. Capillary pressure–saturation relationships also exhibit marked hysteresis effects. Several mathematical models exist to treat hysteretic capillary pressure curves, including the one proposed by Killough. From a practical point of view, however, capillary pressure effects are often negligible at the time of numerically simulating field-scale displacements, when the characteristic capillary length is much smaller than the grid resolution (Aziz and Settari, 1979).

The above mentioned state of the art implies that laboratory data are available. Efforts have been made to obtain the maximum gas saturation values from correlation to other standard petrophysical properties (Keelan and Pugh, 1975; Batycky et al., 1988; Hamon et al., 2001; Holtz and Major, 2002). Maximum residual gas saturation (S_{grm}) is what initially results from imbibition on rock at irreducible water saturation (S_{wirr}). S_{grm} results from gas acting as the non-wetting phase during imbibition hysteresis as pressure is depleted in a gas reservoir and an aquifer encroaches in pore space that was once filled with gas. Numerous influences may affect S_{grm}: (1) how the wetting fluid gets in (either forced or spontaneous imbibition), (2) type of wetting fluid, (3) rate of imbibition, (4) rock type (lithology, grain size and sorting), (5) pore type, (6) wettability and (7) interfacial tensions.

Porosity has been shown to have the strongest relationship to S_{grm}. Nearly all studies involving a porosity-S_{grm} relationship indicate that S_{grm}, increases as porosity decreases (Keelan and Pugh, 1975; Jerauld, 1996; McKay, 1974; Delclaud, 1991). With water acting as the wetting phase and gas acting as the non-wetting phase, S_{grm} results from pore scale capillary forces. S_{grm} is the trapped non-wetting phase when the wetting phase has been imbibed into the rock from a state of irreducible water saturation to a state of zero capillary pressure. The models that describe how this trapping occurs are pore-geometry dependent. Three trapping models are possible (Figure 7). The pore doublet model is more likely to occur in poorly sorted rock or in rock with dual-porosity networks. The pore snap-off and dead-end models are more likely to occur in lower porosity rocks.

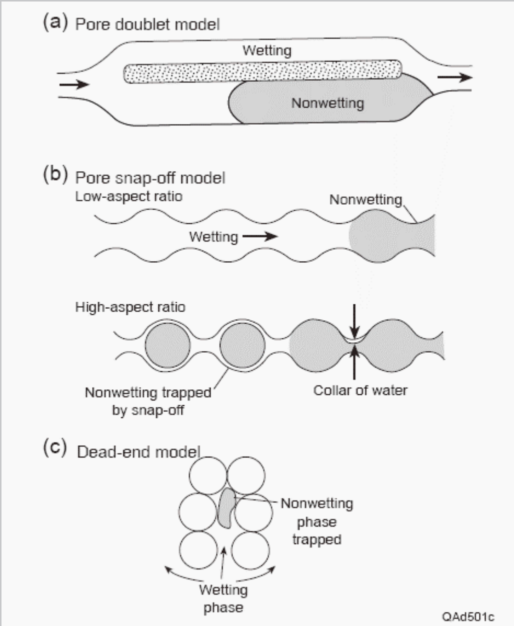

Figure 7 Three conceptual trapping models.

Different S_{gr}-PHI relationships are shown in Figure 8.

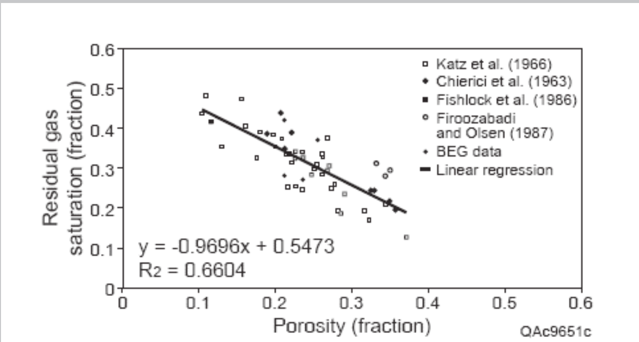

Figure 8 Different experimental data relating porosity to residual gas saturation.

Thus, one can use for S_{grm} the correlation above or make use more generally of a relationship which conciliates petrophysical properties such as permeability (K), irreducible water saturation (S_{wirr}) and S_{grm}. They must be integrated in such a way that S_{grm} is a function of S_{wirr} so that the initial condition of S_{grm} being less than or equal to the initial gas saturation is met. This initial condition is met with the development of an initial residual non-wetting phase curve (IR curve). The general shapes of IR curves are shown in Figure 9 (modified from Lake, 1996). These curves represent the character of an individual rock sample. The end point to the curve is the S_{grm} value. The shape of the initial-residual wetting phase saturation curves displays the effect of rock type. As sandstone becomes cleaner, better sorted, and less cemented (higher porosity), the curves move farther away from the 1 to 1 line, increasing in slope as S_{grm} decreases.

The curves must stay below the 1 to 1 line, terminate at a given S_{grm}-S_{gi} position, and decrease in slope with higher quality rock. The modified Land's equation below meets these criteria:

$$S_{gr} = \frac{1}{\left[\left(\frac{1}{S_{grm}} - 1\right) + \left(\frac{1 - S_{wirr}}{Sg}\right)\right]} \tag{5}$$

Thus, given a set of S_{wirr}-S_{grm} values, the S_{gr} can be determined for a given S_g. It is to be noted that a relationship between residual gas saturation and porosity is given with data obtained from the Frio pilot project (Figure 10).

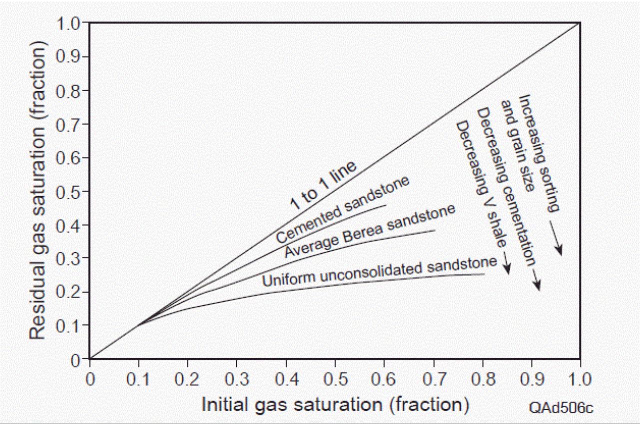

Figure 9 IR curves.

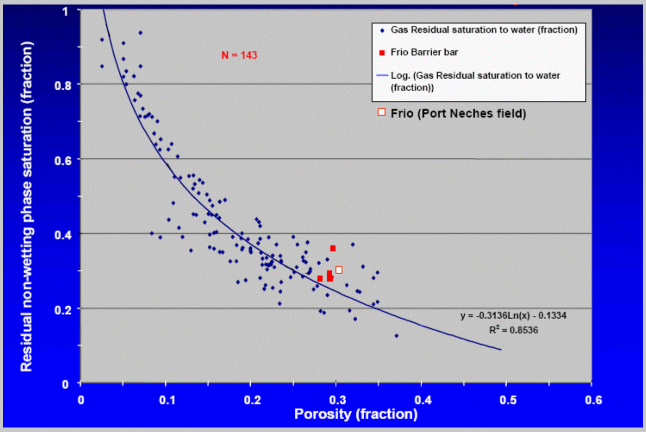

Figure 10 Residual gas saturation vs porosity (Holtz, 2005).

4.1.2 Reservoir-scale study

During injection of CO_2 in a storage compartment, the ambient fluids in the reservoir are displaced. In the case of P18-4, the injected CO_2 enters the available pore-space involving displacement and mixing processes with the remaining natural gas molecules. In this situation the water phase is not or hardly displaced. During the event of venting, the re-production should therefore not be subject to hysteresis. In the case of an aquifer, the CO_2 is injected in a pore-space, which is already occupied by the brine phase. This means that the wetting fluid is displaced (so-called drainage process). Reversal of the flow during the event of venting would result in hysteresis and relative permeability-saturation curves, which are a function of the displacement history (reversal points, entrapment etc.). Several models have been derived for describing hysteretic relationships. Examples are Lenhard and Parker (1987), Parker and Lenhard (1987). Oak (1990), however, mentions that many data sets are at best limited to just a couple of saturation history cases. Besides during venting, reversal of displacement also occurs when brine re-imbibes into areas, vacated by the CO_2 during redistribution within the aquifer. The entrapment, associated with hysteresis, also increases the interfacial area between the CO_2 and the brine. This leads to more rapid dissolution and thus to more rapid pressure reduction.

The starting point was a non-hysteretic reservoir model, which was one of the deliverables of the aforementioned feasibility study. The relative permeability-saturation curves for the carbon dioxide were made hysteretic, while those of the wetting fluid (brine) were left non-hysteretic. With this model, a number of simulations were carried out. Back production of CO_2 as predicted by the reservoir model with and without a hysteretic description was compared. A limited sensitivity analysis was carried out for various bottom-hole pressures, periods between the end of injection and the actual reproduction etc.

Future investigation would involve: 1) The impact of hysteresis on the long term extent of the migration, 2) massive water injection to immobilize (by entrapment) and pushing the CO_2 away from a possible faulty well.

4.2 Well effects during back production

The back production of CO_2 reverses the flow direction and multiphase flow phenomena occur that are fundamentally different as those from the injection. During injection only one operational state exists, changing the injection rate induces gradual differences in the injection pressure. In contrast, the back production phase can be described by three different operational modes. At small production rates $r_{CO2} < r_{cl}$ pure CO_2 can be produced continuously at wellhead elevation (Figure 11a). However, at reservoir elevation both, CO_2 and brine are extracted from the sandstone. The water has a higher density than CO_2 and remains in the lower part of the well where it reinfiltrates into the formation. Therefore a water cone develops (Figure 11a-c).

With increasing rates more water is produced and the reinfiltration capacity of the formation is exceeded. This occurs when the critical rate r_{cl} is exceeded. This rate depends on the CO_2 saturation, distribution and reservoir petrophysical properties. The water level rises above the well filter and the CO_2 passes through the water column in the form of bubbles (Figure 11b). The water column has a higher density than the CO_2 column and therefore, the bottom-hole pressure is reduced. Depending on the control mode at the outlet and the reservoir behavior, the water column may rise such that the CO_2 flux decreases below the nominal rate.

In case the rate of CO_2 exceeds the Turner velocity ($r_{CO2} > v_{Tur}$) the brine is dispersed and entrained by the CO_2, transported upwards and arrives at the wellhead. No accumulation occurs (Figure 11c).

For the Ketzin case, production rates will be between 800 and 3200 kg/h. The magnitude of the critical rate r_{cl} is not known prior to the test. The critical rate r_{Tur} is about 2700 to 3800 kg/h (Bannach et al., 2014), depending on the test conditions.

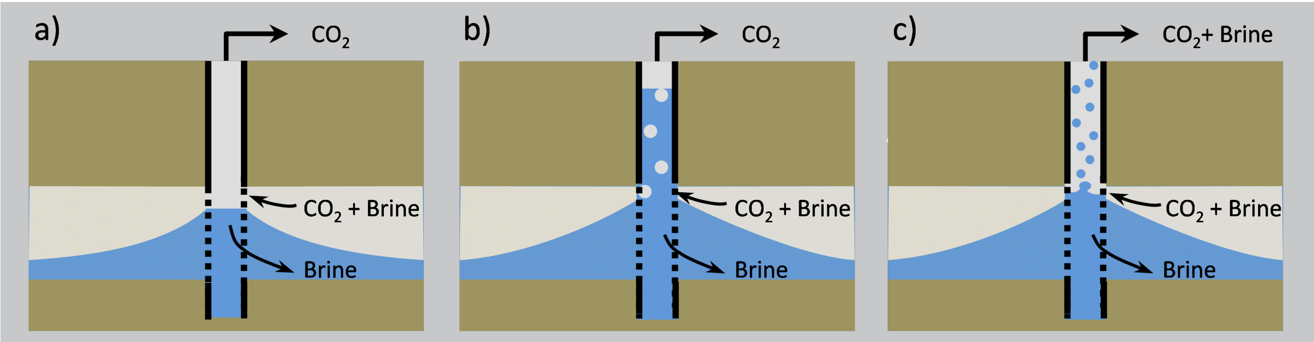

Figure 11 Three operational modes during the back production test.

4.3 Application of nanoparticles

The application of nanoparticles may improve the performance of CO_2 injection and storage and has potential as a remediation method in the case of leakage. Nanoparticles can potentially increase the dissolution of CO_2 and promote the formation of emulsions and foams with the reservoir brine. The main benefits are:

1. Reduction of the pressure
2. Decrease the amount of undissolved CO_2 that can potentially leak: dissolved CO_2 is trapped. An additional benefit is the fact that the density of the brine increases due to the dissolution of CO_2, which makes it less buoyant or even negatively buoyant.

The primary application of nanoparticles that is considered is the remediation of leakage scenarios with comparatively low rates. This is based in the comparatively slow reaction rates in comparison to hydraulic processes.

Task 4.5 addresses enhanced CO_2 dissolution by application of nanoparticles to enhance the process of convective mixing.

Nanoparticles (solid particles in the size range $<$ µm) can be used to stabilize emulsions by interfacial adsorption to form so-called solid-stabilized or Pickering emulsions. The adsorbed particle layer provides a steric barrier that prevents the coalescence of emulsion droplets. The driving force for interfacial adsorption is the reduction of the interfacial area of the two phases (in our case CO_2 and brine) and a corresponding reduction in the interfacial energy. Molecular surfactants can also be used for the stabilization of emulsions, but the working principle is different. Molecular surfactants stabilize emulsions by reducing the interfacial tension and not so much the interfacial area. In general it can be stated that Pickering emulsions are more stable against coalescence as otherwise stabilized emulsions. To achieve Pickering stabilization, the nanoparticles should have an intermediate wettability with respect to CO_2 and brine. Potential particles might be silica, clay (Planomer® technology), cellulose fibers (Greenanofilm, EU FP7), soot, and carbon black. All particles can be coated (engineered nanoparticles as e.g. Aminzadeh et al., 2013). The major advantage of Pickering stabilization is the stability under the extreme conditions underground (high pressure, temperature, salinity etc.) and the possibility to increase density by selecting nanoparticles with high density.

Most literature on CO_2 and nanoparticles discusses the creation of stable emulsions or foams of CO_2 and brine for different purposes: for CO_2 storage in aquifers (Espinosa et al., 2010; Hariz, 2012; Aminzadeh et al., 2013), for CO_2 storage in deep ocean environments (Golomb et al., 2006; Golomb et al., 2007), or for enhanced oil recovery using CO_2 (e.g. Jikich, 2012; Worthen et al., 2012; Al-Otaibi et al., 2014). The goal of the stable foams or emulsions is always to decrease the mobility of the CO_2, because the mobility of the foam is lower than that of the individual pure phases (DiCarlo et al., 2011). Nanoparticles can be used in three different ways:

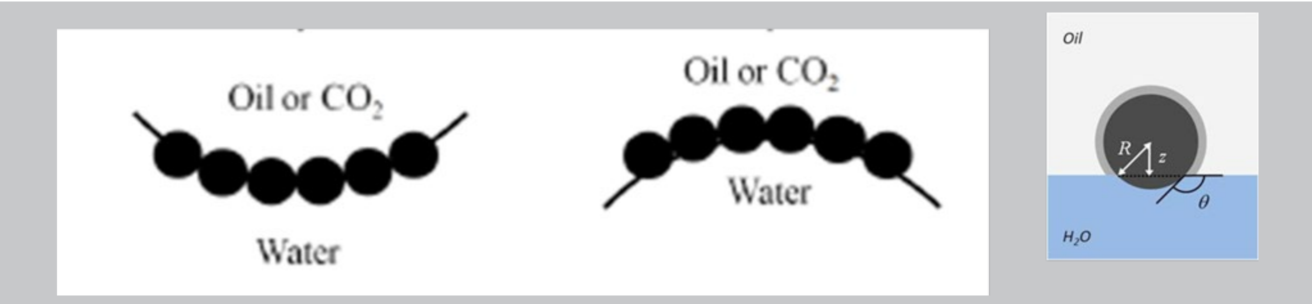

Figure 12 Interfacial adsorption of emulsion by solid nanoparticles.

1. Increase CO_2 dissolution by enhancing convective mixing.
Convective mixing is a process that occurs in CO_2 underlain by brine (Green and Ennis-King, 2013; Huppert and Neufeld, 2014; Szulczewski et al., 2013). The CO_2 dissolves in the underlying brine via diffusion, which increases the density of the brine and creates an inherently unstable, high density boundary layer. At some point, downward flow will start via fingering, which replaces the saturated brine in the boundary layer with fresh, unsaturated brine. This process significantly enhances the dissolution of CO_2. The nanoparticles could be used to enhance the onset and efficiency of the convective mixing (Javadpour and Nicot, 2011; Singh et al., 2012). The two questions addressed are to determine the injection method and the type of applicable particles.

2. Increase CO_2 dissolution during CO_2 injection and the subsequent convection of the CO_2 plume.
The application of a disperser during CO_2-injection can reduce droplet size and increase the dissolution of CO_2. Reduction of the droplet size could also be achieved by pumping the CO_2 through the porous formation itself. Upon passing through the pores, the super critical CO_2 deforms, increases the interfacial area with brine and allows particle adsorption. The created interfacial area is then stabilized against coalescence. This might have the unwanted side-effect that the smaller CO_2 droplets can pass more easily through pore throats and become more mobile because of that. The question is really how small the droplets will become during injection. The amount of brine present in the vicinity of the well is not sufficient to store the CO_2. The accumulation of CO_2 is the limiting factor, rather than the speed of dissolution of CO_2. This means that CO_2 needs to be mixed with water/brine and disperser in the well. Consequently, research needs to consider that large amounts of water or brine are required. If it becomes apparent that the use of nanoparticles is not suitable as a remediation method, it will not be further investigated in this task.

3. For immediate remediation in case of high-rate leakage through a fault or along a spill point
Nanoparticles could be injected close to the area of leakage with the goal of reducing the mobility of the CO_2 by creating foams and/or emulsions and possibly immobilizing the leaking CO_2 by increasing the dissolution. Main questions are how much the mobility of the CO_2 can be reduced and whether the dissolution can be accelerated sufficiently and whether there is sufficient storage capacity. Also it should be studied how the nanoparticles can be transported to the required location, for example via hydraulic fractures. This scenario and the associated research questions are addressed in Tasks 6.3 and 6.4.

5. INDUSTRY PRACTICE

Flow diversion methods (control of the plume position) are currently applied for oil fields, since these frequently comprise a high number of wells. The operational mode is changed on the breakthrough of gas or water to production wells. There is no knowledge about predictive modelling here. Gas fields in contrast typically have a lower number of wells and typically not a defined breakthrough, wherefore flow diversion is not applicable. Direct CO_2 injection for enhanced gas recovery is not carried out since the natural gas would be contaminated and require subsequent separation. Natural gas storage is carried out in formations with a natural boundary, which may be a close boundary in case of reservoir compartments or an open boundary in case of anticline structures. These boundaries control the plume shape, wherefore active plume management is not carried out.

The plume migration direction is considered the dominating risk at the In Salah test site for CO_2 injection (Dodds et al., 2011). Furthermore, a spill point is another significant risk, wherefore the corresponding plume distance is regularly monitored and the injection was interrupted when spill point was approached.

Traditionally the reservoir pressure is observed top-hole. In the mid 90's the first bottom-hole equipments have been installed in North Sea fields, and in the US this instrumentation spreads out with the beginning of the 2000 years. There is actually a lot of technical progress in this field of application and bottom-hole gauges are almost standard now. Frequently they are based on fiber optics with distributed temperature and pressure management and the possibility to connect additional sensor types. However, the devices can be easily damaged during installation, which was the case at the Cranfield (Mississippi, USA) and In Salah (Algeria) site. At the Ketzin site bottom-hole pressure is observed with a Weatherford optical sensor. Similar pressure and temperature sensors have been installed at the Aquistore test site (Canada). It has to be considered, that bottom-hole pressure frequently means that the sensor is close to the reservoir, but some distance above the reservoir elevation. At the Ketzin test site, the sensor is located at 550m, about 90 m above the reservoir.

The primary control variable for natural gas storage is the maximum pressure. The maximum limit is the allowable pressure to stay well below fracture pressure, but the maximum operational pressure of the compressor type may also be a practical limit. Currently there are no cases known where a remediation of a natural gas storage became necessary.

Heuristic analytical models based on Darcie's Law are used as straightforward solution for vertical wells with either closed or open boundaries. Since horizontal wells became standard and numerical methods improved, most of them are not applicable any more. Numerical models are used instead and are nowadays standard method for reservoir management. A prognosis typically predicts an interval of 3-6 months. There are three big families for reservoir models, they are the Eclipse family from Schlumberger, the Stars system from CMG and Quiklook reservoir simulator from Halliburton. There is no commercial application of nanoparticles yet.

Suggestions:

- Microgravity is rapidly evolving for reservoir monitoring with the focus to offshore applications. It should be considered to include this in MiReCOL.
- Tracers are important to distinguish injected from natural CO_2 to improve leakage detection. An alternative to SF6 would be desirable. Some research on this is carried out art Snovit, in Edinburgh research on nitrogen and helium is carried out.

The Interview was based on the following questions

- Are there standard procedures in which flow diversion methods are applied?
- In which cases is the plume shape explicitly considered?
- How is the reservoir pressure observed? Top- or bottom-hole? Which are the most common gauges applied in industrial fields?
- Are there differences for application in
  - natural gas fields?
  - underground gas reservoirs?
  - oil fields?
  - others (e.g. salt caverns)
- Most relevant to MiReCOL are gas reservoirs which comprise an aquifer.
  - Which are the control variables? Which are the parameters to be optimized?
  - Which analytical approximations are applied?
  - Which numerical models are applied for predicting pressure and the effect of management methods?
  - What kind of remedial activities do you consider, when a spill point in natural gas storage may/is reached. How do you monitor that?
  - Under what situation would you consider venting as a final remedial action?
- Nanoparticles
  - Are you aware of any use of substances like nanoparticles used for pressure management (rather than tertiary recovery)?
  - Do you know of any field-scale or test implementations of nanoparticles for CO_2-EOR?

6. SUMMARY

This report should summarize the state of the art of pressure management in petroleum industry practice. As an intensive literature study has shown, pressure management does not play an important role in industrial context of oil and gas production. For CO_2 storage reservoirs, however, pressure is a critical parameter because reservoirs are filled up overpressured and, as consequence, the caprock integrity might be compromised. The leakage from an overpressured reservoir has high potential for environmental pollution. Research is required to assess its potential for operation and remediation of CO_2 storage reservoirs. The present report outlines the state of the art and the planned workflow within the project topic "Pressure management".

The natural reservoir features, such as type of reservoir, type of boundary conditions, hysteresis properties etc. have a dominating impact on reservoir behaviour and, therefore, on the pressure management. A careful assessment of these conditions is the prerequisite for the choice of an appropriate remediation method. It is crucial to reduce the number of potential remediation methods a priori, because the second step of numerical modelling requires much larger effort and only allow a limited number of simulations. Numerical modelling is necessary for quantification of the remediation efficiency, comparison of different remediation methods and optimization of the operational scheme. The models within this report are site specific but it is intended to derive generally valid best practice rules and to quantify the remediation success.

References

Al-Otaibi, F.M. et al Gelled emulsion of CO_2 Water Nanoparticles (2014), Saudi Aramco Journal of Technology.

Aminzadeh, B., D.H. Chung, S.L. Bryant, C. Huh and D. A. DiCarlo (2013), CO_2 leakage prevention by introducing engineered nanoparticles to the in-situ brine. Energy Procedia 37, 5290 – 5297.

Aziz, K., and A. Settari (1979), Petroleum Reservoir Simulation, Elsevier, New York.

Ref.14 - Keelan D.K., and Pugh V.J.: "Trapped-Gas Saturation in Carbonate Formations," paper SPE 4535 presented at the 1975 SPE-AIME 48th Annual Fall Meeting, April. Bannach, A., Eberth, K., Pippig, P., Schlichenmayer, 2014, Rückfördertest Bohrung Ktzi 201 - Vorplanungen zum Test Design, ESK Freiberg.

Batycky, J., Irwin, D., and Fish, R.: "Trapped Gas Saturation in Leducage Reservoirs," J. Can. Pet. Techn. (Feb. 1988) 32. Benson, S., Hepple, R., 2005, Prospects for Early Detection and Options for Remediation of Leakage from CO_2 Storage Projects.

Birkholzer, J., Cihan, A., Zhou, Q. (2012), Impact-driven pressure management via targeted brine extraction-Conceptual studies of CO_2 storage in saline formations, International Journal of Greenhouse Gas Control, 7, 168-180.

Breunig, H., Birkholzer, J., Borgia, A., Oldenburg, C., Price, P., McKone, T. (2013), Regional evaluation of brine management for geologic carbon sequestration, International Journal of Greenhouse Gas Control, 14, 39-48.

Buscheck, T.A., Sun, Y., Hao, Y., Wolery, T.J., Bourcier, W., Tompson, A.F., Jones, E.D., Friedmann, S.J., Aines, R.D. (2011), Combining brine extraction, desalination, and residual-brine reinjection with CO_2 storage in saline formations: Implications for pressure management, capacity, and risk mitigation, Energy Procedia , 4, 4283 - 4290, DOI: http://dx.doi.org/10.1016/j.egypro.2011.02.378.

Chen, F., Wiese, B., Zhou, Q., Kowalsky, M., Norden, B., Kempka, T., Birkholzer, J. (2014), Numerical modeling of the pumping tests at the Ketzin pilot site for CO_2 injection: Model calibration and heterogeneity effects, International Journal of Greenhouse Gas Control, 22, 200-212.

Delclaud, J.: "Laboratory Measurements of the Residual Gas Saturation," Second European Core Analysis Symposium, London (20-22 May 1991).DiCarlo, D. A., B. Aminzadeh, M. Roberts, D. H. Chung, S. L. Bryant, and C. Huh (2011), Mobility control through spontaneous formation of nanoparticle stabilized emulsions, Geophysical Research Letters, 38(L24404), 5.

Ennis-King, J., and L. Paterson (2002), Engineering aspects of geological sequestration of carbon dioxide, SPE Pap. 77809-MS, Soc. of Pet. Eng., Richardson, Tex.

Espinosa, D., Caldelas, F., Johnston, K., Bryant, S. L., Huh, C. (2010), Nanoparticle-Stabilized Supercritical CO_2 Foams for Potential Mobility Control Applications. Proceeding of the 2010 SPE Improved Oil Recovery Symposium Tulsa, Oklahoma, USA, 24–28 April 2010.

Flett, M., R. Gurton, and I. Taggart (2004), The function of gas– water relative permeability hysteresis in the sequestration of carbon dioxide in saline formations, SPE Pap. 88485-MS, Soc. of Pet. Eng., Richardson, Tex. Golomb, D., E. Barry, D. Ryan, P. Swett and H. Duan (2006) Macroemulsions of Liquid and Supercritical CO_2-in-Water and Water-in-Liquid CO_2 Stabilized by Fine Particles. Ind. Eng. Chem. Res. 2006, 45, 2728-2733.

Golomb, D., S. Pennel, D. Ryan, E. Barry and P. Swett (2007), Ocean Sequestration of Carbon Dioxide: Modeling the Deep Ocean Release of a Dense Emulsion of Liquid CO_2-in-Water Stabilized by Pulverized Limestone Particles. Environ. Sci. Technol. 2007, 41, 4698-4704.

Green, C.P. and J. Ennis-King (2013), Convective mixing in geology. Report EP13096. Earth science & resource engineering, CSIRO.

Hamon, G., Suzanne, K., and Billiotte, J.: "Field-Wide Variations of Trapped Gas Saturation in Heterogeneous Sandstone Reservoirs," paper SPE 71524 presented at the SPE Annual Tech. Conf. and Exh., New Orleans, LA, 30 Sept.–3 Oct, 2001.

Hariz, T.R. (2012), Nanoparticle stabilized CO_2 foams for potential mobility control applications. PhD thesis, University of Texas, Austin, TX.

Holtz, M.H., and Major, R.P.: "Petrophysical Characterization of Permian Shallow-Water Dolostone," paper SPE 75214 presented at the 2002 SPE/DOE IOR Conference.

Holtz, M. H., Reservoir characterization applying residual gas saturation modeling, example from the Starfak T1 reservoir, middle Miocene Gulf of Mexico, M.Sc. Thesis, University of Texas at Austin, 2005.

Hovorka, S. D., C. Doughty, and M. H. Holtz (2004), Testing efficiency of storage in the subsurface: Frio brine pilot experiment, paper presented at International Conference on Greenhouse Gas Control Technologies (GHGT-7), Int. Energy Agency, Vancouver, B. C., Canada.

Huppert, H.E. and J.A. Neufeld (2014), The fluid mechanics of carbon sequestration. Annu. Rev. Fluid Mech. Vol. 46, p 255-272.

Javadpour, F. and J.-P. Nicot (2011), Enhanced CO_2 storage and sequestration in deep saline aquifers by nanoparticles: commingled disposal of depleted uranium and CO_2.

Jerauld, G.R.: "Gas-Oil Relative Permeability of Prudhoe Bay," paper SPE 35718 presented at the 1996 Western Meeting.

Jikich, S. (2012), CO_2 EOR: Nanotechnology for Mobility Control Studied. Technology update JPT, July 2012.

Kempka, T., Kühn, M. (2013), Numerical simulations of CO_2 arrival times and reservoir pressure coincide with observations from the Ketzin pilot site, Germany, Environmental Earth Sciences, 70 (8), 3675-3685.

Killough, J. E. (1976), Reservoir simulation with history-dependent saturation functions, Soc. Pet. Eng. J., 16(1), 37–48.

Kumar, A., R. Ozah, M. Noh, G. A. Pope, S. Bryant, K. Sepehrnoori, and L. W. Lake (2005), Reservoir simulation of CO_2 storage in deep saline aquifers, Soc. Pet. Eng. J., 10(3), 336– 348.

Lake, Larry: Enhanced Oil Recovery, Prentice Hall (1996), 550.

Lenhard, R. J., and J. C. Parker (1987), A model for hysteretic constitutive relations governing multiphase flow: 2. Permeability-saturation relations. Water Resources Research 23: 2197-2206.

Lenormand, R., C. Zarcone, and A. Sarr (1983), Mechanisms of the displacement of one fluid by another in a network of capillary ,J. Fluid Mech.135123–132.

Maulbetsch, J., DiFilippo, M. (2010), Performance, cost and environmental effects of saltwater cooling towers, Public Interest Research Program Final Project Report, California Energy Comission, CEC-500-2008-043.

McKay, B.A.: "Laboratory Studies of Gas Displacement from Sandstone Reservoirs Having Strong Water Drive," APEA Journal (1974), 189.

Mijic, A., Mathias, S., Laforce, T. (2013), Multiple well systems with non-darcy flow, Groundwater, 51 (4), 588-596.

Moore, C., Doherty, J. (2006), The cost of uniqueness in groundwater model calibration, Advances In Water Resources, 29 (4), 605-623.

Oak, M.J. (1990), Three-Phase relative Permeability of water-wet Berea. SPE/DOE 20183.

Obi, E.-O. I., and M. J. Blunt (2006), Streamline-based simulation of carbon dioxide storage in a North Sea aquifer, Water Resour. Res., 42.

Parker, J.C. and Lenhard, R.J. (1987), A model for hysteretic constitutive relations governing multiphase flow: 2. Saturation-Pressure relations. Water Resources Research 23: 2187-2196.

Singh H., S.A. Hosseini, F. Javadpour (2012), Enhanced CO_2 storage in deep saline aquifers by nanoparticles: numerical simulation results. SPE 156983.

Pruess, K., and J. Garcıa (2002), Multiphase flow dynamics during CO_2 disposal into saline aquifers, Environ. Geol., 42(2–3), 282– 295.

Pruess, K., T. Xu, J. Apps, and J. Garcia (2003), Numerical modeling of aquifer disposal of CO_2, Soc. Pet. Eng. J., 8(1), 49–60.

Riaz, A., M. Hesse, H. A. Tchelepi, and F. M. Orr Jr. (2006), Onset of convection in a gravitationally unstable, diffusive boundary layer in porous media, J. Fluid Mech., 548, 87–111.

Szulczewski, M.L., M.A. Hesse and R. Juanes (2013), Carbon dioxide dissolution in structural and stratigraphic traps. J. Fluid. Mech., vol. 736, p 287-315.

Wellman, T. P., R. B. Grigg, B. J. McPherson, R. K. Svec, and P. C. Lichtner (2003), The evaluation of CO_2 – brine-rock interaction with laboratory flow test and reactive transport modeling, in SPE/DOE International Symposium on Oilfield Chemistry, Houston, Texas, (SPE 80228).

Wiese, B., Nimtz, M., Klatt, M., Kühn, M. (2010), Sensitivities of injection rates for single well CO_2 injection into saline aquifers, Chemie der Erde - Geochemistry, 70 (Supplement 3), 165-172.

Worthen, A.J., Bagaris, H.G., Chen, Y., Bryant, S.L., Huh, C., and Johnston, K.P. (2012), Nanoparticle-Stabilized Carbon Dioxide in Water Foams for Enhanced Oil Recovery. Paper SPE 154285, presented at the SPE Improved Oil Recovery Symposium, Tulsa, 16–18 April. http://dx.doi.org/10.2118/10.2118/154285-MS.

Zhou, Q., Birkholzer, J. (2011), On scale and magnitude of pressure build-up induced by large-scale geologic storage of CO 2, Greenhouse Gases: Science and Technology, 1 (1), 11-20.

Zhou, Q.L., Birkholzer, J.T., Mehnert, E., Lin, Y.F., Zhang, K. (2010), Modeling Basin- and Plume-Scale Processes of CO_2 Storage for Full-Scale Deployment, Ground Water, 48 (4), 494-514, DOI: 10.1111/j.1745-6584.2009.00657.x.

Xu, T. F., J. A. Apps, and K. Pruess (2003), Reactive geochemical transport simulation to study mineral trapping for CO_2 disposal in deep arenaceous formations, J. Geophys. Res., 108.

Chapter VII

The impact of hysteresis effects on brine/CO_2 relative permeability and CO_2 recovery as remediation measure

Cor Hofstee[1]
[1] TNO, The Netherlands

SUMMARY

This deliverable reports on the impact of hysteretic relative permeability on intended or unintended venting of the aquifer. Furthermore, the impact of hysteresis is compared with the role of diversion of the CO_2 by the injection of brine. To avoid increasing the definition of the storage complex, the injected brine was produced from the same compartment.

Dynamic flow simulations were applied to selected reservoir models to test the effects of hysteresis on CO_2 recovery and reservoir pressure management. A limited sensitivity study was conducted to determine the impact of duration of redistribution, permeability, pore volume and amount injected on the venting process. In addition it was attempted to lower the CO_2 emissions during a venting procedure, by injection of water into the CO_2 zone.

1 NUMERICAL MODELLING OF A SALINE DEEP AQUIFER

During injection of CO_2 in a storage compartment of a gas field, the ambient fluids in the reservoir are displaced. In the case of the mature gas field P18-4, for example, the injection CO_2 enters the available pore space involving displacement and gradually mixes with the remaining natural gas molecules. In this situation the water phase is not or hardly displaced. During the event of venting, the re-production should therefore not be subject to hysteresis. In the case of an aquifer, the CO_2 is injected in a pore space, which is occupied by the brine phase. This means that the wetting fluid (= brine) is displaced (so-called drainage process). The space occupied by the injected CO_2 is created by the increase of the reservoir pressure, which leads to compression of the brine. Reversal of the flow during the event of venting (opening injector) would result in hysteresis and relative permeability-saturation curves, which are a function of the displacement history (reversal points, entrapment etc.) (Corey, 2004). Although hysteretic characteristic curves are routinely employed by the petroleum industry, researchers in other fields, such as those of geothermal energy systems and CO_2 storage, tend to assume non-hysteretic conditions (Doughty, 2007). Several expressions have been derived for describing hysteretic relationships. Examples are Lenhard and Parker (1987) and Parker and Lenhard (1987). Oak (1990), however, mentioned that many data sets (used in CCS studies), are at best limited to just a couple of measured saturation history cases. Recent work by Benson et al. (2015) indicated that the situation has hardly improved in the last 25 years. Besides during venting, reversal of displacement also occurs when brine re-imbibes (displacement of non-wetting (= CO_2) by wetting fluid) into areas, vacated by the CO_2 during its redistribution within the aquifer. The entrapment, associated with hysteresis, also increases the interfacial area between the CO_2 and the brine. This leads to more rapid dissolution.

Venting as a remediation technique was studied in a simulations study by Esposito and Benson (2012). They considered the removal of as much as possible gaseous CO_2 from shallow (100 m deep) aquifers. These aquifers received various quantities (up to 50000 ton) of CO_2 through a faulty well. Depending on the shape of the CO_2 plume, horizontal or vertical wells were used. Injection of water was also considered. While this study demonstrated that CO_2 removal is possible, the effectivity of various remediation approaches was found to vary depending on the quantity of CO_2, and the permeability distribution in the aquifer. For this project, a static geological model of an actual unnamed aquifer was selected. Furthermore, venting of CO_2 works also as potential corrective measure to reduce the overpressure, typically around 10-20 % over the initial pressure, as shown by Neele et al., 2011.

After a description of the simulation approach, we first demonstrate the importance of including hysteretic properties in the simulation of venting procedures (Section 3). This is done by comparing the results of non-hysteretic prediction with hysteretic modelling. This is followed by a sensitivity analysis of the venting procedures, where parameters, such as permeability, injection rates and the pore volume will be varied. In Section 4, the hysteresis is further enhanced by the injection of large volumes of water. To avoid increases in the reservoir pressure, this injected brine is produced in the same aquifer. Again a sensitivity analysis is done with various water injection schemes and the cumulative CO_2 injection.

2 MATERIAL AND METHODS

The starting point of the current study was a non-hysteretic reservoir model. The non-hysteretic relative permeability-saturation curves (Figure 1) of the carbon dioxide and the brine were made hysteretic by applying the EHYSTER keyword (Eclipse reservoir simulation software), with an entrapped non-wetting fluid saturation of 0.1. This means that below a minimum CO_2 saturation (0.1 in this case), the gaseous phase is considered to be discontinuous and the relative permeability of the CO_2 phase goes to zero.

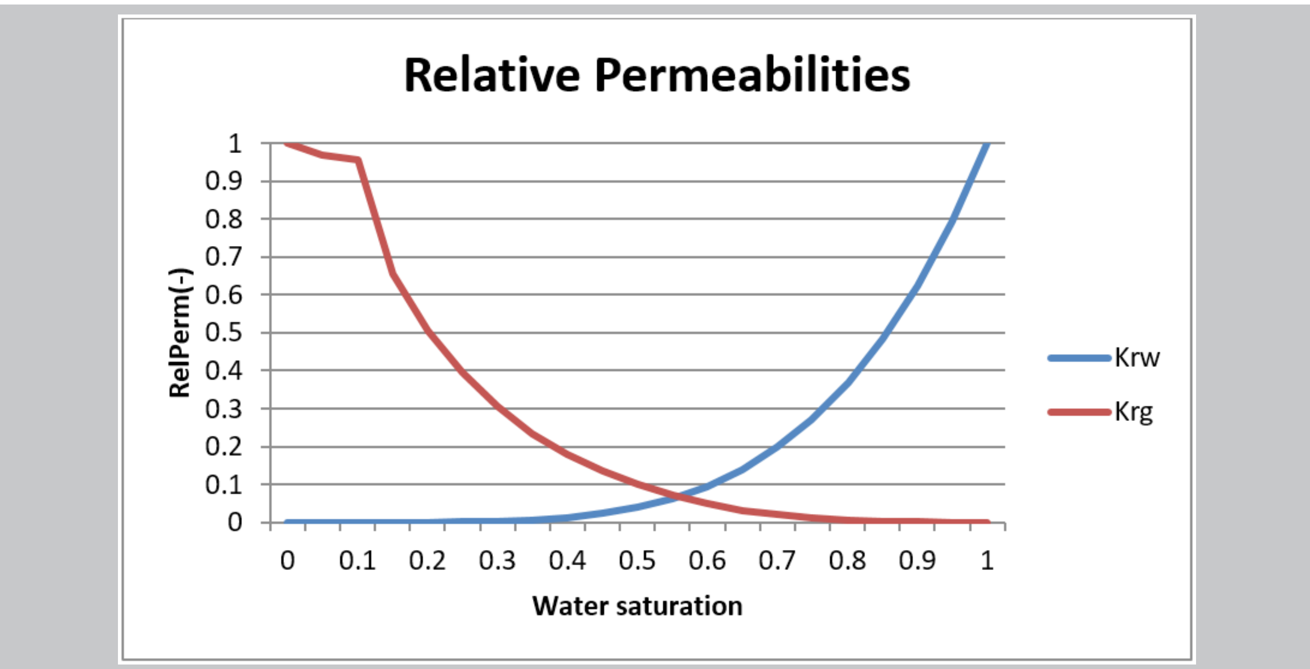

Figure 1 Original non-hysteretic relative permeability values, where the subscript w and g stand for water and brine, respectively.

Prior to further simulation, the aquifer underwent a cumulative injection of $3.2*10^{10}$ Sm^3 (58 Mt), between 2009 and 2018 (Figure 2). The post-injection saturation distribution and reservoir pressure are shown in Figure 3 and Figure 4, respectively.

With this model, a number of simulations were carried out. Back production of CO_2 as predicted by the reservoir model was compared with and without a hysteretic description. A sensitivity analysis was carried out concerning periods between the end of injection, and the actual back production. Further investigations involved 1) The impact of hysteresis on combined water injection and venting mitigation technique (Section 3). 2) Massive water injection was applied in an attempt to immobilize and/or push the CO_2 away from a possible faulty well (Section 4).

Simultaneous water injection and venting was simulated by introducing a seperate injector at the location of the CO_2 injector. For these scenario's only hysteretic predictions were made.

Figure 2 Injection profile (Red) for around 60 Mt CO_2 and bottom hole pressure (BHP) of the injector (green), as used as starting point for all scenarios.

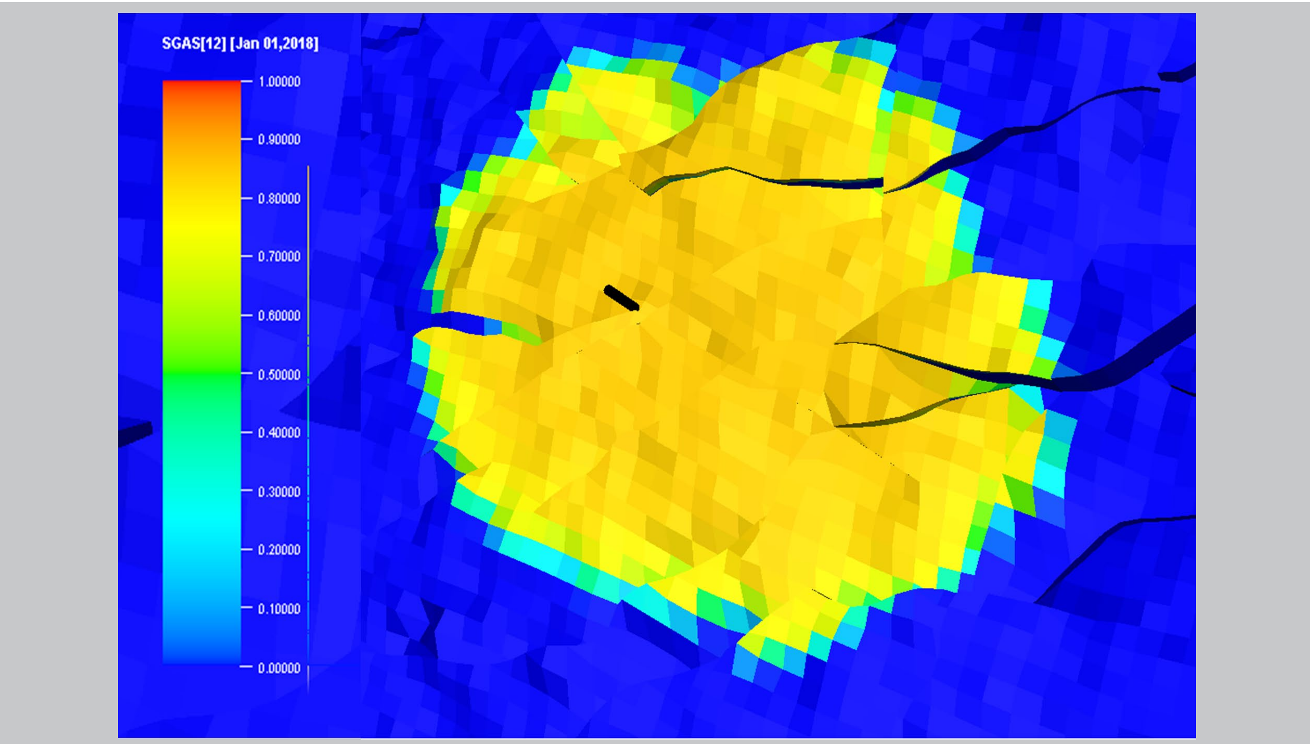

Figure 3 CO_2 saturation distribution around two injectors, at end of injection period. The size of the CO_2 plume is around 6.8 by 4.7 km.

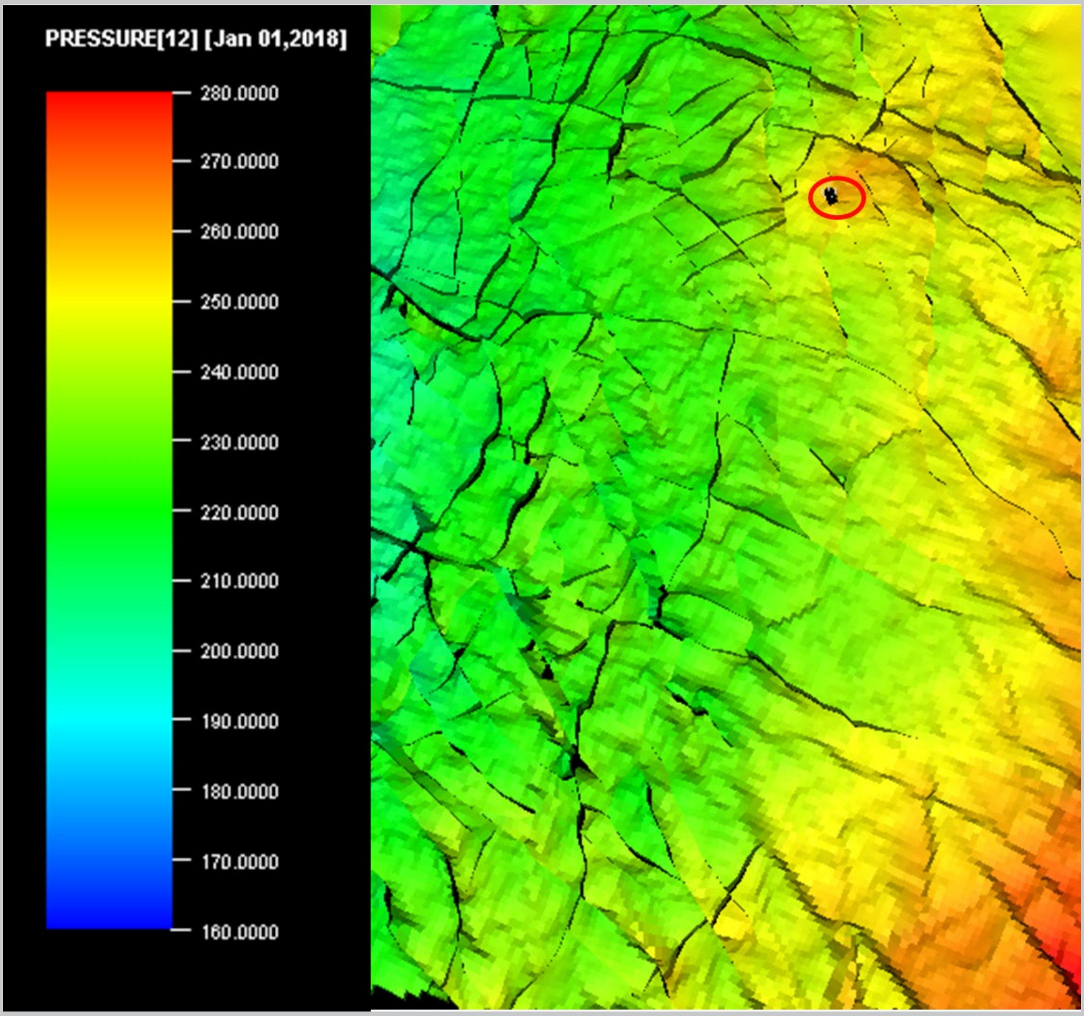

Figure 4 Constant pressure (around 240 bar) distribution at the end of injection, indicating good overall connectivity throughout the reservoir. The red circle indicates the position of the injector.

It should be noted that the reservoir simulator reports several predictions at selected times only. This means that figures in this report may show steps functions, which in reality should be smooth continuous lines.

Venting was initiated by changing the injector into a producer and applying a minimum bottom hole pressure (BHP) constraint to that producer. Simultaneous water injection and venting was simulated by introducing a separate injector with the same completion/ coordinates of the venting well, This injector was constrainted with an injection rate constraint. The earlier studies confirmed that the injection pressure did not exceed the maximum reservoir pressure. Figure 3 shows the impact of the many faults in the area on the migration of the injected CO_2. During the aformentioned feasibility study, each fault in the aquifer was evaluated. Although many of the faults show some connectivty issues, the overal pressure buildup was practically homogeneous, throughout the aquifer (Figure 4). The only exception was the higher pressure near the injector during injection.

3 THE IMPACT OF HYSTERESIS ON THE LONG-TERM EXTENT OF THE MIGRATION.

In the following, the role of hysteresis on the venting process will be demonstrated by comparing a hysteretic with a non-hysteretic prediction of several scenarios (Table 1). In addition, the impact of time between the end of injection and the unwanted flow is looked at. This is done by comparing 2190 days (6 years) of redistribution time with 11315 days (31 years), prior to the start of the CO_2 back production procedure.

Table 1 Overview of scenarios looking at the impact of post-injection redistribution time and hysteresis on the emission rates during venting.

Scenario	Redistribution time (years)	Permeability
2a	6	non-hysteretic
2b	6	hysteretic
3a	31	non-hysteretic
3b	31	hysteretic

Figure 5 and Figure 6 show the back production rates as a function of time as predicted by a non-hysteretic and hysteretic model, respectively. The hysteretic case shows both lower initial production rates (4.4 versus 5.6 MSm³/day) and ultimate back production (27 versus 48 % of the injected CO_2 ($3.2*10^{10}$ Sm³), lower, than in the non-hysteretic case. This is as expected as hysteresis allows for capillary entrapment of the CO_2 and also the differences (between hysteretic and non-hysteretic cases) in relative permeability at specific saturations.

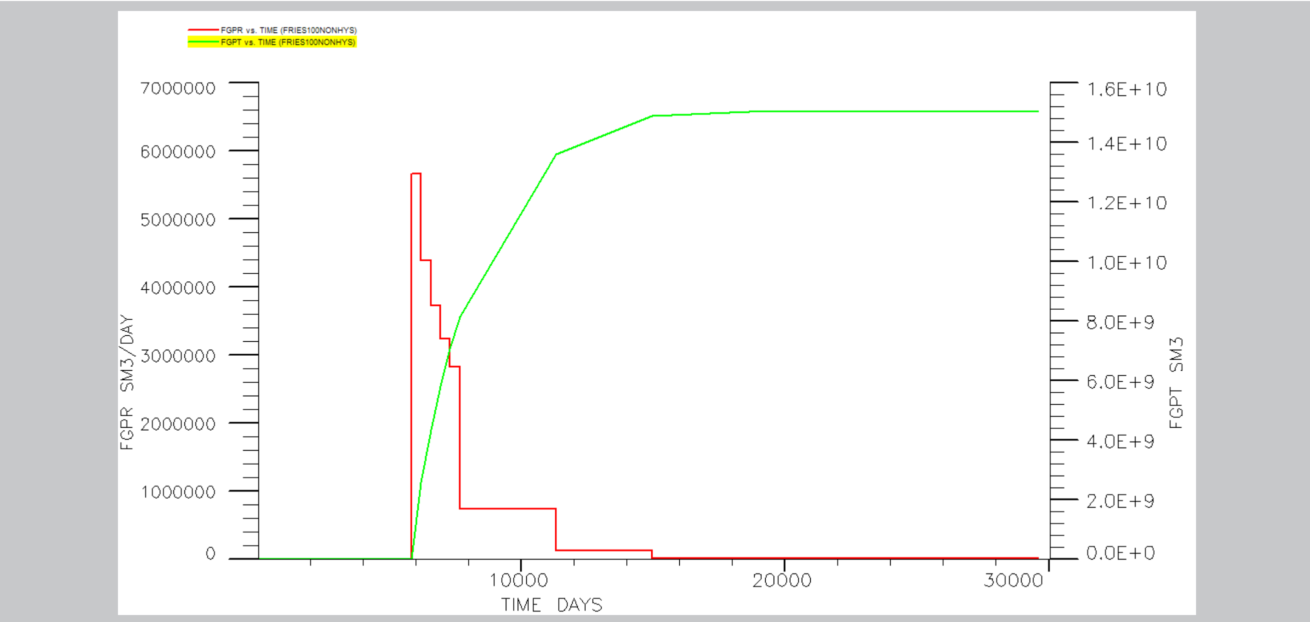

Figure 5 Venting rates (in red) and cumulative emission (in green) as a function of time for the non-hysteretic venting (scenario 2a), 2190 days or 6 years after the end of injection. It should be noted that the number of days on the x-axes include the time of injection.

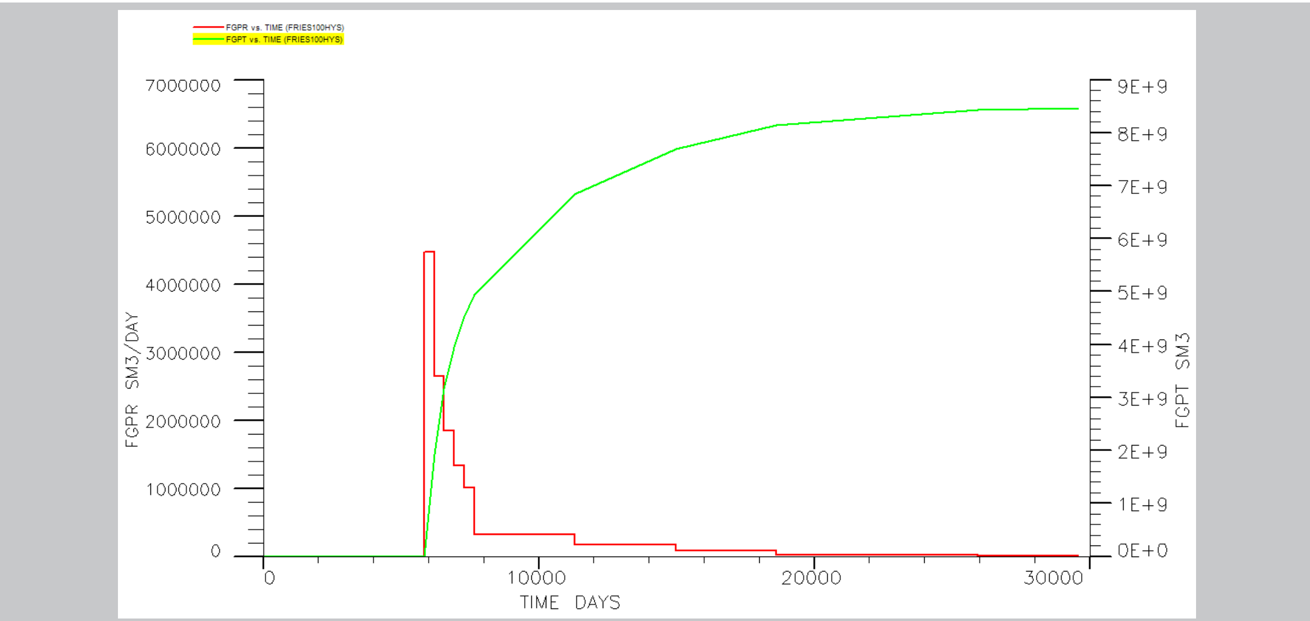

Figure 6 As Figure 5 but with hysteretic relative permeabilities (scenario 2b) for the CO_2 phase.

Figure 7 and Figure 8 show the venting rates, after the CO_2 was allowed to migrate for 11315 days (31 years) before the start of this venting.

Table 2 reveals that the process of hysteresis has a significant impact on emission rates during venting. As expected, the initial venting rate of the hysteretic case is lower than the corresponding rate for the non-hysteretic scenario, and drops faster with time. Unexpectedly, the hysteresis has a little bit more impact after 6 years of redistribution of the CO_2, then after 31 years. The saturation distribution after the venting during scenario 3b is shown in Figure 9. The faults in the reservoir are likely to have attributed to the no-uniform gas saturation distribution. It can be concluded that for an accurate prediction of the emission rates during venting, hysteresis should be included in the simulation.

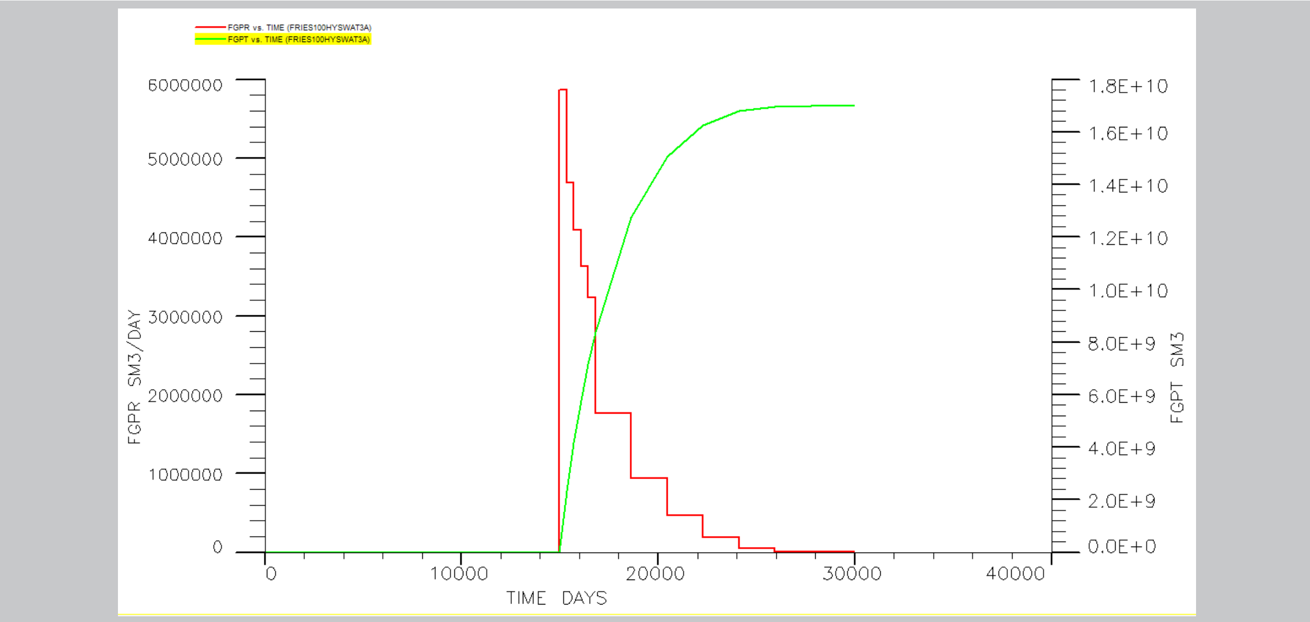

Figure 7 Back production 11315 days, or 31 years, after end of the injection (non-hysteretic simulation).

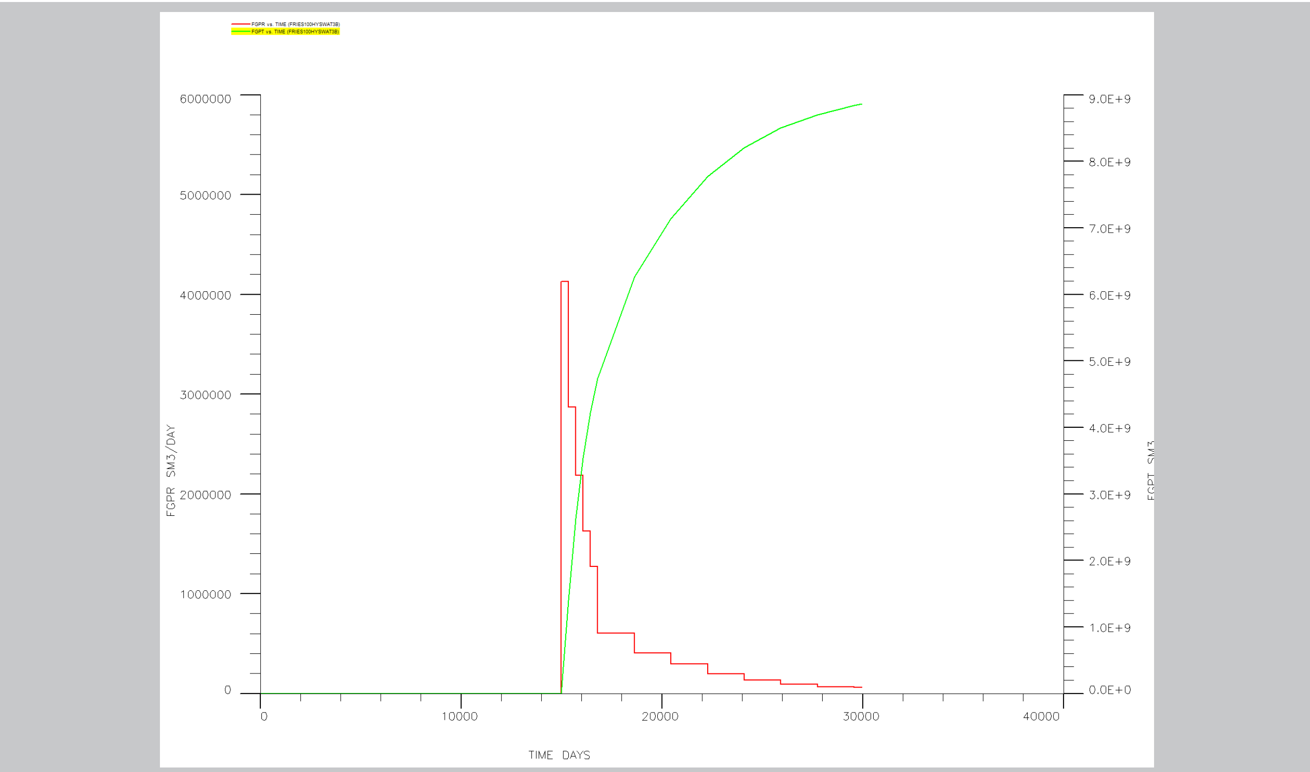

Figure 8 Back production 11315 days, or 31 years, after end of the injection (hysteretic).

Additional simulations showed that the emission rates increased with reducing the pore-volume (by a factor 2). This can be attributed to the higher saturations near the injector.

In addition, Table 2 shows that the pore volume and permeability adjustment have limited effect on the cumulative emission during venting. These can therefore not been seen as key factors. The percentages of back production reduce with lower amount of CO_2 in the aquifer. This can be attributed to more relative migration (extra space due to lower volume in same aquifer) and also more impact of hysteresis. This also explains why venting experiments in current aquifer storage pilots shows limited emissions. An example is the Frio test, where limited venting rates were reported after a small injection of 1.6 tonnes of CO_2 (Hovorka, 2006). The figures of the 7 last predictions in Table 2 can be found in the Appendix. These cases were run with the hysteretic mode, only.

Table 2 Overview of the cumulative emission for the various scenarios.

Scenario	Cumulative emission ($\cdot 10^9$ Sm³)	% of total injected CO_2
2a	15.5	48.0
2b	8.4	26.3
3a	17	53.0
3b	8.8	27.5
Multipv 0.5 compensated elsewhere	10	31
Multipermx 4	12.4	38.7
Multipermx 0.5	12.5	39.1
0.5 injection	2.16	13.1
0.25 injection	$3.4 \cdot 10^{-2}$	0.43
0.125 injection	$7.8 \cdot 10^{-4}$	0.20
0.0625 injection	0	0

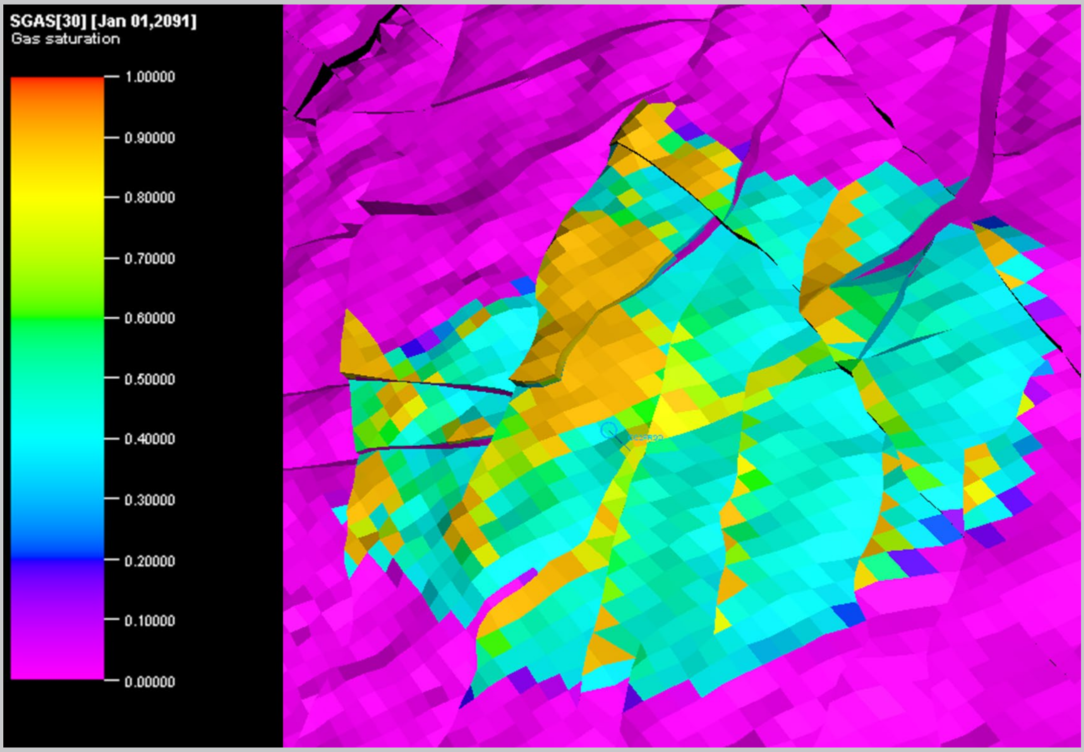

Figure 9 Non uniform CO_2 saturation profile after the venting of CO_2 (scenario 3b).

4 WATER INJECTION COMBINED WITH WATER PRODUCTION AT A LARGE DISTANCE.

In an effort to further enhance hysteresis, in the following simulations, large amounts of water will be injected. By itself this would lead to unwanted increase in the reservoir pressure. To avoid this, a water producer was installed outside the CO_2 plume (Figure 10). The production rate of this producer was set at 77000 Sm³/d for a duration of 13 years. This produced water was re-injected in the injection well. This means that the average reservoir pressure is constant during this operation. After the water production/ reinjection was halted, the previously closed injector was opened completely. The 7 years between the end of injection and the start of back production represents the required time for detection of the leakage and also to allow some time for migration of the injected CO_2.

Four scenarios were tested:

- Scenario 4a) 12 years of water injection, starting 2555 days or 7 years after the end of CO_2 injection, followed by continued CO_2 back production.
- Scenario 4b) Continuous simultaneous venting and water injection in at same injector location, starting 7 years after the end of the injection scheme. This scenario was repeated 3 times (scenario f, g, and h) with increasing reduced amounts of stored CO_2.

- Scenario 4c) Simultaneous water injection/production period, starting 2190 days or 7 years after the end of the CO_2 injection, and continuing for a total of 4745 days or 13 years. Continued venting of CO_2 (without water injection) starts 1825 days after start water injection.
- Scenario 4d) as for 4c but with a longer period (7665 days, or 21 years) of simultaneous production and injection of water.
- Examples of the injection/production procedures of scenario 4a and 4b are shown in Figure 11 and Figure 13, respectively.

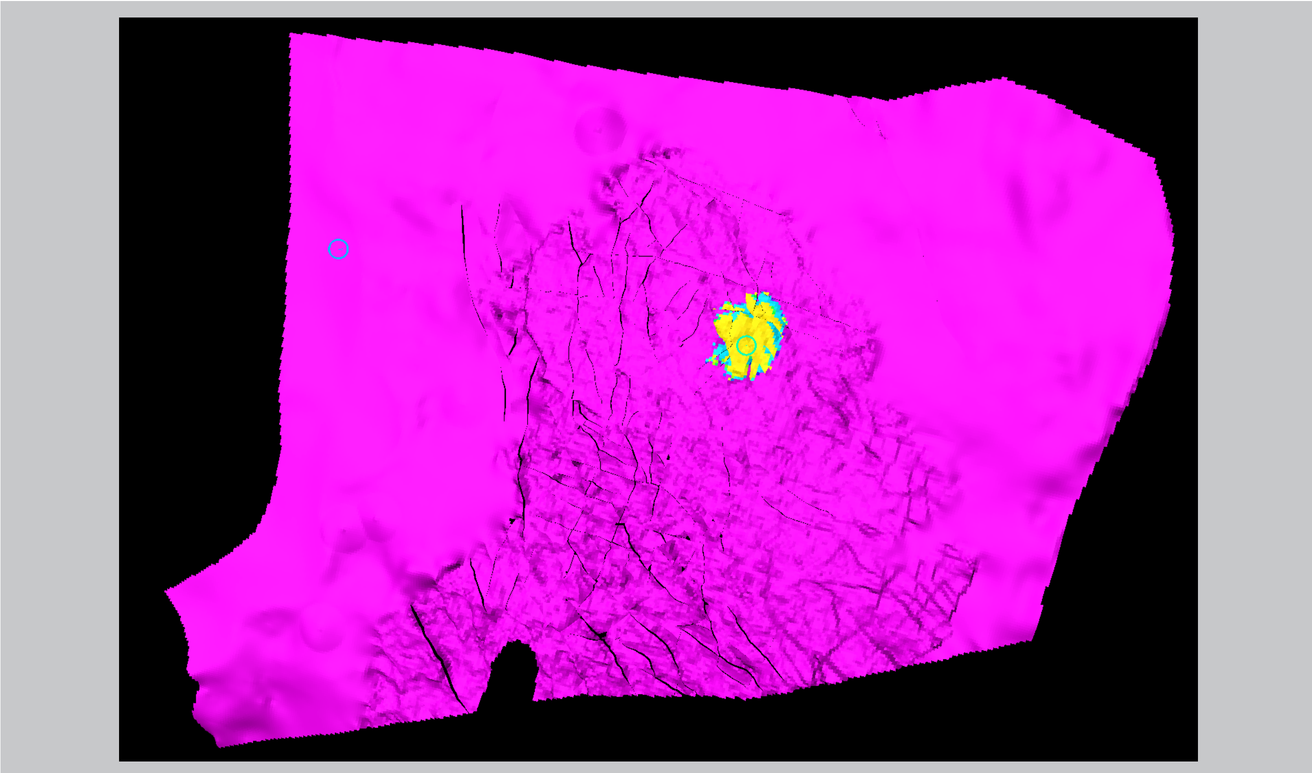

Figure 10 Position of water production well (to the left, at a distance of 33600 m), relative to that of the injection/venting wells (to the right) as shown in a gas saturation plot of the aquifer.

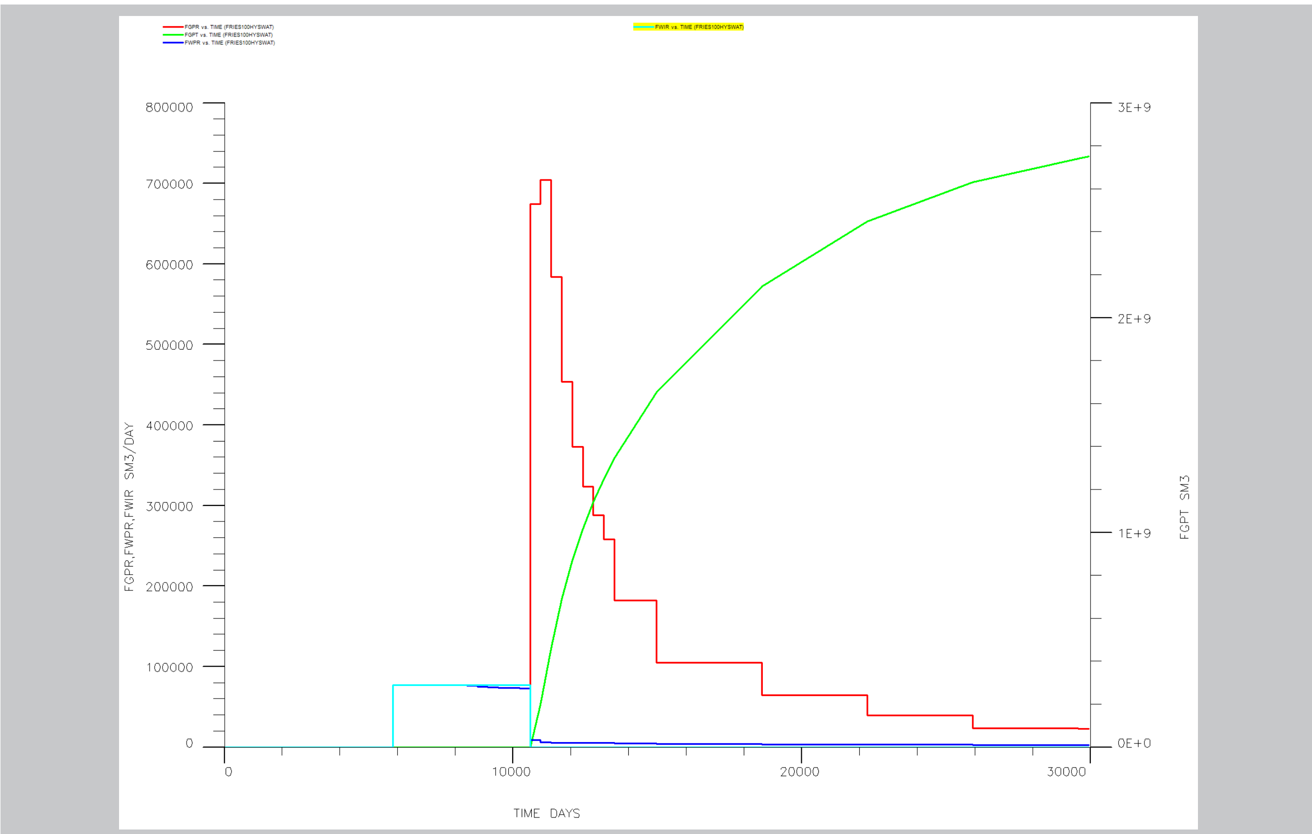

Figure 11 The produced/injected water rates (dark and light blue, respectively), the vented CO_2 rate (red) and cumulative amount of reproduced CO_2 (green) of scenario 4a.

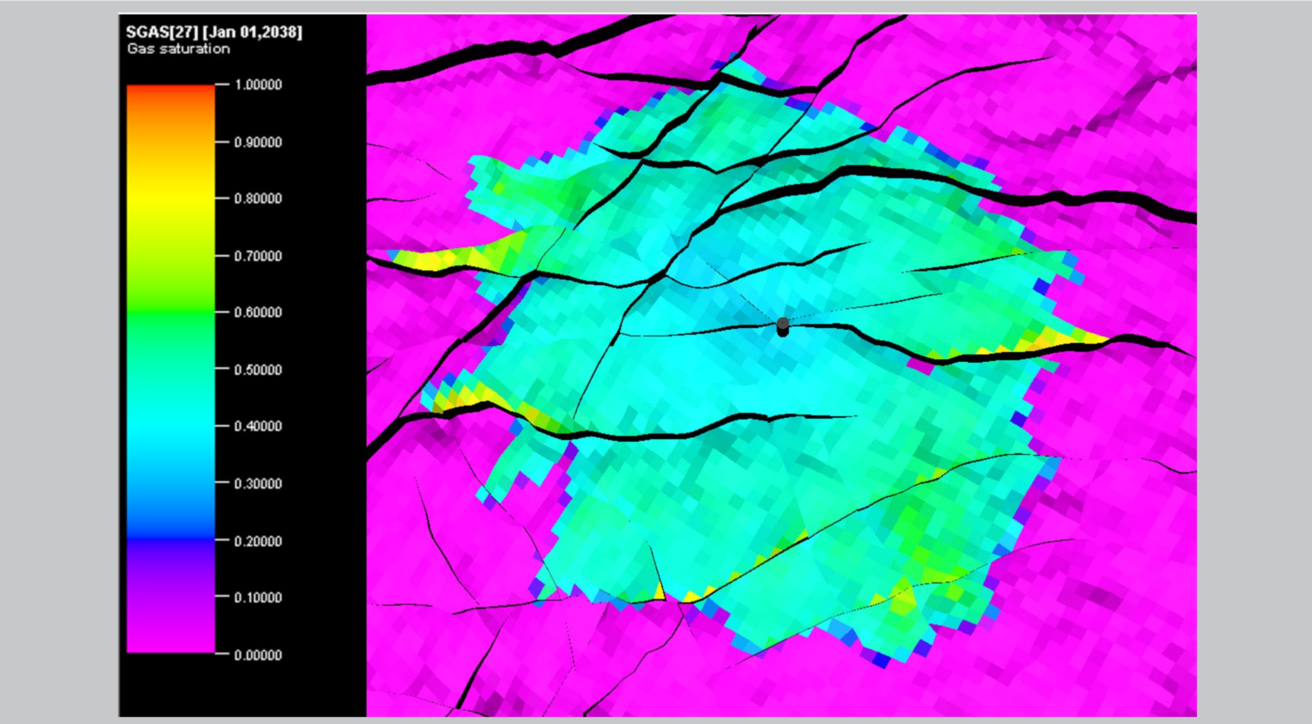

Figure 12 Final CO_2 saturation distribution (size around 8.2 by 7.2 km) after water injection (scenario 4a). The green colour indicates saturation values around 0.4 to 0.5. More yellow stands for higher saturations, with red indicating a saturation of 1.0.

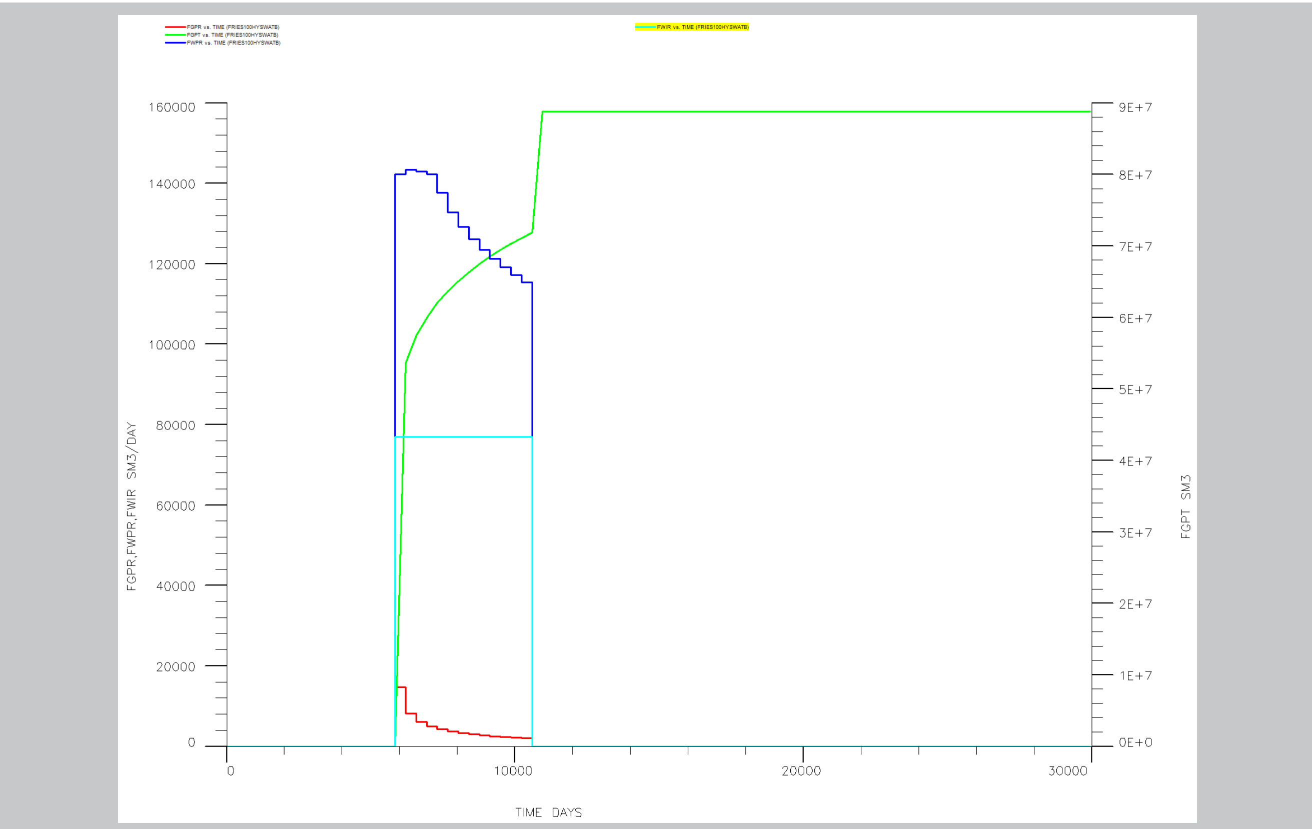

Figure 13 Continuous simultaneous venting (red is rate and green is cumulative) and water injection/production (light and dark blue, respectively) in same injection location, starting 7 years after the end of the injection scheme (scenario 4b).

Figure 11 shows that venting of CO_2 cannot be prevented by this approach. This means that the anticipated hysteresis (entrapment) has not lead to complete immobilization of the CO_2 phase, Figure 12 indicates indeed gas saturation levels in the range of 0.4 to 0.5. This is above the maximum entrapment saturation of 0.1. The CO_2 is still mobile.

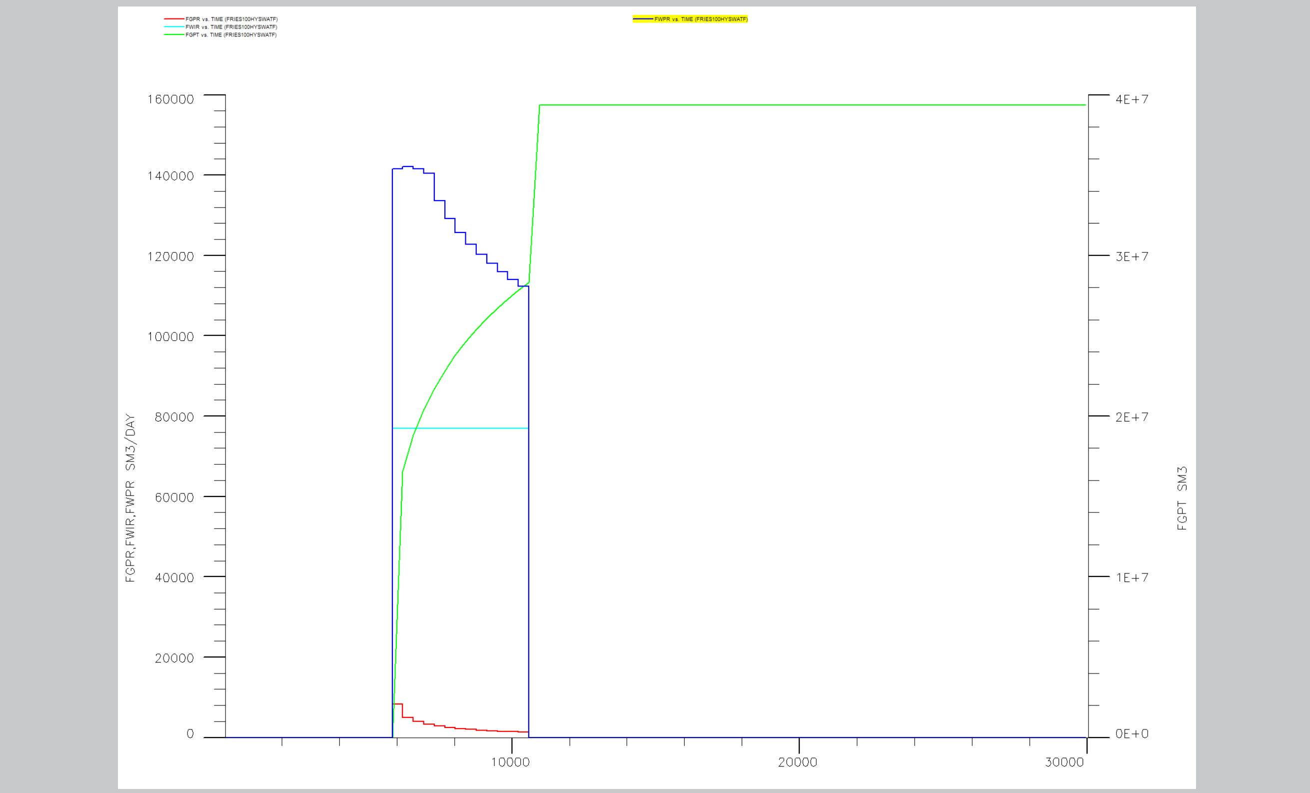

Figure 14 As scenario 4b, but with less CO_2 injection (2.26*10[10] Sm³).

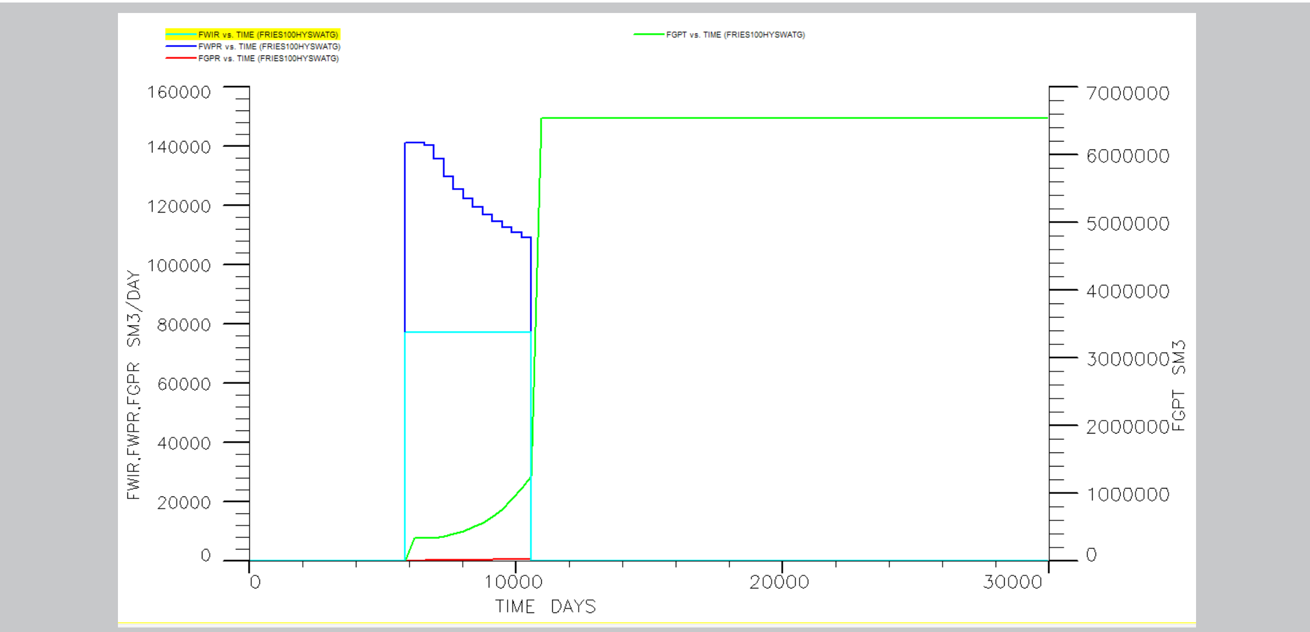

Figure 15 As scenario 4b, but with less CO_2 injection (1.15*10[10] Sm³).

Scenario 4a assumes that one has the luxury of having prior knowledge on a future issue with the integrity of the storage capacity leak. The following scenario starts the water injection at the time of the first emissions of CO_2. This second set of simulation was conducted with hysteretic relative permeability, only.

Figure 13 shows the CO_2 back production rates as a function of time after the venting was started at the start of the water production and re-injection. Unfortunately, the simultaneous venting and injection of water again lead to some emission of CO_2. Figure 17 shows areas with high CO_2 saturation along areas which are more water rich. The amount of emission, however, is much lower than for scenario 4a.

Scenario 4b was repeated several times with reducing amount of stored CO_2. Figure 14, Figure 15 and Figure 16 show the emission of CO_2 decrease with the amount of CO_2, which is stored. In Figure 16, the water injection almost complexly eliminates the emissions.

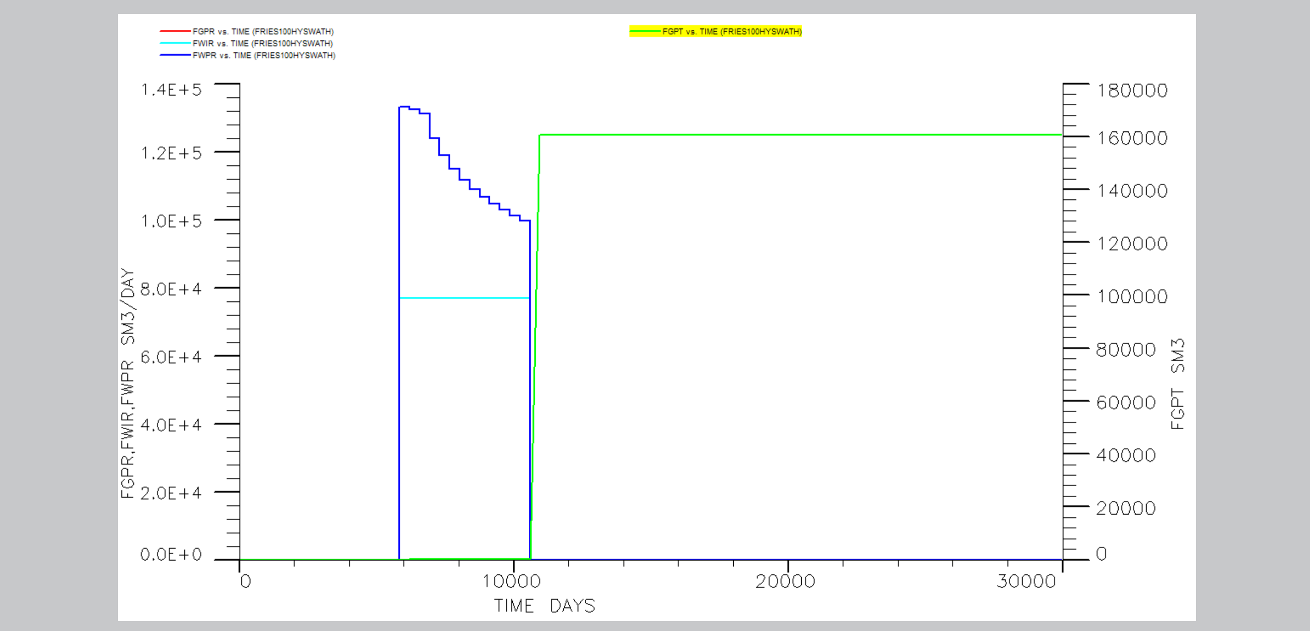

Figure 16 As scenario 4B, but with less CO_2 injection ($9.8*10^8$ Sm^3)

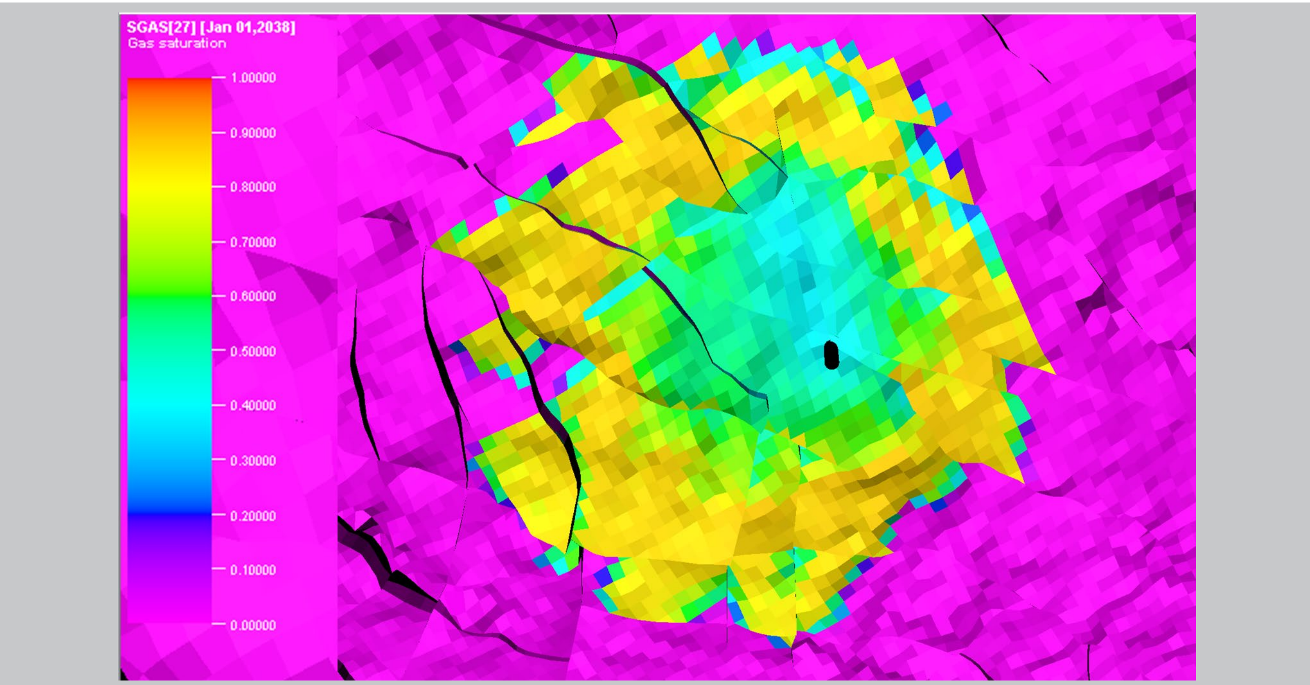

Figure 17 High CO_2 saturation (0.8-0.9) (in red) and lower (0.4-0.5) CO_2 saturation (green/yellow) distribution, after simultaneous venting and massive water injection (scenario 4b).

In simulations of scenario 4c, the water recirculation was continued for just 6 years after the CO_2 back production started. This limited period of the water injection clearly lead to a second peak in venting rates (Figure 18).

The second peak in venting rates (Figure 18) can be avoided when the period of production/injection of water is extended to 4745 days or 13 years (Figure 19, scenario 4d). In this scenario, the emission of CO_2 stops together with the injection of brine. This can be attributed to the sudden drop in pressure at the site of the injector below the pressure constraint of the venting well.

Comparing Table 2 and Table 3 reveals that water injection is far more efficient in reducing emission rates during venting then hysteresis by itself. The results in Table 3 also show that simultaneous water injection with the venting is more efficient as water injection prior to the venting procedure. That indicates that injection of water to displace the CO_2 from the venting injector is more efficient than relying on immobilizing the CO_2 phase by capillary entrapment (part of the hysteresis process).

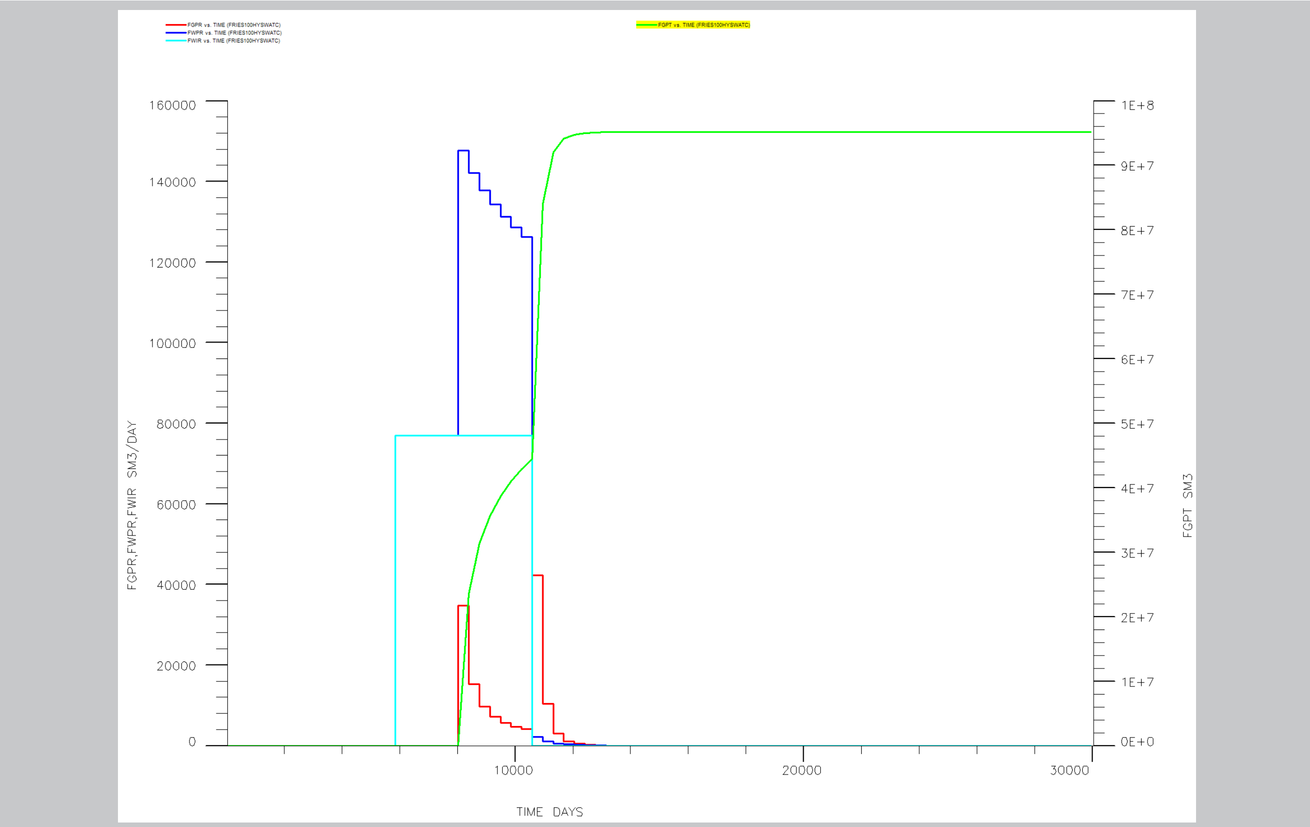

Figure 18 Leakage rates (red) as a function of time in a situation where the initial leak starts 6 years (2091 days) after the massive water production and injection (blue) has started. Furthermore this water production/injection continues another 7 years (scenario 4c).

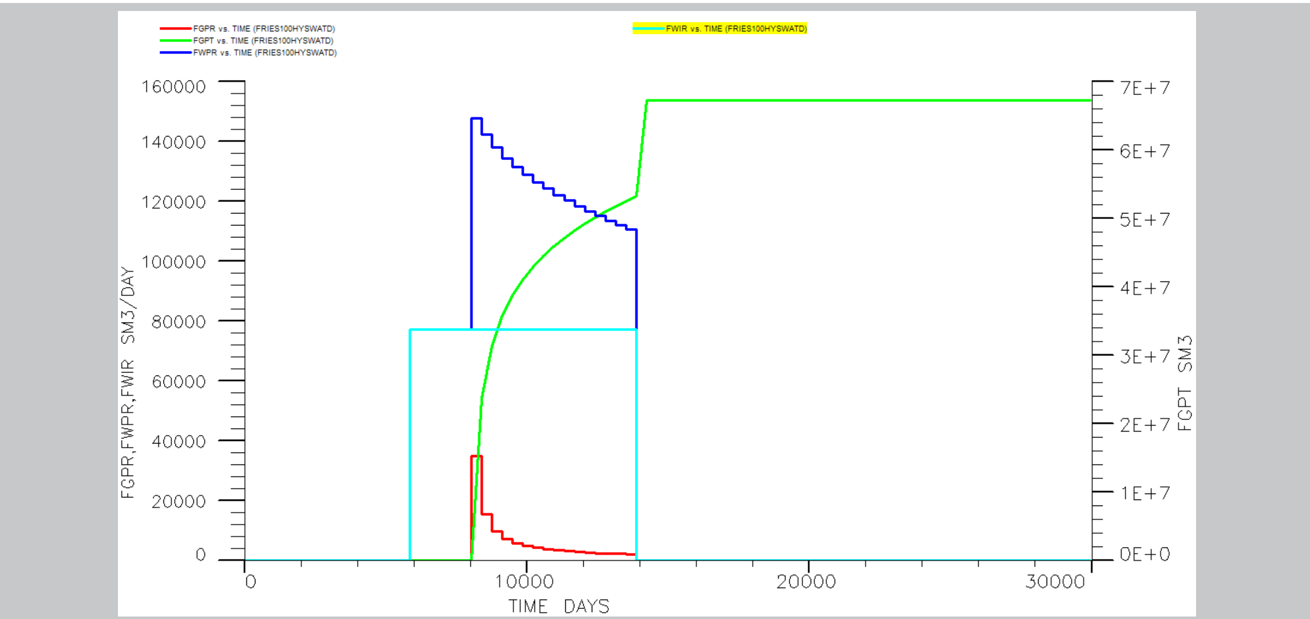

Figure 19 Venting rates (red) as a function of time in a situation where the initial leak starts 2190 days or 6 years after the massive water production and injection (blue) has started. Furthermore this production/injection of water continues another 4745 days (scenario 4d).

Table 3 Overview of the cumulative emission for the scenarios 4a, 4b, 4c 4d, 4e, 4f, 4g and 4h.

Scenario	Cumulative emission ($\cdot 10^7$ Sm^3)	% of total injected CO_2
4a	275	8.6
4b	8.85	0.28
4c	9.51	0.30
4d	6.77	0.21
4f	3.95	0.17
4g	0.658	0.057
4h	0.16	0.016

5 CONCLUSIONS

Although hysteresis and the associated entrapment of CO_2 somewhat suppresses the amount of emitted CO_2 during unintended flow of CO_2 towards the surface, they generally cannot stop the unwanted flow of CO_2 from large injection sites. The amount of vented CO_2 decreases with the time-span between the end of CO_2 injection and opening of the injector. This is due to the migration and spreading of CO_2 within the aquifer. This spreading means that more CO_2 is captured by the brine imbibition after the well is opened and it is also more likely that this imbibing process may disconnect the otherwise continuous CO_2 phase

The relative permeability's during the imbibition cycle were estimated using a software algorithm. Using actual measured hysteretic relative permeability's may lead to more or less favorable results of emissions during venting as the actual entrapment of CO_2 may be affected. It should also be noted that hysteresis is a natural process, and that non-hysteretic conditions only occur within reservoir models. The results show that the venting emissions are overestimated when the hysteresis process is ignored.

Results of back production should be independent of the size of the aquifer, as the volume of the compressed water is far greater than the volume of CO_2. The permeability did not have a large effect on the amount of back production. The amount of injected CO_2 was by far the most important parameter in determining the amount of back productions.

With hysteresis being a natural process and the limited impact of permeability, pore-volume (all within the range seen in actual aquifer storage projects) on the predicted emission rates during venting, the only remaining key factor is the amount of injected CO_2.

It is also complicated to stop the back production of CO_2 in an opened well by the injection of brine at the same reservoir location, but emission rates of CO_2 can be strongly reduced. Again the fraction of stored CO_2, which is emitted, depends on the amount of CO_2 stored. At low values for the stored CO_2, simultaneous injection of water at the site of the venting came very close (less than 1 % of the stored CO_2) to a complete elimination of the unwanted CO_2 flow.

It should be noted that this report deals with rather extreme leakage scenarios including the very large potential flow caused by a completely opened injector in combination with an aquifer in which a massive amount of CO_2 was injected (for comparison 5 times as much as currently in the Sleipner field).

Although the injection of up to 3.65 105 m^3 of brine was unable to entrap all this CO_2. The process of diverting the CO_2 away from the injector was far more efficient in eliminating the CO_2 emissions during the venting procedure.

Combining venting and water injection as a corrective measurement may therefore be useful in situations where reducing the reservoir pressure is required but significant venting rates should be avoided. Examples could be urban settings. Injection of water to displace the CO_2 away from potential leak may also be useful. When CO_2 is leaking though a faulty injector, the water injection near the perforations will also reduce the emissions.

References

Benson, S.M. Pini, R., Reynolds, S.V.C., Niu, B., Calvo, R. and Niemi, A. (2015). Relative permeability for multiphase flow in CO_2 storage reservoirs. Part II Resolving fundamental issues and filling data gaps. Global CCS Institute Report (GLOBALCCSINSTITUTE.COM).

Corey, A.T. (1994). Mechanics of immiscible fluids in porous media. Water Resources Publications, Highlands Ranch, CO, USA, 252 pp.

Doughty, C. (2007) Modeling geologic storage of carbon dioxide: Comparison of non-hysteretic and hysteretic characteristic curves.48: 1768–1781

Esposito, A. and S.M. Benson (2012). Evaluation and development of options for remediation of CO_2 leakage into groundwater aquifers from geologic carbon storage. International Journal of Greenhouse Gas Control 7 (2012) 62–73

Hovarka, S.D. (2006). Frio brine storage experiment –lessons learned. GCCC Digital Publication Series #06-13.

Lenhard, R.J and Parker, J.C (1987) A model for hysteretic constitutive relations governing multiphase flow: 2. Permeability-saturation relations. Water Resources research 23; 2197-2206.

Neele, F., Nepvue, M., Hofstee, C., and W. Meidertsma (2011). CO_2 storage capacity assessment methodology. TNO-report: TNO-060-UT-2011-00810

Oak, M.J. (1990). Three-phase relative permeability of water-wet Berea. In: Seventh Symposium on Enhanced Oil Recovery, Paper SPE/Doe 20183. Tulsa, OK, April 22-25

Parker, J.C and Lenhard, R.J. (1987). A model for hysteretic constitutive relations governing multiphase flow: 1. saturations-pressures relations. Water Resources Research 23; 2187-2196.

Juanes, R., E. J. Spiteri, F. M. Orr Jr., and M. J. Blunt (2006). Impact of relative permeability hysteresis on geological CO_2 storage, Water Resour. Res., 42, W12418, doi:10.1029/2005WR004806.

APPENDIX

In this appendix, several additional simulations will be discussed, such as a sensitivity analysis of the venting procedure as described in Chapter 3.

The first simulation concerns a reduction of the pore volume in half the aquifer (around the injector) by a factor 0.5. To compensate for this reduction, the pore volume in the rest of the aquifer was multiplied by a factor 2, so that the total pore volume of the aquifer remained the same. This is to avoid any issues with the reservoir pressure. Figure A.1 shows that the back production is still high and close to the earlier hysteretic models.

Although, as expected, the initial back production rates are higher for the high permeability than the low permeability, the cumulative back production quantities are very similar.

In the following scenarios, an analysis will be conducted in which the quantity of CO_2 injection is systematically reduced (the following prediction using half the previous amount, until the back production stops).

After $2*10^9$ Sm^3 of injection, no back production was predicted (Figure A.7). Further reduction of the injection was therefore not conducted. The results of all scenarios in this Appendix are summarized in Table 2.

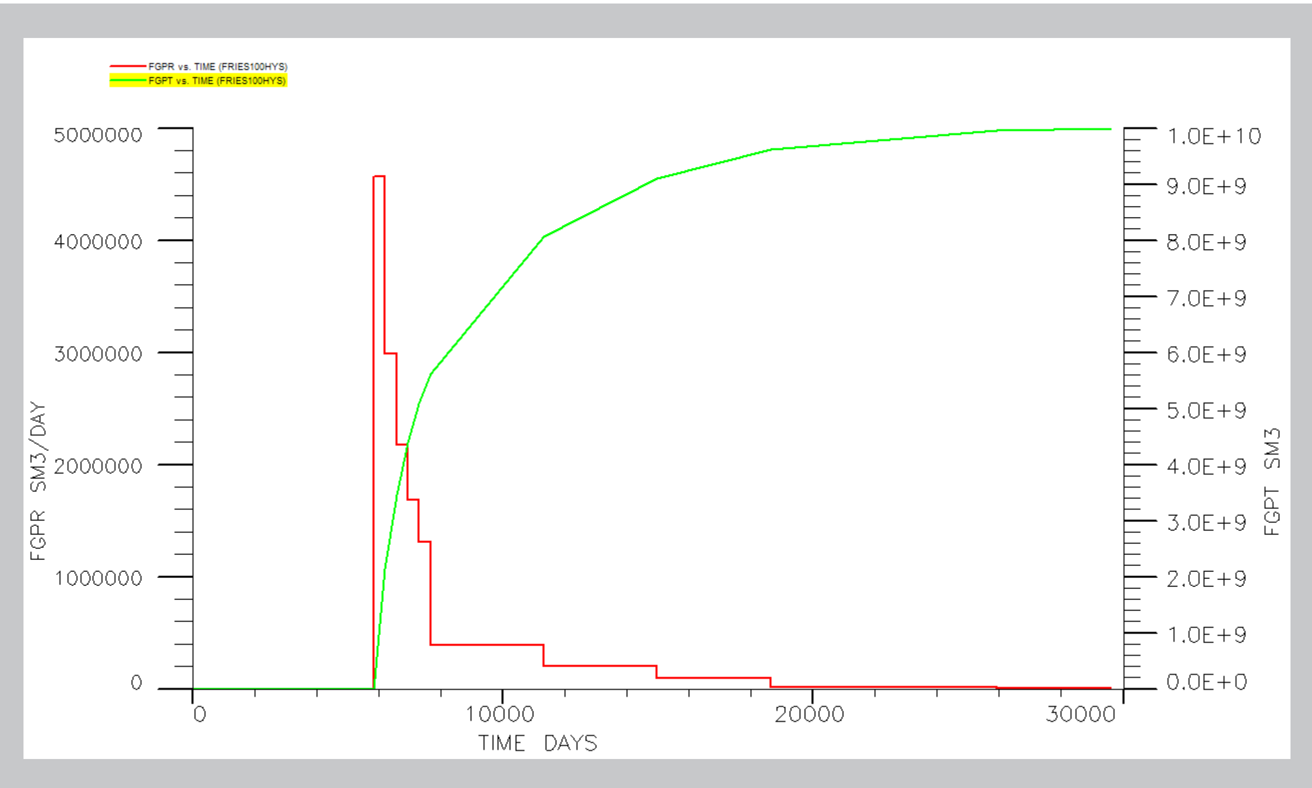

Figure A.1. The back-production rate and cumulative production for a simulation with pore volume multiplier of 0.5 around the injector.

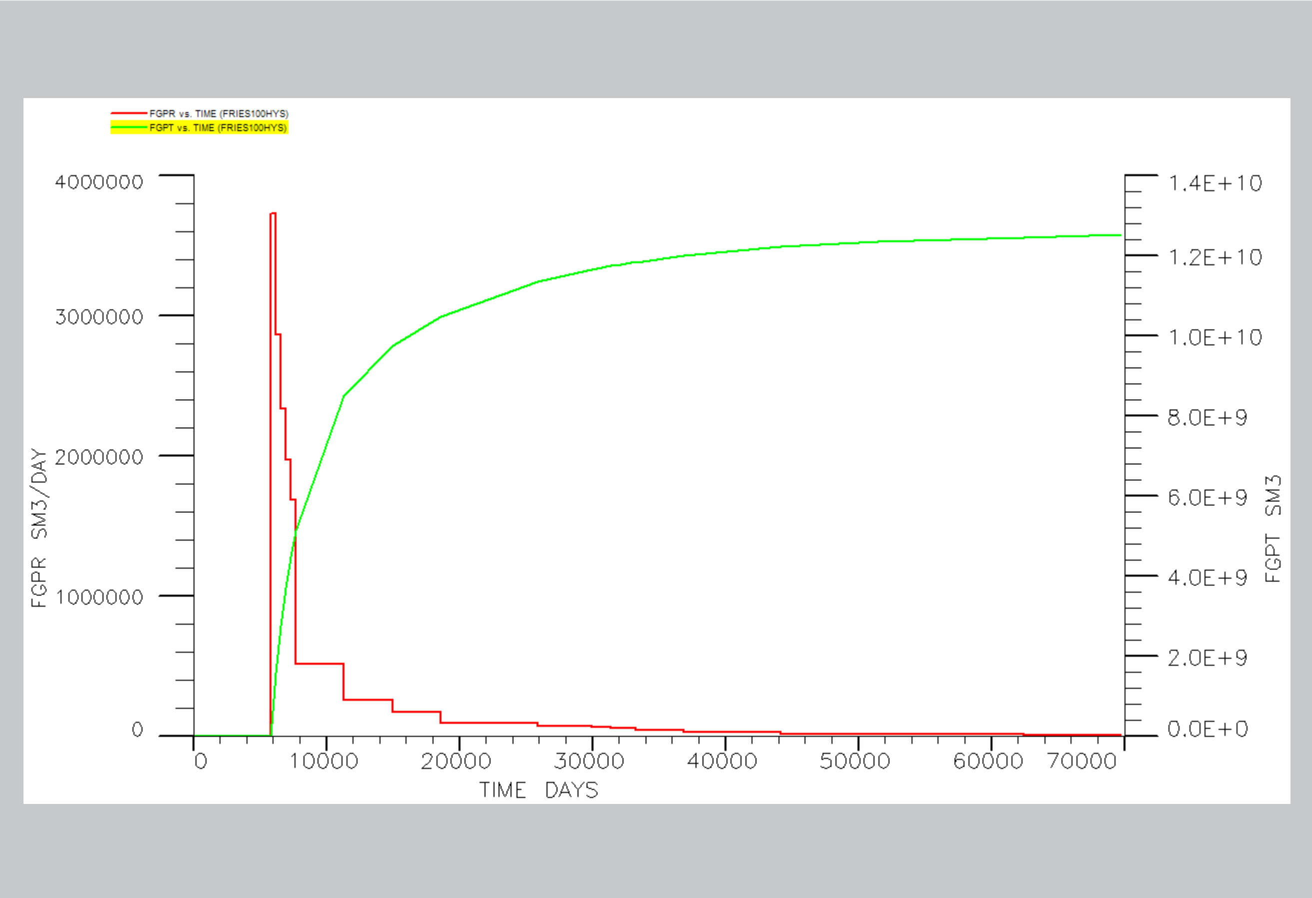

Figure A.2. The back-production rate and cumulative production for a simulation with permx multiplier of 4 on the horizontal permeability.

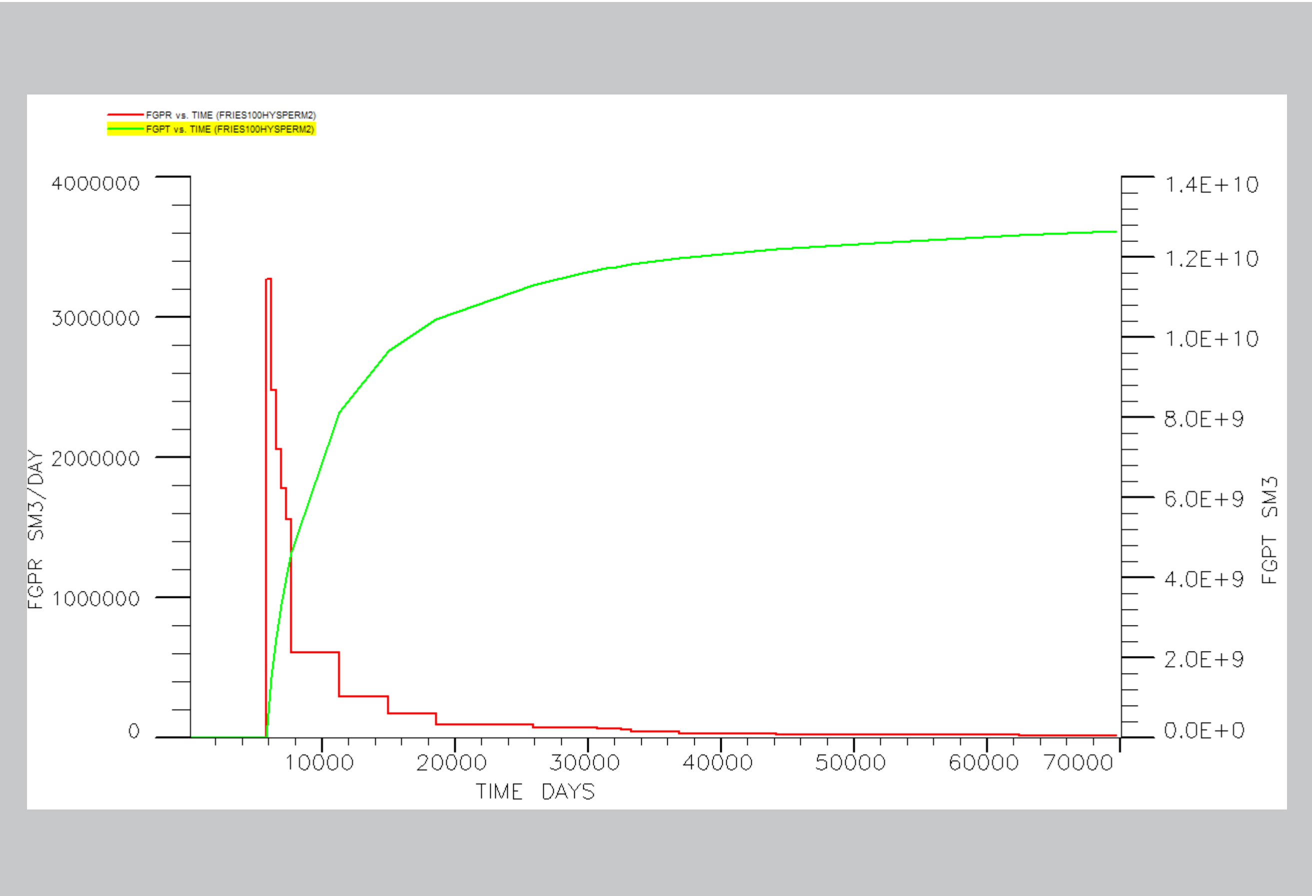

Figure A.3. As Fig. A.2, but with a global multiplier of 0.5 on the horizontal permeability .

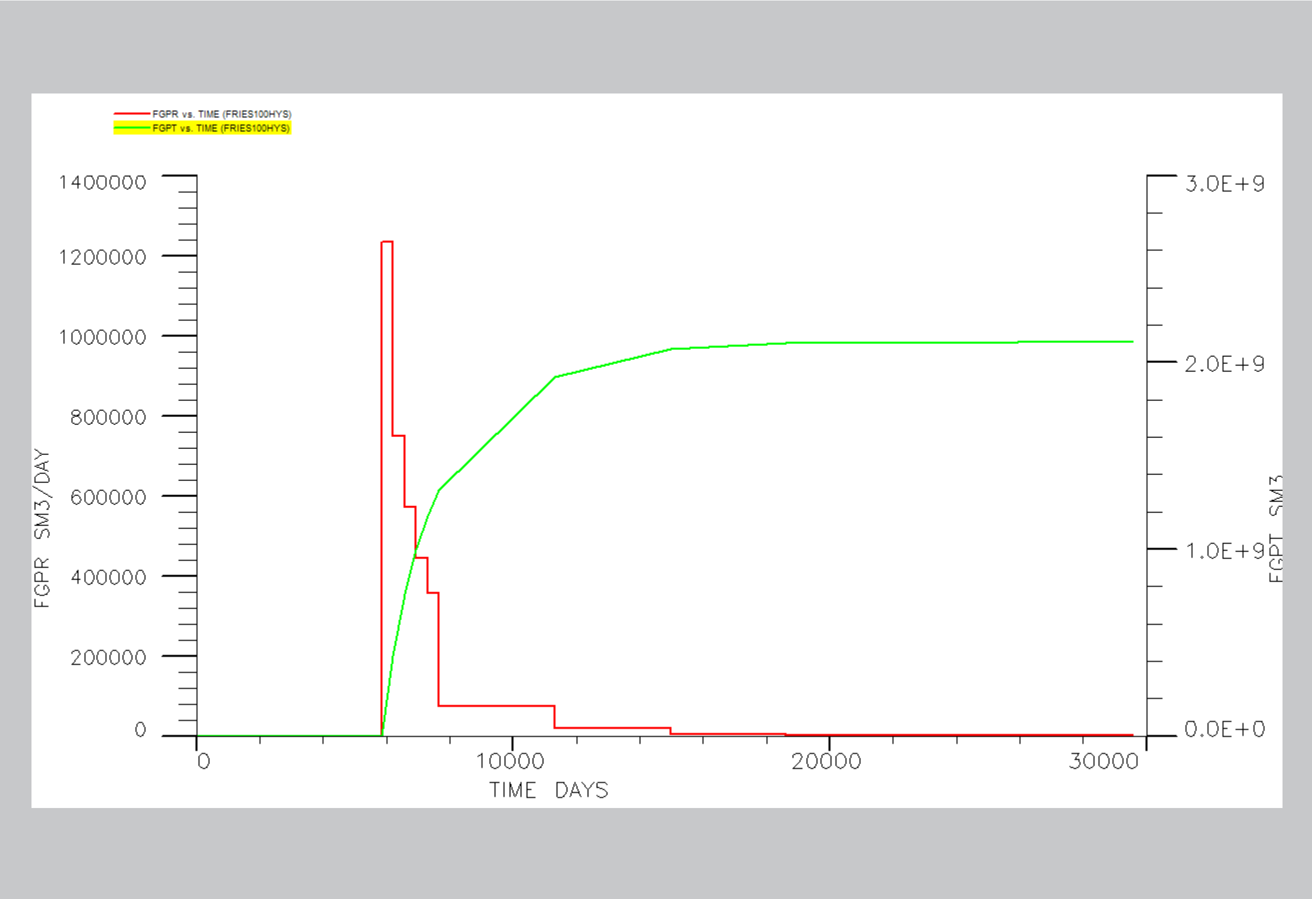

Figure A.4. Venting rates and cumulative back production after an injection of 16*10⁹ Sm³ of CO_2 (half than that in Chapter 3).

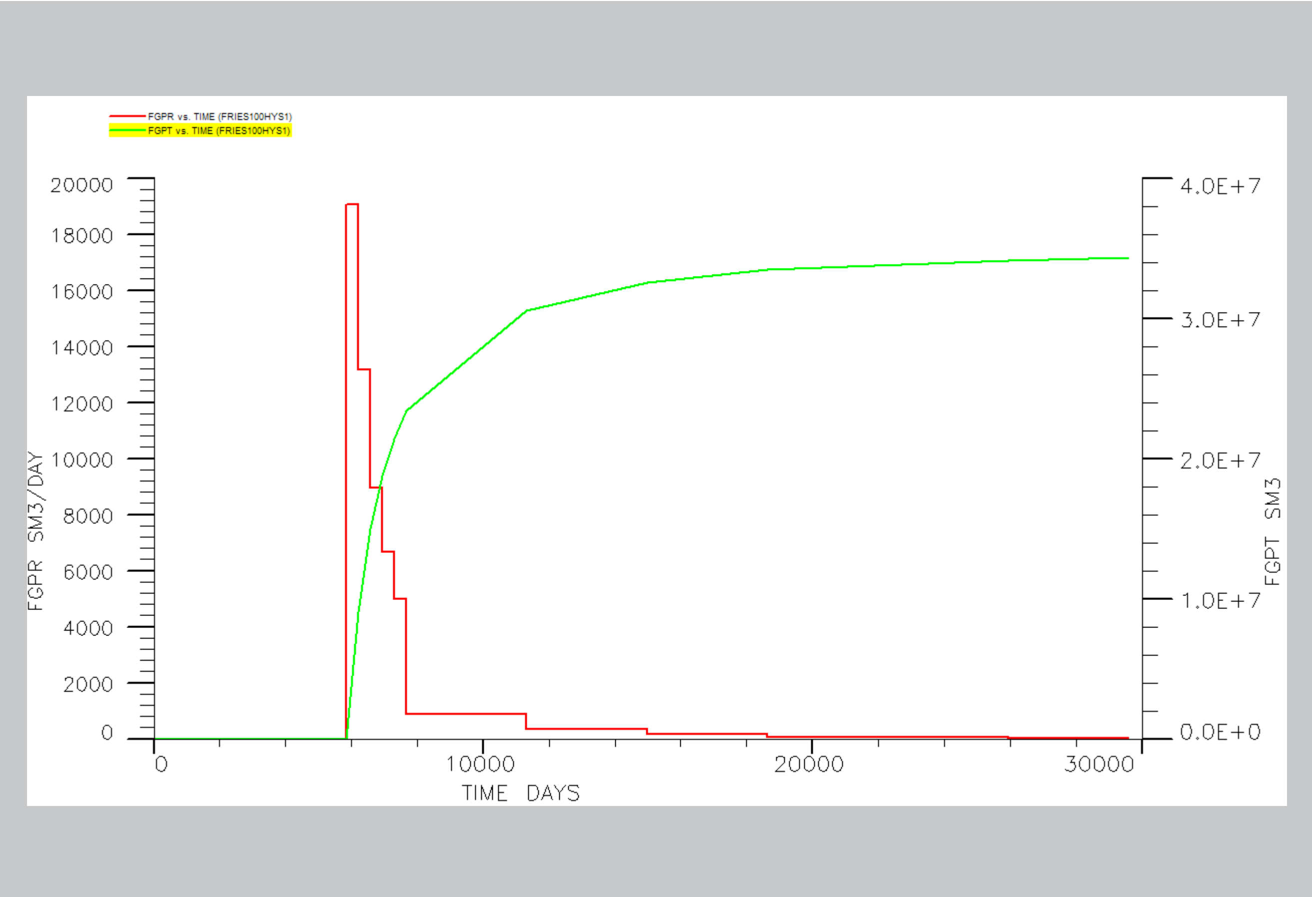

Figure A.5. As Fig A.4, but after 8*10⁹ Sm³ Mton of CO_2 injection.

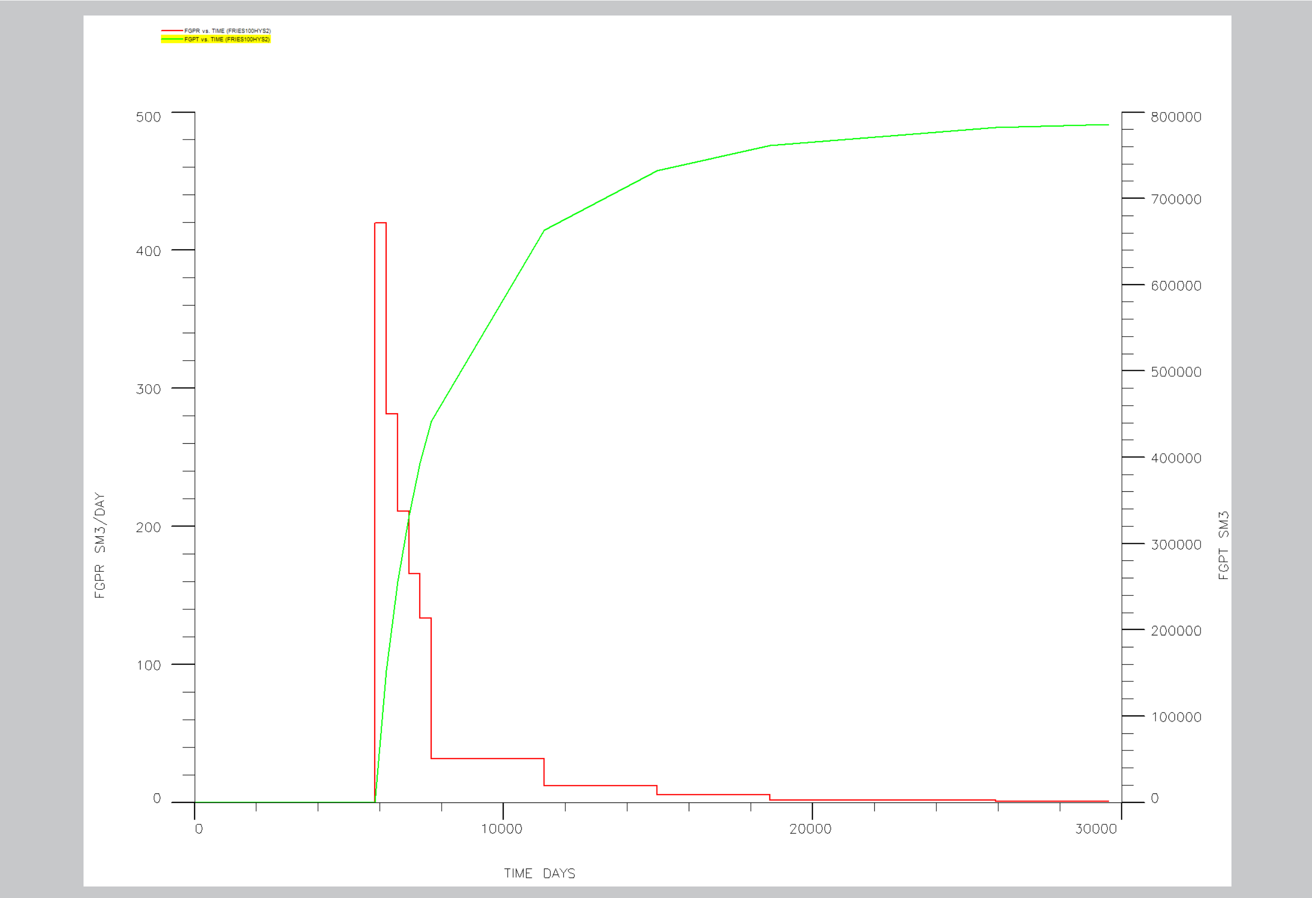

Figure A.6. As previous figure, but with half the cumulative injection (4*10^9 Sm^3).

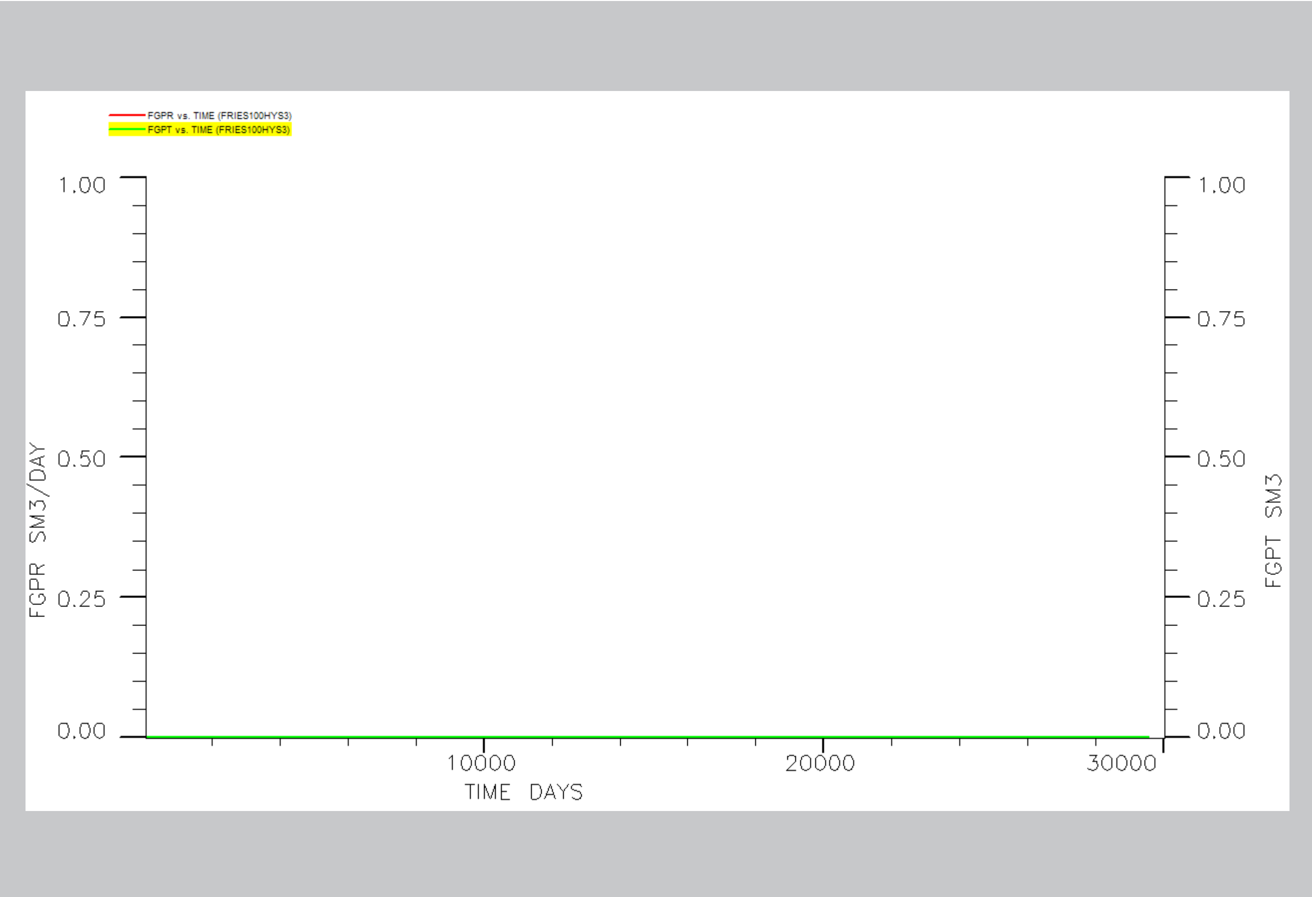

Figure A.7. As previous Figure, but with 2*10^9 Sm^3 injection.

Chapter VIII

CO_2 back-production at the Ketzin and K12-B sites

Cornelia Schmidt-Hattenberger[1], Bernd Wiese[1], Axel Liebscher[1], Fabian Möller[1],
Sevket Durucan[2], Anna Korre[2], Rajesh Govindan[2], Guangyao Si[2], Cor Hofstee[3]
[1] GFZ, Germany
[2] Imperial College, UK
[3] TNO, The Netherlands

SUMMARY

The report summarizes the studies regarding a "Feasibility test and numerical modelling of CO_2 back-production as remediation measure to reduce reservoir pressure", conducted at the Ketzin CO_2 pilot site, Germany. The report represents a description of the technical operation as well as results of numerical simulations of the pressure evolution and produced CO_2/brine volumes. Conclusions on the deployment of this type of pressure management techniques as corrective measures are drawn. Results from the Ketzin pilot study are compared with those of the K12-B gas field (Dutch North sea sector), a real-production case study where two back-production periods have been investigated.

1 INTRODUCTION

CO_2 migration and leakage through faults, wellbores and non-sealing cap rock have been studied in various simulations by several authors (see for example Celia et al., 2005; Nordbotten et al., 2005; Pruess, 2006; Pruess, 2008; Yamamoto et al., 2009; Birkholzer et al., 2009). Mitigation and remedial measures of these potential undesired migration/leakage scenarios are mainly associated with operational activities, some of which could be implemented immediately, whereas others require more time and technical effort (Manceau et al., 2014).

During regular injection operation, a temporary cease or reduction of injected CO_2 is the most immediate remedial action that can be implemented if a leakage is detected. Reducing the amount of injected gas will lower the rate of pressure increase as potential driving factor causing the undesired migration of CO_2.

In the post-injection phase, a back-production process of formerly injected CO_2 may provide a suitable technique to (i) mitigate undesired migration of CO_2 in the reservoir by inducing a pressure-gradient driven directed flow of CO_2 and (ii) manage the reservoir pressure. Furthermore, the production of CO_2 will also form an integral part of any temporary storage of CO_2 in the frame of a different carbon capture storage & utilisation (James, 2013) and/or power-to-gas concepts (Grond and Holstein, 2014). In CO_2 storage combined with enhanced hydrocarbon recovery CO_2 will be co-produced with the recovered hydrocarbons. The production ratio of gas to reservoir fluid is an important design parameter in all contexts. Below a minimum flow velocity in a well, the critical Turner velocity vTur, no fluid is produced and well load up (cone shaped brine accumulation) occurs.

To study its general feasibility, a CO_2 back-production experiment was conducted in October 2014 at the Ketzin pilot site, Germany (Martens et al., 2015). Over a two-week period a total amount of 240 tonnes of CO_2 and 55 m^3 of brine were safely extracted from the reservoir. Geoelectrical monitoring by means of a permanent electrode array at the production well was capable of tracking the back-production process and the back flow of brine into the parts previously filled with CO_2. Preliminary results also show that the back-produced CO_2 at Ketzin has a purity >97 %. Secondary component in the CO_2 stream is N_2 with <3 %, which probably results from previous field tests. The geochemical results will help to verify laboratory experiments which are typically performed in simplified synthetic systems. Numerical simulations were carried out (i) in advance of the field test to support its design and (ii) after the field test in order to demonstrate the performance of the history-matched model. Considering the effective time schedule and the maximum allowed flow rates, the total amount of back-produced CO_2 was underestimated by about 14 % in the numerical simulations (Martens et al., 2015a).

The results obtained at the Ketzin site refer to the pilot scale field trial. Upscaling of the results to industrial scale is possible and has been underlined by further numerical simulations, but should be first tested and validated at demonstration projects.

The case study of the K12-B gas field in the North Sea demonstrates the injection into a mature gas field as potential option for long-term CO_2 storage. Frequently, the injection process is initially also aimed for enhancing the gas recovery (EGR). The K12-B gas field is one of the first and only gas fields in the Netherlands where injection of CO_2 was carried out. Residual CO_2 from the gas production was re-injected into different compartments of the field during different injection intervals. After the injection periods a number of back-production test have been carried out. These operations are numerically analysed for key factors such as recovery rate, CO_2 ratio, well pressure and water coproduction. In addition, the measured data as well as observations at the field are history matched with a compositional reservoir simulator.

2 TECHNICAL IMPLEMENTATION AND MONITORING RESULTS

The German Research Centre for Geosciences operates the Ketzin CO_2 pilot site, the first European on-shore geological storage experiment in a saline aquifer of the North East German Basin (Liebscher et al., 2013). The active CO_2 injection and storage phase covers the period from June 2008 to August 2013. During this time, a total amount of approximately 67 kt of carbon dioxide (CO_2) was stored in the sandstone layers of the Stuttgart formation (Martens et al., 2015b). In the frame of several Ketzin project phases, the behavior of CO_2 in the storage reservoir and the resulting behavior of the storage complex have been studied by a multi-disciplinary scientific monitoring concept, comprising geophysical and geochemical methods, as well as numerical modelling studies.

To test the general feasibility of storage, including the retrievability of the injected CO_2, a so-called back-production experiment was carried out in October 2014. Along with the technical and operational details, the following questions should be examined:

- Recovery of process parameters (temperature profiles along the production tubing, well-head and bottom-hole pressures, flow rates) to assess the reservoir and wellbore behavior and to evaluate the technical feasibility
- Investigation of the composition of the back-produced CO_2
- Does the gas quality adequately fit into the context of carbon capture storage and utilization (CCSU), i.e. in particular to “power to gas” concepts?
- What quantities of formation water are simultaneously produced and what is the composition?
- What technical and organisational measures have to be taken for a safe back-production operation of CO_2?

- The overarching objective of this experiment was evaluating whether this technical operation can be used as a corrective measure for pressure management of a storage reservoir. Among other techniques of pressure regulation and CO_2 plume management, the conversion of an injection well into a producing well for accelerating the pressure reduction may be considered (Manceau et al., 2014). For simplification purposes, one can assume that the well is producing at a constant rate which is equal to the previous injection rate (CO_2 injection rate at Ketzin: ~min 1.6 t/h to max. 3.2 t/h). This corresponds to 0.5 kg/s – 0.8 kg/s and is in the order of magnitude of a standard water pump (~ 1kg/s or 1liter/s). During the CO_2 extraction, pressure in the injection zone declines. When the extraction stops, the pressure field is equilibrated in the reservoir leading to a pressure recovery in the injection zone.

2.1 Organisation of the operation

The CO_2 back-production was conducted from October 15, 2014 until October 27, 2014. GFZ had commissioned the company Weatherford Energy Services for conduction all technical operations. A professional safe guard as well as scientific personnel of GFZ was on site every day.

The test operation at the Ketzin pilot site took place around the clock seven days a week. A corresponding exemption according the German law (ArbZG) was submitted together with the technical procedures and received approval from the Mining Authority of the Federal State of Brandenburg. In order to estimate a possible noise pollution of the neighborhood by the CO_2 back-production, an acoustic certificate was conducted by an engineering bureau on October 15, 2014, during the peak hours from 10:00 am to 4:00 pm. In this period, all intended production rates were tested. The result showed that the CO_2 back-production does not cause any harmful effects by noise pollution.

2.2 Technical description of facility

Weatherford Energy Services provided the technical equipment for conducting the back-production test (Figure 1), as well as the skilled engineering personnel for the operation.

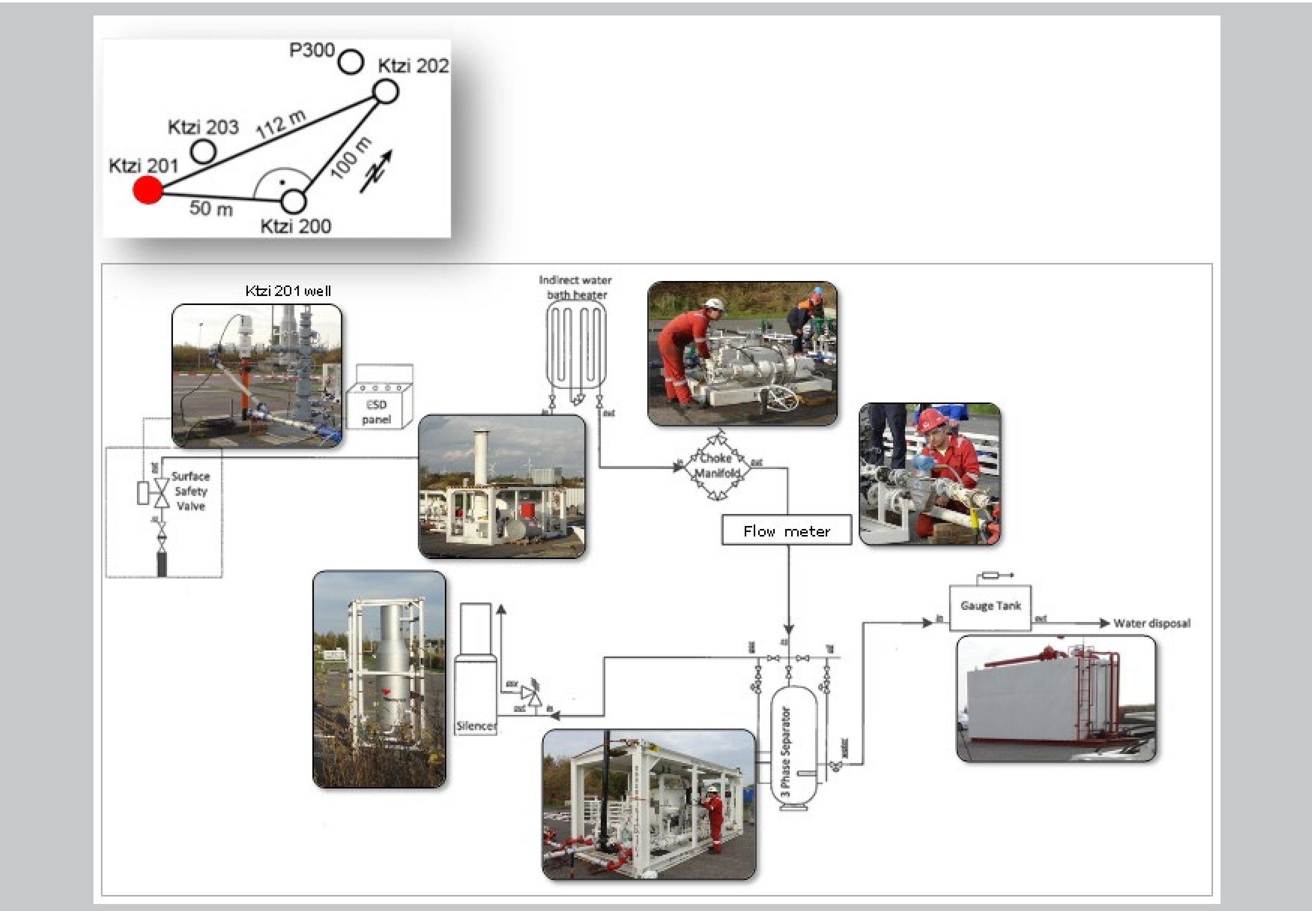

Figure 1 Technical components for the back-production test (Martens et al., 2015). In the schematic borehole layout (top left), the well Ktzi 201 is marked by a red dot. The CO_2 was flowing at the wellhead of Ktzi 201 through a surface safety valve (Figure 1).

Thereafter, it was heated by means of a diesel-powered waterbath-heater to about 50 °C to prevent dry ice formation. After preheating, a manual volume control was carried out by means of a choke manifold. Co-produced brine from the reservoir was separated in a separator, stacked in a tank on site and properly disposed (see also section 2.4). The CO_2 was vented via a silenced 6 m high stack system in the ambient air. Gas and water samples for further investigation were taken at the separator (see sections 3.3 and 3.4).

2.3 Test procedure

On October 15, 2014 at 10:50 am, extraction rates of about 900 kg/h, 2.000 kg/h and 3.500 kg/h were conducted for at least one hour each, in order to demonstrate the general feasibility and to carry out a meaningful measurement of the noise level (see section 2.1). The operational protocol is presented in Table 1.

Table 1 Operational protocol during the back-production experiment.

Start time	End time	Rate
15.10.2014 (4:00 pm)	20.10.2014 (12:00 am)	continuously, about 800 kg/h
20.10.2014 (12:00 am)	22.10.2014 (5:00 pm)	continuously, ca. 1.600 kg/h
23.10.2014 (11:00 am)	27.10.2014 (8:00 pm)	alternating regime with a mean flow rate of 800 kg/h during day shift (8:00 am - 8:00 pm); and switch off during night shift (8:00 pm – 8:00 am)

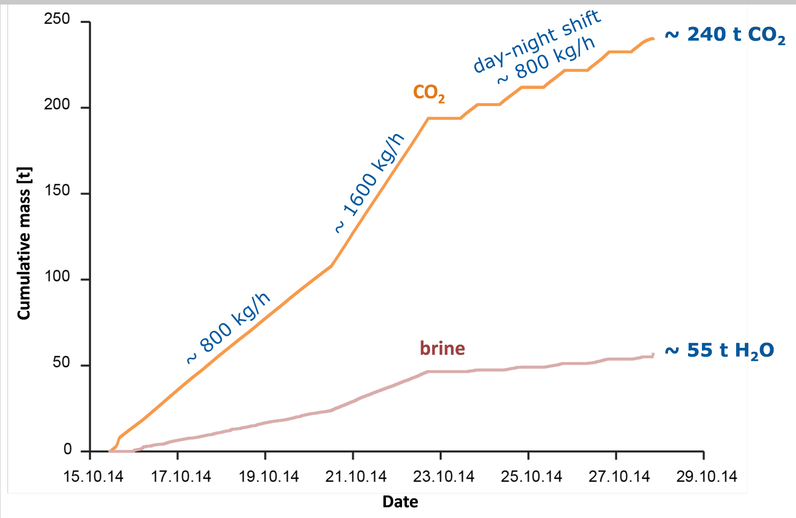

Figure 2 Cumulative mass of produced CO_2 and brine, with various rates during a period of two weeks.

Before the experiment ended, the rates were successively decreased every hour by 100 kg/h, starting from 800 kg/h towards 200 kg/h, in order to determine the final rate of co-produced formation water. This was the case at a rate of 500 kg/h. The experiment was terminated on 27.10.2014 at 8:00 pm. The total amount of produced CO_2 and brine is presented in Figure 2.

2.4 Safety measures

Before starting the experiment, a safety-training meeting with all personnel involved was conducted. Major objective of this instruction was the fulfilling of the establishment order. Particular working conditions have been discussed and appointed. A locked security zone (about 28 m x 35 m) around the stack system was set up as safety measure against possible increased CO_2 concentrations in the ambient air. In addition, the duration of stay for the staff in the environment of facility components (choke manifold, separator, etc.) has been limited to a minimum to control and monitor the experiment. For permanent CO_2 concentration measurements within the safety zone of the technical facility, the field crew used a typical handheld instrument. After October 16, the CO_2 concentrations outside of the safety zone were recorded by Weatherford or GFZ, measured at least every four hours with the same instrument. A total of 72 measurement patrols were carried out. For the majority of measurements (57 of 72) CO_2 concentrations <0.5% by volume, usually in the range of 0.04 vol% (in ambient air), have been recorded. It was also found that CO_2 concentrations show temporarily - highly dependent on wind conditions – a local increase (> 0.50 vol .-%). In the case of 5 measurement patrols local CO_2 concentrations > 1% by volume were recorded due to very calm weather conditions. 1% by volume represents the critical short-term exposure value for CO_2 (acc. To TRGS 900, Class II, overload factor 2). To take into account of the strict health and safety regulations, the back-production rate was reduced to 800 kg /hours after October 23, 2014 and the operation was carried out only during the day shift. From October 20, 2014, two additional mobile fan systems were made available and have been used in the work area for a more rapid mixing of the CO_2 with the ambient air.

2.5 Disposal of co-produced brine

A total amount of 61.74 tonnes of co-produced brine with a high salinity (see subsection 2.9) had to be disposed. This was carried out by a commissioned company. In addition, measurement of radioactivity of each fetched batch of formation water has been conducted. No radioactivity has been detected. Also, the final measurement of all technical system components by Weatherford revealed no radioactive contamination.

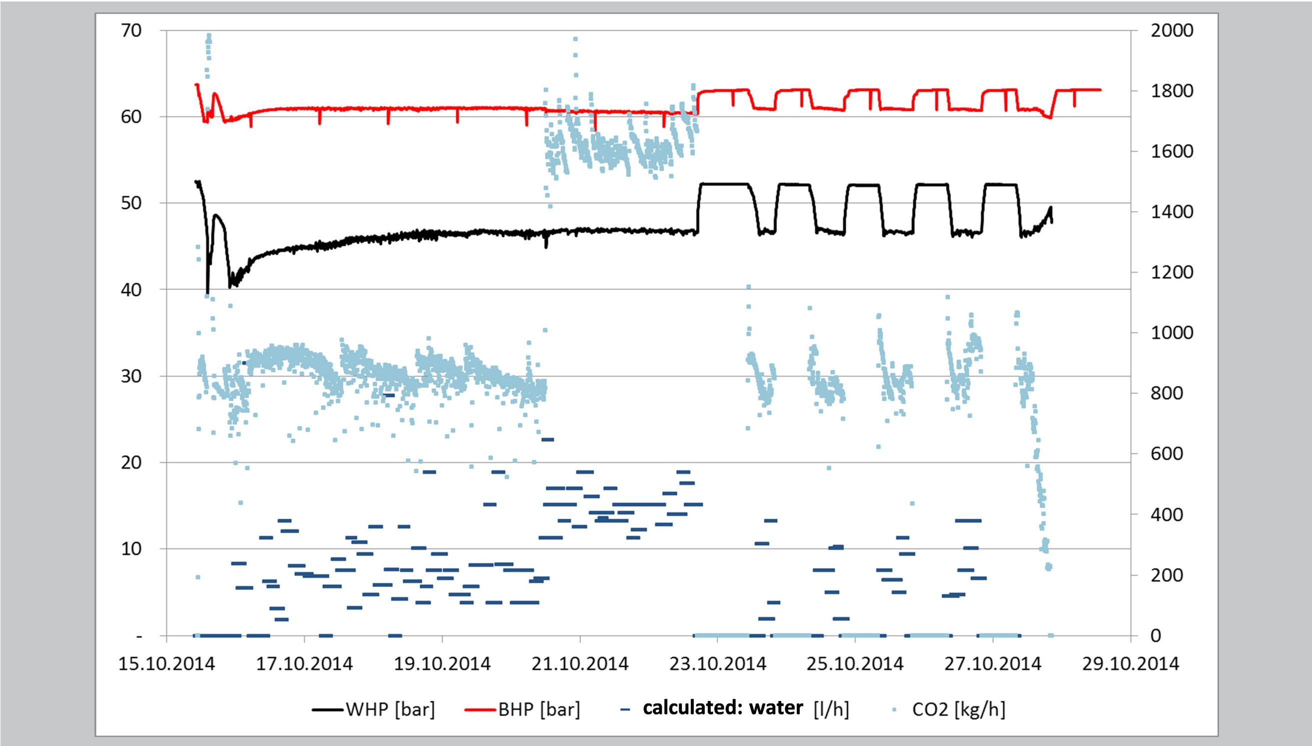

Figure 3 Overview of the measured parameters during the CO_2 back-production experiments at Ktzi 201: WHP (wellhead pressure), BHP (bottomhole pressure) @ 550 m depth. Formation water has been co-produced until a rate of 500 kg/h CO_2.

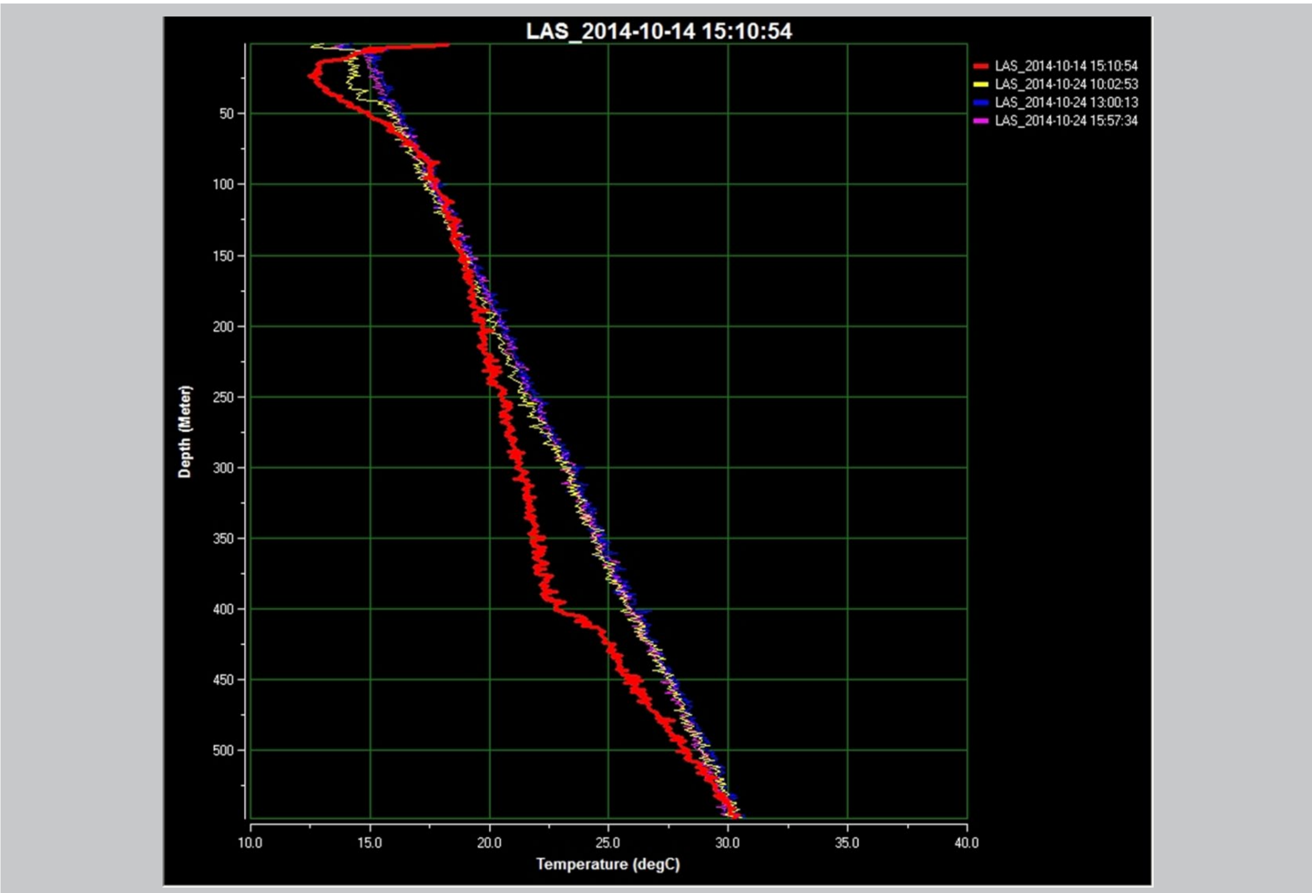

Figure 4 Temperature profiles of production well Ktzi 201 during the back-production experiment. Baseline (14.10.2014/red curve) and three different measurements (various times at 24.10.2014).

2.6 Pressure and temperature behaviour

For the whole test period, besides the continuous measurement of CO_2 and brine production rates, well-head and bottom-hole pressure at Ktzi 201 was recorded (Figure 3). After adjusting a continuous production rate the pressure sensor of the well Ktzi 201 at 550 m depth displayed a dynamic equilibrium pressure of approximately 61 bar from October 16, 2014, and a dynamic equilibrium pressure of around 46 bar at the wellhead since October 18, 2014, . The dynamic equilibrium was not significantly disturbed by doubling the production rate at 1,600 kg/h on October 20, 2014. After October 23, 2014, when the alternating regime of 12 hours production at a rate of 800 kg/h with subsequent shutting off the wellbore for another 12 hours was introduced, a very rapid adjustment of the pressure to the level before the start of back-production (~ 65 bar) was observed. The pressure readings during the continuous production operation were comparable at ~ 61 bar.

The very short periodic pressure drops (daily at 5:20 am) were caused by technical reasons. The data acquisition system has been re-started automatically on a daily basis during the night-time in order to increase the stability of the measurements.

Figure 4 displays temperature profiles, continuously recorded by a distributed temperature sensing (DTS) system at the fibre-optic cables along the 3.5" production tubing of Ktzi 201. The baseline measurement (red curve) was recorded before the start of back-production and represents the temperature profile of the stagnant wellbore. It shows the continuous re-allocation of CO_2 with condensation in the upper region and evaporation in the lower area of the wellbore, known as heat pipe effect. After starting the back-production, a linear temperature profile (different colored curves of Figure 4) occurs, presenting gaseous CO_2 in the entire well. This condition was observed during the entire back-production process.

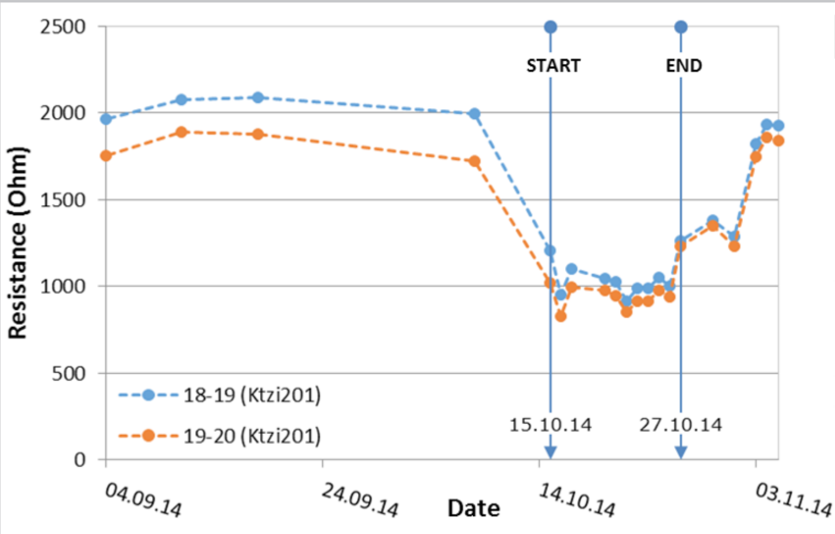

Date	#18-#19	#19-#20
04.09.2014	1966	1751
11.09.2014	2075	1889
18.09.2014	2086	1878
08.10.2014	1993	1724
15.10.2014	1208	1021
16.10.2014	949	828
17.10.2014	1098	993
20.10.2014	1043	977
21.10.2014	1026	944
22.10.2014	916	850
23.10.2014	988	916
24.10.2014	988	911
25.10.2014	1048	977
26.10.2014	999	938
27.10.2014	1262	1229

Figure 5 Display of contact resistance values measured at the permanent downhole electrodes #18-#19 and #19-#20 at the Ktzi 201 well, recorded from Sep-04 until Oct-27, 2014. The time window of Oct 15th until Oct 27th, 2014 indicates the back-production process, where the variations of the contact resistances correlate with the pressure fluctuations (measured as BHP @ 550 m). Data loss took place between Oct-18/Oct-19, 2014.

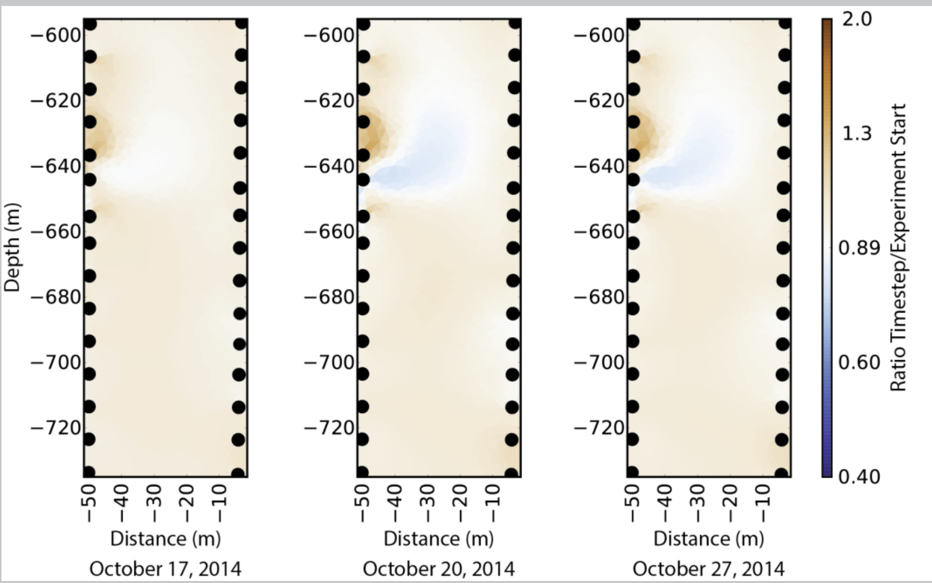

Figure 6 Tomographic results show the baseline (1) and two following time steps (2, 3), where stimulation of formation water (blue colored) is seen together with the ascending CO_2 (brown colored).

2.7 Geoelectric measurements

The back-production test has been accompanied by regular geoelectrical measurements based on the permanent downhole electrodes of the crosshole plane Ktzi 201-Ktzi 200 (Martens et al., 2015). Daily recordings have been carried out but some data was lost due to remote-control interruption. A direct indication of the near-wellbore processes during the back-production experiment is given by the contact resistances, which represent raw data of the electrode array. The data describe the coupling behavior of the electrodes with the surrounding rock mass, and image the contact with high-conductive brine or high-resistant CO_2. Usually, the electrodes are grouted by cement and provide stable contact resistance values during all measurement phases. In case of the injection/production well Ktzi 201, a partially open annular space exists where fluid exchange between brine and CO_2 occurs. Therefore, the contact resistances directly indicate the type of fluid in the borehole.

As seen in Figure 5, the observed electrodes start with high resistance values which indicates CO_2 in the annulus, equilibrated during the previous post-injection phase. The back-production causes a significant decrease in the resistance values due to ascending brine, which occurs together with the vented CO_2. This behavior can also be demonstrated by the tomographic results of Figure 6, where a comparison between the baseline situation (October 14, 2014) and various time-steps from the back-production phase is given.

2.8 Gas analysis

To determine the composition of the back-produced gas, a special pipe from the separator gas outlet to the analyser in the scientific cabin has been installed. For continuous gas analysis, a mass spectrometer, a gas chromatograph and a photoacoustic sensor were used. Every day, gas sample tubes were repeatedly filled for a subsequent study of stable carbon isotopes in the laboratory.

The extracted gas consisted of > 97% of CO_2 (Figure 7). The second most component was nitrogen, the concentration of which continuously decreased towards October 23, 2014 (3 to 1.4%), the beginning of the alternating load regime. During the day shift a mixture of ~ 98.5/~ 1.5% CO_2/N_2 were recorded, with slightly increased nitrogen levels in the morning after the re-start.

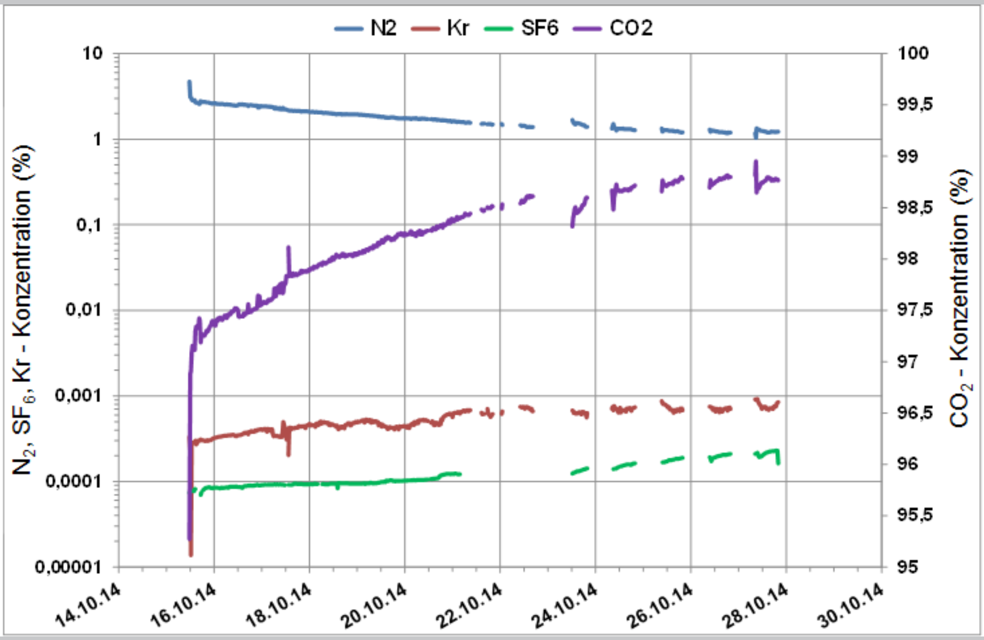

Figure 7 Composition of the back-produced gas.

Furthermore, small amounts of methane, carbon monoxide and hydrogen (<0.01%) as well as krypton and sulfur hexafluoride (concentrations <0.001%, e.g., used in 2013 as a gaseous tracer during the injection) were measured.

It is known from gas measurements on fluids of Ktzi 200 before the start of injection that the original pore fluid (LGas/LFluid: 0,017) contains methane, CO_2, H2 and N_2 (0.17 / 0.08 / 0.14 / 17.9 mg/l). After the arrival of CO_2 at Ktzi 200 increased concentrations of methane and hydrogen (1.44 & 0.43 mg/l) were measured. Nitrogen was also detected, although at low concentrations (1.48 mg/l). In particular, the nitrogen can thus originate from either the injection operation or the CO_2-N_2 co-injection test in 2013, and/or from the original pore fluid. Investigations on the isotopic composition are still in progress.

To answer the question, whether the composition of the produced gas will allow application of carbon capture, storage and usage (CCSU), gas samples were provided to the Brandenburg Technical University Cottbus (BTU). In cooperation between GFZ and BTU, catalytically guided methanation of CO_2 samples from Ketzin is under investigation. The results are also currently pending.

2.9 Water analysis

Water samples at the separator were taken to study the chemical composition of the entrained water from the Ktzi 201 during the back-production process. The electrical conductivity of the samples was in the range 206 to 225 mS/cm. The pH ranged from 5.7 to 6.0.

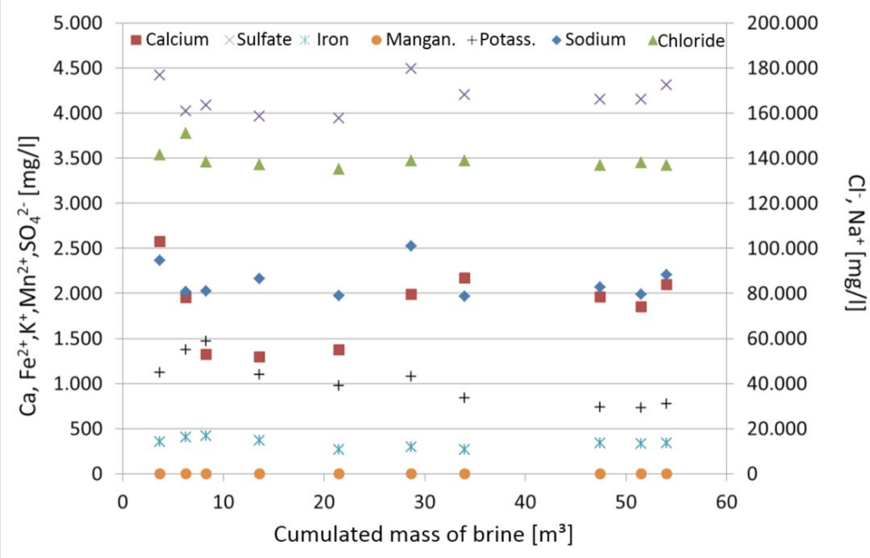

Figure 8 Analysis of water samples taken at the separator during the back-production process.

In addition, 10 samples were analysed by the Potsdam Water and Environmental Laboratory regarding inorganic parameters and selected heavy metals (iron, manganese).

Figure 8 shows the results of the water sample analysis based on the cumulative mass of brine. In the 10 samples, stable values of analysed parameters versus cumulative amount of brine are shown. Over the test period, no substantial changes were determined in the water composition.

In particular, the measured values for chloride, sulfate, sodium and the electrical conductivity show that the produced water represents highly concentrated salt water. Concentrations remain comparatively constant during the experiment. Nevertheless, some variations in Calcium and Sulphate may indicate geochemical processes. There is a certain decrease of the Iron concentration, although a little bit masked by the axis scale. This is partially attributed to borehole corrosion. Compared to pre-injection conditions, the Iron concentrations in the reservoir are increased by more than factor 2. Since this increase is comparatively constant and does not have a strong correlation to the borehole, it is considered to be the result of geochemical reactions of pyrite or iron-oxides.

3 NUMERICAL SIMULATIONS AND RESULTS

3.1 Numerical simulations in advance of the field test

A predictive simulation run was carried out to elaborate estimates on the potential well flow rates of gaseous CO_2 and formation water during the scheduled field-test (Martens et al., 2015). The simulation results have been considered in the planning and design of the field test, i.e., for refinement of monitoring layout and cost estimations on required brine intermediate storage and disposal. Thereafter, the valve-determined flow rates applied during the field test were used as limiting boundary condition in a second simulation run, considering the effective time schedule of the test and the maximum allowed flow rates adjusted at the release valve.

Both simulation runs were based on the history-matched reservoir model (Kempka and Kühn, 2013; Kempka et al., 2013). This calibrated reservoir model is applicable to establish reliable short- to mid-term predictions of reservoir pressure development by numerical simulations (Class et al., 2015). The Schlumberger ECLIPSE 100 black-oil simulator (Schlumberger, 2009) was employed, using a minimum downhole pressure of 59 bar at 620 m depth and atmospheric pressure conditions at the wellhead as boundary conditions for the well model in both simulation runs. An effective maximum well flow rate limit was set in the second simulation run, determined by the valve settings made during the field test to consider all manual flow rate reductions, while the first run used the scheduled maximum allowed flow rates. Since the initially scheduled and effective flow rates used in the field experiment differ in their magnitudes and time, only the results of the second simulation run are discussed in the following paragraph.

Figure 9 shows the comparison between the simulated and observed cumulative produced CO_2 and formation water. Simulated CO_2 back-production amounts to about 205 metric tonnes at the end of the field test, while the observed CO_2 back-production is about 240 metric tonnes (underestimation by about 14 %). Total co-production of brine is overestimated by about 39 % in the numerical simulations (about 91 sm^3) compared with the observed coproduction (about 55 sm^3). These deviations are expected to result from the wellbore model implementation, i.e., the lack of vertical flow profiles for the Ktzi 201 well, the relatively coarse lateral grid size (5 m x 5 m) in the well block elements and potential differences in the near-well (<5 m radius) CO_2 saturation. Detailed investigations are scheduled to assess the simulated gaseous CO_2 saturation in the near-well area by comparing simulation results with data from ERT and pulsed-neutron gamma (PNG) logging campaigns.

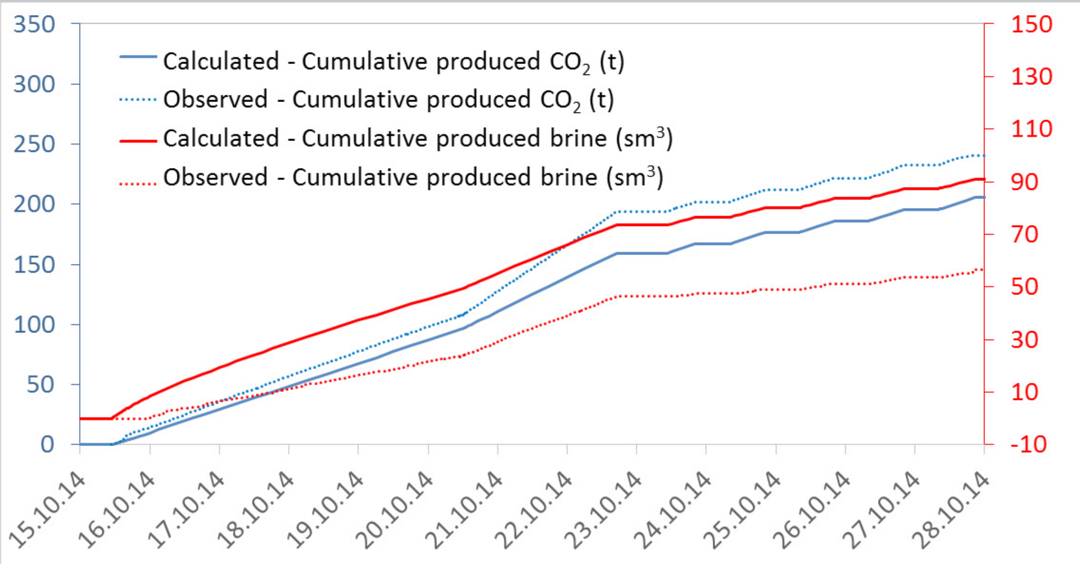

Figure 9 Comparison between the observed (dotted lines) and simulated (solid lines) back-produced gaseous CO_2 (blue lines, values on primary y-axis) and co-produced formation brine (red lines, values on secondary y-axis). Total CO_2 back-production is underestimated by about 14 %, while co-production of brine is overestimated by about 39 % in the numerical simulations based on the history-matched reservoir model of the Ketzin pilot site.

3.2 Numerical simulations after the field test (Imperial)

Imperial and GFZ made collaborative efforts to implement the Ketzin reservoir model and history match the bottomhole pressures recorded during the back-production experiment for 14 days. Scenarios of the back-production of larger volumes of CO_2 were also simulated for an extended period so as to assess the effects of associated pressure changes on the geomechanical integrity of the wellbore infrastructure and surrounding rock formation.

CO_2 back-production modelling for the Ketzin field

The back-production simulations were set up in Schlumberger's ECLIPSE 300 (E300) software using the geological model and dynamic reservoir parameters based on previous studies carried out by Kempka and Kühn (2013). The history-matched results obtained for gas saturation and bottomhole pressures during the CO_2CARE project (Govindan et al., 2014) for the CO_2 injection period at Ketzin (June 2008 - August 2013), as illustrated in Figure 10 and Figure 11 respectively, were used in order to assume the initial reservoir condition prior to back-production.

The CO_2 back-production rates (in kg/hour) were implemented and the model was simulated for 14 days. It was noted that the bottom-hole temperature data did not show much variation during this period, with average values of 29.5°C and 33°C at Ktzi 201 and Ktzi 203 respectively. The history matching results for the bottom-hole pressures at the wells and CO_2 production rates obtained are illustrated in Figure 12.

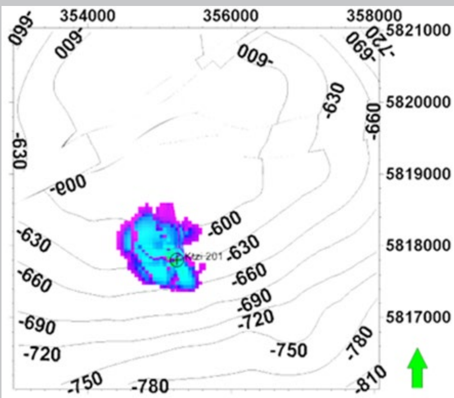

Figure 10 Simulated gas saturation distribution at the end of injection (August 2013) at Ketzin; the contour lines indicate the depth of the top surface of the reservoir model.

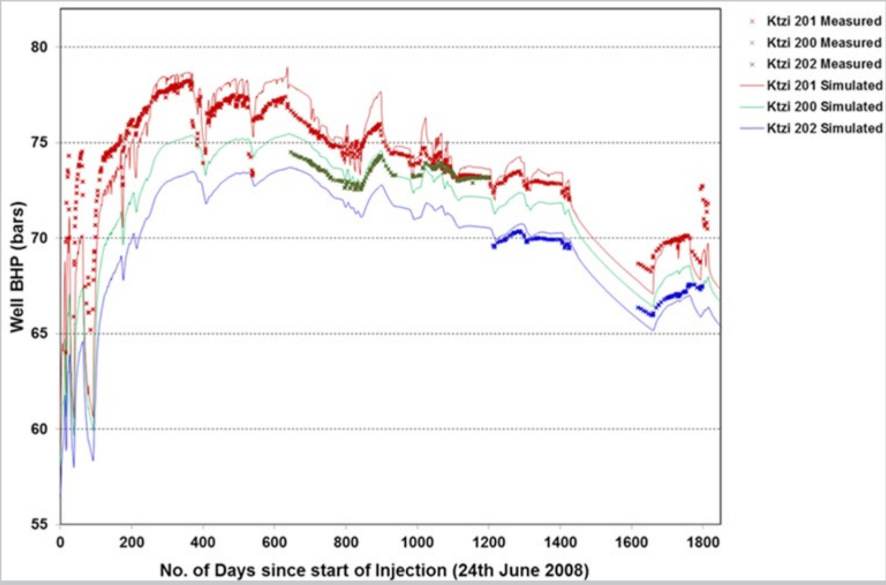

Figure 11 Comparison of measured (dotted lines) and simulated (solid lines) well BHPs during CO_2 injection at Ketzin.

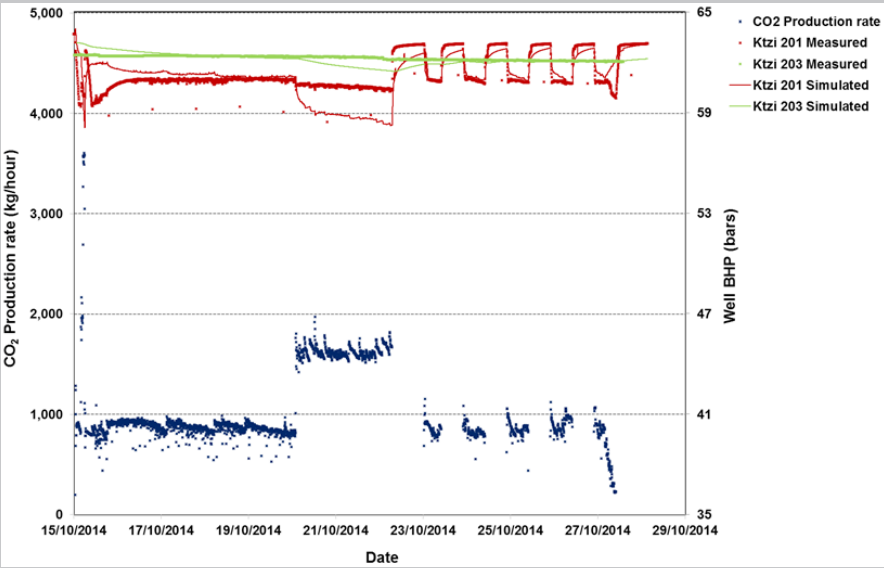

Figure 12 Comparison of the measured (dotted lines) and simulated (solid lines) well BHPs during CO_2 back-production at Ketzin.

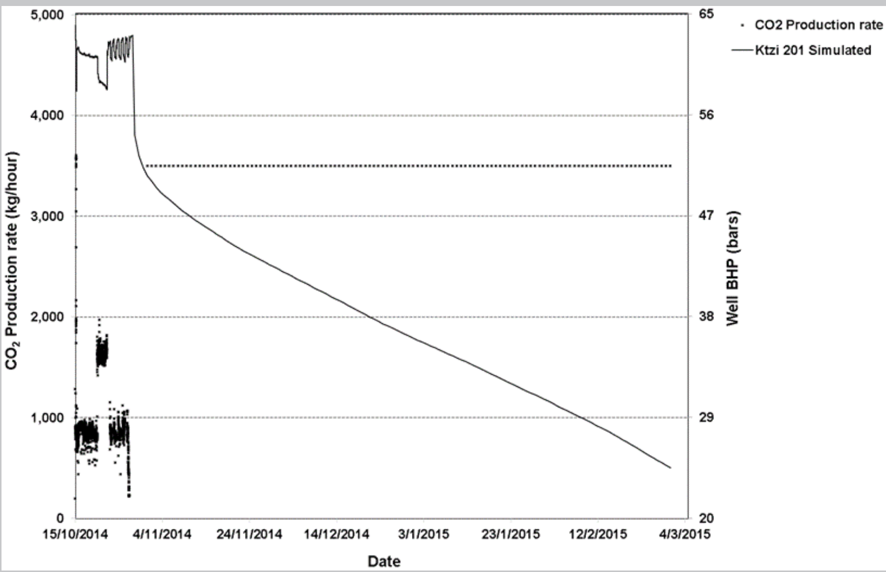

Figure 13 Simulated long-term well BHP at Ktzi 201 for a scenario considering CO_2 back-production at a constant rate.

Two scenarios were subsequently considered for extended periods of CO_2 back-production (for four months, until March 2015) including: (a) constant production rate, assumed at a peak rate of 3,500 kg/hour (Figure 14); and (b) variable production rate, switching periodically between 0 and 3,500 kg/hour every month (Figure 14). The results for the simulated bottom-hole pressures at Ktzi 201 indicate that the change in pressure would range between 10-40 bars in these long-term back-production scenarios.

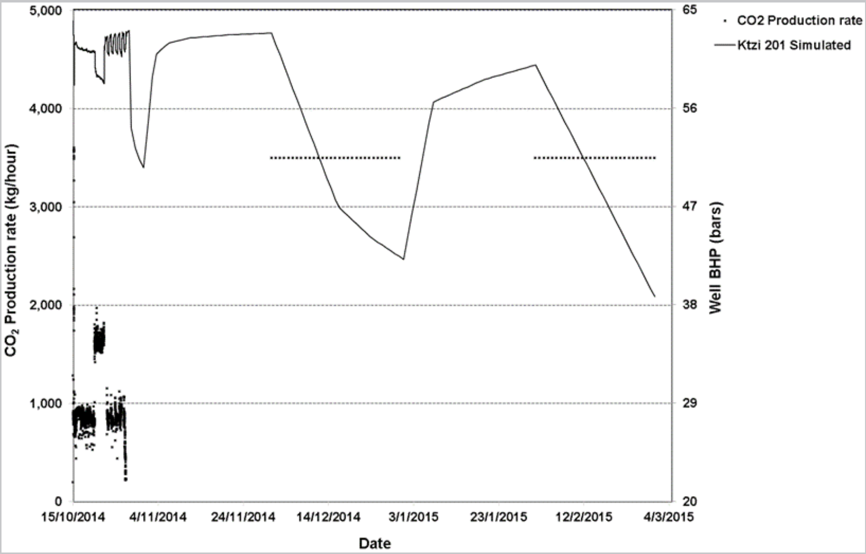

Figure 14 Simulated long-term well BHP at Ktzi 201 for a scenario considering CO_2 back-production at a variable rate.

Near wellbore geomechanical model for the Ketzin field

The near wellbore model developed aims at assessing the potential for failure zone development during both CO_2 injection and back-production period at the Ketzin site. Since the temperature monitoring results suggested that there was no significant temperature change during the operational period, only the effect of pressure change on near wellbore behaviour was considered in this model.

As illustrated in Figure 15, increasing pore pressure may push the Mohr circle beyond the failure envelope and result in shear failure. Excessive pressure increase ($p>\sigma_3$) can also induce tensile failure and thus fracture the reservoir. On the other hand, reducing the pore pressure moves the Mohr stress circle further away from the Mohr failure envelope, which makes failure less likely to happen.

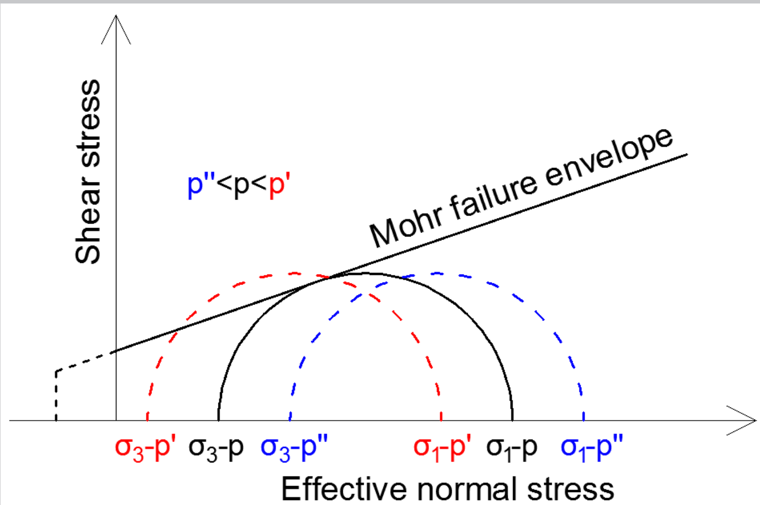

Figure 15 Pore pressure dependent failure behaviour of rock formations.

Model development

Numerical models to assess near wellbore stress and failure behaviour during CO_2 injection and back-production at Ketzin were developed in FLAC^{3D}, an advanced geomechanical analysis software. As shown in Figure 16a, the physical dimensions of the model are 10×10×10m (length×width×height) and a cylindrical zone at the centre of the model is refined to accommodate the simulated wellbore. Figure 16b shows the detailed model design of the near wellbore, which covers two concentric rings of cement and casing. The entire model domain was assumed to be within the Stuttgart formation at depth from -640 to -650 m.

In the model, the σ_v is assumed to be the intermediate principal stress and its magnitude is close to the load induced by overburden weight, which is 15.1 MPa. As reported by Klapperer et al. (2011), the maximum principal stress σ_H is in NE-SW direction parallel to the axis of the anticline. The magnitudes of σ_H and σ_h are suggested to be lower than 2.8 σ_v and higher than 0.62σ_v, respectively. Therefore, σ_H and σ_h are assumed to be the maximum (42.3 MPa) and minimum (9.4 MPa) values at each range. Y-axis was assumed to be the vertical direction, z-axis (positive) was assumed to be pointing the North, and the angle between σ_H and z-axis is 60°. The boundary conditions of the model were such that it is laterally confined and the model base is fixed.

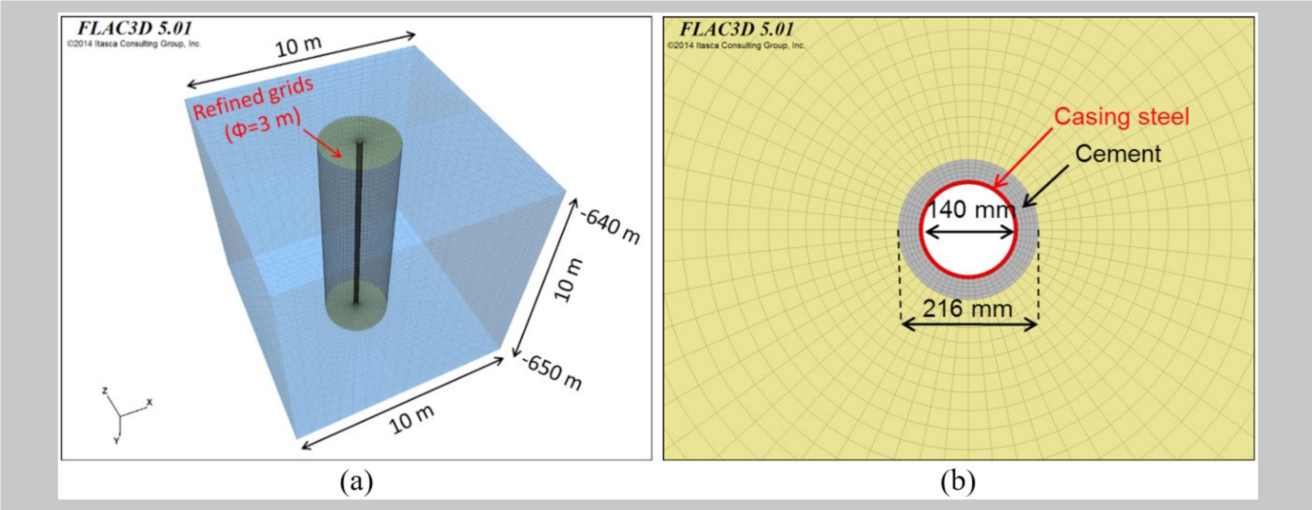

Figure 16 Model geometry and the central refined area.

Table 2 Rock mechanical and strength properties of the Stuttgart formation and the wellbore material.

Layer	K (GPa)	G (GPa)	φ (°)	C (MPa)	t (MPa)
Stuttgart formation	6.06	3.13	25	11.47	-1.15
Cement	19.43	6.14	-	-	-
Casing steel	160.31	80.47	-	-	-

Rock mechanical properties used in this model, which are summarised in Table 2, were adopted from the paper published by Ouellet et al. (2011). The constitutive model used here was assumed to be the classical Mohr-Coulomb model in FLAC^{3D}. Cement and casing steel were modelled as elastic and their properties are based on literature (BGS, 2008). The initial reservoir pore pressure was assumed to be uniform at 6 MPa within the model domain.

The simulation consists of five consecutive procedures: (1) initial equilibrium, (2) well drilling, (3) wellbore completion, (4) CO_2 injection, and (5) CO_2 back-production. Well drilling was simulated in the model by assigning the 'NULL' property (no mechanical stiffness and strength) to the grids representing the well at 216 mm diameter. In the wellbore completion stage, the grids representing the cement and casing were reinstated and the well diameter was reduced to 140 mm. The coupling between casing and cement, cement and rock were simply assumed to be fully bonded.

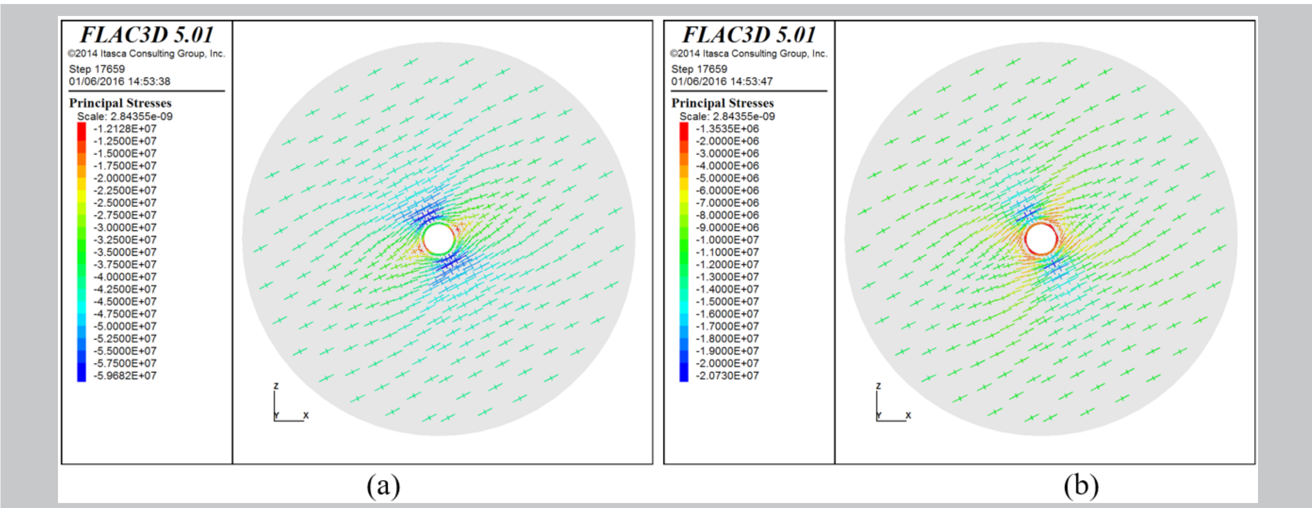

Figure 17 Principal stress tensors after well completion: (a) tensors coloured by the maximum principal stress and (b) tensors coloured by the minimum principal stress.

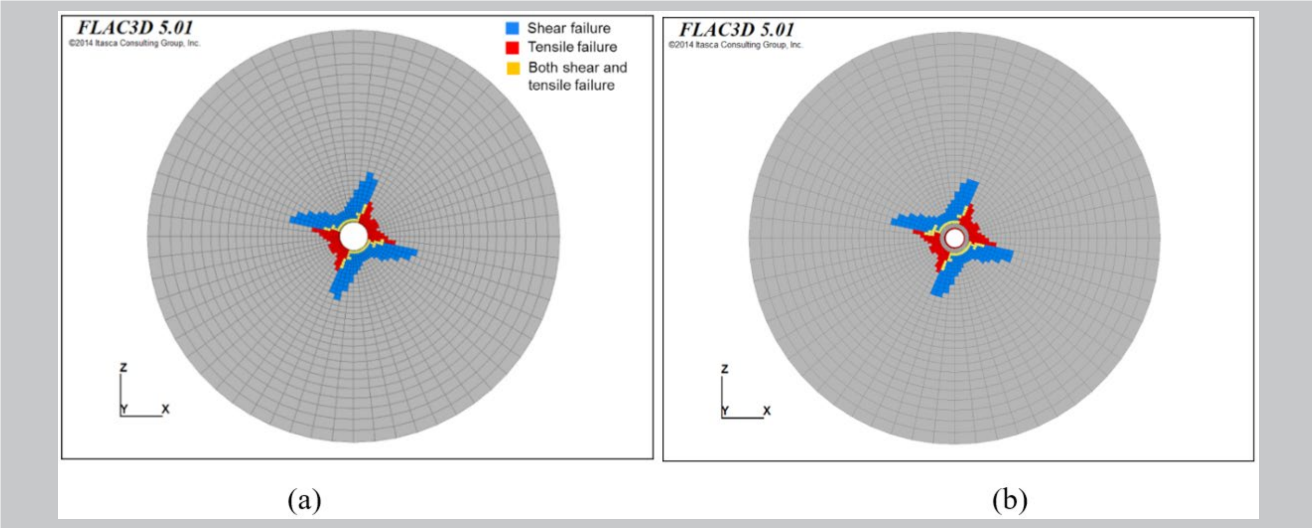

Figure 18 Near wellbore failure zones after (a) well drilling and (b) well completion.

The stress distribution estimated after well completion is shown in Figure 17. As expected, in the near wellbore grids, notable stress concentration can be observed along the direction of minimum principal stress. On the other hand, along the direction of maximum principal stress, near wellbore grids experienced dramatic stress relief. As a response to the stress change, the failure zone near the wellbore is presented in Figure 18, which forms the baseline for further injection/backproduction processes. Shear failure was shown in the large compressive stress zone and tensile failure was found in the stress relief zone. Well completion process has no direct impact on the development of near wellbore failure zone.

Geomechanical response to CO_2 injection and back-production

Near wellbore stress and failure behaviour during the CO_2 injection phase was first evaluated. The pore pressure within the model domain was gradually elevated from 6 MPa to 8 MPa to simulate the CO_2 injection process. In the meantime, the percentage of failure

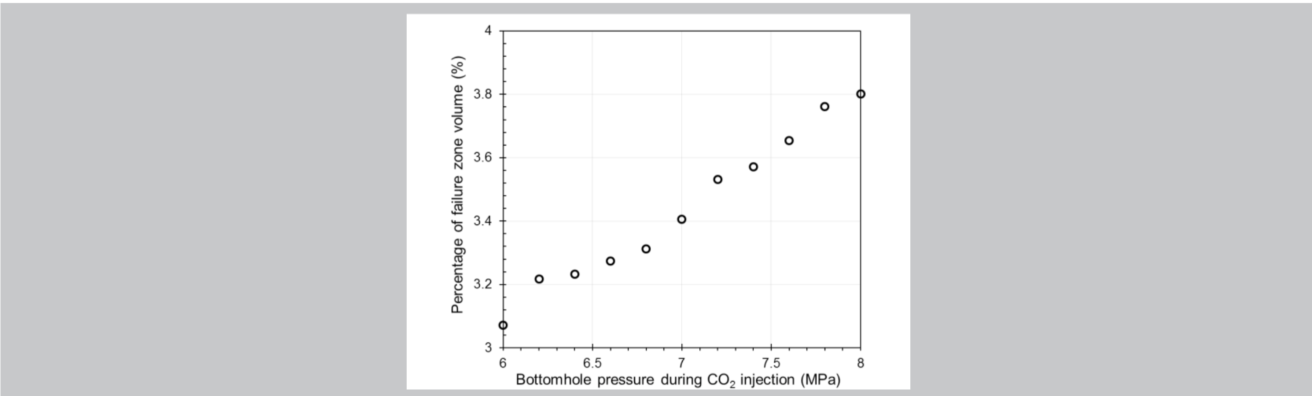

Figure 19 Failure zone development during the CO_2 injection process.

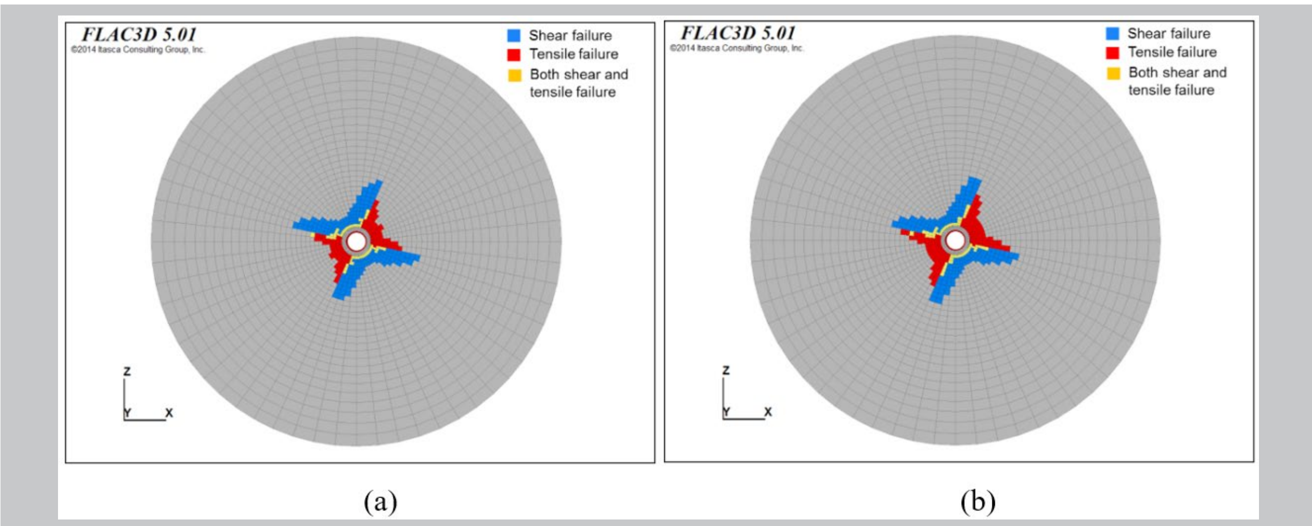

Figure 20 Distribution of the near wellbore failure zone when the CO_2 injection pressure is (a) 7 MPa and (b) 8 MPa.

zone volume within the refined area was recorded at different pressure levels (see Figure 19). As shown in Figure 19 and Figure 21, the failure zone size near the wellbore increased slightly with the increase of CO_2 injection pressure.

Next, the wellbore model was used to reduce the pore pressure gradually from 8 MPa to 4 MPa to mimic the period of CO_2 back-production.

Figure 21 illustrates that decreasing the near wellbore pore pressure has almost no effect on the failure zone developed earlier, and its size remains the same after CO_2 back-production.

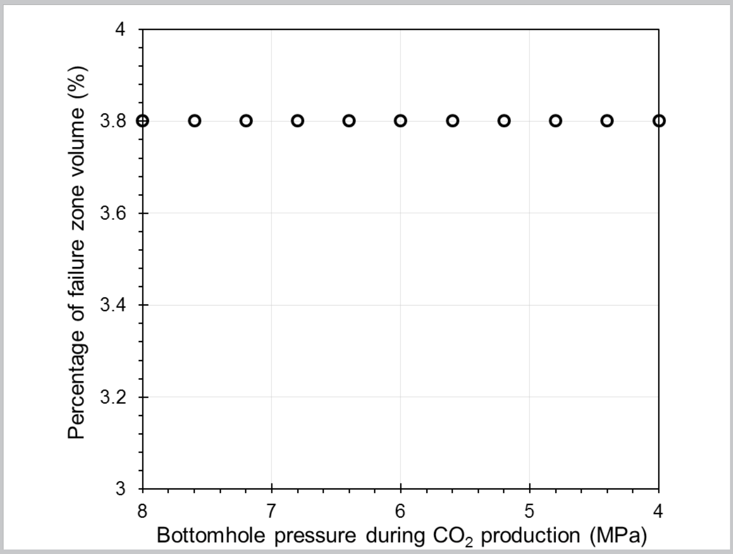

Figure 21 Failure zone development (or lack of it) during the CO_2 production process.

3.3 Development of an inverse Ketzin model for near-wellbore studies (GFZ)

Previous Ketzin reservoir modelling work focused on reservoir CO_2 pressure and arrival times (Kempka and Kühn, 2013). It captured the arrival times and the long term trend of CO_2 reservoir pressure reasonably well. This model significantly underestimates short term variations wherefore the modelling was strongly constrained with observation data. Therefore, it was decided that the CO_2 back-production experiment should be modelled during the MiReCOL project. The modelling work includes short term pressure variations with time scales from hours to days. The predictive capabilities of this kind of models partly rely on data that is observed after the experiment. Consequently a model with improved short term behaviour was developed.

Back-production of CO_2 is connected with shifting the brine/CO_2 interface. Brine is accumulated by coning in the vicinity of the wellbore. This effect is theoretically known and described for natural gas production. However, this experience cannot be directly

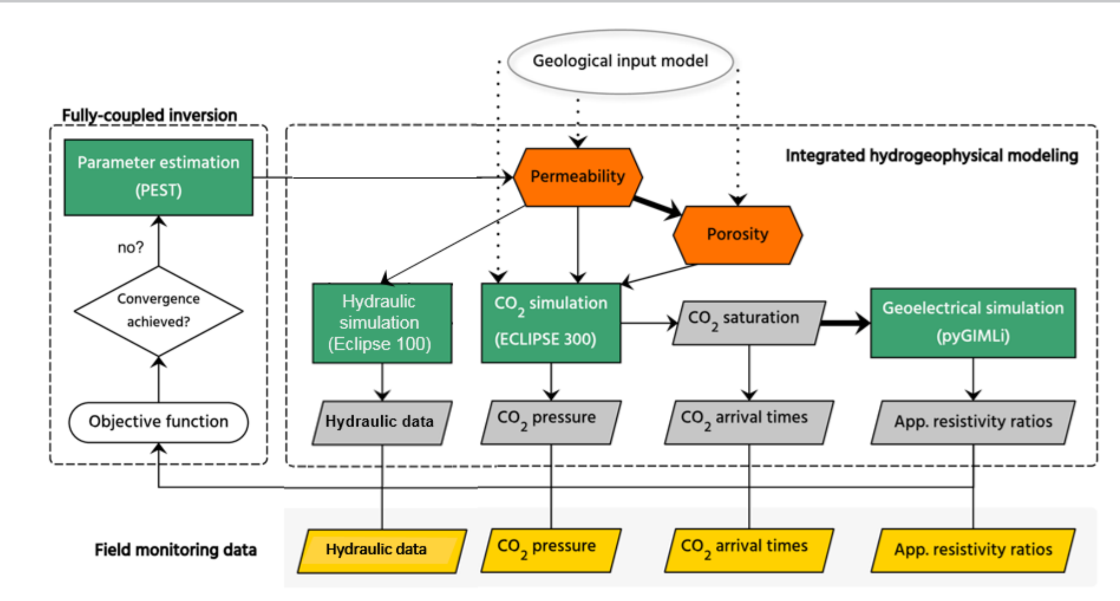

Figure 22 Flow chart of the hydrogeophysical inversion framework. Green fields indicate active modelling tools, orange field indicate parameter fields, grey fields show simulated physical properties. Monitoring data are represented by yellow fields.

applied to CO_2 back-production (Liebscher et al., 2016) and should be investigated in detail with the in situ condition of reservoir. Therefore, the new model aims to include resistivity data for an improved imaging of near wellbore changes in saturation.

A novel inverse model has been established for the Ketzin pilot site. It integrates three pre-CO_2-injection hydraulic tests and the first 270 days of CO_2 injection. It comprises 500 free parameters and is feasible to model channeling effects due to layered permeability. It is an advanced continuation of the hydraulic modelling work of Chen et al. (2014) and forms a necessary complement for description of near wellbore effects and consistency with hydraulic testing, which is not covered by the recent large scale Ketzin model. The task requires high technical prerequisites: Coupling of a single phase model with a multiphase model, coherent time stepping adaptation during the inversions, online observation of model results during runtime. A significant reduction of model runs could be achieved by application of singular value decomposition assistant. In the last report period the model was extended to a full hydrogeophysical inversion environment.

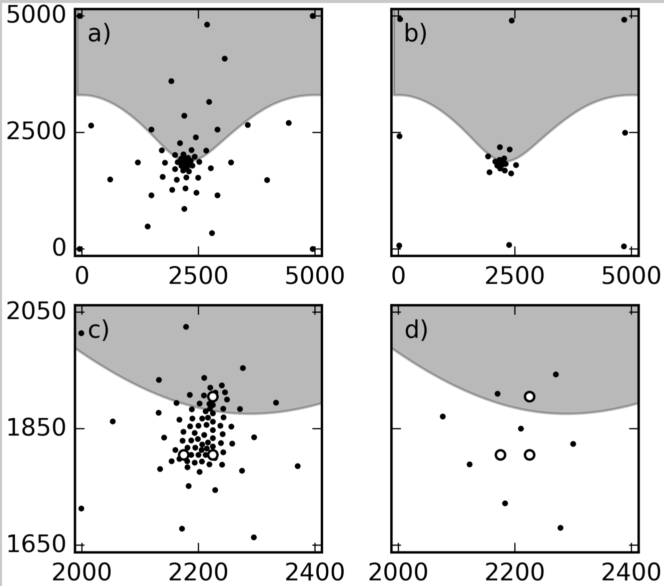

Figure 23 Permeability parameterisation of model layers with spatially distributed permeability. Dots indicate pilot points, circles indicate the wells, which are pilot points as well. The main reservoir aquifers (a,c) are discretised by 194 pilot points, the aquitard anhydrite layer (b,d) is discretised by 25 pilot points. The grey area indicates a low permeability area. The scale is in metres from the model origin, subplots c and d are details from subplots a and b, respectively.

The hydrogeophysical inversion framework is shown in Figure 22. The parameter estimation Tool PEST forms the central part. An initial permeability field is generated based on user setting. Based on an empirical petrophysical relation (Norden and Frykman, 2013) this is transferred to a porosity field. These two fields form the main input data to hydraulic simulation with Eclipse 100 and multiphase CO_2 simulation with Eclipse 300. These models generate hydraulic data and CO_2 pressure, which are compared to their respective observation counterpart. Eclipse 300 furthermore generates a spatial CO_2 saturation which forms the input to the geoelectrical simulations carried out with pyGIMLi.

The model is spatially parameterised with a pilot point approach. Pilot points are spatially distributed over the model area with each pilot point representing one model parameter. They form a grid on top of the numerical model grid. Hydrological parameters i.e. permeability or porosity are interpolated between the pilot points and assigned to each model cell. This resulting parameter fields are closer to reality than using traditional zonation approach which was applied by Chen et al. (2014).

The pilot points are heterogeneously distributed with higher density in areas with much information, i.e. in vicinity to the wells and lower density in at larger distances (Figure 23). The same principle applies to different lithological units. The higher importance of the aquifers relative to the aquitards is honoured by higher pilot point density (Figure 24).

Convergence problems of the hydraulic model have been addressed. Previous versions of the model resulted in very heterogeneous parameter distributions. A detailed analysis shows that two (obs200_p201, obs201_p200) of nine hydraulic time series are mutually exclusive, only either of them can be calibrated. This is surprising since both are reciprocal, i.e. only pumping and observation well are switched. Furthermore, when including one of the abovementioned time series the calibrated permeability is outside the range of realistic values that can be expected in the reservoir (Figure 24). Time series obs200_p201 and obs201_p200 were recorded consecutively with the same data logger, which was just shifted from one well to the other. Consequently, both time series are removed from the dataset.

The reduced set of observations results in better inversion convergence. Simulations based on the entire dataset show pronounced artifacts in the permeability distribution (Figure 25a). The parameters hit their upper and lower boundaries, the high permeability contrasts appear unrealistic. In the model, the near wellbore permeabilities are constrained to their observed values which are comparatively similar (Norden et al., 2010).

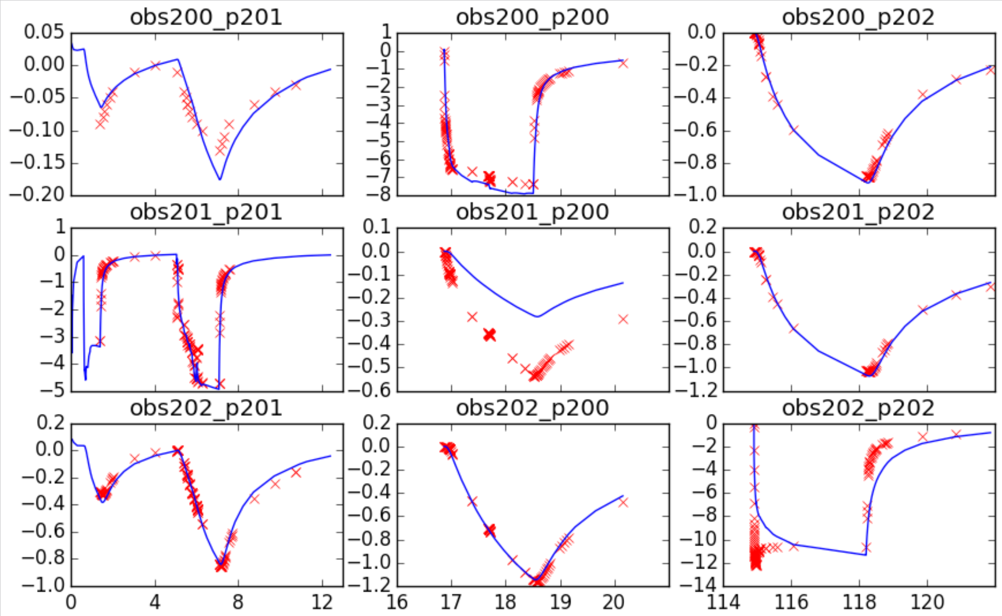

Figure 24 Results of the hydraulic model. The x axis shows days since the first pumping test, the y axis shows drawdown. Red crosses indicate observed, blue lines indicate simulated values. The first part of the subplot titles indicate the observation well, the second part the pumping well, e.g. obs200_p201 are hydraulic observations in well Ktzi200 during pumping in well Ktzi 201.

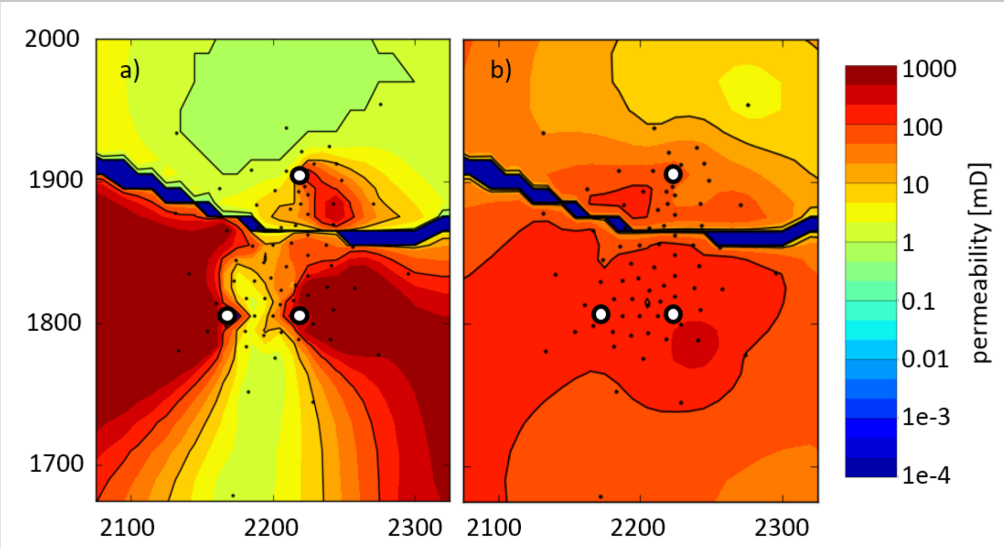

Figure 25 Calibrated permeability distribution a) including all hydraulic time series b) excluding time series obs200_p201 and obs201_p200. The white circles indicate wells, the black dots indicate pilot points. Map units are metres from the model origin.

In the resulting parameter map the wells are located at the inflection points of the permeability (Figure 25a). It appears arbitrary that the wells penetrate just the areas with average permeability. The permeability distribution in Figure 25b is more realistic. The contrasts within the aquifer are similar to the permeability contrasts observed in the wells. Although it might be critical to exclude incompatible observations from a model, these indications appear strong enough that the respective observations are considered as erroneous.

Significant progress was made in including electrical resistivity tomography (ERT) into the model. The pyGIMLi geoelectrical forward code was coupled successfully into the inversion framework (Figure 22). While convergence for the individual data types hydraulics, CO_2 pressure and arrival times can be achieved, the convergence of geoelectric data is not satisfying. The observations show a higher dynamic than simulated values. Exemplarily one of over 1000 electrode configurations is shown in (Figure 26). The next step is to find an appropriate data filtering criterion. Although the reciprocal observations should match and provide identical values, there is typically a certain mismatch between the data. For the current example in Figure 26 both curves show the same dynamic, but the signal of the reciprocal configuration (blue curve) is about twice as high compared to the base configuration (green curve).

The example of hydraulic data described above emphasizes that unreliable data can cause significant deterioration of the model performance. Consequently, further investigation will identify appropriate statistical criteria for selecting only the most reliable data for the inversion.

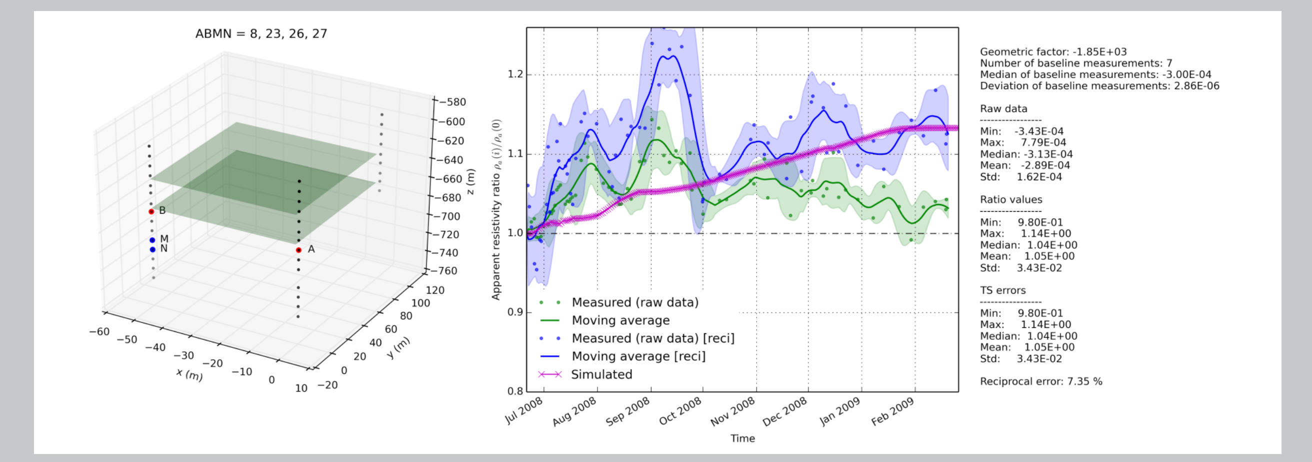

Figure 26 The left part shows the current electrode configuration. Red circles indicate current injection electrodes, blue circles indicate voltage observation electrodes. Grey dots indicate inactive electrodes attached to the borehole casing. The right part shows the apparent resistivity ratio. Observed values have green and blue colour, simulated values are presented in pink.

4 PRACTICAL UNDERSTANDING OF WELL LOAD-UP BEHAVIOUR

4.1 Well effects during back-production

Assessing the feasibility of CO_2 back-production from a storage reservoir does not only require knowledge of the near-well and far-field reservoir behaviour but also of the in-well conditions.

As shown in report D4.1, the back-production of CO_2 reverses the flow direction and multiphase flow phenomena occur that are fundamentally different as those from the injection. The back-production phase can be described by three different operational modes, depending from the actual production rate rCO_2 (Table 1, Figure 27). At reservoir elevation both, CO_2 and brine are extracted from the sandstone. The water has a higher density than CO_2 and remains in the lower part of the well where it reinfiltrates into the formation. Therefore a water cone develops as seen in Figure 27.

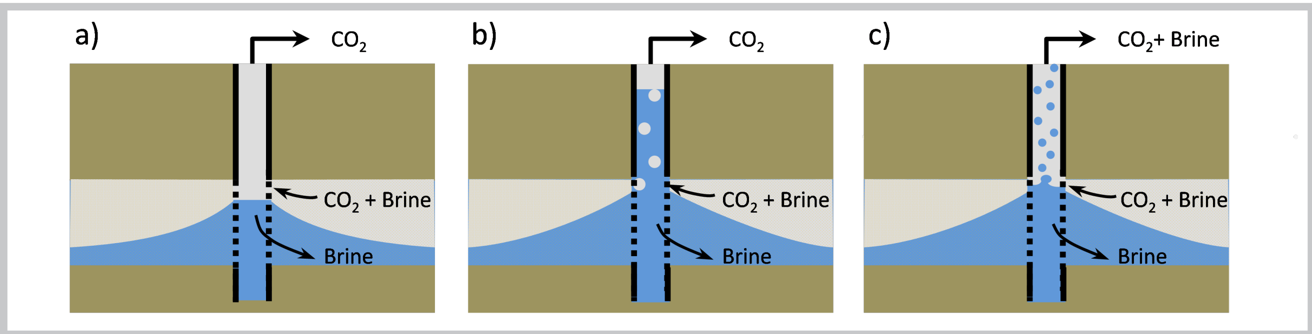

Figure 27 Three operational modes during the back-production test: (a) At low production rates $r_{CO2} < r_{cl}$, pure CO_2 can be produced continuously at wellhead elevation. (b) At production rates $r_{CO2} > r_{cl}$, the water level rises above the well filter and the CO_2 passes through the water column in form of bubbles. (c) In case the production rate exceeds the Turner velocity ($r_{CO2} > v_{Tur}$), the brine is dispersed and entrained by the CO_2, transported upwards and arrives at the wellhead.

4.2 Turner criterion

The back-production experiment was monitored by continuous pressure and temperature measurements in the producing well at 550 m depth at the lower end of the production tubing – i.e. ~ 80 m above the reservoir – and at the wellhead; flow rate of the produced stream was measured by a Coriolis type mass flow meter and controlled by a choke manifold. After initial commissioning and testing of the equipment during the first hours, the experiment was performed in three main stages: Continuous operation with mean flow rates of ~ 800 kg/h from 15th to 20th October 2014 and ~ 1,600 kg/h from 20th to 22nd October and an alternating regime from 22nd to 27th October with a mean flow rate of ~ 800 kg/h during day shift and shut-in during night shift. At the end of the experiment flow rate was ramped down over 6 hours in 100 kg/h steps from 800 kg/h to 200 kg/h. Throughout the back-production downhole pressure and temperature conditions were very stable at ~ 29 °C/61 bar as was wellhead pressure at ~ 46 bar; wellhead temperature showed stronger variations reflecting day-night changes of ambient air temperature and solar radiation. The actual measured downhole and wellhead pressure and temperature data for density calculations were used based on an EOS for pure CO_2 in combination with inner wellbore diameters of 73 mm for the production tubing and 121 mm for the production string to calculate minimum (critical) gas flow rates and velocities according to the Turner criterion as developed for natural gas-well load-up.

For the 51/2"casing, the calculated minimum (critical) velocities based on the Turner criterion are notably higher (up to one order of magnitude) than the actual velocities during the back-production experiment, wherefore well load-up was expected (Figure 28). However, the very stable downhole pressure conditions precludes any well load-up due to accumulation of reservoir brine below the production tubing indicating that flow rates were high enough for entraining any co-produced reservoir fluid to the surface. This is supported by a constant gas/fluid ratio during the different rate stages of the experiment. The data suggest that it is not sufficient to change EOS based fluid properties of a traditionally developed Turner criterion that is adjusted to natural gas production. The criterion still overestimates the minimum (critical) velocity for fluid entrainment in a CO_2 dominated well. For future experimental and operational design it is required to modify the entire set of empirical parameters to calculate an accurate Turner criterion.

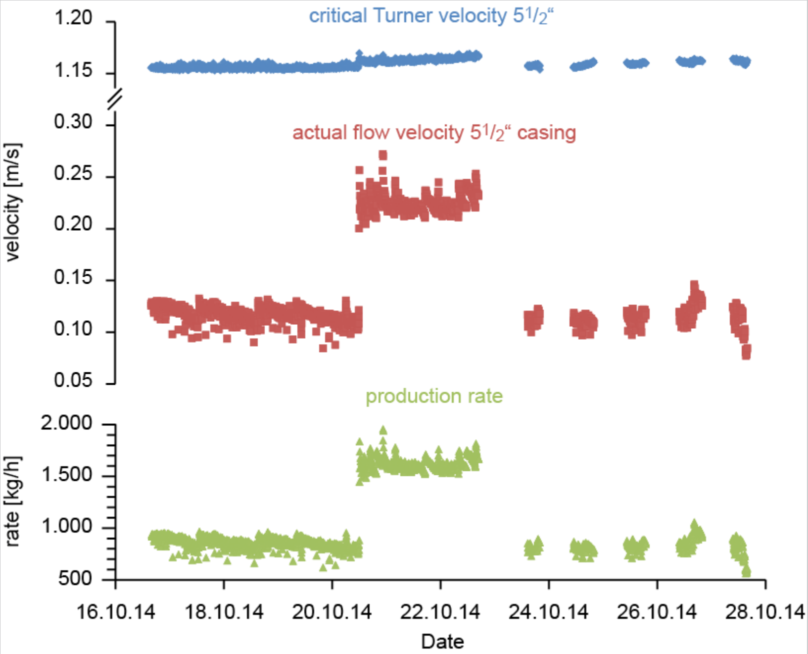

Figure 28 Calculated critical Turner velocity (blue) compared to actual flow velocity (red) for the 51/2" casing. The actual flow velocity positively correlates with production rate (green) but is notably lower than calculated critical Turner velocity throughout the entire back-production experiment.

5 CASE STUDY OF THE K12-B GAS FIELD

5.1 Field site

The K12-B gas field is located in the Dutch sector of the North Sea, some 150 km northwest of Amsterdam (Figure 29). It has been producing natural gas from 1987 onwards and is operated by Engie E&P Nederland B.V.

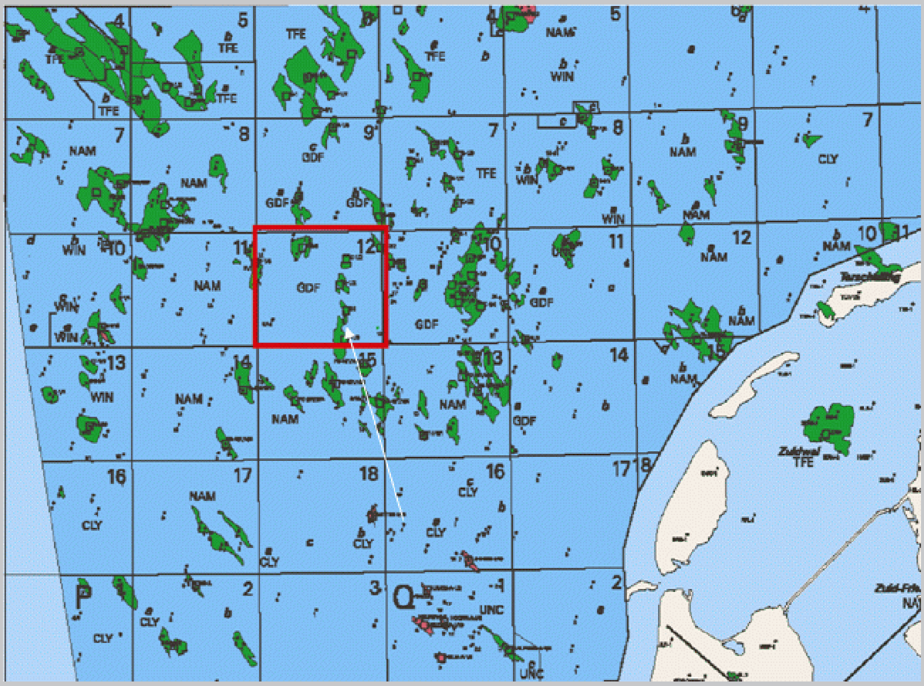

Figure 29 Location of the K12-B reservoir in the Dutch part of the North Sea (supplied by operator).

The K12-B structure was discovered in 1982 by the K12-6 exploration well. Gas production started in 1987. Gas is produced from the Upper Slochteren Formation of Permian age (Rotliegend). The reservoir lies at a depth of approximately 3800 meters below sea level, and the temperature of the reservoir is about 128 ºC. The gas contains 13% CO_2 which is removed from the gas stream at the production platform. Gas is produced from the Upper Slochteren Formation of Permian age (Rotliegend). The K12-B gas reservoir is the first and so-far only gas reservoir in the Netherlands in which industrially produced and captured CO_2 was re-injected in the reservoir. The K12-B field consists of several compartments that are hydraulically separated by several faults. The current investigation concentrates on compartment 4, where two back-production operations have been carried out. More info on the CO_2 injection at this site can be found in Vandeweijer et al, 2011 and Van der Meer et al, 2009.

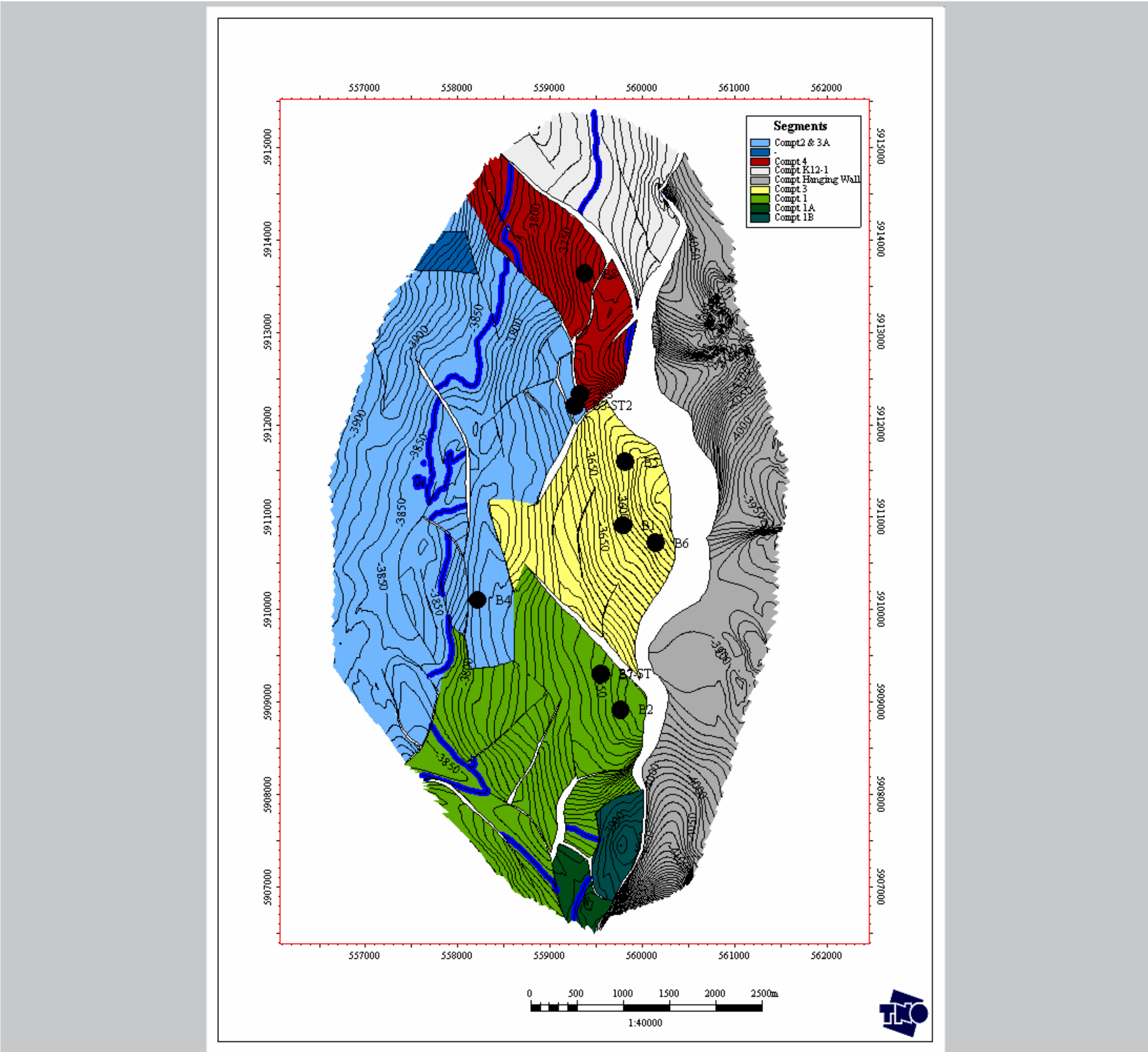

Figure 30: Compartment structure of the K12-B gas field. Compartment 4 (dark red) is under investigation in this report. Wells are indicated by black circles, with B8 located in compartment 4 (modified after Vandeweijer et al., 2008).

5.2 Back-production experiments

In 2004, the well K12-B8 had ceased conventional gas production and was converted into an injection well. More than 10 kt CO_2 had been injected into compartment 4, and after that, well B8 was closed again (Vandeweijer et al, 2008). The well was re-opened at the end of 2007, and significant amounts of CH_4 and CO_2 were produced simultaneously.. After one year, the production stopped again. In 2012, a further CO_2 injection period was carried out, followed by a brief back-production period in 2014.

The water production was not measured individually for compartment 4, but values were measured at the separator for the entire field. The water rate was around 40 m^3/mlnNm^3 (40 m^3 water in 1 million m^3 gas at 0oC and 1.01325 Bar), with a low salt content. This indicates that the K12-B aquifers were in not-active state. The water was probably a result of condensation at the surface from the wet gas due to decreasing temperature and pressure.

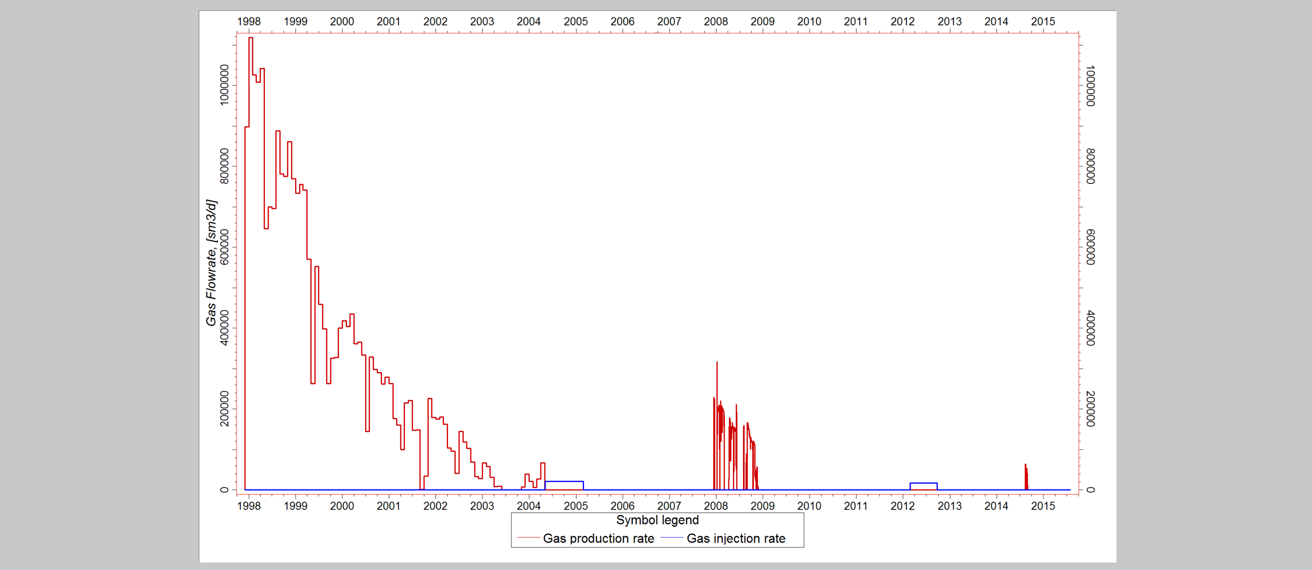

Figure 31 Gas production (red) and CO_2 injection rates (blue) in the well B8 as supplied by the operator. Back-production periods are from the end of 2007 until the end of 2008 and also in late 2014.

When well B8 was put in back-production in December 2007, the well head pressure (WHP) was significantly higher than that at the time of the end of the CO_2 injection (early 2005, see Vandeweijer et al, 2008). This indicates that the compartment and its gas had been under influence of processes not formerly taken into account. Potential underlying processes are: (i) leakage from neighbouring/ internal compartments, (ii) not yet identified sub-compartments, (iii) leakage from tighter parts of the reservoir, (iv) aquifer support or (v) compaction. A combination of the processes is possible.

5.3 Modelling approach

The geological model is based on the general K12-B static model (Van der Meer et al, 2005). To avoid as much water production as possible a vertical permeability anisotropy kv/kh of 0.1 was used and all faults were closed, with the exception of Faults 2, which had a limited transmissivity of 0.1.

The compositional reservoir simulator Eclipse 300 was used for simulations. The PVT (pressure-volume-temperature) model was taken from a previous study on compartment 3 of K12-B. Production and injection data for the compartment were received from the operator. Figure 31 shows the various production and injection procedures, which took place in compartment 4. The schedule of the history match was based on these production and injection data. The history match was conducted using the supplied gas production and injection rates as constraints.

Data on the composition of the produced gas during the first back-production were taken, as well as further observations during that test were taken by Vandeweijer et al, 2008. From the second back-production tests, only indirect observations, such as short duration and high CO_2 concentrations, were available (supplied by operator). Other observations from K12-B (such as actual gas-water-ratios) were also obtained from the operator ENGIE.

5.4 Results

Figure 32 shows the simulated gas and water production rates. The maximum simulated water production is around 120 m^3/mlnNm^3 and drops with the reduced gas production rates. This is considerably higher than the observed value of 40 m^3/mlnNm^3. A possible explanation is the high salinity of the reservoir fluid. Although the ratio of free water is negligible, a considerable amount of pore water is present. Therefore, the vapour pressure in the gas is in equilibrium with this pore water. The high salinity of the pore water reduces the vapor pressure, and therefore, the water content in the gas compared to low salinity conditions (Panin and Brezgunov, 2006). The vapour pressure in the reservoir simulator is not a function of pore water salinity but is referenced to freshwater conditions. Therefore, the simulations overestimate the vapor pressure, and as a result the water production rate.

The measured CO_2 content data of the off-shore detection equipment was assumed to be based on molar fractions. Comparing the simulated CO_2 concentration with the measured values (Figure 34) indicates that the simulated CO_2 concentration in the produced gas is initially higher than the measured values. This can probably attributed to more distinct spreading and dispersion of the CO_2 in reality in comparison to the simulations.

The second group of measurement were taken around November 2008 (Figure 34), which is 11 months after the start of the resumed production. The measured value of 0.2 again are similar to the simulated values at that time.

The CO_2 content remains constant during the 2.5 years after the first back-production period (Figure 33). Careful examination of the production rates revealed production rates of very short duration during that period. Apparently the operator was attempting to reopen the well B8 during this period.

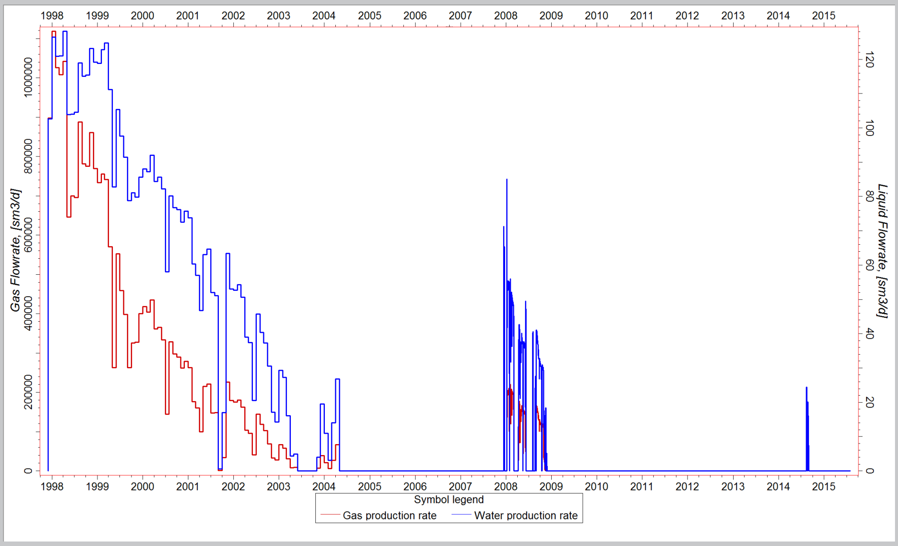

Figure 32 Simulated gas production rate (red) and water production rates (blue).

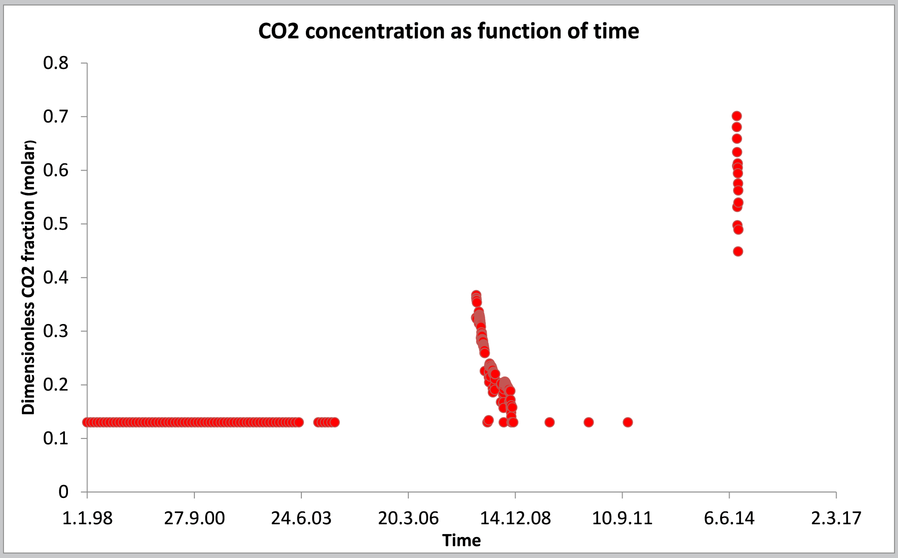

Figure 33 Simulated CO_2 mole fraction of the produced gas, as function of time.

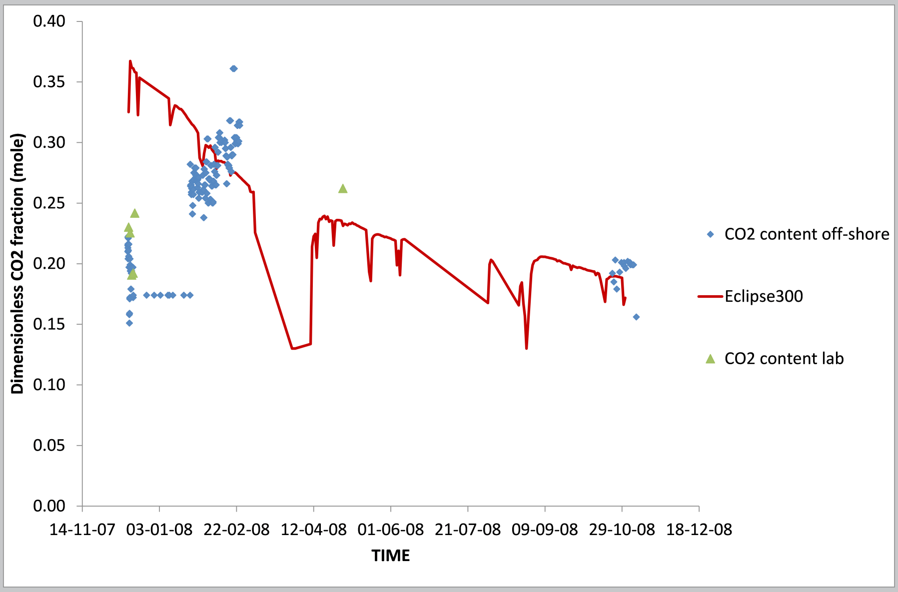

Figure 34 Simulated (red line) versus measured (green for lab analyzed gas samples, and blue for in-situ detection at the platform) CO_2 molar fractions during the first back-production experiment.

Figure 33 shows that the simulated CO_2 mole fraction in the second back-production period is 0.7. The measured concentrations for the second back-production experiment were in the range of 0.45-0.5. This indicates that the spreading away of from the well B8 is more pronounced in reality than simulated by the reservoir model.

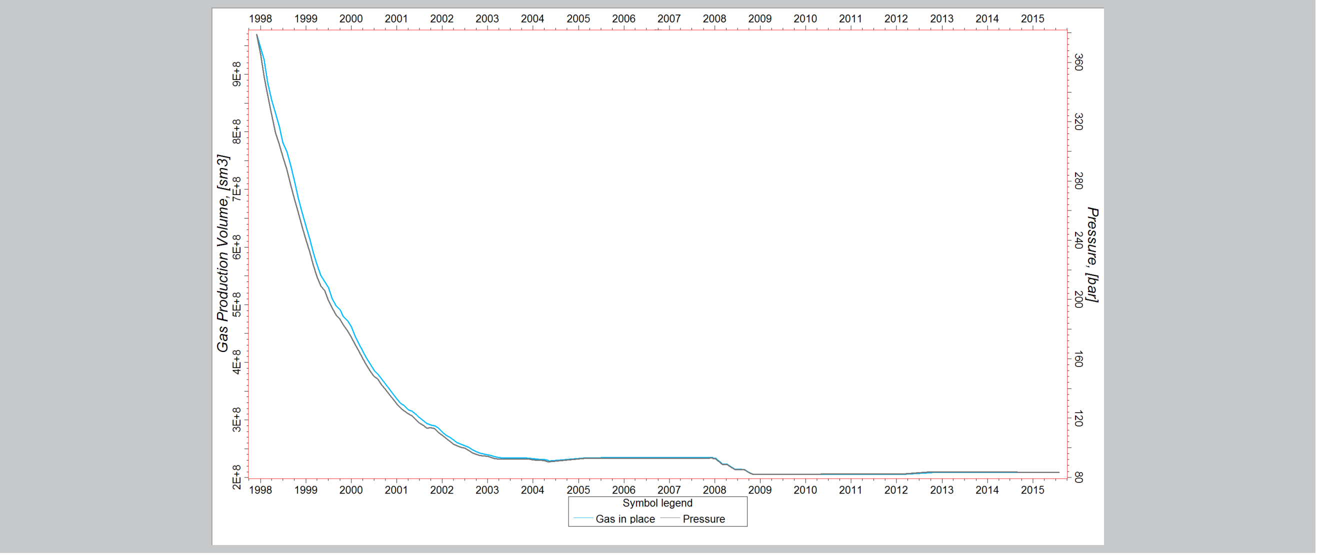

Figure 35 Gas production volume and corresponding reservoir pressure as a function of time.

Figure 35 shows that the gas-initially in place (GIIP) of the simulation is 9.6 *108 Sm^3, which is similar to the estimations of the 8.8 and 9.7 * 108 Sm^3 of the GIIP acceding to the volumetric and material balance calculations, respectively.

Figure 35 shows that the simulated reservoir pressure rises slightly during the suspended state of the well B8 between 2005 and 2008. This rise in pressure can be attributed to a subdivision of compartment 4. Apparently two sub-compartments exist that are divided by a low transmissivity fault. Due to the fault, a higher pressure was conserved in one sub-compartment that gradually releases its pressure to the main sub-compartment where well B8 is located.

However, a comparison between the simulated and measured CO_2 fractions during first back-production experiments in 2007-2008 shows that simulated values are too high and also provide a different temporal pattern. This means that the actual fate and transport of the CO_2 in the reservoir cannot be fully captured by the simulator.

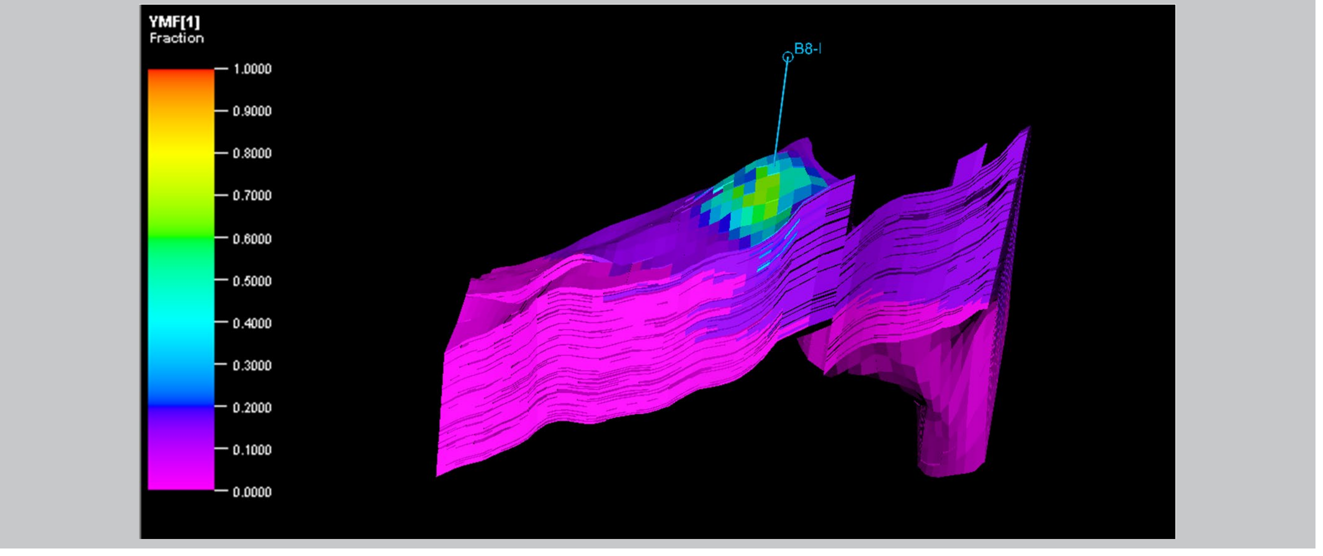

Figure 36 Cross section of molar CO_2 fraction prior to first back-production on November 1st, 2007.

The hypothesis of two sub-compartments that are connected by a low transmissitiy fault is illustrated in Figure 36 and Figure 37. The injected CO_2 does not spread across the reservoir but stays rather close to the injector (Figure 36, Figure 37). After the second back-production period the molar fractions near the well B8 are even higher in early 2015. This corresponds to the simulation result, that simulated concentrations are higher than observed concentrations at the beginning of both back-production periods. It appears that the back-production pulls the CO_2 closer to the well.

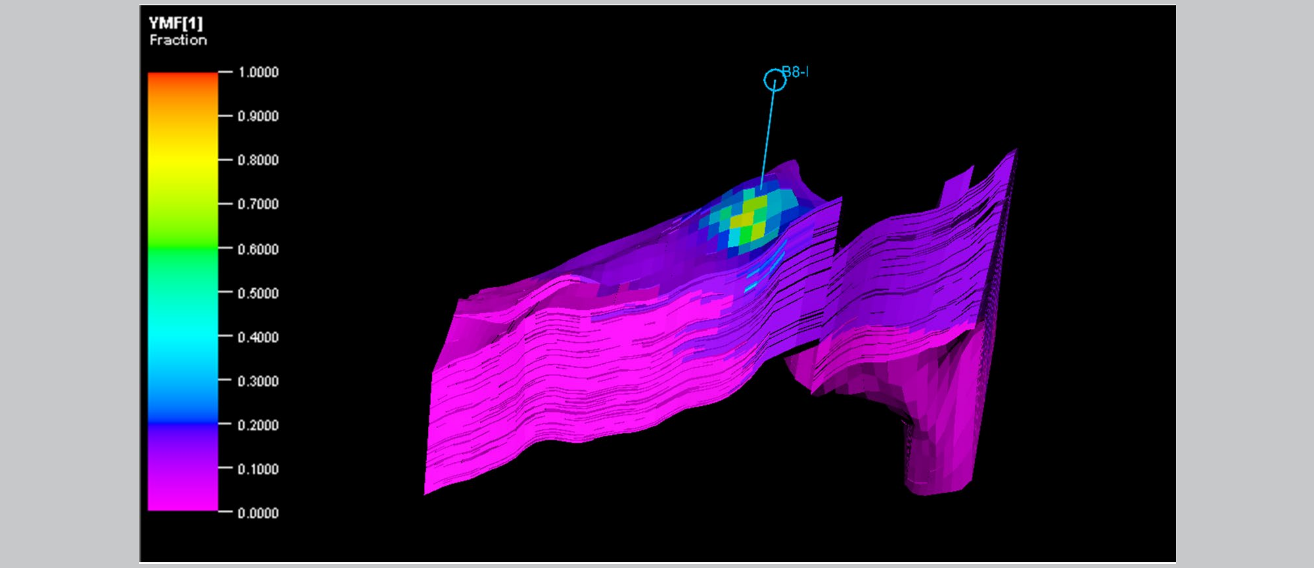

Figure 37 Cross section of molar CO_2 fraction after second back-production period on January 1st, 2015.

The cumulative injection into the B8 well is 18,710 t, from which 11,974 t was injected before the first back-production test and 6,736 t after the first back-production test

The amount of produced CO_2 was 300 t (along significant amounts of natural gas) during the first test and 20 t (at much higher concentration) during the second test, in 2014. This means that 2.5 % of injected CO_2 was produced in the first test and 0.11 % of injected CO_2 was produced during the second test.

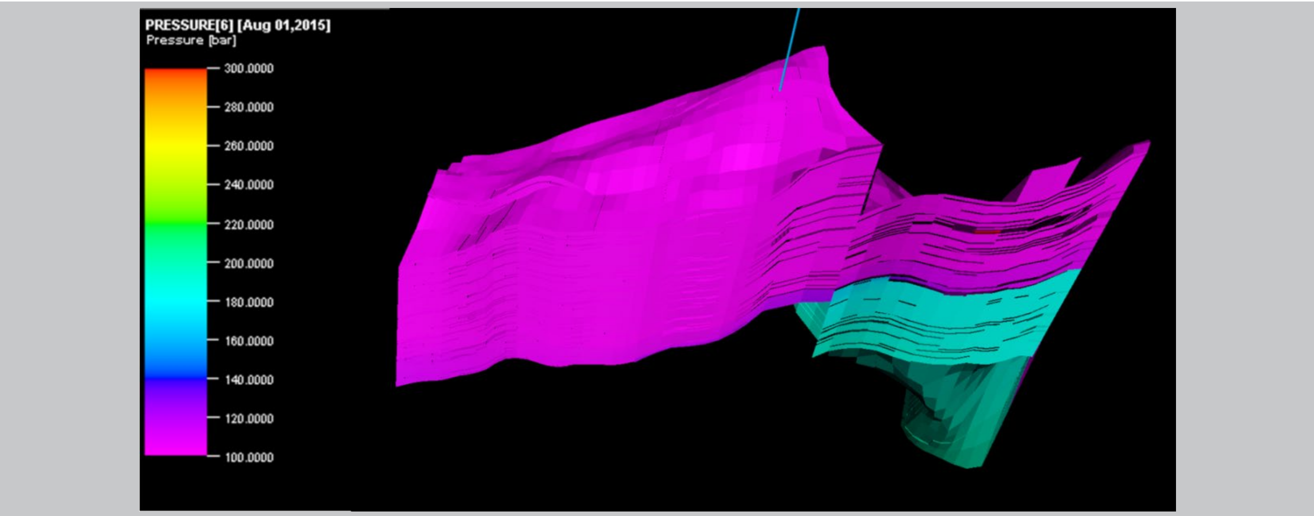

Figure 38 Pressure distribution in the K12-B reservoir at 1 November 2006. Higher pressure in the sub-compartment on the lower right.

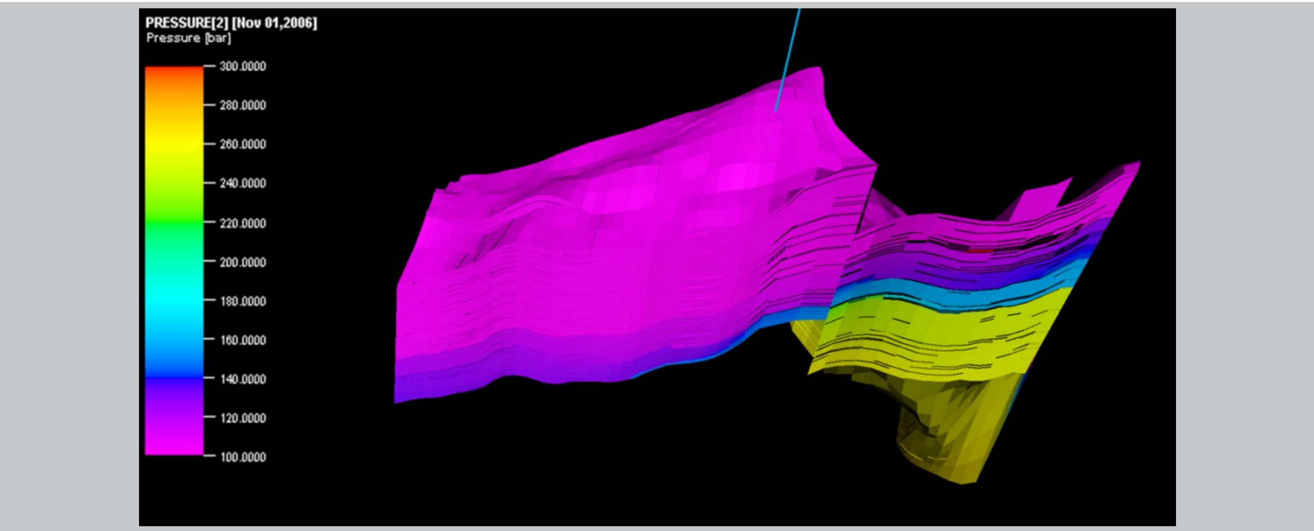

Figure 39 Pressure distribution in the K12-B reservoir at 1 August 2015. Both sub-compartments are near pressure equilibrium.

Figure 38 shows the pressure distribution on November 1st 2006. At this time the conventional production at the well B8 has ceased. The pressure in the right sub-compartment is higher than that in the left sub-compartment with the well B8. This is due to the low transmissivity of faults between the two sub components. The success during the first back-production can possibly be attributed to a delayed pressure support through fault 2.

Figure 39 shows that the pressure is almost at equilibrium in 2015. This explains the short second re-production period. If the hypothesis of two sub-compartments connected by a low transmissivity fault it true, a third re-production period would also not be successful.

5.5 Discussion

A compositional model was applied for history matching two back-production experiments at the mature gas field K12-B. Although the predictions are close to the actual measurements, it cannot completely reproduce the measured values as a function of time. A considerable amount of gas could be produced on the first back- production period, only a very small amount was retrieved during the second back-production period. A plausible explanation for this behaviour was found. The reservoir is divided in two sub-compartments that are connected by a low transmissivity fault. After the end of the regular gas production, the second sub-compartment was still pressurized with the consequence of continous gas flow into the main sub-compartment with the producing well B8. During a further waiting period the overpressure of the small sub-compartment was nearly equilibrated and only very little amount of gas could penetrate into the main sub-compartment. Therefore only a small amount of gas could be retrieved during the second back-production period. A further back-production period does not appear to be successful. The amount of back-produced CO_2 was 2.5 % during the first and around 0.1 % during the second back-production period. As the two tests were ended when the production had ceased, the maximum possible volume of CO_2 was back-produced. The back-production experiments were carried out when the gas reservoir was very mature and reservoir pressure decreased to around 80 bar. The back-production rates can be expected to be higher when the gas reservoir filled until values close or equal to the initial reservoir pressure (around 380 bar), commonly used for CCS projects.

6 SUMMARY

The field experiment at the Ketzin pilot site has shown that a safe back-production of CO_2 is generally feasible, and can be performed at both stable reservoir and wellbore conditions. The official permission document by the Mining Authority of the Federal State of Brandenburg for starting the experiment, and a brief summary of key operational data were provided as Milestones 10 and 11. The recorded pressure and temperature data were released to the modelling groups.

Over the entire test period, the back-production of CO_2 at the pilot site Ketzin ran stable and reliable regarding the CO_2 production rates and the corresponding pressure values above and below ground. There were no work accidents or environmental-related events.
From October 15 to 27, 2015, approximately 240 tonnes of CO_2 and around 62 tonnes of deposit water were produced from the wellbore Ktzi 201. The extracted gas consisted of> 97% of CO_2. As second most component nitrogen was observed. The gas was released by a stack system in the ambient air. The co-produced high-saline formation water has been disposed as waste.

The back-production experiment at Ketzin shows that the reservoir pressure can be effectively lowered by the back-production of CO_2. However, the pressure level reestablishes rapidly after the back-production is stopped. No permanent reduction of the reservoir pressure could be observed. Even at low rates significant amounts of brine are produced at a much higher rate than previously expected. Hence, its disposal requires additional effort. In conclusion, it can be said that back-production of small amounts is feasible as a temporal remediation measure.

The reservoir model developed for the Ketzin field was history-matched using the bottomhole pressure data recorded during the CO_2 back-production experiment. Scenarios considering back-production for an extended period were also simulated assuming both constant and variable production rates in order to understand the associated reservoir pressure behaviour. The simulated bottomhole pressures at the well Ktzi 201 indicate that the decrease in pressure would potentially range between 10-40 bars if the back-production is sustained for a period of four months.

A near wellbore geomechanical model based on Ketzin field has been developed. The whole cycle of well drilling, completion, CO_2 injection and back-production was simulated. It has been found that the pressure increase induced by CO_2 injection can marginally enlarge the failure zone around the wellbore. On the other hand, decreasing the near wellbore pore pressure has almost no effect on the failure zone developed earlier, and its size remains the same after CO_2 back-production.

For the K12-B gas field as a real-production case study, two back-production periods have been investigated. Although the numerical predictions are close to the actual measurements, they cannot completely reproduce the measured values of gas and water production as a function of time. The given structure of the reservoir (compartments with different pressure levels, low transmissivity faults) constitute challenging constraints for the applied compositional reservoir simulator. Further numerical studies needs to be applied here.

References

BGS, 2008. A joint research project report on "Reactions between CO_2 and borehole infrastructure" by British Geological Survey, Imperial College, IFP Energies Nouvelles and Bureau de Recherches Géologiques et Minières (2008): Report submitted to European Commission during the CO_2GeoNet project.

Birkholzer, J. T., Zhou, Q., and Tsang, C.-F., 2009. Large-scale impact of CO_2 storage in deep saline aquifers: A sensitivity study in pressure response in stratified systems. International Journal of Greenhouse Gas Control 3, 181-194.

Celia, M.A., Bachu, S., Nordbotten, J. M., Gasda, S.E. and Dahle, H.K. (2005): Quantitative Estimation of CO_2 Leakage from Geological Storage: Analytical Models, Numerical Models and Data Needs. In Rubin, E.S., Keith, D.W. and Gilboy C.F. (eds.) Proceedings of 7th International Conference on Greenhouse Gas Control Technologies (GHGT-7). September 5-9, 2004, Vancouver, Canada, v.I, 663–672

Chen, F., Wiese, B., Zhou, Q., Kowalsky, M., Norden, B., Kempka, T., Birkholzer, J. (2014): Numerical modeling of the pumping tests at the Ketzin pilot site for CO_2 injection: Model calibration and heterogeneity effects, International Journal of Greenhouse Gas Control 22, 200-212.

Class, H., Mahl, L., Ahmed, W., Norden, B., Kühn, M., Kempka, T. (2015): Matching pressure measurements and observed CO_2 arrival times with static and dynamic modelling at the Ketzin storage site. European Geosciences Union General Assembly 2015, EGU, Division Energy, Resources & Environment, ERE, Energy Procedia 76, 623 - 632, doi: 10.1016/j.egypro.2015.07.883.

Grond, L. and Holstein, J. (2014): Power-to-gas: Climbing the technology readiness ladder. Gas for Energy 2, 20-25.

James, R. (2013): Novel CO_2 Utilization Concepts: Working Paper. US Department of Energy DOE/NETL-2012/1588.

Kempka, T., Kühn, M. (2013): Numerical simulations of CO_2 arrival times and reservoir pressure coincide with observations from the Ketzin pilot site, Germany, Environmental Earth Sciences, 70 (8), 3675-3685.

Kempka,T., Class, H., Görke, U.-J., Norden, B., Kolditz, O., Kühn, M., Walter, L., Wang, W., Zehner, B. (2013): A Dynamic Flow Simulation Code Intercomparison based on the Revised Static Model of the Ketzin Pilot Site. Energy Procedia, Volume 40, Pages 418-427, doi:10.1016/j.egypro.2013.08.048.

Manceau, J.-C., Hatzignatiou, D. G., de Lary, L., Jensen, N. B., Réveillère, A. (2014): Mitigation and remediation technologies and practices in case of undesired migration of CO_2 from a geological storage unit - Current status. International Journal of Greenhouse Gas Control 22, 272–290. doi: 10.1016/j.ijggc.2014.01.007

Martens, S., Kempka, T., Liebscher, A., Möller, F., Schmidt-Hattenberger, C., Streibel, M., Szizybalski, A., Zimmer, M. (2015): Field experiment on CO_2 back-production at the Ketzin pilot site. European Geosciences Union General Assembly 2015, EGU, Division Energy, Resources & Environment, ERE, Energy Procedia 76 (2015) 519 - 527, doi: 10.1016/j.egypro.2015.07.902.

Neele, F., Quinquis, H., Read, A., Wright, M., Lorsong, J., Poulussen, D. F., 2014. CO_2 storage development: Status of the large European CCS projects with EEPR funding. Energy Procedia 63, 6053-6066.

Nordbotten, J.M., Celia, M.A., Bachu, S., Dahle, H.K. (2005): Semi-analytical Solution for CO_2 Leakage through an Abandoned Well, Environ. Sci. Technol. 39, 602-611.

Norden, B. & Frykman, P. (2013): Geological modelling of the Triassic Stuttgart Formation at the Ketzin CO_2 storage site, Germany, International Journal of Greenhouse Gas Control 19, 756-774.

Panin, G.N. and Brezgunov, V.S. (2006): Influence of the salinity of water on its evaporation. Atmospheric and Oceanic science 43-663-665.

Pruess, K. (2006): On CO_2 Behaviour in the Subsurface, Following Leakage from a Geologic Storage Reservoir. Lawrence Berkeley National Laboratory, 12. PROCEEDINGS, CO_2SC Symposium Lawrence Berkeley National Laboratory, Berkeley, California, March 20-22, 2006, 178-181. www.osti.gov/scitech/servlets/purl/881621

Pruess, K. (2008): Leakage of CO_2 from geologic storage: Role of secondary accumulation at shallow depth. International Journal of Greenhouse Gas Control 2, 37-46.

Schlumberger. Eclipse Technical Manual 2009.

Vandeweijer, V. P., Van der Meer, L. G. H, Hofstee, C. (2008): Monk Monitoring K12-B. TNO Report 2008-U-R1329/B

Vandeweijer, V. P., Van der Meer, L.G.H, Hofstee, C., Mulders, F. M. M, D'Hoore, D., Graven, H. (2011): Monitoring the CO_2 injection site: K12-B. Energie Procedia 4, 5471-5478.

Van der Meer, L. G. H, Kreft, E and Geel, C. R. (2005): K12-B: A test site for CO_2 storage and enhanced gas recovery. SPE 94128.

Van der Meer, L. G. H., Arts, R. J., Geel, C. R., Hofstee, C., Winthaegen, P., Hartman, J., D'Hoore, D. (2009), K12-B: Carbon dioxide injection in a nearly depleted gas field offshore the Netherlands, in M. Grobe, J. C. Pashin, and R. L. Dodge, eds., Carbon dioxide sequestration in geological media—State of the science: AAPG Studies in Geology 59, p. 379–390.

Yamamoto H., Zhang K., Karasaki K., Marui A., Uehara H. and Nishikawa N. (2009): Numerical investigation concerning the impact of geologic storage on regional groundwater flow. International Journal of Greenhouse Gas Control 3, 586-599.

Chapter IX

Brine/water withdrawal as pressure management and flow diversion option for a CO_2 storage operation

Rajesh Govindan[1], Zhenggang Nie[1], Sevket Durucan[1], Anna Korre[1]
[1] Imperial College, UK

SUMMARY

This element of the MiReCOL project aims to investigate the feasibility of brine withdrawal technique and test its effectiveness for pressure management and CO_2 flow diversion in a storage reservoir. The study uses a field-scale reservoir model of the P18-A block, which represents a group of three depleted gas fields, namely the P18-2, P18-4 and P18-6 fields, located in the Dutch offshore region, 20 km north-west of Rotterdam, at an average depth of 3,500m below sea level. The model was made available by TNO in the MiReCOL project model database. Three scenarios were investigated by selecting the largest field in the block, namely the P18-2 field, which is broadly divided into three compartments. The results obtained using the CO_2 injection and brine production simulations were individually analysed and the key performance indicators (KPIs) for each scenario, namely: (a) well layouts for remediation; (b) volume of extracted brine; (c) longevity of remediation; (d) response time of remediation; (e) spatial extension of remediation; and (f) the estimated costs of remediation, are summarised in this report.

1 INTRODUCTION

A number of risks are associated with the underground storage of CO_2. The risks are mechanisms that could lead to the migration of CO_2 outside the storage complex, into the shallower formations, and ultimately resulting in surface emissions to the atmosphere. These include CO_2 leakage through: (a) sub-seismic faults that were undetected during the site characterisation phase prior to injection; (b) geomechanical effects, such as the reactivation of faults and the creation of new fractures in the caprock due to reservoir over-pressure created during injection (Rutqvist et al., 2007, 2008); (c) presence of improperly plugged abandoned wells in the field (Carroll et al., 2009; Zheng et al., 2009; Apps et al., 2010); and (d) geochemical reactions between CO_2 and the caprock (IEAGHG Report, 2007). In particular, over-pressurisation of the reservoir is of concern because it could have a large-scale impact, namely interference with the operations in neighbouring oil and gas fields, or CO_2 storage sites that could co-exist in the same formation. Such interference also has regulatory implications since issuing permits to operators would then be based on the outcome of a multi-site process evaluation, which can be quite involved, and rather unnecessary (Birkholzer and Zhou, 2009).

In view of the potential risks, contingency planning and analysis of leakage remediation is thus a requirement in order for the operator to obtain a permit for CO_2 storage. Some of the remediation options that were investigated in the current MiReCOL project include: (a) injection of sealant materials, such as polymer-gel solutions to create a localised reduction in permeability, either inside the reservoir or above the caprock, in order to divert the migration of the plume; (b) injection of brine in the reservoir to create a competitive fluid movement or enhance CO_2 dissolution; (c) injection of brine in a high permeability formation above the caprock in order to create a pressure (hydraulic) barrier; and (d) production of brine from the reservoir in order to regulate its pressure during injection, enhance the efficiency of CO_2 storage (or capacity utilisation), and possibly induce plume steering.

1.1 Review of the application of reservoir brine production in CO_2 storage

Benson and Hepple (2005) investigated scenarios wherein the leakage of CO_2 through various pathways, such as faults and fractures, were modelled. It was demonstrated that by producing brine from the reservoir, the pressure-driven leakage was minimised and consequently the net of amount of leakage is largely buoyancy-driven, thus reducing the rate of leakage. While pressure management via brine extraction is not be considered a mandatory component for large-scale CO_2 storage projects, it could also potentially provide many other benefits, such as increased storage capacity utilisation, simplified permitting, smaller area of review for site monitoring, and the manipulation of CO_2 plume in order to increase its sweep efficiency (Birkholzer et al., 2012).

Buscheck et al. (2011) coined the acronym 'ACRM', which stands for active CO_2 reservoir management, wherein CO_2 injection is combined with simultaneous brine production for the storage in saline formations. The specific reservoir performance objectives of ACRM are to relieve pressure build-up, increase CO_2 injectivity, increase available pore space and storage capacity, manipulate CO_2 migration, and constrain brine migration. In summary, ACRM enables greater control of subsurface fluid migration and pressure perturbations. Additionally, Buscheck et al. (2012) provide a qualitative overview of the subsequent options to handle the produced brine, including desalination, saline water for cooling the towers at the CO_2 capture facility, source of makeup water for enhanced oil recovery (EOR) systems, and geothermal energy production. Various industries provide evidence that brine-sourced heat, minerals, and water are marketable products that present an opportunity for considering the brine as a resource (Breunig et al., 2013).

In terms of plume steering, the use of brine production has been analysed for CO_2 injection from a single vertical well surrounded by a ring of vertical brine production wells (Buscheck et al., 2011; Court et al., 2011). Court et al. (2011) found a single ring of four vertical production wells, has a negligible steering potential on the CO_2 plume and concluded that complex well placement strategies would need to be devised. On the other hand, Buscheck et al. (2011) showed significant steering potential with the availability of many more brine producing wells in the neighbourhood. However, this option is economically viable for depleted oil and gas reservoirs that could have a myriad of exploration and hydrocarbon production wells.

Buscheck et al. (2011) also showed that by extracting brine from the lower portion of the storage formation, much of the buoyancy force that tends to drive CO_2 to the top of the storage formation is counteracted, thereby higher storage efficiency is obtained, and injectivity is improved. However, Bergmo et al. (2011) concluded that in order to utilise an additional fraction of 1-2% of the pore volume for CO_2 storage, it is necessary to produce significant amounts of brine from the reservoir.

Another important aspect in brine production is considering the possibility of eventual CO_2 breakthrough at brine production wells (Buscheck et al., 2012). Therefore, the general challenge for brine production is to determine the operational parameters, such as the number, location and type (vertical or horizontal) of wells, spacing between the wells, and the corresponding rates of brine production so that while the targeted pressure relief is achieved, CO_2 breakthrough time is also delayed. Solving this trade-off requires separate process-optimisation studies in order to determine the best CO_2 injection-brine production strategy, including cost optimisation, for each storage site that is selected.

1.2 Objectives of the study

The objectives of the study described in this report is to perform numerical modelling of brine withdrawal technique and test its effectiveness for pressure management and CO_2 flow diversion in a storage reservoir. Different scenarios were considered to determine the key performance indicators (KPIs) of the technique under the scope of the MiReCOL project, namely: (a) well layouts for remediation; (b) volume of extracted brine; (c) longevity of remediation; (d) response time of remediation; (e) spatial extension of remediation; and (f) the estimated costs of remediation.

In particular, the study area and the reservoir model characteristics are described in section 0. It is one of many models in the MiReCOL project model database, and represents an offshore and compartmentalised depleted gas reservoir. In section 0, the scenarios considered are described and the results and their KPI analyses are presented. The conclusions from this study and some recommendation for future work are made in section 0.

2 DESCRIPTION OF THE STUDY AREA

2.1 P18-A block

The P-18A block represents a group of three depleted gas fields, namely the P18-2, P18-4 and P18-6 fields, located in the Dutch offshore region, 20 km north-west of Rotterdam, at an average depth of 3,500m below sea level. The clastic reservoir rocks in these fields form a part of the Triassic Main Buntsandstein Subgroup with a discomformably overlying primary seal comprising of siltstones, clay stones, evaporates and dolostones. The gas fields are heavily faulted, hence forming hydraulically isolated compartments that are either fully or partially closed to their surroundings, as illustrated in Figure 1.

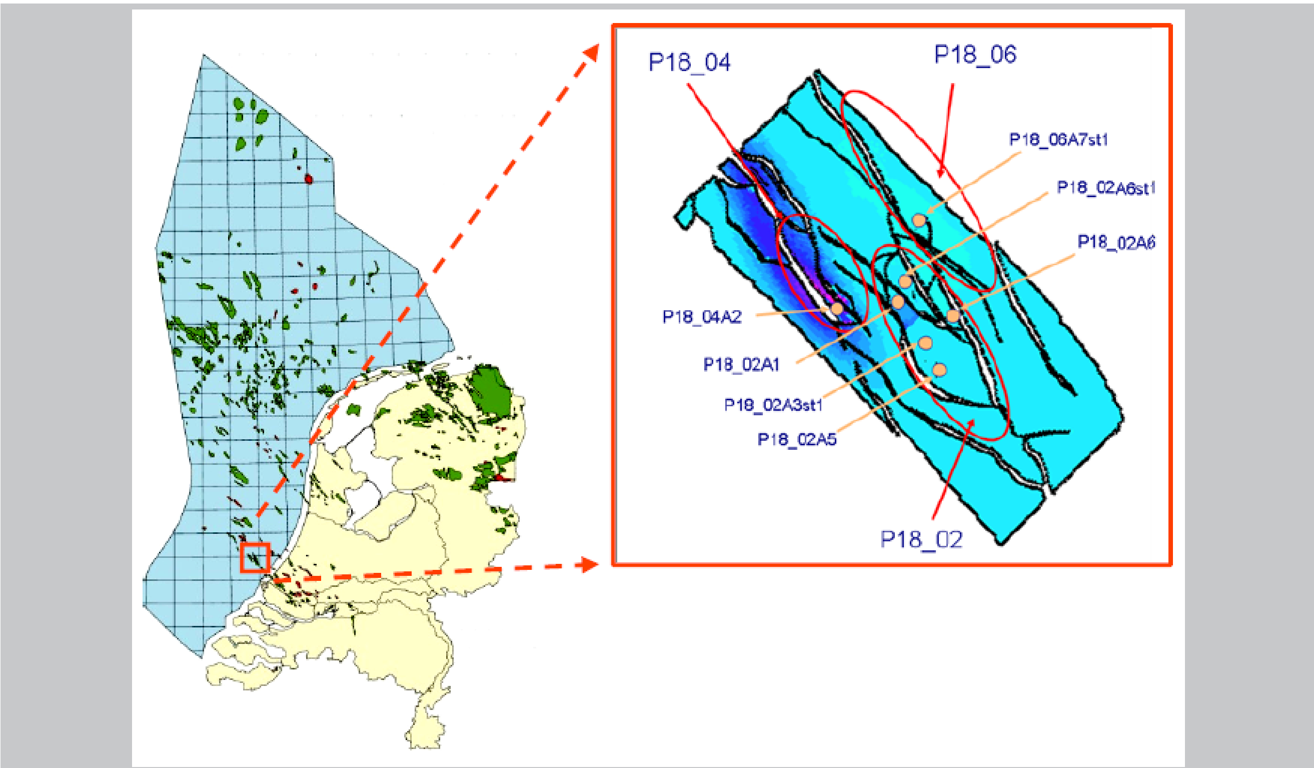

Figure 1 The offshore location of the P18-A block, comprising of the depleted gas fields P18-2, P18-4 and P18-6 (after Gutierrez-Neri et al. (2012), the CATO-2 project).

2.1.1 Structural history

The deposition and deformation of the P18-A block was strongly controlled by a sequence of rift pluses that started during the Late Triassic period (Arts et al., 2012). Prior to the rifting events, sedimentation initially included the lacustrine sediments, followed by sandy fluvial and Aeolian successions that constitute the Main Buntsandstein Subgroup. During the active rifting period, several rift pulses broke up the basin into a number of NW-SE trending compartments bounded by faults (De Jager, 2007). Figure 2 illustrates the compartments that resulted from the rifting events in the P18-A block.

2.1.2 Reservoir geology

The structures containing the depleted gas reservoirs are bounded by the faults in a horst and graben configuration, with a sinistral strike-slip component. The reservoir rocks are broadly divided into three formations formed by the cyclic alternation of arkosic sandstones and clayey siltstones of approximately 200m in thickness (Arts et al., 2012).

The Volpriehausen formation at the bottom part of the reservoir is mainly fluvial, but also contains some aeolian sediments. It consists of braided river deposits interbedded with subordinate flood-plain and crevasse-splay and locally dune deposits (Ames and Farfan, 1996).

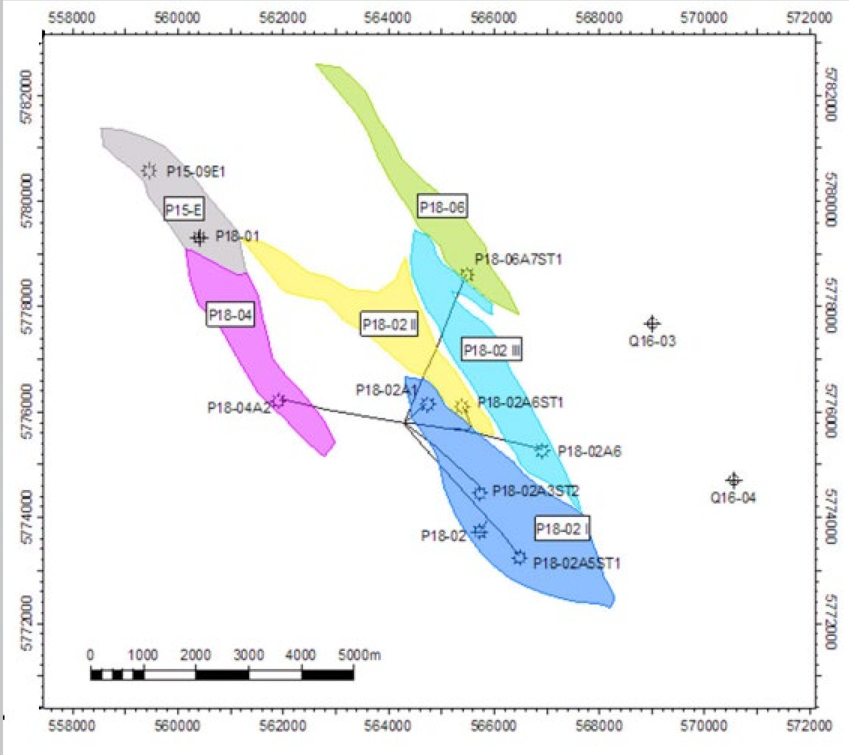

Figure 2 The compartmentalisation of the P18-A block (after Paginer et al. (2011), the CATO-2 project).

The overlying Detfurth formation comprises mainly of aeolian sediments (dunes), with some fluvial deposits (Ames and Farfan, 1996). It is generally marked by low gamma-ray values owing to the presence of quartz-cementation (Geluk et al., 1996). The upper part of the formation is distinctly separated from the lower part by a well-correlatable interval of relatively higher gamma-ray values and a single coarsening-upward sequence.

The Hardegsen formation is the youngest part of the Main Buntsandstein Subgroup. It mainly consists of aeolian deposits overlain by the Solling sandstone member at the top part of the reservoir, which is characterised by an increase in the gamma-ray values compared to the underlying Detfurth formation.

2.2 P18-A reservoir model

2.2.1 Structural and geological model

A field-scale reservoir model of the P18-A block was made available by TNO in the MiReCOL project model database. The model was previously developed and history matched using gas production data within the Dutch CATO-2 research program. The model grid spans an area of approximately 20.5km×7.5km and includes several faults whose structural characteristics result in variable horizontal transmissibility ranging from sealing to non-sealing nature.

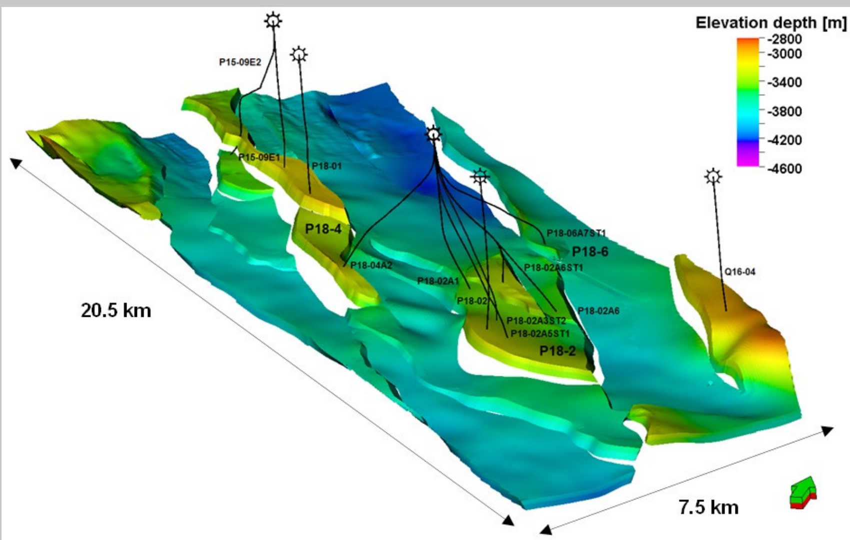

Figure 3 The structural model of the P18-A block and well locations.

The grid represents the Main Buntsandstein reservoir subdivided into four zones, namely (from bottom to top): (1) the Volpriehausen formation with an average thickness of 115m and resolution of 50m×50m×115m; (2) the lower Detfurth formation with an average thickness of 22m and resolution of 50m×50m×22m; (3) the upper Detfurth formation with an average thickness of 48m and resolution of 50m×50m×48m; and (4) the Hardegsen formation with an average thickness of 30m and resolution of 50m×50m×30m. The depth of the model ranges between 2,850m and 4,500m. Figure 3 illustrates the structural model of the depleted gas fields in the P18-A block and well locations previously used for gas production.

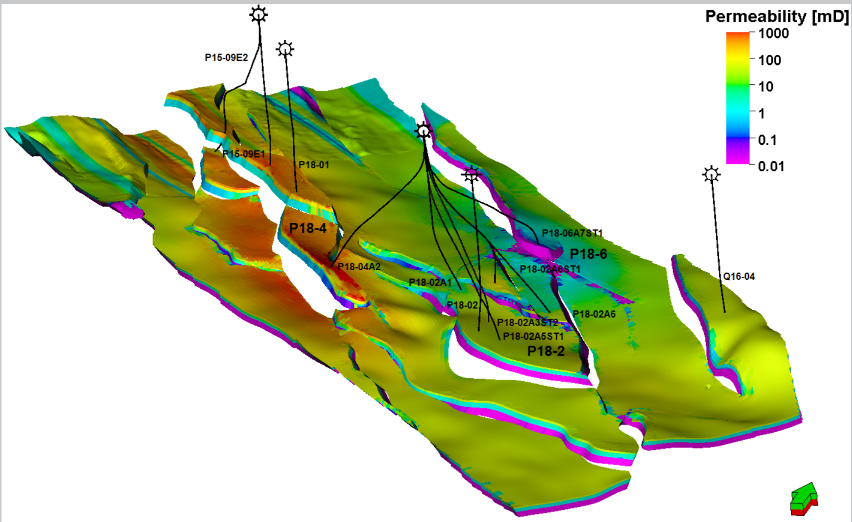

Figure 4 The horizontal permeability distribution of the P18-A block.

The MiReCOL database also includes the petrophysical property attributions for porosity, permeability and net-to-gross ratio that were generated by TNO from the information available in the well logs using the block kriging technique. Figure 4 illustrates the horizontal permeability distribution as an example. In addition, Table 1 summarises the petrophysical properties for different reservoir zones in the model.

Table 1 The summary of petrophysical properties in the model.

Reservoir zones	Porosity				Horizontal Permeability (mD)*				NTG			
	min	mean	max	st.dev	min	mean	max	st.dev	min	mean	max	st.dev
Hardegsen	0.01	0.08	0.18	0.03	10^{-4}	130	1,977	206	0.01	0.96	1	0.1
Upper Detfurth	0.01	0.05	0.13	0.02	10^{-4}	34	751	93	0.01	0.77	1	0.3
Lower Detfurth	0.01	0.05	0.11	0.02	10^{-5}	24	1,133	97	0.01	0.83	1	0.3
Volpriehausen	0.01	0.03	0.11	0.01	10^{-5}	0.16	307	1.8	0.01	0.25	1	0.3

* Vertical permeability = 0.1 × Horizontal permeability (Arts *et al.*, 2010)

2.2.2 Dynamic properties of the reservoir model

The initialisation for CO_2 injection and brine production simulations performed in this study is based on the depletion condition of the fields. The pressure in the fields of the P18-A block during the post-production period in 2015 was estimated to be in the range of 25-30 bars (Arts et al., 2012; Tambach et al., 2015). Previous simulation studies have also estimated that the dynamic capacity for CO_2 storage is 30.4Mt, 8.1Mt and 0.6Mt for the P18-2, P18-4 and P18-6 fields respectively, assuming a maximum allowable pressure limit of 350 bars according to the pre-production field conditions (Paginer et al., 2011). The reservoir temperature was set to be constant at 120°C.

3 CO_2 FLOW DIVERSION AND PRESSURE MANAGEMENT IN THE RESERVOIR WITH BRINE WITHDRAWAL

A dynamic model for the simulation of CO_2 flow diversion with brine withdrawal was set up in Schlumberger's Eclipse 300 (E300) software using the static geological model and the dynamic reservoir parameters described in the previous section. It is based on the compositional option for simulating CO_2 storage in depleted reservoirs, enabled by the CO_2SOL option, wherein CO_2 can be present in three phases (Schlumberger, 2014). The modelling broadly comprise of three stages: CO_2 injection; termination of injection when plume migration beyond the field boundary (due to overfilling of the reservoir) is detected; and flow diversion of the plume with brine production.

The P18-2 field was selected for the purposes of the study in this report since it is a relatively larger field in comparison to P18-4 and P18-6 (see Figure 2). As illustrated in Figure 5, it is sub-divided into three compartments, namely P18-2 (1), P18-2 (2) and P18-2 (3), that are penetrated by six wells used for gas production.

3.1 CO_2 injection: plume migration and pressure analyses

Since the current study deals with a compartmentalised field model, it was deemed necessary to initially investigate the maximum possible CO_2 injection rates that could be implemented for each of the three compartments, the migration of the plume in the reservoir, and the pressure communication amongst the compartments, including the far-field region which lies beyond the boundary of the P18-2 field (see Figure 5). Suitable injection rates were thus chosen in order to maximise their respective dynamic capacities.

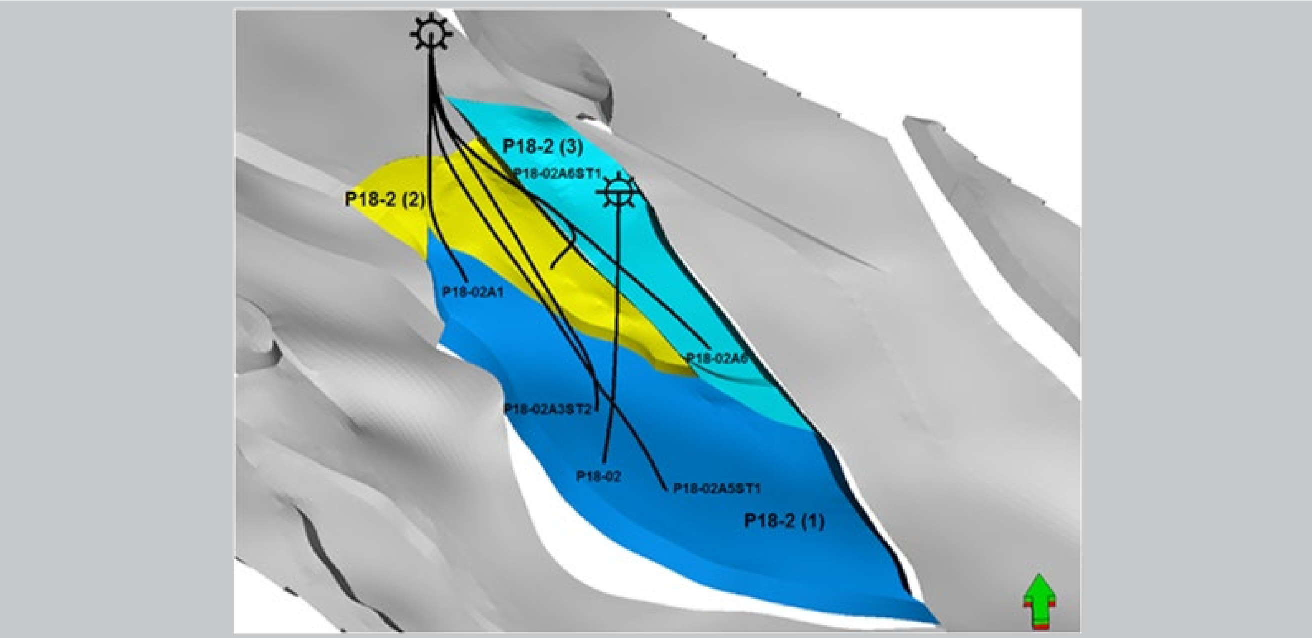

Figure 5 The P18-2 field compartments and well locations.

The migration of the plume in the reservoir was observed by visualising the gas saturation distribution and noting the fractions of the cumulative mass of injected CO_2 available in each of the compartments and the far-field region during the simulation period of 30 years.

The pressure in the compartments were also monitored during the simulation period in order to check if it ranges within the fracture pressure limit, which is assumed as 1.5 × initial reservoir pressure, prior to gas production (=350 bars).

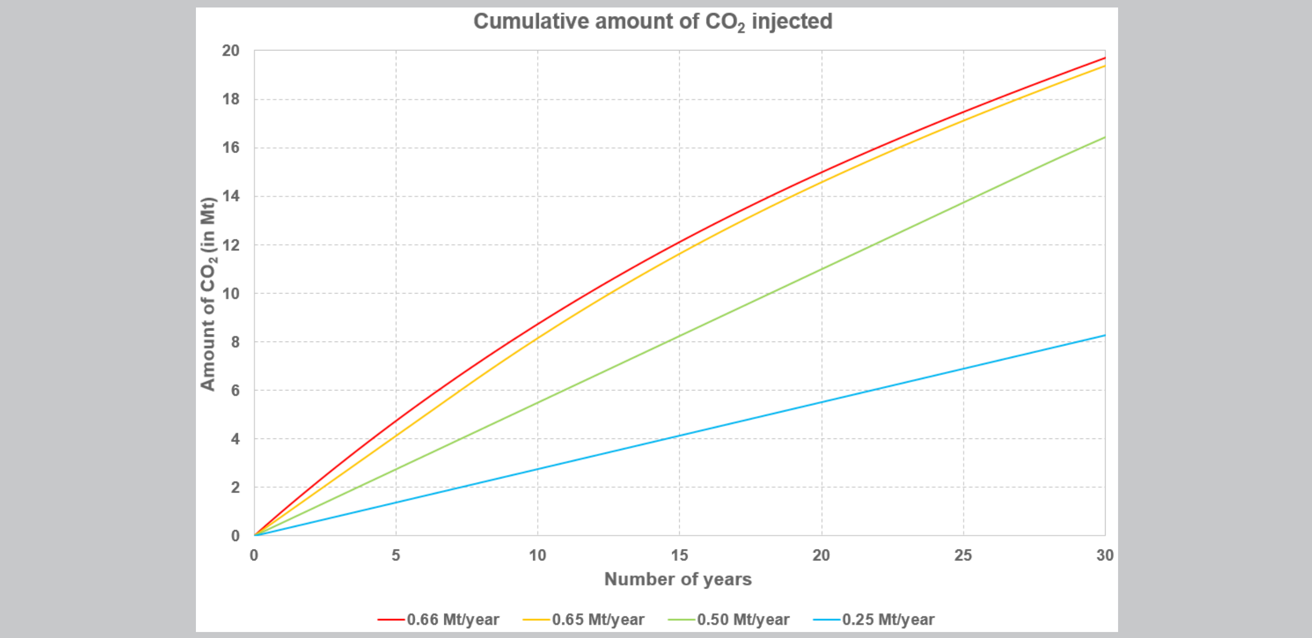

Figure 6 Cumulative amount of CO_2 injected into the P18-2 (1) compartment for different injection rates.

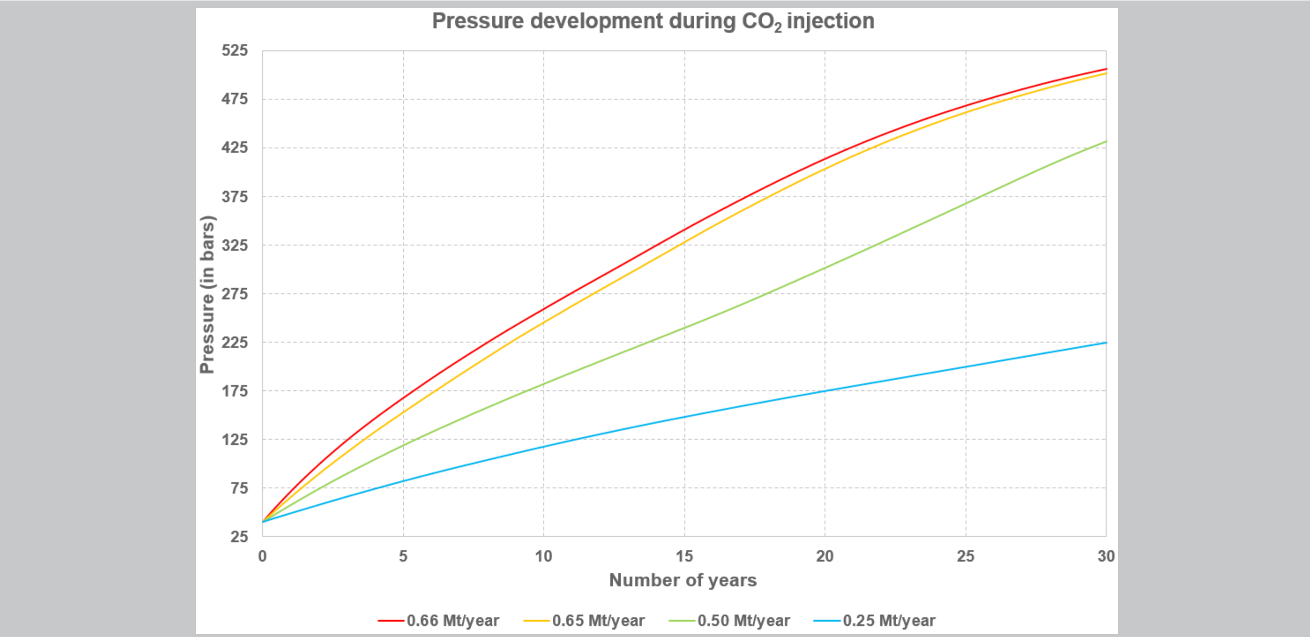

Figure 7 Pressure development in the P18-2 (1) compartment for different injection rates.

3.1.1 Compartment P18-2 (1)

The simulations for CO_2 injection in the 18-2 (1) compartment were carried out using the well P18-02. Multiple injection rates were assumed between 0-1Mt/year. The cumulative amount of CO_2 injected and the corresponding pressure build-up in the compartment were noted. The highest possible rate of injection in the compartment is 0.66Mt/year (Figure 6) while ensuring that the pressure is being maintained within the fracture pressure limit of 525 bars during the simulation period (Figure 7). Hence, the cumulative amount of CO_2 injected is 19.8Mt in 30 years. Figure 8 illustrates the plume migration in and outside the P18-2(1) compartment during CO_2 injection at 0.66Mt/year.

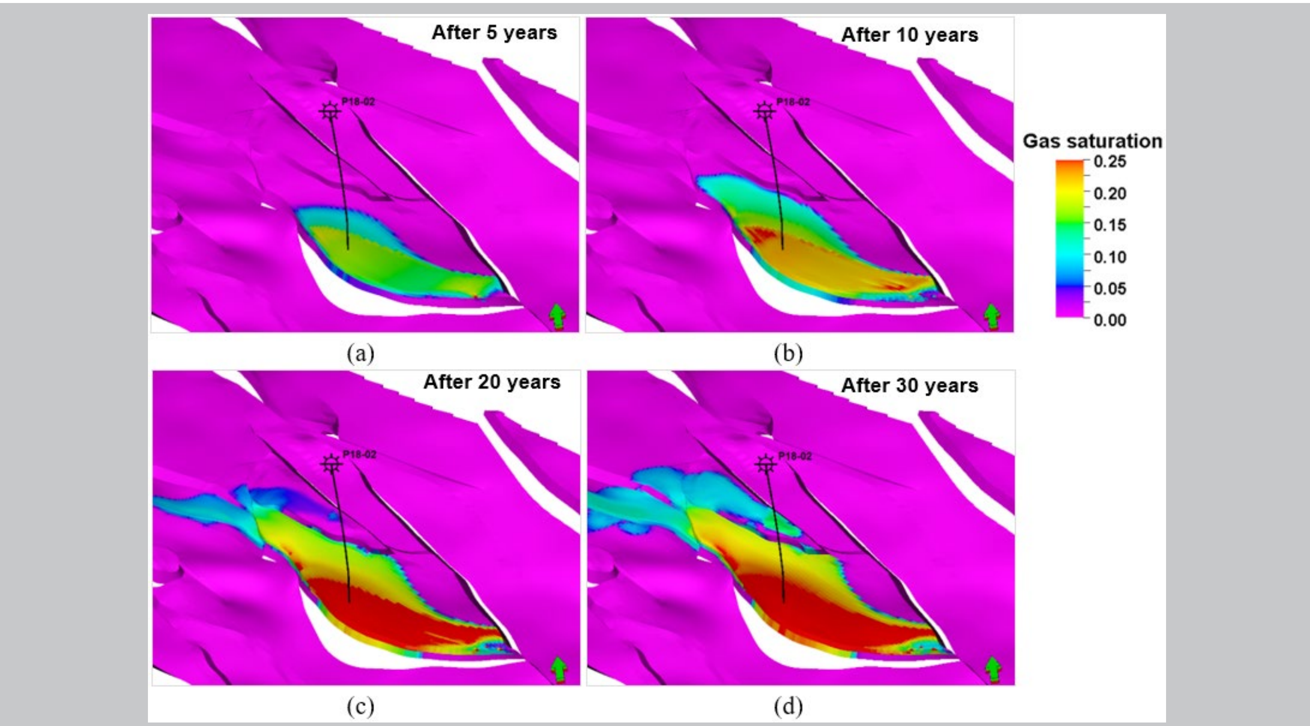

Figure 8 The estimated CO_2 plume distribution and its evolution in and outside the P18-2(1) compartment during CO_2 injection at 0.66Mt/year: (a) after 5 years; (b) after 10 years; (c) after 20 years; (d) after 30 years.

The fractions of the plume migrating outside the compartment, as illustrated in Figure 9, is related to the reservoir permeability, horizontal fault transmissibility and pressure build-up in the neighbouring compartments. For example, the highest fractional amount of plume migration occurring outside the P18-2 field, which corresponds to 1.19Mt CO_2, is caused by the relatively higher dynamic pressure gradient created between the compartments during injection (Figure 10).

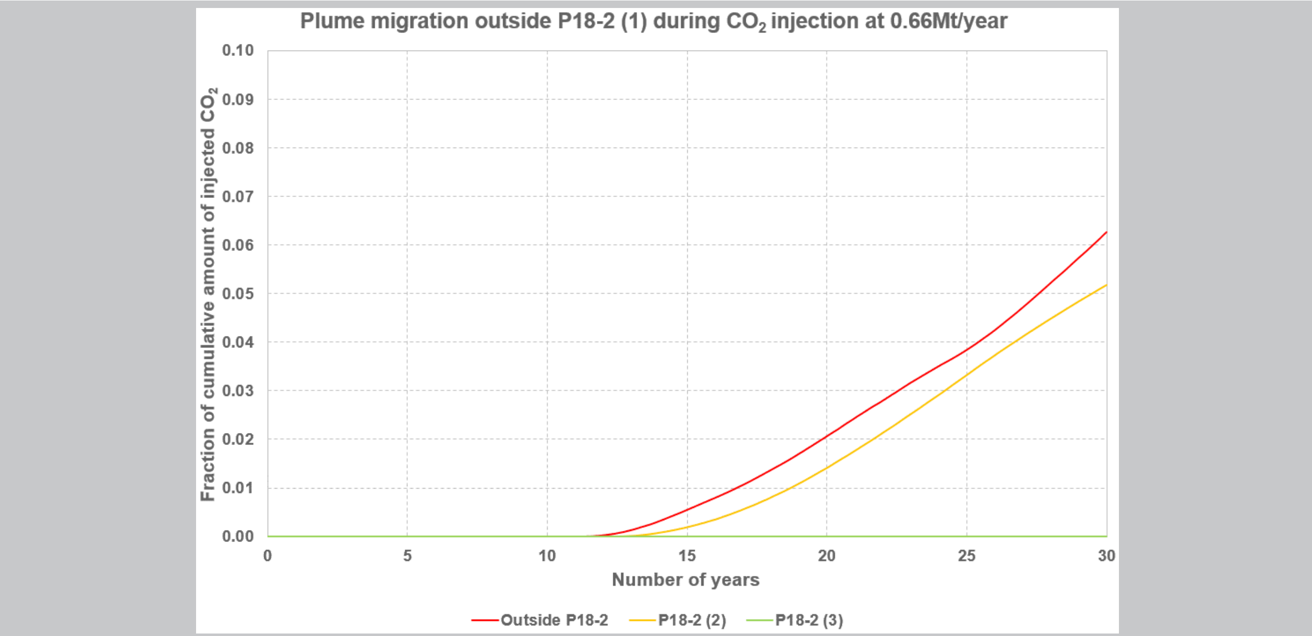

Figure 9 Plume migration outside the P18-2 (1) compartment during CO_2 injection at 0.66Mt/year, expressed as the fraction of the cumulative amount of CO_2.

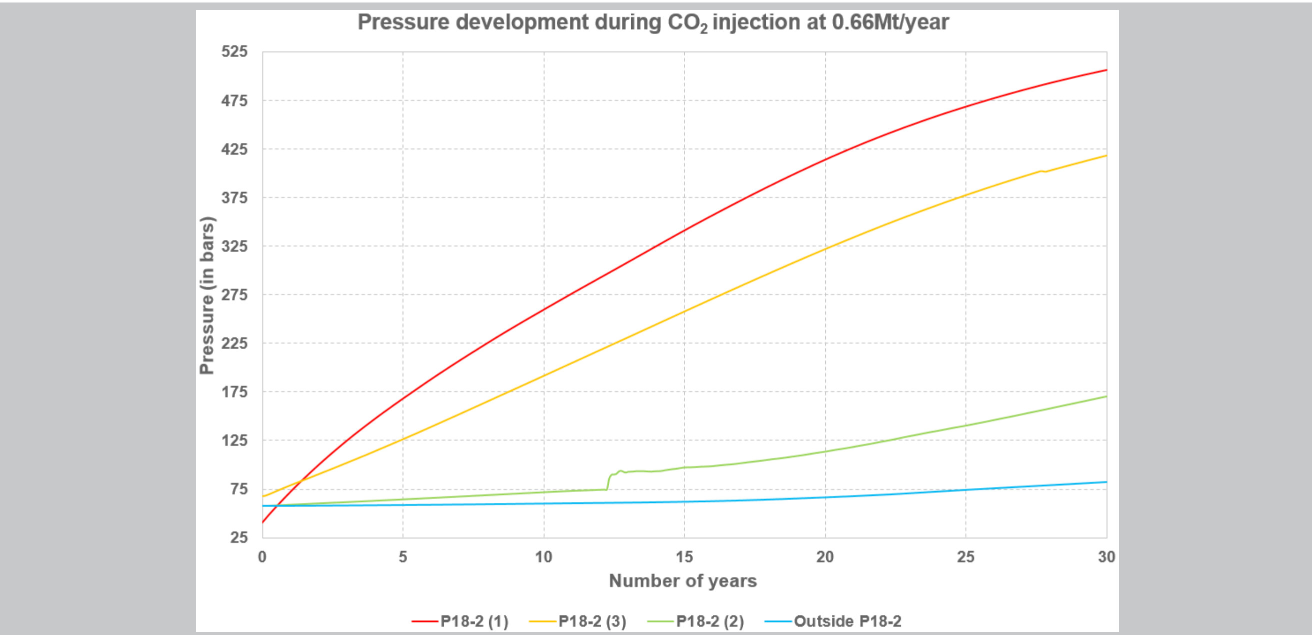

Figure 10 Pressure development in different compartments during CO_2 injection at 0.66Mt/year.

3.1.2 Compartment P18-2 (2)

The simulations for CO_2 injection in the 18-2 (2) compartment were carried out using the well P18-02A6ST1. Multiple injection rates were assumed between 0-1Mt/year. The cumulative amount of CO_2 injected and the corresponding pressure build-up in the compartment were noted.

The simulations suggest that the highest possible rate of injection in the compartment is 0.17Mt/year (Figure 11). The pressure increase is also well within the fracture pressure limit during the simulation period (Figure 12). Hence, the cumulative amount of CO_2 injected is 5.1Mt in 30 years.

Figure 13 illustrates the plume migration in and outside the P18-2(2) compartment during CO_2 injection at 0.17Mt/year.

The highest fractional amount of plume migration of 1.33Mt CO_2 occurs outside the P18-2 field. Correspondingly, a large fraction of 26% indicated in Figure 14 suggests that owing to its smaller size, the P18-2 (2) compartment is able to contain a lesser amount of CO_2 at the end of the simulation period (see Figure 13d) when compared to CO_2 injection in the P18-2 (1) compartment described previously.

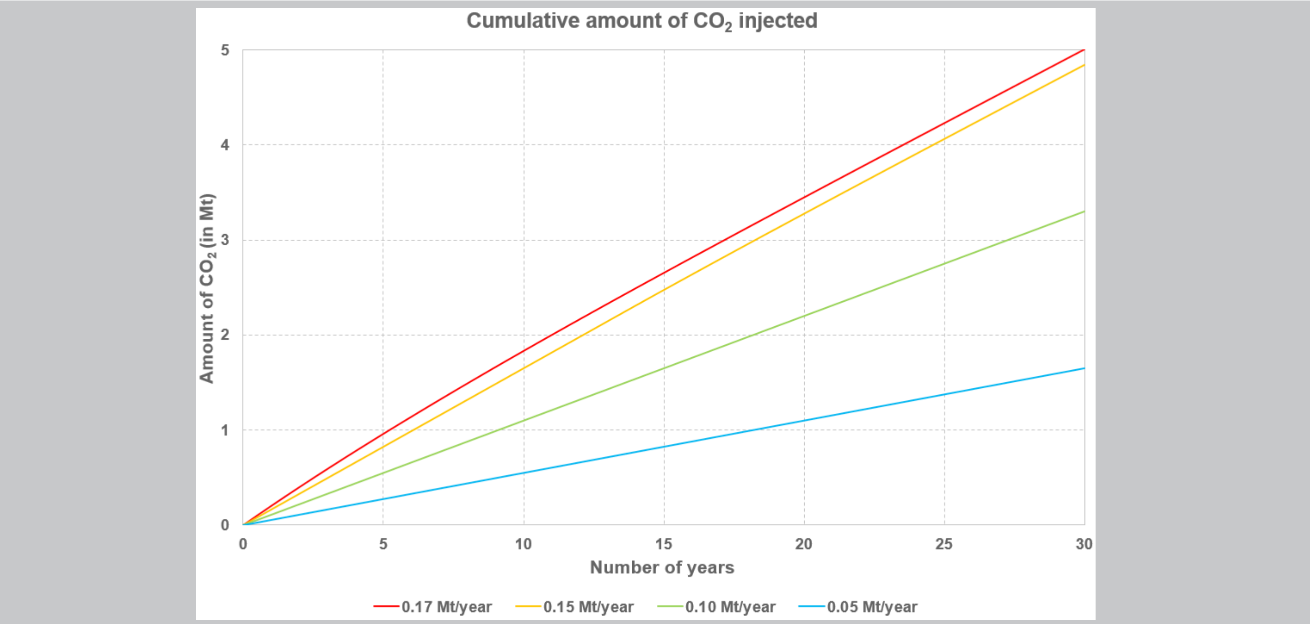

Figure 11 Cumulative amount of CO_2 injected into the P18-2 (2) compartment for different injection rates.

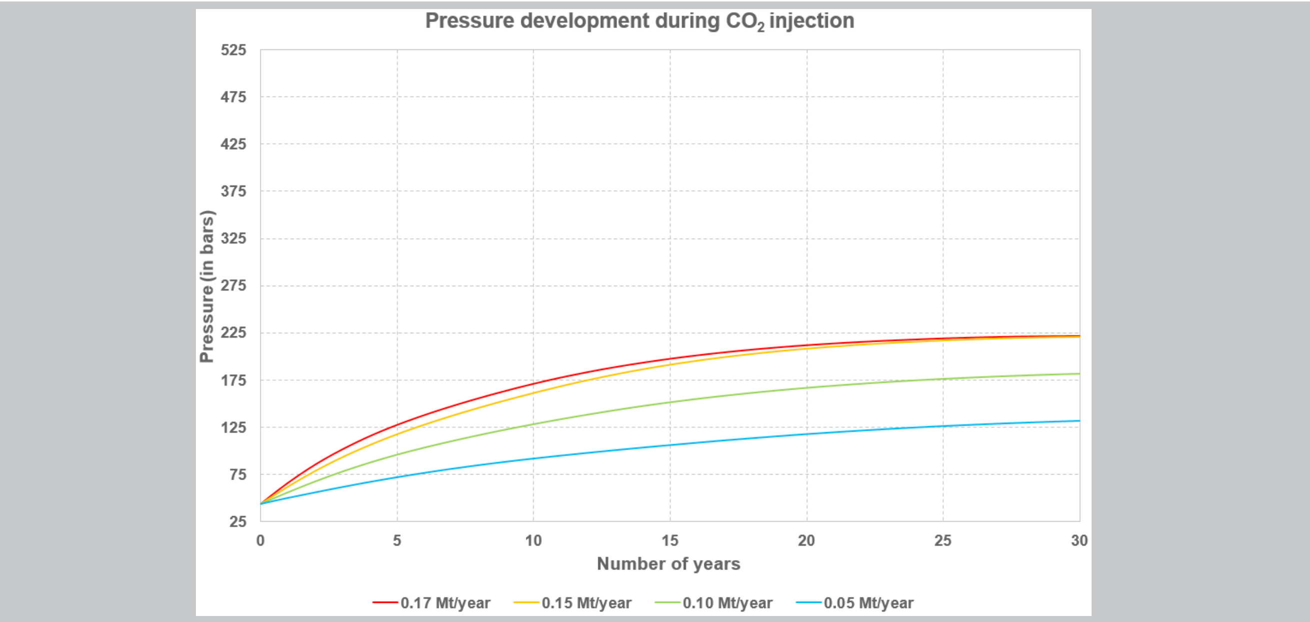

Figure 12 Pressure development in the P18-2 (2) compartment for different injection rates.

In addition, the pressure development in various compartments as illustrated in Figure 15 suggests that the pressure gradient is largely isotropic in all directions (towards the P18-2 (1) and P18-2 (3) compartments, and outside the P18-2 field). Hence, when injection occurs in the P18-2 (2) compartment, there is a preferential migration of the plume outside the P18-2 field which is attributed to relatively higher horizontal transmissibility across the relevant faults.

3.1.3 Compartment P18-2 (3)

The simulations for CO_2 injection in the 18-2 (3) compartment were carried out using the well P18-02A6. Multiple injection rates were assumed between 0-1Mt/year. The cumulative amount of CO_2 injected and the corresponding pressure build-up in the compartment were noted.

The highest possible rate of injection in the compartment is found to be 0.05Mt/year (Figure 16). This is unlike the previous scenarios (injection in the P18-2 (1) and P18-2 (2) compartments) because Figure 17 suggests that, for the injection rates that were simulated, the pressure build-up in the P18-2 (3) compartment exceeds the fracture pressure limit during the simulation period. This is largely due to relatively lower horizontal transmissibility of the bounding faults and lower reservoir permeability in the compartment. Hence, the highest cumulative amount of CO_2 achieved is 0.875Mt in 17.5 years, as a trade-off when injected at a lower injection rate of 0.05Mt/year. The simulation results also suggest that injection at higher rates ideally requires termination within five years of operation (Figure 17), although for the sake of the discussion of the results, all simulations were run for 30 years (see Figure 16). Figure 18 illustrates the plume migration in and outside the P18-2(3) compartment during CO_2 injection at 0.05Mt/year.

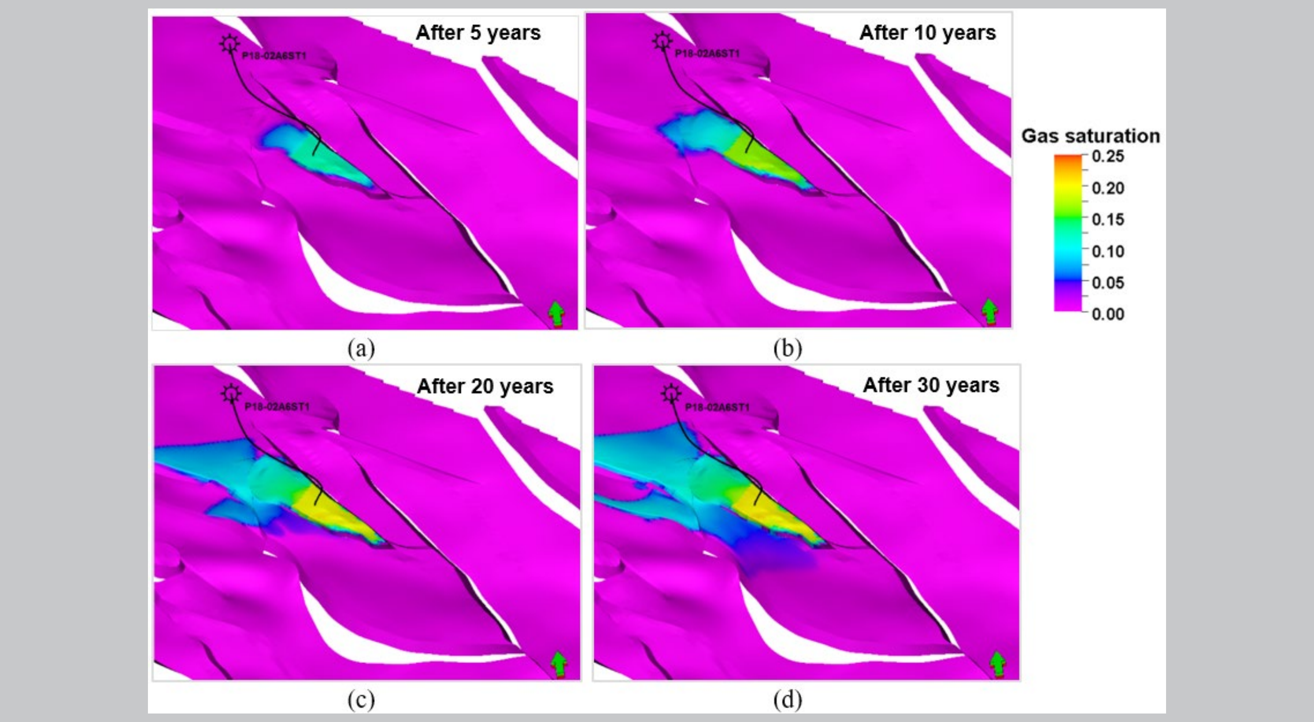

Figure 13 The estimated CO_2 plume distribution and its evolution in and outside the P18-2 (2) compartment during CO_2 injection at 0.17Mt/year: (a) after 5 years; (b) after 10 years; (c) after 20 years; (d) after 30 years.

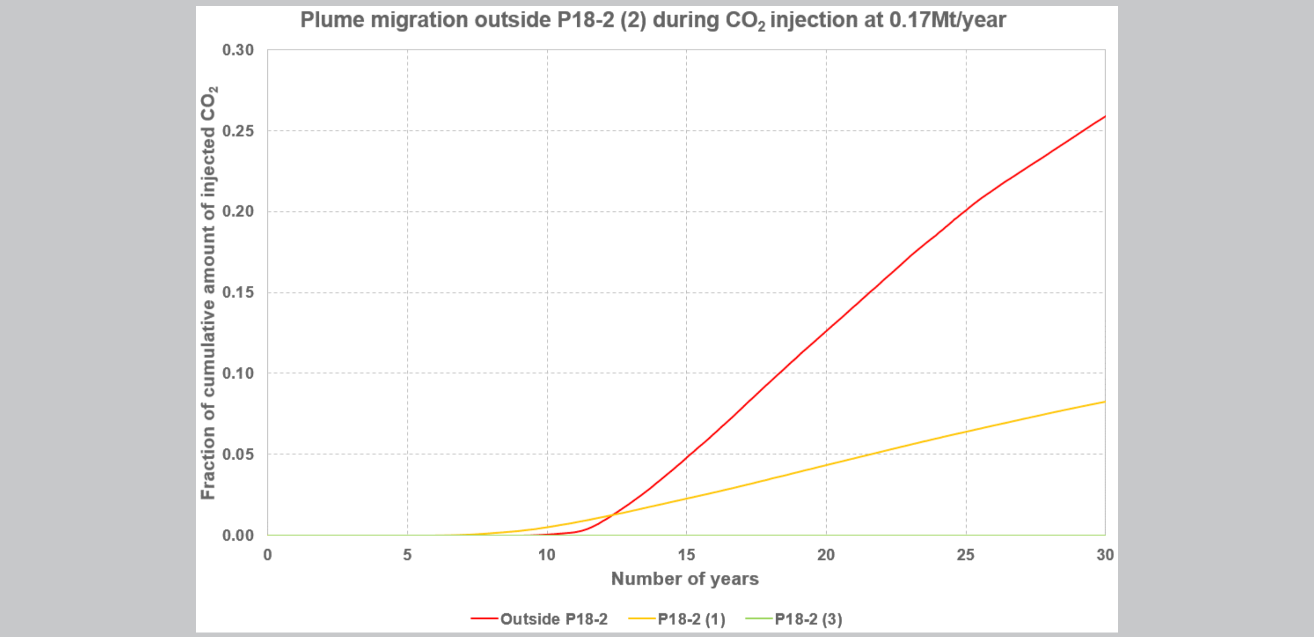

Figure 14 Plume migration outside the P18-2 (2) compartment during CO_2 injection at 0.17Mt/year, expressed as the fraction of the cumulative amount of CO_2.

The highest fractional amount of plume migration of 0.375Mt CO_2 occurs in the P18-2 (1) compartment. This plume migration is desirable since it shows that CO_2 storage occurs within the limits of the P18-2 field, as illustrated in Figure 19.

On the contrary, the pressure development results in Figure 20 clearly suggests that the available storage capacity would be underutilised if the injection needs to be stopped after 17.5 years of operation (an example for plume distribution is shown for 20 years in Figure 18c), as opposed to the planned period of 30 years. Moreover, the reservoir topography suggests that the P18-2 (3) is a low-lying compartment when compared to P18-2 (1), and hence buoyancy would also enhance the dynamic storage capacity during injection, provided suitable measures are taken to maintain the compartment pressure within the fracture pressure limit. In this context, brine production has been investigated as an option for pressure management, which is to be discussed in the following sections, although re-starting CO_2 injection after pressure management is not in the scope of this study.

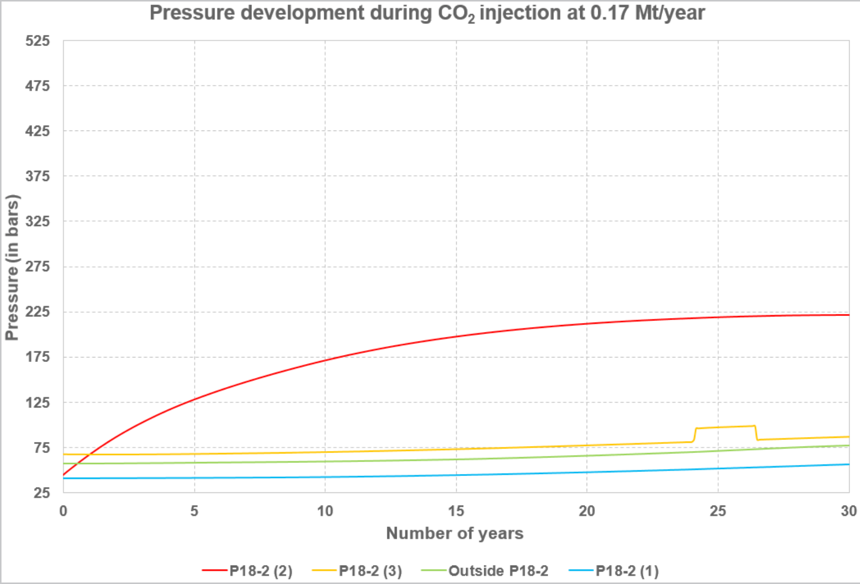

Figure 15 Pressure development in different compartments during CO_2 injection at 0.17Mt/year.

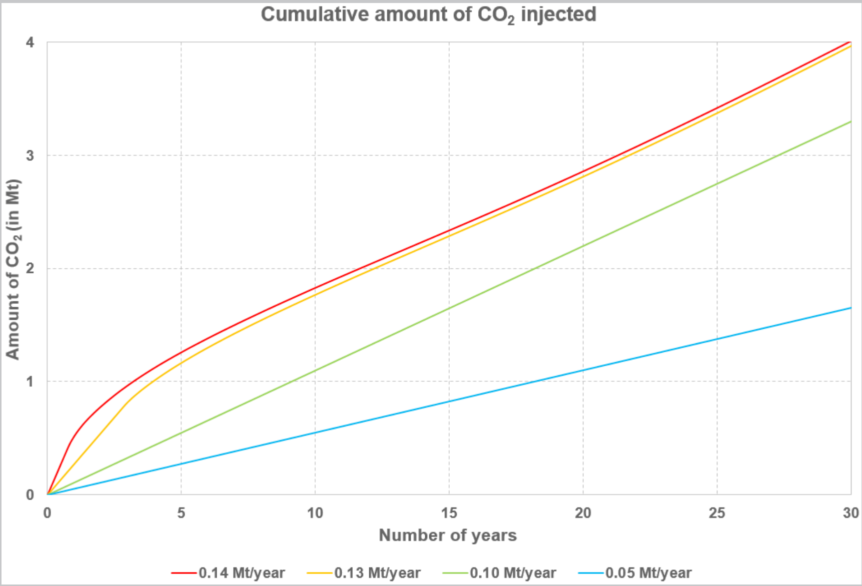

Figure 16 Cumulative amount of CO_2 injected into the P18-2 (3) compartment for different injection rates.

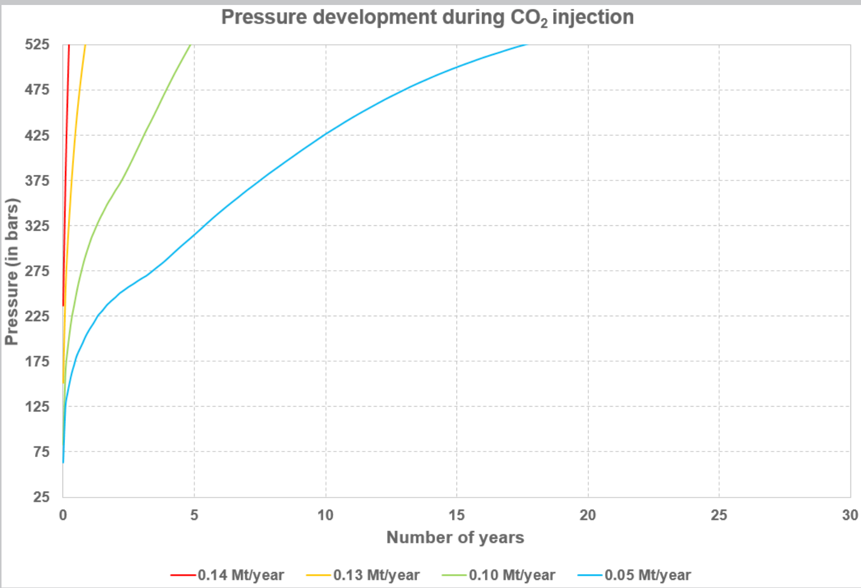

Figure 17 Pressure development in the P18-2 (3) compartment for different injection rates.

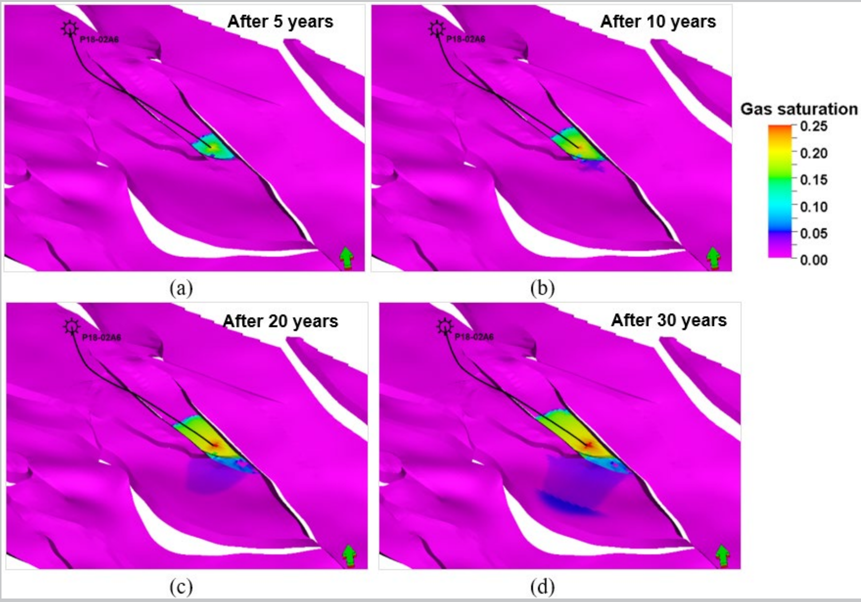

Figure 18 The estimated CO_2 plume distribution and its evolution in and outside the P18-2 (3) compartment during CO_2 injection at 0.05Mt/year: (a) after 5 years; (b) after 10 years; (c) after 20 years; (d) after 30 years.

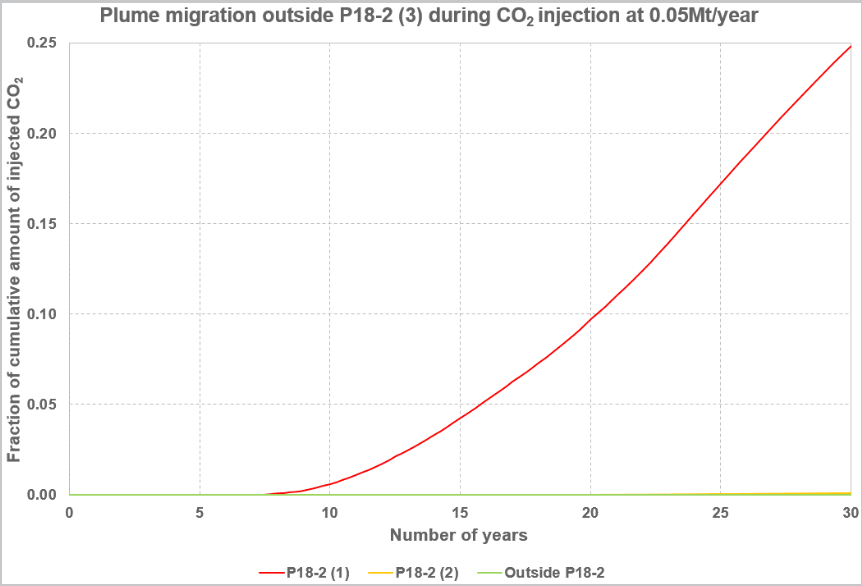

Figure 19 Plume migration outside the P18-2 (3) compartment during CO_2 injection at 0.05Mt/year, expressed as the fraction of the cumulative amount of CO_2.

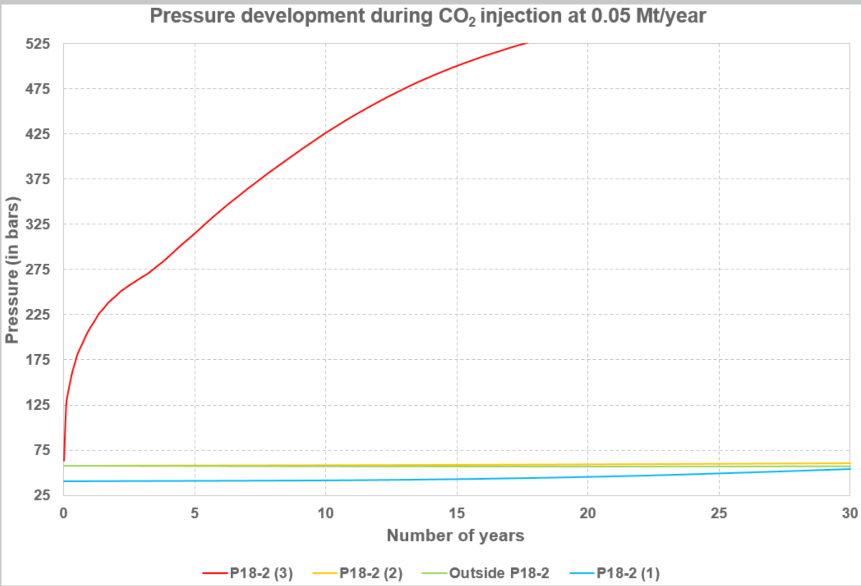

Figure 20 Pressure development in different compartments during CO_2 injection at 0.05Mt/year.

3.2 Relaxation of the reservoir

Based on the discussion of the results obtained in the previous sections, two stopping criteria for CO_2 injection were thus assumed: (a) when the plume migrates beyond the boundary of P18-2 field (all three compartments taken together) during CO_2 injection in the P18-2 (1) and P18-2 (2) compartments; and (b) when the pressure in the P18-2 (3) compartment approaches the fracture pressure limit during injection.

3.2.1 Compartment P18-2 (1)

The simulation for CO_2 injection in the 18-2 (1) compartment was carried out at a rate of 0.66Mt/year using the well P18-02. It was observed that after 13 years of simulation, the plume migrates outside the P18-2 field. This corresponds to 5000 tonnes CO_2 in the far-field which was assumed as the lower detection limit (Benson, 2006). The injection was stopped and the reservoir was allowed to equilibrate during the remaining period of the simulation.

Figure 21a illustrates the plume distribution after 13 years, when the migration occurring outside the P18-2 field boundary was detected. The cumulative amount of CO_2 injected in the compartment is 8.58Mt.

The fractional amount of CO_2 which migrates outside the field during the remaining period of equilibration (Figure 21b) corresponds to 0.39Mt CO_2, and it is smaller when compared to 1.19 Mt CO_2 if the injection were sustained for 30 years (Figure 22), as described previously.

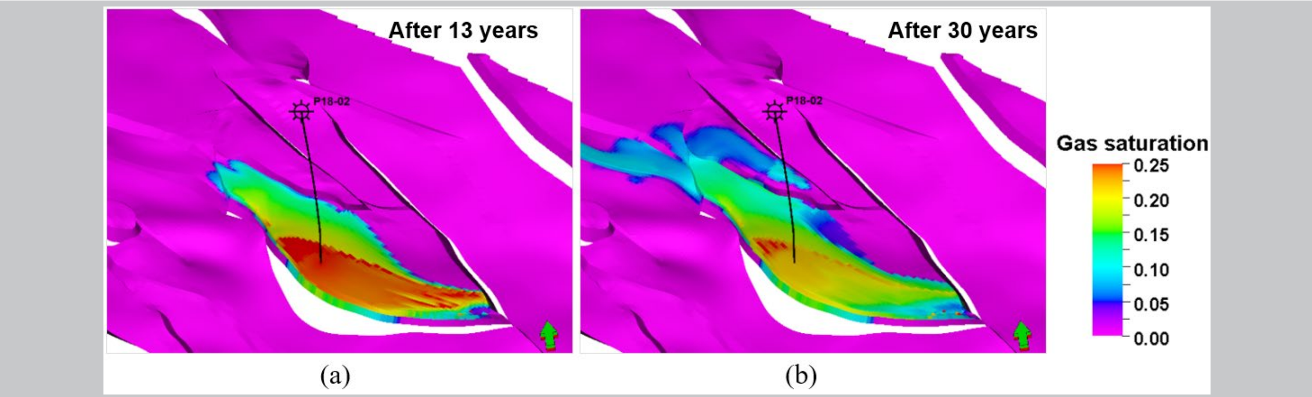

Figure 21 The estimated CO_2 plume distribution and its evolution in and outside the P18-2 (1) compartment: (a) after 13 years when the plume migrates outside the P18-2 field and CO_2 injection simulation was stopped; (b) after 30 years.

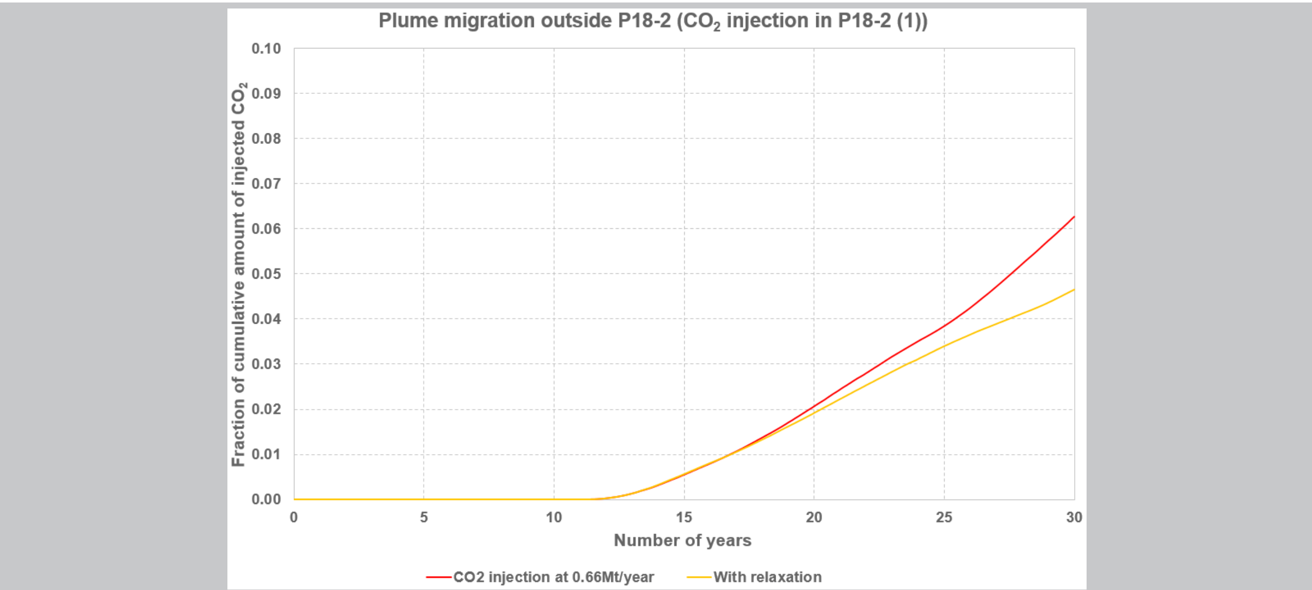

Figure 22 Comparison of plume migration outside the P18-2 field, expressed as the fraction of the cumulative amount of CO_2.

Hence, by stopping CO_2 injection, it is estimated that approximately 23% reduction in plume migration beyond the field boundary was achieved per unit Mt of injected CO_2.

3.2.2 Compartment P18-2 (2)

The simulation for CO_2 injection in the 18-2 (2) compartment was carried out at a rate of 0.17Mt/year using the well P18-02A6ST1.

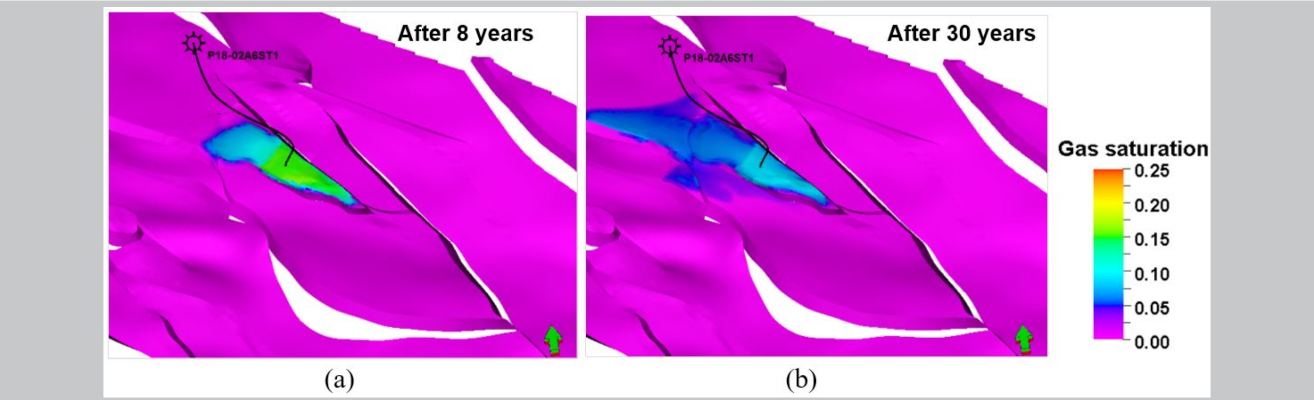

Figure 23 The estimated CO_2 plume distribution and its evolution in and outside the P18-2 (2) compartment: (a) after 8 years when the plume migrates outside the P18-2 field and CO_2 injection simulation was stopped; (b) after 30 years.

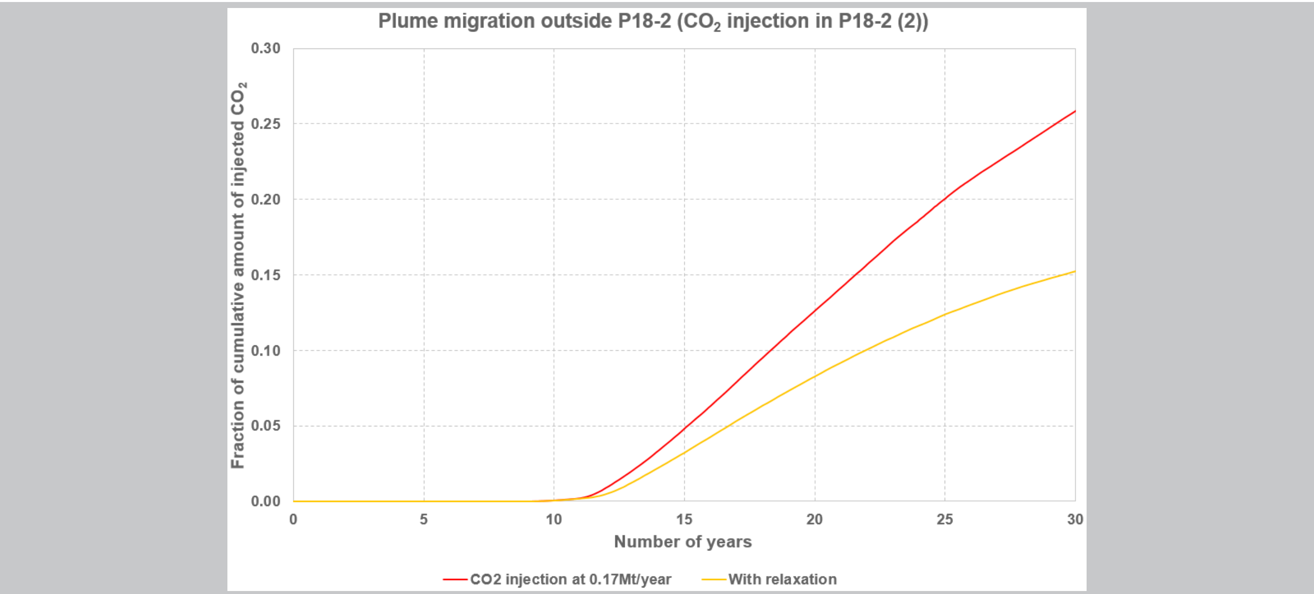

Figure 24 Comparison of plume migration outside the P18-2 field, expressed as the fraction of the cumulative amount of CO_2.

It was observed that after 8 years of simulation, the plume migrates outside the P18-2 field, and thus the stopping criterion was applied thereafter. Figure 23a illustrates the plume distribution after 8 years, when the cumulative amount of CO_2 injected in the compartment is 1.36Mt.

The fractional amount of CO_2 which migrates outside the field during the remaining period of equilibration (Figure 23b) corresponds to 0.2Mt CO_2, and it is smaller when compared to 1.33Mt CO_2 if the injection were sustained for 30 years (Figure 24), as described previously. Hence, by stopping CO_2 injection, it is estimated that approximately 42% reduction in plume migration beyond the field boundary was achieved per unit Mt of injected CO_2.

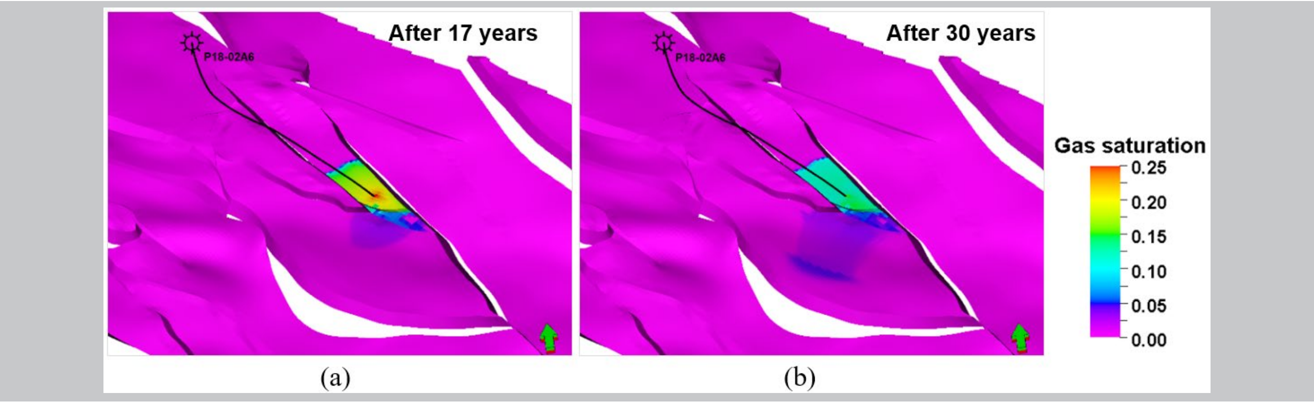

Figure 25 The estimated CO_2 plume distribution and its evolution in and outside the P18-2 (3) compartment: (a) after 17 years when the pressure in the compartment approaches the fracture pressure (525 bars) and CO_2 injection simulation was stopped; (b) after 30 years.

3.2.3 Compartment P18-2 (3)

The simulation for CO_2 injection in the 18-2 (3) compartment was carried out at a rate of 0.05Mt/year using the well P18-02A6. It was observed that after 17 years of simulation, the pressure in the compartment approaches the fracture pressure of 525 bars, and thus the stopping criterion was applied thereafter. Figure 25a illustrates the plume distribution after 17 years, when the cumulative amount of CO_2 injected in the compartment is 0.85Mt.

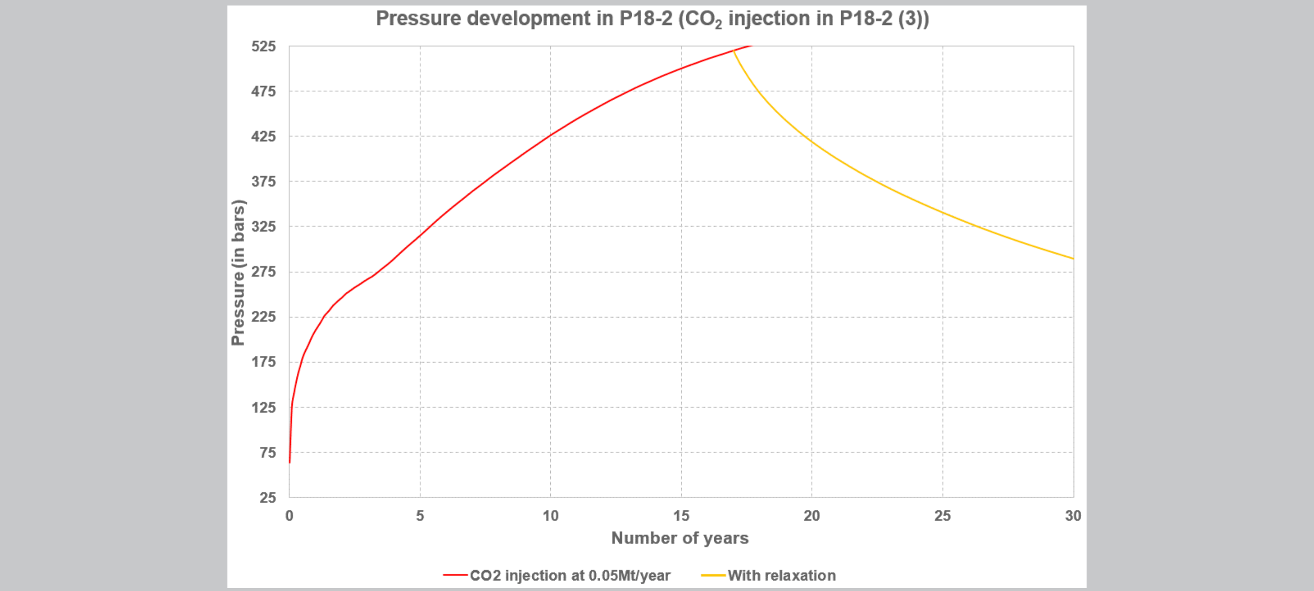

Figure 26 Pressure development in the P18-2 (3) compartment during CO_2 injection at 0.05Mt/year (for 17 years) and after the relaxation criterion is applied (for 13 years).

A pressure reduction of approximately 45% was achieved as a result of pressure equilibration to 290 bars (Figure 26), while the plume is retained within the P18-2 field (Figure 25b). It thus provides the necessary and sufficient condition to re-start CO_2 injection after 30 years. However, this would fall under a separate study on the maximisation of reservoir capacity utilisation, which is currently outside the scope of the current objectives.

3.3 Brine withdrawal

Brine withdrawal simulations were carried out for each scenario by making similar assumptions for the injection stopping criteria as discussed for reservoir relaxation. The brine production well layouts were chosen in such a way that there is a minimum risk of CO_2 breakthrough during the simulation period is expected. The issues related to CO_2 breakthrough would fall under a separate study on risk assessment, which is currently outside the scope of the current objectives.

3.3.1 Compartment P18-2 (1)

The simulation for CO_2 injection in the 18-2 (1) compartment was carried out at a rate of 0.66Mt/year using the well P18-02 (Figure 27a). When the plume migration occurs outside the P18-2 field after 13 years of simulation, CO_2 injection was stopped and brine production at the vertical well P18-02A6 (Figure 27b) was started simultaneously.

Figure 27 illustrates the plume distribution at the end of the simulation period. The cumulative amount of CO_2 injected in the compartment is 8.58Mt. The fractional amount of CO_2 which migrates outside the field with brine production (Figure 28) corresponds to 0.34Mt CO_2. It is estimated that approximately 33% reduction in plume migration beyond the field boundary was achieved per unit Mt of injected CO_2 when brine production was applied.

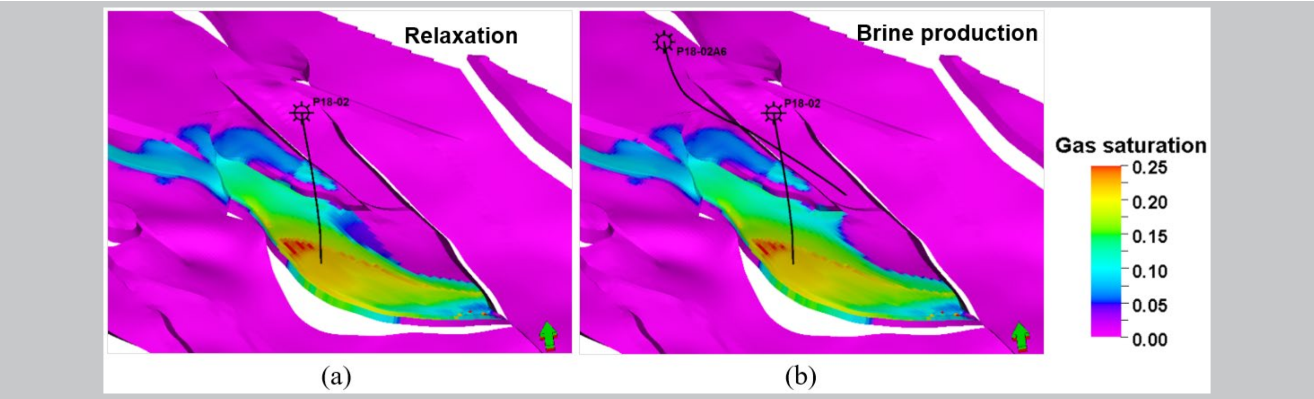

Figure 27 Comparison of the estimated CO_2 plume distribution in and outside the P18-2 (1) compartment after 30 years: (a) relaxation; (b) brine production.

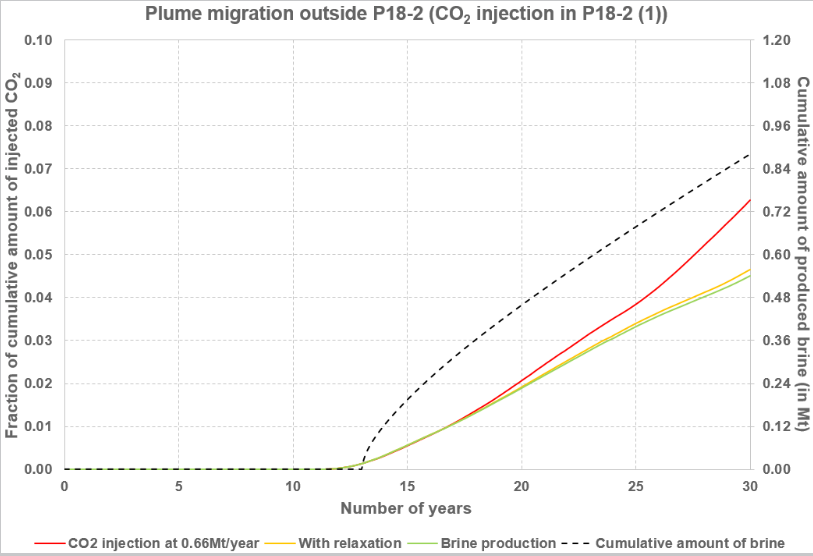

Figure 28 Comparison of plume migration outside the P18-2 field, expressed as the fraction of the cumulative amount of CO_2 and the cumulative amount of brine produced, represented on the secondary axis.

3.3.2 Compartment P18-2 (2)

The simulation for CO_2 injection in the 18-2 (2) compartment was carried out at a rate of 0.17Mt/year using the well P18-02A6ST1 (Figure 29a). When the plume migration occurs outside the P18-2 field after 8 years of simulation, CO_2 injection was stopped and brine production at four vertical wells, namely P18-02, P18-02A3ST2, P18-02A5ST1 and P18-02A6 (Figure 29b) was started simultaneously. Figure 29 illustrates the plume distribution at the end of the simulation period. The cumulative amount of CO_2 injected in the

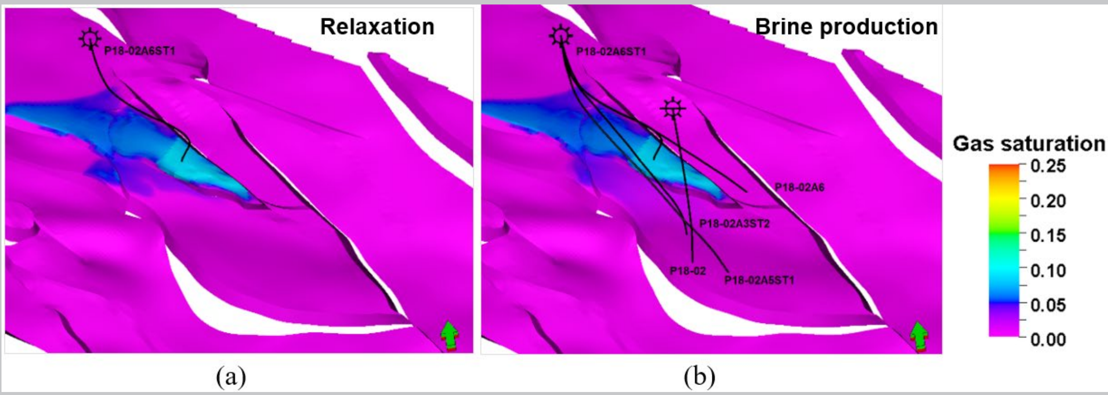

Figure 29 Comparison of the estimated CO_2 plume distribution in and outside the P18-2 (2) compartment after 30 years: (a) relaxation; (b) brine production.

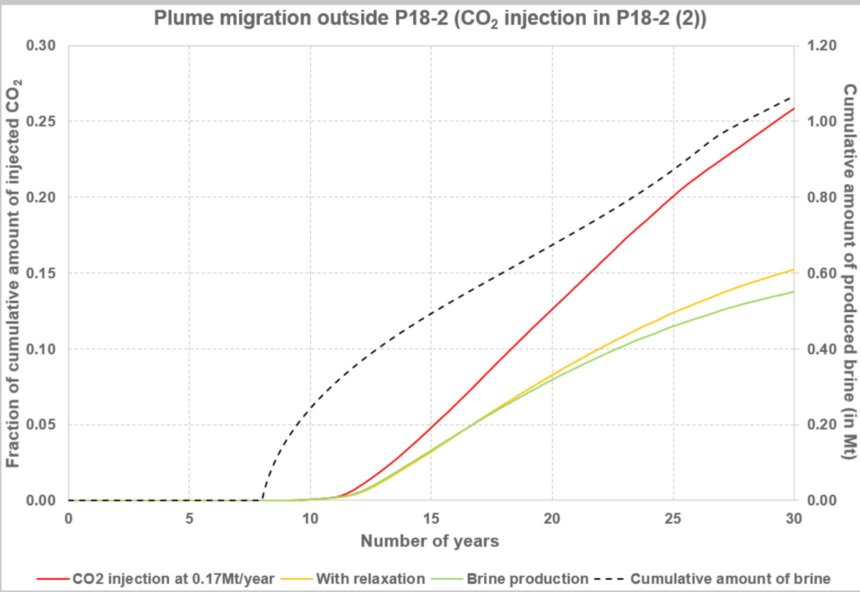

Figure 30 Comparison of plume migration outside the P18-2 field, expressed as the fraction of the cumulative amount of CO_2 and the cumulative amount of brine produced, represented on the secondary axis.

compartment is 1.36Mt. The fractional amount of CO_2 which migrates outside the field with brine production (Figure 30) corresponds to 0.19Mt CO_2. It is estimated that approximately 46% reduction in plume migration beyond the field boundary was achieved per unit Mt of injected CO_2 when brine production was applied.

Figure 30 Comparison of plume migration outside the P18-2 field, expressed as the fraction of the cumulative amount of CO_2 and the cumulative amount of brine produced, represented on the secondary axis.

3.3.3 Compartment P18-2 (3)

The simulation for CO_2 injection in the 18-2 (3) compartment was carried out at a rate of 0.05Mt/year using the well P18-02A6 (Figure 31a). When the pressure in the compartment approaches the fracture pressure of 525 bars after 17 years of simulation, CO_2 injection was stopped. It was assumed that a horizontal well extension is drilled, essentially deeper (-3,640m) than the injection interval (-3,490m) to ensure no immediate CO_2 breakthrough occurs.

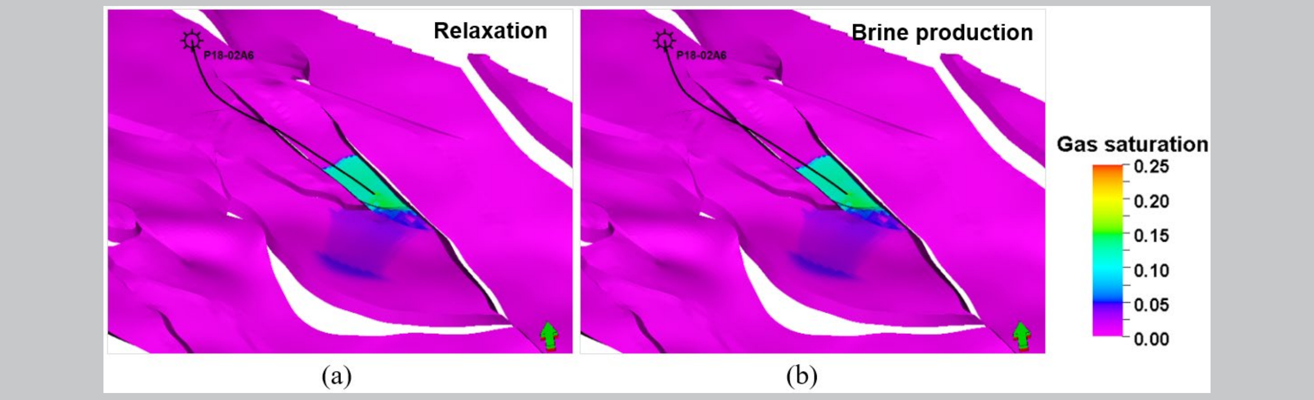

Figure 31 Comparison of the estimated CO_2 plume distribution in and outside the P18-2 (3) compartment after 30 years: (a) relaxation; (b) brine production.

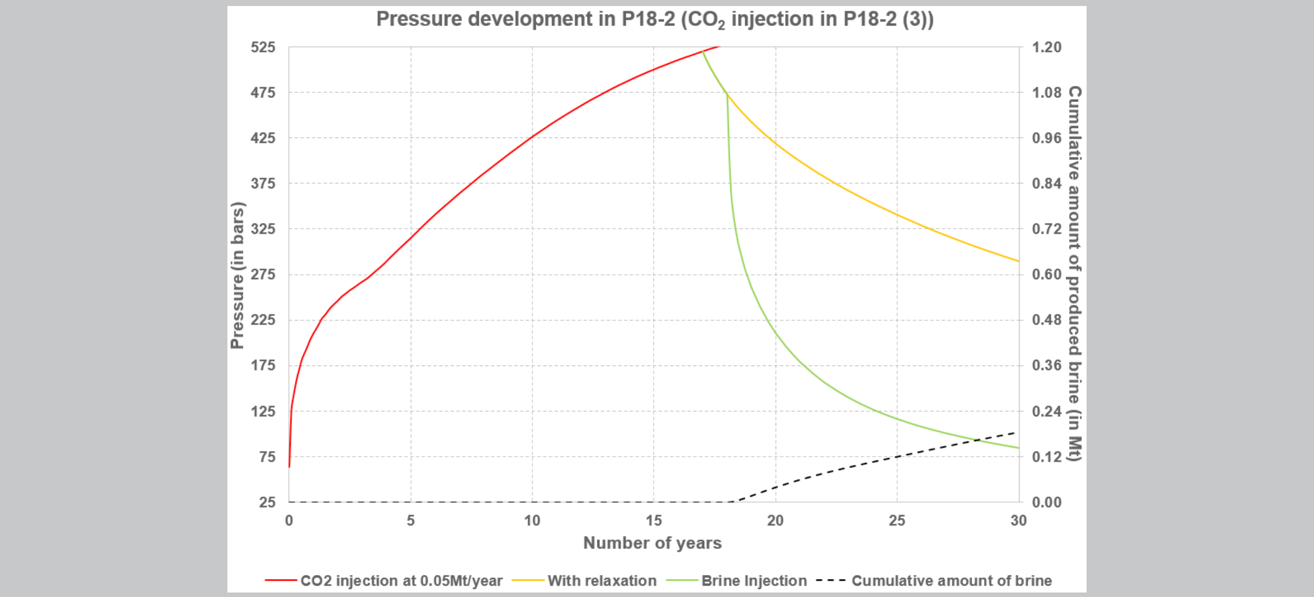

Figure 32 Comparison of pressure development in the P18-2 (3) compartment and the cumulative amount of brine produced, represented on the secondary axis.

Prior to brine production, it was also assumed that drilling a horizontal well extension of 250m in the reservoir would require one year. Figure 31 illustrates the plume distribution at the end of the simulation period indicating that the plume is retained within the P18-2 field at the end of the simulation period. Figure 32 illustrates that a significant pressure reduction of approximately 84% was achieved as a result of brine production (to 85 bars).

3.3.4 Summary of the key performance indicators

Table 2 lists a summary of the KPIs determined for each of the scenarios for brine production assessed in this study.

Table 2 The summary of KPIs.

KPI	Scenario 1: CO_2 injection in 18-2 (1)	Scenario 2: CO_2 injection in 18-2 (2)	Scenario 3: CO_2 injection in 18-2 (3)
Well Layout	1 vertical well	4 vertical wells	1 horizontal well
Volume of Brine extracted (in Mt)	0.9 (see Figure 28)	1.1 (see Figure 30)	0.2 (see Figure 32)
Longevity (in years)	17 (see Figure 28)	22 (see Figure 30)	12 (see Figure 32)
Response time (in years)	5 (see Figure 28)	3 (see Figure 30)	0 (see Figure 32)
Spatial extension (in km^2)	9.5 (see Figure 33a)	11.8 (see Figure 33b)	2.7 (see Figure 33c)
Estimated annual costs* (in Million €)	0.82	0.81	3.54

*Costs estimated at an inflation rate of 2.1% p.a., include seismic monitoring every 5 years for 10% of the model area, capital cost for drilling a horizontal well extension (scenario 3 only), and operational cost (including brine handling and treatment).

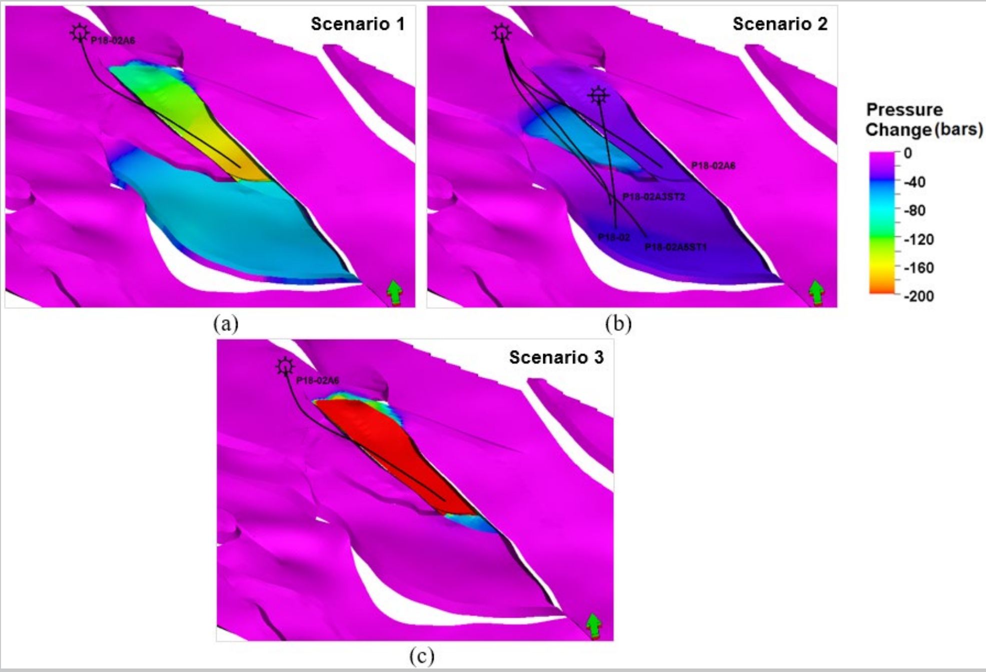

Figure 33 The footprint of pressure change indicating the area of influence of brine production: (a) CO_2 injection in compartment 18-2 (1); (b) CO_2 injection in compartment 18-2 (2); (c) CO_2 injection in compartment 18-2 (3).

4 CONCLUSIONS

In this report, the results obtained from the simulations for brine production and its assessment as a technique for CO_2 flow diversion and pressure management in a compartmentalised reservoir were presented. The factors determining the plume migration and pressure communication in the reservoir are reservoir permeability, horizontal fault transmissibility and relative pressure build-up in the compartments.

Three scenarios, namely CO_2 injection and brine production in three compartments of the P18-2 field, were considered separately. The results generally shows that the amount of flow diversion achieved is limited for the brine production layouts that were discussed. On the other hand, it is clear that there is a huge benefit of using brine production for pressure management since the associated costs could be offset by the reduction in risks induced by geomechanical failure and potentially consequent CO_2 leakage, the reduction in the area of review associated with monitoring, and the increase in storage capacity utilisation.

Further modelling work is thus required in two different aspects. One is to investigate an optimisation framework in order to maximise flow diversion of the plume considering the well layouts and CO_2 injection-brine production strategies. The other is carry out a detailed risk assessment of the strategies adopted in order to avoid early CO_2 breakthroughs at the production wells, especially in compartmentalised reservoirs.

References

Ames, R., Farfan, P. F., 1996. The environment of deposition of the Triassic Main Buntsandstein Formation in the P and Q quadrants offshore the Netherlands. In: Rondeel, H. E., Batjes, D. A. J., Nieuwenhuijs, W. H. (Eds.), Geology of Gas and Oil under the Netherlands. Kluwer Academic Publishers, Dordrecht, pp. 167-178.

Apps, J. A., Zheng, L., Zhang, Y., Xu, T., Birkholzer, J. T., Evaluation of Potential Changes in Groundwater Quality in Response to CO_2 Leakage from Deep Geologic Storage. Transport in Porous Media, 82(1), pp. 215-246.

Arts, R. J., Vandeweijer, V. P., Hofstee, C., Pluymaekers, M. P. D., Loeve, D., Kopp, A., Plug, W. J., 2012. The feasibility of CO_2 storage in the depleted P18-4 gas field offshore the Netherlands (the ROAD project). International Journal of Greenhouse Gas Control, 11, pp. S10-S20.

Benson, S.M., 2006. Monitoring carbon dioxide sequestration in deep geological formations for inventory verification and carbon credits. Society of Petroleum Engineers, SPE 102833.

Benson, S. M., Hepple, R., 2005. Prospects for early detection and options for remediation of leakage from CO_2 storage projects. Carbon dioxide capture for storage in deep geologic formations - results from the CO_2 capture project, 2, pp. 1189-1203.

Bergmo, P. E. S., Grimstad, A.-A., Lindeberg, E., 2011. Simultaneous CO_2 injection and water production to optimise aquifer storage capacity. International Journal of Greenhouse Gas Control, 5(3), pp. 555-564.

Birkholzer, J. T., Cihan, A., Zhou, Q., 2012. Impact-driven pressure management via targeted brine extraction - Conceptual studies of CO_2 storage in saline formations. International Journal of Greenhouse Gas Control, 7, pp. 168-180.

Birkholzer, J. T., Zhou, Q., 2009. Basin-scale hydrogeologic impacts of CO_2 storage: Capacity and regulatory implications. International Journal of Greenhouse Gas Control, 3(6), pp. 745-756.

Breunig, H. M., Birkholzer, J. T., Borgia, A., Oldenburg, C. M., Price, P. N., McKone, T. E., 2013. Regional evaluation of brine management for geologic carbon sequestration, International Journal of Greenhouse Gas Control, 14, pp. 39-48.

Buscheck, T. A., Sun, Y., Hao, Y., Wolery, T. J., Bourcier, W., Tompson, A. F., Jones, E. D., Friedmann, S. J., Aines, R. D., 2011. Combining brine extraction, desalination, and residual-brine reinjection with CO_2 storage in saline formations: Implications for pressure management, capacity, and risk mitigation, Energy Procedia, 4, pp. 4283-4290.

Buscheck, T. A., Sun, Y., Chen, M., Hao, Y., Wolery, T. J., Bourcier, B. Court, M. A., Celia, S., Friedmann, S. J., Aines, R. D., 2012. Active CO_2 reservoir management for carbon storage: Analysis of operational strategies to relieve pressure build-up and improve injectivity. International Journal of Greenhouse Gas Control, 6, pp. 230-245.

Carroll, S., Hao, Y., Aines, R., 2009. Geochemical detection of carbon dioxide in dilute aquifers. Geochemical Transactions, 10:4.

Court, B., Elliot, T. R., Dammel, J., Buscheck, T. A., Rohmer, J., Celia, M. A., 2011. Promising synergies to address water, sequestration, legal, and public acceptance issues associated with large-scale implementation of CO_2 sequestration. Mitigation and Adaptation Strategies for Global Change, 17(6), pp. 569-599.

De Jager, J. J., 2007. Geological development. In: Wong, et al. (Eds.), Geology of the Netherlands. Royal Netherlands Academy of Arts and Sciences, Amsterdam, pp. 5-26.

Geluk, M. C., 1999. Palaeogeographic and structural development of the Triassic in the Netherlands - new insights. In: Bachmann, G. H., Lerche, I. (Eds.), The Epicontinental Triassic, Zentralblatt für Geologie und Paläontology Teil I, 1998, Heft 7-8, pp. 545-570.

Gutierrez-Neri, M., Ganji, Z., van Breukelen, B., Kooi, H., 2012. CO_2 geological storage: injection into depleted gas fields. The CATO-2 project.

IEAGHG Report, 2007. Remediation of leakage from CO_2 storage reservoirs. IEA Greenhouse Gas R&D Programme, Report No. 2007/11.

Pagnier, H., Hofstee, C., Arts, R. J., vd Weijer, V., Loeve, D., Pluymaekers, M. P. D., Benedictus, T., 2012. The feasibility of CO_2 storage in the offshore P18 depleted gas reservoir (EEPR-ROAD). The CATO-2 project.

Rutqvist, J., Birkholzer, J.T., Cappa, F., Tsang, C-F., 2007. Estimating maximum sustainable injection pressure during geological sequestration of CO_2 using coupled fluid flow and geomechanical fault-slip analysis. Energy Conversion and Management, 48(6), pp. 1798-1807.

Rutqvist, J., Birkholzer, J.T., Tsang, C-F., 2008. Estimating maximum sustainable injection pressure during geological sequestration of CO_2 using coupled fluid flow and geomechanical fault-slip analysis. International Journal of Rock Mechanics and Mining Sciences, 45(2), pp. 132-143.

Tambach, T. J., Loeve, D., Hofstee, C., Plug, W-J., Maas, J. G., 2015. Effect of CO_2 Injection on Brine Flow and Salt Precipitation after Gas Field Production. Transport in Porous Media, 108(1), pp. 171-183.

Zheng, L., Apps, J.A., Zhang, Y., Xu, T., Birkholzer, J.T., 2009. On mobilization of lead and arsenic in groundwater in response to CO_2 leakage from deep geological storage. Chemical Geology, 268(3-4), pp. 281-297.

Chapter X

Novel approaches to lower reservoir pressure by accelerating convective mixing between brine and CO_2

Lies Peters[1], Joris Salari[1]
[1]TNO, The Netherlands

SUMMARY

In this report, it is investigated whether it is possible to enhance dissolution of CO_2 in brine using nanoparticles (NPs) as a remediation and/or mitigation option for unwanted migration of CO_2. The idea is to inject a homogeneous mixture of NPs and CO_2 into the stored CO_2. The heavier NP-CO_2 mixture spreads on the interphase between the CO_2 and brine. The heavier NPs move into the brine together with the CO_2 and increase the density of the brine. This will enhance the process of convective mixing which increases the dissolution rate of CO_2. However, it was found that the method is very inefficient in terms of the amount of NPs needed compared to the increase in CO_2 dissolution. For example, to achieve an increase of 50% in the CO_2 dissolution rate, 1 kg of NP is needed to dissolve 3 kg extra CO_2 for an example case at 1 km depth. This makes the method unattractive both technically and economically, because:

- a large effort is required for engineering NPs with the correct properties
- the risks associated: risk of clogging and pressure increase
- the method is expensive: for dissolving 5 Mton CO_2 at doubled dissolution rate, costs in excess of 1 trillion € were estimated.
- the method is very slow (order 10-100 years).

1 INTRODUCTION

This report is part of the research project MiReCOL (Mitigation and Remediation of CO_2 leakage) funded by the EU FP7 programme. Research activities aim at developing a handbook of corrective measures that can be considered in the event of undesired migration of CO_2 in deep subsurface reservoirs. MiReCOL results support CO_2 storage project operators in assessing the value of specific corrective measures if the CO_2 in the storage reservoir does not behave as expected. MiReCOL focuses on corrective measures that can be taken while the CO_2 is in the deep subsurface. The general scenarios considered in MiReCOL are 1) loss of conformance in the reservoir (undesired migration of CO_2 within the reservoir), 2) natural barrier breach (CO_2 migration through faults or fractures), and 3) well barrier breach (CO_2 migration along the well bore).

This report investigates the possibilities for enhancing dissolution of CO_2 in brine. Dissolution of CO_2 in brine has two safety advantages:

- The pressure is lowered.
- The dissolved CO_2 can no longer migrate as a separate phase but its migration is restricted to migration of the brine.

For enhancing CO_2 dissolution during the injection phase several possibilities are discussed in the literature:

- Alternate injection with water/brine (Emami-Meybodi et al., 2015)
- Co-injection of CO_2 with SO_2 (Crandell et al., 2010)
- Co-injection of CO_2 with nanoparticles (NPs) to enhance convective mixing (Javadpour and Nicot, 2011 and Singh et al., 2012)

From these methods, the last method was selected in MiReCOL to be investigated as potential remediation method in this work package. The proposed method enhances the natural process of convective mixing by increasing the density of the CO_2-saturated brine by using NPs. Convective mixing can develop when CO_2 is stored on top of brine: the CO_2 dissolves into the underlying brine which increases the density of the brine. The heavier, CO_2-saturated brine on top of the lighter, normal brine is unstable and at some point in time the layer of heavy brine becomes unstable and the heavy, CO_2-saturated brine starts to move downward. As a result, fresh (unsaturated) brine is transported to the CO_2-brine interface. In case of enhancement using NPs, the heavy NPs (e.g. metals and/or metaloxides which are in the order of 1-50 nm in size) move into the brine together with the CO_2. This increases the density of the CO_2-saturated brine which in turn increases the rate of convective mixing.

Natural CO_2 dissolution is a relatively slow process even when enhanced by convective mixing and is important for the long-term storage of CO_2 (Huppert and Neufeld, 2014). Therefore, this remediation strategy is aimed at undesired migrations of a relatively slow rate or as a complementary measure for another remediation strategy. Maybe it is also possible to use this for mitigation rather than remediation at a very early stage before an actual leak has developed.

To evaluate the feasibility of using NPs for remediation and/or mitigation, two aspects are evaluated:

- Placement of the NPs: how do you get the NPs where you need them
- Assuming that the NPs are where you need them, how much do they enhance convective mixing and thus increase the dissolution of CO_2 into the brine.

For the first aspect (placement), for both remediation and mitigation, it is most likely that the NPs are injected when (part of) the CO_2 is in place. This means that a mixture containing the NPs will need to be injected in such a way that the NPs reach the boundary between the CO_2 and the brine. A strategy to achieve this is discussed in section 2.1. To simulate the placement of the NPs on the boundary, numerical simulation is used. This method is discussed in section 2.3. The main point addressed by the NP placement simulation is:

- What is an acceptable density of the NP-CO_2 mixture for injection?

For the acceptable density range, the NP-CO_2 (homogeneously mixed) should obviously be heavier than CO_2, but lighter than the brine. If the NP-CO_2 is too heavy, then it will move into the brine and not spread on the interface. If the NP-CO_2 is too light (i.e. density difference with the CO_2 is small), the spreading is not efficient.

For the second aspect, a situation is assumed where a mixture of free CO_2 and NPs is present on top of brine (both stationary). In that case, the use of equations for the estimation of CO_2 dissolution resulting from convective mixing as derived by Szulczewski et al. (2013) is justified. This method is described in section 2.4.

The results of the analysis of both aspects are discussed in section 3. Also some economic aspects and potential risks are discussed there. The report will be concluded with a discussion and conclusions.

2 METHODS

2.1 Injection strategy of nanoparticles (NPs)

Since we are investigating the use of NPs for remediation and/or mitigation measures, the NPs are not injected together with the CO_2 from the start. The NPs need to be injected when (part of) the CO_2 is in place. For an effective remediation strategy it is necessary to place the NPs on the interface between brine and CO_2 where the CO_2 dissolution takes place. Two basic strategies for placing the NPs are:

1. Injection of a mixture of NPs and CO_2 (NP-CO_2) into the CO_2 phase with a density intermediate between CO_2 and brine. The NP mixture will move down through the CO_2 and spread on the CO_2-brine interface.
2. Injection of a mixture of NPs and CO_2 (NP-CO_2) into the brine phase with a density intermediate between CO_2 and brine. The NP mixture will move up through the brine and then spread on the interface.

The NPs cannot be injected alone but need to be injected in combination with another substance as a (homogeneous) mixture. Obvious candidates for mixing with the NPs are brine and CO_2, but other substances would also be possible (e.g. methane, nitrogen, alcohol). To simplify matters for now, we will assume that the NPs are injected together with CO_2. Since the NPs should have high density in order to increase the convective mixing, an appropriate mixture of NPs and CO_2 should result in a density which is intermediate to the CO_2 and brine. This will be investigated in section 3.1.

Placing strategy 1 (injection of NPs into the CO_2) is illustrated in Figure 1. For strategy 2, the injection phases and strategy are similar. In this report, we focus on strategy 1.

The placing of NP-CO_2 via injection can be divided in three phases (see Figure 1):

1. Injection phase: a homogeneous mixture of the CO_2 with NPs (NP-CO_2) is injected in supercritical phase in the CO_2. Flow in the reservoir is dominated by advection and pressure differences caused by injection. This means that the CO_2 moves laterally away from the well. Some losses and retention of NPs are to be expected.
2. Spreading phase: once injection is stopped the NP-CO_2 moves down due to the density difference with the surrounding supercritical CO_2. The flow is still dominated by advection. Once the NP-CO_2 reaches the interface with the brine, NPs will gradually move into the brine. This phase already starts during injection
3. Dissolution phase: NPs move into the brine, effectively increase the density and thereby enhance convective mixing.

At this stage, the processes inside the well during injection are not investigated. It is assumed that it is possible to inject the required homogeneous NP-CO_2 mixture at the required depth. As long as the CO_2 is super-critical (with relatively high density), it is likely that a sufficiently stable mixture can be created. This may however require engineering of the NPs, which can increase the cost of the particles.

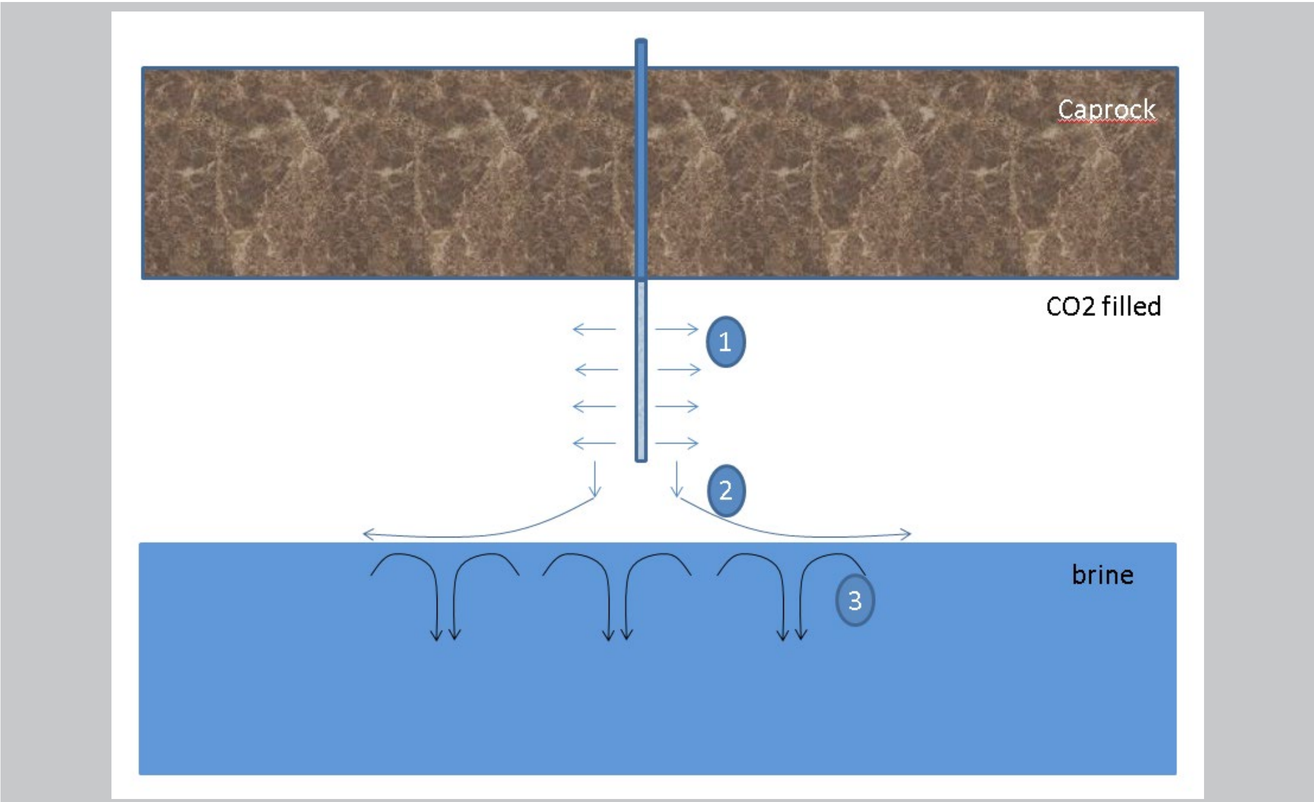

Figure 1 Overview of the injection of CO_2 with NPs (NP-CO_2) into CO_2 overlying brine,with three distinct phases of placing NP-CO_2: (1) Injection phase, (2) spreading phase, (3) dissolution phase.

2.2 Properties of NP-CO_2

Since the NPs will be present in both, CO_2 and brine, we define the following volume (V) fractions of NPs:

The volume fraction of NPs in brine saturated with CO_2 (f_b) is defined as:

$$f_b = {}^{V_{NP}}\!/_{V_{NPCO2satbrine}} \tag{1}$$

with $V_{CO2satbrine} + V_{NP} = V_{NPCO2satbrine}$

The volume fraction of NPs in (free) CO_2 (f_c) is defined as:

$$f_c = {}^{V_{NP}}\!/_{V_{NPCO2}} \tag{2}$$

with $V_{CO2} + V_{NP} = V_{NPCO2}$

2.2.1 Density

The density of CO_2 as a function of pressure and temperature is taken from Lemmon et al. (2015). The density of the CO_2-saturated brine is calculated from the correlation by Garcia (2001).

Density (ρ) of the NP mixtures is based on the equations provided by Javadpour and Nicot (2011):

$$\rho_{NPCO2satbrine} = (1 - f_b)\rho_{CO2satbrine} + (f_b)\rho_{NP} \tag{3}$$
$$\rho_{NPCO2} = (1 - f_c)\rho_{CO2} + (f_c)\rho_{NP} \tag{4}$$

2.2.2 Viscosity

The viscosity of the CO_2 is taken from Lemmon et al. (2015). The viscosity of the brine is calculated from Batzle and Wang (1992). The viscosity of the CO_2-saturated brine is assumed to be the same as that of normal brine. Solubility of CO_2 in brine is calculated according to Duan et al. (2006).

The viscosity (μ) of the NP-mixtures is based on the equations provided by Javadpour and Nicot (2011) using Einstein's viscosity relation:

$$\mu_{NPCO2satbrine} = (1 + 2.5\, f_b)\mu_{CO2satbrine} \tag{5}$$
$$\mu_{NPCO2} = (1 + 2.5\, f_c)\mu_{CO2} \tag{6}$$

2.3 Reservoir simulation for NP placement

As discussed in the introduction, the main point addressed by the NP placement simulations is:

- What is an acceptable density of the NP-CO_2 for injection?

To calculate the placement of the NP-CO_2, a numerical reservoir simulator is used (industry-standard code Eclipse 100, black-oil simulator). We assume that the CO_2 is stationary and is not moving up-dip any more. Since the reservoir simulator is not able to simulate NPs explicitly, a simplified approach is followed in which CO_2 is simulated as the gas phase, NP-CO_2 as the (dead) oil phase (with properties matching those of the NP-CO_2) and brine as the water phase. Convective mixing is not included in these simulations, since the focus here is to investigate whether it is feasible to place the NP-CO_2 on the interphase between CO_2 and brine and what acceptable densities are to achieve this.

Below is a list of other processes which might be relevant, but are not taken into account.

- The degree of dispersion and stability of the NPs. Phase separation due to gravity might occur.
- NP losses to ambient CO_2 or brine other than on the interface, which changes the properties of the NPs-CO_2. In other words, the fraction NP in the NP-CO_2 is fixed.
- Retardation of the NPs (Kampel and Goldsztein, 2011)
- Miscibility: the phases CO_2 (simulated as gas phase) and NP-CO_2 (simulated as oil phase) are assumed to be immiscible.
- Clogging of pores: pore throats for high permeability sand are generally >1 µm, whereas the particles have size of 10-100 nm. In case of aggregation, the particle size gradually increases and might lead to clogging of the pore throats. This is undesirable. Additional stabilization/functionalization of the NPs with a partly CO_2-philic layer might be needed in that case. A potential candidate might be polyethylene glycol.
- Foam formation which reduces injectivity.

Most of these processes can be avoided to a large extent by proper engineering of the particles. Miscibility cannot be avoided, but is more important on long time scales. It is expected that this simplified approach provides sufficient information to reach the goal of these simulation, namely estimate a suitable density range.

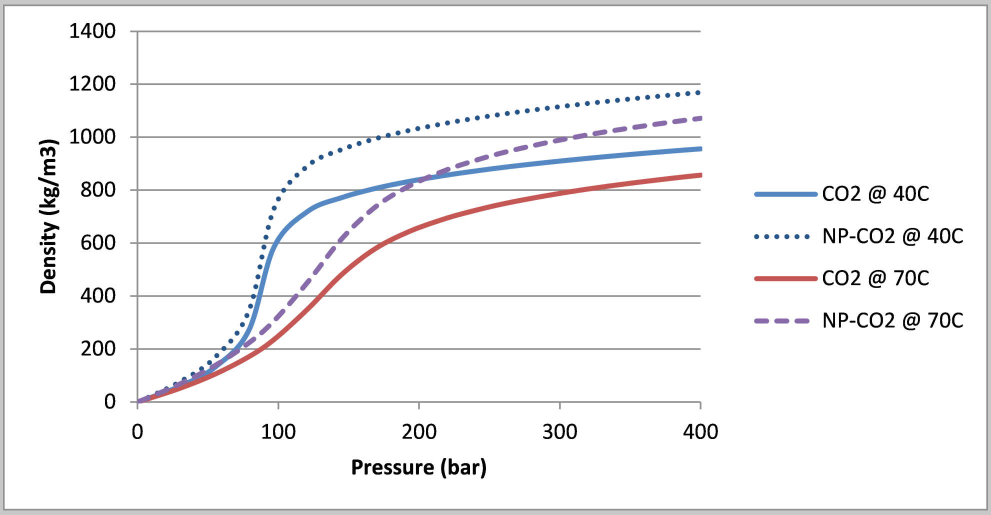

Figure 2 Density of CO_2 and NP-CO_2 as a function of pressure for a temperature of 40°C and 70°C for NP density of 5000 kg/m³ and mass fraction of 1E-4.

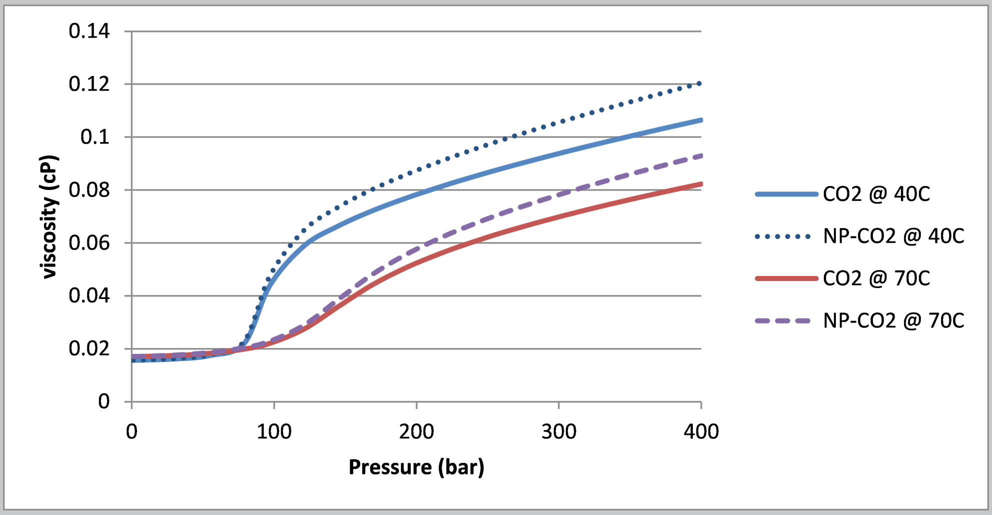

Figure 3 Viscosity of CO_2 and NP-CO_2 as a function of pressure for a temperature of 40°C and 70°C for NP density of 5000 kg/m³ and mass fraction of 1E-4.

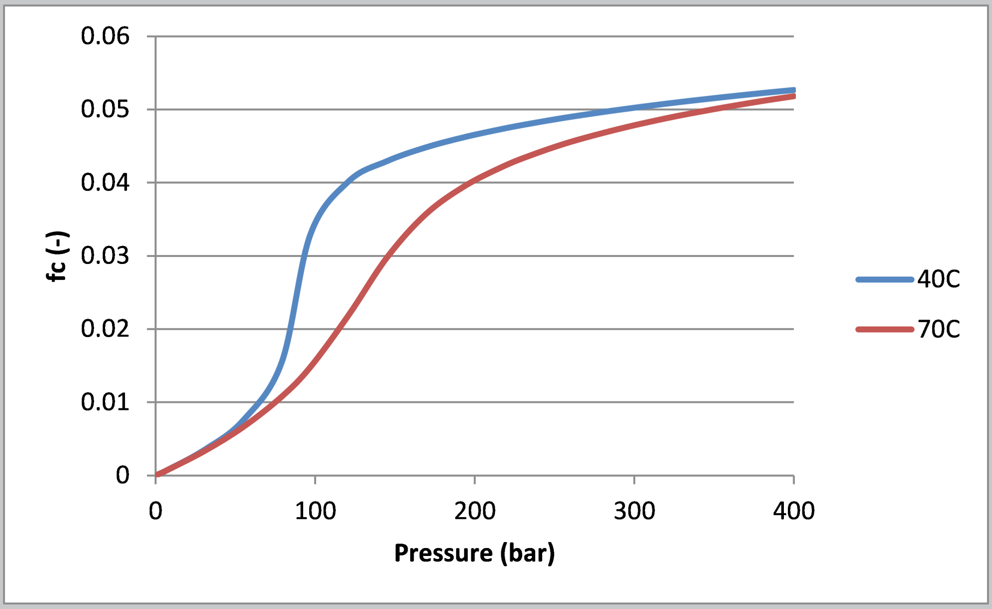

Figure 4 Volume fraction NPs in NP-CO_2 (f_c) as a function of pressure for temperatures of 40°C and 70°C for NP density of 5000 kg/m³ and mass fraction of $1{\cdot}10^{-4}$.

For the reservoir simulation, the PVT properties of the NP-CO_2 are required as a function of pressure. To calculate this, a constant mass fraction of NPs is assumed and the corresponding properties calculated. The calculation of properties for CO_2 and NP-CO_2 has been described in Section 2.2. In Figure 22, Figure 23 and Figure 24 the resulting properties are presented as a function of pressure for an NP density of 5000 kg/m^3 and mass fraction of 1E-4.

To determine the range of acceptable densities for placement of the NPs, 5 cases are simulated. In Table 1 the settings of the 5 cases are presented.

Table 1 Overview of the reservoir input settings for five cases.

	Case 1a	**Case 1a_brine**	**Case 1b**	**Case 2a**	**Case 2b**
Depth	1000 m			2000 m	
Pressure	105 bar @ CO_2-brine contact			205 bar @ CO_2-brine contact	
Temperature	40 °C			70 °C	
Permeability (horizontal)	1000 mD			1000 mD	
Permeability (vertical)	100 mD			100 mD	
Porosity	0.2			0.2	
CO_2 density (@ reservoir conditions)	656 kg/m^3			668 kg/m^3	
NP density	5000 kg/m^3		7500 kg/m^3	5000 kg/m^3	7500 kg/m^3
Injection into phase	**CO_2**	**brine**	**CO_2**	**CO_2**	

The placing was simulated as follows: first one year of injection into the CO_2 at a rate of 1·106 sm^3/day in a vertical injection well, then another year of spreading of the NP-CO_2 without further injection. Two different NPs were tested: one with a density of 5000 kg/m^3 (properties in Figure 22, Figure 23 and Figure 24) and one with a density of 7500 kg/m^3 (Javadpour and Nicot, 2011). The volume fraction of the NPs is the same in both cases (Figure 24). The mass fraction of NPs is 50% higher for the heavier particles.

2.4 Calculation of CO_2 dissolution flux with NPs

For the calculation of the dissolution flux of CO_2 into the brine (enhanced by convective mixing) that could be achieved by adding NPs, we can assume that NP-CO_2 is in contact with the brine. The CO_2 dissolution flux (FCO_2) in case of convective mixing (also named the fingering regime) is calculated as presented by (Szulczewski et al., 2013):

$$F_{CO2} \approx 0.017\ c_s V \qquad (7)$$

with

$$V = \frac{\Delta\rho g k}{\mu\varphi} \qquad (8)$$

Where:

c_s : saturated concentration of CO_2 [kg/m^3]
V : characteristic velocity of the fingers [m/s]
$\Delta\rho$: density difference between CO_2-saturated brine and brine without CO_2 [kg/m^3]
g : gravitational acceleration [m/s^2]
k : permeability [m^2]
μ : dynamic viscosity [Pa·s]
φ : porosity [-]

The properties affected by the NPs are V, $\Delta\rho$ and μ. Thus the CO_2 dissolution flux with and without NPs can be calculated. Table 2 shows the input settings for the calculations. A density of 10.000 kg/m^3 was used here to make the chance for success as large as possible.

Table 2 Input settings for calculating the efficiency of enhancing CO_2 dissolution by convective mixing.

Pressure	100 bar
Temperature	40 °C
Vertical permeability	500 mD
Porosity	0.35
Salinity	3.5 %
Density NPs	10.000 kg/m^3

2.4.1 Partitioning of NPs between CO_2 and brine

To calculate the properties of the NP-CO_2 and NP-CO_2 saturated brine for eq. 7 and eq. 8, the volume fraction of NPs is required. The volume fraction NPs in free CO_2 (f_c (eq. 1)) is determined by the injection strategy. However, the volume fraction NP in the brine (f_b) cannot be determined easily. It depends on the partitioning of the NPs over the CO_2 and the brine, which depends on the properties of the surface of the NPs and the relative affinity for CO_2 and/or brine. Javadpour and Nicot (2011) assumed that the brine at the interface would get the same volume fraction of NPs as the injected NP-CO_2, or in other words f_b=f_c. This presents a problem though: if the CO_2-saturated brine that moves away from the interface due to convection contains a volume fraction f_b=f_c, then the CO_2 at the interface would quickly become depleted of NPs. In general three cases can be identified:

1. The rate of NPs moving to the brine is faster w.r.t. the CO_2.
2. The rate of NPs moving to the brine is the same w.r.t. the CO_2 (thus the amount of NPs that move into the brine can be calculated from the CO_2 solubility).
3. The rate of NPs moving to the brine is slower w.r.t. CO_2.

For case 1, NP-CO_2 at the CO_2-brine interface will become depleted of NPs (f_c will decrease). For the assumption under case 3, NPs will remain behind in the CO_2 (f_c will increase). For case 2, f_c will remain constant. So, even though the partitioning of the NPs between brine and CO_2 in no way depends on the solubility of CO_2, for evaluation purposes it is useful to derive f_b based on case 2 and calculate any other cases based on that f_b. Thus f_b can be calculated from f_c, the solubility of CO_2 and the different densities. The derivation will be presented below.

Please note that it is assumed that the NPs are stable particles and do not dissolve in either the CO_2 or the brine.

The solubility s of CO_2 in the brine is defined a:

$$s = \frac{m_{CO2}}{m_{brine}} = \frac{\rho_{CO2}V_{CO2}}{\rho_{brine}V_{brine}} \tag{9}$$

with f_b defined in (Eq. 1).

With the definition of f_c (Eq. 2), this can be written as:

$$f_b = f_c \times \frac{V_{NPCO2}}{V_{NPCO2satbrine}} = f_c \times \frac{V_{NP}+V_{CO2}}{V_{NP}+V_{CO2satbrine}} \tag{10}$$

As an intermediate step we multiply with $1/V_{brine}$, resulting in:

$$f_b = f_c \times \frac{V_{NP}/V_{brine} + V_{CO2}/V_{brine}}{V_{NP}/V_{brine} + V_{CO2satbrine}/V_{brine}} \tag{11}$$

The four fractions in the equation (9) above can be rewritten into known variables. This will be explained below. From the definition of solubility s above, it follows that:

$$V_{CO2}/V_{brine} = s\, \rho_{brine}/\rho_{CO2} \tag{12}$$

From the definition of f_c:

$$V_{NP} = f_c(V_{NP} + V_{CO2}) \tag{13}$$

$$V_{NP} - f_c V_{NP} = V_{NP}(1 - f_c) = f_c V_{CO2} \tag{14}$$

$$V_{NP}/V_{brine} = \frac{f_c}{1-f_c}\frac{V_{CO2}}{V_{brine}} \tag{15}$$

And

$$V_{CO2satbrine}/V_{brine} = \frac{(1+s)m_{brine}/\rho_{CO2satbrine}}{m_{brine}/\rho_{brine}} = (1+s)\, \rho_{brine}/\rho_{CO2satbrine} \tag{16}$$

Substituting Eq. 10, 13 and 14 in Eq. 9 results in the equation to calculate the volume fraction of NPs in brine (f_b) based on the volume fraction in the CO_2 (f_c) and the solubility of CO_2 in brine:

$$f_b = f_c \times \frac{\left(\frac{f_c}{1-f_c}+1\right)\left(\rho_{brine}/\rho_{CO2}\right)s}{\frac{f_c}{1-f_c}\left(\rho_{brine}/\rho_{CO2}\right)s + (1+s)\left(\rho_{brine}/\rho_{CO2satbrine}\right)} \tag{17}$$

3 RESULTS AND DISCUSSION

3.1 NP Placement

Table 3 shows the results of the cases described in Table 1. In section 2.3, the simulation approach was described.

The radius listed in the last column is the maximum radius reached by the NP-CO_2 after 2 years (1 year of injection and a year time for spreading). The sensitivity of spreading to the density of the injected NP-CO_2 is not very large. So for acceptable spreading, a density of NP-CO_2 between 750 and 950 kg/m^3 at reservoir conditions is probably acceptable. Figure 6 shows the density of NP-CO_2 as a function of the volume fraction of the NPs in the injected CO_2 at reservoir conditions. From this plot, the acceptable range for the volume fraction of the NPs in the NP-CO_2 to be used for the calculations of the increase in CO_2 dissolution flux in the next section, can be derived. For these calculation a density of the NPs of 10.000 kg/m^3 was used in order to get the highest possible benefit from the NPs. The radius presented in Table 3 is after 2 years (of which only in the first year injection occurred). The spreading continues after this time. For example for case 1a, after another year of spreading the radius has grown with another ~40 m. This is similar for the other cases. However, the assumptions of immiscible flow and no loss of particles become less valid as spreading continues.

Table 3 Results of the placement simulations.

Case	Density NP	Density NP-CO_2 @ $P_{reservoir}$	Radius (after 2 yrs)
Case 1a	5000 kg/m^3	785 kg/m^3	420 m
Case 1a_brine	5000 kg/m^3	785 kg/m^3	400 m
Case 1b	7500 kg/m^3	872 kg/m^3	440 m
Case 2a	5000 kg/m^3	844 kg/m^3	400 m
Case 2b	7500 kg/m^3	946 kg/m^3	400 m

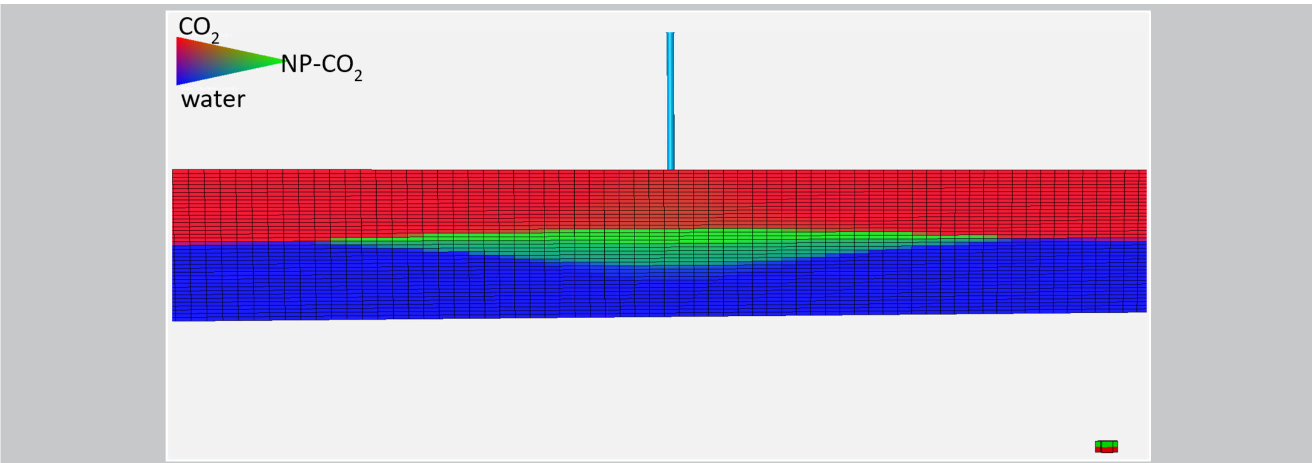

Figure 5 Spreading 2 years after the start of injection for case 1 (Table 3) with NP-CO_2 injection in a vertical well with NP density of 7500 kg/m^3 (horizontal grid block size = 40 m). The cross section shows the CO_2 in red, the NP-CO_2 in green and in blue the brine.

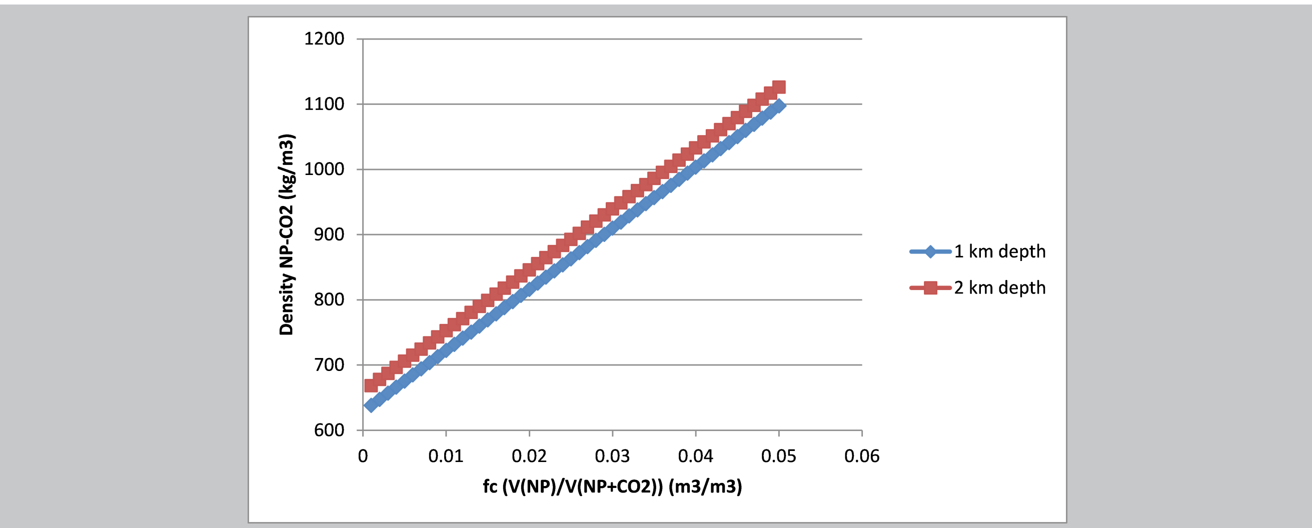

Figure 6 Density of NP-CO_2 as a function of the volume fraction of NPs with a density of 10.000 kg/m^3 (all at reservoir conditions) for case 1 (1 km depth) and case 2 (2 km depth).

To check whether injection strategy 2 (injection into the brine) significantly affects the results, case1a was also simulated for injection into the underlying brine. The differences were small: for the same settings, the NP-CO_2 spread a bit further for the injection in CO_2 than for the injection in brine (420 m away from the well after 2 years for injection into CO_2 (Figure 7) versus 400 m away from the well for injection into brine (Figure 8)). Also, more NP-CO_2 was trapped due to residual trapping in the case of injection into the brine.

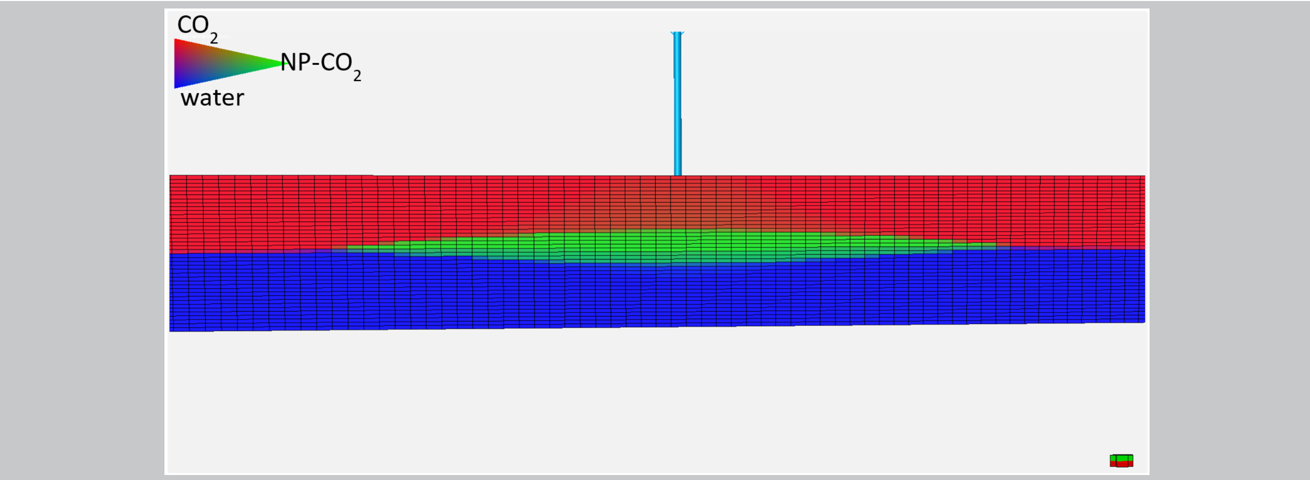

Figure 7 Spreading 2 years after the start of injection for case 1a for injection in the CO_2 (see Table 3). The cross section shows the CO_2 in red, the NP-CO_2 in green and in blue the brine.

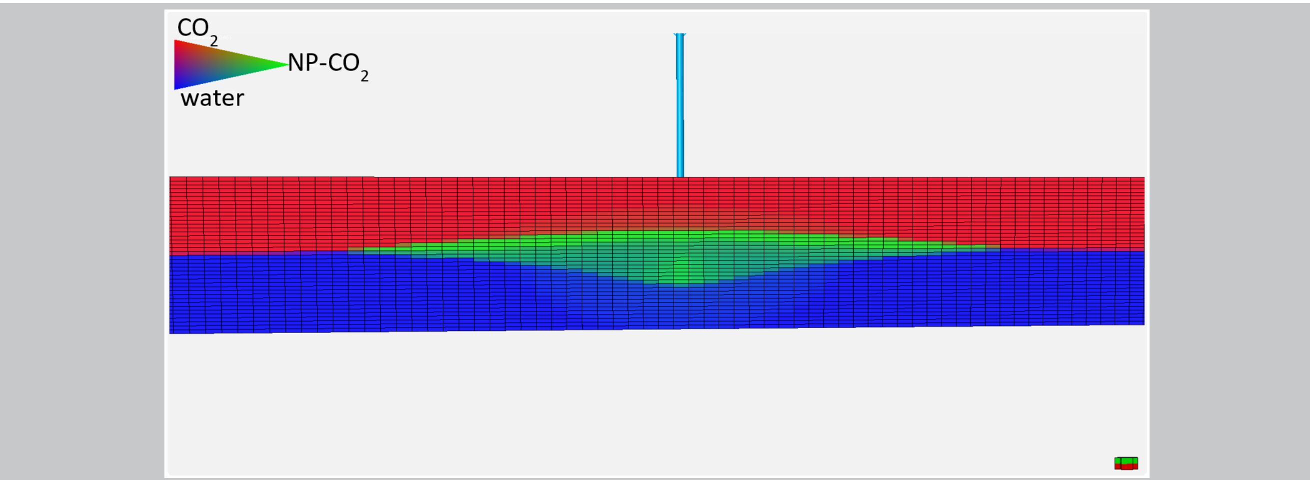

Figure 8 Spreading 2 years after the start of injection for case 1a_brine with injection into the brine below the CO_2. The cross section shows the CO_2 in red, the NP-CO_2 in green and in blue the brine.

3.2 Efficiency of increasing CO_2 dissolution flux

To determine the efficiency of the mitigation measure the next step is to calculate, for the values of f_c determined in the previous section, the increase in convective mixing and in CO_2 dissolution. To characterize the efficiency, the following numbers are calculated:

- Percentage increase in CO_2 dissolution flux (flux in kg/m²/yr) (*I*):

$$I = 100\% * \left(\left(F_{CO2,NP} - F_{CO2}\right)/F_{CO2}\right) \tag{18}$$

Where:

$F_{CO2,\,NP}$: CO_2 dissolution flux with NP-CO_2 (kg/m²/yr)
F_{CO2} : CO_2 dissolution flux with only CO_2 (kg/m²/yr)

- Ratio of additional CO_2 dissolution flux and the required NP flux to reach that CO_2 flux (R):

$$R = \left(F_{CO2,NP} - F_{CO2}\right)/F_{NP} \tag{19}$$

Where:

F_{NP} : flux NPs in the flux $F_{CO2,\,NP}$ (kg/m²/yr)

Ratio of the additional CO_2 dissolution flux and the CO_2 input required to inject the relevant amount of NPs (R_{CO2}) (also expressed as a flux in kg/m²/yr):

$$R_{CO2} = \left(F_{CO2,NP} - F_{CO2}\right) / \left(F_{NP} * \frac{(1-f_{c,m})}{f_{c,m}}\right) \tag{20}$$

Where $f_{c,m}$ is the mass fraction of NP in NP-CO_2, calculated from:

$$f_{c,m} = f_c * \frac{\rho_{NP}}{\rho_{NPCO2}} \tag{21}$$

The three numbers defined above (Eq. 18-20) are presented as a function of f_c (at downhole conditions) in Figure 9 to Figure 11 for case 1 (see Table 2 for details on the input). The values of f_c are chosen to get acceptable densities of the NP-CO_2 in terms of placement (see Section 3.1 and Figure 32). Four different levels of partitioning in brine were investigated: 100%, 50%, 20% and 10%. 100% means that the volume fraction of the NPs with respect to the CO_2 in the CO_2-saturated brine is the same as the volume fraction in the free CO_2. In the other cases, the volume fraction NPs in brine is reduced compared to that scenario.

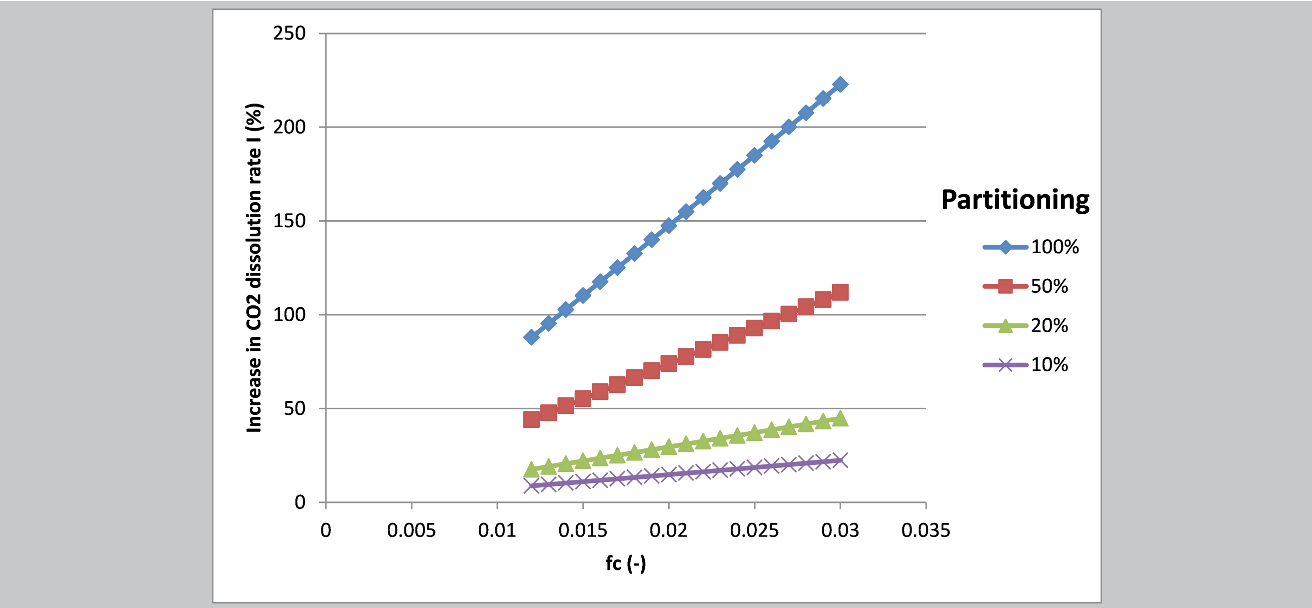

Figure 9 Percentage increase in CO_2 dissolution flux (I, Eq. 18) as a function of f_c for 4 different scenarios of partitioning of NPs over CO_2 and brine (100% is equal partitioning, 10% indicates a strong preference for the CO_2 phase).

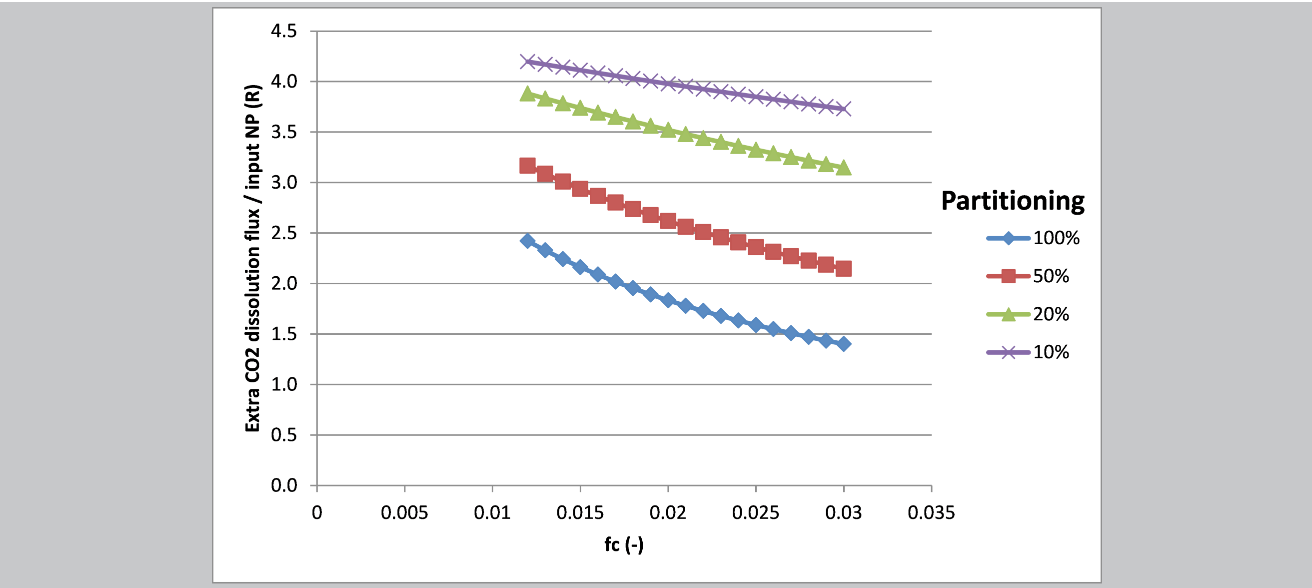

Figure 10 Ratio of additional CO_2 dissolution flux and the required NP flux (R, Eq. 19) as a function of f_c for 4 different scenarios of partitioning of NPs over CO_2 and brine (100% is equal partitioning, 10% indicates a strong preference for the CO_2 phase).

The results in the Figure 9 and Figure 10 show a clear trade-off: with more NPs moving into the brine, the increase in dissolved CO_2 becomes larger, but the efficiency decreases. The efficiency with which the NPs are used is low: even for the most efficient cases only 4.5 kg of CO_2 is dissolved additionally for every kg of NP added (per m² per year). Figure 12 illustrates this trade-off in one figure.

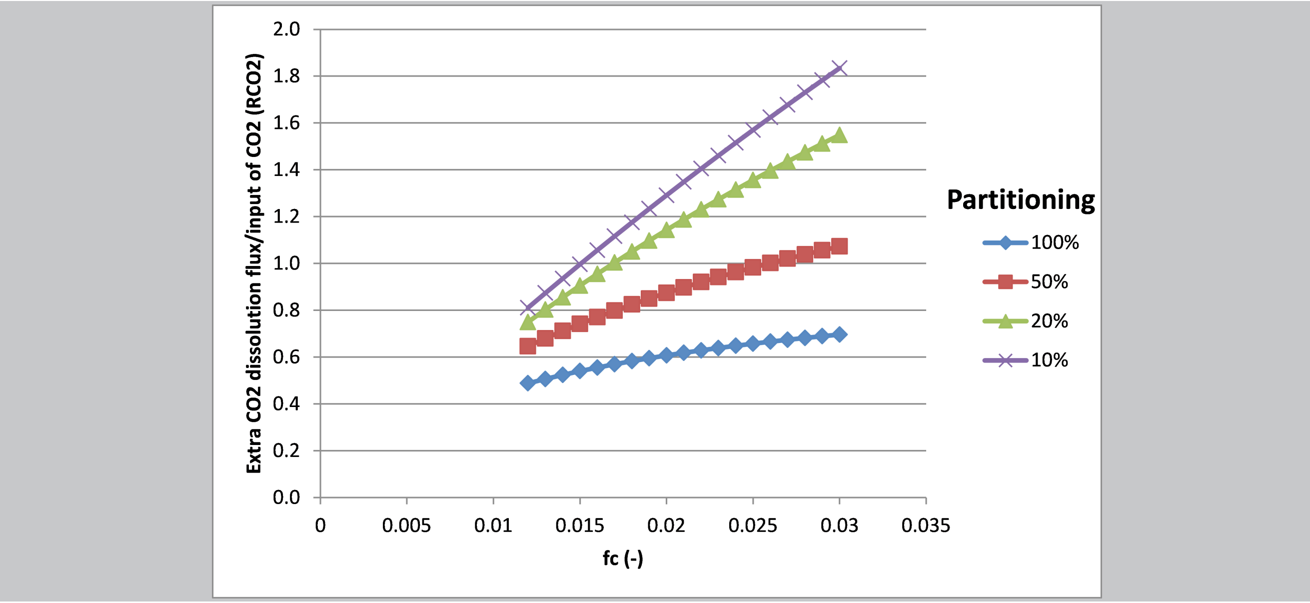

Figure 11 Additional CO_2 dissolution flux compared to the CO_2 input associated with the input in NPs (RCO_2, Eq. 20) as a function of f_c for 4 different scenarios of partitioning of NPs over CO_2 and brine (100% is equal partitioning, 10% indicates a strong preference for the CO_2 phase).

Figure 11 shows the amount of CO_2 necessary for injection with the NPs compared to the amount of CO_2 dissolved extra. Values above 1 mean that more CO_2 is dissolved than added. For all the cases below 1, more CO_2 is added when injecting the NPs than is additionally dissolved. This means that for many cases more CO_2 needs to be added than is dissolved. This is not a problem if the method is used in cases where CO_2 injection for storage is continued: a mitigation measure rather than remediation (see also the discussion in the Introduction and the next section). However, the amount of NPs to be injected is very large in any case.

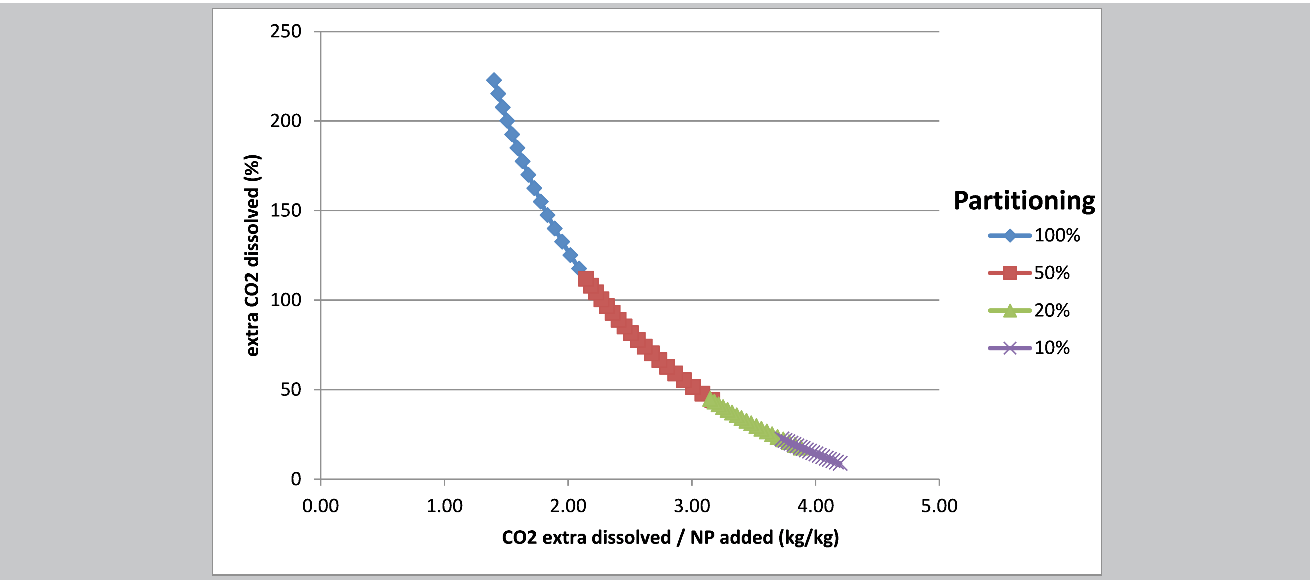

Figure 12 Illustration of the trade-off between a large increase in dissolution and efficient use of the NPs.

The efficiency of the method in terms of pressure decrease has not been simulated. Since NP require to be co-injected with a solvent/ carrier medium, typically CO2, the method requires injection of large volumes, initial pressure increase can be expected. If pressure increase is an issue, this method is obviously not suitable.

3.3 NP injection from the start

So far only the injection of NPs as a mitigation or remediation option have been discussed: i.e. when (part of) the CO_2 has already been injected. Javadpour and Nicot (2011) investigate the co-injection of NPs with CO_2 from the start of the injection of CO_2. Javadpour and Nicot (2011) stated that for co-injection of NPs from the start only a small volume fraction in the CO_2 was needed (0.001) to achieve an increase in convective mixing of 50%, suggesting that the process is quite efficient. The main reason for the difference with the results shown in this paper is the partitioning: Javadpour and Nicot assumed that the volume fraction NPs in the brine would be identical to the volume fraction NPs in the CO_2 (see section 2.2.3), whereas we assume that the NPs and CO_2 move into the brine together at the same volume fraction. With the assumption of Javadpour and Nicot, the CO_2 would become depleted of NPs very quickly. A second difference is that we compare the mass of the required NPs to the mass of CO_2. Due to the large difference in density between CO_2 and NPs (roughly a factor of 10), the mass fraction NPs in CO_2 is much larger than the volume fraction.

Thus for upfront injection, the required amounts and efficiency of NPs are the same as for injection when the CO_2 is in place. A disadvantage of injecting the NPs with CO_2 from the start is that usually the plume moves up dip first, which might result in loss of NPs. An advantage is that the presence of the NPs can reduce the time necessary for convective mixing to start.

An extreme option, especially for deep injection would be to add so many NPs that the density of the NP-CO_2 would become heavier than the brine and would sink rather than rise enhancing storage safety.

3.4 Associated risks

To evaluate the potential of this technique for remediation purposes, associated risks of the method need to be evaluated. An important side effect, is the rise in pressure caused by this method on the short term due to the required injection of quite large volumes. The amount of NPs to be injected is large, certainly if you also consider the amount of gas that needs to be co-injected with the NPs. The effect of the rise in pressure might be mitigated by brine withdrawal at the same time as (continued) injection of CO_2.

Another potential risk is loss of injectivity due to clogging of pores. This might happen if the selected NPs are too large compared to the pore throats (e.g. Mohamed, 2011) or if they aggregate. See also Section 2.3.

3.5 Cost

The costs of NPs is an important part of the feasibility of the suggested approach. Since we are particularly aiming for high density NPs, such as metal NPs (Pb, Fe, Cu, Ag or Au). The costs of such NPs is in the order of 5 – 25 k€/kg.[1] The costs of the common metal NPs (Pb, Fe and Cu) is in the lower range, while the noble metal NPs (Ag and Au) are clearly in the upper price range. On the other end of the price spectrum are clay nanoparticles. They are used in a variety of applications, among which is the oil and gas industry. The price for these mineral NPs is in the order of 0.1 k€/kg.[2] The price is lower than the metal NPs. However, the density of minerals is significantly lower than for metals and therefore they might be less effective in enhancing convective mixing. Given the range of possible prices for NPs and the need for a high density, a price of 1 k€/kg is assumed for further calculations.

Example calculation:

The goal is to dissolve 5 Mton CO_2 at doubled dissolution rate at a pressure of 100 bar and temperature of 40°C (density CO_2 is 629 kg/m^3). For an average thickness of the CO_2 layer of 10m, the surface area of CO_2 is 7.95E5 m^2. From Figure 35, it can be seen that this is possible in two ways which are summarized in Table 4.

Table 4 Example of calculation of cost for use of NPs.

	Partitioning 100%	**Partitioning 50%**
f_c (reservoir conditions)	0.014	0.027
Density NPs (kg/m^3)	10.000	10.000
Density NP-CO_2 (kg/m^3)	760	882
CO_2 dissolution flux (kg/m^2/yr)	8.89	8.79
Time to full dissolution (yrs)	707	715
NP flux (kg/m^2/yr)	2.01	1.94
Co-injected CO_2 flux (kg/m^2/yr)	8.89	4.40
Required Mass NP (kg)	1.13E9	1.10E9
Price NP (€)	1.13E9	1.10E9

From this table, it is clear that the cost are prohibitive: for dissolving 5 Mton CO_2 already more than 1 Mton NP is necessary which would cost 1 trillion € at a price of 1 €/kg, which doesn't even include the cost of transport and the required injection wells.

Even when using waste (depleted uranium oxides) as suggested by Javadpour and Nicot (2011), costs are associated with the NPs. Creating particles of the right size can be expensive and is not straightforward (Hasan et al., 2011). For example, Javadpour and Nicot (2011) cite the work by Hastings et al. (2008), in which particles are created. However the created particles are in the µm range rather than in the nm range, which would be too large to inject in a reservoir because of the risk of clogging the pores.

1 http://www.sigmaaldrich.com/materials-science/material-science-products.html?TablePage=18010474
2 https://www.sigmaaldrich.com/catalog/product/aldrich/682659?lang=en&region=NL

4 CONCLUSIONS

In this report it was investigated whether injecting NPs to enhance CO_2 dissolution via convective mixing is a viable mitigation strategy. However, it was found that the method is very inefficient in terms of the amount of NPs needed compared to the increase in CO_2 dissolution. For example, to achieve an increase of 50% in the CO_2 dissolution rate, 1 kg of NP is needed to dissolve 3 kg extra CO_2 for an example case at 1 km depth. This makes the method unattractive both technically and economically, because:

- a large effort is required for engineering NPs with the correct properties
- the risks associated: risk of clogging and pressure increase
- the method is expensive: for dissolving 5 Mton CO_2 at doubled dissolution rate, costs in excess of 1 trillion € were estimated.
- the method is very slow (order 10-100 years).

The only way to make this work applicable is to also enhance the solubility of the CO_2 at the same time.

References

Crandell, L.E., B. R. Ellis, C.A. Peters (2010) Dissolution potential of SO_2 co-injected with CO_2 in geologic sequestration. Environ. Sci. Technol. 44(1), pp 349-355. Doi: 10.1021/es90261m.

Duan, Z., Sun, R., Zhu, C. and Chou, I-M. (2006): An improved model for calculation of CO_2 solubility in aqueous solutions containing Na^+, K^+, Ca^{2+}, Mg^{2+}, Cl^- and SO_4^{2-}. Marine Chemistry 98, p 131-139.

Emami-Meybodi H., H. Hassanzadeh, C.P. Green, J. Ennis-King (2015) Convective dissolution of CO_2 in saline aquifers: Progress in modeling and experiments. Int. J. of Greenhouse Gas Control 40, pp 238-266. Doi: 10.1016/j.ijggc.2015.04.003.

Garcia, J.E., 2001. Density of aqueous solutions of CO_2, Lawrence Berkley National Laboratory Report, LBNL 49023.

Hasan S. et al. (2011).Synthesis of uraniumoxide nanoparticles in aqueous solutions (2011) Nuclear Technology 173, 3, 310-317.

Hastings, E.P., C. Lewis, J. Fitzpatrick, D. Rademacher, L. Tandon (2008) Characterization of depleted uranium oxides fabricated using different processing methods. Journal of Radioanalytical and Nuclear Chemistry 276(2), pp 475-481. Doi: 10.1007/s10967-008-0529-6.

Huppert H.E. and J.A. Neufeld (2014) The Fluid Mechanics of Carbon Dioxide Sequestration. Annu. Rev. Fluid Mech. 46, p 255-272. Doi: 10.1146/annurev-fluid-011212-140627.

Javadpour, F. and J.-P. Nicot (2011) Enhanced CO_2 storage and sequestration in deep saline aquifers by nanoparticles: commingled disposal of depleted uranium and CO_2.

Kampel, G. and G. H. Goldsztein (2011) Transport of non-brownian particles in porous media. Siam J. Appl. Math. 71(3), pp 773-790. Doi: 10.1137/090780687.

Lemmon, E. W., M.O. McLinden and D.G. Friend, “Thermophysical Properties of Fluid Systems” in NIST Chemistry WebBook, NIST Standard Reference Database Number 69, Eds. P.J. Linstrom and W.G. Mallard, National Institute of Standards and Technology, Gaithersburg MD, 20899, http://webbook.nist.gov, (retrieved July 17, 2015).

Mohamed, M. 2011. Engineerd particle size distribution while drilling helped minimize wellbore damage in sandstone reservoirs. SPE 141752.

Szulczewski, M.L., M.A. Hesse and R. Juanes (2013) carbon dioxide dissolution in structural and stratigraphic traps. J. Fluid. Mech., vol. 736, p 287-315.

Singh H., S.A. Hosseini, F. Javadpour (2012) Enhanced CO_2 storage in deep saline aquifers by nanoparticles: numerical simulation results. SPE 156983.

Section III

REMEDIATION LINKED TO TRANSPORT PROPERTIES OF FAULTS AND FRACTURE NETWORKS

Chapter XI

Report to partners justifying the choice of models (Remediation scenarios linked to CO_2 migration through faults and fractures)

Bogdan Orlic[1], Alexandre Lavrov[2], Andreas Busch[3], Dusan Karas[4]
[1] TNO, The Netherlands
[2] SINTEF PR, Norway
[3] Shell, The Netherlands
[4] NIS, Serbia

SUMMARY

Because most fractures are stress-sensitive, we investigate the feasibility of modifying the stress field to decrease the leakage rate through faults and fractures. In this study, the effect of the in-situ stress regime on possible fracture and fault reactivation scenarios has been qualitatively analysed for two kinds of CO_2 storage: deep saline reservoirs; and depleted oil and gas reservoirs. Literature review was performed to summarise the current knowledge on fracture closure laws. In the follow-up study, the effect of stresses on fracture permeability under normal or shear deformation will be quantitatively studied in detail using a hydro-mechanically coupled numerical framework. Closure laws derived in this study will thereupon be used to perform numerical simulations of realistic leakage scenarios through the caprock. This will be done by means of prototypical models, or for a real field case (e.g. Bečej field in Serbia), if enough input data becomes available for the latter. The effect of changing stress field under different injection schedules will be specifically addressed for different tectonic regimes (extensional, compressional, strike-slip).

Another remediation scenario considers mitigation of leakage by diverting CO_2 to nearby reservoir compartments in the storage reservoir. This scenario requires creating a pathway for fluid migration between the injected, leaky compartment and neighbouring compartments, as the injected and neighbouring compartments are originally not connected. A geological setting suitable to investigate the feasibility of remediation by flow diversion comprises a compartmentalized gas reservoir or aquifer. Such structural settings are quite common: e.g. the depleted P18-4 gas reservoir, planned to be used for CO_2 storage in the Rotterdam Capture and Storage Demonstration Project (ROAD), is separated by a sealing fault from the neighbouring P15 depleted gas field. Another example relevant for CO_2 storage in both depleted gas fields and aquifers, are the Rotliegendes reservoir rocks, which are compartmentalized throughout north-western Europe. The feasibility of remediation by flow diversion will be tested in a follow-up study; first on a generic model with two reservoir compartments separated by a fault. In the subsequent phase a realistic reservoir model will be used.

1 INTRODUCTION AND OBJECTIVES

The MiReCOL project investigates existing and new techniques for remediation and mitigation of leakage from geological CO_2 storage sites. The present study investigates remediation options linked to transport properties of faults and fracture networks. Fractured caprocks and faults intersecting the caprock are of primary concern as they can act as conduits for CO_2 migration out of the storage reservoir. Faults and fractures can act either as permeability barriers or preferential pathways for fluid flow, depending on their infill and the stresses acting on them. As the state of stress changes during geological history, reservoir production and injection operations, faults and fractures can open and become conductive at some time, or close and become non-conductive at other times.
The main objectives of the research are as follows:

- Review state of the art techniques for assessing leakage rates in faults and fracture networks; describe the possible leakage scenarios and the controlling factors; describe the modelling approaches that will be used in follow-up studies to investigate the feasibility of proposed remediation scenarios.
- Evaluate the impact on leakage rates of changing stress field by decreasing reservoir pressure.
- Test an original approach consisting of transferring CO_2 to another compartment originally unconnected to the storage compartment.

The present study describes remediation scenarios linked to CO_2 migration through faults and fractures. Literature study was performed to summarise the current knowledge on stress-dependent permeability, fracture closure laws, hydro-mechanical behaviour of faults and hydraulic fracturing practices in the oil and gas industry. Subsequently, the methods and approaches are described that will be used in follow-up studies to investigate the feasibility of the proposed remediation scenarios by means of numerical simulations.

2 MODIFYING THE STRESS FIELD TO DECREASE LEAKAGE RATES

The flow rates through fracture systems and faults are usually stress-dependent. If a leak through a fractured caprock or a fault is detected during CO_2 injection, the pressure in the reservoir can be relieved. The pressure change in the reservoir will affect the stress state not only in the reservoir rock, but also in the caprock, surrounding formations and nearby faults. As a consequence, the leakage rates controlled by fractures and faults will also be affected. In this chapter we investigate the feasibility of decreasing the leakage rates controlled by faults and fractures by manipulating the pressure field in the reservoir.

2.1 State-of-the-art review of CO_2 migration rates and stress conditions

2.1.1 Relevant events at storage sites

Underground storage of CO_2 requires a good understanding of CO_2 trapping and migration in subsurface. Natural analogues of CO_2 storage sites may contribute to such understanding, especially with regard to long-term effects since the lifetime of such sites is significantly longer than what ongoing engineered CO_2 pilot projects can offer. There are usually considered three possible types of leakage scenarios in natural CO_2 sites (Fessenden et al., 2009):

- focused leakage, e.g. in the form of a geyser, which can be considered as analogue to a leaking well in an engineered site;
- diffuse leakage, through a fracture system leading towards but not reaching the surface, which can be considered as analogue to a leakage through a fracture / fault system in caprock of an engineered storage site;
- no leakage.

In practice, the "no leakage" situation might be difficult to achieve in long term. Very slow seepage through porous matrix may occur in a very long term even for a rock with the lowest permeability.

The term 'diffuse leakage' in the above list is not related to the mechanism, i.e. diffusion or viscous flow, but rather to the appearance of the leak in space and time. 'Diffuse leakage' can thus be due to either diffusion or viscous flow (or both). Likewise, 'focused' leakage' can be caused by different mechanisms, e.g. a reactivated fault or a gas chimney.

An example of focused leakage from a natural site is the Crystal Geyser in Utah created by a well drilled into a natural-CO_2-bearing formation. The geyser has an average CO_2 release rate of 40-50 t/day (Friedman, 2007).

An example of diffuse leakage can be found e.g. in California, at the base of Mammoth Mountain, with CO_2 flux of 7.5 kg/(m^2/day) over an area of 5-10 ha (Fessenden et al., 2009). In the case of diffuse leakage, CO_2 typically spreads horizontally through a system of connected fractures and faults. This particular site started to leak in 1989 after a series of seismic events that supposedly opened up fractures and activated faults.

An example of a natural CO_2 site with no detectable leakage is Bravo Dome in the US (Fessenden et al., 2009).

It was emphasized by Fessenden et al. (2009) that "natural analogues can greatly help… since they provide information about the long term fate of CO_2 in a natural system". Extrapolation of results from a leaking or not leaking natural site onto engineered storage sites calls for a closer look at possible similarities and differences in stress variation and fracture/fault dynamics at natural and engineered CO_2 storage sites.

Leakage scenarios during underground storage of CO_2 are often classified into two categories: (1) abrupt leakage caused by a well failure; (2) gradual and diffuse leakage through faults, fractures or wells (Metz et al., 2005). The focus in this Section is on potential leakage through natural or induced fractures, and geological faults.

It should be noted that engineered storage sites, from stress history point of view, can belong to one of two types:

- depleted oil and gas reservoirs;
- deep saline (undepleted) aquifers.

Stress changes during production of oil and gas have been studied in reservoir geomechanics for the last 20 years (Fjær et al., 2008; Segall and Fitzgerald, 1998; Zoback and Zinke, 2002). Stress dynamics during depletion of an oil reservoir can be briefly summarized as follows, assuming pore pressure only changes inside the reservoir, and the stiffness of the reservoir is not much different from those of the over-, under- and sideburden (Fjær et al., 2008; Segall and Fitzgerald, 1998; Zoback and Zinke, 2002).

- In the reservoir: The total vertical stress may become somewhat less compressive due to arching effect. The effective vertical stress becomes more compressive. The total horizontal stress becomes less compressive. The effective horizontal stress becomes more compressive; its change however is smaller than the change in the vertical effective stress. The above stress changes typically promote normal faulting in the reservoir if the overall in-situ stress regime is extensional. They also promote closure of pre-existing vertical fractures in the reservoir.
- In the overburden: The vertical stress (total or effective) is unchanged or becomes less compressive due to the effects of the Earth surface. The horizontal stress (total or effective) becomes more compressive. These stress changes may promote reverse faulting if the initial in-situ stress regime was compressional. They also promote closing of vertical fractures.

Field observations at Valhall and Ekofisk fields suggest that normal faulting is indeed promoted in the reservoir during depletion (Zoback and Zinke, 2002). Caution should however be exercised when applying the above qualitative picture for specific fields since it is valid for a perfectly elastic isotropic case with no elastic contrast between the reservoir and the surroundings. Effects of elastic contrast are very significant, as is effects of tilt – so the in situ stress paths may be quite different. It needs to be estimated from case to case using e.g. coupled geomechanical simulations.

2.1.2 Stress alteration under injection into an undepleted aquifer

If CO_2 is injected into a deep saline aquifer surrounded by low-permeability rocks, and the reservoir has not been previously depleted, the stress dynamics will be opposite to that under depletion. Namely:

- In the reservoir: The total vertical stress may become somewhat more compressive. The effective vertical stress becomes less compressive. The total horizontal stress becomes more compressive. The effective horizontal stress becomes less compressive; its change however is smaller than the change in the vertical effective stress.
- In the overburden: The vertical stress (total or effective) is unchanged or becomes more compressive due to the effects of the Earth surface. The horizontal stress (total or effective) becomes less compressive.

Here, again, it has been assumed that pore pressure only changes inside the reservoir, and the stiffness of the reservoir is not much different from those of the over-, under- and sideburden. In reality, the cap rock is in undrained state and is typically represented by plastic and anisotropic shale, with mechanical properties different from the reservoir rock. Under such conditions, the pore pressure in the cap rock may change instantly albeit there is no flow, provided the mean stress changes.

The above stress changes will have different implications in different tectonic environments. This is illustrated by Mohr circles in Figure 1, Figure 2 and Figure 3 for extensional (normal faulting), compressional (reverse faulting) and strike-slip regimes, respectively. Note that the stress changes in the overburden appear inconsistent with results of (Vilarrasa, 2014). The reason is that a reservoir of infinite horizontal extension was analysed in the latter. We are considering a reservoir having finite dimensions in all directions.

The reservoir part of Figure 1 can be found e.g. in Magri et al. (2013) for a specific field case.

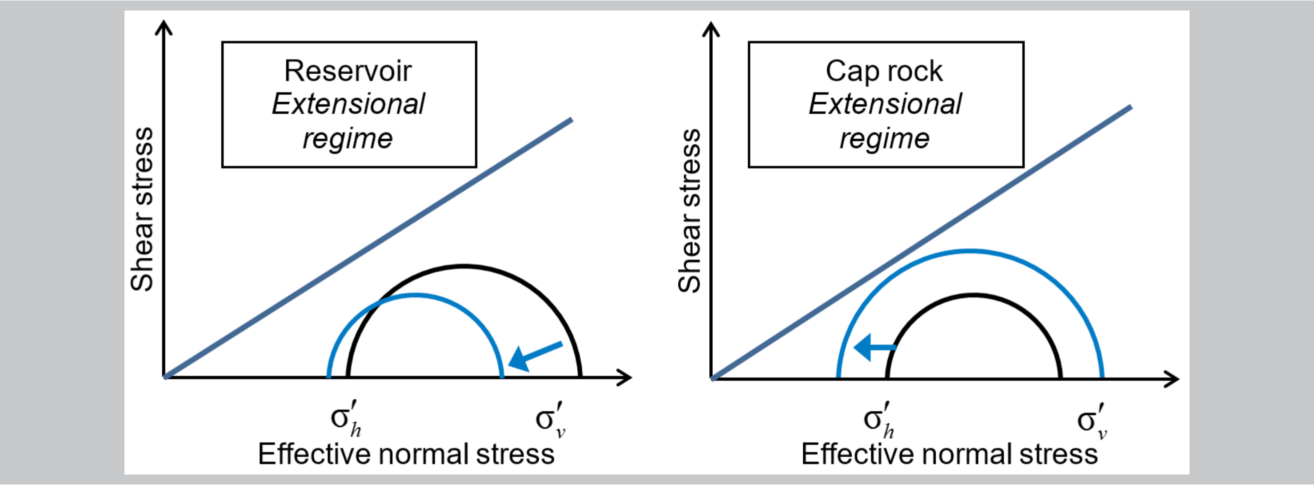

Figure 1 Schematic illustration of effective stress alterations in reservoir and overburden (caprock) during injection into an undepleted deep saline aquifer of finite horizontal and vertical dimensions. Extensional (normal faulting) in-situ stress regime is assumed. Pore pressure is assumed to remain constant outside the reservoir. Mechanical properties of the reservoir and surrounding rocks are assumed to be the same. Black Mohr circle: before injection. Blue Mohr circle: during injection (pore pressure increase in the reservoir). Blue arrow indicates possible change of the Mohr circle caused by injection. Subscripts 'v' and 'h' refer to the vertical and minimum horizontal stresses, respectively.

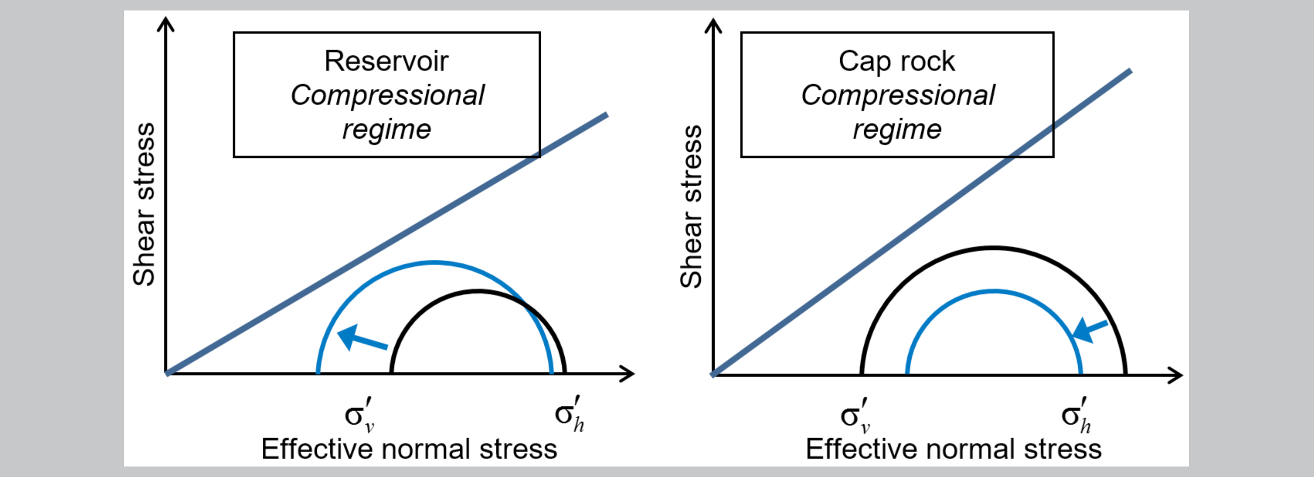

Figure 2 Schematic illustration of effective stress alterations in reservoir and overburden (caprock) during injection into an undepleted deep saline aquifer of finite horizontal and vertical dimensions. Compressional (reverse faulting) in-situ stress regime is assumed. Pore pressure is assumed to remain constant outside the reservoir. Mechanical properties of the reservoir and surrounding rocks are assumed to be the same. Black Mohr circle: before injection. Blue Mohr circle: during injection (pore pressure increase in the reservoir). Blue arrow indicates possible change of the Mohr circle caused by injection. Subscripts 'v' and 'h' refer to the vertical and minimum horizontal stresses, respectively.

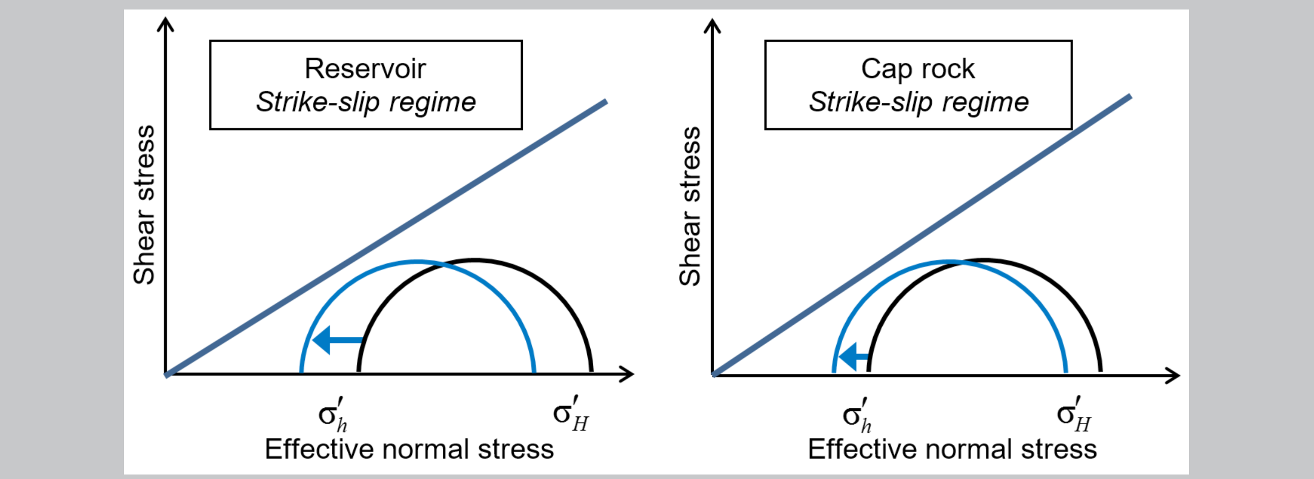

Figure 3 Schematic illustration of effective stress alterations in reservoir and overburden (caprock) during injection into an undepleted deep saline aquifer of finite horizontal and vertical dimensions. Strike-slip in-situ stress regime is assumed. Pore pressure is assumed to remain constant outside the reservoir. Mechanical properties of the reservoir and surrounding rocks are assumed to be the same. Black Mohr circle: before injection. Blue Mohr circle: during injection (pore pressure increase in the reservoir). Blue arrow indicates possible change of the Mohr circle caused by injection. Subscripts 'H' and 'h' refer to the maximum and minimum horizontal stresses, respectively.

2.1.3 Stress alteration under injection into a depleted reservoir

Injection of CO_2 into geological formations increases the pore pressure. As a result, the effective normal stress on pre-existing faults and shear fractures is generally reduced. This, in turn, reduces frictional resistance on the fracture surfaces, thus facilitating reactivation of faults and shear fractures by slip. In addition, increasing the pore pressure above a certain level may induce hydraulic fracturing in the reservoir that might or might not propagate into the overburden. Finally, injection changes the overall state of stress in and around the reservoir because of poroelastic effects.

An important aspect during injection into depleted reservoirs is the effect of reservoir stress path. Stress path can be defined as the ratio of the increase in the total horizontal stress to the increase in the pore pressure that caused it, $\beta_h = \Delta\sigma_h/\Delta P_p$ or $\beta_H = \Delta\sigma_H/\Delta Pp$. While the stress path during depletion can often be about 0.5-0.8 (Nelson et al., 2005), it can be much smaller, down to almost zero, during subsequent injection into the depleted field (Santarelli et al., 1998). More research on stress path during depletion – reinjection is needed in order to find out how common the abnormally low stress paths reported in the literature are under different tectonic regimes and geological settings.

From geomechanical viewpoint, depletion corresponds to reservoir loading (increase of effective stresses). Subsequent injection into a depleted reservoir corresponds to its unloading. Zero (or low) stress path is believed to be due to plastic deformation created in the reservoir by its loading during depletion. Detrimental role of possibly zero stress path during injection of CO_2 into a depleted field was recognized in a recent publication (Vidal-Gilbert et al., 2010).

Assume that during both depletion and subsequent injection the pore pressure only changes inside the reservoir, and the stiffness of the reservoir is not much different from those of the over-, under- and sideburden. Under these assumptions, stress changes under depletion and injection are illustrated in Figure 4, Figure 5 and Figure 6 for extensional (normal faulting), compressional (reverse faulting) and strike-slip regimes, respectively. The reservoir parts of Figure 4 and Figure 6 can be found in (Vidal-Gilbert et al., 2010) for a specific field case. Stress changes during depletion are shown by black arrows in these Figures. Two cases are illustrated in each Figure: Stress changes with zero reservoir stress path during injection are shown by yellow arrows. Stress changes with unchanged, original stress path during injection are shown by blue arrows. The latter case corresponds to reversible reservoir deformation during depletion-injection. The stress path in the overburden (caprock) is assumed to be the same under depletion and injection, i.e. no irreversible deformation occurs in the caprock under depletion. Moreover, the stress path in the overburden (caprock) is assumed to be unaffected by possibly zero reservoir stress path. In reality, the latter might not be the case. The stress paths for the minimum and maximum horizontal stresses are assumed to be equal in Figure 2.6 ($\beta_h = \beta_H$).

Non-zero stress path and non-unity Biot effective stress coefficient reduce the risk of fault reactivation in the reservoir in normal and strike-slip regimes (Orlic et al., 2011; Vidal-Gilbert et al., 2010).

Irreversibility represented by zero (or very low) stress path is expected to have profound effects on the reservoir and caprock integrity. In particular, if normal faults have been reactivated in the reservoir during depletion, they will not be able to return to their initial state during injection because it is not possible to reconstruct the pre-depletion state of stress by simply re-pressurizing the reservoir to the same pressure. In addition, hydraulic conductivity of fractures subject to shear deformation is irreversible (Esaki et al., 1999) and thus may persist even in the case of a sufficiently high stress path, β_h, during injection.

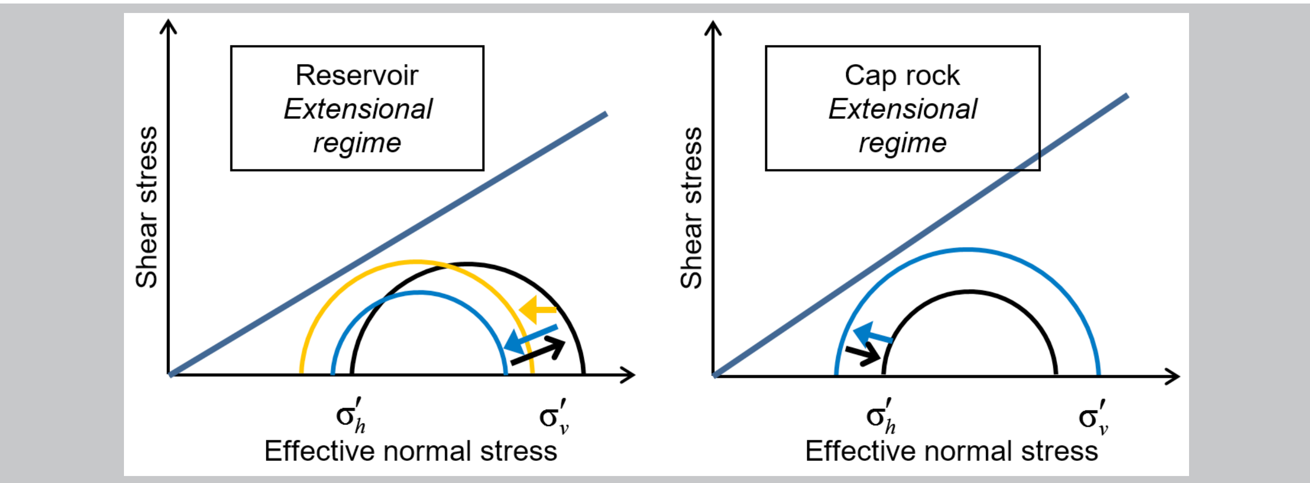

Figure 4 Schematic illustration of effective stress alterations in reservoir and overburden (caprock) during injection into a depleted reservoir of finite horizontal and vertical dimensions. Extensional (normal faulting) in-situ stress regime is assumed. Pore pressure is assumed to remain constant outside the reservoir. Mechanical properties of the reservoir and surrounding rocks are assumed to be the same. Black Mohr circle: after depletion. Blue Mohr circle: during injection (pore pressure increase in the reservoir), assuming unchanged stress path (reversible deformation). Yellow Mohr circle: during injection (pore pressure increase in the reservoir), assuming zero stress path. Subscripts 'v' and 'h' refer to the vertical and minimum horizontal stresses, respectively.

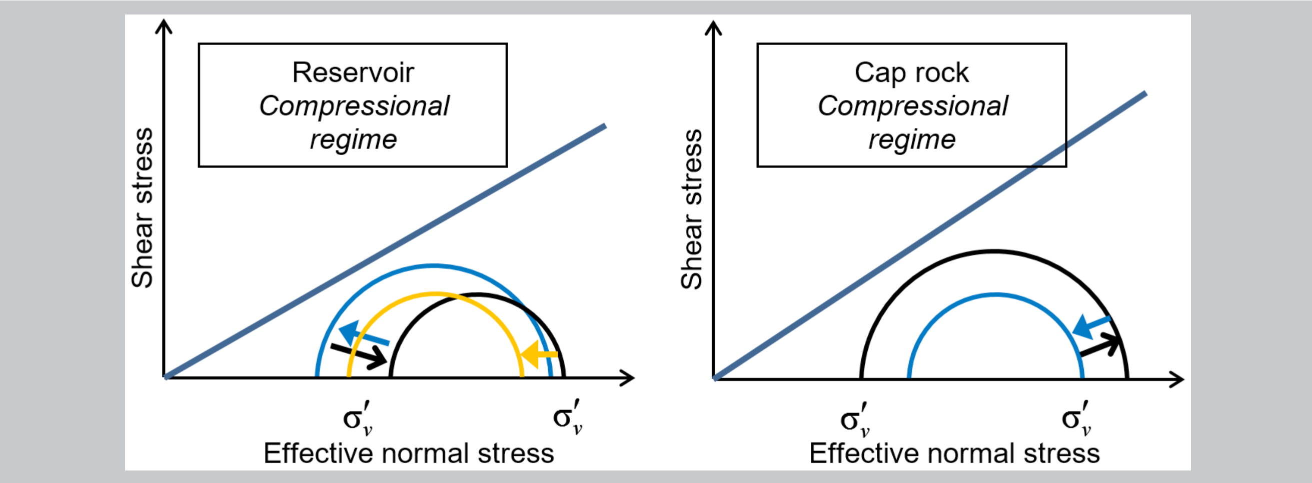

Figure 5 Schematic illustration of effective stress alterations in reservoir and overburden (caprock) during injection into a depleted reservoir of finite horizontal and vertical dimensions. Compressional (reverse faulting) in-situ stress regime is assumed. Pore pressure is assumed to remain constant outside the reservoir. Mechanical properties of the reservoir and surrounding rocks are assumed to be the same. Black Mohr circle: after depletion. Blue Mohr circle: during injection (pore pressure increase in the reservoir), assuming unchanged stress path (reversible deformation). Yellow Mohr circle: during injection (pore pressure increase in the reservoir), assuming zero stress path. Subscripts '*v*' and '*h*' refer to the vertical and minimum horizontal stresses, respectively.

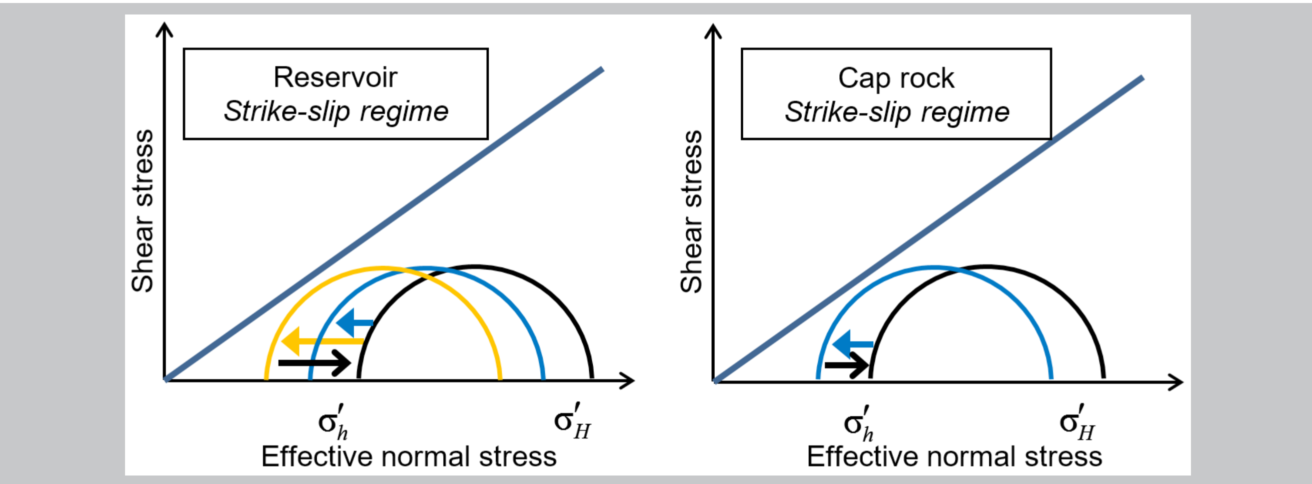

Figure 6 Schematic illustration of effective stress alterations in reservoir and overburden (caprock) during injection into a depleted reservoir of finite horizontal and vertical dimensions. Strike-slip in-situ stress regime is assumed. Pore pressure is assumed to remain constant outside the reservoir. Mechanical properties of the reservoir and surrounding rocks are assumed to be the same. Black Mohr circle: after depletion. Blue Mohr circle: during injection (pore pressure increase in the reservoir), assuming unchanged stress path (reversible deformation). Yellow Mohr circle: during injection (pore pressure increase in the reservoir), assuming zero stress path. Subscripts '*H*' and '*h*' refer to the maximum and minimum horizontal stresses, respectively.

2.1.4 Effect of stress alteration on fractures and faults in reservoir and caprock.

Stress changes that can be expected during CO_2 injection into a deep saline aquifer or a depleted oil reservoir were summarised above. Due to large variation and heterogeneity in rock properties and complex geological structures, the stress variations can be much more complex in real life. However, our simplified treatment still provides some hints about the geomechanical effects on reservoir and caprock stability during injection. Mechanisms affecting stability can be derived from Figure 1 to Figure 6 and are summarized in Table 1. In addition to the effects listed in Table 1, reactivation of shear fractures and faults may enhance permeability in the direction of the intermediate in-situ stress due to the “tubular” effect at shear fracture intersections (Sibson, 1996). This may, consequently, facilitate horizontal spreading of CO_2 under extensional and compressional stress regimes.

It is important to emphasize that possible activation of each of the mechanisms listed in Table 1, such as e.g. tensile fractures or thrusts, ultimately depends on mechanical properties of rocks and faults, and on the specific values of pore pressure and stress magnitudes before, during and after injection. The descriptions in Table 1 only indicate what can possibly happen, provided e.g. that the fluid pressure becomes high enough or the rock strength is sufficiently small. Also, in real life, the picture can and probably will be complicated by pore pressure diffusion from the reservoir into the surrounding low-permeability rock that was neglected when constructing Figure 1 to Figure 6. Moreover, even when fracturing occurs, it will not necessarily lead to leakage. For instance, fractures may fail to establish a connected network. Some fractures might close after injection is finished provided that shear displacement was sufficiently small on those fractures. A detailed analysis is required for each specific case in order to assess the risks associated with stress changes and possible fracturing during CO_2 injection.

Table 1 Possible fracturing scenarios during CO_2 injection in different tectonic regimes. 'Pore pressure' in the Table refers to the reservoir pore pressure. Pore pressure in the caprock is assumed to remain unchanged.

Type of storage	Stress regime	Reservoir	Caprock
Deep saline aquifer	Extensional (normal faulting)	Possible opening of subvertical fractures if pore pressure becomes sufficiently high.	Possible reactivation of normal faults and shear fractures. Possible opening of subvertical fractures if pore pressure becomes sufficiently high.
	Compressional (reverse faulting)	Possible reactivation of thrusts and shear fractures. Possible opening of subvertical fractures if pore pressure becomes sufficiently high.	
	Strike-slip	Possible reactivation of strike-slip faults and shear fractures. Possible opening of subvertical fractures if pore pressure becomes sufficiently high.	Possible reactivation of strike-slip faults and shear fractures. Possible opening of subvertical fractures if pore pressure becomes sufficiently high.
Depleted reservoir	Extensional (normal faulting)	Possible reactivation of normal faults if stress path is sufficiently low during injection. Possible opening of subvertical fractures if stress path is sufficiently low compared to its value during depletion, and pore pressure becomes sufficiently high.	Possible reactivation of normal faults after pore pressure becomes sufficiently larger than it was before depletion.
	Compressional (reverse faulting)	Possible reactivation of reverse faults if stress path during injection is sufficiently high (i.e. unchanged with regard to its value during depletion).	
	Strike-slip	Possible reactivation of strike-slip faults and shear fractures if stress path is sufficiently low during injection. Possible opening of subvertical fractures if pore pressure becomes sufficiently high.	Possible reactivation of strike-slip faults and shear fractures becomes sufficiently larger than it was before depletion. Possible opening of subvertical fractures if pore pressure becomes sufficiently high.

It should be noted that shear and tensile fractures generated or reactivated in the reservoir might improve the injectivity by reducing the flow resistance (Nelson et al., 2005). However, propagation of such fractures into the caprock may represent a risk factor for caprock integrity (Orlic et al., 2011; Streit and Hillis, 2004). And so may fault reactivation inside the reservoir if the slip displacement propagates into the caprock. In any event, the effect of changing reservoir pressure on the stress state in the caprock is typically smaller than on the stress state in the reservoir itself (Orlic et al., 2011). Therefore fracture and fault reactivation scenarios in the caprock under depletion shown in the last column of Table 2.1 will most likely be able to develop only after the onset of fracture or fault reactivation in the reservoir. Another important contributing factor that should be carefully examined for storage in depleted reservoirs is damage that possibly has been created in the caprock during depletion (Orlic et al., 2011; Streit and Hillis, 2004). This may include fault reactivation, wellbore casing failure or formation of new fractures (Streit and Hillis, 2004).

2.1.5 Rock fractures and their role in possible leakage of CO_2

One of the main factors controlling possible leakage of CO_2 from underground storage facilities is believed to be flow through fractures and faults, either in the near-well area, or farther away in the caprock (Fessenden et al., 2009; Orlic et al., 2011).

Fractures are present in most rocks. Intergranular microcracks, extensional fractures, joints, shear fractures are all examples of fractures found on different scales. Given the abundance of fractures and faults in the Earth crust, it is important to be able to predict the risk and extent of leakage through fractures and faults at CCS sites. This requires a good understanding of hydro-mechanical behaviour of fractures and faults.

It should be noted that being able to predict CO_2 flow in natural fractures is important not only because of possible leakage but also because it may influence the injectivity and the storage capacity of the CCS site. Experiments and numerical simulations suggest that CO_2 can bypass the matrix if fractures of sufficient permeability are available in the formation (Oh et al., 2013). This may reduce the matrix storage capacity and the overall storage capacity of the reservoir. It is conceivable that this might also impact plume migration along such fractures and the predictability of it. It is not improbable that channelization through fractures might deliver CO_2 into parts of the reservoir where it is actually not supposed to be, such as e.g. close to faults or abandoned wells.

Hydraulic properties of fractures; implications for CCS; concept of hydraulic aperture

Fracture surfaces are rough. In particular, landscapes of natural tensile fracture surfaces are known to exhibit more or less regular structures reflecting their growth process, such as hackle plumes (Bahat et al., 2005). Roughness, contact points and mineral deposits between fracture faces contribute to flow tortuosity which effectively means an increase in flow resistance.

In flow modelling, the fracture conductivity is usually characterized by the so called hydraulic aperture which is the aperture of a conduit with smooth parallel plane walls that exhibits the same flow rate under a given pressure gradient as the rough-walled fracture does. The mechanical aperture is defined as an average geometric distance between fracture faces. Numerous studies suggest that the hydraulic aperture of rock fractures is smaller than the mechanical aperture, sometimes by a factor of 5-6 (Esaki et al., 1999). It is the hydraulic, not mechanical, aperture, wh, that controls the flow rate through the fracture.

At low Reynolds numbers, the flow rate, q, of a Newtonian fluid in the fracture is given by the “cubic law” (Brown, 1987; Zimmerman et al., 1991):

$$\mathbf{q} = -\frac{w_h^3}{12\eta}\nabla P \quad (1)$$

where P is the fluid pressure; η is the dynamic viscosity of the fluid.

Fracture initiation, propagation and reopening in CO_2 storage

Natural and induced fractures represent potential escape paths for fluids injected into geological formations. In particular, faults and fractures are found to be the most common leakage pathway in natural CO_2 leakage incidents reviewed by (Lewicki et al., 2007).

Fractures can be natural (pre-existing), or be created by pressurization during injection, or be due to damage incurred during fault reactivation. How much a particular fracture contributes to leakage depends on its morphology, connectivity to other fractures, orientation with respect to in-situ stresses etc. These factors are discussed further in this Section.

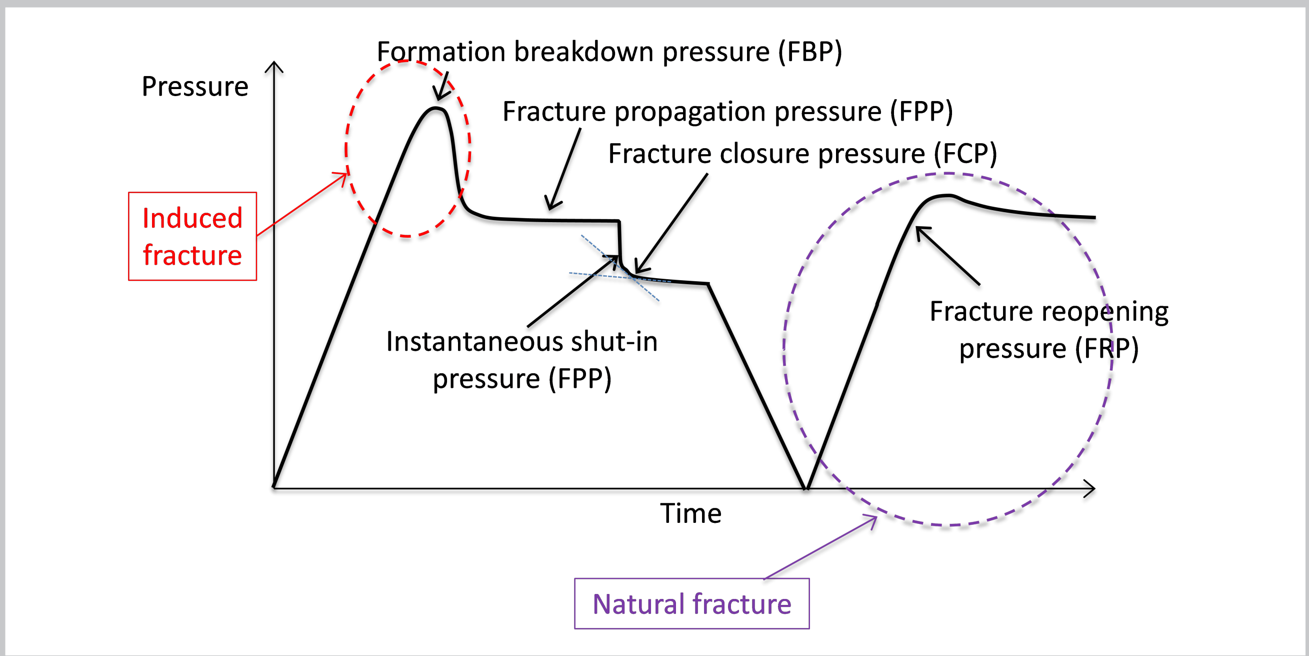

Figure 7 Injection pressure vs time in an extended leak-off test (XLOT). Origin corresponds to the pressure equal to the pore pressure (formation fluid pressure).

Behaviour of natural or induced fractures during CO_2 injection into subsurface can be illustrated by means of the extended leak-off test (XLOT) used in oil and gas industry to evaluate the minimum in-situ stress. During this test, fluid is injected into the formation until the formation fractures, and beyond. A typical pressure vs time curve obtained in an XLOT is schematically shown in Figure 7. A detailed coverage of XLOT can be found e.g. in (Fjær et al., 2008; Raaen et al., 2006).

After the first injection and the subsequent shut-in and bleed-off (flow-back) phases, a repeat cycle of the test is performed. This repeat cycle, on the right in Figure 7, can be used to illustrate the behaviour of a pressurized natural fracture located in the near-well area or farther away from the injector. The first injection cycle, on the left in Figure 7, is illustrative of induced fractures in the near-well area.

Leakage through natural fractures and faults

Three flow situations can be conceived, depending on the fluid pressure at the entry point into the fracture, P, relative to the formation fluid pressure, Pp, and the in-situ stresses.

$$P = P_p$$

The fracture is hydraulically closed in this case. There is hydraulic equilibrium, i.e. there is no hydraulic gradient between the entry point into the fracture and the rest of the fracture. There is therefore no flow. “Entry point” here means e.g. the spot where the injection wellbore intersects the fracture.

$$P_p < P < P_{FRP}$$

When the fluid pressure at the point of entry into the fracture, P, exceeds the formation pore pressure, P_p, but is below the fracture re-opening pressure, P_{FRP} (Figure 8), the fracture is “closed”, but only in the sense that the opposing fracture faces touch each other at asperities. There is a hydraulic gradient inside the fracture. If there were no asperities, i.e. no roughness, the fracture would have zero mechanical and hydraulic aperture, and there would be no flow. However, due to roughness, the fracture is hydraulically opened albeit its hydraulic aperture is significantly smaller than it would be if the fracture faces had been kept apart. Flow is therefore possible although contact spots increase the flow tortuosity and thereby reduce the hydraulic aperture. CO_2 should be able to flow through the fracture under such conditions, albeit its flow rate, being proportional to , would be much smaller than in the case of an open fracture ($P > P_{FRP}$) considered below.

$$P > P_{FRP}$$

When the fluid pressure inside the fracture, P, exceeds the fracture re-opening pressure, the fracture opens up, i.e. asperities on the opposite sides are not in contact any more. As the fracture opens up, its hydraulic aperture increases, and, as Eq.(3) shows, it has a dramatic impact on the fracture conductivity. Under such conditions, supercritical CO_2 ($scCO_2$) will eventually be able to flow in the fracture as it becomes sufficiently wide.

In addition, if the natural fracture has a limited extent, and the fluid pressure is increased so as to pass the peak in the repeat cycle (Figure 7), the fracture may start propagating (see plateau in the rightmost part of Figure 7). Whether such scenario is realistic is an open question.

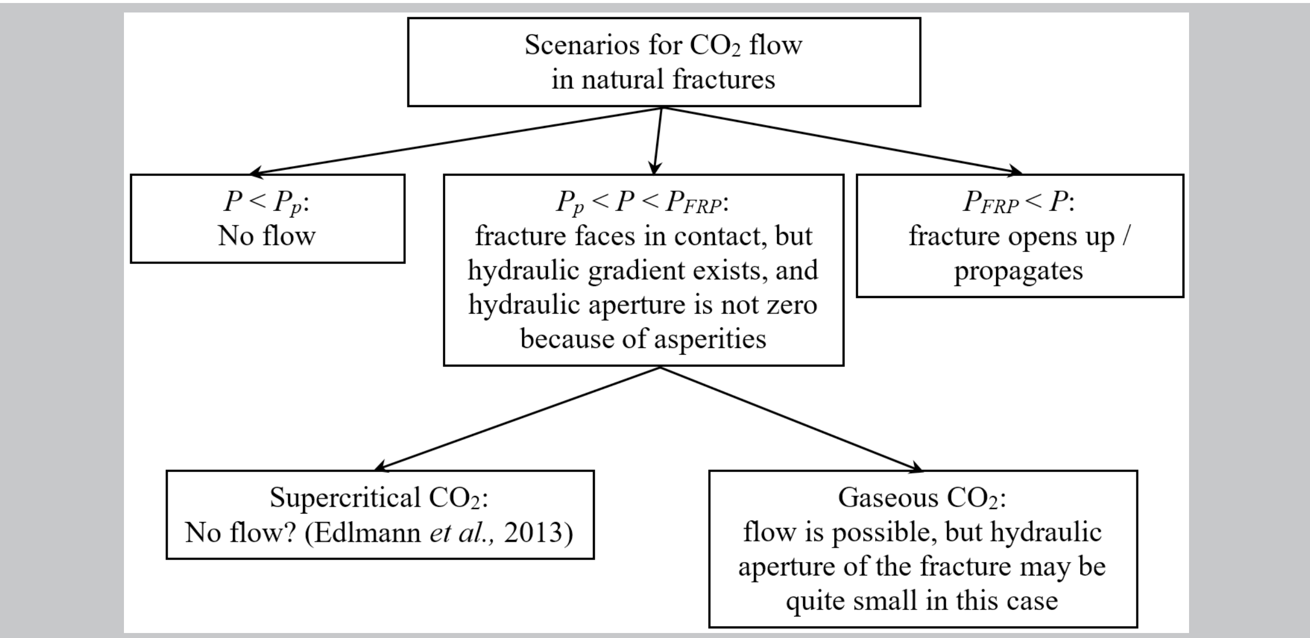

Figure 8 Scenarios for CO_2 flow in natural fractures.

The scenarios for CO_2 flow in fractures described above are summarized in Figure 8.

Experimental data on CO_2 flow in fractures

Only few experimental studies on flow of gaseous or supercritical CO_2 in rock fractures have been published.

Edlmann et al. (2013) reported that supercritical CO_2 could not flow in closed fractures in their laboratory experiments. Gaseous CO_2 (gCO_2), on the other hand, could flow in the same fractures and under the same pressure gradient. The inability of $scCO_2$ to flow in closed fractures was not supported by experiments of (Oh et al., 2013). In any event, the experiments by Edlmann et al. (2013) indicate that fracture permeability to $scCO_2$ can be considerably smaller than to gCO_2.

Oh et al. (2013) performed laboratory experiments on fracture flow of $scCO_2$, supported by numerical simulations. The specimen contained one throughgoing artificial fracture. At low injection rates, the CO_2 flow was only through the fracture. As the injection rate was increased, flow through the matrix started, but was considerably slower than in a specimen that did not contain a fracture.

Fracture permeability under stress

Hydraulic aperture of a fracture may change as a result of fracture opening/closing, or due to shear. Moreover, natural fractures, unless they are completely filled with precipitated minerals or gouge, or unless their faces perfectly fit (due to creep on geological time scale, for instance), may have an initial aperture that will contribute to their permeability even if no opening / closing or shear at recent time has occurred. Initial apertures, opening/closing and shear contribute to flow re-distribution during reservoir depletion and re-pressurization under CO_2 injection. They are the most essential components of any numerical model of leakage through fractures. Therefore, the remainder of this Section provides a brief overview of fracture deformation and flow under stress, to be used in the later stages of the project when performing coupled geomechanical simulations of CO_2 flow in fractured rock.

Fracture opening / closing and normal stiffness

If no shear stress is applied on the fracture, and the effective normal stress changes (by changing fluid pressure inside the fracture or by changing the applied normal stress), the fracture will open or close. The fracture faces move in the direction normal to the fracture faces in this case. This is known as mode I in fracture mechanics. The change in the mechanical and, thereby, hydraulic aperture is controlled by the fracture normal stiffness in this case, K_n. The fracture normal stiffness depends on the spatial distribution and the amount of contact spots between the fracture faces (Pyrak-Nolte, 1996). Flow in the fracture depends on the amount and spatial distribution of opened apertures in between the contact spots.

Fracture deformation in mode I is nonlinear: The normal stiffness increases as the applied compressive stress increases (or, equivalently, the fluid pressure inside the fracture decreases) (Pyrak-Nolte, 1996).

Since both fracture permeability and normal stiffness depend on the amount and distribution of contact spots, there is a relationship between these two properties schematically shown in Figure 9.

Figure 9 Fracture permeability versus normal stiffness under applied normal stress, after (Pyrak-Nolte, 1996).

Fracture shearing and shear stiffness

When a shear stress is applied to a fracture or a cohesionless fault, the necessary condition for sliding to commence is given by the Coulomb criterion (Nemoto et al., 2008):

$$\tau = \mu(\sigma_n - P) \quad (2)$$

where τ and σ are the shear and normal stress on the fracture surface, respectively; μ is the coefficient of friction, P is the fluid pressure inside the fracture. After the peak in the shear displacement – shear stress curve is reached, the shear stress typically drops to its residual value of about 50% of the peak stress (Figure 10) (Esaki et al., 1999). The shear displacement corresponding to the peak was found to be about 1% of the fracture size in laboratory tests (Yeo et al., 1998).

During shear caused by increasing shear stress under a constant normal load, the fracture conductivity increases up until it levels off (Figure 11; Esaki et al., 1999). The increase can be 1-2 orders of magnitude. This increase is due to dilatancy caused by surface roughness: Asperities slide over one another, and the fracture opens up (Nemoto et al., 2008).The maximum value of conductivity achievable during the sliding is a function of the maximum height of asperities.

During reverse shearing, the fracture conductivity drops only slightly, and significant conductivity is still maintained when the fracture faces return to their initial position (Figure 11). The drop in conductivity during reverse shearing is larger under higher applied normal stress, which was attributed by (Esaki et al., 1999) to fracture plugging by gouge formed by crushing of asperities under elevated normal stress. Irreversible shear deformation of fractures may contribute to their elevated conductivity during the depletion-injection cycle when CO_2 is stored in a depleted reservoir.

It should be noted that the experiments on which Figure 10 and Figure 11 are based were performed on a hard crystalline rock that does not exhibit swelling and self-sealing. Shear-induced permeability changes can be considerably more complicated in shales due to swelling and smearing of clay minerals under shear displacement (Cuss et al., 2011).

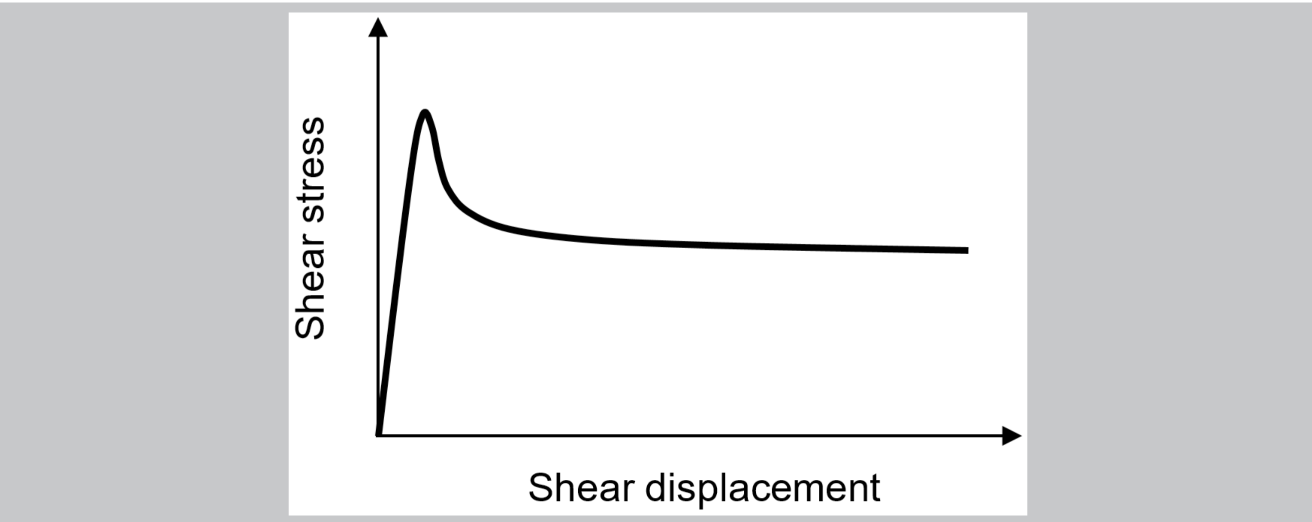

Figure 10 Shear stress versus shear displacement during sliding under constant applied normal stress, after (Esaki et al., 1999).

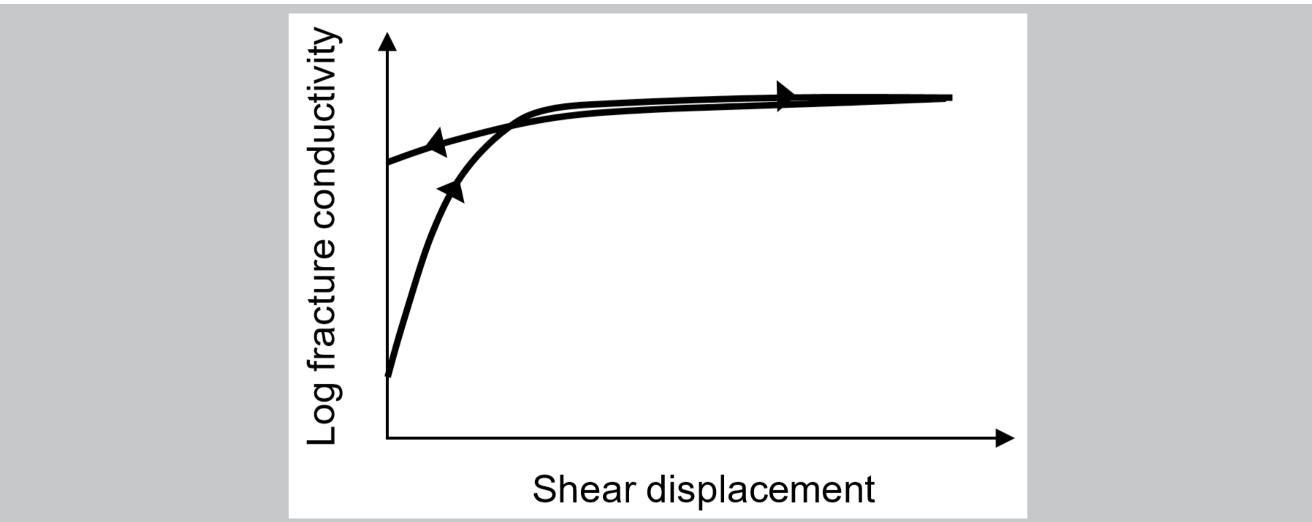

Figure 11 Log fracture conductivity vs shear displacement during forward and reverse shearing under constant applied normal stress, after (Esaki et al., 1999).

Key parameters controlling CO_2 leakage through fractures and faults

CO_2 leakage through fractures and faults is mainly controlled by the following factors:

- in-situ pore pressure (currently existing pressure – as affected by depletion or previous injections);
- locations and dimensions of faults, and their hydraulic and mechanical properties;
- number and orientation of fracture sets;
- spacing of fractures in each set;
- connectivity of the fracture network;
- extent of the fractures and fracture networks in vertical and horizontal directions;
- tectonic regime; magnitude and orientation of in-situ principal stresses (current status – as affected by depletion or previous injections);
- hydraulic aperture of fractures in each set;
- filling of fractures – gouge, mineralization;
- self-sealing potential of fractures (in the long-term perspective)

Moreover, fracture surface roughness and aperture distribution can provide additional information on mechanical and hydraulic behavior of fractures.

2.1.6 Model requirements and description of the CO_2 migration scenarios

The CO_2 mitigation scenarios consider modifying the stress field to decrease the leakage rate.

Model requirements

Since the procedures proposed are quite innovative, much can be learnt from considering, at first, some simplified prototype models of processes that we are dealing with, such as stress-dependent fracture permeability or influence of large-scale stress variations on flow dynamics controlled by fractures and faults. Numerical simulations of a well-documented field case of CO_2 leakage are envisaged at a later stage of the project.

Description of the models selected

Sufficient characterization of the site will be an important criterion for selecting the field case. This should include rock properties, fracture properties (as listed in the section on Key parameters controlling CO_2 leakage through fractures and faults), orientation and magnitude of in-situ stresses, fault locations, dimensions and hydro-mechanical properties. In the case of a leaking natural CO_2 site, the data should also include the history of leakage. We intend to focus in particular on the Bečej natural CO_2 field (provided by NIS) in which secondary accumulations of CO_2 have been formed in the overburden above the main reservoir. The Bečej model is currently under construction and will be described in the subsequent reports. The use of the Bečej field implies that enough input data becomes available to us in order to build a representative geomechanical model. In case such data cannot be procured during the project lifetime, we shall perform an extended study of stress field modification effects by means of prototypical models. This will allow us to draw generic conclusions regarding the effects of stress state modification on CO_2 leakage.

Planned model procedure I

The key parameters controlling migration caused by fractures and faults will be addressed through numerical simulation in this project. Fracture simulation requires that deformation and flow in fractures are first quantified as function of applied stresses (or displacements, normal or shear). Fracture permeability as a function of stresses/displacement then enters as a closure law in the hydro-mechanically coupled simulation framework. Therefore, the following plan of actions can be proposed:

1. Quantify stress-dependent fracture permeability to provide a closure law for coupled geomechanical simulation of leakage through fractures and faults in caprock (Y2014-2015).
2. Establish prototype models of typical expected leakage scenarios in CO_2 storage sites caused by fractures and faults, and taking into account the effect of stress regime on the leakage mechanism as discussed in this report (Y2015).
3. Perform simulations with prototype models (numerical or semi-analytical) (Y2015).
4. Simulate numerically a field case that can be used to investigate the roles and contributions of the leakage mechanisms revealed in prototype models. Pre-requisite for such a simulation is sufficiently detailed characterization of the site, in particular the geomechanical data and the fracture properties listed in Section 3.1.1 (Y2015).
5. Based on the modelling results, provide recommendations on prevention and remediation of leakage under different stress regimes (Y2016).

Quantification of stress-dependent fracture permeability (step 1 in the above plan) will be done by performing simulations of individual fracture deformation (normal or shear) with the finite-element code ABAQUS, taking into account plasticity at contacts between rough fracture surfaces (e.g. Walsh et al., 2013), and possible breakage of asperities. Extended finite-element method (XFEM) available in ABAQUS can be used to model crushing of asperities and nonlinear effects it may cause. Flow in tensile or shear fractures will then be quantified as a function of applied stresses by using the fracture flow code PROPANICA developed at SINTEF

(Lavrov, 2013a; b). This modelling workflow is illustrated in Figure 12. The computational framework will allow us to establish and test a procedure for providing critically important closure laws for geomechanical simulations of leakage through fractures.

Simulations of leakage in prototypical and real cases (steps 2-5) will be performed by using another fracture modelling framework. Hydro-mechanically coupled fracturing simulator based on the hybrid finite-element / discrete-element fracturing code MDEM developed at SINTEF (Alassi et al., 2011; Lavrov et al., 2014) and the reservoir simulator TOUGH2 developed at Lawrence Berkeley National Laboratory (Pruess et al., 2012) can be used as such framework (Figure 13). Other possible choices of the modelling tool will be considered as well.

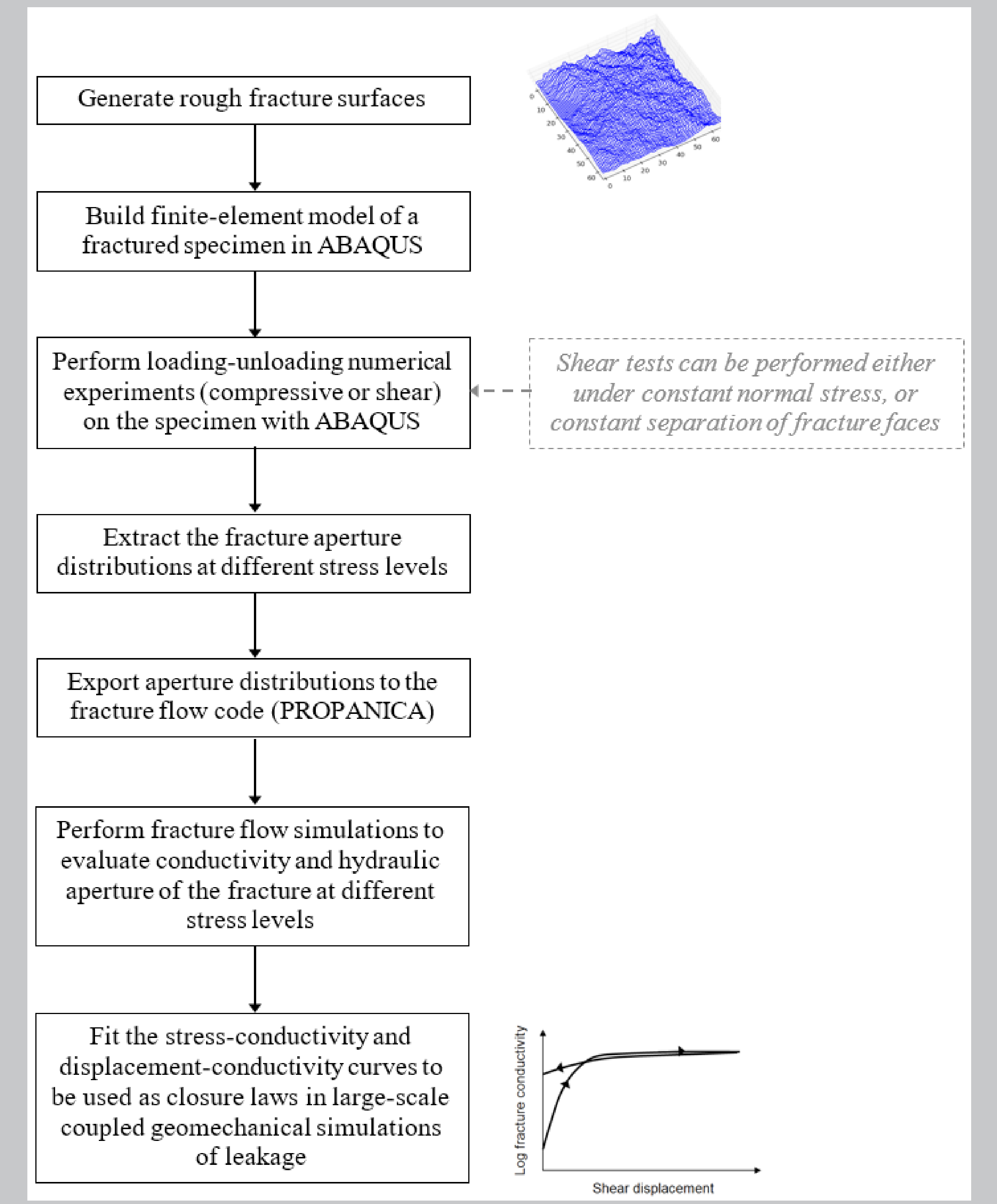

Figure 12 Schematic view of the work flow for deriving closure laws for coupled geomechanical simulations of leakages caused by normal and shear fractures.

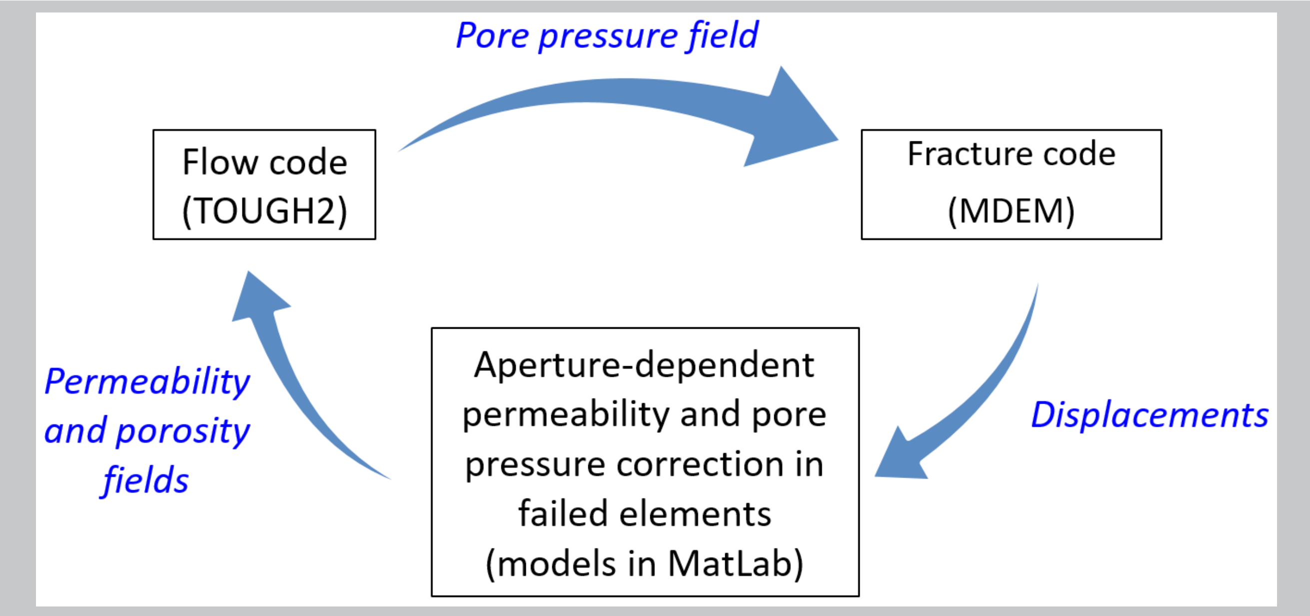

Figure 13 Computational flow in hydro-mechanically two-way coupled fracture simulation framework used at SINTEF.

Planned model procedure II

The proposed CO_2 migration scenario is based on the Bečej field case. The scenario considers leakage through a channel in the caprock created by a well blowout. This scenario is inspired by a real incident in the Bečej field that happened in 1968 (Lakatos et al., 2009).

Gas migration through a channel created by a well blowout is very similar to migration through fractures and faults. A channel consists of a collapsed zone, filled-in by secondary material, and a heavily fractured damaged zone, possibly forming a system of (small) caverns.

The field study of CO_2 leakage will be based on a detailed geological model of the Bečej field. Such a model comprises the main gas-saturated reservoir and the complex overburden structure with several shallow aquifers (Figure 14).

In the first phase of dynamic modelling, a near-well sector model will be developed, with a leakage channel through the caprock created by a well blowout. The channel connects the main CO_2 reservoir with the shallow overburden, which were initially isolated by the caprock. The near-well model will be based on all the available field information and other reported cases of well blowouts. Such a model will allow calculating the volume of gas that can be released from the reservoir at specific PVT conditions.

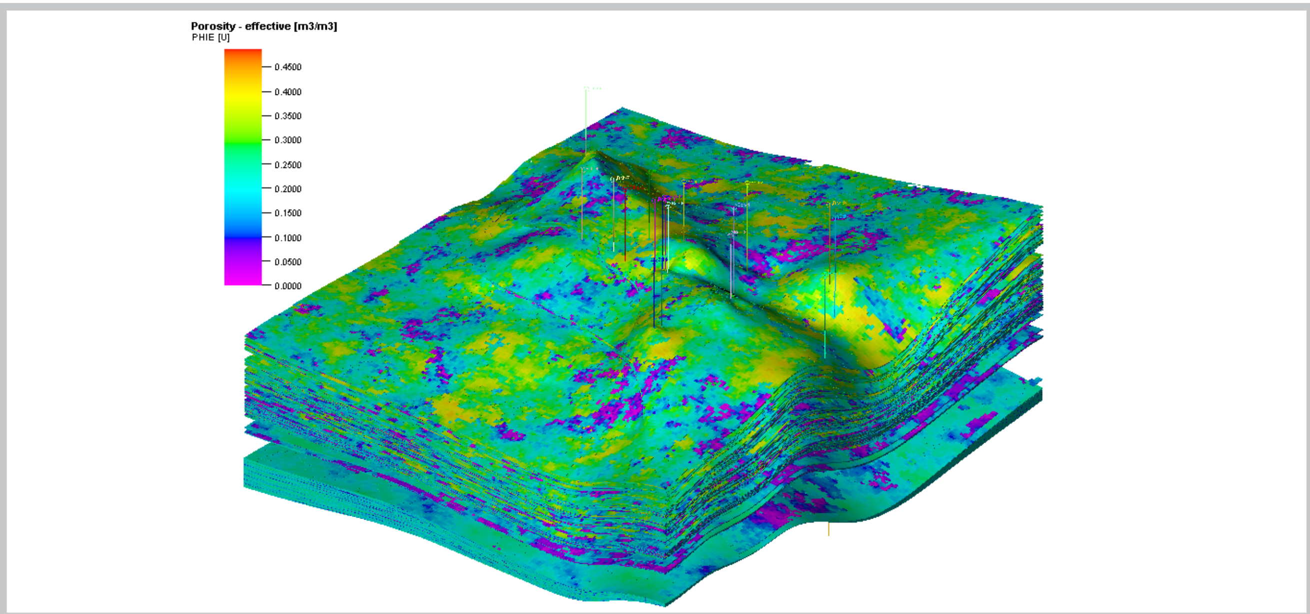

Figure 14 Petrel model of the Becej CO_2 field showing permeability distribution in the main reservoir and the overburden with several aquifers.

In the second phase of dynamic modelling, a full-field reservoir simulation model of the Bečej field will be developed. Geological model of the Bečej field in Petrel project format, which contains all available geological and petrophysical information, will be used to develop a full-field simulation model. Suitable methods available in the reservoir simulator will be chosen to adequately represent the geometry and the flow properties of a flow channel (e.g. gridding techniques). The dynamic model will be developed in Eclipse and history-matched with the available pressure data (Figure 15).

The full-field model will be used to explore the characteristics and behaviour of a complex flow system consisting of several aquifers in shallow overburden (Figure 2.16). Such a model will also be used to investigate the effectiveness of various mitigation scenarios.

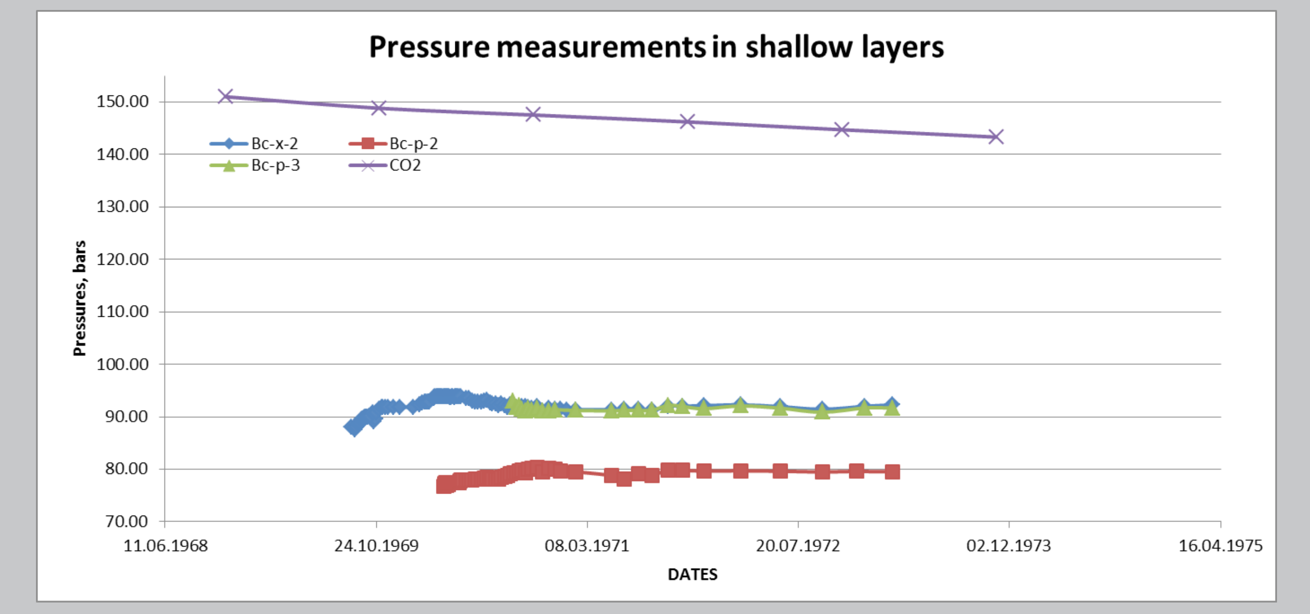

Figure 15 Pressure measurements in the shallow layers of the Becej CO_2 field.

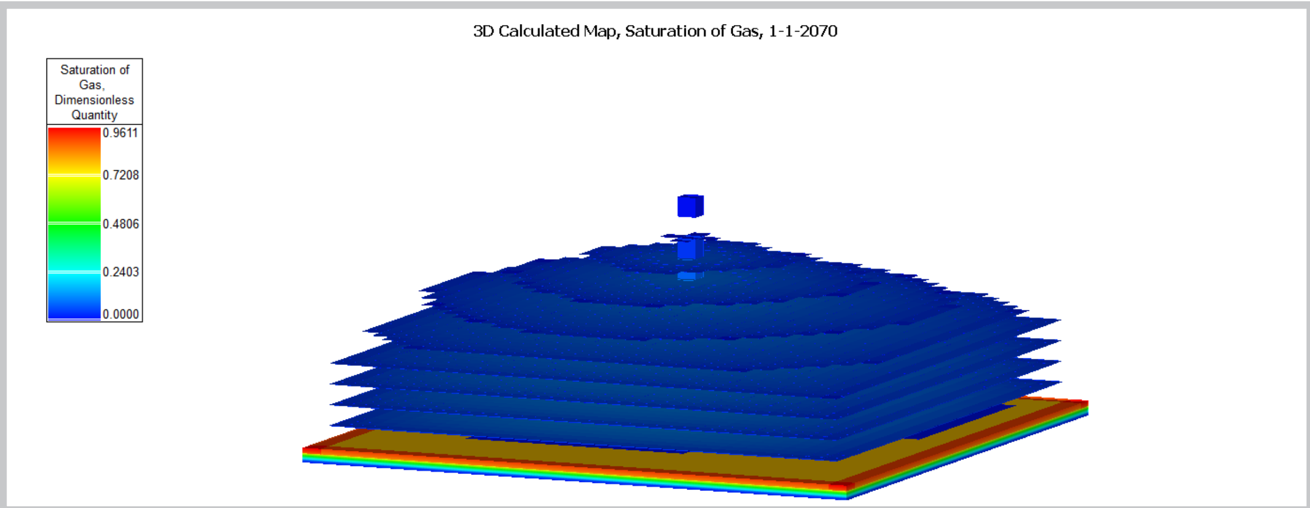

Figure 16 Gas saturation due to CO_2 leakage into the overburden from initial reservoir simulations.

2.1.7 Concluding remarks

Leakage through natural or induced fractures in caprock may develop under certain circumstances, under CO_2 injection into either undepleted deep saline or depleted reservoirs. Development of fractures and reactivation of faults is controlled by the reservoir pressure dynamics, rock properties, fracture and fault properties, and by the in-situ stress state. In addition, in the case of depleted reservoirs, fractures created during depletion might contribute to flow. The uncertainty, in the case of depleted reservoirs, is exacerbated by possibly zero or very small stress path, which may result in irreversible behaviour of faults and fractures. In addition, irreversible (hysteretic) behaviour of shear fractures is their inherent property, and may persist even in the case of fully reversible reservoir stress dynamics. This makes numerical modelling of long-term caprock integrity inherently difficult, and requires a good understanding of fracture behaviour under cyclic loading. This issue will be addressed in the project. After the necessary stress-permeability closure laws are obtained for some example fractures by means of numerical simulations, hydro-mechanically two-way coupled fracturing simulations under injection will be performed for prototype models as well as for a chosen field case scenario. As a field case scenario, a natural CO_2 analogue site or an engineered site can be used.

3 REMEDIATION OF LEAKAGE BY DIVERSION OF CO_2 TO NEARBY RESERVOIR COMPARTMENTS

Remediation of leakage can be attempted by diversion of CO_2 to a nearby compartment originally unconnected to the main reservoir. Remediation by diversion can be attempted in a compartmentalized gas field or aquifer initially without cross fault communication. Breaching of a fault seal, which separates two neighbouring compartments, can be attempted by multi-stage hydraulic fracturing. Hydraulic fractures represent pathways for transferring CO_2 between two neighbouring, partially juxtaposed reservoir compartments. A realistic reservoir model with a suitable geological and structural setting will be used to test a flow diversion option. Initial simulations will consider a generic model with two compartments separated by a fault. Numerical models will be used to investigate the role of key parameters controlling CO_2 migration between two compartments, such as the number and the flow characteristics of hydraulic fractures.

3.1 State-of-the-art review of fault sealing behaviour and hydraulic fracturing in the oil and gas industry

Literature review considers topics relevant for developing a scenario for remediation of leakage by diversion to nearby compartment. The topics reviewed comprise: fluid flow and geomechanical properties of faults, hydraulic fracturing and the interaction between a hydraulic fracture and a fault.

3.1.1 Faults

Faults have been intensively studied in the petroleum industry as they play an important role in the formation of hydrocarbon accumulations and affect fluid flow during hydrocarbon production. Faults can act as seals and hold the hydrocarbons, or function as conduits and provide a migration route. Faults can be barriers to fluid moving across faults, or can enhance flow in the up-dip direction along faults. Besides in the petroleum industry, faults and fault mechanics have been widely studied in seismology, as the main cause of an earthquake is a sudden movement on a fault (i.e. fault re-activation).

Faults are generally complex zones consisting of a fault core (with sharp fault surfaces, gouge and cataclasite) surrounded by a fault damage zone (with fractures and deformation bands). Typical fault zone structures can have a single core (as shown in Figure 17) or multiple cores (e.g. Faulkner et al., 2010). Mechanical and fluid flow properties of fault zones are closely related to the fault zone structure as discussed in detail in review papers by Wibberly et al. (2008) and Faulkner et al. (2010).

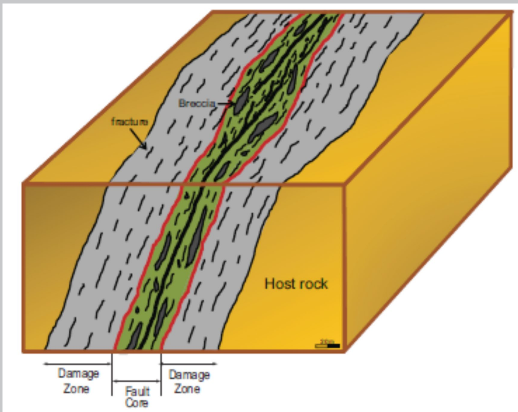

Figure 17 Typical fault zone structure with a single fault core surrounded by a fractured damage zone (Ligtenberg et al., 2011).

3.1.1.1 Fluid flow properties of faults

Fluid flow properties of fault zones generally depend on several factors such as the host rock lithology, the amount of shale in the surrounding rocks, the dip and strike of faults, the fault throw, the tectonic history and fault diagenesis.

The juxtaposition pattern of different lithological units across a fault is of primary importance for prediction of fault sealing behaviour. The sealing behaviour can arise from a juxtaposition seal (i.e. reservoir-against-nonreservoir juxtaposition) or a fault rock seal (i.e. reservoir-against-reservoir juxtaposition). In the case of a juxtaposition seal, faults are acting as barriers to fluid flow. In the case of a fault rock seal, this is often not the case. Analysis of the petrophysical properties of fault rocks gathered from over 50 oil and gas fields in the North Sea and Norwegian Continental Shelf by Fisher and Knipe (2001) showed that in many cases faults are likely to allow some flow to occur. In this case, faults are partially transmissible and act as flow baffles.

The common way of modelling faults in industry-standard fluid flow simulators is to introduce transmissibility multipliers (e.g. Jolley et al., 2007). Transmissibility multipliers are the derived numerical parameters assigned to grid-blocks or grid-block faces adjacent to faults in order to take into account the influence of fault rocks on fluid flow. Transmissibility multipliers are generally a function of the fault zone and of the grid-blocks to which they are assigned. In the method proposed by Manzocchi et al. (1999), the fault is conceptualized as a volume of a particular thickness and shale content, and the proportion of shale in the volume is assumed to be the main control on the fault permeability. The latter was also evident from experimental data, which showed that the permeability reduced log-linearly over four orders of magnitude with increasing clay content (Crawford et al., 2008). The shale content of the fault zone is calculated as a function of the faulted sequence using the Shale Gouge Ratio (SGR) method. The SGR method is generally applicable to clastic (sand-shale) sequences. The SGR method calculates the proportion of shale along each part of the fault (Yielding et al., 1997; Yielding, 2002). For a sequence of reservoir layers of different thickness and shale content, the SGR-value can be calculated using the following expression:

$$SGR = \frac{\sum(Vsh * \Delta z)}{t} x100\% \tag{3}$$

SGR is the Shale Gouge Ratio, Vsh is the shale content in a particular layer, Δz is the thickness of a particular layer and t is the fault throw.

In the next step an empirical relation can be used to predict fault zone permeability as a function of shale content (calculated by the SGR method) and fault displacement. Finally, an up-scaled fault transmissibility value can be derived, which is equal to the mean permeability of the juxtaposed cells, weighted by the cross-sectional contact area and the inverse of the distance between their centers (for details refer to Manzocchi et al., 1999).

Another method for calculation of transmissibility multipliers proposed by Zijlstra et al. (2007) can account for the two-phase flow properties of fault rocks. This is done by: (i) making the faults totally sealing to gas for a height above the free water level determined from the capillary entry pressure of the fault rock; and (ii) at greater distances above the free water level relative transmissibility multipliers are calculated based on estimates of the relative permeability of the fault rock. The authors present successful application of the method in three North Sea field simulation studies.

3.1.1.2 Geomechanical properties of faults

Fault zone mechanical properties and fault mechanics have been extensively studied in relation to earthquakes, which are the results of ruptures due to shear failure along pre-existing faults (Scholz, 2002).

Mechanical properties of fault zones, similar to fluid flow properties, depend on several factors such as the host rock lithology, fault-gouge composition, fault zone diagenetic history, offset, etc.

Elastic properties
The elastic properties of fault zones show a reduction in Young's modulus and an increase in Poisson's ratio with increasing damage within the damage zone to the fault core (Faulkner et al., 2006).

Shear strength and constitutive models for shear failure
Shear failure of a fault can be brittle or ductile. Earthquakes result from brittle failure, which has been studied far more extensively in the literature than ductile failure. Brittle shear failure under compressive stress states is commonly described with the empirical Coulomb failure criterion:

$$\tau = c+\mu_s\sigma_n \tag{4}$$

τ is the critical shear stress at failure, c is the cohesion and μ_s is the static friction coefficient which can be calculated as $\mu_s = tan(\varphi)$ (φ is the friction angle).
The fluid pressure is coupled to the stress by the effective stress law of Terzaghi:

$$\sigma'_n = \sigma_n\text{-}p \tag{5}$$

σ'_n is the effective normal stress acting on a fault, σ_n is the total normal stress and is the fluid pressure.

The coupling between the fluid pressure and the stress enables estimation of the fluid pressures required to initiate shear failure and fault reactivation in a CO_2 storage reservoir.

The static coefficient of friction varies between 0.6 and 0.85 (Byerlee, 1978). This range is valid for different mineralogical composition with exception of phyllosilicates and rock salts, where coefficients of friction are typically lower (e.g. Moore and Rymer, 2007). A frictional coefficient of 0.6 is, in many cases, adopted as a lower limit value, and faults are assumed cohesionless.

Coulomb failure criterion with the static coefficient of friction is, however, not sufficient to describe dynamic fault rupture. Experimental data showed that the force necessary to initiate the shear movement along two surfaces in contact is larger than the force required to maintain the motion. Therefore two coefficients of friction were distinguished: the static coefficient of friction (μ_s), which is necessary to initiate sliding, and the kinetic or dynamic coefficient of friction (μ_{ks}), which is necessary to maintain sliding.

Static friction was found to increase logarithmically with hold time. The kinetic coefficient of friction was observed to vary with sliding velocity; it may either become stronger (velocity strengthening) or weaker (velocity weakening).

Rabinowicz (1951) showed experimentally that the static and kinetic friction can be related. The transition from static to dynamic friction occurs over a critical distance D_c. This led to the development of a slip weakening law (Figure 18). An important shortcoming of this law is that it can not account for healing and is therefore limited to one stick-slip cycle.

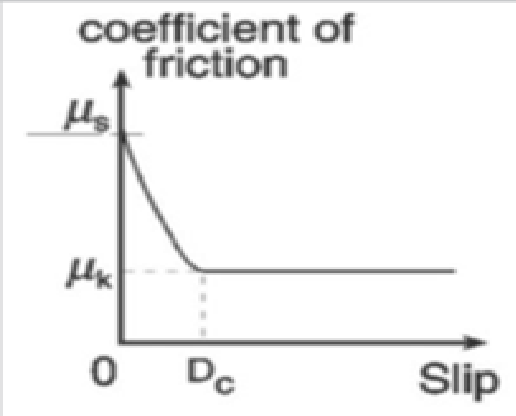

Figure 18 Linear slip weakening law showing the transition between static and dynamic friction during sliding (Rabinowicz, 1951).

The shortcoming of a slip weakening law was overcome by an empirical Rate-and-State Friction (RSF) model, which can describe many aspects of the observed seismic and inter-seismic frictional behavior (e.g. pre-seismic slip, earthquake nucleation, after-slip, etc.; Dieterich, 1979; Ruina, 1983; Marone, 1998). The RSF does not make a distinction between a static and dynamic friction coefficient; it uses a single coefficient of friction, which is a function of sliding velocity and a state variable Θ that represents a memory of past sliding history. The expressions to calculate the friction coefficient and the evolution of a state variable according to Dieterich (1979) are as follows:

$$\mu = \mu_0 + a\ln\left(\frac{V}{V_0}\right) + b\ln\left(\frac{V_0\theta}{D_c}\right), \qquad \frac{d\theta}{dt} = 1 - \left(\frac{V\theta}{D_c}\right) \tag{6}$$

μ_0 is the steady state friction coefficient at reference velocity V_0, V is the new velocity, D_c is the characteristic or critical slip distance (equal to the distance required for the frictional resistance to reach 1/e of its original value) and a and b are dimensionless empirical parameters. D_c, a and b are determined from laboratory data in which velocity is changed (Figure 19).

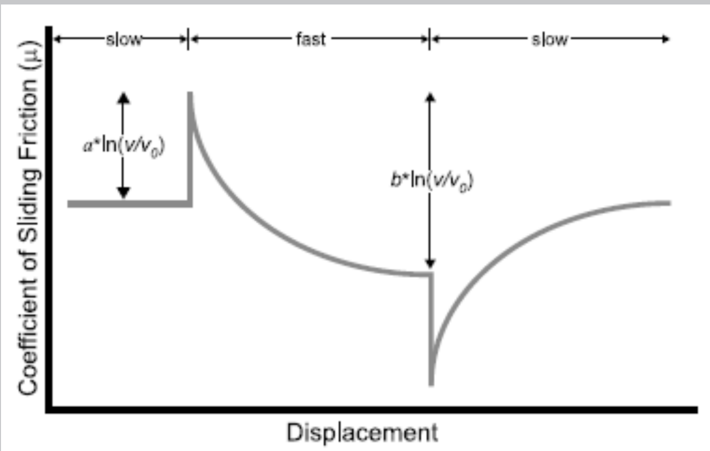

Figure 19 Results from velocity step experiments are shown to illustrate the concept of rate-and-state dependent friction. Idealized frictional response in velocity step experiments in which a gouge layer is sheared until a friction has reached a steady state and then the velocity is changed instantaneously. For a step increase in loading velocity, friction increases by $a*ln(V/V_0)$ and then decays over a characteristic sliding distance (D_c) by an amount $b*ln(V/V_0)$ to a new steady state value. $(a\text{-}b)>0$ implies a velocity strengthening material. $(a\text{-}b)<0$ (as in the figure) is a velocity weakening material (Samuelson et al., 2009).

Tensile strength and tensile failure

Tensile opening of a single fracture in Mode I will occur when the effective normal stress acting on a cohesionless fault becomes tensile. Possible cause for fracture dilation and opening is pore pressure increase within the fracture (Eq.3.5).

Hydromechanical behaviour of faults

Fault zone permeability predicted by a fault seal algorithm (such as the SGR method described earlier) can be changed on production/ injection time-scales due to geomechanical effects. Production- or injection-related geomechanical stress changes, arising from pore pressure changes, can trigger fault slip and re-activate faults changing (mainly increasing) their permeability. Coupling of the interactions between fluid flow and related geomechanical effects on faults cannot be done in production simulation models as they do not have appropriate constitutive models for frictional fault behavior, which are available in coupled stress-flow simulators.

Modelling of coupled deformation and permeability evolution during fault re-activation was performed in the context of geological CO_2 sequestration to assess the geological risks of induced seismicity and fluid leakages (Rutqvist et al., 2007). Cappa and Rutqvist (2011) describe three modeling approaches that have been considered to analyze multi-phase fluid flow and stress coupling with the TOUGH-FLAC simulator. Fault behavior was represented in hydromechanical models using slip zero-thickness interface and finite-thickness elements with isotropic or anisotropic elasto-plastic constitutive models. The results of this investigation showed that fault hydromechanical behavior can be appropriately represented with the least complex alternative, using a finite-thickness element and isotropic plasticity.

In the context of petroleum production, fault behavior is incorporated in coupled hydromechanical models developed to assess the potential for fault re-activation either as a cause of seismicity or well damage, and rarely in connection to fluid migration. An example of the latter is given in Cuisat et al. (2010). The study objective was to assess the potential for developing hydraulic communication between Statfjord and Snorre fields separated by a horst structure during final depressurization of the Statfjord field. Mechanical and sealing integrity of the horst-bounding faults and the horst structure were assessed by coupled single-phase fluid flow and elastic stress simulations with the Plaxis simulator. The results indicated that the geomechanical stress changes and the associated deformation will not affect significantly sealing integrity of faults.

The initial stress field (i.e. pre-depletion for CO_2 storage in depleted gas fields) can significantly affect fault zone permeability. According the critically-stressed-fault hypothesis by Zoback (2007, p.341), faults, which are in a state of failure equilibrium, are hydraulically conductive. This is supported by deep crustal permeability data acquired from in situ hydraulic tests and induced seismicity (Townend and Zoback, 2000). Critically stressed faults with a static friction coefficient μ=0.6 to 1.0 have in situ permeability in the range 0.01 to 0.1 mD, which is three to four orders of magnitude higher than measured on core samples. However, the hypothesis of the critically stressed deep subsurface is not generally applicable to shallower depths (< 4 km) where depleted gas reservoirs, which could be used for CO_2 storage, are usually found. For example, the faults involved in induced seismicity associated with gas extraction in the Netherlands are not critically stressed at the onset of depletion. This can explain the delay of seismic events which occur not prior to 28% of depletion (Van Wees et al., 2014).

3.1.2 Hydraulic fracturing

Hydraulic fracturing is a well stimulation technique to increase the productivity of hydrocarbon production wells. Wells are stimulated by initiating and propagating a tensile fracture from wellbore into the hydrocarbon-bearing rock formation by injecting large quantities of fluids at high pressure. Hydraulic fractures, varying in length from a few meters to a few hundreds of meters, are formed perpendicular to the minimum in situ stress direction. The technique has been in use in the oil and gas industry since 1947 (DOE, 2004).

Hydraulic fracturing is used in both conventional and unconventional reservoirs. In conventional reservoirs, fracturing is typically used to: (i) increase the permeability of reservoirs; (ii) restore the impaired permeability in the near well area; and (iii) control sand production. Besides improving well production, conventional reservoirs are fractured to increase the injectivity of rock formation for re-injection of produced water (PWRI) or slurry containing drill cuttings. In unconventional reservoirs, hydraulic fracturing is used for stimulations of shale formations, coalbed methane reservoirs and geothermal systems. In the mining industry, hydraulic fracturing is sometimes used for pre-conditioning of the rock to promote caving during mining operations.

Small scale fracturing is used in field tests to measure the in situ stresses and to aid the design of conventional fracturing treatments. In these tests a very small hydraulic fracture (a few decimeters to a few meters) is induced by pumping a small quantity of the injected fluid, compared to the conventional fracturing, without proppant. The field tests comprise micro- and a mini-frac tests, leakoff and extended leakoff tests, etc..

In conventional reservoirs, hydraulic fracturing commonly creates a single fracture that propagates in two directions from the wellbore forming two wings (Figure 20). The commonly used geometry models for a fracture comprise a vertical (or horizontal) ellipsoidal fracture (Figure 20a) or a constant height fracture (Figure 20b). The geometry of the created fracture is primarily driven by the in situ stress field with fracture growth perpendicular to the direction of the least principal stress. Other reservoir parameters controlling the fracture growth include the layering or interfaces between different rock strata and the mechanical properties of these strata. In addition, the fracture growth will be affected by the fracture treatment itself, the characteristics of the fraccing fluid, chemical reactions between the fluid and the rock, etc..

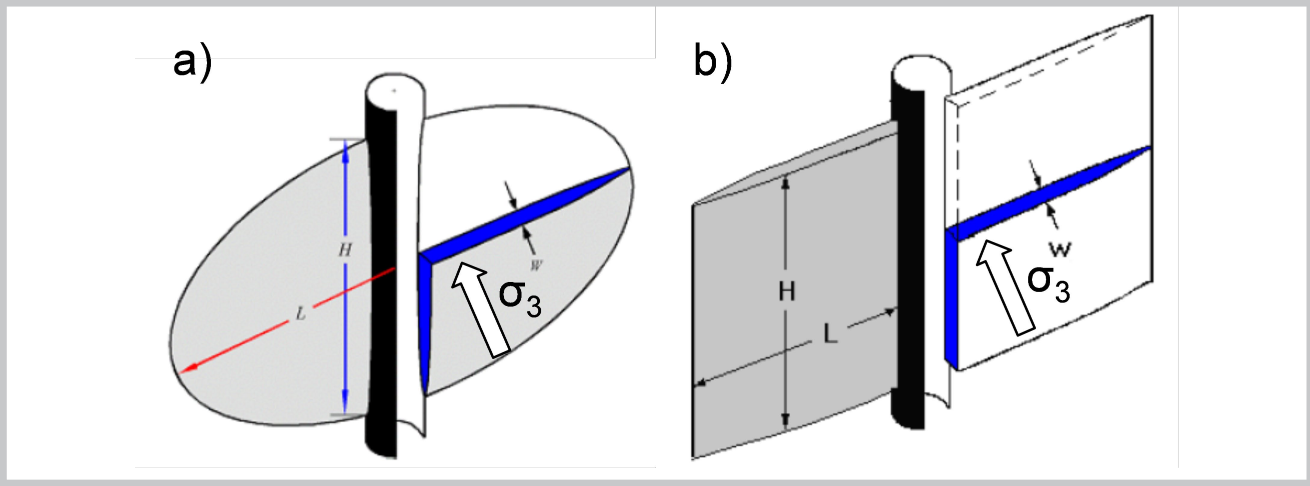

Figure 20 a) Vertical ellipsoidal fracture geometry and b) constant height fracture geometry (Meyer, 2013). The fracture is induced at 90° to the direction of the minimum in situ stress σ_3.

In unconventional reservoirs and naturally fractured reservoirs, hydraulic fracturing induces fractures that propagate and interact with a system of natural fractures already present in the reservoir rock. The interaction between an induced fracture and a natural fracture system, i.e. a Discrete Fracture Network (DFN), is usually quite complex (as illustrated in Figure 21). The most recent advances in fracturing of unconventional reservoirs have been achieved in development of shale gas resources. In shale gas development, aggressive hydraulic fracturing is used to generate an interconnected open fracture network with a large internal surface area for gas drainage towards a well. The emplacement of horizontal wells more than 1 km long, which became economical by the late 1990's, and development of Multi-Stage Hydraulic Fracturing[1] (MSHF) in the period 2000–2008, are the two key technologies that made the "shale gas revolution" in the United States and Canada possible (Dusseault, 2013).

Horizontal drilling and MSHF are the two technologies particularly relevant for the CO_2 mitigation scenario described in section 3.1.3 in which the MSHF from a long horizontal well will be used to connect two neighboring reservoir compartments.

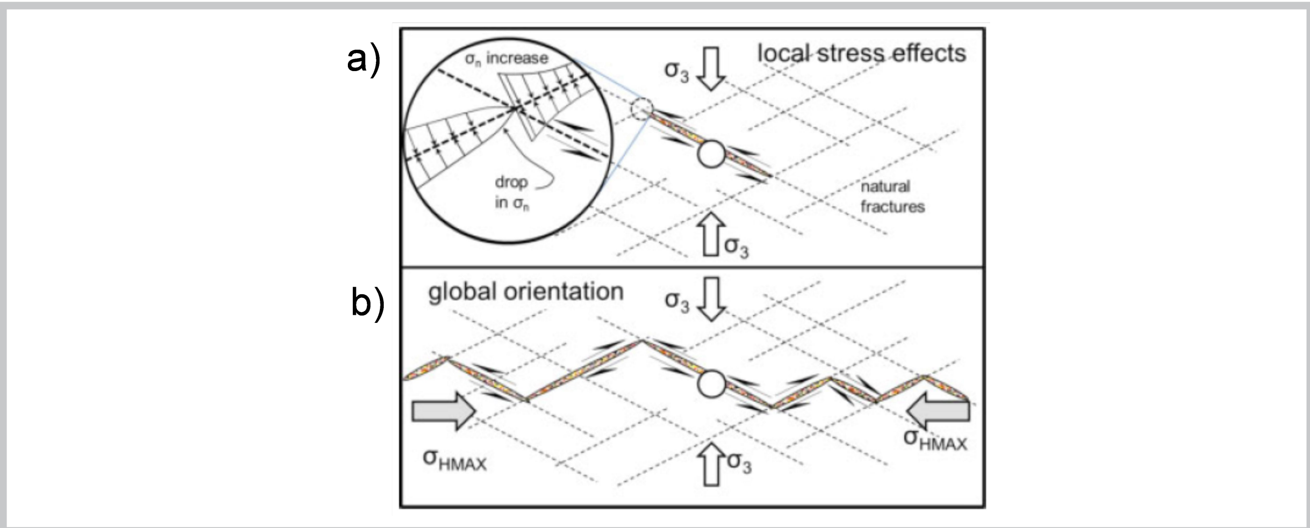

Figure 21 a) Local and b) large scale effects on fracture propagation in naturally fractured formation (Dusseault, 2013). At the local scale, a fracture will tend to follow approximately natural fractures rather than initiate new ones through the intact rock. At the large scale, the fractures will tend to remain on average at 90° to the direction of σ_3.

3.1.2.1 Hydraulic fracturing across geological discontinuities

The flow diversion option of transferring CO_2 to a neighboring compartment by a fault-seal breach requires consideration of the interaction between a hydraulic fracture propagating from the wellbore and an existing fault. A brief literature review showed that this particular topic has been explored in only a limited manner, typically considering the interaction between two discrete mechanical discontinuities representing a hydraulic fracture and a natural fracture. Representing a fault with a single discontinuity may not always be sufficient because the fault architecture is usually more complex: it comprises the damaged rock, the fault gouge

1 Creation of hydraulic fractures at multiple locations in a single well.

and several slip surfaces, with the distinct material properties. The literature on hydraulic fracturing mainly focuses on the fracture design and prediction of fracture initiation and growth.

The criterion for fracture initiation was defined by Haimson and Fairhurst (1967): a fracture will be initiated when the fluid pressure in the wellbore exceeds the minimum in situ stress (assuming that the host rock has a negligible tensile strength).

Early studies carried out in 1980's focused on determining the factors affecting the propagation and containment of a hydraulic fracture in a layered rock mass. Anderson (1979) conducted hydraulic fracture experiments to observe the growth of hydraulic driven fractures in the vicinity of an unbonded interface in rocks. The two factors were identified which determine whether a hydraulic fracture would cross the interface: the normal stress acting on the interface and the frictional properties of the interface.

Teufel and Clark (1984) demonstrated that two distinct geologic conditions can inhibit or contain the vertical growth of hydraulic fractures in layered rock: a weak interfacial shear strength of the layers and an increase in the minimum horizontal in situ stress in the bounding layers. The in situ stress distribution is thought to be more important for the fracture growth and containment. Differences in elastic properties within a layered rock mass could also be important because variations in elastic properties influence the vertical distribution of the minimum horizontal stress.

The importance of the in situ stress distribution on fracture growth was also observed in the field tests and the mineback experiments carried out by Warpinski and Teufel (1987; Figure 3.6). The confinement resulting from a high-stress region is a first order effect, whereas interfaces, strength changes, fluid pressure gradients have only second-order effects on fracture growth. Geologic discontinuities can affect the overall geometry of hydraulic fractures by arresting the growth of the fracture, increasing fluid leakoff, enhancing the creation of multiple fractures, etc.. The ability of a crack to propagate across the natural discontinuity depends on the in-situ stresses and the coefficient of friction of the interface. Fractures will generally cross discontinuities at high angles of approach and large stress differences (Figure 22).

Zhang and Jeffry (2004) developed a numerical fracture model for solving the problem of coupled rock deformation, fluid transport and interface slip associated with hydraulic fracture propagation across frictional interfaces. The authors found that the approaching hydraulic fracture can induce a new fracture in rocks of low tensile strength. However, there is a critical range of tensile strengths that result in the fracture penetrating the interface without offset. Beyond the maximum of this range, the fracture cannot induce a new fracture, based on the tensile strength criterion and is diverted into and grows along the interface instead.

Wu et al. (2004) demonstrated both numerically and experimentally that when a fracture propagates from a rigid layer toward a softer layer, the fracture will break through the interface. However, when a fracture propagates from a soft layer to a rigid or stiffer layer, crack arrest can occur and other fracture mechanisms such as the formation of secondary fractures across the interface (again leading to fracture breakthrough), delamination along the interface, or crack kinking resulting in fracture containment, can occur. The authors proposed a fracture mechanisms map (FMM) in the vicinity of an interface to assist in hydraulic fracture treatment design.

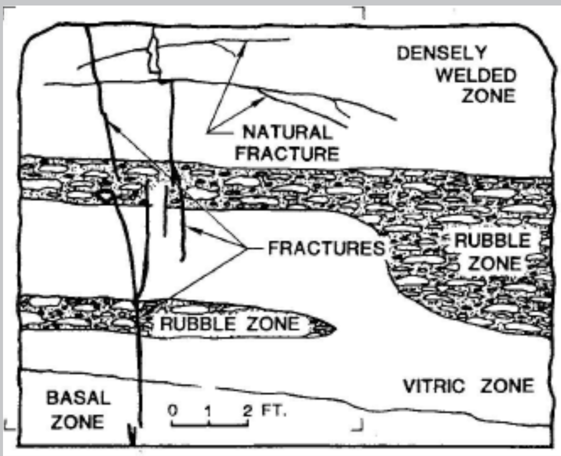

Figure 22 Complex fracture behavior from a mineback experiment at the Nevada Test Site in the U.S. The sketch shows that induced fractures intersect the natural fracture system (Warpinsky and Teufel, 1987).

Chuprakov et al. (2013) studied hydraulic fracture propagation across a weak discontinuity controlled by fluid injection. This research was mainly focused on the result of fracture interaction in terms of crossing or arresting of the hydraulic fracture at the natural fracture. The key parameters controlling the crossing/non-crossing interaction behavior were identified: in-situ stress parameters, interaction angle, the injection rate, viscosity of fracturing fluid and the fracture aperture. When the pre-existing aperture of the natural fracture is as large as that of the hydraulic fracture, the hydraulic fracture is likely to arrest.

One case was reported of hydraulic fracturing during a gas well stimulation, which induced movement on a nearby fault (Maxwell et al., 2009).

3.1.2.2 Implications for fracture containment in CO_2 storage reservoirs

Practical implications of the importance of stress distribution on fracture containment are that it is much easier to constrain the vertical fracture growth in a depleted gas reservoir (being re-filled with CO_2) than in an aquifer. In the case of CO_2 storage in a depleted gas reservoir, the minimum in situ stress in the reservoir will be lower than in the pre-depleted state (assuming a normal-faulting stress regime and re-pressurization with the injected CO_2 below the initial reservoir pressure) while the stress in the caprock will stay largely unchanged. Change in the minimum in situ stress in the reservoir due to pore pressure change can be estimated by the following expression:

$$\Delta Sh\min = \alpha\ dP\frac{1-2\nu}{1-\nu} \tag{7}$$

ΔSh is the minimum stress change, α is the Biot's constant, dP is the depletion and ν is the Poisson's ratio.

The minimum stress in the caprock will always be higher than the pressure in a depleted, or partially re-pressurized, storage reservoir. As a consequence, the vertical growth of a hydraulic fracture will be naturally constrained by the presence of a high-stress region in the caprock. In contrast to the CO_2 storage in a depleted reservoir, the minimum in situ stress in the reservoir will be increasing during the CO_2 injection, and the vertical fracture growth will be difficult to constrain.

3.1.2.3 Hydraulic fracturing simulators

Fracture design and treatment rely on a good understanding and prediction of fracture initiation and growth. Hydraulic fracturing simulators are used for the design, analysis and monitoring of hydraulic fractures (Figure 23 and Figure 24). The first simulators appeared in the late 1980's (Meyer, 1989). Nowadays, fracturing simulators are developed and used as in-house tools in some of the major oil companies (e.g. Van den Hoek et al., 1999; Noirot et al., 2003) or are available as commercial software packages (e.g. the Meyer Fracturing Software suite; Meyer, 2013). The Meyer fracturing simulator, which is a state-of-the-art fracturing simulator with several modules. The most relevant modules are those for simulating fracture propagation as well as the interaction between the hydraulic fracture and natural fractures or a fault. These modules are:

- MFrac - a three-dimensional hydraulic fracturing simulator accounting for the coupled parameters affecting fracture propagation and proppant transport, and including three-dimensional fracture geometry.
- MPwri – a three-dimensional hydraulic fracturing waterflood simulator designated for simulating produced water reinjection (PWRI).
- MShale - a Discrete Fracture Network (DFN) simulator designated for simulating three-dimensional hydraulic fracture propagation in discrete fracture networks.

The major fracture, rock and fluid mechanics phenomena included in the Meyer suite of fracturing simulators are: (1) multilayer unsymmetrical confining stress contrast; (2) multilayer leakoff; (3) fracture toughness and dilatancy (tip effects); (4) variable injection

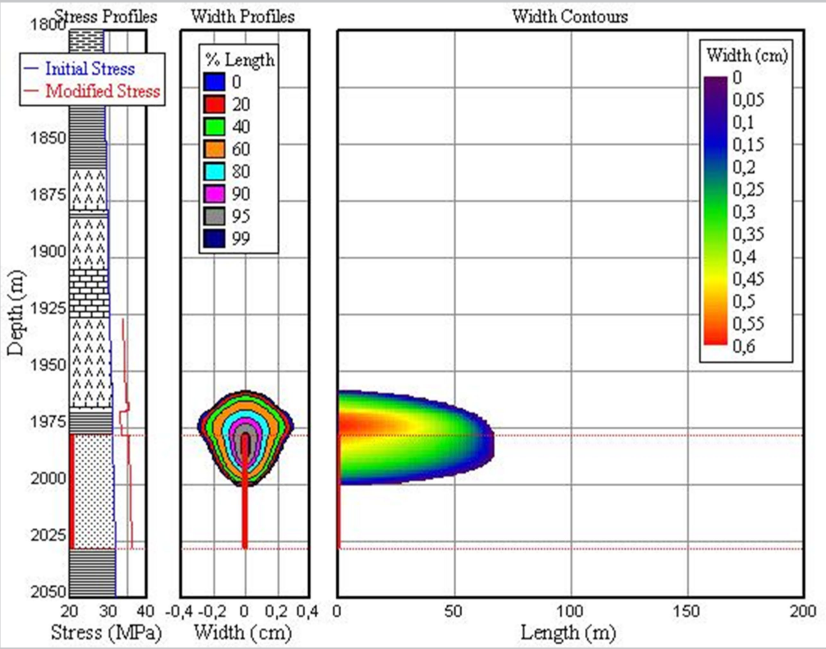

Figure 23 Typical simulation of hydraulic fracture obtained using MFrac/MPwri fracturing simulator. The graphs show (from left to right) stress profiles, width profiles and contours of the hydraulic fracture (Hofstee et al., 2009).

rate and time dependent fluid rheology; (5) vertical and lateral rock deformation; (6) wall roughness and (7) coupled proppant transport, heat transfer and fracture propagation (Appendix A; Meyer, 2013).

The shortcomings of the MFrac/MShale are due to the following assumptions: (1) horizontal layering; (2) homogeneity in the rock properties within model layer; (iii) pre-defined and simple geometry of the DFN represented by two orthogonal fracture systems; (iv) simple criteria for fracture initiation and propagation.

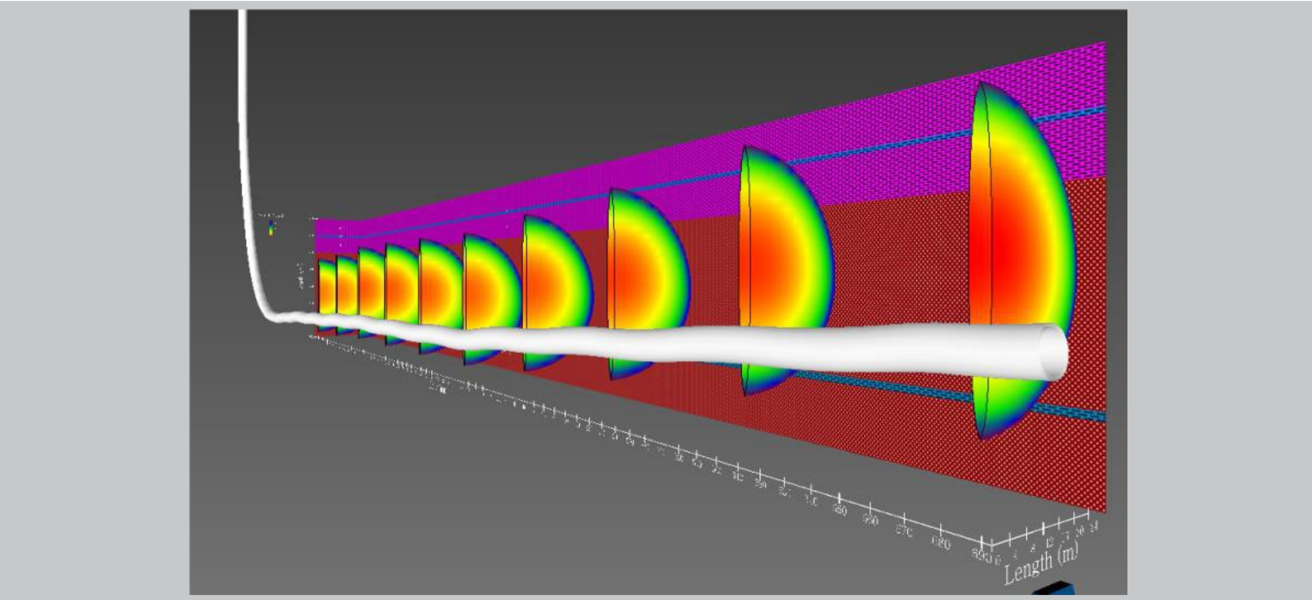

Figure 24 Simulation of multistage hydraulic fracturing from a horizontal well using MFrac/MShale (source: TNO).

3.1.3 Model requirements and description of the CO_2 mitigation scenarios

The CO_2 mitigation scenario considers flow diversion to a neighbouring compartment separated by a fault from the main compartment, which shows signs of leakage of deviations from the expected flow behaviour. The fault seal has to be breached in order to make transferring of CO_2 between the compartments possible. Seal breach can be attempted by multistage hydraulic fracturing from a horizontal well drilled through the main compartment approximately parallel to the fault strike.

Model requirements

The reservoir model should represent a compartmentalized gas field or aquifer initially without cross fault communication between

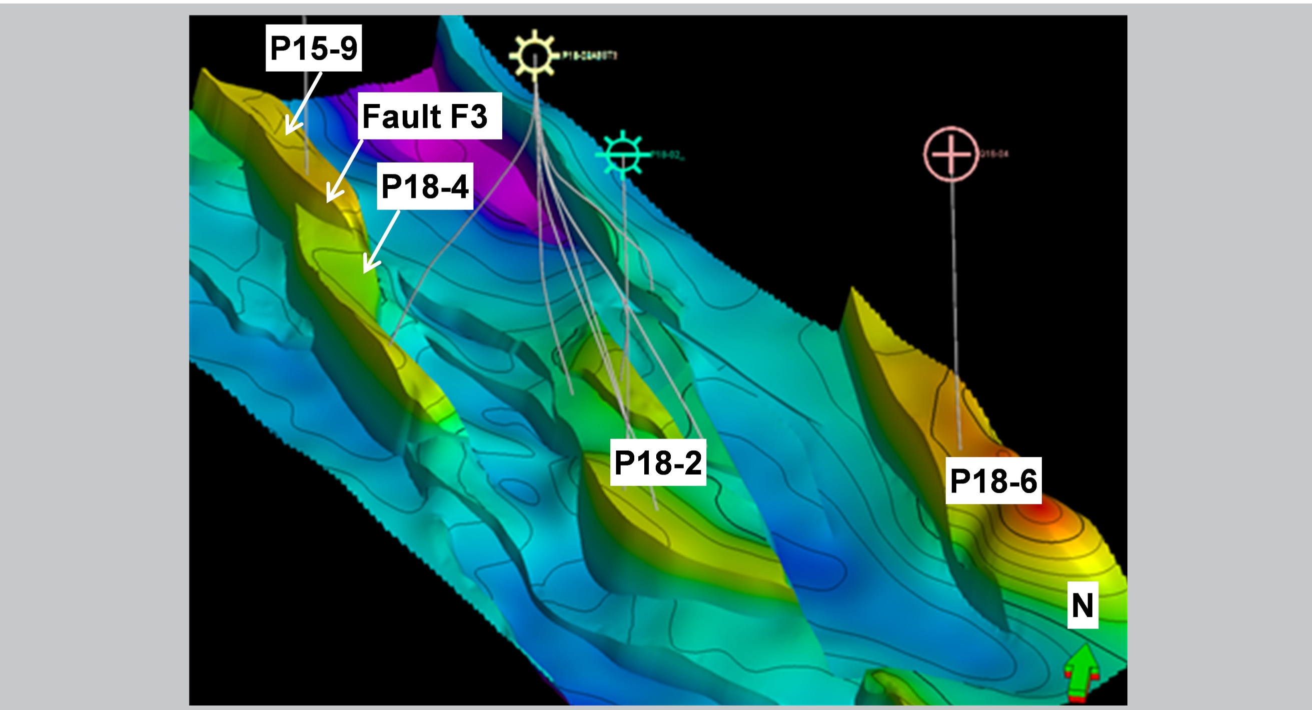

Figure 25 An example of the structural setting with two neighboring depleted gas reservoirs separated by a sealing fault (P18-4 and P15; Arts et al., 2012).

neighbouring compartments. The main reservoir and the neighbouring compartment planned to be used for flow diversion must be partially juxtaposed. Fluid pressure in the neighbouring compartment should preferably be lower than in the main compartment to facilitate buoyancy-driven CO_2 flow during flow diversion. The latter requirement is fulfilled when the neighbouring compartment is upthrown and/or depleted. The model must contain migration pathways for CO_2 leakage through the fractured caprock or reservoir bounding faults.

Description of the model selected

A geological setting suitable to investigate the feasibility of remediation by flow diversion comprises a compartmentalized gas reservoir or aquifer. Such structural settings are quite common: e.g. the depleted P18-4 gas reservoir, planned to be used for CO_2 storage in the Rotterdam Capture and Storage Demonstration Project (ROAD), is separated by a sealing fault from the neighbouring P15 depleted gas field (Figure 25). The feasibility of CO_2 storage in the depleted P18-4 gas reservoir was studied in the Dutch national programme on Carbon Capture and Storage - CATO-2 (Arts et al., 2012, Arts et al., 2011; Vandeweijer et al., 2011).

Another field example relevant for CO_2 storage in both depleted gas fields and aquifers, are the Rotliegendes reservoir rocks, which are compartmentalized in the Netherlands and also throughout north-western Europe (Figure 26).

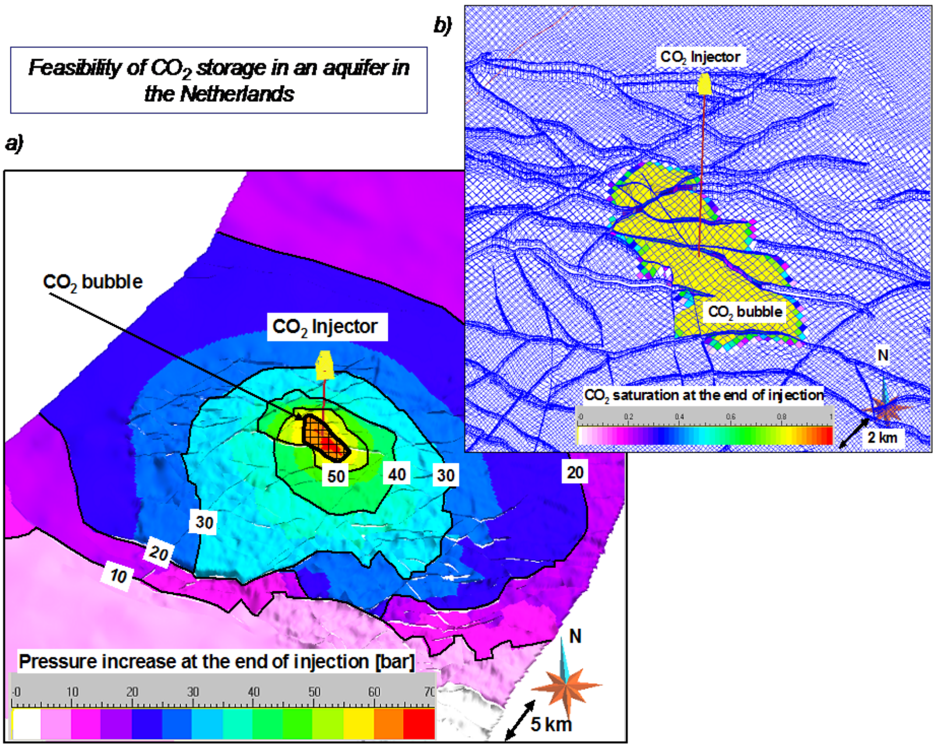

Figure 26 An example of the structural setting with multiple aquifer compartments. Reservoir simulation results of CO2 injection assuming that all the faults are conductive. a) Footprint area of elevated pressures; b) footprint area of the CO_2 plume (Orlic et al., 2011).

Planned model procedure

The feasibility of remediation by flow diversion will be tested in a follow-up study on a generic model with two reservoir compartments separated by a sealing fault (Figure 27). Leakage scenarios may consider leakage through one of the bounding faults, implemented as a line sink, and leakage through the caprock, implemented as an areal sink. The geometry of the compartments in the synthetic model will be fairly simple. Models with various fault offsets can be considered (e.g. 10 to 50%). Also, differences in permeability between the two neighbouring compartments can be considered, e.g. the case where a low-permeability reservoir is juxtaposed against a high-permeability reservoir, and vice-versa. Various grid configurations and resolutions can be explored for inclusion of hydraulic fractures in a reservoir simulation grid. The initial volumes of gas, the volumes of gas produced and CO_2 injected in a generic model will be kept realistic for the case of industrial-scale CO_2 storage. The effects of flow diversion as a mitigation measure can be tested for the option of CO_2 storage in a depleted gas field and in an aquifer.

In the second phase of the project, a realistic field-scale model with two neighbouring compartments will be developed. Model adjustments can be implemented based on the outcome of generic model simulations. Envisaged leakage scenarios are the same for the generic and the realistic model: a leakage through a bounding fault and a leakage through the caprock. The leakage may be initiated at the start of injection period or at some point during injection. The total amount of CO_2 that escaped from the storage reservoir must be above detectable thresholds before starting the proposed mitigation action: drilling a new well and creating hydraulic fractures through the fault seal to connect with the nearby compartment. Geometry and hydraulic properties of induced fractures will be obtained from hydraulic fracturing simulations. Transmissibility multipliers will be derived from fracturing simulations and applied in a realistic reservoir simulation model to account for the fluid flow through the newly created hydraulic fractures.

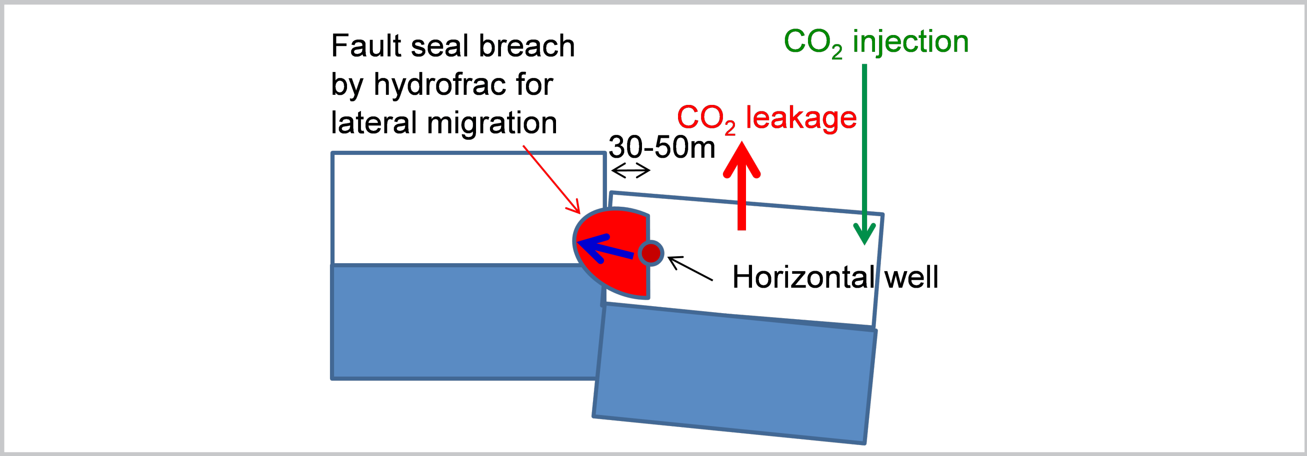

Figure 27 Side-view of a generic model with two reservoir compartments separated by a sealing fault. Connection to a neighbouring compartment for diversion of CO_2 is achieved by hydraulic fracturing.

Simulations will be used to investigate:

- The diversion rates through a single and multiple hydraulic fractures.
- The effect of fracture dimensions and flow properties on the diversion rates.
- The duration needed to release the reservoir pressure and the leakage rates to an admissible level.

3.1.4 Concluding remarks

A CO_2 mitigation scenario by flow diversion from the main, leaky compartment to a neighbouring compartment separated by a sealing fault, has been developed. The fault seal must be breached in order to make transferring of CO_2 between two neighbouring compartments possible. Seal breach can be attempted by multistage hydraulic fracturing from a new horizontal well drilled approximately parallel to the fault strike. Several newly created hydraulic fractures will act as high-permeability pathways for CO_2 migration from the main reservoir to a neighbouring compartment in the storage reservoir, releasing the pressure and decreasing the migration rates out of the main reservoir.

The feasibility of the described CO_2 mitigation scenarios will be investigated by numerical simulations of fluid flow in a fault-compartmentalized gas reservoir or aquifer. The CO_2 mitigation scenario by flow diversion will be first tested on a generic model, which consists of two reservoir compartments, separated by a sealing fault. The role of key parameters controlling CO_2 migration between two compartments, such as the number and the flow characteristics of hydraulic fractures, will be investigated. In the subsequent phase a realistic reservoir model will be used.

References

Alassi, H.T., Holt, R., Nes, O.-M., Pradhan, S., 2011. Realistic geomechanical modeling of hydraulic fracturing in fractured reservoir rock. CSUG/SPE paper 149375, in the Canadian Unconventional Resources Conference held in Calgary, Alberta, Canada, 15-17 November 2011.

Anderson, G.A., 1979. Effects of friction on hydraulic fracture growth near unbonded interfaces in rock, SPE 54th Annual Technical Conference and Exhibition, Las Vegas, SPE 8347.

Arts, R., Hofstee, C., Vandeweijer, V., Pluymaekers, V., Loeve, D., Orlic, B., Koenen, M., Tambach, T., Spiers, C., Samuelson, J., 2011. Status report on remaining issues identified after the feasibility study for CO_2 injection in the depleted P18 gas field. CATO-2 report CATO-2-WP3.9-D14.

Arts, R.J, Vandeweijer, V.P, Hofstee, C., Pluymaekers, M.P.D., Loeve, D., Kopp, A., Plug, W.J., 2012. The feasibility of CO_2 storage in the depleted P18-4 gas field offshore the Netherlands (the ROAD project), International Journal of Greenhouse Gas Control, 11, S10–S20.

Bahat, D., Rabinovitch, A., Frid, V., 2005. Tensile Fracturing in Rocks: Tectonofractographic and Electromagnetic Radiation Methods, 584, Springer, Berlin.

Brown, S.R., 1987. Fluid flow through rock joints: the effect of surface roughness, Journal of Geophysical Research, B, 92, 1337-1347.

Byerlee, J.D., 1978. Friction of rocks, Pure and Applied Geophysics, 116: 615-626.

Cappa, F., Rutqvist, J., 2011. Modeling of coupled deformation and permeability evolution during fault reactivation induced by deep underground injection of CO_2, International Journal of Greenhouse Gas Control, 5, 336–346.

Chuprakov, D., Melchaeva, O., Prioul, R., 2013. Hydraulic fracture propagation across a weak discontinuity controlled by fluid injection, In Bunger, McLennan, and Jeffrey (eds): Proceedings of the International Conference for Effective and Sustainable Hydraulic Fracturing, An ISRM specialized Conference, Brisbane, Australia, May 2013, http://dx.doi.org/10.5772/55941.

Crawford, B.R., Faulkner, D.R., Rutter, E.H., 2008. Strength, porosity, and permeability development during hydrostatic and shear loading of synthetic quartz-clay fault gauge, Journal of Geophysical Research, 113, B03207, doi:10.1029/2006JB004634.

Cuisat, F., Jostad, H.P., Andresen, L., Skurtveit, E., Skomedal, E., Hettema, M., Lyslo, K., 2010. Geomechanical integrity of dealing faults during depressurisation of the Statfjord Field, Journal of Structural Geology, 32, 1754-1767.

Cuss, R. J., Milodowski, A., Harrington, J. F., 2011. Fracture transmissivity as a function of normal and shear stress: First results in Opalinus Clay, Physics and Chemistry of the Earth, Parts A/B/C, 36, 1960-1971.

DOE, 2004, Department of Energy - Hydraulic Fracturing White Paper, Appendix A, EPA 816-R-04-003.

Dieterich, J. H., 1979. Modeling of rock friction 1. Experimental results and constitutive equations, Journal of Geophysical Research B: Solid Earth, 84(B5), 2161-2168.

Dusseault, M., 2013. Geomechanical aspects of shale gas development, In Proceedings of EUROCK 2013 - The 2013 ISRM International Symposium, M. Kwaśniewski and D. Łydżba (eds.), Wrocław, 21-26 September, 969-975, London, Taylor & Francis Group.

Edlmann, K., Haszeldine, S., McDermott, C.I., 2013. Experimental investigation into the sealing capability of naturally fractured shale caprocks to supercritical carbon dioxide flow, Environmental Earth Science, 70(7), 3393-3409.

Esaki, T., Du, S., Mitani, Y., Ikusada, K., Jing, L., 1999. Development of a shear-flow test apparatus and determination of coupled properties for a single rock joint, International Journal of Rock Mechanics and Mining Sciences, 36(5), 641-650.

Faulkner, D.R., Jackson, C.A.L., Lunn, R.J., Schlisch, R.W., Shipton, Z.K., Wibberley, C.A.J., Withjack, M.O., 2010. A review of recent developments concerning the structure, mechanics and fluid flow properties of fault zones, Journal of Structural Geology, 32, 1557-1575.

Faulkner, D.R., Mitchell, T.M., Healy, D., Heap, M.J., 2006. Slip on 'weak' faults by the rotation of regional stress in the fracture damage zone, Nature, Letters, 444, 922-925.

Fessenden, J.E., Stauffer, P.H., Viswanathan, H.S., 2009. Natural Analogs of Geologic CO_2 Sequestration: Some General Implications for Engineered Sequestration, in Geophysical Monograph Series. Vol.183, AGU.

Fisher, Q.J., Knipe, R.J., 2001. The permeability of faults within siliciclastic petroleum reservoirs of the North Sea and Norwegian Continental Shelf, Marine and Petroleum Geology, 18, 1063-1081.

Fjær, E., Holt, R.M., Horsrud, P., Raaen, A.M., Risnes, R., 2008. Petroleum Related Rock Mechanics, 2nd ed., 491, Elsevier, Amsterdam.

Friedman, S.J., 2007. Geological carbon dioxide sequestration, Elements, 3(June), 179-184.

Haimson, B.C., Fairhurst, C., 1967. Initiation and extension of hydraulic fractures in tocks, Society of Petroleum Engineers Journal, 7, 310-318, SPE 1710.

Hofstee, C., Benedictus, T., Ter Heege, J. H., Huibregtse, J., Van der Meer, B., Nelskamp, S., Orlic, B., Pluymaekers, M., Tambach, T., 2009. Feasibility of CO_2 storage in the Friesland platform, TNO Built Environment and Geosciences report TNO-034-UT-2009001084.

Jolley, S.J., Dijk, H., Lamens, J.H., Fisher, Q,J., Manzocchi, T., Eikmans, H., Huang, Y., 2007. Faulting and fault sealing in production simulation models: Brent Province, northern North Sea, Petroleum Geoscience, 13, 321-340.

Lakatos, I., Medic, B., Jovicic, D., Basic, I., Lakatos-Szabo, J., 2009. Prevention of vertical gas flow in a collapsed well using silicate/plolymer/urea method, SPE International Symposium on Oilfield Chemistry, Woodlands, Texas, SPE 121045.

Lavrov, A., 2013a. Numerical modeling of steady-state flow of a non-Newtonian power-law fluid in a rough-walled fracture, Computers and Geotechnics, 50(0), 101-109.

Lavrov, A., 2013b. Redirection and channelization of power-law fluid flow in a rough-walled fracture, Chemical Engineering Science, 99(0), 81-88.

Lavrov, A., Larsen, I., Holt, R.M., Bauer, A., Pradhan, S., 2014. Hybrid FEM/DEM simulation of hydraulic fracturing in naturally-fractured reservoirs. ARMA paper 14-7107, in the 48th US Rock Mechanics/Geomechanics Symposium held in Minneapolis, MN, USA, 1-4 June 2014.

Lewicki, J., Birkholzer, J., Tsang, C.-F., 2007. Natural and industrial analogues for leakage of CO_2 from storage reservoirs: identification of features, events, and processes and lessons learned, Environmental Geology, 52(3), 457-467.

Ligtenberg, H., Okkerman, J., De Keijzer, M., 2011. Fractures in the Dutch Rotliegend – an overview, Society for Sedimentary Geology Special Publication 98, 229-244.

Magri, F., Tillner, E., Wang, W., Watanabe, N., Zimmermann, G., Kempka, T., 2013. 3D Hydro-mechanical Scenario Analysis to Evaluate Changes of the Recent Stress Field as a Result of Geological CO_2 Storage, Energy Procedia, 40(0), 375-383.

Manzocchi, T., Walsh, J.J., Nell, P.,Yielding, G., 1999. Fault transmissibility multipliers for flow simulation models, Petroleum Geoscience, 5, 53-63.

Marone, C., 1998. Laboratory-derived friction laws and their application to seismic faulting. Annual Review of Earth and Planetary Sciences, 26, 643-696.

Maxwell, S.C., Jones, M., Parker, R., Miong, S., Leaney, S., Dorval, D., D'Amico, D., Logel, J., Anderson, E., Hammermaster, K., 2009. Fault activation during hydraulic fracturing, SEG Houston 2009 International Exposition and Annual Meeting.

Meyer, B.R., 1989. Three-dimensional hydraulic fracturing simulation on personal computers: theory and comparison studies, Eastern Regional SPE Meeting, Morgantown, West Virginia, SPE 19329.

Meyer, B. R., 2013. Meyer Fracturing Simulators, Programs and User's Guide Tenth Edition, Baker Hughes Incorporated, Meyer Fracturing Software Group http://www.mfrac.com/.

Metz, B., Davidson, O., de Coninck, H., Loos, M., Meyer, L., 2005. IPCC Special Report on Carbon Dioxide Capture and Storage, Cambridge University Press, Cambridge.

Moore, E.D., Rymer, M.J., 2007. Talc-bearing serpentinite and the creeping section of the San Andreas fault. Nature 448:795–797.

Nelson, E.J., Hillis, R.R., Meyer, J.J., Mildren, S.D., Van Nispen, D., Briner, A., 2005. The reservoir stress path and its implications for water-flooding, Champion Southeast field, Brunei. ARMA/USRMS paper 05-775, in Alaska Rocks 2005, The 40th U.S. Symposium on Rock Mechanics (USRMS): Rock Mechanics for Energy, Mineral and Infrastructure Development in the Northern Regions, held in Anchorage, Alaska, June 25-29, 2005.

Nemoto, K., Moriya, H., Niitsuma, H., Tsuchiya, N., 2008. Mechanical and hydraulic coupling of injection-induced slip along pre-existing fractures, Geothermics, 37(2), 157-172.

Noirot, J.C., Van den Hoek, P.J., Zwarts, D., Bjoerndal, H.P., Stewart, G., Drenth, R., Al-Masfry, R., Wassing, B., Saeby, J., Al-Masroori, M., Zarafi., A., 2003. Water injection and water flooding under fracturing conditions, SPE 81462.

Oh, J., Kim, K.-Y., Han, W.S., Kim, T., Kim, J.-C., Park, E., 2013. Experimental and numerical study on supercritical CO_2/brine transport in a fractured rock: Implications of mass transfer, capillary pressure and storage capacity, Advances in Water Resources, 62, Part C(0), 442-453.

Orlic, B., ter Heege, J., Wassing, B., 2011. Assessing the integrity of fault- and top seals at CO_2 storage sites, Energy Procedia, 4(0), 4798-4805.

Pruess, K., Oldenburg, C., Moridis, G., 2012. TOUGH2 User's Guide v2..

Pyrak-Nolte, L. J., 1996. The seismic response of fractures and the interrelations among fracture properties, International Journal of Rock Mechanics and Mining Sciences & Geomechanics Abstracts, 33(8), 787-802.

Rabinowicz, E., 1951. The nature of the static and kinematic coefficients of friction, Journal of Applied Physics, 22, 1373-1379.

Raaen, A.M., Horsrud, P., Kjørholt, H., Økland, D., 2006. Improved routine estimation of the minimum horizontal stress component from extended leak-off tests, International Journal of Rock Mechanics and Mining Sciences, 43(1), 37-48.

Ruina, A., 1983. Slip instability and state variable friction laws, Journal of Geophysical Research, 88(B12), 10359-10370.

Rutqvist, J., Birkholzer, J.T., Cappa, F., Tsang, C.-F., 2007. Estimating maximum sustainable injection pressure during geological sequestration of CO_2 using coupled fluid flow and geomechanical fault-slip analysis, Energy Conversion and Management, 47, 1798–1807.

Samuelson, J, Elsworth, D., Marone, C., 2009. Shear-induced dilatancy of fluid-saturated faults: Experiment and theory, Journal of Geophysical Research, 114:B12404, doi:10.1029/2008JB006273.

Santarelli, F.J., Tronvoll, J.T., Svennekjaer, M., Skeie, H., Henriksen, R., Bratli, R.K., 1998. Reservoir stress path: the depletion and the rebound. SPE/ISRM paper 47350, in the SPE/ISRM Eurock'98 held in Trondheim, Norway, 8-10 July 1998.

Scholz, C.H., 2002. The Mechanics of Earthquakes and Faulting (second edition), Cambridge University Press.

Segall, P., Fitzgerald, S.D., 1998. A note on induced stress changes in hydrocarbon and geothermal reservoirs, Tectonophysics, 289(1–3), 117-128.

Sibson, R.H., 1996. Structural permeability of fluid-driven fault-fracture meshes, Journal of Structural Geology, 18(8), 1031-1042.

Streit, J.E., Hillis, R.R., 2004. Estimating fault stability and sustainable fluid pressures for underground storage of CO_2 in porous rock,

Energy, 29(9–10), 1445-1456.
Teufel, L.W., Clark, J.A., 1984. Hydraulic fracture propagation in layered rock: experimental studies of fracture containment, Society of Petroleum Engineers Journal, SPE 9878.
Townend, J., Zoback, M.D., 2000. How faulting keeps the crust strong, Geology, 28:5, 399-402.
Van den Hoek, P.J., Matsuura, T., De Kroon, M., Gheissary, G., 1999. Simulation of produced water reinjection under fracturing conditions, SPE Prod. & Facilities 14 (3), SPE 57385.
Vandeweijer, V.P., Groenenberg, R., Donselaar, R., Pluymaekers, M., Loeve, D., Hofstee, C., Nepveu, M., Orlic, B., Akemu, O., Miersemann, U., Benedictus, T., Arts, R., Neele, F., Meindertsma, W., 2011. Feasibility study P18. CATO-2 report CATO2-WP3.01-D06.
Van Wees, J.D., Buijze, L., Van Thienen-Visser, K., Nepveu, M., Wassing, B.B.T., Orlic, B., Fokker, P.A., 2014. Geomechanics response and induced seiamicity during gas field depletion in the Netherlands, Geothermics, http://dx.doi.org/10.1016/j.geothermics.2014.05.004.
Vidal-Gilbert, S., Tenthorey, E., Dewhurst, D., Ennis-King, J., Van Ruth, P., Hillis, R., 2010. Geomechanical analysis of the Naylor Field, Otway Basin, Australia: Implications for CO_2 injection and storage, International Journal of Greenhouse Gas Control, 4(5), 827-839.
Vilarrasa, V., 2014. Impact of CO_2 injection through horizontal and vertical wells on the caprock mechanical stability, International Journal of Rock Mechanics and Mining Sciences, 66(0), 151-159.
Walsh, S.C., Du Frane, W., Mason, H., Carroll, S., 2013. Permeability of Wellbore-Cement Fractures Following Degradation by Carbonated Brine, Rock Mechanics and Rock Engineering, 46(3), 455-464.
Warpinski, N.R., Teufel, L.W., 1987. Influence of geological discontinuities on hydraulic fracture propagation, Journal of Petroleum Technology, 209-220, SPE 13224.
Wibberly, C.A.J., Yielding, G., Di Torro, G., 2008. Recent advances in the understanding of fault zone internal structure: a review, In Wibberly, C.A.J., Kurz, A.J., Imber, J., Holdsworh, R.E., Colletinni, C. (eds), The Internal Structure o Fault Zones: Implications for Mechanical and Fluid-Flow Properties, Geological Society of London Special Publication 299, 5-33.
Wu, H., Chudnovsky, A., Dudley, J.W., Wong, G.K., 2004. A map of fracture behavior in the vicinity of an interface, Gulf Rocks 2004, Proceedings of the 6th North American Rock Mechanics Symposium, Houston, Texas, June 5-9, ARMA/NARMS 04-620.
Yeo, I.W., de Freitas, M.H., Zimmerman, R.W., 1998. Effect of shear displacement on the aperture and permeability of a rock fracture, International Journal of Rock Mechanics and Mining Sciences, 35(8), 1051-1070.
Yielding, G., 2002. Shale Gouge Ratio – calibration by geohistory, In Koestler, A.G., Hunsdale, R. (eds), Hydrocarbon Seal Quantification, NPF Special Publication 11, 1–15, Elsevier Science.
Yielding, G., Freeman, B., Needham, D., 1997. Quantitative fault seal prediction, AAPG Bulletin, 81:6, 897-917.
Zhang, X., Jeffry, R.G., 2004. Hydraulic fracture propagation across frictional interfaces, US Rock Mechanics / Geomechanics Symposium, ARMA-07-2004.
Zijlstra, E.B., Reemst, P.H.M., Fisher, Q.J., 2007. Incorporation of fault properties into production simulation models of Permian reservoirs from the southern North Sea, In: Jolley, S.J., Barr, D., Walsh, J.J., Knipe, R.J. (eds), Structurally Complex Reservoirs, Geological Society, London, Special Publications, 292, 295–308.
Zimmerman, R.W., Kumar, S., Bodvarsson, G.S., 1991. Lubrication theory analysis of the permeability of rough-walled fractures, International Journal of Rock Mechanics and Mining Sciences & Geomechanics Abstracts, 28(4), 325-331.
Zoback, M.D., 2007. Reservoir Geomechanics, Cambridge.
Zoback, M., Zinke, J., 2002. Production-induced Normal Faulting in the Valhall and Ekofisk Oil Fields, in The Mechanism of Induced Seismicity, edited by C. Trifu, 403-420, Birkhäuser Basel.

Chapter XII

The effects of stress on leakage through faults and fracture networks

Alexandre Lavrov[1], Andrey Antropov[2], Dusan Karas[2], Bogdan Orlic[3]
[1] SINTEF PR, Norway
[2] NIS, Serbia
[3] TNO, The Netherlands

SUMMARY

The MiReCOL project investigates existing and new techniques for remediation and mitigation of leakage from geological CO_2 storage sites. WP5 of this project is concerned with remediation options linked to transport properties of faults and fracture networks. This report is the second deliverable of WP5 (D5.2). The report investigates the effect of in-situ stress alterations on flow through faults and fractures in the cap rock. Deliverable D5.2 consists of three parts:

1. an Energy Procedia paper presented at the 13th International Conference on Greenhouse Gas Control Technologies (GHGT-13) held in Lausanne: Lavrov et al., 2016, Diversion of CO_2 to nearby reservoir compartments for remediation of unwanted CO_2 migration. GHGT-13, Lausanne;
2. a peer-reviewed paper published in the Journal of Petroleum Exploration and Production Technology: Lavrov, A., 2016, Fracture permeability under normal stress: a fully computational approach. DOI 10.1007/s13202-016-0254-6;
3. a report on coupled numerical simulations of stress-dependent CO_2 flow through faults in the cap rock, conducted on the semi-synthetic model of the Bečej natural CO_2 field, Serbia.

First paper (by SINTEF, NIS and TNO) describes a semi-analytical model of flow through a vertical fracture penetrating cap rock taking into account the stress-dependent fracture permeability. The semi-analytical model of leakage developed in this study allows a quick estimation of the leakage potential without the need for a complicated and time-consuming coupled reservoir simulation. The model enables to obtain first-order estimates of the leakage rate.

Second paper (by SINTEF) presents a numerical approach for predicting the fracture permeability as a function of the effective normal stress taking into account the fracture roughness. This computational approach provides an insight into the actual mechanics of the fracture deformation under stress, and the effect of stress on the permeability.

The third and final part of this report (by NIS) describes a workflow for coupled stress-flow reservoir simulations implemented in the numerical geomechanical simulator Visage. The workflow is applied on a semi-synthetic model of the Bečej natural CO_2 field to investigate the effect of stress on CO_2 flow through a hypothetical fault in the overburden. For the simulated cases and selected ranges of input parameters, the effects of injection-induced stress changes on flow rates through faults were minor.

1 EFFECT OF IN-SITU STRESS ALTERATIONS ON FLOW THROUGH FAULTS AND FRACTURES IN THE CAP ROCK

13th International Conference on Greenhouse Gas Control Technologies, GHGT-13, 14-18 November 2016, Lausanne, Switzerland
Andrey Antropov, Alexandre Lavrov, Bogdan Orlic

ABSTRACT

Cap-rock integrity is of paramount importance during injection and subsequent long-term storage of CO_2 in the subsurface. Pre-existing (natural) and man-induced fractures in the cap rock represent potential flow paths out of the storage formation. In this study, a first-order semi-analytical model of flow through a vertical fracture penetrating cap rock is constructed taking the stress-dependent fracture permeability into account. The model is then applied to study the effects of in-situ stress normal to fracture on the flow rate through the fracture. The flow rate increases nonlinearly with the reservoir pressure, which is due to a combined effect of nonlinear fracture deformation law and the cubic law governing the flow rate.

1.1 Introduction

Cap-rock integrity is of paramount importance during injection of CO_2 and during subsequent long-term storage of CO_2 in the subsurface. Fractures and faults in the cap rock represent potential flow paths for CO_2 migration out of the storage formation. Pre-existing sealing fractures and faults may open and thereby become hydraulically conductive if the compressive normal stress acting on the fracture plane is reduced during injection or during subsequent lifetime of the storage site.

Stress changes leading to fracture opening can be caused by natural geological processes, but may also result from the stress re-distribution accompanying the injection of CO_2 into the reservoir [1, 2]. For instance, injection into a reservoir is known to increase the total horizontal stresses in the reservoir and to reduce the total (and effective) horizontal stresses in the overburden (Fig. 1) [3]. Such stress alteration will lead to dilation, and possibly the opening of pre-existing, natural vertical fractures that often exist in siliciclastic (shales, claystone) and evaporitic (anhydrite) cap rocks. Fracture reopening will increase the permeability of the overlying formation, which may allow CO_2 to migrate upwards through the cap rock. For example, at the In Salah CO_2 injection project in Algeria, CO_2 injection in well KB-502 caused tensile opening of an existing fracture zone in the caprock and upward migration of the injected CO_2 into the lower part of the caprock [4, 5]. Another type of fractures that may create flow paths through the cap rock are fractures in the near-well area. Since a wellbore serves as a stress concentrator, alterations of in-situ stresses caused by injection are likely to be amplified in the vicinity of the well. Such amplified stresses may induce new fractures or activate the already existing ones, enabling upward migration of CO_2 across the cap rock.

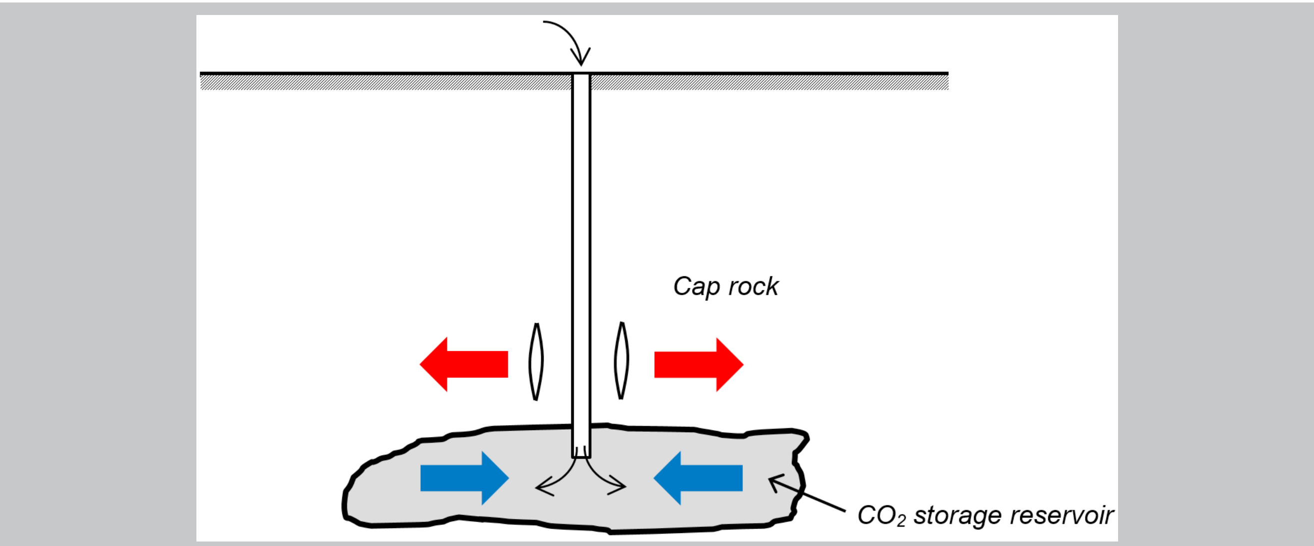

Figure 1 (a) Schematic view of vertical fracture opening in the cap rock caused by CO2 injection into the underlying reservoir. Blue arrows indicate increase of horizontal total stresses in the reservoir (stresses becoming more compressive). Red arrows indicate decrease of horizontal total stresses in the overburden (stresses becoming less compressive). Aperture of pre-existing, natural vertical fractures in the overburden is likely to increase as a result of these stress changes. This will increase the permeability of the cap rock.

In this study, we focus on the effect of a single, individual vertical fracture in the cap rock on leakage from a CO_2 storage reservoir. The effect of an individual vertical fracture on CO_2 leakage was previously addressed in refs. [6, 7]. However, geomechanical effects were neglected in those earlier studies, and only the hydraulic problem was treated. In reality, the permeability of a fracture (and thus the flow through the fracture) depends on the effective normal stress acting on the fracture plane and given by:

$$\sigma'_n = \sigma_n - p \quad (1)$$

where σ'_n is the effective normal stress; σ_n is the total normal stress; p is the fluid pressure inside the fracture. It is assumed in Eq. (1) that the Biot effective stress coefficient for the fracture deformation is equal to one, which is a common assumption for fractures in geomechanics. When the effective normal stress increases, either due to an increase in the in-situ horizontal stress or due to a reduction in the fluid pressure, the fracture closes, and its permeability decreases. Conversely, when the effective normal stress decreases, e.g. due to a fluid pressure increase caused by fluid injection or due to a reduction in the in-situ horizontal stresses, the fracture opens, and its permeability increases. The decrease in the permeability in the former case and the increase in the latter are typically nonlinear: it takes more effort to close the fracture as its aperture becomes smaller since more asperities come into contact, and the normal stiffness of the fracture increases.

In this paper, remediation by flow diversion is first analyzed using a synthetic test case and then applied to a real field case. The findings inferred from these cases are discussed. Finally, more general conclusions are drawn on the use of flow diversion as a remediation measure in the context of geological CO_2 storage.

Consider a vertical fracture (a "joint") penetrating the cap rock from the reservoir to an upper aquifer. In reality, it can be an isolated fracture, a fracture network or a pre-existing fault. For the sake of simplicity, the case of an isolated fracture is considered in this study. During CO_2 injection, the fluid pressure front might eventually reach the fracture, and the fluid pressure in the fracture will increase. This will induce the flow (of CO_2 or brine) in the fracture in the vertical direction unless the fracture is completely closed and thus has zero permeability (this may happen e.g. if the fracture is filled with gouge or is mineralized). At the same time, the fracture might start opening as the pressure increases along the fracture height. This will increase the fracture permeability. Therefore, we are dealing here with a two-way coupled problem: The fracture aperture affects the fluid flow, and the fluid pressure affects the fracture aperture. The coupling strength depends on the fracture properties, in particular the normal stiffness.

As the CO_2 injection proceeds, the horizontal in-situ stresses in the cap rock may eventually decrease. This will further increase the fracture permeability and thus the leakage rate.

Fractures may have different orientation. Even in the same fracture set, the fracture orientations may slightly vary. Thus, the normal stress acting on each vertical fracture is different unless the horizontal in-situ stresses are isotropic. Moreover, different normal stresses may act on different parts of the same fracture if the fracture surface is not a perfect plane. These considerations suggest that the total normal stress plays a crucial role in determining the fracture permeability.

The objective of this study was to investigate the effect of a single vertical fracture in the cap rock on the integrity of a CO_2 storage site. To this end, we construct a simple semi-analytical model in Section 2 that can be used to estimate the leakage flow rate as a function of the reservoir pressure. The model is then applied to demonstrate the effect of in-situ stresses on the leakage flow rate in Section 3. The paper concludes with a discussion and recommendations on CO_2 storage site selection and pressure management that would take into account geomechanical effects and stress-dependent fracture permeability.

1.2 Semi-analytical model of leakage through a vertical fracture

The geometry of the model is shown in Fig. 2. The fracture height and length are equal to H and L, respectively. The fracture width is equal to w and can be different at different vertical locations. However, the fracture width is assumed to be the same at all points located at the same depth, i.e. at a given z.

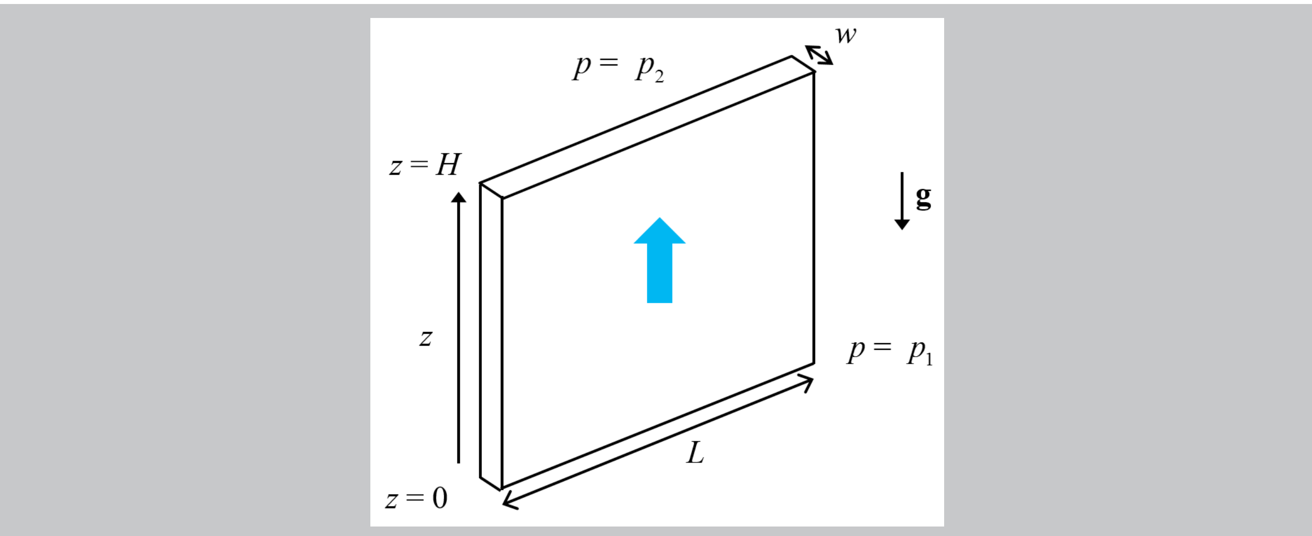

Figure 2 Geometry of the vertical fracture in the cap rock. Blue arrow indicates the direction of flow (upwards). Fracture width, height, and horizontal length are denoted by w, H, and L, respectively.

There are many correlations between the normal stress and the fracture permeability available in the literature. For instance, the following correlation was reported for shale in ref. [8]:

$$k = k_0\, exp(-C'\sigma'_n) \tag{2}$$

where C' is a fitting parameter, equal to e.g. 0.27 for Kimmeridge shale [8]; k_0 is the permeability of a fracture at zero effective normal stress. Two examples of k vs. σ'_n dependency are shown in Fig. 3, for two different values of C'.

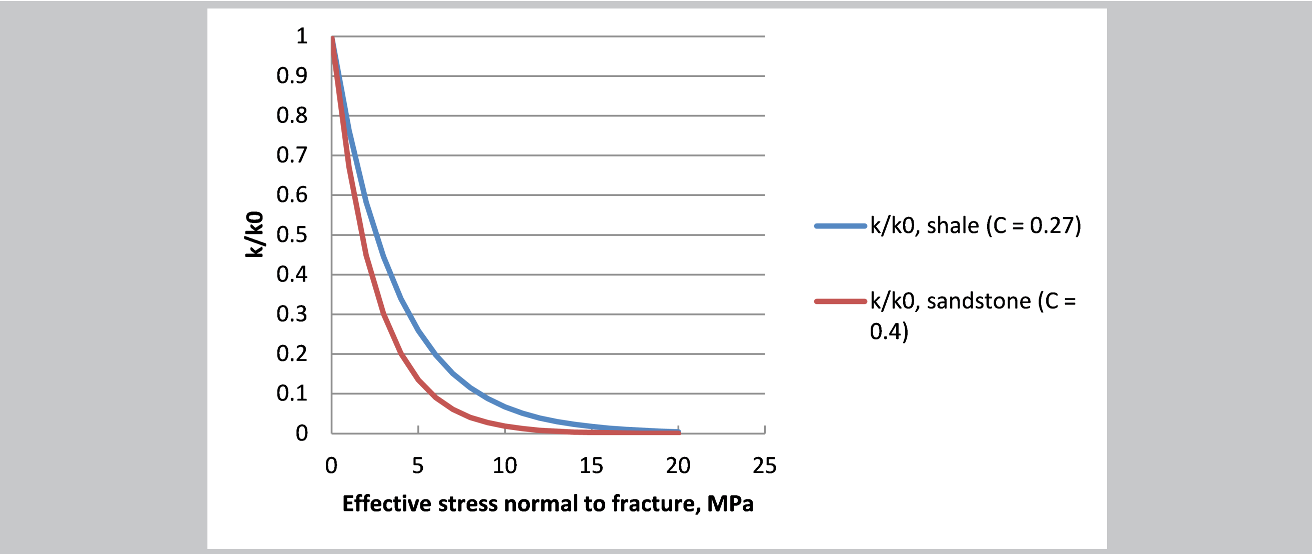

Figure 3 Fracture permeability vs. effective normal stress for $C' = 0.27$ (blue) and $C' = 0.4$ (red), according to Eq. (2).

Assuming single-phase flow (e.g. CO_2 dissolved in brine), the superficial fluid velocity in the fracture along the vertical direction is given by:

$$v = -\frac{w^2}{12\mu}\frac{d}{dz}\left(p + \rho_f g z\right) \tag{3}$$

where ρ_f and μ are the density and the dynamic viscosity of the fluid, respectively; g is the acceleration of gravity; z is the vertical coordinate (Fig. 2). The aperture, w, in Eq. (1) should be hydraulic rather than mechanical aperture. In this model, we make no distinction between the two, thereby implying that the mechanical and hydraulic apertures are equal. Since the fracture is assumed to have the same aperture at all locations at a given z, the horizontal components of the superficial fluid velocity are equal to zero at all locations inside the fracture.

We assume that the fracture permeability can be approximated locally with Eq. (2). For a Newtonian fluid, the local fracture permeability is given by $w^2/12$. Thus, the aperture is given by:

$$w = w_0\, exp(-C'\sigma'_n/2) \tag{4}$$

where w_0 is the aperture at zero effective normal stress. Assume that the horizontal in-situ stress acting normal to the fracture plane is a linear function of depth:

$$\sigma_n = \sigma_0 - \beta\rho_b g z \tag{5}$$

where σ_0 is the horizontal in-situ stress at the bottom of the fracture ($z = 0$); ρ_b is the bulk density of the rock; β is a dimensionless coefficient. In extensional tectonic regime, e.g. in stable intercontinental areas, $\beta<1$. In compressional stress environment, e.g. in tectonically active areas, $\beta>1$. Substituting Eqs. (4) and (5) into Eq. (3) yields the following pressure equation for the fracture:

$$\frac{dp}{dz} + \rho_f g = -\frac{12\mu Q}{L w_0^3}\exp\left[C\left(\sigma_0 - \beta\rho_b g z - p\right)\right] \tag{6}$$

where Q is the flow rate through the fracture (m^3/s), and $C = 3C'/2$.

After introducing dimensionless pressure, flow rate, z-coordinate, σ_0, rock bulk weight, and fluid bulk weight as follows:

$$\tilde{p} = \frac{p}{\rho_f g H}\ ,$$
$$\tilde{Q} = \frac{12\mu Q}{L\rho_f g w_0^3}\ ,$$
$$\tilde{z} = z/H\ , \qquad (7)$$
$$\tilde{\sigma}_0 = C\sigma_0\ ,$$
$$\tilde{\gamma}_b = C\beta\rho_b g H\ ,$$
$$\tilde{\gamma}_f = C\rho_f g H\ ,$$

the pressure equation reduces to:

$$\frac{d\tilde{p}}{d\tilde{z}} + \tilde{Q}\exp\left(\tilde{\sigma}_0 - \tilde{\gamma}_b\tilde{z} - \tilde{\gamma}_f\tilde{p}\right) + 1 = 0 \qquad (8)$$

As a boundary condition, we specify pressure, p_2 at the top of the fracture (Fig. 2):

$$\tilde{p} = \tilde{p}_2 \quad \text{at} \quad \tilde{z} = 1 \qquad (9)$$

1.3 Effect of in-situ stresses on leakage flow rate

We now perform computations for different flow rates, Q, and different in-situ stress values at the fracture bottom, σ_0. The dimensional input parameters for the simulations are listed in Table 1. Dimensionless parameters derived from Table 1 using Eqs. (7) are listed in Table 2. Table 2 demonstrates how the number of parameters has been reduced by non-dimensionalization.

Eq. (8) with the boundary condition given by Eq. (9) was solved numerically using the spatial discretization step $\Delta\tilde{z}=10^{-4}$. Computations were performed for a wide range of flow rates and for two values of the in-situ stress at the fracture bottom (see Tables 1 and 2).

The results in form of pressure curves at different flow rates are presented in Figure 4 for two values of the dimensionless horizontal in-situ stress: $\tilde{\sigma}_0=10.8$ (Figure 4a) and $\tilde{\sigma}_0=8.1$ (Figure 4b). The red lines in Figure 4 represent the fracture reopening pressure. Fracture reopening occurs when the fluid pressure in the fracture is equal to the total normal stress, $p=\sigma_n$. In dimensionless parameters, the fracture reopening is thus given by:

$$\tilde{p} = \frac{\tilde{\sigma}_0 - \tilde{\gamma}_b\tilde{z}}{\tilde{\gamma}_f} \qquad (10)$$

As evident from Figure 4, the pressure stays below the fracture reopening pressure at all flow rates except the highest one.

Flow rate through the fracture increases nonlinearly with the fluid pressure applied at the fracture bottom. This nonlinearity is a combined result of two mechanisms: the nonlinear fracture deformation law (Eq. (4)) and the “cubic law” describing the dependency of the flow rate on the local fracture aperture (Eq. (3)). According to Eq. (4), the fracture aperture increases faster as the effective

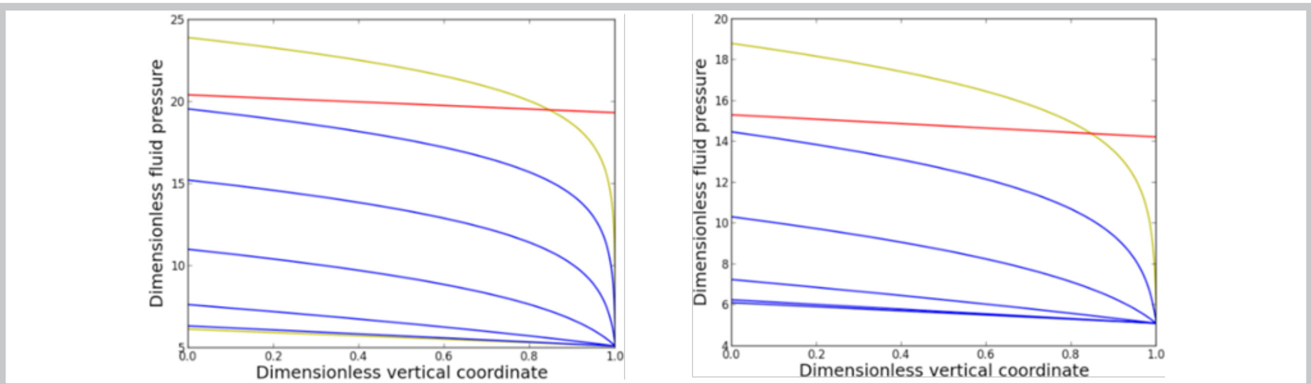

Figure 4 Dimensionless fluid pressure in the fracture as a function of depth at different leakage rates. The red line shows the fracture reopening pressure. The top yellow line corresponds to $\tilde{Q}$=12.2. The bottom yellow curve corresponds to $\tilde{Q}$=1.22 10^{-5} The blue curves correspond, in ascending order, to $\tilde{Q}$=1.22 10-4, 1.22 10-3, 1.22 10-2, 1.22 10-1, 1.22. The dimensionless horizontal in-situ total stress, $\tilde{\sigma}_0$, is equal to 10.8 (a) or 8.1 (b). The bottom yellow line is indistinguishable from the bottom blue line in (b).

stress becomes smaller, i.e. as the pressure increases and the fracture opens up. According to the "cubic law" [9, 10], the flow rate is proportional to w^3 [cf. Eq. (3)]. Thus, both mechanisms result in the flow rate increasing more rapidly as the pressure in the reservoir builds up.

Table 1 Dimensional input parameters for semi-analytical simulations.

Dimensional parameter	Value
C, Pa^{-1}	$0.27{\cdot}10^{-6}$
β	0.4
ρ_b, kg/m^3	2700
ρ_f, kg/m^3	1000
g, m/s^2	9.8
H, m	200
L, m	100
μ, Pa·s	0.001
w_0, m	0.001
p_2, Pa	$10{\cdot}10^6$
σ_0, Pa	$40{\cdot}10^6$; $30{\cdot}10^6$
Q, m^3/s	10^{-6}..1

Table 2 Dimensionless input parameters for semi-analytical simulations; based on Table 1 and Eqs. (7).

Dimensionless parameter	Value
$\tilde{\gamma}_b = C\beta\rho_b gH$	0.572
$\tilde{\gamma}_f = C\rho_f gH$	0.529
$\tilde{p}_2 = p_2/(\rho_f gH)$	5.102
$\tilde{Q} = 12\mu Q/(L\rho_f g w_0^3)$	$1.22{\cdot}10^{-5}$..12.2
$\tilde{\sigma}_0 = C\sigma_0$	10.8; 8.1

1.4 Discussion and conclusion

The semi-analytical model constructed in Section 2 is a simple and fast computational tool that enables risk assessment of leakage through a vertical fracture in the cap rock caused by pressure increase in the reservoir. Computations presented in Section 3 demonstrate that the nonlinear fracture deformation may lead to a rapid increase of the fracture permeability and thus the leakage rate when the fluid pressure front propagates upwards in the fracture. It is therefore important to characterize fractures present or suspected in the cap rock. In-situ investigation of fracture properties at CO_2 storage sites is, in practice, difficult or impossible. Numerical simulations of fracture deformation and flow under stress can therefore be used, as explicated in another recent publication from the MiReCOL project, ref. [11].

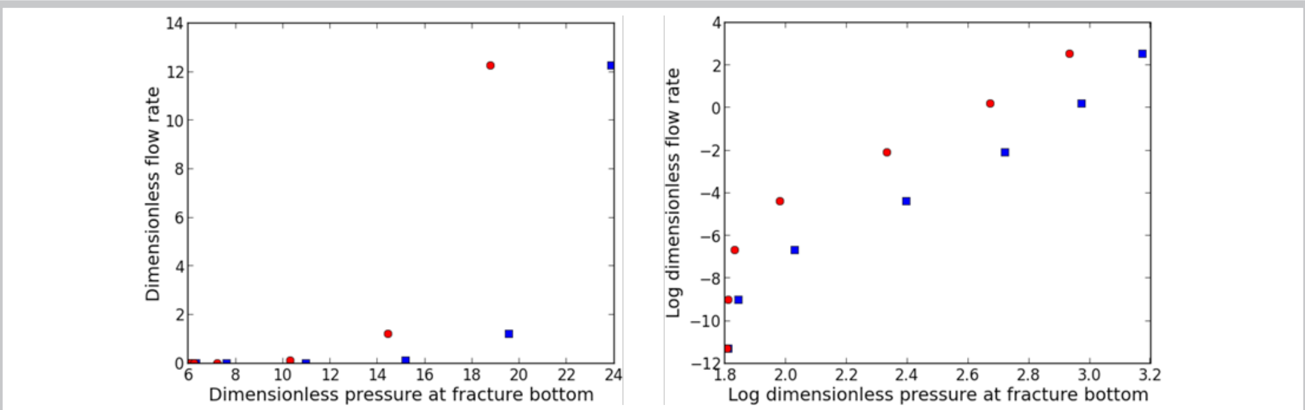

Figure 5 Dimensionless flow rate through the fracture as a function of fluid pressure at the bottom of the fracture (the "reservoir pressure") for $\tilde{\sigma}_0$=10.8 (blue squares) and $\tilde{\sigma}_0$=8.1 (red circles) in linear-linear (a) and log-log (b) coordinates.

The in-situ stress normal to fracture is or paramount importance for leakage prediction through vertical fractures, as Fig. 5 shows. Therefore, in-situ stress measurements are crucial for risk assessment of leakage in CO_2 storage sites. Such measurements can be performed by means of extended leakoff tests, breakout analysis, deformation rate analysis, etc. Fractures can have different orientations in the cap rock. The fractures normal to the minimum horizontal stress have the lowest reopening pressure and thus are most prone to leakage, other parameters being equal.

The variation of the fracture reopening pressure with the fracture orientation lead recently one of the authors to introduce two new concepts in drilling-related geomechanics: the spectrum of fracture reopening pressures and the spectrum of lost-circulation pressures [12, 13]. These are to replace the commonly used (e.g., in drilling) fracture reopening pressure and lost-circulation pressure. The analyses presented in this paper demonstrate that the knowledge of the fracture reopening pressure spectrum is essential for leakage risk assessment in CO_2 storage projects, too.

Nonlinearity of the leakage rate as a function of the reservoir pressure evident in Figure 5 suggests that the role of monitoring becomes even more important as the injection proceeds. Increasing the reservoir pressure by 1 bar at a later stage of injection is likely to have a larger impact on the leakage risk than the same increase at the beginning of injection.

The semi-analytical model of leakage through a vertical fracture in the cap rock developed in this study allows a quick estimation of the leakage potential without the need for a complicated and time-consuming coupled reservoir simulation. The model enables to obtain first-order estimates of the leakage rate. Based on this initial assessment, more detailed, site-specific numerical models (e.g. coupled reservoir-geomechanical models) can be developed.

Such detailed coupled simulations are indeed required for assessment of long-term effects of CO_2 injection on the stress field and, thus, on the fracture permeability. Such effects are due to the stress path, i.e. the change of the total in-situ stresses in the reservoir and in the cap rock caused by the pore pressure variation in the reservoir [14]. During CO_2 injection, the total horizontal stresses in the reservoir increase, while the total horizontal stresses in the cap rock slightly decrease. This will increase the permeability of the vertical fractures penetrating the cap rock, as evident from Fig. 5 (compare the red and blue data points).

The importance of fracture characterization in the cap rock of a CO_2 storage site is obvious from our analysis. Fracture properties are crucial for application of even the simplest models, such as the semi-analytical model introduced in Section 2. In particular, not only fracture permeabilities, but also fracture aperture, orientation, morphology, and stress-displacement behaviour should be characterized by field and laboratory measurements as accurately as possible. This will improve the overall risk assessment of CO_2 storage sites in both short-term and long-term perspectives.

Acknowledgements
Research reported in this paper has been conducted with funding from the European Commission FP7 project MIRECOL (www.mirecol-CO_2.eu), Grant Agreement No. 608608. The project received additional funding from Statoil, ENGIE and Shell.

References

1. Lavrov A Dynamics of stresses and fractures in reservoir and cap rock under production and injection. Energy Procedia 2016; 86: 381-90.
2. Orlic B, Heege Jt, Wassing B Assessing the integrity of fault- and top seals at CO_2 storage sites. Energy Procedia 2011; 4: 4798-805.
3. Fjær E, Holt RM, Horsrud P, Raaen AM, Risnes R. Petroleum related rock mechanics. 2nd ed. Amsterdam: Elsevier; 2008.
4. Shi J-Q, Sinayuc C, Durucan S, Korre A Assessment of carbon dioxide plume behaviour within the storage reservoir and the lower caprock around the kb-502 injection well at in salah. International Journal of Greenhouse Gas Control 2012; 7: 115-26.
5. Rinaldi AP, Rutqvist J Modeling of deep fracture zone opening and transient ground surface uplift at kb-502 CO_2 injection well, in salah, algeria. International Journal of Greenhouse Gas Control 2013; 12: 155-67.
6. Selvadurai APS Fluid leakage through fractures in an impervious caprock embedded between two geologic aquifers. Advances in Water Resources 2012; 41: 76-83.
7. Zeidouni M Analytical model of leakage through fault to overlying formations. Water Resources Research 2012; 48: n/a-n/a.
8. Gutierrez M, Øino LE, Nygård R Stress-dependent permeability of a de-mineralised fracture in shale. Marine and Petroleum Geology 2000; 17: 895-907.
9. Brown SR Fluid flow through rock joints: The effect of surface roughness. J. Geophys. Res. B 1987; 92: 1337-47.
10. Zimmerman RW, Kumar S, Bodvarsson GS Lubrication theory analysis of the permeability of rough-walled fractures. International Journal of Rock Mechanics and Mining Sciences & Geomechanics Abstracts 1991; 28: 325-31.
11. Lavrov A Fracture permeability under normal stress: A fully computational approach. Journal of Petroleum Exploration and Production Technology 2016; 1-14.
12. Lavrov A. Lost circulation: Mechanisms and solutions. Oxford: Elsevier; 2016.
13. Lavrov A From fracture gradient to the spectrum of lost-circulation pressures: A paradigm shift? Energy procedia, proceedings of ghgt-13 (this volume). 2016.
14. Holt RM, Gheibi S, Lavrov A. Where does the stress path lead? Irreversibility and hysteresis in reservoir geomechanics. Arma paper 16-496 presented at the 50th us rock mechanics / geomechanics symposium, houston, texas, USA, 26-29 june 2016. In.; 2016.

2 FRACTURE PERMEABILITY UNDER NORMAL STRESS: A FULLY COMPUTATIONAL APPROACH

Alexandre Lavrov
SINTEF Petroleum Research, Trondheim, Norway
Email: alexandre.lavrov@sintef.no
Tel.: +47 98 28 66 58

Abstract
Fractures contribute significantly to the overall permeability of naturally- or hydraulically-fractured reservoirs. In the cap rock, fractures may provide unwanted pathways for reservoir or stimulation fluids. Predicting fluid flow in naturally-fractured rocks under production or fluid injection requires that permeability of a single, rough-walled fracture be well understood and accurately described as a function of the effective stress. The lack of information about the properties of fractures at depth calls for a numerical approach that would enable predicting the fracture permeability as a function of the effective normal stress. Such fully computational approach is developed in this study. The fracture deformation is calculated by solving the contact problem using the finite-element method. At each deformation step, the steady-state fluid flow in the fracture is computed in two orthogonal directions using the lubrication theory approximation, in order to evaluate the permeability and the hydraulic aperture of the fracture. The computational approach is tested on two examples: a "brittle rock" (linear elastic) and a "ductile rock" (linear elastic perfectly plastic). Both mechanical and hydraulic behaviour of the fracture under cyclic normal loading are found to be in qualitative agreement with the results obtained in a number of published experimental studies. The computational approach provides an insight into the actual mechanics of the fracture deformation under stress, and the effect of the latter on the permeability. In particular, hysteresis in the fracture roughness is obtained with the "ductile rock" suggesting that (at least some) fractured rocks may retain "memory" about their loading history imprinted in the fracture landscapes.

Acknowledgment
The research leading to these results received funding from the European Union Seventh Framework Programme (FP7/2007-2013), subprogramme ENERGY.2013.5.2.1 "Mitigation and remediation of leakage from geological storage", under grant agreement No. 608608 ("Mitigation and remediation of CO_2 leakage"). The project receives additional funding from Statoil, GDF SUEZ and Shell.

2.1 Introduction
The importance of fracture for fluid flow in subsurface rocks has been recognised in hydrology, geophysics and reservoir engineering for at least three decades. In petroleum engineering, the naturally-fractured reservoirs (carbonates, gas shale) stand out as a subject of their own, because of their remarkably different behaviour (Aguilera 1980). Naturally-fractured reservoirs are those where fractures contribute crucially to storage and / or permeability. In reality, all rocks contain fractures, spanning in size from microcracks at grain scale to master joints extending for hundreds of meters (Twiss and Moores 2007).

Fracture permeability is a function of (i) the average opening of the fracture (which is often called the mechanical aperture); (ii) the roughness of the fracture faces caused by asperities. The roughness creates tortuous flow paths for the fluids (Brown 1987; Muralidharan et al. 2004). Hydraulic aperture of a fracture, w_h, is defined as the aperture of a smooth-walled conduit that has the same permeability as the real rough-walled fracture (Brown 1987; Zimmerman et al. 1991). The permeability of a fracture is thereby equal to $w_h^2/12$.

Note that the terms "mechanical aperture", "average aperture" and "mean aperture" are used interchangeably throughout this manuscript, just as they are in modern rock mechanical and hydrogeological literature.

When compressive normal stresses in the rock are increased, a fracture closes, and its permeability declines. At the same time, the fracture stiffness increases since more contacts between the fracture faces are created, and the area of the existing contacts increases (Chen et al. 2000; Pyrak-Nolte and Morris 2000). Similar effects, i.e. fracture closure and permeability reduction, are observed when the fluid pressure inside the fracture is reduced. Apart from direct reduction of the aperture, fracture closing increases the flow tortuosity since more asperities come into contact, and the flowing fluid has to go around them. This effectively increases the length of streamlines and pathlines, further reducing the hydraulic aperture of the fracture.

Unloading of a fracture, i.e. reduction of the normal stress, is usually accompanied with hysteresis in the fracture permeability: the fracture permeability is different during unloading from what it was at the same stress during loading (Gutierrez et al. 2000). Hysteresis of the fracture permeability under normal loading is a manifestation of a more general irreversibility of rock deformation that also includes, e.g., the "stress memory" capacity of rocks (Becker et al. 2010; Lavrov 2005).

Depletion of oil and gas reservoirs is known to be accompanied with fracture closure, which is one of the reasons for notoriously low recovery factors in naturally-fractured reservoirs (e.g. recovery factors down to 10-15% in some fractured carbonates). A recent study suggests that stress-dependent fracture permeability can reduce the cumulative ten-year production from an unconventional gas field by 10% (Aybar et al. 2014). Designing hydrocarbon production from and fluid injection into such fields requires a good grasp of the basic mechanisms affecting fracture behaviour during depletion and injection. It also calls for quantitative estimates of fracture permeability as a function of drawdown (reservoir pressure reduction).

It should be noted that very little information about fracture morphology (incl. roughness) and properties of the fracture network is available in practice when a field is developed. This information is usually gathered by interpreting image logs (acoustic or electric). Such logs show only traces of the fractures on the borehole wall. The resolution of the currently available equipment is not sufficient to quantify the fracture aperture, let alone provide information about fracture roughness. Under these circumstances, use of analogues, e.g. fractured outcrop rocks, for deriving fracture behaviour of fractures at depth becomes difficult, if possible at all, since fracture properties at depth can only be guessed.

The inaccessibility of fractures at depth, and unavailability of information on their properties, motivate the development of a computational approach that would allow an engineer to derive fracture properties such as stiffness and permeability from the limited information about the rock and fractures that is available. The first objective of this study is to demonstrate the viability of such approach for a fracture subject to normal stress.

Many empirical and semi-empirical fracture deformation laws have been proposed in the literature over the past 40 years. These laws are typically obtained for specific rocks. Each of such laws is therefore not particularly useful for other rocks. A number of empirical and semi-empirical laws governing fracture deformation under normal stress are discussed in (Gangi 1978; Malama and Kulatilake 2003). As pointed out in (Gangi 1978), the empirical and semi-empirical laws, albeit useful for matching the experimental data for a specific rock, provide no insight into the physical mechanisms of stress-dependent fracture permeability.

The limited validity and applicability of empirical and semi-empirical fracture deformation laws has motivated the development of numerical models of fracture deformation under normal stress. Most of these models are based on the approach of a “bed of nails” advocated in (Gangi 1978). In that study, asperities were considered as a collection of cylinders deforming independently of each other. It was shown that “nails” of different shapes could be used and could bring about the same fracture deformation law as the cylinders, provided that the length distribution of the “nails” is adjusted accordingly. A similar approach was taken in (Brown and Scholz 1986) where the Hertzian model was used to describe the interaction between asperities in contact. Independent interaction of asperities in models of this kind is a crude approximation. Another drawback of these models is the need for their calibration in terms of micromechanical parameters that cannot be easily obtained from a direct rock mechanical test. Despite the above weaknesses, tuning the model parameters enabled a good approximation of the measured normal stress vs fracture closure curves in (Brown and Scholz 1986; Gangi 1978). The Hertzian model was used to describe contact interaction between asperities also in a number of subsequent studies, e.g. (Lespinasse and Sausse 2000). A simplified description of the contact interaction was employed also in the work of (Pyrak-Nolte and Morris 2000) and (Detwiler and Morris 2014) who modelled asperities as circular cylinders behaving elastically at any stress.

It should be noted that, even though the above mentioned simplified treatments of fracture deformation do provide a valuable insight into the mechanics of fracture closure, it is difficult to establish a relationship between the parameters of such models and measurable rock properties. Modern finite-element codes offer a more accurate, and consistent, description of contact interactions, without the major simplifications used in the above earlier works. In addition, the hard contact model implemented e.g. in the finite-element package ABAQUS and used in this study, involves only measurable, macro-scale properties of the rock, such as the Young’s modulus and the Poisson’s ratio, and is therefore more suitable for practical applications. Unlike its empirical and semi-empirical counterparts, the finite-element model of the contact problem allows one to study directly the effect of different factors, such as the rock plasticity, on the fracture deformation.

It should be noted that most of the experiments on fracture deformation and fracture permeability under stress have been performed on brittle, crystalline rocks such as granite, quartzite, marble etc. Studies on rocks showing some degree of plasticity, e.g. shale, are rare. Experiments of (Gutierrez et al. 2000) performed on Kimmeridge shale revealed irreversible, hysteretic fracture deformation under cyclic normal load. The fracture had nonmatching rough walls in that study. As a result, it was not possible to completely close such fracture by applying normal load. Even at normal stresses on the order of or higher than the unconfined compressive strength of the shale, the fracture permeability was several orders of magnitude higher than the matrix permeability of the rock. In contrast, experiments performed on an artificial, smooth-walled fracture using another shale (Opalinus Clay) demonstrated that the permeability of such fracture could be reduced virtually down to matrix permeability by applying a sufficiently large normal stress (Cuss et al. 2011). The above two studies demonstrate the essential role of asperities in governing the mechanical and hydraulic behaviour of fractures in a ductile rock. It should be noted that asperities also have a significant impact on particle transport. In particular, surface roughness gives rise to hydrodynamic dispersion during particle transport in fractures (Bauget and Fourar 2008; Cumbie and McKay 1999; Koyama et al. 2008; Nowamooz et al. 2013).

The role of plastic deformation in contact interactions between asperities was recognised and confirmed via SEM analyses already by (Brown and Scholz 1986). However, their plasticity model, being part of the Hertzian contact model, was severely oversimplified. The objectives of this study, in addition to demonstrating the viability of the computational approach, were: to look into the effect of rock ductility (plasticity) on fracture permeability under normal stress; to look into the effect that normal stress might have on the roughness-induced anisotropy of the fracture permeability, in a relatively brittle rock and in a relatively ductile rock.

2.2 Computational workflow

The numerical workflow used for deriving fracture permeability as a function of normal stress in this work is as follows:

1. Generate two fracture surfaces. This is done numerically in this study. Alternatively, profilometry can be performed on geological samples of a fractured rock.
2. Use the two landscapes obtained in 1) to make two rock blocks (prisms), with each of the two landscapes being a face on one of the prisms. The prisms are then placed so that the two rough sides face each other (Figure 1).
3. Import the two rock blocks into a finite-element software.
4. Fix one block and apply a desired history of normal loading-unloading to the other block, under displacement control.
5. At each displacement step, export the distribution of the fracture aperture and construct an updated fracture aperture landscape.
6. For each exported distribution of aperture, perform fracture flow simulations to derive the fracture permeability (the hydraulic aperture).

Items 1, 2 and 3 in the above list are pre-processing. Item 5 is post-processing. Items 4 and 6 are the actual numerical simulations.

The recursive subdivision technique was used in this study to generate two fracture faces numerically (step 1 in the above list) (Fournier et al. 1982). Both fracture surfaces were generated using the same parameters, in particular the Hurst exponent (a parameter linked to the fractal dimension of the fracture surfaces) equal to 0.7, and had the same in-plane dimensions of 32 cm × 32 cm. The Hurst exponent is typically around 0.8 for natural fractures in rocks (Detwiler and Morris 2014). The in-plane grid spacing was equal to 1 cm, thus the fracture plane had à 33 nodes in the x- and y-directions. The discretization was thus quite coarse. However, as shown by (Schmittbuhl et al. 2008), viscous flow in a fracture is controlled by long wavelengths of the fracture aperture landscape, at least when the fracture is opened. Therefore, as a first approximation, a coarse model was deemed sufficient. Using a fine grid would induce a prohibitive computational cost for the FEM model of mechanical deformation since the mechanical model was 3D, while the flow model was effectively 2D. All numerical computations in the workflow were performed on a desktop computer in this study. The relatively coarse resolution is sufficient to demonstrate the viability of our fully-computational approach. Finer grids can be used in future work.

It should be noted that the procedure described above and used for generating the fracture faces numerically in this study implies that fracture faces do not match at the beginning of the simulation. According to (Gangi 1978), this is a reasonable conjecture since, even in the case where the fracture faces could potentially be matching (e.g. freshly formed tensile fracture without shear displacement in hydraulic fracturing), the fracture will most likely be kept opened at some spots by gouge (small broken pieces of rock dislodged from the fracture faces). The latter would play the role of asperities even in the rare cases where the fracture faces could match.

The grid spacing of 1 cm ensured that the lubrication theory approximation would hold in flow simulations (step 6 in the above list). It should be noted that, instead of numerical generation of the fracture landscape, a real landscape could be obtained from a real rock sample using e.g. mechanical profilometry (Lespinasse and Sausse 2000) or laser profilometry (Młynarczuk 2010; Schmittbuhl et al. 2008).

A structured mesh of hexahedral elements was then generated in both blocks (step 2 in the above list). The two meshed blocks are shown in Figure 1. The two blocks were then imported into a finite-element code (item 3 in the above list). ABAQUS was used in this study, but any other FEM code capable of handling contact problems could be used as well.

ABAQUS is a commercially-available general-purpose finite-element code widely used for solving problems in solid mechanics. In this work, static stress analysis of fracture deformation under normal displacement was performed with ABAQUS. The following boundary conditions were applied on the bottom block: rollers at the bottom side ($z = 0$), the front side ($y = 0$) and the left-hand side ($x = 0$). See Figure 1 for the coordinate system. For the top block, z-displacement was applied at the top side. The loading was thus displacement-controlled. The intention was to reproduce the boundary conditions of a laboratory test used to study fracture deformation and flow.

After the finite-element simulation of fracture deformation was completed, the reaction force on the top surface of the top block was extracted. From this force, the averaged applied stress was calculated at each displacement step. Furthermore, the distribution of the contact opening was exported for each displacement step. This data was then used to construct an updated fracture aperture profile (step 5 in the above list).

For each updated fracture profile, a steady-state flow simulation was performed to assess the fracture permeability and the hydraulic aperture. To this end, the updated fracture profiles were imported into a fracture flow code, and a steady-state simulation of unidirectional flow of an incompressible Newtonian fluid was performed by applying a pressure gradient in the x-direction, i.e.

between the sides x = 0 and x = 32 cm of the fracture. It should be noted that the fracture permeability is usually so much greater than the matrix permeability that matrix porosity and permeability were neglected in this study, and only flow inside the fracture was considered (with no matrix-fracture fluid exchange and no poroelastic effects in the matrix).

The fracture flow code solved the problem under the assumptions of the lubrication theory approximation. These assumptions are as follows (Zimmerman et al. 1991):

1. the inertial effects are negligible, i.e. the Reynolds number is smaller than 1;
2. the velocity gradient in the fracture plane is much smaller than in the direction normal to fracture. This means in practice that the standard deviation of the aperture distribution is smaller than the largest wave length of the aperture profile.

Under the above assumptions, the flow equation is given by (Brown 1987; Keller et al. 1999):

$$\frac{\partial}{\partial x}\left(w^3\frac{\partial p}{\partial x}\right)+\frac{\partial}{\partial y}\left(w^3\frac{\partial p}{\partial y}\right)=0 \qquad (1)$$

where p is the fluid pressure inside the fracture; w is the local fracture aperture; x, y are Cartesian coordinates in the fracture plane. Eq. (1) was solved on a regular Cartesian grid using the finite-volume method described and benchmarked elsewhere (Lavrov 2014). It should be noted that numerical modelling of this type has been used for evaluation of fracture permeability in many previous studies, e.g. (Brown 1987; Koyama et al. 2008).

From the flow simulation (step 6 in the above list), the hydraulic fracture aperture was obtained as a function of the normal stress or displacement. Other outputs, at each loading step, included: distributions of fluid pressure and velocity in the fracture plane; maximum and average (mechanical) aperture of the fracture.

The numerical roadmap laid out above was tested on two examples:
1. a linear-elastic rock (“brittle rock”);
2. an elastic perfectly plastic rock (“ductile rock”).

The “brittle rock” may serve as a model for a fracture in a brittle, hard, crystalline rock. The “ductile rock” may serve as a model for a fracture in a soft, sedimentary rock showing significant plasticity, such as some shales.

2.3 Results

2.3.1 Brittle rock

The material properties of the rock are given in Table 1. The rock was linear elastic and might serve as analogue to a hard rock under stresses that do not exceed its yield point.

The two blocks were initially placed in such way that the initial mechanical aperture (the average distance between the rough fracture faces) was equal to 2 mm. There were no contact spots between the fracture faces at the beginning of the simulation. The displacement of the top surface of the top block was then increased from 0 to 5 mm so as to close the fracture. Since the material was linear elastic, the deformation was reversible, and no loading-unloading cycles were therefore performed in this simulation.

The averaged stress at the top surface of the top block vs applied displacement is shown in Figure 2 (solid line, diamond markers). The solid line in Figure 2 is quite nonlinear even though the rock is linear elastic. The nonlinearity was due to the fracture progressively closing as the displacement increased. The number and area of the contact spots were increasing with displacement, making the fracture effectively stiffer. This behaviour is well-known from laboratory tests, e.g. (Pyrak-Nolte and Morris 2000). The rate of stiffness increase depends on the rate of formation of new contacts as the fracture surfaces are pressed against each other.

The plot in Figure 2 is qualitatively similar to the stress-displacement plots in (Koyama et al. 2008; Malama and Kulatilake 2003). The displacement values represented by the solid line in Figure 2 contains both, the deformation (closure) of the fracture and the deformation (compression) of the bulk rock. As mentioned in (Koyama et al. 2008), the rightmost part of the solid curve corresponds to the elastic deformation of the bulk rock and is therefore linear in this simulation. The linear component of the deformation is plotted as a dashed line with triangular markers in Figure 2. We now follow the procedure described in (Koyama et al. 2008) to extract the fracture deformation curve from these simulation data. Shifting the solid line leftwards so that it now passes through the origin produces the dashed line with square markers in Figure 2. Shifting the dashed straight line with triangular markers leftwards, so that it now passes through the origin, produces the other dashed line with square markers in Figure 2. Subtracting one dashed line with square markers from the other produces the dotted line, which is the fracture deformation curve. Its shape is similar to the fracture deformation curve in (Koyama et al. 2008). All deformation of the bulk rock material has been removed from the displacement represented by the dotted curve. The dotted curve represents the pure fracture deformation.

The fracture deformation curve in Figure 2 has a vertical asymptote at 1.4 mm which, according to (Koyama et al. 2008), signifies the mechanical aperture of the fracture (i.e. the mean aperture) at zero normal stress. It is the theoretical maximum of the relative normal displacement of the fracture faces that can be achieved by increasing the compressive stress on the fracture.

Analysis of the fracture aperture distributions at subsequent displacement steps has shown that the fracture faces first touched each other when the applied displacement became equal to 1.0 mm. The greatest value of the local fracture aperture as a function of the applied displacement is shown in Figure 3 (dashed line). It is evident from Figure 3 that the fracture became completely closed mechanically at the last loading step, i.e. at the applied displacement of 5 mm. The flow through the fracture in the x-direction ceased, however, already at the displacement of 2 mm, as the hydraulic aperture data suggest (solid curve in Figure 3). Figure 4 illustrates the decay of the mechanical aperture (average distance between the fracture faces) as the stress increases. The shape of the curve in Figure 4 resembles the respective plot obtained in a laboratory experiment on a granitic rock (Chen et al. 2000). The main qualitative difference between the curve in (Chen et al. 2000) and the curve in Figure 4 is that zero aperture was not reached in the former. In the simulation, a zero aperture is eventually reached as the stress becomes sufficiently high. In a real test, the bulk rock may break or the loading capacity of the equipment may be exceeded before that happens.

Note that the hydraulic aperture shown in Figure 3 was obtained when the pressure gradient was applied in the x-direction in the flow simulations, i.e. in the horizontal direction in Figure 5. In the right-hand part of the fracture, a region of small aperture existed from the very beginning (blue region in Figure 5a). As the loading proceeded, this region was closing first, until it completely blocked the flow in the x-direction (Figure 5b). The flow was blocked because the fracture became completely closed along its right-hand side (x = 0.32 m), while a substantial percentage of the fracture area was still mechanically opened, i.e. had nonzero local aperture.

It should be noted that, if the fracture were larger, the fluid would probably be able to find a way around and to bypass the closed area. However, since all fractures, in practice, are finite, the percolating flow path would sooner or later cease to exist at some displacement value, and the hydraulic aperture would drop to zero. In the case of a real, rough-walled fracture with poorly matching faces and/or with gouge deposited inside the fracture, the fracture is likely to remain mechanically opened at some spots when the flow stops. The exact displacement at which the flow stops is expected to depend on the initial aperture, the fracture roughness distribution, and the in-plane dimensions of the fracture.

The difference between the concepts of the hydraulic and the mechanical aperture is evident in Figure 5. Similar to isolated pores in porous media, open parts of the fracture in Figure 5c create mechanical aperture, but do not contribute to the permeability of the fracture. Thus the mean (i.e. mechanical) aperture is nonzero in Figure 5c whereas the hydraulic aperture is zero.

The effect of fracture closure on the fluid velocity and the fluid pressure distributions is evident in Figures 6 and 7, respectively. The pressure gradient is quite uniform at the beginning of the loading, when the fracture is wide open (Figure 7a). As the loading proceeds, increasingly greater pressure drop is needed to flow through the constriction at the right-hand side of the fracture. As a result, most of the pressure drop occurs at the right-hand side in Figure 7b. The fluid velocity field becomes increasingly tortuous as the loading proceeds (compare Figure 6b to Figure 6a).

Figure 8 shows the ratio of hydraulic to mechanical aperture, w_h/w, as a function of the mechanical aperture, w. As w increases, w_h/w asymptotically approaches 1, as expected since the effect of roughness decreases with w (the height of asperities becomes *relatively* small, compared to the steadily increasing fracture aperture).

It seems, from the above exposition that the flow stoppage at displacement 2 mm is controlled by the right-hand constriction in the fracture landscape. What if the flow were in the orthogonal direction? Would the results be different? In order to answer this question, flow simulations were repeated in the y-direction for all displacement steps. In turned out that the flow stopped at the next step, i.e. at 3 mm displacement, in this case. The results were in general quite similar to those obtained with the flow in the x-direction. The results obtained with the flow in the x- and y-directions are juxtaposed in Figure 9. A striking similarity exists between the two curves in Figure 9, despite the fact that the numerical model is relatively small (33 × 33 nodes in the fracture plane), which might be expected to produce greater anisotropy.

As mentioned above, flow in the x-direction stops at displacement 2 mm, while flow in the y-direction stops at displacement 3 mm. A closer look at Figure 5 reveals why and how this happens. It is evident from Figure 5a that percolating clusters in both x- and y-directions do exist at displacement 1 mm. From Figure 5b, a percolating cluster only in the y-direction survives at displacement 2 mm. From Figure 9c, no percolating cluster can be found in the fracture. This is consistent with the difference in the evolution of w_h in the x- and y-directions in Figure 9.

Figure 9 indicates that, although the anisotropy of the fracture permeability is quite small, it is present at all displacement steps. It is instructive to see how the permeability anisotropy evolves as the fracture closes. This is shown in Figure 10 where the anisotropy coefficient is plotted as a function of the mechanical aperture. The permeability coefficient is here defined as the ratio of the hydraulic aperture obtained with the flow in the x-direction to the hydraulic aperture obtained with the flow in the y-direction. Figure 10 suggests that the permeability anisotropy is indeed quite small, and the fracture becomes more isotropic as it opens. In the limit of an infinitely wide fracture, the anisotropy coefficient would be equal to 1 for any fracture since the effect of the (finite) roughness becomes negligible as $w \rightarrow \infty$.

To conclude the elastic case, aperture histograms are presented Figure 11 for increasing displacements. The distribution of the aperture changes shape after the fracture faces come into contact. Contact spots emerge as a peak at the leftmost bin in Figure 11c. Concurrently, the distribution acquires a "fat tail" in Figure 11c.

2.3.2 Ductile rock

The material properties used in the simulation of a "ductile rock" are given in Table 2. The rock is linear elastic perfectly plastic, and represents a ductile rock. As evident from Table 2, the elastic properties of the ductile rock were chosen equal to those of the brittle rock (see Section 3.1 and Table 1). This was done in order to single out the effect of rock plasticity on fracture behaviour. Thus, the two cases (ductile vs brittle) differ only with regard to the plastic behaviour, while the elastic properties are identical. In reality, a "typical" ductile rock would typically have elastic moduli lower than a "typical" brittle rock.

Similarly to the elastic rock, the two rock blocks were initially placed in such way that the initial mechanical aperture was equal to 2 mm. There were no contact spots between the fracture faces at the beginning of the simulation. The displacement of the top surface of the top block was then increased from 0 to 5 mm. After the maximum displacement value of 5 mm had been reached, the applied displacement was decreased through the same steps from 5 mm to 0. After that, a second loading cycle was performed: the displacement was again increased, retracing the same steps from 0 to 5 mm.

Averaged stress at the top surface of the top block vs applied displacement is shown in Figure 12. The curve in Figure 12 is nonlinear and has a significantly different shape than the respective curve for an elastic rock (Figure 2, solid line). Namely, the curve is S-shaped during loading of the ductile rock. The nonlinear part at the beginning of the loading in Figure 12 is caused by the same mechanism as the nonlinearity in the case of the elastic rock, i.e. an increase in the contact area. The nonlinear part at the end of the loading (rightmost part of the S-shaped curve in Figure 12) is caused by plastic yield at contact points. Plastic yield leads to the flattening of the fracture faces by the end of the load increase. As a result, the aperture of the fracture is smaller and more evenly distributed than at the end of loading of the elastic model. The hysteresis caused by plastic deformation at the fracture faces is evident in the evolution of the hydraulic aperture (Figure 13). The evolution of wh during loading resembles that in the elastic rock (cf. Figure 3). However, whereas the same curve would be traced by an elastic rock during unloading as during loading, plastic deformation leads to a hysteretic loop in Figure 13. The unloading branch is reversible. In addition, the unloading branch is linear, apart from a slight nonlinearity at the rightmost end (at the very beginning of unloading). The latter is caused by an elastic rebound of the fracture faces. After that, the two fracture faces become completely separated, and the increase in the aperture follows the displacement applied at the top side of the top block. Irreversible, plastic deformation of asperities experienced during compression in the first cycle results in the hydraulic aperture being virtually equal to the average (i.e. mechanical) aperture during subsequent unloading and reloading. This is evident in Figure 14 (red curve).

The hysteresis evident in Figures 13 and 14 results in different relationships between wh and w at the initial loading and during subsequent unloading-reloading. During the initial fracture closing, the relationship between wh and w is similar to that of an elastic rock. During unloading, the fracture surfaces are quite smooth because of the plastic deformation induced in the preceding loading. In subsequent loading cycles, the asperities do not cause so much flow tortuosity as they did in the original fracture, prior to the first loading cycle. Thus, repeated normal loading/unloading of a ductile rock reduces the permeability anisotropy of a fracture.
In addition to affecting the value of the hydraulic aperture, the repeated loading also affects the anisotropy of the fracture permeability. It is evident from Figure 14 that the fracture was slightly anisotropic during the initial loading, just as its elastic counterpart was. During unloading and subsequent reloading, the fracture opened for flow, and its permeability was virtually identical in the x- and y-directions since the asperities were smoothed out by plastic deformation, and their impact on the flow tortuosity was thereby significantly reduced.

To conclude the ductile case, aperture histograms are presented Figure 15 for successive loading and unloading steps in the first cycle. Note that the initial distribution, prior to the first cycle, is identical to the brittle case and is shown in Figure 11a. After the fracture faces come into contact, the distribution rapidly changes shape acquiring a fat tail in Figure 15b, just as it did in the brittle rock. During unloading, an elastic rebound occurs, and the distribution becomes quite close to normal in Figure 15c. The distribution of the aperture in the fracture that experienced plastic deformation is much narrower than it was in the original fracture (notice the scale of the horizontal axis in Figures 15b and 15c). Subsequent parting of the faces of the already opened fracture shifts the distribution towards higher apertures without altering its shape (Figure 15d).

2.4 Discussion

Hysteresis in the fracture permeability vs normal stress exhibited by the ductile rock suggests that caution should be exercised when transferring the results of laboratory measurements of the fracture permeability under stress onto in-situ (reservoir) conditions. The

rock could have been subject to a complex loading history in situ. Performing a single loading in the laboratory with an uncomplicated stress path is therefore likely to produce the fracture permeability figures that are not very relevant for an in-situ fracture.
Simulations suggest that there is no direct proportionality between the mechanical and the hydraulic aperture, even if the rock were perfectly elastic. Moreover, there might be a nonzero mechanical aperture below which there is no flow, i.e. below which the hydraulic aperture is zero. This is evident in Figure 8.

The results presented in Figure 8 are inconsistent with the empirical law of (Barton et al. 1985) which suggests that the ratio w_h/w should linearly increase with w:

$$\frac{w_h}{w} = \frac{w}{\mathrm{JRC}^{2.5}} \quad (2)$$

where JRC is the joint roughness coefficient of the fracture surfaces. Earlier, (Chen et al. 2000) pointed out that Barton's formula was inconsistent with their experimental results. In the case of our Figure 8, the inconsistency with Eq. (2) is mainly in the existence of a threshold value of w below which there is no flow in our simulation. This might be the effect of finite fracture dimensions. However, even in a very large fracture, some isolated spots might remain opened after the flow is blocked as the fracture closes, thereby creating some nonzero, "residual" mechanical aperture (similar to isolated pores creating porosity but not contributing to permeability in porous media). Therefore, the existence of a threshold value of w seems plausible albeit contradicting Eq. (2). This is also consistent with the discussion of flow in fractures of correlated vs uncorrelated landscapes in (Pyrak-Nolte and Morris 2000). In a fracture having a correlated aperture distribution (or, more precisely, when the correlation radius is the same order of magnitude as the in-plane fracture dimensions), the fluid flow is dominated by few preferential flow paths similar to those appearing in Figure 6b. When these channels are closed during fracture deformation, the flow rate will drop to zero. On the other hand, in the case of uncorrelated landscapes (or, more precisely, in the case of a fracture with large in-plane dimensions compared to the correlation radius), asperities are distributed evenly across the fracture, and therefore multiple flow paths are available even at large normal displacements.

Different behaviour of the fracture permeability in the first vs subsequent loading cycles in the ductile rock suggests that different fracture permeability closure laws might be applicable for mature fractures and fresh (newly created) fractures. The hysteresis in the mechanical behaviour of a fracture and in the fracture permeability under cyclic normal loading is known from experiments. An example is provided in (Gangi 1978) where it was attributed to the breakage of asperities in the first cycle. In our model of the "ductile rock", the asperities irreversibly deform rather than break. It should be noted that irreversible (hysteretic) behaviour of fracture permeability was observed also in experiments on brittle rocks, e.g. (Scholz and Hickman 1983).

Experiments suggest that, in some cases, plasticity at contacts may contribute significantly to fracture-permeability reduction at elevated normal stresses. This is corroborated, for instance, by digital strain imaging of a fracture formed at the interface between cement and rock (Walsh et al. 2012). In the latter experiment, plastic deformation was observed in the amorphous silica regions and regions depleted of Portlandite cement adjacent to the fracture faces. These chemical alterations were induced by exposure to CO_2. As a result, the reduction in the fracture permeability under stress was significantly greater than what could be attributed to the elastic deformation of contacts alone.

In real rock formations, the flattening effect observed in the simulation on the ductile rock and caused by plastic deformation of asperities, could be further enhanced by shear displacement under stress that may further smooth the fracture faces out by shearing the asperities off. The gouge (pieces of broken rock) produced during such slip may further complicate the picture by blocking the flow in the fracture and thereby reducing the fracture permeability (Lorenz 1999; Smart et al. 2001).

The changes of the aperture distribution as the fracture closes (see the histogram evolution from Figure 11a to Figure 11c) is quite similar to the changes observed in experiments by Muralidharan et al., who used CT scans to quantify the development of fracture aperture under normal stress (Muralidharan et al. 2004). In particular, the emergence of the "fat tail" in the distribution evident in our Figure 11c (and Figure 15b) was observed in Muralidharan et al.'s experiments.

The effect of irreversible, plastic normal deformation on the fracture aperture is to compress the statistical distribution of the aperture, so that the apertures fall into a narrower range than they do in a virgin fracture (Figure 15). The statistical distribution of apertures in a fracture that underwent plastic deformation is different than it was before such deformation. The loading of a fractured rock leaves therefore an "imprint", or "memory", about the loading that then stays in the fracture. The roughness of the fracture faces thus carries information about the stress history. This is in a way similar to other stress-memory effects in rocks, such as the Kaiser effect in acoustic emission, a phenomenon well-known in rock mechanics (Becker et al. 2010; Lavrov 2003).

Fracture permeability is often anisotropic. For instance, anisotropy can be created by shear displacement (slip) of the fracture faces (Detwiler and Morris 2014). Our simulations show that normal loading is likely to increase the anisotropy of the fracture permeability. This confirms the earlier results of Detwiler and Morris obtained with a much simpler fracture deformation model (Detwiler and Morris 2014).

It should be noted that properties of the rock were identical in the entire rock block in this study. In reality, fracture surfaces can be weathered or damaged, making the strength and stiffness of asperities different from the properties of the bulk material. Incorporating such alterations into the finite-element model of fracture deformation should be trivial, but would require information about the distribution of, e.g., cohesion and internal friction angle in the rock, in the direction normal to the fracture face. Such information could be obtained, e.g., by a hardness test or a scratch test that enable estimation of rock properties at different depths from the free surface.

In order to use the proposed computational approach, a validation against experiments is needed. Calibration and validation of the model against experiments for specific rocks is an outstanding task. In order to perform such a calibration properly, a larger fracture model would need to be used.

2.5 Conclusions

A computational framework for evaluating the fracture permeability under normal stress has been developed and tested on two examples: a perfectly elastic ("brittle") rock and an elastic perfectly plastic ("ductile") rock. The two types of rock exhibit significantly different behaviour of fracture permeability under repeated loading. Both mechanical and hydraulic behaviour of the fracture under cyclic normal loading are found to be in qualitative agreement with the results obtained in a number of published experimental studies. The computational approach provides an insight into the actual mechanics of the fracture deformation under stress, and the effect of the latter on the permeability. In particular, a hysteresis in the fracture roughness is obtained with the "ductile rock" suggesting that (at least some) fractured rocks may have "memory" about their loading history imprinted in the fracture landscapes. The anisotropy of fracture permeability is reduced as the fracture opens and is increased as the normal stress increases. During repeated loading/unloading of a fracture in a ductile rock, asperities are smoothed out. Therefore, repeated loading/unloading cycles reduce the flow tortuosity and the anisotropy of the fracture permeability. The effect of repeated loading of a ductile rock is also to compress the statistical distribution of the local fracture apertures.

References

Aguilera R (1980) Naturally fractured reservoirs. The Petroleum Publishing Company, Tulsa

Aybar U, Eshkalak MO, Sepehrnoori K, Patzek TW (2014) The effect of natural fracture's closure on long-term gas production from unconventional resources Journal of Natural Gas Science and Engineering 21:1205-1213 doi:http://dx.doi.org/10.1016/j.jngse.2014.09.030

Barton N, Bandis S, Bakhtar K (1985) Strength, deformation and conductivity coupling of rock joints International Journal of Rock Mechanics and Mining Sciences & Geomechanics Abstracts 22:121-140 doi:http://dx.doi.org/10.1016/0148-9062(85)93227-9

Bauget F, Fourar M (2008) Non-Fickian dispersion in a single fracture Journal of Contaminant Hydrology 100:137-148 doi:http://dx.doi.org/10.1016/j.jconhyd.2008.06.005

Becker D, Cailleau B, Dahm T, Shapiro S, Kaiser D (2010) Stress triggering and stress memory observed from acoustic emission records in a salt mine Geophysical Journal International 182:933-948 doi:10.1111/j.1365-246X.2010.04642.x

Brown SR (1987) Fluid flow through rock joints: the effect of surface roughness J Geophys Res B 92:1337-1347

Brown SR, Scholz CH (1986) Closure of rock joints Journal of Geophysical Research: Solid Earth 91:4939-4948 doi:10.1029/JB091iB05p04939

Chen Z, Narayan SP, Yang Z, Rahman SS (2000) An experimental investigation of hydraulic behaviour of fractures and joints in granitic rock International Journal of Rock Mechanics and Mining Sciences 37:1061-1071 doi:http://dx.doi.org/10.1016/S1365-1609(00)00039-3

Cumbie DH, McKay LD (1999) Influence of diameter on particle transport in a fractured shale saprolite Journal of Contaminant Hydrology 37:139-157 doi:http://dx.doi.org/10.1016/S0169-7722(98)00156-9

Cuss RJ, Milodowski A, Harrington JF (2011) Fracture transmissivity as a function of normal and shear stress: First results in Opalinus Clay Physics and Chemistry of the Earth, Parts A/B/C 36:1960-1971 doi:http://dx.doi.org/10.1016/j.pce.2011.07.080

Detwiler RL, Morris JP (2014) Transmissivity anisotropy in rough-walled fractures: The combined influence of shear offset and normal deformaion. Paper ARMA 14-7539 presented at the 48th US Rock Mechanics / Geomechanics Symposium held in Minneapolis, MN, USA, 1-4 June 2014.

Fournier A, Fussell D, Carpenter L (1982) Computer rendering of stochastic models Commun ACM 25:371-384 doi:10.1145/358523.358553

Gangi AF (1978) Variation of whole and fractured porous rock permeability with confining pressure International Journal of Rock Mechanics and Mining Sciences & Geomechanics Abstracts 15:249-257 doi:http://dx.doi.org/10.1016/0148-9062(78)90957-9

Gutierrez M, Øino LE, Nygård R (2000) Stress-dependent permeability of a de-mineralised fracture in shale Marine and Petroleum Geology 17:895-907 doi:http://dx.doi.org/10.1016/S0264-8172(00)00027-1

Keller AA, Roberts PV, Blunt MJ (1999) Effect of fracture aperture variations on the dispersion of contaminants Water Resources Research 35:55-63 doi:10.1029/1998wr900041

Koyama T, Li B, Jiang Y, Jing L (2008) Numerical simulations for the effects of normal loading on particle transport in rock fractures during shear International Journal of Rock Mechanics and Mining Sciences 45:1403-1419 doi:http://dx.doi.org/10.1016/j.ijrmms.2008.01.018

Lavrov A (2003) The Kaiser effect in rocks: principles and stress estimation techniques International Journal of Rock Mechanics and Mining Sciences 40:151-171 doi:http://dx.doi.org/10.1016/S1365-1609(02)00138-7

Lavrov A (2005) Fracture-induced Physical Phenomena and Memory Effects in Rocks: A Review Strain 41:135-149 doi:10.1111/j.1475-1305.2005.00233.x

Lavrov A (2014) Radial Flow of Non-Newtonian Power-Law Fluid in a Rough-Walled Fracture: Effect of Fluid Rheology Transp Porous Med 105:559-570 doi:10.1007/s11242-014-0384-6

Lespinasse M, Sausse J (2000) Quantification of fluid flow: hydro-mechanical behaviour of different natural rough fractures Journal of Geochemical Exploration 69–70:483-486 doi:http://dx.doi.org/10.1016/S0375-6742(00)00111-4

Lorenz JC (1999) Stress-sensitive reservoirs Journal of Petroleum Technology 51:61-63

Malama B, Kulatilake PHSW (2003) Models for normal fracture deformation under compressive loading International Journal of Rock Mechanics and Mining Sciences 40:893-901 doi:http://dx.doi.org/10.1016/S1365-1609(03)00071-6

Młynarczuk M (2010) Description and classification of rock surfaces by means of laser profilometry and mathematical morphology International Journal of Rock Mechanics and Mining Sciences 47:138-149 doi:http://dx.doi.org/10.1016/j.ijrmms.2009.09.004

Muralidharan V, Chakravarthy D, Putra E, Schechter DS (2004) Investigating fracture aperture distributions under various stress conditions using X-ray CT scanner. paper 2004-230 presented at the Petroleum Society's 5th Canadian International Petroleum Conference (55th Annual Technical Meeting), Calgary, Alberta, Canada, June 8-10, 2004.

Nowamooz A, Radilla G, Fourar M, Berkowitz B (2013) Non-Fickian Transport in Transparent Replicas of Rough-Walled Rock Fractures Transp Porous Med 98:651-682 doi:10.1007/s11242-013-0165-7

Pyrak-Nolte LJ, Morris JP (2000) Single fractures under normal stress: The relation between fracture specific stiffness and fluid flow International Journal of Rock Mechanics and Mining Sciences 37:245-262 doi:http://dx.doi.org/10.1016/S1365-1609(99)00104-5

Schmittbuhl J, Steyer A, Jouniaux L, Toussaint R (2008) Fracture morphology and viscous transport International Journal of Rock Mechanics and Mining Sciences 45:422-430 doi:http://dx.doi.org/10.1016/j.ijrmms.2007.07.007

Scholz CH, Hickman SH (1983) Hysteresis in the closure of a nominally flat crack Journal of Geophysical Research: Solid Earth 88:6501-6504 doi:10.1029/JB088iB08p06501

Smart BGD, Somerville JM, Edlman K, Jones C (2001) Stress sensitivity of fractured reservoirs Journal of Petroleum Science and Engineering 29:29-37 doi:http://dx.doi.org/10.1016/S0920-4105(00)00088-7

Twiss RJ, Moores EM (2007) Structural Geology., 2nd ed. edn. W.H. Freeman,

Walsh SDC, Du Frane WL, Sholokhova Y, Settgast R, Johnson SM, Carroll SA (2012) Chemo-mechanical permeability evolution in wellbore-cement fracures exposed to carbon-dioxide-rich brines. Paper ARMA 12-426. Paper presented at the the 46th US Rock Mechanics / Geomechanics Symposium held in Chicago, IL, USA, 24-27 June 2012,

Zimmerman RW, Kumar S, Bodvarsson GS (1991) Lubrication theory analysis of the permeability of rough-walled fractures International Journal of Rock Mechanics and Mining Sciences & Geomechanics Abstracts 28:325-331 doi:http://dx.doi.org/10.1016/0148-9062(91)90597-F

APPENDIX

Table 1 Material properties in the simulation of a "brittle" rock.

Property	Value
Young's modulus, GPa	5.0
Poisson's ratio	0.3

Table 2 Material properties in the simulation with linear elastic perfectly plastic rock.

Property	Value
Young's modulus, GPa	5.0
Poisson's ratio	0.3
Cohesion, MPa	5.0
Angle of internal friction, °	30
Angle of dilatancy, °	25

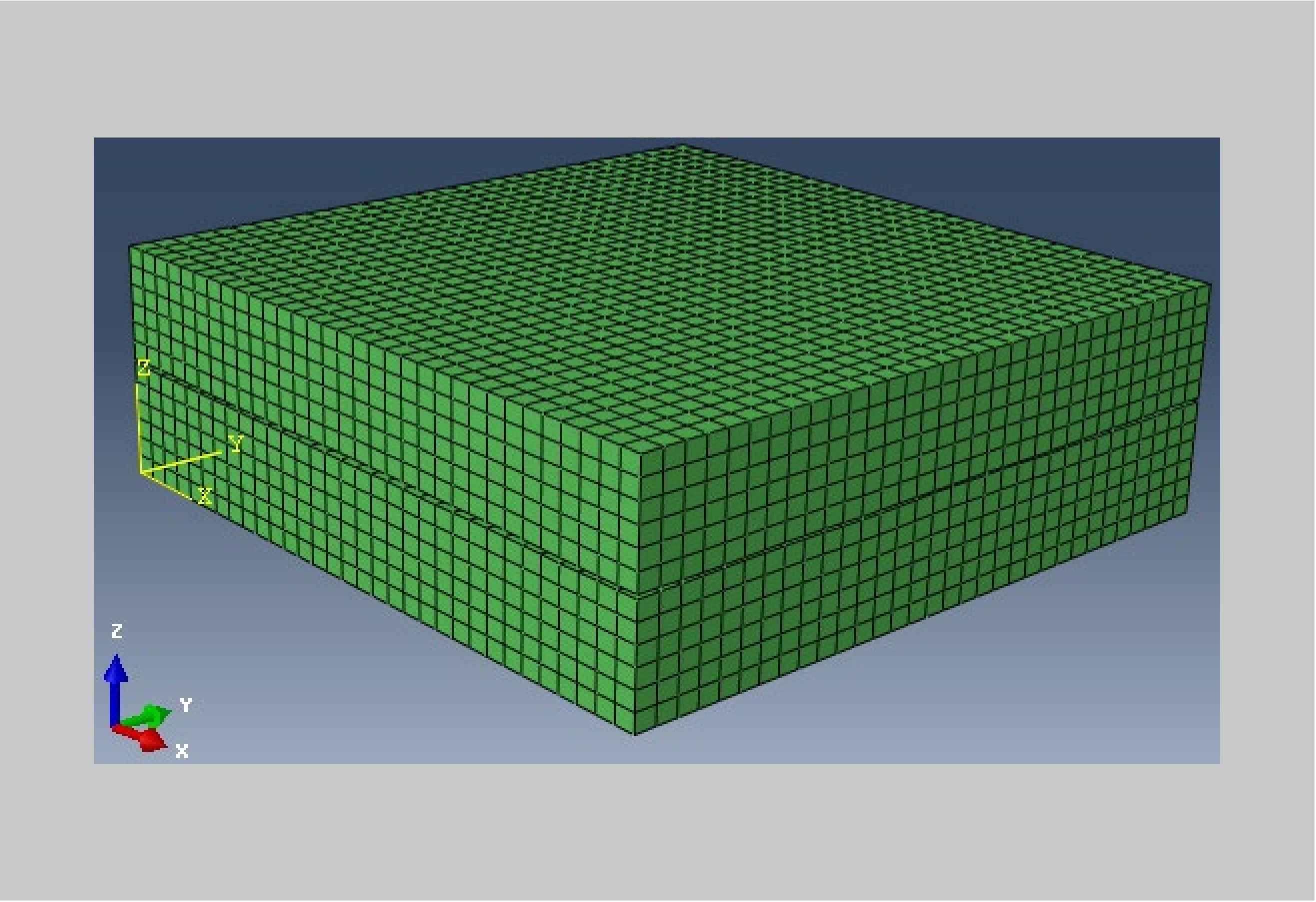

Figure 1 Two rock blocks with the fracture between them

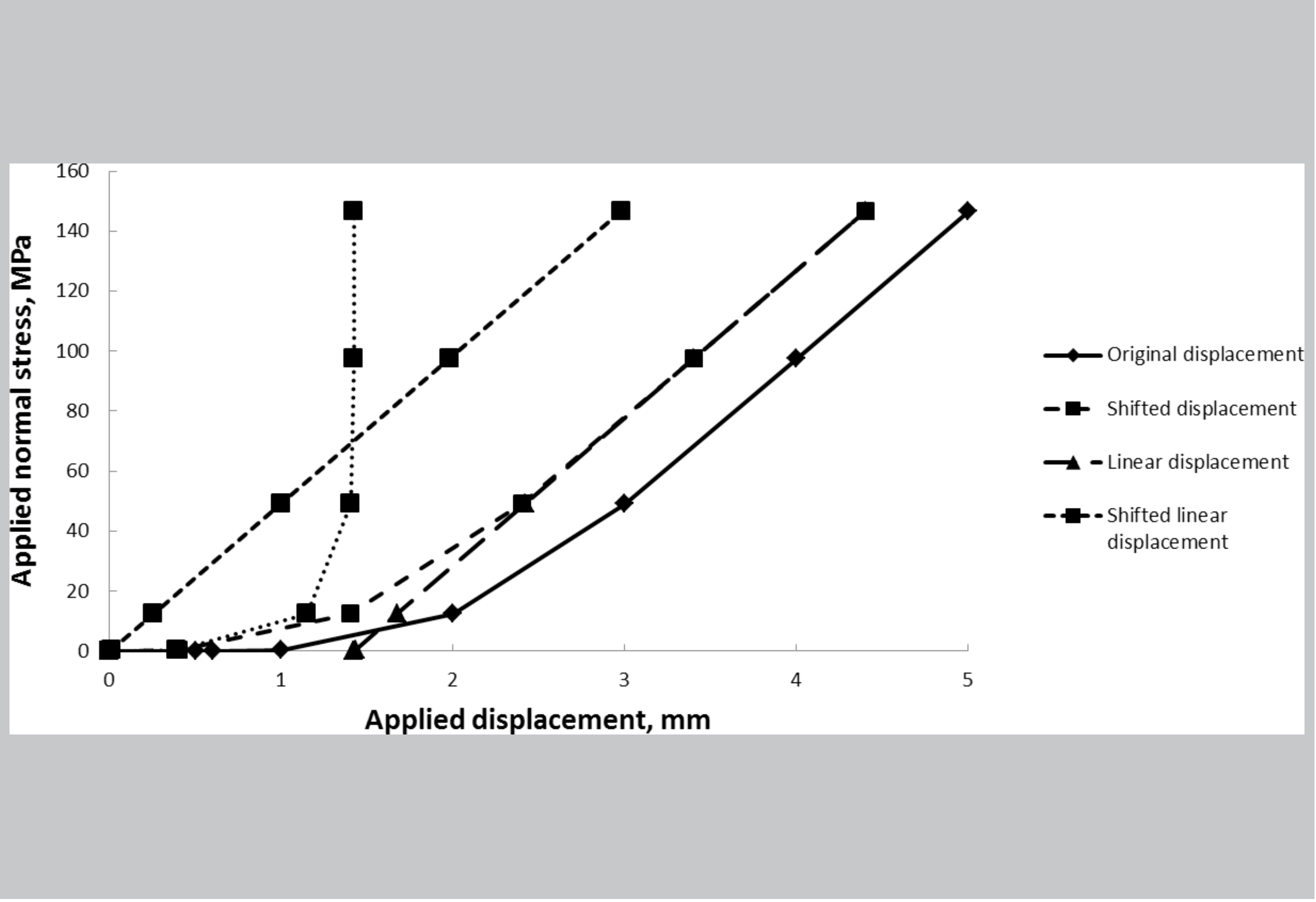

Figure 2 Stress vs displacement obtained in the simulation of a "brittle" rock

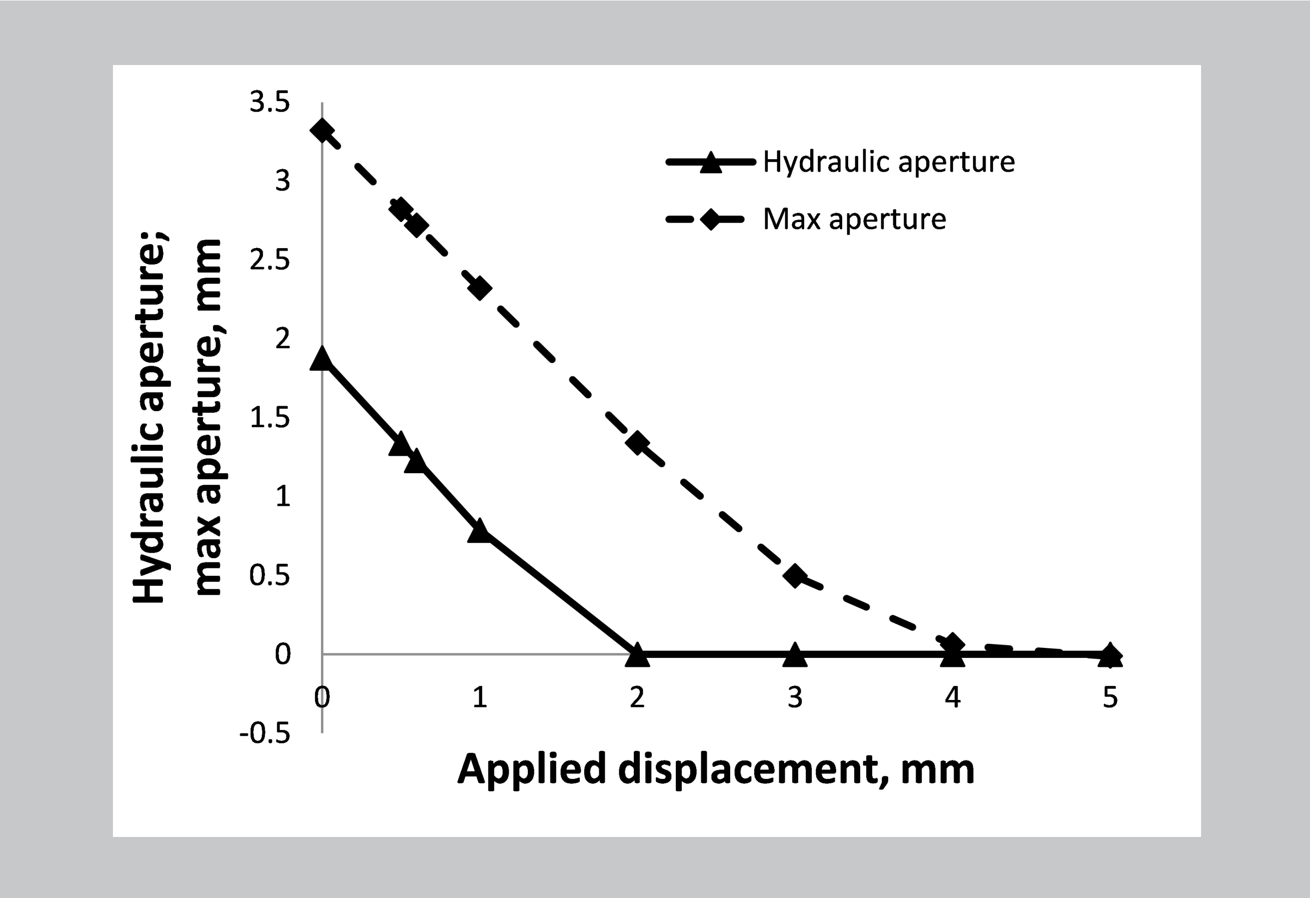

Figure 3 Hydraulic and maximum apertures vs applied displacement obtained in the simulation of a "brittle" rock. Hydraulic aperture obtained with for flow in x-direction

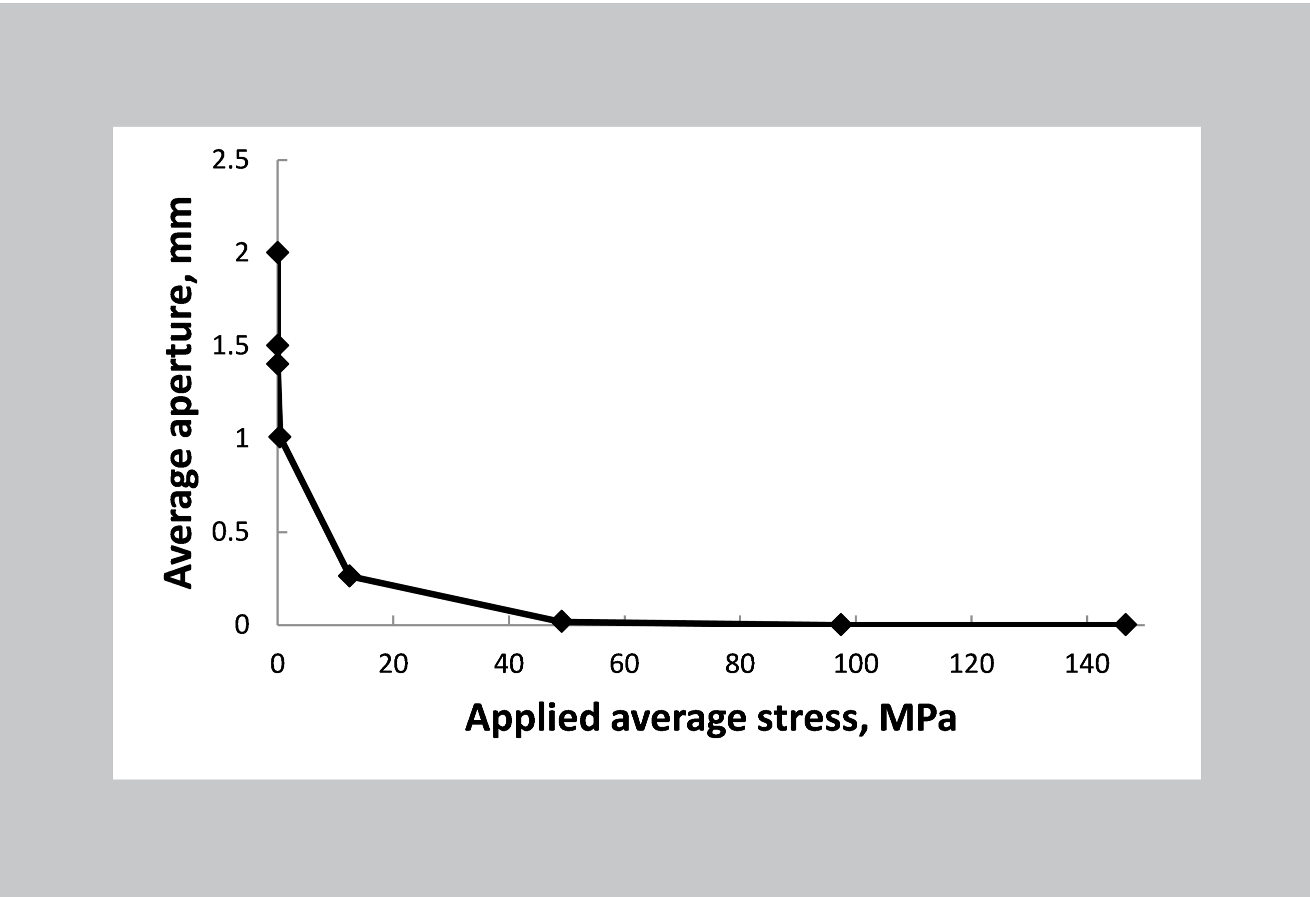

Figure 4 Average aperture vs applied normal stress obtained in the simulation of a "brittle" rock

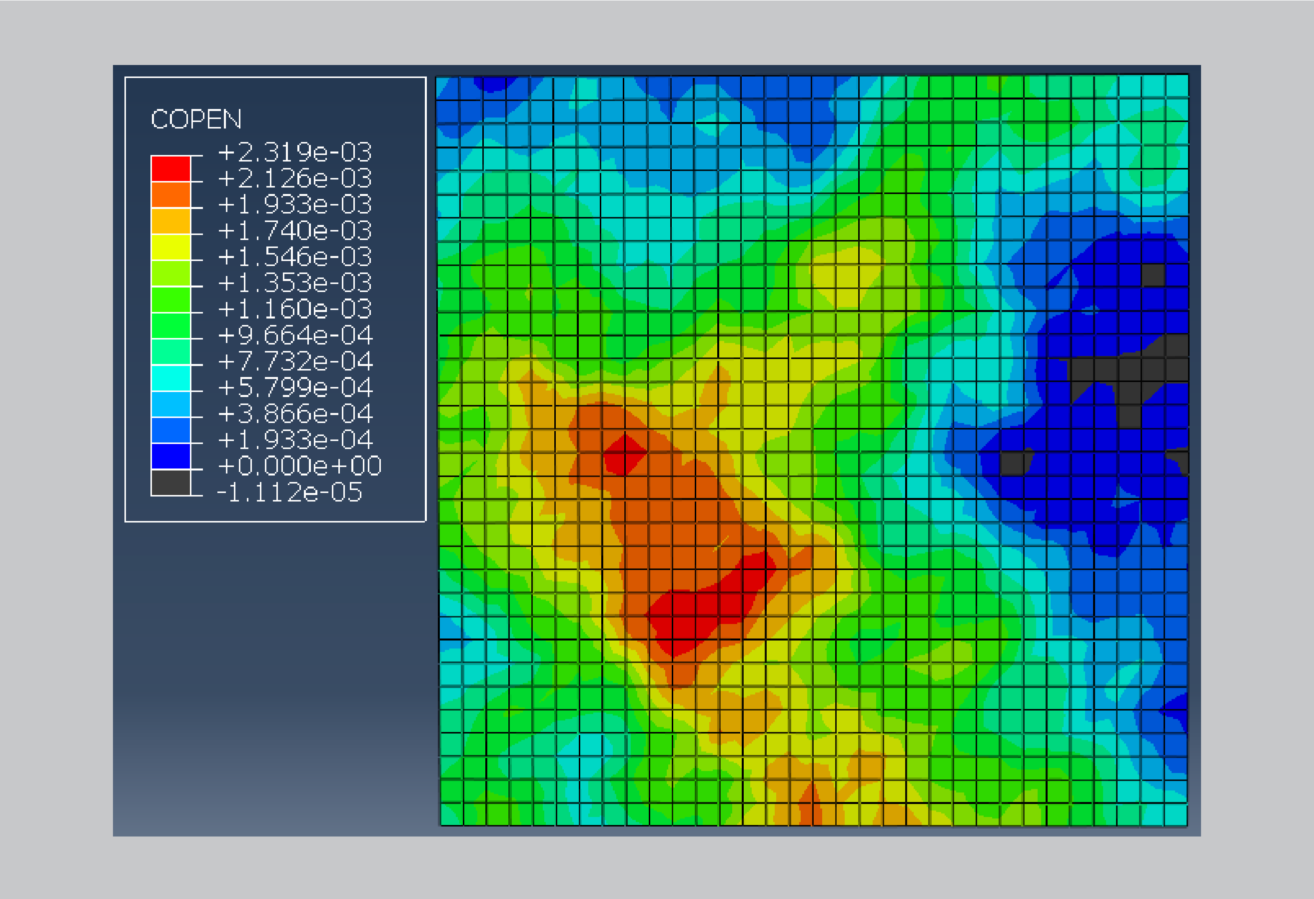

Figure 5a Fracture aperture distributions at successive applied displacements in the simulation of a "brittle" rock (unit of aperture in the legend: m). Dark grey areas: closed fracture (contact between the faces). Axis directions: x vertical, y horizontal (cf. Figure 1). (a) displacement 1.0 mm

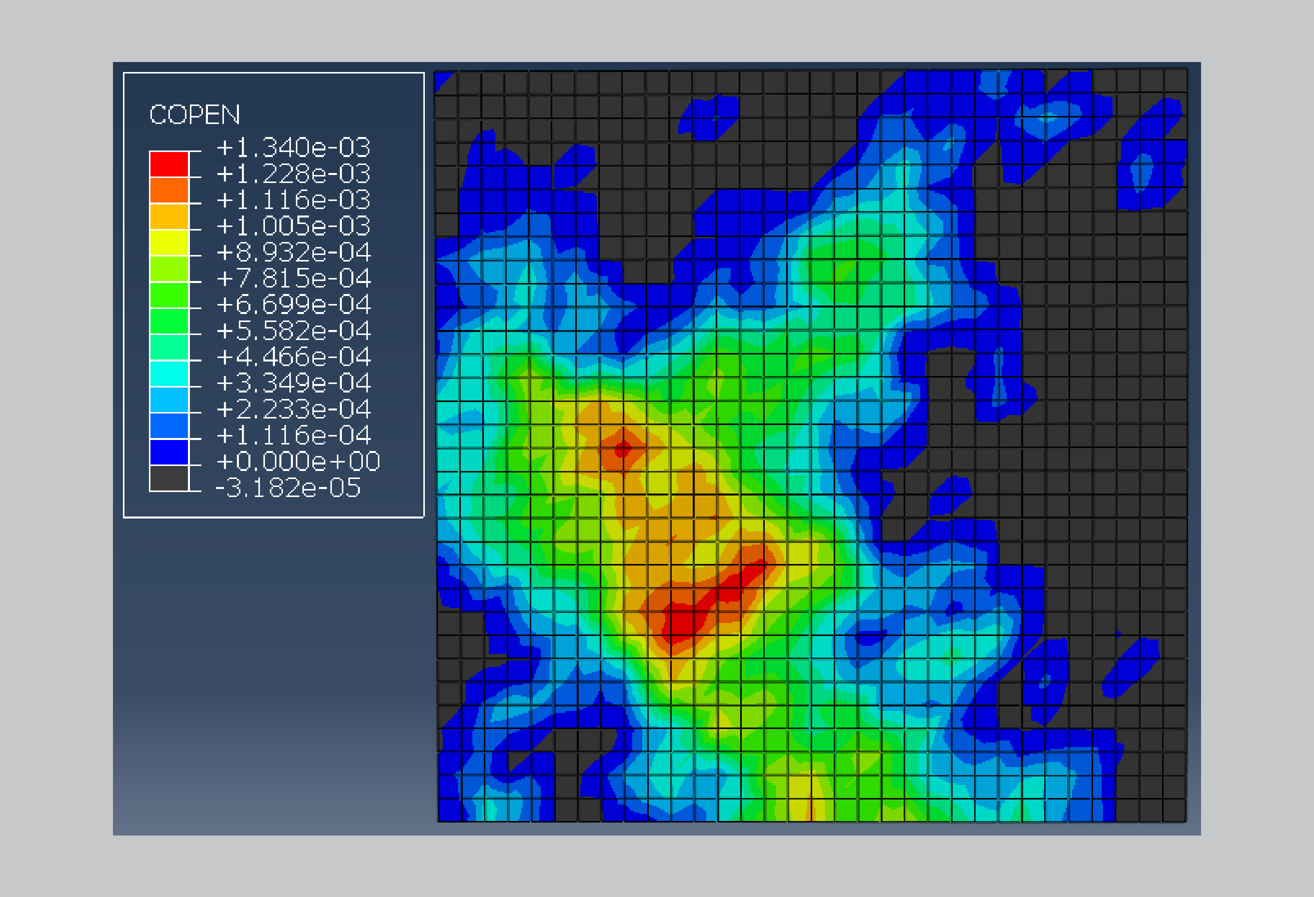

Figure 5b Fracture aperture distributions at successive applied displacements in the simulation of a "brittle" rock (unit of aperture in the legend: m). Dark grey areas: closed fracture (contact between the faces). Axis directions: x vertical, y horizontal (cf. Figure 1). (b) displacement 2.0 mm

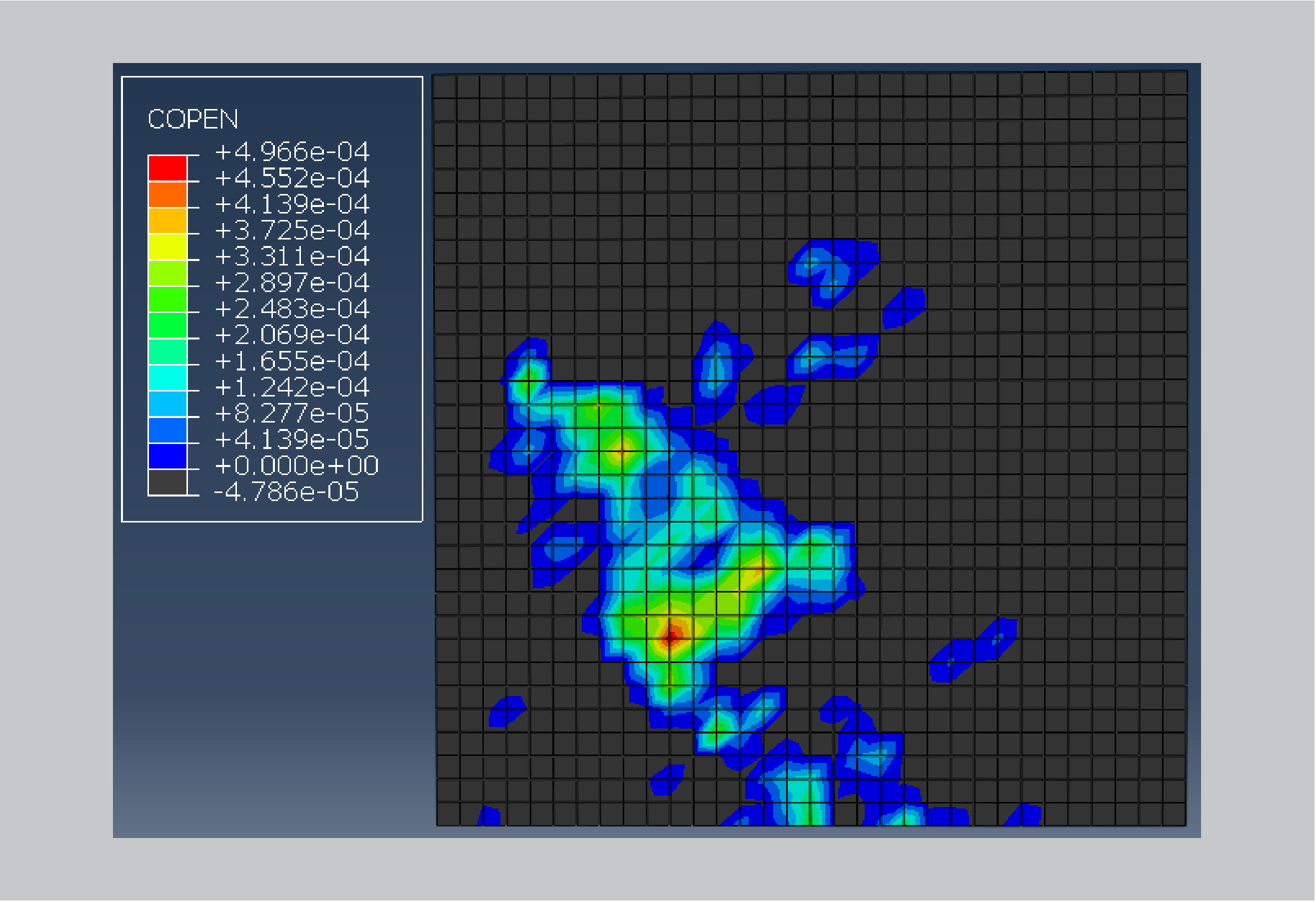

Figure 5c Fracture aperture distributions at successive applied displacements in the simulation of a "brittle" rock (unit of aperture in the legend: m). Dark grey areas: closed fracture (contact between the faces). Axis directions: x vertical, y horizontal (cf. Figure 1). (c) displacement 3.0 mm

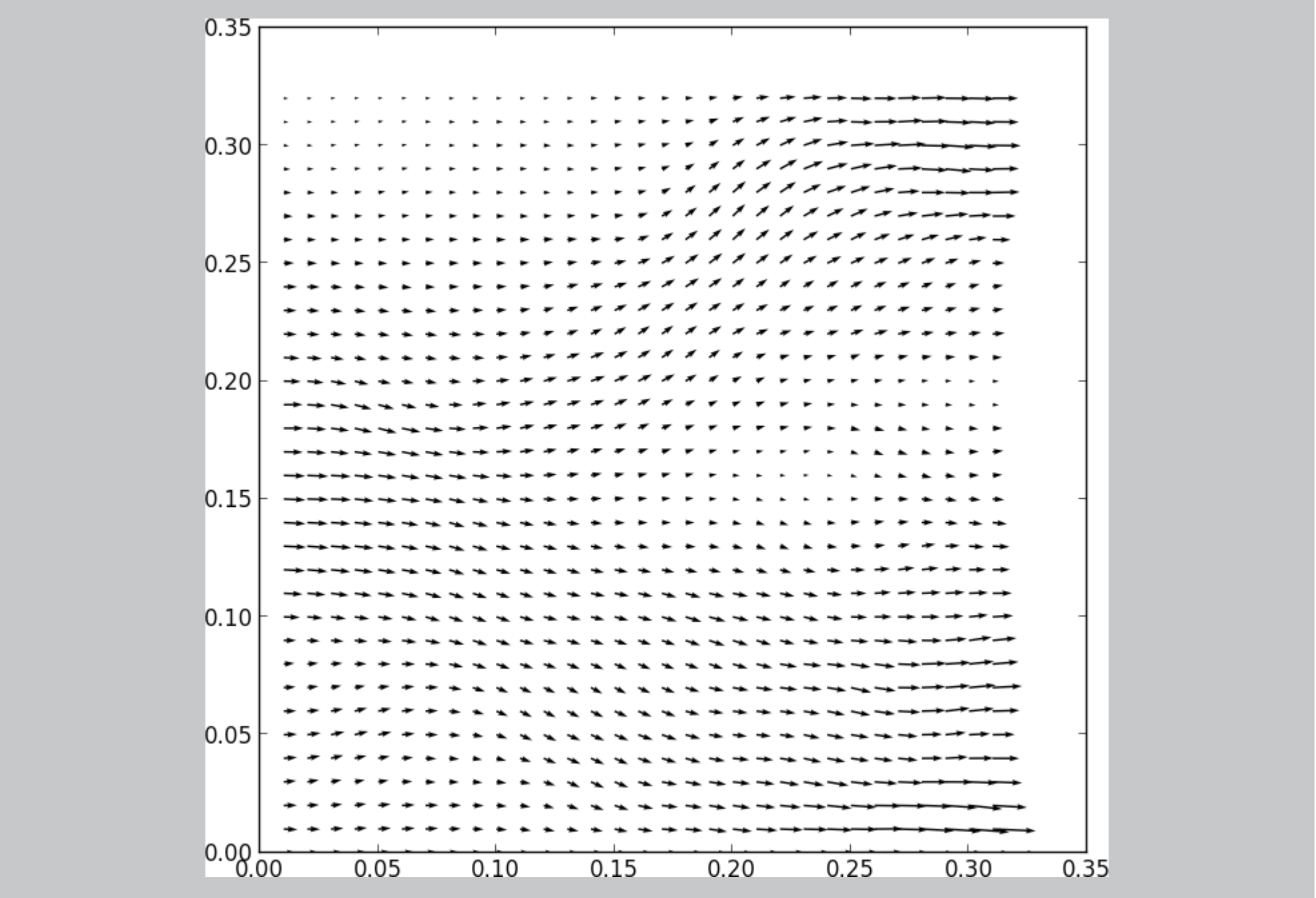

Figure 6 Fluid velocity distributions at successive applied displacements in the simulation of a "brittle" rock. Units along x- and y-axes are m. Axis directions: x vertical, y horizontal (cf. Figure 1). (a) initial state, zero displacement of top surface

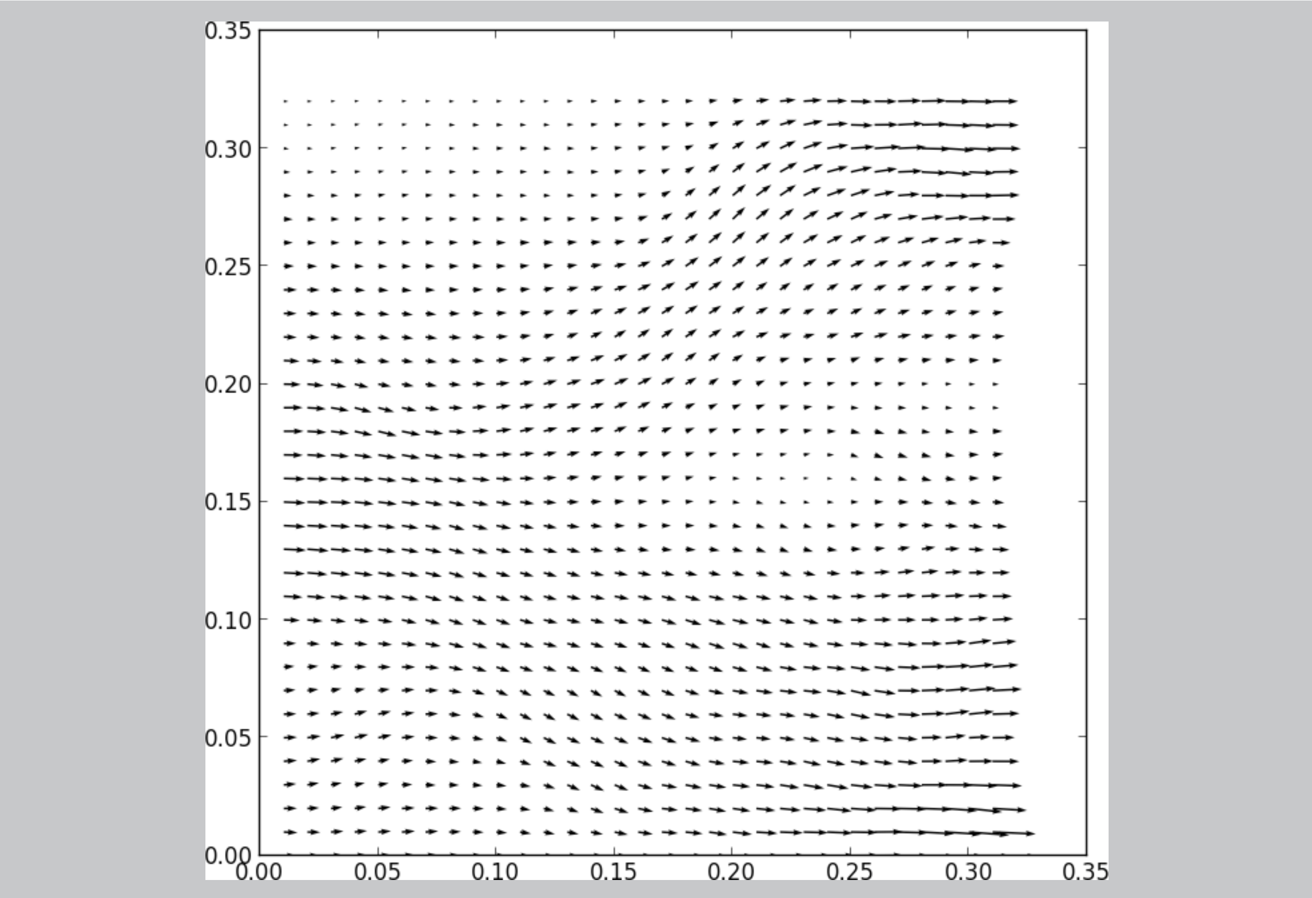

Figure 6a Fluid velocity distributions at successive applied displacements in the simulation of a "brittle" rock. Units along x- and y-axes are m. Axis directions: x vertical, y horizontal (cf. Figure 1). (a) initial state, zero displacement of top surface

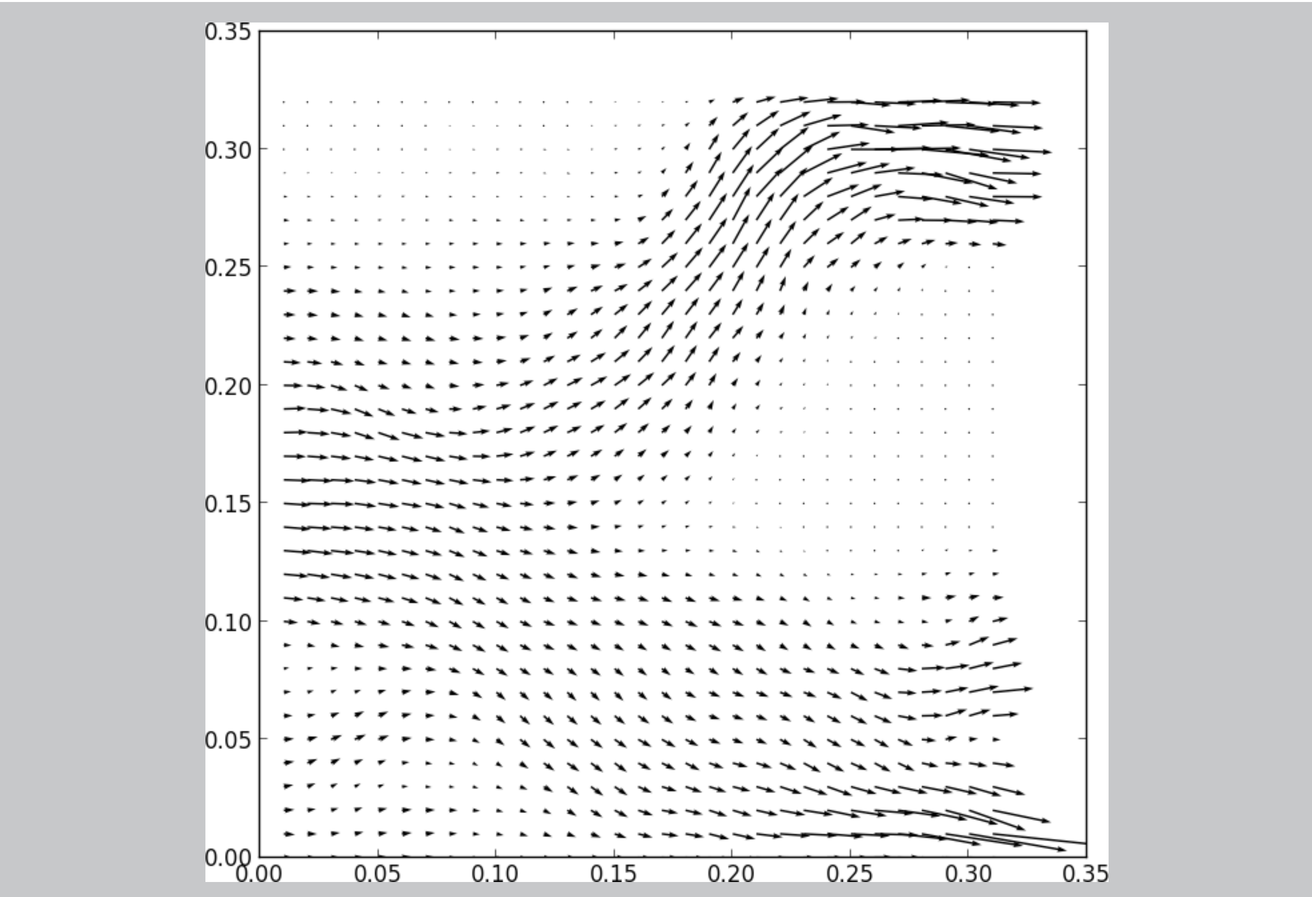

Figure 6b Fluid velocity distributions at successive applied displacements in the simulation of a "brittle" rock. Units along x- and y-axes are m. Axis directions: x vertical, y horizontal (cf. Figure 1). (b) displacement 1.0 mm

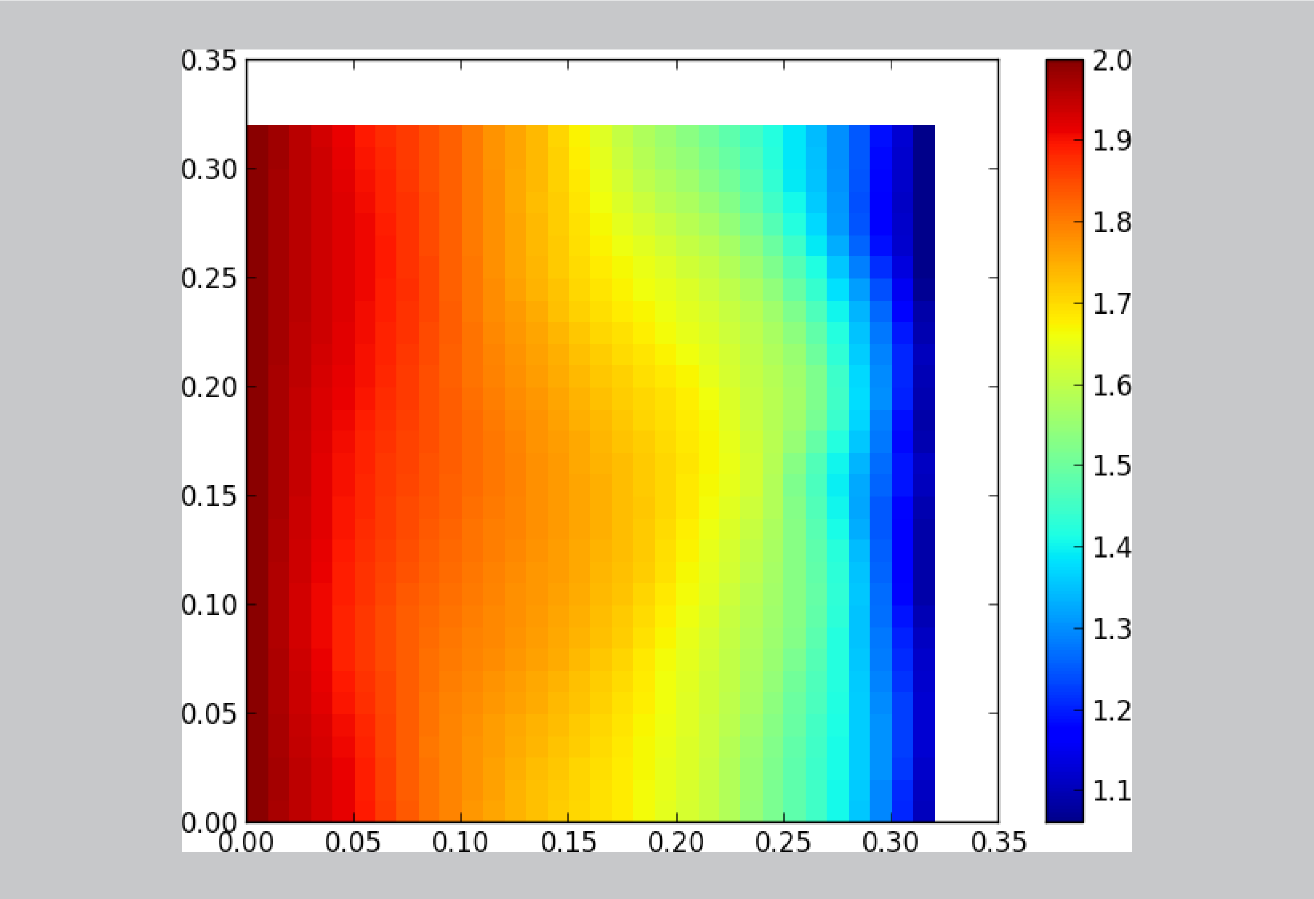

Figure 7a Fluid pressure distributions at successive applied displacements in the simulation of a "brittle" rock. Units along x- and y-axes are m. Pressure units in the legend are Pa. Pressure applied at the left-hand boundary is 2 Pa. Pressure applied at the right-hand boundary is 1 Pa. Axis directions: x vertical, y horizontal (cf. Figure 1). (a) initial state, zero displacement of top surface

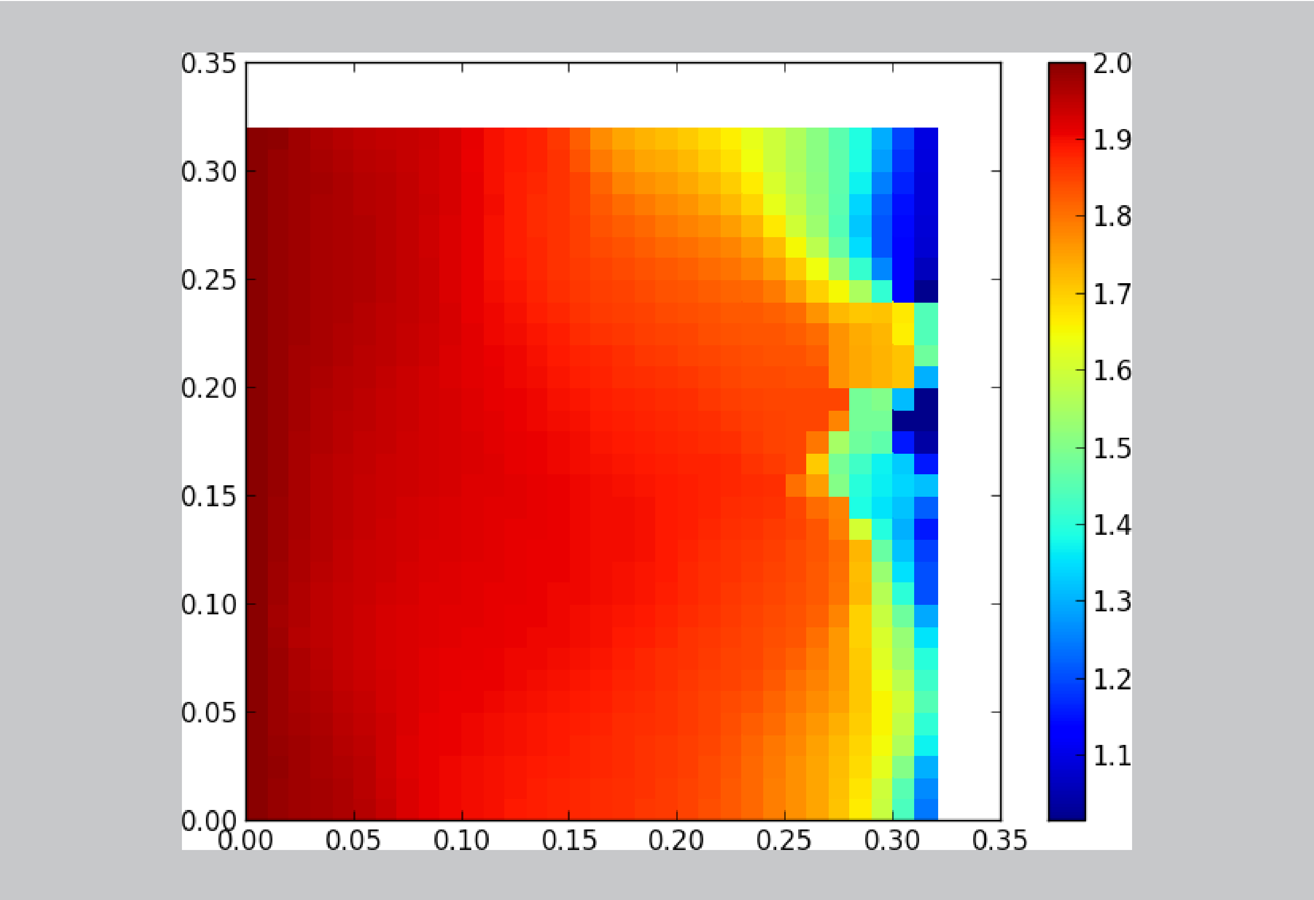

Figure 7b displacement 1.0 mm

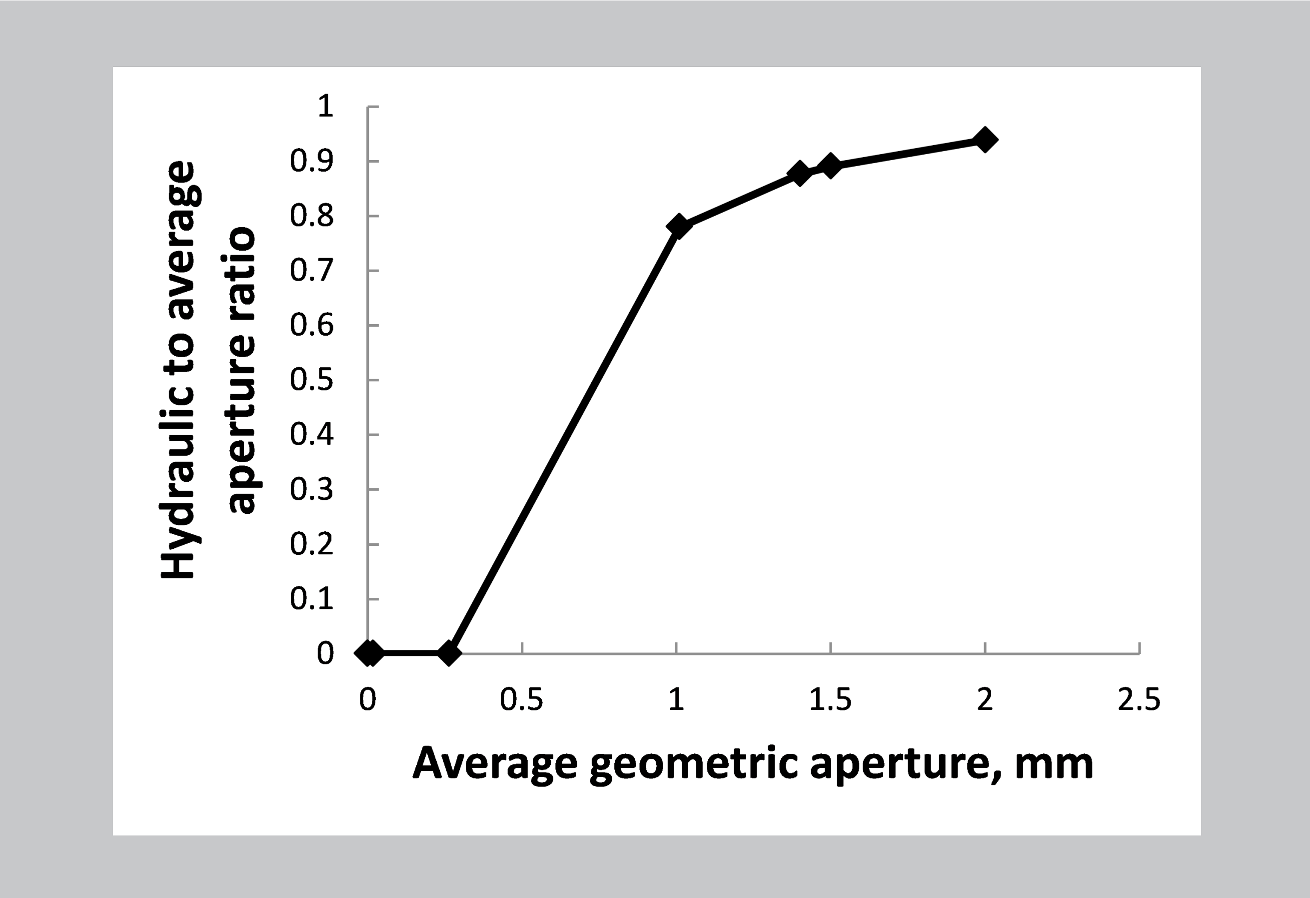

Figure 8 Hydraulic-to-average aperture ratio vs average aperture in the simulation of a "brittle" rock

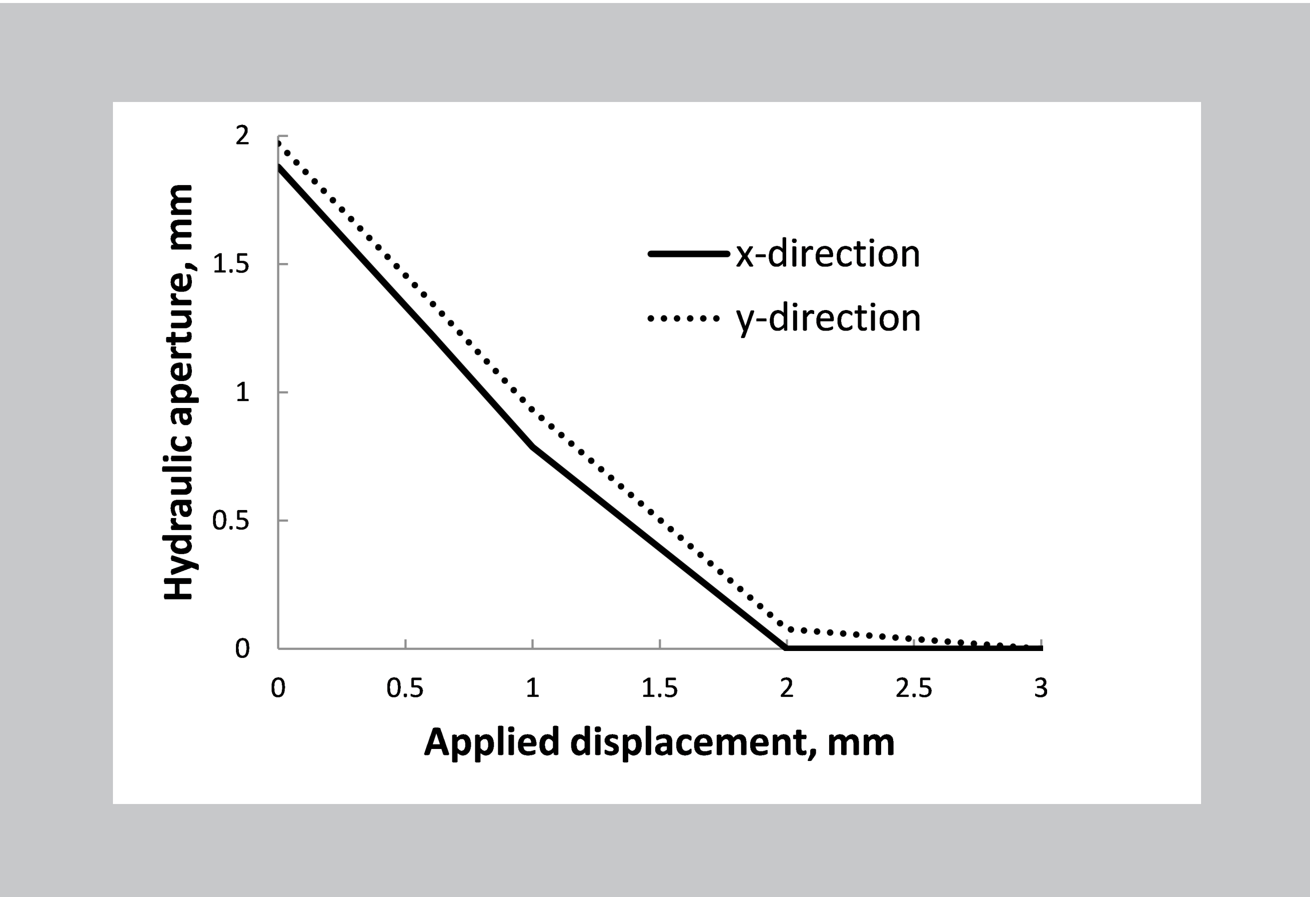

Figure 9 Hydraulic aperture obtained with flow in x- or y-direction vs applied displacement in the simulation of a "brittle" rock

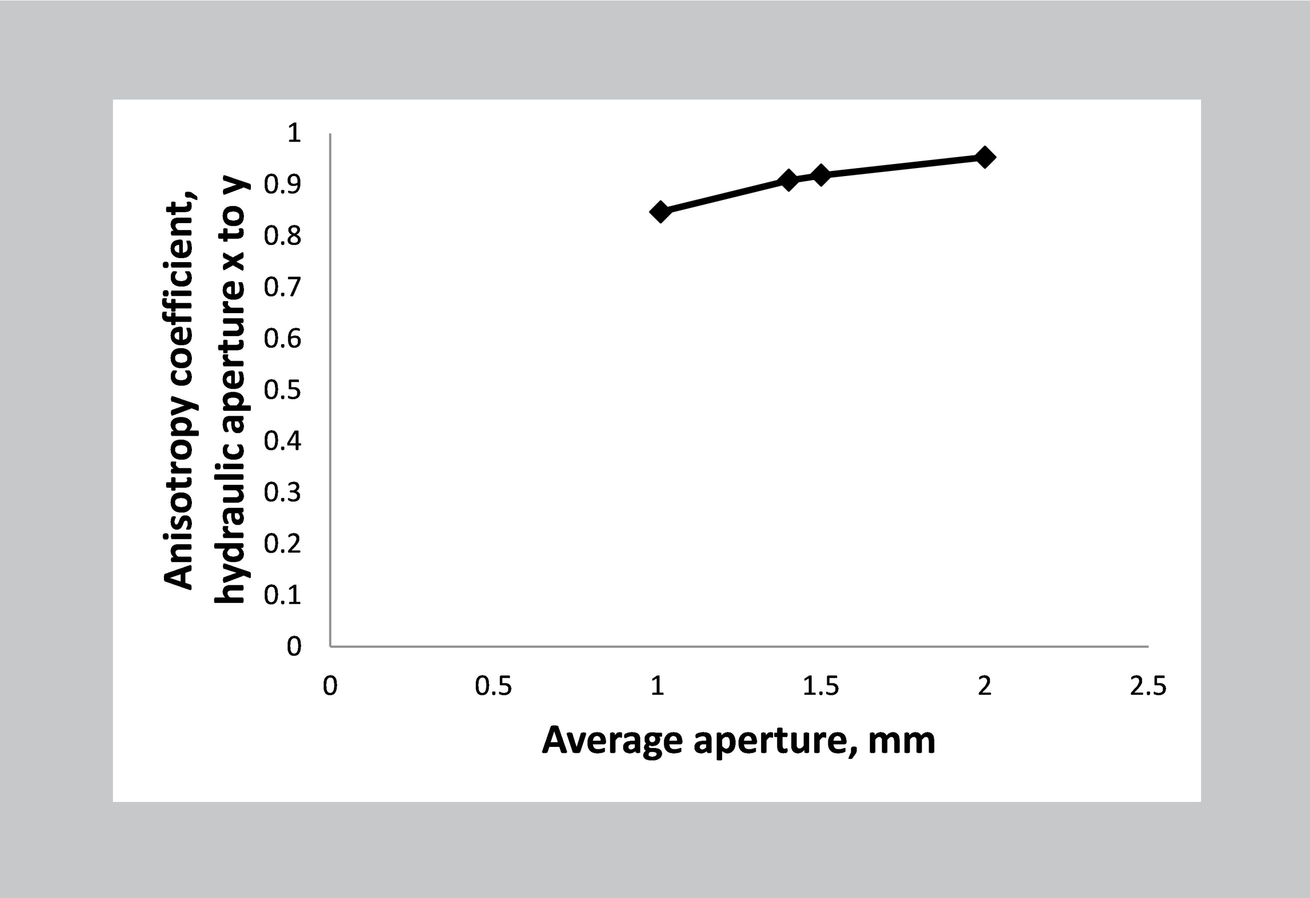

Figure 10 Anisotropy coefficient vs average aperture in the simulation of a "brittle" rock

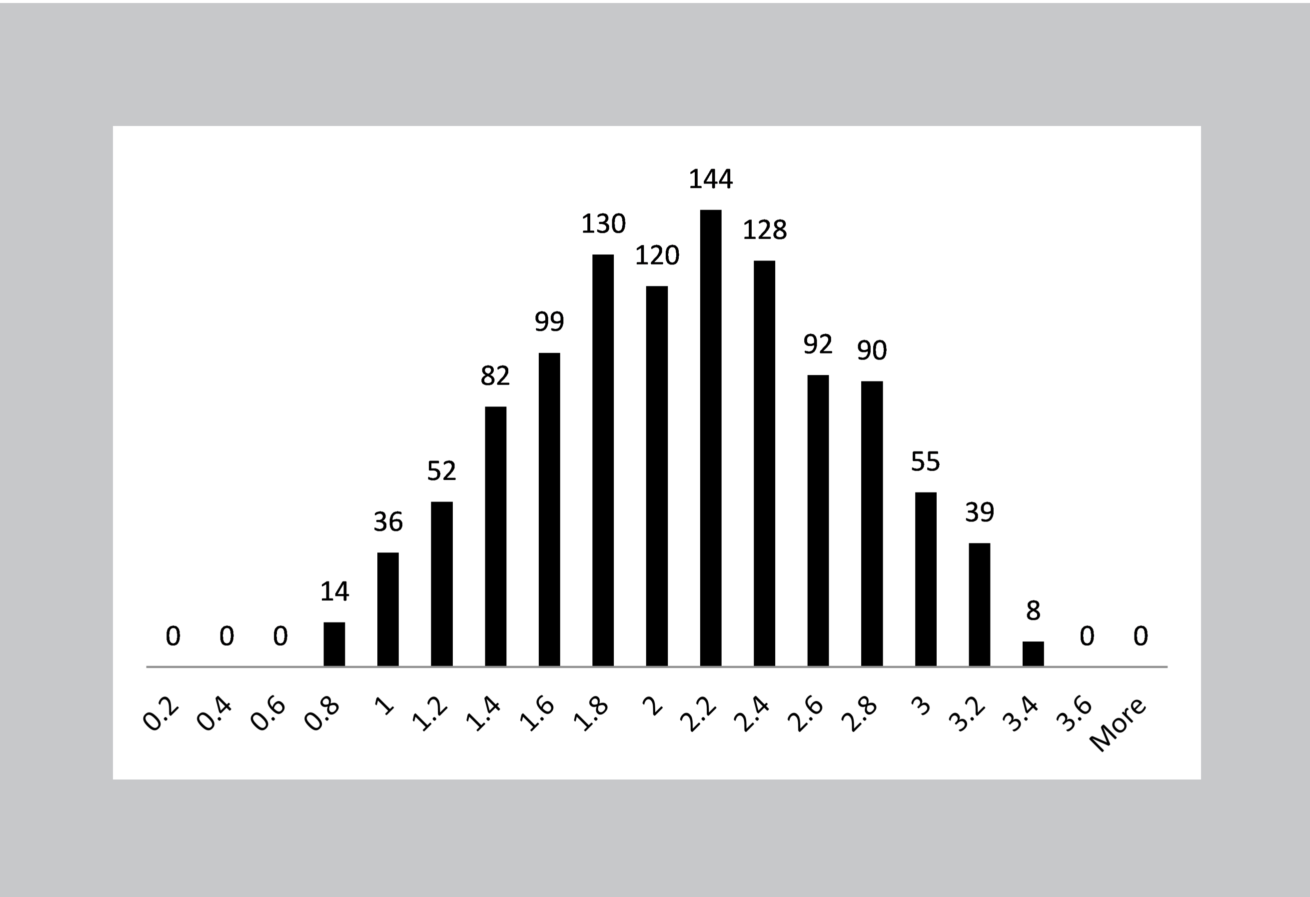

Figure 11a Histograms of mechanical aperture (mm) at successive applied displacements in the simulation of a "brittle" rock: (a) initial state, zero displacement of top surface;

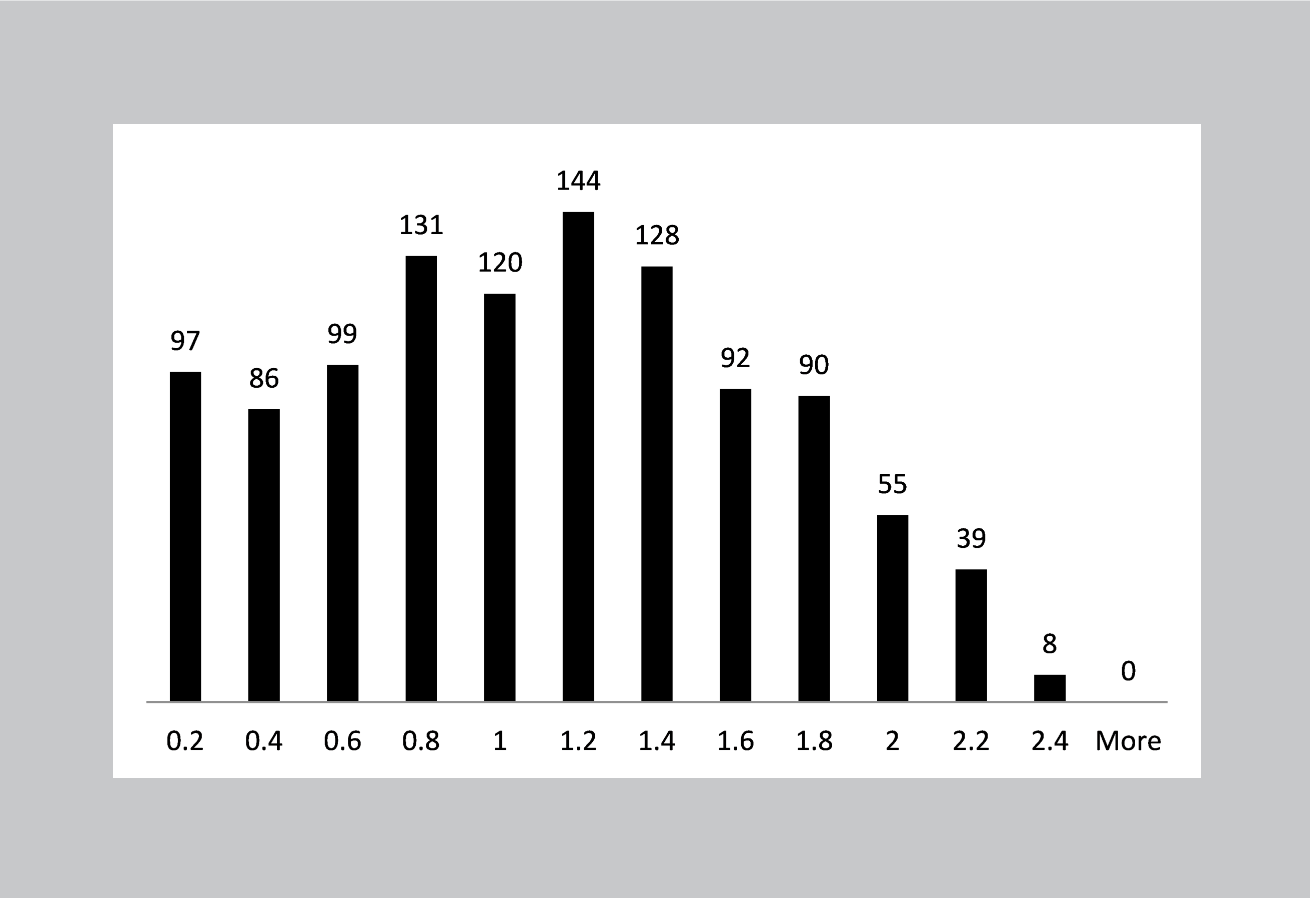

Figure 11b Histograms of mechanical aperture (mm) at successive applied displacements in the simulation of a "brittle" rock: (b) displacement 1.0 mm;

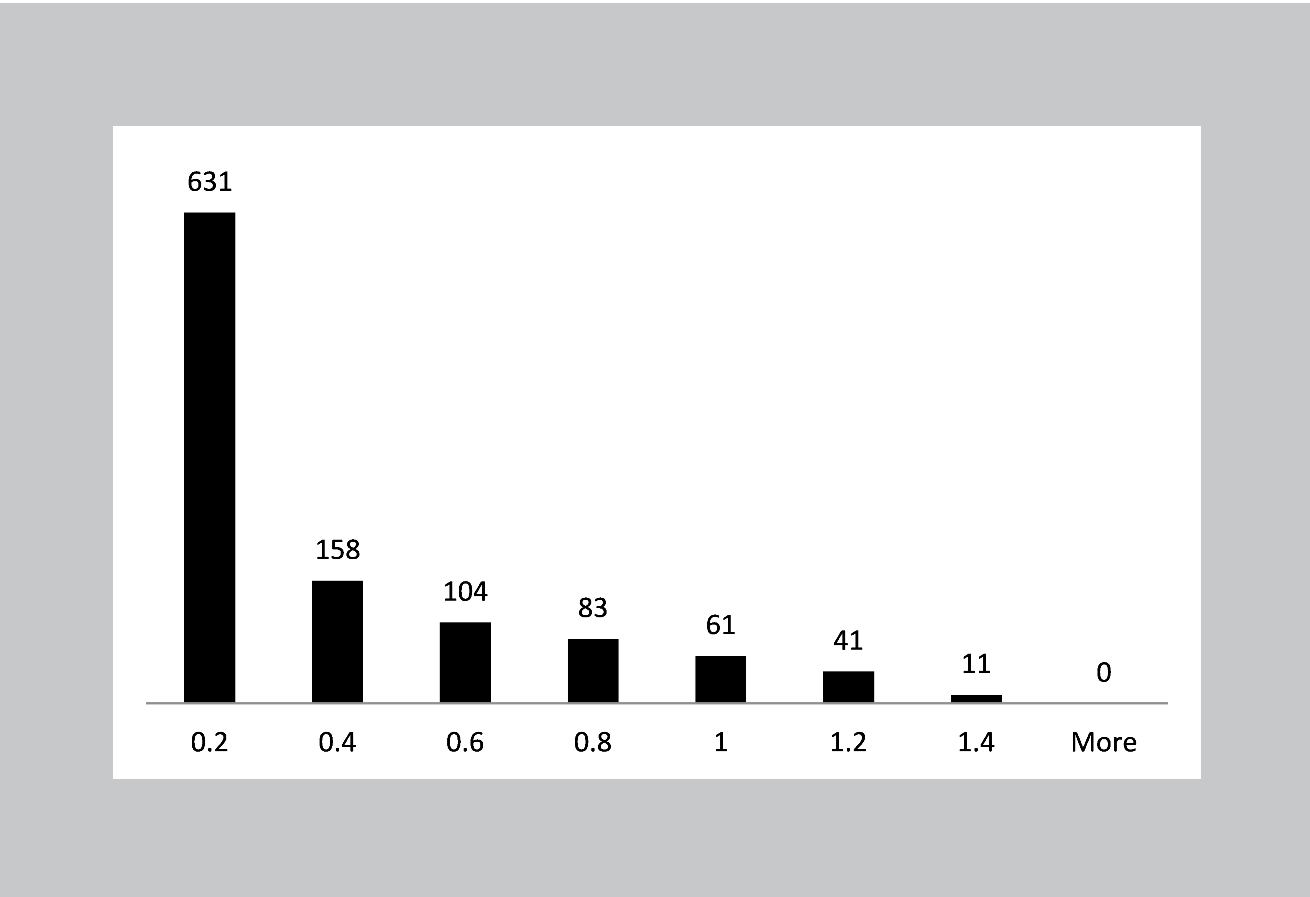

Figure 11c Histograms of mechanical aperture (mm) at successive applied displacements in the simulation of a "brittle" rock: (c) displacement 2.0 mm

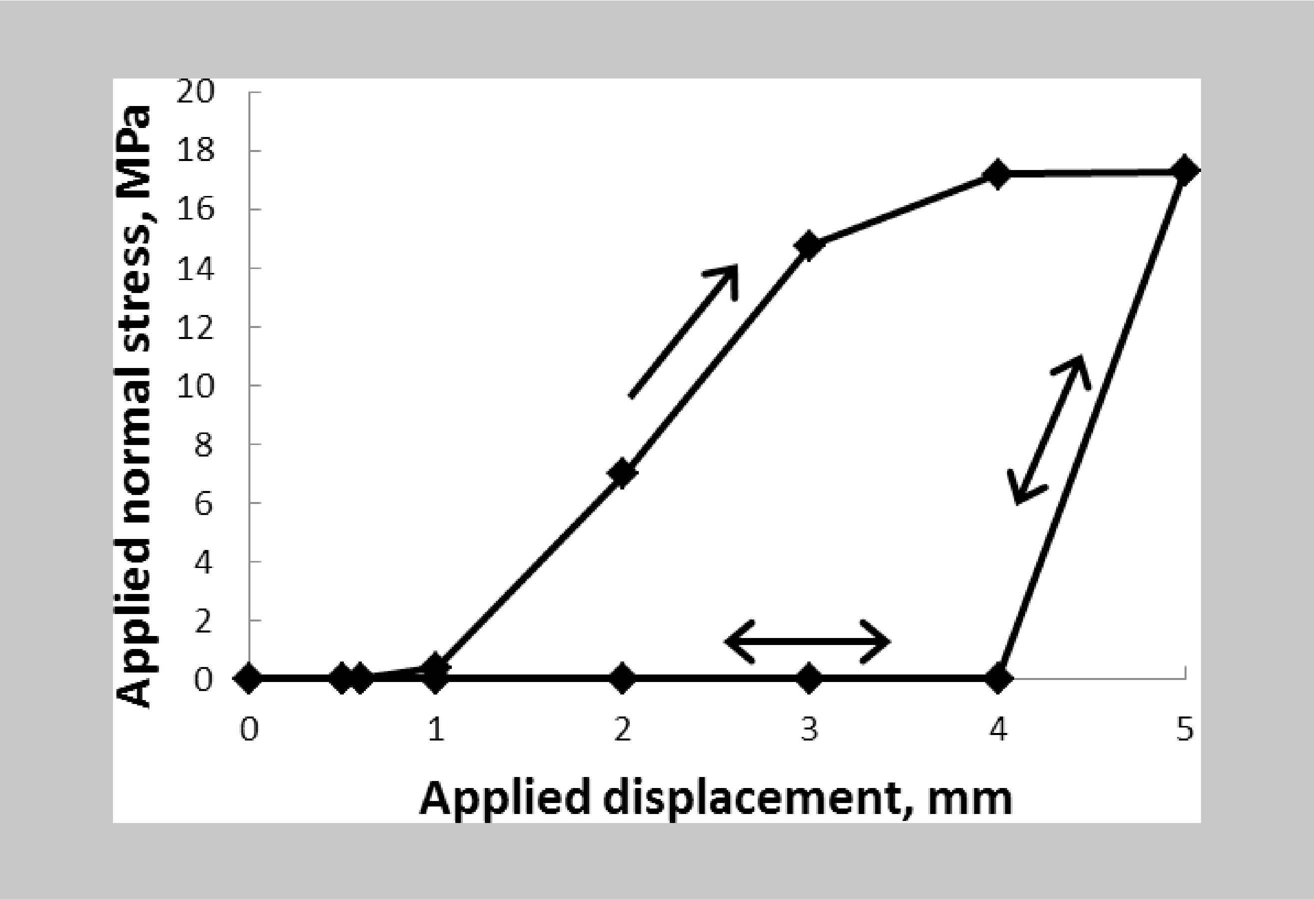

Figure 12 Stress vs applied displacement in the simulation of a "ductile" rock

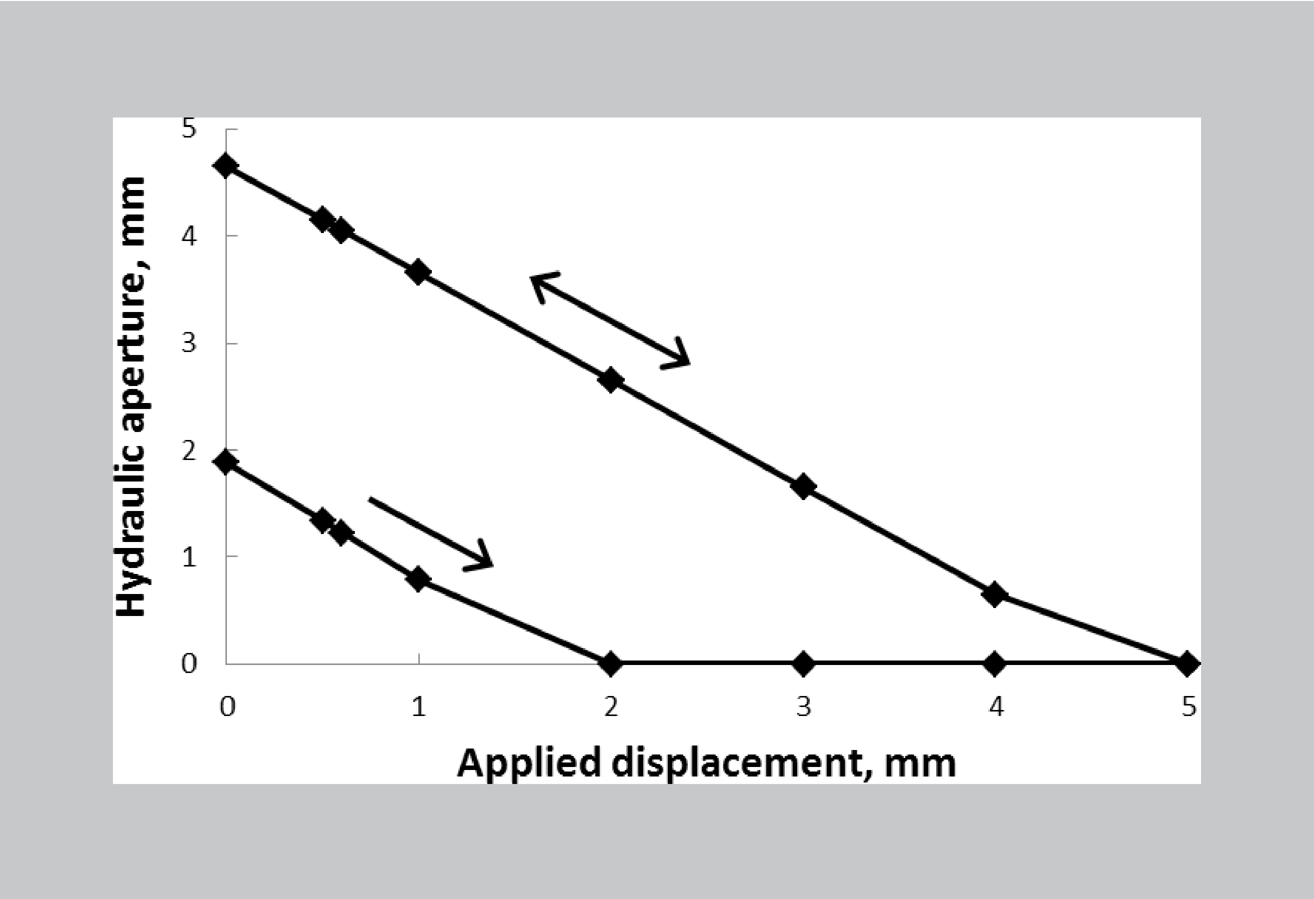

Figure 13 Hydraulic aperture vs applied displacement in the simulation of a "ductile" rock

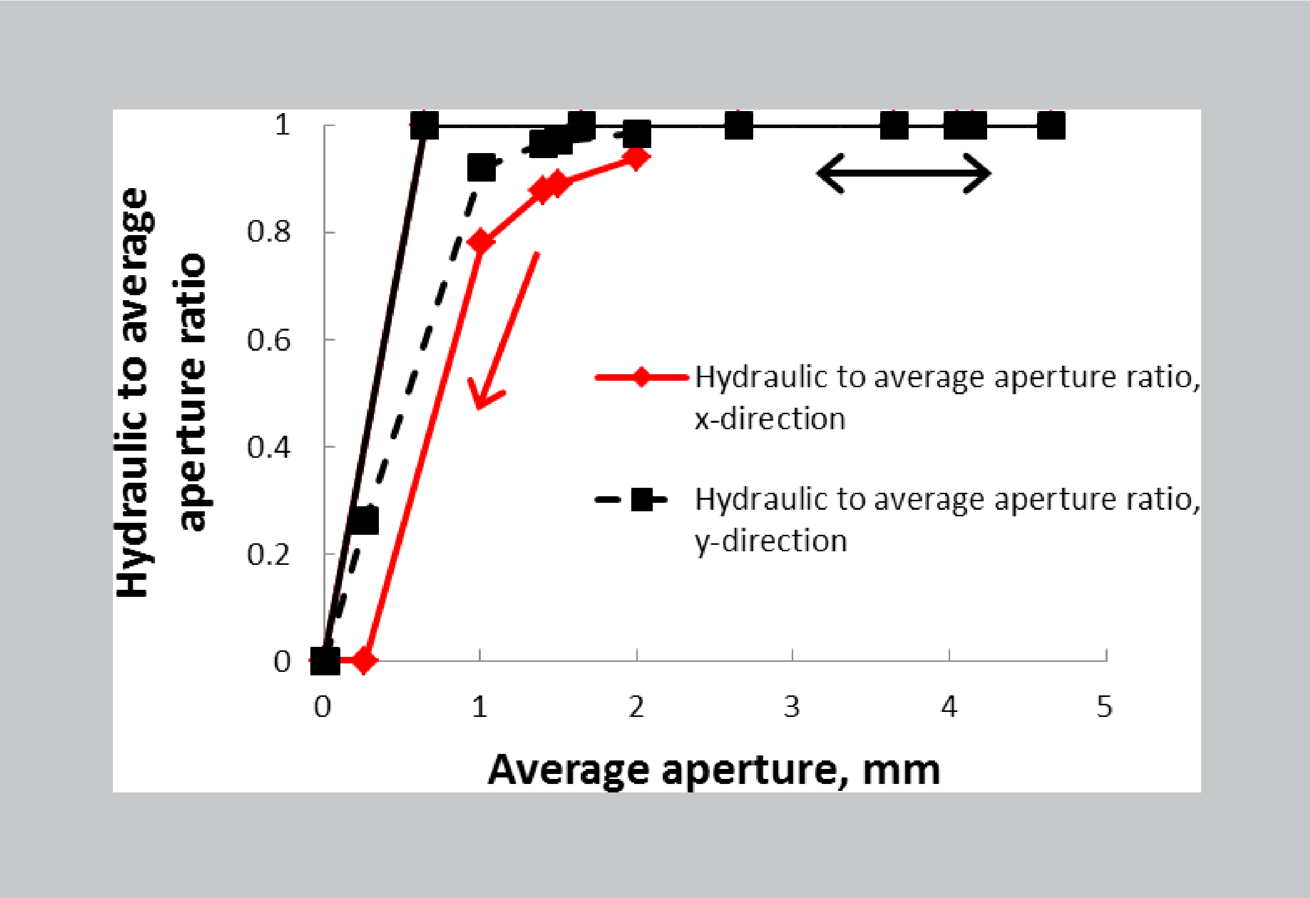

Figure 14 Hydraulic-to-average-aperture ratio (flow in x- or y-direction) vs average (i.e. mechanical) aperture in the simulation of a "ductile" rock

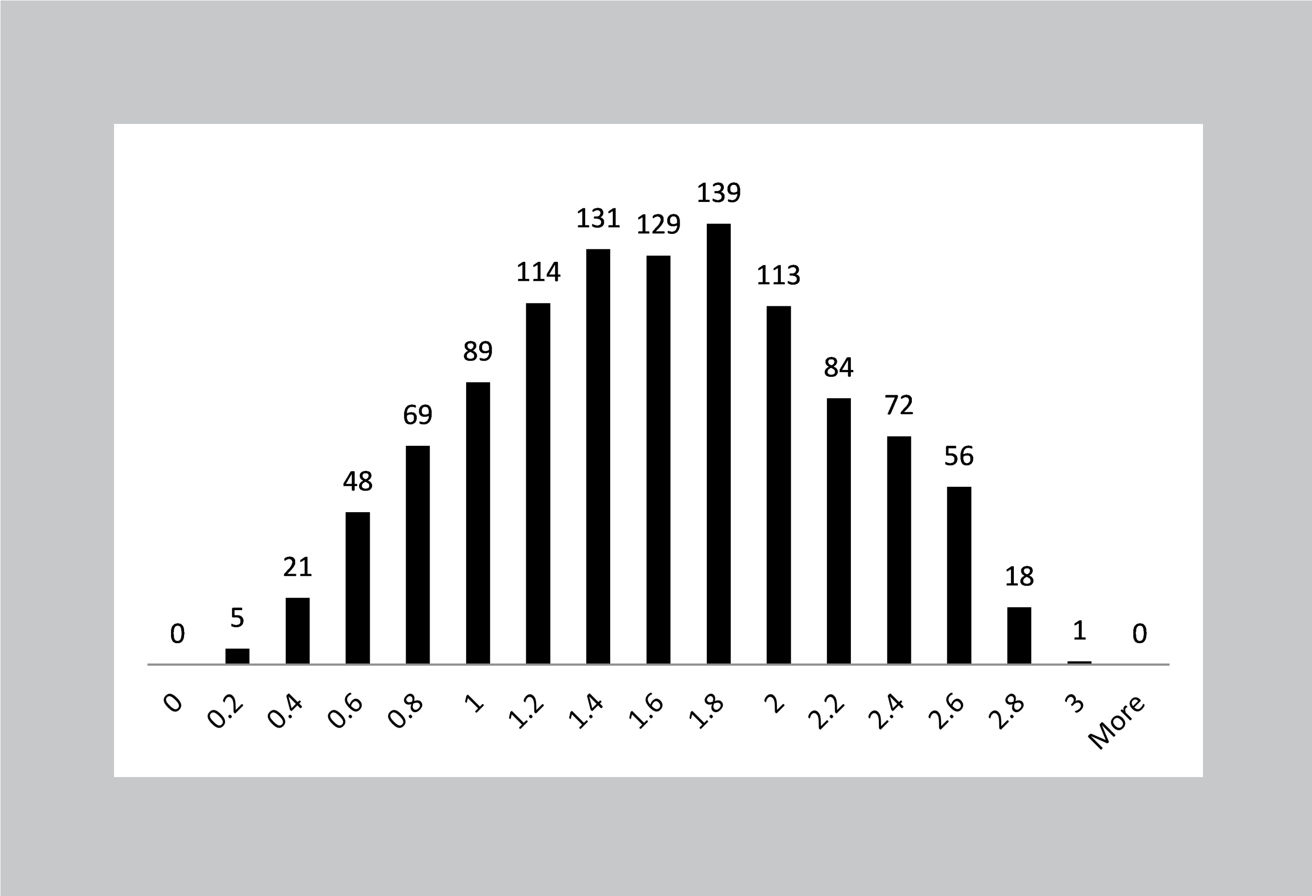

Figure 15a Histograms of mechanical aperture (mm) at successive applied displacements in the simulation of a "ductile" rock. (a) displacement 1.0 mm, loading (first cycle);

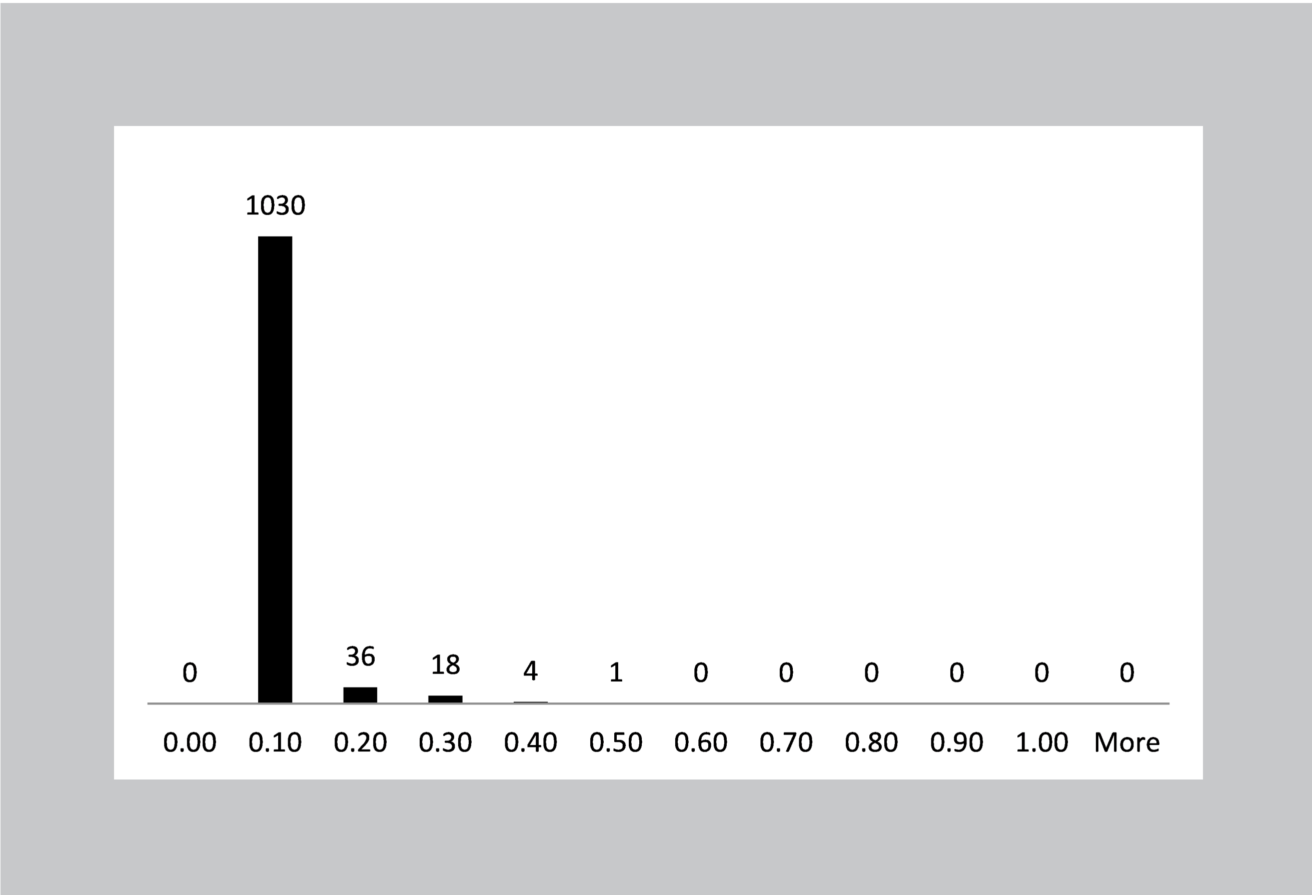

Figure 15b Histograms of mechanical aperture (mm) at successive applied displacements in the simulation of a "ductile" rock. (b) displacement 3.0 mm, loading (first cycle);

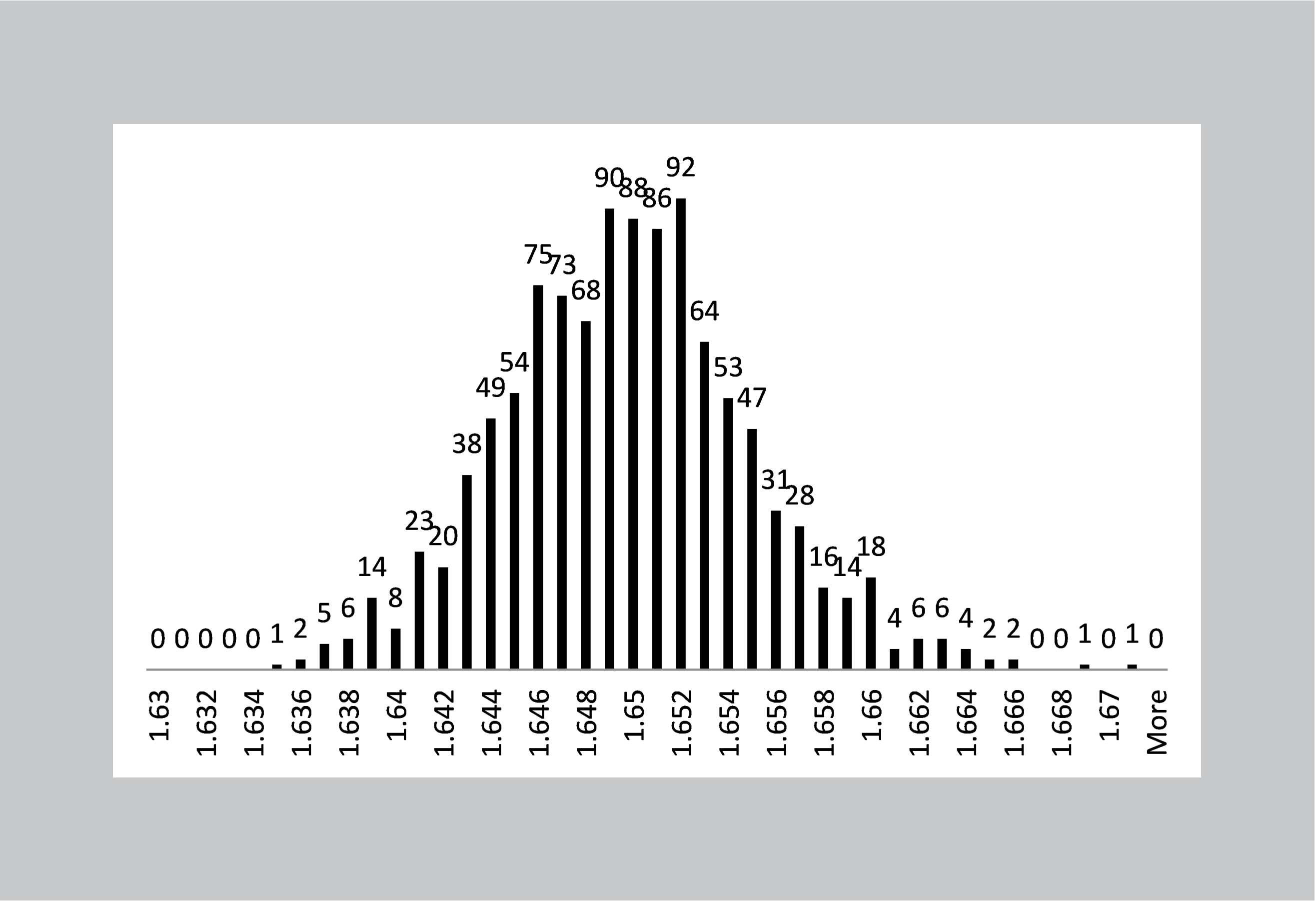

Figure 15c Histograms of mechanical aperture (mm) at successive applied displacements in the simulation of a "ductile" rock. (c) displacement 3.0 mm, unloading (first cycle);

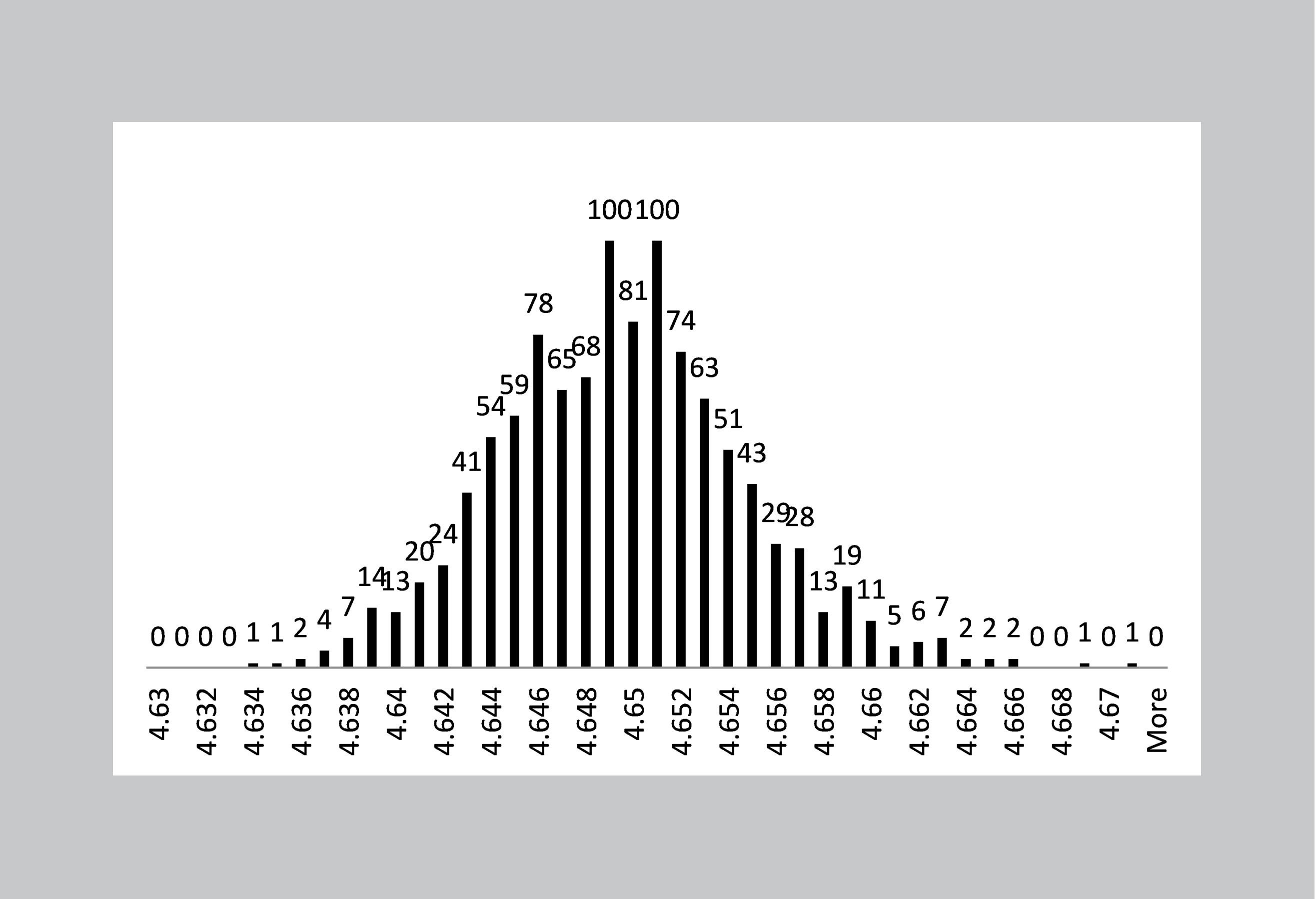

Figure 15d Histograms of mechanical aperture (mm) at successive applied displacements in the simulation of a "ductile" rock. (d) zero displacement, end of unloading from the first cycle

3 COUPLED NUMERICAL MODELLING OF STRESS-DEPENDENT CO_2 FLOW THROUGH FAULTS IN THE CAP ROCK

3.1 Introduction

This part of report describes coupled numerical simulations of stress-dependent CO_2 flow through faults that connect the main storage reservoir with the overlying aquifers. Geological model of the Bečej CO_2 gas field [1] was used as a basis to define various simulation cases.

The geological model of the Bečej field comprises:

- main gas storage reservoir;
- three shallow aquifers at different depths (-50, -400 and -1200 m);
- four vertical fault zones that connect the main gas reservoir with the shallow aquifers.

Using the coupling of two simulators Eclipse and Visage, we investigated the effect of stress and the associated permeability change on flow rates through faults.

3.2 Simulation cases

For this study a set of simulation cases was defined.

Base case

In the base case, initial pressure in the main reservoir was 151 bar and there was no additional CO_2 injection. Flow simulations were performed by Eclipse without coupling to geomechanics. The permeability update option for the flow through faults was not used here. The amount of CO_2 which migrated through faults to the shallow compartments was calculated without taking into account induced stress changes and the associated permeability changes of faults.

Case 1

In this case two-way coupled hydrodynamic-geomechanical simulations were used to calculate leakage rates assuming the same initial pressure as in the base case and no additional CO_2 injection. Permeability update functions were implemented and used for fault zones. This approach allows a stress-dependent estimate of the amount of CO_2 leakage through faults.

Case 2

Eclipse simulations without coupling to geomechanics were used to assess the case of additional CO_2 injection in the main reservoir. Three wells near the fault zones inject the CO_2 with bottom hole pressure of 250 bars (gas rate unlimited). This causes rapid increase of the reservoir pressure and also enhances the amount of gas leakage through faults.

Cases 3 and 4

These cases use the two-way coupled approach and assume that CO_2 is injected in the main reservoir. The difference between cases 3 and 4 is in the value of a fitting parameter C used to update permeability function. In case 3, C has a value representative of Kimmeridge shales – 0.27 [2]; in case 4, a value representative of sandstones – 0.4.

3.3 Model setup

3.3.1 Model geometry and flow properties

Previously constructed geological model of the Bečej field [1] was used to develop a semi-synthetic model for coupled stress-flow simulations. Because of specific features of Visage simulator, and to reduce calculation times, reservoir simulation grid was simplified. A regular vertical grid was used with cells of 100 m x 100 m (Figure 1). Porosity and permeability were assumed constant for all reservoir layers (Table 1).

Table 1 Porosity and permeability of reservoirs and fault zones.

	Porosity, %	Horizontal permeability, mD	Vertical permeability, mD
Main gas reservoir and shallow aquifers	30	1000	300
Faulted zones	1	1000	0.1

The fault zones were constructed around the fault surfaces. An additional fault was added near well Bč-6 to have faults in the model, which are oriented parallel and perpendicular to the assumed directions of the principal horizontal in-situ stresses. Fault locations are shown in Figure 2.

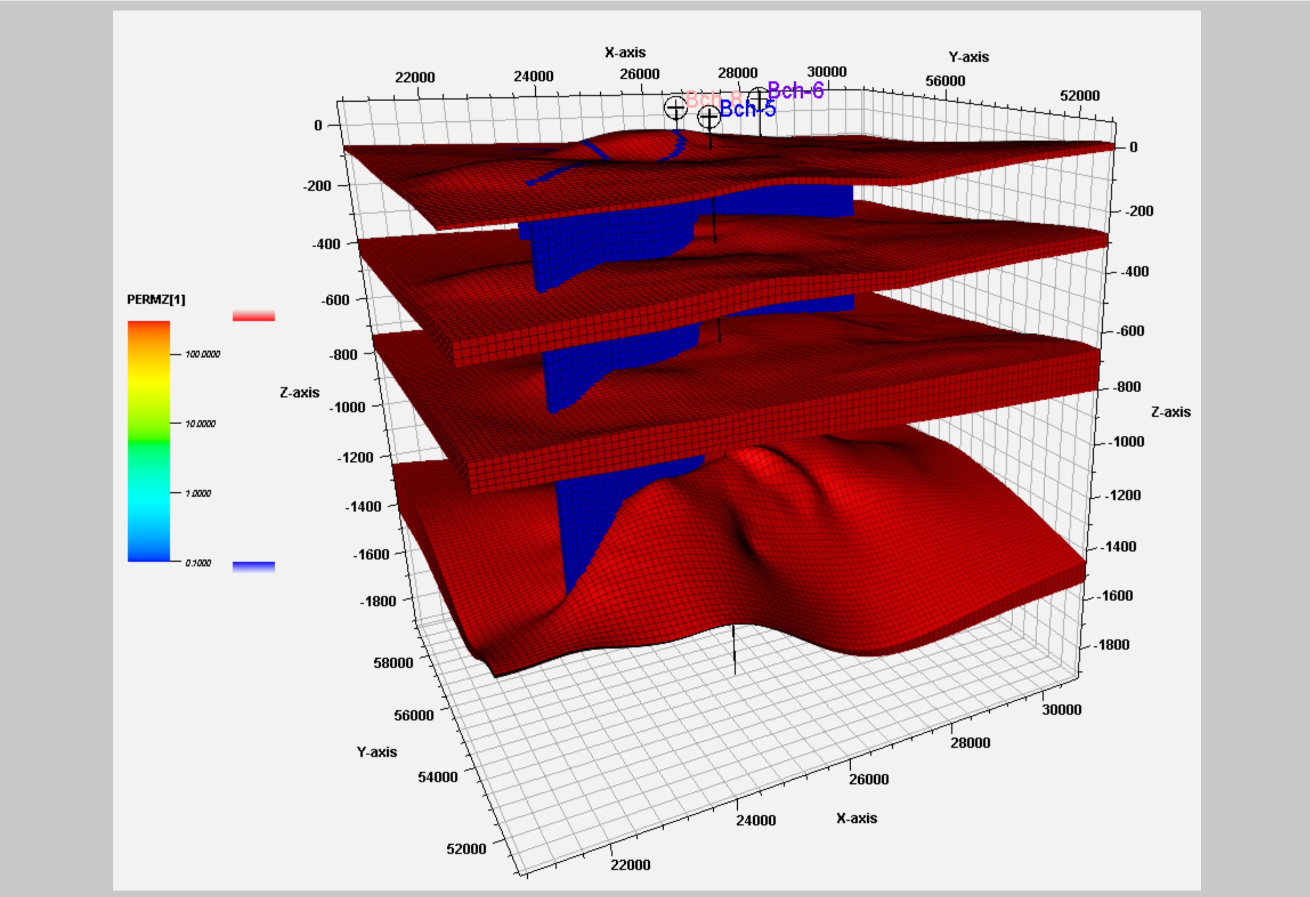

Figure 1 3D view of the vertical permeability cube.

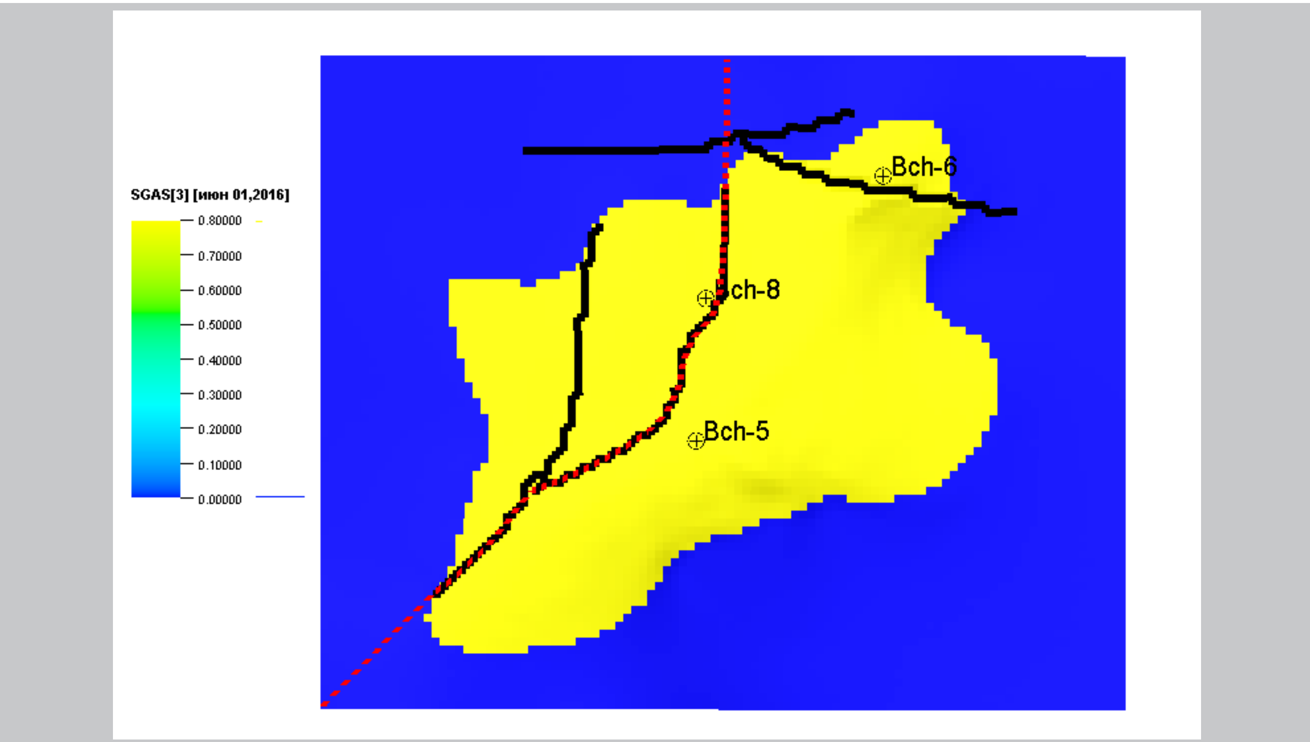

Figure 2 Top view of the main reservoir with faults.

3.3.2 Geomechanical grid

To reduce edge effects in geomechanical simulations, the geological grid was extended by adding the overburden, sideburden and underburden compartments (Figure 3). Size of the resulting geomechanical grid was 70.8 km x 57.5 km x 25 km (Figure 4).

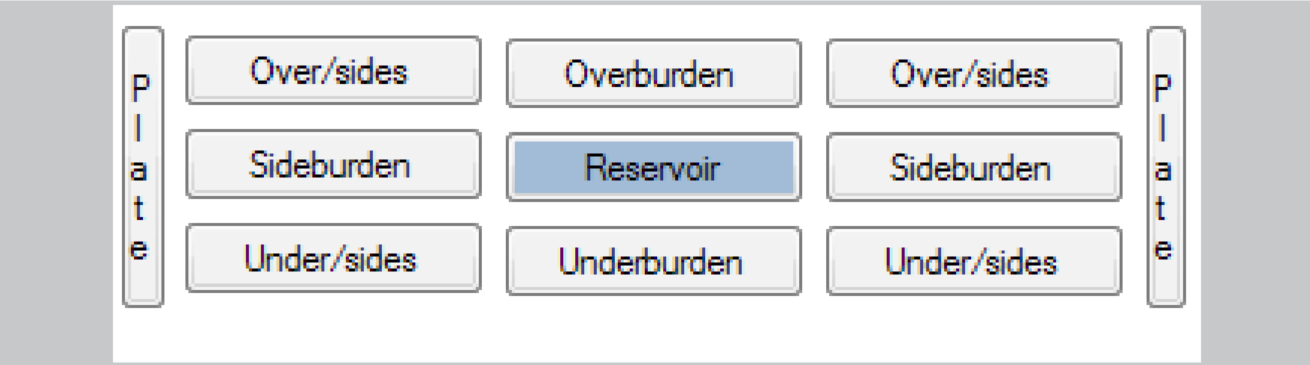

Figure 3 Schematic representation of the geomechanical grid.

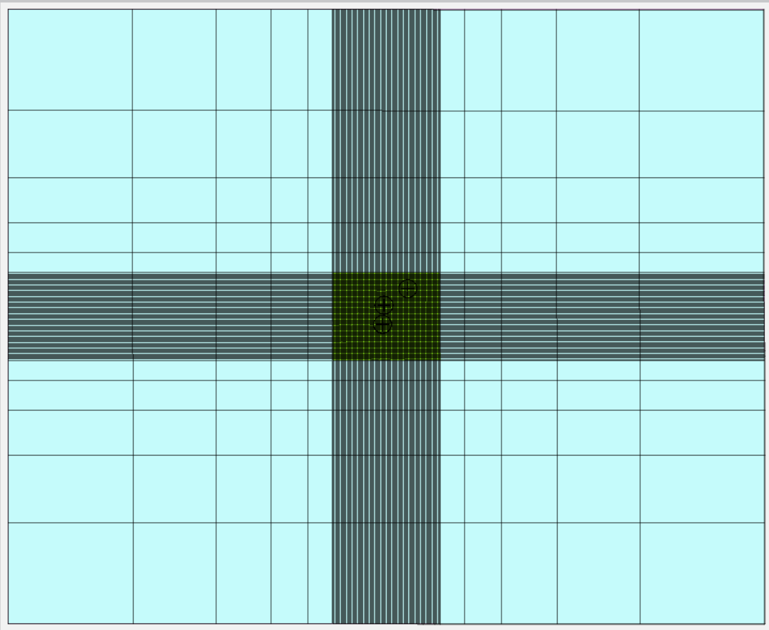

Figure 4 Geomechanical grid.

3.3.3 Geomechanical properties

After building, the geomechanical grid was populated by geomechanical properties. For this purpose the Petrel Reservoir Geomechanics material library was used. For all geological compartments "Sandstones" material was used. Properties of "Steel" were selected for the stiff plates. Elastic properties of materials are listed in Table 2. Yield criteria and material properties are given in Table 3.

Table 2 Elastic properties of model materials.

	Young's Modulus, GPa	Poisson's Ratio	Bulk Density, g/cm3
Sandstones	15.8	0.13	2.45
Steel	200	0.27	7.8

Table 3 Yield criteria and plastic properties of model materials.

Property	Value
Unconfined Compressive Strength, bar	670
Friction Angle, deg	40
Dilation Angle, deg	17.45
Tensile Stress Cut-off, bar	75
Hardening/Softening Coefficient	0

Fault zones were defined as a discontinuity type of material with properties listed in Table 4.

Table 4 Discontinuity properties of fault zones.

Property	Value
Fault normal stiffness, bar/m	20000
Fault shear stiffness, bar/m	10000
Cohesion, bar	0.01
Friction Angle, deg	20
Dilation Angle, deg	10
Tensile Strength, bar	0.01
Initial Opening	0

Young's modulus (E), Poisson's ratio (μ) and Unconfined Compressive Strength (q_u) were assumed to be depth-dependent. The values of these parameters were calculated using the following empirical relationships:

$$\begin{aligned} &E = 9.16*\exp(0.004*D) + 1, \\ &\mu = -5.75 * 10^{-5}*D + 0.2, \\ &q_u = (2.28 + 4.1089*E)*10, \end{aligned} \qquad (1)$$

where D is the absolute depth. For a depth of 1200 m, the updated value of Young's modulus amounts to 15.8 GPa and Poisson's ratio is equal to 0.13.

3.3.4 Permeability update

In two-way coupled simulations, the permeability of fault zones is dependent on shear strain and normal strain. Permeability multipliers used to update normal permeability and shear permeability dependent on shear strain are listed in Table 5 and shown in Figure 5.

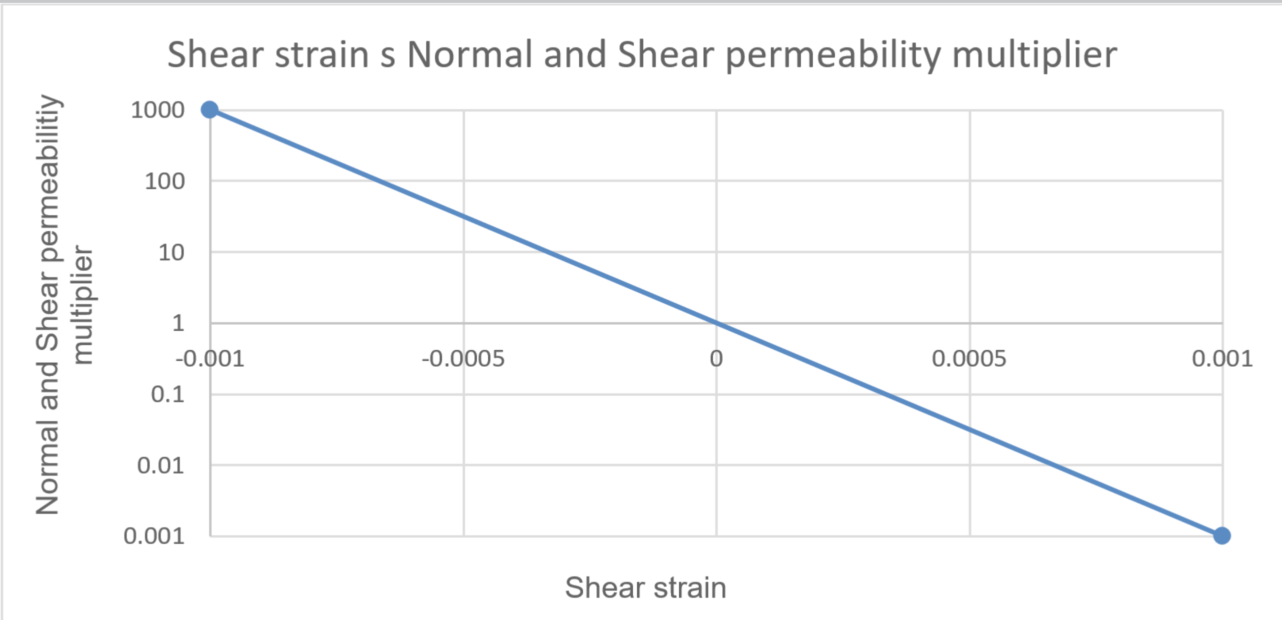

Figure 5 Normal and Shear permeability multiplier vs Shear strain.

Table 5 Shear strain and corresponding Normal and Shear permeability multipliers.

Shear strain	Normal and Shear permeability multiplier
-0.001	1000
0	0
0.001	0.001

Permeability multipliers used to update the shear permeability dependent on normal strain were calculated using the equation given in [2]:

$$k = k_0 \, exp(C'\sigma'_n) \tag{2}$$

where k is the fracture permeability, k_0 is the permeability of a fracture at zero effective normal stress, C' is a fitting parameter and σ_n' is the effective normal stress. Assuming a fault stiffness of 20000 bar/m, the values of permeability multipliers obtained for the two different values of C' are given in Table 6 and Table 7, and shown in Figure 6.

Table 6 Normal strain and corresponding Shear permeability multiplier for C'= 0.27, representative of Kimmeridge shale.

Normal strain	Shear permeability multiplier
-0.001	1.71600
0	1
0.0025	0.25924
0.005	0.06720
0.0075	0.01742

Table 7 Normal strain and corresponding Shear permeability multiplier for C'= 0.4, representative of sandstone.

Normal strain	Shear permeability multiplier
-0.001	2.2255
0	1
0.0025	0.13533
0.005	0.01831
0.0075	0.00247

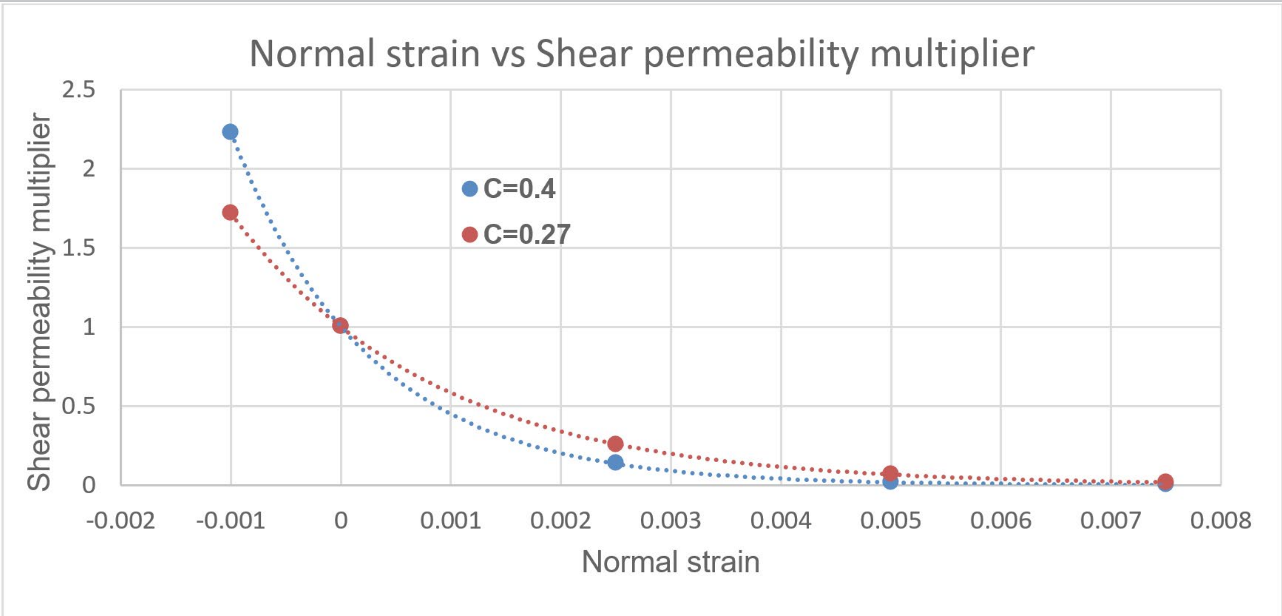

Figure 6 Shear permeability multiplier vs. Normal strain for C' =0.27(red) and C'=0.4(blue).

3.3.5 Geomechanical model initialization

The geomechanical model was initialized by applying the stress conditions determined by the parameters given in Table 8.

3.3.6 Flow model initialization

Reservoir simulation model was initialized as compositional with two components – water and pure CO_2. CO_2-water solubility option was not used.

Table 8 In-situ stress parameters.

Parameters	Values
Sh gradient, bar/m	0.135
Sh offset, bar	0
SH/Sh	1.15
Sh azimuth, deg	110

Shallow aquifers were initialized as separate equilibrium regions with the same pressure and 100% water saturation.

The initial pressure in the main reservoir, at the gas water contact (-1225 m), was 151 bar.

Relative permeabilities were defined by Corey-Brooks correlation for shaly-sand collectors.

The initial gas in place was 89.2×10^9 m^3.

3.4 Simulation results

3.4.1 Cases without gas injection

First we compare results of the cases without CO_2 injection, calculated with uncoupled simulations (base case) and two-way coupled simulations (case 1). The effects of stress-dependent permeability of fault zones on flow rates are plotted in Figure 7.

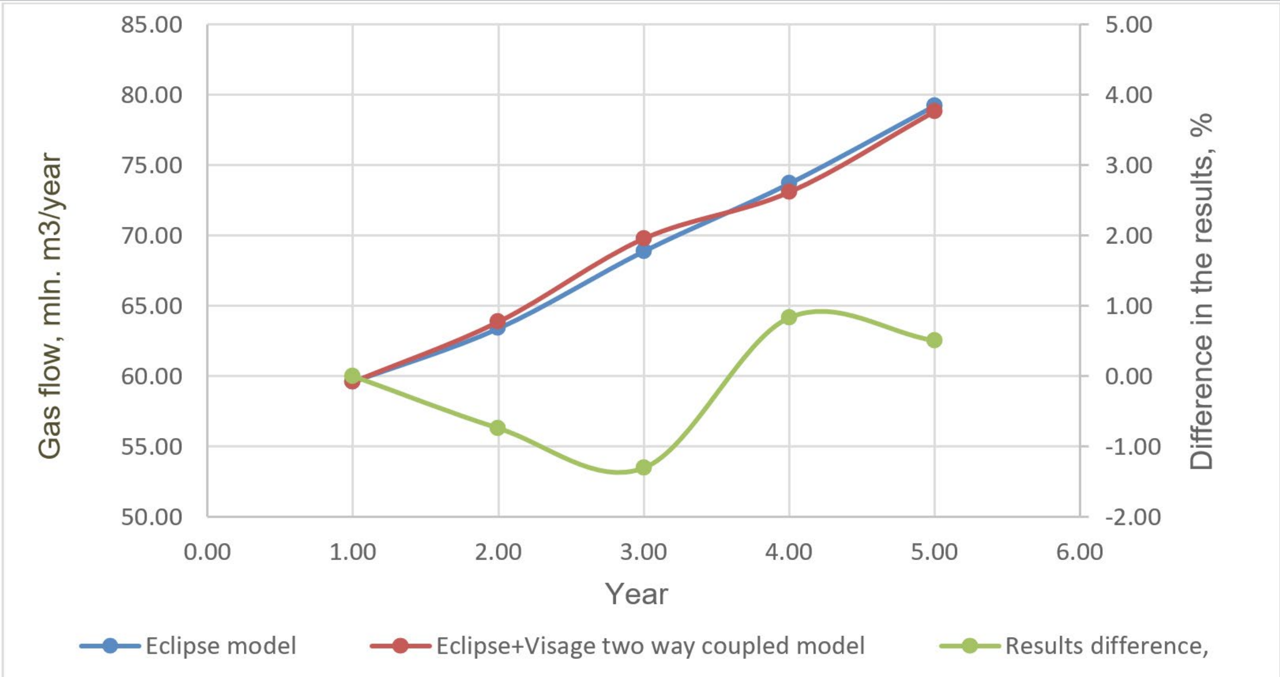

Figure 7 CO_2 flow rates through the central fault from uncoupled (base case) and two-way coupled (case 1) simulations.

Simulation results indicate that the differences in CO_2 flow rates through fault zones in uncoupled and coupled simulations are very small, max 1%. This can be explained by small changes in permeability associated with stress change. During 5 calculation steps, the vertical permeability of some cells decreased from 0.1 mD to 0.083 mD, whereas in other cells the permeability increased to 0.116 (Figure 8). Relatively small increase in fault zone permeability of 16 % had a very small effect on flow rates through fault zones in the model.

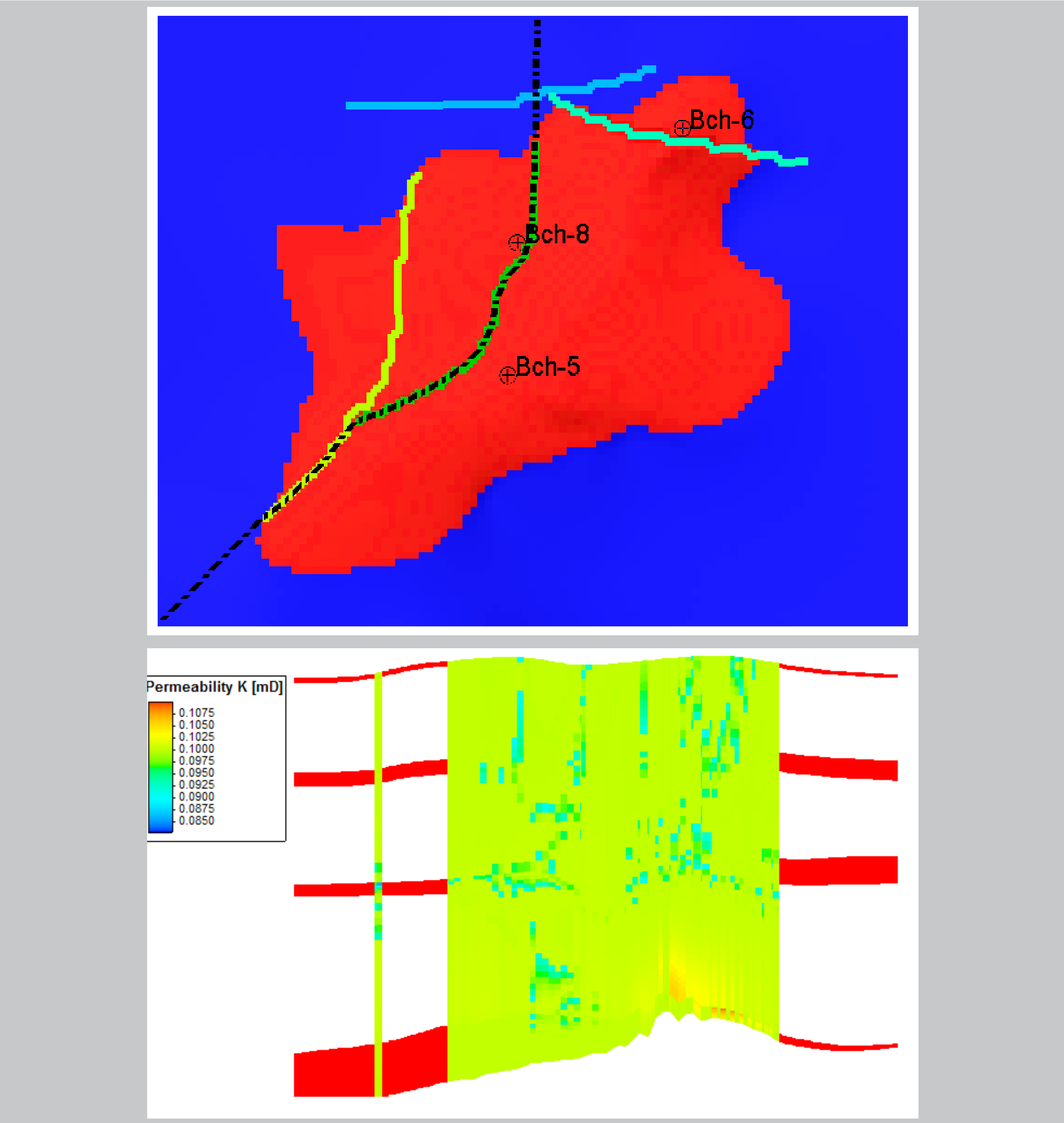

Figure 8 Top view of the main reservoir (top) and vertical cross-section (bottom) showing the vertical permeability cube along the central fault line (indicated by black line in top figure).

Cases with gas injection

In the cases with CO_2 injection (cases 2-4), gas is injected through three wells with constant tubing-hole pressure of 250 bar. The average field pressure increased from the initial 151 bar to 250 bar (Figure 9) and the volume of free gas in the reservoir increased to 151.9*109 m^3.

Results of the cases with CO_2 injection are compared in Figure 10. Case 2 was calculated with uncoupled simulations, while cases 3 and 4 with coupled simulations.

Figures 10 and 11 indicate that the differences between the three cases are very small. This can be explained by very small stress-dependent permeability changes of fault zone (Figure 12). In cases 3 and 4, vertical permeability even decreased from 0.1 mD to 0.08 mD.

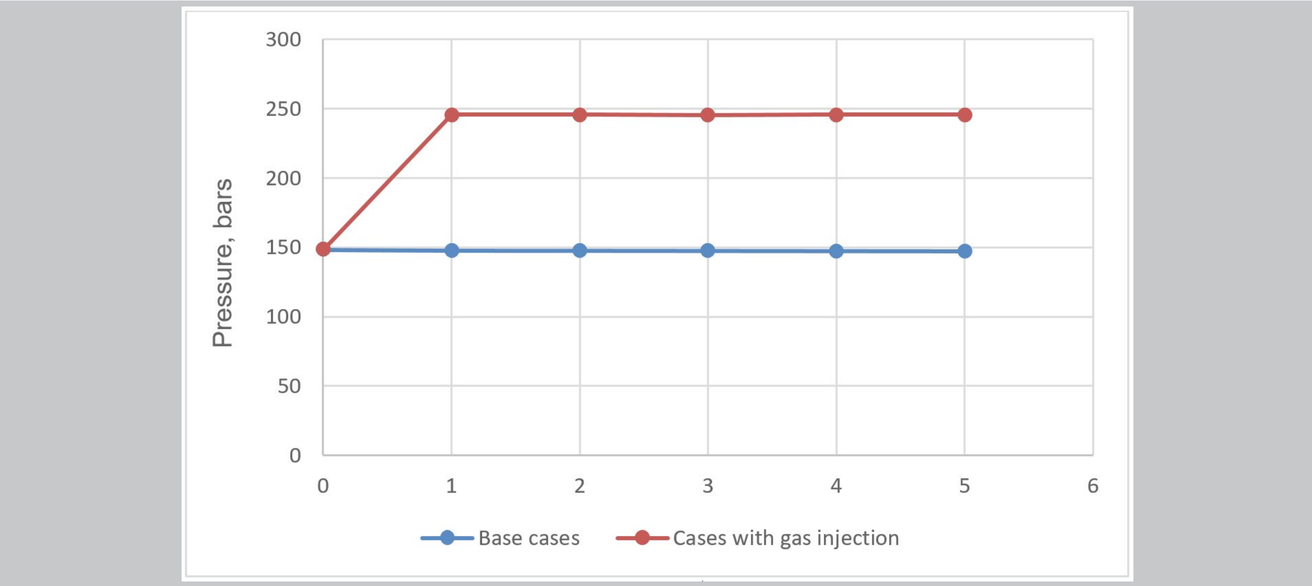

Figure 9 Average field pressure in the main reservoir in the cases without CO_2 injection (blue line) and the cases with CO_2 injection (red line).

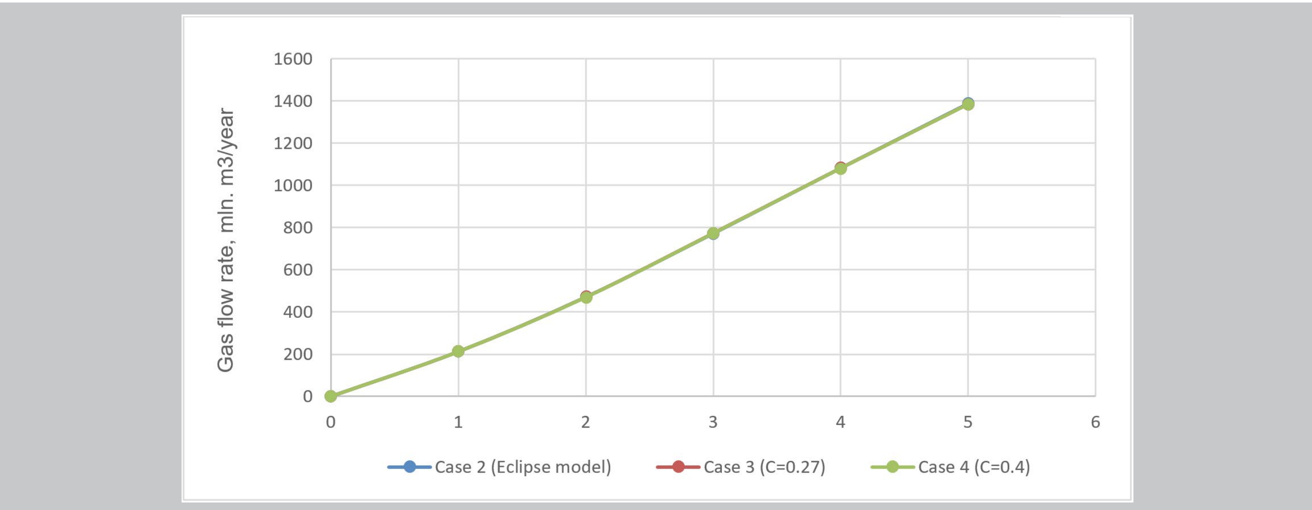

Figure 10 CO_2 flow rates through the central fault from uncoupled simulations(case 2) and coupled simulations(cases 3 and 4). Scenarios 2-4 assume additional CO_2 injection in the main reservoir.

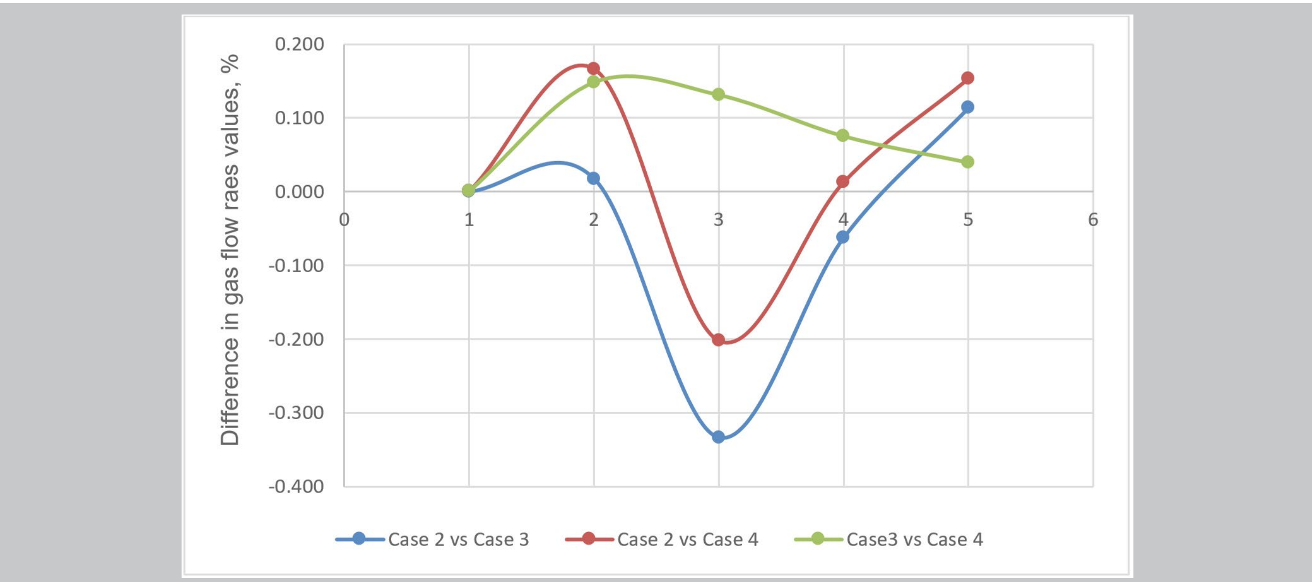

Figure 11 Differences in CO_2 flow rates between different scenarios that assume additional CO_2 injection in the main reservoir.

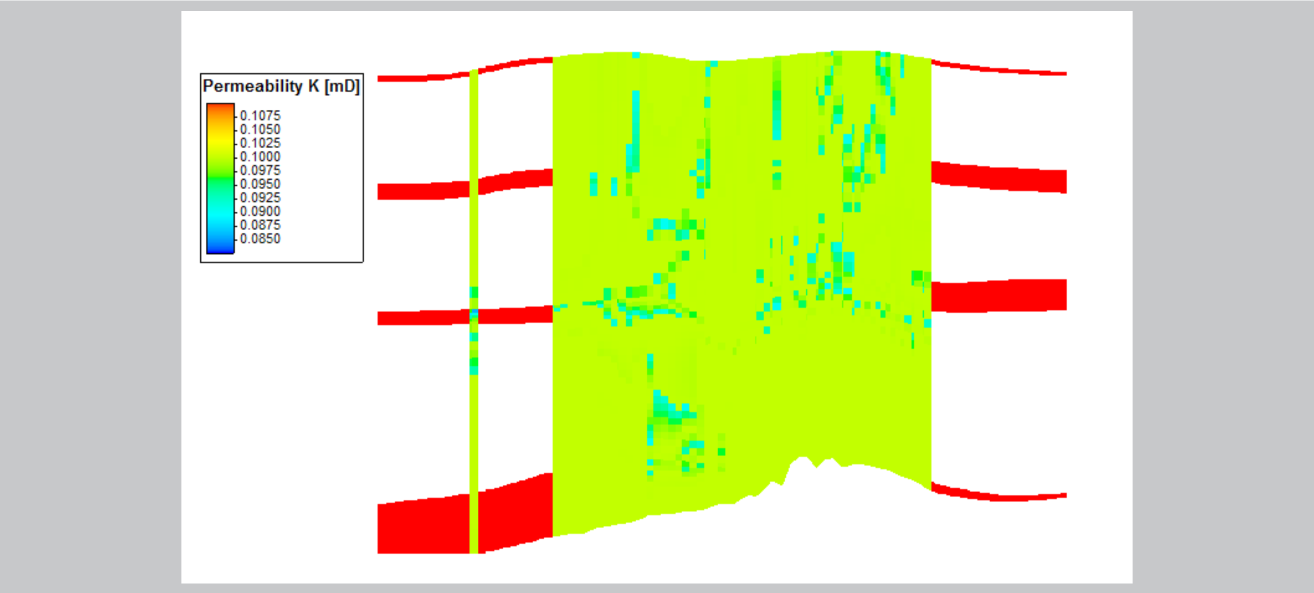

Figure 12 Vertical cross-section showing the vertical permeability cube along the central fault line for case 4.

3.5 Conclusions

Coupled flow-stress simulations were conducted on a semi-synthetic model of the Bečej natural CO_2 field to investigate the effect of stress on CO_2 flow rates through a hypothetical fault in the overburden. The workflow for coupled simulations was successfully developed in the Eclipse and Visage simulators. For the simulated cases and the selected ranges of input parameters, the pore pressure changes and the associated stress changes induced very small changes in the fault zone permeability leading to minor changes of flow/leakage rates. The simulation time of 5 years was relatively short, due to long computational times, and should be extended in future simulations.

For future work, we propose to develop a coupled model of stress-dependent CO_2 flow through a single fracture. Multiple fractures could also be introduced to simulate more realistically CO_2 leakage through a fractured fault zone.

References

1. Karas D., Kultysheva K., Demic I., Antropov A., Blagoevic M., Pluymaekers M., Orlic B. Pertel model of the Bečej field. Deliverable D12.2 of the MiReCOL project: Mitigation and remediation of leakage from geological storage. 2015.
2. Gutierrez M, Øino LE, Nygård R. Stress-dependent permeability of a de-mineralised fracture in shale. Marine and Petroleum Geology. 2000; 17(8):895-907.

Chapter XIII

Remediation of leakage by diversion of CO_2 to nearby reservoir compartments

Bogdan Orlic[1], Daniel Loeve[1], Lies Peters[1]
[1] TNO, The Netherlands

SUMMARY

This study describes mitigation of leakage by diverting CO_2 from the storage compartment to nearby reservoir compartments through fractures. Study results are published in an Energy Procedia paper presented at the 13th International Conference on Greenhouse Gas Control Technologies (GHGT-13) held in Lausanne in 2016 (Loeve et al., 2016, Diversion of CO_2 to nearby reservoir compartments for remediation of unwanted CO_2 migration). The mitigation method requires creating a pathway for fluid migration between the injected, leaky compartment and neighbouring compartments, as the injected and neighbouring compartments are originally not connected. Compartmentalized gas reservoirs or aquifers represent geological settings potentially suitable for remediation by flow diversion. Such structural settings are quite common in the Dutch and the North Sea reservoirs; for example, the depleted P18-4 gas reservoir, planned to be used for CO_2 storage in the Rotterdam Capture and Storage Demonstration Project (ROAD), is separated by a sealing fault from the neighbouring P15 depleted gas field. Another example relevant for CO_2 storage in both depleted gas fields and aquifers, are the Rotliegendes reservoir rocks, which are compartmentalized throughout the North-western Europe.

Our study demonstrates that in the event of significant irregularities and leakage from a CO_2 storage site, pressure relief can be achieved by diverting the CO_2 from the storage compartment to non-connected parts of the reservoir, or to adjacent reservoirs and aquifers. Fluid migration between the two originally non-connected reservoirs could be enabled by hydraulic fracturing across a sealing fault that separates adjacent compartments, or by drilling a well or laterals. The effects of flow diversion as a remediation option are evaluated through numerical simulations of idealized synthetic case and a real field case from the North Sea. The results show that flow diversion is a possible remediation option for a specific setup of depleted gas fields or saline aquifers, which is common in the Dutch and the North Sea portfolio of reservoirs. The key factors controlling the efficiency of flow diversion are the conductivity of the created pathways between the two reservoirs, the pressure difference between the reservoirs and the permeability of the receiving reservoir. In the case of CO_2 diversion into an undepleted saline aquifer, the remediation is relatively slow, compared to diversion into an adjacent depleted gas field, due to the small pressure difference between the two compartments. The simulations of the real case show that the diversion strategy needs to be optimized for the specific conditions and structural setting of the storage site. For the conditions evaluated in the real case, the remediation using a well is much more effective than remediation using hydraulic fractures.

This chapter is published as an Energy Procedia paper presented at the 13th International Conference on Greenhouse Gas Control Technologies (GHGT-13) held in Lausanne in 2016 (Loeve et al., 2016, Diversion of CO_2 to nearby reservoir compartments for remediation of unwanted CO_2 migration).

DIVERSION OF CO_2 TO NEARBY RESERVOIR COMPARTMENTS FOR REMEDIATION OF UNWANTED CO_2 MIGRATION

D. Loeve, E. Peters, M.P.D. Pluymaekers, F. Jedari-Eyvazi, F. Neele, B. Orlic

ABSTRACT

In the event of significant irregularities and leakage from a CO_2 storage site, pressure relief can be achieved by diverting the CO_2 from the storage compartment to unconnected parts of the reservoir or to adjacent reservoirs and aquifers. Fluid migration between the two originally unconnected reservoirs could be enabled by hydraulic fracturing across a sealing fault that separates adjacent compartments or by drilling a well or laterals. The effects of flow diversion as a remediation option are evaluated through numerical simulations of an idealized synthetic case and a real field case from the North Sea. The results show that flow diversion is a possible remediation option for a specific setup of depleted gas fields or saline aquifers, which is common in the Dutch and the North Sea portfolio of reservoirs. The key factors controlling the efficiency of flow diversion are the conductivity of the created pathways between the two reservoirs, the pressure difference between the reservoirs and the permeability of the receiving reservoir. In the case of CO_2 diversion into an undepleted saline aquifer, the remediation is relatively slow, compared to diversion into an adjacent depleted gas field, due to the small pressure difference between the two compartments. The simulations of the real case show that the diversion strategy needs to be optimized for the specific conditions and structural setting of the storage site. For the conditions evaluated in the real case, the remediation using a well is much more effective than remediation using hydraulic fractures.

1 INTRODUCTION

Geological CO_2 storage in depleted gas fields and saline aquifers is considered one of the most promising technologies for a low-carbon energy future. The goal of geological CO_2 storage is permanent and safe storage of substantial quantities of CO_2 in the subsurface formations. In the event of undesired migration of CO_2 within or out of the storage reservoir, corrective measures need to be taken to mitigate the unwanted migration and reduce the possible consequences of a leak. The feasibility of existing and new techniques that are potentially relevant to remediation and mitigation of leakage from geological CO_2 storage sites has been investigated in the MiReCOL (Mitigation and Remediation of CO_2 Leakage) project (2014-2017; http://www.mirecol-CO_2.eu/). The aim of this project is to develop a handbook of corrective measures that can be considered in the event of undesired migration of CO_2 in deep subsurface reservoirs

In this study we investigate one possible corrective measure, which is diversion of the injected CO_2 from a leaky storage compartment to an adjacent compartment to achieve pressure relief in the storage formation. Although different remediation methods were considered in several earlier publications (e.g. [1-5]), flow diversion as a remediation option has to the best of our knowledge not been studied so far. A suitable structural setting for flow diversion comprises two reservoir compartments separated by a sealing fault (Fig. 1a). Flow diversion requires creating a pathway for fluid migration between the two originally unconnected reservoirs, which can be achieved, for example, by hydraulic fracturing across the fault or by drilling a well or lateral(s) (Fig. 1b). The creation of a pathway will cause pressure equilibration between the two compartments. In our analysis, we assume that the pressure reduction in the leaking compartment will be sufficient to stop unwanted migration of CO_2.

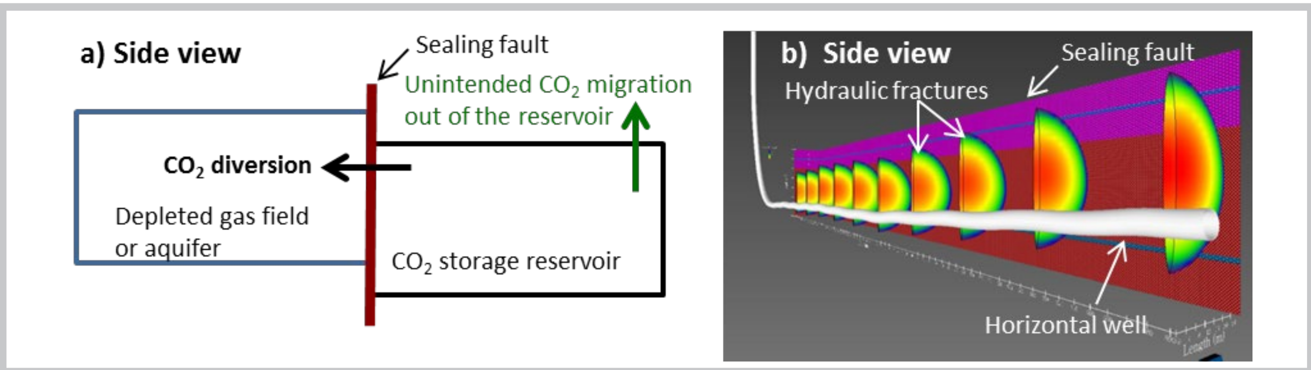

Figure 1 (a) Schematic representation of the structural setting possibly suitable for flow diversion. The CO_2 storage reservoir and the depleted reservoir are separated by a sealing fault (side view). (b) Breaching of a fault seal by multi-stage hydraulic fracturing will enable flow diversion, i.e. lateral migration of fluids between the two adjacent reservoir compartments through fractures.

Remediation by flow diversion can be relevant for CO_2 storage in a depleted gas field, which is adjacent to other depleted gas fields. Structural settings where several depleted gas reservoirs or compartments are transected or separated by sealing faults are common for Dutch onshore fields, North Sea fields and many other petroleum provinces. Remediation by flow diversion can also be relevant for storage in aquifers with undetected sealing faults, which becomes apparent during the injection phase. In both cases, creating a flow conduit across the fault/barrier that separates the adjacent compartments will allow CO_2 and/or water to flow out of the storage compartment and therefore will lower the pressure.

In this paper, remediation by flow diversion is first analyzed using a synthetic test case and then applied to a real field case. The findings inferred from these cases are discussed. Finally, more general conclusions are drawn on the use of flow diversion as a remediation measure in the context of geological CO_2 storage.

2 MODEL SETUP AND PARAMETERS

Initial tests were performed on synthetic models. Then, the effectiveness of remediation by flow diversion is investigated on a real field case from the North Sea. This section provides description of the flow models, model parameters and simulation scenarios. Simulations of the synthetic case were conducted with ECLIPSE, while simulations of the real case were done with Shell's in-house reservoir simulator MoReS.

2.1 Synthetic case

The synthetic case comprises an idealized representation of two depleted, adjacent reservoir compartments separated by a sealing fault. CO_2 is injected into one of the compartments. At some point during injection, CO_2 starts leaking from the storage reservoir due to, for example, the presence of fractures within the caprock or leaky wells. After leak detection, it is decided to divert CO_2 into the adjacent compartment with a lower pressure, which has sufficient capacity to store the diverted CO_2. A long horizontal well is drilled parallel to the sealing fault, which separates the two reservoirs (Fig. 1b and Fig. 2a). Then, multi-stage hydraulic fracturing is performed to create pathways for fluid migration across the fault from the storage compartment to the receiving neighboring compartment. We assume that it is possible to create hydraulic fractures across the fault interface. As all the fractures in the synthetic model are identical and equidistant, the model can be reduced to a single slice with only one fracture (Fig. 2b).

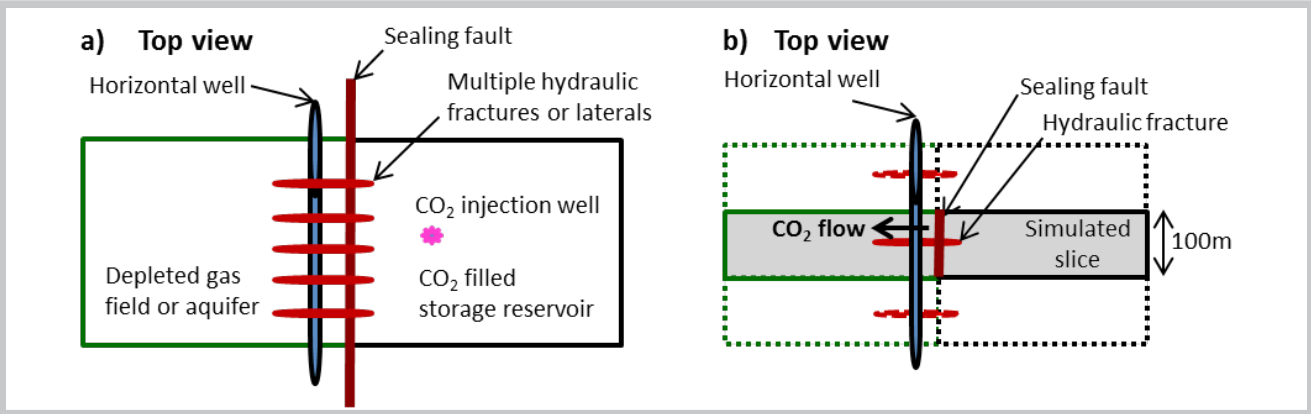

Figure 2 (a) Schematic representation of the synthetic model with two adjacent reservoir compartments and a sealing fault intersected by multiple hydraulic fractures (top view). (b) Due to symmetry, the model can be reduced to a single slice with one fracture. The model is delineated by no flow boundaries (solid lines).

2.2 Synthetic model and simulation scenarios

The synthetic model setup is shown in Fig. 3. The model size is 100 m x 2000 m x 180 m with a grid block size of 10 m x 5 m x 5 m. The initial pressure in the storage compartment is 300 bar and 20 bar in the receiving (depleted) compartment, which are typical initial- and depleted pressures of gas reservoir in the Netherlands. The storage compartment has a dip of 5°, and the receiving compartment is horizontal. The juxtaposition of reservoir blocks across the fault is 30%. In the reservoir, two zones are identified: a 60m-thick top zone with good reservoir properties (permeability, k = 100 mD, porosity, ϕ = 0.12) and a 120m-thick bottom zone with poor reservoir properties (k = 5 mD, ϕ = 0.05). Vertical permeability is equal to horizontal permeability and the net-to-gross (NTG) ratio is 1. Both compartments are initialized with CO_2 and no gas-water contact is present. The storage capacity of the depleted compartment is about 0.5 million tonnes (Mt) of CO_2 for re-pressurization from the initial pressure of 20 bar to the pre-depletion pressure of 300 bar. For comparison, the estimated storage capacity of the real reservoir considered in the next section 2.3 is about 8 Mt, which implies that 16 synthetic symmetry elements (i.e. single slices) would be needed to store the same mass of CO_2. The hydraulic fracture is represented by a single column of 5m-wide grid blocks with a transmissibility of 1,000 mD*m (400 D * 2.5 mm). Thus, the permeability of the 5m-wide grid block representing the fracture is 200 mD.

The unintended CO_2 migration is defined at 10,000 sm^3/d and stops when pressure (P) is lower than 200 bar. The reason that the leakage stops due to a pressure reduction in the reservoir (at an arbitrary threshold of 200 bar) is, for example, the stress-sensitive fluid flow in a fracture or fracture network in the caprock leading to unwanted migration of CO_2 out of the storage complex. Because fracture permeability is sensitive to the effective stress and therefore also to the pore pressure changes, pressure reduction will cause closure of open fractures in the caprock making them non-conductive. The CO_2 leakage rate of 10,000 sm^3/d corresponds to a pressure reduction of 100 bar in 27 years (3.7 bar/yr). This is significantly higher than a pressure reduction of 0.03 to 0.9 bar/yr observed in the Bečej natural CO_2 field due to the leak caused by the uncontrolled migration of CO_2 through the caprock damaged by a blown-out well in 1968 [6]. The leakage rates used in our simulations are more in line with the rates used in [2]: 200-10,000 t/yr (~300-15,000 sm^3/d).

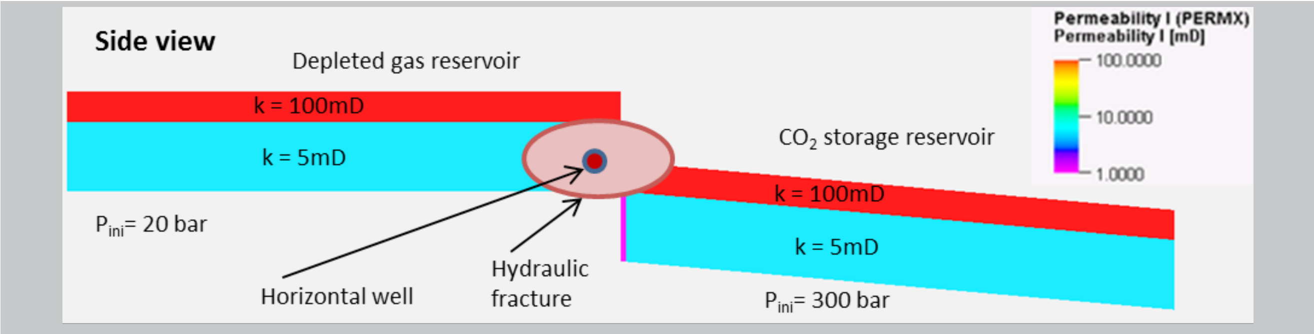

Figure 3 Synthetic model with the base case parameters (side view).

A number of sensitivities was modelled to investigate the effect of important controlling factors on the efficiency of flow diversion (Table 1). In the geological scenarios 1-7 we varied the juxtaposition of the reservoir compartments across the fault (scenarios 1 and 2), the dip of the storage compartment (scenarios 3 and 4), the permeability of the lower part of the reservoirs (scenarios 5 and 6) and pore volume of the receiving compartment (scenario 7).

The sensitivity of the results with respect to the setup of the remediation is investigated in scenarios 8-12. The sensitivities considered variation in fracture permeability (scenarios 8 and 9) and the initial pressure in the receiving compartment (scenario 10).

In scenario 11, a pathway is created across the fault using a lateral well instead of a hydraulic fracture. In this case a radial well is considered [7]. In this type of well, small-diameter laterals are jetted from the main well bore using hydraulic jetting. For the radial wells, the same modelling approach is used and only one slice consisting of one radial well is modelled. The created well is 100 m long and has a diameter of 2 inch (5 cm). Pressure drop in the well is not simulated.

In scenario 12, the receiving compartment is not a depleted gas filed, but an aquifer. The pressure in both compartments is changed to be more representative of CO_2 storage in aquifers. The pressure in the aquifer is assumed to be hydrostatic; in the storage compartment, the pressure is 110% of hydrostatic. The unintended migration of CO_2 from the storage compartment stops when the pressure in the storage compartment is reduced to 105% of hydrostatic. It is assumed that the receiving compartment is very large to avoid rapid pressure build-up in that compartment.

Table 1 Simulation scenarios of the synthetic test case.

No.	Name	Description
Geological scenarios		
	Base case	The juxtaposition across the fault is 30% The dip of the storage compartment is 5° The permeability of the lower zone is 5 mD Fracture permeability is 400 D Initial pressure in the receiving compartment is 20 bar The receiving compartment is a depleted gas field
1	Juxtaposition = 10%	The juxtaposition across the fault is 10%
2	Juxtaposition = 50%	The juxtaposition across the fault is 50%
3	Dip = 0	The dip of the storage compartment is 0°
4	Dip = 10	The dip of the storage compartment is 10°
5	k = 0.1 mD	The permeability of the lower zone is 0.1 mD
6	k = 100 mD	The permeability of the lower zone is 100 mD
7	Pore volume x 2	Pore volume of the receiving compartment is multiplied by 2
Remediation scenarios		
8	Frac perm x 0.1	Fracture permeability is 40 D
9	Frac perm x 0.01	Fracture permeability is 4 D
10	P_INI = 80 bar	Initial pressure in the receiving compartment is 80 bar
11	P_INI = 80 bar + Well	Initial pressure in the receiving compartment is 80 bar and a lateral instead of a fracture is used as remediation
12	Aquifer	The receiving compartment is an aquifer instead of a depleted gas field

2.3 Real case
In the second part of the study, flow diversion is studied in a model representing the structure and the dynamics of a real reservoir, namely the depleted P18-4 gas field located in the North Sea about 20 km off the coast of Rotterdam. The model represents two adjacent, single-compartment gas fields formed in fault-bounded horst structures at a depth of about 3500 m. The southern compartment (P18-4) is considered for future CO_2 storage (Fig. 4a). The estimated storage capacity of the P18-4 reservoir is about 8 Mt of CO_2. The northern compartment (P15-9) also contained gas initially and has been depleted. The volume of the P15-9 reservoir is about 2.2 times larger than that of the P18-4 reservoir. A fault towards the north separates the P18-4 gas field from the adjacent P15-9 gas field (Fig. 4b). The reservoir thickness of about 200 m is approximately equal to the vertical fault throw; therefore, permeable reservoir facies are not juxtaposed across the fault. The fault appears to be sealing on a production time scale [8].

The P18 gas reservoirs belong to the Main Buntsandstein Subgroups. The oldest Volpriehausen Formation has low porosities (~5%) and permeabilities (~1 mD). The Volpriehausen is overlain by the Detfurth Formation, which is composed of the Lower and Upper Detfurth Sandstone Members. The youngest reservoir formation is the Hardegsen Formation. Parts of the Detfurth and the Hardegsen Formation (with porosities of 9-12% and permeabilities of 100-200 mD) contribute the most to gas production.

The model of the depleted P18-4 gas field used in previous studies for storage- and injectivity capacity estimations was extended and modified as described below to suit the analysis of potential remediation options. In the remainder of this paper, we will refer to the modified version of the P18-P15 model as the real case model. The structure, reservoir properties and gas properties for the real case model are taken from the P18-P15 gas fields.

2.4 Real case model and simulation scenarios
The thickness of the northern compartment is increased by adding an additional zone to the bottom of the original reservoir model. This zone, which is composed mostly of shale, is now juxtaposed against the upper, permeable part of the southern compartment (Fig. 4b). Permeability of the newly created zone is 0.01 mD in the horizontal direction and 0.0001 mD in the vertical direction. Porosity and NTG are 0.07 and 0.1, respectively. Similar to the synthetic case, the reservoir properties (permeability and porosity) in both reservoirs decrease with depth and the fault between the adjacent compartments is fully sealing (Fig. 4b).

The southern depleted compartment is filled with CO_2 to a pressure of approximately 350 bar over 5 years (from 1-1-2010 to 1-1-2015), which was the initial plan of the Rotterdam Capture and Storage Demonstration Project (ROAD) [8]. The northern compartment is depleted to approximately 20 bar and is still partially filled with the original hydrocarbon gas. In the simulation model, the northern

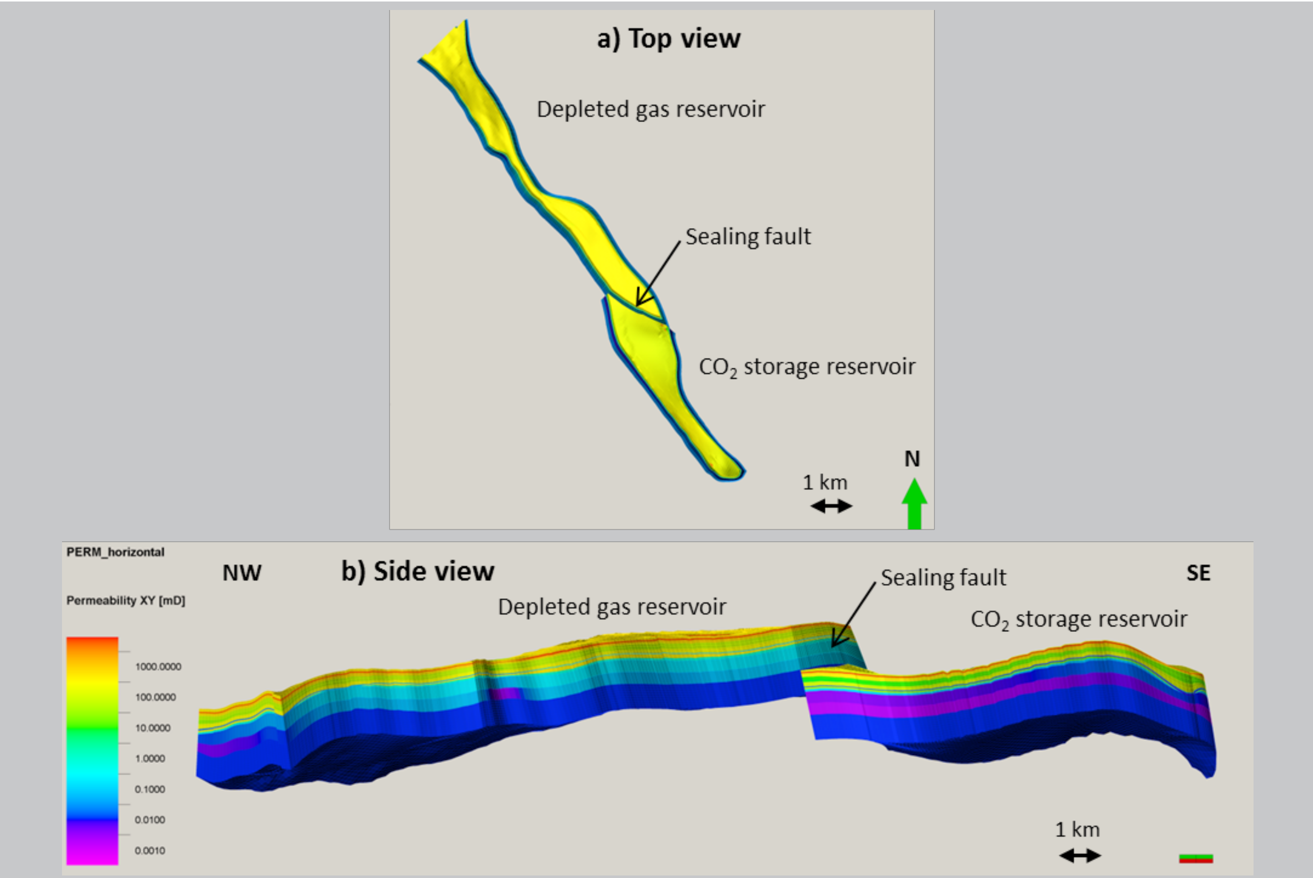

Figure 4 (a) Top view and (b) side view of the real case model.

depleted compartment was initialised at 20 bar without simulation of gas production, while the gas production from the southern compartment, and the subsequent CO_2 injection, were fully simulated.

The remediation case setup for the real case is similar to the synthetic case: a horizontal well is drilled parallel to the fault in the low-permeability zone which is juxtaposed to the CO_2-filled reservoir and hydraulic fracturing is performed to create the pathways for fluid migration across the fault (Fig. 5). We assume that hydraulic fractures can propagate in the direction approximately perpendicular to the strike of the fault. In reality, hydraulic fracture will propagate in the direction of the present-day maximum stress, which is NW-SE in the Netherlands. Further, we assume that it is possible to create a few-hundred-meters-long hydraulic fracture using an appropriate treatment plan, as shown for the similar geological setting in [9]. We also assume that the hydraulic fractures, when propagating from a low permeable and more rigid layer towards a high permeable, less rigid layer will break the fault interface as shown in [10, 11]. The remediation starts directly after the end of the CO_2 injection period, on 1-1-2015.

In the base case scenario, we use two hydraulic fractures instead of multiple fractures to reduce the computational effort. The characteristics of these fractures (Table 2) are chosen to be optimal for remediation, but the same effects could be achieved using multiple fractures with lower permeabilities, as in the case of synthetic model (section 2.2). The fractures are not simulated explicitly in the reservoir model, but as non-neighboring connections. The permeability of the shale zone in which the fractures are created is 0.01 mD in the horizontal direction and 0.0001 mD in the vertical direction. NTG of the zone is 0.1 (this only affects the horizontal permeability).

Table 2 Characteristics of the hydraulic fractures in the base case scenario.

Property	Value
Half length	350 m
Total height	100 m
Permeability	1000 D
Width	0.025 m

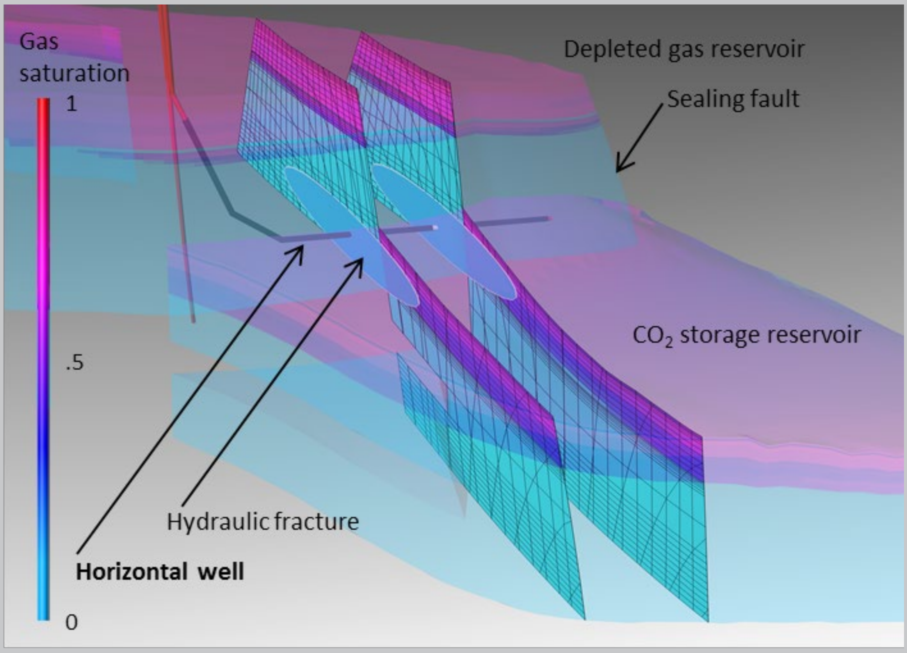

Figure 5 Remediation with two fractures in the real case model.

In the sensitivity analysis we investigated the effect of different geological factors and remediation characteristics on the efficiency of flow diversion (Table 3). The focus of geological scenarios 1-4 is on the permeability of the receiving compartment, because this is the main limiting factor for efficient remediation. The sensitivity of the results with respect to the setup of the remediation is investigated in scenarios 5-8. All the remediation scenarios with fractures (scenarios 5-7) have been run with the increased permeability in the shale zone. In scenario 8, a deviated well instead of fractures is used to divert the CO_2 (Fig. 6). The well is perforated in both reservoir sections, and cross-flow in the well is allowed. The well diameter is 12 inches (0.30 m) and no tubing is assumed. Pressure drop in the well is not simulated.

Table 3 Simulation scenarios of the real field case.

No.	Name	Description
Geological scenarios		
1	2 fracs	Base case remediation with 2 fractures
2	2 fracs, kxy low zone x 100	Horizontal permeability in the shale zone multiplied by 100
3	2 fracs, kxyz low zone x 100	Horizontal and vertical permeability in the shale zone multiplied by 100
4	2 fracs, kxyz low zone x 1000	Horizontal and vertical permeability in the shale zone multiplied by 1000
Remediation scenarios		
5	3 fracs, kxyz low zone x 100	Remediation with 3 fractures Horizontal and vertical permeability in the shale zone multiplied by 100
6	High well, 2 fracs, kxyz low zone x 100	The horizontal well is located 40 m higher than in the base case Horizontal and vertical permeability in the shale zone multiplied by 100
7	High well, 2 fracs high, kxyz low zone x 100	The horizontal well is located 40 m higher than in the base case The two fractures are 200 m high and have a half-length of 250 m Horizontal and vertical permeability in the shale zone is multiplied by 100
8	Deviated well	Diversion of CO_2 is done by means of a deviated well (Fig. 6)

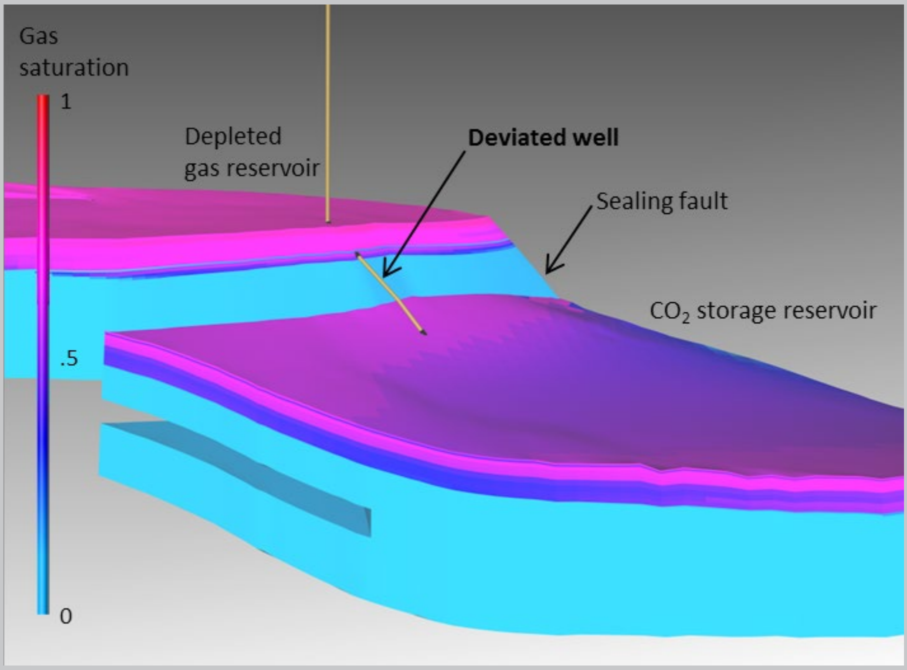

Figure 6 Remediation with a deviated well used to divert the flow of CO_2 from the storage compartment to the neighboring compartment.

3 RESULTS

3.1 Synthetic case

Fig. 7 shows the evolution of leakage rate and pressure with time for the synthetic case without remediation. As expected, the pressure in the storage compartment decreases slowly due to continuous leakage. After approximately 27 years, the pressure has dropped to 200 bar, i.e. the assumed threshold at which the leak stops. In case of remediation with the simulation parameters corresponding to the base case scenario from Table 1, pressure in the storage compartment decreases much faster. After 40 days the pressure has dropped sufficiently to stop the leakage (Fig. 8). The pressure in the storage compartment and the receiving compartment equilibrate in about half a year.

Fig. 9 compares the duration of remediation in the synthetic model for different scenarios. The time period until the unintended migration stops varies from 1 to 16 months for the range of input parameter values considered in the sensitivity study. For scenarios 1-10 with a hydraulic fracture, the duration of remediation depends primarily on the following key parameters: permeability of the adjacent reservoir sections connected by the created fracture (scenarios 5 and 6), the conductivity of the created fracture (scenarios 8 and 9) and the pressure difference between the two compartments (scenario 10). The higher the permeability of the connected reservoirs, the conductivity of hydraulic fractures and the pressure difference between the compartments, the shorter the duration of remediation.

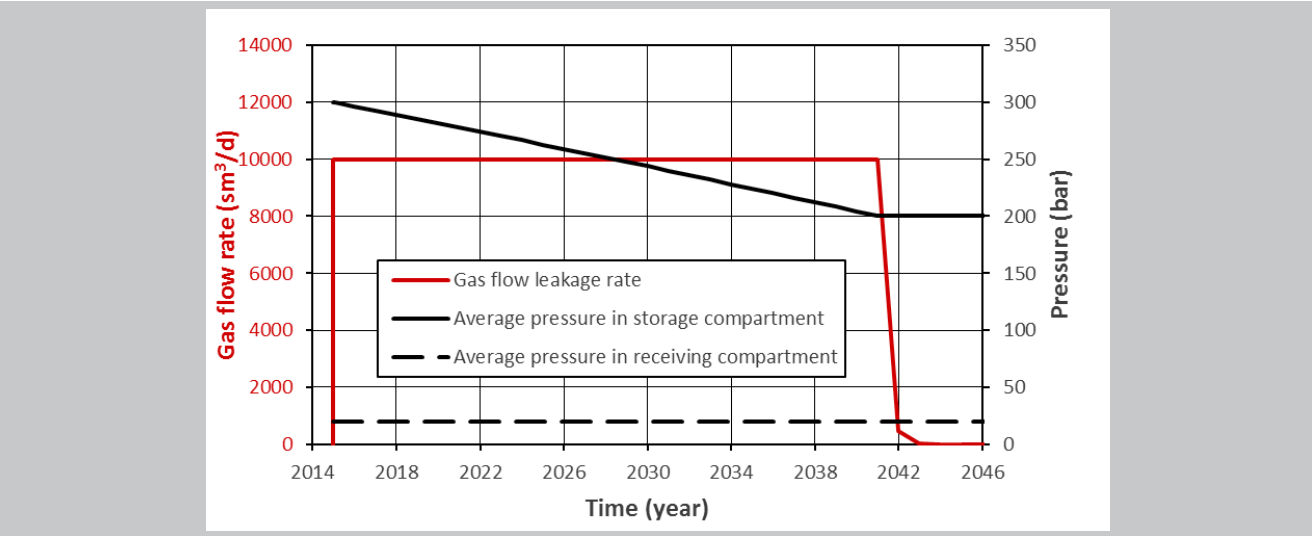

Figure 7 Evolution of leakage rate and pressure in the synthetic model without remediation.

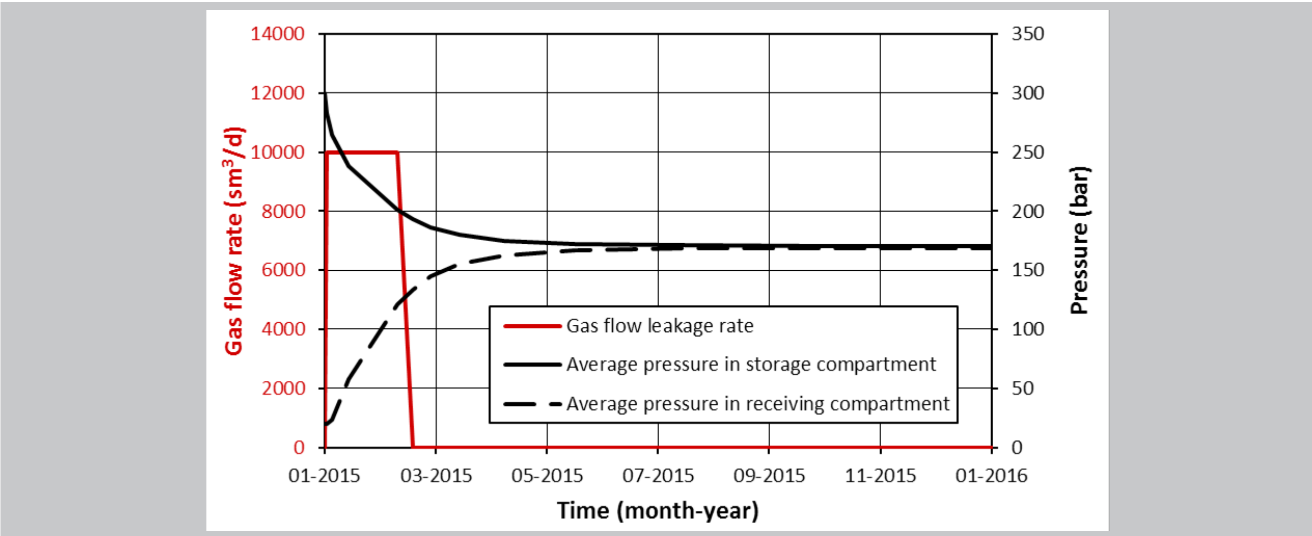

Figure 8 Evolution of leakage rate and pressure in the synthetic model for the base case remediation scenario.

The juxtaposition of more permeable parts of the reservoir across the fault is an important factor controlling possible connectivity of the reservoirs by a hydraulic fracture (scenarios 1 and 2). The longest duration of remediation that exceeds 500 days is obtained when a part of the storage reservoir with higher permeability is juxtaposed against a part of the receiving compartment with a very low permeability (~0.1 mD in scenario 5 instead of 5 mD in the base case). The sensitivity of the synthetic model to the considered variations in the inclination of the storage compartment appears to be low (scenarios 3 and 4).

In scenario 11, a 2-inch diameter lateral well is used to create a conduit between the two compartments. The duration of remediation with a lateral well of 130 days is almost twice as long compared to the similar scenario (10) with a fracture, where it amounts to 70 days. The time to stop leakage in scenario 11 is somewhat overestimated because the pressure drop in the well has not been taken into account in simulations. In a real case, a larger diameter for lateral wells may be feasible.

For the aquifer scenario 12, it takes much longer (~330 days) for the unintended migration to stop. The pressure difference between the two compartments is here much smaller compared to other scenarios that assume a depleted receiving compartment. Also, the CO_2 moves slower into the receiving compartment as the effective permeability for gas is lower, due to the presence of water in the receiving compartment. After one year, lateral movement of water from the receiving aquifer compartment into the storage compartment is observed, due to the density difference between the CO_2 and brine (Fig. 10). As a consequence, more CO_2 will flow into the receiving compartment.

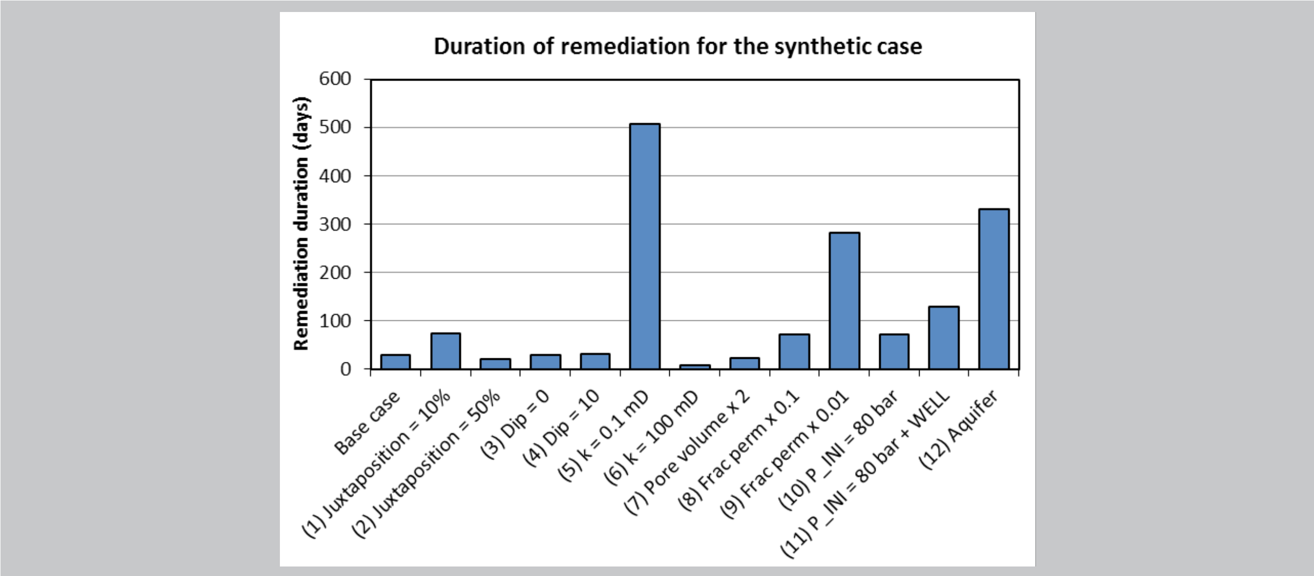

Figure 9 Duration of remediation in the synthetic model for different scenarios (see Table 1 for scenario description).

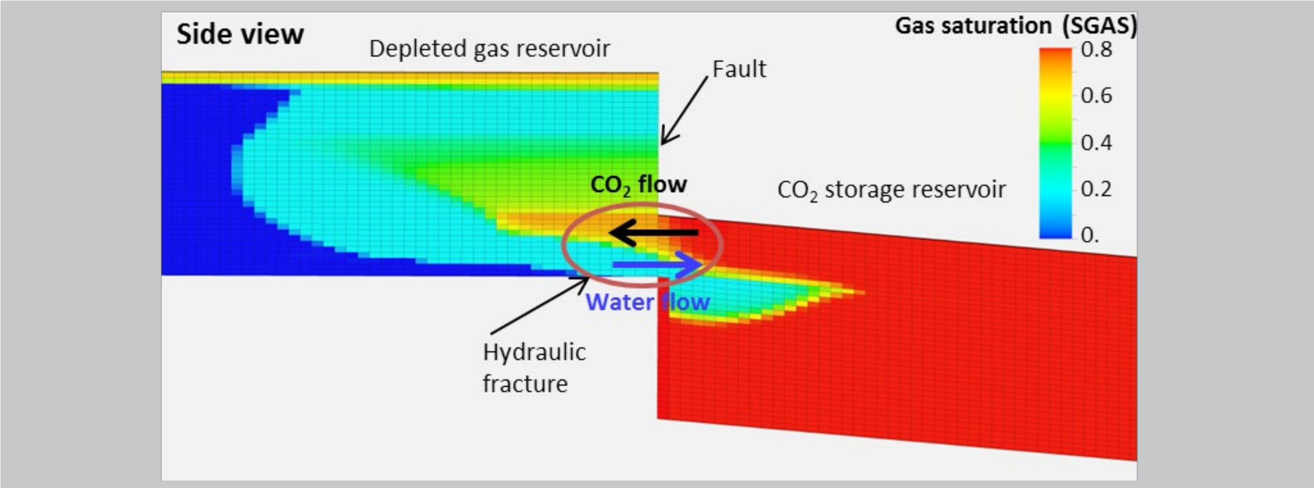

Figure 10 Gas saturation in the synthetic model after 10 years of remediation in case when the receiving compartment is an aquifer (scenario 12 in Table 1).

3.2 Real case

The base case remediation scenario for the real case (scenario 1 in Table 3) has two hydraulic fractures, which connect the shale zone below the receiving reservoir with the storage reservoir (Fig. 4b). In Fig. 11, the results of the base case remediation scenario are compared to the case without remediation. The pressure drop in the storage compartment without remediation is due to pressure dissipation after termination of CO_2 injection. In the scenario with remediation, the amount of CO_2 diverted away from the storage compartment is very small: only 20 thousand tonnes of CO_2 in 5 years. The receiving compartment already contains some CO_2 because the original hydrocarbon gas also contained CO_2. The resulting additional pressure drop in the storage compartment at the injection well is less than 2 bar. The main reason for the poor effects of remediation is the low reservoir quality of the zone in the receiving compartment where the hydraulic fractures are created.

In the geological scenarios (Table 3), we investigated the effect of the horizontal and vertical permeabilities on the remediation efficiency by increasing the horizontal permeability only by a factor of 100 (scenario 2), the horizontal and vertical permeabilities by a factor of 100 (scenario 3), and the horizontal and vertical permeabilities by a factor of 1,000.

In Fig. 12 the pressure is shown over a period of 5 years for all geological scenarios. The impact of an increase in vertical permeability is much larger (a decline of 51 bar compared to no remediation) than in horizontal permeability (a decline of 9 bar compared to no remediation). Overall, the remediation using fractures is not very effective in this case: even when the permeability is increased by a factor of 1,000, the pressure drops only 92 bar over 5 years.

Weak effects of remediation in the real case compared to the synthetic case (with the remediation duration of 1 to 16 months) are largely due to a much smaller permeability and NTG in the real case. In the synthetic case, vertical permeability (kz) is equal to horizontal permeability (kxy) and NTG=1, while in the real case kz is 100 times smaller than kxy and NTG=0.1. This explains why the method is more effective in the synthetic case than in the real case.

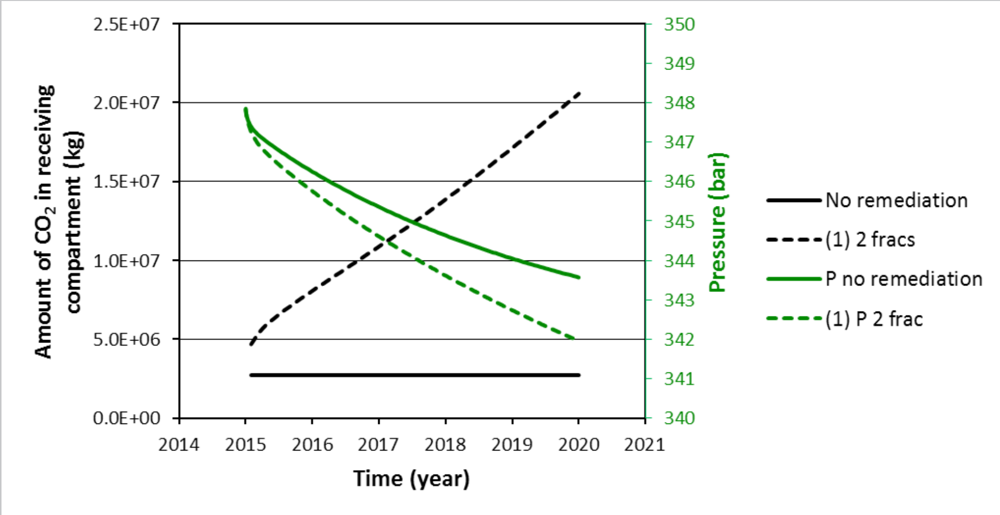

Figure 11 The amount of CO_2 in the receiving compartment (black lines) and the pressure in the storage compartment (green lines) for the real case without remediation and the real case with remediation with 2 fractures (base case remediation scenario 1 in Table 3).

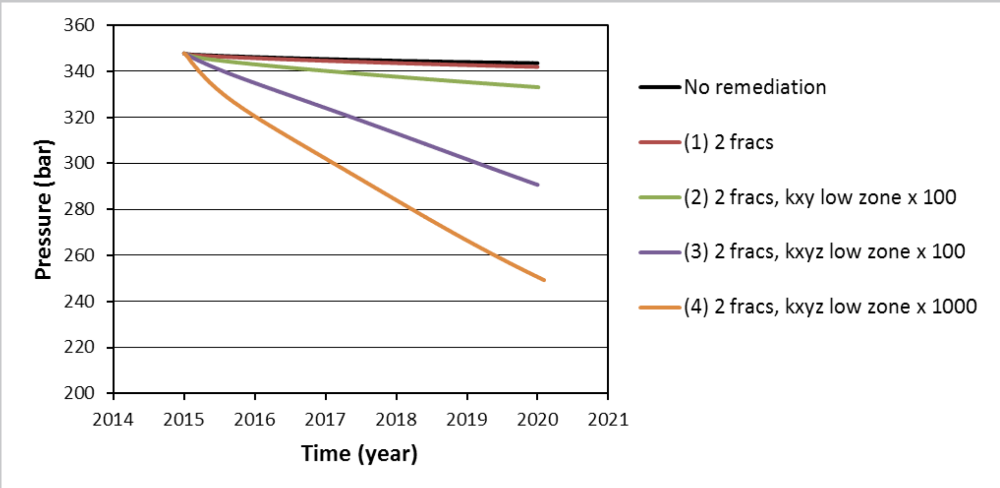

Figure 12 Evolution of pressure in the storage compartment for different geological scenarios (the real case, scenarios 1-4 in Table 3).

The results for the remediation scenarios 5-8 are summarized in Fig. 13. As can be seen, the remediation using a well (scenario 8) is much more effective than the remediation using hydraulic fractures (scenarios 5-7). The reason is that the well connects the CO_2-storage reservoir with a highly permeable upper part of the receiving reservoir rather than with the shale layers below the reservoir, which is the case for hydraulic fractures. In less than a year, sufficient CO_2 has been diverted through a deviated well to equilibrate the pressure in the two compartments. In reality, it would take somewhat longer, because the rates in the first month are unrealistically high (> 15 million sm^3/d). However, even assuming that the rates in this first month are half of the calculated rates, diversion of the CO_2 and equilibration would be fast.

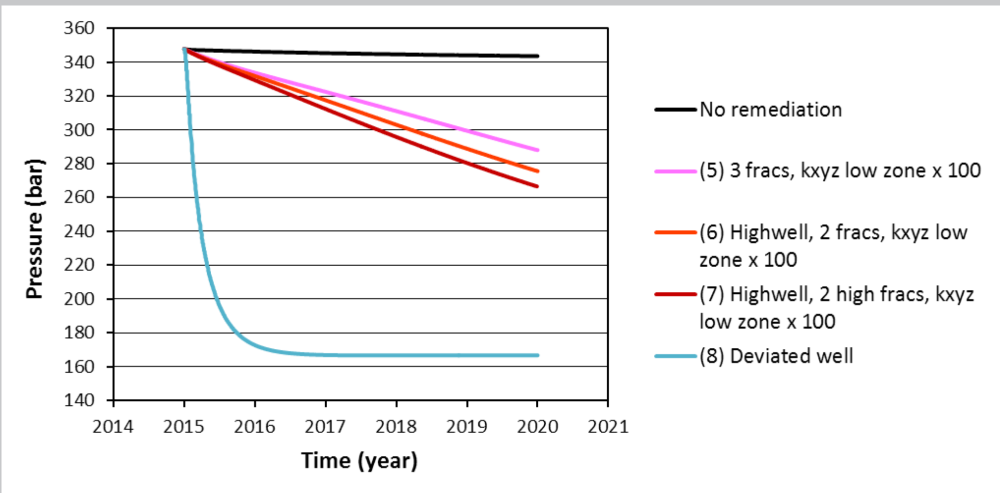

Figure 13 Evolution of pressure in the storage compartment for different remediation scenarios (the real case, scenarios 5-8 in Table 3).

For the scenarios with hydraulic fractures, Fig. 13 shows that adding additional fractures only marginally increases the efficiency of remediation (scenario 5). The efficiency improves when the fractures are created to connect to the upper, more permeable part of the storage reservoir because the reservoir permeability decreases with depth (scenario 7 with “high fracs” gives better effects than scenario 6).

4 CONCLUSIONS

In the case of unwanted migration of CO_2 from the storage compartment, pressure relief in the storage formation can be achieved by diverting the CO_2 to unconnected parts of the reservoir, or to the adjacent reservoirs and aquifers. Flow diversion requires creating a pathway for fluid migration between the two originally unconnected reservoirs, which can be achieved by hydraulic fracturing across the fault or by drilling a well or laterals. This paper evaluates the effects of flow diversion as a remediation option through numerical simulations of an idealized synthetic case and a real field case from the North Sea, which was modified and then used to simulate hypothetical remediation scenarios.

From numerical modelling it is clear that the key factors controlling the efficiency of flow diversion are the conductivity of the created pathways between the two reservoirs, the pressure difference between the reservoirs and the permeability of the receiving reservoir. In the case of CO_2 diversion into an undepleted saline aquifer, the remediation is relatively slow due to the small pressure difference between the CO_2 storage compartment and the receiving aquifer.

The simulations of the real case showed that the diversion strategy needs to be optimized taking into account site-specific parameters and in-situ conditions. In particular, CO_2 needs to be diverted to a zone of the receiving compartment with sufficient permeability. For the conditions evaluated in the real case, the remediation using a well is much more effective than the remediation using hydraulic fractures.

ACKNOWLEDGEMENTS

The research leading to the results reported in this paper received funding from the European Community’s Seventh Framework Programme (ENERGY.2013.5.2.1) under grant agreement no 608608 (“Mitigation and remediation of CO_2 leakage”). The project received additional funding from Statoil, ENGIE and Shell. The in-house simulator MoReS used in this study was kindly provided by Shell.

References

[1] IEA Greenhouse Gas R&D Programme (IEA GHG), Remediation of Leakage from CO2 Storage Reservoirs. 2007/11, September 2007.

[2] Esposito A, Benson SM. Optimization of remediation of possible leakage from geologic CO2 storage reservoirs into groundwater aquifers. SPE Western regional meeting, Anaheim, California, 2010. SPE paper 133604.

[3] Rohmer JR, Le Guenan TLG, Réveillère AR, Vong CQV. Remediation of CO2 leakage from deep saline aquifer storage based on reservoir and pollution engineering techniques. Second EAGE CO2 Geological Storage Workshop, Berlin, Germany, 11-12 March 2010.

[4] Réveeillère, A, Rohmer J, Manceau J-C. Hydraulic barrier design and applicability for managing the risk of CO2 leakage from deep saline aquifers. Int J Greenh Gas Con 2012;9:62-71.

[5] Manceau J-C, Hatzignatiou DG, Lary de L, Jensen DB, Réveillère A. Mitigation and remediation technologies and practices in case of undesired migration of CO2 from a geological storage unit – Current status. Int J Greenh Gas Con 2014;22:272-290.

[6] Karas D, Demić I, Kultysheva K, Antropov A, Blagojević M, Pluymaekers M, Orlić B. First field example of remediation of unwanted migration from a natural CO2 reservoir: The Bečej Field, Serbia. The 8th Trondheim Conference on CO2 Capture, Transport and Storage, Trondheim, Norway, June 16-18 2015.

[7] Ragab AMS. Improving well productivity in an Egyptian oil field using radial drilling technique. J Petrol Gas Eng 2013;4:103-117.

[8] Arts RJ, Vandeweijer VP, Hofstee C, Pluymaekers MPD, Loeve D, Kopp A, Plug WJ. The feasibility of CO2 storage in the depleted P18-4 gas field offshore the Netherlands (the ROAD project). Int J Greenh Gas Con 2012;11S:S10-S20.

[9] Pizzocolo F, Hewson CW, Ter Heege JH. Polymer-gel remediation of CO2 migration through faults and numerical simulations addressing feasibility of novel approaches. The 50th US Rock Mechanics / Geomechanics Symposium, Houston, Texas, USA, June 26-29 2016. ARMA paper 16-100.

[10] Warpinski NR, Teufel LW. Influence of geological discontinuities on hydraulic fracture propagation. J Petrol Technol 1987:209-220. SPE paper 13224.

[11] Wu H, Chudnovsky A, Dudley JW, Wong GK, 2004. A map of fracture behavior in the vicinity of an interface. Gulf Rocks 2004, Proceedings of the 6th North American Rock Mechanics Symposium, Houston, Texas, USA, June 5-9. ARMA/NARMS paper 04-620.

Section IV

REMEDIATION AND MITIGATION METHODS USING SEALANTS IN FAULT AND FRACTURES

Chapter XIV

Report to partners summarizing the choice of models (Use of sealant as a corrective measure to stop CO_2 flow through fault: review and work-plan)

Lahcen Nabzar[1], Marc Fleury[1], Sevket Durucan[2], Francesco Pizzocolo[3], Jan ter Heege[3], Lies Peters[3]
[1] IFPEN, France
[2] Imperial College, UK
[3] TNO, The Netherlands

SUMMARY

This document summarizes the approach that will be taken in the case of breach of the caprock, typically along a fault or a fracture zone. Here, we consider two methods: 1) methods using polymer based gels and 2) methods using foams or gel-foams.

The oil and gas industry has long-term experience in reducing the flow rate of a given fluid, or maximizing oil or gas recovery by injecting viscous fluids or foams with specific properties. The objective is to select or adapt such techniques for reducing or stopping the migration of CO_2 through faults and fractures.

In general, two potential leakage pathways will be considered: (i) Leakage through an areal sink, represented by a fracture zone in the caprock, (ii) Leakage through a line sink, represented by a fault extending through the caprock into the overlying formation. Polymer-gels are expected to be injected at the top of the caprock using a permeable layer. Foams or gel-foams are expected to be injected below the caprock at the top of the storage zone.

Laboratory work will be performed to define the best formulations and performances of polymers and foams. This work will be complemented by numerical simulations to study essentially the radius of effective intervention.

1 INTRODUCTION

This report is part of the research project MiReCOL (Mitigation and Remediation of CO_2 leakage) funded by the EU FP7 programme. Research activities aim at developing a handbook of corrective measures that can be considered in the event of undesired migration of CO_2 in the deep subsurface reservoirs. MiReCOL results support CO_2 storage project operators in assessing the value of specific corrective measures if the CO_2 in the storage reservoir does not behave as expected. MiReCOL focuses on corrective measures that can be taken while the CO_2 is in the deep subsurface. The general scenarios considered in MiReCOL are 1) loss of conformance in the reservoir (undesired migration of CO_2 within the reservoir), 2) natural barrier breach (CO_2 migration through faults or fractures), and 3) well barrier breach (CO_2 migration along the well bore).

This document summarizes the approach that will be taken in the case of breach of the caprock, typically along a fault or a fracture zone. We consider two methods: 1) methods using polymer based gels and 2) methods using foams or gel-foams.

Describing in some details the planned work performed by several teams from different institutions is an important step to insure a coherent and complementary approach at the beginning of the project, both in the laboratory and for numerical simulations. Hence, this document constitutes an important reference to guide the research efforts for the next two years.

For both methods, a brief state-of-the-art review is provided, essentially with publications originating from the oil and gas literature. For CO_2 applications, we can indeed benefit from a large knowledge from the Oil & Gas industry in which these techniques are used for many purposes. Then the scenarios envisaged are described, followed by a description of the models and/or the different steps for demonstrating the efficiency of these remediation methods, but also clearly stating their limitations.

2 METHODS USING POLYMERS

The oil and gas industry has long-term experience in reducing the flow rate of a given fluid, or maximizing oil or gas recovery by injecting viscous fluids or other fluids with specific properties. The objective of WP6 in the MiReCOL project is to select or adapt such techniques for reducing or stopping the migration of CO_2 through faults and fractures. Work includes the validation of a method in the laboratory, and the description of the possible range of action when injecting the sealant from a well. The latter is performed by numerical simulations. The possibility of accessing an out of range leaky location by hydraulic fracturing will also be considered.

2.1 Background and review of the state of the art in the use of gels in industry

Crosslinked hydrolysed polymer-gel injection is used in petroleum industry to improve conformity of fluid flow in the reservoir, remediate leakage around wells and also used in conjunction with the prospect of enhanced oil recovery under various temperature and pressure conditions [1, 2, 3, 4, 5, 6, 7, 8, 9, 10, 11, 12, 13, 14, 15, 16, 17] and to improve miscible CO_2 floods [18, 19].

The majority of field practice in applying gel treatments aimed to reduce channeling in high-pressure gas floods and to reduce water production from gas wells [20, 21, 22, 23]. Often referred to as relative permeability modification (RPM) or disproportionate permeability reduction (DPR) and water shut off (WSO) treatments, there are many examples of production performance modeling data for gel treated wells in the literature [24, 25]. In the early days of the technology, RPM treatment was mainly used in controlling flow in matrix-rock porous media. More recent research have reported successful treatment of fractured rock where relatively strong gels impart RPM/DPR to fluid flow within gel filled fractures and achieve total shutoff [13].

Hydrolysed polyacrylamide (Figure 1a), in various proportions, is one of the widely used polymers within the petroleum industry [26, 27]. The polymer exists as loose molecular chains in the aqueous solution. When appropriate crosslinker is added, these polymer chains are aligned and this polymer solution is turned into a solid gel which resembles the structure illustrated in Figure 1b. Metal ions such as Cr^{3+} [28, 29, 30, 31] and Aluminum [32, 33] are widely used as a crosslinkers, although occasional use of organic crosslinkers such as formaldehyde [34] was also observed. Polyacrylamide based-gel solutions are used in the industry to selectively shut off undesired gas influx in production fields [35, 12, 36, 37] and sometimes in combination with other surfactants [38]. Application of polyacrylamide-gel solution for modifying injectant flow profile are also noted [39] in addition to remediating non conformal flow within the reservoir [40].

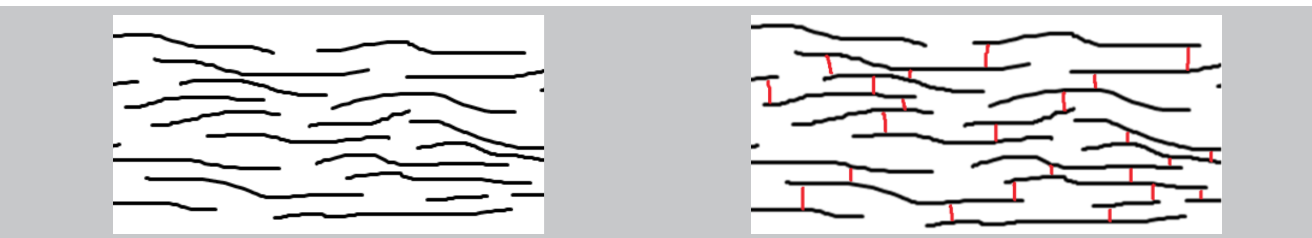

Figure 1 (a) Artistic representation of polymer chains in carrier fluid and (b) effect of crosslinker on the arrangement of polymer molecules in the solution.

The rheological characteristics of polymers injected into the subsurface reservoir are modified in time either by adding an additive, or just by interaction with the environment such as variation in temperature, pressure or surrounding fluids. These changes are observed to be accomplished either through the injection of individual components ie., monomer, cross linker and other additives or through injection of crosslinked polymer directly into the reservoir [41].

The time taken for hydrolysed polymer to be converted into polymer gel upon the addition of cross linker is generally termed as gelation time, which is also an indicator of the possible penetration of the injected polymer gel solution into the reservoir before it solidifies. Gelation time is also defined as the time when the elastic and viscous moduli of the gel are equal [42]. This time is dependent on the characteristics such as chemical composition, molecular weight and concentration of the polymer, temperature and cross-linker type. Hence, the temperature and salinity of the reservoir are important factors in the selection of appropriate concentration of a polymer and the cross-linker. Addition of organic ligands and pre formed Cr^{3+} complexes with suitable ligands added to the polymer solution were found to control the gelation time over the temperature range of 60-135 °C [43]. Furthermore, aqueous solution of dilute polyacrylamide was reported to be reasonably stable under shear. The stability of a polymer-gel system was reported to be dependent on the stability of polymer molecules themselves [44, 45].

Preliminary laboratory characterisation and assessment for field application of one polyacrylamide based polymer gel system was carried out as part of the EU funded CO_2CARE project. The important conclusions of the work are summarised here:

1. The gelation time decreases with increase in polyacrylamide concentration; furthermore, for identical combination of polyacrylamide and Cr^{3+}, the gelation time was found to decrease with increase in temperature.
2. CO_2 permeability reduction of more than 99% can be achieved in high permeability sandstones
3. An increase in irreducible brine salinity generally leads to the destruction of the polymer chains and a notable reduction in permeability. However, almost 90% reduction in permeability was still achieved in higher salinity environments (12 to 25%).
4. Water slug experiments in the laboratory have confirmed that the negative impact of high salinity on permeability reduction in aquifers can be reduced by this technique.

In summary, high molecular weight, anionic and hydrolised polymer chains such as poly acrylamide along with a cross linker can be used to remediate leakage of CO_2 if the area of influence is carefully evaluated and the injection process designed accordingly.

The design of an efficient remediation strategy using polymer gel for possible CO_2 leakage would depend on engineering the gelation time of the polymer and crosslinker combination for the targeted subsurface reservoir conditions, which would be investigated though the current research.

2.2 Envisaged scenarios

Two storage models will be used in the study: the Imperial College Saline Aquifer Model (ICSAM) model and another model representing a typical reservoir containing a fault, here named Px model. In general, two leakage pathways will be considered:

- Leakage through an areal sink, represented by a fracture zone in the caprock
- Leakage through a line sink, represented by a fault extending through the caprock into the overlying formation

The polymer gel is intended to be injected in one permeable layer in the overlying structure above the caprock.

Previous research has shown that gelation time and effectiveness of polymers depend on temperature, pressure and salinity of the reservoir fluid. Therefore, for each leakage pathway, the following key features will be considered and implemented to form a number of modelling scenarios:

- Storage reservoir depth (formation pressure and temperature)
- Caprock thickness/distance to the permeable layer above the storage reservoir
- Permeable layer permeability/porosity
- Permeable layer brine salinity

Polymer gel injection scenarios will investigate the effectiveness of the selected polymers in terms of:

- Radius of effective intervention for different polymer types and concentrations
- Composition of the leaked CO_2 plume and CO_2 mobility with and without polymer-gel remediation

In leakage scenario simulations, the amount of CO_2 leaked out of the target storage reservoir at a selected location is continuously monitored, and the injection is terminated once a pre-set detection threshold is exceeded. The leakage, however, is allowed to continue until its source (the free CO_2 in the storage reservoir available for leakage) is exhausted to yield the total leakage potential. In this way, potential leakage risk profiles through the leaky caprock/faults may be established to provide a benchmark for evaluating the effectiveness of any remediation measure.

In a study of a depleted gas field, several CO_2 migration scenarios have already been studied by Vandeweijer et al. [46], to determine the risk of migration of CO_2 through the overburden. In particular three migration paths had been taken into account: through the aquifer reservoir spill point, through an induced fracture into the primary seal with a migration of CO_2 into the overlying sandstone and, finally, through a wellbore shortcut. For these migration analysis a Petrel model of the overburden was constructed. Vandeweijer et al. [46] concluded that for the depleted gas field studied the most plausible migration pathway of the stored CO_2 to the surface was via leaking wells; a pathway that developed within the overburden was considered highly unlikely.

Following the results presented by Vandeweijer et al. [46], we have constructed a model of reservoir plus cap rock structure and geology that is best suited to simulate the case of CO_2 leakage through existing faults, using induced hydro-fractures to transport the sealant to the leaking location.

2.3 Numerical modeling of gel remediation

The main requirement of the reservoir model(s) are: inclusion of a caprock and the presence of at least one permeable layer in the overlying structure above the caprock where polymer solutions can be injected. The second requirement is the presence of migration pathways through the caprock, in the form of fracture zones or faults.

2.3.1 ICSAM Model

Leakage through an areal sink represented by a fracture zone in the caprock

Guided by the above model requirements, the Imperial College Saline Aquifer Model (ICSAM) developed in CO_2CARE project has been chosen as the base model to carry out the polymer injection scenarios for the areal sink case.

The ICSAM model measures 36 km x 10 km and includes several faults (Figure 1a). The depth of target storage formation ranges from 1,082 to 3,484 m across the model domain, dipping considerably. The injection well is located at a location where the storage reservoir is between 1,973 to 2,181 m deep (Figure 2a). The model has a more or less uniform grid block size of 200 m x 200 m in the lateral direction.

The storage reservoir, which has a thickness of approximately 240 m, consists of 6 layers of varying properties both within each layer and across the layers. The overlying formation (caprock) is considered to be impermeable, except for a 60 m thick layer situated at 180 m above the reservoir, which is assigned a permeability of 10 mD (Figure 2b). The reservoir/overburden is initially at hydrostatic pressure, and the reservoir temperature is 92 °C.

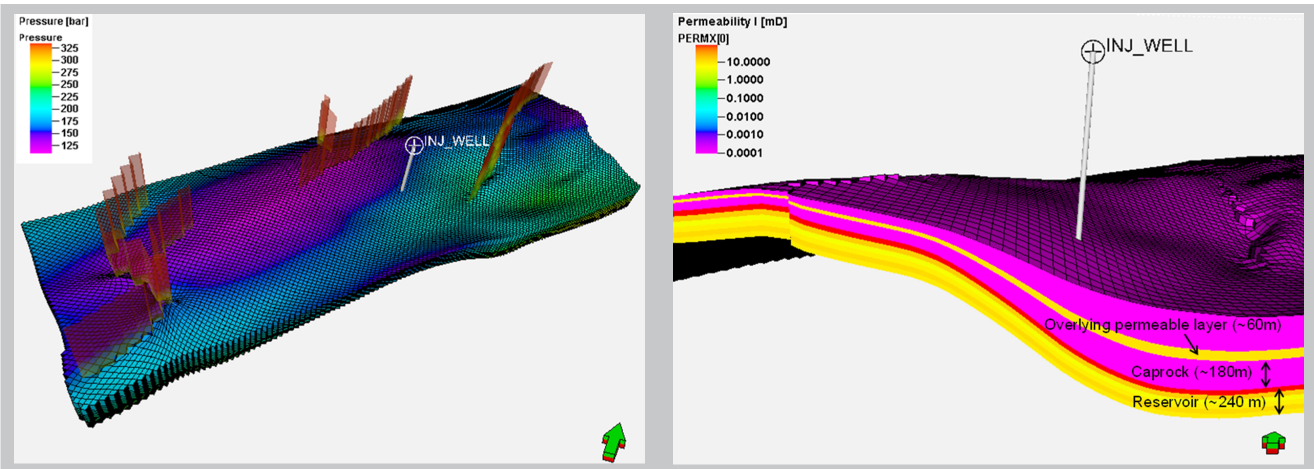

Figure 2 Imperial College Saline Aquifer Model (ICSAM). (a) Hydrostatic pressure distribution, (b) A close-up showing the caprock and overburden layers.

2.3.2 Notional storage model

There are already many different mitigation and remediation technologies to apply in case of unwanted migration of CO_2 from CO_2 geological storage units. Some of them have already been used in real cases, while others only in laboratory tests. An interesting overview of these different techniques can be found in Manceau et al. [47] (2014). The characteristics, the viscous, mechanical and chemical properties of polymer gels match perfectly the needs of a method to mitigate leakages. Our idea is to create and use hydro-fractures to transport the sealant gel to the leaky fault to mitigate or remediate the CO_2 leakage. Another interesting option would be to stimulate a horizontal hydro-fracture to create a sort of blanket that act like an impermeable barrier (see Figure 3). This would be possible only for shallow reservoirs in which the vertical stresses horizontal fractures to be formed.

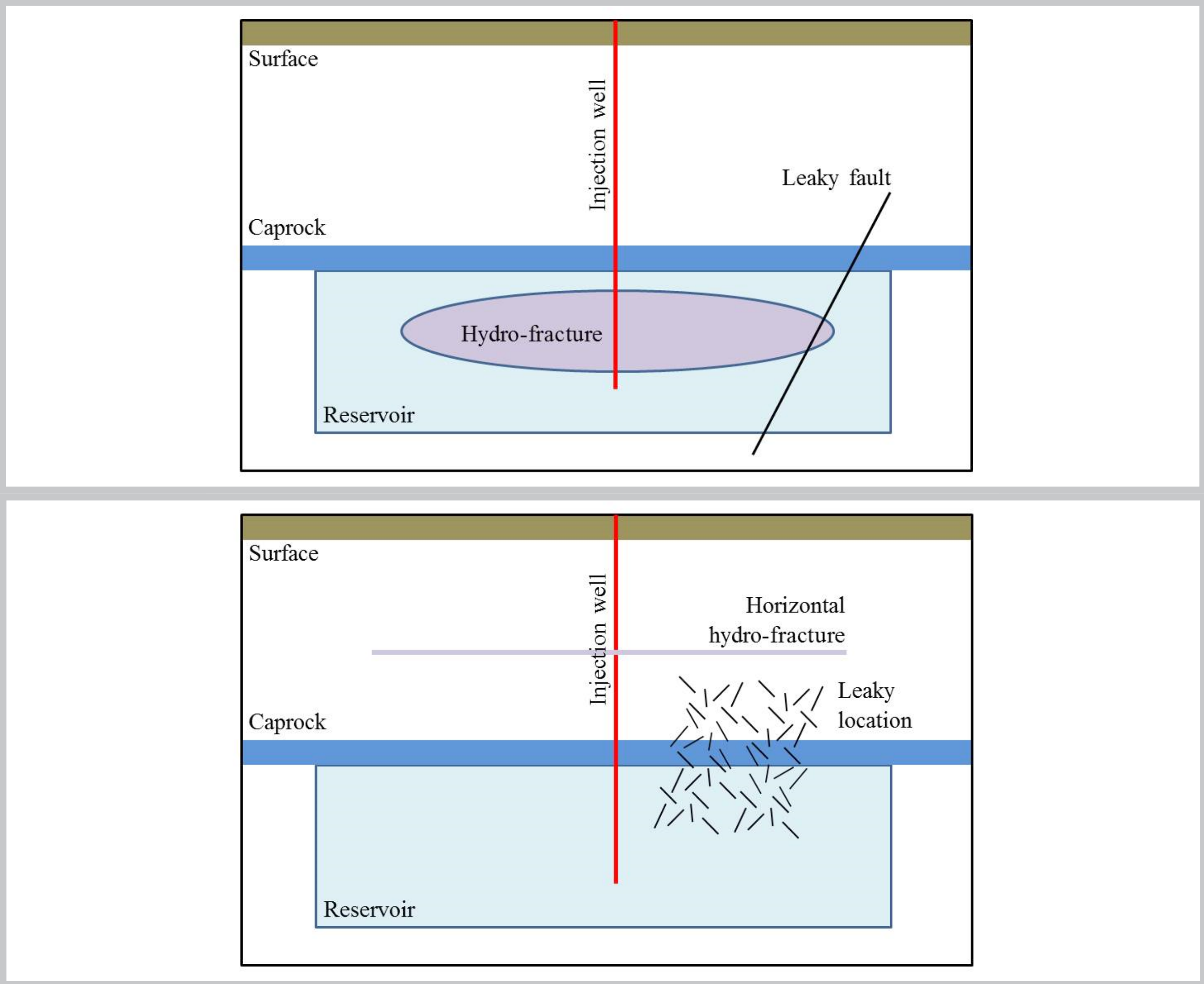

Figure 3 Schematic representation of the methods.

We will perform the numerical simulations with the software MFRAC. After creating the 1D geomechanical model, such as shown in Figure 3, we will import the 1D model into the software and we will try different kind of injection rates and replace the proppant by polymer based gels. Playing with different viscosity, mechanical and chemical properties of the gel and with different injection rate of the fluid, we want to study how far, how well and how accurate we can transport the sealant to a leaky location. The aim of this work is to define which parameters control the effectiveness of the two methods that we proposed, to allow operators to use these solutions also for other fields.

2.4 Summary

The injection of polymer gel will be studied, with the objective of reducing CO_2 leakage through the caprock. Two leakage situations are considered:

- Leakage through an areal sink, represented by a fracture zone in the caprock
- Leakage through a line sink, represented by a fault extending through the caprock in to the overlying formation

The required characteristics of the polymer gel will be studied in the laboratory: gelation time, crosslinker combination for the targeted subsurface reservoir conditions. The large experience gained in the oil and gas industry will be used for the choice of the best adapted polymers.

Large scale numerical modeling will be performed to study the effectiveness of the method. For this purpose, two models will be used: a saline aquifer model (ICSAM) and a model of a notional storage site that includes reservoir, cap rock and overburden.

3 METHODS USING FOAMS

Foams have been used in Enhanced Oil Recovery (EOR) as the most promising and cost effective means to alleviate the drawbacks associated with gas-based EOR processes such as viscous fingering, channelling, gravity override and early gas breakthrough.

Indeed, generation of strong foams could drastically reduce gas mobility improving volumetric sweep efficiency.

Foams can be used for in-depth gas mobility control, as blocking agents (thief zones, Gas-oil-Ratio reduction) and conformance control (fractures, large permeability contrast, and layered reservoirs). Thus, besides their use for EOR purposes, they can be also used to secure gas storage operations through gas confinement and gas leakage prevention/remediation. Indeed, one can increase considerably the apparent viscosity by injecting water with a foaming agent. In this situation, the simultaneous flow of gas and water will generate a foam depending on certain conditions. The onset of a foam depends primarily on the gas to liquid velocity ratio, and also on the choice of surfactant quality and concentration.

We propose to study in the laboratory the conditions of generation of a CO_2-brine foam in a fracture and to study using numerical simulations the conditions for accessing the bottom of the fracture in the caprock.

3.1 State of the art

Although a significant volume of theoretical, laboratory and pilot work has been dedicated to foam processes [48, 49, 50, 51, 52, 53, 54, 55, 57, 58], it is still a developing technology and significant uncertainties still remain regarding the actual physics underlying foam generation/ propagation in porous media. The main challenges are to bring this promising technology to the field and to perform field trials and pilots. This requires being able to probe the feasibility and predict the effectiveness and the added value of this method compared to other means to justify the associated investments and risks. In turn, this requires an effective synergy between simulations and experimental work in order to convert laboratory data to reliable field scale predictions.

Regarding CO_2 storage operations, gas confinement is of outmost importance to ensure that such process can be used as a safe and effective solution for greenhouse mitigation. A clear insight on the associated risks, their sound evaluation and the development of means for their prevention and mitigation are thus needed. Among these risks, CO_2 leakage through/along wells, faults and fractures and through the sealing cap-rock are the most important to consider. Indeed, due its low density and high mobility, gas might potentially migrate out of the storage zone towards the upper formation due to gravity segregation and finally might leak into the atmosphere. This leakage potential is mainly dependent on well and sealing cap rock integrity.

Due to their ability to preferentially restrict fluid flow in the most permeable areas, foams are particularly indicated to address the leakage from high-permeability areas or through fracture and fissures that are considered as the most important leakage pathways [59].

3.1.1 Brief on foam description and use

As mentioned above, foams could be used for different purposes including gas mobility control, conformance improvement and as blocking agents. For each application, specifically designed foam systems should be designed to meet the application requirement under controllable conditions. For in depth gas mobility control for example, a "weak foam system" providing moderate gas mobility reduction is preferable as it requires to be propagated deeply inside the reservoir. In turns, "strong foam system" opposing high resistance to fluid flow up to its complete plugging is required for conformance improvement and blocking purposes of specific areas.

3.1.1.1 General aspects

A foam system classically consists of water continuous phase and dispersed gas (bubbles) at a given volumetric fraction usually termed foam quality. Gas bubble formation requires a certain amount of energy (shear) and are stabilized by foaming agents (surfactant) that are classically dissolved in the water phase (but could be also in the gas phase: CO_2).

The characterization of foam in bulk solution is usually based on several properties such as [60]:

- Foam quality or the volumetric gas fraction. Foam with large foam quality (that can be as large as 97%) are referred to as dry foams while wet foams are those with low foam quality. There exists an upper foam quality limit above which foam collapse (dry out effect). For EOR, usual foam quality are between 70 and 90%.
- Foam texture that refers to gas bubble size. At the same foam quality, more finely "textured" foam contains a larger number of bubbles and lamellae (see section 3.1.1.2).
- Bubble size distribution
- Stability that is usually quantified by the foam half-life parameter that measures the time for a column of foam to decrease to the half of its initial height.

Among these properties, the stability is of utmost importance for foam application. Foams are dispersed systems and, as such, they are intrinsically unstable with time. However, for gas mobility control in EOR, foam should be stable and propagate inside the reservoir and for conformance and blocking purposes, they should remain stable in place for a given time that ensure the economic viability of the process (frequent treatment could be detrimental to the economics).

The stability of foam is mainly dependent on the chemical and physical nature of the surfactant (or surfactant formulation) used as foaming agent, but of course also on the system nature (gas, brine and oil for EOR operation) and application conditions (P, T and formation properties: mineralogy, permeability, etc.).

Finally, foam usually has a low density compared to the liquids present in the injection formation. Several applications (gas coning prevention and GOR reduction, injection of low interfacial-tension formulation in the gas cap) take advantage from this property for foam emplacement in the targeted upper part of the reservoir.

3.1.1.2 Foam behavior in porous media

Foam generation and transport in porous media result from a dynamic equilibrium between lamellae creation and destruction. This equilibrium determines foam texture in porous media, that is usually different from that in bulk solution, and which, in turn, governs to the flow behavior (finely textured foams with a large number of lamellae are expected to induce higher resistance to flow). Foam stability equilibrium could be impacted by a huge number of parameters including reservoir properties (rock type, K, heterogeneity, wettability, P, T), fluid properties: oil/gas/brine (compositions, density and saturations), surfactant properties (nature and concentration) but also fluid/fluid and fluid/rock interactions (adsorption, solubility/partition, dissolution). Foam destabilization could result from several effects including excessive film thinning and rupture, diffusion of gas from smaller bubbles into the larger bubbles (coarsening or Ostwald effect), lack of surfactant because of excessive adsorption on the surface of reservoir rock or precipitation due to adverse brine salinity and hardness, high capillary pressure and presence of oil61.

Currently, large uncertainties and incompletely understood areas still remain regarding the actual physics underlying foam flow in porous media. Though the previous studies [49, 50, 51, 52, 53, 54] did not allow to propose a comprehensive and satisfactory physical modeling of foam flow and propagation, they allowed to come up with a general, yet useful, phenomenological description of the rheological behavior of foams in porous media:

Foam generation and stability

- Lamellae creation results from different mechanisms such as leave-behind, snap-off and lamellae division [52] (see Figure 4)..

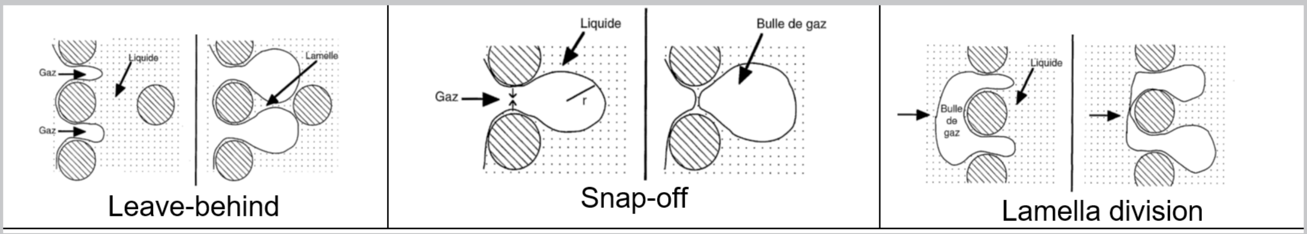

Figure 4 Main lamellae generation mechanisms

- Lamellae destruction and film rupture result mainly from: capillary pressure (when $Pc{=}Pc{*}{=}\ P_d^r$, critical disjoining pressure) [55], oil impact if present (nature and saturation: existence of a critical saturation) [61,62], very low water saturation (below a critical value S_{wmin}), insufficient or excess shear and from gas trapping (depending on fluid saturation, pressure gradient and pore structure).
- Two categories of foams are usually distinguished: "weak foams" and "strong foams". The transition between the two types of foam is often abrupt and requires a minimum pressure gradient (ΔPc [49] or a minimum critical velocity Vc [49]. Weak or coarse foams induce only low resistance to flow (low gas mobility reduction factor, or MRF) while strong foam leads to much larger resistance to flow (with non-dense gas like N_2 the induced MRF can reach values greater than 1000). For CO_2, the mobility reduction factor is usually much lower and the maximum attainable value decreases rapidly with CO_2 density [63, 64, 65]. With supercritical dense CO_2 it was inferred from laboratory study, using classical foaming agent, that probably only coarse foams-emulsions could be formed. However, more recent results [62] showed that, even with dense-CO_2 and using dedicated surfactant formulations, gas mobility reduction factors as high as 25 could be obtained indicating the formation of strong foams.

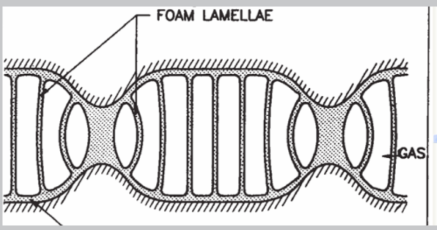

Figure 5 Bubble trains in a pore

Foam flow: rheology and transport

- In porous media, foams consist mainly in “bubble trains” that increase gas viscosity/ decrease gas mobility.
- The resistance to gas flow is usually evaluated using the gas *MRF* calculated as:

$$MRF = \Delta P_{Foam} / \Delta P_{no\ Foam} \quad (1)$$

  - *MRF* determined by the resistance of the lamella to coalescence
  - Apparent foam viscosity is due to pressure required to displace bubbles:
    - Continuous gas foam causes high mobility or low apparent viscosity
    - Discontinuous gas foam causes low mobility or high apparent viscosity

$$\mu_{app} = (Krw.\Delta P)/(Vint.\Phi.L) \quad (2)$$

where μ_{app}: apparent foam viscosity; Krw: effective brine permeability at residual oil saturation; *Vint*: interstitial velocity (= $Q/S\Phi$); Φ, L: porosity and core length

- Strong foam flow exhibits two flow regimes depending on foam quality *fg* [$fg = q_g/(q_g+q_w)$] (high quality regime and low quality regime). The transition occurs at an optimal foam quality *fg** corresponding to the critical capillary pressure *Pc** and to the maximum in pressure drop. Below *fg** (wet foam with low quality), the pressure drop is almost independent of liquid flow rate and above *fg**(dry foam with high quality) it becomes almost independent of gas flow rate (Figure 6) [56, 66].

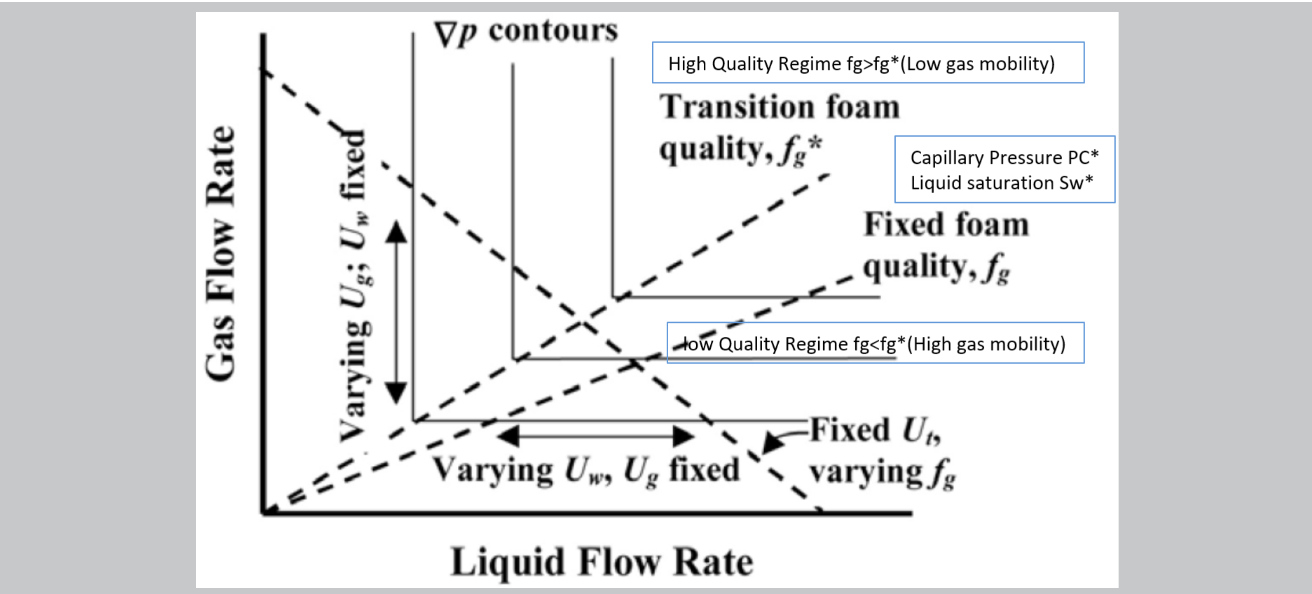

Figure 6 The two flow regimes for strong foams [56]

Thus, according to this view, the foam-induced pressure drop usually exhibits a maximum when plotted against foam quality [56, 63, 67, 68]. This maximum is reached at the optimal foam quality *fg** that depends on system characteristics and especially on formation permeability, surfactant and flow rate. This optimal foam quality is a very important parameter to determine for a given application case. It has been demonstrated that for strong foam generation, a minimum pressure gradient or a minimum critical velocity is

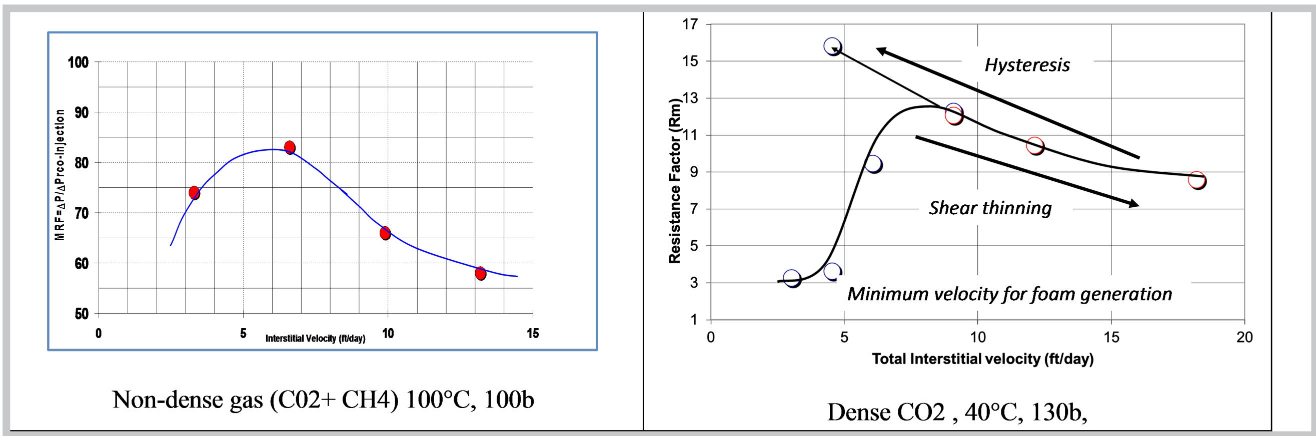

Figure 7 Typical foam rheological behavior (IFPEN results).

required [49]. Once these strong foams are generated inside the porous media, their rheological behavior shows the following main trends:

- First, MRF increases with increasing velocity up to a maximum.
- Then, MRF decreases upon further increasing the velocity beyond the maximum (shear thinning behaviour).
- Finally, MRF shows an hysteresis effect when the velocity is decreased.

Most of the foams exhibit the shear thinning behavior. This is an important advantage for the use of foams in EOR for sweep improvement. Indeed, foams are usually generated in situ in the near wellbore area where the velocity is high, leading to low MRF that mitigate the injectivity issue. Far way from wellbore, the velocity decreases leading to higher MRF with better sweep efficiency. Such typical rheological l behavior is illustrated on Figure 7.

Foam flow modelling

Several approaches have been proposed to model foam flow in porous media. These include empirical, semi-analytical and mechanistic approaches. Mechanistic approaches are based on the dynamic mechanisms of lamella generation/destruction and make use of population balance equation for bubbles [48, 69, 70, 71, 72, 73, 74, 75]. They attempt to take into account the space-time variation of foam structure/properties and their relation to rheology. These models use conservation and rate equations for bubbles and take into account trapped gas. The use of such comprehensive models is however limited due to the number of parameters that are difficult to obtain, measure and scale-up at larger scale. The semi-analytical approach is based on the application of fractional flow theory of Buckley/Leverett to foam flow [76, 77]. This approach has of course the limitation of the fractional flow theory. Though this type of model is able to reproduce the general foam behavior described above, its use for foam is limited due to the assumptions used. Therefore, in the absence of a comprehensive, simple, yet useful, physical modeling of foam flow in porous media, only the empirical approach is currently used in most of the reservoir simulators. Within this approach, based on the local steady-state model, the effect of foam on gas mobility is modeled through a simple modification (parameterization) of the relative gas permeability in presence of foam using a functional form FM

$$[Krg^{foam}(S_g) = FM.K_{rg}^{no\text{-}foam}(S_g)] \quad (3)$$

Thus, the functional form FM controls the gas mobility reduction in presence of foams and is written as follows [78]:

$$FM = 1/(1+(Mref\text{-}1) \times F1 \times F2 \times F3 \ldots Fn) \quad (4)$$

The functions Fi $(0 \leq Fi \leq 1)$ take into account the contribution of the main parameters impacting the gas mobility. If all the Fi's are set to unity, then $FM = Mref$. $Mref$ is the maximum gas mobility reduction factor that could be obtained from the gas MRF obtained from laboratory experiments (see eq. (1)).

For example, if we consider only the impact of surfactant concentration (F1), water saturation (F2), capillary number (F3) and oil saturation (F4), FM becomes:

$$FM = 1/(1+(Mref\text{-}1) \times F1 \times F2 \times F3 \times F4) \quad (5)$$

Such an empirical model has no predictive abilities and needs to be calibrated (Fi determination) for each application case before its use [66]. It cannot describe the variability in foam properties with time and space inside the reservoir as it does not include any actual physics of foam process.

Simulation at pilot and field scale of foam process is a perquisite to convert laboratory data into field predictions, as well as for foam process optimization. Such optimization includes:

- Injection strategy to maximize oil production and/or for a proper emplacement and a clear identification of the targeted area for conformance and blocking purposes.
- To optimize the volume to be injected which is of the utmost importance for the economics of the process.

Foam use

Foams have been widely used during EOR operations both for conformance improvement and in-depth gas mobility control, with varying success. The main successes were for conformance purposes while disappointing results were obtained for in-depth gas mobility control. A detailed literature review, including pilot trial analysis, is available in the literature [53, 87].

Foams have also been tested, both at laboratory and pilot scale, as blocking agents mainly for GOR reduction through gas coning limitation [79, 80, 81, 82, 83]. For underground gas storage, the use of foams to improve and secure these operations has been investigated by several authors [84, 85, 86]. The objective of using foam in these operations is to prevent gas leakage or the increase the storage volume. Foam could also be used to block water flow or to modify gas mobility. The use of foam for gas leak remediation during gas storage operations could greatly benefit from the experience gained from the use of foams as blocking agent in the oil industry, especially for conformance issue remediation and GOR reduction through gas coning limitation from the gas cap.

For the use of foams as gas flow blocking agents, the foam emplacement and its resistance to gas flow as well as its durability and stability are of the utmost importance for the efficiency and economics of the process. Though the use of "classical" foams for controlling excessive GOR has been considered as a promising technology [81, 83, 88, 89], it was shown that these foams have limited lifetime (weeks to months) and the treatment often needs to be repeated [89]. Cubillos et al. showed that stable foams are formed in a sand pack plug with alkyl olefin sulfonate (AOS C14-16) by injecting gas at 2 m/d behind a surfactant slug. The pressure drop reached was about 35 bar with an estimated mean value of MRF of about 100. However, when the gas rate was increased to 4 m/d, a rapid foam decay was observed with a decrease of MRF by a factor of about four after 20 PV were injected (the pressure drop fell from 35 bar to only 8 bar over six days). Thus, the classical foams:

- are unlikely to completely block gas flow,
- provide only limited durability and stability with time,
- do not induce residual permeability reduction after foam decay.

These aspects are even more crucial in the case of the use of CO_2-foams for gas leakage prevention/remediation during CO_2 storage operations. Indeed, compared to other foam systems like N_2-foams or natural gas-foams, CO_2-foamss usually generate much lower MRF due to the impact of CO_2 on the interfacial tension [49, 62, 63, 64, 65]. In addition, the CO_2-foam-induced MRF are very sensitive to the CO_2 density and thus to injection and reservoir conditions of pressure and temperature [65]. Solbakken et al. [65] studied the impact of CO_2 density on MRF using AOS-based foaming agents and found that the MRF is strongly affected by the supercritical CO_2 ($scCO_2$) density, with MRF values of about 55 at a density of around 0,2 g/cm^3 and less that 5 at a density of 0,85 g/cm^3, the latter value indicating the presence of only coarse foam. Chabert et al. [62] infered from a laboratory study that $scCO_2$-dedicated surfactant could improve $scCO_2$-foam resistance to flow and showed that MRF as high as 23 could be reached even with high CO_2 density. However, even such MRF are not high enough to block gas flow and to consider CO_2-foams as a promising method for gas leak blockage.

Alternatively, several improvements have been proposed with the objective of increasing the foam system strength, its resistance to gas flow and its durability once emplaced in the targeted area. This includes mainly polymer enhanced foams (PEF) and gel foams [89, 90, 91, 92]. From these previous studies, gel-foam appeared to be the more promising technology for gas flow blockage, but it requires a careful design together with an optimization of the strategy of injection and emplacement. This, in turn, requires a tight synergy between laboratory experiment for the design and testing and simulation for the process optimization.

3.1.2 Brief on gel foams

Gel foam: what is about?

Gel foams consist in forming foams by creating and stabilizing gas bubbles in a liquid solution that is able to undergo gelation. Foam is formed and stabilized using a foaming agent (surfactant). The liquid solution usually consists of a solution of high molecular weight polymer with reactive ends (ionic groups for example) distributed along the molecular chains. Gelation is provoked by incorporating in the polymer solution a specific crosslinker that is able to react with the polymer reactive ends to form intermolecular bridges and polymer gel. Initiation of this gelation reaction is usually controlled using a delaying chemical agent (ligand) that is also incorporated in the polymer solution at the desired dosage. Thus, a gel-foam formulation (liquid solution) usually contains:

- A polymer with reactive ends along the molecular chains,
- A crosslinker,
- A delaying ligand, and
- A surfactant (foaming agent).

This liquid solution is, of course, to be customized (formulated and optimized) for the targeted application to reach the desired objectives.

Gel foam: what is it for?

For EOR and well productivity improvement gel-foams are used as blocking agent to prevent fluid flow (gas or water) into or out of an undesired area. Thus, gel-foam could be used to block thief zones, for conformance control in fractured/layered reservoir or in presence of high permeability contrast. One of their most interesting and promising applications is to increase well productivity through GOR reduction by blocking gas influx. Similarly, they could be used also for confinement purposes to prevent CO_2 leak across the cap-rock in a CO_2 storage reservoir. Taking advantage from their low density, gel foams could be placed toward a gas gap for gas coning blocking or just beneath the cap rock as sealing agent of leakage zone through the cap rock.

However, gel-foam application is a very complex process that requires careful and thorough investigation and optimization to produce a customized, effective and safe solution for a given reservoir application. Two main issues should be mentioned here and are actually common to all the in-situ gelation processes: injectability of the delayed gel-foam that, actually is a PEF, and placement.

Indeed, gelation is initiated in-situ once the non-gelled foam (PEF delayed foam) is placed in the area targeted to be blocked. Delayed gel-foams should be strong and stable in order to be propagated inside the reservoir and to form strong gel upon gelation initiation. Such strong delayed gel-foam, or PEF foams, should however exhibit acceptable injectability (to avoid exceeding reservoir fracturing pressure for example or to avoid excessive injection energy cost). The second issue is related to the emplacement and is more difficult. To take benefit from the process, it is a prerequisite to create gel only in the targeted area and to avoid blocking unwanted ones. Therefore, developing a customized gel-foam solution for a given application requires a good reservoir knowledge and careful and extensive optimization study as a function of product (polymer, surfactant, crosslinker, delaying agent) nature and concentration, injection conditions (flow rate, foam quality) and reservoir properties.

3.2 Scenario

The basic scenario is that injection of gel-foam takes place below the caprock from a well as close as possible to the leaky fault (Figure 8). Typically, the well is a rescue well rather than an existing one. Indeed, it is unlikely to drill a well close to a fault, unless such fault/fracture has not been detected initially. Due to a large density contrast, the gel-foam will migrate upward and reach the base of the caprock, where it can block the gas flow. The distance between the injector and the leaky fault is an important parameter that will be determined during the study. A key parameter for the propagation of the foam around the well is the adsorption of the surfactant on the rock mineral surface.

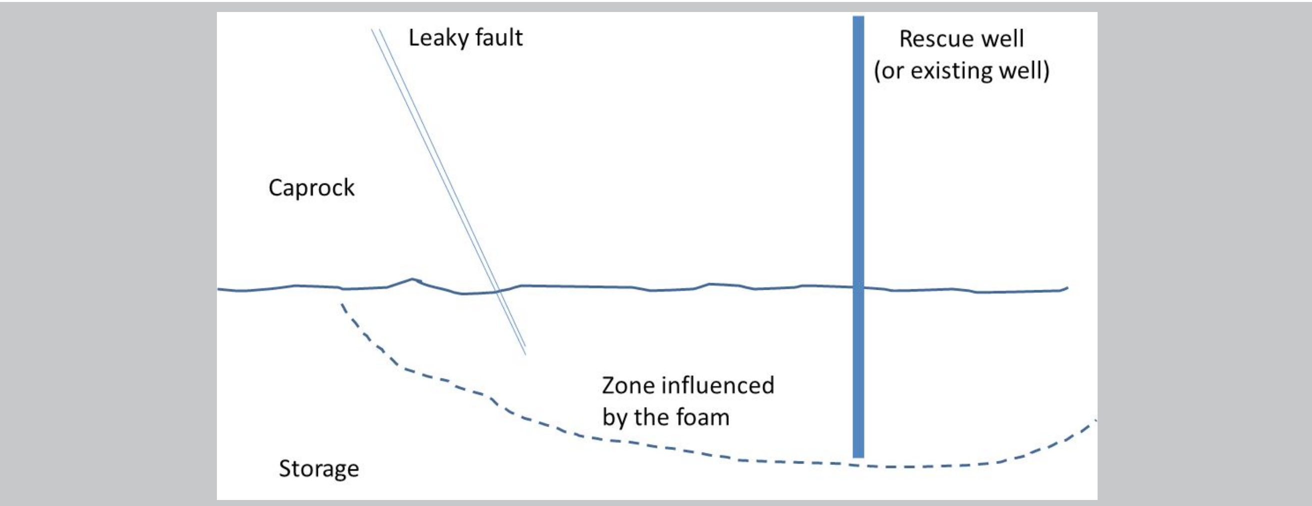

Figure 8 Schematic of the scenario envisaged for gel-foam remediation.

In the study of gel-foams, we will not consider a specific storage model due to the limited radius of influence that are inherent to these methods. For these reasons, it is sufficient to use generic models in which a layer of uniform porosity and permeability is implemented.

3.3 Study of gel-foam

As detailed above, the gel-foam technology appears to be a much better solution than foam alone for blocking fluid motions in a certain area. Although it combines two technical difficulties (foam and gelation), gel-foams have the essential advantage of a much longer stability if the gelation time can be tuned appropriately. The study of gel-foam contains two important steps:

Part 1: Feasibility Study

The objective of this first part is not to come up with a customized and optimized solution. It is a preliminary feasibility study to evaluate and check for the efficiency of gel-foam to block gas influx. It will consist of carrying out gel-foam system screening /design and petrophysics evaluations in core flooding tests in order to study the potential added value of gel foams as compared to classical and polymer enhanced foam.

This preliminary part will consist mainly of the following tasks

- Screening and selection of the gel foam system based on bulk properties
  - Polymer selection: nature and concentration
  - Surfactant selection: nature and concentration
  - Crosslinker selection (based on gel strength determination): nature and concentration
  - Delaying ligands screening vs. gelation time
- Qualification and characterization in core floods
  - Characterization of the rheological behaviour in porous media of the polymer and polymer-enhanced foams
    - Brine, polymer, (polymer+CO_2), (polymer+surfactant+ gas) and finally gas
  - Characterization on the rheological behavior in porous media of the delayed gel-foam (with crosslinker)

- Brine, polymer, (polymer+ gas), (polymer + surfactant + gas), (polymer+ surfactant + gas + crosslinker + delaying agent), gas (after shut-off and allowing gelation to occur)

At the end of injection sequences performed (PEF and gel-foams), the resistance ability of PEF or gel-foam to displacement with gas will be evaluated: the injection will be stopped and a low differential pressure will be first applied across the core (no gas at the outlet). The differential pressure will then and increased stepwise until gas breakthrough. Comparison of gas breakthrough onset differential pressure for PEF and Gel-foam will allow to evaluate the potential added value of gel-foam in the ability to block gas influx. Finally, the residual resistance factor to gas flow (gas injection) will be also determined.

Part 2: Optimization study
One the feasibility has been demonstrated, the objective here is to optimize the solution including

- Gel strength,
- Delaying time (gelation kinetics),
- Propagation facility of PEF.
- Defining precisely the targeted area
- Injection strategy and emplacement
- Injection volumes

This optimization part will be carried out in close connection between formulation, petrophysics and simulation works.

3.4 Numerical modeling

The goal for the numerical modelling work is to assess the radius of intervention and placement of the different injected foams, gel foams or PEFs. Thus this work is not aimed at optimizing a site-specific (gel) foam injection, but to investigate the field scale behaviour for different realistic settings of an injected (gel-)foam.

Field scale simulation of (gel-)foam is necessarily limited to a more empirical approach. Such approaches are implemented in industry-standard simulators such as STARS [93], or Eclipse or in dedicated applications such as those of the University of Texas (UTGEL [94, 95]). These tools need to be calibrated based on field tests to make reliable predictions. However, for the current application, it is by definition impossible to perform such tests. In fact, the level of uncertainty is likely to be higher than for conventional oil reservoirs, especially for CO_2 storage in aquifers. Therefore the approach here is to investigate a range of effective properties of the (gel-)foam to be injected. The goal is to provide an overview of 'what if' scenarios: if a stable foam can be created with a viscosity reduction of x times the original viscosity of CO_2, how effective would that be? Also it will be investigated how robust the scenarios are and whether their robustness can be improved by for example injecting CO_2 with a different temperature to improve placement of the foam.

Important aspects of the model work are:

- the effective properties of the created foam (viscosity, density, (relative) permeability reduction, adsorption (mainly of the surfactant)),
- geometry and position of the injection well (vertical, horizontal),
- geometry of the leakage area (fracture (line sink), areal sink),
- CO_2 leakage rate (to estimate the transport of the (gel-)foam into the fractures or fault),
- size and/or boundary conditions of the model (to estimate the pressure increase as a result of the injection).
- Possible dip of the caprock

To take the aspects listed above, a 3D model will need to be used with fine grids near the injection well and the fracture/fault.

The flow of the (gel-) foam in the leaking fault/fracture itself is not included in this part of the work, because it does not contribute to answering the question of the radius of influence.

Scenarios
As a real case for this part of the work package a model of a notional CO_2 storage formation has been chosen, which consists of a reservoir formation, a cap rock and a fault intersecting the cap rock. The model is the same as that used in study described in section 2.

Figure 9 gives an overview of the model setup. Both a horizontal and vertical injection well will be tested, because this well configuration strongly affects the potential radius of influence and the pressure increase around the injection well. The pressure increase should be limited as much as possible to avoid increasing the leakage problem. Of course, the choice of well also affects the pressure gradient and thus the creation of the foam, however that will not be taken into account since the actual process of foam creation is not simulated.

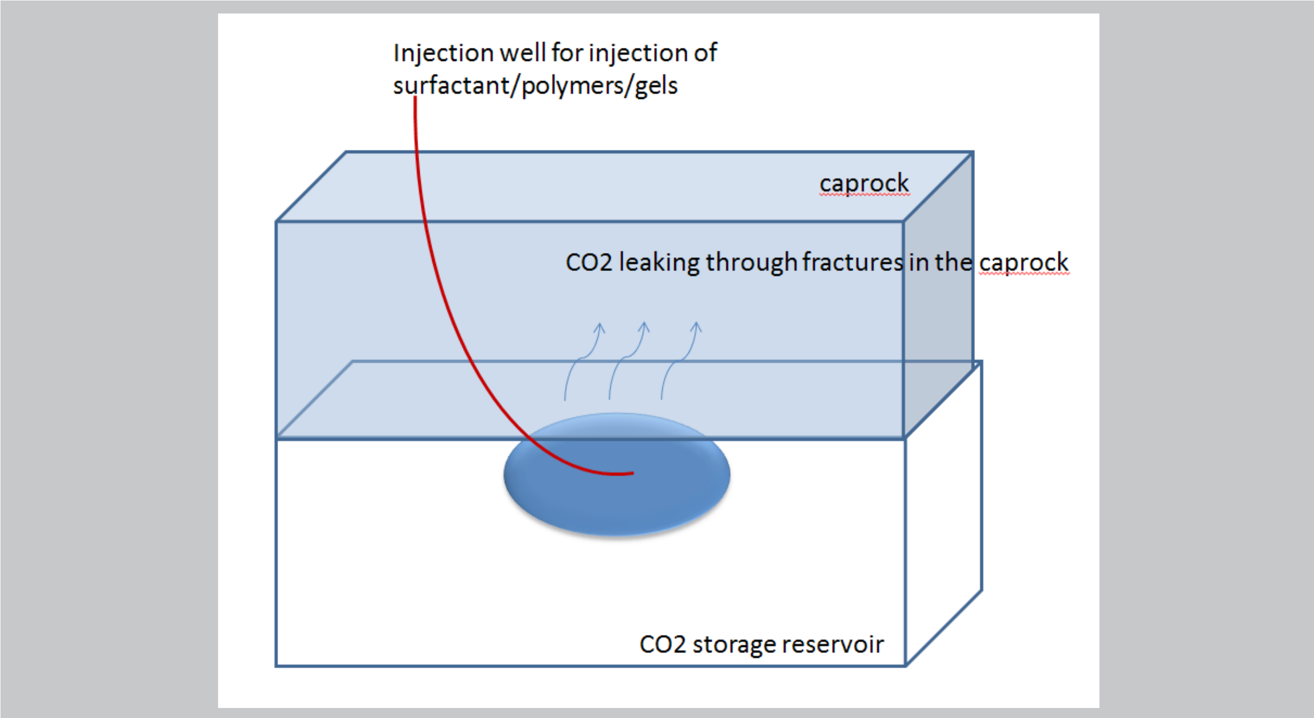

Figure 9 Setup of the model.

By not taking into account the fact that the gel-foam is formed inside the reservoir, the model might experience unrealistic injectivity problems. These can be alleviated by changing the relative permeability model of the well or by setting a negative skin. This should not affect the overall results much.

3.5 Summary

Foams have the ability to restrict or block the flow in high permeability zones. In the context of CO_2 flowing through a leaky fault across a caprock, it is preferable to use gel-foams that have attractive stability properties.

The typical scenario envisaged is the injection of gel-foams below the caprock, as close as possible to the leaky fault in which CO_2 is flowing.

Gel foams will be studied in the laboratory. Due to their complexity, a feasibility study will first be performed, before optimizing some important aspects such gel strength, gelation time. Through numerical simulations, we will study the injection strategy and provide estimates of volumes needed for the desired distance of influence.

References

1. Sydansk, R. D., 1988. A new conformance improvement treatment Chromium(III) gel technology, in SPE Enhanced Oil Recovery Symposium, Tulsa, Oklahoma.
2. Hunter, B., Buell, R. and Abate, T., 1992. Application of a polymer gel system to control steam breakthrough and channeling, in SPE Western Regional Meeting, Society of Petroleum Engineers Inc., Bakersfield, California.
3. Gao, H. W., Chang, M.-M., Burchfield, T. E. and Tham, M. K., 1993. Permeability modification simulator studies of polymer-gel-treatment initiation time and crossflow effects on waterflood oil recovery, SPE Reservoir Engineering, 8(3), 221-227.
4. Whitney, D., Montgomery, D. and Hutchins, R., 1996. Water shutoff in the North Sea: Testing a new polymer gel system in the Heather field, UKCS block 2/5, SPE Production & Operations, 11(2), 108-112.
5. Hutchins, R., Dovan, H. and Sandiford, B., 1996. Field applications of high temperature organic gels for water control, in SPE/DOE Improved Oil Recovery Symposium, Society of Petroleum Engineers, Inc., Tulsa, Oklahoma.
6. Bryant, S. L., Rabaioli, M. and Lockhart, T. P., 1996. Influence of syneresis on permeability reduction by polymer gels, SPE Production & Operations, 11(4), 209-215.
7. Kantzas, A., Marentette, D. F. and Allsopp, K., 1999. Utilization of polymer gels, polymer enhanced foams, and foamed gels for improving reservoir conformance, Journal of Canadian Petroleum Technology, 38(13).
8. Ricks, G., and Portwood, J. T., 2000. Injection-side application of marcit polymer gel improves waterflood sweep efficiency, decreases water-oil ratio, and enhances oil recovery in the Mcelroy field, Upton county, Texas, in SPE Permian Basin Oil and Gas Recovery Conference, Society of Petroleum Engineers Inc., Midland, Texas.
9. Sydansk, R. D., and Southwell, G. P. 2000. More than 12 years experience with a successful conformance-control polymer-gel technology, SPE Production & Operations, 15(4), 270-278.
10. Wouterlood, C., Falcigno, E., Gazzera, C. and Norman, C., 2002. Conformance improvement with low concentration polymer gels in a heterogeneous, multilayer reservoir, in SPE/DOE Improved Oil Recovery Symposium, Society of Petroleum Engineers Inc., Tulsa, Oklahoma.
11. Herbas, J., Kumar, S., Moreno, R., Romero, M.F and Avendano, H., 2004. "Reservoir Simulations of Gel Treatments to Control Water Production, Improve the Sweep Efficiency and the Conformance Factor in Eastern Venezuelan HPHT Fractured Reservoirs" Paper Presented at the SPE Int. Petroleum Conf., Mexico, SPE 92003.
12. Sydansk, R., Al-Dhafeeri, A., Xiong, Y. and Seright, R., 2004. Polymer gels formulated with a combination of high- and low molecular weight polymers provide improved performance for water-shut off treatments of fractured production wells, SPE Production & Operations, 19(4), 229-236.
13. Sydansk R.D., Xiong, Y., Al-Dhafeeri, A.M., Schrader, R.J. and. Seright, R.S., 2005. "Characterisation of Partially Formed Polymer Gels for Application to Fractured Production Wells for Water-Shutoff Purposes" SPE Production & Facilities, 20(3), pp.240-249, SPE 89401.
14. Norman, C., Turner, B. O., Romero, J. L., Centeno, G. A. and Muruaga, E., 2006. A review of over 100 polymer gel injection well conformance treatments in Argentina and Venezuela: Design, field implementation, and evaluation, in First International Oil Conference and Exhibition in Mexico, Society of Petroleum Engineers, Cancun, Mexico.
15. Zhao, H., Zhao, P., Bai, B., Xiao, L. and Liu, L. 2006. Using associated polymer gels to control conformance for high temperature and high salinity reservoirs, Journal of Canadian Petroleum Technology, 45(5).
16. Turner, B. O., and Zahner, R. L., 2009. Polymer gel water-shut off applications combined with stimulation increase oil production and life of wells in the Monterey formation offshore california, in SPE Western Regional Meeting, Society of Petroleum Engineers, San Jose, California.
17. Al-Muntasheri, Sierra, G. A., L., Garzon, F. O., Lynn, J. D. and Izquierdo, G. A., 2010. Water shut-off with polymer gels in a high temperature horizontal gas well: A success story, in SPE Improved Oil Recovery Symposium, Society of Petroleum Engineers, Tulsa, Oklahoma, USA.
18. Hild, G., and Wackowski, R., 1999. Reservoir polymer gel treatments to improve miscible CO_2 flood, SPE Reservoir Evaluation & Engineering, 2(2), 196-204.
19. Saez, M., Paponi, H. M., Cabrera, F. A., Muniz, G., Romero, J. L. and Norman, C., 2012. Improving volumetric efficiency in an unconsolidated sandstone reservoir with sequential injection of polymer gels, in SPE Improved Oil Recovery Symposium, Society of Petroleum Engineers, Tulsa, Oklahoma, USA.
20. Seright, R. S., 1995. "Reduction of Gas and Water Permeabilities using Gels" SPE Production & Facilities pp.103-108.
21. Raje, M., Asghari, K., Vassoughi, S., Green, D.W. and Willhite, G.P., 1999. "Gel Systems for Controlling CO_2 Mobility in Carbon Dioxide Miscible Flooding" SPE Reservoir Eval. & Eng., 2(2), pp. 205-210. SPE 55965, Paper presented at the SPE/DOE Symp. on Improved Oil Recovery, Tulsa.

22. Grattoni, C.A., Jing, X.D. and Zimmerman, R.W, 2001. "DisproportionatePermeability Reduction When a Silicate Gel is Formed in-Situ to Control Water Production". Paper SPE 69534 presented at the SPE Latin American and Caribbean Petroleum Engineering Conference, Buenos Aires, 25-28 March.
23. Sydansk R.D. and. Seright, R.S., 2007. "When and Where Relative Permeability Modification Water-Shutoff Treatments Can be Successfully Applied" SPE Production and Operations, pp.236-247. SPE 99371, Paper presented at the SPE/DOE Symp. on Improved Oil Recovery, Tulsa.
24. Wassmuth, F.R., Green, K, and Hodgins, L., 2004. "Water Shutoff in Gas Wells: Proper Gel Placement is the Key to Success" SPE Production & Facilities, pp.217-227. SPE 89403, Paper presented at the SPE/DOE Symp. on Improved Oil Recovery, Tulsa.
25. Herbas, J., Moreno, R., Romero, M. F. and Coombe, D., 2004. Reservoir simulation of non selective placement of a polymer gel treatment to improve water injection profiles and sweep efficiency in the lagomar field western venezuela, in SPE International Petroleum Conference in Mexico, Society of Petroleum Engineers, Puebla Pue., Mexico.
26. Flew, S., and Sellin, R. H. J., 1993. Non-newtonian flow in porous media-a laboratory study of polyacrylamide solutions, Journal of Non-Newtonian Fluid Mechanics, 47(0), 169-210.
27. Rodriguez, S., Romero, C., Sargenti, M. L., Mueller, A. J., Saez, A. E. and Odell, J. A., 1993. Flow of polymer solutions through porous media, Journal of Non-Newtonian Fluid Mechanics, 49(1), 63{85.
28. Prud'homme, R., and Uhl, J., 1984. Kinetics of polymer/metalion gelation, in SPE Enhanced Oil Recovery Symposium, Tulsa, Oklahoma.
29. Sydansk, R. D., 1990. A newly developed Chromium(III) gel technology, SPE Reservoir Engineering, 5(3), 346-352.
30. Lockhart, T. P., and Albonico, P., 1994. New chemistry for the placement of chromium(lli)/polymer gels in high-temperature reservoirs, SPE Production & Operations, 9(4), 273-279.
31. Lu, X., Wang, W., Wang, R., Liu, Y. and Shan, J., 2010. The performance characteristics of Cr^{3+} polymer gel and its application analysis in Bohai oilfield, in International Oil and Gas Conference and Exhibition in China, Society of Petroleum Engineers, Beijing, China.
32. Dovan, H.T., 1987. Development of a new Aluminium/polymer gel system for permeability adjustment, SPE Reservoir Engineering, 2(2), 177-183.
33. Smith, J., 1995. Performance of 18 polymers in Aluminum citrate colloidal dispersion gels, in SPE International Symposium on Oilfield Chemistry, Society of Petroleum Engineers, Inc., San Antonio, Texas.
34. Albonico, P., Bartosek, M., Malandrino, A., Bryant, S. and Lockhart, T., 1995. Studies on phenol-formaldehyde crosslinked polymer gels in bulk and in porous media, in SPE International Symposium on Oilfield Chemistry, Society of Petroleum Engineers, Inc., San Antonio, Texas.
35. Sanders, G., Chambers, M. and Lane, R., 1994. Successful gas shut off with polymer gel using temperature modeling and selective placement in the Prudhoe bay field, in SPE Annual Technical Conference and Exhibition, 1994 Society of Petroleum Engineers, New Orleans, Louisiana.
36. Simjoo, M., Koohi, A. D., Seftie, M. V. and Zitha, P. L. J., 2009. Water shut-off in a fractured system using a robust polymer gel, In 8th European Formation Damage Conference, Society of Petroleum Engineers, Scheveningen, The Netherlands.
37. Reddy, B. R. R., Crespo, F. and Eoff, L. S., 2012. Water shut off at ultralow temperatures using organically crosslinked polymer gels, in SPE Improved Oil Recovery Symposium, Society of Petroleum Engineers, Tulsa, Oklahoma, USA.
38. Woo, G., Lopez, H., Metcalf, A. and Boles, J., 1999. A new microemulsion polymer gelling agent with an external surfactant gellant activator improves acid fracturing, in Latin American and Caribbean Petroleum Engineering Conference, Society of Petroleum Engineers, Caracas, Venezuela.
39. Chan, K. S., 1989. Injection profile modification with a new non-polymer gelling system, in Annual Technical Meeting, Petroleum Society of Canada, Banff.
40. Mebratu, A., Nerland, B. and Kleppan, T., 2004. Annular barrier re-establishment using a long-life, high-strength polymer gel system, in SPE International Symposium and Exhibition on Formation Damage Control, Society of Petroleum Engineers, Lafayette, Louisiana.
41. Hubbard, S., Roberts, L.J. and Sorbie, K.S., 1998. Experimental and theoretical investigation of time setting polymer gels in porous media, SPE Reservoir Engineering, 3 (4), 1257-1267.
42. Tung, C.-Y. M., and Dynes, P. J., 1982. Relationship between viscoelastic properties and gelation in thermosetting systems, Journal of Applied Polymer Science, 27(2), 569-574.
43. Albonico, P., and Lockhart, T., 1993. Divalent ion-resistant polymer gels for high-temperature applications: Syneresis inhibiting additives, in SPE International Symposium on Oilfield Chemistry, Society of Petroleum Engineers, Inc., New Orleans, Louisiana.
44. Albonico, P., Burrafato, G., Di Lullo, A. and Lockhart, T.P., 1993. Effective gelation delaying additives for Cr^{3+}/ polymer gels. In SPE International Symposium on Oilfield Chemistry, New Orleans, 2-5 March.
45. Moradi-Araghi, A., Bjornson, G. and Doe, P., 1993. Thermally stable gels for near-wellbore permeability contrast corrections, SPE Advanced Technology Series, 1(1), 140-145.
46. Vandeweijer, V., et al., Feasibility study P18 (final report), Doc.nr: CATO2-WP3.01-D06, 2011.
47. Manceau J.-C. et al., Mitigation and remediation technologies and practices in case of undesired migration of CO_2 from a geological storage unit – Current status, Intern. J. of Greenhouse Gas Control, 22, 272-290, 2014.
48. Kovscek, T. Patzek, C. Radke, Mechanistic prediction of foam displacement in multidimensions: a population balance approach, SPE/DOE 27789 (1994)
49. Gauglitz, A., Friedmann, F., Kam, I., and Rossen, R. [2002] Foam generation in homogeneous porous media. Chemical Engineering Science, 57, 4037-4052

50. Skauge, A., Aarra, M. G., Surguchev, L., Martinsen, H. A., and Rasmussen, L. [2002] Foam-Assisted WAG: Experience from the Snorre Field. SPE 75157
51. Farajzadeh, R., Andrianov, A., and Zitha, P. L. J. (2009). Investigation of Immiscible and Miscible Foam for Enhancing Oil Recovery. Industrial & Engineering Chemistry Research 49:1910-1919.
52. Dickson Tanzil, Goerges Hirasaki and Clarence A. Miller, "Conditions of foam generation in Homogeneous Porous Media", SPE/DOE IOR Symp., Tulsa, Oklahoma, 13-17 April 2002
53. Enick, R. M. and Olsen, D. K. [2012] Mobility and Conformance Control for Carbon Dioxide Enhanced Oil Recovery (CO_2-EOR) via Thickeners, Foams, and Gels - A Detailed Literature Review of 40 Years of Research. DOE/NETL-2012/1540.
54. Max Chabert (Rhodia), Lahcen Nabzar (IFPEN), Siti Rohaida, Pauziyah Hamid (Petronas PRSB), M.Faizal Sedaralit (Petronas EPTC) & N. Darman (Petronas EPTC), An integrated laboratory workflow for the design of a foam pilot in Malaysia, IOR 2013 – 17th European Symposium on IOR. St. Petersburg, Russia, 16-18 April 2013
55. Khatib, G. Hirasaki, A. Falls, Effects of capillary pressure on coalescence and phase mobilities in foams flowing through porous media, SPE Reservoir Engineering, August 1988, pp. 919-926
56. J.M. Alvarez, H.J. Rivas and W.R. Rossen, "Unified Model for Steady-state Foam Behavior at High and Low Foam Quality" , September 2001 SPE Journal
57. Bachu S., Gunter W.D. and Perkins E.H.: 1994, 'Aquifer disposal of CO_2: hydrodynamic and mineral trapping', Energy Conversion and Management, 35, 269-279.
58. Ennis-King J. and Paterson L.: 2001, 'Reservoir engineering issues in the geological disposal of carbon dioxide', in Williams D., Durie B., McMullan P., Paulson C. and Smith A. (eds), Fifth International Conference on Greenhouse Gas Control Technologies, Cairns, vol. I, CSIRO, Collingwood, pp. 290-295.
59. Damen, Kay J.; Faaij, A.P.C.; Turkenburg, W.C. Health, safety and environmental risks of underground CO_2 storage: overview of mechanisms and current knowledge, Climatic Change, volume: 74, issue: 1-3 (2006), pp. 289 – 318
60. Schramm, L.L. and Wassmuth, F. 1994. Foams: Basic Principles. Foams: Fundamentals and Applications in the Petroleum Industry, L.L. Schramm ed., 3-45. Washington, DC: Advances in Chemistry Series 242, American Chemical Soc.
61. Mannhardt, K. and Svorstol, I. [1999] Effect of oil saturation on foam propagation in Snorre reservoir core. Journal of Petroleum Science and Engineering, 23, 189-200.
62. Max Chabert, Lahcen Nabzar, Virginie Beunat, Emie Lacombe, Amandine Cuenca, Impact of Surfactant Structure and Oil Saturation on the Behavior of Dense CO_2 Foams in Porous Media , SPE 169176, SPE Improved Oil Recovery Symposium held in Tulsa, Oklahoma, USA, 12–16 April 2014.
63. M. Chabert, M. Morvan and L. Nabzar, "Advanced screening technologies for the selection of dense CO_2 foaming surfactants", Eighteenth SPE Improved Oil Recovery Symposium, Tulsa,Oklahoma, USA, 14-18 April 2012.
64. Max Chabert (Rhodia), Mikel Morvan (Rhodia), Lahcen Nabzar (IFPEN) Advanced Screening Technologies for the Selection of Dense CO_2 Foaming Surfactants. 33rd IEA EOR Symp. August 26-30, 2012
65. J.S Solbakken, A. Skauge and MG. Aarra, Spercritical CO_2 foam- The importance of CO_2 density on Foam Performance, SPE 165296, SPE EOR Conf§;, Kuala Lumpur, Malaysia, 2-4 July 2013
66. Kun Ma, Jose L. Lopez-Salinas, Maura C. Puerto, Clarence A. Miller, Sibani Lisa Biswal, and George J. Hirasaki, Estimation of Parameters for the Simulation of Foam Flow through Porous Media. Part 1: The Dry-Out Effect, Energy Fuels 2013, 27, 2363–2375
67. Ma, K., Lopez-Salinas, J. L., Puerto, M. C., Miller, C. A., Biswal, S. L. & Hirasaki, G. J., "Estimationof Parameters for the Simulation of Foam Flow Through Porous Media, Part 1: The Dry-Out Effect," Energy & Fuels 27 (2103), 2363–2375.
68. Moradi-Araghi, A., Johnston, E. L., Zornes, D. R., and Harpole, K. J., "Laboratory Evaluation of Surfactants for CO_2-Foam Applications at the South Cowden Unit", paper SPE 37218 presented at the 1997 SPE International Symposium on Oilfield Chemistry, Houston, 18-21 February.
69. Falls AH, GJ Hirasaki, TW Patzek, PA Gauglitz, DD Miller, and T Ratulowski. 1988. "Development of a mechanistic foam simulator: The population balance and generation by snap-off." Soc. Petr. Eng. Res. Eng. 3(3):884–892.
70. Falls AH, JJ Musters, and J Ratulowski. 1989. "The Apparent Viscosity of Foams in Homogeneous Beadpacks." Soc. Petr. Eng. Res. Eng. 4(2):155–164.
71. Friedmann F, WH Chen, and PA Gauglitz. 1991. "Experimental and Simulation Study of High-Temperature Foam Displacement in Porous Media." Soc. Petr. Eng. Res. Eng. 6(1):37–45.
72. Kam SI, and WR Rossen. 2003. "A Model for Foam Generation in Homogeneous Porous Media." SPE J., 8(4):417–425.
73. Kovscek AR, TW Patzek, and CJ Radke. 1995. "A Mechanistic Population Balance Model for Transient and Steady-State Foam Flow in Boise Sandstone." Chemical Engineering Science, 50(23):3783–3799.
74. Kovscek AR, TW Patzek, and CJ Radke. 1997. "Mechanistic Form Flow Simulation in Heterogeneous and Multidimensional Porous Media." Soc. Pet. Eng. J. 2:511–517.
75. Kovscek AR and CJ Radke. 1994. "Fundamentals of From Transport in Porous Media." In: LL Schramm (Ed.), Foam: Fundamentals and Applications in the Petroleum Industry. American Chemical Society, Washington, D.C.
76. Zhou ZH and WR Rossen. 1995. "Applying Fractional-Flow Theory to Foam Processes at the Limiting Capillary Pressure." SPE Adv. Technol. 3(1):154–162.
77. Dholkawala ZF, HK Sarma, and SI Kam. 2007. "Application of Fractional Flow Theory to Foams in Porous Media." Journal of Petroleum Science and Engineering 57, 152–165.
78. Cheng, L., Reme, A.B., Shan, D., Coombe, D.A, and Rossen, W.R, Simulating Foam Processes at High and Low Foam Qualities, SPE59287, SPE/DOE symp. On IOR, Tulsa, OK, 3-5 April, 2000.

79. Rossen, W.R. 1996. Foams in Enhanced Oil Recovery. Foams—Theory, Measurement, and Applications, R.K. Prud'homme and S.A. Khan ed., 413-464. New York: Marcel Dekker Inc.

80. Rossen, W.R. 1988. Theories of Foam Mobilization Pressure Gradient. Presented at the SPE Enhanced Oil Recovery Symposium, Tulsa, Oklahoma, 16-21 April 1988. SPE-17358-MS.

81. Albrecht, R.A. and Marsden, S.S. 1970. Foams as Blocking Agents in Porous Media. SPE J. 10 (1): 51–55. SPE-2357-PA.

82. Svorstol, I. et al.: "A production well foam pilot in the North Sea Snorre Field," paper 001 presented at the 1997 European Symposium on Improved Oil Recovery, The Hague, 20–22 October.

83. Wong, F. et al.: "Design and field trial application of foam in production wells to improve conformance," J. Cdn. Pet. Tech. (February1997)

84. Bernrad G.G.,and Holm, L.W, Model study of foam as a sealant for leak in gas storage reservoir, Soc.Petrol.Eng. J. (1964), 4, 9-16

85. Persoff, P., Preuss, K., Benson, S.M. and Wu, Y.S, "Aqueous Foams for Control of Gas Migration and Water Coning in Aquifier Gas Storage ", Energy Sources, Vol. 12, 479-497, 1990

86. Smith, D.H, and Jikich, S.A, "Foams and Surfactants for Improved Underground Storage of Natural Gas by Blockage of water Coning", SPE 26908, SPE Eastern Regional Meeting, 2-4 Nov. Pittsbourg, 1993

87. Enick, R.M,Olsen, D.,Ammer, J. and Schuller, W., Mobility and Conformance Control for CO_2-EOR via Thickeners, Foams, and Gels- A Litterature Review of 40 Years of Research and Pilot Tests,SPE 154122, SPE IOR symposium, Tulas, Oklahoma, 14-18 April 2012

88. Cubillos, H., Montes, J. Prieto, C. and Romero, P., Assessment of foam for GOR control to optimize miscible gas injection recovery, SPE 152113, SPE IOR symposium, Tulsa, Oklahoma, 14-18 April 2012

89. Wassmuth, FR, Hodgins, L.A., Schramm, L.L., and Kutay, S.M., Screening and coreflood testing of gel foams to control excessive gas production in oil wells, SPE Resrevoir Evaluation & Engineering, June 2001

90. Dalland, M. and Hanssen, J.E.: "Enhanced Foams for Efficient Gas Influx Control," paper SPE 37217 presented at the 1997 SPE International Symposium on Oilfield Chemistry, Houston, 18–21 February.1997

91. Friedmann, F., Hughes, T.L., Smith, M.E., Hild, G.P., Wilson, A., and Davies, S.N., Development and testing of a foam-gel technology to improve conformance of Rangely CO_2 flood, SPE Reservoir Evel & Eng 2 (1), February 1999

92. Hughes, T.L., Friedmann, F., Johnson, D., Hild, G.P., Wilson, A., and Davies, S.N., Large-volume foam-gel treatment to improve conformance of the Rangely CO_2 flood, SPE reservoir Eval. & Eng., 2 (1), February 1999

93. Herbas J., R. Moreno, Amaury Marin T., M. F. Romero, D. Coombe. 2004. Reservoir Simulation of Non Selective Placement of a Polymer Gel Treatment to Improve Water Injection Profiles and Sweep Efficiency in the Lagomar Field Western Venezuela. http://dx.doi.org/10.2118/92025-MS.

94. Delshad, M., Varavei, J., and Sepehrnoori, K. The University of Texas at Austin Gel Simulator (UTGEL), 2011.

95. Taksaudom, P. 2014. Simulation Study of Preformed Particle Gel for Conformance Control. Msc thesis, University of Texas at Austin.

Chapter XV

Laboratory characterisation of polymer-gels

Mojgan H. Mosleh[1], Sevket Durucan[1], Anna Korre[1]
[1] Imperial College, UK

SUMMARY

This report provides the results of the study on the use of polymer-gel technology as an option to remediate non-conformal flow behaviour of CO_2 within the storage reservoir or leakage through faults and fractures. Several polymer-gels with crosslinkers were tested. The rheology, gelation and working times of these polymer-gels at various concentrations were investigated under different temperatures representative of CO_2 storage reservoirs.

Laboratory core flooding experiments were carried out on high permeability core samples to test the suitability of polymer-gels for the flow through and containment of CO_2 in porous media. The core samples saturated with brine were subjected to polymer-gel injection. Core sample permeabilities for N_2 and CO_2 were measured and the change in permeability of the samples before and after the polymer-gel injection was noted. In order to assess the effect of reservoir temperature on gelation process and effectiveness of the polymer-gel for permeability reduction, core flooding experiments were conducted at temperatures ranging from ambient up to 60°C. The results are presented and discussed in this report.

Note: this report has not been made publicly available, thus only the title and public abstract are provided.

Chapter XVI

Gel and foam injection as leakage remediation through caprock and fractures

Mojgan Hadi Mosleh[1], Rajesh Govindan[1], Ji-Quan Shi[1], Anna Korre[1], Sevket Durucan[1],
Francesco Pizzocolo[2]
[1] Imperial College, UK
[2] TNO, The Netherlands

SUMMARY

This element of the MiReCOL project aims to investigate the effectiveness of polymer-gel solutions in remediation of CO_2 leakage from storage reservoirs. The report is presented in two distinct Sections. The first Section presents work carried out to assess the effectiveness of polymer-gel injection by converting the CO_2 injection well or newly drilled wells for use as polymer-gel injectors. In this respect, the report addresses both CO_2 flow diversion within the reservoir and the remediation of leakage through faults and/or fracture zones in the caprock using polymer-gel injection in a shallower, high permeability formation above the caprock. In this Section, the first part provides the results of numerical simulations of polymer-gel injection process using a chemical flooding simulation software UTCHEM in order to investigate the effect of various reactant parameters, such as polymer and crosslinker concentration, on the gelation process and its area of influence. The second and third parts of the first Section of the report provide the results of numerical simulations of polymer-gel injection for flow diversion of the CO_2 plume in the reservoir and the remediation of leakage through fractured caprock using Schlumberger's Eclipse (E300) simulator. Here, it was assumed that leakage through a sub-seismic fault was detected in the shallow aquifer during CO_2 injection. A realistic reservoir model developed by Imperial College was used to study a number of leakage and remediation scenarios. The results obtained from laboratory investigations of polymer-gel characterisation and core flooding experiments that were conducted in the MiReCOL project were used to define a range of permeabilities for the polymer-gel treatments modelled. Depending of proximity of injection well to target area and type of polymer used, the amount of polymer solution, area of influence, and cost of treatments were estimated for the remediation cases considered.

The second Section of the report presents research carried out to assess the potential for using hydraulically created fractures to deliver a sealant gel (or foam) to a leaky fault or a leaky zone to create a barrier. Modelling work performed by TNO used the P18 gas field to demonstrate the technology in a real field site. This section presents a brief summary of the geology of the P18 field, the leakage scenarios that have been analysed, and the methods that were used to evaluate the mitigation and remediation of CO_2 leakage.

1 INTRODUCTION

The effectiveness of low permeability polymer-gel barriers in diverting the CO_2 plume from a sub-seismic fault in the reservoir and caprock was previously investigated by considering different layouts of the barrier in the storage reservoir. In a previous report, an assessment of the effectiveness of local permeability reduction in the reservoir caused by the polymer-gel barrier was made by drawing a comparison between the estimated amounts of CO_2 that leaked into shallow aquifer before and after the placement of the barrier.

In this report, the results of numerical simulations of polymer-gel injection into the targeted zones of both the reservoir and shallow high permeability formations overlying the caprock for the flow diversion of the plume and the consequent remediation of leakage through the fractured caprock are presented as a follow up. In both the cases, the area of influence of polymer-gel remediation and the volume of the polymer-gel required for effective treatment have also been estimated for a number of cases considered.

A chemical flooding reservoir simulation software UTCHEM was used to simulate polymer injection and its subsequent gelation process in a saline aquifer model. Parameters such as polymer concentration, polymer-to-crosslinker ratio and its influence on the gelation process, and the area of influence were investigated. In addition, the effect of delaying agent on the gelation process and area of influence was investigated by considering a range of kinetic rate constants for the reaction between the polymer and crosslinker.

Furthermore, using Schlumberger's Eclipse 300 (E300) software, the injection of polymer-gel solution was simulated and the area of influence and volume of polymer-gel needed were estimated for each case. The effect of the delaying agent on the area of influence was considered by using a range of polymer viscosity values. Based on the proximity of the polymer injection well to target zone and viscosity of the solution, a range of polymer treatment cases were defined. The cost of polymer-gel treatment has also been estimated for the scenarios considered.

1.1 Polymer-gel remediation as a flow diversion option

In comparison to other likely storage sites, such as the depleted hydrocarbon fields, knowledge on the geological and petrophysical properties of saline aquifers is extremely limited. Hence, a considerable degree of uncertainty in the conformance of CO_2 flow in the subsurface in comparison to that estimated by theoretical/numerical computations is expected. This uncertainty may lead to undesired and unpredicted preferential flow of CO_2 into parts of the host reservoir, or leakage into shallower formations. Mechanisms that could lead to migration or leakage of CO_2 into shallower formation and ultimately leakage to the atmosphere could include: unwarranted intrusion, equipment failure e.g. abandoned wells, faults reactivation due to over-pressurisation, or geochemical reactions between the CO_2 and the cap rock, and sub-seismic faults undetected during the site characterisation phase prior to CO_2 injection (IEAGHG Report, 2007).

In order to mitigate undesired CO_2 plume migration and its leakage into shallower formations, flow diversion measures may be implemented, such as: i) localised injection of brine creating a competitive fluid movement, ii) change of injection strategy, or iii) localised reduction in permeability by the injection of gels or foams, or by immobilising the CO_2 in the pore space.

Crosslinked hydrolysed polymer-gel injection is used in petroleum industry to improve conformity of fluid flow in the reservoir, remediate leakage around wells, and also used in conjunction with enhanced oil recovery at various temperature and pressure conditions (Sydansk, 1998; Hild and Wackowski, 1999; Sydansk and Southwell, 2000; Sydansk, et al., 2004; Turner and Zahner, 2009; Al-Muntasheri et al., 2010; Saez et al., 2012). Water-based gels are highly elastic semi-solids with high water content, trapped in the three-dimensional polymer structure of the gel (Vossoughi, 2000). Polyacrylamide (PAM) is the main crosslinked polymer used mostly by the industry (Flew and Sellin, 1993; Rodriguez et al., 1993). The use of biopolymers is more challenging as compared to the synthetic polymers due to chemical degradation at higher temperatures, causing the loss of mechanical strength (Sheng, 2011). Most of polymer-gel systems are based on crosslinking of polymers with a heavy metal ion. The most common heavy metal ion used is chromium III. However, in view of its toxicity and related environmental concerns (Stavland and Jonsbraten, 1996; Vossoughi, 2000), its application in reservoir conformance and CO_2 leakage remediation is considered to be limited. Therefore, more environmental friendly crosslinkers such as boron (Sun and Qu, 2011; Legemah et al., 2014), aluminium (Smith, 1995; Stavland and Jonsbraten, 1996) and zirconium (Lei and Clark, 2004) have been proposed and used in recent years.

Several commercial and research-purpose simulators have been used to simulate chemical/polymer injection into deep geological formations, most of which was developed for the purpose of Enhanced Oil Recovery (EOR) from hydrocarbon reservoirs. For instance, a two phase, four component polymer EOR model was developed by Wegner and Ganzer (2012) using COMSOL to simulate the displacement of oil by aqueous polymer solutions. Gharbi et al. (2012) performed history-matching to assess the potential of surfactant/polymer flooding in a Middle Eastern reservoir, using the chemical flood reservoir simulator (UTCHEM) developed at The University of Texas at Austin. In addition, Schlumberger's simulator, Eclipse, has also been used for polymer flooding and EOR in the Norne Field E-Segment, e.g. by Sarkar (2012) and Amirbayov (2014).

2 NUMERICAL MODELLING OF POLMER INJECTION AND ITS GELATION PROCESS

The UTCHEM software was used to simulate polymer injection and its subsequent gelation process in a saline aquifer model.

The model represents a simplified homogenous reservoir at approximately 1,600m depth and dipping at 22°. The grid spans an area of 750m×750m, and consists of a single layer with a resolution of 25m and a thickness of 15m. The initial pressure distribution of the formation is assumed to be hydrostatic, with an average of 174bar, as illustrated in Figure 1. The fracture pressure of the formation was assumed to be 1.5 times the initial hydrostatic pressure.

The petrophysical properties of the saline aquifer, such as porosity, permeability, salinity and temperature were assumed to be uniform in order to study the gelation process (Table 1). These values are based on previous studies that were reported for the North Sea-type reservoir conditions (Durucan et al., 2016).

Table 1 Static properties of the saline aquifer considered for the model setup.

Property	Value
Porosity [%]	20
Horizontal permeability [mD]*	3,000
Salinity [%]	12
Temperature [°C]	92

*Vertical permeability = 0.1 × Horizontal permeability

The polymer injection well is located at the centre of the model. As part of the injection strategy, the period of injection and observation (shut-in) were considered to be fixed as 10 and 40 days respectively.

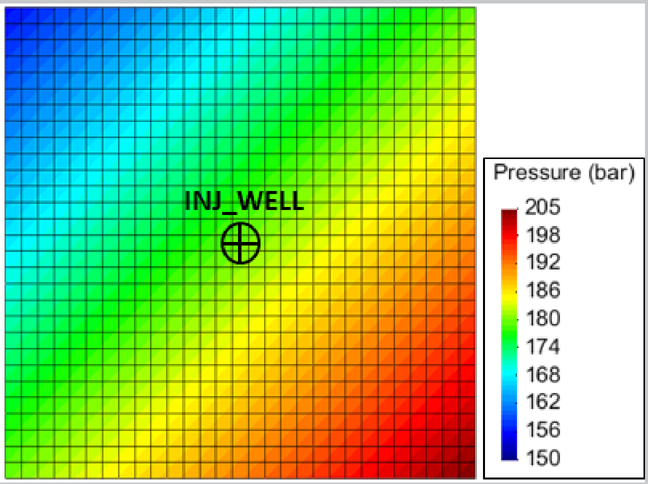

Figure 1 The numerical reservoir model with a resolution of 25m×25m grid blocks.

2.1 Modelling the gelation process

The gelation process for the polyacrylamide-based polymers and chromium crosslinker was investigated by simulating the injection of a solution of 300ppm polymer and 50ppm crosslinker into the porous medium. Figure 2 shows the area influenced by the polymer-gel plume and its concentration at different time steps.

A lower gel concentration is observed at the centre of the plume. This is owing to the fact that the polymer solution is a non-Newtonian fluid and its viscosity is affected by the shear rate induced at the location of injection. Figure 3 presents changes in gel concentration around the injection well with time. After 10 days, when the injection was stopped, the effect of shear rate disappears and hence the gel concentration in the near-well region attains its maximum value of approximately 260ppm.

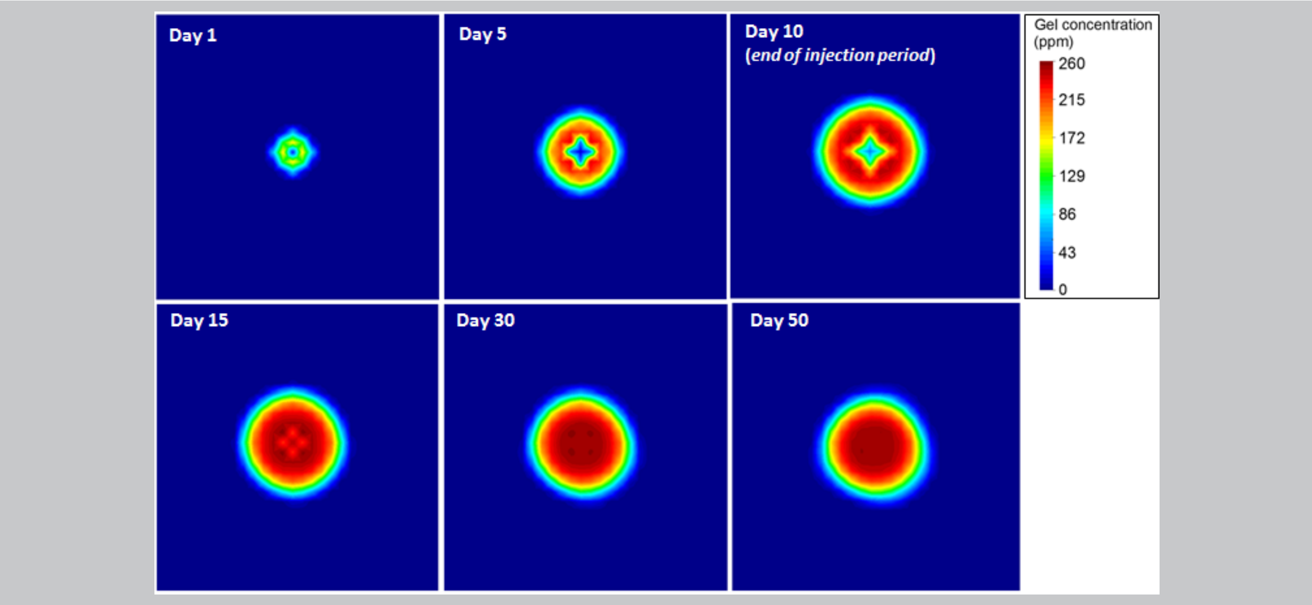

Figure 2 Gel concentration and the area of influence at different time steps.

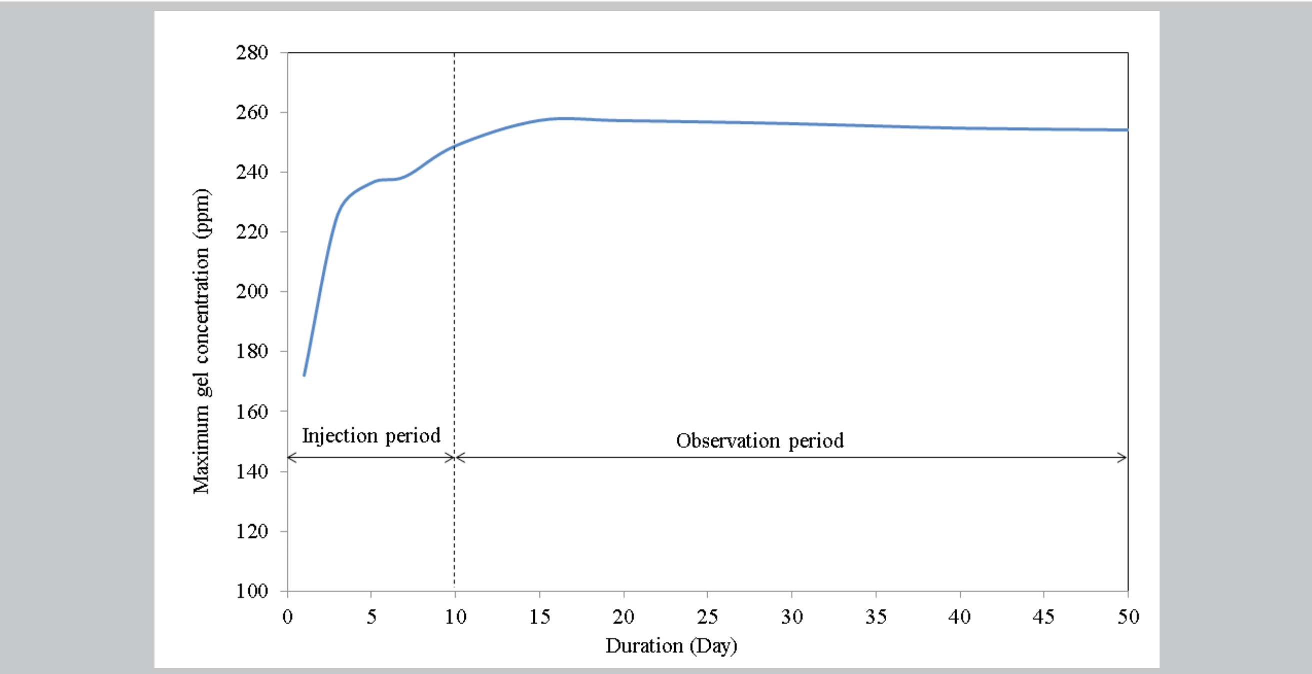

Figure 3 The variation of gel concentration with time.

2.2 The effect of initial formation permeability

The effect of the initial formation permeability on polymer distribution inside the reservoir was investigated by performing simulations for permeability values ranging from 1,000mD to 3,000mD in the saline aquifer model. A solution with concentrations of 300ppm polymer and 50ppm crosslinker was injected into the formation. The results of the simulation runs for the final time step (day 50) are presented in Figure 4 for each case.

The results show that, for the given reservoir conditions and polymer solution, the area of influence increases as the reservoir permeability increases (Figure 4). This is expected and is also partly attributed to the fact that at constant injection rates, lower permeability of the formation leads to rapid bottomhole pressure increase, reaching the maximum allowable pressure limit in order to avoid induced fractures in the system.

Figure 5 presents the changes in gel concentrations with time when the formation permeability is varied. For simulation runs with lower concentrations of the polymer, the permeability of the formation does not affect the gelation process. For higher polymer concentrations, however, the gel concentration reduces with decreased permeability. This is due to the development of higher shear rates during the injection of the polymer solution, which in turn reduces the gel viscosity.

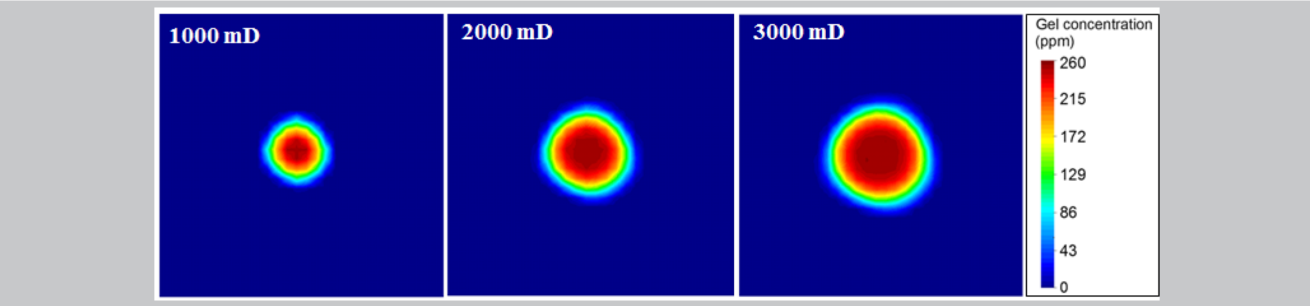

Figure 4 Effect of initial formation permeability on polymer-gel treatment in terms of the area of influence (300ppm polymer and 50ppm crosslinker solution injected).

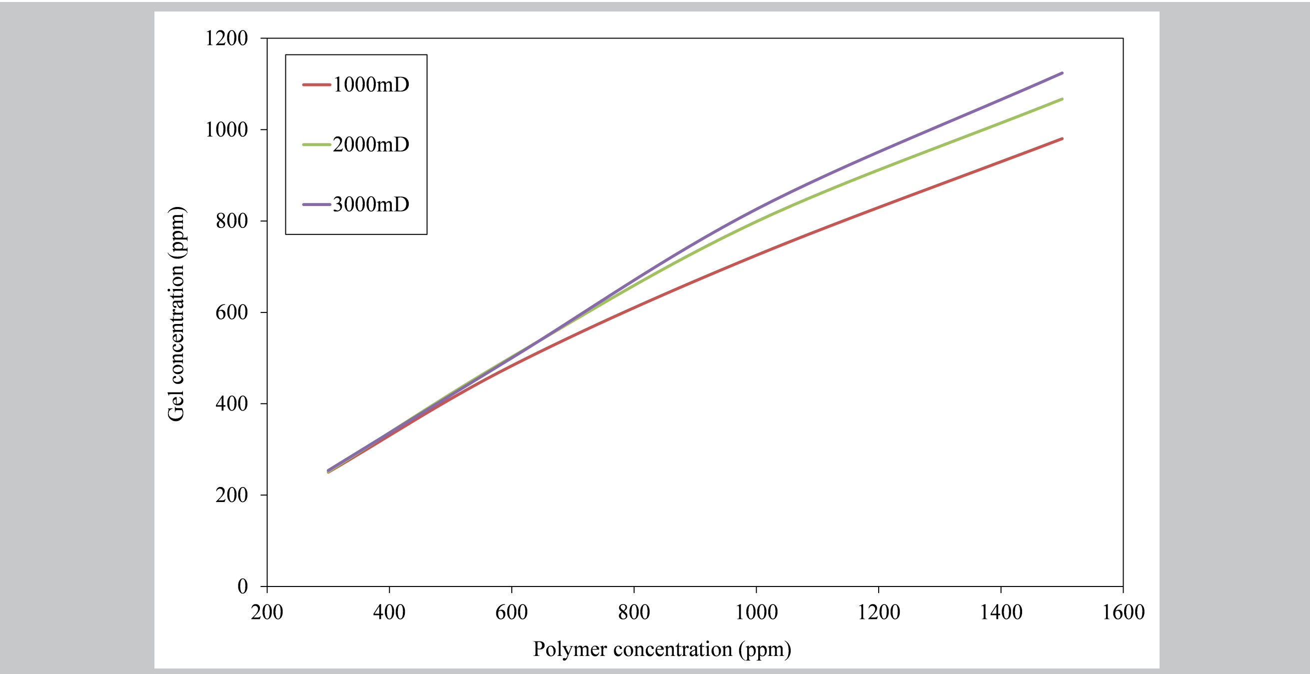

Figure 5 Gel concentration achieved at different polymer concentrations and reservoir permeabilities.

2.3 Effect of polymer and crosslinker concentrations

In order to assess the effect of polymer-to-crosslinker ratio on the effectiveness of polymer-gel treatments a number of simulations were performed for a range of polymer and crosslinker concentrations. The key output parameters that have been considered were: i) the gel strength and ii) the area of influence. The gel strength is characterised by the concentration of the produced gel; in general, the higher the concentration of produced gel, the stronger and more stable the gel is. The area of influence is also an important factor especially for cases where far-field gel treatments are required. To evaluate the polymer-gel treatment process, simulations have been run with concentrations at 300ppm, 600ppm, 1,000ppm and 1,500ppm. For each case, the polymer to crosslinker ratio was varied between 2 and 20. The results of simulations are presented in Figures 6a and 6b.

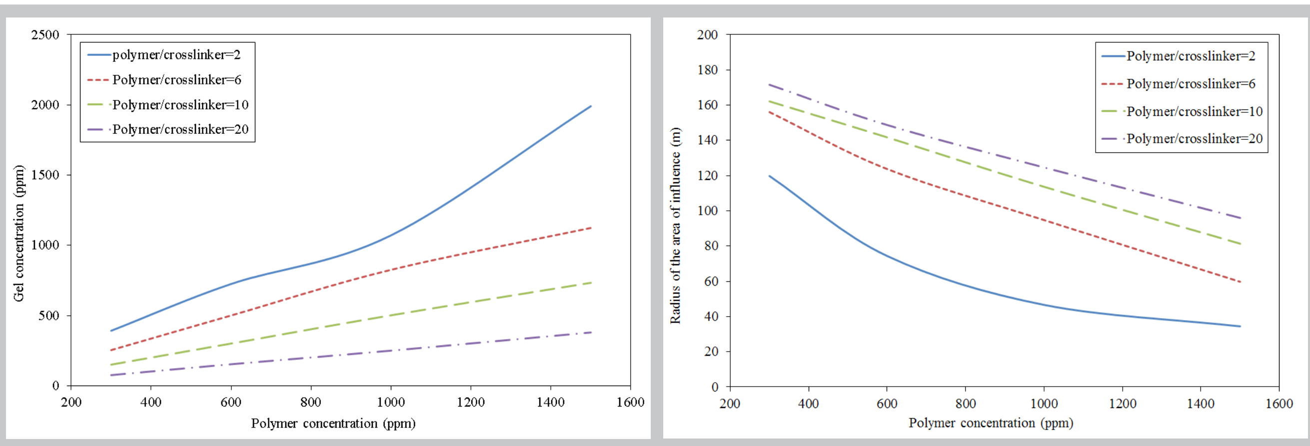

Figure 6 Effect of polymer and crosslinker concentrations on: a) gel concentration; and b) the area of influence.

The results of the simulations show that the concentration of the produced gel increases with increased polymer and crosslinker concentrations. In other words, at lower polymer to crosslinker ratios a relatively higher gel concentration is achieved, and therefore a stronger gel can be expected (Figure 6a). On the other hand, the area of influence increases with a decrease in crosslinker concentrations for a given polymer concentration (Figure 6b). This is mainly to the effect of decreased viscosity and slower gelation at lower crosslinker concentrations.

2.4 The effect of pH

The effect of pH on the gelation process and the area of influence was investigated by varying the concentration of H^+ in the range of 0 to 6.3×10-5 meq/ml. The initial concentration of H^+ in the formation pore fluid is estimated by the simulation software as 1.26×10-8 meq/ml. A solution of 300ppm polymer and 50ppm crosslinker was injected for 10 days, followed by 40 days of observation. The results of polymer gel concentration at various H^+ concentrations are presented in Figures 7a-c.

In the first case (Figure 7a), only polymer and crosslinker were included in the injection stream, therefore the pH of the injected solution is expected to be slightly higher than the pH of the surrounding formation fluid. In the second case (Figure 7b), the concentration of H^+ in the injection stream was increased to that of the concentration in the formation fluid. In the third case (Figure 7c), the H^+ concentration in the injection stream was further increased to 6.3×10-5 meq/ml and therefore the pH of the injected solution was lower than the pH of the formation fluid.

In the simulation software, the concentration of H^+ is a controlling parameter on the kinetics of the gelation process, i.e. the higher the concentration of H^+, the slower the crosslinking process. As a result of delayed crosslinking, polymer viscosity does not increase and therefore polymer slug migrates to the far-field region of the reservoir formation before it gels (Figure 7c).

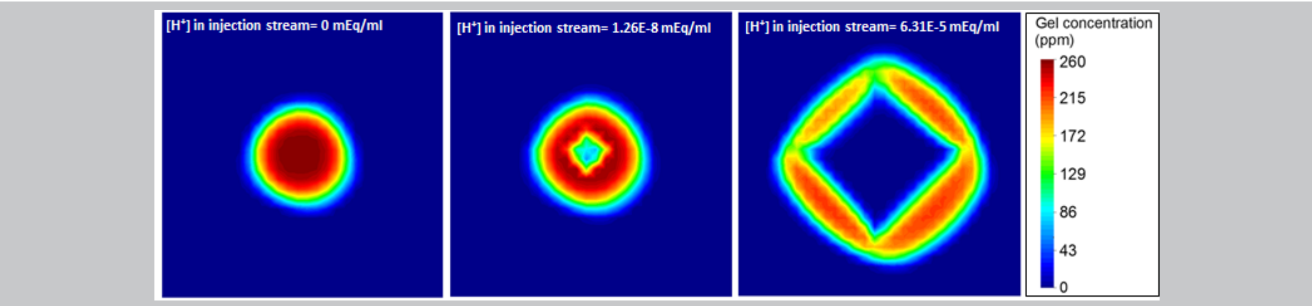

Figure 7 Effect of H^+ concentration on gelation process and the area of influence.

2.5 Effect of gelation kinetics

The kinetic rate constant used for the reactions between polymer and crosslinker in the model defines the viscosity and mobility of the gel, which can be considered as the effect of delaying agent on the gelation process. The reaction rate can also be controlled by adding delaying/accelerating agents to the solution. In particular, the reaction kinetics is described by the following equations (Lockhart, 1992):

$$[polymer]+n[Cr(III)]=[gel] \tag{1}$$

$$\frac{d[\mathrm{Cr\ (III)}]}{dt} = -k\frac{[\mathrm{Cr\ (III)}]^{0.6}[\mathrm{polymer}]^{2.6}}{[\mathrm{H}^+]^{1.0}} \tag{2}$$

$$\frac{d[\mathrm{gel}]}{dt} = -\frac{1}{n}\frac{d[\mathrm{Cr\ (III)}]}{dt} \tag{3}$$

where, k is the reaction rate constant. A sensitivity analysis was carried out by considering a range of rate constants for the crosslinking process. A series of simulations were performed to investigate the effect of delaying/accelerating agents on the gelation process. The results are presented in Figure 8a and 8b.

The results show that the decrease in reaction rate constant, i.e. adding delaying agents (see equations (2) and (3)), leads to production of gel at lower concentrations (Figure 8a). This type of treatment can be useful for far field treatments, where the area of influence of a larger size is required (Figure 8b).

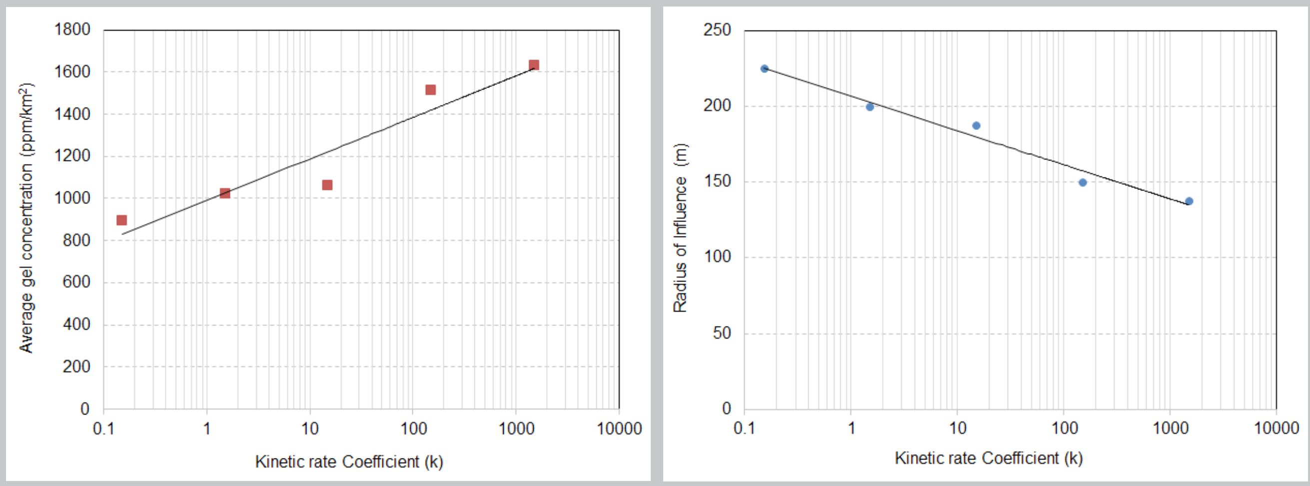

Figure 8 Effect of gelation rate on: a) gel concentration; and b) the area of influence.

3 NUMERICAL SIMULATION OF CO_2 LEAKAGE REMEDIATION USING POLYMER-GEL INJECTION

This section presents the results of the numerical modelling carried out to investigate the application of polymer-gel solutions for flow diversion of CO_2 plume within the storage reservoir. The objective of this work was: i) to perform simulations of polymer-gel injection with different remediation layouts after CO_2 leakage has been detected, ii) to estimate the area of influence and volume of polymer gel solution required for each remediation case. The results of laboratory investigations on polymer-gel characterisation and core flooding experiments conducted in the MiReCOL project were used to define a range of permeabilities of the polymer-gel barriers.

3.1 Reservoir model description

3.1.1 Structural and geological model

A numerical reservoir model was set up to study the mobility control of CO_2 plume using polymer-gel injection within a heterogeneous saline aquifer. The structural model used in this study represents a saline aquifer with a broad and considerably dipping anticlinal structure (Figure 9), where the containment of CO_2 is envisaged. The model grid spans an area of 36km×10km and includes five major sealing faults. The grid broadly comprises of three layers, namely: (1) a reservoir layer with an average thickness of 240m and resolution of 200m×200m×4m; (2) a caprock (seal) layer with an average thickness of 225m and resolution of 200m×200m×225m; and (3) a shallow aquifer layer with an average thickness of 175m and resolution of 200m×200m×20m. The depth of the model ranges between 1,087m and 3,471m.

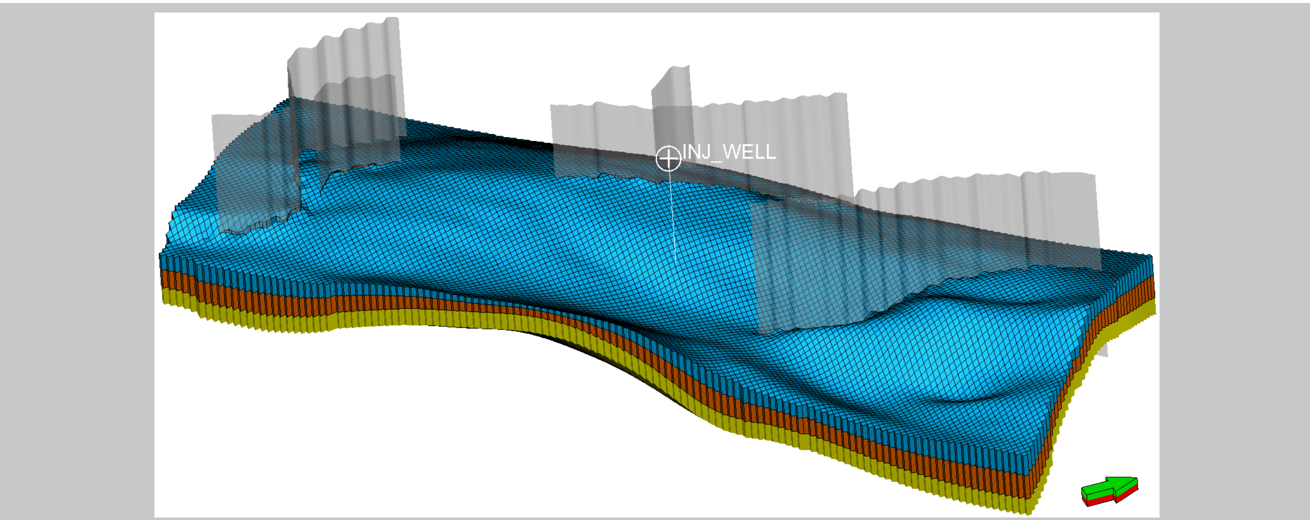

Figure 9 The structural model of the numerical saline aquifer (36km×10km) containing five major faults and three stratigraphic layers: reservoir layer, caprock (seal) layer and shallow aquifer layer.

The geological model of the reservoir layer is represented by a fluvial-channel system, typically containing braided sandstone channels and interbedded floodplain deposits (the inter-channel region) of mudstone or siltstone. These generally represent the fluviodeltaic progradation and floodplain deposition formations found in the Triassic of the Barents Sea. The channel layout parameters implemented in the model to represent the fluvial-channel system are given in Table 2. The range of the petrophysical properties used in the static geological model attribution (Table 3) are based on the Late Triassic Fruholmen Formation in the Hammerfest Basin (NPD, 2013), which is located at depths similar to those considered in this model. The petrophysical attributions of the geological model were generated using Sequential Gaussian Simulation (SGS) in order to represent the variability in the distribution of these values. Example realisations of the porosity and horizontal permeability distributions for the top reservoir layer are illustrated in Figure 10.

Table 2 Channel layout parameters used in the reservoir layer of the geological model.

	Min	Mean	Max
Amplitude [m]	400	500	600
Wavelength [m]	14,000	15,000	16,000
Width [m]	1,400	1,500	1,600
Thickness [m]	4	8	12

Table 3 Petrophysical properties used in the geological model.

Petrophysical properties		Channels	Inter-channel region	Caprock	Shallow aquifer
Porosity	Min, Mean, Max	0.1, 0.18, 0.25	0, 0.1, 0.25	0.01	0.05, 0.15, 0.25
	Standard deviation	0.05	0.05	0	0.05
Horizontal Permeability [mD] *	Min, Mean, Max	125, 3000, 7000	0.1, 10, 100	0.0001	100, 3000, 5000
	Standard deviation	2000	40	0	1000
NTG	Min, Mean, Max	0.6, 0.9, 1	0, 0.2, 0.5	0.01	0.6, 0.9, 1
	Standard deviation	0.05	0.05	0	0.05

*Vertical permeability = 0.1 × Horizontal permeability

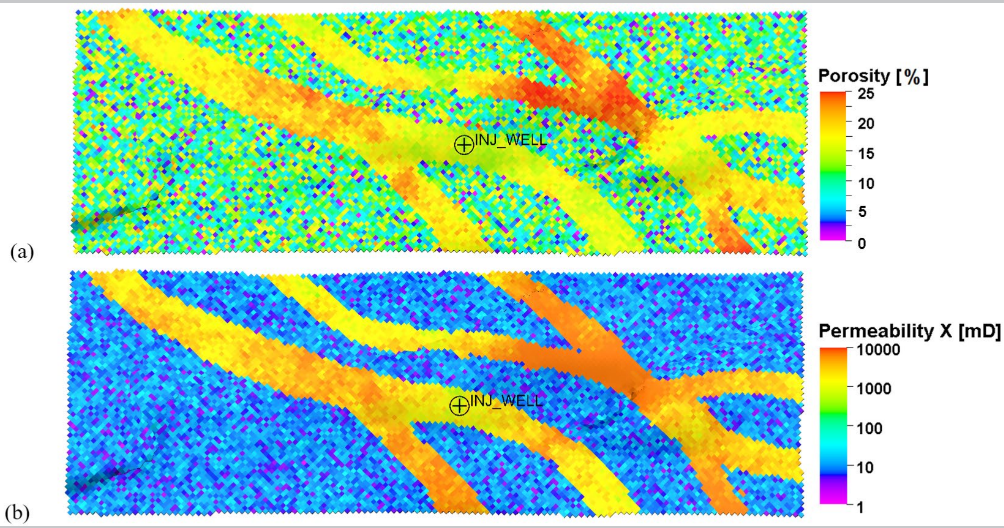

Figure 10 Example realisations of petrophysical properties distribution for the top layer of the reservoir: (a) Porosity; (b) Horizontal permeability covering the area of the reservoir model (36km×10km).

3.1.2 Dynamic properties of the reservoir model

Similar to the petrophysical properties of the geological model attribution, the dynamic properties of the reservoir model have been selected based on the values reported for the reservoir conditions found in the corresponding or neighbouring Barents Sea formations. The salinity of the formation water was chosen to be 14% based on the values reported for the Tubåen formation of the Snøhvit field (Benson, 2006), which is also part of the Realgrunnen Subgroup overlying the Fruholmen. The reservoir temperature was set at 93°C and the initial pressure of the reservoir model was assumed to be at hydrostatic pressure.

The dynamic model was set up in Schlumberger's Eclipse 300 (E300) software using the static geological model and the dynamic reservoir parameters described in the previous sections. The compositional flow simulation of CO_2 storage in the saline aquifer model was carried out by implementing a quasi-isothermal, multi-phase, and multi-component algorithm, enabled by the CO2STORE option, wherein mutual solubilities of CO_2 and brine are considered. Simulations were carried out for 30 years, comprising of the CO_2 injection at a rate of 1Mt/year, leakage detection, remediation, and post-remediation CO_2 injection periods.

A sub-seismic fault was introduced in the model at a distance of 1km away from the injection well, located at the flank of the anticline (Figure 11). The fault has a lateral dimension of 1600m×2m, with a uniform vertical permeability of 105mD and spanning the reservoir and the caprock thickness (approximately 450m).

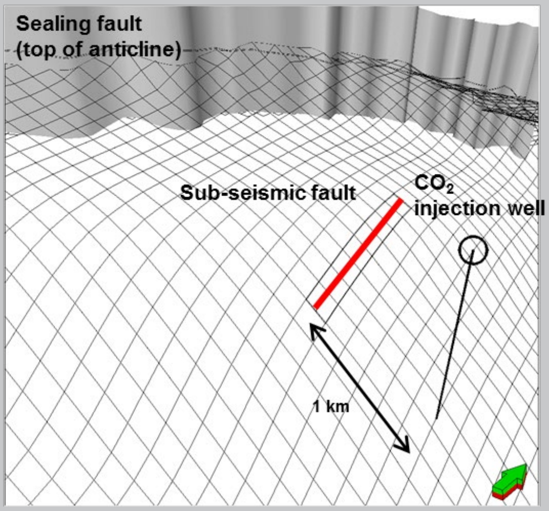

Figure 11 Numerical modelling of field polymer-gel injection.

3.2 Modelling CO_2 leakage remediation using polymer injection in the reservoir

Leakage through the fault was detected inside the shallow aquifer within a few months of injection, assuming 5,000 tonnes of mobile CO_2 as the lower limit for detection (Benson, 2006). CO_2 injection was temporarily terminated until polymer gel treatment in the reservoir was carried out. The remediation was subsequently assessed for the remaining time left during the simulation period of 5 years.

A number of scenarios were considered for the remediation of CO_2 leakage using polymer injection using horizontal well configurations (Figure 12). The scenarios are based on three factors:

- polymer gel viscosity.
- depth of polymer injection in the reservoir.
- proximity of polymer injection to the leaky sub-seismic fault.

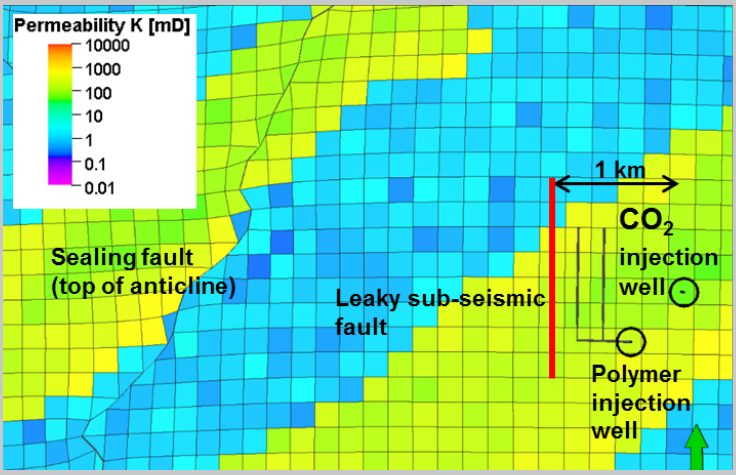

Figure 12 Location of polymer injection well, sub-seismic fault and CO_2 injection well.

3.2.1 Effect of polymer viscosity on its area of influence

The relationship between the polymer concentration and water viscosity multiplier was varied in the Eclipse simulation software as a proxy for the inclusion of delaying agents in the polymer solution (Table 4). Three cases were simulated for a fixed polymer injection period of 20 days and their radii of influence were noted.

Table 4 The relationship between the polymer concentration and water viscosity multiplier as a proxy for the inclusion of delaying agents in the polymer solution.

Polymer concentration (kg/m^3)	Water viscosity multiplier		
	High viscosity 0.005Mt polymer injected	Intermediate viscosity 0.08Mt polymer injected	Low viscosity 0.2Mt polymer injected
0	1	1	1
0.1	5	2	2
0.2	7	3	3
0.3	10	5	4
0.4	15	10	5
0.5	20	15	6
0.6	2000	100	10

Figure 13 shows the results of numerical simulations for three cases of polymer-gel injections with high, intermediate and low viscosity ranges, assuming a distance of 800m between the horizontal polymer injection well and the sub-seismic fault.

3.2.2 The proximity of polymer injection well to the sub-seismic leaky fault

From the previous set of cases, it was observed that a period of injection longer than 20 days may be required to mobilise the polymer towards the fault and potentially help in CO_2 flow diversion. Therefore, the period of injection was further increased to 60 days to allow a larger quantity of polymer in the reservoir. In addition, the distance between the polymer injection well and the fault was reduced to 400m (Figure 14). The depth of injection was varied between: i) at the bottom of the reservoir: 2050m, and ii) at the

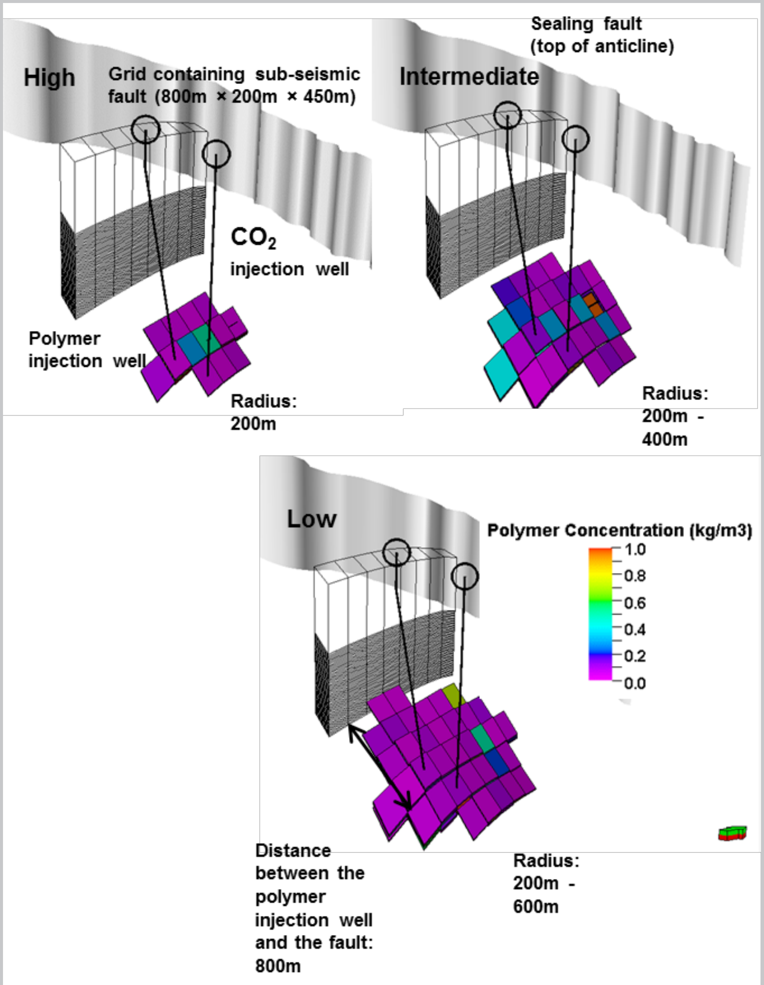

Figure 13 Area of influence after 20 days of polymer-gel injections for a) high, b) intermediate, and c) low viscosity cases.

top of the reservoir: 1800m. For both cases, the intermediate polymer viscosity was implemented.

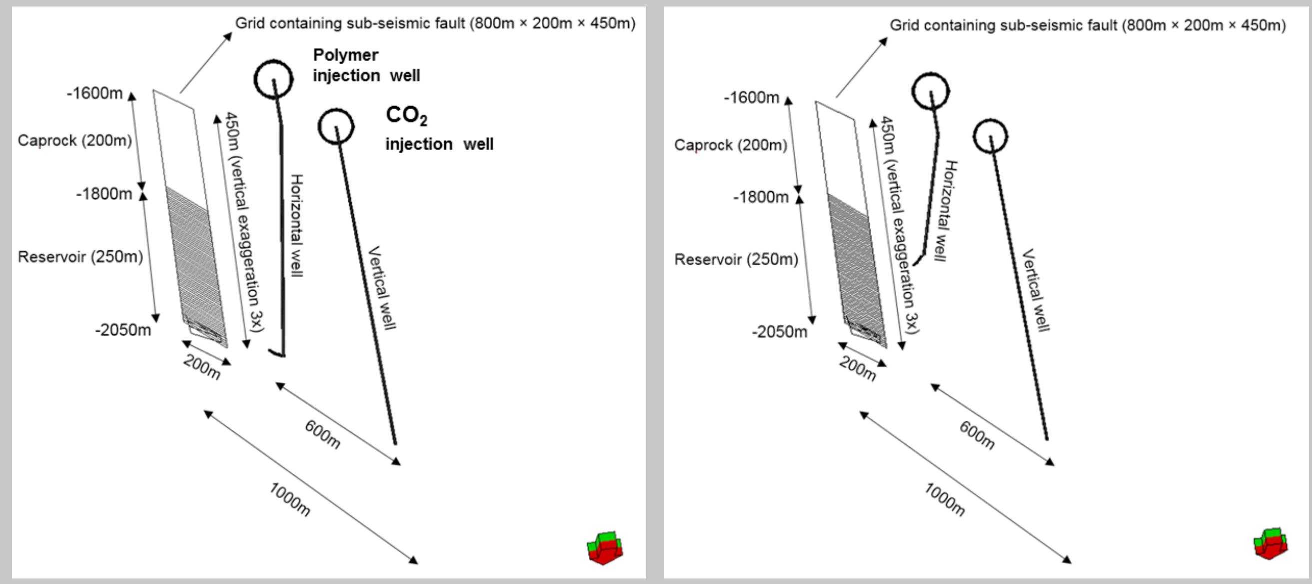

Figure 14 Layout of polymer injection well for cases of a) injection at the bottom of reservoir, and b) injection at the top of the reservoir.

The results show that increasing the period of injection, potentially clogs the CO_2 injection well when the polymer is injected at the bottom of the reservoir (Figure 15). Hence, polymer injection just below the caprock using the horizontal well configuration was found to be more suitable. The amount of polymer required is also potentially less when injected at shallower intervals.

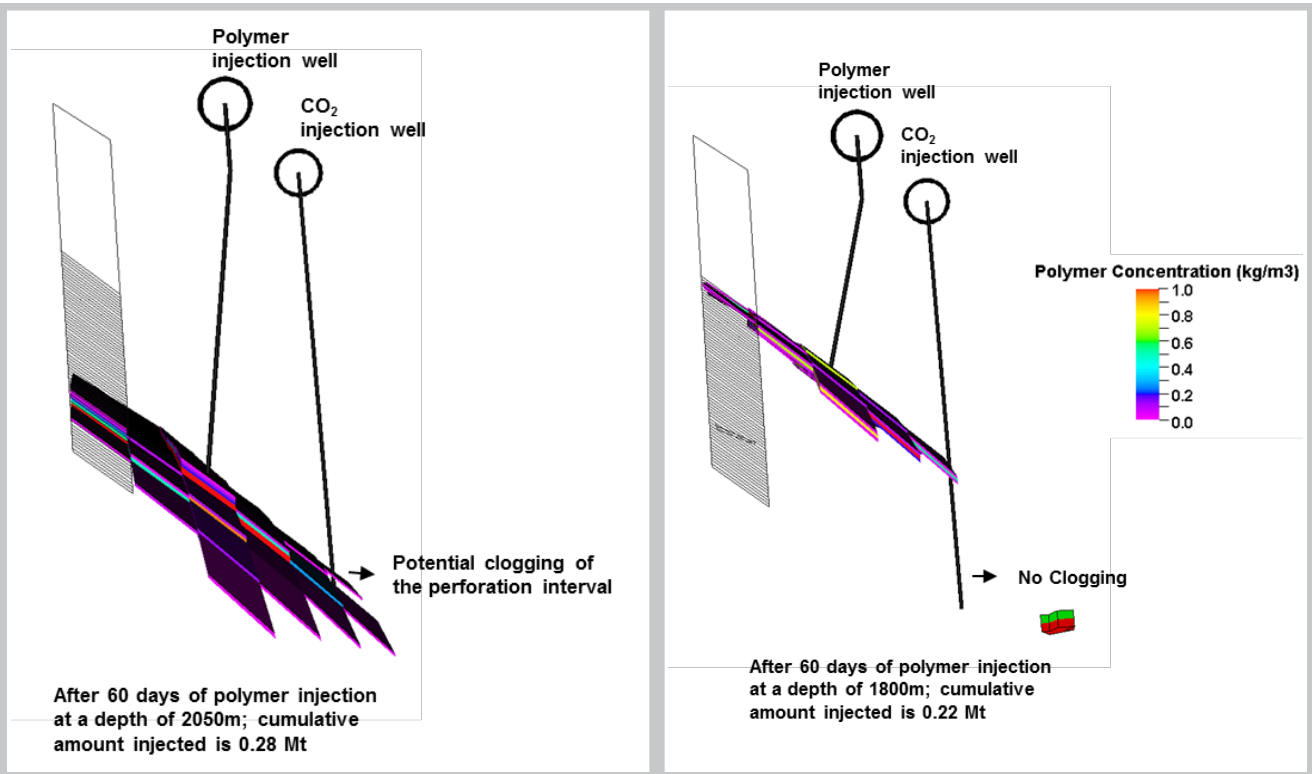

Figure 15 Numerical simulations of polymer injection at the a) bottom of the reservoir, and b) top of the reservoir.

Four cases in which the distance between the polymer injection well and the fault were reduced to200m and 400m from the fault and the results were compared. For all cases, the injection was performed at the top of the reservoir (depth of 1,800m). The effect of varying polymer viscosity was also considered for low and intermediate viscosity ranges (Table 5). The results of simulations are presented in Figure 16.

3.2.3 CO_2 leakage remediation results

To assess leakage remediation, it was assumed that gelation occurs almost immediately after the polymer injection was stopped. For example, considering case 1 in Table 5, after the polymer-gel treatment (assuming a high permeability reduction from 3000mD to 10-3mD, illustrated by the grey region in Figure 17b), CO_2 injection was resumed for the remaining simulation period. Figure 17 shows the results of CO_2 plume distribution after 1.7years when the CO_2 leakage was detected (Figure 17a), and after 5 years of post-remediation CO_2 injections (Figure 17b).

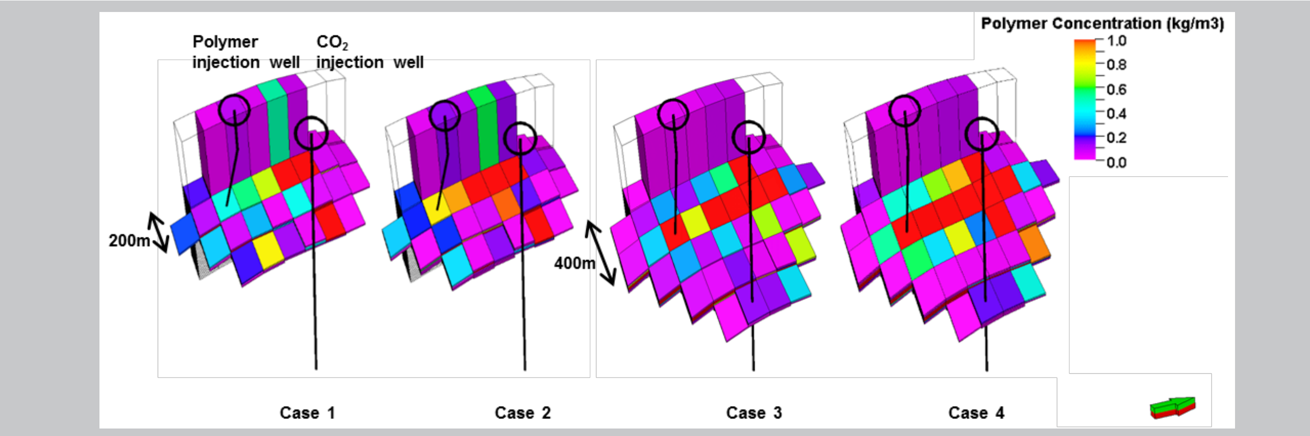

Figure 16 The results of numerical simulations for polymer-gel injections at different distances to the leaky fault and with various viscosities.

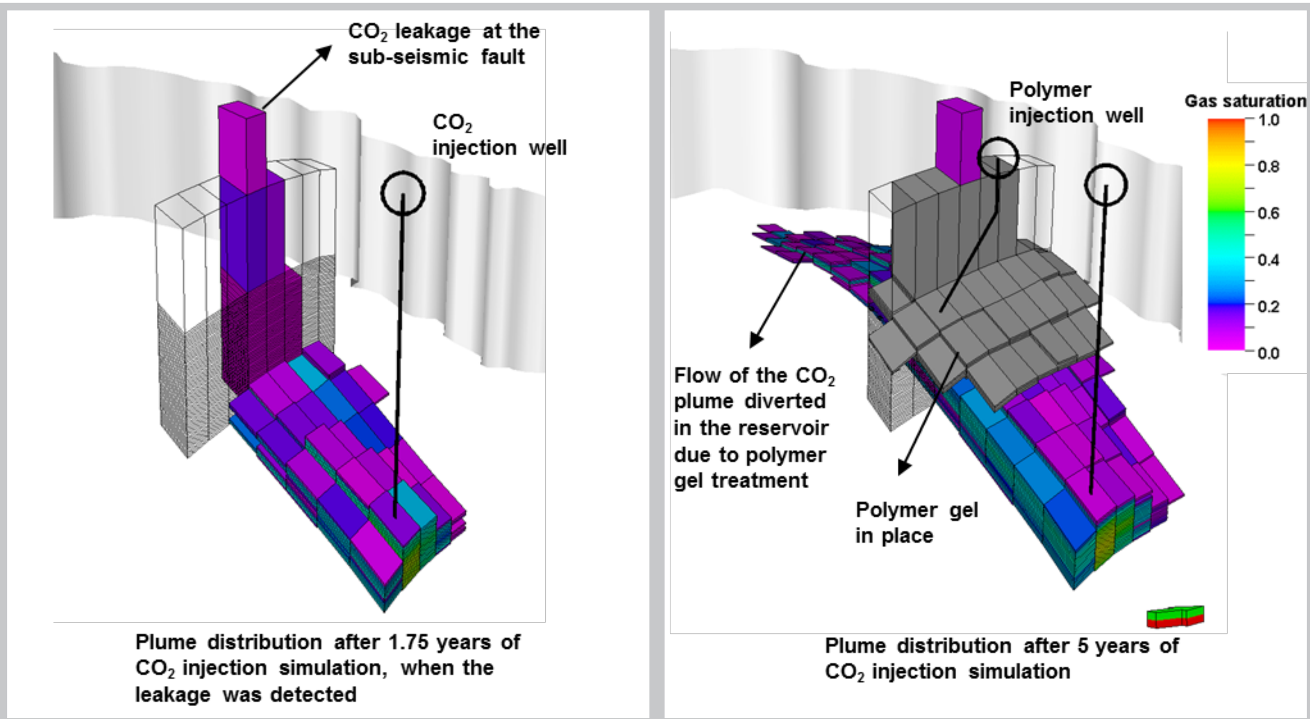

Figure 17 The results of numerical simulations of CO_2 plume distribution: (a) at the time of leakage detection, and (b) after 5 years of post-remediation CO_2 injections.

Table 5 Polymer-gel injection cases considered to assess the effect of proximity of the injection well to the leaky fault.

Distance of polymer injection from the fault (m)	Polymer Viscosity	Case #	Amount of polymer injected (Mt)	Time period of injection (days)
200	Low	1	0.29	30
	Intermediate	2	0.34	95
400	Low	3	0.59	60
	Intermediate	4	0.63	185

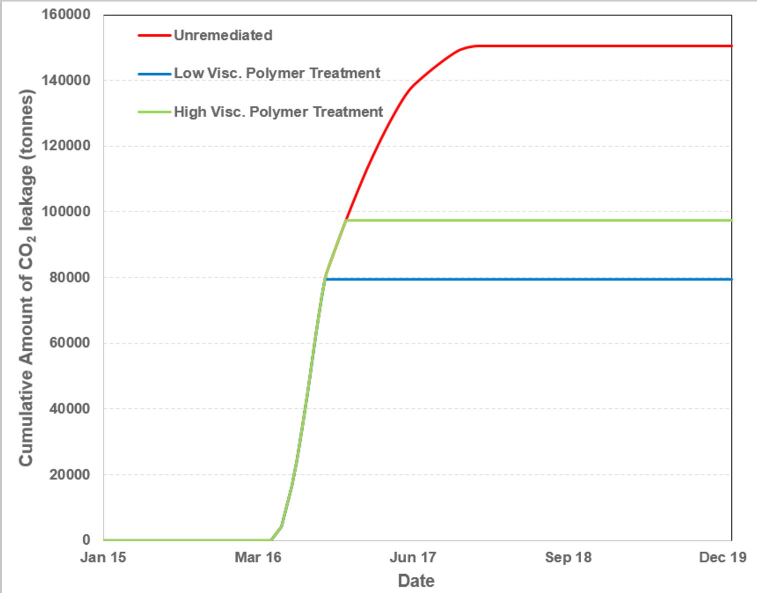

Figure 18 The results of CO_2 leakage remediation for cases of unremediated leakage, low and high viscosity polymer-gel treatments.

Figure 18 shows the comparison between of the amounts of CO_2 leaked into the shallower formations for the unremediated case, as well as the remediated cases using low and intermediate polymer viscosity ranges. For the unremediated case, the total amount of CO_2 loss from the reservoir without polymer treatment after the leakage was detected to be 160kt. For the remediated cases of intermediate and low polymer viscosities, the total amount of CO_2 leakage was estimated to be 80kt and 100kt respectively. The results showed that the polymer-gel solution seals the fault and diverts the CO_2 flow as desired. In the scenarios considered, an appreciable reduction in CO_2 leakage was thus achieved depending on the viscosity of the polymer-gel used and no CO_2 leakage was observed after the implementation of polymer-gel treatments.

3.3 Modelling CO_2 leakage remediation using polymer injection in a shallower aquifer above the caprock

A number of scenarios were considered for the remediation of CO_2 leakage through a subseismic fault in the caprock, using polymer injection via both horizontal and vertical well configurations (Figure 19). The vertical well configuration here was considered to be the CO_2 injection well. The scenarios are based on three factors:

- polymer gel viscosity.
- The layout of polymer injection well (vertical and horizontal configurations) and its proximity to the leaky sub-seismic fault.

CO_2 leakage remediation was assessed during a total simulation period of 5 years.

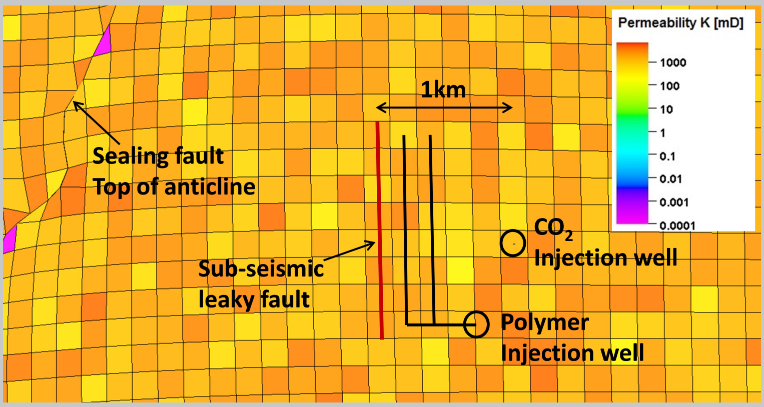

Figure 19 Location of polymer injection well in the shallow aquifer, sub-seismic fault and CO_2 injection well.

3.3.1 Effect of polymer viscosity on its area of influence

The relationship between the polymer concentration and water viscosity multiplier was varied in the Eclipse simulator as a proxy for the inclusion of delaying agents in the polymer solution (see Table 4). Figure 20 shows the results obtained from numerical simulations for two cases of polymer-gel injection into the shallow aquifer formation with intermediate and low viscosity ranges.

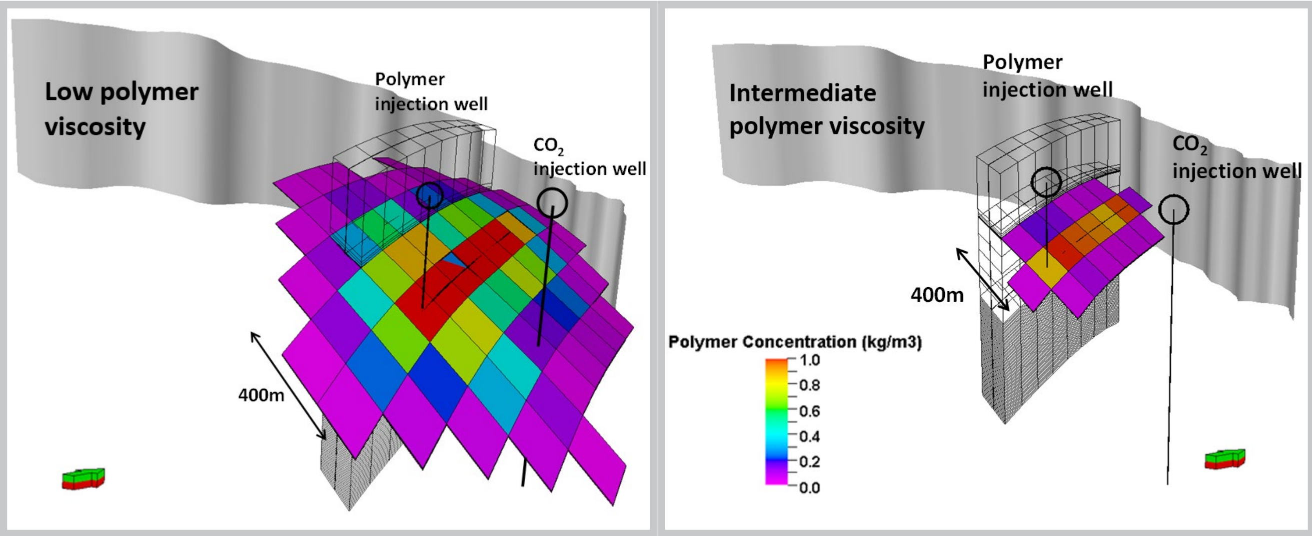

Figure 20 Area of influence after 7 months of polymer-gel injections for a) low, and b) intermediate viscosity cases.

3.3.2 The polymer injection well layout and its proximity to the leaky fault

The time period and amount of polymer required to seal the leaky fault at the top of the caprock was assessed. Four cases were considered in which the injection of polymer-gel at distances of less than 50m, 200m, 400m and 1000m from the fault were compared. For the first three cases, a horizontal injection well was used, whereas for the final case, the CO_2 injection well was used to inject polymer gel solution of low viscosity. In all the cases, the injection was performed at a depth just above the caprock (approximately 1,500m). The results of simulations are presented in Figure 21.

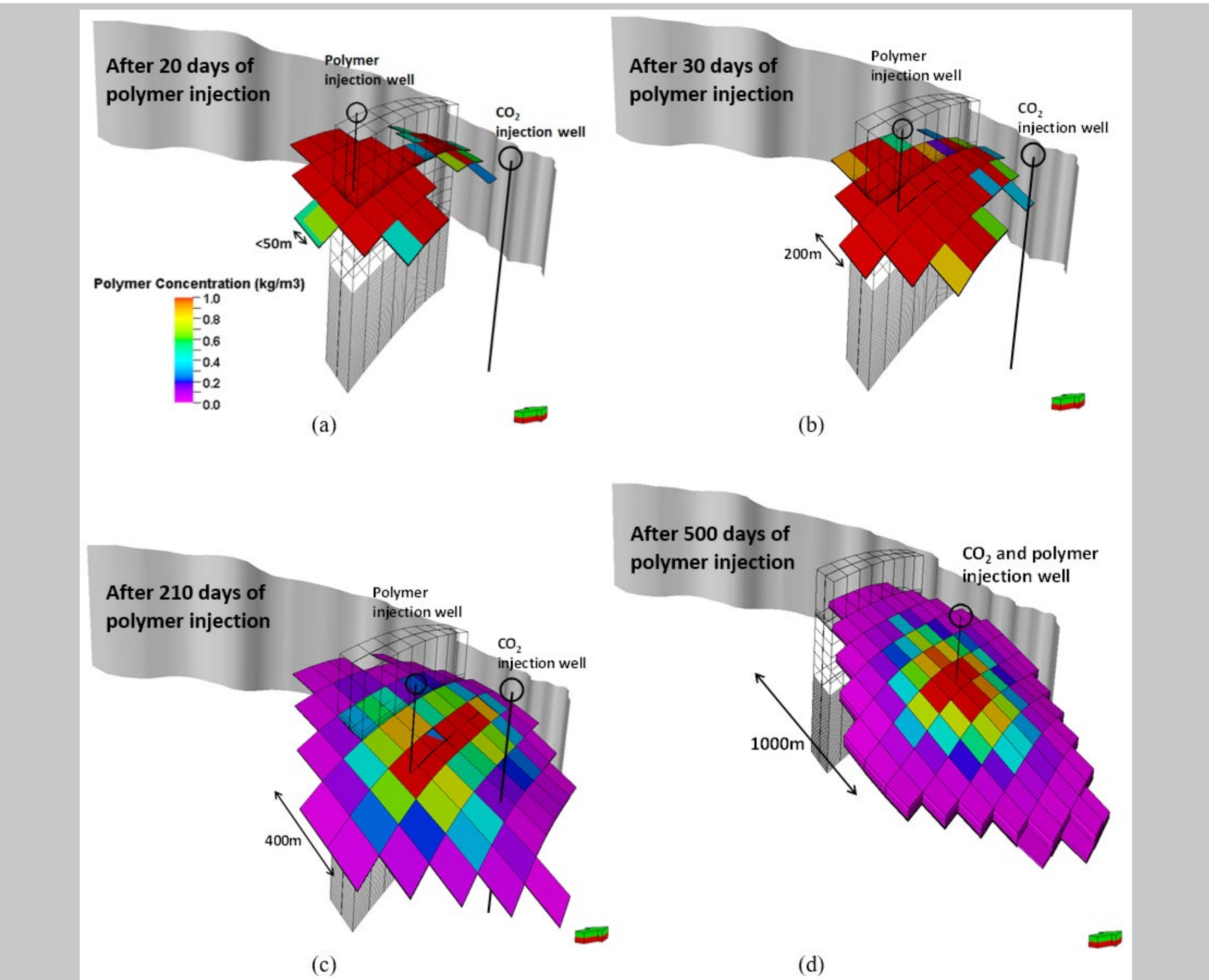

Figure 21 The results of numerical simulations for polymer-gel injections at different distances to the leaky fault and with horizontal (a, b and c) and vertical (d) layouts.

The results show that with increase in distance between polymer injection well and leaky fault, the time period required for effective polymer injection increases significantly. For instance, if polymer injection well located near the leaky faults (with less than 50m distance), the injection duration of 1 month would be sufficient to seal the fault, whereas, for the case of polymer injection location at 400m away from the fault, at least 7 months of polymer injection is to be expected. The amount of polymer required is also higher when injected at longer distances.

3.3.3 CO_2 leakage remediation results

To assess leakage remediation, it was assumed that gelation occurs almost immediately after the polymer injection was stopped. Table 6 presents a summary of polymer remediation cases including the amount of polymer gel and time period of injection required for each case. After polymer-gel treatment (case 5 in Table 6), CO_2 injection was resumed for the remaining simulation period. Figure 22 shows the results of CO_2 plume distribution after 9 months when the leakage was detected (Figure 22a), and after 5 years during the post-remediation period when CO_2 injection was resumed (Figure 22b).

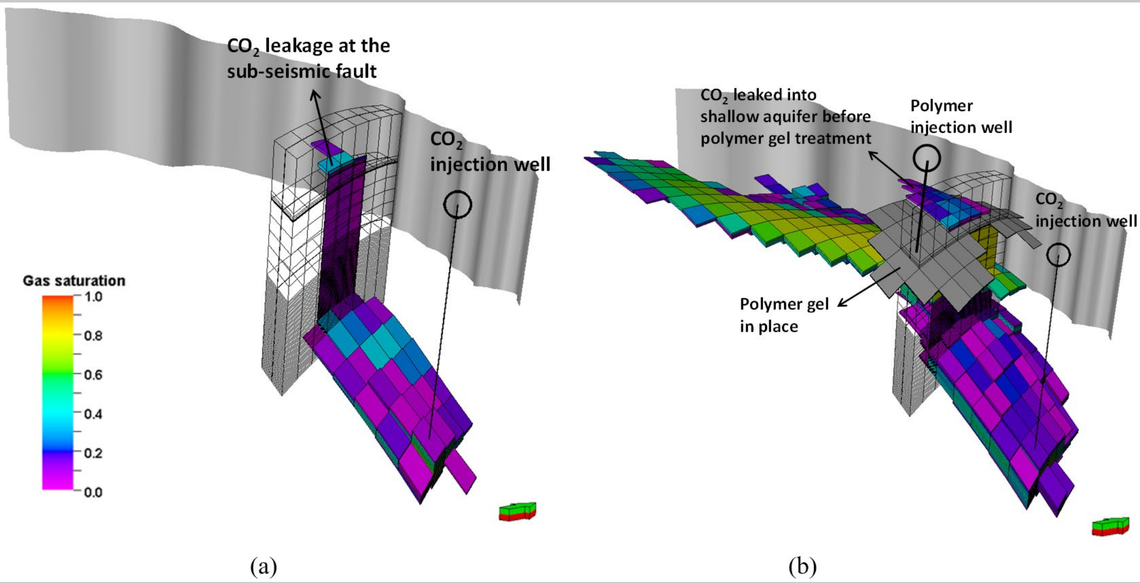

Figure 22 The results of numerical simulations of CO_2 plume distribution: (a) at the time of leakage detection, and (b) after 5 years of post-remediation CO_2 injections.

Table 6 The amount of polymer-gel and time period required for each polymer-gel remediation cases considered.

Distance of polymer injection from the fault (m)	Polymer Viscosity	Case #	Amount of polymer injected (Mt)	Time period of injection (days)
Less than 50m*	Low	5	0.15	20
200*	Low	6	0.24	30
	Intermediate	7	0.27	360
400*	Low	8	2.0	210
	Intermediate	9	0.4	400
1000**	Low	10	3.2	500

* Polymer-gel is injected using a horizontal well.
** Polymer-gel is injected using the main CO_2 injection well.

Figure 23 shows the results of the amount of CO_2 leakage into shallower formations for the unremediated case as well as the remediated cases of low and intermediate polymer viscosity ranges. Depending on the remediation case, the time period required for polymer-gel treatment (including well drilling and injection) varied between 7 to 29 months. Therefore, the amount of CO_2 leakage after detection and stopping of injection varies slightly. The total amount of CO_2 leaked into the shallow aquifer after the leakage was detected and CO_2 injection stopped was about 60kt. For remediated cases, this value lies between 55kt and 60kt. In these cases however, re-injection of CO_2 into the reservoir did not lead to further CO_2 leakage. In other words, for the scenarios considered no significant CO_2 leakage was observed after the polymer-gel treatments and subsequent re-injection of CO_2. The results showed that the polymer-gel solution seals the fault (assuming a high permeability reduction from 3000mD to 10-3mD, illustrated by the grey region in Figure 22b) and stops further CO_2 leakage into shallow aquifer as desired.

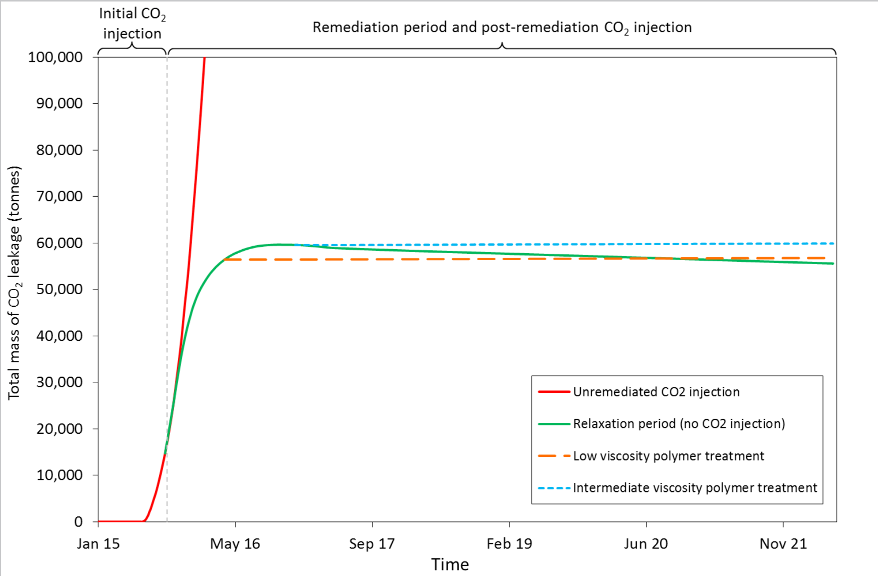

Figure 23 The results of CO_2 leakage remediation for cases of unremediated leakage, low and intermediate viscosity polymer-gel treatments.

4 COST ESTIMATION FOR THE POLYMER-GEL REMEDIATION CASES CONSIDERED

Depending on the type of polymer and crosslinker, different factors should be taken into account, depending on whether the polymer considered is present in emulsion or powder form. For instance, the AN1506 polymer used for the experimental studies in the project conducted at Imperial, its cost in powder form is estimated to be 3.2 €/kg. If a polymer solution with a concentration of 1,000ppm AN1506 is considered, and for every metre cube of solution prepared, 1 kilogram of powder AN1506 is required.

For the crosslinker, the cost of Tyzor 217 (with 5.6% Zr^+ concentration) manufactured by Dorf Ketal, is estimated to be €40 per gallon (equivalent to 10,000 €/m^3). Based on a 50ppm Zr^+ concentration in the final solution, for every metre cube of polymer solution to be injected, 0.001 m^3 (1L) of Tyzor 217 is required.

Table 7 Summary of the operational parameters assumed.

Polymer injection	Offshore cases
Depth of the sea water	120 m
Area for seismic (3D streamer)	16 km^2
Number of seismic surveys required*	2
Number of injection well	1
Number of pressure relief wells	1
Length of horizontal well	1600 m

** Assuming 2 seismic are required after the polymer injection.*

Table 8 Summary of the cost estimation for polymer-gel treatment cases considered for flow diversion option.

Case number	1	2	3	4
Time period of injection (days)	30	95	60	185
Amount and Time period of injection, (Mt) days	0.29	0.34	0.59	0.63
Depth at which polymer is injected (m)	1750	1750	1800	1800
Cost of polymer (M€)	0.92	1.08	1.88	2
Cost of crosslinker (M€)	3.09	3.63	6.29	6.72
Injection well: drilling new wells (M€)	20.40	20.40	20.45	20.45
Relief well: Re-use of abandoned wells (M€)	5.75	5.75	5.75	5.75
Injection well and relief well operation cost (M€)	0.05	0.16	0.10	0.31
Well plugging after the injection (M€)	2.90	2.90	2.90	2.90
Cost of seismic monitoring (M€)	1.28	1.28	1.28	1.28
SUM (M€)	34.39	35.20	38.65	39.41

In order to estimate the total cost of polymer-gel remediation, other components should be taken into account, such as the cost of drilling a new well (if required) and its orientation (vertical or horizontal), the cost of polymer solution preparation, transport, and equipment. In addition, depending on the zone (offshore or onshore), the constraints (ATEX area), the type of formation (permeability, salinity, pressure, temperature), and the pumping rates, the cost of remediation can be different. Table 7 provides a summary of the operational parameters assumed for the cost estimation polymer-gel treatment. Tables 8 and 9 present summary of cost estimations for polymer-gel treatment cases considered for flow diversion option and caprock leakage remediation option, respectively.

Table 8 Summary of the cost estimation for polymer-gel treatment cases considered for flow diversion option.

Case number	5	6	7	8	9	10
Time period of injection (days)	20	30	360	210	400	500
Amount and Time period of injection, (Mt) days	0.15	0.24	0.27	2	0.4	3.2
Depth at which polymer is injected (m)	1500	1550	1550	1600	1600	1800
Cost of polymer (M€)	0.48	0.76	0.86	6.36	1.27	10.18
Cost of crosslinker (M€)	1.6	2.55	2.88	21.33	4.27	34.14
Injection well: drilling new wells (M€)	20.19	20.22	20.22	20.26	20.26	5.75
Relief well: Re-use of abandoned wells (M€)	5.75	5.75	5.75	5.75	5.75	5.75
Injection well and relief well operation cost (M€)	0.03	0.05	0.60	0.35	0.66	0.29
Well plugging after the injection (M€)	2.90	2.90	2.90	2.90	2.90	2.90
Cost of seismic monitoring (M€)	1.28	1.28	1.28	1.28	1.28	1.28
SUM (M€)	32.24	33.51	34.49	58.23	36.40	60.29

SEALANT DELIVERY USING HYDRAULICALLY CREATED FRACTURES

5 INTRODUCTION

In MiReCOl project, new methods to remediate CO_2 leakage using sealant and faults have been studied. In particular, it was evaluated to establish if it is possible to use hydraulically created fractures to transport sealant gel (or foams) to a leaky faults or, more in general, to a leaky areas or to create an impermeable horizontal barrier. In the literature, it is possible to find many publications that describe methods of intervention on leaking wells, like wellhead repair, patching casing and more, because leaking wells are probably to most common situation that leads to CO_2 migration to the surface. Figure 24 presents different leakage mechanisms in CO_2 storage (Tongwa et al., 2013).

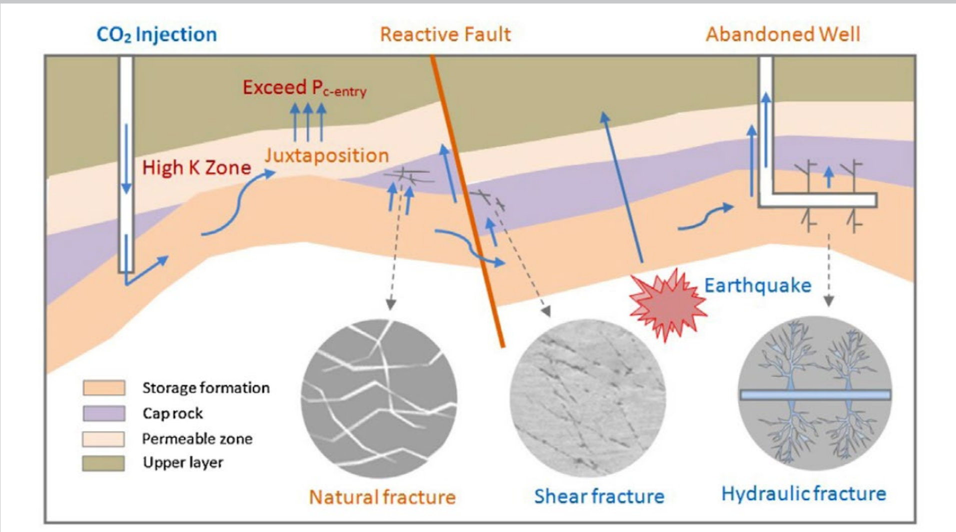

Figure 24 Possible CO_2 leakage mechanisms: through naturally occurring high permeability zones, through natural conduits and wells (after Tongwa et al., 2013).

This report does not address CO_2 leakage through wells, but other problematic cases: for example through caprock failings or leaking faults and fractures or high permeability areas. The most common solution adopted in these situations is perhaps to relieve the pressure in the CO_2 storage formation. Decreasing the pressure in the formation by dissolving CO_2 or stopping the injection of CO_2, can be a successful technique to reduce the leakage or avoid that the CO_2 reaches potentially dangerous area, like faults or highly permeable layers. In some cases this system might not be enough to prevent leakage, and other approaches, such as drilling new injection wells may be necessary. Research carried out under this part of the project investigated the possibility of transporting sealing material, such as gel-based polymers or foam, through hydraulically created fractures to the leaking location. Polymers and foam have been already used to seal leaking wells, but the plume penetrates the matrix only for few inches because of the low applied pressures. Geopolymers have the capability to resist to corrosion and the chemical resistance to CO_2 over a long period of time. For this reason, these polymers are already a valid option to substitute the conventional cements in CO_2 sequestration wells. Several potential fracture sealing materials have been already texted. In particular in Tongwa et al. (2013) the focus was on materials that can seal or at least reduce the permeability of faults and fractures. In their paper they have shown that paraffin wax, silica- and polymer-based gel and micro-cement have the capability to significantly reduce the fracture permeability. They conclude that for fractures larger than 0.5 mm, the micro-cement would be the material of choice to seal CO_2 leakage pathways, despite this cement might not be chemically stable because of carbonation. In case of smaller cracks, with width smaller than 0.25 mm, polymer gels with a polymer concentration between 4,000 and 8,500 ppm are efficient sealants and chemically stable when in contact with CO_2. In this project a model was built using the commercial software MFRAC to study how well one can distribute the sealant and how far one can take it by creating a hydrofracture, implementing the mechanical properties of the polymer gel or the micro-cement. The performance of different kind of sealing materials, in combination or not with a proppant, was investigated to determine the ones that better deliver this new technique.

5.1 THE P18 FIELD

5.2 Geology

As already mentioned in the introduction, the P18 field is located offshore, around 20 km off the coast of the Netherlands, in proximity of the port of Rotterdam. This field is contained into sandstones from the Triassic age, below impermeable layers of clay. This field is divided into 3 main blocks, bounded by a system of NW-SE oriented normal faults. The top of these 3 blocks is in between 3175 and 3455 m depth below sea level. The area that comprehend the P18 field is very faulted and consist on fault bounded compartments. Production data indicate that most of the faults between the various compartments are sealing, at least on production time scale. The cap rock (primary seal) of the P18 is 150 meters thick and it directly covers the reservoir's blocks. In the overburden, directly above the primary seal, it is present a secondary seal, the Altena group, which is roughly 500 meters thick. The remaining of the overburden is constituted by different geological formations, some of which also have sealing properties. In figure 25 and 26, taken from (Arts et al. 2012) it is presented the geology and a 3D view of the P18 gas field.

For a more detailed description of the geology, the available data and the studies about the P18 field that already have been made, refer to (Arts et al., 2012 and Brouwer et al., 2011).

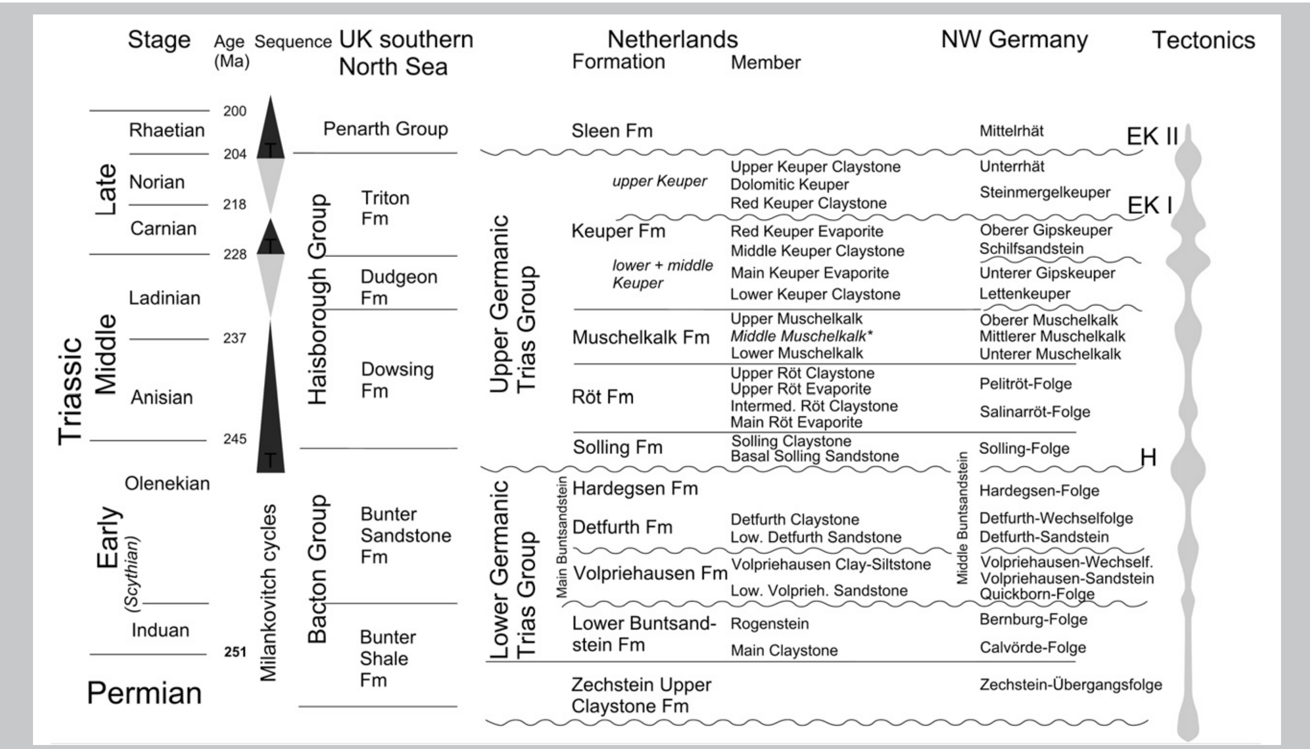

Figure 25 Overview of group and formation names and stages and sequences.

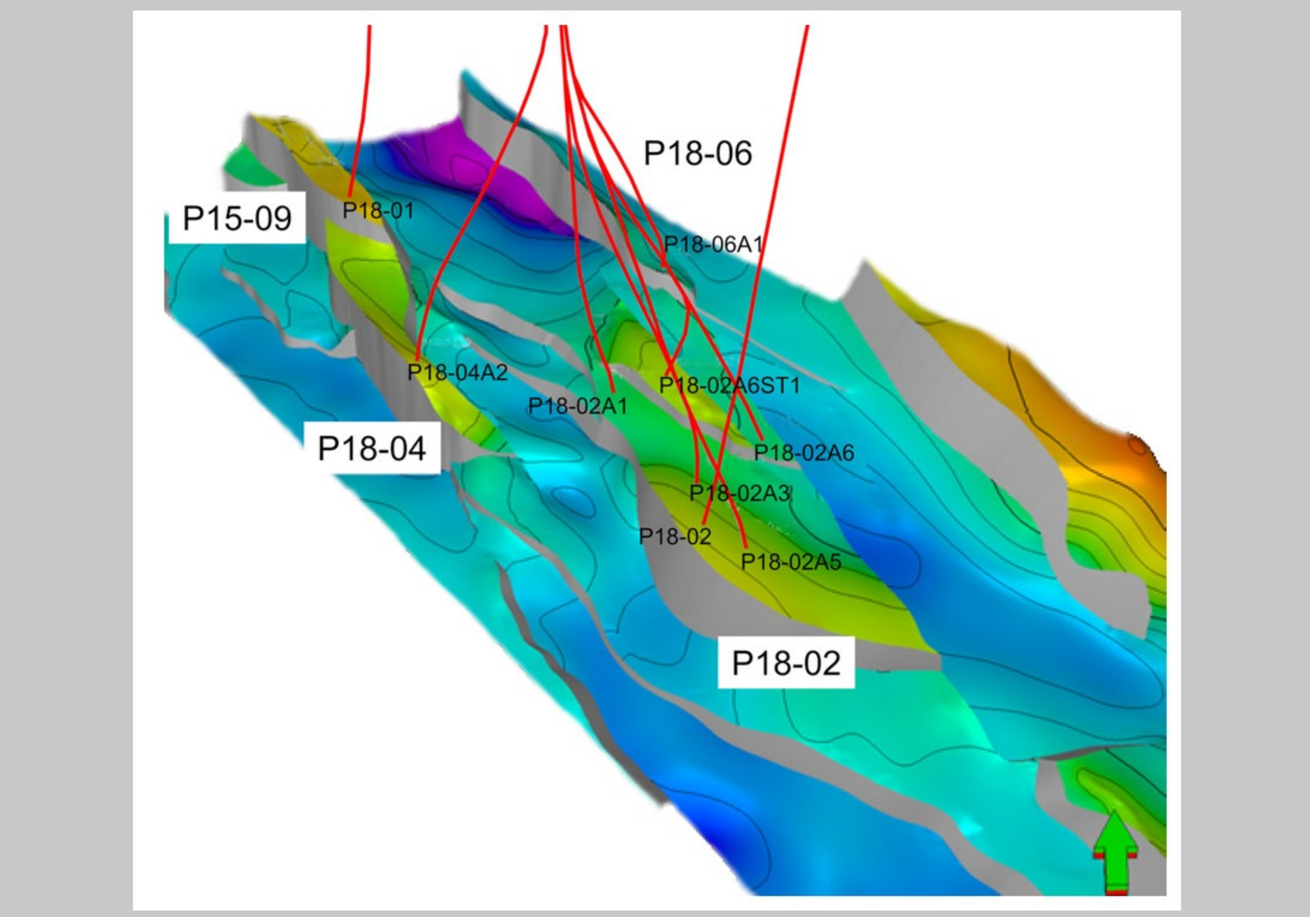

Figure 26 3D view of the top of the P18 fields. Faults are shown in grey, well traces are shown in red.

5.3 Leakage scenarios

Several CO_2 migration scenarios have already studied in the Feasibility study P18 (final report) (Brouwer et al., 2011) (in Chapter 8), to determine the risk of migration of CO_2 through the overburden. In particular 3 migration paths had been taken into account: through the aquifer spill reservoir, through an induced fracture into the primary seal with a migration of CO_2 into the sandstone and through a wellbore shortcut. For these migration analysis it has been built and used a Petrel model of the overburden. In this study it has been concluded that the most plausible migration pathway of the stored CO_2 to the surface is via leaking wells and that the CO_2 would reach directly the atmosphere through the wells and not via pathway that developed within the overburden. Despite the conclusion of the Feasibility study P18 (Brouwer et al., 2011), we believe that the structure and geology of the P18 reservoir is optimal to simulate as well the case of CO_2 leakage through existing faults. Case that is ideal to test the method, use hydro-fractures to transport the sealant to a leaking location that we want to apply.

5.4 Methodology

There are already many different mitigation and remediation technologies to apply in case of unwanted migration of CO_2 from CO_2 geological storage units. Some of them have already been used in real cases, while others only in laboratory tests. An interesting overview of these different techniques can be found in (Manceau et al., 2014). The characteristics, the viscous, mechanical and chemical properties of polymer gels match perfectly the needs of a method to mitigate leakages. Our idea is to create and use hydro-fractures to transport the sealant gel to the leaky fault to mitigate or remediate the CO_2 leakage. Another interesting option would be to stimulate a horizontal hydro-fracture to create a sort of blanket that act like an impermeable barrier (see Figure 27). This would be possible only for shallower reservoir than the P18 field because at the depth of the P18 reservoir the vertical stresses would be too high to create a horizontal fracture.

We will perform the numerical simulations with the software MFRAC. After creating the 1D geomechanical model of a section of the P18 field, we will import the 1D model into the software and we will try different kind of injection rates and replace the proppant by polymer based gels. Playing with different viscosity, mechanical and chemical properties of the gel and with different injection rate of the fluid, we want to study how far, how well and how accurate we can transport the sealant to a leaky location. We do not want to constrain the results of our study only to the P18 gas field, but to define which parameters control the effectiveness of the 2 methods that we proposed, to allow operators to use these solutions also for other fields.

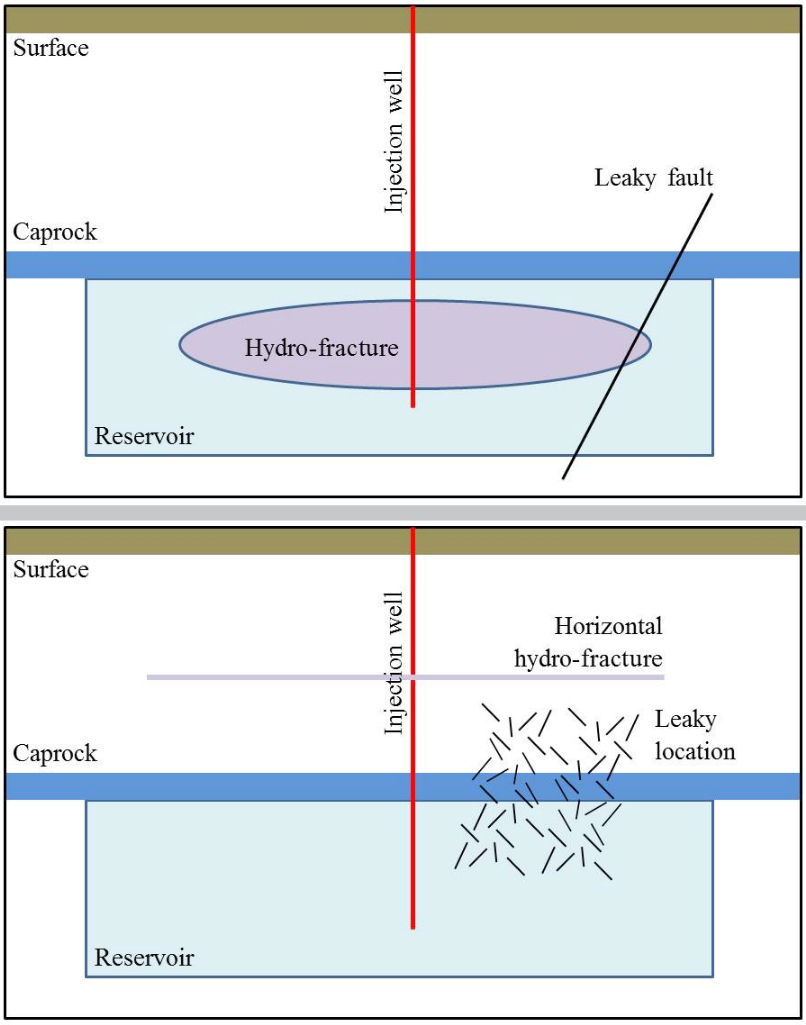

Figure 27 Schematic representation of the methods.

5.5 Selection of the model

We decided to proceed with the first model that has been presented in the previous section (inducing a hydrofracture to transport the sealant to the leaky location). Before beginning to develop such a model, we analysed the advantages and disadvantages of this approach.

We want to reach a leaking fault (or fracture) in the reservoir and spread as more sealant as we can on a surface as wide as possible. Faults and fractures are surrounded by a damaged zone with permeability much higher than the reservoir (up to 10 times higher) and we can use this higher permeability to spread the sealant polymer on a wider surface.

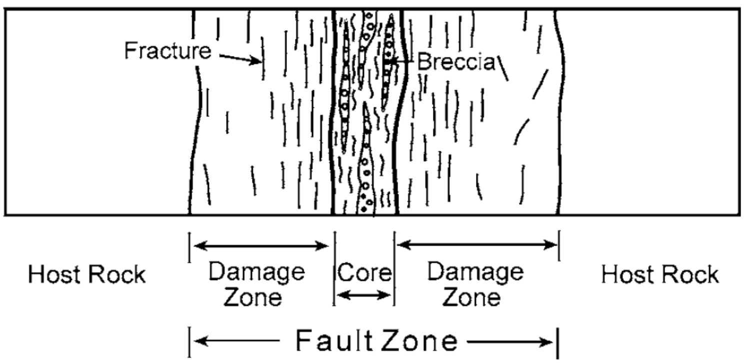

Figure 28 The fault zone is composed of 2 main mechanical units: a core and a damaged zone. (Gudmundson, 2003).

The first important choice we needed to take it was about the orientation of the well: vertical or horizontal.

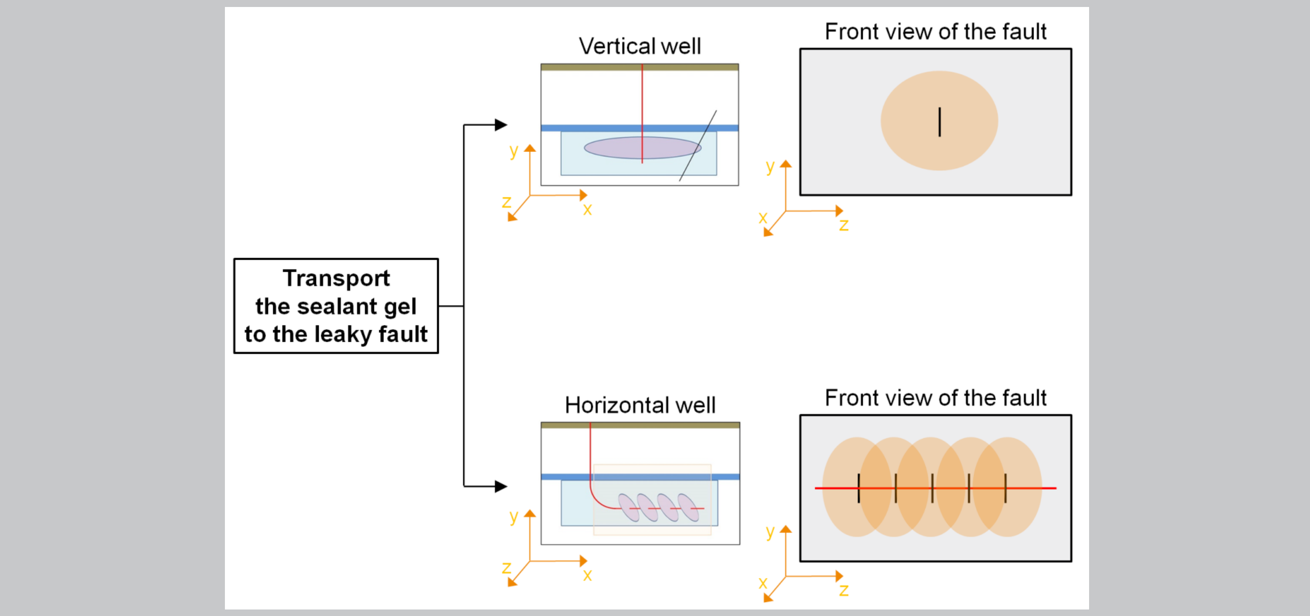

Figure 29 Hydraulic fracturing via vertical or horizontal well.

If we hydrofracture the reservoir using a vertical well, we can induce one hydrofracture at the time. Because of that we need to locate the leaking area with good precision to be able to transport the sealant where it is needed. With an horizontal well it is possible to create several hydrofractures simultaneously. In this case we can potentially cover a much wider area of the fault's surface with the sealant. On the other hand, because of the high permeable damaged zone around the fault's surface, a single hydrofracture might also be enough to reach the degree of mitigation that we desire. Unfortunately in out model it was not possible to incorporate the higher permeability of the damaged zone. Therefore we can only speculate about the influence that the enhanced permeability of the damaged zone has on the surface of the fault that it is covered by the sealant. As final remark, it is important to keep in mind that to drill an horizontal well it is much more expensive than a vertical one and that, at least in the case of the P18-4, the vertical well is already in place without the need of any extra costs.

The second choice was related to the location of the hydrofracture: above or inside the reservoir. This choice is strictly correlated with the weight of the sealant polymer that it is used to create the hydrofracture.

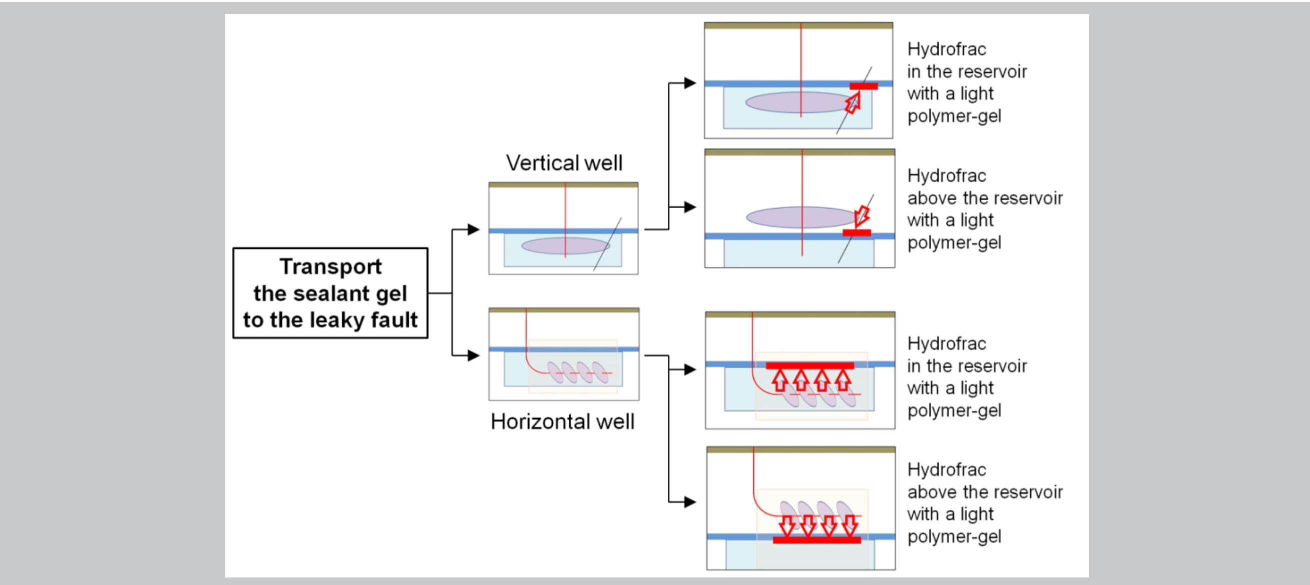

Figure 30 Hydraulic fracturing above (with heavy polymer-gel) or within (with light polymer-gel) the reservoir.

If we provoke an hydrofracture within the reservoir, we have to be careful to not damage the caprock. We have to take in some way under control the vertical propagation of the hydrofracture. If we hydrofracture above the reservoir we would not risk to damage the cap rock. Another advantage of hydrofracturing above the caprock is related to the rock permeability: within the reservoir the permeability is much higher than above the caprock and it is much more complicated to hydrofrac a rock with high permeability than a rock with low permeability (because of the leak off). For the P18-4 case, for example, above the caprock the permeability of the rock matrix is in the range of the 0.1 mD and within the reservoir is in the range of 150 mD. In case we would induce an hydrofrac within the reservoir, we would choose a light polymer as sealant (to have a flow in the direction of the surface) while for the other case, fracturing above the caprock, we would need a heavy polymer, to have a flow in opposite direction and to reach the leaking fault from the top.

Considering the physical advantages and disadvantages together with the financial considerations and with the fact that probably no institution would allow to hydrofrac above the caprock, especially it is already leaking, we decided to model the case with the vertical well and to hydrofrac within the reservoir using a light polymer gel.

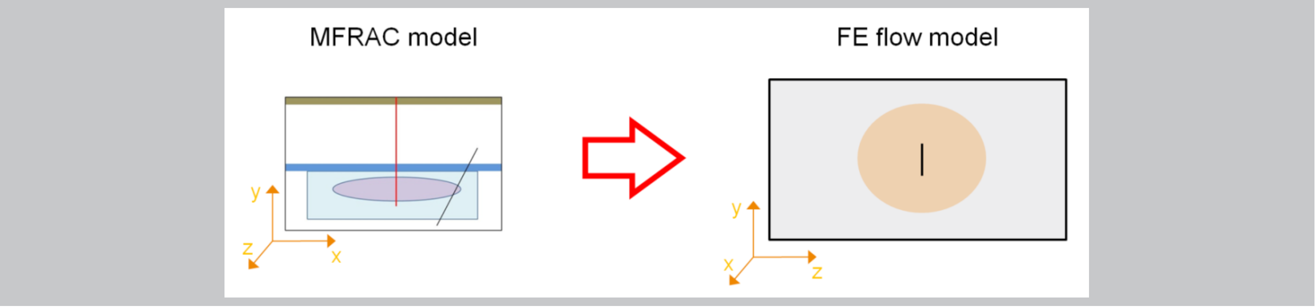

Figure 31 Modelled scenario: vertical well and hydrofracture inside the reservoir.

5.6 Results

The P18-4 well has been modelled using the commercial software MFRAC.

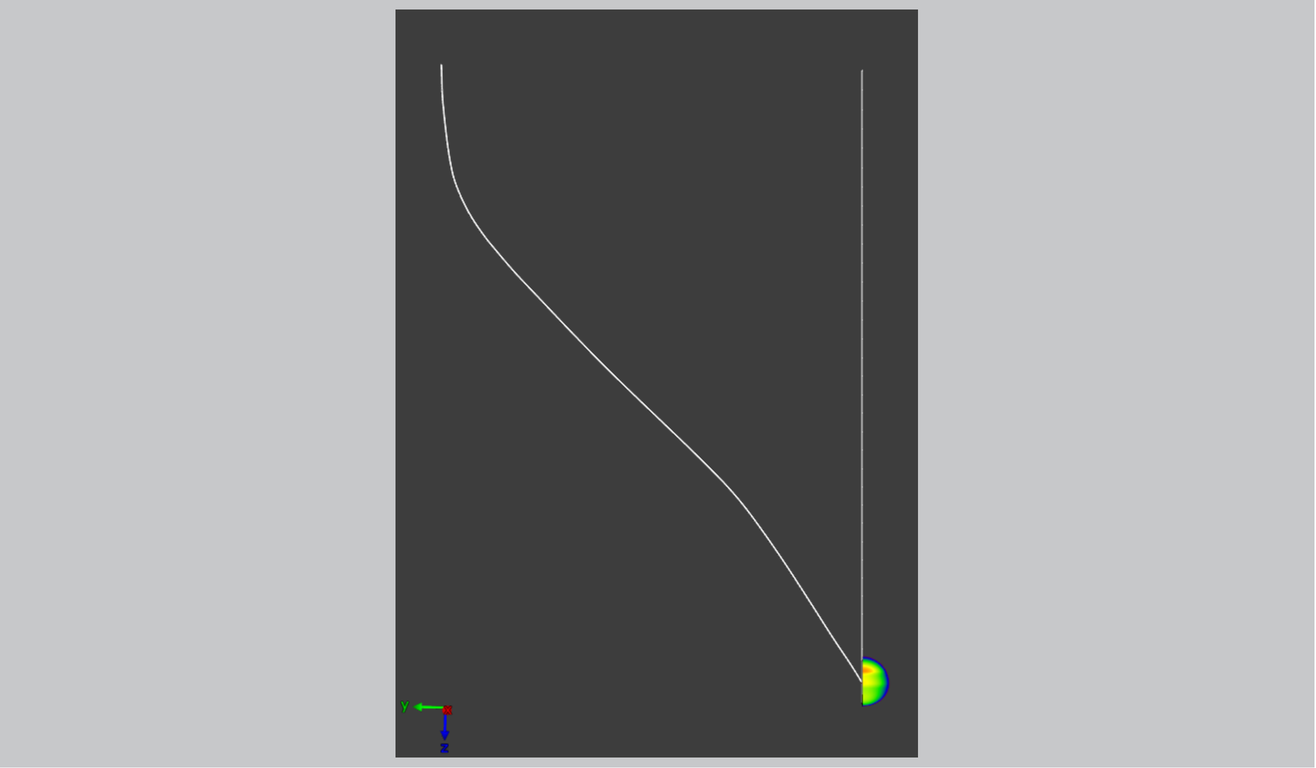

Figure 32 Side view of the well P18-4 in MFRAC with an hydraulically induced fracture.

The mechanical properties adopted are shown in Figure 34.

For the reservoir has been considered a permeability of 100 mD.

To induce the hydrofracture, we considered 100 perforations of 0.39 inches of diameter between 4244 m and 4261 m MD (3340-3355 m TVD).

In Figure 35, 36 and 37 it is presented the treatment schedule that has been adopted to perform the crack job.

As it has been mentioned earlier in this report, we are hydrofracking an exhausted reservoir that has high permeability. For this reason the leak off is high and therefore unfavourable to perform a crack job. The distance that we can reach with the sealant

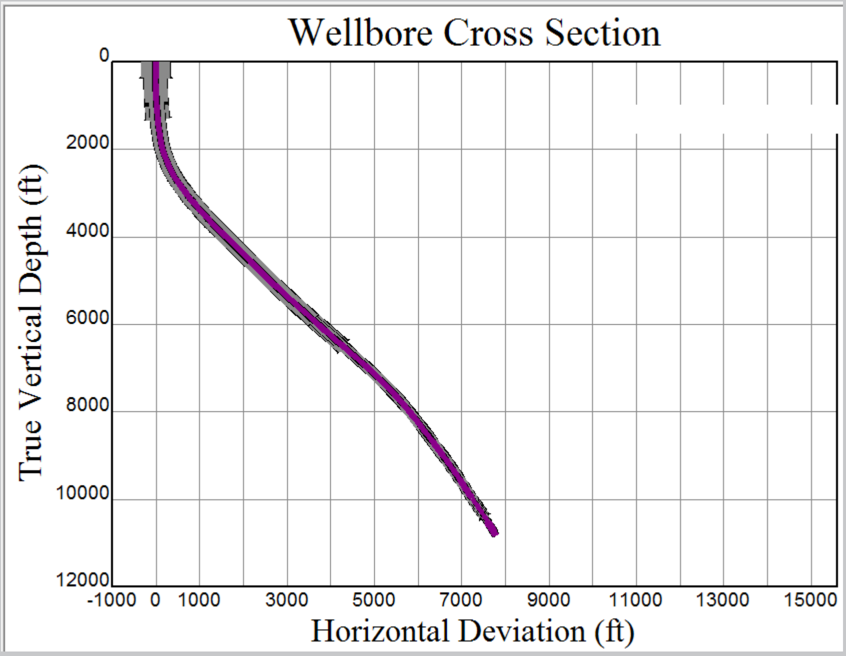

Figure 33 P18-4 wellbore cross section.

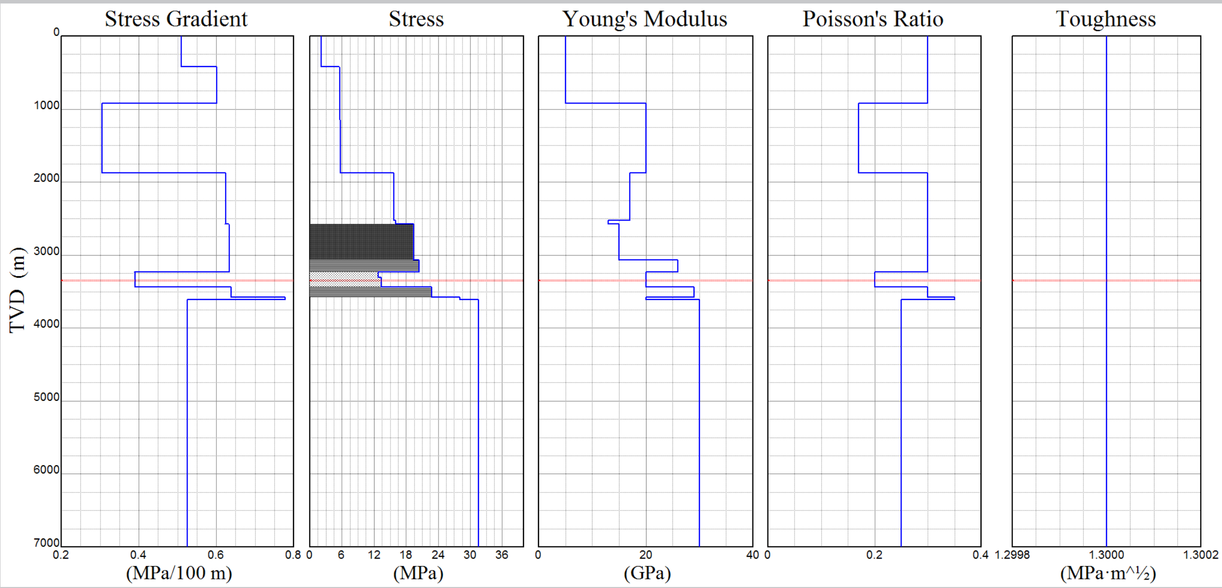

Figure 34 Mechanical properties. The red line indicates the perforations interval (3340-3355 m TVD).

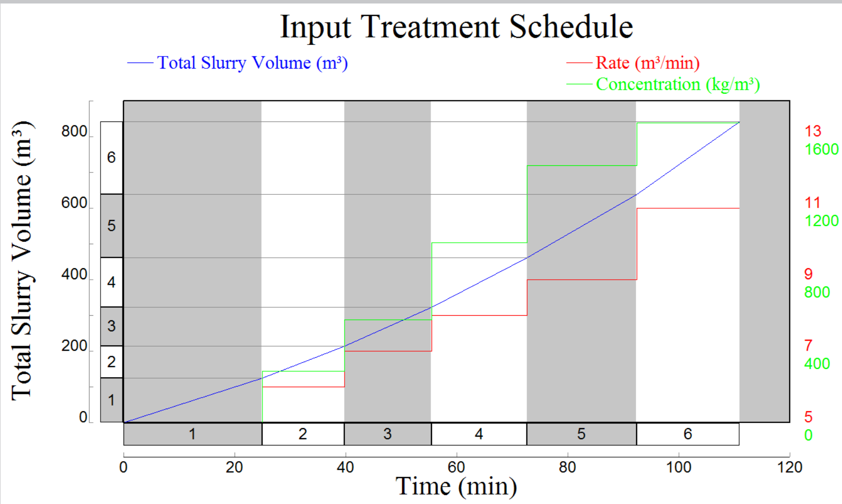

Figure 35 Input treatment schedule: tot al slurry volume, rate and concentration.

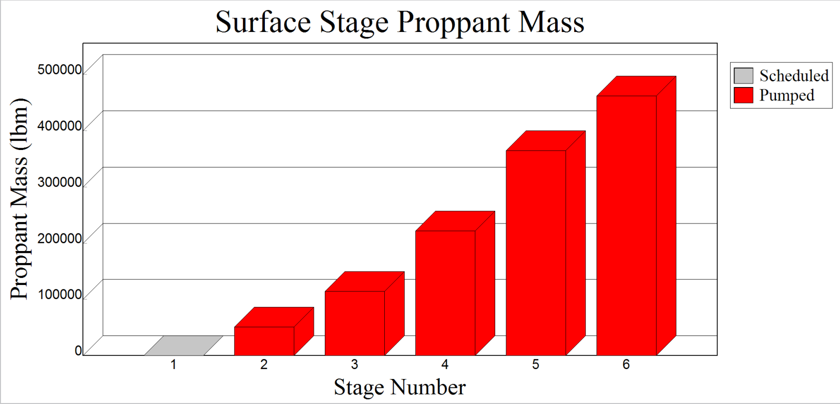

Figure 36 Input treatment schedule: surface stage proppant mass.

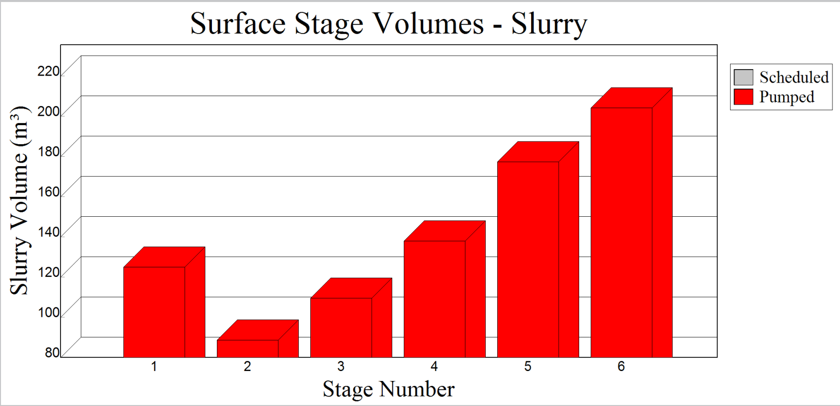

Figure 37 Input treatment schedule: surface stage volumes for the slurry.

strongly depends on the leak off coefficient. For low leak off coefficient the crack develops along the border with the caprock. For higher values of the leak off, the crack does not risk to penetrate into the caprock.

As it is shown in Figure 38, in the geological configuration of the P18 field, the hydrofracture tends to develop more in the vertical direction than in the horizontal direction. In the figure below it is shown the shape of the hydrofrac related to the leakoff of 10-5 ft/min$^{1/2}$.

In this situation we created a fracture 185 meter long. Assuming, for example, to intersect the leaking fault after 140 meters, we would be able to cover 26500 m^2 with the sealing polymer. The surface of the leaking fault that is covered by the sealing polymer obviously depends from the distance of the leaking fault from the injection well.

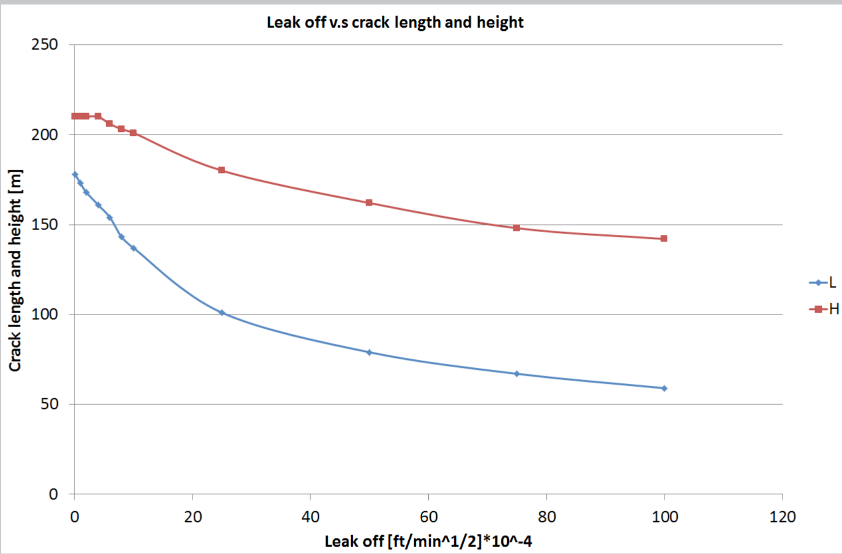

Figure 38 Leak off versus crack length and height.

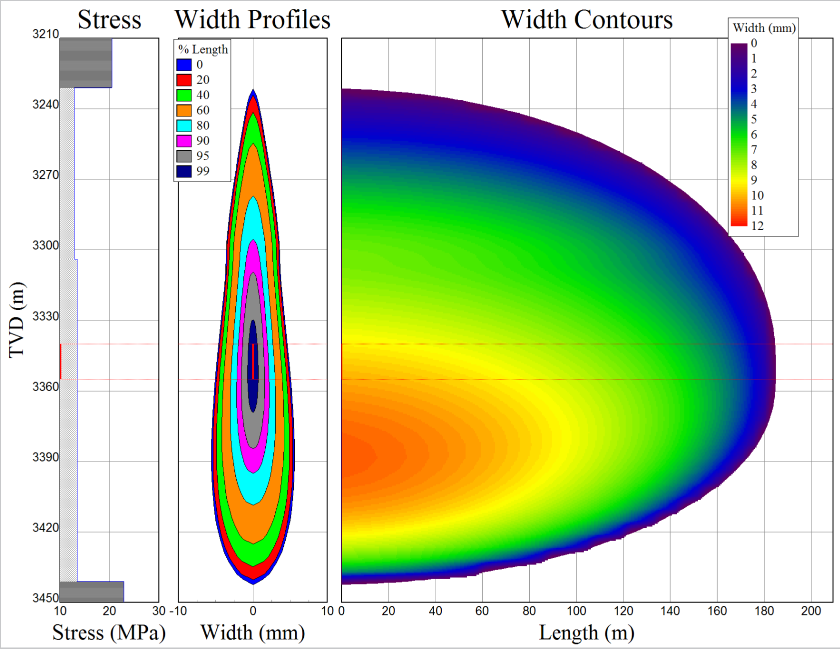

Figure 39 Width and length of an hydrofracture (leak off 10-5 ft/min^1/2).

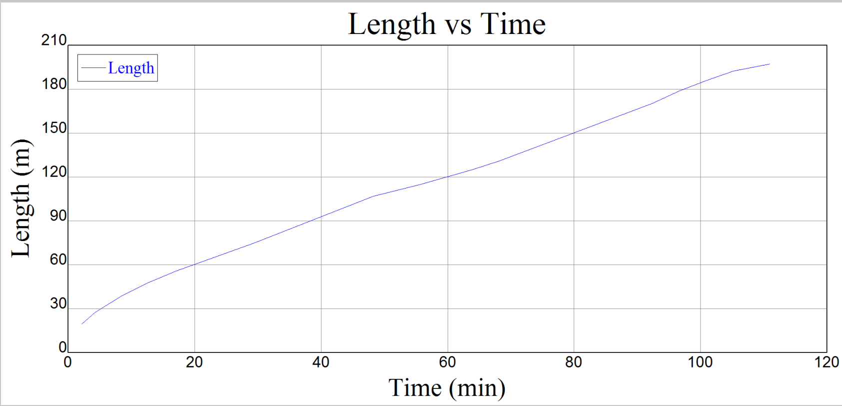

Figure 40 Fracture length versus time.

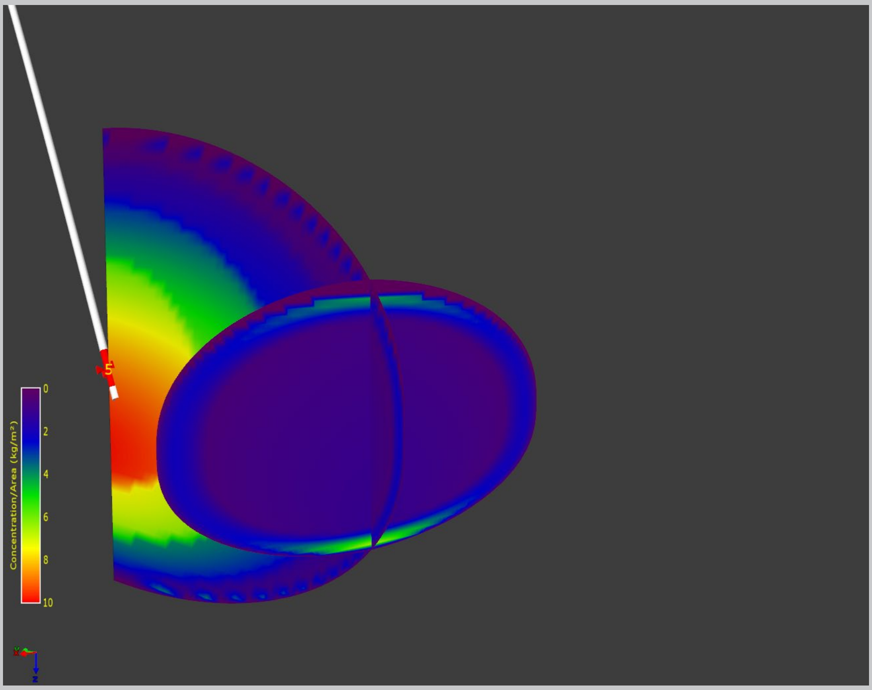

Figure 41 Area of the leaking fault covered by the sealing polymer.

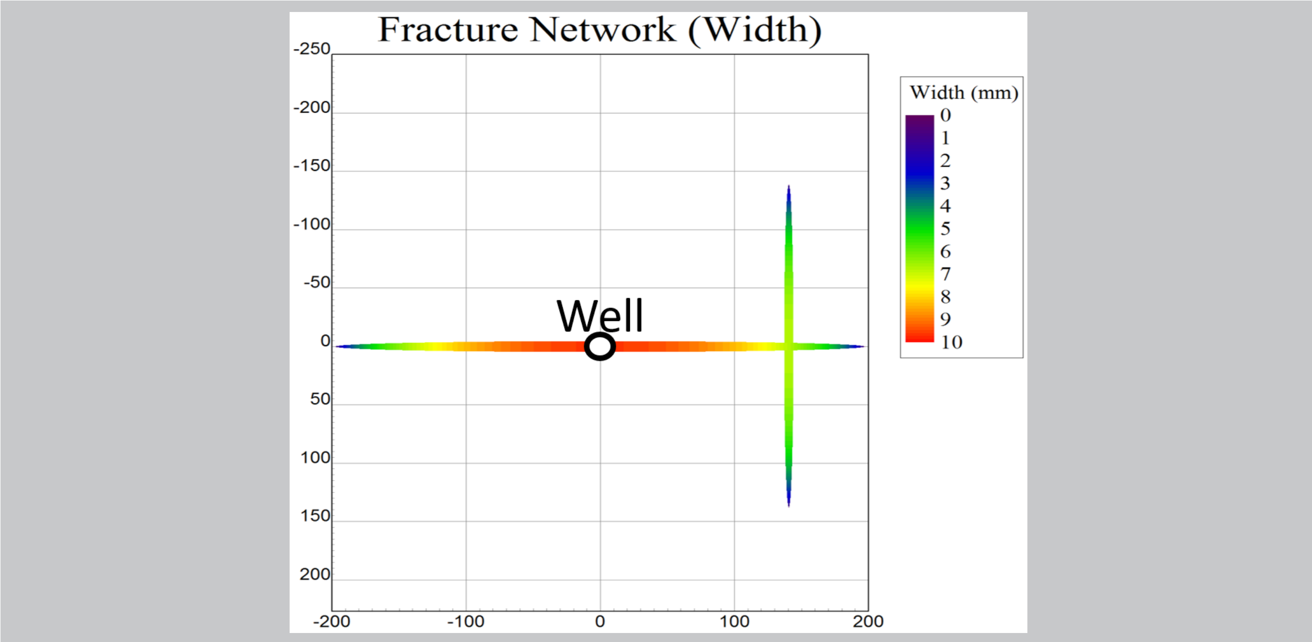

Figure 42 Top view of the fracture network (hydrofracture and leaking fault).

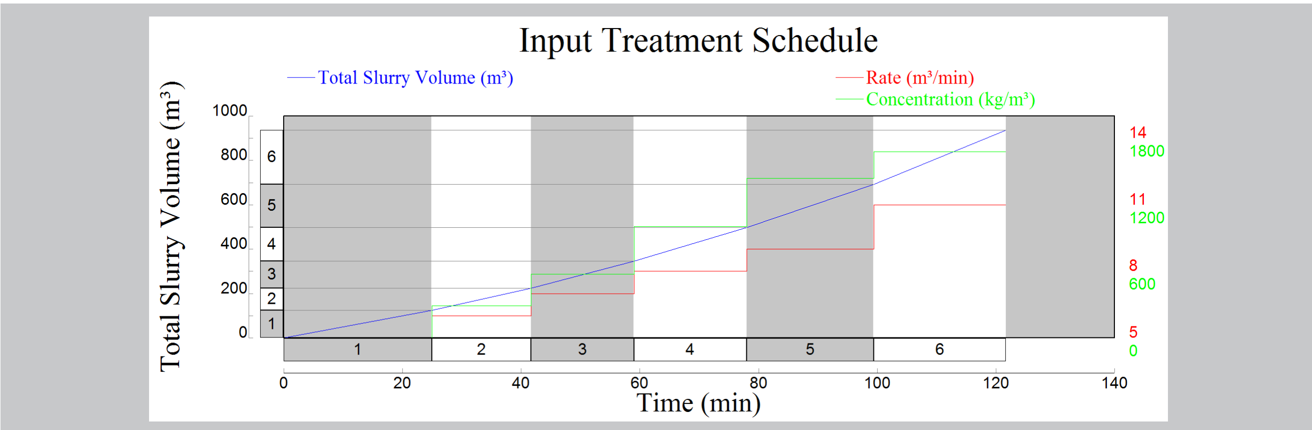

Figure 43 Input treatment schedule: tot al slurry volume, rate and concentration.

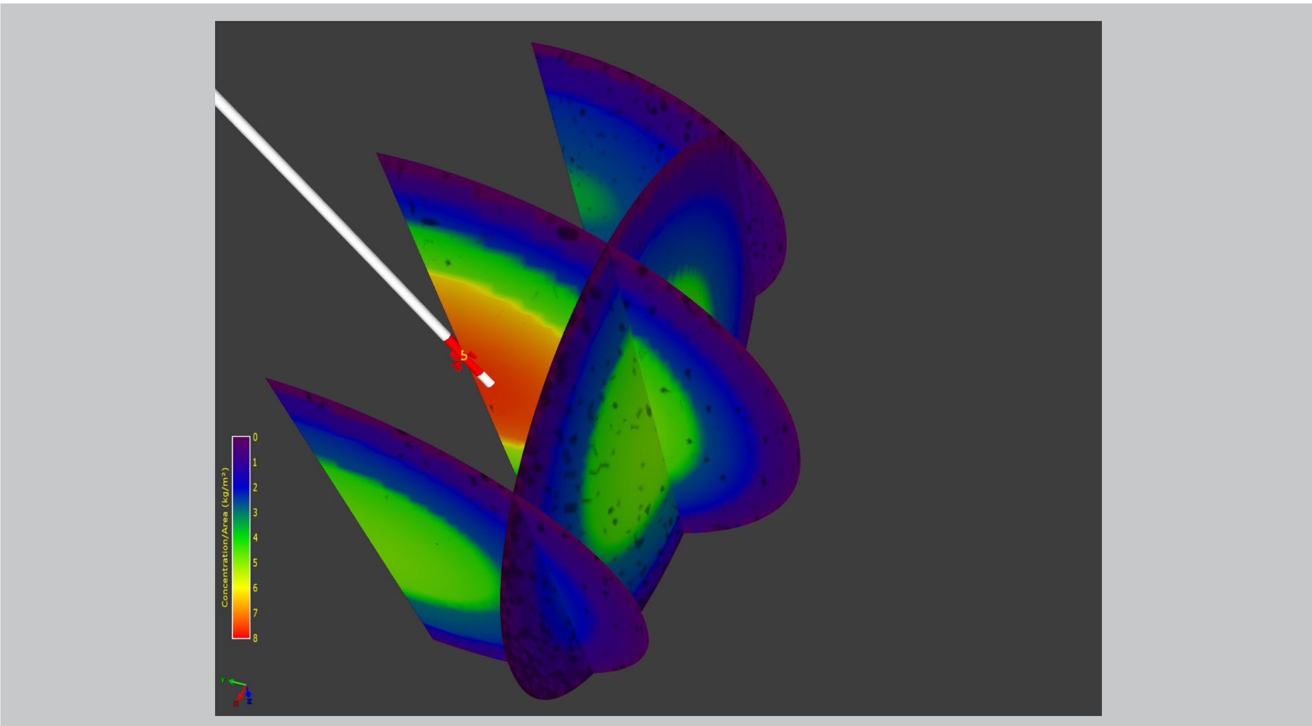

Figure 44 Area of the leaking fault covered by the sealing polymer.

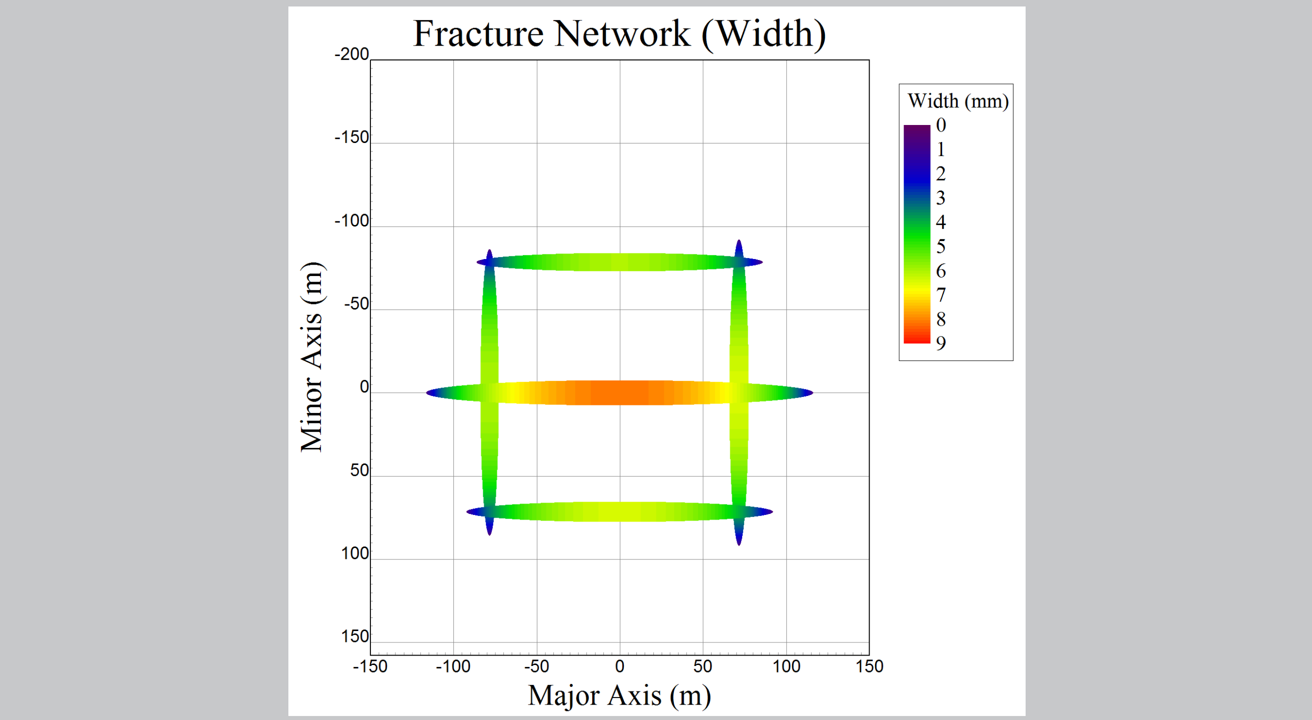

Figure 45 Top view of the fracture network (hydrofracture, leaking fault and lateral faults).

This method can result also successful if the well would be placed inside a block in the reservoir. In this case the sealant would also be transported in the lateral walls (faults) of the block. To analyse this case we adopted the treatment schedule shown in Figure 43.

Under these circumstances we developed an hydrofracture 112 meters long that intersect a leaking fault after 78 meters. The fault surface cover with the sealing polymer will be of 20600 m^2.

6 CONCLUSIONS

This report presented two different approaches to leakage remediation using sealants, namely the injection of sealants from wells and transport through porous structures and the use of hydraulically created fractures to deliver the sealants to leaky zones as the second alternative.

The results obtained from numerical simulations using the UTCHEM simulation software show that the area of influence increases with the decrease in crosslinker concentration for a given polymer concentration. This is mainly due to the decreased viscosity and slower gelation rate.

The results of polymer-gel injection using Eclipse (E300) show that polymer-gel injection (with delaying agents) from a horizontal well close to the leaky fault and directly above the caprock can effectively remediate the CO_2 leakage through a leaky sub-seismic fault in the caprock.

For the cases of flow diversion within the storage reservoir, the simulation results show that increasing the period of injection, potentially clogs the CO_2 injection well when the polymer is injected at the bottom of the reservoir. Therefore, polymer injection just below the caprock using the horizontal well configuration was found to be more suitable.

For the cases of polymer injection above the caprock, simulation results show that polymer injection from CO_2 injection well, which is at a distance of approximately 1k from the leaky fault, is the least favourable option as the duration of polymer gel treatment (500 days) and volume of polymer solution required would increase the cost of operation significantly.

In conclusion, an appreciable reduction in CO_2 leakage was achieved depending on the permeability reduction caused by the polymer-gel treatment.

In the second section where hydraulically created fractures were tested to deliver the sealants to leaky zones the P18 field was used as a real case scenario and the methodology proposed was described. The advantages and disadvantages of this approach were discussed. The results have shown that this method (combined with a proper choice of a polymer gel) can be an option to mitigate CO_2 leakage of a leaking fault. This model has, of course, some limitations. For example, the work could only considered vertical faults and it was not possible to introduce the enhanced permeability of the damaged zone that surrounds a fault.

References

Abbas, S., Donovan, J.C., and Sanders, A. 2013. Applicability of hydroxyethylcellulose polymers for chemical EOR. Society of Petroleum Engineers, SPE-165311-MS.

Amirbayov, T., 2014. Simulation study of the polymer flooding applied to the Norne Field E-Segment. MSc Thesis, Norwegian University of Science and Technology.

Al-Muntasheri, G.A., Sierra, L., Garzon, F.O., Lynn, J.D. and Izquierdo, G.A. 2010. Water shut-off with polymer gels in a high temperature horizontal gas well: A success story. Society of Petroleum Engineers, SPE-129848-MS. Annunziatellis A. et al. 2008. Gas migration along fault system and through the vadose zone in the Latera caldera (central Italy): implications for CO_2 geological storage, Intern. Jou. of Greenhouse Gas Control, 2, 353-372.

Arts R.J. et al. 2012. The feasibility of CO_2 storage in the depleted P18-4 gas field offshore the Netherlands (the ROAD project). Intern. Jou. of Greenhouse Gas Control, 11S, S10-S20.

Benson, S.M., 2006. Monitoring carbon dioxide sequestration in deep geological formations for inventory verification and carbon credits. Society of Petroleum Engineers, SPE 102833.

Brouwer J. et al. 2011. Feasibility study P18 (final report), Doc.nr: CATO2-WP3.01-D06.

Ciotoli G. et al. 2005. Migration of gas injected into a fault in low-permeability ground, Quart. Jou. of Eng. Geol. and Hydrog., 38, 305-320.

Durucan, S., Korre, A., Shi, J-Q., Govindan, R., Hadi Mosleh, M., and Syed, A. 2016. The use of polymer-gel solutions for CO_2 flow diversion and mobility control within storage sites. Energy Procedia, Elsevier, 86C, pp. 450-459.

Flew, S., Sellin, R.H.J., 1993. Non-Newtonian flow in porous media-a laboratory study of polyacrylamide solutions. Journal of Non-Newtonian Fluid Mechanics, (47) 169-210.

Gharbi, R., Alajmi, A., and Algharaib, M. 2012. The Potential of a Surfactant/Polymer Flood in a Middle Eastern Reservoir. Energies 5(1): 58.

Gudmundson A. 2003. Effect of Young's modulus on fault displacement, Geodynamics.

Hild, G.P., and Wackowski, R.K. 1999. Reservoir polymer gel treatments to improve miscible CO_2 flood. Society of Petroleum Engineers, SPE-56008-PA.

IEAGHG Report, 2007. Remediation of leakage from CO_2 storage reservoirs. IEA Greenhouse Gas R&D Programme, Report No. 2007/11.

Kim, H. 1995. A Simulation Study of Gel Conformance Treatments. PhD Thesis, the University of Texas, Austin, TX, USA.

Legemah, M., Guerin, M., Sun, H., and Qu, Q., 2014. Novel high-efficiency boron crosslinkers for low-polymer-loading fracturing fluids. Society of Petroleum Engineers, SPE 164118.

Lei, C., and Clark, P.E., 2004. Crosslinking of guar and guar derivatives. Society of Petroleum Engineers, SPE 90840.

Liang J., Sun H., and Seright R.S., 1992. Reduction of oil and water permeabilities using gels. Society of Petroleum Engineers, SPE-24195-MS.

Littmann, W. 1988. Polymer Flooding, Developments in Petroleum Science 24, Elsevier.

Lockhart, T.P. 1992. A New Gelation Technology for In-Depth Placement of Cr^{3+}/Polymer Gels in High Temperature Reservoirs. SPE/DOE 24194, presented at the SPE/DOE Eighth Symposium on Enhanced Oil Recovery, Tulsa, OK, April 22-24.

Manceau J.-C. et al. 2014. Mitigation and remediation technologies and practices in case of undesired migration of CO_2 from a geological storage unit – Current status, Intern. Jou. of Greenhouse Gas Control, 22, 272-290.

Chapter XVII

Remediation techniques based on foam injection

Guillaume Batôt[1], Marc Fleury[1], Chris Hewson[2], Lahcen Nabzar[1]
[1] IFPEN, France
[2] TNO, The Netherlands

SUMMARY

We studied in the laboratory the capacity of foams to reduce gas flow for CO_2-brine systems in rock core sample with common surfactants, as a function of interstitial velocity and gas to water fraction. All experiments were carried out in similar Clashach sandstones with permeability between 220 and 1500 mD, and porosity in the range 10-20%. The gas and the surfactant-brine solution were co-injected at the core inlet face with a gas fraction around 0.7. We vary the interstitial velocity within two decades from about 3 ft/day up to 100 ft/day.

The performance of the generated foams was evaluated from the relative foam viscosity, the ratio of the measured pressure drop in the presence of foam to the pressure drop in single phase condition for the same interstitial velocity. Whatever the pressure and permeability/porosity, the relative foam viscosity can be described as a power law vs. the shear rate evaluated from the interstitial velocity, permeability and porosity. The exponent is close to -1 describing the shear-thinning behavior.

Based on this experimental correlation the technical feasibility of foam injection, as a mitigation method, was numerically explored from reservoir simulations. The scenario studied is the case of a leak through a fracture in the caprock. The foam is injected at the top of the reservoir below the caprock. We show that foams can effectively reduce the leak provided the well is not too far from the leak, typically of the order of 50-10 m. The advantages and drawbacks of this remediation method are discussed.

This work was partially presented during the Society of core Analysts meeting in Snow Mass, Colorado, USA (August 2016) and during the Green House Gas Technology meeting (GHGT13) in Lausanne, Switzerland (November 2016).

1 INTRODUCTION

The oil and gas industry has a long-term experience in reducing the flow rate of a given fluid, or maximizing the oil and gas recovery, by injecting fluids with specific properties into rock formations containing hydrocarbons. As it has already been stated [1], Carbon Capture and Sequestration programs (CCS) could benefit from the CO_2-Enhanced-Oil-Recovery knowledge. Indeed, in the EOR context, the gas-based injections are now the most common methods since the decline of the thermal ones in the early 2000's [2]. Due to its unique properties such as low minimum miscibility pressure, CO_2 has been mainly used in such techniques.

Beyond their use for mobility control in EOR, foams can also be adequate to secure gas storage operations through gas confinement and leakage prevention/remediation. Regarding CO_2 storage operations, gas confinement is of great importance to ensure that such process can be used as a safe and effective solution for greenhouse mitigation. A clear insight on the associated risks, their sound evaluation and the development of means for their prevention and mitigation are thus needed. Risks of CO_2 leakage through/along wells, faults and fractures and through the sealing cap-rock are among the most important. Indeed, due to its low density and high mobility, gas might potentially migrate out of the storage zone towards the upper formation due to gravity segregation and finally might leak into the atmosphere. This leakage potential is mainly determined around the well and on the sealing cap rock integrity. Due to their ability to preferentially restrict fluid flow in the most permeable areas, foams are particularly indicated to address the leakage from high permeability areas or through fracture and fissures that are considered as the most important leakage pathways [3].

The foam lifetime in the porous media may be about few weeks, at best, thus the use of classical foams in a CCS context is adapt for emergency remediation but for mid-term prevention gel-foam [4] can be designed. For both, classical and gel foams, laboratory experiments in rock samples are based on the evaluation of the gas flow resistance of the foam lamellae. The gel-foam implies a complementary chemical study on the relevant cross-linkers needed to gel the foam. In the following we focus only on the foam generation, propagation, and its ability to reduce the gas flow rate in porous media.

1.1 Foam generation and propagation in porous media

Despite numerous theoretical studies [5, 6], experimental works [4, 7, 8] and field/pilot tests [9–11] dedicated to foam processes, it is still a developing technology and uncertainties remains regarding the governing parameters of this complex physics. On several aspects, foams generated in rock formations are very different from the "everyday life" or "bulk" foam that we are familiar with. In porous media they can be seen as finely-textured gas bubbles, such as nitrogen, methane or carbon dioxide, dispersed within brine. Their formation requires a certain amount of energy, which is provided by shearing along the porous structure, and are stabilized by surfactants that are generally solubilized in the water, but could also be dissolved into the CO_2 [12, 13]. The gas bubbles are separated by liquid films called lamellae, responsible for the reduction of the gas flow. In homogeneous structure, lamellae creation results from two main identified mechanisms [6]: the lamellae division and the gas bubble snap-off. A third mechanism is also identified, the leave-behind, but it can be seen as a specific case of the lamellae division. Thus, the gas transport properties may result from a dynamic equilibrium between lamellae creation and destruction.

At the laboratory scale, the resistance to gas flow, i.e. the resistance of the lamellae to coalescence, is evaluated macroscopically within rock core sample from the pressure drop ΔP_{foam} along the core. The so-called gas Mobility Reduction Factor (MRF) is defined as the following ratio $\Delta P_{foam} / \Delta P_{ref}$, which can be seen as a relative and apparent viscosity of the generated foam at a given flow rate. The reference pressure drop can be the water pressure drop (monophasic reference) or the pressure drop measured from a water and gas co-injection (diphasic reference).

In the absence of oil, the lamellae coalescence seems to be mainly governed by the capillary pressure P_c and the local water saturation S_w. Two regimes of foam flow have been distinguished [7]: in the P_c^* regime, when the P_c is close, or equal, to the limiting value P_c^*, the generated foam is "strong" and provides high MRF; below the P_c^* the foam is "weak" and does not give large resistance to gas flow. At a given total flow rate, the capillary pressure can be increased with the gas fractional flow, or foam quality, denoted as $f_g = Q_g / (Q_w + Q_g)$ the gas flow rate divided by the total flow rate. When the limiting capillary pressure P_c^* is reached, further increase in the foam quality induces instabilities through coarsening of the foam texture. There is an upper limit, mostly over f_g ~ 0.9, above which foam collapses due to "dry out" effect.

In the P_c^* regime two flow regimes exist and the transition occurs at a critical or optimal gas fraction f_g^* corresponding to the critical capillary pressure and to the maximum in pressure drop at a given total flow rate. With low quality wet foam, $f_g < f_g^*$, the pressure drop is almost independent of the liquid flow rate while for dry foam at high quality, $f_g > f_g^*$ it becomes almost independent of the gas flow rate [14]. The optimal foam quality is usually obtained between 0.7 and 0.9 [15]. Thus, according to this view, the foam-induced pressure drop usually exhibits a maximum when plotted against foam quality [15–18]. This maximum is reached at the optimal foam quality f_g^* that depends on system characteristics and especially on formation permeability, surfactant and flow rate. This optimal foam quality is a very important parameter to determine for a given application case.

It has been demonstrated that for strong foam generation, a minimum pressure gradient or a minimum critical velocity is required [4]. Once these strong foams are generated, inside the porous media, their rheological behavior shows the following main trends:

first, MRF increases with increasing velocity up to a maximum. Then MRF decreases when increasing further the velocity beyond the maximum (shear thinning behavior). Finally, MRF shows hysteresis effect when the velocity is decreased. Such typical rheological behavior is illustrated on Figure 1.

Most of the foams exhibit the shear thinning behavior. This is an important advantage for the use of foams in EOR for sweep improvement. Indeed, foams are usually generated in situ in the near wellbore area where the velocity is high leading to low MRF that mitigate the injectivity issue. Far away from wellbore, the velocity decreases leading to higher MRF with better gas blocking performance.

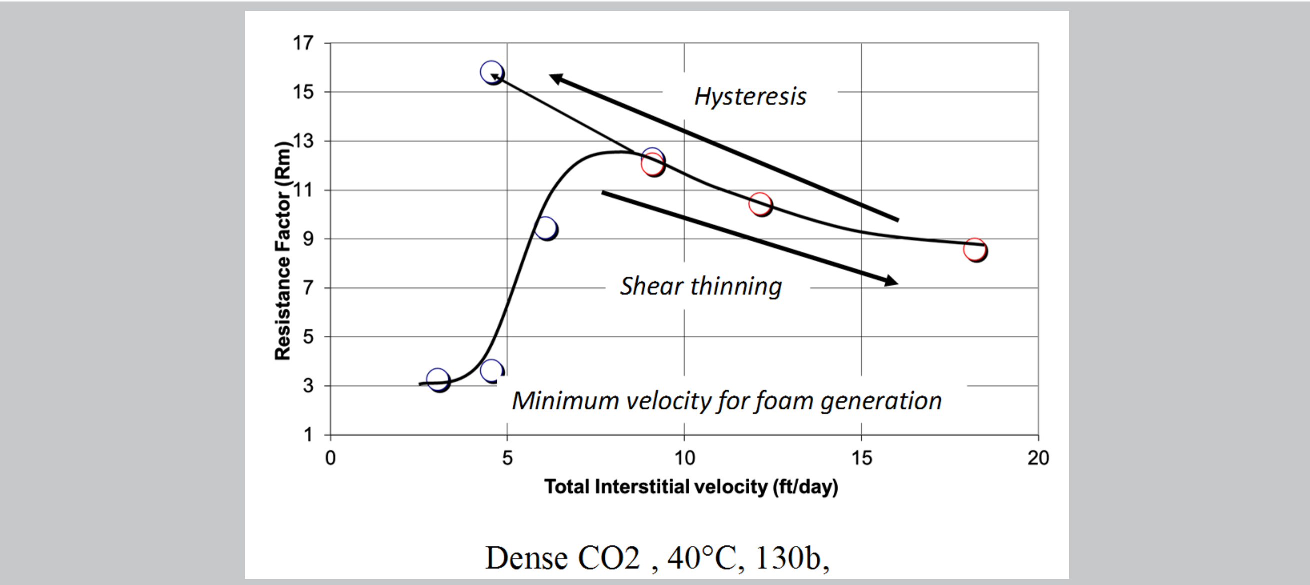

Figure 1 Typical behavior of foam when increasing the total interstitial velocity. Hysteresis may occur with decreasing velocity, yielding higher resistance to gas far from the well (Nabzar, 2014, ADRAC, Abu Dhabi). Conditions: 40°C, 130 bar.

1.2 Numerical simulation of foam

Empirical [19], semi-analytical [20, 21] and mechanistic [22, 23] approaches have been proposed to model foam flow in porous media [24]. The mechanistic models are based on the population balance equation taking into account lamellae creation and destruction in order to predict the dynamics of the foam bubbles. They aim at describing the relation between the space-time variation of the foam structure and its rheological properties. The use of such comprehensive models is however limited due to the number of parameters that are difficult to obtain, measure and scale-up at larger scale. The semi-analytical approach is based on the application of the fractional flow theory of Buckley-Leverett to foam flow [20, 21]. Though such model is able to reproduce the general foam behavior described above, its use for foam is limited due to the assumptions used. Therefore, in the absence of a comprehensive, simple, yet useful, physical modeling of foam flow in porous media, only the empirical approach, is currently used in most of the reservoir simulators. Within this approach, based on the local steady state model, the effect of foam on gas mobility is modeled through a simple modification of the relative gas permeability k_{rg} in presence of foam $k^f_{r,g}$:

$$k^f_{r,g} = k_{r,g} M_{rf} \tag{1}$$

The mobility reduction factor M_{rf} are input values obtained from the experimental measurements. A functional form or a tabular form can be use depending on the available data.

2 MATERIAL AND METHODS

2.1 Core-flood experiments

Experiments presented in this work were carried out in Clashach sandstones with a water permeability between 225 mD and 1550 mD and a porosity between 10% and 20%. Depending on the experimental set-up, two different plug sizes are used, the smallest ones have a pore volume of 1.5 and 2.5 ml with a length of 4.0 cm and a radius of 1.0 cm, while the largest has a pore volume of 25 ml with a length of 10.0 cm and a radius of 2.0 cm. The water used is a 3.5 wt% NaCl brine. Surfactant is a classical AOS type (Rhodacal® A-246/L manufactured by Solvay) prepared at the concentration of 0.5 wt. % in this brine.

A typical experiment consists in first co-injecting brine and pure CO_2, and then brine is replaced by a solution of the same brine but containing a surfactant. In all these experiments CO_2 and surfactant-brine are co-injected at the core inlet to make sure that the foam is generated by shearing through the porous structure, and not before. The foam quality f_g, or gas fraction, is fixed around 0.7. Various total flow rates varying from near wellbore to in depth fluid velocities can be explored in an experiment.

2.1.1 MRI system at low pressure

With the MRI small core-flood set-up (Figure 2), brine and pure CO_2 are co-injected at the top inlet face of the sample. The flooding cell is custom built and specifically designed for MRI systems: sample diameter is 2.0 cm with a maximum sample length of 5.0 cm; NMR probe diameter is 3.0 cm; the maximum confining pressure is 80 bar and 10 bar pore pressure is imposed by a membrane back-pressure regulator (BPR); the temperature is fixed around 30°C (MRI magnet temperature). The liquid and gas flow rates are respectively imposed using a pump (QX-6000 from Quizix) and a gas controller (EL-Flow® from Bronkhorst®). We vary the total flow rate Q_t by a factor of 100, from 1 cm³/h up to 100 cm³/h, corresponding in this case to interstitial velocity $v_i = Q_t(S\phi)$ between 1.6 and 160 cm/h, or between 1.22 and 122 ft/day in usual engineering units. During injection, we continuously measure by standard MRI techniques the saturation profiles (a spin echo sequence) and the T_2 relaxation time distributions typically every minute.

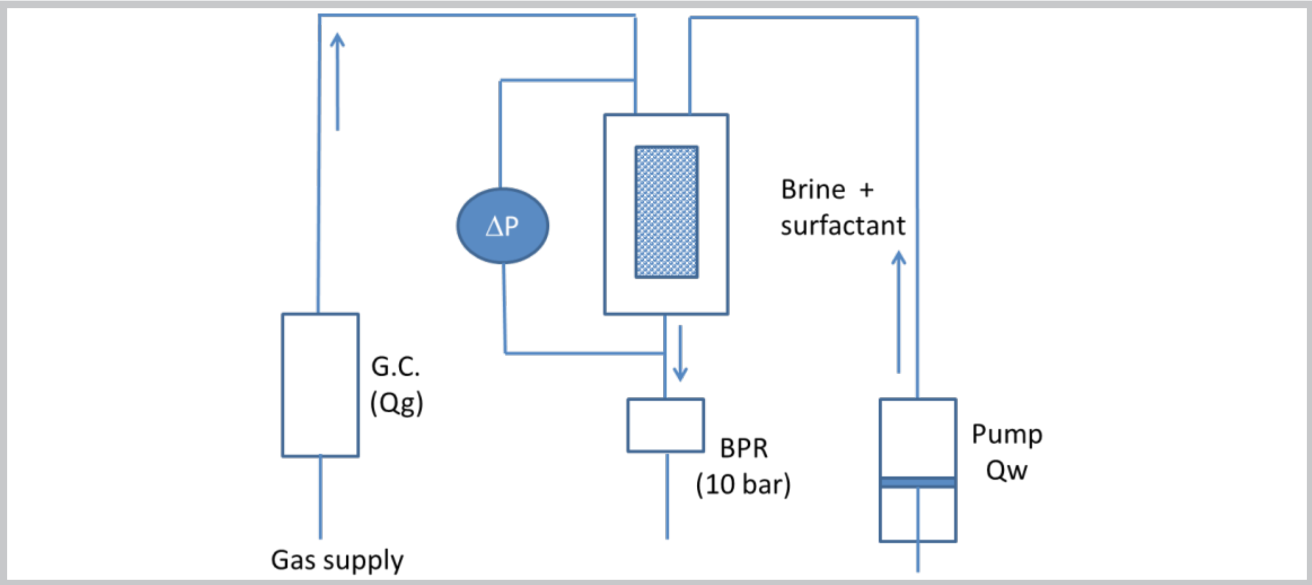

Figure 2 Schematic of the experimental set-up using NMR imaging. Gas controller (G.C.) to impose a fixed gas flow rate. Back pressure regulator (BPR): used to set the outlet pressure. The MRI system is a 20 MHz compact permanent magnet system from Oxford Instrument.

2.1.2 X-Ray system at high pressure

The high pressure system is conceptually similar and is composed of a horizontal composite core holder with low X-ray attenuation. The X-ray generator (90keV – Ta filter) and the detector can move along the heated Hassler cell using a step by step motor. A full-length scan every 5 mm takes about 15 min. A saturation profile is calculated from the measured X-ray profile and two calibration profiles (sample fully saturated with brine and dry). The CO_2 is injected from a high pressure piston-cylinder cell at the chosen working pressure and temperature; experiments were carried out at 40°C and 130 bar pore pressure with 180 bar of overburden pressure; the core sample used had a water permeability of 820 mD and a porosity of 20.2 %. The total flow rate was changed from 10 to 300 cm³/h yielding interstitial velocities between 3.9 and 119.3 cm/h (3.1 and 94.0 ft/day) in the same range as in the MRI setup. At 40°C and 130 bars, the injected CO_2 is in a supercritical dense state with a density of 743 ± 3.7 kg/m³ (from NIST database).

2.2 Numerical simulation

The technical feasibility of foam injection as a remediation method was explored using Schlumberger's commercial reservoir simulator Eclipse 100.

2.2.1 Reservoir model

A reservoir model was created to study the mobility control of CO_2 with the use of a foam in a depleted gas field considered for CO_2 storage (P18-4 [25]). The model was purposely simplified and was created with similar properties.. The structural model was a tilted box (10º dip) so that the gravity effects of the fluid could be studied. The bounds were no flow boundaries to emulate the P18-4 field compartments. The extent of the model was 1075 m x 1925 m x 130 m with a grid block size of 25 m x 25 m x 5 m (x, y, and z direction respectively) as to not have the bounds interfere with the determination of the radius of investigation. The injection well was perforated in the top 50 m of the reservoir (Figure 3). The relatively high resolution of the model was used to properly model the dispersion of the foam. The permeability field was chosen to be homogenous with 200 mD in the horizontal direction and 20 mD in the vertical direction. The porosity was also homogenous throughout the reservoir and was chosen as 0.15.

For this study, the overburden was not considered. Instead a production well was used to model the effect of a leakage zone in the cap rock. The size of the leak in the reservoir section was chosen as 2m x 2m x 25m. It was assumed that the cap rock would leak after the reservoir pressure reached 400 bars (reactivation pressure).

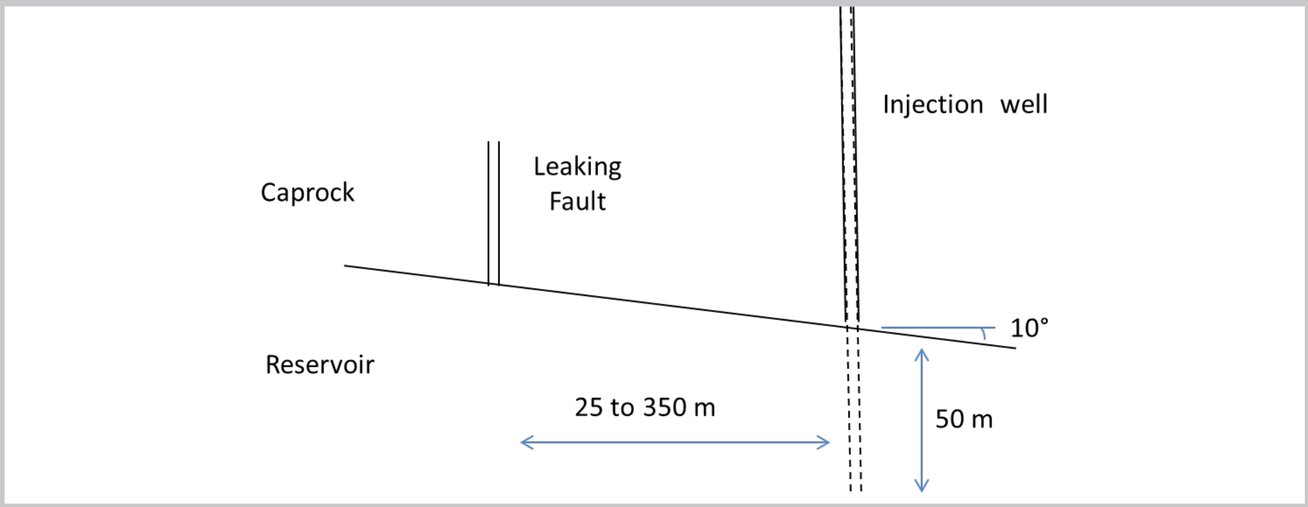

Figure 3 Sketch of the injection well and leaky fault in the caprock. The injection is perforated over the top 50m of the reservoir. The distance between the well and leaking fault was varied from 25 up to 350m.

The leakage through the cap rock (i.e. leak well) was under rate control with a minimum pressure limit of the aquifer above (we assume that at that point no more CO_2 can leak from the reservoir). The parameters used to model the leak are presented in Table 1. Additionally, a rate control was imposed on the leak using a combination of Buckingham's equation [26] for flow through slots of fine clearance (eq. 3) and Darcy's law (eq. 2) :

$$q_f = -\frac{k_f A}{\mu}\left(\frac{\Delta p}{L}\right) \tag{2}$$

$$k_f = \frac{\phi_f w_f^2}{12\tau} \tag{3}$$

where

Δp	= differential pressure [Pa]
k_f	= fracture permeability [m^2]
μ	= fluid viscosity [Pa*s]
L	= length of fracture (i.e. thickness of the caprock) [m]
A	= cross-sectional area [m^2]
q_f	= volumetric flow rate through fracture [m^3/s]
ϕ_f	= fracture porosity [-]
w_f	= fracture width [m]
τ	= fracture tortuosity [-]

Table 1 Parameters values for the leak model.

Fracture Permeability [D]	29
Length of Fracture [m]	20
Cross-sectional Area [m^2]	0.01181
Fracture Porosity [-]	0.43
Fracture Width [m]	0.000009
Fracture Tortuosity [-]	0.01

The implementation of two separate operating constraints for the leak allow for sufficient modelling of the leakage zone without the inclusion of a complex geological model or a large fracture extent. The leak permeability was taken to be 29 D, correlating to a leak flow rate of approximately 200 kg/day. The leakage rate was chosen based on a worst case scenario cap rock failure and was checked for a basis in reality from a previous study on CO_2 leakage from geological storage [27].

2.2.2 Transport equation

The commercial reservoir simulation software, Schlumberger's Eclipse 100, was used to model the depletion of the gas field, injection of CO_2, the leakage of CO_2 from the reservoir, and the injection of foam to mitigate the leak. The foam is modeled as a tracer in the gaseous phase of the reservoir simulator. The foam can be thought of as being dependent on the surfactant concentration that exists in foam form. The simulation software models the amount or concentration of surfactant that is able to reach different points of the reservoir (in terms of both flow and degradation effects) and directly relates this to a parameter known as foam concentration. A conservation equation is used within Eclipse to determine the concentration of the activated surfactant in each grid block (in the numerical simulator's conservation equation this is referred to as the foam concentration). The mobility reduction factor, M_{rf}, is introduced into the local conservation equation (without adsorption effect) for the gas phase and is shown in equation 4:

$$\frac{d}{dt}N_f = \sum\left[\frac{Tk_{r,g}}{\mu_g}M_{rf}\left(\delta P_g - \rho_g g D_z\right)\right]C_f + Q_T f_g C_f \tag{4}$$

with N_f the number of foam tracers in a simulation block, C_f is the foam concentration, ρ_g the gas density, T the absolute permeability (transmissivity), P_g the gas pressure, g the gravitational constant, D_z the cell center depth, Q_T the total flow rate, and f_g is the gas fractional flow. The summation is performed over all neighboring cells in 3 dimensions.

Foam propagation using numerical simulators has been well documented in previous studies [19, 24, 28]. Eclipse uses a set of user defined parameters to model transport, adsorption, decay and the mobility reduction factor M_{rf}. The gas mobility reduction can be calculated either using tables or functional parameters. In this work, the tabular model was chosen as we can use the M_{rf} obtained from the corefloods experiments as direct input. The tabular model includes surfactant concentration, pressure, and shear dependent terms. Equations 5 and 6 display the equations Eclipse uses to determine the mobility reduction factor (M_{rf}) of the foam:

$$M_{rf} = \left(1 - M_{rf}^{cp}\right)M_v\left(V_g\right) + M_{rf}^{cp}, \tag{5}$$

$$M_{rf}^{cp} = \left(1 - M_c\left(C_f\right)\right)M_p(P) + M_c\left(C_f\right), \tag{6}$$

where $M_v(V_g)$ is the mobility reduction modifier due to interstitial velocity, $M_c(C_f)$ is the gas mobility reduction modifier due to the foam concentration and $M_p(P)$ is the gas mobility reduction modifier due to pressure. The foam does require a minimum concentration of 0.05 to be effective, below that concentration in a grid block, the foam begins to collapse. In our modeling, foam does not degrade over time and the surfactant does not adsorb on the surface of the rock. This assumption is not always verified, especially in the presence of hydrocarbons and biological impurities within the rock matrix [29, 30]. Hence, we consider an ideal foam with the objective of studying the main mechanisms.

3 RESULTS

3.1 Low pressure system: transient regime before foam formation

Here we focus on the onset of foam at the lowest flow rate (1 cm³/h or 1.6cm/h, Figure 3). The sample is a Clashach sandstone of porosity 20.2% and water permeability 1550 mD. The sample was used for several foam experiments before this one and therefore adsorption of the surfactant on the solid surface is stabilized. A foam generating a strong pressure drop is only observed when the

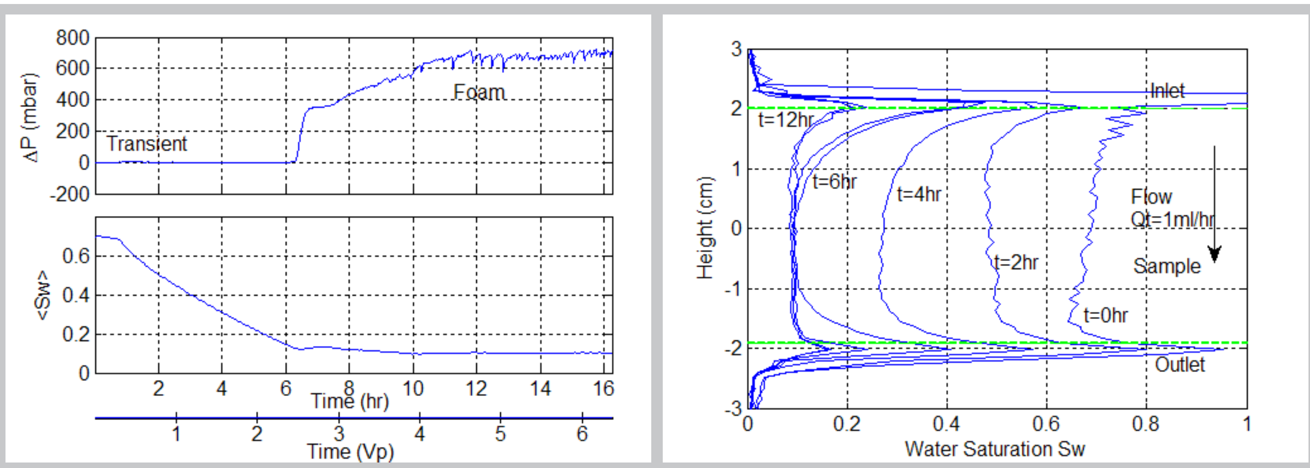

Figure 4 [Left] Generation of foam at a low interstitial velocity (1 ml/h, 1.6 cm/h) : Clashach sandstone, porosity 20.2%, 1550 mD, f_g=0.6, brine 35 g/l, AOS type surfactant concentration 0.5 wt%. [Right] Local saturation profiles corresponding to the left graph every 2 hours. At t=6 hr, a strong foam is present. The spikes at the inlet and outlet correspond to the liquid present in the injectors. The average saturation is calculated with the values between the green horizontal lines.

water saturation is low enough (~15%), corresponding to high capillary pressure close to irreducible water saturation (Figure 3 – left). This is achieved after a few pore volume (PV). Then, at a nearly constant water saturation and during a few pore volume also, a strong foam is abruptly formed as indicated by the sharp increase of the pressure drop after injection of 2 PV or at this low flow rate after t = 6.2 hr. Interestingly, the saturation profiles (Figure 3 - right) are nearly uniform for strong foams and this uniform profile is gradually achieved starting from the middle of the sample.

3.2 Low pressure system: foam apparent viscosity

At steady state, the mobility reduction factor is calculated as the ratio of the measured pressure drop in the presence of foam ΔP_{foam} $(Q_t;f_g \sim 0.7)$ to the one during a single phase brine injection $\Delta P_{brine}(Q_t)$ at the same total flow rate Q_t:

$$\mathrm{MRF}\left(Q_t; f_g\right) = \frac{\Delta \mathrm{P}_{\mathrm{foam}}(Q_t;f_g \sim 0.7)}{\Delta \mathrm{P}_{\mathrm{brine}}(Q_t)}. \tag{7}$$

Indeed, as shown by 3D CT-scan imaging [8], defining the mobility reduction factor with the pressure drop in two phase flow conditions (co-injection of gas and brine without surfactants) in such short samples has little meaning due to severe digitation problems. Based on the Darcy law, with this definition the MRF can be seen as the foam relative apparent viscosity, denoted as η_r^f in the following, which corresponds to the ratio of the foam apparent viscosity to the brine viscosity $\eta_{app}^f / \eta_{brine}$.

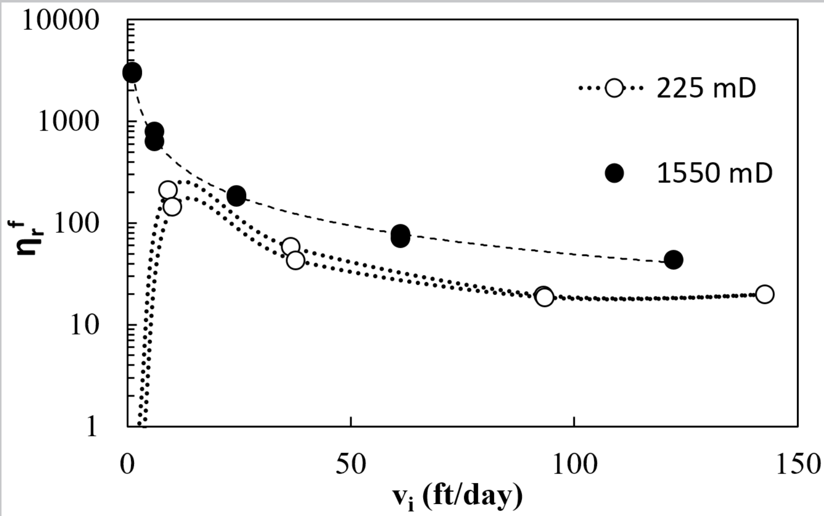

Figure 5 Foam relative viscosity in a small core of Clashach sandstone plotted against the interstitial velocity. Full circles correspond to the date obtain with a core of 1550 mD water permeability and 20.2% of porosity. Empty circles are the data for 225 mD and 12.1% porosity. Points are obtained with both increasing and decreasing velocities (duplicate points).

On Figure 5 the foam relative viscosity η_r^f is plotted against the total interstitial velocity for the two permeability values. The data obtained from increasing and decreasing total flow rate are very similar (duplicate points). In the less permeable rock sample, at the lowest interstitial velocity of 2.2 ft/day, the measured apparent viscosity is very close to 1, suggesting that there is strictly speaking no foam generated at this point. At 9.2 ft/day we observed a rise of the pressure drop and strong water desaturation of the porous media, leading to a relative viscosity about 100-200. No such critical velocity is observed with the more permeable core, as it may be too small to be measured with the present experimental set-up.

3.3 High pressure system: foam apparent viscosity

The flooding cell used with the high pressure setup allows working with longer core sample (10 cm) and denser gas. Hence, we first measured reference pressure drops when water and CO_2 are simply co-injected without any surfactant for a range of velocities used later in the presence of foam (Figure 6). The data are well described by linear relationships and both linear regressions can be used to evaluate either the performance ratio between foam and gas/water co-injection $MRF = \Delta P_{foam} / \Delta P_{water\text{-}gas}$, or the relative foam viscosity $\Delta P_{foam} / \Delta P_{water}$.

During the foam generation and propagation in the porous media, the mean water saturation is recorded from X-ray absorbance technique. During the first four injected pore volumes, at the total flow rate of 10 cm^3/h (or 3.1 ft/day interstitial velocity), the transient regime of the initial foam formation is clearly observed and correlated to a fast water desaturation (Figure 7). Increasing the total flow rate increases the pressure drop as expected if the foam still exists and does not coalesce.

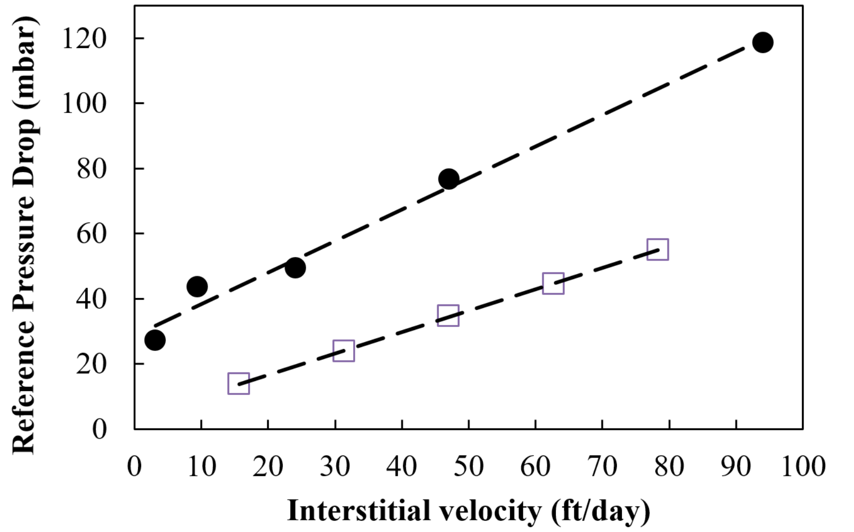

Figure 6 Pressure drops for several interstitial velocities. Empty squares are the measurements from the injection of water without surfactants, while the full circle from the co-injection of gas and water still without surfactants. Dotted lines are linear regressions.

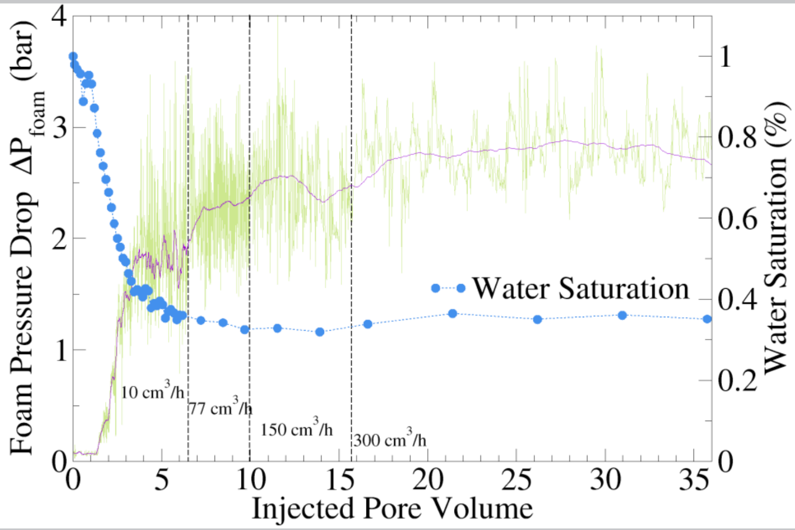

Figure 7 Dense supercritical CO_2-foam generation in a 820 mD Clashach sandstone. The line in dark purple is a running average of 200 points of the raw pressure drop measurement represented here in light green. The full circles represent the mean water saturation along the core. Data are plotted against the total injected pore volume and thus not linear in time as the total flow rate was increased from 10 up to 300 cm³/h.

When scaled by the water-gas pressure drop at the same velocities (Figure 6), the MRF does not express anymore a relative viscosity (Figure 8) but the "true" effect of the foam compared to a situation in which both gas and water are flowing in the absence of foam (i.e. it includes relative permeability effects). Then, the mobility reduction factor ranges between 20 and 50 with a less pronounced shear thinning evolution.

3.4 Synthesis

As the interstitial velocity takes into account the porosity, it is not an adequate variable to compare results between plugs with different porosity but having the same permeability. We suggest to use the shear rate noted $\dot{\gamma}$ which is however not a quantity directly available from measurements in complex geometries. The shear rate is critical for polymer systems flowing in porous media and an empirical law has been established by Chauveteau [31] in sandstones and bead-packs. Very recently Pedroni [32] have shown that this law can be successfully used for foam flow in homogeneous sandstones. From a classical rheological point of view the Chauveteau law can be expressed as follow:

$$\dot{\gamma} = 4\frac{v_i}{l_s}\alpha(K_w) \qquad l_s = \sqrt{8K_w/\Phi} \tag{8}$$

with v_i the interstitial velocity, l_s the typical length scale of the sheared zone and α an empirical correction which is a decreasing function of the water permeability K_w. The length l_s is the pore throat estimated from conduit flow model as $\sqrt{(8K_w/\Phi)}$. Extrapolating

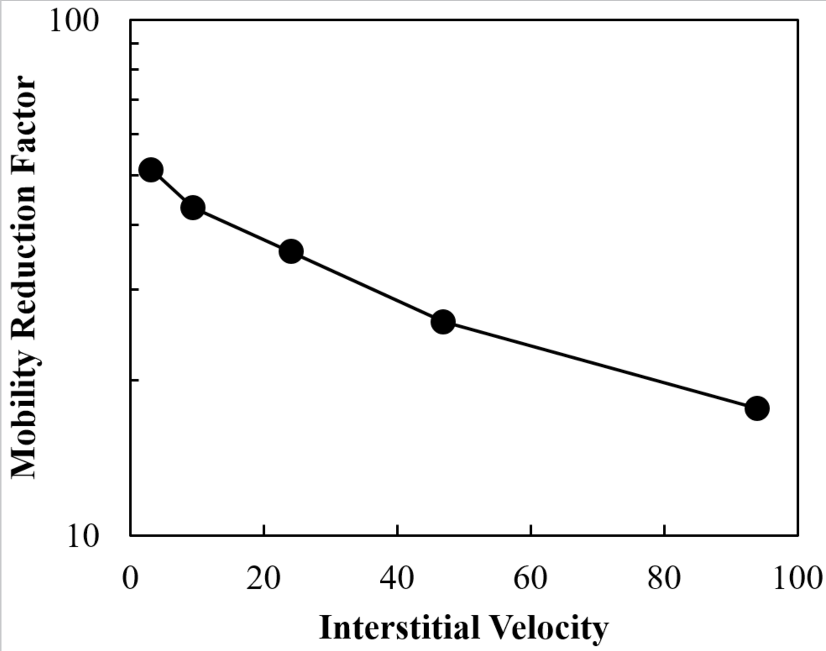

Figure 8 Mobility Reduction Factor evaluated from the performance ratio between foam and gas/water co-injection $MRF=\Delta P_{foam} / \Delta P_{water\text{-}gas}$. The $\Delta P_{water\text{-}gas}$ is extracted from the linear regression of raw data (Figure 6).

the relation $\alpha = 16.71 \times K_w^{-0.277}$ from the data obtained by Chauveteau et al. [31], we found $\alpha \approx 3.7275$ for 225 mD and $\alpha \approx 2.189$ for 1550 mD. Plotting the foam apparent viscosity against the shear rate calculated with the above coefficients yields a unique curve (Figure 9). Thus the data obtained from different permeability and porosity are reduced to a single power law curve with exponent close to -1 (between -0.90 and -0.95).

The water saturation (also plotted on Figure 9) increases monotonously, from 10 to 20%, as the foam relative viscosity decreases with the shear rate. As η_r^f decreases the foam becomes less effective in reducing the CO_2 flow and the gas may flow more easily along the preferential paths, resulting in an increase of the water saturation. Furthermore one could also observe that water saturation is always below the injected water fraction $f_w = 1 - f_g = 30\%$. It means that the gas mobility is well reduced within the rock and the generated foam is very efficient for the whole range of interstitial velocity used here: from 3 ft/day to 100 ft/day, representative range from in depth fluid velocities to near wellbore.

Performing the same analysis for the high pressure data, the shear rate $\dot{\gamma}$ was estimated from eq. 8 with $\alpha = 2.605$ for $K_w = 820$ mD and $\Phi = 20.0$ %. We observed that the foam relative viscosity η_r^f can be described with the same power law for both low and high pressure measurements (Figure 10). The exponents are respectively -0.94 and -0.92 for the low and high pressure conditions. Thus, at steady state, the generated CO_2-foam shows the same ability to reduce the gas flow, whatever the pressure.

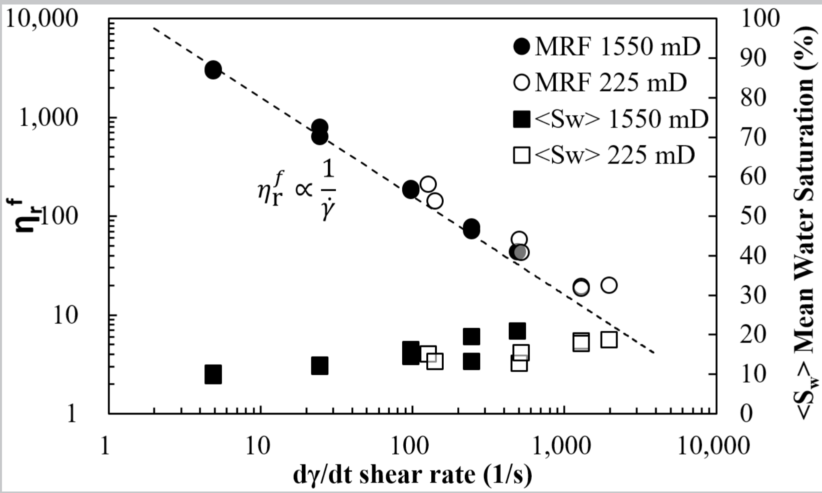

Figure 9 The foam relative viscosity η_r^f (circles) and the mean water saturation <Sw> (squares) vs. the shear rate $\dot{\gamma}$ computed from eq. 8 in Clashach sandstone at 30°C and a pore pressure of 10 bar. The full symbols represent data for a 1550 mD sandstone with a porosity about 20%. The empty symbols for 225 mD with a porosity about 12%. The dotted line corresponds to the equation η_r^f=16000/ $\dot{\gamma}$.

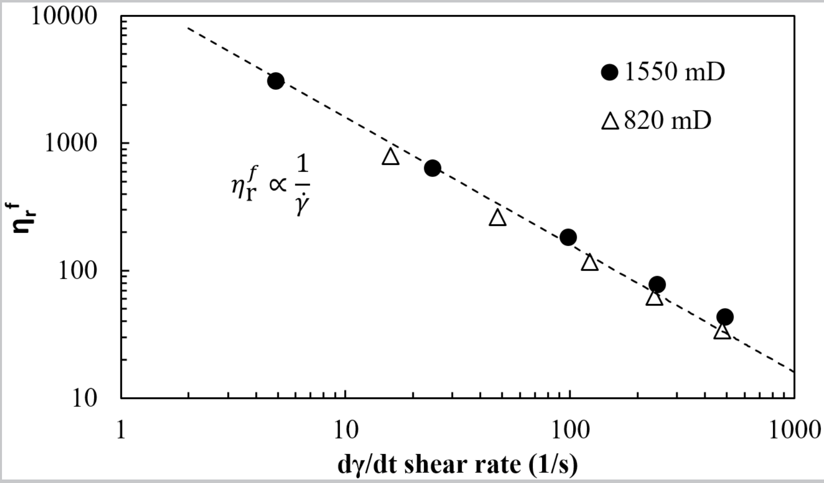

Figure 10 Comparison between low (full circle - 1550 mD) and high pressure (empty triangles - 820 mD) experiments for the decreasing velocities (as in reservoir application). The shear rate is computed from eq. 8. The dotted line is the same power law as plotted on Fig. 8 : η_r^f=16000/ $\dot{\gamma}$.

The effective viscosity of the foam can finally be modeled for all conditions as a function of the shear rate (eq. 8) according to:

$$\eta_r^f = \frac{16000}{\dot{\gamma}} \tag{9}$$

in which we impose an exponent -1 close to the measured ones. This relation includes the effect of permeability and porosity and can be used for foam simulations. Indeed, for a given formation of permeability K and porosity Φ one can calculate the velocities according to equation 8, and the effective foam viscosity function of velocity according to equation 9. Hence, the MRF curve function of velocity can be entered as input parameter, as shown later.

3.5 Foam Simulations : Radius of Investigation

Since the relationship in equation 9 cannot be entered directly as an input in the simulator, the tabulated values $M_v(V_g)$, $M_c(C_f)$, and $M_p(P)$ were first adjusted in order match the experimental pressures and saturations observed, i.e. the foam effective viscosity follows a power law function of total interstitial velocity. Since the experiments show no pressure effect, the foam pressure parameter (M_p) takes a very small value. However, Eclipse does not allow for MRF values to increase with increasing shear rates and hence, the typical foam behavior shown in Figure 1 with the inflection point cannot be explicitly modelled in the simulator.

The radius of investigation was looked at to determine how far the foam could reach a leak in the cap rock. Leak distances of 25 m, 75 m, 175 m, and 350 m from the injection well location were looked at to determine the time of intervention and the volume of foam that was able to reach the site relative to the injected volume of foam. A surfactant-alternating-gas (SAG) process was used to generate the foam in situ. For our study, one slug of surfactant solution was injected at a rate of 100 m³/day for 2 months, followed by a CO_2 gas slug of 200 t/day for 3 months in order to prevent injectivity issues of surfactant and gas around the near wellbore region.

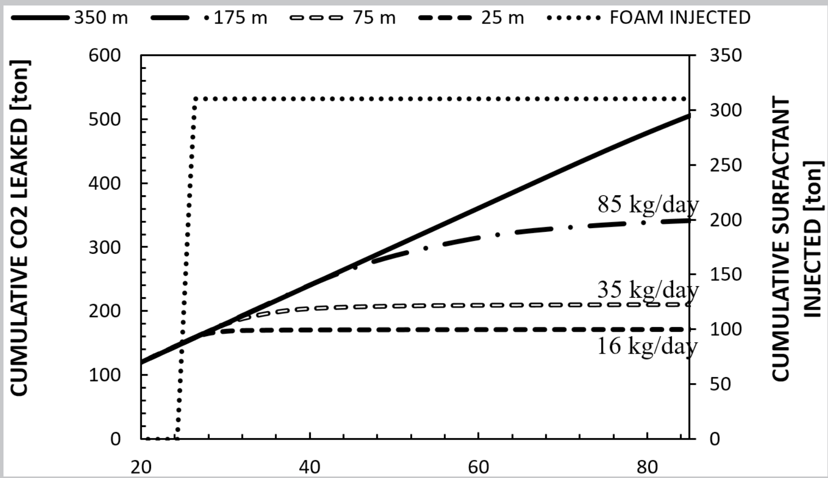

Figure 11 Cumulative CO_2 production through the leak at various distances from the injection site. The dotted line indicates the start of surfactant injection into the reservoir. The final CO_2 leak rate obtained at the end of the simulation is indicated near the corresponding curve, it should be compared to the initial value of 200 kg/day.

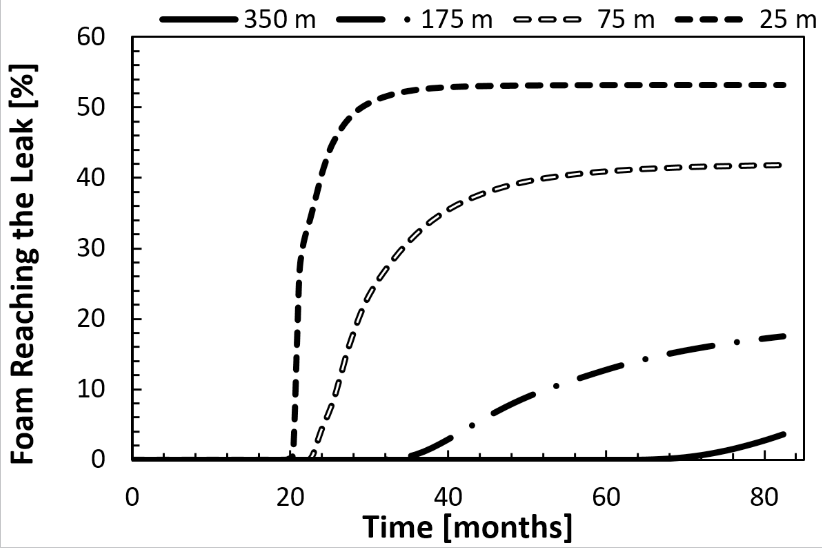

Figure 12 Cumulative percentage of injected foam (injection period of 180 days) reaching the leak location with varying distance from the foam injection location.

As the leak distance increases, the amount of CO_2 that can be prevented from leaking decreases (Figure 11). The leak rate decreases from the initial value of 200 kg/day down to 16, 35 and 85 kg/day respectively for distances of 25, 75 and 175m. As well, the amount of the surfactant and gas mixture and the time at which the foam reaches the leak location is greatly affected by the distance of the injection well from the leak. The percentage of injected foam contacting the leak site is shown in Figure 12. The amount of time that it takes for the foam to have an effect on the CO_2 leakage for the 175 m case (500 days) makes the foam mitigation technique ineffective as it requires such a large amount of time. Figure 12 shows that a low percentage of the foam has actually reached the leak. The rest of the foam has spread itself throughout the reservoir as there is no way to direct the foam to the leak site. Not only does the foam have a larger distance to travel for the 175 m leak distance, but the plume of foam is also much wider in such a case. More foam is thus transported to parts of the reservoir/cap rock that do not benefit from the mobility reduction provided by the foam. The minimum shear velocity is not always satisfied for all cases, the only really effective case was seen in the 25 m distance scenario presented in Figure 13. We present the foam and shear rate 6 years after the end of injection for highlighting more clearly the foam flow but it is not expected that the foam would last for such a large duration. Although the minimum velocity condition for foam is not always satisfied when being transported to the leakage site (Figure 13 (c) and (d)), the velocity caused by the high flow rate at the leak site allow for the foam to be regenerated at the site of the leak if it had collapsed previously. The spread of the foam (Figure 13(a) and (b)) show that the foam is able to spread in the lateral directions in order to prevent further CO_2 leakage from occurring.

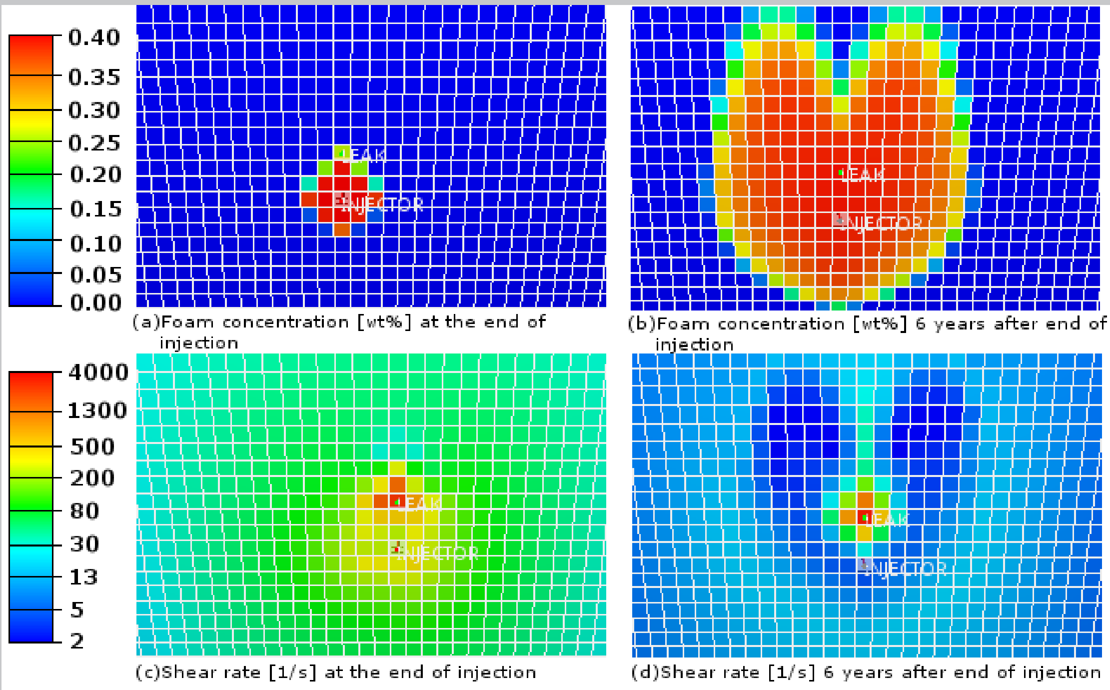

Figure 13 Comparison of the interstitial velocity and foam concentration for the 75 m leak distance situation in the grid block of the leak location.

At 25 m, the CO_2 leakage was reduced to a very low rate (16 kg/day) and rather quickly (31 days from the start of foam injection). The foam injection can be tailored for different leakage scenarios in order to effectively mitigate a leak with different parameters.

4 DISCUSSION

Using foam injection, the leakage of CO_2 was reduced in a relatively short amount of time as shown in Figure 10. This shows promising results for leaks that are relatively close to the injection well site. With large distances (greater than ~150 m), it is very difficult to reach the leak site as the foam will spread in all directions and will require large volumes of foam to reach the leak site in a realistic amount of time. Previous works [33] investigated using a hydraulic fracture to better transport a substance to the leak site, where a more concentrated solution could be placed at the leak site, which would overcome this issue of spreading.

The ability of the foam to flow and reach the leak site is greatly improved for a high permeability reservoir and it is more likely that the foam would flow to the leak due to the pressure gradient in the leak being encountered further from the leak site. In terms of controllable factors, the amount of foam injection added the greatest benefit for leak mitigation as the leaked foam would be replenished by the extra foam that was injected.

Similar to what was seen in previous literature [34, 35], the leak was able to be slowed by the foam injection due to the reduced gas mobility induced by the foam. The effectiveness of this foam injection is highly dependent on the ability of the foam to reach the leak site and to do so in a reasonable amount of time. Foam injection is also a temporary solution, as the real situation would exhibit foam degradation over time. Additionally, foam will leak through the leak in the same manner as CO_2 would. The CO_2 would in essence be replaced with the foam leaking through the cap rock, potentially creating more problems than it has solved. The use of a gel-foam could be a solution to this problem, but the strength and stability of this substance should be investigated further, as well as the chemical interactions between all components. Considering the large quantities injected, the surfactant contained in the foam should be considered for potential environmental impact and weighed against the impact of CO_2.

5 CONCLUSIONS

We studied the performance of CO_2 foams as a mean to reduce the gas flow rate in the vicinity of fractures or reactivated faults in the context of CO_2 storage. The laboratory experiments were conducted on typical sandstones representative of storage formations, with permeabilities in the range 200-1500 mD, and porosities between 10 and 20 %. The surfactant-brine solution and the CO_2 were co-injected at the inlet face of the sample using two different set-ups, in which the local saturation profiles are measured either by magnetic resonance imaging or by X-ray attenuation. These set-ups allowed observing the onset of foam as a function of interstitial velocity, in the largest possible range from about 3 ft/day up to 100 ft/day. The performance of the generated foams was evaluated from the relative foam viscosity corresponding to the ratio of the measured pressure drop in the presence of foam to the pressure drop in single phase condition for the same interstitial velocity. Whatever the pressure and permeability/porosity, the relative foam viscosity can be described as a power law vs. the shear rate evaluated from an empirical law established for polymer systems in which the interstitial velocity, permeability and porosity are the main variables. The exponent is close to -1 describing the shear-thinning behavior.

By using foam injection in reservoir simulations, it was shown that the rate of CO_2 leakage could be significantly slowed in order to allow for further remediation. Assuming an ideal foam (no adsorption, no degradation over time), a typical radius of investigation is 50 m. For field applications, it is unlikely that the precise leak location would be known. Hence, the radius of investigation for treatment thus becomes an important parameter to consider when designing the foam mitigation technique. The maximum distance to be considered for the leak location thus becomes more important than the precise leak location in order for the injected foam to reach the leak. Since a large quantity of CO_2 is injected to create the foam and reach the leak location, another remediation method should be applied in the long term. From this point of view, we believe that a gel-foam would be more appropriate for mid-term remediation.

6 ACKNOWLEDGEMENTS

We acknowledge Solvay for providing the surfactant used in this study. Research in this paper was conducted with funding from the European Commission FP7 project MiReCOl, Grant Agreement n°608608.

References

(1) MIT Energy Initiative Symposium. Role of Enhanced Oil Recovery in Accelerating the Deployment of Carbon Capture and Sequestration 2010.

(2) Thomas, S. Enhanced Oil Recovery - An Overview. Oil & Gas Science and Technology - Rev. IFP 2008, 63 (1), 9–19. DOI: 10.2516/ogst:2007060.

(3) Damen, K.; Faaij, A.; Turkenburg, W. Health, Safety and Environmental Risks of Underground CO_2 Storage – Overview of Mechanisms and Current Knowledge. Climatic Change 2006, 74 (1-3), 289–318. DOI: 10.1007/s10584-005-0425-9.

(4) Gauglitz, P. A.; Friedmann, F.; I. Kam, S.; R. Rossen, W. Foam generation in homogeneous porous media. Chemical Engineering Science 2002, 57 (19), 4037–4052. DOI: 10.1016/S0009-2509(02)00340-8.

(5) Kovscek, A. R.; Patzek T. W.; Radke, C. J. Mechanistic Prediction of Foam Displacement in Multidimensions: A Population Balance Approach 1994, SPE/DOE 27789.

(6) Dicksen Tanzil, George J. Hirasaki, Clarence A. Miller. Conditions for Foam Generation in Homogeneous Porous Media.

(7) Khatib Z.I.; Hirasaki, G. J.; Falls A. H. Effects of Capillary Pressure on Coalescence and Phase Mobilities in Foams Flowing Through Porous Media. SPE Reservoir Engineering 1988, 919–926.

(8) Batôt, G.; Fleury, M.; Rosenberg E.; Nabzar, L.; Chabert, M. Foam Propagation in Rock Samples: Impact of Oil and Flow Caracterization. SPE EOR OGWA Oman 2016, SPE-179855-MS.

(9) Skauge, A.; Aarra, M. G.; Surguchev, L.; Martinsen, H. A.; Rasmussen L. Foam-Assisted WAG: Experience from the Snorre Field. SPE/DOE IOR 2002, SPE 75157.

(10) W.R. Brock, L.A. Bryan. Summary Results of CO_2 EOR Field Tests, 1972-1987 1989.

(11) Enick, R. M.; Olsen D. K. Mobility and Conformance Control for Carbon Dioxyde Enhanced Oil Recovery (CO_2-EOR) via Thickeners, Foams, and Gels - A detailed Literature Review of 40 years of Research. DOE/NETL-2012/1540 2012.

(12) Bernard G.G.; Holm L.W. Method for recovering oil from subterranean formations 1967, US patent 3 342 256.

(13) McLendon, W. J.; Koronaios, P.; Enick, R. M.; Biesmans, G.; Salazar, L.; Miller, A.; Soong, Y.; McLendon, T.; Romanov, V.; Crandall, D. Assessment of CO_2-soluble non-ionic surfactants for mobility reduction using mobility measurements and CT imaging. Journal of Petroleum Science and Engineering 2014, 119, 196–209. DOI: 10.1016/j.petrol.2014.05.010.

(14) W.T. Osterloh and M.J. Jante Jr. Effects of Gas and Liquid Velocity on Steady-State Foam Flow at High Temperature 1992, SPE/DOE 24179.

(15) J.M. Alvarez, H.J. Rivas, and W.R. Rossen. Unified Model for Steady-State Foam Behavior at High and Low Foam Qualities. SPE journal 2001, SPE 74141.

(16) Chabert M.; Morvan M.; Nabzar, L. Advanced screening technologies for the selection of dense CO_2 foaming surfactants 2012, SPE 154147.

(17) Ma, K.; Lopez-Salinas, J. L.; Puerto, M. C.; Miller, C. A.; Biswal, S. L.; Hirasaki, G. J. Estimation of Parameters for the Simulation of Foam Flow through Porous Media. Part 1: The Dry-Out Effect. Energy Fuels 2013, 27 (5), 2363–2375. DOI: 10.1021/ef302036s.

(18) Moradi-Araghi, A.; Johnston, E. L.; Zornes, D. R.; Harpole, K. J. Laboratory Evaluation of Surfactants for CO_2-Foam Applications at the South Cowden Unit 1997, SPE 37218.

(19) Rossen, W. R.; Boeije C. S. Fitting Foam Simulation Model Parameters for SAG Foam Applications. SPE 2013.

(20) Zhou, Z. H.; Rossen, W. R. Applying Fractional-Flow Theory to Foam Processes at the "Limiting Capillary Pressure". SPE Advanced Technology Series 1995, 3 (1).

(21) Dholkawala, Z. F.; Sarma, H. K.; Kam, S. I. Application of fractional flow theory to foams in porous media. Journal of Petroleum Science and Engineering 2007, 57 (1-2), 152–165.

(22) A. H. Falls, G. J. Hirasaki, T. W. Patzek, D. A. Gauglitz, D. D. Miller, T. Ratulowski. Development of a Mechanistic Foam Simulator: The Population Balance and Generation by Snap-Off. SPE Reservoir Engineering 1988.

(23) Kovscek, A. R.; Patzek T. W.; Radke, C. J. Mechanistic Prediction of Foam Displacement in Multidimensions: A Population Balance Approach. SPE/DOE 1994, 27789.

(24) Rossen, W. R. Numerical Challenges in Foam Simulation: A Review. SPE 2013.

(25) Arts, R. J.; Vandeweijer, V. P.; Hofstee, C.; Pluymaekers, M.; Loeve, D.; Kopp, A.; Plug, W. J. The feasibility of CO_2 storage in the depleted P18-4 gas field offshore the Netherlands (the ROAD project). International Journal of Greenhouse Gas Control 2012, 11, S10-S20. DOI: 10.1016/j.ijggc.2012.09.010.

(26) Dake, L. P. Darcy's Law and Applications. Fundamentals of Reservoir Engineering; pp 103–131.

(27) Review of Leakage from Geological Storage Reservoirs. International Energy Agency Greenhouse Gas R&D Programme 2003, 21.

(28) Spirov P.; Rudyk N. S.; Khan A. A. Foam Assisted WAG, Snorre Revisit with New Foam Screening Model. SPE 2012.

(29) Tsau, J.-S.; Heller, J. Evaluation of Surfactants for CO_2-Foam Mobility Control. SPE PBOGRC 1992, SPE-24013-MS.

(30) Manlowe, D. J.; Radke, C. J. A Pore-Level Investigation of Foam/Oil Interactions in Porous Media. SPE Reservoir Engineering 1990, 5 (04).

(31) Chauveteau, G.; Zaitoun, A. Basic rheological behavior of xanthan polysaccharide solutions in porous media: effects of pore size and polymer concentration 1981, Developments in Petroleum Science 13, Enhanced Oil Recovery: Proceedings of the Third European Symposium on Enhanced Oil Recovery, 197–212.

(32) L. Pedroni. Private communications.

(33) Pizzocolo, F.; Hewson, C. W.; ter Heege, J. H. Polymer-Gel Remediation of CO_2 Migration through Faults and Caprock: Numerical Simulations Addressing Feasibility of Novel Approaches. ARMA proceedings 2016, 50th U.S. Rock Mechanics/Geomechanics Symposium, 26-29 June, Houston, Texas.

(34) Bernard G.G.; Holm L. W. Model Study of Foam as a Sealant for Leaks in Gas Storage Reservoirs. SPE 2353.

(35) Wassmuth; L. H. Hodgins; L. L. Schramm; S. M. Kutay. Screening and Coreflood Testing of Gel Foams To Control Excessive Gas Production In Oil Wells. SPE 59283.

Section V

REMEDIATION AND PREVENTATIVE MEASURES USING HYDRAULIC AND GAS BARRIERS

Chapter XVIII

Short report summarizing the choice of models (Hydraulic and gas barriers as a corrective measure for undesired CO_2 migration: review and work-plan)

Dan Bossie-Codreanu[1], Marc Fleury[1], Sevket Durucan[2], Anna Korre[2],
Bernd Wiese[3], Andreas Busch[4]
[1] IFPEN, France
[2] Imperial College, UK
[3] GFZ, Germany
[4] Shell, The Netherlands

SUMMARY

This short document summarizes the approach that will be taken to study two methods to prevent CO_2 migration across and above the caprock: 1) the injection of nitrogen; 2) the creation of a hydraulic barrier using water injection in a permeable layer above the caprock.

The principle of nitrogen injection is to increase the interfacial tension between water and gas. Since N_2 is lighter than CO_2, the fluid system effective at the base of the caprock will be nitrogen-water, and not CO_2-water. Therefore, higher overpressures are allowed, or from a safety perspective, the safety margin is increased.

The principle of the hydraulic barrier is to inject water continuously in an aquifer above the caprock in order to decrease the pressure gradient across the caprock, or if possible create an inverse pressure gradient. Such measure will decrease the leakage rate occurring across the caprock. This remediation technique can be applied at low cost but is only temporary. The Imperial College Saline Aquifer Model (ICSAM) developed in CO_2CARE project has been chosen as the base model to carry out brine injection simulations. Two potential leakage pathways have been envisaged and a number of modeling scenarios have been identified for each leakage pathway.

1 INTRODUCTION

This report is part of the research project MiReCOL (Mitigation and Remediation of CO_2 leakage) funded by the EU FP7 programme. Research activities aim at developing a handbook of corrective measures that can be considered in the event of undesired migration of CO_2 in the deep subsurface reservoirs. MiReCOL results support CO_2 storage project operators in assessing the value of specific corrective measures if the CO_2 in the storage reservoir does not behave as expected. MiReCOL focuses on corrective measures that can be taken while the CO_2 is in the deep subsurface. The general scenarios considered in MiReCOL are 1) loss of conformance in the reservoir (undesired migration of CO_2 within the reservoir), 2) natural barrier breach (CO_2 migration through faults or fractures), and 3) well barrier breach (CO_2 migration along the well bore).

This short document summarizes the approach that will be taken in work package 7 (WP7) entitled "Hydraulic and gas barriers", part of sub-project 2 "Leakage through fault of caprocks". The objectives of WP7 are two folds: 1) test a mitigation technique to prevent CO_2 migration in the caprock using nitrogen injection; 2) test a hydraulic barrier method after CO_2 migration in the caprock using water injection.

The principle of nitrogen injection is to increase the interfacial tension between water and gas. Since N_2 is lighter than CO_2, the fluid system effective at the base of the caprock will be nitrogen-water, and not CO_2-water. Therefore, higher overpressures are allowed, or from a safety perspective, the safety margin is increased.

The principle of the hydraulic barrier is to inject water continuously in an aquifer above the caprock in order to decrease the pressure gradient across the caprock, or if possible create an inverse pressure gradient. Such measure will decrease the leakage rate occurring across the caprock. This remediation technique can be applied at low cost but is only temporary.

2 GAS BARRIER

Nitrogen injection within the context of CO_2 storage is used as a mean to secure the injected CO_2, taking advantage of the N_2 interfacial tension properties regarding the cap-rock. By comparison to CO_2, the N_2 interfacial tensions are higher than CO_2 ones, thus allowing higher overpressures to be reached within the storage complex (Figure 1). The figure is valid for pressures from 1-30Mpa and temperatures between 298-373 °K.

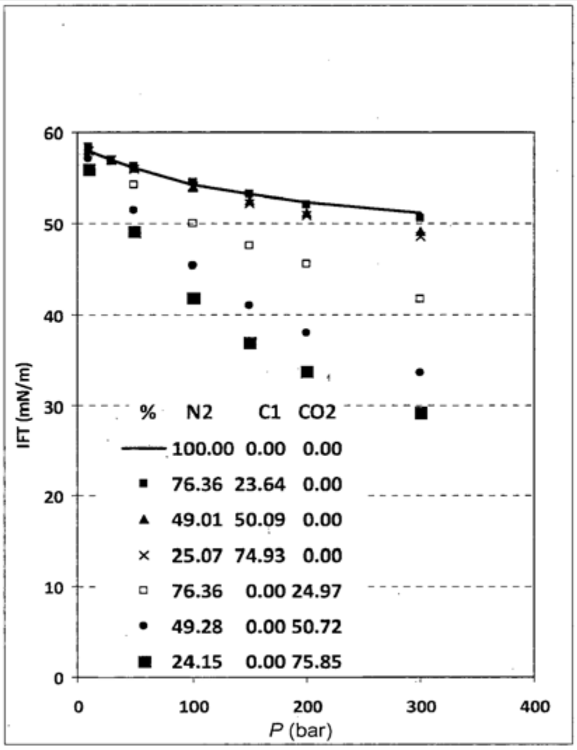

Figure 1 Interfacial tension (IFT) comparison (CO_2 - N_2 - C1) - [1]

When considering the full process, several aspects must be known, namely:

- thermodynamic properties of the nitrogen gas,
- injection position and vertical conformance (including gravity effects on the vertical N_2 saturation, regarding reservoir K_v properties),
- areal conformance with regard to the areal extent of the CO_2 "bubble" sought after by design.

There is enough knowledge about the thermodynamic properties of CO_2-N_2 mixture and therefore, we will study only the two last aspects using numerical simulations.

As such, N_2 injection represents one method of CO_2 injection management, aiming at reducing the leaking risk after the injection period, including its long-term fate, if the N_2 treatment spreads over large distances.

2.1 Background and review of the state of the art

2.1.1 Plume extension

N_2 injection is not any different than any gas injection in a reservoir. Consequently, given its specific PVT properties the operational sequence should be:

- determination of the CO_2 bubble extent in-situ, given (a) the allowable overpressure imposed by the cap-rock properties and (b) the rock properties - dynamic and static - of the reservoir.
- choice of the N_2 injection point given the well completion in such a way as to enhance the viscous gradient while minimizing the gravity one, thus as close as possible to the base of the cap-rock.
- injection of a volume of N_2 corresponding to the difference of overpressure allowance for N_2 and overpressure allowance of CO_2. The viscosity of N_2, lower than CO_2 should favor the lateral mobility (K/μ) of the N_2, thus covering the CO_2 bubble.

The entry pressure of a gas in the caprock is given by:

$$Pe = \frac{2\sigma\cos(\theta)}{r} \tag{1}$$

where σ is the water-gas interfacial tension (IFT), θ is the contact angle, and r a pore radius characterizing the porous media. When looking at data concerning the IFT of different gases (N_2, CO_2, CH_4), see Figure 2 it is clear that N_2 IFT's are higher than CO_2 IFT's. ([2 to 5) - roughly doubling the IFT for the experimental data used. Hence, if the IFT is increasing by a factor of two, the entry pressure will increase accordingly, assuming there is no modification of the contact angle θ. Recent work [12] indicate only a slight modification of the contact angle in the presence of CO_2 (less water wet) and replacing CO_2 by N_2 will be even more favorable (strictly water wet).

Systems	Conditions	IFT (mN/m)
CH_4/water	10–30 MPa, 40–80 °C	48.6–61.7
N_2/water	10–30 MPa, 40–80 °C	53.7–67.2
Medium oil/water	>6.9 MPa, 54.4–81.1 °C	30–35
N-alkane (C_6–C_{16})/water	10–30 MPa, 25-50 °C	49–54
CO_2/water	10–30 MPa, 40–80 °C	16–30

Figure 2 IFT for different fluid systems

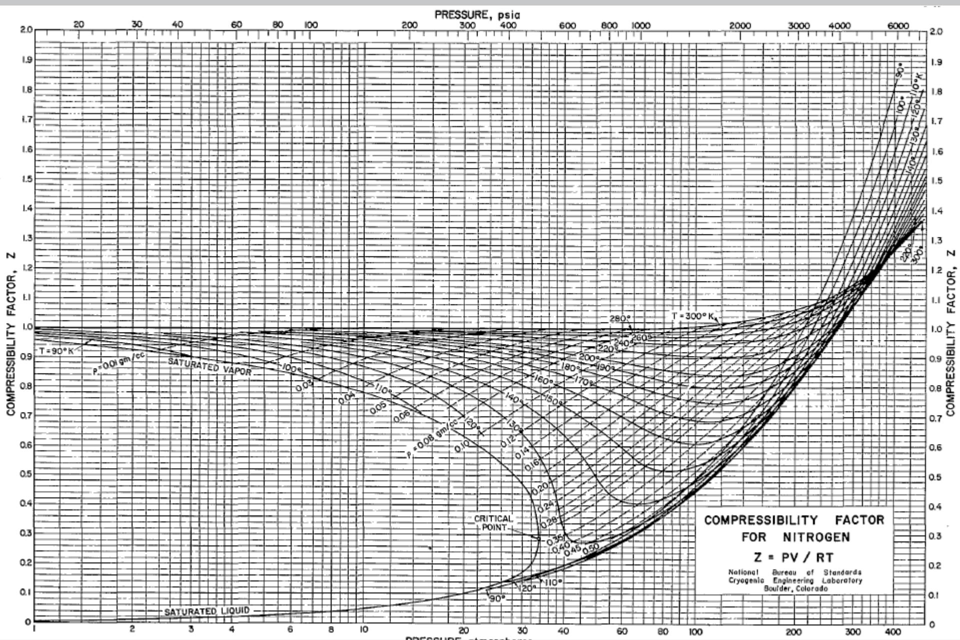

Figure 3 Compressibility, Z of N_2 [6]

Concerning injection, the common rule used for the injection of CO_2 is to consider that the maximum reservoir pressure which the reservoir can reach, P_{max} is P_{max} = 1.2/1.3 $P_{res.init.}$. Given the above, it means that the use of N_2 can increase the P_{max}, , potentially reaching a value P_{max} = 1.4/1.6 $P_{res.init.}$ available for the N_2/CO_2 system.

At typical reservoir pressure and temperatures N_2 is a gas. The specific PVT properties of N_2 are calculated using an EOS (Peng-Robinson) – density, compressibility while viscosity is calculated using the LBK equation. Here-below we can see a few correlations which can provide some orders of magnitude concerning some of these values – Z-factor and viscosity (Figure 3 and Figure 4).

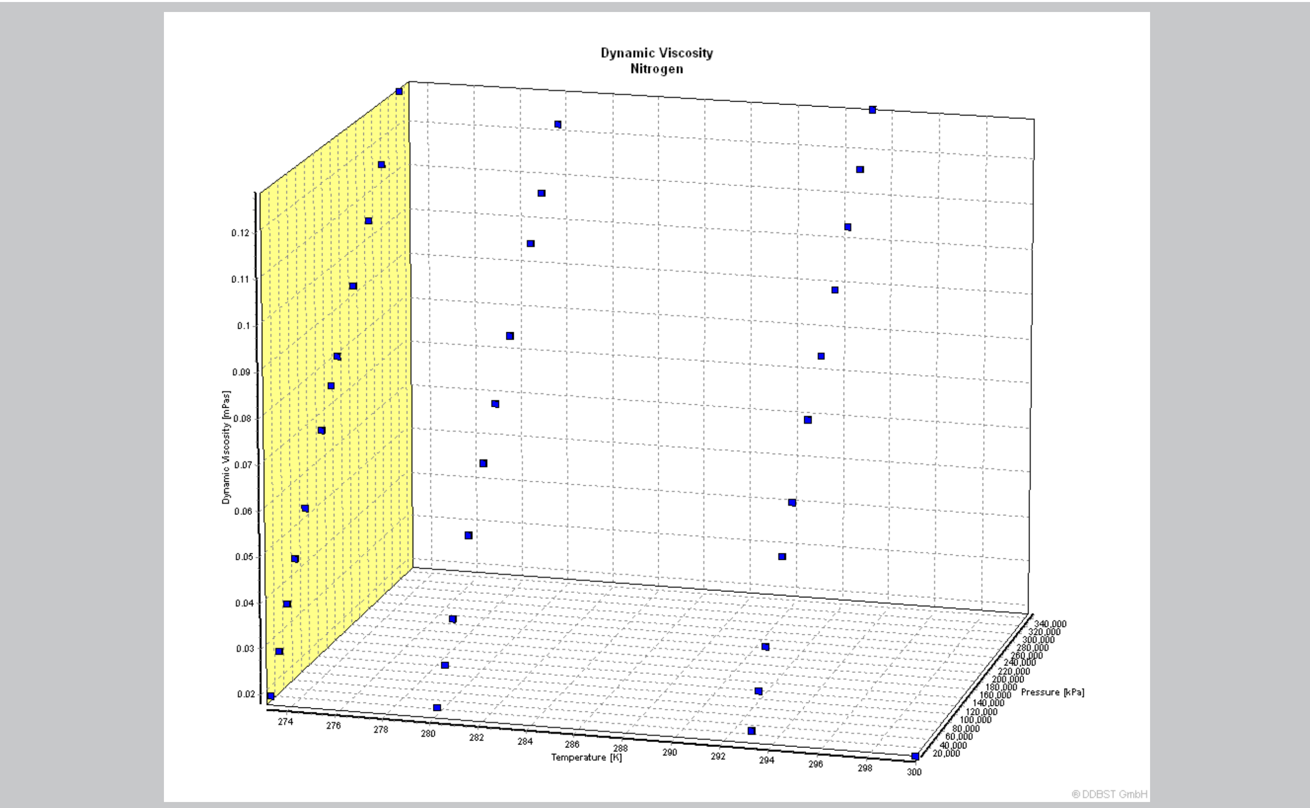

Figure 4 N_2 viscosity [7]

Solubility in water will be calculated and input in the form of K-values using [8], see Figure 5.

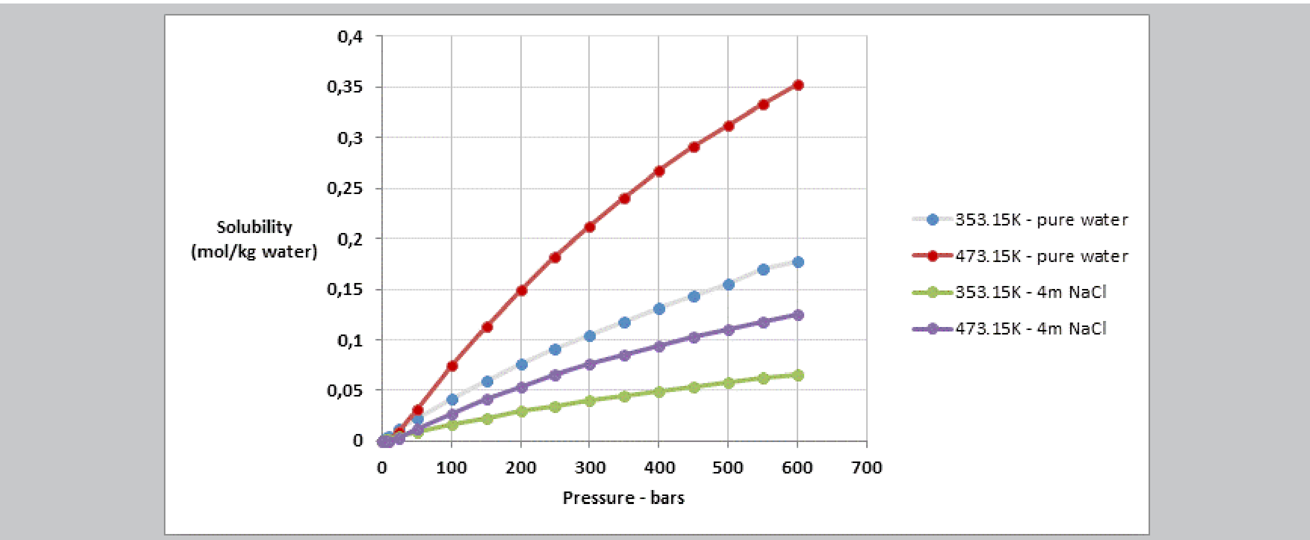

Figure 5 Solubility of N_2 in pure water and 4m NaCl [8]

Plume extension

Considerations concerning "reservoir engineering" aspects applicable to the N_2 injection can be easily understood through the use of an analytic model. Instead of developing yet an "other" analytic tool, let's take one commonly applied for CCS [9].

The analytic model assumes radial flow around an injection which penetrates a horizontal aquifer of constant thickness H, porosity φ and permeability k. In this case the location of the interface between the two fluids is a function only of distance from the injection well and time. As a result, the following equation can be written that relates pressures at the top and bottom of the aquifer:

$$p(r,H)=p(r,0)-\rho_{g,w}gh_{g,w}(r)-\rho_g g\left[H-h_{g,w}(r)\right] \quad (2)$$

Where: p = Pressure
g = Gravitational constant
h_g = Plume thickness
r = distance (radius) from the injection well
and the subscripts (g) and (w) stand for the injected gas and aquifer brine, respectively.

If the density and viscosity of the injected acid gas are considered constant (at values corresponding to the in-situ aquifer pressure and temperature), which can be considered as a fairly reasonable approximation when the pressure decay due to the injection build-up is rapid (errors will be existent only at the near-vicinity of the well), we can write for the fluid flow:

$$Q_{g,w}=-2\pi r h_{g,w}(r)\frac{kkr_{g,w}}{\mu_{g,w}}\frac{\partial p_{g,w}}{\partial r} \quad (3)$$

where (g) and (w) stand for either gas or water and:
k = permeability
$kr_{g,w}$ = relative permeability of either gas or water
$h_{g,w}$ = fluid thickness (or column height) for gas or water at location r
$Q_{g,w}$ = fluid flux through a well of radius r

In the equation above, $h_w = H - h_g$ when $kr_{g,w} = 1$ since full saturation was assumed for each phase. Also, the total volume must be conserves locally, thus:

$$Q_w + Q_g = Q \quad (4)$$

where Q is the gas injection rate (assumed constant). The change in thickness for either fluid is given by the accumulation of that fluid in the cylindrical volume from the injection well to radius r, according to:

$$\frac{\partial h_{g,w}}{\partial t}=\frac{-1}{2\pi\varphi r}\frac{\partial}{\partial r}\left(rQ_{g,w}\right) \quad (5)$$

where t is time.

The above equations form a system of four equations (three of them differential) with four unknowns: $h_{g,w}$, $Q_{g,w}$, $p(r,0)$ and $p(r,H)$. The solution is based on energy minimization and variational calculus principles. Details of the solutions can be found in the original paper [9]. The fluids in the system will arrange themselves at any time to minimize the amount of energy required to inject the given mass of fluid. In this case energy (work) includes injection, viscous flow (energy dissipation) and buoyancy caused by density differences between the two fluids. In seeking a solution, the following dimensionless variables are introduced:

$$\lambda = \frac{\mu_w}{\mu_g} \quad (6)$$

which is the mobility and:

$$\Gamma = \frac{2\pi\phi\Delta\rho g k kr_w H^2}{\mu_w Q} \quad (7)$$

represents the ratio of buoyant versus viscous and pressure forces, and is an indication of the importance of buoyancy (density differences) in driving the flow of the injected acid gas. This shows that the whole gas injection process (whether CO_2 or N_2) is described by two independent parameters only, the mobility ratio λ and the dimensionless number Γ.

Examination of the latter is very instructive in indicating when buoyancy needs to be taken into account and when it can be neglected. For Γ <0.5 hydrodynamic and viscous forces dominate and buoyancy can be neglected. This situation will happen for:

- high injection rate (strong hydrodynamic force)
- small density difference between the injected gas and formation water (low buoyancy)
- injection into a thin and/or low porosity and permeability aquifer.

At the other end of the spectrum, buoyancy strongly dominates for Γ > 10. Such cases will occur for a combination of the following factors:

- large density differences between the injected fluid and formation water,
- injection into a thick aquifer characterized by high porosity and permeability,
- low injection rate (small hydrodynamic force).

In these cases, because of high buoyancy, the plume will, most likely, not reach the bottom of the aquifer. Thus, for 0.5 < Γ < 10, buoyancy, hydrodynamic and viscous forces are comparably important and the full system of equations described previously has to be solved. The boundaries between the various domains of buoyancy importance and solution applicability (i.e., Γ = 0.5 and Γ = 0) are not definite, but rather fuzzy. These values are only indicative of the region in the Γ space where the transition from one flow regime to another starts to occur.

In the case of Γ < 0.5, when buoyancy is negligible, the profile of the plume (given as a fraction of the total height) of injected gas is given by the equation:

$$\frac{h_g(r,t)}{H} = \frac{1}{\mu_w - \mu_g}\left[\sqrt{\frac{\mu_g \mu_w V(t)}{\pi \phi H r^2}} - \mu_g\right] \tag{8}$$

where: $V(t)$ = Volume of injected gas since inception of injection.

This simplified solution corresponds to the radial Buckley-Leverett solution. For values of Γ > 0.5 solutions are more complicated, necessitating numerical approaches. The Dirac Delta function governs the segregation within the reservoir toward the cap-rock, whereas the above equation governs the plume displacement over the “reservoir” layer where the CO_2 is injected (often considered to be governed by viscous forces alone).

The discussion above is meant to clarify which parameters will govern simulations and therefore the data needs, as well as characterization and overall interaction during simulation.

2.1.2 Pore radius approach

The injection of Nitrogen increases the entry pressure of gas into the caprock. This section describes the underlying physical processes of the interaction with CO_2 that should be considered during application of this technique. The aim is to provide guidelines about applicability of Nitrogen to reduce leakage through a porous caprock.

Here the link to existing geology shall be made. Two kinds of percolation pathways through a caprock exist. Geomechanical failure occurs if the fracture pressure of the caprock is exceeded and fractures open up in the rock. As consequence CO_2 may percolate though the emerging fractures. This mechanical failure provides a constraint to a CO_2 reservoir operation. The maximum reservoir

Table 1 Critical pore radius for a 76% CO_2 gas mixture and pure N_2. Interfacial tensions are extracted from Figure 1.

Depth [m]	Hydrostatic pressure [bar]	Maximum reservoir pressure [bar]	Over-pressure [bar]	Interfacial tension 76% CO2, 24% N2 [mN/m]	Interfacial tension 100% N2 [mN/m]	critical pore diameter 76% CO2 [µm]	critical pore diameter 100% N2 [µm]
500	55	82.5	27.5	44	55	6.4E-02	8.0E-02
1000	110	165	55	36	53	2.6E-02	3.9E-02
1500	165	247.5	82.5	31	52	1.5E-02	2.5E-02
2000	220	330	110	28	51	1.0E-02	1.9E-02

overpressure is related to the hydrostatic pressure. Percolation failure occurs when the entry pressure of the caprock is exceeded and gas percolates into its pore network. In this case N_2 injection can increase the gas entry pressure and therefore can counteract percolation.

The reservoir should be operated such that both failure conditions, geomechanical failure and percolation failure do not occur. Both failure conditions impose constraints to the reservoir pressure do not interact with each other and therefore have both to be fulfilled, independently of the results of the other constraint.

As a practical approach, it is analysed under which conditions both failures can be avoided. N_2 injection can only improve storage security if the pressure is below the geomechanical fracture pressure. The feasible pressure to avoid fracturing of the cap rock is determined. For this pressure it is evaluated whether N_2 injection can increase the storage safety.

Considering a hydrostatic gradient of 11 kPa per m and a geomechanical failure pressure of 1.5 times the hydrostatic pressure, the maximum reservoir pressure is obtained dependent on the reservoir depth (Table 1). The interfacial tension between brine and CO_2/N_2 is a function of depth (Table 1). Based on these values it is determined, which is the maximum pore size of the caprock that should not be exceeded. It is shown that the maximum pore size increases by 25% in a depth of 500 m and by 82 % in a depth of 2000 m. This means that the effectivity of N_2 injection increases with reservoir depth. The pore diameter where N_2 injection may increase storage safety is between 10-8 and 8 10-8, which corresponds to a caprock facies of tight sandstone or shale (Nelson, 2009). This window for potential nitrogen injection is also shown in Figure 6. As further task it shall be determined, which is an appropriate cutoff radius to determine the critical pore radius on the basis of a pore size distribution obtained by experimental methods such Nuclear Magnetic Resonance or mercury injection.

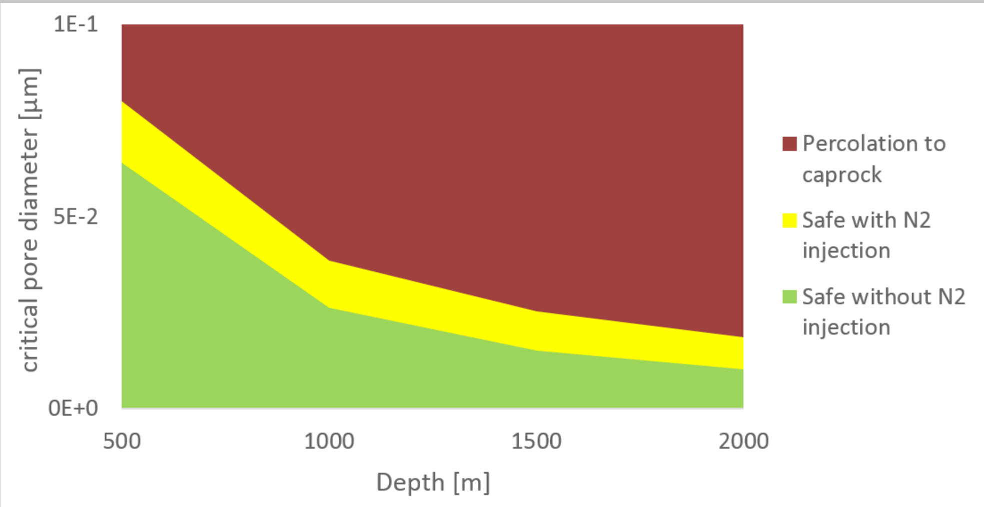

Figure 6 Maximum allowable caprock pore size as function of depth. The green area indicates safe CO_2 storage without Nitrogen injection. The safe storage can be extended by the yellow area when applying N_2 injection. For a larger pore radius safe storage cannot be guaranteed. The results are presented for a mechanical cap rock failure of 1.5 times hydrostatic pressure.

2.1.3 Diffusive Mixing

Nitrogen and carbon dioxide are well miscible in all ratios above the critical point of CO_2 (31.1 °C, 73.8 bar), which is typically fulfilled for storage reservoirs. Several processes exist that induce mixing between CO_2 and N_2. This mixing should be avoided since it lowers the N_2 concentration at the caprock and therefore deteriorates the beneficial effect. The mixing is affected by different processes which counteract each other (Table 2). The two main effects are molecular diffusion increasing the mixing and gravity segregation causing separation of N_2 and CO_2.

Table 2 Processes involved in the mixing between CO_2 and N_2

Process	*Effect on N_2 concentration*
Molecular diffusion	decreasing
Increasing temperature	decreasing
Increasing pressure	stabilizing
Gravity segregation	stabilizing

The physics of the diffusion process is well known and the diffusion coefficients can be derived from existing PVT correlations. The results depends on the boundary conditions and geological configuration. An analytical solution is given below, which is valid for infinite boundary conditions. Effectively this approach is applicable if the thickness of the diffusive layer is smaller than the extent of the different gas components. Figure 7 shows the erosion of a formerly sharp concentration gradient with infinite extent boundaries.

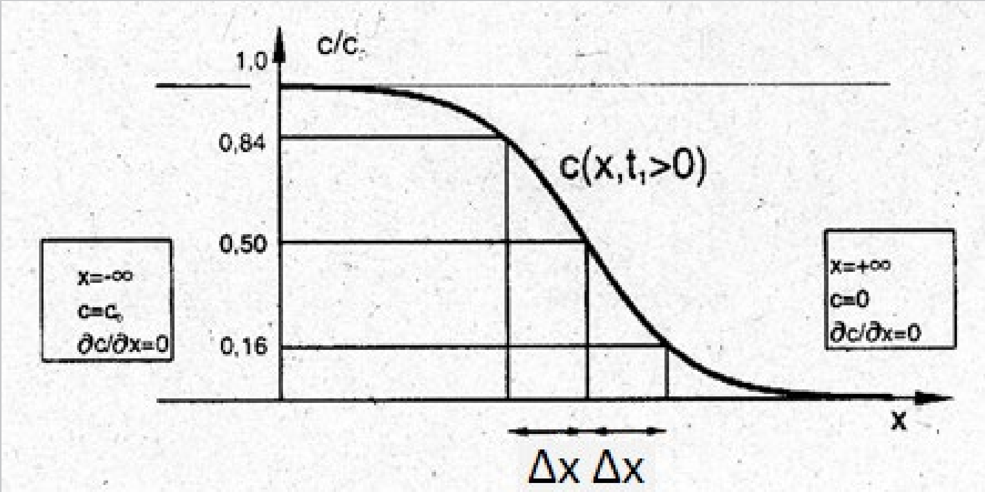

Figure 7 Erosion of a formerly sharp concentration front by diffusion.

The corresponding characteristic length Δx from Figure 7 is calculated according to equation 9.

$$\Delta x = \sqrt{(2\,D\,t)} \qquad (9)$$

With Δx as the characteristic distance where the initially pure N_2 phase is mixed with 16% CO_2. Binary diffusion coefficients for a 50% CO_2 and 50% N_2 mixture and geologic conditions are provided in Table 3. The resulting characteristic lengths are provided in Table 4. For example, if the N_2 layer has a thickness of 3 m, after 1000 days the N_2 concentration caprock will be decreased to 84%.

Table 3 Diffusivities for a 50% CO_2/N_2 mixture with respect to different pressure conditions and geothermal temperature.

Depth [m]	Hydrostatic pressure [bar]	Maximum pressure [bar]	Temperature [°C]	Diffusivity hydr. pressure [m²/s]	Diffusivity max. pressure [m²/s]
500	55	82.5	26.5	2.7E-07	1.7E-07
1000	110	165	43	1.3E-07	7.8E-08
1500	165	247.5	59.5	9.3E-08	5.5E-08
2000	220	330	76	7.5E-08	4.5E-08

Table 4 Characteristic diffusion lengths for a 1500 m deep reservoir at maximum pressure for different durations.

time [days]	Δx [m]
1	0.1
10	0.3
100	1.0
1000	3.1

The presented approach provides a general idea about necessary scales and times that are required for the application of N_2 as remediation measure. It is simplified, since the lateral extent is assumed as infinite. For a limited layer thickness, concentration levels out faster. Gravity segregation will induce a static vertical concentration gradient and prevent complete mixing. These effects will be further studied in the project (Table 2.2). During the fluid injection phase convective mixing will further contribute to decrease the maximum concentration of N_2. Furthermore, the tortuosity of the pore matrix is not considered. Tortuosity typically decreases diffusion coefficients and therefore reduces mixing of N_2 and CO_2.

2.2 Work program

2.2.1 Plume extension and injection strategy

For the study of N_2 injection, many models are suitable. N_2 injection can be considered both as a preventive and remediation measure. Globally, such measure considers a migration of CO_2 into the caprock but without precise localization, generated by a global weakness of the caprock in terms of entry pressure.

Viewed as a preventive measure, N_2 could be injected before CO_2, with the main objective of producing the largest possible horizontal plume extension below the caprock (Figure 2-6). However, since N_2 injection will also increase the pressure in the reservoir, the overall benefit must be studied carefully and the process optimized. Such optimization will be studied on a synthetic case using analytical formulation or numerical simulation before considering a real case.

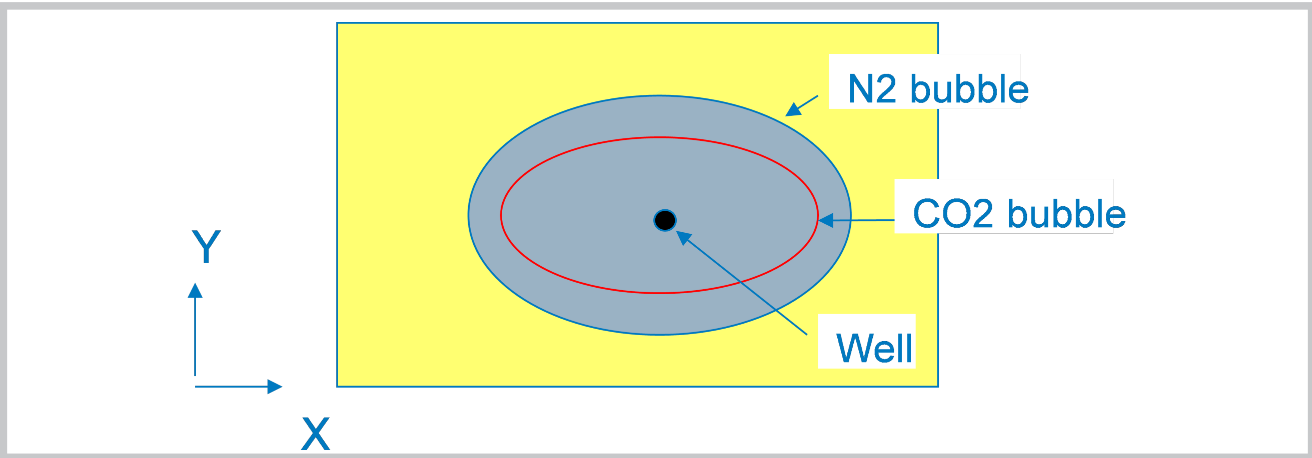

Figure 8 Schematic showing the desired effect in terms of areal conformance

Viewed as a remediation measure, N_2 injection is more complex and its effectiveness must be studied. If one injects N_2 in the presence of CO_2 while it is migrating into the caprock, the resulting increase of pressure may not produce the desired effect, (i.e. limiting the migration). Therefore, it is anticipated that one should most likely, first, back-produce a certain amount of CO_2, and then inject N_2 at an appropriate location in the well.

In order to obtain general conclusions, we will use generic models to study N_2 injection, rather than considering a single situation taken from a detailed geological case. The generic models will be build using a methodology described in appendix 2.4. Shortly, a storage will be described by about 8 non-dimensional numbers representing various physical characteristics of interest for the studied process (aspect ratio, dip angle, mobility ratio, buoyancy, heterogeneity, capillarity, pressure). Then, a data base of existing or potential storage sites will be compiled in order to have typical and extreme values of these non-dimensional numbers. Using an experimental design approach, a sufficient number of generic models will be created to represent the most probable cases; theoretically, with a two level approach and 8 parameters, $2^8 = 256$ cases need to be created and simulated; however, this number may be reduced by eliminating un-necessary parameters. In all these simulations, the N_2 injection will be evaluated based for example on the following criteria:

- over-pressure due to N_2 injection,
- added capacity for CO_2 storage,
- conformance,
- gravity effect and mixing.

Such approach has the advantage of clarifying in which case the N_2 injection is useful.

2.2.2 Mixing modeling

During injection of Nitrogen into a carbon dioxide reservoir both components tend to mix. These mixing processes are affected as well by local geologic parameters and also on the mixing processes that are described in section 2.1.3. The processes are difficult to predict and should be evaluated on the basis of field experiments.

In the pre-injection phase of the Ketzin pilot site 123 m^3 of N_2 were injected into the reservoir. This induces a Nitrogen pre-flush of the reservoir during CO_2 injection. In addition to Nitrogen also smaller amounts of Argon, Krypton and Helium are injected as tracer gases.

The experimental conditions mimic a potential scenario for industrial application of the technique. The experiment allows to identify mixing between CO_2 and Nitrogen under reservoir conditions. The relevant mixing processes as described in section 2.1.3 will be identified and a quantification of their importance carried out.

The work will be related to reservoir simulations carried out in WP3 and WP4. A short overview on these simulation is given below, more information can be found in the report for the respective work package.

Numerical Modeling of the Ketzin pilot site
A simple inverse model exists for the Ketzin Pilot site. It integrates three hydraulic tests and the first thirty days of CO_2 injection. The model focuses on the joint inversion of the observed pressure during the hydraulic test, injection pressure in the CO_2 injection well and the arrival time of CO_2 arrival data. It contains 30 free parameters and is feasible to model channeling effects due to layered permeability. It is an advanced continuation of the hydraulic modeling work [13] and a necessary complement to the general Ketzin reservoir modelling work [14].

Modelling approaches that consider only single phase hydraulic tests indicate a region of low permeability between the injection well Ktzi 201 and observation well Ktzi 200. Multiphase simulations of CO_2 injection in contrast indicate a high permeability between both wells. Single phase simulations predict a higher effective permeability than constrained multiphase simulations. The problem is resolved by joint inversion of one single and one multiphase model. It is crucial for this calibration to develop a geological concept that contain the relevant features that allow to reproduce the different type of observations. Generally, the large amounts of data that are recollected from the tests site represent different aspects of the same geological features.

This model shall be used to model the spreading and transport of CO_2 injection experiment at the beginning of the CO_2 injection at the pilot site Ketzin. The model is set up with the simulator Eclipse 300, which allows for modelling multicomponent gas composition including dissolution effects. It will be investigated, whether the flow and transport processes in the reservoir are affected significantly by alteration of interfacial pressure for the gaseous phase containing variable ratios of CO_2 and N_2.

2.3 Summary

The injection of N_2 below the caprock can be used as mean to secure a CO_2 storage. The method is based on the increase of the interfacial tension when N_2 instead of CO_2 is present as the base of a caprock. This process may not be useful in all situations and a large number of generic models will be used to determine in which situations it is useful. A compromise must be found between the over-pressure due to N_2 injection, the added capacity, the conformance and the mixing effect. A specific study will focus on the mixing effect.

2.4 Appendix: Method for generating synthetic reservoir models

Synthetic models will be generated by making use of dimensionless numbers characterizing a CO_2 storage, listed hereafter:

- Effective Aspect ratio (R_L)

$$R_L = \frac{L}{H}\sqrt{\frac{k_z}{k_x}} \tag{10}$$

where: L = reservoir length
H = reservoir height
k_z = vertical permeability
k_x = horizontal permeability

The effective aspect ratio is related to cross-flow within the reservoir. It is a measure of the communication between fluids in the horizontal direction relative to the vertical one. The aspect ratio governs the vertical equilibrium (VE), representing the state of maximum cross-flow, occurring when the forces in the transverse direction is zero. The greater the aspect ratio, the closer it is to vertical equilibrium (well approximated for aspect ratios greater than 10).

- Dip angle group (N_α)

$$N_\alpha = \frac{L}{H}\tan\alpha \tag{11}$$

where: α = dip angle of the reservoir to the horizontal.

Long, thin, dipping reservoirs will have greater values of N_α, lessening the potential impact of gravity overriding, while thicker, shorter reservoirs (low N_α) increase the potential impact of gravity overriding.

- Mobility ratio (M)

$$M_g^w = \frac{k_{rg}^o \mu_w}{k_{rw}^o \mu_g} \tag{12}$$

where: μ_g and μ_w = gas (CO_2 and/or N_2) and water viscosity
K_{rg}^o and K_{rw}^o = relative permeability end-points for gas and water

Mobility relates the ability of gas and water to move relative to each other.

- Buoyancy Number (N_g)

$$N_g = \frac{H \Delta \rho g \cos \alpha}{\Delta P} \tag{13}$$

where: H = reservoir thickness
$\Delta\rho$ = density difference between gas and water
g = gravity constant
α = dip angle
ΔP = pressure difference between the well and reservoir pressure

The buoyancy number is the ratio of the gravity forces resulting of the density difference to the viscous forces in a reservoir. Larger values of N_g indicate larger density differences between fluids and therefore a higher potential for segregation. Thus, the N_g value governs the shape of the CO_2 from its injection point (lower N_g values favoring a more cylindrical shape).

- Capillary Number

$$N_{Pc} = \frac{\Delta P}{\sigma} \sqrt{\frac{k}{\phi}} \tag{14}$$

where: σ = Interfacial tension between gas and water
φ = porosity
K = permeability

The capillary number is the ratio of the viscous forces to the capillary ones. It governs the amount of trapping which may occur in an aquifer storage. Capillary forces increase with capillary pressure.

One of the most favorable cases (from the point of view of storage) in case of CO_2 injection is one in which capillary forces dominate over viscous forces and viscous forces in turn dominate over gravitational forces.

- Heterogenity (VDP) – Dykstra-Parsons method
This method is simple, allowing the generation of a vertical (and possibly horizontal) permeability heterogeneity. It is expressed as a variance of the permeability and written as:

$$VDP = \frac{K_{50} - K_{84.1}}{K_{50}} \tag{15}$$

Where K_x is the permeability with a probability of x % . The significance of such a definition can be seen in the Figure 9.

A homogeneous system has a VDP = 0 and a completely heterogeneous system a VDP = 1. In our case the VDP is given, from which a vertical permeability is generated. This vertical distribution can be generated horizontally (areal distribution). The fact that areal distributions are often more homogeneous than vertical ones is accounted for. Similarly, porosity distributions are adjusted accordingly.

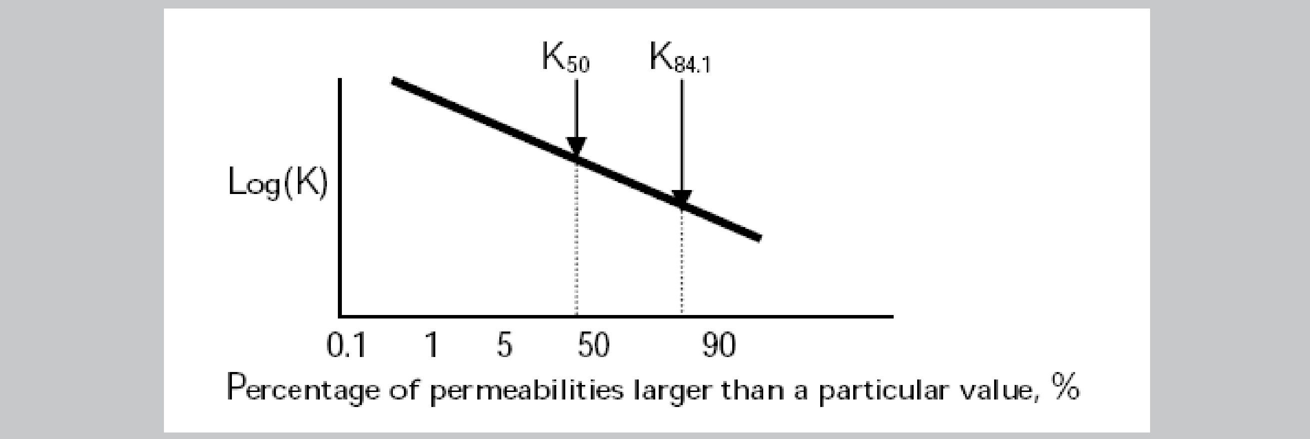

Figure 9 Permeability distribution plot.

The question may be raised on why geostatistical methods are not used here. The answer is simple. Geostatistical data such as correlation lengths obtained from variogram analysis imply the existence of many wells so as to determine the existence of such correlations lengths. Furthermore, if correlations can be found at the facies "level", thus eventually for porosity (for particular deposition environments) it is hardy seen at the permeability level (outcrop studies have proven that). Data base of geostatistical parameters for aquifers or hydrocarbon reservoirs are not easy to come by. By opposition, VDP statistics for many reservoirs have been collected and thus we can use these for our modeling purpose. Given its simplicity, we will use this method in order to introduce heterogeneity in our model.

- Injection pressure

$$P_i = \frac{P_{inj}}{P_{fract}} \tag{16}$$

This ratio determines the dimensionless injection pressure with regard to the fracturing pressure, considered as a limiting pressure for CO_2 operations.

- Residual gas saturation S_{gr}

The above parameters will be collected for a large variety of storage sites, giving a realistic range of values. Then, one can build a simplified reservoir model by choosing a combination of parameters and taking values within the observed range. An experimental design approach will be taken to generate these various situations. In principle, with a 2 level approach and with 8 parameters, $2^8 = 256$ cases need to be constructed. However, not all parameters are relevant for a given process and one can also use a fractional factorial approach, decreasing the number of simulations to be performed to more practical values (e.g. 32).

3 HYDRAULIC BARRIER

Injection of high pressure saline water above a fractured cap rock or a fault, if maintained at a higher pressure than the CO_2 pressure in the reservoir, would not only create an inverse pressure gradient to reverse the flow direction, it would also increase the solubility of CO_2 in the saline water barrier formed, and prevent or at least limit leakage. This procedure could enable fast and reasonably low cost mitigation measures once a leakage is detected, however, this technology can only be used as a temporary measure and allow for more permanent remediation techniques to be prepared and implemented with time.

The efficiency of this technology relies upon continuous injection of brine above the leakage area and a number of site specific reservoir conditions represented by static and dynamic rock and fluid characteristics, geometry and position of the leakage. Furthermore, unless carefully assessed and designed, this methodology may fail to deliver under certain reservoir conditions. Proposed research will involve testing realistic reservoir and CO_2 leakage scenarios representative of selected models from SP5 as described under Task 7.1 and focus on the role of controlling parameters which may affect the success or failure of the hydraulic barrier technology considered.

3.1 Background and review of the state of the art

It was Celia et al. [15] who initially carried out numerical experiments to investigate remediation options near a leaky injection well during CO_2 storage. It was suggested that injection of brine above the caprock, at a higher pressure than the CO_2 pressure in the reservoir, would create an inverse pressure gradient to reverse the flow direction and also increase the solubility of CO_2 in the saline water barrier formed, and thus prevent or limit leakage. Furthermore, coupled with fluid management procedures during aquifer storage (saline water extraction and re-injection above the caprock), this methodology can also be used to minimise displacement and migration of native brine, and avoid pressure build up in closed or semi-closed structures.

In a more recent study, Reveillere et al. [16] conducted a numerical study on the same phenomenon using an overly simple 3D flow model with flat layers (thus buoyancy-driven flow was not accounted for). They reported that this technique may efficiently stop leakage in a relatively short time or may be effectively used as a preventive measure, while continuing injecting CO_2. It is believed that such a procedure could enable fast and relatively low cost mitigation action once a leakage is detected. On the other hand, the results illustrated in the literature are valid for an idealized case and the methodology may have limitations which need to be investigated further through exhaustive analysis of field based properties.

As part of recently completed CO_2CARE project, funded by European Commission under the Seventh Framework Programme, a preliminary assessment of the effectiveness of the pressure gradient reversal (PGR) method as a potential remediation technique for CO_2 leakage from deep saline aquifers was investigated using a realistic 3D reservoir/caprock model. A hypothetical CO_2 storage operation involving CO_2 injection at 1 Mt/year for up to 30 years down-dip of a structure high in the model domain was considered. Separate leakage scenario simulations were carried out for 30 different/assumed leakage point sources (18 in the transient zone and 12 in the non-transient zone) independently. At each simulation, the amount of CO_2 leaked out of the target storage reservoir at a selected location was continuously monitored, and the injection terminated once a pre-set detection threshold is exceeded. The brine injection simulation results indicate that the performance of PRG is strongly affected by how early leakage is detected from the start of injection (time-to-detection), which in turns is controlled by the CO_2 leakage detection threshold (in thousands of tonnes), leakage pathway permeability and the distance to the injection well.

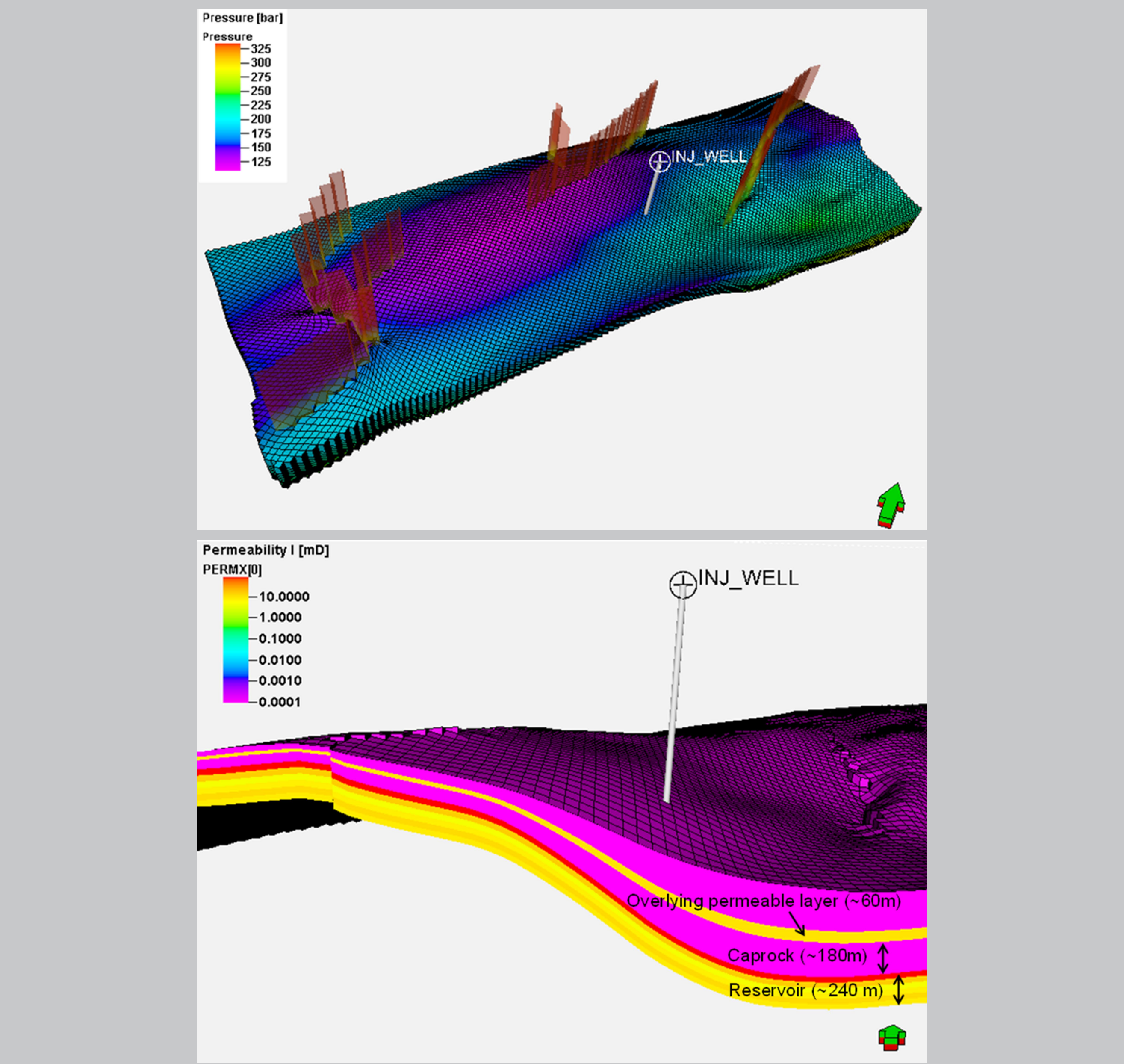

Figure 10 Imperial College Saline Aquifer Model (ICSAM). a) Hydrostatic pressure distribution; b) a close-up showing the caprock and overburden layers.

3.2 Model requirements and description of the CO_2 mitigation scenarios setup

Model requirements

The basic requirements of the reservoir model(s) are: inclusion of a caprock and the presence of at least one permeable layer in the overburden formations which is suitable for brine/water injection.

Description of the model selected

Guided by these considerations, a review of the currently available reservoir models from the database in SP 5 has been carried out and the Imperial College Saline Aquifer Model (ICSAM) developed in CO_2CARE project has been chosen as the base model to carry out brine injection simulations.

The ICSAM model measures 36 km x 10 km and includes several faults (Figure 10a). The depth of target storage formation ranges from 1,082 to 3,484 m across the model domain, dipping considerably. The injection well is located at a location where the storage reservoir is between 1,973 to 2,181 m deep (Figure 10a). The model has a more or less uniform grid block size of 200 m x 200 m in the lateral direction.

The storage reservoir, which has a thickness of approximately 240 m, consists of 6 layers of varying properties both within each layer and across the layers. The overlying formation (caprock) is considered to be impermeable, except for a 60 m thick layer situated at 180 m above the reservoir, which is assigned a permeability of 10 mD (Figure 10b). The reservoir/overburden is initially at hydrostatic pressure, and the reservoir temperature is 92 °C.

Scenarios

Two leakage pathways are envisaged:

- Leakage through an areal sink in the caprock
- Leakage through a fault/fault zone (line sink)

For each leakage pathway, the following key features of the storage reservoir will be considered and implemented to form a number of modelling scenarios

- Storage reservoir depth (formation pressure and temperature)
- Top of reservoir topography
- Caprock thickness/distance to the permeable layer above the storage reservoir
- Permeable layer permeability/porosity

For each scenario the base reservoir model will be modified accordingly for CO_2 and brine injection simulations and associated remediation performance evaluation.

Other elements to be evaluated in terms of their impact on the effectiveness of the remediation technique are

- Leakage pathway geometry and dimensions
- Leakage pathway permeability and distance to injection well
- Leakage detection threshold and amount of CO_2 injected prior to remediation

In leakage scenario simulations, the amount of CO_2 leaked out of the target storage reservoir at a selected location is continuously monitored, and the injection is terminated once a pre-set detection threshold is exceeded. The leakage, however, is allowed to continue until its source (the free CO_2 in the storage reservoir available for leakage) is exhausted to yield the total leakage potential. In this way, potential leakage risk profiles through the leaky caprock/faults may be established to provide a benchmark for evaluating the effectiveness of any remediation measure, including PGR.

3.3 Summary

For hydraulic barriers, guided by the basic requirements of the reservoir model(s): inclusion of a caprock and the presence of at least one permeability layer in the overburden formations which is suitable for brine/water injection, the Imperial College Saline Aquifer Model (ICSAM) developed in CO_2CARE project has been chosen from the database in SP 5 as the base model to carry out brine injection simulations. Two potential leakage pathways have been envisaged and a number of modeling scenarios have been identified for each leakage pathway.

References

[1] W. Yan, Zhao GY, Chen Guo and GJ TM: " Interfacial Tension of (Methane + Nitrogen) + Water and (Carbon Dioxide + Nitrogen) + Water Systems", Journal of Chemical and Engineering Data, Vol. 46, No. 6, 2001, 1545

[2] Ren QY, Chen GJ, Yan W, Guo TM. Interfacial tension of (CO_2 + CH_4) + water from 298 K to 373 K and pressures up to 30 MPa. J Chem Eng Data 2000;45:610–2.

[3] Yan W, Zhao GY, Chen GJ, Guo TM. Interfacial tension of (methane + nitrogen) + water and (carbon dioxide + nitrogen) + water. J Chem Eng Data 2001;46:1544–8.

[4] Hocott CR. Interfacial tension between water and oil under reservoir conditions up to pressure of 3800 psia and temperatures of 180 F. AIME Trans 1938;132:184–90.

[5] Cai BY, Yang JT, Guo TM. Interfacial tension of hydrocarbon + water/brine systems under high pressure. J Chem Eng Data 1996; 41:493–6.

[6] National Bureau of Standards, Cryogenic Engineering Laboratory, Boulder, Colorado

[7] DDB (Dortmund Data Bank) and DDBSP data

[8] Rui Sun, Wenxuan Hu, and Zhenhao Duan "Prediction of Nitrogen Solubility in Pure Water and Aqueous NaCl Solutions up to High Temperature, Pressure, and Ionic Strength" Journal of Solution Chemistry, Vol. 30, No. 6, 2001

[9] Nordbotten, J.M., M.A. Celia, and S. Bachu. 2004. Injection and storage of CO_2 in deep saline aquifers: analytical solution for CO_2 plume evolution during injection. Transport in Porous Media

[10] Di Pasquoa B., P. de Montleau, J.M. Daniel, D. Bossie Codreanu, Qualification of a CO_2 storage site using an integrated reservoir Study, , 7th Trondheim CCS Conference, TCCS-7, June 5-6 2013, Trondheim, Norway

[12] Tonnet N., Broseta D., Mouronval G. (2010) Evaluation of the petrophysical properties of a carbonate-rich caprock for CO_2 geological storage purposes. SPE 131525, 12 p.

[13] Chen, F., Wiese, B., Zhou, Q., Kowalsky, M., Norden, B., Kempka, T., Birkholzer, J., 2014, Numerical modeling of the pumping tests at the Ketzin pilot site for CO_2 injection: Model calibration and heterogeneity effects, International Journal of Greenhouse Gas Control, 22, 200-212.

[14] Kempka, T., Kühn, M., Class, H., Frykman, P., Kopp, A., Nielsen, C., Probst, P., 2010, Modelling of CO_2 arrival time at Ketzin - Part I, International Journal of Greenhouse Gas Control, 4 (6), 1007-1015.

[15] Celia, M. A., Peters, C. A., and Bachu, S., 2002, Geologic Storage of CO_2: Leakage Pathways and Environmental Risks, PowerPoint Presentation, accessed 18 September 2002:
http://www.slidefinder.net/g/geologic_storage02/geologic_storage02/2766438

[16] Réveillère, A., Rohmer, J., Manceau, J.C., 2012. Hydraulic barrier design and applicability for managing the risk of CO_2 leakage from deep saline aquifers. International Journal of Greenhouse Gas Control 9, 62-71.

Chapter XIX

Study of N_2 as a mean to improve CO_2 storage safety

Dan Bossie-Codreanu[1]
[1] IFPEN, France

SUMMARY

Current CO_2 storage operations in aquifer reservoirs are naturally limited, among other parameters, by entry pressures encountered in cap-rocks, thus limiting over-pressures allowed during the storage process. The injection of nitrogen in a zone just below the cap-rock, prior CO_2 injection, could be a viable protective measure to increase the storage safety by lowering the leakage risk and increasing the maximum allowable reservoir pressure.

The physical background of the beneficial impact of Nitrogen on the caprock entry pressure is based on the higher N_2-brine interfacial tension (IFT) compared to CO_2-brine. As a maximum possible effect (for pure N_2-brine systems), IFT could increase by a factor of two, yielding correspondingly to the same increase of allowable pressure. However, the N_2 injection decreases the storage volume and the trade-off must be studied carefully. The IFT spread decreases rapidly with the mixing ratio of CO_2 in the N_2. Mixing can occur due to advective processed induced by differential absolute pressure due to CO_2 injection and also due to vertical mixing due to different partial pressure. Injection placement is carefully studied carefully, especially the vertical conformance as well as saturation rarefaction.

In order to study the feasibility of such approach for different storage conditions, a series of CO_2 injection simulations were performed within a generic characterization framework based on dimensionless numbers. A database of dimensionless numbers governing the storage was built, using literature information. The application of an experimental design based on the minimum/maximum values found within the data-base identified a series of cases to be simulated, further reduced by a fractional approach of such design. The scenarios simulated consisted in a CO_2 injection within a reservoir storage zone found at some distance from the N_2 zone, just below the cap-rock, followed by a resting period during which the CO_2 saturation is monitored. The N_2 zone is refined, rendering possible the study of the potential mixing and contamination with CO_2. For all case members of the data base, the CO_2 conformance was studied in terms of possible mixing and override of the CO_2 plume. Discussion of the potential benefits and possible difficulties are addressed. Conclusions were drawn considering the possible field application of such a technique, identifying a-priori sites more suitable for such a technique, based on the dimensionless numbers characterizing them.

This report has been submitted for publication as: Bossie-Codreanu, D., Study of N_2 as a means to improve CO_2 storage safety, Energy Procedia, in press, April 2017.

1 INTRODUCTION

Storage of CO_2 currently is naturally limited by entry-pressure values of the cap-rock, which is a limiting factor in terms of storage capacity. One method which has been suggested as being effective in protecting the cap-rock is the injection of N_2, which is supposed to act not only in shielding the cap-rock from the CO_2 but also increasing the IFT which controls the CO_2 entry.
The concept governing the injection of N_2 is summarized below.

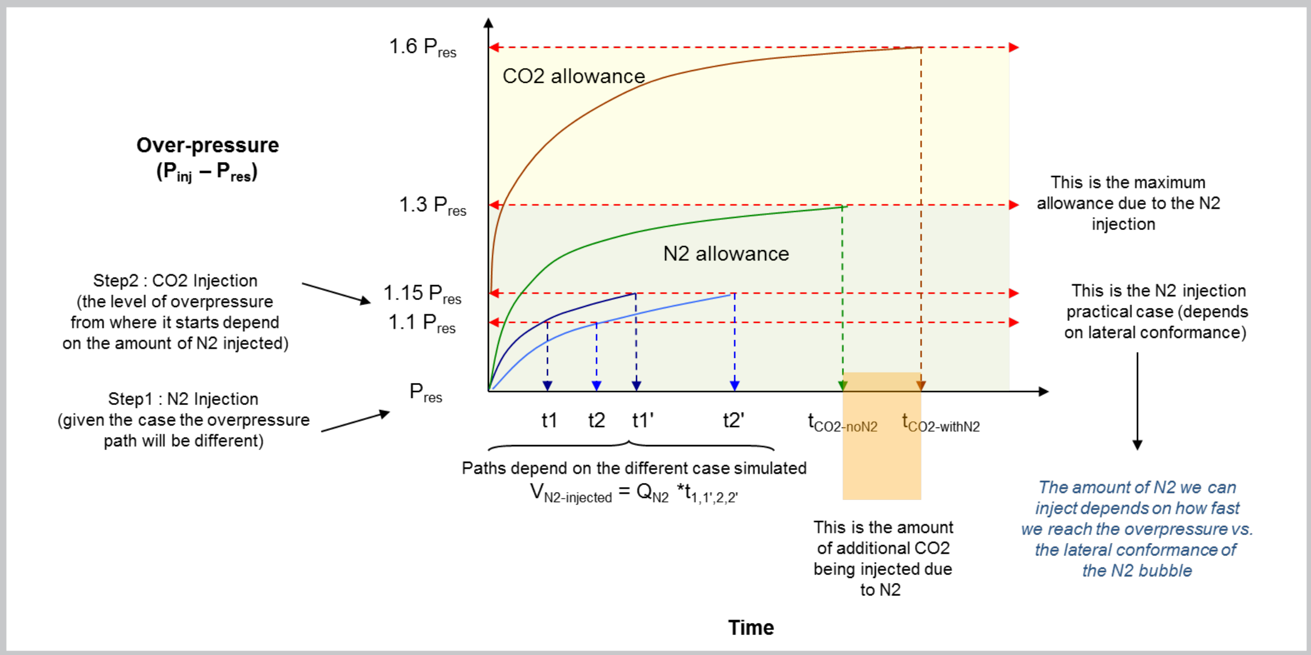

Figure 1 Conceptual design of an N_2 injection prior to a CO_2 injection

The conceptual schematic showing the N_2 injection (Figure 1) considers a first injection step made up only of the N_2, followed by the injection of the CO_2. Within this scheme, the allowable overpressure for the N_2 needs to be set with regard to the cap-rock, which subsequently defines how much CO_2 can be injected in a second step. This implies a double design; one concerning the injection of the N_2, followed by the CO_2, within a framework in which the overall overpressure allowance is studied and decided for the storage, considering both gases instead of only one (the CO_2). Furthermore, the areal conformance of the N_2 within the injection layer should be considered since the protective nature of the N_2 should cover the entire CO_2 plume extension.

Considerations above concern a possible injection of N_2 as a mean to increase capacity while protecting the storage site against leaking risks. The process of the N_2 injection envisioned as a cushion gas as well as possibly enhancing storage capacities has been patented by IFPEN (Barroux, [24]). Several authors have recently shown interest in the co-injection of CO_2 and N_2 (Fisher et al. [25] and Wei et al. [26]). Yet, their interest concerned more the N_2 as a tracer rather than a gas to be used as a cushion gas. From the thermodynamic point of view the IFT properties are a-priori favorable for the design of such a process.

Yet, issues have been raised about the possible mixing between the CO_2 and the N_2 occurring below the cap-rock, where in principle the N_2 needs to be placed, thus lessening the potential protection caused by this gas cushion. Before discussing more critical issues such as the effective volumes needed to provide a thorough conformance of the N_2 below the cap-rock, or the study of the overall overpressure allowance, the present study investigates the possibility of mixing between the two gases. The N_2 is supposed to have been injected in a layer below the cap-rock. Several CO_2 injection scenarios within a reservoir storage zone are, below the protecting N_2 zone, followed by a resting period, are simulated, investigating the CO_2 movement within the full field (during the injection, after the injection and finally at the end of a 10 year period of rest – the resting period was chosen ad-hoc). For that a dimensionless approach, consisting in generating numbers governing the CO_2 injection were generated, studying the gas saturation corresponding to a typical CO_2 injection, followed by a resting period during which the movement of the CO_2 is recorded, along with the overpressure. The goal of the study is to determine which dimensionless numbers govern favorable conditions for the CO_2 confinement within the storage zone, including the resting period.

The CO_2 saturation is analyzed using the dimensionless numbers supposed to characterize the different reservoirs, drawing conclusions about the mixing characteristics below the cap-rock in regard to the dimensionless numbers characterizing the storage setting.

2 BUILDING THE PROBLEM

2.1 Theoretical Foundations

The movement of CO_2 in the groundwater aquifer during injection, potential leaking and possible remediation is complex and depends on the interplay of many factors. These factors include gravity effects, capillary forces, and viscous forces as well as the impacts from dissolution/ex-solution of the CO_2 with the water. In order to obtain a "generic" simulation framework, the following methodology followed was applied:

Step 1: Dimensionless Numbers and Experimental Design Definition

Definition of process dimensionless Numbers (DN). A series of pertinent dimensionless numbers governing injection and evolution of the CO_2 plume, using pertinent knowledge obtained by the oil industry (reservoir engineering).

Building a data base (DB) of DN. Based on parameters making up the dimensionless numbers, an investigation of their value was collected from field cases already performed, using literature data, and a DB build accordingly.

Using the value range of each DN, a Min/Max criteria allowed a fractional experimental design, thus reducing the number of cases.

Step 2: Definition of a series of scenarios of CO_2 production

Based on the above a series of simulation covering all possible cases was build and several production scenarios were considered, stemming from a common initial CO_2 injection scheme which establishes an average original saturation field. These scenarios account for the rate production, acknowledging the possibility of water coning, which in the case of CO_2 production can be favorable, since it will favor the production of water which is probably easier to dispose.

Step 3: Perform simulations on all cases defined in Step 2

Step 4: Analyze results and define criteria by which simulations will be evaluated in terms of safety and process performance (ex. % of CO_2 recovered by comparison to CO_2 injected)

Theoretically, the dimensionless numbers which can used have been identified using literature of CO_2-EOR which aimed originally at scaling the CO_2 injection Shook et al. [1], Rivas et al. [2], Diaz et al. [3]. Scaling consists in extrapolating results obtained at one scale size to another scale. This process produces dimensionless groups, which then serve as a basis of comparison between scales. These are combination of properties such that the dimensions of the properties composing the dimensionless group cancel each other to produce a final group with no dimensions. A process can be described by independent and dependent dimensionless variables. When the independent dimensionless groups for that group are identical, the dependent dimensionless group will also be identical. This implies that systems with completely different dimensional properties but similar dimensionless properties have a similar dimensionless response, allowing a comparison between scales. The dimensionless groups retained for the description of the injection/production CO_2 process are:

Aspect Ratio (RL): This is a measure of the communication between fluids in the horizontal direction relative to the vertical one. The aspect ratio governs the vertical equilibrium (VE), representing the state of maximum cross-flow, occurring when the forces in the transverse direction is zero. The greater the aspect ratio, the closer it is to vertical equilibrium (well approximated for aspect ratios greater than 10).

$$R_L = \frac{L}{H}\sqrt{\frac{k_z}{k_x}} \tag{1}$$

where L is the reservoir length, H is the thickness, k_z is the vertical permeability and k_x is the horizontal permeability.

Dip angle group (N_α): Long, thin, dipping reservoirs will have greater values of N_α, lessening the potential impact of gravity overriding, while thicker, shorter reservoirs (low N_α) increase the potential impact of gravity overriding.

$$N_\alpha = \frac{L}{H}\tan\alpha \tag{2}$$

where α is the reservoir angle with the horizontal

Mobility Ratio (M): Mobility relates the ability of gas and water to move relative to each other and are used to evaluate sweep efficiencies.

$$M_g^w = \frac{k_{rg}^o \mu_w}{k_{rw}^o \mu_g} \tag{3}$$

where μ_g and μ_w are gas and water viscosity and $K_{rg}{}^{\circ}$ and $K_{rw}{}^{\circ}$ are relative permeability end-points for gas and water

Buoyancy Number (N_g): The buoyancy number is the ratio of the gravity forces resulting of the density difference to the viscous forces in a reservoir. Larger values of N_g indicate larger density differences between fluids and therefore a higher potential for segregation. Thus, the N_g value governs the shape of the CO_2 from its injection point (lower N_g values favoring a more cylindrical shape).

$$N_g = \frac{H \Delta \rho g \cos \alpha}{\Delta P} \tag{4}$$

where $\Delta\rho$ is the density between gas sand water, g is the gravity constant and ΔP is the difference in pressure between the injection and the reservoir.

Capillary Number (N_{Pc}): The capillary number is the ratio of the viscous forces to the capillary ones. It governs the amount of trapping which may occur in an aquifer storage. Capillary forces increase with capillary pressure.

$$N_{Pc} = \frac{\Delta P}{\sigma} \sqrt{\frac{k}{\phi}} \tag{5}$$

where σ is the interfacial tension and φ is the porosity.

Heterogeneity (VDP) – Dykstra-Parsons method: This method is simple, allowing the generation of a vertical (and possibly horizontal) permeability heterogeneity. It is expressed as a variance of the permeability where K_x is the permeability with a probability of x %. The index is expressed by:

$$VDP = \frac{K_{50} - K_{84.1}}{K_{50}} \tag{6}$$

The significance of such a definition can be seen in Figure 2.

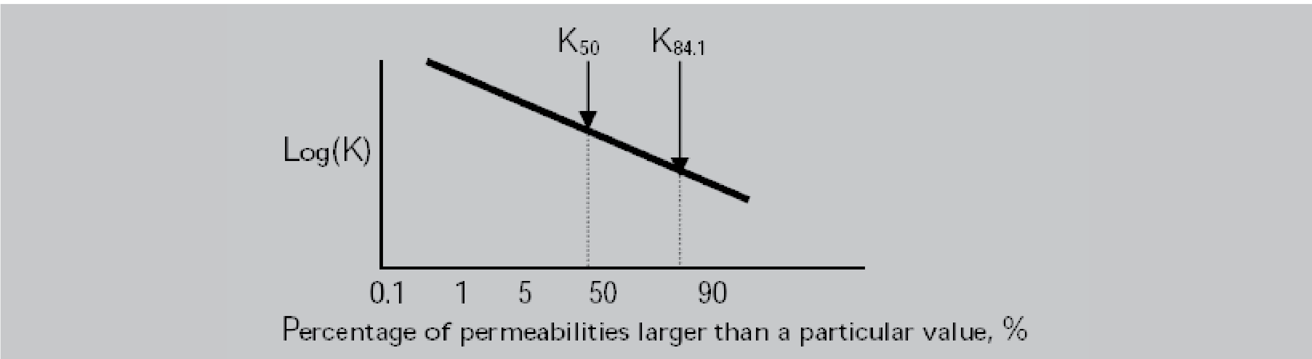

Figure 2 Illustration of the VDP concept

A completely homogeneous system has a VDP = 0 and a completely heterogeneous system has a VDP = 1. Heterogeneity is viewed as a layered system to which a permeability is assigned per layer. Thus, the method used in this study consists in assuming some VDP value (from statistics issued from hydrocarbon reservoirs), and then assign a permeability to each layer, inverting the VDP function. Vertical permeability is calculated from the horizontal value (ex. $K_z = 0.1\ K_x$). Porosity is assigned from the K-PHI relationship corresponding to the field under study, often available.

The question may be raised on why geostatistical methods are not used here. The answer is simple. Geostatistical data such as correlation lengths obtained from variogram analysis imply the existence of many wells so as to determine the existence of such correlations lengths. Furthermore, if correlative relations could be found at the facies "level", such as porosity which can be correlated for particular deposition environments it is hardy the case for permeability (outcrop studies have proven that). Using petrophysical properties for characterization would need the development of flow-units, which is not easy to Data base of geostatistical parameters for aquifers or hydrocarbon reservoirs are not easy to come by. By opposition, VDP statistics for many reservoirs have been collected (Hirasaki et al [4], Jensen et al. [5], Dykstra et al. [6]) and thus we can use these for our modeling purpose. While recognized as being imperfect, this method accounting for heterogeneity, given its simplicity, is considered as adequate for this study.

In our case, two representative values of VDP were considered - VDP = 0.6 and 0.8 as seen in Figure 3 below (Hirasaki et al [5]).

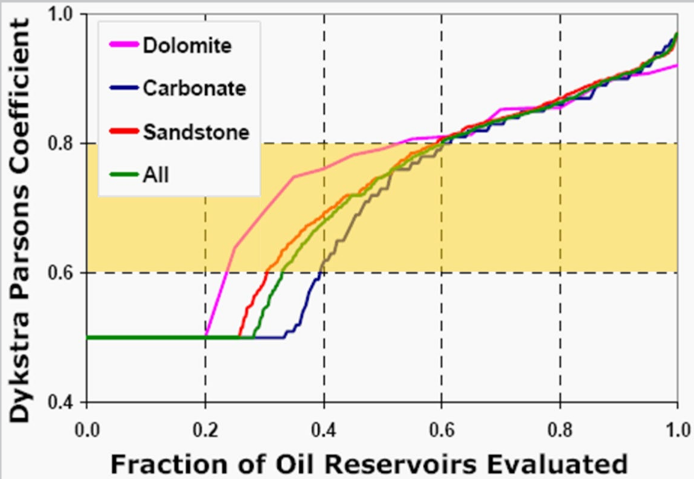

Figure 3 VDP value depending on the reservoir type

Injection pressure (P_i): This ratio determines the dimensionless injection pressure with regard to the fracturing pressure, considered as a limiting pressure for CO_2 operations. For all simulations cases two scenarios were chosen, based on over-pressure data obtained from traditional CH_4 storage operations.

$$P_i = \frac{P_{inj}}{P_{fract}} \quad (7)$$

Residual gas saturation (S_{gr}): Residual gas saturation controls the volume of gas trapped in that portion of the reservoir that has experienced water encroachment. As water moves into a rock volume filled with gas, the water displacement of the gas is incomplete. The water fills pores and pore throats, causing capillary pressure and relative permeability effects to stop the flow of gas and allow only water to pass through the rock volume. This results in gas being trapped behind the encroaching waterfront as residual gas. The volume and location of the residual gas are controlled by the distribution of the petrophysical properties. The trapping characteristics used were calculated from the relation of Holtz [22].

2.2 Data Base Building

The data-base of dimensionless numbers was built from information obtained from different publications describing field injections (Bachu et al. [7]., Bachu S. [8], Flett et al. [9], Hosa et al. [10]). The total number of sites qualifying for the data base is 60, of which 40 are aquifers and 20 reservoirs.

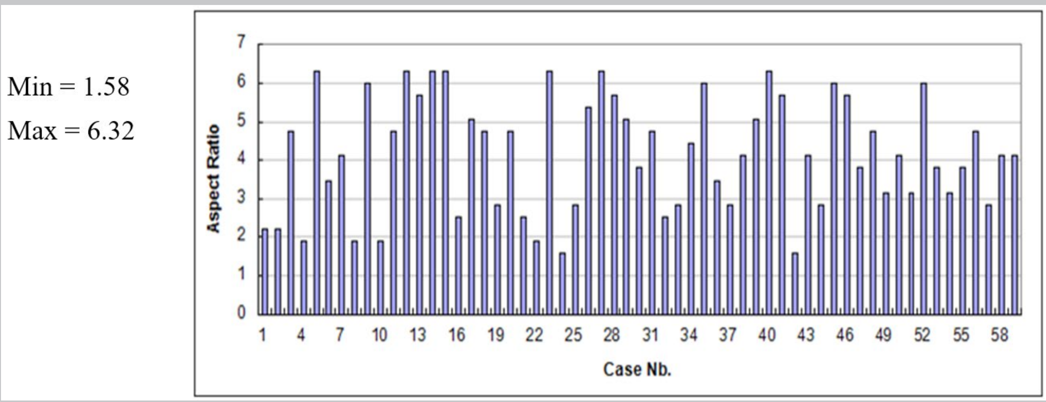

Figure 4 Aspect Ratio obtained for all investigated cases

The theoretical analysis identified eight dimensionless groups characterizing the CO_2 storage. Further analysis of the available data lead to a reduction of the groups considered. Thus, only five groups were retained to represent the variability of all cases, namely the Aspect Ratio (R_L), the Dip angle group (N_α), the Mobility Ratio (M), the Buoyancy Number (N_g) and the Capillary Number (N_{Pc}). The other groups, namely the Residual gas saturation, VDP and Injection Pressure are estimated, making up the different simulation group scenarios. Results from the Data-Base are shown below in Figure 4 through 9.

Aspect ratio

As seen, no value among all cases considered reaches a value of 10, which is theoretically a value approximating a perfect vertical equilibrium.

Dip Number

Long, thin dipping reservoirs have greater Dip Angle numbers, lessening the potential impact of gravity overriding. It also has an impact on the shape of the interface between displaced and displacing fluids. The lower the value of the number the more the interface parallel to the fluid movement. By opposition, the higher the value, the is most perpendicular to the fluid movement. In developing the statistic angle values varying between 1 and 10 degrees were used.

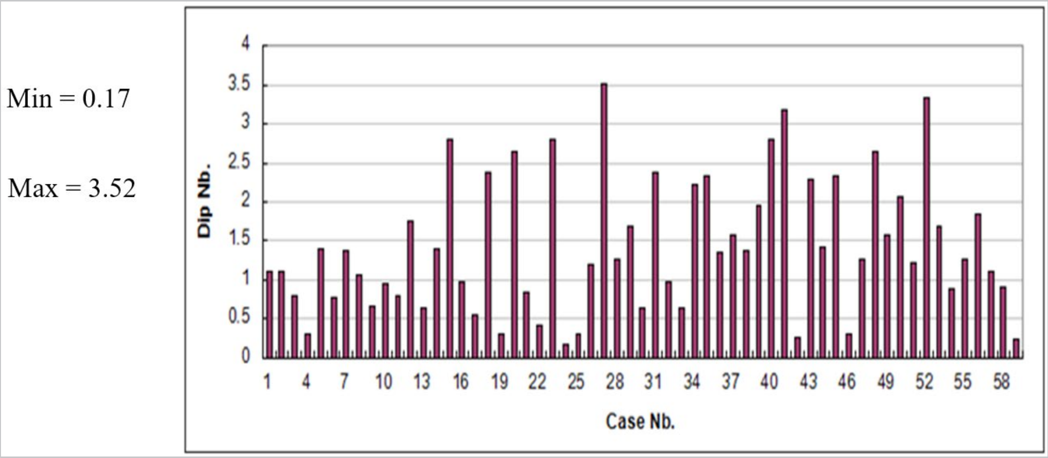

Figure 5 Aspect Ratio distribution obtained for all investigated cases

Mobility Ratio

This is the ratio of the viscous forces of one fluid relative to the other. In theory the closest the ratio is to 1.0 the more stable the recovery of CO_2 will be. High values such as the ones recorded here using our data base of aquifer projects shows values up to 54.0 (for oil reservoirs it can go up to 45.0), indicative of conditions where displacement will be highly unfavorable.

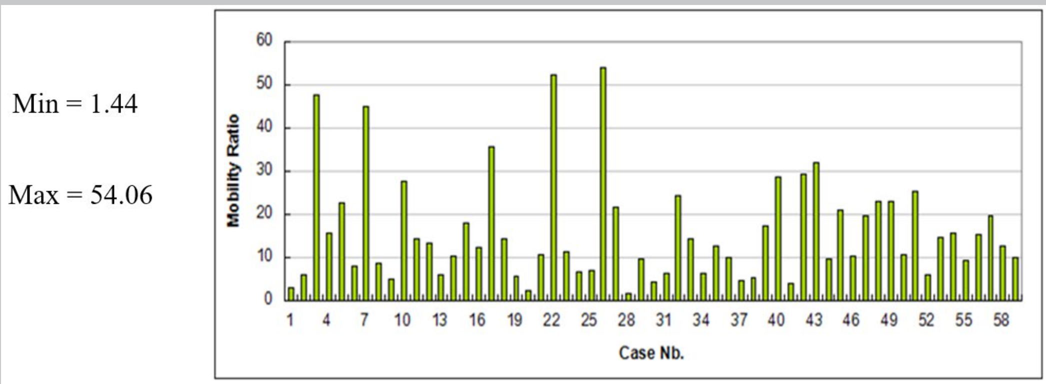

Figure 6 Mobility Ratio distribution obtained for all investigated cases

Buoyancy Number

The buoyancy group requires a ΔP term between the injection pressure and the reservoir pressure. The injection pressure is related to the fracturing pressure which represents a potential risk when storing the CO_2 - the risk not being necessarily the fracture itself, but the potential impact it could create on the well completion (cementation), thus creating a potential leaking path. Thus, two hypothesis are made. The first one assumes that $P_{inj} = 1.1P_{res}$ (option a) while the second one is that $P_{inj} = 1.8P_{res}$ (option b). Results are shown below. Given the fact that the only values changing between the two options are the injection pressure, the variability among values stays the same.

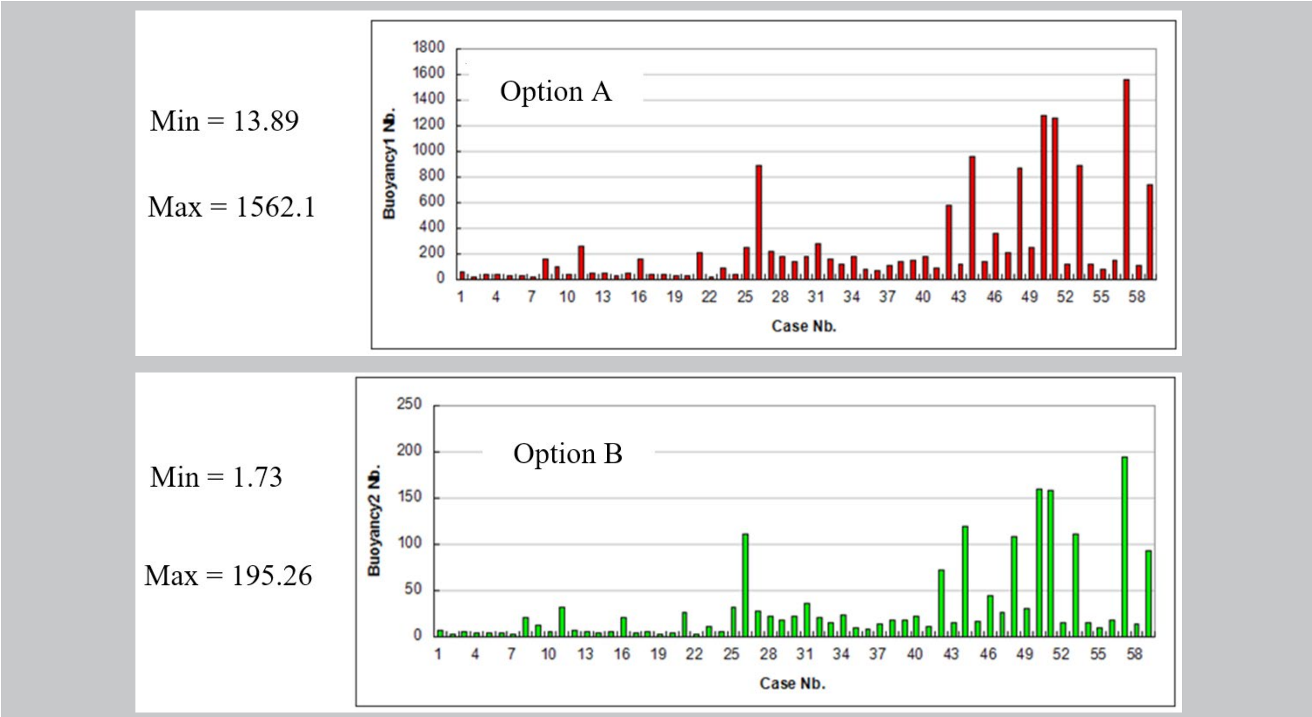

Figure 7 Buoyancy Number distribution obtained for all investigated cases (Option A -Top and B - Bottom)

Capillary Number

The capillary group variability is shown below (Figure 8).

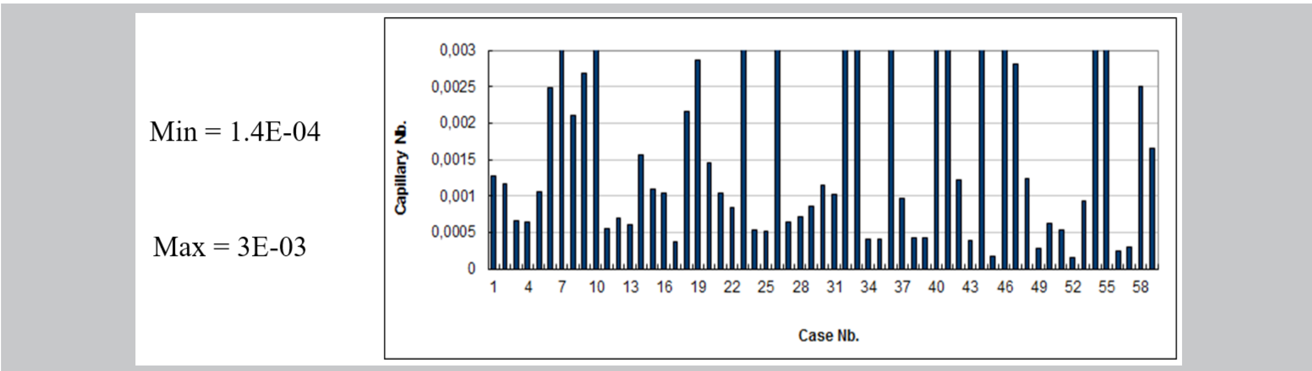

Figure 8 Capillary Number distribution obtained for all investigated cases

Like the other constitutive relationships describing multiphase flow, capillary pressure and relative permeability, the IR characteristic of a rock is considered to be invariant across a wide range of fluid pairs and conditions of temperature, pressure and brine salinity so long as the wetting state of the system remains similar between systems.

It is well known that these properties will vary, however, and if these conditions control the wetting state of the system (Salathiel [11]) or the flow velocity v, viscosity μ and interfacial tension σ combine in a way such that the dimensionless capillary number, $Nc = v\mu/\sigma$, exceeds a critical value for desaturation. For Berea sandstone, for example, this has been observed to be in the range $Nc > 10^{-5}$ - 10^{-4} (Taber [12]). For natural rocks representative of a wide variety of pore structures the range of capillary numbers for desaturation extends to $Nc > 10^{-7}$ - 10^{-4} (Lake et al., [13]). Observations of the wetting state of the CO_2 brine system have raised doubts about whether these general observations extend to CO_2 displacement. Contact angle, conventionally measured in the wetting phase, water, was observed to increase (weakening water wetting) with pressure in work of Broseta et al. [14] Chiquet et al. [15] or Iglauer et al. [16], by opposition to the work of Espinoza et al. [17], Farokhpoor et al. [18], and Wang et al. [19]. Contact angle was observed to increase significantly with brine salinity in work by Espinoza et al. [17], but not in Broseta et al. [14], Chiquet et al. [15]. The work of Farokhpoor et al. [18], Saraji et al. [20] investigated the dependency of contact angle on temperature but a clear trend was not observed. A recent review of the subject (Iglauer et al [21].) highlights the challenging nature of these experiments and summarizes that the wide range of behavior observed can be attributed largely to differences in surface roughness and surface contamination between studies. Thus, it is difficult a-priori to estimate the role this number will play during the simulation of an injection/production process as envisioned here. We expect the residual saturation to play a larger role through the Kr trapping effects and thus indirectly reflecting the importance of capillary trapping.

The S_{gr} term

In addition to all the dimensionless groups chosen as representative of the CO_2 storage, the maximum gas strapping saturations are shown, in order to define a representative value range to be used with all scenarios (see Figure 9).

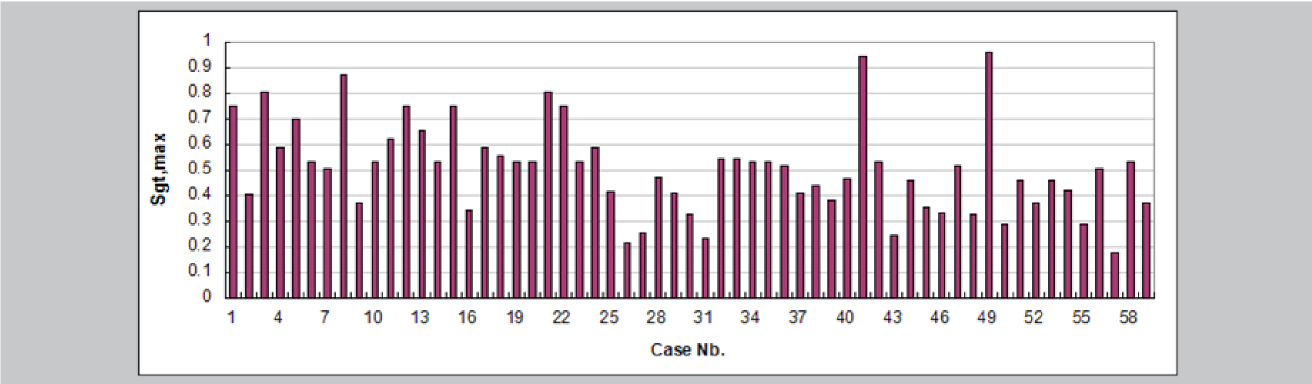

Figure 9 Sgt_{max} distribution obtained for all investigated cases

When studying the distribution of reservoirs within our data-base by Sgt_{max} class-values, we observe very high values of trapped gas saturations for reservoirs of low porosity values. These potential candidates should be excluded from potential storage sites given their porosity values which in term controls the storage capacity.

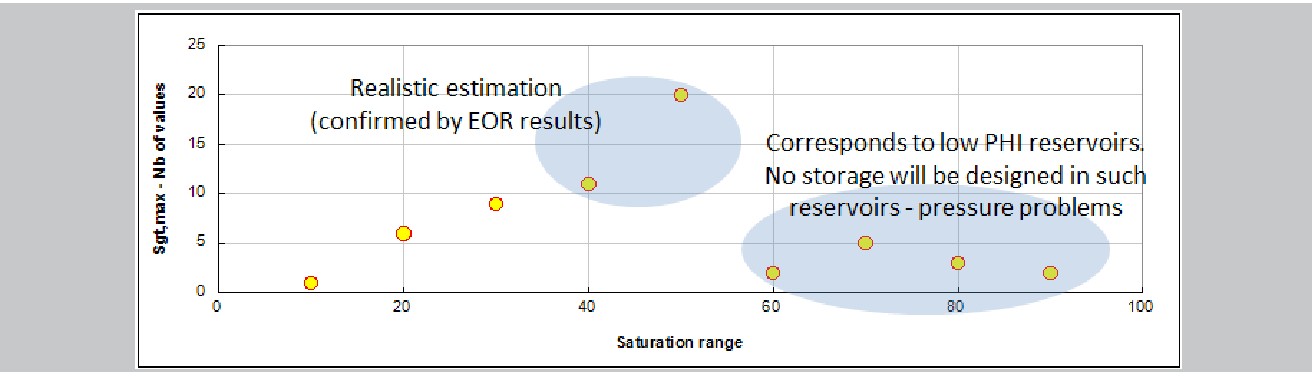

Figure 10 Reservoir distribution classified by trapped gas saturation values

The value most representative are considered as Sgt_{max} = 0.45. The EOR operations have shown from a simple material balance (amount of CO_2 injected – amount of CO_2 produced) that about 40 to 50 % of the CO_2 injected stays trapped. These numerical figures are worth considering over eventual core-floods since they are obtained at a macroscopic scale (realistic scale), as seen in Figure 10.

Scenario 1	-1	1
VDP	0.6	
	Min	Max
Aspect Ratio	1.58	6.32
Dip	0.17	3.52
Mobility Ratio	1.44	54.06
Buoyancy1	13.89	1562.1
Capillary	0.000301	4.68

Scenario 2	-1	1
VDP	0.6	
	Min	Max
Aspect Ratio	1.58	6.32
Dip	0.17	3.52
Mobility Ratio	1.44	54.06
Buoyancy1	1.73	195.26
Capillary	0.000301	4.68

Scenario 3	-1	1
VDP	0.8	
	Min	Max
Aspect Ratio	1.58	6.32
Dip	0.17	3.52
Mobility Ratio	1.44	54.06
Buoyancy1	13.89	1562.1
Capillary	0.000301	4.68

Scenario 4	-1	1
VDP	0.8	
	Min	Max
Aspect Ratio	1.58	6.32
Dip	0.17	3.52
Mobility Ratio	1.44	54.06
Buoyancy1	1.73	195.26
Capillary	0.000301	4.68

Figure 11 All scenarios considering values of dimensionless numbers

From all the dimensionless terms defined above, considering a representative variability we are looking after, and considering the min/max values of all dimensionless groups, we designed 4 main scenarios, shown below in Figure 11.

The Scenarios above consider two VDP values (0.6 and 0.8), along with two buoyancy numbers (corresponding to two injection conditions; one leading to higher overpressures after 4 years than the other – these numbers being derived from a pressure difference formulation between reservoir pressure and injection pressure.

In summary six numbers are considered (including two different buoyancy numbers) but only five are considered for an experiment design for each VDP chosen (in our case 0.6 and 0.8)

2.3 Experimental Design & Optimization

The design of experiments (in our case simulations) is a planned approach aiming to determine cause and effect relationships, applied to any process with measurable inputs and outputs. The aim of designing experiments is to identify the factors which cause changes in the responses, and predicting them in a simple mathematical form. In our case we used a fractional factorial design to reduce the number of simulations to be run in order to obtain a representative response relationship.

Factorial design means that all possible combinations of the levels of the factors are investigated in each complete trial or replication of the experiment (simulation). One of the most widely used case of factorial design is using K factors with two levels. These two levels are denoted as (-1) for the minimum value and (+1) for the maximum one. Therefore, a 2^k factorial design requires 2^k runs to perform the analysis. For a five dimensionless group problem, considering the maximum and minimum values, the total number of simulations to perform are 32. In our case since four main scenarios are considered, 128 simulation in theory cover the entire "experiment", including all interactions. This is shown in Figure 11 in which A = Aspect Ratio, B = Dip Number, C = Mobility Ratio, D = Buoyancy Number (either 1 or 2 depending on the injection scheme chosen) and E = Capillary Number.

	A	B	C	D	E	ABCDE	AB	AC	AD	AE	BC	BD	BE	CD	CE	DE	ABC	ACD	ADE	BCD	BDE	CDE	ABCD	BCDE	Sum
1	1	1	1	1	1	1	1	1	1	1	1	1	1	1	1	1	1	1	1	1	1	1	1	1	18
2	-1	1	1	1	1	-1	-1	-1	-1	-1	1	1	1	1	1	1	-1	-1	-1	1	1	1	-1	1	2
3	1	-1	1	1	1	-1	-1	1	1	1	-1	-1	-1	1	1	1	-1	1	1	-1	-1	1	-1	-1	0
4	1	1	-1	1	1	-1	1	-1	1	1	-1	1	1	-1	-1	1	-1	-1	1	-1	1	-1	-1	-1	-2
5	1	1	1	-1	1	-1	1	1	-1	1	1	-1	1	-1	1	-1	1	-1	-1	-1	-1	-1	-1	-1	-4
6	1	1	1	1	-1	-1	1	1	1	-1	1	1	-1	1	-1	-1	1	1	-1	1	-1	-1	1	-1	2
7	-1	-1	1	1	1	1	1	-1	-1	-1	-1	-1	-1	1	1	1	1	-1	-1	-1	-1	1	1	-1	-4
8	1	-1	-1	1	1	1	-1	-1	1	1	1	-1	-1	-1	-1	1	1	-1	1	1	-1	-1	1	1	0
9	1	1	-1	-1	1	1	1	-1	-1	1	-1	-1	1	1	-1	-1	-1	1	-1	1	-1	1	1	1	0
10	1	1	1	-1	-1	1	1	1	-1	-1	1	-1	-1	-1	-1	1	1	-1	1	-1	1	1	-1	1	0
11	-1	-1	-1	1	1	-1	1	1	-1	-1	1	-1	-1	-1	-1	1	-1	1	-1	1	-1	-1	-1	1	-4
12	1	-1	-1	-1	1	-1	-1	-1	-1	1	1	1	-1	1	-1	-1	1	1	-1	-1	1	1	-1	-1	-2
13	1	1	-1	-1	-1	-1	1	-1	-1	-1	-1	-1	-1	1	1	1	-1	1	1	1	1	-1	1	-1	0
14	-1	-1	-1	-1	1	1	1	1	1	-1	1	1	-1	1	-1	-1	-1	-1	1	-1	1	1	1	-1	2
15	1	-1	-1	-1	-1	1	-1	-1	-1	-1	1	1	1	1	1	1	1	1	1	-1	-1	-1	-1	1	2
16	-1	-1	-1	-1	-1	-1	1	1	1	1	1	1	1	1	1	1	-1	-1	-1	-1	-1	-1	1	1	6
17	1	-1	-1	-1	-1	1	-1	-1	-1	-1	1	1	1	1	1	1	1	1	1	-1	-1	-1	-1	1	2
18	-1	1	-1	-1	-1	1	-1	1	1	1	-1	-1	-1	1	1	1	1	-1	-1	1	1	-1	-1	-1	0
19	-1	-1	1	-1	-1	1	1	-1	1	1	-1	1	1	-1	-1	1	1	1	-1	1	-1	1	-1	-1	2
20	-1	-1	-1	1	-1	1	1	1	-1	1	1	-1	1	-1	1	-1	-1	1	1	1	1	1	-1	-1	4
21	-1	-1	-1	-1	1	1	1	1	1	-1	1	1	-1	1	-1	-1	-1	-1	1	-1	1	1	1	-1	2
22	1	1	-1	-1	-1	-1	1	-1	-1	-1	-1	-1	-1	1	1	1	-1	1	1	1	1	-1	1	-1	0
23	-1	1	1	-1	-1	-1	-1	-1	1	1	1	-1	-1	-1	-1	1	-1	1	-1	-1	1	1	1	1	0
24	-1	-1	1	1	-1	-1	1	-1	-1	1	-1	-1	1	1	-1	-1	1	-1	1	-1	1	-1	1	1	0
25	-1	-1	-1	1	1	-1	1	1	-1	-1	1	-1	-1	-1	-1	1	-1	1	-1	1	-1	-1	-1	1	-4
26	1	1	1	-1	-1	1	1	1	-1	-1	1	-1	-1	-1	-1	1	1	-1	1	-1	1	1	-1	1	0
27	-1	1	1	1	-1	1	-1	-1	-1	1	1	1	-1	1	-1	-1	-1	-1	1	1	-1	-1	-1	-1	-6
28	-1	-1	1	1	1	1	1	-1	-1	-1	-1	-1	-1	1	1	1	1	-1	-1	-1	-1	1	1	-1	-4
29	1	1	1	1	-1	-1	1	1	1	-1	1	1	-1	1	-1	-1	1	1	-1	1	-1	-1	1	-1	2
30	-1	1	1	1	1	-1	-1	-1	-1	-1	1	1	1	1	1	1	-1	-1	-1	1	1	1	-1	1	2
31	1	-1	1	-1	1	1	-1	1	-1	1	-1	1	-1	-1	1	-1	-1	-1	-1	1	1	-1	1	1	-2
32	-1	1	-1	1	-1	-1	-1	1	-1	1	-1	1	-1	-1	1	-1	1	1	1	-1	-1	1	1	1	2
Sum	0	0	0	0	0	0																			

Figure 12 Setting up the experimental design including interactions

Results of the full experimental design are shown in Figure 12, including the interaction terms, considering all parameters (5 parameters) or any combination (2, 3 or 4 parameters). Along with the full experimental design, the sum of all parameters is shown in the last column, helping in reducing the number of simulations.

In order to reduce the number of simulations we can reduce use a "balance" method which adds all coefficients (1 and -1 corresponding the min and max values), including all interaction terms among all 5 dimensionless terms considered, and choose only those cases

		A	B	C	D	E	ABCDE	AB	AC	AD	AE	BC	BD	BE	CD	CE	DE	ABC	ACD	ADE	BCD	BDE	CDE	ABCD	BCDE	Sum
1	3	1	-1	1	1	1	-1	-1	1	1	1	-1	-1	-1	1	1	1	-1	1	1	-1	-1	1	-1	-1	0
2	8	1	-1	-1	1	1	1	-1	-1	1	1	1	-1	-1	-1	-1	1	1	-1	1	1	-1	-1	1	1	0
3	9	1	1	-1	-1	1	1	1	-1	-1	1	-1	-1	1	1	-1	-1	-1	1	-1	1	-1	1	1	1	0
4	10	1	1	1	-1	-1	1	1	1	-1	-1	1	-1	-1	-1	-1	1	1	-1	1	-1	1	1	-1	1	0
5	13	1	1	-1	-1	-1	-1	1	-1	-1	-1	-1	-1	-1	1	1	1	-1	1	1	1	1	-1	1	-1	0
6	18	-1	1	-1	-1	-1	1	-1	1	1	1	-1	-1	-1	1	1	1	1	-1	-1	1	1	-1	-1	-1	0
7	23	-1	1	1	-1	-1	-1	-1	-1	1	1	1	-1	-1	-1	-1	1	-1	1	-1	-1	1	1	1	1	0
8	24	-1	-1	1	1	-1	-1	1	-1	-1	1	-1	-1	1	1	-1	-1	1	-1	1	-1	1	-1	1	1	0

Figure 13 Final experimental design covering all simulations per scenario

for which the sum is null. In such a way we have a balance effect of all parameters among themselves. This leads us a fractional experimental design showing 8 cases. The summary of this simple method is shown in Figure 13.

3 SIMULATIONS SET-UP

In order to perform simulations one needs to define as input a geometry (grid properties), which should be refined within the storage zone. The grid shown below is common to all simulations. Below (Figure 14) we show first an X-Y view followed by a X-Z or Y-Z view of the layering chosen.

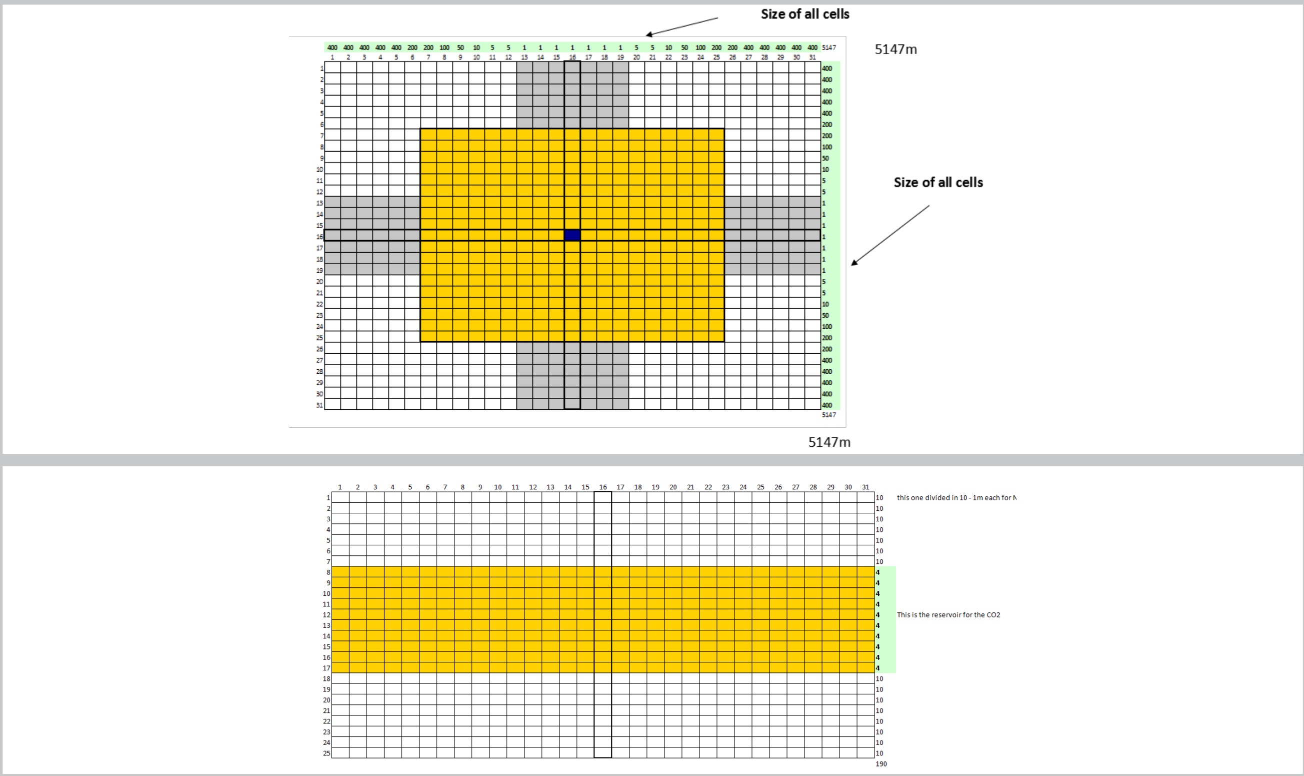

Figure 14 Grid used in X, Y and Z for all simulations: (a) X-Y and (b) X-Z or Y-Z

As seen the injection zone has been refined, in order to minimize gridding effects. The layer below the cap-rock is also refined, in order to catch a possible saturation evolution within the zone where the N_2 is supposed to be placed. The full reservoir zone is closed, considered as an injection storage zone, isolated from the rest of the field.

A petrophysical relationship between K and PHI as well as a spatial distribution of these properties has been developed using the two VDP values chosen (0.6 and 0.8), considered to cover the entire range of possible heterogeneity variation. The average permeability used is 200md and the average porosity is 0.2.

Given the VDP used the minimum permeability is 43md while the maximum is 912md for VDP = 0.6 and the minimum permeability is 13md and 2874md for VDP = 0.8. Results corresponding to a stochastic draw of 8 realizations (corresponding to the 8 cases identified as representative by the experimental design) are shown below when considering an PHI range of 0.15 to 0.24, considered as representative of reservoirs in which CO_2 storage will be considered (Figure 15).

These values were generated at the level of the reservoir (See grid representation above) while for the rest of the simulation domain average values were used.

The actual K vs. PHI distributions are shown below. In principle the VDP concept implies an ordering of layers within the reservoir. In our case this is not the case and all values within layers are drawn randomly within the petrophysical range values indicated. The procedure consisted to first determine a unique K-PHI relationship within a porosity range 0.15 and 0.24 (typical of potential storage aquifers). To these porosity values are associated permeability values obtained from the VDP centered around an average permeability of 200md (again typical of what storage aquifers ought to have). The final step is to draw randomly from the porosity and permeability distribution 8 realizations which establishes 8 distributions. Results are shown in Figure 16.

A dynamic petrophysical data set (Relative permeability Kr curves for water and CO_2). Aside from the saturation and individual curves end-points, exponents of the curves are also needed.

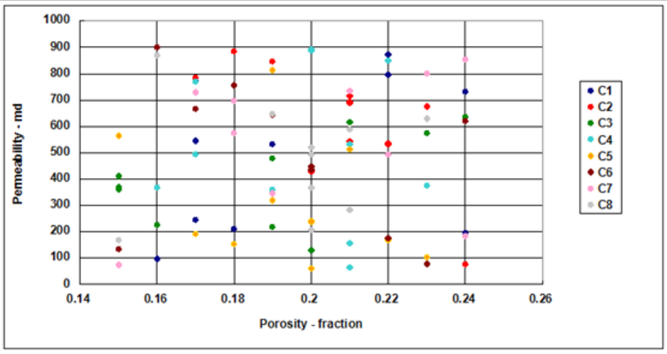

VDP = 0.6 / K = 200 md
Min = 43 / Max = 912
8 realizations using for each realization 10 layers

VDP = 0.8 / K = 200 md
Min = 13 / Max = 2874
8 realizations using for each realization 10 layers

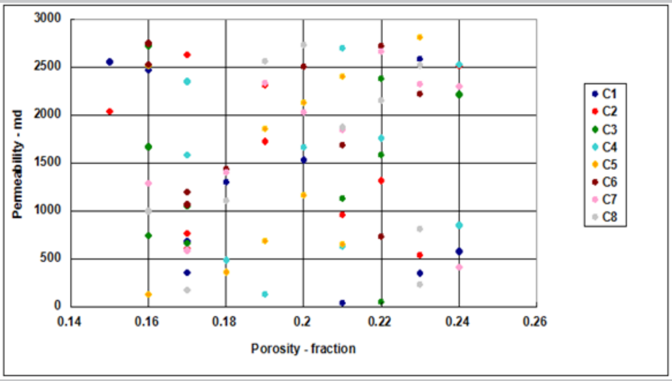

Figure 15 Permeability realizations obtained for a VDP of (a) 0.6 and (b) 0.8

For VDP = 0.6

PHI	K	PHI	K	PHI	K	PHI	K	PHI	K	PHI	K	PHI	K	PHI	K
0.24	732	0.21	691	0.15	362	0.16	367	0.22	169	0.24	620	0.21	734	0.19	646
0.24	196	0.22	534	0.15	411	0.19	361	0.2	62	0.2	448	0.24	184	0.2	521
0.22	796	0.17	784	0.23	574	0.17	769	0.21	513	0.19	645	0.24	854	0.23	630
0.17	245	0.23	676	0.2	129	0.22	850	0.19	320	0.17	667	0.18	574	0.16	868
0.18	210	0.21	715	0.24	635	0.23	374	0.15	565	0.18	756	0.18	698	0.21	283
0.17	774	0.2	428	0.15	369	0.21	64	0.17	191	0.16	901	0.22	493	0.2	495
0.16	98	0.24	76	0.21	616	0.21	531	0.18	154	0.2	437	0.23	801	0.15	169
0.22	874	0.18	884	0.16	226	0.17	495	0.19	814	0.22	175	0.15	74	0.21	589
0.19	532	0.19	847	0.19	479	0.21	156	0.2	239	0.23	78	0.17	729	0.2	368
0.17	545	0.21	543	0.19	219	0.2	890	0.23	104	0.15	134	0.19	347	0.2	206

For VDP = 0.8

PHI	K	PHI	K	PHI	K	PHI	K	PHI	K	PHI	K	PHI	K	PHI	K
0.17	354	0.17	765	0.17	1054	0.21	2697	0.2	1165	0.16	2744	0.17	588	0.17	177
0.23	2584	0.23	536	0.22	2379	0.17	1579	0.19	685	0.22	732	0.22	2657	0.18	1103
0.2	1530	0.19	2312	0.22	49	0.24	2526	0.21	651	0.17	1065	0.18	1398	0.22	2150
0.15	2554	0.22	1317	0.21	1132	0.17	2348	0.23	2806	0.18	1435	0.24	411	0.16	998
0.18	1295	0.19	1725	0.22	1583	0.21	632	0.19	1855	0.17	1197	0.2	2023	0.19	2560
0.21	37	0.15	2036	0.16	2724	0.2	1663	0.16	127	0.22	2719	0.21	1847	0.21	1870
0.24	578	0.17	607	0.24	2213	0.24	852	0.16	2517	0.23	2216	0.23	2323	0.23	811
0.16	2466	0.17	2624	0.16	1668	0.22	1757	0.21	2396	0.2	2503	0.24	2295	0.2	2732
0.17	683	0.21	958	0.16	741	0.19	127	0.2	2124	0.16	2525	0.16	1285	0.23	234
0.23	352	0.24	2514	0.17	664	0.18	487	0.18	363	0.21	1682	0.19	2330	0.23	2519

Figure 16 K-PHI distributions for all simulations

VDP = 0.6

Sim 1	Sim2	Sim3	Sim4	Sim5	Sim6	Sim7	Sim8
0.381106893	0.363649342	0.396969158	0.378157216	0.383057333	0.384259012	0.373317673	0.381504725

VDP = 0.8

Sim 1	Sim2	Sim3	Sim4	Sim5	Sim6	Sim7	Sim8
0.384822981	0.38422881	0.386291817	0.368941326	0.38439346	0.386921737	0.367989639	0.370658978

Figure 17 Trapped CO_2 saturation for all simulations using Holtz correlation

The first step of this data generation is to define the maximum gas saturation trapped (Sgt_{max}). Since for all realizations a different porosity distribution is used, we considered the average porosity of each realization and then using the correlation of Holtz [22] we generated the corresponding trapping gas saturation. Results are show in Figure 17.

The second step is to generate the other end-point of the Kr curves, such as the Swi (for both imbibition and drainage curves since injection and imbibition have to be considered. The other factors concern the M and N Corey shape factors which have to be used. Since no clear data base is currently available in the literature we used values given by Bachu [8], concerning aquifers in Canada. We considered them as representative (Figure 18).

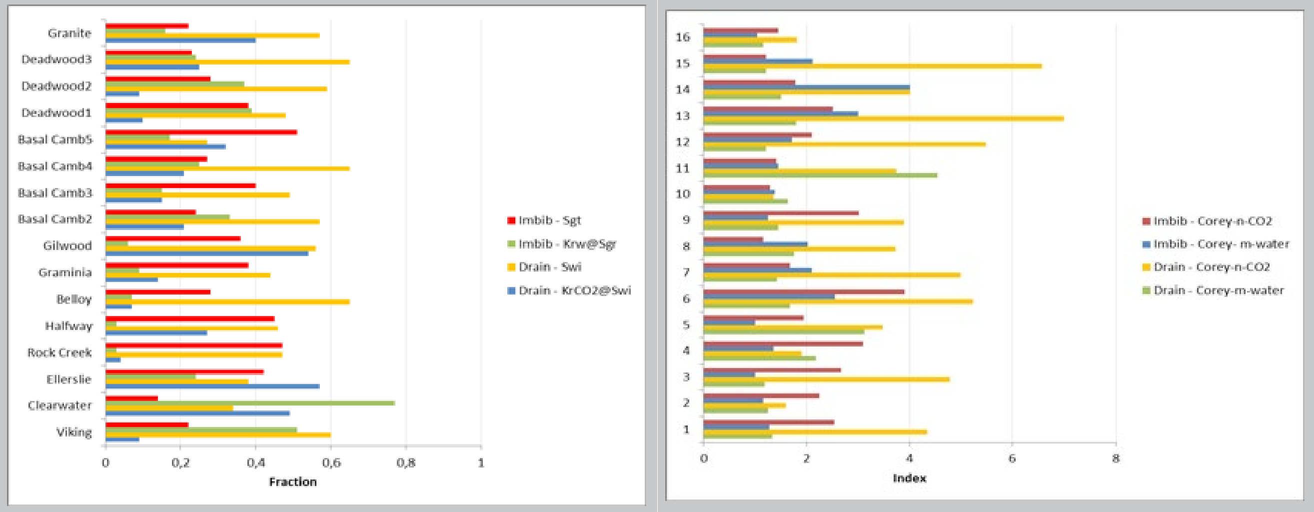

Figure 18 (left) Sgt and Swi including end-points and (right) M and N Corey exponents

When summarizing all results and grouping them according to all cases simulated, for drainage and imbibition, results can be seen below (Figure 19).

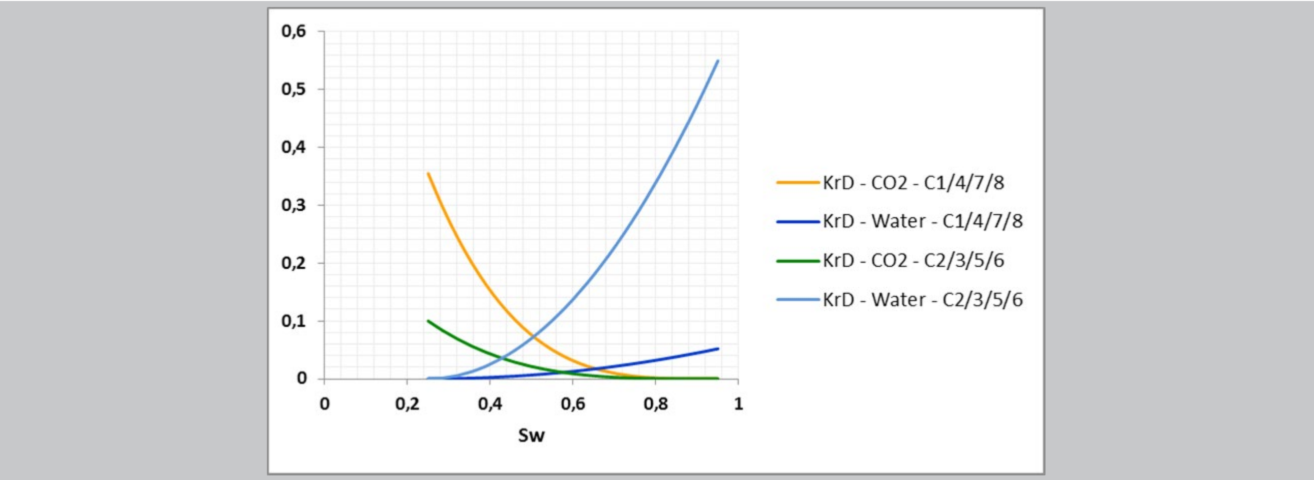

Figure 19 Kr for all cases for drainage

Given all of the above we can summarize all simulation cases along one injection scenarios corresponding to allowable overpressures varying between 1.1 P_{res} and 1.2 P_{res}. These values are considered as typical low overpressures which are seen during the storage of CH_4 which are the only reliable historical record of storage gas overpressure in our possession. This is why we considered these values for the simulations undertaken.

In summary, what has been developed are the formulation of a few dimensionless numbers characterizing the storage, the minimum and maximum values of these from a realistic data-base of reservoirs and a few simulations based on various combinations of maximum and minimum values of these dimensionless numbers. The last step is to find common values of the parameters making up these dimensionless numbers, coherent throughout and meeting the requirements of the min. and max. values. This step was done through an iterative, trial-and error process, leading to a data set of values which fit the best all dimensionless values.

Results are given in the next figures (Figure 20), for both injection schemes, leading to different overpressures expected during the various simulations undertaken.

Summary	Scenario 1 (Plim from 1.1Pres to 1.23Pres)							
	1	2	3	4	5	6	7	8
L	800	800	800	800	800	800	800	800
H	40	40	40	40	40	40	40	40
Kx	200	200	200	200	200	200	200	200
Kz	20	20	20	20	20	1,25	1,25	1,25
alpha	5	5	5	5	5	5	5	5
Krw'	0,052	0,55	0,55	0,052	0,55	0,55	0,052	0,052
KrCO2'	0,355	0,1	0,1	0,355	0,1	0,1	0,355	0,355
Muw	0,8	0,8	0,8	0,8	0,8	0,8	0,8	0,8
MuCO2	0,1	0,1	0,1	0,1	0,1	0,1	0,1	0,1
rhow	1200	1200	1200	1200	1200	1200	1200	1200
rhoCO2	500	500	500	500	500	500	500	500
Pres	14000	14000	14000	14000	14000	14000	14000	14000
Pinj	15400	15400	15400	25200	25200	25200	25200	15400
PHI	0,25	0,25	0,25	0,25	0,25	0,25	0,25	0,25
sigma	40	40	40	40	40	40	40	40

Figure 20 All cases for the injection scenarios $P_{inj} = 1.1/1.2P_{res}$

An initial temperature and pressure: the initial temperature was set at 54°C (ad-hoc) whereas the initial pressure is taken as 140bars, in the middle of the perforated interval.

An injection rate corresponding to the CO_2 placement stage - injection stage: the injection rate chosen is 1M tons CO_2/year. This value is often used as a "standard" in CO_2 injection scenarios. The injection is supposed to occur over the entire reservoir height. The reservoir height considered are supposed to be realistic. Injection is set to occur for 4 years. This is followed by a resting period set to 10 years during which time the saturation is slowly equilibrates as the pressure diffuses throughout the reservoir.

The total number of simulations is 16 corresponding to the injection scenario, for the two heterogeneity factors used. Throughout the full simulation the CO_2 saturation is monitored so as not to contaminate the layer below the cap-rock (refined into 10 thin layers) where the N_2 is supposed to be injected as a protective, cushion measure.

4 RESULTS AND DISCUSSION

Among all results (16 cases simulated) only 5 are recognized as being favorable for an eventual N_2 injection as a preventive leaking measure, since no CO_2 reached the upper layer, neither at the end of the injection period, nor after the resting period of 10 years. The favorable cases were Case 6/7/14/15 and 16. These cases show the following dimensionless numbers (see Figure 21).

Case	Aspect Ratio	Dip	Mobility Ratio	Buoyancy Nb.	Capillary Nb.	Sgr	VDP
6	1.58	3.52	1.45	13.89	0.000301	0.38	0.6
7	1.58	3.52	54.61	13.89	0.000301	0.37	0.6
14	1.58	3.52	1.45	13.89	0.000301	0.38	0.8
15	1.58	3.52	54.61	13.89	0.000301	0.37	0.8
16	1.58	0.17	54.61	1562.1	0.000301	0.38	0.8

Figure 21 Dimensionless numbers for all favorable N_2 cases

The first remark when inspecting these results is the fact that two have a VDP of 0.6 (more homogeneous) while three cases have a VDP of 0.8 (more heterogeneous). Thus, heterogeneity doesn't play an important role in the CO_2 placement with regard to the cap-rock. All favorable cases have the same aspect ratio (low), the same capillary number, almost the same S_{gr} and the same buoyancy number, N_g (low). The role of the vertical movement due to low N_g and low vertical permeability Kz, which enters in the aspect ratio term is evident. Those two numbers drive the CO_2 setting, and therefore the capacity of the CO_2 to eventually contaminate the upper layer where the N_2 would be injected. The role of the mobility ratio is more ambiguous and plays a role when the gravity number is high (Case16). Let's look at the regulating role of the mobility ratio by comparing Cases 6 and 7.

For case 6 (considered as a typical favorable case) the situation at the end of the injection period (4 years) shows a favorable CO_2 saturation, which has not reached the upper layer. When looking at the evolution of the saturation during the resting period, the CO_2 remains within the original region of storage, moving only slightly. The lateral movement, governed by the mobility number, compensates the vertical movement adequately. This is shown in Figure 22.

When looking at Case 7, for which the Mobility number is higher, the general saturation shows a propensity to spread more, given the K-PHI distribution (comparison of the CO_2 saturation zone between Case 6 and 7) which are certainly different yet both having variance values corresponding to a common VDP (0.6), thus statistically equivalent.

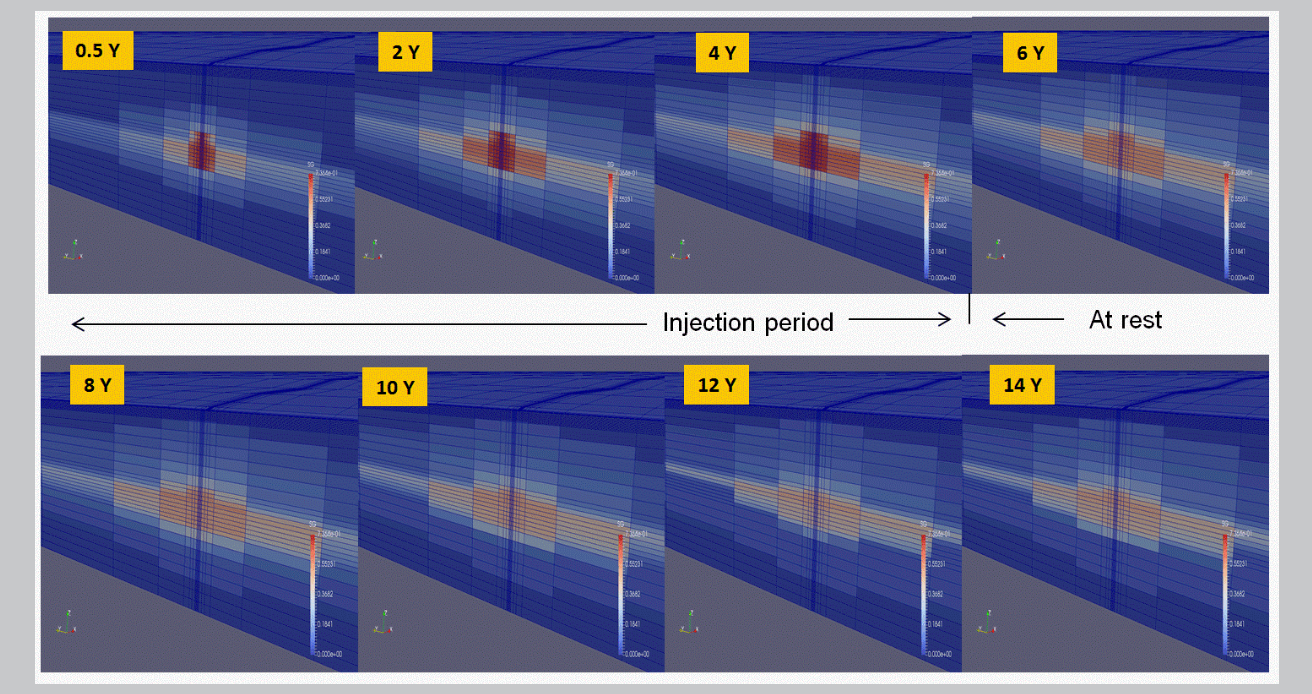

Figure 22 Case 6 - CO_2 saturation evolution

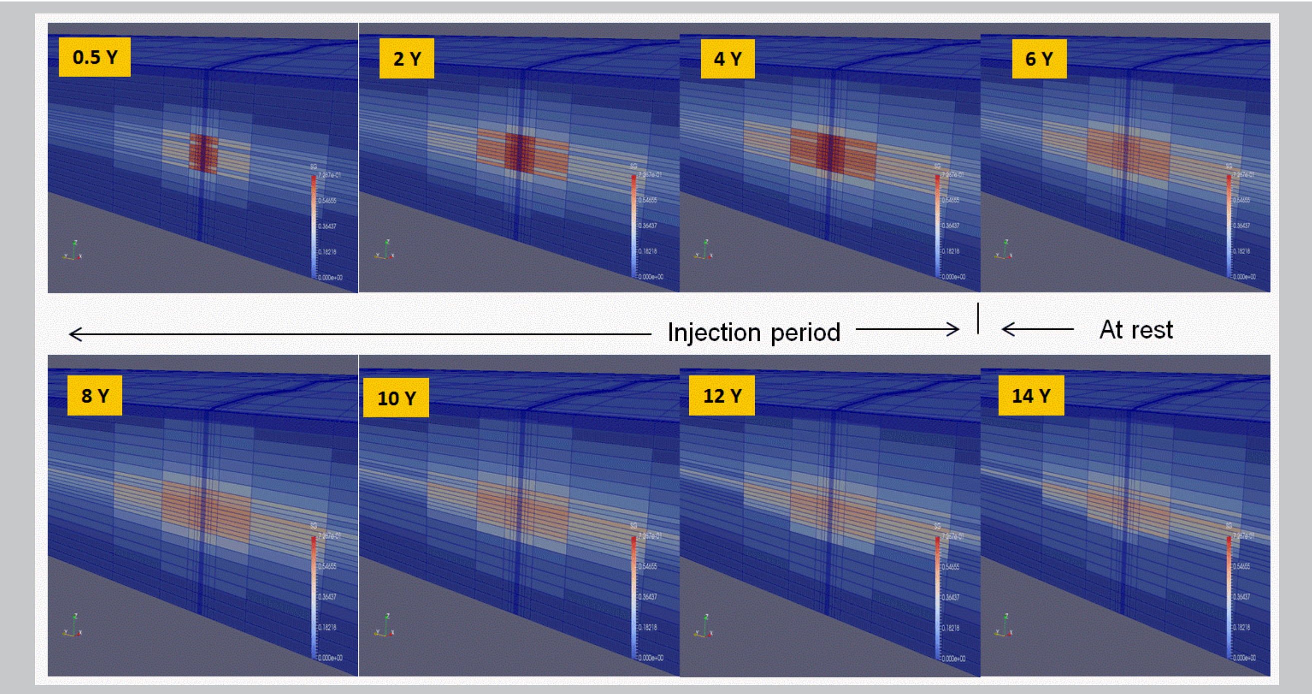

Figure 23 Case 7 saturation evolution

For both cases the maximum CO_2 saturation obtained at the end of 4 years of injection is almost identical, namely 0.7364 and 0.7267. Therefore, comparing the spread between these two cases can become significant. The situation can be seen in Figure 23.

By opposition, if we look at an unfavorable case (Case9) the aspect ratio is 6.32 (max) instead of 1.38 (min) implying that the favorable vertical permeability favors the vertical movement. This can be seen in Figure 24.

The same situation occurs for all the other cases. For example the maximum saturations reached for Cases 14, 15 and 16 are respectively 0.688, 0.672 and 0.677. A different situation occurs for Case 16 which shows, when looking at the dimensionless numbers, a high Gravity number and a high Mobility number. This is the only case for which the saturation distribution is still favorable for the CO_2 saturation (Figure 25).

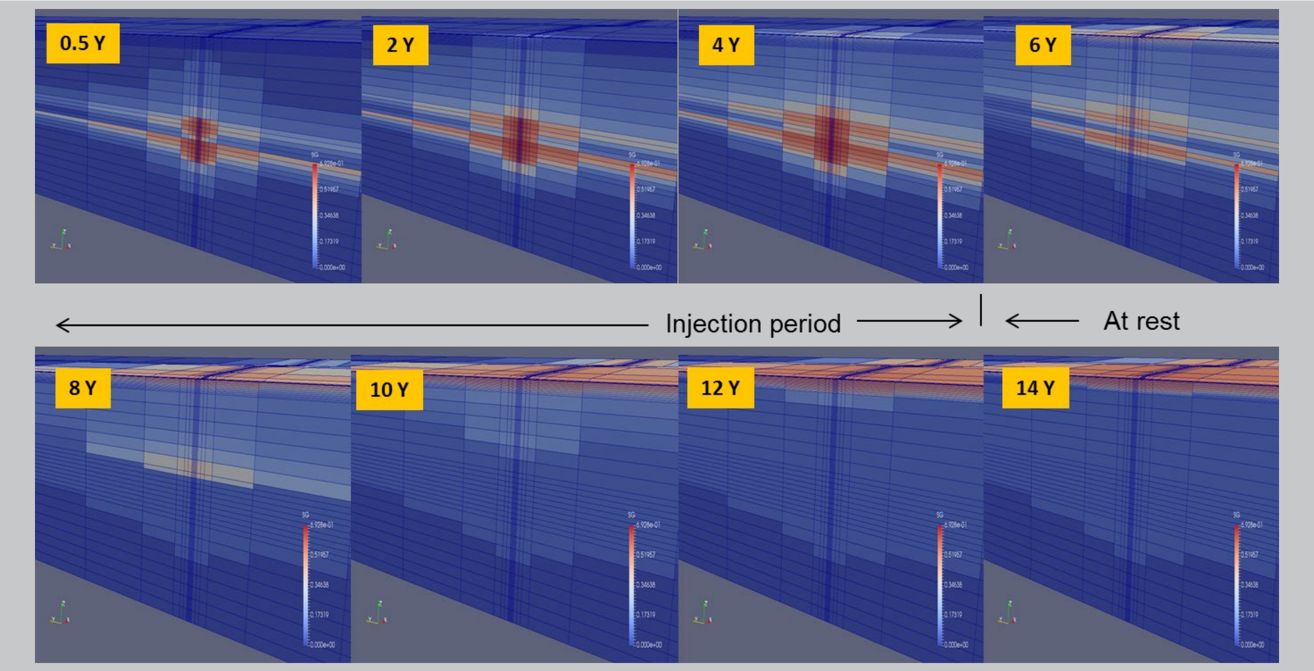

Figure 24 Case 9 - CO_2 saturation evolution (unfavorable)

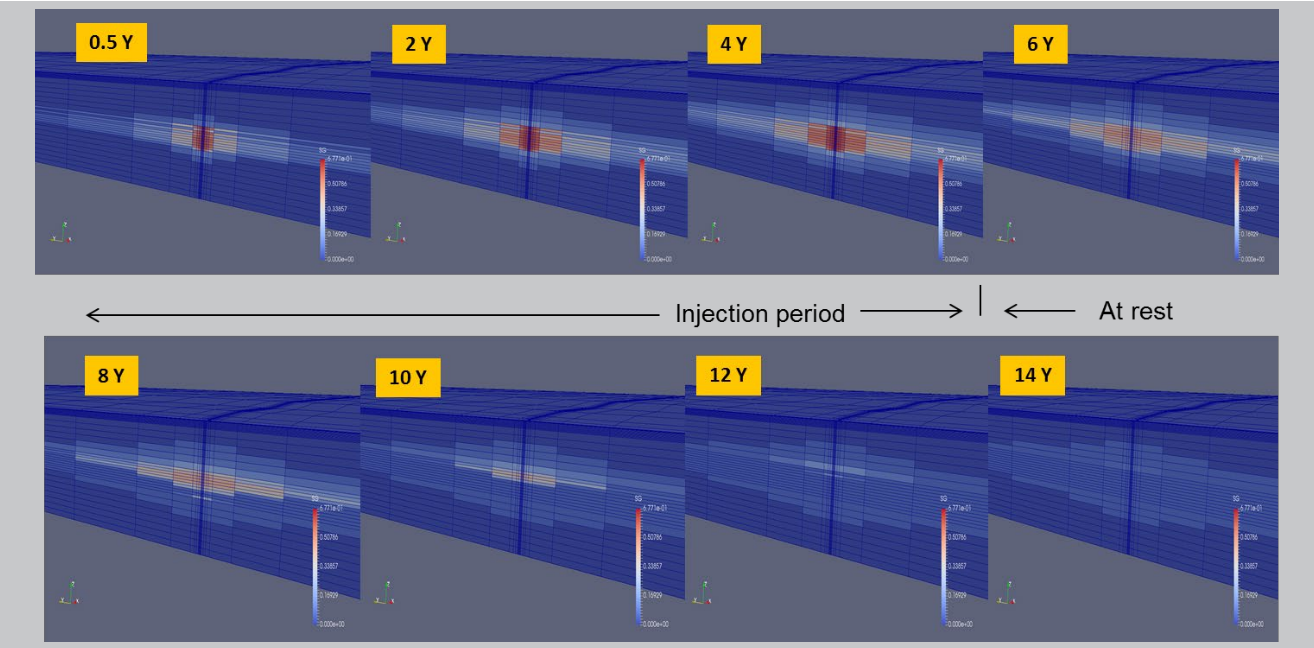

Figure 25 Case 16 - CO_2 saturation evolution

The situation is similar to Case 9, shown above. Yet, the difference is that for this particular case, a low Aspect Ratio is present (1.58) which proves that the Aspect Ratio is very important. In conclusion we can state that a low Aspect Ratio, high Mobility and low Gravity number are important parameters to estimate, prior to the possible injection of N_2.

5 CONCLUSIONS

A realistic set of dimensionless numbers, characterizing the storage of CO_2 has been developed.

Based on these dimensionless numbers, a database of values from different projects currently operating, or to be operated has been developed. Using minimum and maximum values of these numbers, a full experimental design, followed by a simplification, led to a minimal set of simulations studying the movement of the CO_2 in relation to a potential storage layer containing N_2.

N_2 is conceptually imagined as a potential shield agent against CO_2 leaking, while potentially increasing the storage capacity of a site.

The study of the CO_2 saturation distribution throughout the reservoir in regard to a potential layer containing the shielding N_2, has identified three main factors keeping the CO_2 in place. These are the Aspect Ratio, the Buoyancy number (Gravity Number) and the

Mobility Ratio. While the first two govern the vertical movement of the CO_2, the last one controls the lateral extension of the CO_2. For these numbers, a low aspect ratio, combined with low Gravity number and a High Mobility number insures that CO_2 stays within the reservoir throughout the injection period.

It is clear that the cases studied correspond to a specific injection rate, distance between the reservoir and the N_2 storage layer, and a specific period time of injection. A more refined study is needed to determine the relationship between injection rate, distance between reservoir and N_2 and time of injection. Within the range of values chosen, out conclusions are valid for the design of a N_2 placement prior to the injection of CO_2.

References

[1] Shook, M. Lake, L.M. and Li, D.: "Scaling Immiscible Flow Through Permeable Media by Inspectional Analysis" In Situ, 16(4), 311-349, 1992.
[2] Rivas, O., Embid, S. and Bolivar, F.: "Ranking Reservoirs for CO_2 Flooding Processes", SPE 23641 presented at the 1992 SPE Latin American Petroleum Engineering Conference, Caracas, March 8-11.
[3] Diaz, D., Bassiouni, Z., Kimbrell, W., and Wolcott, J. : "Screening Criteria for Application of Carbon Dioxide Miscible Displacement in Waterflooded Reservoirs Containing Light Oil", SPE 35431 presented at the 1996 SPE Improved Oil recovery Symposium, Tulsa, April 21-24.
[4] Hirasaki, G., Steward W.C., Elkins, L.E., Wilhite, P.G. "Reply to Discussion of the National Petroleum Council Study on EOR", SPE 20007, Journal of Petroleum Technology, Nov. 1989.
[5] Jensen JL, Lake LW, Corbett P, Goggin D. Statistics for petroleum engineers and geoscientists: Handbook of petroleum exploration and production 2 (HPEP). Elsevier, 2000.
[6] Dykstra, H, and R,L, Parsons: "The Prediction of Oil Recovery by Water Flood," Secondary Recovery of Oil in the United States, Principles and Practice, 2nd ed, Amer, Pet. Inst, (1950), 160-174.
[7] Bachu, S., Nordbotten, J.M., Celia, M.A. "Evaluation of the spread of acid gas plumes injected in deep saline aquifers in western Canada as an analogue for CO_2 injection in continental sedimentary basins" GHGT-7 Paper ID Nb.12 revised.
[8] Bachu, S., 2013. Drainage and imbibition CO_2/brine relative permeability curves at in situ conditions for sandstone formations in Western Canada. Energy Proc. – 11th Int. Conf. Greenhouse. Gas Control Technol. 37, 4428–4436.
[9] Flett, M., Taggart, I., Lewis J., and Gurdon, R. "Subsurface sensitivity Study of Geologic CO_2 Sequestration in Saline Formations" 2nd Annual Conf. on Carbon Sequestration, Alexandria, VA May 5-8, 2003.
[10] Hosa, A., Esentia, M., Stewart, J., Haszeldine S., "Benchmarking worldwide CO_2 saline aquifer injections" Scottish Center for Carbon Capture and Storage, March 2010.
[11] Salathiel, R., 1973. Oil recovery by surface film drainage in mixed-wettability rocks. J. Petrol. Technol. 25, 1216–1224.
[12] Taber, J., 1969. Dynamic and static forces required to remove a discontinuous oil phase from porous media containing both oil and water. SPE J. 9, 3–12.
[13] Lake, L., Johns, R., Rossen, B., Pope, G., 2014. Fundamentals of Enhanced Oil Recovery. Society of Petroleum Engineers, TX, USA.
[14] Broseta, D., Tonnet, N., Shah, V., 2012. Are rocks still water-wet in the presence of dense CO_2 or H_2S? Geofluids 12, 280–294.
[15] Chiquet, P., Broseta, D., Thibeau, S., 2007. Wettability alteration of caprock minerals by carbon dioxide. Geofluids 7, 112–122.
[16] Iglauer, S., Pentland, C., Bush, A., 2014a. CO_2 wettability of seal and reservoir rocks and the implications for carbon geosequestration. Water Resour. Res.
[17] Espinoza, D.N., Santamarina, J.C., 2010. Water-CO_2-mineral systems: Interfacial tension, contact angle, and diffusion–implications to CO_2 geological storage. Water Resour. Res. 46, W07537.
[18] Farokhpoor, R., Bjorkvik, B., Lindeberg, E., Torsaeter, O., 2013. Wettability behaviour of CO_2 at storage conditions. Int. J. Greenh. Gas Control 12, 18–25.
[19] Wang, F., 1988. Effect of wettability alteration on water/oil relative permeability, dispersion, and flowable saturation in porous media. SPE Reserv. Eng. 3, 617–628.
[20] Saraji, S., Goual, L., Piri, M., Plancher, H., 2013. Wettability of supercritical carbon dioxide/water/quartz systems: Simultaneous measurement of contact angle and interfacial tension at reservoir conditions. Langmuir 29, 6856–6866.
[21] Iglauer, S., Salamah, A., Sarmadivaleh, M., Liu, K., Phan, C., 2014b. Contamination of silica surfaces: Impact on water-CO_2-quartz and glass contact angle measurements. Int. J. Greenh. Gas Control 22, 325–328.
[22] Holtz, M.H., "Residual Gas Saturation to Aquifer Influx: A Calculation Method for 3-D Computer Reservoir Model Construction", SPE 75502, SPE Gas Technology Symposium held in Calgary, Alberta, Canada, 30 April–2 May 2002.
[23] Hadlow, R.E. "Update of Industry Experience with CO_2 Injection" SPE 24928, 67th ATCE held in Washington, DC, October 4-7, 1992.
[24]Barroux C. Method for maintaining a gas volume in an underground geological reservoir by nitrogen injection - EP 2565371 A1.
[25] Fischer S., Szizybalski A., Zimmer M., Kujawa C., Plessen B., Liebscher A., Moeller F. "N2-CO_2 co-injection field test at the Ketzin pilot CO_2 storage site" Energy Procedia 63 (2014) 2848 – 2854.
[26] Wei N., Li X., Wang Y., Wang Y., Kong W. "Numerical study on the field-scale aquifer storage of CO_2 containing N2" Energy Procedia 37 (2013) 3952 – 3959.

APPENDIX A

Case 1

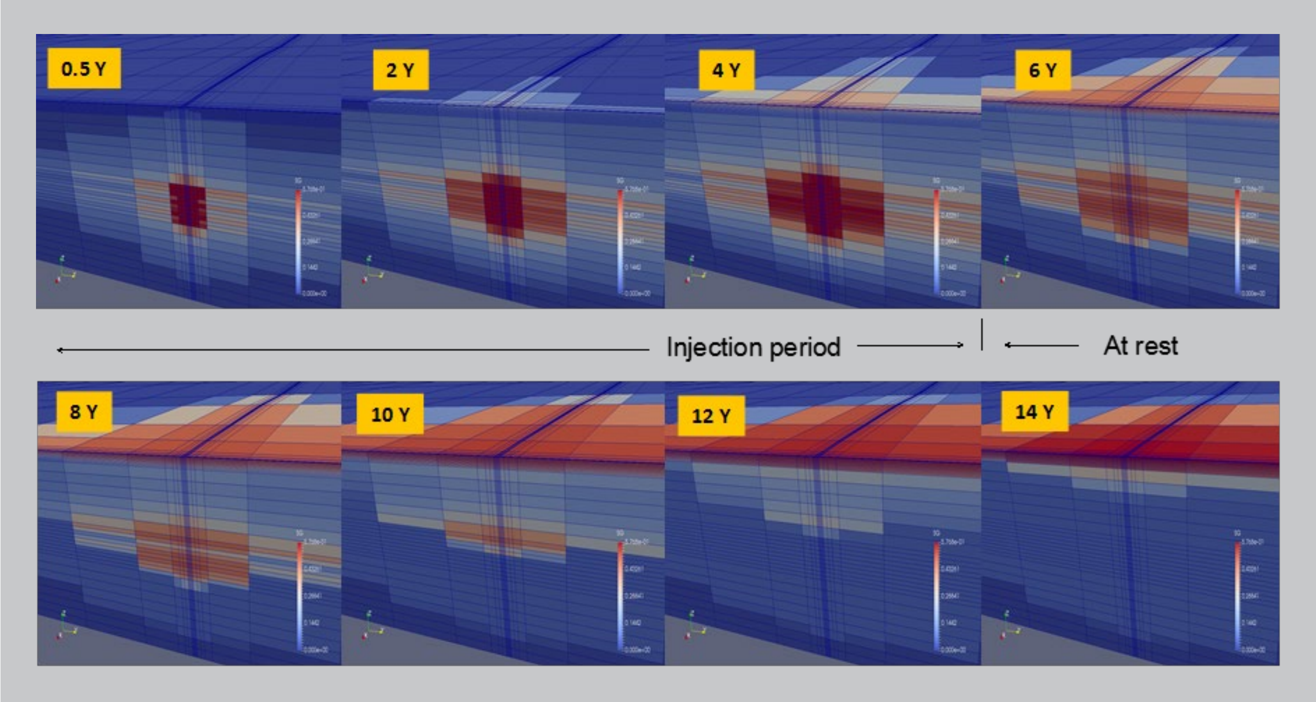

Case 2

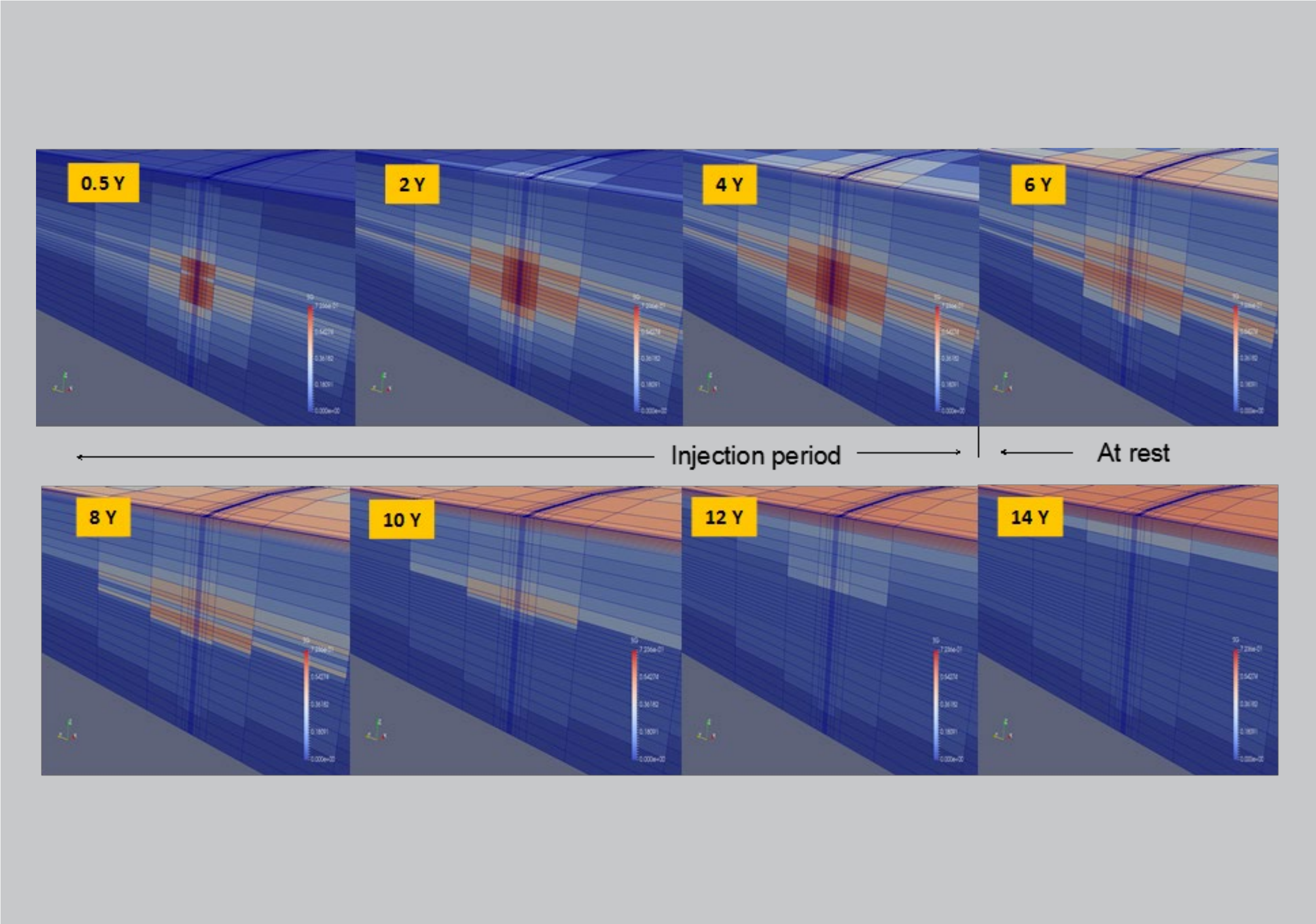

Case 3

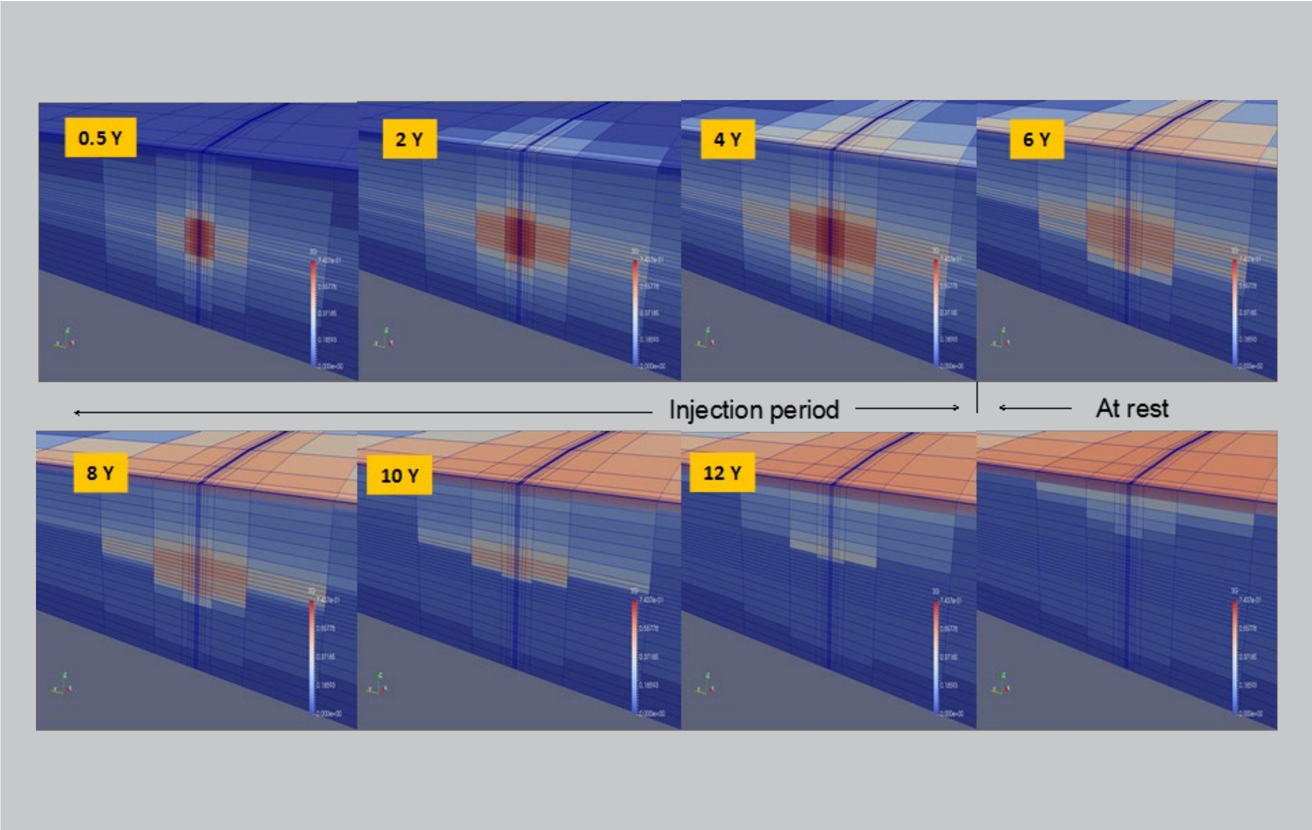
0.5 Y
2 Y
4 Y
6 Y
Injection period
At rest
8 Y
10 Y
12 Y

Case 4

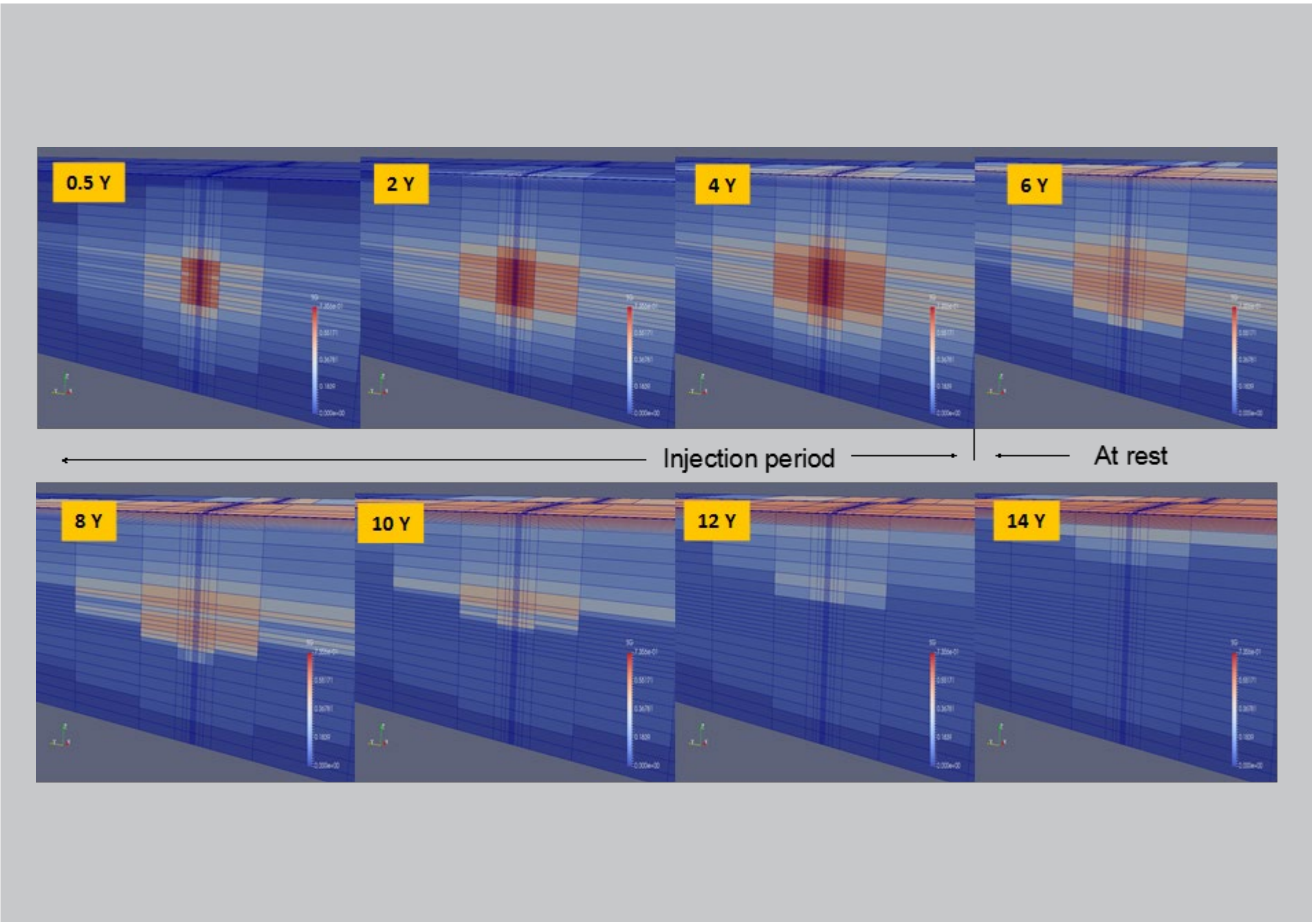
0.5 Y
2 Y
4 Y
6 Y
Injection period
At rest
8 Y
10 Y
12 Y
14 Y

Case 5

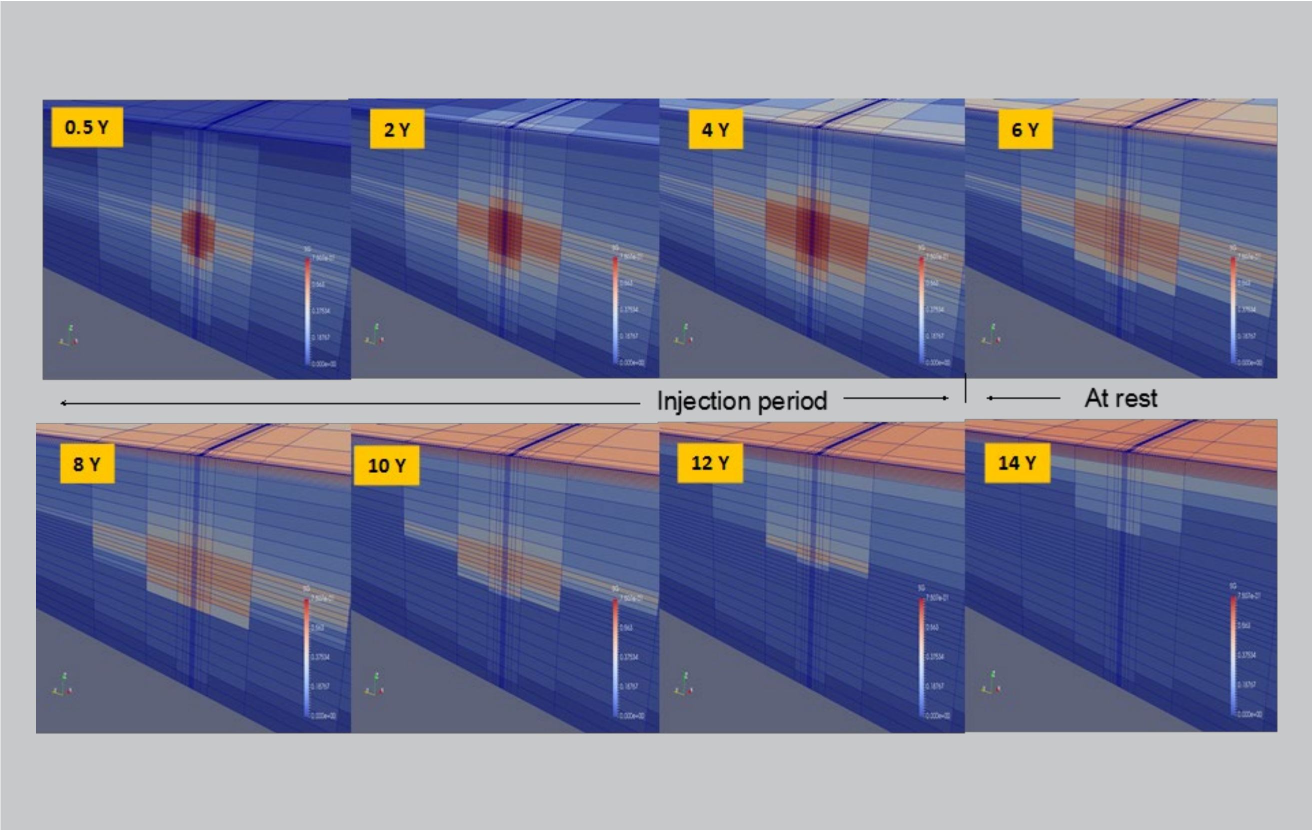
0.5 Y
2 Y
4 Y
6 Y
Injection period
At rest
8 Y
10 Y
12 Y
14 Y

Case 6

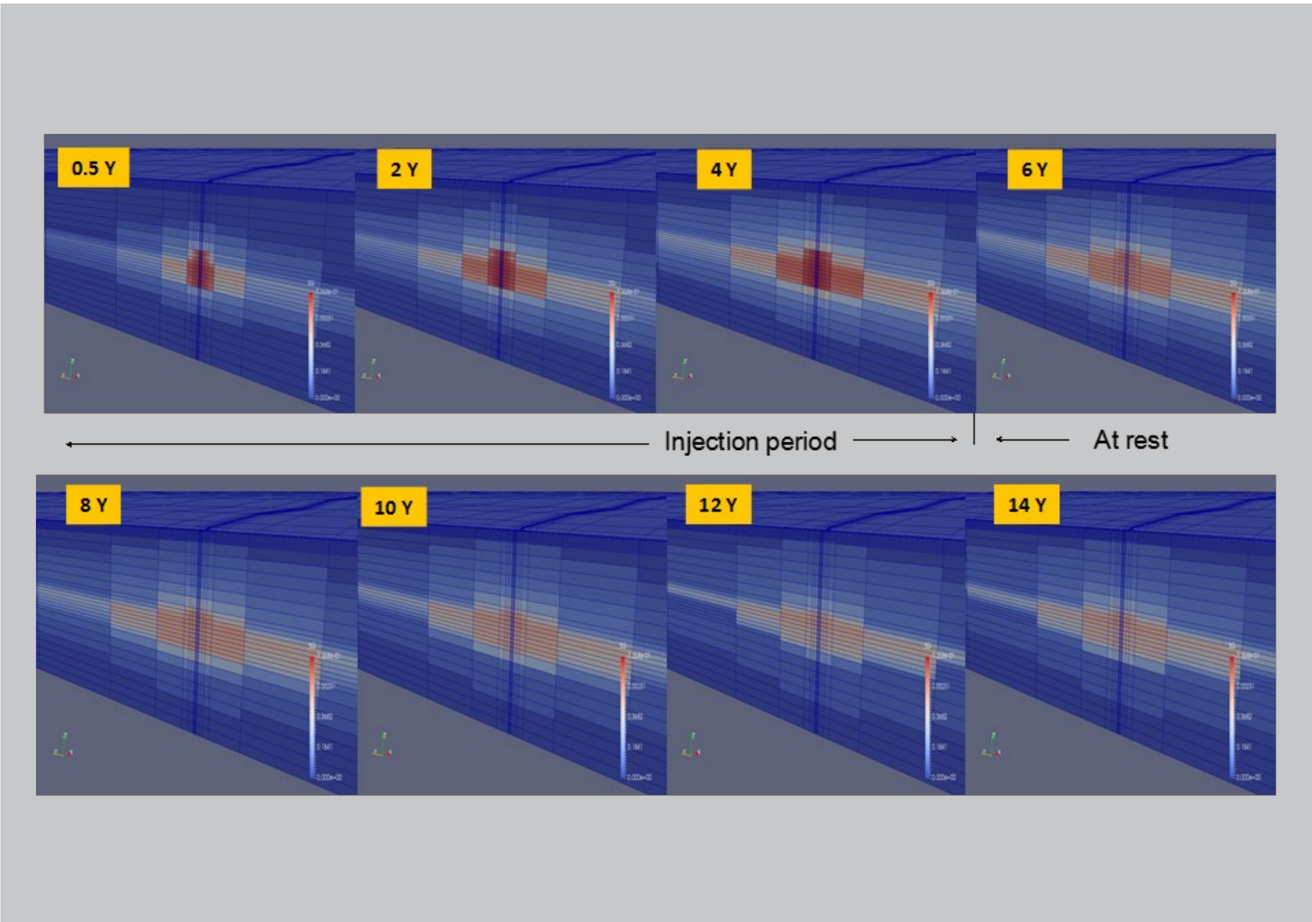
0.5 Y
2 Y
4 Y
6 Y
Injection period
At rest
8 Y
10 Y
12 Y
14 Y

Case 7

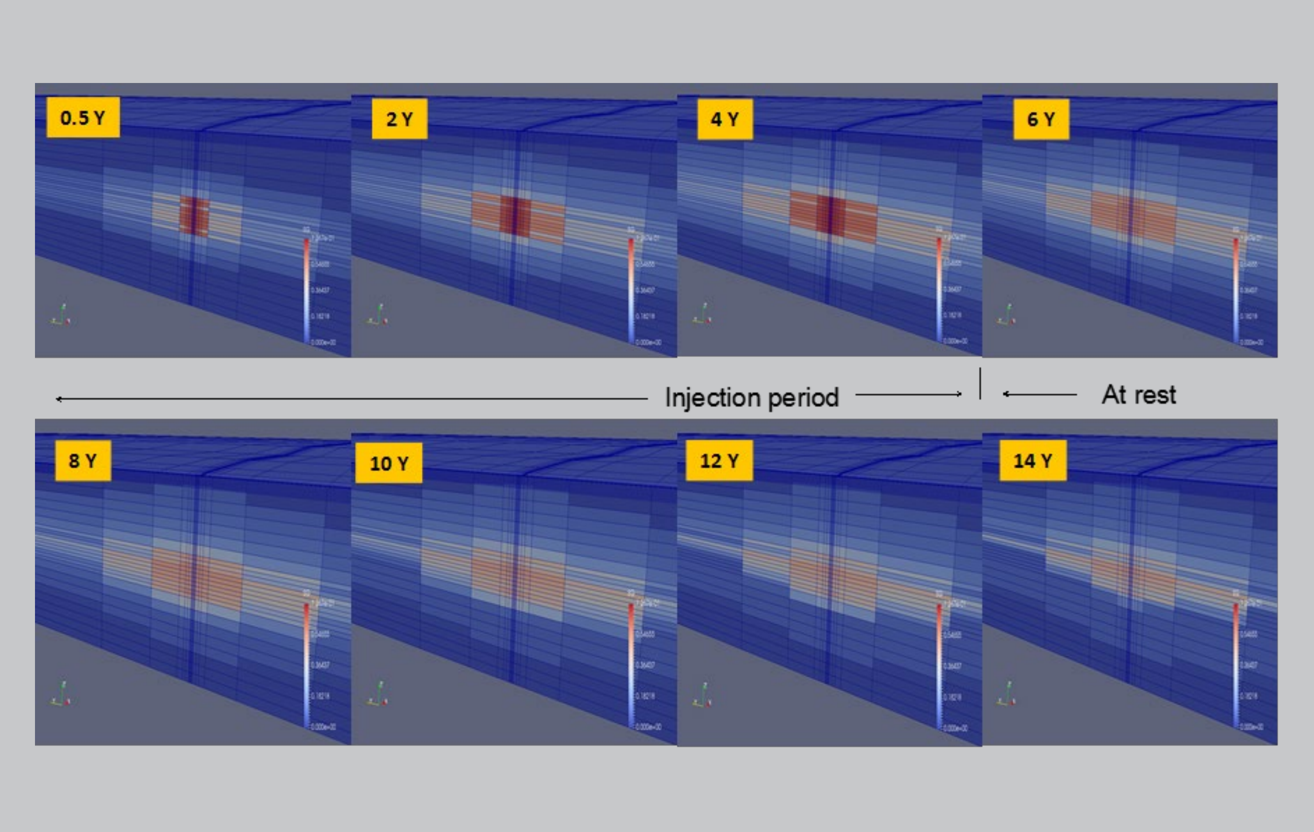
0.5 Y
2 Y
4 Y
6 Y
Injection period
At rest
8 Y
10 Y
12 Y
14 Y

Case 8

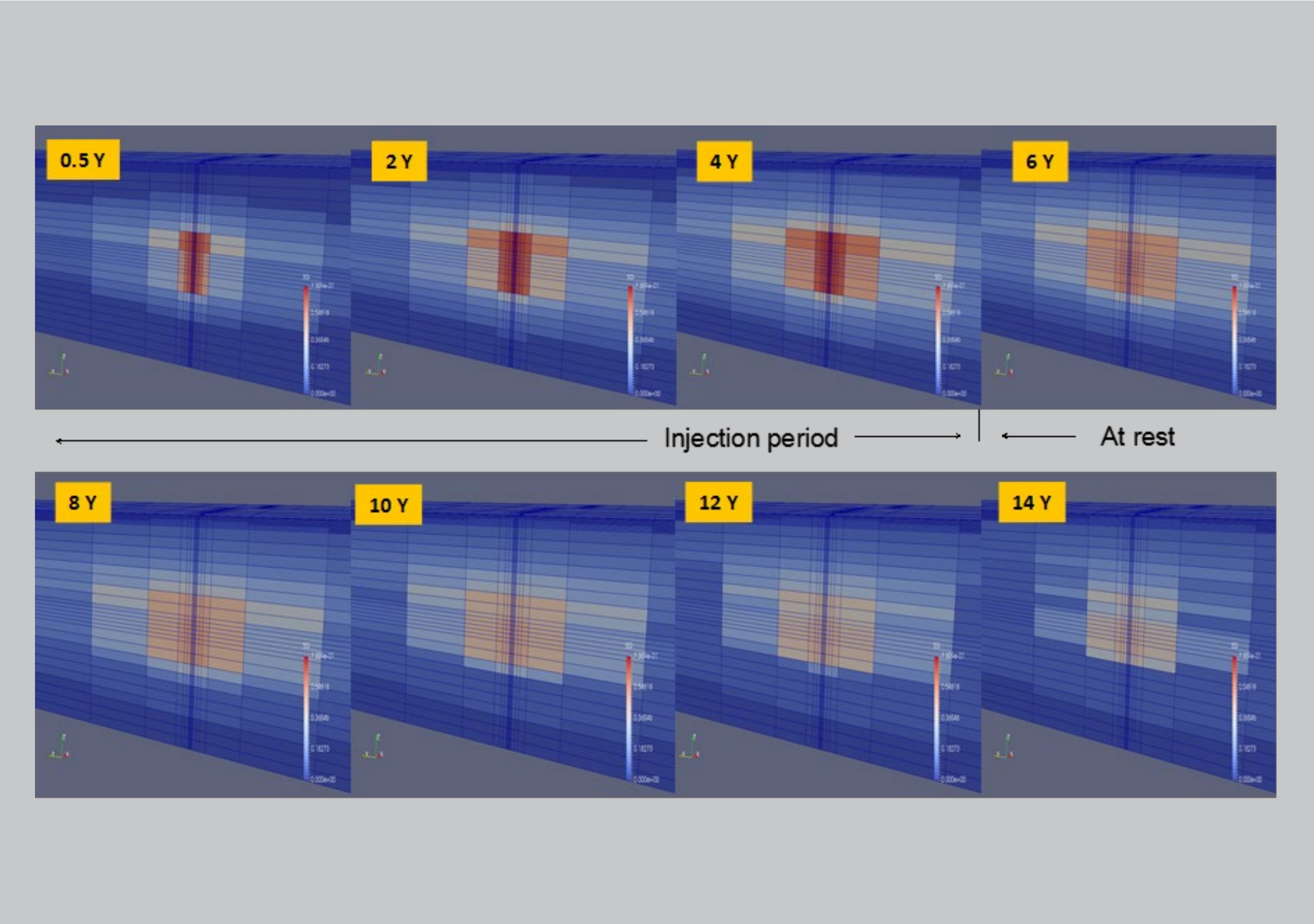
0.5 Y
2 Y
4 Y
6 Y
Injection period
At rest
8 Y
10 Y
12 Y
14 Y

Case 9

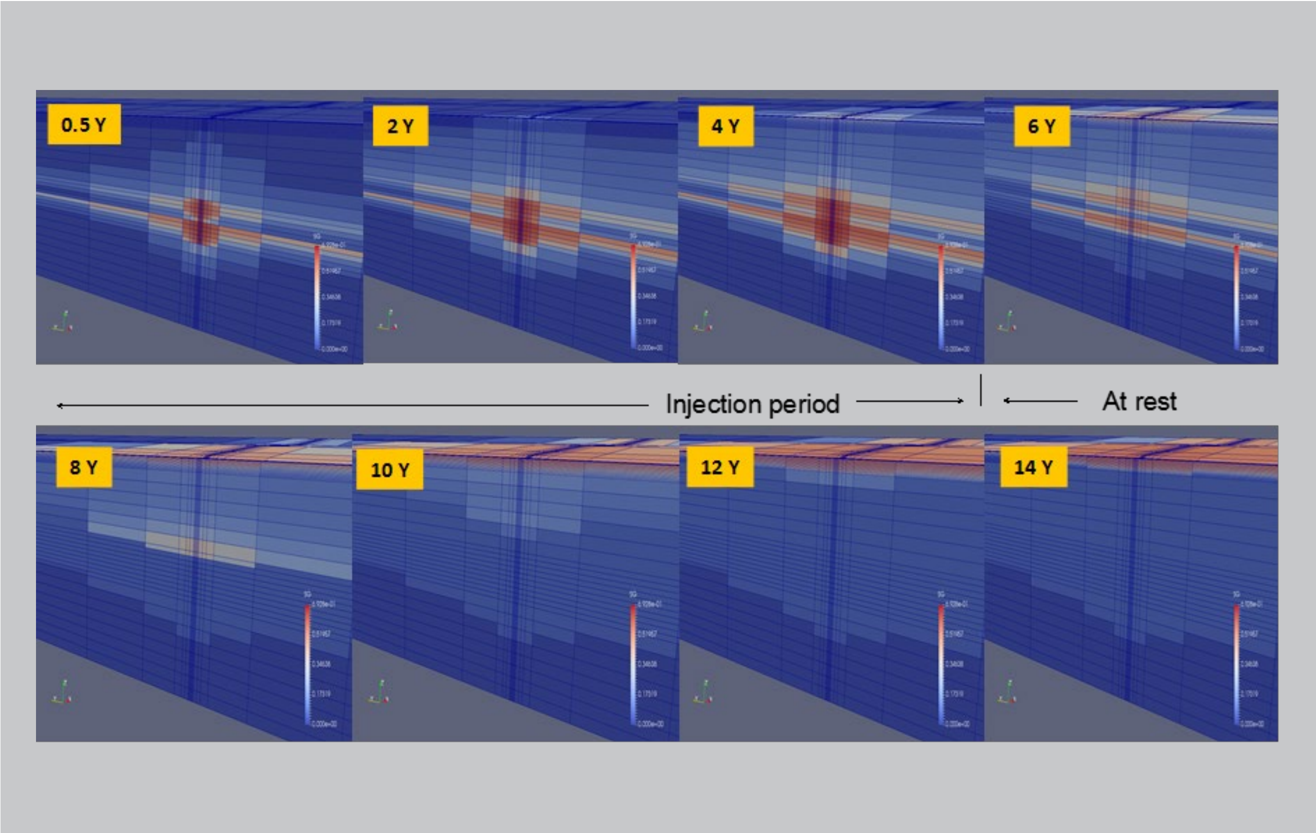

Case 10

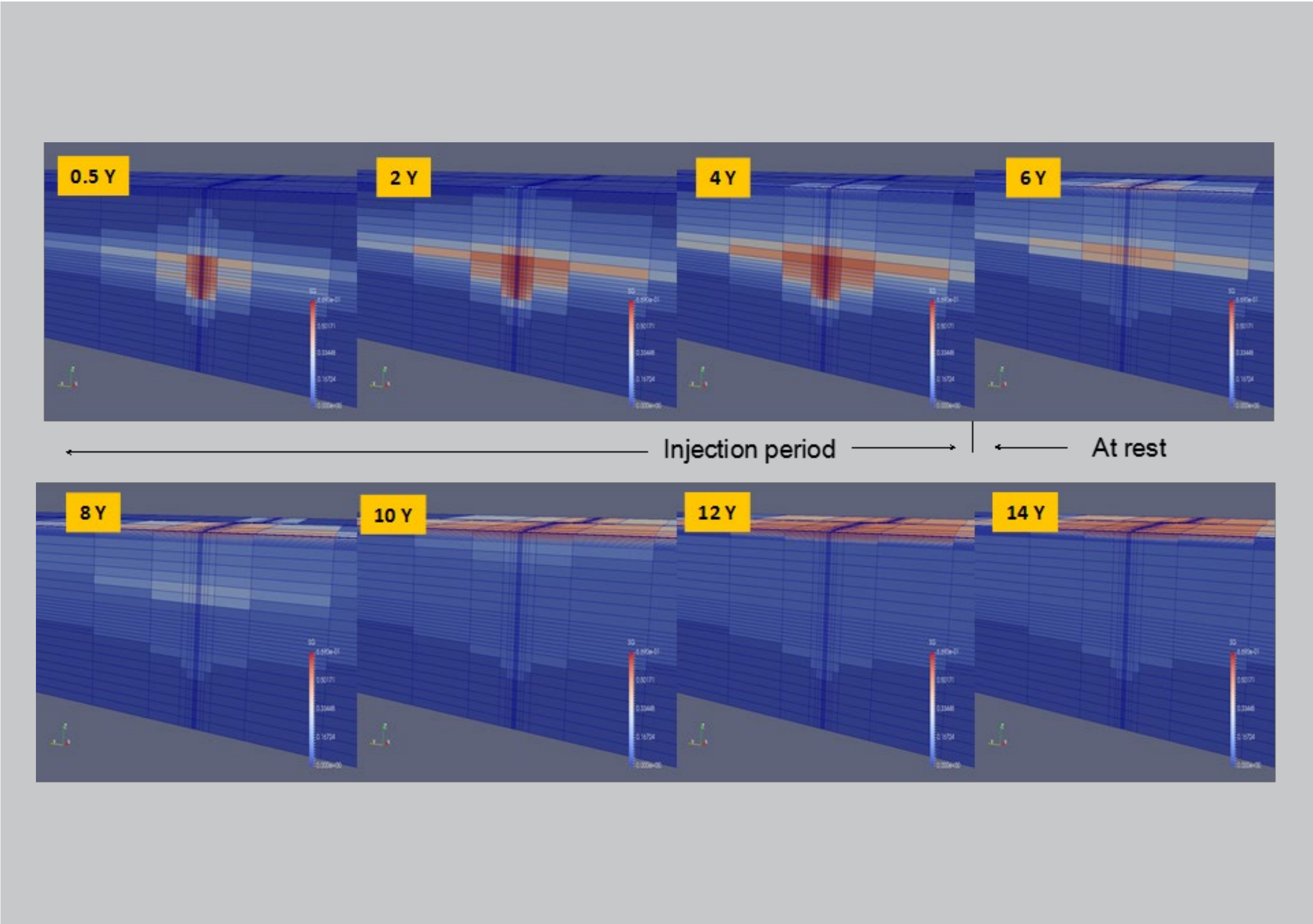

Case 11

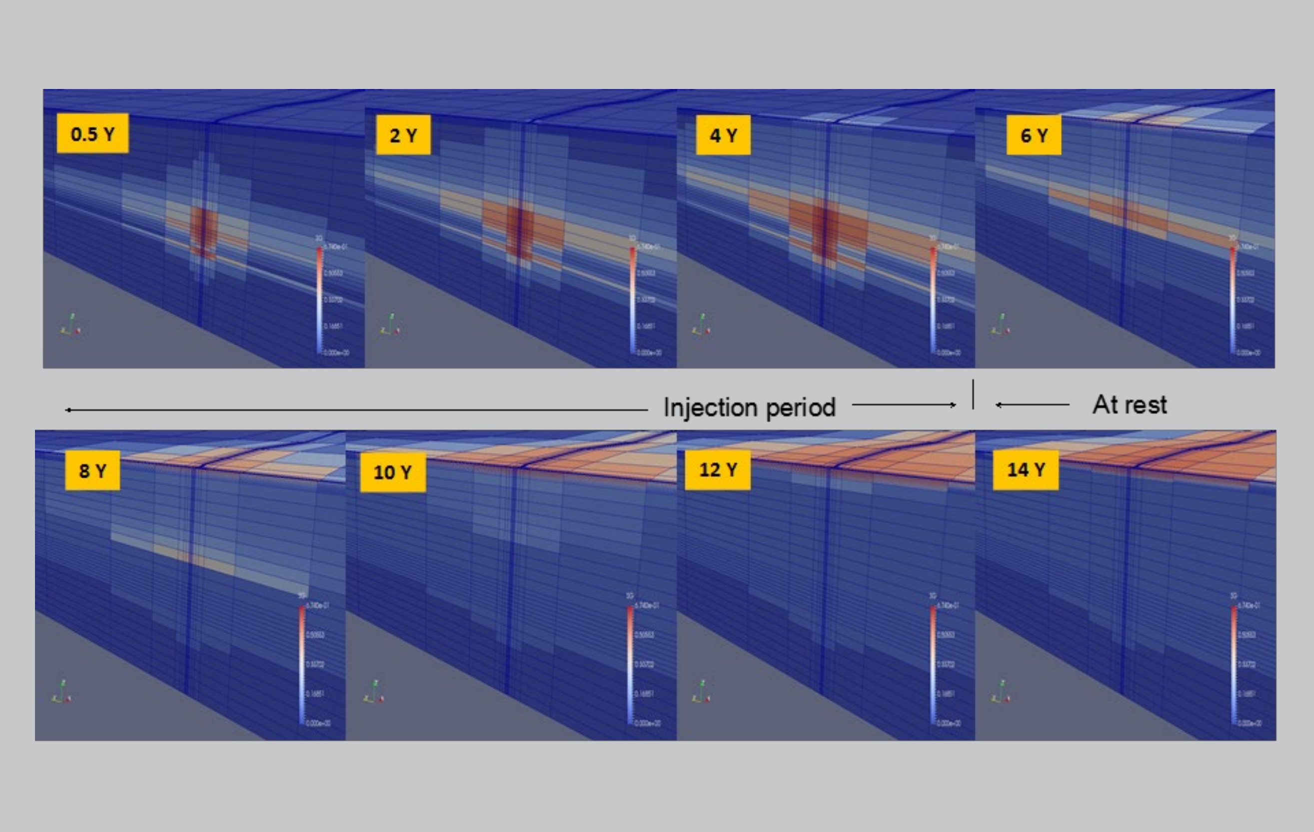

Case 12

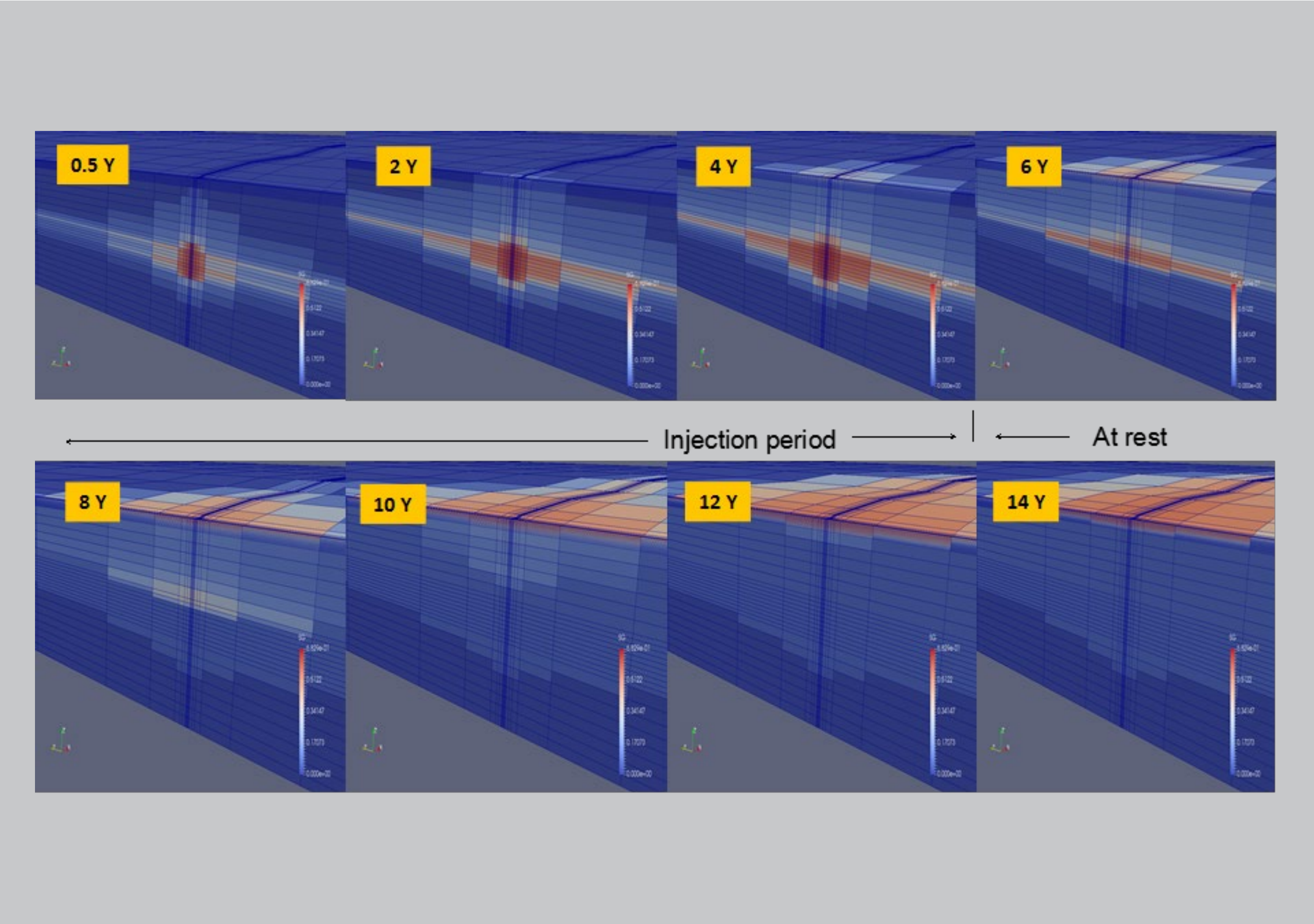

Case 13

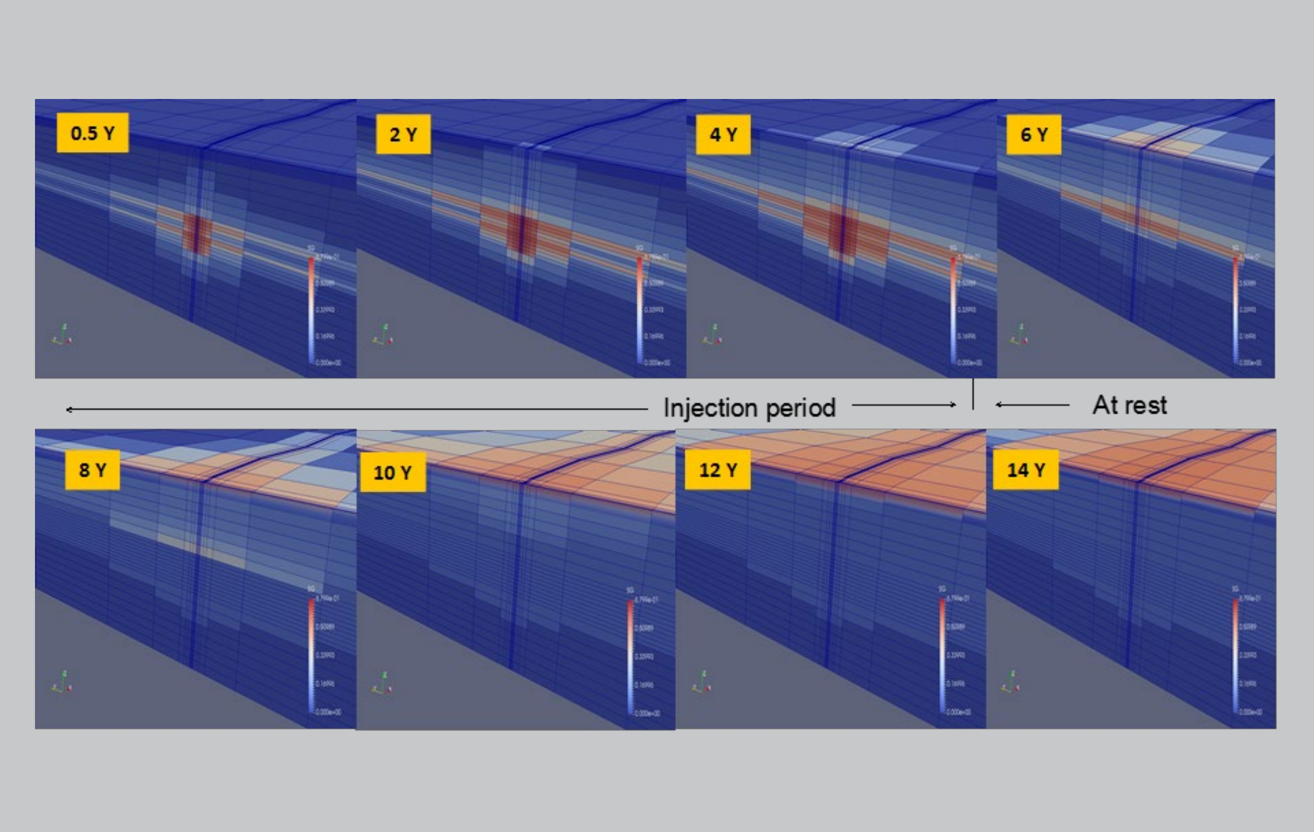

Case 14

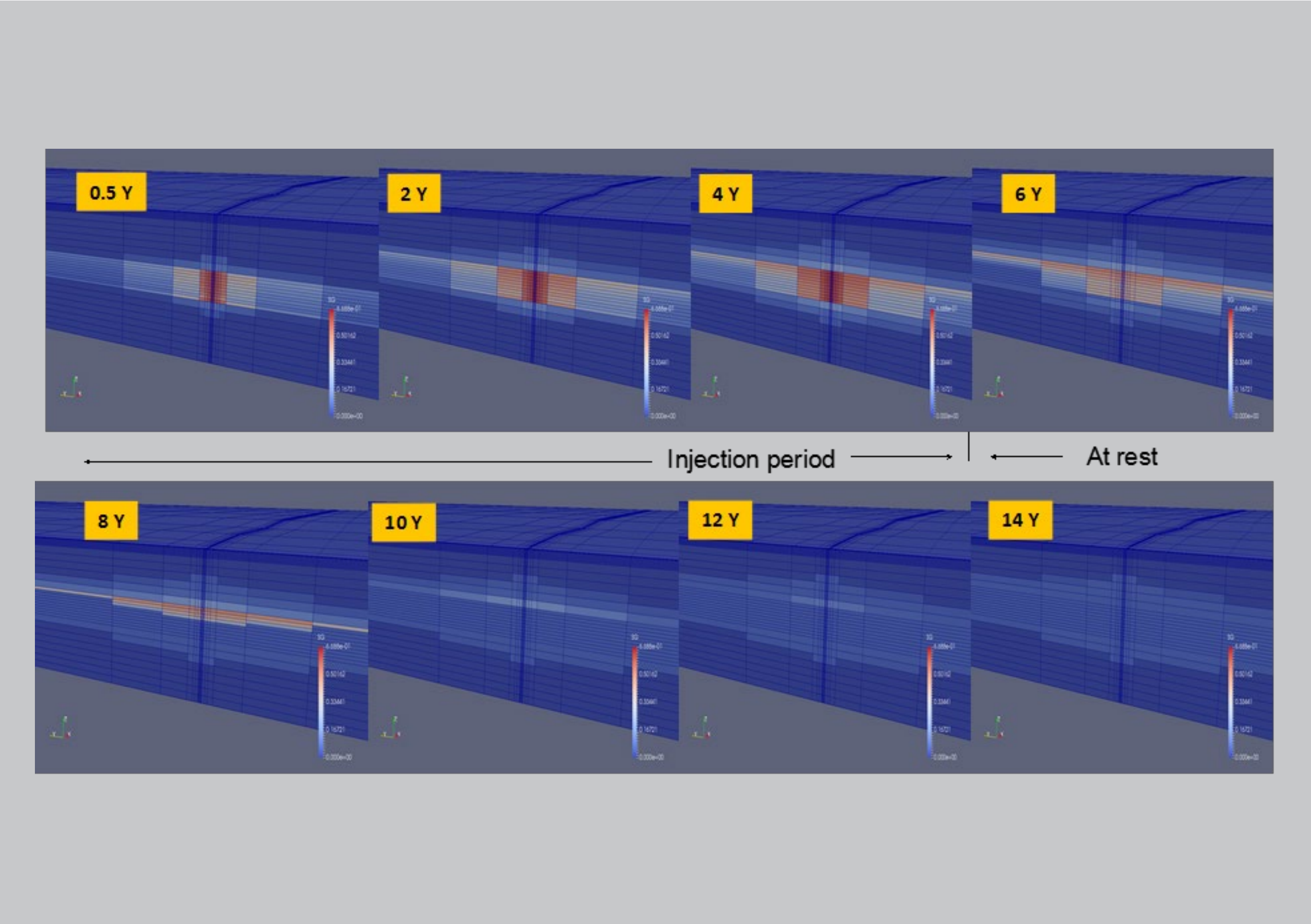

Case 15

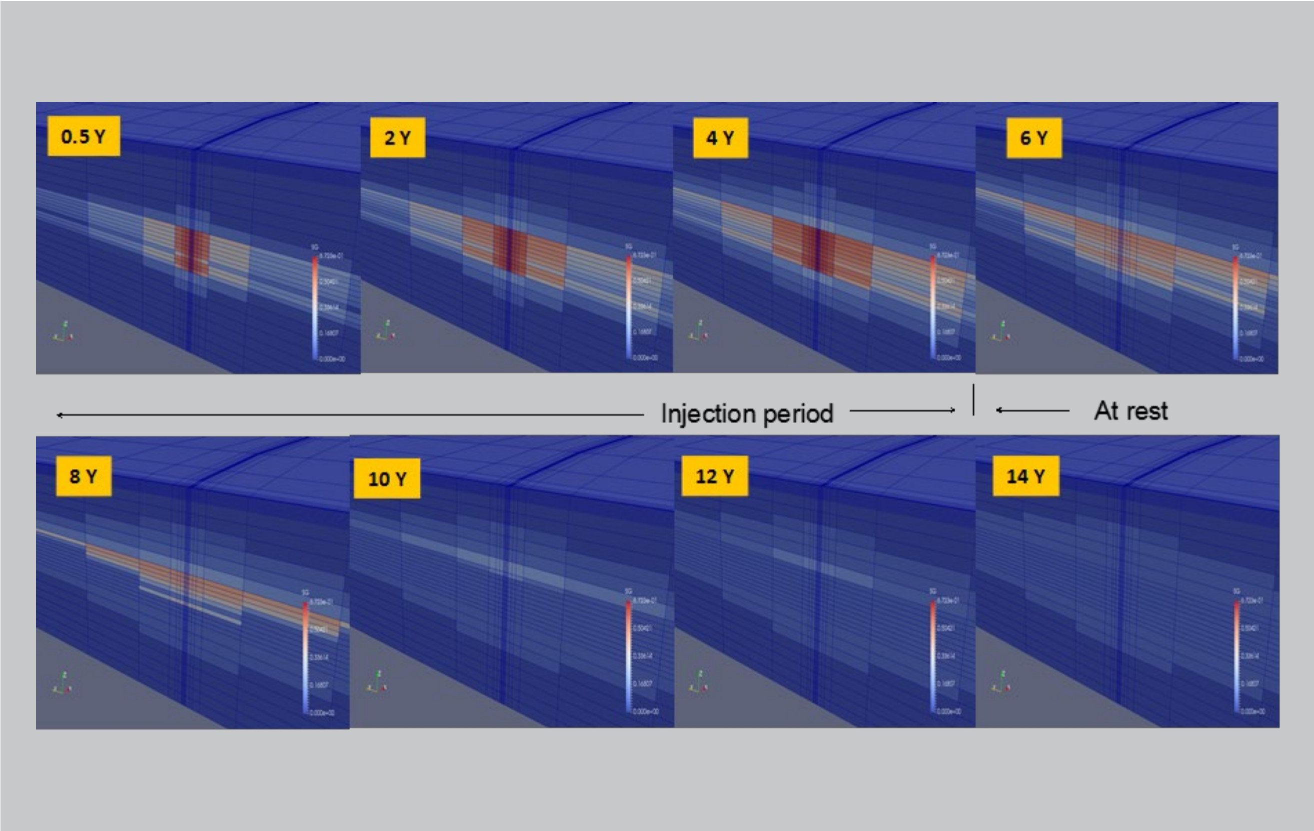

Case 16

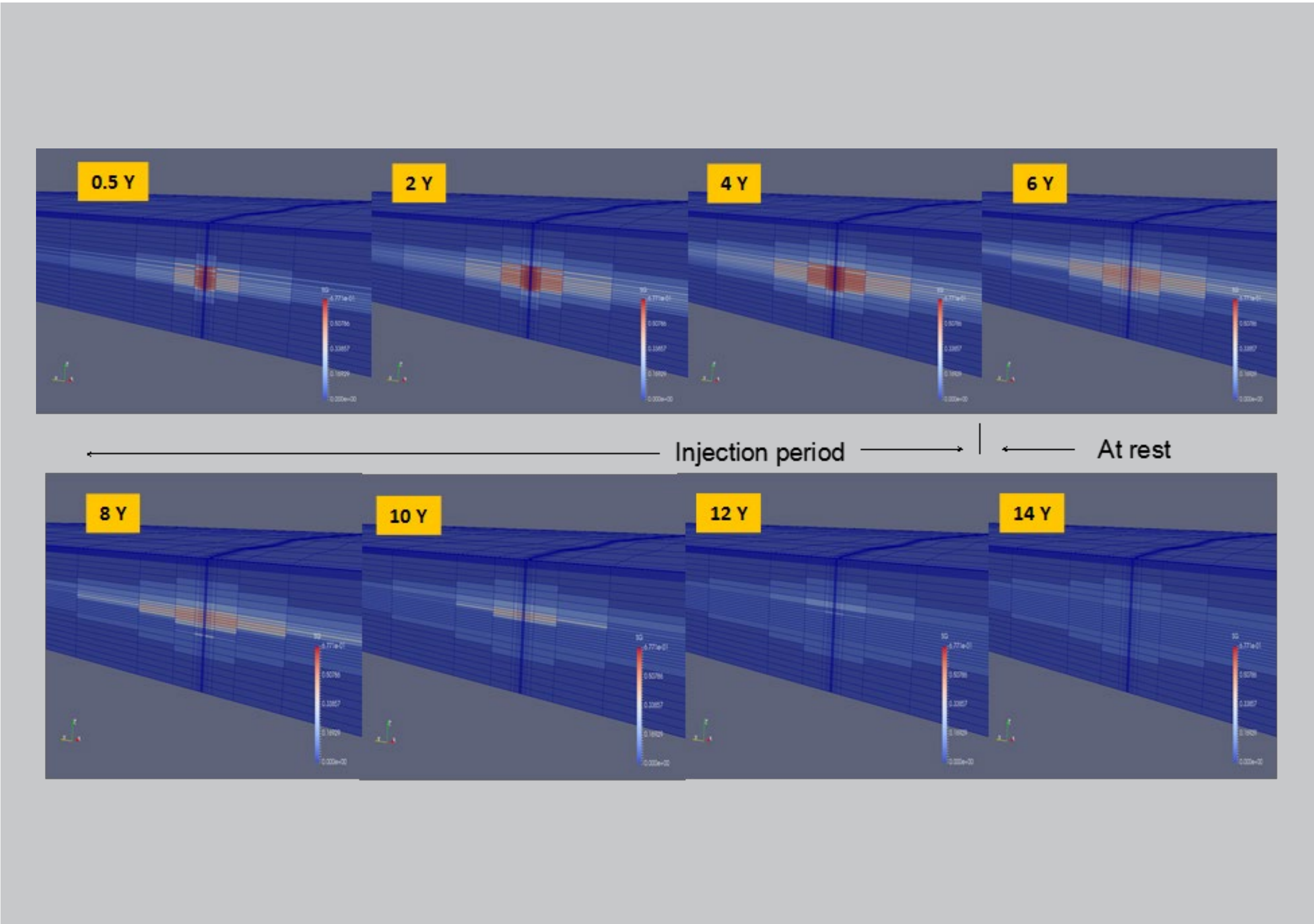

Chapter XX

Remediation and preventive measures using hydraulic barrier method

Ji-Quan Shi[1], Sevket Durucan[1], Anna Korre[1], Dong Chen[1]
[1] Imperial College, UK

SUMMARY

This element of the MiReCOL project aims to investigate the feasibility of brine injection above a fractured cap rock or a fault at high pressure to create an inverse pressure gradient to reverse the flow direction of CO_2 plume. Research involved testing realistic reservoir and CO_2 leakage scenarios representative of the subsurface and focused on the role of controlling parameters which may affect the success or failure of the hydraulic barrier technology considered.

Using the Imperial College Saline Aquifer Model (ICSAM) chosen from the project database as the base model, two potential leakage pathways have been investigated. The potential leakage pathways include 1) an areal sink in the caprock; and 2) fault/fault zone (elongated sink). For each leakage pathway, the following key features of the storage reservoir were considered and implemented to form a number of modelling scenarios:

- Storage reservoir depth (formation pressure and temperature)
- Top of reservoir topography
- Caprock thickness/distance to the permeable layer above the storage reservoir
- Permeable layer permeability/porosity

The modelling results in terms of time-to-detection and cumulative CO_2 leakage for with/without remediation for all the scenarios are presented and the pressure gradient reversal (PGR) performances are compared. The results suggest that, for the areal sink favourable performance of PGR may be achieved when the shallow aquifer has a significantly larger permeability, whereas PGR is less well suited for a thicker caprock compared to the base case. For the case of elongated sink, the results suggest that better performance of PGR technique may be achieved in the reservoir with flatter slope or at a shallower depth than the base case.

1 INTRODUCTION AND OBJECTIVES

It has been suggested (Celia et al., 2002) that injection of brine above the caprock, at a higher pressure than the CO_2 pressure in the reservoir, would create an inverse pressure gradient to reverse the flow direction and increase the solubility of CO_2 in the saline water barrier formed, and prevent or limit leakage. Furthermore, coupled with fluid management procedures during aquifer storage (saline water extraction and re-injection above the caprock), this methodology can also be used to minimise displacement and migration of native brine, and avoid pressure build up in closed or semi-closed structures. In a more recent study, Reveillere et al. (2012) conducted a numerical study on the same phenomenon using an overly simple 3D flow model with flat layers (thus buoyancy-driven lateral migration of CO_2 was absent). They reported that this technique may efficiently stop leakage in a relatively short time or may be effectively used as a preventive measure, while continuing injecting CO_2. The effectiveness of above zone brine injection for CO_2 leakage remediation has also been investigated by Zahasky (2014).

It was thus suggested that, such a procedure could enable fast and relatively low cost mitigation action once a leakage is detected. On the other hand, the results illustrated in the literature are valid for a specific case and the methodology may have limitations which needed to be investigated further through exhaustive analysis of field based properties.

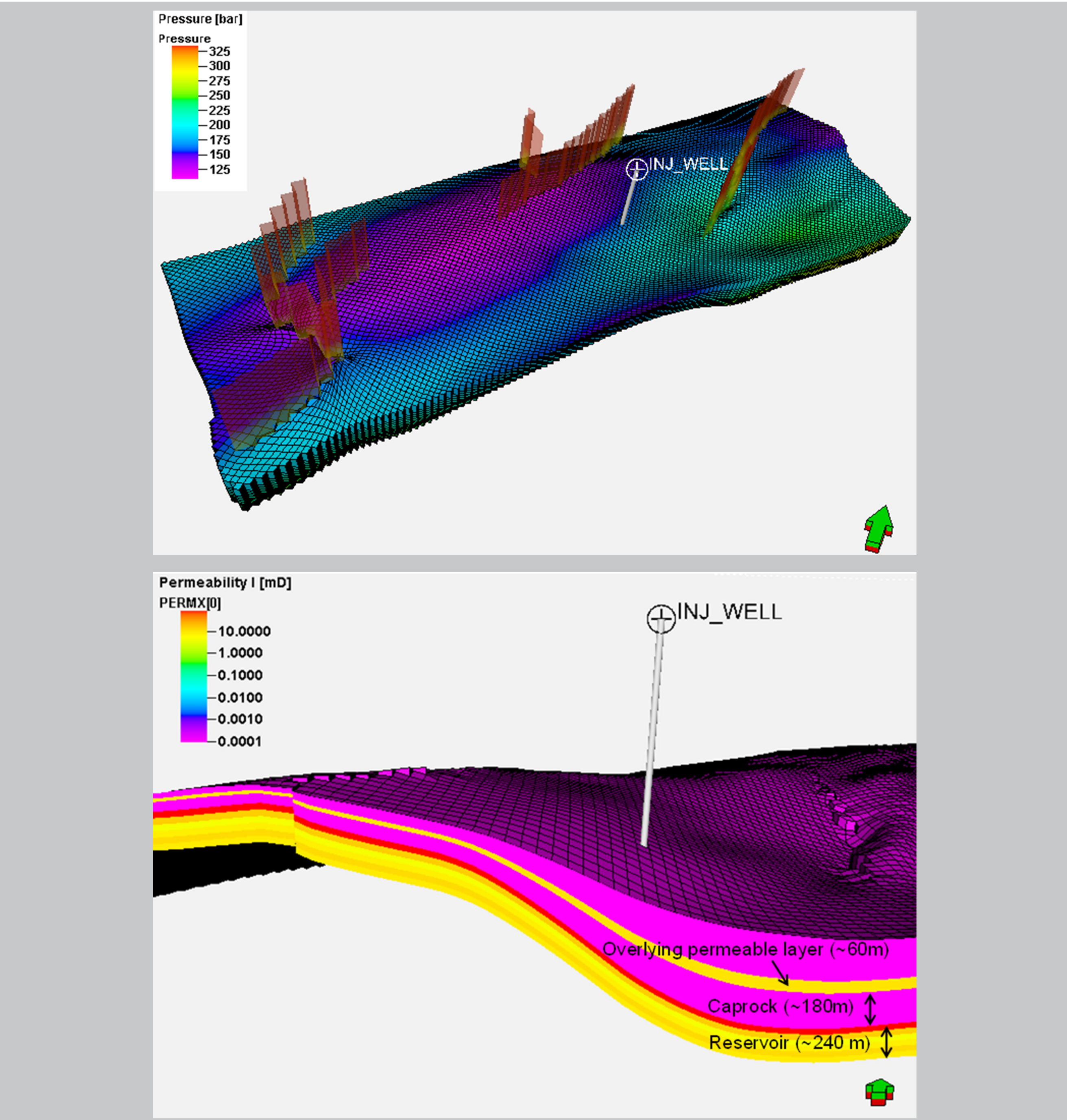

Figure 1 ICSAM reservoir/overburden model. (a) Hydrostatic pressure distribution, (b) A close-up showing the caprock and overburden layers.

In the research reported here, the effectiveness of the pressure gradient reversal (PGR) method as a potential remediation technique for CO_2 leakage from deep saline aquifers was investigated using a realistic 3D reservoir/caprock model.

The objective of this research was to test a hydraulic barrier method to mitigate against CO_2 migration through the caprock using water injection, and specifically, to testing realistic reservoir and CO_2 leakage scenarios representative of selected models from the project database. The focus was on the role of controlling parameters which may affect the success or failure of the hydraulic barrier technology considered.

1.1 Imperial College Saline Aquifer Model

The Imperial College Saline Aquifer Model (ICSAM) has been chosen as the base model to carry out brine injection simulations. The key requirements in model selection were 1) inclusion of a caprock and 2) the presence of at least one permeability layer in the overburden formations which is suitable for brine/water injection. The ICSAM model measures 36 km x 10 km and includes several faults (Figure 1a). The model has a uniform grid block size of 200 m x 200 m in the lateral direction.

The depth of target storage formation ranges from 1,082 to 3,484 m across the model domain, dipping considerably. The injection well is located at a location where the storage reservoir is between 1,973 to 2,181 m deep. The storage reservoir, which has a thickness of approximately 240 m, consists of 6 layers of varying properties both within each layer and across the layers (Figure 1b). The overlying formation (caprock) is considered to be impermeable, except for a 60 m thick layer situated at 180 m above the reservoir, which is assigned a permeability of 10 mD in the base case scenario. The reservoir/overburden is initially at hydrostatic pressure, and the reservoir temperature is 92 °C. Figure 2 shows the gas-water relative permeability curves used for the storage reservoir and the shallow aquifer in the research. The relatively high irreducible water saturation is noted.

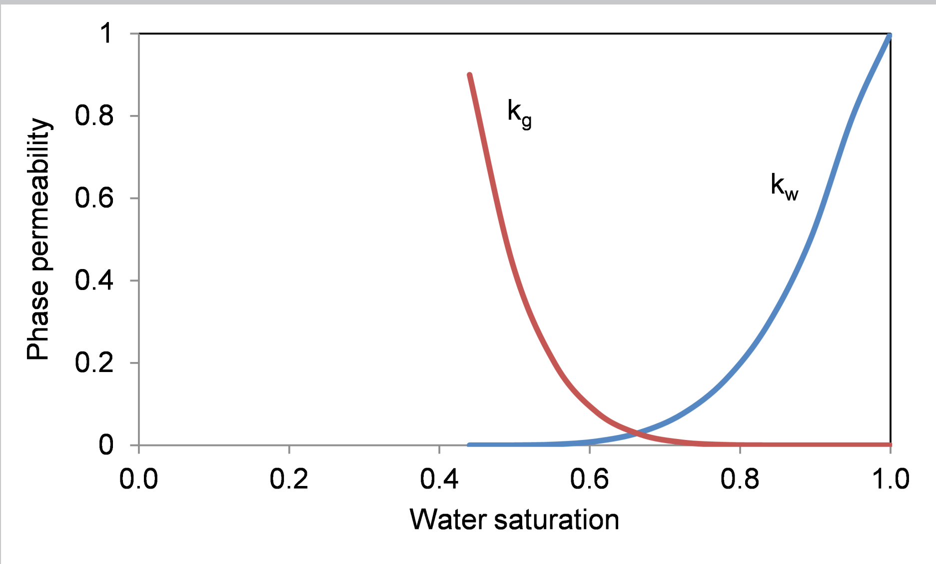

Figure 2 CO_2-water relative permeability curves used in the model.

2 TRANSIENT AND NON-TRANSIENT CO_2 PLUME REGIONS AND LEAKAGE ASSESSMENT

Reservoir simulation of CO_2 injection at a rate of 1 Mt/year for 30 years was carried out to evaluate the plume migration behaviour during injection and after the termination of injection. A pore volume multiplier of 100 was used during simulations to represent the connected pore volume beyond the model domain. It was found that the plume largely stabilised at about 120 years from the start of injection. Figure 3 presents snapshots of the CO_2 plume at different stages of plume migration up dip following the formation topography.

Based upon this plume migration behaviour, the plume footprint may be broadly divided into (Figure 4):

- the transient region (where the free CO_2 largely has a limited residence time), and
- the non-transient region (where the free CO_2 residence is more or less stable),

In the transient region (Figure 4), the free mobile CO_2 represents a moving, dynamic source for potential CO_2 leakage (or migration) out of the storage reservoir if an undetected and characterised leakage zone (sink) exists along this path. Free CO_2 accumulated in the non-transient region (top of an anticline in this case), on the other hand, represents a largely stationary (or stabilised) source for potential CO_2 leakage out of the storage reservoir. This distinction has been found to have a direct bearing on the potential leakage profiles in the two regions.

In an earlier study, the potential leakage risk profiles, i.e. the total amount of leaked CO_2 through the caprock, and the leakage time periods, at various locations in both the transient and non-transient regions were computed and mapped. The leakage scenario considers one leaky block at one time iteratively. To simulate CO_2 leakage, a leakage pathway is intentionally created by assigning a permeability of between 1 and 10 mD to the column of grid blocks in the caprock between the storage reservoir and the permeable layer above (Figure 1a). During simulations, the cumulative leakage from the storage reservoir was monitored and injection is terminated when a pre-set leakage detection threshold/limit is exceeded. Based upon the findings from these early simulations, a detection threshold between 1,000 to 10,000 tonnes of CO_2 was used.

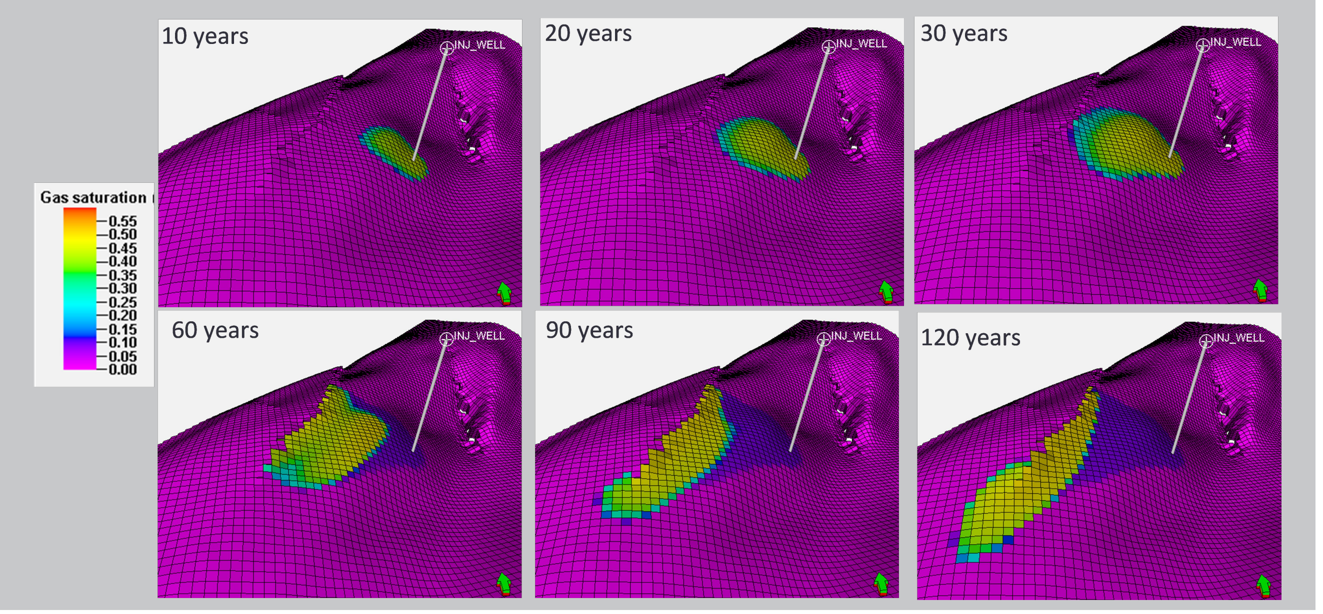

Figure 3 Simulated CO_2 plume migration in the reservoir during injection and post-injection periods.

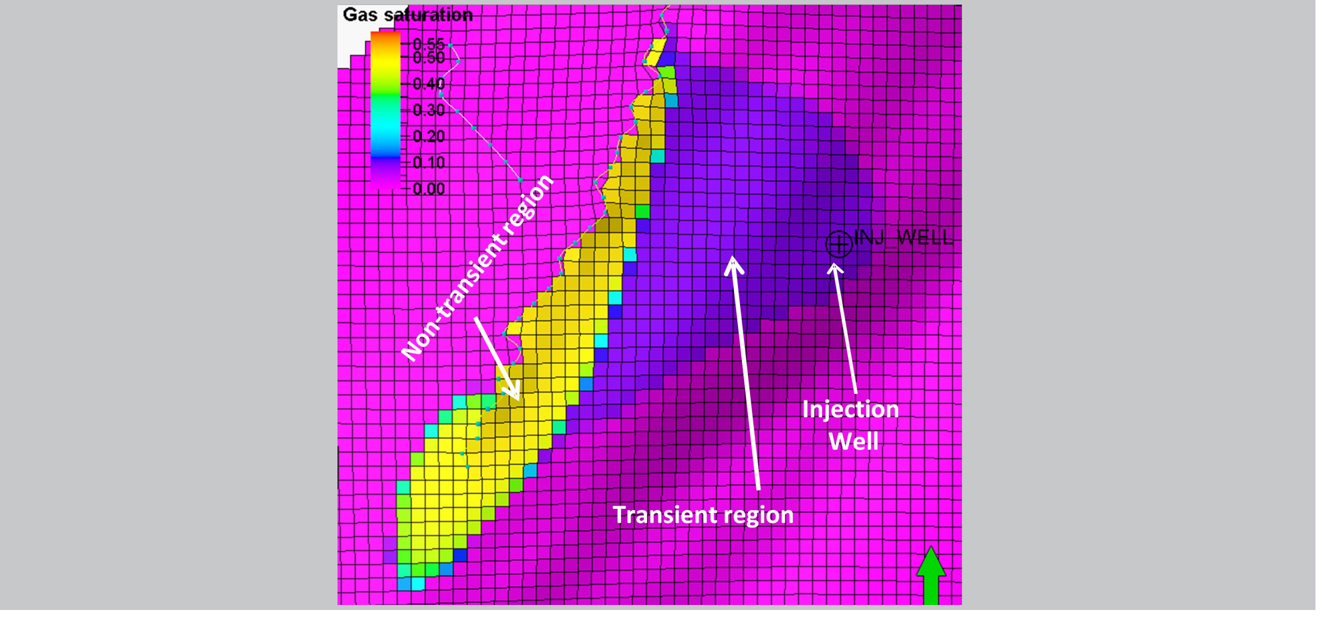

Figure 4 The CO_2 plume footprint is divided into transient and non-transient regions.

One important parameter is the time (year) it takes for the leakage to be detected during the simulation, i.e. time-to-leakage detection, referred to for simplicity as the time-to-detection (TTD). Clearly it is expected to vary spatially within the CO_2 plume footprint. Furthermore, the TTD at a given leakage location depends on the combined effect of a detection threshold applied and the leakage pathway permeability assigned (Table 1).

Although CO_2 injection is terminated once leakage is detected during CO_2 injection simulations, leakage is continuously monitored until its source (the free CO_2 in the storage reservoir available for leakage at that grid) is exhausted. In this way, potential leakage profile, including the total leakage duration and the cumulative CO_2 leakage, may be obtained to provide a benchmark for evaluating the effectiveness of any remediation measure. The simulation results have shown that the computed leakage profiles display very different trends in the transient and non-transient regions (Figure 5).

Table 1 Computed time-to-detection, cumulative CO_2 leakage and total leakage duration for three grid blocks marked in Figure 5 in the transient region.

	Time-to-detection (year)	Cumulative CO_2 leakage (Mt)	Total leakage duration (year)
P44	8 months	0.13	5
P43	5	0.46	20
P42	12	0.97	48

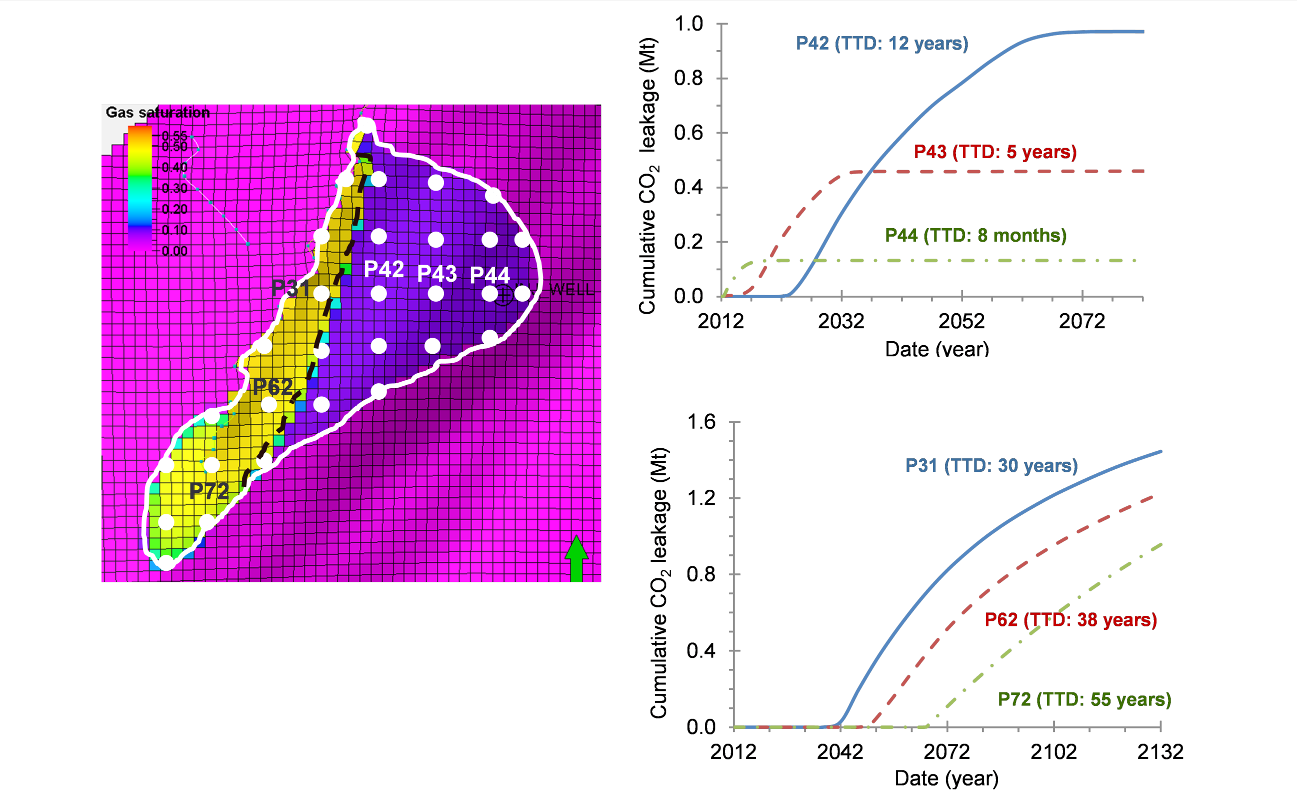

Figure 5 Computed potential CO_2 leakage profiles at selected points in the transient and non-transient regions, showing distinctive region-wise trends.

Two leakage locations (grid blocks P44 and P43) in the transient source region, at a distance of 200m and 1,200 m, respectively, to the CO_2 injector were selected for conducting above-zone brine injection simulations. The focus of the injection and leakage modelling work was mainly on P44, which is much closer than P43 is to the injection well. In addition to the base case (detection threshold = 10,000 tonnes, leakage pathway permeability = 10 mD), three other cases with a lower detection threshold (1,000 tonnes) and leakage pathway permeabilities (1 mD) or both were also considered to assess the effectiveness of PGR under different conditions.

The performance of brine injection into an overlying permeable layer (Figure 6) as a potential means for leakage remediation was evaluated through reservoir simulations. In the simulations, brine was injected into the original CO_2 injection well immediately following the detection of leakage and the termination of CO_2 injection. In other words, time which would normally be required for the conversion from a CO_2 injector to a brine injector was not considered. Brine injection into the overlying permeable layer was subject to a constant bottom hole pressure limited to 1.3 times of the hydrostatic pressure to prevent fracturing the reservoir and caprock.

Varying brine injection durations (4 – 16 months) were simulated and it was found that the optimal injection duration was 12 months. The brine injection simulation results indicate that the performance of PGR is strongly affected by how early leakage is detected from the start of injection (time-to-detection), which in turns is controlled by the detection threshold, leakage pathway permeability and the distance to the injection well. The following conclusions may be drawn:

- Above-zone brine injection not only brings down the pressure difference between the storage reservoir and the overlying permeable layer, as is intended, but also the CO_2 saturation in the reservoir around the leakage block. The reduction in CO_2 leakage potential is contributed to both the factors.
- PRG is more effective the earlier the leakage is detected and the closer is the leakage location to the injection well.

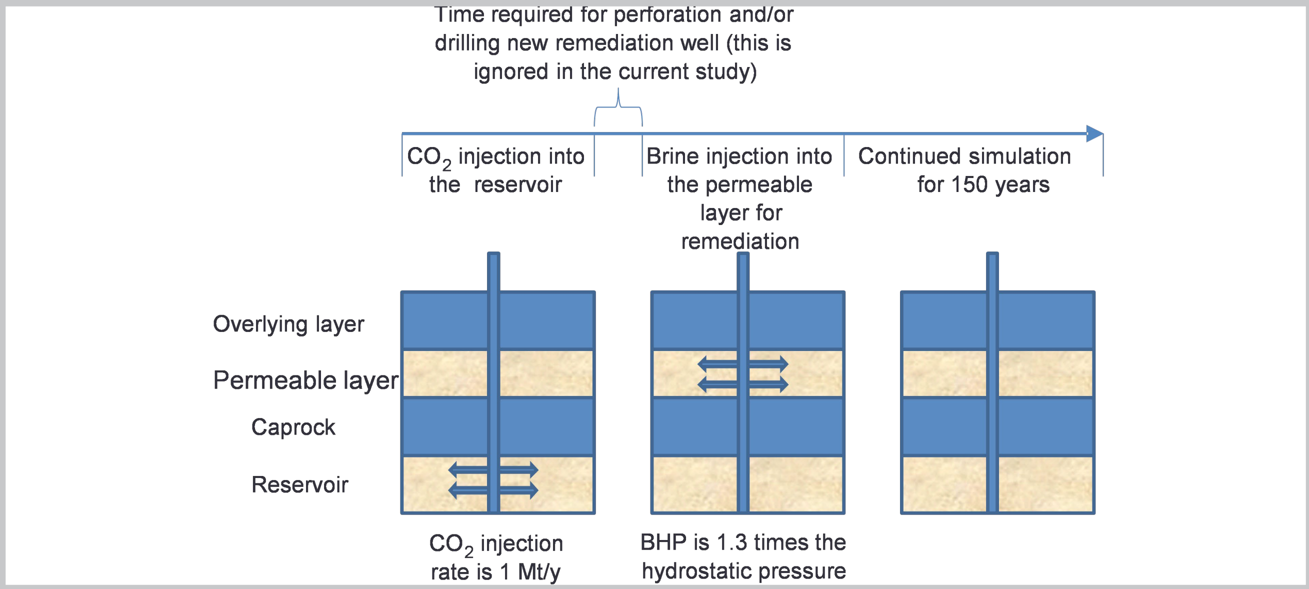

Figure 6 A schematic showing the simulation procedure for PGR method.

3 LEAKAGE REMEDIATION SCENARIO ANALYSIS

The leakage remediation model scenarios considered in the project builds upon the early leakage assessment work carried out. In addition to an areal sink, an elongated sink to represent a fault/fault zone was also considered. As before, the areal sink flow path is represented by a single column of grid cells (~200m x ~200m) across the caprock in the model, along which CO_2 in the storage reservoir can migrate to the shallow aquifer. The elongated sink at the caprock is modelled through performing local grid refinement on the selected grids to yield rectangular cells with large aspect ratio.

For each leakage pathway, the following key features of the storage reservoir are considered and implemented to form a number of modelling scenarios

- Storage reservoir depth (formation pressure and temperature)
- Top of reservoir topography
- Caprock thickness/distance to the permeable layer above the storage reservoir
- Shallow aquifer permeability/porosity

For each scenario the base reservoir model is modified accordingly for CO_2 and brine injection simulations and associated remediation performance evaluation.

3.1 CO_2 leakage and brine injection remediation scenario results

CO_2 is injected at 1 Mt/y into the injection well (Figure 1a). The leakage column permeability and leaked CO_2 detection threshold in the shallow aquifer is assumed to be 10 mD and 10,000 tonnes respectively. Following the detection of CO_2 leakage, brine is injected at a target rate of ~1 Mt/year into the overlying permeable formation (shallow aquifer, Figure 1b) through the same CO_2 injection well, subject to the BHP limit of 1.3 times the hydrostatic pressure at the injection point, for a period of 12 months. In these new and comprehensive remediation scenarios, the simulation is run for a total of 150 years.

3.1.1 Remediation of leakage through an areal sink

As discussed above for the leakage assessment simulations, grid P44 (Figure 7), which is 200m away from the injection well, is selected for conducting CO_2 leakage and subsequent brine injection simulations for the areal sink scenarios. The results for the base case scenario are presented first. Different scenarios implemented to evaluate the effects of

1. storage reservoir depth (with associated pressure and temperature variations),
2. the top of reservoir topography,
3. caprock thickness,
4. permeability and
5. porosity of the shallow aquifer

on the effectiveness of pressure gradient reversal (PGR) on CO_2 leakage remediation are then presented here.

The simulation results for each scenario include time-to-detection (TTD), cumulative leakage for without remediation and with brine injection. These are summarised in Table 2.

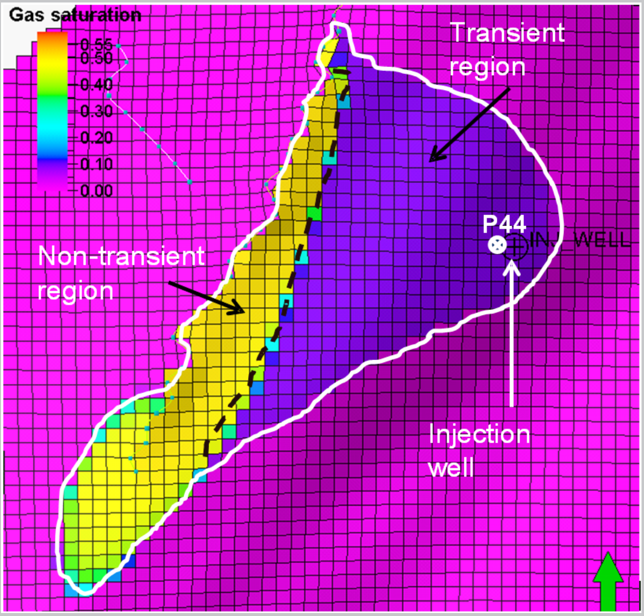

Figure 7 The CO_2 leakage location at grid 44 in transient region selected for above-zone brine injection simulations.

Table 2 Pressure gradient reversal performance for different areal sink scenarios.

			Time-to-detection (month)	Cumulative leakage 10^3 tonne
Base Case		No remediation/ with PGR (%)	8	97/ 25 (26%)
Reservoir depth	Shallower (-350m)	No remediation/ with PGR (%)	7	80/ 26 (33%)
	Deeper (+350m)	No remediation/ with PGR (%)	9	113/ 21 (19%)
Reservoir top slope (16°)	Gentler (7°)	No remediation/ with PGR (%)	9	116/ 29 (25%)
	Steeper (22°)	No remediation/ with PGR (%)	9	74/ 26 (35%)
Caprock thickness (180m)	Thinner (60m)	No remediation with PGR (%)	7	81/ 26 (32%)
	Thicker (360m)	No remediation/ with PGR (%)	10	123/ 92 (75%)
Shallow aquifer permeability (10 mD)	Lower (1mD)	No remediation/ with PGR (%)	11	60/ 30 (50%)
	Higher (100 mD)	No remediation/ with PGR (%)	7	93/ 11 (12%)
Shallow aquifer porosity (10%)	Lower (5%)	No remediation/ with PGR (%)	8	98/ 21 (21%)
	Higher (20%)	No remediation with PGR (%)	8	96/ 31 (32%)

Base case scenario

For the base case scenarios, the leakage detection threshold (10,000 tonnes) at P44 was reached in the 8th month of CO_2 injection at a rate of 1 Mt/y, as illustrated in Figure 8a. With the determination of TTD, two subsequent simulation runs were performed where CO_2 injection is terminated after 8 months, one followed by brine injection at ~1 Mt/y for a fixed period of 12 months and one without. Figure 8b presents the simulated cumulative CO_2 leakage for the two runs. The results show that the cumulative CO_2 leakage would be reduced from the bench mark 97 kt (without remediation) to 25 kt (or 26%) with brine injection, a reduction of 74%.

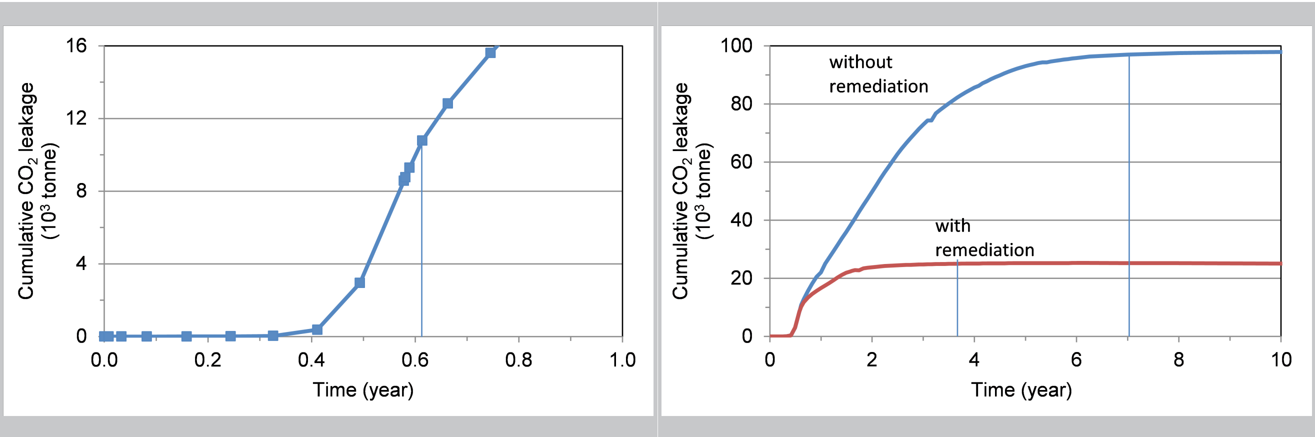

Figure 8 a) Determination of time-to-detection and b) leakage profiles with and without brine injection for the base case scenario.

Effect of storage reservoir depth (with associated pressure and temperature variations)

The reservoir formation (with a reservoir temperature 92˚C) in the base model was shifted up and down by 350 m to create a shallower (with reservoir temperature 80.75˚C) and a deeper case (with reservoir temperature 105.25˚C). As a consequence, the corresponding injection bottomhole pressure during brine injection was also limited to 189.8 and 276.9 bars respectively, compared to 232.3 bars for the base case. For the shallower/deeper case, leakage detection threshold at P44 was reached on the 7th/9th month of CO_2 injection at a rate of 1 Mt/y (Table 2). In this scenario, the cumulative CO_2 leakage would be reduced from the bench mark 80/113 kt (without remediation) to 26/21 kt (or 33%/19%) with brine injection, a reduction of 67%/81% (Table 1, Figure 9).

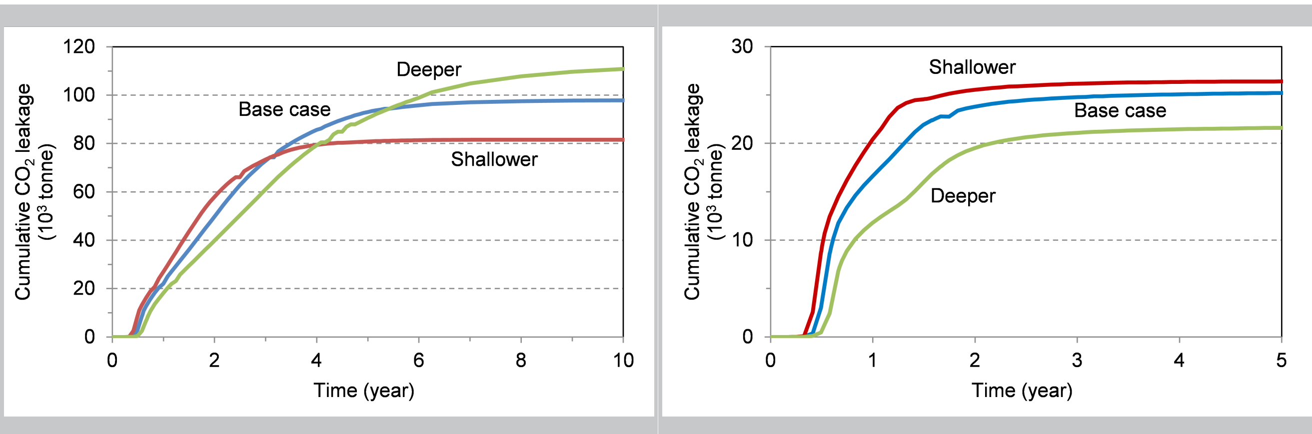

Figure 9 The effect of varying the storage formation depth on CO_2 leakage profiles without (top) and with brine injection (bottom).

Effect of storage reservoir topography

In this scenario, the reservoir top slope was varied from the base case (16˚ near the CO_2 injection well) to represent a flatter (7˚ near the CO_2 injection well) or a steeper (22˚ near the CO_2 injection well) slope. For the flatter/steeper cases, leakage detection threshold at P44 was reached on the 9th/9th month of CO_2 injection at a rate of 1 Mt/y (Table 2). Then, the cumulative CO_2 leakage would be reduced from the bench mark 116/76 kt (without remediation) to 29/26 kt (or 25%/35%) with brine injection, a reduction of 75%/65% (Table 2, Figure 10).

Effect of caprock thickness

As shown in Figure 1b, the caprock thickness is 180m in the base case. For the thinner/thicker cases, it was reduced/increased to 60m/360m in the model. For the thinner/thicker cases, leakage detection threshold at P44 was reached on the 7th/10th month of CO_2 injection at a rate of 1 Mt/y (Table 2). For this scenario, the cumulative CO_2 leakage would be reduced from the bench mark 81/123 kt (without remediation) to 26/92 kt (or 32%/75%) with brine injection, a reduction of 68%/25% (Table 2, Figure 11).

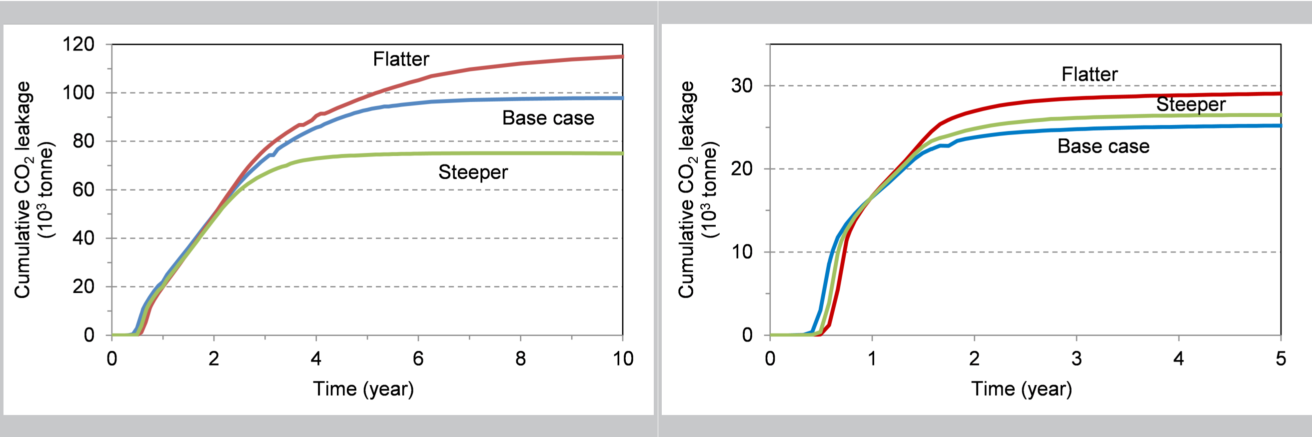

Figure 10 The effect of varying the storage reservoir topography on CO_2 leakage profiles without (top) and with brine injection (bottom).

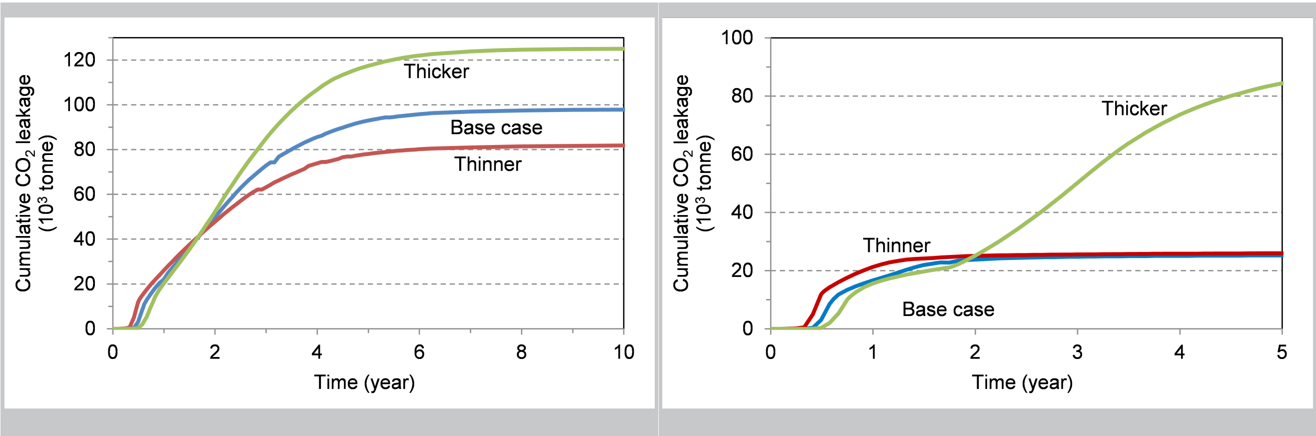

Figure 11 The effect of varying caprock thickness on CO_2 leakage profiles without (top) and with brine injection (bottom).

Effect of shallow aquifer permeability

The shallow aquifer has a permeability of 10 mD in the base case. For this scenario, the permeability was reduced/increased to 1 mD/100 mD in the model to evaluate its impact on the PGR performance. For the lower k/higher k cases, leakage detection threshold at P44 was reached on the 11th/7th month of CO_2 injection at a rate of 1 Mt/y (Table 2). The cumulative CO_2 leakage would then be reduced from the bench mark 60/93 kt (without remediation) to 30/11 kt (or 50%/12%) with brine injection, a reduction of 50%/88% (Table 2, Figure 12).

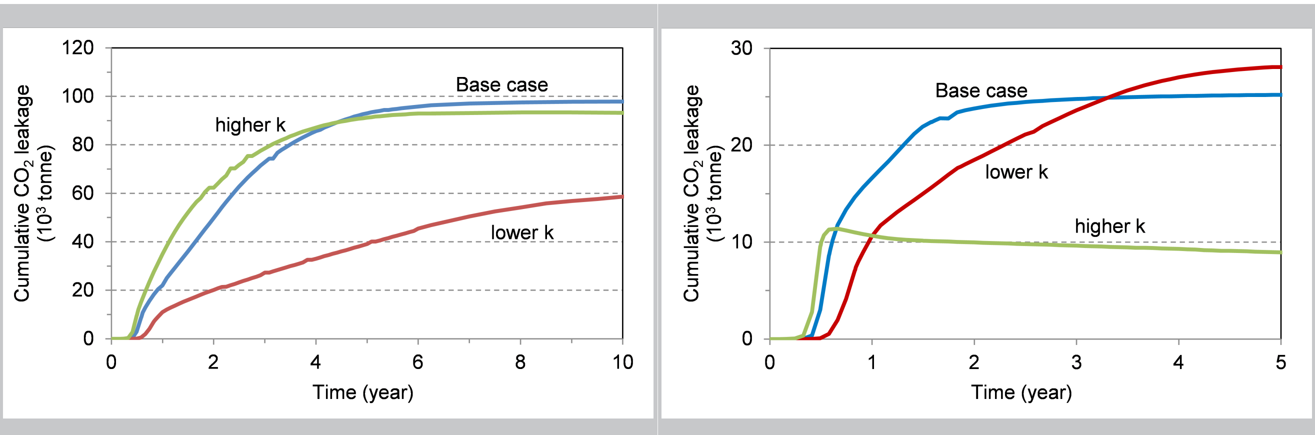

Figure 12 The effect of shallow aquifer permeability on CO_2 leakage profiles without (top) and with brine injection (bottom).

Effect of shallow aquifer porosity

In this scenario, the base case shallow aquifer porosity of 10% was reduced/increased to 5%/20 % to evaluate its impact on the PGR performance. For the lower Φ/higher Φ cases, leakage detection threshold at P44 was reached on the 8th/8th month (unchanged from the base case) of CO_2 injection at a rate of 1 Mt/y (Table 1). This has indicated that the cumulative CO_2 leakage would be reduced from the bench mark 98/96 kt (without remediation) to 21/31 kt (or 21%/32%) with brine injection, a reduction of 79%/68% (Table 2, Figure 13).

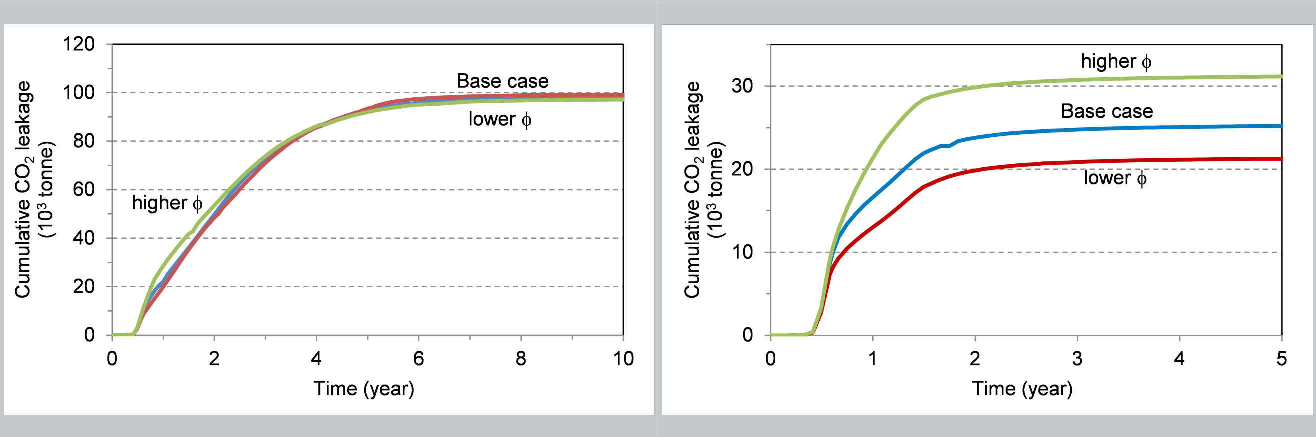

Figure 13 The effect of shallow aquifer porosity on CO_2 leakage profiles without (top) and with brine injection (bottom).

Summary of the results of areal sink scenarios

The modelling results in terms of time-to-detection, cumulative CO_2 leakage for with/without remediation for all the cases presented above are compared in Figures 14 and 15. It can be seen from Figure 14 that, for the different scenarios tested, time-to-detection (10,000 tonnes of leakage to the shallow aquifer) was between 7 to 11 months depending on the reservoir properties and the reservoir top topography selected. It was found that, the permeability of shallow aquifer has the largest impact on the detection time, increasing to 11 months from 8 months (base case and 10 mD permeability) for an order of magnitude reduction in its permeability, followed by the caprock thickness (10 months for doubling the thickness from 180m).

The results in Figure 15 suggest that favourable performance of PGR may be achieved when the shallow aquifer has a significantly larger permeability (an order of magnitude increase in permeability leads to 89% reduction in the cumulative CO_2 leakage compared to 74% for the base case permeability of 10 mD), whereas PGR is less well suited for a thicker caprock compared to the base case.

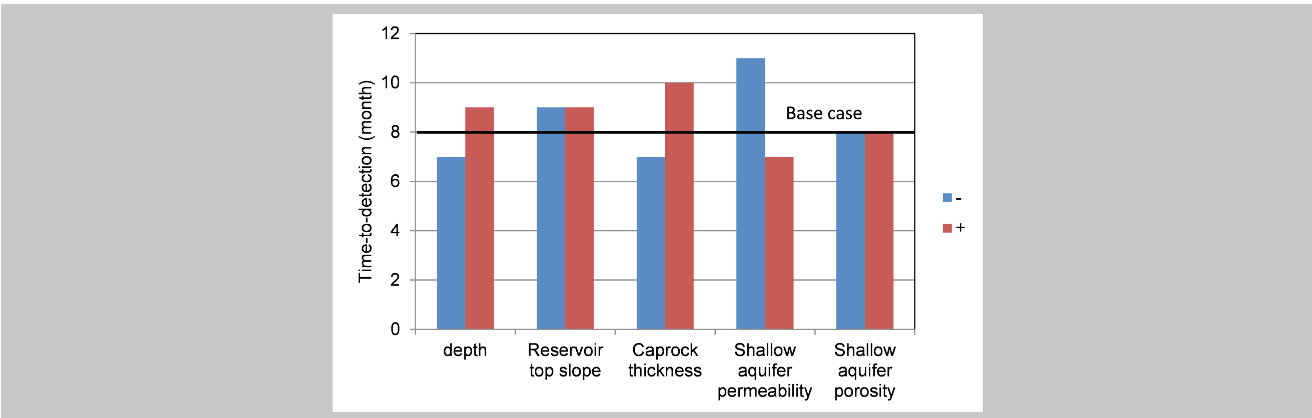

Figure 14 Comparison of time-to-detection for areal-sink scenarios (P44).

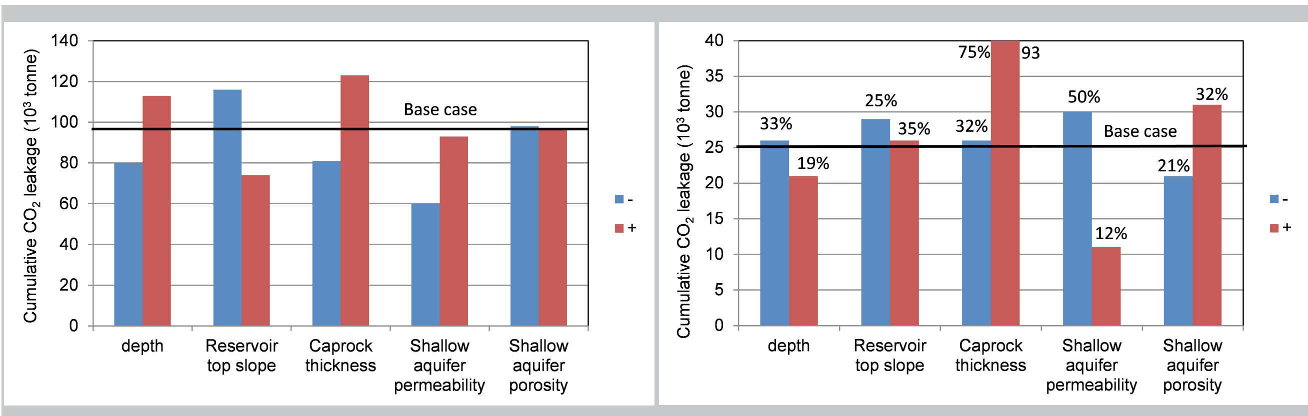

Figure 15 Comparison of cumulative CO_2 leakage for areal scenarios without (left) and with remediation (right).

3.1.2 Remediation of leakage through an elongated sink

An elongated sink (10m x 600m) at the location of P44 for modelling CO_2 leakage along a fault/fault zone is presented in Figure 16. The central 400m length is used as a sink. The elongated sink is assigned a vertical permeability of 100mD so that the product of leakage sink permeability and its area remains unchanged from that for the areal sink. The results for the base case scenario are presented first. Different scenarios to evaluate the effects of:

1. storage reservoir depth (with associated pressure and temperature variations),
2. the top of reservoir topography,
3. caprock thickness,
4. permeability and
5. porosity of the shallow aquifer

on the effectiveness of PGR on CO_2 leakage remediation are then presented.

The simulation results for each scenario include time-to-detection (TTD), cumulative leakage for without remediation and with brine injection. They are summarised in Table 3.

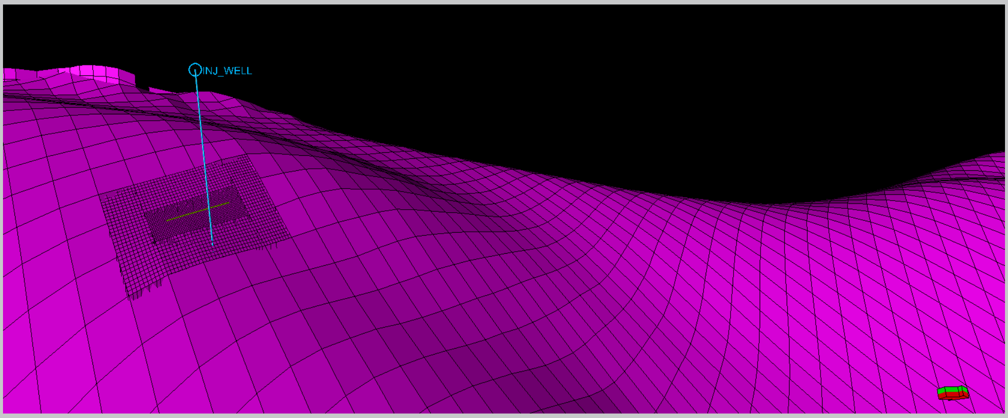

Figure 16 An elongated sink (20m x 600m) at the location of P44 for modelling CO_2 leakage along a fault/fault zone. The central 400m length is used as a sink.

Table 3 PRG performance for different elongated sink scenarios.

			Time-to-detection (month)	Cumulative leakage 10^3 tonne
Base Case		No remediation/ with PGR (%)	7	111/46 (41%)
Reservoir depth	Shallower (-350m)	No remediation/ with PGR (%)	7	90/32 (36%)
	Deeper (+350m)	No remediation/ with PGR (%)	8	133/43 (32%)
Reservoir top slope (16°)	Gentler (7°)	No remediation/ with PGR (%)	10	130/30 (23%)
	Steeper (22°)	No remediation/ with PGR (%)	9	78/36 (46%)
Caprock thickness (180m)	Thinner (60m)	No remediation with PGR (%)	9	69/33 (48%)
	Thicker (360m)	No remediation/ with PGR (%)	8	118/39 (33%)
Shallow aquifer permeability (10 mD)	Lower (1mD)	No remediation/ with PGR (%)	12	64/41 (64%)
	Higher (100 mD)	No remediation/ with PGR (%)	6	105/59 (56%)
Shallow aquifer porosity (10%)	Lower (5%)	No remediation/ with PGR (%)	7	109/45 (41%)
	Higher (20%)	No remediation with PGR (%)	7	115/47 (41%)

Base case scenario

In the base case scenario, leakage detection threshold (10,000 tonnes) at the elongated sink was reached on the 7th month of CO_2 injection at a rate of 1 Mt/y, as illustrated in Figure 17a. With the determination of TTD, two subsequent simulation runs were performed where CO_2 injection is terminated after 7 months, one followed by brine injection at ~1 Mt/y for a fixed period of 12 months and one without. Figure 17b presents the simulated cumulative CO_2 leakage for the two runs. The results show that the cumulative CO_2 leakage would be reduced from the bench mark 111 kt (without remediation) to 46 kt (or 41%) with brine injection, a reduction of 59%.

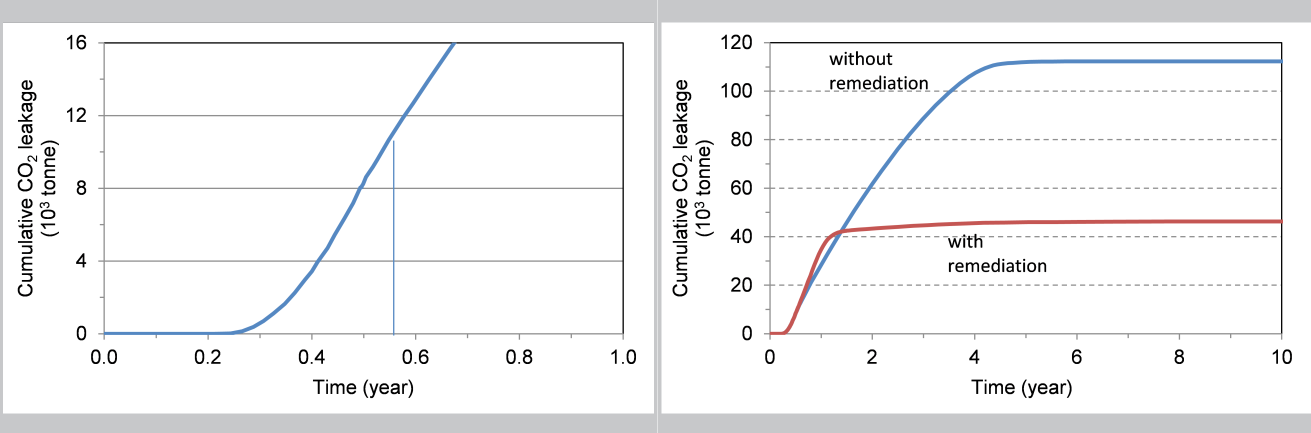

Figure 17 a) Determination of time-to-detection and b) leakage profiles with and without brine injection for the base case scenario.

Effect of storage reservoir depth (with associated pressure and temperature variations)

The reservoir formation (with a reservoir temperature 92˚C) in the base case model was shifted up and down by 350 m to create a shallower (with reservoir temperature 80.75˚C) and a deeper case (with reservoir temperature 105.25˚C). The corresponding injection bottomhole pressure during brine injection was also limited to 189.8 and 276.9 bars respectively, compared to 232.3 bars for the base case. For the shallower/deeper case, leakage detection threshold at the elongated sink was reached on the 7th/8th month of CO_2 injection at a rate of 1 Mt/y (Table 3). The cumulative CO_2 leakage would be reduced from the bench mark 90/133 kt (without remediation) to 32/43 kt (or 36%/32%) with brine injection, a reduction of 64%/68% (Table 3, Figure 18).

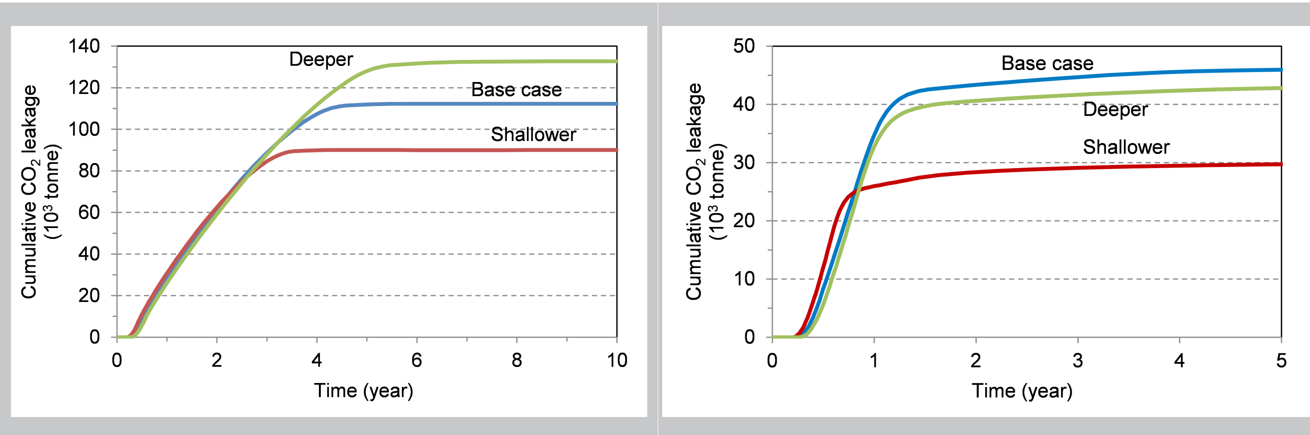

Figure 18 The effect of varying the storage formation depth on CO_2 leakage profiles without (left) and with brine injection (right).

Effect of storage reservoir topography

In this case the reservoir top slope was varied from the base case (16˚ near the CO_2 injection well) to represent a flatter (7˚ near the CO_2 injection well) or a steeper (22˚ near the CO_2 injection well) slope. For the flatter/steeper case, leakage detection threshold at the elongation sink was reached on the 10th/9th month of CO_2 injection at a rate of 1 Mt/y (Table 3). The cumulative CO_2 leakage would be reduced from the bench mark 130/78 kt (without remediation) to 30/36 kt (or 23%/46%) with brine injection, a reduction of 75%/64% (Table 3, Figure 19).

Effect of caprock thickness

As shown in Figure 1b, the caprock thickness is 180m in the base case. For the thinner/thicker case, this was reduced/increased to 60m/360m in the model. For the thinner/thicker cases, leakage detection threshold at P44 was reached on the 9th/8th month of CO_2 injection at a rate of 1 Mt/y (Table 3). It was found that the cumulative CO_2 leakage would be reduced from the bench mark 69/118 kt (without remediation) to 33/39 kt (or 48%/33%) with brine injection, a reduction of 52%/67% (Table 3, Figure 20).

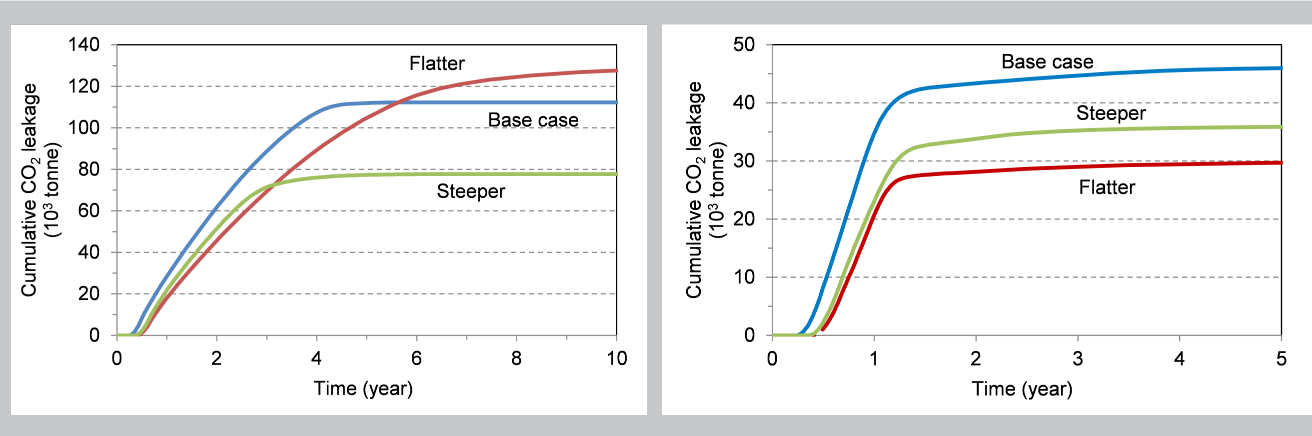

Figure 19 The effect of varying the storage reservoir topography on CO_2 leakage profiles without (left) and with brine injection (right).

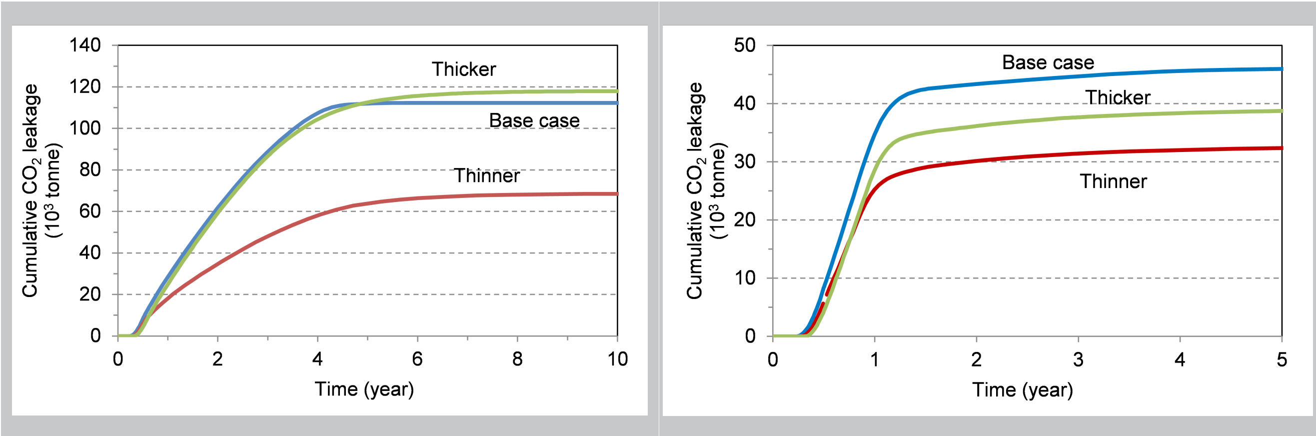

Figure 20 The effect of varying caprock thickness on CO_2 leakage profiles without (left) and with brine injection (right).

Effect of shallow aquifer permeability

The shallow aquifer has a permeability of 10 mD in the base case. The permeability was reduced/increased to 1 mD/100 mD in this scenario to evaluate its impact on the PGR performance. For the lower k/higher k cases, leakage detection threshold at P44 was reached on the 12th/6th month of CO_2 injection at a rate of 1 Mt/y (Table 2). In this scenario, the cumulative CO_2 leakage would be reduced from the bench mark 64/105 kt (without remediation) to 41/59 kt (or 64%/56%) with brine injection, a reduction of 36%/44%. (Table 3, Figure 21).

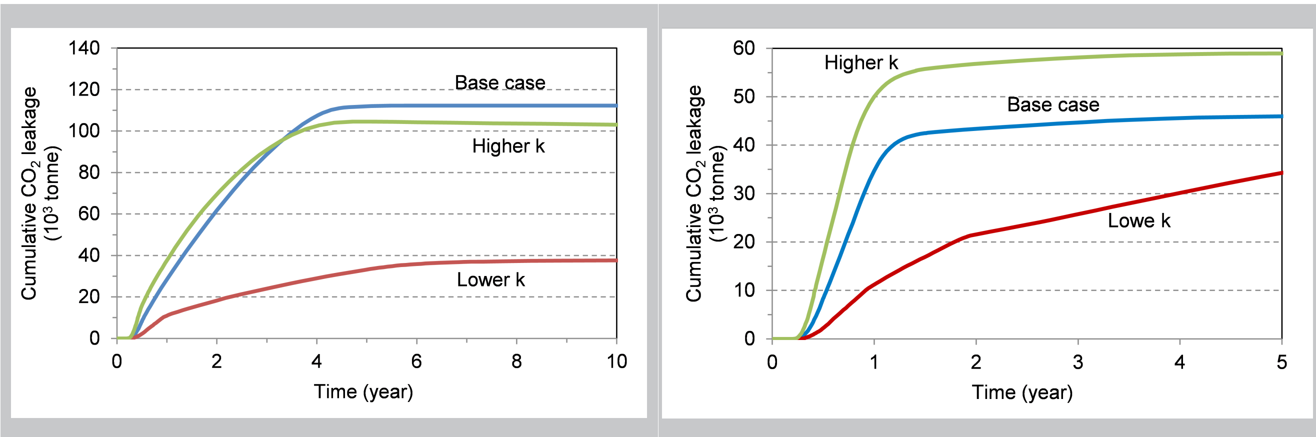

Figure 21 The effect of shallow aquifer permeability on CO_2 leakage profiles without (left) and with brine injection (right).

Effect of shallow aquifer porosity

The base case shallow aquifer porosity of 10% was reduced/increased to 5%/20 % to evaluate its impact on the PGR performance. For the lower Φ/higher Φ cases, leakage detection threshold at P44 was reached on the 7th/7th month (unchanged from the base case) of CO_2 injection at a rate of 1 Mt/y (Table 2). The cumulative CO_2 leakage would be reduced from the bench mark 109/115 kt (without remediation) to 45/47 kt (or 41%/41%) with brine injection, a reduction of 59%/59% (Table 3, Figure 22).

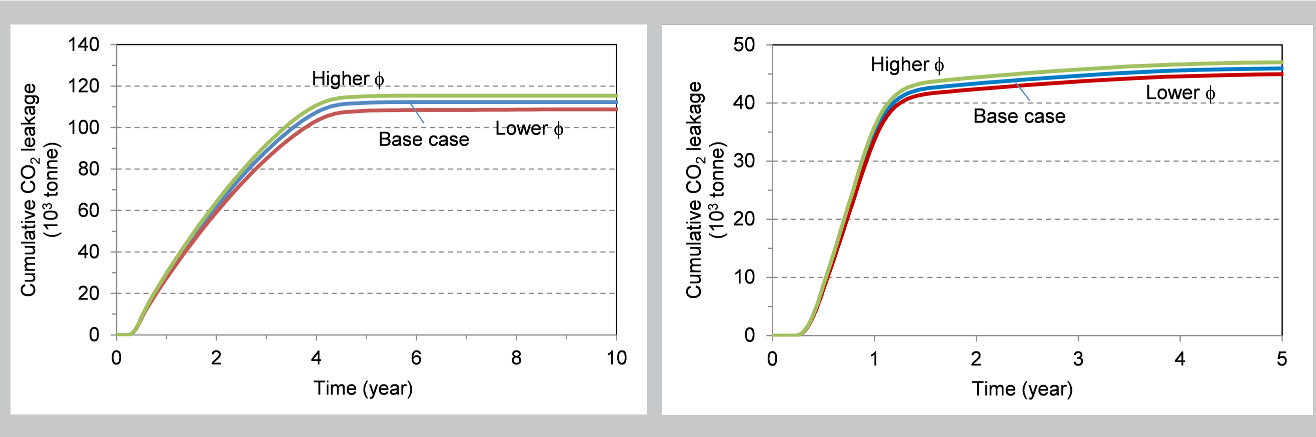

Figure 22 The effect of shallow aquifer porosity on CO_2 leakage profiles without (left) and with brine injection (right).

Summary of the remediation findings for the elongated sink scenarios

The modelling results in terms of time-to-detection, cumulative CO_2 leakage and the leakage period after detection with/without remediation for all the cases presented above are compared in Figures 23 and 24. It can be seen from Figure 23 that, for the different scenarios tested, time-to-detection (10,000 tonnes of leakage to the shallow aquifer) was between 7 to 12 months depending on the reservoir properties and the reservoir top topography selected. It was found that, the permeability of shallow aquifer has the largest impact on the detection time, increasing to 12 months from 8 months (base case and 10 mD permeability) for an order of magnitude reduction in its permeability, followed by the reservoir top slope (10 months for reducing it to 7º from 16º).

The results in Figure 24 suggest that better performance of PGR technique may be achieved in the reservoir with flatter slope (9o reduction in the slope of the reservoir top leads to 77% reduction in the cumulative CO_2 leakage compared to 59% for the base case slope of 16o), or at a shallower depth than the base case (65% reduction in the cumulative CO_2 leakage).

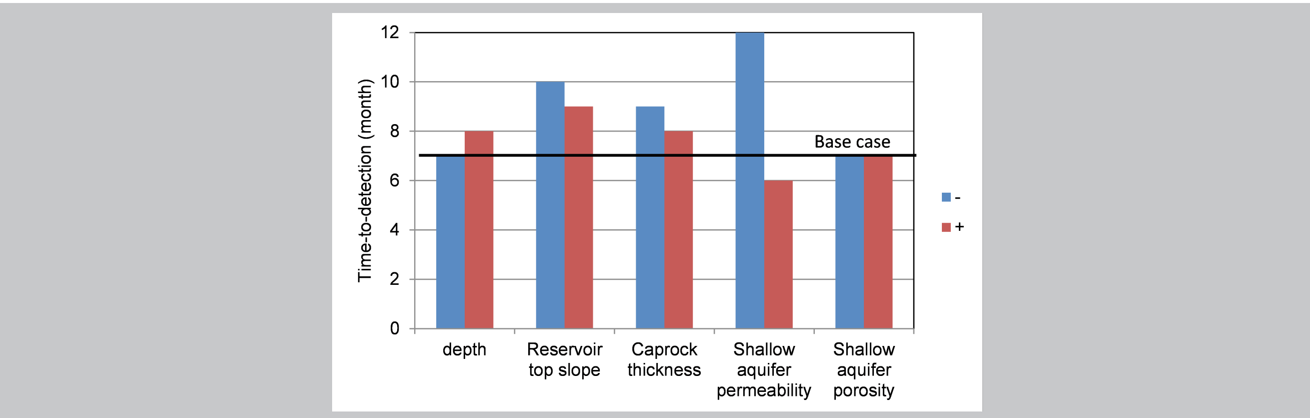

Figure 23 Comparison of time-to-detection for elongated-sink scenarios.

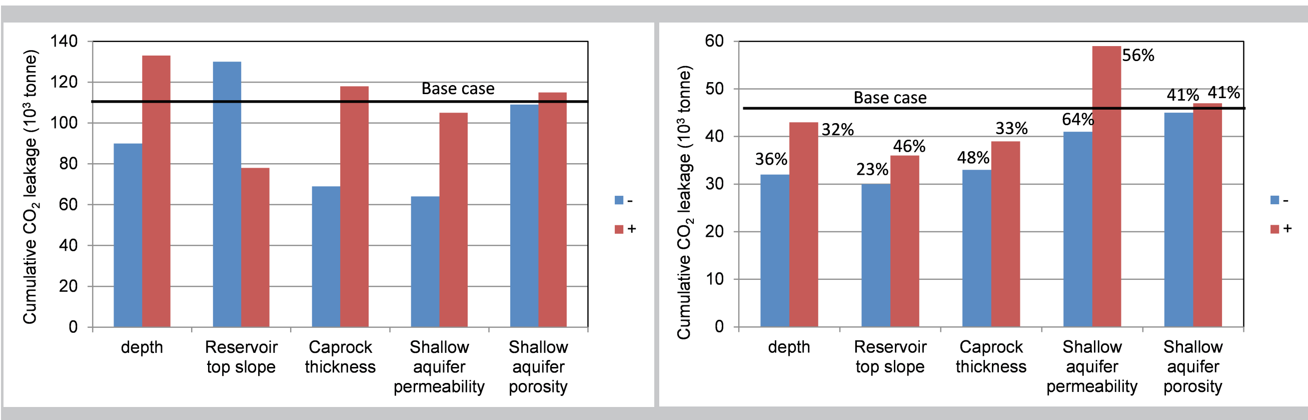

Figure 24 Comparison of cumulative CO_2 leakage for elongated scenarios without (left) and with remediation (right).

4 CONCLUSIONS

Injection of brine above a fractured cap rock or a fault, if maintained at a higher pressure than the CO_2 pressure in the reservoir, can create an inverse pressure gradient to reverse the flow direction of CO_2 and form a barrier to prevent or at least limit leakage. This procedure could enable fast and reasonably low cost mitigation measures once a leakage is detected, however, this technology can only be used as a temporary measure and allow for more permanent remediation techniques to be prepared and implemented with time. The efficiency of this technology relies upon continuous injection of brine above the leakage area and a number of site specific reservoir conditions represented by static and dynamic rock and fluid characteristics, geometry and position of the leakage.

Using the Imperial College Saline Aquifer Model (ICSAM) as the base model, a large number of brine injection simulations to remediate leakage scenarios have been carried out. Two potential leakage pathways have been investigated with a number of modelling scenarios for each leakage pathway. For each scenario, time-to-detection was set as 10,000 tonnes of injected CO_2 reaching the shallow aquifer. Remediation was implemnted through the injection of 1 Mt of brine over 12 months. The modelling results in terms of time-to-detection, and cumulative CO_2 leakage for with/without remediation for all the scenarios are presented and the PGR performances were compared.

The results suggest that, for the areal sink scenarios tested, time-to-detection was between 7 to 11 months depending on the reservoir properties and the reservoir top topography selected. It was found that, the permeability of shallow aquifer has the largest impact on the detection time, increasing to 11 months from 8 months (base case and 10 mD permeability) for an order of magnitude reduction in its permeability, followed by the caprock thickness (10 months for doubling the thickness from 180m). It was also found that favourable performance of PGR may be achieved when the shallow aquifer has a significantly larger permeability (an order of magnitude increase in permeability leads to 89% reduction in the cumulative CO_2 leakage compared to 74% for the base case permeability of 10 mD), whereas PGR is less well suited for a thicker caprock compared to the base case.

In the case of elongated sink scenarios, such as a fault or a fracture zone, the time-to-detection was between 7 to 12 months depending on the reservoir properties and the reservoir top topography selected. It was found that, the permeability of shallow aquifer has the largest impact on the detection time, increasing to 12 months from 8 months (base case and 10 mD permeability) for an order of magnitude reduction in its permeability, followed by the reservoir top slope (10 months for reducing it to 7o from 16o). Better performance of PGR technique may be achieved in a reservoir with flatter slopes (9o reduction in the slope of the reservoir top leads to 77% reduction in the cumulative CO_2 leakage compared to 59% for the base case slope of 16o), or at a shallower depth than the base case (65% reduction in the cumulative CO_2 leakage).

References

Celia, M. A., Peters, C. A., and Bachu, S., 2002, Geologic Storage of CO_2: Leakage Pathways and Environmental Risks, PowerPoint Presentation, accessed 18 September 2003: http://www.slidefinder.net/g/geologic_storage02/geologic_storage02/27664384.

Reveillere, A, Rohmer, J, Manceau, JC, 2012. Hydraulic barrier design and applicability for managing the risk of CO_2 leakage from deep saline aquifers, International Journal of Greenhouse Gas Control 9:62-71.

Zahasky, C, 2014. Quantification and intervention strategies for potential leakage from carbon storage reservoirs, Msc thesis Stanford University.

Section VI

O&G INDUSTRY BEST PRACTICE FOR REMEDIATION OF WELL LEAKAGE

Chapter XXI

Description of leakage scenarios for consideration in the work in SP3

Torbjørn Vrålstad[1], Jelena Todorovic[1], Jens Wollenweber[2], Jafar Abdollahi[3], Dusan Karas[4], Maike Buddensiek[1]
[1] SINTEF PR, Norway
[2] TNO, The Netherlands
[3] Weatherford, Norway
[4] NIS, Serbia

SUMMARY

Wells are generally considered to be the most likely path for leakage in a CO_2 storage project. Such leakages are caused by failure of one or more well barrier elements (WBE); otherwise the well integrity would be intact. Generally, WBEs that are exposed to CO_2 are most prone to leakage.

This first deliverable on the subject of well leakage remediation best practice describes the well barriers of active and abandoned wells and causes and consequences of leakage through the well barrier elements (WBE). Aging issues with cement degradation, casing corrosion and wear, and thermal loads imposed on the well infrastructure are examples of the most likely causes for well leakages. The tubing is the WBE that is by far the most likely to fail; probably due to corrosion and/or connection failures. Also, the casing and the cement have a considerable record of failure.

A wide range of technologies and methods from the oil & gas industry are available that can also be used for the remediation and mitigation of leakage from CO_2 wells. In the following deliverables, available remediation technologies from the O&G industry and previous EU projects will be reviewed and evaluated towards their application to CO_2 wells.

1 INTRODUCTION

This report is part of the research project MiReCOL (Mitigation and Remediation of CO_2 leakage) funded by the EU FP7 programme. Research activities aim at developing a handbook of corrective measures that can be considered in the event of undesired migration of CO_2 in the deep subsurface reservoirs. MiReCOL results support CO_2 storage project operators in assessing the value of specific corrective measures if the CO_2 in the storage reservoir does not behave as expected. MiReCOL focuses on corrective measures that can be taken while the CO_2 is in the deep subsurface. The general scenarios considered in MiReCOL are 1) loss of conformance in the reservoir (undesired migration of CO_2 within the reservoir), 2) natural barrier breach (CO_2 migration through faults or fractures), and 3) well barrier breach (CO_2 migration along the well bore).

In a CO_2 storage project, well integrity failure is generally considered to represent one of the highest risks of leakage. Generally, WBEs that are exposed to CO_2 are most prone to leakage. Ageing issues with cement degradation, casing corrosion and wear, and thermal loads imposed on the well infrastructure are examples of causes of well leakages. Such well integrity failure has the potential to lead to catastrophic CO_2 leakages with large safety and environmental consequences.

As the technology for drilling and completion of wells for CO_2 storage is largely the same as is used by the oil and gas (O&G) industry, much of that experience of causes of leakage and remediation methods can be directly transferred. Other aspects that are more relevant to CO_2 wells, such as chemistry and time effects, require some additional consideration.

The objective of this first deliverable related to well leakage remediation best practice is to describe the most relevant scenarios for leakage of CO_2 from storage reservoirs from active and abandoned wells, and to evaluate the consequences of the leak in each scenario. The partners agreed to approach this task in terms of well barrier element failure, conceptually following the NORSOK D-010 standard from the O&G industry, instead of a qualitative Features-Events-Processes (FEP) approach. If needed for the assessment of large scale processes, such as reservoir pressure and regional stress changes, a FEP analysis will be applied.

This report presents a brief introduction to well barriers and well barrier elements (WBE), followed by a description of WBE failure modes and consequences of leakage through those failed WBEs.

Next, the report describes the dramatic case of a blow-out during drilling operations in 1968 at the Bečej natural CO_2 field, which was followed by uncontrolled migration of gas from the reservoir into the overburden that lasted until 2007 when remediation actions were successfully applied. Although this blowout occurred while drilling into a natural CO_2 field and is therefore not directly relevant for active and abandoned CO_2 injection wells, the description of the remedial actions taken afterwards provide valuable input for the work to be done in SP3. Our project partner NIS is the operator of the Bečej natural CO_2 field and thus brings first-hand experience with CO_2 well leakage and remediation to the Consortium.

As a knowledge base and to avoid duplication of work, an overview of the work related to well integrity and well leakage scenarios in the EC projects CO_2CARE, SiteChar and ULTimateCO_2 is given in the following chapter.

Finally, the report closes with some concluding remarks.

1.1 Objective of this report

This report is the first deliverable within the sub-project "Leakage along wells" of the MiReCOL project. The aim of this subproject is to review and assess the efficiency of measures for mitigation and remediation of CO_2 leakages from wells. Both best practices and current remediation technologies from the oil and gas industry as well as new developments and emerging technologies will be included in the analysis. Future work will focus on the review and assessment of O&G mitigation and remediation measures, the experimental assessment of various novel materials and the review of the new developments in well leakage remediation techniques.

This deliverable aims at describing the most relevant scenarios for leakage of CO_2 from storage reservoirs via different types of wells. Following reports will review measures in the O&G best practice portfolio and assess the efficiency of these as measures for mitigation of CO_2 leakage for the most relevant leakage scenarios. This work will contribute to the integration of the findings from all subprojects, in particular to the discussion of possible new risks associated with the use of wells in the mitigation and remediation measures that are discussed in other subprojects. Furthermore, current knowledge gaps will be highlighted and recommendations for improvements will be provided.

2 WELL INTEGRITY AND WELL BARRIERS

Requirements and guidelines for well integrity can be found in the NORSOK D-010 standard, which describes well integrity for all well operations in Norway. Norwegian regulations are considered as some of the most stringent in the world, and the NORSOK D-010 standard is generally deemed to be a good example for obtaining and managing well integrity; including the two-barrier philosophy.

Well integrity is defined as "the application of technical, operational, and organizational solutions to reduce risk of uncontrolled release of formation fluids and well fluids throughout the life cycle of the well" (NORSOK D-010). The "technical" aspect of well integrity refers to the installation and use of well barriers to prevent leakages from the well.

2.1 Two-barrier principle

The central aspect of the NORSOK D-010 standard is the "two-barrier principle", which implies that two independent well barriers shall be present at all times, where "Well barrier" and "Well barrier element" are defined as:

Well barrier: Envelope of one or several well barrier elements preventing fluids from flowing unintentionally from the formation into the wellbore, into another formation or to the external environment.

Well barrier element (WBE): A physical element which in itself does not prevent flow but in combination with other WBE's forms a well barrier.

In other words, each well barrier can be seen as a chain of connecting well barrier elements (i.e. well components such as tubing, cement, etc.) that constitute a well barrier envelope, as illustrated in Figure 1 below. There shall be at least two such independent well barrier envelopes in the well, the primary and secondary envelope, respectively, and these should not have common well barrier elements.

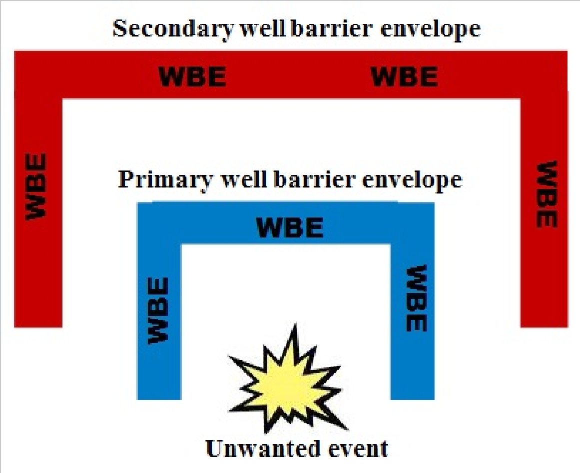

Figure 1 Illustration of the two-barrier principle: Two well barrier envelopes that consist of different well barrier elements (WBEs) that contains the leakage (unwanted event).

3 DESCRIPTION OF WELL BARRIER ELEMENTS (WBE)

Well leakages are caused by failure of one or more well barrier elements; otherwise the well integrity would be intact. Below is a description of the most common WBEs found in CO_2 wells, categorized for active wells (i.e. injection/production/monitoring wells) and abandoned wells, respectively.

3.1 Active wells

An example of a well barrier schematic for an active CO_2 well (i.e. injection/ production/monitoring) is shown in Figure 3.1 below, where both primary and secondary well barrier envelopes consisting of different WBEs are shown. Note that this example is for a platform well; the well barrier schematics for a subsea well can be slightly different.

Descriptions of all the WBEs found in Figure 2 with possible preventative measures are given below in alphabetical order:

Casing cement: Cement in annulus between casing and formation. The cement is placed as a slurry in the annulus during well construction, and hardens in-situ to support the casing and provide zonal isolation in the annulus.

> Possible preventive measures: Ensure good mud removal during cement placement to avoid mud channels in cement and microannuli. Rotate casing during cementing and use sufficient number of centralizers. Material selection: use expandable cement to avoid shrinkage and formation of microannuli, and use flexible cement systems that can withstand the tensile stresses and loads the cement will be exposed to during the well lifetime. Consider using CO_2-resistant cement if directly exposed to CO_2.

Casing hanger: A hanger element made of steel that supports the weight of the casing and provides a seal between the casing, wellhead and Christmas tree.

> Possible preventive measures: Material selection; use high-quality corrosion resistant steel that avoids corrosion and that withstands the expected loads and pressures during well lifetime.

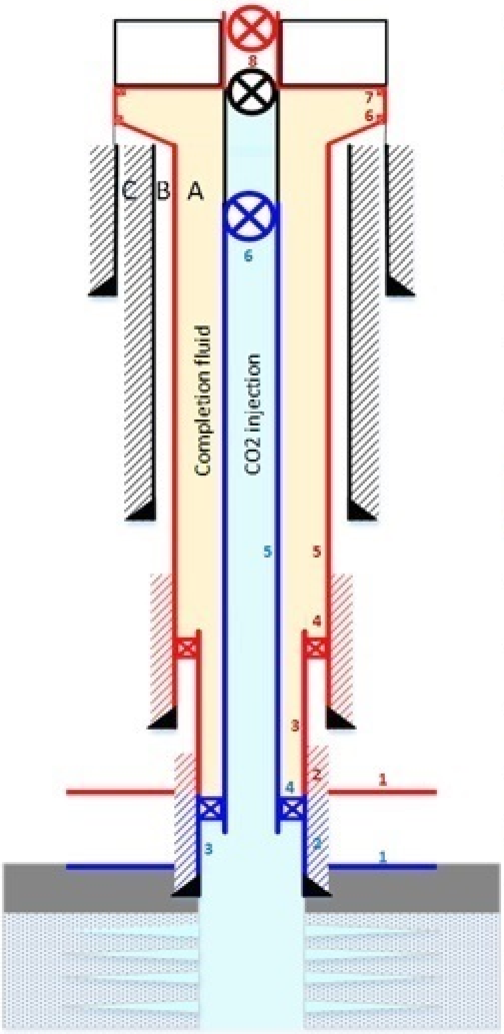

No.	Well barrier element
PRIMARY WELL BARRIER ENVELOPE	
1	In-situ formation
2	Liner cement (below production packer)
3	Liner (below production packer)
4	Production packer
5	Completion string (Production tubing)
6	Downhole safety valve (DHSV)
SECONDARY WELL BARRIER ENVELOPE	
1	In-situ formation
2	Casing cement (above production packer)
3	Liner (above production packer)
4	Liner packer
5	Production casing
6	Casing hanger
7	Tubing hanger (neck seal)
8	Wellhead / X-mas tree with valves

Figure 2 Example of a well barrier schematic with WBEs for a CO_2 injection well. Primary and secondary well barrier envelopes in blue and red colors, respectively.

Completion string (i.e. production tubing): Steel tubular that is the conduit for injection fluids into the well or production fluids from the well, depending on well type.

> Possible preventive measures: Avoid casing wear during well construction. Material selection: use high-quality corrosion resistant steel that avoids corrosion and withstands the expected loads and pressures during the well lifetime. Use premium connections that are gas-tight and that can withstand the expected loads and pressures.

Dowhole safety valve (DHSV): Valve inside tubing with a close/open mechanism that seals off the tubing bore. The valve is controlled by hydraulic pressure through a control line, and is operated in a fail-safe mode.

> Possible preventive measures: Use qualified DHSV designs and materials, and avoid corrosion/leak in hydraulic control line, regular maintenance. For production wells avoid potential scale formation.

In-situ formation: The formation that has been drilled through and is located adjacent to the annulus cement. The formation strength must exceed the maximum wellbore pressures expected during the well lifetime in order to be qualified as a WBE.

> Possible preventive measures: Good knowledge of the subsurface/formation properties, by logging and by performing XLOT tests.

Liner: Steel tubular, with similar function as casing, that does not extend all the way to surface.

> Possible preventive measures: Avoid casing wear during well construction. Material selection; use high-quality corrosion resistant steel that avoids corrosion and that withstands the expected loads and pressures during the well lifetime. Use premium connections that are gas-tight and that can withstand the expected loads and pressures.

Liner cement: Cement in annulus between liner and formation. The cement is placed as a slurry in the annulus during well construction, and hardens in-situ to support the liner and provide zonal isolation in the annulus.

Possible preventive measures: Ensure good mud removal during cement placement to avoid mud channels in cement and microannuli. Rotate liner during cementing and use sufficient number of centralizers. Material selection; use expandable cement to avoid shrinkage and formation of microannuli, and use flexible cement systems that can withstand the tensile stresses and loads the cement will be exposed to during well lifetime. Consider using CO_2-resistant cement if directly exposed to CO_2.

Liner packer: Sealing device made of steel and/or elastomer that seals the annulus between the liner and production casing.

Possible preventive measures: Material selection: ensure that the sealing elements in packer withstand the chemical and physical environment throughout the well lifetime. Avoid casing wear at the packer setting depth to ensure good seal around the packer.

Production casing: Steel tubular that extends all the way to surface.

Possible preventive measures: Avoid casing wear during well construction. Material selection: use high-quality corrosion resistant steel that avoids corrosion and that withstands the expected loads and pressures during well lifetime. Use premium connections that are gas-tight and that can withstand the expected loads and pressures.

Production packer: Sealing device made of steel and/or elastomer that seals the annulus between the production tubing and production casing/liner.

Possible preventive measures: Material selection: ensure that the sealing elements in packer withstand the chemical and physical environment throughout the well lifetime. Avoid casing wear at packer setting depth to ensure good seal around the packer.

Tubing hanger: A hanger element made of steel that supports the weight of the tubing and provides a seal between the tubing, wellhead and X-mas tree.

Possible preventive measures: Material selection: use high-quality corrosion resistant steel that avoids corrosion and withstands the expected loads and pressures during the well lifetime.

Wellhead/X-mas tree: The wellhead provides mechanical support for casing and tubing strings, and prevents flow from the bore and all annuli to the environment. The X-mas tree, which is supported by the wellhead, consists of a housing with several different valves that controls the flow of injection/production fluids, as well as annuli monitoring.

Possible preventive measures: Material selection: use high-quality corrosion resistant steel that avoids corrosion and withstands the expected loads and pressures during the well lifetime, regular maintenance.

3.2 Abandoned wells

An example of a well barrier schematic for an abandoned CO_2 well is shown in Figure 3.2 below, where both primary and secondary well barrier envelopes consisting of different WBEs are shown.

Descriptions of all the WBEs found in Figure 3 with possible preventive measures are given below in alphabetical order:

Casing: Steel tubular that extends all the way to surface.

Possible preventive measures: Material selection: use high-quality corrosion resistant steel that avoids corrosion. Consider removing the casing by milling prior to abandonment.

Casing cement: Cement in annulus between casing and formation. The cement is placed as a slurry in the annulus during well construction, and hardens in-situ to support the casing and provide zonal isolation in the annulus.

Possible preventive measures: Ensure good mud removal during cement placement to avoid mud channels in cement and microannuli. Rotate casing during cementing and use sufficient number of centralizers. Material selection: use expandable cement to avoid shrinkage and formation of microannuli, and use flexible cement systems that can withstand the tensile stresses and loads the cement will be exposed to during the well lifetime. Consider using CO_2-resistant cement if directly exposed to CO_2.

Cement plug: Solid plug of cement in the wellbore that prevents flow of formation fluids.

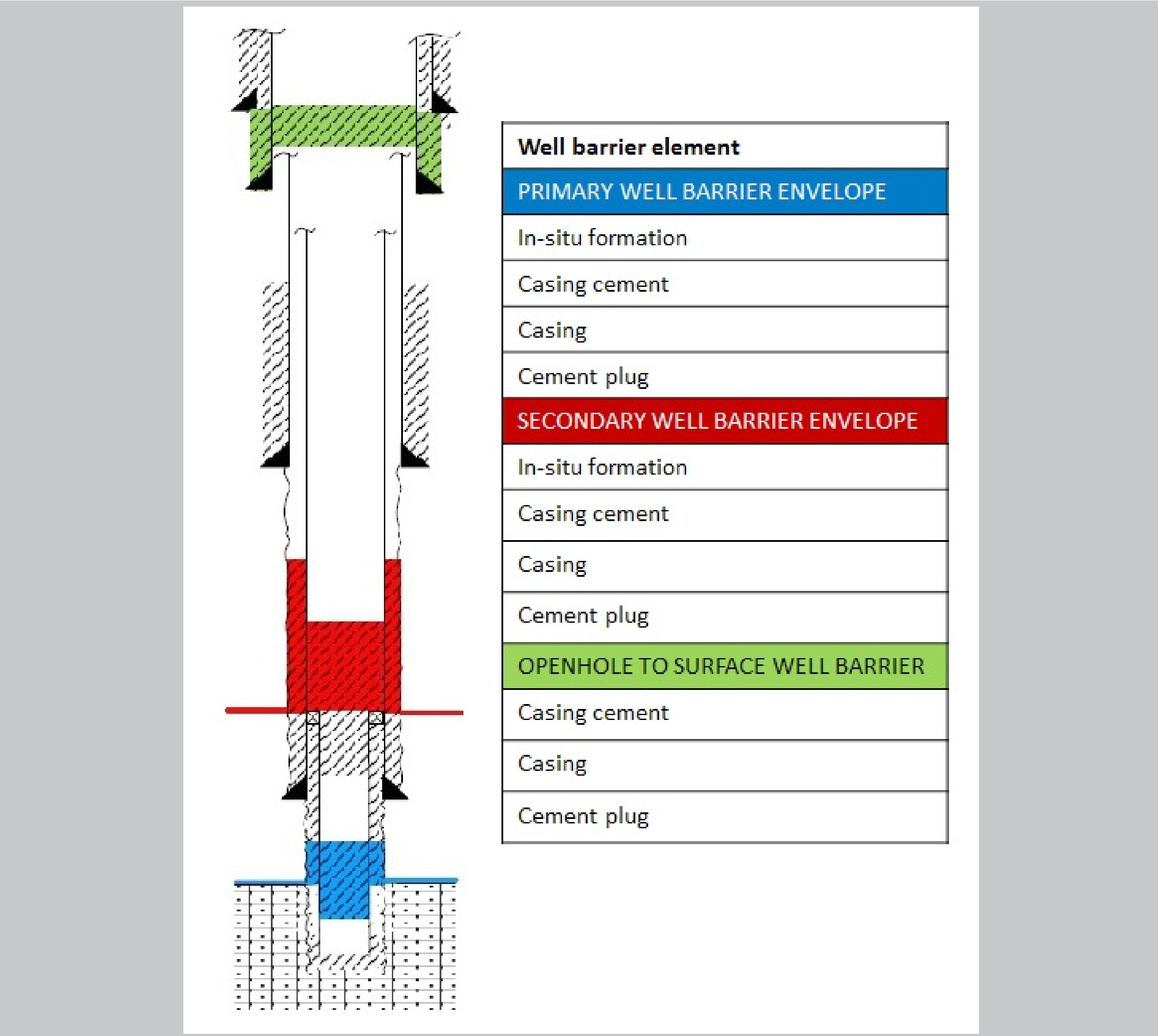

Figure 3 Example of a well barrier schematic with WBEs for an abandoned CO_2 well. Primary and secondary well barrier envelopes in blue and red colors, respectively, with the "openhole to surface" barrier in green (based on NORSOK D-010).

Possible preventive measures: Ensure good mud removal during cement placement to avoid mud channels in cement and microannuli. Material selection; use expandable cement to avoid shrinkage and formation of microannuli, and consider use of flexible cement systems that can withstand the movements/loads the cement will be exposed to after well abandonment. Consider using CO_2-resistant cement if directly exposed to CO_2. Use of a mechanical bridge plug as a foundation to ensure good plug placement.

In-situ formation: The formation that has been drilled through and is located adjacent to the annulus cement or cement plugs placed in the wellbore. The formation strength must exceed the maximum wellbore pressure expected during the life of the well in order to be qualified as a WBE.

Possible preventive measures: Good knowledge of subsurface/formation properties, by logging and by performing XLOT tests.

4 CAUSES AND CONSEQUENCES OF WELL LEAKAGES

If a leak occurs, the first cause of action will be to determine the cause of the leak; i.e. which of the well barrier element(s) has failed. When the cause of the leak has been determined, remedial actions can proceed.

4.1 WBE failures in active wells

Figure 4 shows an illustration of some possible leak pathways due to WBE failures in an active CO_2 well.

An overview of causes and consequences of different WBE failures in active CO_2 wells is listed below in alphabetical order:

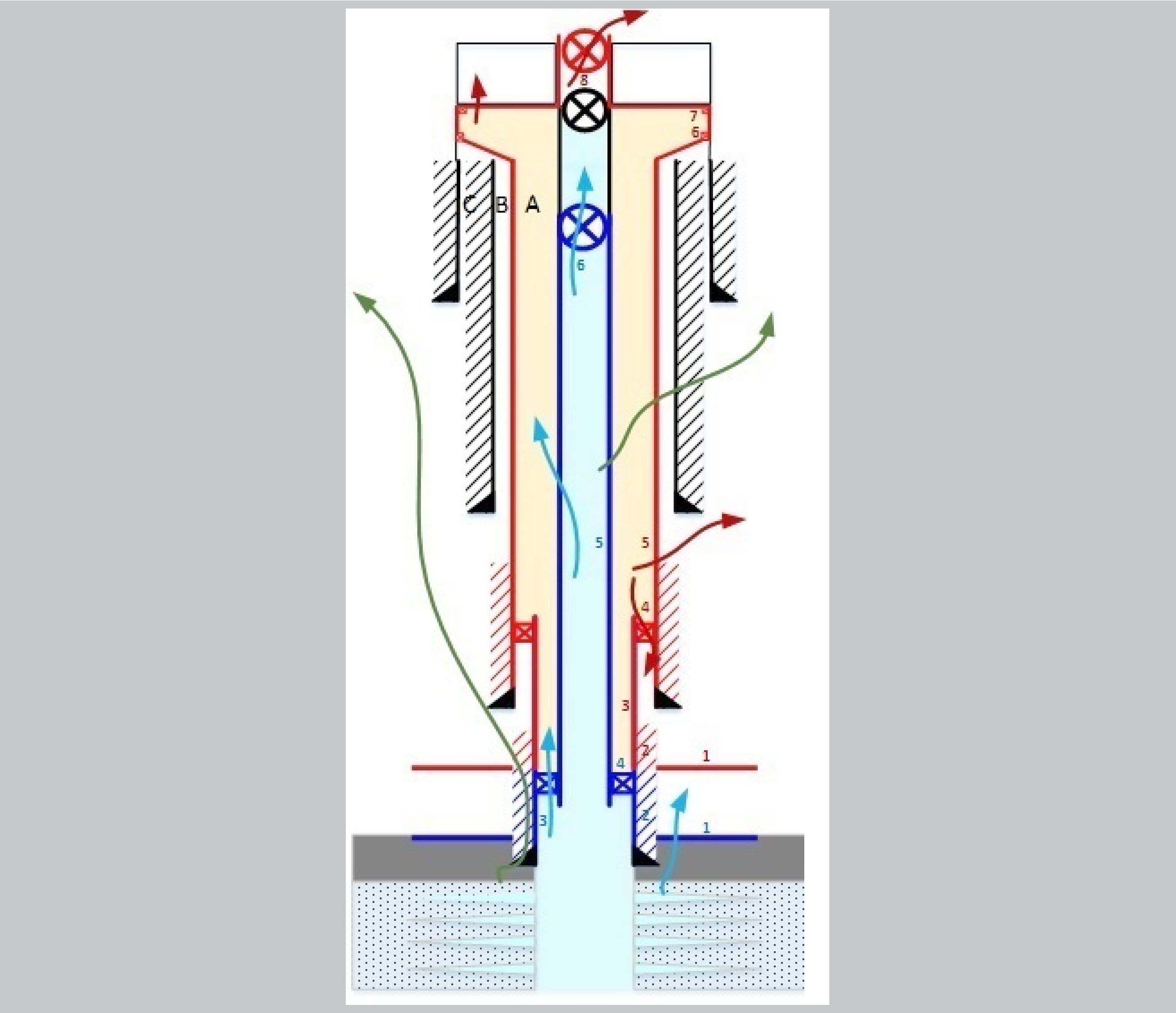

Figure 4 Schematic illustration of some possible leak pathways due to WBE failures in an active CO_2 well. Blue arrows show failure of primary well barrier envelope, red arrows show failure of secondary well barrier envelope, and green arrows show failure of multiple WBEs.

Annulus cement (for casing and liner):
Causes of failure: Presence of mud channels, gas channels or microannuli formed during well construction that act as leak pathways. Formation of radial cracks and microannuli (i.e. de-bonding) due to temperature and pressure cycles during injection/production. Possibly CO_2 degradation.

Consequences: Loss of zonal isolation and pressure build-up in annulus. Possible upwards migration of formation fluids along the outside of the well, if formation strength is too low, i.e. failure of a second WBE and potential leak to the environment.

Casing hanger / Tubing hanger:
Causes of failure: Material degradation due to corrosion and/or fatigue. Poor initial design with respect to material selection and/or expected loads and pressures. Exposure to annulus pressures and loads outside design envelope; for example due to wellhead growth.

Consequences: Leakage into the environment (if the primary WB fails as well).

Completion string (i.e. production tubing):
Causes of failure: Material degradation due to fatigue, corrosion and/or erosion. Failure of tubing connections. Poor initial design with respect to material selection and/or expected loads and pressures.

Consequences: Pressure communication through tubing, resulting in pressure build-up in annulus A.

Downhole safety valve (DHSV):
Causes of failure: Material degradation due to corrosion of flapper valves and/or control line. Scale build-up preventing proper valve closure, overpressure.

Consequences: Loss of sealing ability for flapper valve failure or loss of functionality for control line failure (hydraulic failure).

In-situ formation:
Causes of failure: Drilling-induced damage to formation. Reduced formation strength due to presence of microcracks and fracures. Poor bonding to cement.

Consequences: Fracture propagation and growth upwards through formation or along wellbore. May create leak to surface.

Production casing / liner:
Causes of failure: Material degradation due to corrosion or casing wear. Burst or collapse of casing if internal or external annulus pressures exceed casing strength. Failures of casing connections. Poor initial design with respect to material selection and/or expected loads and pressures.

Consequences: Pressure communication between adjacent annuli through casing, thereby possibly causing pressure build-up in several annuli.

Production packer / liner packer:
Causes of failure: Chemical or thermal degradation of sealing material in packer. Poor sealing towards oval casing damaged by casing wear.

Consequences: Loss of sealing ability. Pressure build-up in annulus above packer, or downwards fluid migration from annulus into surrounding (weak) formation, which may lead to further fracture propagation.

Wellhead / X-mas tree:
Causes of failure: Material degradation due to corrosion and/or fatigue. Poor initial design with respect to material selection and/or expected loads and pressures. Exposure to annulus pressures and loads outside design envelope; for example due to wellhead growth.

Consequences: Leakage into the environment and to the surface, if the primary barrier fails as well.

4.2 WBE failures in abandoned wells

An overview of causes and consequences of different WBE failures in abandoned CO_2 wells is listed below in alphabetical order:

Casing:
Causes of failure: Material degradation due to corrosion. For legacy wells, possible degradation due to vertical stress changes (reservoir de-compaction).

Consequences: Formation of leak paths along/through casing if degraded. Fluid migration upwards through the barrier.

Casing cement:
Causes of failure: Presence of mud channels, gas channels or microannuli formed during well construction that act as leak pathways. Formation of radial cracks and microannuli (i.e. de-bonding) due to previous temperature and pressure cycles during injection/production phase. Possibly CO_2 degradation. For legacy wells, possible cracking and de-bonding due to vertical stress changes (reservoir de-compaction).

Consequences: Loss of zonal isolation, fluid migration upwards through barrier and pressure build-up in well above cement. Possible upwards migration of formation fluids along the outside of the well, if formation strength is too low. For surface barrier: Leakage into the environment.

Cement plug:
Causes of failure: Presence of mud channels or microannuli formed during plug placement that act as leak pathways. Shrinkage of cement during setting can create considerable microannuli/gaps around plug. Possibly CO_2 degradation. For legacy wells, possible cracking and de-bonding due to vertical stress changes (reservoir de-compaction).

Consequences: Fluid migration upwards through cement plug and pressure build-up in well above cement. For surface barrier: Leakage into the environment.

4.3 Most likely WBE failures

Relatively few studies have been published that provide reliable statistical information on the failures of different well barrier elements, but one such study has been published by Vignes and Aadnøy (2008).

In this study, a total of 406 wells from 7 different operators where mapped by the Norwegian Petroleum Safety Authorities (PSA). It was found that 75 of these wells had well integrity issues; i.e. 18 % of all the wells had experienced problems. An overview of which WBEs that failed in these 75 wells was also given in the study. Table 1 lists the failure percentages of the WBEs most relevant for CO_2 wells. As this study surveyed only wells in operation, it is only relevant for active CO_2 wells, not abandoned wells.

From these results it is seen that the tubing is the WBE that is by far the most likely to fail; probably due to corrosion and/or connection failures. The casing and the cement also have considerable failure percentages.

Table 1 Overview of WBE failures for wells in operation (Vignes and Aadnøy, 2008)

Casing	Cement	DHSV	Packer	Tubing	Wellhead
11 % of failures	11 % of failures	3 % of failures	5 % of failures	39 % of failures	5 % of failures

Furthermore, the study also revealed a difference between production and injection wells. Of the 406 wells included in the study, 323 were production wells and 83 were injection wells, as listed in Table 2 below. 48 production well failures were reported (i.e. 15 % of all production wells), whereas 27 injection well failures were reported (i.e. 33 % of all injection wells).

Table 2 Well integrity failures of production and injection wells (Vignes and Aadnøy, 2008)

	Total number wells	Wells with WI failure
Production wells	323	48
Injection wells	83	27
TOTAL	406	75

Injection wells are therefore significantly more likely to fail than production wells, and this finding is very relevant for CO_2 storage since most CO_2 wells are injection wells. The reason for this difference is, however, unknown.

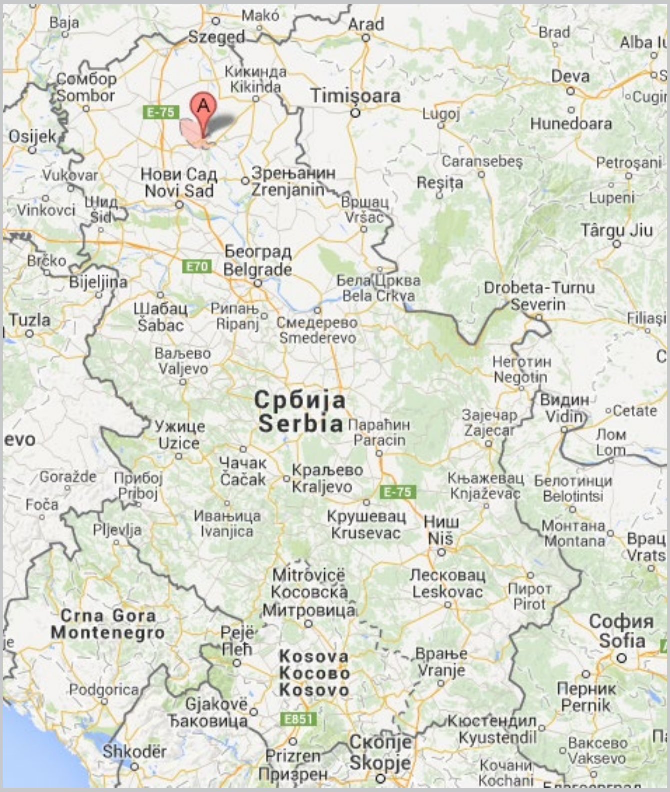

Figure 5 Location of Becej (A) in Serbia (courtesy of Google Maps)

5 BLOW-OUT AT BEČEJ NATURAL CO_2 FIELD IN 1968/69

In the following, the dramatic case of blow-out during drilling operations at the Bečej natural CO_2 field is described. Although this blowout occurred while drilling into a natural CO_2 field and is therefore not directly relevant for active and abandoned CO_2 injection wells, the description of the remedial actions taken afterwards provide relevant input for the work to be done in SP3.

The natural CO_2 gas field Bečej was discovered in 1951 by the borehole Bč-2. It is situated between Bačko Petrovo Selo and Bečej, and extended partially beneath the city Bečej, in northern part of Republic Serbia – Vojvodina Province, at the bank of Tisa River (Figure 5).

During drilling of well Bč-5 by the end of 1968, an uncontrolled and spontaneous gas eruption happened when the bit entered the Miocene layer at the depth of 1,092.50 –1,093.35 m (Figure 6). The blowout could not be controlled and lasted for eight months (until mid 1969 - 209 days) when the lower section of the open borehole collapsed. After that, the blowout continued for another 57 days. During this second period of the blowout, the free gas jet created a crater at the surface around the borehole and discharged high amounts of clay and sand containing slurry (www.youtube.com/watch?v=-riYk2J0B0c 0:46-1:44). Unfortunately, the eruption claimed several human lives and caused serious damages in surface facilities.

After this second period of blowout, the surface eruption ceased, however, gas continued to migrate from the geological reservoir. Regular periodic measurements and monitoring of the reservoir pressure after 1975 showed an intensive leakage/migration of CO_2 into the upper/shallower horizons through the collapsed borehole, i.e. an underground gas migration. This was also supported by chemical analysis of gas stored in those layers. From 1968 to 2001, the reservoir pressure dropped from 150 bar to 117 bar, which cannot solely be accounted to CO_2 production.

Several other issues, especially unfavorable reservoir geological parameters led to the conclusion that the gas migration problem could not be solved by conventional and routine well treatment or work-over techniques such as cementing. In order to control and stop the CO_2 migration (Medic et al. 2008, Lakatos et al. 2009), NIS engaged in 2007 in a series of activities, which are described below.

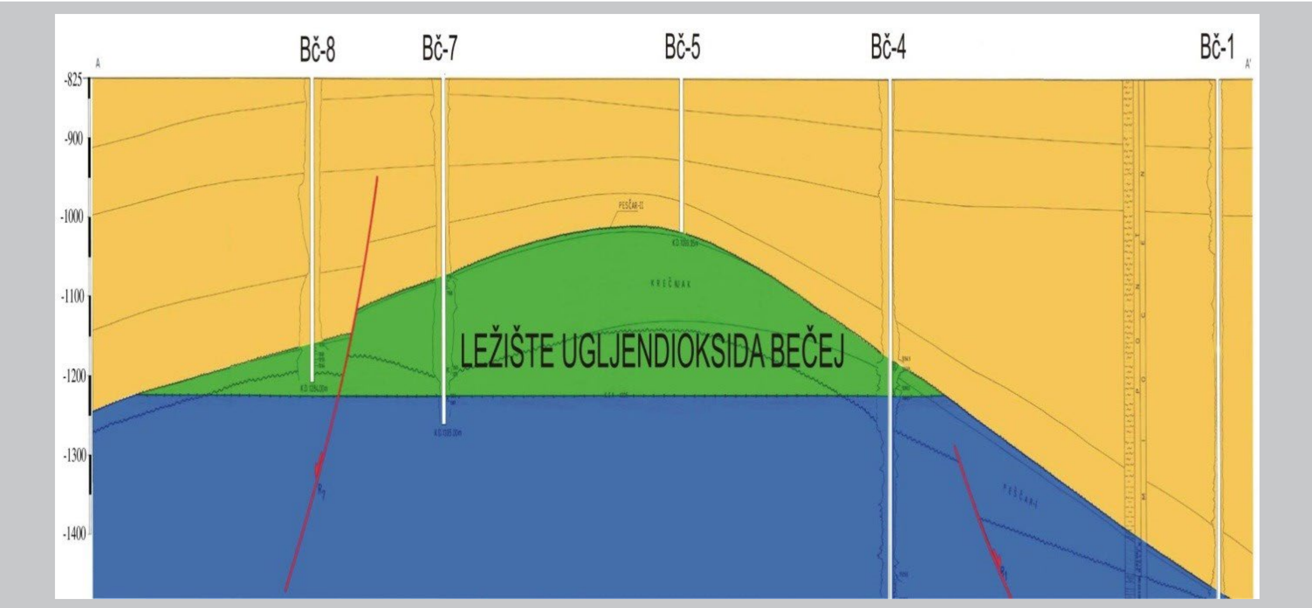

Figure 6 Geologic profile of Bečej field at the location of Bč-5 well.

5.1 Summary of Bč-5 drilling operation and blow-out/eruption

The exploration well Bč-5 was spudded on 30th October 1968. All drilling operations stopped after 12 days on 10th November 1968 due to the blow-out, at total depth of 1092.50 – 1093.25 m in the Miocene sandstone formations. The well Bč-5 was drilled with bentonite mud with sodium hydroxide additive, and occasionally weighted by barite.

During the drilling operation, at a depth of 361m there was gas influx into the mud that reduced the mud density from 1.28 g/cm^3 to 1.17 g/cm^3. On this occasion, the mud was pulsating and spilled out for 2-3 minutes over the flowline. By the end of the third shift the mud was weighted to 1.20 g/cm^3. In the interval of 400-480 m the well continued to pulsate occasionally and mud was increasingly weighted first to 1.24 g/cm^3, and then because of continuing pulsation to 1.28 g/cm^3. Drilling operation was continued during 6th November with this mud weight.

Due to the risk of possible mud loss on 7th November the mud density was reduced to 1.25 g/cm^3 and later to 1.24 g/cm^3. At a depth of 628.30 m, during circulation/washing prior to coring operation (core no. 2), a slight increase of gas concentration in the mud was noticed. During 8th, 9th and 10th November, the mud density ranged from 1.26 to 1.30 g/cm^3 while the viscosity ranged between 38 and 40 sec.

Drilling operations were taking place normally, without major delays or problems, until 10th November at 01:45 h. During drilling at depth 1092.50 – 1093.25 m, the whole assembly of drilling tools suddenly dropped 0.75 m and the tools were pulled up for circulation/washing. During circulation, it was noticed that mud spilled out on the wellhead, over flow line and mud pits. The BOP was activated immediately but was not successfully closed completely. The blowout became more intensive and after 5 minutes the ejected mud column was as high as the drilling rig. After approximately 15 minutes, the well started to blow out only gas; methane for about 30 minutes, and then "pure" CO_2. The blowout could not be stopped after that.

Possible reasons for the blow-out of well Bč-5 are:

- Unfavorable geological (reservoir) parameters, such as very complex geological conditions, tectonic stress, existence of networks of faults and fractures, several superimposed shallower sandy layers/horizons – secondary CO_2 accumulations/ reservoirs/pools, over-pressurized major Bečej CO_2 pool etc.
- Despite the fact that Bč-5 was the fifth well, it can be said that there was not enough data, and that the quality of the data did not give the possibility of creating more accurate/reliable geological model which implies different well construction, mud design etc.
- The technological standard of the time was much lower than today

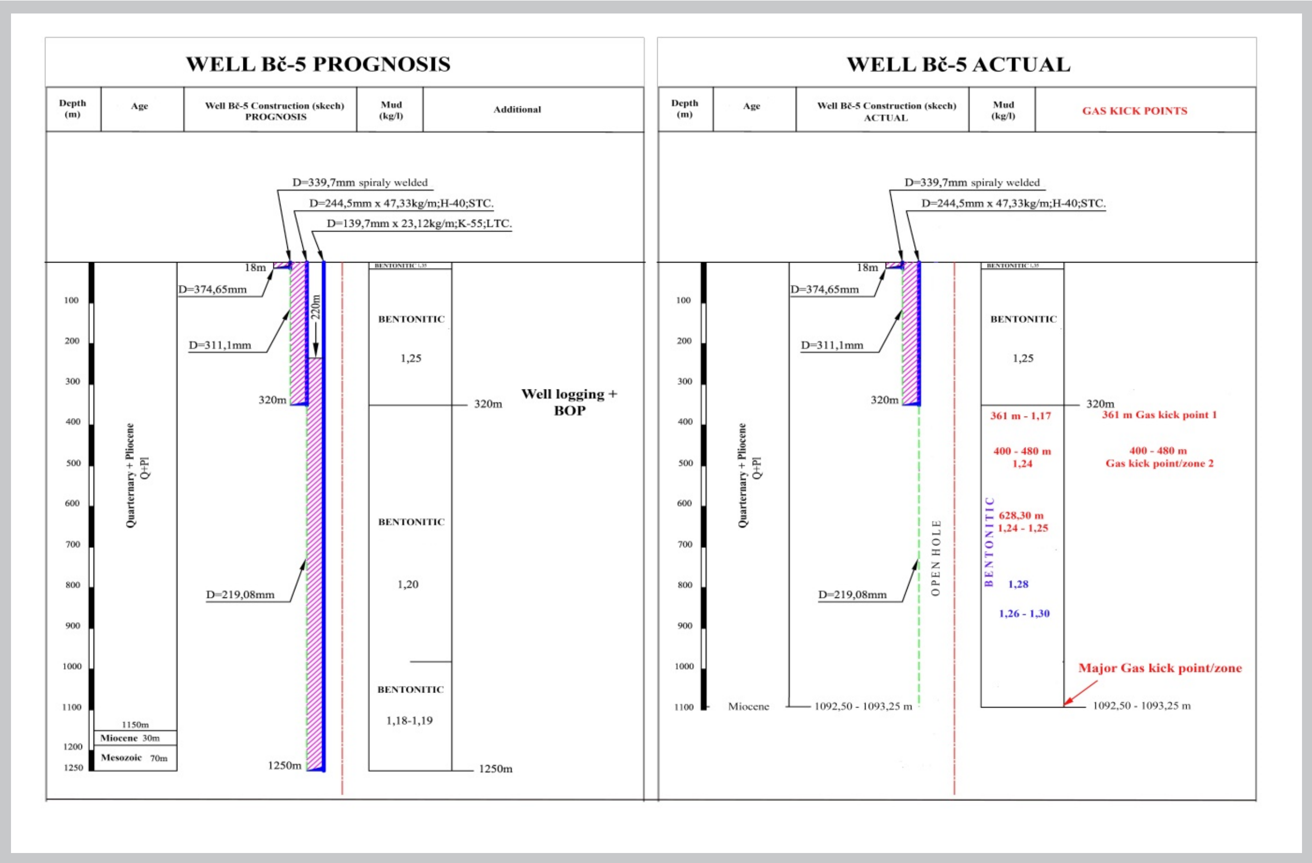

Figure 7 Schematic of prognosticated (left) and actual (right) well Bč-5.

5.2 Implementation of remediation project

In order to remediate the uncontrolled migration of CO_2 gas from Bč-5, a co-operation with the Institute of Applied Chemistry at the University of Miskolc, Hungary, was established in 1991. A project for remediation and mitigation "Revitalization Project for CO_2 gas migration control in the Bečej-5 Well" was initiated in 1992, but was not realized.

During 2007, a remediation operation to stop the uncontrolled gas migration was performed successfully. This operation was performed in a triangular well layout formed by the damaged well Bč-5 and the two directional wells Bč-x1 (Figure 5.4) and Bč-9 (Figure 5.5). The remediation procedure consisted of injecting various chemical solutions to clog the flow paths, via the directional well Bč-9, with constant monitoring of wells Bč-x1 and Bč-5 as control points. This is described in more detail below.

Well Bč-x1, a deviated well, was drilled 240 m away from Bč-5 targeting the bottom hole of the collapsed wellbore, with the aim of mitigating gas loss and observing the underground flow processes. The well Bč-x1 was completed at a depth of 1150.70 m, but mitigation works were not performed because of self-strangulation of well Bč-5. It is assumed that the bottom of well Bč-x1 is located within a diameter of about 15 m from the nominal borehole Bč-5, as shown in Figure 8 below. The deviated, directional well Bč-x1 served as observation well and/or as an alternative remediation well. The Bč-x1 well was reworked and completed in a similar manner as well Bč-9, except that the tubing was equipped for pressure monitoring.

Well Bč-9, another deviated recovery well, was also drilled in the immediate vicinity of the damaged well Bč-5. The well was properly completed with minor issues of kicks and fluid loss. The final depth reached was 15 m above the planned depth of the well, and it approached the nominal shoe of the Bč-5 well to a horizontal distance of 11 m, as shown in Figure 9. The last casing, 5", was completely cemented and perforated in the interval of 1131-1133 m.

Remediation operations took place in the period 01.05.-01.07.2007. The operations were performed with the use of a number of new methods and technical procedures that had not been used before by NIS Naftagas. The operation was performed through the well Bč-9 with the permanent monitoring wells Bč-5 and Bč-xl as control points. In accordance with the designed protocols (physical-chemical properties of the fluids, pressure and volume), a total of 1700 m^3 of different chemical solutions (water glass, polymer, activators, cross linking agent and acid) were injected into the bottom region of the damaged well Bč-5, with 150 m^3 of water as a precursor and 200 m^3 of water to finish. Injection capacity was 50 m^3 per day, and the pressure in the injection well head 5 – 35 bar. A field laboratory was established at the site to check the physical-chemical characteristics of the fluids, and also for fluid preparation such as a new type of gel-breaking polymers. The injection was performed using two triplex pumps plunge Union TD 60 on electric drive, which was also a novelty. Early monitoring measurements in the control wells Bč-5 and Bč-x1 indicated that a positive result could be expected and that the uncontrolled migration of CO_2 would be significantly reduced or completely stopped.

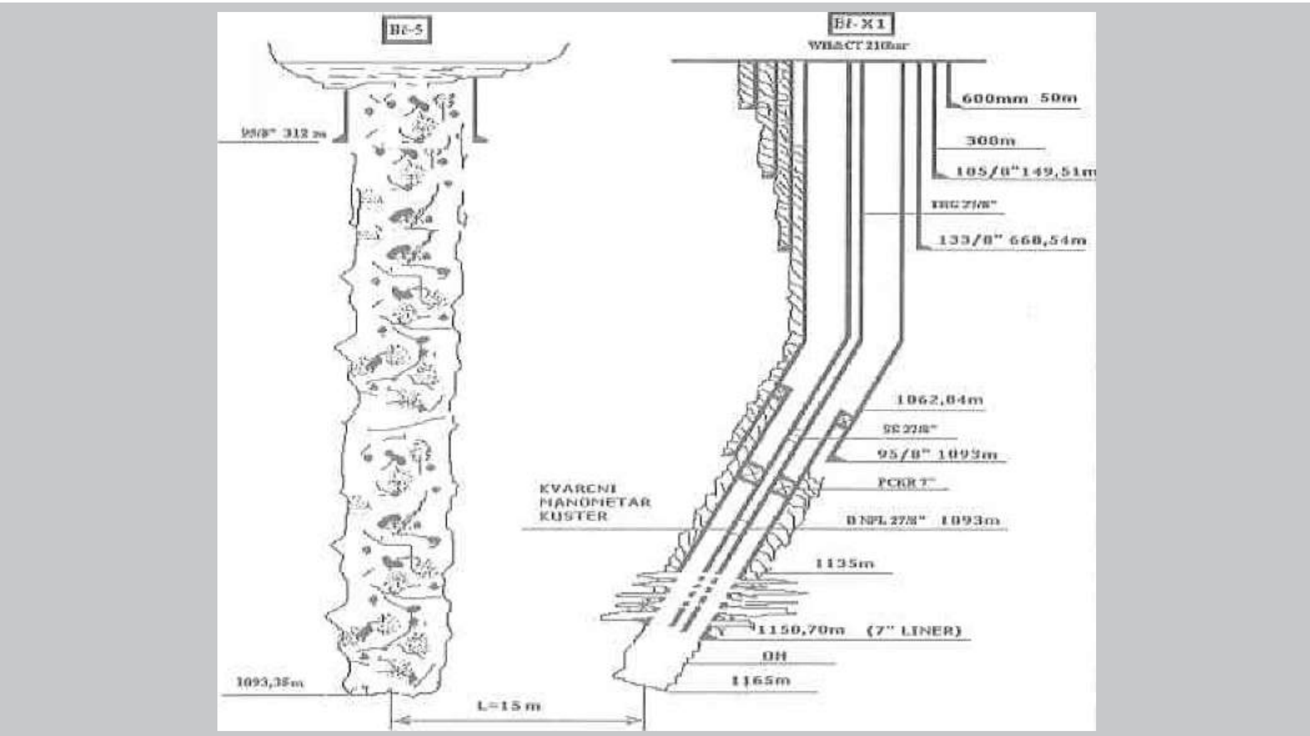

Figure 8 Well schematics for wells Bč-x1 and Bč-5.

5.3 Effect of remediation action

During injection of chemicals into well Bč-9, permanent reduction of gas was registered by accumulation of water in well Bč-5, which at the end of the operation practically ceased. Also, at well Bč-x1, a constant moderate growth of pressure at the bottom of the borehole was recorded during the early phase of operations, and by the confluence of fluids through opened intervals in the last week of the operation and after its completion. The level of fluid in the tubing at Bč-x1 in the period 07.01.2007-28.08.2007 increased from 900 m to 400 m, with an increase in pressure at the bottom of the borehole of 20.8 bar. These were the first encouraging signs that the damaged well Bč-5 and well Bč-x1 were filled with chemicals injected through well Bč-9. Therefore, the remediation procedure seems to have been successful.

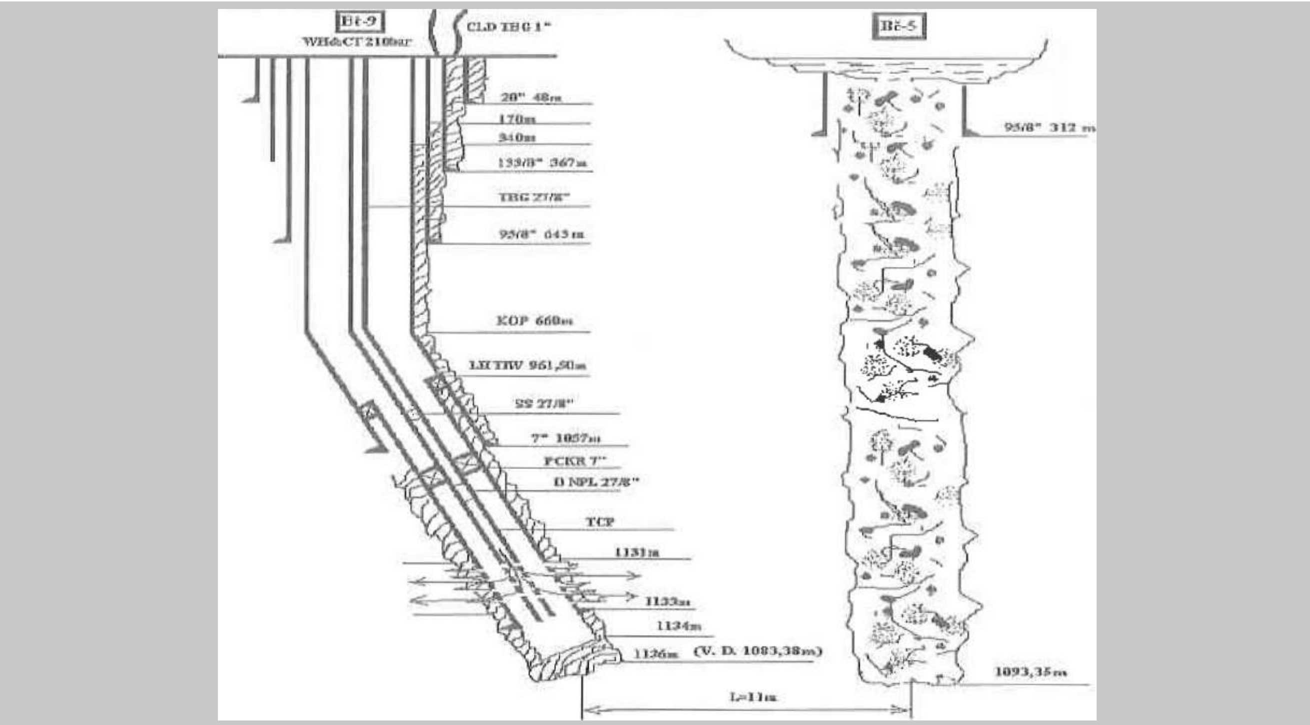

Figure 9 Well schematics for wells Bč-9 and Bč-5.

6 OVERVIEW OF RELEVANT EC PROJECTS ON CO_2 WELL LEAKAGES

This section gives an overview of research on well leakage scenarios performed in preceding EC projects. Previous research will be used in MiReCOL as a knowledge base and this summary will help to avoid duplication of work. Certainly not all relevant work performed earlier can be mentioned here. The work presented in this section can be regarded as exemplary for (some) research performed under the EC FP-7 framework.

Research activities in recent EC projects did not particularly focus on WBEs and their failure modes (to our knowledge). Basic research on degradation mechanisms of steel and cement, also on the long term, and fluid flow behavior through and along wellbore interfaces present the main focus of EC research, at least in EC projects the MiReCOL partners participated in. However, this knowledge can also be seen as highly relevant for work in MiReCOL and will be considered in the ongoing and future research in MiReCOL.

The overview focusses on three previous EC research projects:

- CO_2CARE: “CO_2 Site Closure Assessment Research” Grant agreement no: 256625; THEME ENERGY.2010.5.2-3
- SiteChar: “Characterisation of European CO_2 storage” Grant agreement no : 256705; THEME ENERGY.2010.5.2-1
- ULTimateCO_2: “Understanding the long-term fate of geologically stored CO_2” Grant agreement no.: 281196; THEME ENERGY.2011.5.2-1

6.1 CO_2CARE (2011-2013)

The aim of CO_2CARE was to support the large implementation of CCS demonstration projects by investigating the requirements for CO_2 site abandonment and to develop procedures for site closure. The work focused on three key areas:

- Well abandonment and long-term containment
- Reservoir management from closure to long-term
- Risk management methodologies

The technologies and procedures developed were evaluated on the three real CO_2 injection sites at Ketzin, Sleipner and K12-B; and dry-run applications for site abandonment have been performed for hypothetical closure scenarios.

The work included the review of current regulatory frameworks (CO_2CARE D1.1) and industry best practices (CO_2CARE D1.2) with respect to well and site abandonment.

Examples of relevant work performed:
CO_2CARE report D1.3 “Database of first abandoned CCS/ CO_2- exposed wells” (CO_2CARE,2012) refers to three CO_2 leakage events in the United States related to wellbores all of which can be used as examples and analogues for leakage events related to CO_2 storage operations.

In 1936, an exploration well at Chrystal Geyser (Utah, USA) hit an aquifer with high CO_2 concentrations, which let to regular eruptions and the release of 11.000t of CO_2 per year (Wilson et al., 2007). The well does not have a plug and can therefore act as an analogue for a worst case scenario of a leaking abandoned well. The CO_2 concentration next to the wellbore was found to be lower than environmental and safety thresholds, implicating that the risk for human and nature posed by a leaking abandoned well seems to be low (Wilson et al., 2007). It is recommended to model the impact of CO_2 release scenarios for wells at a potential storage sites before the injection of CO_2 commences to assess the actual risk for humans and environment.

At Sheep Mountain (Colorado, USA) a CO_2 blowout occurred in 1982 from a natural CO_2 reservoir, which led to a loss of well control for 17 days. After five attempts, the well was back under control and no subsequent leakage was reported. The remediation method was not further specified. The total amount of leakage was estimated to be 200.000 t of CO_2. Due to lucky circumstances (terrain, weather) nobody was seriously injured. This event can be seen exemplary for the upper limit leakage rates from a single well (Wilson et al., 2007).

An example of how to deal with legacy well has been shown at the Salt Creek CO_2-EOR operations (Wyoming, USA). It is a reasonable example of leakage over a broad area with many old wells and provides recommendations on remediation. In 2004 and 2005, approximately 0.008% of the total amount of CO_2 injected seeped to the surface in a small area which could be attributed to legacy wells and existing migration pathways in the shallow subsurface (natural oil seeps). Some seepage could be eliminated immediately. "Substantial efforts have been undertaken to locate undocumented old wells that may exist throughout the field which include magnetic detection techniques (aerial and surface), radon, methane, and CO_2 detection (spectroscopy) and well file research" (CO_2CARE D1.3). Many wells, producers, injectors or P&A, were re-worked or re-plugged to bring them up to current safety standards, and sometimes new casing strings have been set. According to the operator, well integrity can still be improved by deploying modern completion tools and advanced cementing techniques, such as cement squeeze. If standard countermeasures were not successful, the detailed remediation plan included retrieval well drains for the extraction of leaking CO_2.

In CO_2CARE WP4 "risk management" well leakage scenarios for Sleipner, Ketzin and K12-B have been investigated that were used to establish a dry-run license application for the (hypothetical) closure of the three sites (CO_2CARE D4.6 and D4.8).

Relevant work performed at the Ketzin pilot site focused on well integrity monitoring. Besides typical operational parameters, such as BHP and BHT, the extensive monitoring program included

- Permanent ring chamber pressure monitoring in all the wells
- Electromagnetic inspection of the casing thickness
- Reservoir Saturation Tool (RST)
- P-T logging
- Magneto-Inductive-Defect Detection (MID) logging measurements
- Camera inspections
- Monitoring of saturation changes is performed in a time-lapse mode by PNG (Pulsed-Neutron-Gamma)
- a Distributed Temperature Sensonr (DTS) string, installed behind the borehole casing and cemented in place

All methods confirmed that there is no risk for the confinement of the CO_2 and no leakage could be detected. The methods listed above represent state-of-the-art measures for the validation (or failure) of well barriers (in particular behind the casing), also after remedial actions have been performed.

A FEP (Features-Events-Processes) approach has been used to assess risk scenarios for Sleipner in CO_2CARE Deliverable D4.8. One of the main risk scenarios is the leakage along wellbores encountered by the CO_2 plume, also associated with earthquakes. Two main risk factors were defined regarding wells (also in combination with natural pathways):

- Corroded annular cement and/or casing of the injector as a result of the dissolution of injected CO_2. Cement plugs would also be affected after abandonment.
- Leakage through an abandoned exploration or appraisal well, if it gets in contact with the CO_2 plume

Further investigation of these scenarios revealed very low likelihood with minor consequences for both. The integrity of the injection well annulus was confirmed e.g. by a leak-off test (below the 13 3/8" casing) and a formation integrity test (FIT) below the 9 5/8" casing. In addition, they used fit-for-purpose well barrier materials, 25% chrome (stainless) duplex casing steel and Class G cement. Additionally, the steel casing joints in the storage formation are made of 13% chrome steel which is much more resistant to corrosion than typical carbon steel casings. Numerical simulations showed that the plume will (probably) not reach legacy wells penetrating the storage complex and it is recommended to have a remediation plan in place for one well close to the plume.

Well leakage scenarios at K12-B can be compared to those at Ketzin and Sleipner and are related to geo-chemical and geo-mechanical attack of the cement sheath, casing and cement plugs. But the fact that K12-B is a depleted gas reservoir requires a different approach. In the first place, the risk scenarios of well leakage in K-12B are related to geo-mechanical issues as a result of compaction of the reservoir (from >350 bars to ~40 bars) and strains along the wellbore due to subsidence, in particular de-bonding. This is representative for all depleted hydrocarbon fields as potential candidates for CO_2 storage. A proper investigation includes reservoir-scale geo-mechanical modelling to assess the strains on the wellbore and the actual condition of well barriers. The favorable geological setting of K12-B with its massive overlaying ductile rock salt layers minimizes this leakage option to almost negligible proportions, also proven by the fact that no migration along any wellbore has been detected.

CO_2CARE WP2 was dedicated to well integrity research and many relevant studies have been performed including e.g. modelling flow along the wellbore, lab experiments on potential sealants for well remediation. However, this work package did not consider leakage scenario and risk assessment procedures in detail.

Main findings of CO_2CARE and recommendations, also with respect to ensure well integrity throughout the entire life-cycle (including post-abandonment) are provided in a Best Practice Guideline and a brochure (open-access). The chapter on wellbore safety with special focus on well abandonment management comprises information on:

- Recommendations from a review of current regulatory frameworks and industry best practices
- Summary of experience with abandoned CO_2 wells
- Summary of the track record of abandoned hydrocarbon wells
- Recommended workflow for geo-mechanical wellbore stability assessment
- Geochemical and geo-mechanical interactions
- Novel well-abandonment methodologies
- Well integrity logging

All public CO_2CARE reports can be downloaded at the CO_2CARE Website.

6.2 SiteChar (2010-2013)

SiteChar aimed to improve and extend site characterization workflows for CO_2 storage and investigated the feasibility of several potential storage complexes in the EU. Main focus was on the assessment of risks and the design of monitoring plans for different storage types. Comparable with CO_2CARE, dry-run applications were developed for storage licenses at the end of the site characterization phase. Site characterization studies that also focused on well integrity were done on a site in Denmark and on a site in Poland:

Examples of relevant work performed:
In Deliverable D4.5 “Old well state, Danish site”, an onshore well in Denmark penetrating a potential storage formation has been investigated with respect to work-over and different options for mitigation and abandonment. The well is not in line with current requirements, and the abandonment method that was used poses the risk of CO_2 leakage and is being considered as not ready for CO_2 storage. Main issues are the lack of isolation between two permeable formations and the insufficient length and unknown quality of the cement plugs.

Different options are discussed for intervention:

1. Remediation could be postponed until the CO_2 plume has reached the well or a leak has been detected. This option poses high safety risks and will probably not be accepted by the competent authority for a storage license, unless the probability is very low that CO_2 reaches the well gets or experiences elevated pressure during injection.
2. The well could be reactivated to be used for monitoring and possibly as a back-up injector/producer. Given the initial results of simulations and analysis, the operational value of the well appears to be small and the option to turn it into a (stand-by) producer or injector is not attractive. To re-complete it and turn it into a monitoring well is costly, but an interesting option. Before this option becomes a viable alternative, various leakage and monitoring scenarios would have to be considered. Overall, however, the only saving that the existing well can bring with respect to a new one is an existing 13 ” casing cemented at shallow depths.
3. It could be plugged and abandoned; or an instrumented abandonment could be attempted. Plugging & Abandonment (P&A) presents the simplest solution at minimum risk, however, at the cost of reduced opportunity. Instrumented abandonment increases the residual risk of hydraulic connection. Additionally, this method has not been tested extensively to the knowledge of the authors, so some research & development work is needed before applying instrumented plugs for CO_2 storage site abandonment.

It was recommended that proper plugging and abandonment after well re-entry is the best option at this point. When further details on injection scenarios and operational plans are available, this decision should be reconsidered. This study can be seen as exemplary for dealing with legacy wells in a potential storage area. Each well and its risks have to be investigated separately, options and costs have to be established and a decision on how to proceed has to be made. For many cases, one can expect that properly re-abandoning the old well is the best possible solution.

Report D5.5 "Qualitative assessment of potential risks, Zalecze & Zuchlow site": To evaluate the risk of the potential Polish storage site, a qualitative risk assessment has been performed using the TNO CASSIF approach (Yavuz et al., 2009) as a first step. The study also included the assessment of well leakage risks. A first generic workshop was followed by another workshop dedicated to well integrity issues. This site can be seen to be representative of a depleted hydrocarbon field in an extensively explored oil & gas area with many abandoned wells. The assessment revealed that the major risk related to wells can be described by two scenarios:

1. Plug failure in older, abandoned wells that do not fulfil CO_2 storage requirements, which could lead to CO_2 migration to a shallow saline aquifer or to potable groundwater resources and soil.
2. Cement sheath failure for all, also recent wells, however with very limited consequences.

It was recommended to monitor annular pressures of old wells. Also soil, adjacent aquifer and groundwater should be monitored chemically for all wells. Remediation plans would have to be in place for working over the leaking wells in case significant leakage is detected; and plans to adapt the injection strategy accordingly would have to be developed and evaluated before injection starts. An appropriate risk assessment should be performed before injection is started, including accurate evaluation of existing and additional wells logs. Typically for this kind of assessment, the lack of information and uncertain condition of well barriers are the major issues to be addressed in every well integrity evaluation of this type.

Main results of SITECHAR, including relevant well integrity research, has been summarised in dry-run storage permit applications for the different European sites. Key messages concerning wellbore integrity drawn from SITECHAR are:

- It can be confirmed that existing or old wells represent the highest risk for all SITECHAR storage sites
- Well integrity evaluation is time consuming depending on the number of wells included in the assessment and turns out most often as insufficient as a result of missing data. As a consequence worst-case scenario (modelling) is required.
- Lack of data is of major concern for a proper well integrity evaluation, particularly for depleted hydrocarbon fields with many of wells
- Downhole monitoring might be necessary to ensure the absence of leakage if old (abandoned) wells are not remediated beforehand. Both operations are very cost-intensive and can be technically challenging.

The FEP method provides a vital tool to assess and evaluate risks related to well integrity

6.3 ULTimateCO$_2$ (2011-2015)

This project aimed at increasing the knowledge of the long-term fate of geologically stored CO_2 and at developing tools for predicting long-term storage site performance. The work focusses on the understanding of chemical and physical processes and their impact on:

- Trapping mechanisms in the reservoir
- Fluid-rock interactions and effects on mechanical integrity of the caprock system
- Leakage due to mechanical & chemical damage in the well vicinity

Since the work on well integrity focusses on the well material testing and investigation of the actual degradation processes, leakage scenario definition plays a minor role. However, the field test at Mont Terri will provide valuable insights on well material behavior, multiphase flow along a wellbore and the evolution of well material failures, which can be relevant for this subproject in MiReCOL. Leakage pathway evaluation is currently performed at small scale (e.g. in the annulus) in Task 5.3 and will be extrapolated to large scale. Both can be of high importance for future work in MiReCOL. Related ULTimateCO$_2$ deliverables on experimental and numerical studies on transport properties and well leakage pathway investigations are due next year. Since several institutes participate in both projects, a regular knowledge exchange takes place with focus on deliverables within "Long-term process study – near-well sealing integrity" work package.

Main outcomes of future ULTimateCO$_2$ deliverables will be monitored and regarded in related work in MiReCol.

7 CONCLUSION

Wells are generally considered to represent the highest risk of leakage in a CO_2 storage project. Such leakages are caused by failure of one or more well barrier elements; otherwise the well integrity would be intact.

The well barriers of active and abandoned wells have been described and causes and consequences of leakage through those well barrier elements (WBE) have been presented. Ageing issues with cement degradation, casing corrosion and wear, and thermal loads imposed on the well infrastructure are examples of the most likely causes of well leakages. The tubing is the WBE that is by far the most likely to fail, probably due to corrosion and/or connection failures. Also the casing and the cement have a significant chance of failure.

A wide range of technologies and methods from the oil & gas industry are available that can also be used for the remediation and mitigation of leakages from CO_2 wells. In the next deliverables available remediation technologies from the O&G industry and previous EU projects will be reviewed and evaluated towards their application to CO_2 wells. The remedial actions taken after the blow-out and following migration of CO_2 at the Bečej natural gas field will provide valuable input for this review.

As future work a number of laboratory tests are planned to examine the merits of new materials for remediation of well leakage. These materials include CO_2-reactive suspensions, polymer-based gels, smart cements with a latex-based component and a polymer resin for squeezing. If possible, the efficiency of a CO_2-reactive suspension will be investigated in a field test at the Serbian Bečej natural CO_2 field.

References

CO_2CARE Deliverable D1.1: Report on the international regulatory requirements on CO_2 geological storage and site abandonment. CO_2CARE report, 2011. www.CO_2care.org/FileDownload.aspx?IdFile=137&From=Publications

CO_2CARE Deliverable D1.2: Report on the current site abandonment methodologies in relevant industries. CO_2CARE report, 2012. www.CO_2care.org/SciPublicationsData.aspx?IdPublication=30&IdType=327

CO_2CARE Deliverable D1.3: Report on Database of first abandoned CCS/CO_2-exposed wells: Relevant practices and characteristics. CO_2CARE report, 2012.

CO_2CARE, Deliverable D5.4: Best Practice Guidelines. CO_2CARE report, 2013. www.CO_2care.org/FileDownload.aspx?IdFile=688&From=Publications

Lakatos I., Medic B., Jovicic D., Bašic I., Lakatos-Szabo J., "Prevention of vertical gas flow in a collapsed well using Silicate/Polymer/Urea Method", SPE-121045, presented at the 2009 SPE International Symposium on Oilfield Chemistry, held in The Woodlands, Texas, USA, 20-22 April 2009.

Medic B., Jovicic D., Basic I., "Rehabilitation of Uncontrolled Migration of CO_2 on the Gas Field Bečej", Association of Engineers and Technicians (DIT, NIS-Naftagas), Volume 38 (2008).

NORSOK D-010 "Well integrity in drilling and well operations", Standards Norway, Rev. 4, June 2013.

SiteChar Deliverable D4.5 Old well state, Danish site. SiteChar report, 2012. www.sitechar-CO_2.eu/SciPublicationsData.aspx?IdPublication=309&IdType=557

SiteChar Deliverable D5.5 Qualitative assessment of potential risks, Zalecze & Zuchlow site. SiteChar report, 2013. www.sitechar-CO_2.eu/SciPublicationsData.aspx?IdPublication=345&IdType=557

Vignes B., Aadnøy B.S., "Well-Integrity issues offshore Norway", SPE-112535, presented at the 2008 SPE/IADC Drilling Conference, held in Orlando, Florida 4-6 March 2008.

Wilson E.J., Friedmann S.J., Pollak, M.F., "Research for Deployment: Incorporating Risk, Regulation, and Liability for Carbon Capture and Sequestration", Environmental Science & Technology 41 (2007) 5945-5952.

Yavuz F., et al., "Second Generation CO_2 FEP Analysis: CASSIF – Carbon Storage Scenario Identification Framework", Energy Procedia 1 (2009) 2479-2485.

Chapter XXII

Overview of available well leakage remediation technologies and methods in oil and gas industry

Jelena Todorovic[1], Torbjørn Vrålstad[1], Maike Buddensiek[1], Jens Wollenweber[2]
[1] SINTEF PR, Norway
[2] TNO, The Netherlands

SUMMARY

The objective of this report is to review remediation measures for well leakage in the oil and gas industry best practice portfolio as well as emerging technologies. The approach is to review the technologies with respect to well barrier element failure. Squeeze cementing methods, as the most commonly used for well leakage remediation, are described in detail for different applications. Squeeze cementing can be applied for annular cement failure or casing/liner failure. A variety of sealants that can be used for squeeze cementing, well abandonment, or possibly during well construction as a prevention measure, are described in this report. Other remediation measures include repairs to or replacement of specific well barrier elements that have failed. These operations can be more or less complicated depending on the type and location of the failure. Repair/replacement operations are thus described in a general manner. Well plugging and abandonment can be considered as a last remedy, if all other options failed or are not economically viable. Plugging & abandonment is not a remediation strategy as such and is not covered in this report.

1 INTRODUCTION

This report is part of the research project MiReCOL (Mitigation and Remediation of CO_2 leakage) funded by the EU FP7 programme. Research activities aim at developing a handbook of corrective measures that can be considered in the event of undesired migration of CO_2 in deep subsurface reservoirs. MiReCOL results support CO_2 storage project operators in assessing the value of specific corrective measures if the CO_2 in the storage reservoir does not behave as expected. MiReCOL focuses on corrective measures that can be taken while the CO_2 is in the deep subsurface. The general scenarios considered in MiReCOL are 1) loss of conformance in the reservoir (undesired migration of CO_2 within the reservoir), 2) natural barrier breach (CO_2 migration through faults or fractures), and 3) well barrier breach (CO_2 migration along the well bore).

The long term safety of CO_2 storage sites is largely dependent on the integrity of wells penetrating the storage site. Loss of well integrity has been identified as a major failure factor in CO_2 storage [1, 2]. Thus prevention and remediation options for any potential leakage through wells, which has been assessed in a risk analysis, play a crucial role in large scale implementation of CO_2 storage. A remediation operation can be described as an attempt to repair a leak in a well barrier (element).

In a previous MiReCOL report [3], well leakage scenarios were described using well-barrier/element failure approach. In order to maintain well integrity two independent well barriers shall be present at all times – this is the essence of the "two-barrier principle" from the NORSOK D-010 standard [4]. In other words, each well barrier can be seen as a chain of connecting well barrier elements i.e. well components that constitute a well barrier envelope. There shall be at least two such independent well barrier envelopes in the well, the primary and secondary envelope respectively, and these should not have common well barrier elements.

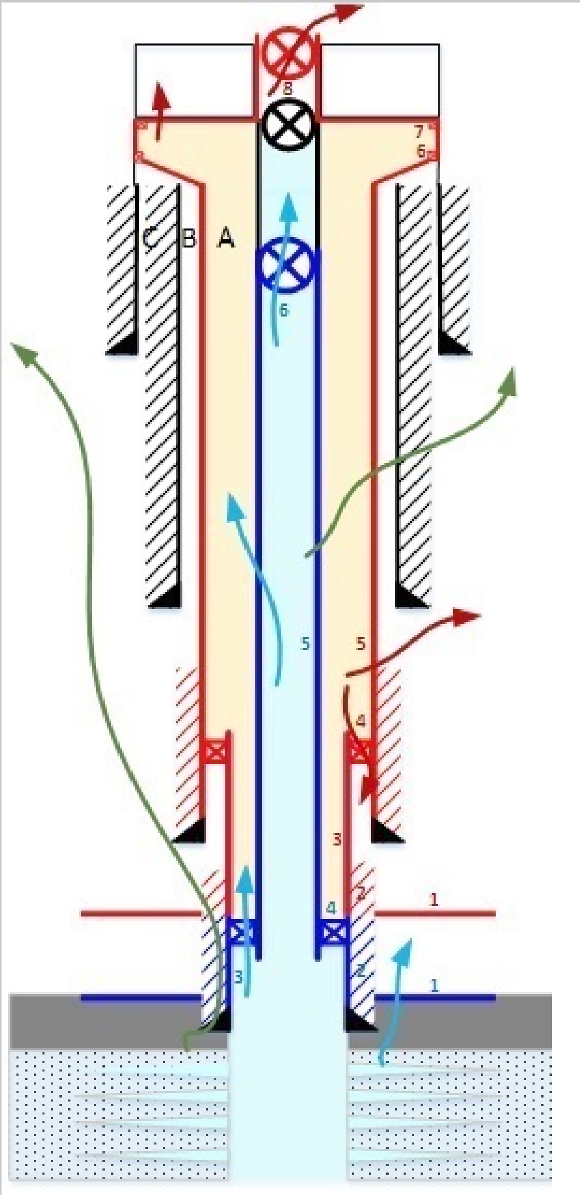

Figure 1 Schematic illustration of some possible leak pathways due to Well Barrier Element failures in an active CO_2 well. Blue arrows show failure of primary well barrier envelope, red arrows show failure of secondary well barrier envelope, and green arrows show failure of multiple Well Barrier Elements. (Acknowledgment to Jafar Abdollahi and Inge Manfred Carlsen, Weatherford Norge).

The primary (blue) and secondary (red) envelope are illustrated in Fig.1. The main elements in the primary envelope are: (1) formation, (2) annular cement, (3) liner, (4) production packer, (5) tubing and (6) downhole safety valve. The secondary envelope contains: (1) formation, (2) annular cement, (3) liner, (4) liner packer, (5) production casing, (6) casing hanger, (7) tubing hanger and (8) wellhead/X-mas tree with valves. In addition, some possible leak pathways due to well barrier envelope failures in an active CO_2 well are indicated: internal – within the well, or external – which may reach the surface. There are a number of reports on the statistics of well integrity failures both in onshore and offshore wells around the world, for example references [5-7]. Ageing issues with cement degradation, casing corrosion and wear, and thermal loads imposed on the well infrastructure are examples of the most likely causes of well leakage. The tubing is the Well Barrier Element that is by far the most likely to fail, probably due to corrosion and/or connection failure. Also the casing and the cement have a significant chance of failure.

The objective of this report is to review remediation measures for oil and gas well leakage presently used by the oil & gas industry. We will review both established best practice methods and novel technologies. Remediation technologies used for oil and gas well leakages can be applied to a great extent to CO_2 wells. Squeeze cementing, as the most commonly used strategy to solve a variety of well problems, is thoroughly described in this report. This includes a review of different squeeze methods, tools and materials for squeezing jobs. In addition, standard casing repair methods are described, including casing patches and expandable casing/liner. Apart from the standard strategies to repair cement and/or casing leaks, there are larger remediation operations such as well-workovers. Cases where it is necessary to remove and replace failed well elements are described in a general way. Novel materials, tools and technologies are presented and their potential for leakage remediation is discussed. Well plugging and abandonment is not a remediation strategy as such and is therefore not considered in this report. A plugging & abandonment operation can be considered as the last remedy which ends the life cycle of a well.

The application of existing and novel oil & gas remediation technologies to CO_2 well leakage will be assessed in the future work. We will discuss strategies for leakage remediation for both active wells and inactive wells. The well barrier breach approach and selected performance criteria will be used to assess and classify the remediation technologies. Risk assessment for various types of leaks and subsequent remediation cost assessment and best practice recommendations will be presented. The next and final report will represent a summary of the work done and the previous report [3].

As future work, a number of laboratory tests are planned to examine the merits of new materials for remediation of well leakage. These materials include CO_2-reactive suspensions, polymer-based gels, smart cements with a latex-based component and a polymer resin for squeezing. If feasible, the efficiency of a designed sealant will be investigated in a field test at the Serbian Bečej natural CO_2 field.

2 SQUEEZE CEMENTING

Squeeze cementing is typically used to repair the annular cement or the casing/liner, or to stop migration of fluids within a well. This operation is usually performed at the time of running the casing. However, it can be used for remediation of leakage later on in the life of a well. General applications of squeeze cementing are:

- Repairing the primary cement job (mud channels, voids, debonding, cement degradation)
- Repairing casing/liner leaks (corrosion, split pipe)
- Sealing lost circulation zones (during drilling)
- Plugging one or more zones in a multi-zone injection well
- Water shut-off
- Isolation of gas or water zones
- Well abandonment

Squeeze cementing operations can be expensive since well workover and wellbore preparation are required. Before squeeze operations are initiated, problem identification, risk and economic analysis need to be performed in order to optimize the success of the operation.

Squeeze cementing is the process of pumping cement slurry through perforations, holes or fractures in the casing or the wellbore annular space into an isolated target interval, behind the casing or into the formation [8, 9]. Squeeze cementing operations start with wellbore preparation. If the slurry needs to be injected bottom-off, a plug must be installed below the squeeze interval to prevent slurry from flowing further downhole. The slurry is pumped through drillpipe or coiled tubing until the wellbore pressure reaches the predetermined value. In most cases the tubing is pulled out of the cement slurry during the setting period. The next step is removal of excess cement which is usually performed by reverse circulation.

Squeeze cementing is a dehydration process. The solid particles in cement slurry are in most cases too large to enter the formation. In case of a permeable formation, the solid particles filter out onto the fracture interface or formation wall, while only a liquid filtrate passes into the formation. This results in a cement filter-cake filling in the perforations, as illustrated in Fig.2. After the accumulation of the filter-cake, cement nodes protrude into the wellbore. Although the filter-cake is not yet set cement, it is impermeable and able to withstand the increased wellbore pressure.

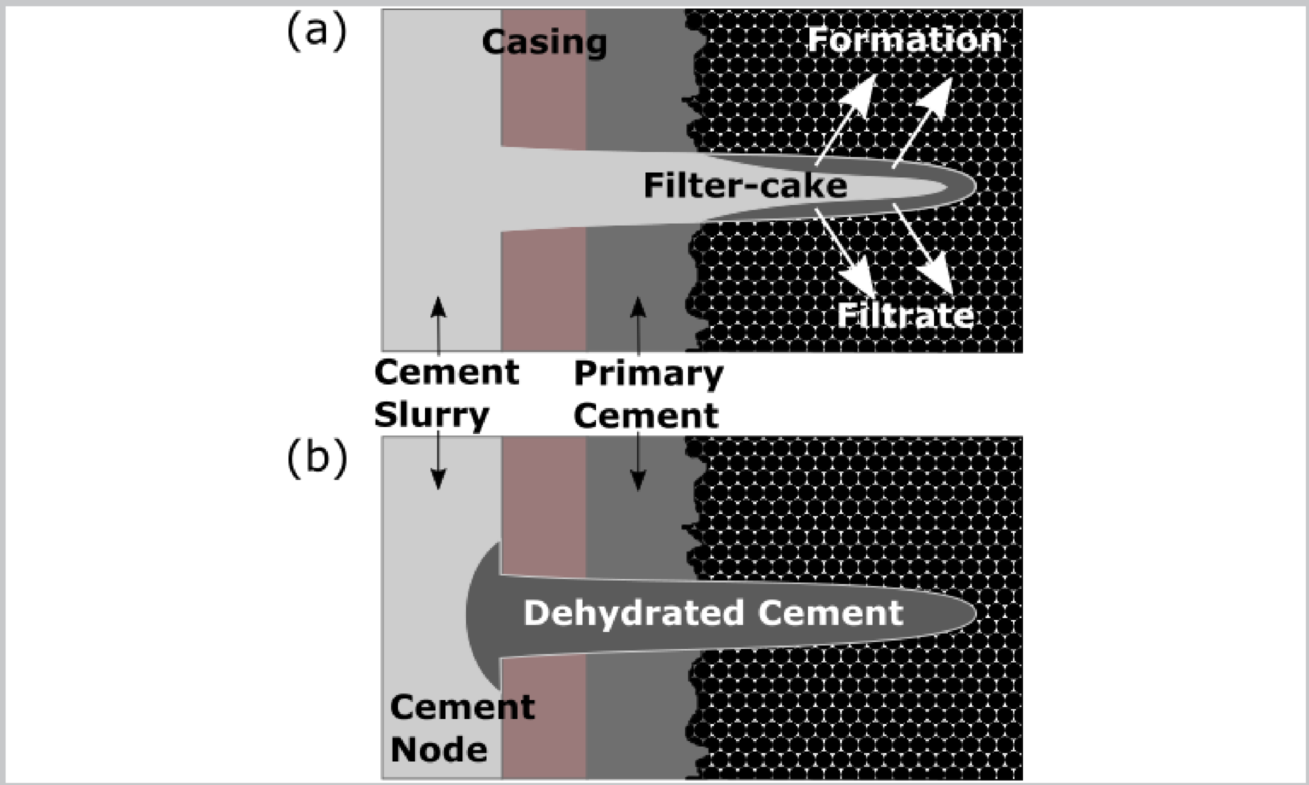

Figure 2 (a) Filter-cake buildup into a perforation channel. (b) Perforation channel filled with dehydrated cement and a cement node is protruding from the perforation.

Squeeze jobs are traditionally classified according to the bottomhole treating pressure into a) low-pressure squeeze (below the formation fracturing pressure) and b) high-pressure squeeze (above the formation fracturing pressure). There are two pumping methods: the running squeeze or the hesitation squeeze which can be applied at low or high pressure. The Bradenhead squeeze is a basic technique which can be applied in different pumping regimes and is usually combined with different squeeze tools. These basic techniques, methods and squeeze tools are described in the following sections.

2.1 Low-Pressure Squeeze

Low-pressure squeeze is the best option for remediation operations in the production zone. This technique avoids fracturing the formation by precise pressure control of the pump pressure and the hydrostatic pressure of the cement slurry [8]. Since no cement slurry is pumped into the formation, the slurry volume used is small. For successful application, it is essential to have the perforations and channels/interconnected voids cleared from mud and solids. If the slurry is properly designed, only a small node of cement filter-cake will remain inside the casing. Since there are many sensitive parameters, low-pressure squeeze requires careful design and execution. This technique is applied in multiple zones, long intervals and wells with low bottomhole pressure.

2.1.1 Circulating Squeeze

Circulating squeeze is a low-pressure method. This procedure involves circulating cement slurry between two sets of perforations, isolated by a packer or cement retainer. A cement retainer is preferable because it is easier to remove after the squeezing operation. Initially water or acid are pumped to achieve circulation, followed by a washer fluid. The cement slurry is pumped last. The exact required volume of cement slurry is unknown, so large amounts are pumped into the annulus. Thus there is a risk of cement slurry bypassing the packer/cement retainer and entering tubing, drillpipe, casing or annulus above the retainer. This may lead to stuck drillpipe or tubing if the excess cement sets. To minimize this risk, the cement retainer is placed as close as possible to the upper perforations and the stinger assembly is removed after cement placement. The excess cement slurry can be reverse circulated out of the well.

2.2 High-pressure Squeeze

When there are small cracks or micro-annuli, or disconnected channels in the annular cement, or when it is impossible to remove wellbore fluids and debris at low pumping pressures, then low-pressure squeeze is not appropriate remediation option [8]. In such cases fractures need to be induced in the formation at or near-by the perforated interval to allow the placement of cement slurry. Further application of pressure initiates slurry dehydration and filter-cake builds up against the formation walls and in all channels and fractures.

Since a high-pressure squeeze induces fractures in the formation, larger cement slurry volumes are needed to fill the additional voids created. This technique is applied when wellbore fluids or mud must be displaced to allow placement of cement slurry into the voids. High-pressure is also used for shoe squeeze, block squeeze and cementing liner top. One drawback is that the location and orientation of created fractures cannot be controlled. Other challenges are that the required squeeze pressure and build-up of filter cake may be difficult to attain. It is useful to wash the target interval with water or acid solution before the squeezing operation, to clean the perforations and open smaller fractures. This reduces the pressure required to initiate the fracture and the necessary slurry volume.

2.2.1 Block Squeeze

Block cementing is a high-pressure method, used to prevent leakage either above or below a producing zone which has poor zonal isolation. For this purpose the sections above and below the target formation are perforated and squeezed. This requires isolation of the permeable zone with a packer or retainer. The permeable interval below the producing zone is perforated and squeezed first, then the permeable interval above. The two residual cement plugs are drilled out after squeezing. Then the production zone is ready for perforation.

2.3 Pumping Methods

2.3.1 Running Squeeze Method

The running squeeze method is continuous pumping of the cement slurry until the final desired squeeze pressure is obtained [8]. If the pressure drops after the pumping stops, more cement slurry is injected until the pressure stabilizes without further pumping. The pumping rate should be low to avoid fracturing the formation and to fill narrow microannuli. Thus, fluid-loss control is not necessary and cement slurry design is simple. However, large volumes of cement slurry need to be injected.

This pumping method is applied only when:

- The wellbore fluids are clean.
- The formation has no fractures and no interconnected voids.
- The operation can be performed below formation fracturing pressure.

Design and application of running squeeze operation is simple, but the operation itself is difficult to control, because it is difficult to determine the rate of pressure increase and final squeeze pressure. Thus the pump rate should be reduced as the pressure builds up. There is a good chance to obtain the final squeeze pressure, but this is not a certain indicator of success. Another disadvantage is that it cannot be expected that all voids will be filled.

2.3.2 Hesitation Squeeze Method

The hesitation squeeze involves periodic pumping of cement slurry while monitoring the pressure on the surface [8]. In most cases during squeeze cementing, the formation absorbs the cement filtrate slower than the minimum pumping rate applied. Maintaining a constant differential pressure while not exceeding formation fracture pressure is therefore challenging, and the hesitation squeeze pumping method provides a solution.

Cement slurry must be carefully designed and shutdown periods between pumping cycles estimated accordingly. For example, a cycle can be 20 min pumping at ¼ - ½ bbl/min, followed by 10-20 min shutdown. The initial hesitation period depends on the formation and will be longer for loose formations. During the shutdowns the pressure drops due to filtrate loss to the formation. In the first pumping cycles, leak-off to the formation is quick. As the filter-cake builds up, the pressure increases, shutdown periods become longer and the difference between pumping and shutdown pressure diminishes. A nearly unchanged pressure during a shutdown indicates the end of the squeeze job.

This pumping method is used for all types of wellbore problems. The hesitation squeeze is more efficient in filling all the voids than the running squeeze, and in this case obtaining the final squeeze pressure is a sign of success. This technique requires much smaller slurry volumes than the running squeeze but the procedure is much more complex. The hesitation squeeze may be characterized as follows:

- Longer cement placement time and increased waiting-on-cement time.
- Squeeze tool placement is critical.
- Pumping rate, cement volume and hesitation time need to be carefully estimated.
- Cement slurry design is complex (fluid loss control, low gel strength).

2.4 Bradenhead Squeeze

The bradenhead squeeze technique is a low-pressure squeeze applied when it has been ensured that casing can withstand the squeeze pressure [8]. This technique owes its popularity to the simplicity of the squeeze procedure (no special tools involved) and a good success rate. As illustrated in Fig.3, an open-end tubing is run to the bottom of the perforated interval. A bridge plug may be used below the perforated interval to isolate the lower part of the wellbore. No squeeze fluid ahead of cement is needed, since the cement slurry is injected directly into the perforated interval. After the slurry is set in place, the tubing is pulled above the cement top and pressure is applied through the tubing with the blowout preventer rams closed. After waiting-on-cement time interval, a reverse circulation of the excess cement is performed through the tubing, providing an easy clean-up procedure.

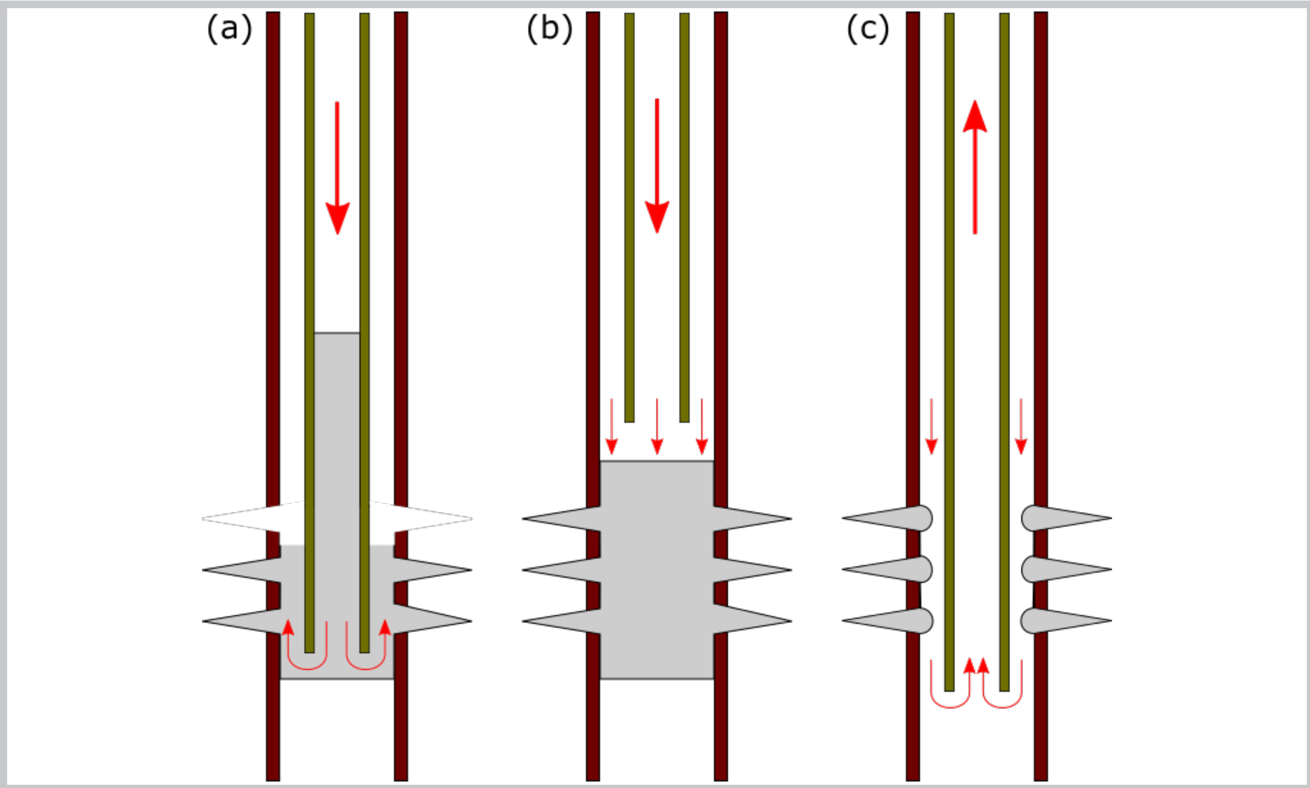

Figure 3 Bradenhead squeeze technique.(a) Cement slurry injection into the perforated interval. (b) The tubing is pulled out of the cement slurry and pressure is applied through the tubing. (c) Reverse circulation of the excess cement slurry.

This technique is often applied when lost circulation occurs during drilling or soon after primary cementing to fix a weak casing shoe. A hesitation squeeze pumping method is often used to force the cement slurry more effectively into the voids. Most coil-tubing squeeze applications are performed using a Bradenhead squeeze.

Drawbacks of the bradenhead squeeze include:

- The whole casing is exposed to the pressure during waiting-on-cement time. Casing integrity must be guaranteed (no corrosion, fatigue, splits).
- During the squeeze, the casing expands and restricts the flow of cement slurry through the microannuli/channels in the annular cement. These channels may not be completely filled with the slurry and will reopen after pressurizing is stopped.

2.5 SQUEEZE TOOLS

The main of objective of using squeeze tools is to isolate the squeeze target or the wellhead and the casing from high pressures applied downhole. Squeeze tools increase control over the cement slurry volume and the squeeze pressures and more accurately locate the target interval.

2.5.1 Retrievable Squeeze Packer

Compression or tension-set packers are used for squeezing. The packer can be set above/below the target interval or between two intervals. The packer allows circulation of the wellbore before the cement slurry is pumped and seals off the annulus during the squeezing. Retrievable packers have a bypass valve which allows fluid flow while running into the wellbore and after the packer is set. The valve is closed during cement squeezing. After the cement job, the valve allows reverse circulation to clean excess slurry. The main advantage over the drillable retainer is that the packer can be recovered and reused. Some possible disadvantages of using a packer are:

- Backflow cannot be prevented.
- Reversing excess slurry may damage the squeezed cement.
- Mechanical problems during running/placement.
- Contamination of the cement slurry is possible during placement.

- Build-up of cement on the packer/string.
- Valve opening during squeeze job.

2.5.2 Drillable Cement Retainer

Cement retainers are drillable packers with a controllable valve. Cement retainers or bridge plugs are used to create a false bottom and isolate the wellbore below the squeeze target. Cement retainers are used to prevent backflow or when there is a high negative differential pressure which disturbs filter-cake build-up. A cement retainer has an advantage that it can be placed more precisely than a packer, close to formation or between perforations. Disadvantages of the retainer are that it takes an additional trip to set it, can be used only once and drilling-through takes time.

2.5.3 Coiled-Tubing Squeeze

Coiled-tubing squeeze is a popular technique that has been in use since the 1980s [8]. This method dramatically reduces workover costs and enables accurate placement of small volumes of cement slurry. A tubing with a packer is used to guide the smaller coiled-tubing with a nozzle down the wellbore to the squeeze interval. The subsequent procedure is as follows:

- Viscous mud is injected into the well until its level is just below the perforations, which acts as a supporting column for the squeeze job. The mud contaminated with wellbore fluids is circulated via the coiled-tubing, and then water or diesel is injected above the mud column.
- The coiled-tubing nozzle is placed just above mud-water interface and cement slurry is pumped in until the perforations are covered. Then the squeeze pressure is applied with the nozzle located below the water-cement interface.
- When the squeeze pressure is reached, a contaminant fluid is injected to dilute the excess slurry and the wellbore is reverse-circulated.

Drawbacks of this technique are:

- Poor depth control.
- The coiled-tubing volume should be directly measured to enable placement of small slurry volumes.
- Fluid contamination can be prevented with use of additional plugs.

2.6 Cement Slurry Design for Squeeze Cementing

Certain factors have to be taken into account for optimal cement slurry design for each squeezing operation [8]:

- Rheology and sedimentation. Low viscosity allows pumping through coiled-tubing and penetration into small cracks and voids. Too low viscosity may result in free water and sedimentation. On the other hand, thick slurries are useful for cementing large voids.
- Low gel-strength during placement is important since gelation restricts slurry flow and increases surface pressure.
- The choice of cement particle size depends on the type of leak and the formation. Engineered micro-cement can be used for small casing leaks or low-permeability formations. For fixing leaks in unconsolidated formations, gravel/grain size, permeability and pore size of the formation are used to determine the appropriate cement particle size.
- Absence of free water is desirable.
- Appropriate fluid-loss control ensures optimal filter-cake build-up within cracks and perforations. The fluid-loss rate can be adjusted from low (<50-100 mL/30 min) for small cracks or to match formation permeability, to high (300-500 mL/30 min) for large cracks/voids behind the casing.
- The thickening time for squeeze job is designed in a way that squeezing and placement is possible as well as subsequent well cleanout. Thickening time generally depends on pressure and temperature. The temperature during squeeze cementing is usually higher than during primary cementing, which should be taken into account when designing the slurry.
- Higher slurry density results in better quality of the set cement but it causes higher hydrostatic pressure during placement. By engineering the particle size in the slurry it is possible to achieve low-density slurry with good mechanical properties or high-density slurry with relatively low viscosity.
- Chemical resistance: the usual requirement is resistance to acidic environment ($HF/HCl/H_2S$).
- Economic cement slurry design: the cement itself usually costs less than 10% of the total squeeze operation costs. Choosing the cement system that increases chance of squeeze job success is thus recommended.

2.7 Squeeze Cementing Summary

Examples of squeeze cementing techniques and possible applications focusing on failure of the cement sheath as a Well Barrier Element are given in Table 1. Squeeze cementing is used both during drilling and completion, and after primary cementing during the production or injection phase. In case of annular cement failure it is challenging or sometimes impossible to determine the nature of the failure (mud channels, fractures, debonding from the casing or formation, cement degradation). But detecting the location of the leak and its severity are some of the essential factors for planning the squeeze operation.

Table 1 Examples of squeeze cementing techniques and possible applications.

Squeeze Technique	Application
Low-pressure squeeze	Loss of well integrity in production zone
Circulating squeeze at low pressure with cement retainer/packer	Annular cement failure; casing/liner leak
High-pressure squeeze	Mud channels, cracks, micro-annuli in cement; casing shoe or liner top cementing
Block squeeze at high pressure with cement retainer/packer	Zonal isolation of a permeable zone – leakage prevention
Bradenhead squeeze with coiled-tubing and retainer/packer; hesitation pumping	Loss of circulation during drilling; cementing casing shoe; annular cement failure; casing/liner leak

3 OTHER SEALANT TECHNOLOGIES

3.1 Pressure Activated Sealants

Pressure-activated sealant technology was at first developed to remediate leaks in hydraulic control lines and surface controlled subsurface safety valves (SCSSV) [10, 11]. Since its development, this technology was expanded to various applications:

- Surface leaks - valves, pinholes, weld defects, etc.
- Wellhead leaks – pack-offs, bradenheads, casing/tubing hangers
- Casing/tubing leaks
- Cement leaks - microannuli, plugs, cavern casing shoe
- Downhole leaks – SCSSVs, umbilical lines, subsea well control systems, packers, pressure and temperature gauge mandrels, etc.

An example of this technology which is presently in use is Seal-Tite®. The pressure-activated sealant formula consists of a super-saturated mixture of short-chain polymers, monomers and other components [10]. High differential pressure at the leak site causes polymerization of the sealant into a flexible solid, as illustrated in Fig.4. The sealant polymerizes first at the edges of the leak site and gradually bridges across the leak site and closes it. The reaction stops when the pressure drops. The resulting plug is flexible and fills in holes/cracks at the leak site. At first the plug is fragile, but it develops strength over time while it retains its flexibility. The plug withstands the pressures up to pressure that activated its polymerization. The remaining injected sealant remains liquid – it will not clog nor plug the hydraulic system. The efficiency of sealing mechanism is not affected by pressure, temperature and time needed to reach the leak site, since each sealant formula is developed for that particular problem.

The advantage of pressure-activated sealant remediation is that there is no need for workover which dramatically reduces the costs. So, this technology has become popular in subsea applications, offshore and in arctic/remote locations. It has been used worldwide and a high success rate of 80% is claimed for the period of 2005-2012 [10, 11].

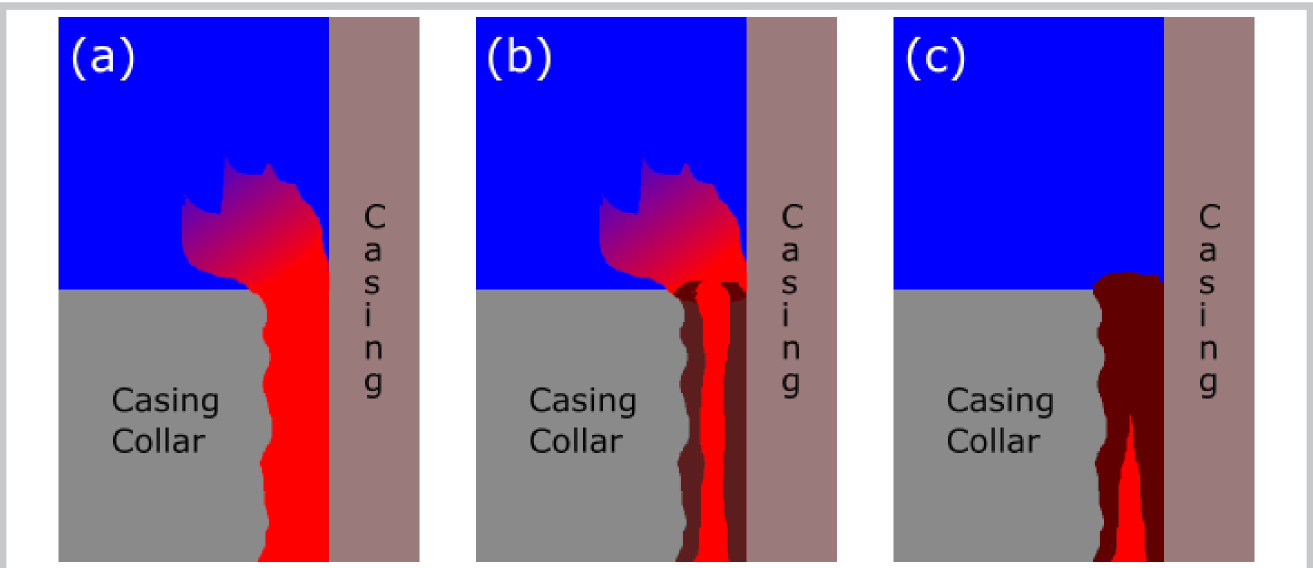

Figure 4 Illustration of pressure-activated sealant mechanism: (a) Sealant (red) forced through the leak site under pressure. (b) Pressure drop causes polymerization along sides of the sides of the leak. (c) The leak is plugged and the remaining sealant is liquid.

The majority of repairs concern wellhead pack-offs. However the development of ultrasonic leak detection has enabled the use of this sealant technology for the repair of small casing/tubing leaks without pulling the tubulars.

3.2 Temperature Activated Sealants

Temperature activated sealants are polymer resin systems designed to cure at a specific temperature. This allows placement, pumping or squeezing while in the liquid state into a desired interval in a well and subsequent curing when the resin reaches the appropriate temperature. Curing temperature, density, viscosity and curing time can be accurately designed for a particular application. In general, polymer resins tolerate some degree of contamination and are compatible with most wellbore fluids and cements. Treatments with polymer resin systems can be reversible (milling, acid treatment). A couple of examples of commercially available temperature activated sealants are described in the following.

ThermaSet® (WellCem) is a polymer resin system that is developed for solving problems such as loss of circulation [12], consolidation of loose formations, channels behind the casing, casing leaks and plugging in general [13], but can be used for many other well integrity issues. Some properties of Thermaset® are:

- Penetrates into permeable formation and narrow channels.
- Cures into a strong and flexible plug that withstands thermal expansion.
- Good bonding to steel and rock.

Thermatek® (Halliburton) is a temperature-activated rigid-setting fluid with a controlled right angle set that quickly develops high compressive strength. Some of the applications are consolidation of loose formations, plugging in general, annular seals behind or between casing/liner sections and fixing casing or packer leaks. Exothermic reaction when mixed initiates the setting process. Additional heat of formation as the fluid is pumped downhole speeds up the setting process. Setting time can be controlled by the addition of a retarder. Some properties of Thermatek® are:

- Controllable right angle set.
- Rapid build-up of compressive strength.
- No shrinkage.
- Zero static gel generation.
- Will not invade formation.

Temperature-activated sealants can in principle be used for squeeze-cementing and remediation of casing and annular cement integrity loss.

3.3 Silicate-based Sealants

Silicate-based methods, although not as widely used as polymers, have a potential for treating many production/injection problems as well as well for leakage remediation [14]. Silicate/polymer methods have been extensively used in Hungarian fields within last decades for water shut-off, profile correction in water injection wells, stabilization of reservoir rocks, etc. Silicate-based treatment was also deployed in the Bečej field (Serbia) in 2007 for mitigation of vertical CO_2 migration as a consequence of the CO_2 blowout in 1968 [15], as described in Report D8.1 [3].

Some advantages of silicate systems are low viscosity, good placement, can be gelled by a variety of inorganic and organic compounds and environmental friendliness [14]. Disadvantages are for example gel rigidity, shrinkage, short setting time and precipitation instead of gelling.

Development of polymer/silicate methods started at the end of the 1970s. The polymer/silicate technique is based on simultaneous cross-linking of hydrolized polyacrylamide and polymerization of sodium ortho-silicate [15]. In this method two solutions are used, with the following main components:

- Partially hydrolyzed polyacrylamide and Na or K ortho-silicate
- Potassium aluminum sulfate, calcium chloride, hydrochloric acid.

These solutions can be injected sequentially or mixed depending on the desired penetration depth. In the example of Bečej 5 well remediation, a sequential injection procedure was applied to avoid premature plugging effect. In the mixing zone, the following chemical reactions take place:

- Cross linking of polymers
- Gelation (polymerization) of silicates
- Precipitation of polymers, silicates and aluminum hydroxides.

If these solutions are injected into in porous formations, absorption of chemicals and entrapment of microgels, clusters, or hydroxides occur at the interfaces with the porous medium. The gelation process is terminated when viscosity reaches 8000-12000 mPa s [15]. The penetration efficiency mostly depends on the viscosity of both solutions. The cross-linking solution has similar viscosity to water and poses no issue. The content of polymer affects the viscosity more dramatically than silicates, increasing with polymer concentration. After curing, the permeability of the treated region is reduced by 4-5 orders of magnitude, the gel strength exceeds 10 bar/m and the barrier is stable up to 150 °C.

The limitation of this technique is that it was primarily developed to treat the formation in the vicinity of the wells and as such it is not focused on well integrity issues, but on formation related problems.

4 CASING REPAIR

Leakage through the casing (or tubing) is usually caused by mechanical erosion, wear and/or corrosion. In oil & gas production wells such leaks may result in loss of production, crossflow, production of unwanted fluids, etc. CO_2 injection wells face the same risks with casing/tubing leaks, especially if a well was originally designed as production well and has been already in operation for many years.

Casing leaks can be repaired by squeeze cementing, but this is an expensive and not a very successful technique. The squeeze operation may damage the casing further due to pressure applied during squeezing. Another option is to set a cement plug within the damaged casing which is more successful than squeezing [8], but this solution is part of the plugging & abandonment phase. The focus of this section is on alternative methods, involving casing manipulation, which allow continued operation of the wellbore. Some these methods are also used to repair cement leaks behind the casing.

4.1 Patching Casing

This method is an alternative to squeeze cementing for repairing casing/liner leaks when squeeze cementing has failed or is not applicable. A casing patch can be placed over or completely replace the damaged/corroded/weakened interval of the existing casing [9]. In the latter case, the inner well diameter is preserved.

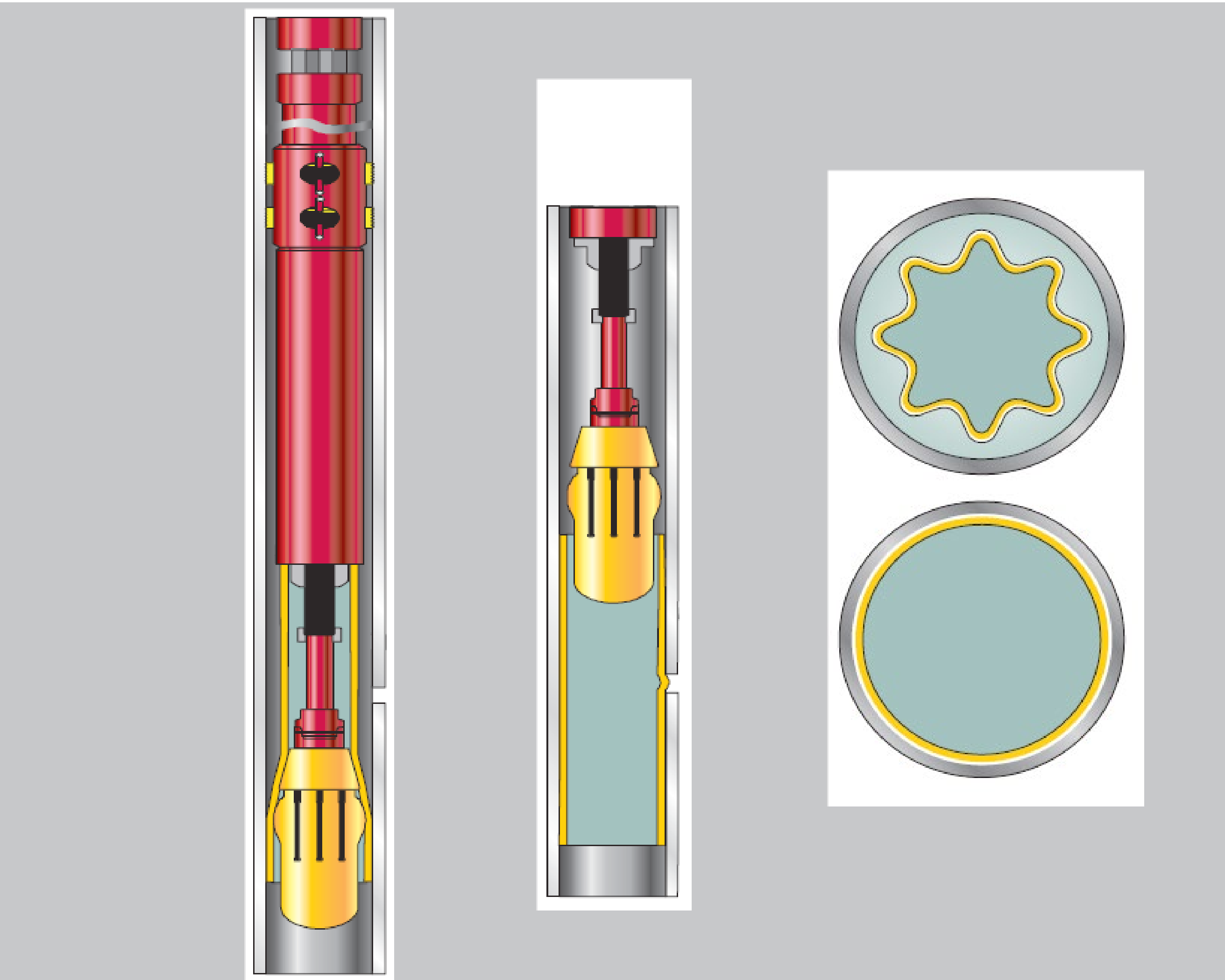

Figure 5 HOMCO® Internal Steel Liner Casing Patch short installation procedure: (a) After placing over desired interval, the patch is expanded, (b) fully expanded patch covering the leak site, (c) top view of the casing patch before and after expanding. Illustration taken from Weatherford.

Casing patch can be coated with epoxy resin on the outer surface prior to placement across the desired interval. Expander assembly is used to expand the patch against the casing. A simplified example of casing patch installation is illustrated in Fig.5. The expanded casing patch is anchored to the casing wall by the friction caused by compressive hoop stress. During the expanding, the epoxy resin fills the voids in the casing and becomes an additional sealant. This technique creates a hydraulic and gas-tight connection between the old and the new casing. Patching casing operation normally takes less than a week. This technique proved to be successful in many cases.

4.2 Expandable Casing/Liner

Use of expandable casing has become a standard technique in the oil & gas industry over the past 10-15 years. Expandable casing technology is commonly used in extended reach drilling but can also be applied for remediation of leakage in the existing wells. It is especially used for casing-off perforations and damaged casing sections. After installation of the expandable casing, perforation can be repeated.

Wellbore cleaning is essential before the expandable casing/liner is installed, to ensure free expansion and proper sealing of the elastomers. The expandable liner is run downhole together with the expander assembly which contains a solid cone. When the expandable liner is set in place, the cone is driven through the liner bottom-up using mechanical force or hydraulic pressure. During the expansion process, the liner diameter increases causing shortening of the overall liner length, but at the same time the wall thickness decreases only slightly. The expansion is completed when the anchor hanger seals the expandable liner against the original casing. The expandable liner can comprise many joints to create necessary length.

The expandable liner technology can be used during drilling and primary cementing as well, this being an open-hole liner expansion operation. In this case, drilling is performed with the expandable liner run down-hole together with the drill bit. The expansion of the liner hanger is performed after cement slurry placement in the annulus. Such an operation drastically reduces the rig time during well completion by avoiding unnecessary trips.

Another option is to expand the existing casing/liner that is cemented in place. During casing expansion, the hydrated cement in the annular space behind the casing is compressed. In laboratory scale experiments [16], it was observed that the cement becomes softer and changes consistency after expansion. But after a certain rehydration period (in contact with water), the cement regains its compressive strength and solid structure.

4.3 Swaging

When casing becomes deformed or collapses into the well, a swaging technique is used to restore it to its correct form [9]. A swaging tool is used to force the tubing or casing walls out while it is driven through deformed/collapsed section. This tool can also be used to expand casing or liner.

4.4 Tubing replacement/repair

Tubing replacement requires a well workover, so the costs are comparable to packer replacement. This operation is applied when other simpler solutions cannot be used to remediate the leakage. When the tubing is pulled out, the leaking joint(s) are replaced and the whole tubing is inspected so that other repairs can be conducted.

5 OTHER REMEDIATION STRATEGIES

5.1 Wellhead and X-mas tree repair

Well head equipment can be easily inspected and repaired for onshore or platform wells. For subsea wells, well head/X-mas tree repair involves a well service vessel and remotely operated vehicle [9]. Depending on the type of the problem, it may be solved at the sea bottom or X-mas tree may be removed and repaired on-shore. The latter operation requires well killing.

5.2 Packer Replacement

A packer leak is detected through the drop in annular pressure when the casing and tubing are known to be intact [9]. The removal and replacement of a production or injection packer is a complicated operation. Such workover includes killing the well, X-mas tree removal, tubing retrieval and finally packer removal. The whole operation takes about two weeks.

A permanent packer is removed using a packer mill. After milling, the remaining packer parts are retrieved and the well is flushed to remove the debris. A retrievable packer is pulled out together with the tubing and then replaced.

6 NOVEL REMEDIATION TECHNOLOGIES

6.1 CannSealTM

CannSeal™ was developed within a DEMO 2000 Project with the support of Statoil, Eni, Total and Shell in the period of 2005-2009, and was launched by AGR CannSeal AS in 2010. This technology features epoxy-based annular zonal isolation and a specially developed tool for sealant placement, as illustrated in Fig.6. The tool is based on an extension to existing perforating/punching technology to create a channel through the tubing/casing into the annulus. A container device is also incorporated into this tool to deliver a sealant precisely into the perforated interval. This tool allows use of more environmentally friendly sealing materials.

The sealing material used is an epoxy resin with adjustable viscosity, setting temperature, elasticity, etc. An example of this epoxy resin cured in the annular space is shown in Fig.7. The epoxy properties can be tailored both prior to hardening (to optimize deployment) and after hardening (to enhance the durability of the seal) according to the needs of the application.

The sealant can be deployed either in an open annulus or in a gravel pack. The treatment effectively seals off unwanted fluid flow behind liners, tubing and screens by placing a solid external annular plug. Other annulus sealing/repair applications, such as placing a plug just above a leaking packer, are also achievable with the tool. This technology can be also used for plugging & abandonment or could replace the traditional cement squeezing in future.

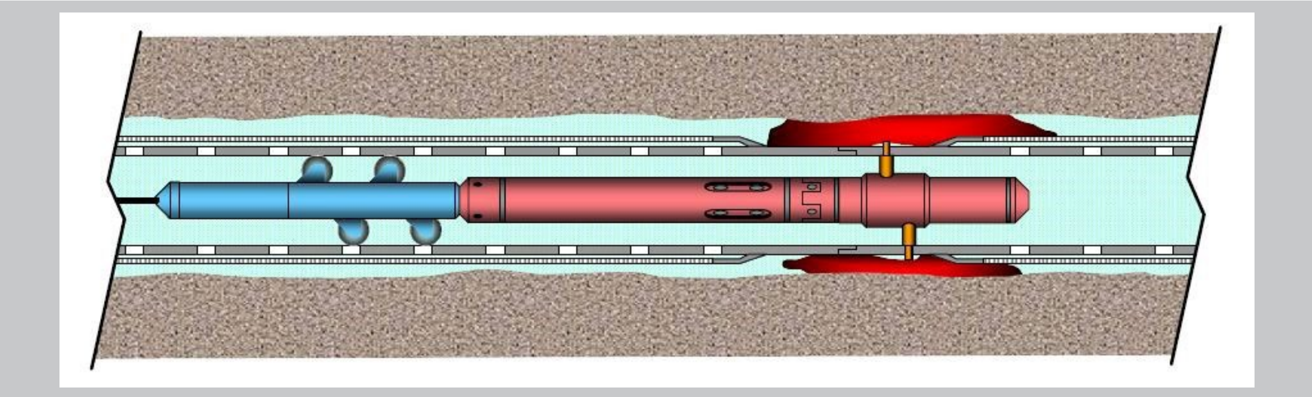

Figure 6 Illustration of Cannseal tool and remediation method.

Figure 7 Cured Cannseal epoxy-resin.

7 CONCLUSION

A wide range of technologies and methods from the oil & gas industry are available that can also be used for the remediation and mitigation of leakages from CO_2 wells. These include:

- Squeeze cementing - pumping cement slurry into an isolated target interval through perforations in the casing/liner to repair the primary cement job or casing/liner leaks.
- Casing/liner repair by patching, expandable casing, welding, or replacement.
- Sealant technologies for zonal isolation, such as pressure- or temperature- activated sealants, polymer-based gels and different cement systems.
- Well workover and replacement of failed Well Barrier Element.

A summary of the main Well Barrier Elements (WBE) coupled with oil & gas remediation methods & technologies that have been described in this report is presented in Table 2. Note that recurring Well Barrier Elements in the primary and secondary barriers are not distinguished since the remediation methods are independent of which barrier the Well Barrier Element belongs to.

The existing technologies mainly focus on the repair of the annular cement and casing/liner/tubing. Valves, packers, wellhead are examples of Well Barrier Elements that can be replaced. Replacement of any Well Barrier Element in general is not a simple operation and it may involve long downtime and well workover. Some Well Barrier Elements may be difficult to access or even inaccessible, such as formation, or annular cement behind several casings/liners; such leaks may lead to sustained casing pressure and are challenging to repair without plugging the well.

Table 2 Summary of the available remediation methods with respect to failed WBEs.

WBE\Method	Squeeze Cementing/ Other Sealants	Casing/Liner repair	Replacement	Cannseal
Formation	x			
Cement	x	x		x
Tubing		x	x	
Casing/Liner	x	x	x	x
Packers	x		x	
Valves	x		x	
Wellhead			x	

References

1. Metz B., et al., IPCC Special Report on Carbon Dioxide Capture and Storage. 2005, Intergovernmental Panel on Climate Change: Cambridge University Press.
2. Bachu S. and M.A. Celia, Assessing the Potential for CO_2 Leakage, Particularly Through Wells, From Geological Storage Sites. Carbon Sequestration and Its Role in the Global Carbon Cycle, Geophysical Monograph Series, 2009. 183: p. 203-216.
3. Vrålstad, T., Description of CO_2 well failure modes, causes and consequences, in Mirecol report D8.1. 2015, SINTEF Petroleum Research.
4. NORSOK Standard D-010: Well integrity in drilling and well operations. Rev. 4. 2013, Standards Norway.
5. Vignes B. and B.S. Aadnøy, Well-Integrity issues offshore Norway. SPE/IADC-112535, 2008.
6. King G.E. and D.E. King, Environmental risk arising from well-construction failure: Difference between barrier and well failure, and estimates of failure frequency across common well types, locations, and well age. SPE 166142, 2013.
7. Davies R.J., et al., Oil and gas wells and their integrity: Implications for shale and unconventional resource exploitation. Marine and Petroleum Geology, 2014. 56: p. 239-254.
8. Nelson E.B. and D. Guillot, Well Cementing. Vol. 2nd edition. 2006: Schlumberger.
9. Manceau J.-C., et al., Mitigation and remediation technologies and practices in case of undesired migration of CO_2 from a geological storage unit – Current status. International Journal of Greenhouse Gas Control, 2014. 22: p. 272-290.
10. Rusch D.W. and B.C. Ellis, Use of Pressure Activated Sealants to Cure Sources of Casing Pressure. SPE 55996, 1999.
11. Julian J.Y., et al., Pressure Activated Sealants-Non-Rig Solutions in Mature Fields in Alaska. SPE 163944, 2013.
12. Knudsen K., et al., First Application Of Thermal Activated Resin As Unconventional LCM In The Middle East. IPTC-18151-MS, 2014.
13. Beharie C., Francis S., and K.H. Øvestad, Resin: An Alternative Barrier Solution Material. SPE-173852-MS, 2015.
14. Lakatos I., et al., Application of Silicate-Based Well Treatment Techniques at the Hungarian Oil Fields. SPE 56739, 1999.
15. Lakatos I., et al., Prevention of Vertical Gas Flow in a Collapsed Well Using Silicate/Polymer/Urea Method. SPE 121045, 2009.
16. Kupresan D., Heathman J., and R. M., Experimental Assessment of Casing Expansion as a Solution to Microannular Gas Migration. IADC/SPE 168056, 2014.

Chapter XXIII

Assessment of Oil & Gas remediation technologies for CO_2 wells

Jafar Abdollahi[1], Inge Manfred Carlsen[1], Jens Wollenweber[2]
[1] PRORES AS, Norway
[2] TNO, The Netherlands

SUMMARY

A generic and systematic approach has been used for a discussion of the most critical well barrier elements (WBEs). A large portion of the referred findings and discussions is based on personal field experiences by the authors and well integrity studies for the O&G industry and authorities. Different leakage scenarios for an operating CO_2 well with 14 WBEs have been mapped and discussed together with preventive actions based on field experience. Technology gaps for mitigation and remediation operations for leaking wells are given.

The following topics are addressed:

- Key well barrier elements and monitoring methods connected to technology solutions
- Summary of well leakage scenarios as described in a previous report (Chapter XXII, D 8.1) to address remediation methods
- Common O&G remediation actions
- Common O&G preventive measures to reduce risk of well barrier failures
- Technology gaps

ABBREVIATIONS

C	Cost impact for risk assessment
CBL	Cement bond log
Cr	Chromium
CT	Coiled tubing
FIT	Formation integrity test
HSE	Health, safety and environment
LOT	Leak-off test
MTTF	Mean time to failure
NCS	Norwegian continental shelf
O&G	Oil and Gas
P&A	Plug and abandonment
PBR	Polished-bore receptacle
PIT	Pressure integrity test
PWC	Perforation, washing, and cementing
T	Time and schedule impact for risk assessment
V0	Special grade V0 gas test
WBE	Well barrier element
WH	Wellhead
WIMS	Well integrity management system
XLOT	Extended leak- off test
XT	X-mas tree

1 INTRODUCTION

This report is part of the research project MiReCOL (Mitigation and Remediation of CO_2 Leakage) funded by the EU FP7 programme. The research activities aim at developing a handbook of corrective measures that can be considered in the event of undesired migration of CO_2 in subsurface reservoirs both through geology formations and along wells. Work package 8 (WP8) addresses the O&G industry best practices for remediation of well leakages and consists of three tasks: Task 8.1 Description of leakage scenarios, Task 8.2 Overview of available technologies and methods, and Task 8.3 Assessment of remediation technologies and gaps. This report addresses Task 8.3 and provides main inputs to SP5 containing models and guidelines.

For this study, a generic and systematic approach has been used for a discussion of the most critical well barrier elements (WBEs). A large portion of the referred findings and discussion is based on personal field experience and well integrity studies for the O&G industry and authorities. Different leakage scenarios for an operating CO_2 well with 14 WBEs have been mapped and discussed together with preventive measures based on field experience. Technology gaps for mitigation and remediation operations for leaking wells are given.

2 WELL BARRIER ELEMENTS

The NORSOK standard D-010 (Rev.4, June 2013), the Norwegian Standard for well integrity in drilling and well operations, has been used as a useful reference for this study.

Different types of CO_2 wells can be referred to such as; producer, injector, monitoring, temporary and permanently plugged and abandoned wells (P&A). The well barrier envelopes and barrier elements can be different for each of the well applications. However, for simplicity only one type of well has been chosen and a typical CO_2 well injector is being used for this report to demonstrate the well integrity envelope with different WBEs and leakage scenarios. The schematics of such a well are illustrated in Figure 1 and used as a reference case.

Due to limited CO_2 well integrity data, experience and best practice from the oil and gas industry have been used. It can be noted that the best analogue O&G well for CO_2 applications is an operating gas well with high CO_2 content and high gas oil ratio (GOR). The fundamental well design for O&G and CO_2 are almost identical except for material selection which are more critical for CO_2 wells. According to the Oil & Gas UK guidelines, the high concentration of CO_2 can have negative impact on WBEs. Typical effects are:

- Potential faster degrading of cement in the presence of water
- Accelerating the corrosion rate of steel
- Dehydration and fracturing of shales leading to leakage through cement-rock interfaces and cap rock

In this report the overall well integrity of CO_2 well is discussed and mapped based on the individual WBEs. A WBE is defined as a physical element to prevent flow and will in combination with other WBEs form a well barrier. The key WBEs are numbered and labelled as shown in Figure 1and listed in Table 1. The different WBEs are grouped as “primary” and “secondary” well barriers. A primary well barrier is the first well barrier that prevents flow from a potential source of inflow while a secondary well barrier acts as a back-up. The primary well barrier envelope is drawn as a blue line while red is used for the secondary well barrier envelope. The WBEs are mainly consisting of; subsurface formation (rock), metal (e.g. casing), cement, and elastomer (e.g. packer and seals).

In total 14 WBEs have been listed for a typical operating CO_2 well; 6 primary and 8 secondary WBEs.

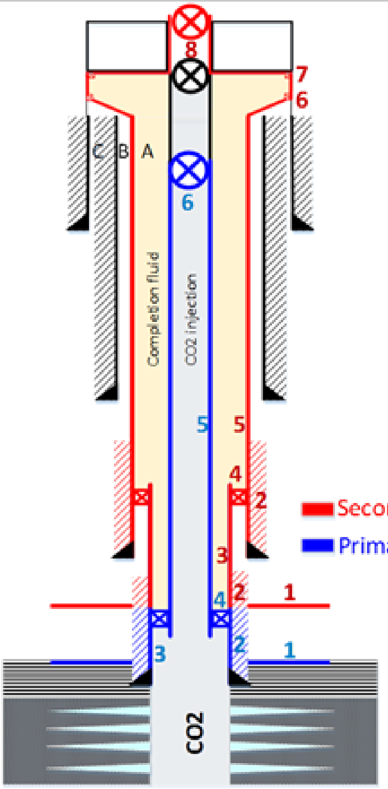

Figure 1 Well barrier schematics with WBE numbering for a typical operating CO_2 well.

Table 1 Key well barrier components.

No.	Well barrier component
PRIMARY WELL BARRIER	
1	In-situ formation (impermeable and moveable)
2	Liner cement (below production packer)
3	Liner tubular (below production packer)
4	Production packer
5	Completion string (tubing, components)
6	Downhole safety valve (including control line)
SECONDARY WELL BARRIER	
1	In-situ formation (impermeable and moveable)
2	Casing cement (above production packer)
3	Production liner (above production packer)
4	Production liner packer
5	Production casing
6	Casing hanger seal
7	Tubing hanger seal (neck seal)
8	Wellhead / surface tree

3 WELL BARRIER TESTING AND MONITORING

Key WBEs for the primary and secondary well barrier envelopes are listed in Table 2 together with initial testing and verification methods during installation and monitoring methods during well operations.

The industry practice for verification of the WBEs during the well construction phase is by pressure testing using drilling fluid (mud). The testing period for an oil and gas well is rather short and typically 10 to 15 minutes. The mud often contains solid particles and also has high viscosity. For gas and CO_2 wells, mud may not be a good test fluid. It has been experienced that in some cases, despite a positive pressure test, the well started to leak once put on operation. For example, this was seen from well integrity data which was collected through a SINTEF task force studies for Norsk Hydro in 2005 – 2007. Gas will leak more easily through seals and tubing connections than mud so it cannot be considered as an ideal testing fluid for gas / CO_2 wells.

The integrity test requirements described in governing guidelines and standards do not distinguish between oil and gas wells. However, it may be beneficial to develop a new and more representative testing criteria's for CO_2 wells. For instance, one should use low or no solid mud for pressure testing during the installation phase if practically feasible and the testing period should be increased. The lack of a fit for purpose integrity testing of CO_2 wells is considered as a technology gap.

In the operation phase the two main well integrity testing and monitoring methods are:

1. Period leak testing of the downhole safety valves, wellhead and X-mas tree valves
2. Continuous pressure monitoring through annuli valves (e.g. production packer, tubing and casing leaks)

For WBEs "in-situ formation" and "casing / liner cement" it may not be possible to implement direct and continuous monitoring solutions after the well has been put into operation. In some cases the leaks occur through a fracture or fault and the released fluid enter to another permeable formation located at a shallower depth. These kind of leaks are referred to as underground leaks or cross flow. The leakage through or along casing / liner cement can be observed as a pressure build-up at the wellhead if a leakage path is present. This is referred to as sustained casing pressure. Even if there is no observed sustained casing pressure at the surface, the well may still have an integrity problem deep down. For instance, a poor liner cement may not be detected if located below good casing cement (WBE number 2 in Table 2).

It will be beneficial to develop new monitoring methods and verification technologies for "in-situ formation" and "casing / liner cement" (WBE 1 & 2). One may use reservoir pressure data in offset monitoring wells to investigate leakages through in-situ formations. For casing / liner cement, one may run advanced logging and imaging tools but this will have impact on the operational costs. In the presence of a production tubing there is no commercial available tools to log through multiple tubulars.

Table 2 Well barrier component and verification and monitoring methods.

No.	Well barrier component	Initial test and verification	Monitoring during operation
PRIMARY WELL BARRIER			
1	In-situ formation (impermeable and moveable)	FIT, LOT, XLOT, field model	n/a after initial verification
2	Liner cement (below production packer)	CBL, PIT, volumetric calculation	n/a after initial verification
3	Liner tubular (below production packer)	Leak test (differential pressure)	n/a after initial verification
4	Production packer	Differential pressure in direction of flow	Pressure monitoring annulus A
5	Completion string (tubing, components)	Pressure testing	Periodic leak testing
6	Downhole safety valve (including control line)	Differential pressure in direction of flow	Periodic leak testing
SECONDARY WELL BARRIER			
1	In-situ formation (impermeable and moveable)	FIT, LOT, XLOT, field model	n/a after initial verification
2	Casing cement (above production packer)	CBL, PIT, volumetric calculation	Pressure monitoring annulus A
3	Production liner (above production packer)	Leak test (differential pressure)	Pressure monitoring annulus A
4	Production liner packer	Differential pressure in direction of flow	Pressure monitoring annulus A
5	Production casing	Leak test (differential pressure)	Pressure monitoring annulus B
6	Casing hanger seal	Leak test	Periodic leak testing
7	Tubing hanger seal (neck seal)	Leak test	Periodic leak testing
8	Wellhead / surface tree	Leak test	Periodic leak testing

4 CLASSIFICATION OF WELL LEAKAGES

Well leakage scenarios were discussed in Task 8.1 (Todorovic et al., 2014). Based upon this, we use a "well leakage classification" based on; type of WBEs, time, and location of leaks. Well leaks can occur through a single or multiple WBEs. The classification system referred to in this report is based on experience from a task force study on the Norwegian Continental Shelf (NCS) including eight fields and several hundred wells (Abdollahi et al., 2007).

If one of the primary WBEs leak, the secondary WBEs may control the leak and this is referred to as an "internal leaks". However, if the leak penetrates through both primary and secondary WBEs, the leak is referred to as an "external leaks" and is more critical as the released fluid may harm both people and the environment.

Figure 2 illustrates the different well leakage scenarios. Leaks that penetrate through primary WBEs are shown in blue arrows while leaks through secondary WBEs are shown in red and leaks through both primary and secondary WBEs are shown in purple.

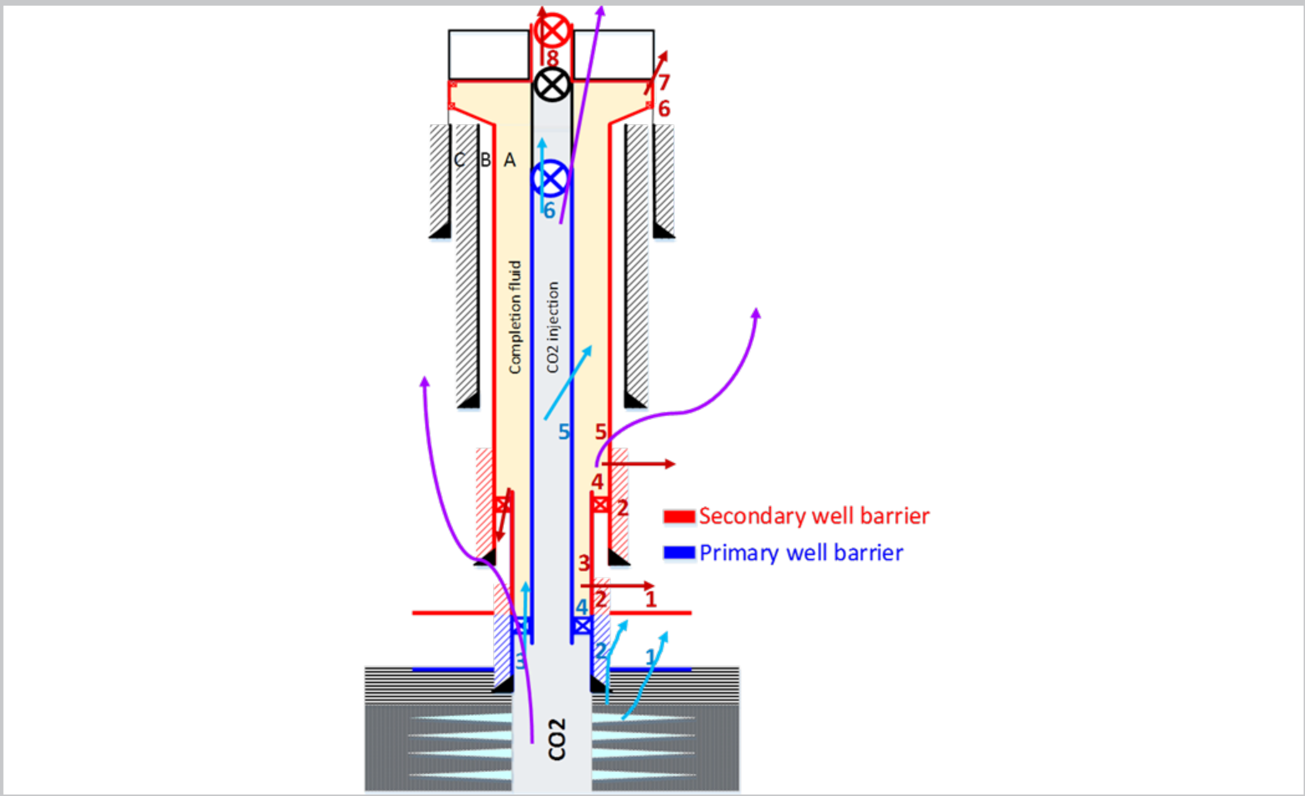

Figure 2 Well leakage scenarios; leak crosses primary (blue) secondary (red) and both primary & secondary (purple), from PRORES.

The Norwegian regulations describe a two independent well barrier philosophy (NORSOK, 2013). Normal well operations are generally stopped and operators have to implement measures to repair any failed WBEs. In some cases, the operator may apply for dispensation if only one barrier fails but a careful monitoring program will be needed with a plan for repair.

The time factor of the leaks is important for investigation of the root causes of the failures. In this report the terminology "early leaks" and "late leaks" are introduced. Early leaks are referred to those leaks that occur after a short period of time after the installation and testing of the WBEs. A typical early leak as reported in well integrity studies on the NCS (e.g. Norsk Hydro task force study) is described as a leak occurring after approximately one month after the well has been put on operation. A late leak are referred to leaks that occur later than this period.

The reasons behind early leaks are often related to:

- Improper well design
- Wrong material selection
- Improper installation of WBEs
- Operational envelope outside the well design envelope
- Insufficient / non effective testing methodology

The reasons behind late leaks are often related to:

- Corrosion and erosion
- Fatigue and degradation of materials
- Loads on WBEs outside initial design due to change of well applications (e.g. converting producer to injector)

Typical conditions leading to leaks are thermal and mechanical loads due to well interventions and stimulations.

5 MITIGATION AND REMEDIATION OF WELL LEAKAGES

The report D8.2 has highlighted on some technologies for remediating of leaking wells (Vrålstad et al., 2014). In this chapter we give some operational practices for mitigation and remediation actions based on individual WBE failures as listed in the previous chapter. Actions are referred to as common practices and technologies implemented in the O&G industry. In addition some new ideas are given, based on personal experiences from the authors. The root causes for the well barrier failures are also given. Probabilities for leakages and level of the complexity for remediation have been considered as well. Table 3 summarizes the findings for the primary well barrier and include well components, cause of failures, remediation practices, probability of failures and consequences. The colour codes are used to define high levels of risk with probability and consequences:

- Green: low
- Yellow: medium
- Red: high

The consequence of failures need to be assessed on a case based study from the individual operator and should be based on: cost impact (C), time and schedule impact (T) and health safety and environment (HSE). The risk evaluation required is qualitative and is based on a detailed description of uncertainty and development of causes and impacts. This has to a large extend to rely on the individual operators experience.

Table 3 List of causes of WBEs failures and proposed mitigation and remediation actions for individual primary well barrier.

No.	Well barrier component	Cause of barrier failure / defect	Mitigation and remediation practice	Probability	Consequences (C, T , HSE)
PRIMARY WELL BARRIER					
1	In-situ formation (impermeable and moveable)	Fractures, faults, permeable cap rock (geology uncertainty), CO2 may cause hydrate and fracturing of shale	• Pump sealing materials (if leakage point is close to the well and possible to access reservoir through well) • Drill relief well, if no access through well		
2	Liner cement (below production packer)	Poor cement bonding, micro channelling, improper displacement, casing movements, improper cement composition	• Section milling – rock to rock • Squeeze cement, one-trip P&A • Perforating Washing and Cementing (PWC) • CannSeal (cure micro channel)		
3	Liner tubular (below production packer)	Casing wear, casing corrosion & erosion, connection leak, deformation due to formation stress	• Straddle packer • MetalSkin, • Liner milling and run new liner • Squeeze cementation		
4	Production packer	Casing wear (non-circular), packer components, casing movements, fatigue	• Run tie-back • Use sealing material on top of packer (CannSeal)		
5	Completion string (tubing, components)	Tubing corrosion and erosion, fatigue, connection leak, leakage through completion components,	• Pull old completion and run new completion • Sealing and coating material		
6	Downhole safety valve (including control line)	Not functioning properly, scale, corrosion, material degradation	• Remove malfunctioning DHSV and install new DHSV • Run new completion string		

According to experience and supporting documents, the production packer including polished-bore receptacle (PBR) together with the completion tubing with downhole equipment and valves have a higher probability for leakages. Production packers are being exposed to high well loads and stresses due to thermal and pressure changes during the well life cycle. Ballooning and piston effects due to pressure changes also generate stresses and loads. In many cases the elastomer material of the packers may not tolerate or even be designed for such higher level of stress.

Table 4 summarizes the findings for the secondary well barrier.

For summary, the mitigation and remediation practices for primary and secondary well barrier leakages are listed below:

- Squeezing different sealing materials (cement, polymer, etc.) in different methodologies (PWC, bullheading, squeeze, etc.)
- Drill relief well, if no access to the leaking well

- Section milling of damaged tubulars
- Cover and isolate the leakage point(s) by use of extra a short tubular (e.g. liner) and straddle packer
- Pull whole leaking completion string and run new completion string
- Pull and remove leaking completion components and install new components

Table 4 List of causes of WBEs failures and proposed mitigation and remediation actions for individual secondary well barrier.

No.	Well barrier component	Cause of failure	Common mitigation remediation practice	Probability	Consequences (C,T, HSE)
SECONDARY WELL BARRIER					
1	In-situ formation (impermeable and moveable)	Fractures, faults, permeable cap rock (geology uncertainty), CO2 may cause hydrate and fracturing of shale	• Pump sealing materials (if leakage point is close well and possible to access reservoir through well) • Drill relief well, if no access through well		
2	Casing cement (above production packer)	Poor cement bonding, micro channelling, improper displacement, casing movements, improper composition	• Section milling – rock to rock • Squeeze cement, one-trip P&A • Perforating Washing and Cementing (PWC) • CannSeal (cure micro channel)		
3	Production liner (above production packer)	Casing wear, casing corrosion & erosion, connection leak,	• Straddle packer • MetalSkin, • Liner milling and run new liner • Squeeze cementation		
4	Production liner packer	Casing wear (non-circular), packer components, casing movements, fatigue	• Run tie-back • Use sealing material on top of packer (CannSeal)		
5	Production casing	Casing wear, casing corrosion & erosion, connection leak,	• Straddle packer • MetalSkin, • Liner milling and run new liner • Squeeze cementation		
6	Casing hanger seal	Wrong material, casing and wellhead movements, design envelope outside operating envelope	• Pull casing and run new liner / casing • Use sealing material on top of packer (CannSeal)		
7	Tubing hanger seal (neck seal)	Wrong material, tubing movements due to hot / cool fluid production / injection, high axial load due to ballooning, design envelope outside operating envelope	• Pull completion tubing and run new completion • Use sealing material on top of packer (CannSeal)		
8	Wellhead / surface tree	Design capabilities exceeded in operation, poor cleanliness, erosion, corrosion, improper sealing element, sand production, vibration,	• Chemical sealant • Workover of XT / WH • Replace valves		

6 PREVENTIVE ACTIONS

The experience from the O&G industry on leaking wells has shown that mitigation and remediation actions can be complex and costly. On this background, a chapter on preventive actions are also included as a guide for the construction of more robust CO_2 wells.

Table 5 and Table 6 list potential preventive actions to reduce the risk of WBE failures. These actions should be implemented in the planning and installation phases.

Table 5 Proposed preventive actions in the planning phase for primary WBEs.

No.	Well barrier component	Leakage preventive measures
Primary well barrier		
1	In-situ formation (impermeable and moveable)	• Provide high quality seismic to improve reservoir imaging and cap-rock sealing. • Provide logs, core, FIT from cap-rock. • Use of abandoned depleted gas fields for CO2 injection (proven cap-rock sealing).
2	Liner cement (below production packer)	• Centralize and rotate liner while cementing to achieve good cement bonding. • Run cement long to verify cement bonding and top of cement. • New cement material and cement compositions to prevent micro channel, resistance against corrosive environment, tolerate against temperature and pressure changes during well life cycle.
3	Liner tubular (below production packer)	• Select fit-for-purpose liner with high connection performance (high Cr percentage, coated pipe). • Minimize casing wear during well construction. • Choose deeper depth for production packer as possible to cover liner.
4	Production packer	• Use high standard sealing element such as V0 elastomer seal, V0 metal-to-metal seal • Optimize packer setting depth (avoid depths with high casing non-circular).
5	Completion string (tubing, components)	• Use high quality tubing, high Cr percentage, coated pipe, metal-to-metal seal connection • Evaluate revolutionary solution such as joint-less pipe (e.g. CT).
6	Downhole safety valve (including control line)	• Deploy high reliable and robust down hole safety valve (e.g. Exprosoft database).

Table 6 Proposed preventive actions in the planning phase for secondary WBEs.

No.	Well barrier component	Leakage preventive measures
Secondary well barrier		
1	In-situ formation (impermeable and moveable)	• Provide high quality seismic to improve reservoir imaging and cap-rock sealing. • Provide logs, core, FIT from formations above cap-rock. • Consider overburden formations (permeable/impermeable) with respect of height of casing cement • Use of abandoned depleted gas fields for CO2 injection (proven cap-rock sealing).
2	Casing cement (above production packer)	• Centralize and rotate liner while cementing to achieve good cement bonding. • Run cement long to verify cement bonding and top of cement. • New cement material and cement compositions to prevent micro channel, resistance against corrosive environment, tolerate against temperature and pressure changes during well life cycle.
3	Production liner (above production packer)	• Select fit-for-purpose liner with high connection performance (high Cr percentage, coated pipe). • Minimize casing wear during well construction. • Choose deeper depth for production packer as possible.
4	Production liner packer	• Use high standard sealing element such as V0 elastomer seal, V0 metal-to-metal seal. • Optimize packer setting depth (avoid depths with high casing non-circular).
5	Production casing	• Select fit-for-purpose casing with high connection performance (metal-to-metal seal, high Cr percentage, coated pipe). • Minimize casing wear during well construction. • Design fit-for-purpose completion fluid (packer fluid), non-corrosive, durable and compatible fluid.
6	Casing hanger seal	• High standard and fit-for-purpose casing hanger for CO2 injection / production, high capacity load, non-corrosive materials.
7	Tubing hanger seal (neck seal)	• High standard and fit-for-purpose tubing hanger for CO2 injection / production, high capacity load, non-corrosive materials.
8	Wellhead / surface tree	• High standard and fit-for-purpose wellhead equipment and X-mas tree, non-corrosive materials.

7 STATISTICS ON LEAKING WELLS

Statistics on leaking wells are important source of information for the improvement of well integrity management. One may investigate robustness and reliability of individual WBEs based on the mean time to failure (MTTF) data. According to the experience of the authors such statistics for CO_2 leaking wells are not yet available. However, there are studies and reports for O&G well integrity that are relevant and can be used. Well integrity studies on the Norwegian Continental Shelf (NCS) have given useful information on the nature of leaks and root causes. Abdollahi (2007) mapped leaking wells from three oil fields on the NCS as a part of his PhD thesis. Eight kinds of leakages were mapped and ranked from a severity point of view as shown in Figure 3. Together with other sources of information such as production history and well operations, important well integrity trends can be revealed and will enhance future well robustness. It is advised to develop well integrity management software and well components reliability data bases for CO_2 wells as been used in the oil and gas industry.

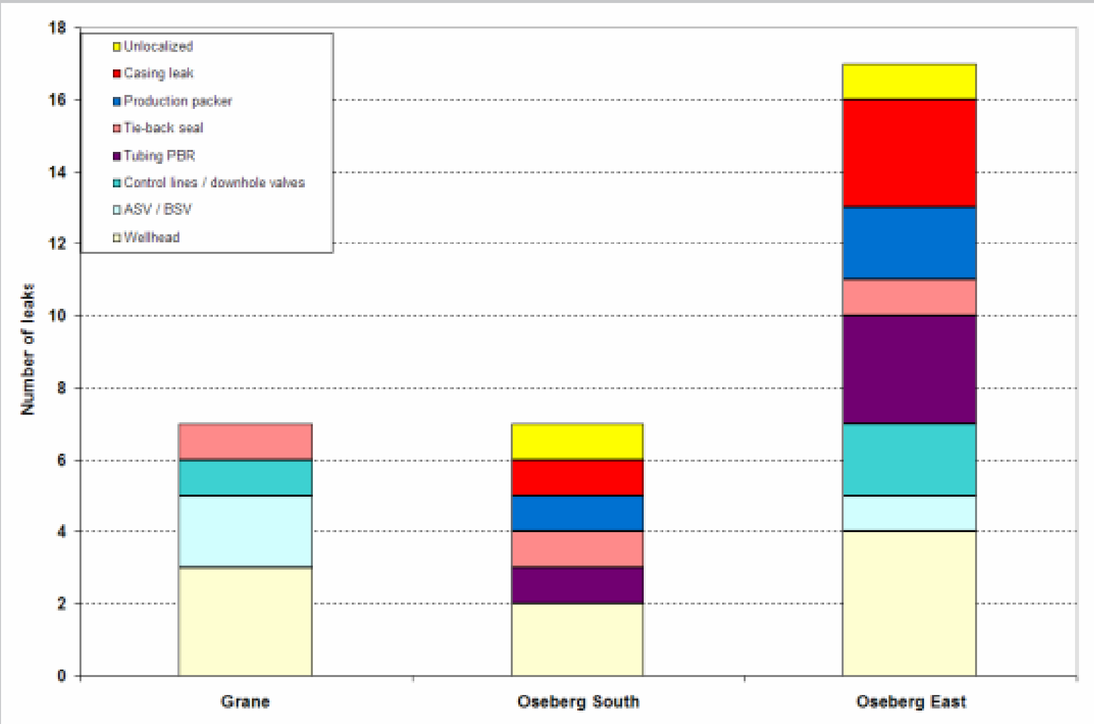

Figure 3 Example showing well leakage statistics for three fields on Norwegian Continental Shelf (Abdollahi, PhD thesis, 2007).

Typical MTTF for an oil production well is experienced to be around seven years (Abdollahi et al., 2007). Injector wells have the tendency to leak earlier due to higher pressure and temperature cycling. For CO_2 wells, the MTTF can be expected to be even shorter due to a more corrosive environment. The use of high quality and corrosive resistant materials and improved testing procedures can prolong the well life cycle for CO_2 wells.

8 TECHNOLOGY GAPS

This chapter summarizes technology gaps for more robust CO_2 well design.

Well integrity testing during the installation phase is critical. The pressure testing procedure should be improved for CO_2 wells. Longer test periods and the use of new testing fluid such as Nitrogen for V0 gas-tight rating of downhole completion and components should be considered.

Another important technology gap is related to the re-installing of annular well barriers and verification. Well integrity failure due to poor annulus cement or lack of integrity behind casing string normally requires section milling. This operation is both expensive and associated with several operational risks. For well plugging and abandonment (P&A), the O&G industry is looking for new and cost efficient technologies for annular barrier replacement without section milling and tubular removal. One approach is the use of so called PWC (perforate, wash and cement) technology. Even more challenging is the placement of annular cement barrier behind multiple casing strings. As an example, the service companies HydraWell and Archer are working on new technologies to fill this technology gap. This technology is still in its infancy and needs further development and qualification. One important challenge is the verification and testing of newly installed annular cement barriers. PRORES is currently working on a concept called One-trip P&A which is targeting operational efficiency for annular cement installation and integrity verification.

Technology gaps are also related to logging of the well status including cement bonding behind two or multiple casing strings. For instance, through tubing logging operations without the need to pull the production tubing has great potential for cement bond logging behind the 9-5/8" casing.

Alternative and improved materials to conventional cement is much sought after and is critical for CO_2 wells. The sealing requirements are related to many parameters such as; long durability, impermeable, non-shrinking, non-brittle, deformable, gas tight, chemically stable, etc. Recent achievements with use of low viscosity and particle free resin systems have a great potential as for example the ThermaSet material from WellCem.

Efficient and reliable downhole sealing material placement techniques are also crucial to achieve a robust WBE installation. The main challenges of today's practices are related to cement contamination and shrinkage.

Continuous barrier monitoring of in-situ formations and cement behind liner is a great challenge. Some of these issues are covered in other MiReCOL work packages under SP2.

9 CONCLUSIONS

Altogether, fourteen key well barrier elements important to the integrity of CO_2 wells have been mapped and discussed in this report. Knowledge and experience from the oil and gas industry relevant to CO_2 wells have been used to classify well leakage scenarios. Methods and technology for mitigation and remediation of leaking CO_2 wells are discussed, including preventive measures.

Important findings on preventive and corrective countermeasures for each WBE are summarized in schematics and tables.

Some of the identified technology gaps are listed below:

- Improved well testing procedures and criteria during the construction and well barrier installation phase to be more suitable for gas / CO_2 wells
- Re-installing of annular cement and barrier verification through multiple casing strings
- Through tubing cement bond logging for external casing cement
- Alternative sealing materials to conventional cement with improved long term properties
- Continuous monitoring of well integrity of in-situ formations and liner cement

In addition, well integrity management system for CO_2 wells should be implemented as routinely used in conventional oil and gas operations.

References

NORSOK Standard D-010, Rev.4, June 2013.
Oil & Gas UK, guidelines on qualification of materials for the suspension and abandonment of wells, issue 1, July 2012.
MiReCOL report D8.1, 2014-2016, SINTEF, T. Vrålstad
MiReCOL report D8.2, 2014 – 2016, SINTEF, J. Todorovic
Analysing Complex Oil Well Problems through Cased-Based Reasoning, PhD thesis, Trondheim, November 2007, J. Abdollahi

Section VII

NOVEL MATERIALS AND TECHNOLOGIES FOR REMEDIATION OF WELL LEAKAGE

Chapter XXIV

CO_2 reactive suspensions

Marc Fleury[1], Olivier Sissmann[1], Etienne Brosse[1], Michel Chardin[1]
[1] IFPEN, France

SUMMARY
This element of MiReCol aims at studying a method for treating the surroundings of a well using a reactive suspension. Ideally, the injected solution should react with the CO_2 present in the formation. Because the amount of CO_2 may be insufficient or even absent, we extended the study to include reactions with an activator (acid). The objective is typically to inject the product around the well, up to a radius of 1 m in order to create a permeability barrier.

The study comprises laboratory tests using sandstones representative of geological formations suitable for CO_2 storage but also specific samples from the Bečej field in collaboration with NIS (Naftna industrija Srbije, Serbia). Indeed, in a second phase of the project, field tests are expected to be implemented to demonstrate the efficiency of the proposed method. Hence, the design of the process is intimately linked to the field constraint, i.e., sufficient time is needed between the preparation at the surface and the injection of the solution into the formation downhole.

Silica-alkaline solutions are aqueous solutions containing high concentrations of SiO_2 and A_2O, where the alkaline element A is generally sodium (Na) or potassium (K). Commercial stable solutions exist with high molar ratio SiO_2/A_2O, spanning from 1.6 up to 3.9 with pH values above 11.5. When the pH is lowered either in contact with CO_2 or using an acid, silica precipitates to form particles. Below a pH of approximately 9 according to the solubility curve, the particles formed are stable and no back-dissolution is possible unless the pH is increased again. Hence, one expects a long-term stable chemical stability.

An experimental investigation of the precipitation of commercial solutions using a weak acid to lower the pH has been performed. Preliminary results using CO_2 indicate that the reaction kinetics are too fast and difficult to control, and the plugging too strong to allow practical field implementation. Various concentrations of acetic acid added to the commercial silica-based solution were tested, and the bulk gelation times measured before the mixture becomes too viscous for injection. The impact of temperature was determined by performing experiments at 20, 40 and 60 °C, with gelation times estimated between a few minutes up to 4 days. To follow the kinetics, several complementary techniques were used: rheological visco-elastic properties to observe the gelling onset, NMR relaxation time measurements to follow the gradual increase of water interactions within the gel.

The ability of the precipitates to plug a porous media was tested on analog sandstone samples representative of CO_2 storage formations, as well as a sample from the Bečej field (Serbia). With a viscosity close to that of water and no particles present in the liquid, injection of such products is possible in almost any permeable media. Using an optimum mixture tuned as described above, the solution is simply injected through the porous media and then kept at constant temperature (e.g. 40 °C) for precipitation. After a few days, a breakthrough experiment is performed by increasing gradually the differential pressure across the sample. The results obtained so far indicate a very large strength of the order of 600 bar/m.

1 GENERAL PRINCIPLES

A large number of methods can be used to treat the surrounding of a well (Manceau et al., 2014). The objective here is to inject a solution around the well in a selected depth interval (a few meters) in order to plug the formation, i.e., reduce porosity and permeability ideally down to zero. Hence, CO_2 flow at this depth interval cannot occur. Schematically, the envisaged process is such that the porosity should be filled with a solid, and this solid is the result of the precipitation of some components of the injected solution.

Some key requirements are:

- long term stability (one year or more),
- injectivity: the solution should not be too viscous, nor contain too large particles,
- reactivity: the solution should not react outside the geologic formation, and especially in the well during injection; i.e., the reaction should not be too fast for practical reasons.

Beside other possibilities such as cement or resins, a first initial choice was to select a process among two main categories: the precipitation of carbonate or silicate alkaline solutions. For example, using a lime solution:

$$Ca(OH)_2 + CO_2 \rightarrow CaCO_3 + H_2O \quad (1)$$

or using a silicate solution (water glass):

$$Na_2O \cdot 3SiO_2 + 2H_2O + 2CO_2 \rightarrow 2NaHCO_3 + 3SiO_2(am) + H_2O \quad (2)$$

In the latter, amorphous silica is formed when the pH is low enough, for example at the plateau value of solubility (other solids are formed at intermediate pH values). The difference can be viewed in terms of the solubility of calcium and silica in alkaline solutions (Figure 1). As a function of pH, the solubility of silica is much higher and potentially, the amount of solid that can be formed is much higher. Another strong argument in favor of silicates is related to their stability: indeed, below a pH of about 9 (Figure 1), no dissolution occurs and a plateau of solubility is present. This is not the case for carbonates for which the solubility is still evolving around a neutral pH and below. In a geological formation containing CO_2, the pH could still change as a function of the brine-rock-CO_2 equilibrium but there is no known process able to bring pH values back to 9 and above. Hence, the generated solids plugging the porous media are fundamentally stable when the initial solution is diluted and the pH drops down below 8.

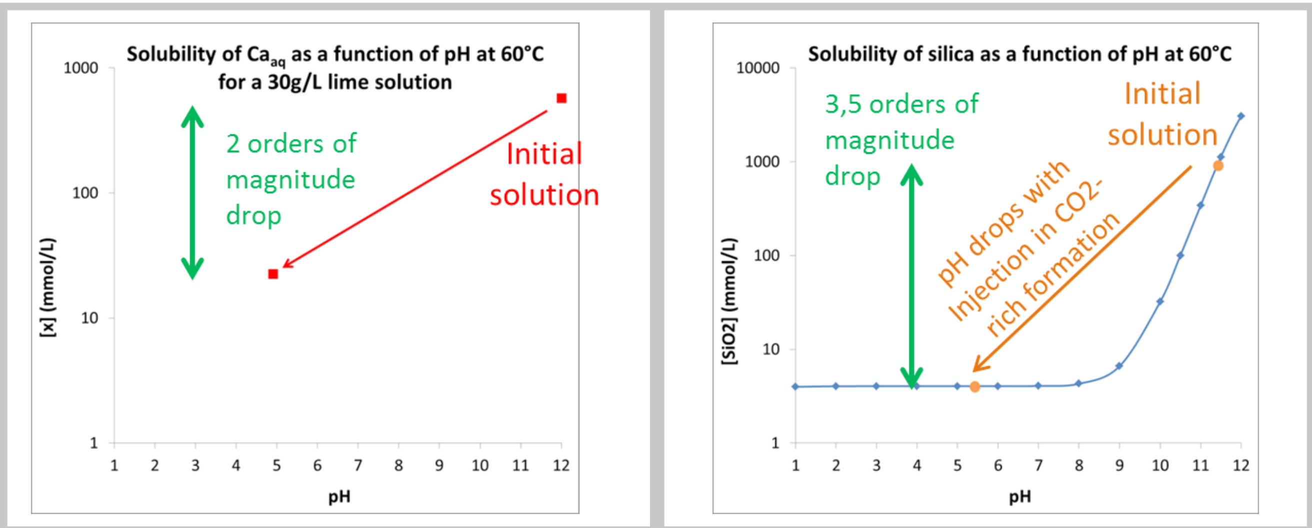

Figure 1 Solubility of Ca and SiO_2 as a function of pH.

The efficiency of carbonate vs. silicate solutions has been investigated recently (Ito et al., 2014) by performing experiments in a bead pack (Figure 2). The reduction of the apparent permeability to CO_2 after precipitation of the injected solution is one order of magnitude larger for silicate solution compared to a lime solution. These observations confirm our reasoning.

In a very general way and in view of field applications, we can list a series of a priori advantages and disadvantages between processes involving carbonates or silicates (Table 1). Mixing at the surface may be easier for silicates because they are less sensitive to atmospheric CO_2; for injection issues; avoiding reaction in the well is possible for both processes; the kinetics of precipitation may be faster for carbonates than for silicates, although this should be compared more carefully; CO_2 gas is needed to lower the pH for carbonates, not necessarily for silicates; the stability w.r.t. pH variations around neutral is better for silicates; carbonates are less costly; the environmental impact is very limited for both processes; and no strong safety issues exist for both processes.

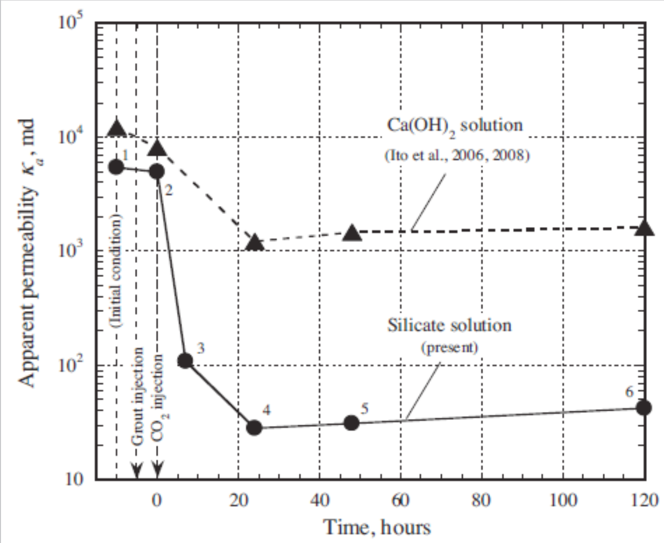

Figure 2 Reduction of the apparent permeability appearing larger when using silicate solution (Ito et al., 2014). From experiments performed in a bead-pack.

The theoretical general approach is to perform 2D reactive transport simulations at the well scale. These simulations should be validated first by 1D reactive transport simulations reproducing laboratory experiments, or some key aspects of laboratory experiments.

Table 1 Comparison of precipitation processes involving carbonates and silicates.

	Carbonate	Silicate
Mixing at the surface	-	+
Reaction in the well	+	+
Kinetics	-	-/+
Need for CO_2	yes	not necessarily
Stability	-	+
Cost	+	-
Environmental impact	+	+
Safety	+	+

2 LITERATURE REVIEW

A literature review shows that silicates in porous media are used in the petroleum industry but also for other applications related to soil consolidation and civil engineering (e.g. Azeiteiro et al., 2014). Besides these two domains, systems made of silica and an alkali metal (e.g. NaOH, KOH) are heavily used in chemical engineering to produce silica particles by precipitation, and nanoporous solids as catalysis support. For this domain, the related knowledge can be found (at least) in two reference books on the subject (Iler, 1979; Bergna and Roberts, 2006). An overview of the general mechanisms involved in the precipitation processes to form particles is given in Figure 3. Starting from a liquid state containing various complexes (described later), the decrease of pH induces the formation of oligomer, followed by the growth of primary particles. If the concentration of these particles is high enough (as the pH is further decreased), the growing aggregates percolate and forms a gel. The gel may precipitate to form solid silica-based porous nano-particles. The sodium silicate chemistry is rather complex and still not fully understood. Quite surprisingly, new precipitation processes to produce silica particles can still be found nowadays (Jung et al., 2010). Unfortunately, as will be seen, some important aspects of interest for our application cannot be found as well.

2.1 Sodium silicate solution as a flow diversion control in the oil industry

Sodium silicate is used for water control in oil reservoirs (Stavland et al., 2011 and references therein). Combined with polymers, it has been used for well treatments or conformance control in order to reduce water production (Lakatos et al., 1999, 2012) and more recently CO_2 gas losses (Lakatos et al., 2014). In the latter, the treatment was applied in one well of the Bečej field and effectively reduced considerably the gas losses. The addition of silicates in polymers (called silica-based gels) improves the gel strength and stability.

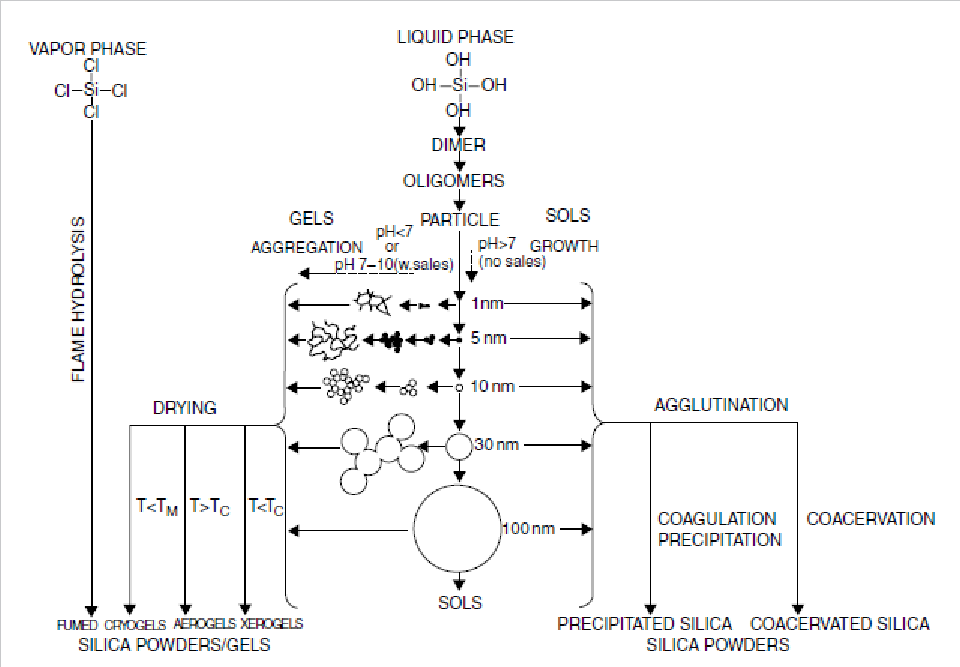

Figure 3 General overview of polymerization and precipitation of alkaline silica solution (Bergna and Roberts, 2006).

For in-depth placement and control, one tries to form a gel after the injection of a silicate solution. The main issues are the following:

- control the gelation time in order to reach a given (or the largest) distance around the well,
- choose an appropriate viscosity in order to generate reasonable pressure increase in the formation, below the fracking limit,
- because the initial solution is often a colloidal suspension containing already particles, an additional issue is to avoid plugging by collective aggregations in the restrictions of the pore network (pore throats) if these particles are large.

The success of the process is quantified by a water mobility reduction factor, comparing the initial permeability of the porous media to that after gelation. But for placement in the formation at a given distance, one should avoid early gelation or precipitation during the injection, and different authors have investigated recently in detail the gelation kinetics as a function of different parameters: pH, dilution in water, dilution in HCl, NaCl salinity and presence of divalent ions. We report below many results that are of high interest for our process.

Dilution and pH

Since the pH is the main parameter triggering the gelation time, the pH was determined for different dilution with distilled water and/or HCl (Hamouda and Amiri, 2014). From the initial solution at pH=11.4 (note that its density is very large), the pH decreases only

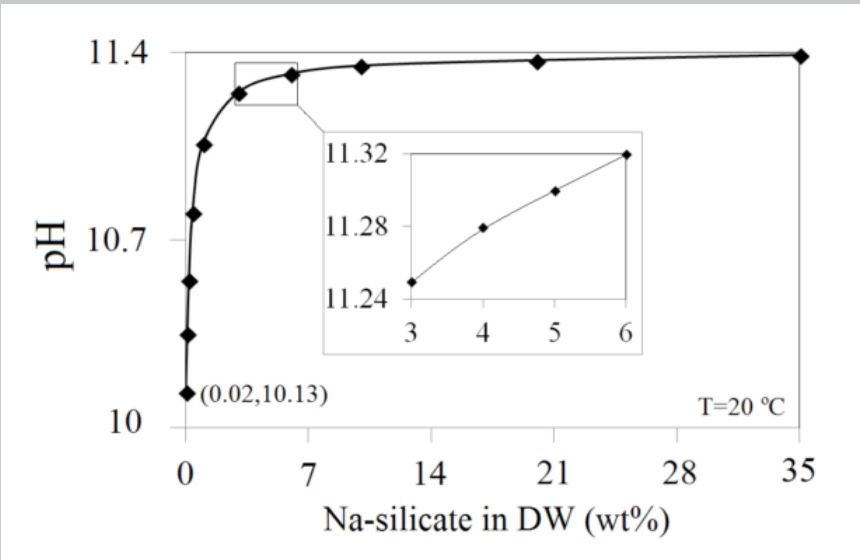

Figure 4 pH of different solution diluted in distilled water. The highest concentration corresponds to the initial solution provided by the manufacturer: Na-Silicate (Na_2OSiO_2) content of 35.7 wt%, molar ratio of 3.35, silicate (SiO_2) content 27.4 wt%, Sodium oxide (Na_2O) of 8.4 wt%, density of 1.368 g/cm3 at 20°C (Hamouda and Amiri, 2014).

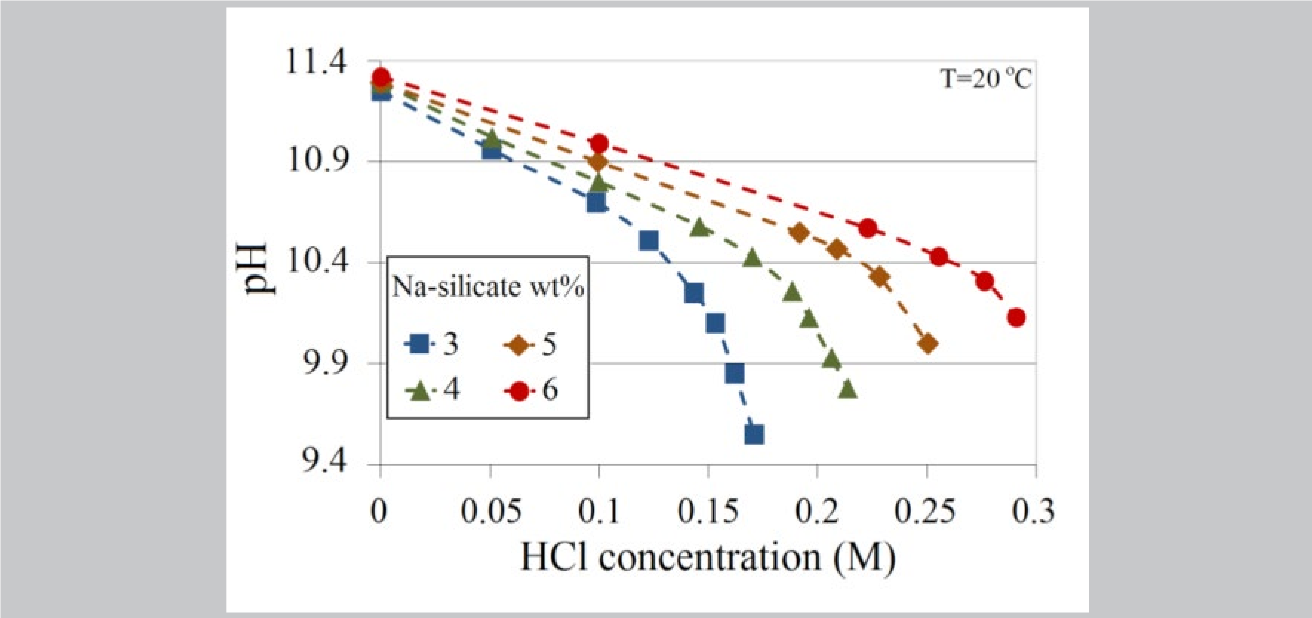

Figure 5 pH of different solutions diluted with hydrochloric acid (Hamouda and Amiri, 2014) . The initial solution (HCl conc. of 0) at different Na-silicate concentration (from 3 up to 6) were obtained by diluting the solution provided by the manufacturer with distilled water (see Figure 4).

when a very large amount of water is added. We used this property to adjust the viscosity of the solution. Another useful curve is the pH when using an acid (HCl, Figure 5). As expected, stronger decreases are observed; with a larger Na-Si concentration, more acid is needed to lower the pH and the different curves appear to be coherent (e.g. the curve for a concentration of 6 can be deduced from the curve at a concentration of 3 by multiplying abscissa values by 2).

Gelation time

The gelation time is typically measured using a rheometer and is defined as the time at which rheological properties are stable. It was studied for the above mentioned solution (Figure 6). As the Na-Si concentration increases, the gelation time becomes very short below pH=10 (a few minutes). These graphs suggest that the gelation may be quasi-instantaneous when using concentrated solution. A more comprehensive explanation of gelation is given by Tognonvi et al. (2011b). The gelation time of an alkaline silica solution ([Si]=3.7 mol/l) diluted in HCl has been studied and the results reported either at a constant Si concentration or at a constant pH to observe the effect of these two parameters independently (Figure 7). The increase of gelation times for increasing pH is interpreted as a competition between poly-condensation reactions and the formation of silicate species due to the dissolution of particles. The decrease of gelation times for increasing concentration is due to a dilution effect, poly-condensation effects becoming more difficult when particles are more dispersed.

Effect of temperature

The temperature effect on gelation times can be described by a Arrhenius type relationship - $exp(Ea/RT)$ - where Ea is an activation energy (J/mol), R is the gas constant (8. 314 J/mol/K) and T is the temperature in Kelvin. Above 40°C, it was found (Hamouda and

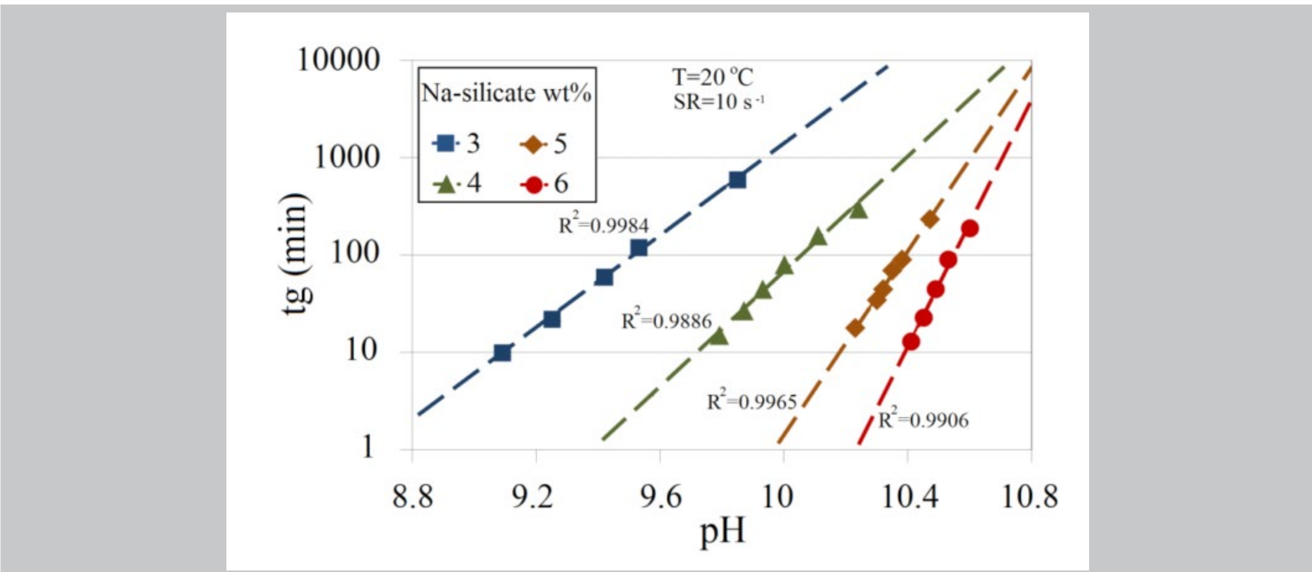

Figure 6 Gelation time tg for the solution described in Figure 5 (Hamouda and Amiri, 2014).

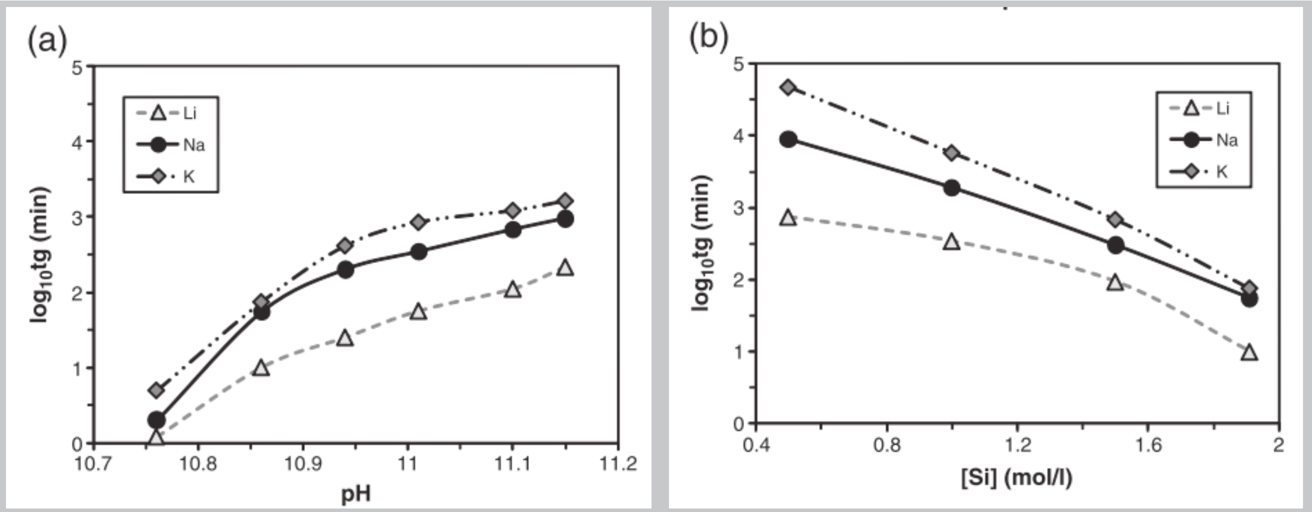

Figure 7 Effect of pH at constant silicon concentration [Si]=1.91 mol/l (a) and concentration at constant pH=10.86 (b) (Tognonvi et al., 2011b).

Amiri, 2014) that the gelation time decreases with Ea=70 kJ/mol (Figure 8), in agreement with other work (when gathering all works, the range is 60-80 kJ/mol). Similarly for the precipitation rate, an Arrhenius relationship was also chosen with an activation energy of -49.8 kJ/mol in the range of temperature relevant for geologic storage (Ito et al., 2014). A representation of such exponential increase indicates that the gelation time may increase by a factor of 5 between 40 and 60°C, and the precipitation rate by a factor of 11 (Figure 9).

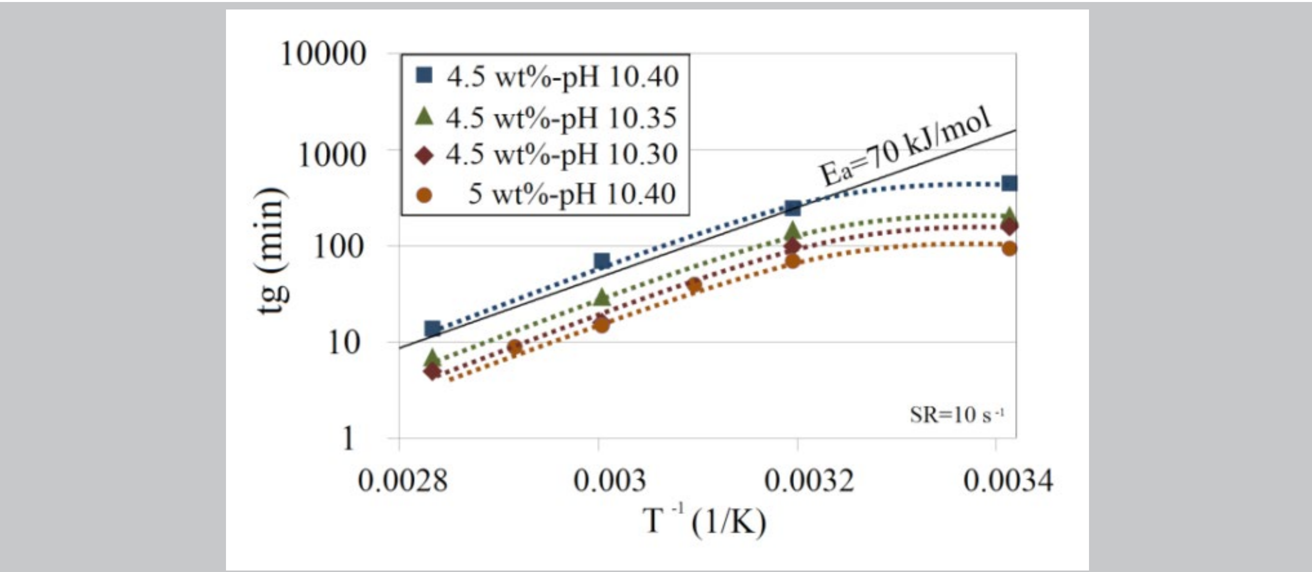

Figure 8 Range of investigated temperature in °C: from 21 up to 84°C. (Hamouda and Amiri, 2014)

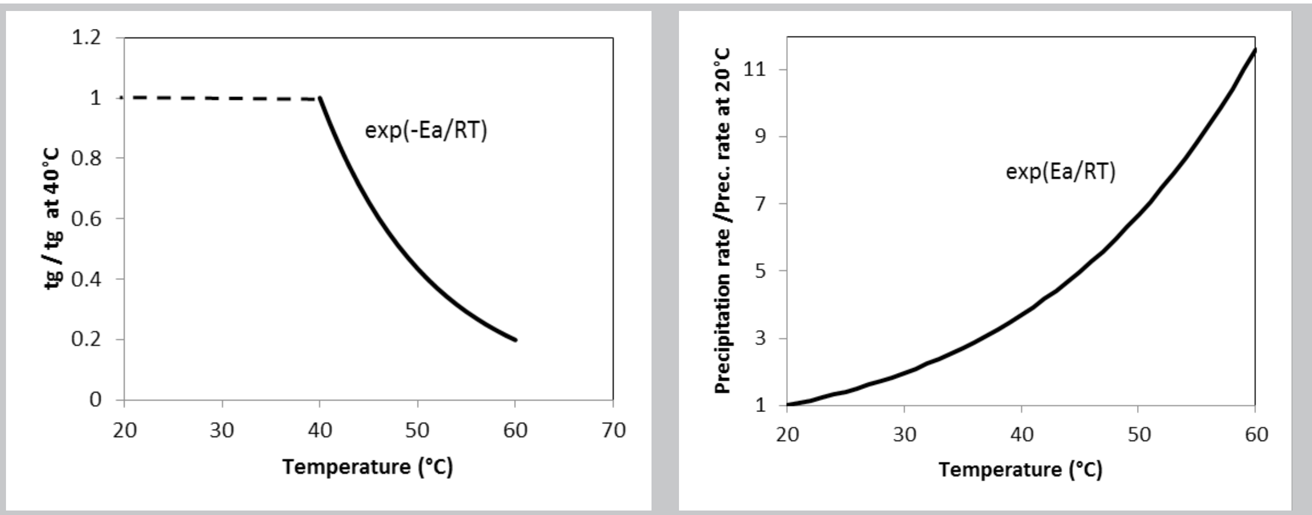

Figure 9 Graphical representation of the variation of gelation time tg and precipitation rate in the range 20-60°C. For gelation Ea=70kJ/mol, for precipitation Ea=49.8 kJ/mol.

Effect of salinity

Similarly to clay suspensions, the presence of salt affects the gelation time or may even generate a gel. In general, dissolved salts tend to reduce repulsive forces between particles, depending also on their surface charges. It was found (Metin et al., 2014) that the gelation time may be severely affected by dissolved salts in the usual range of interest in geological formations (Figure 10). However, in this case, the studied system is different: it is a suspension of non-porous silicate particles of size around 10 nm, in brines with different salinities. The gelation time decreases by several orders of magnitude. It was also observed that divalent ions (Ca^{2+} or Mg^{2+}) also impact the gelation time compared with NaCl brines (Hamouda and Amiri, 2014).

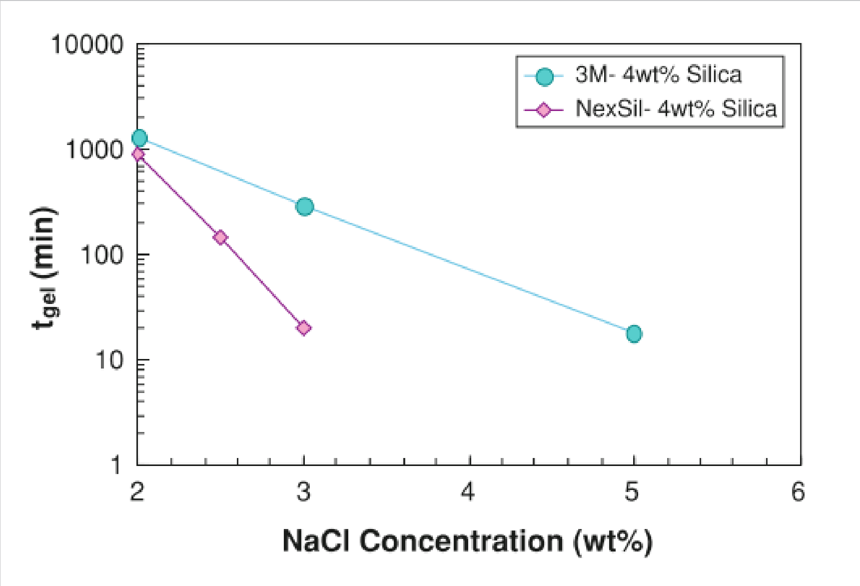

Figure 10 Gelation time for 2 suspensions of silicate nanoparticles in NaCl brine of different concentrations (Metin et al., 2014).

2.2 Sodium silicate solution as a consolidation material

Precipitated silica could also be used as a consolidation material (Kouassi et al., 2011). The study was conducted on sands following the experimental process depicted in Figure 11. A concentrated solution is diluted with acid, then with two types of silica sands, and finally dried. After acidification, the system forms a gel. After drying, a solid is formed binding the grains together, as shown by compressive strength tests. The generation of crystals is very slow (days up to 100 days). We understand this slow generation as due to atmospheric CO_2 inducing a reduction of pH and subsequent crystallization. These experiments show that the silica precipitates are linked to the solid surface presumably through Si-OH bonds. Images of dried precipitates in glass bead packs (Ito et al., 2014) also suggest some interactions with the solid surface.

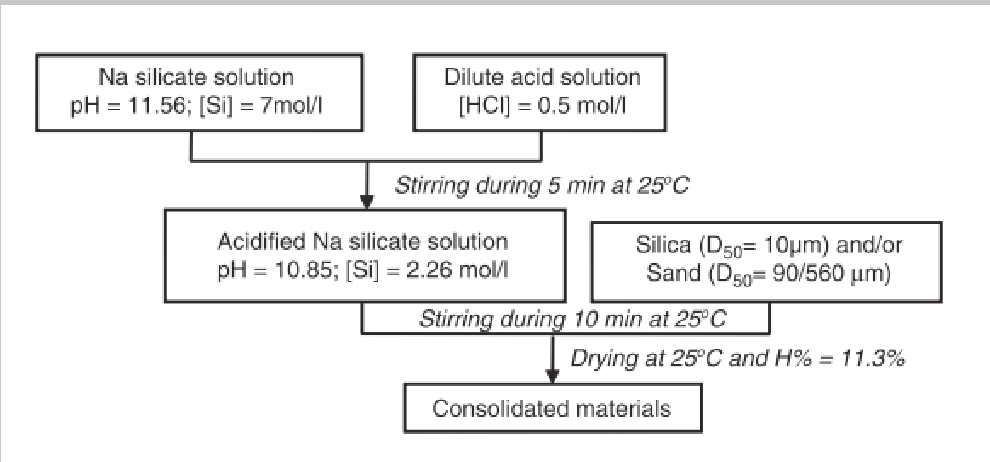

Figure 11 Experimental process to study consolidation of sands (Kouassi et al., 2011).

2.3 Chemical characterization and speciation modelling of silico-alkaline solutions

Silico-alkaline solutions (SAS) are aqueous solutions containing high concentrations of SiO_2 and A_2O, where the alkaline element A is generally sodium (Na) or potassium (K). They are characterized by the molar ratio $(SiO_2)/(A_2O)$, denoted by R_m (commonly 1.6 to 3.9 in commercial solutions, see Iler, 1979). High silica solubility is only possible at high pH (see Fig.I-3 in Tognonvi, 2009), a striking feature of concentrated SAS.

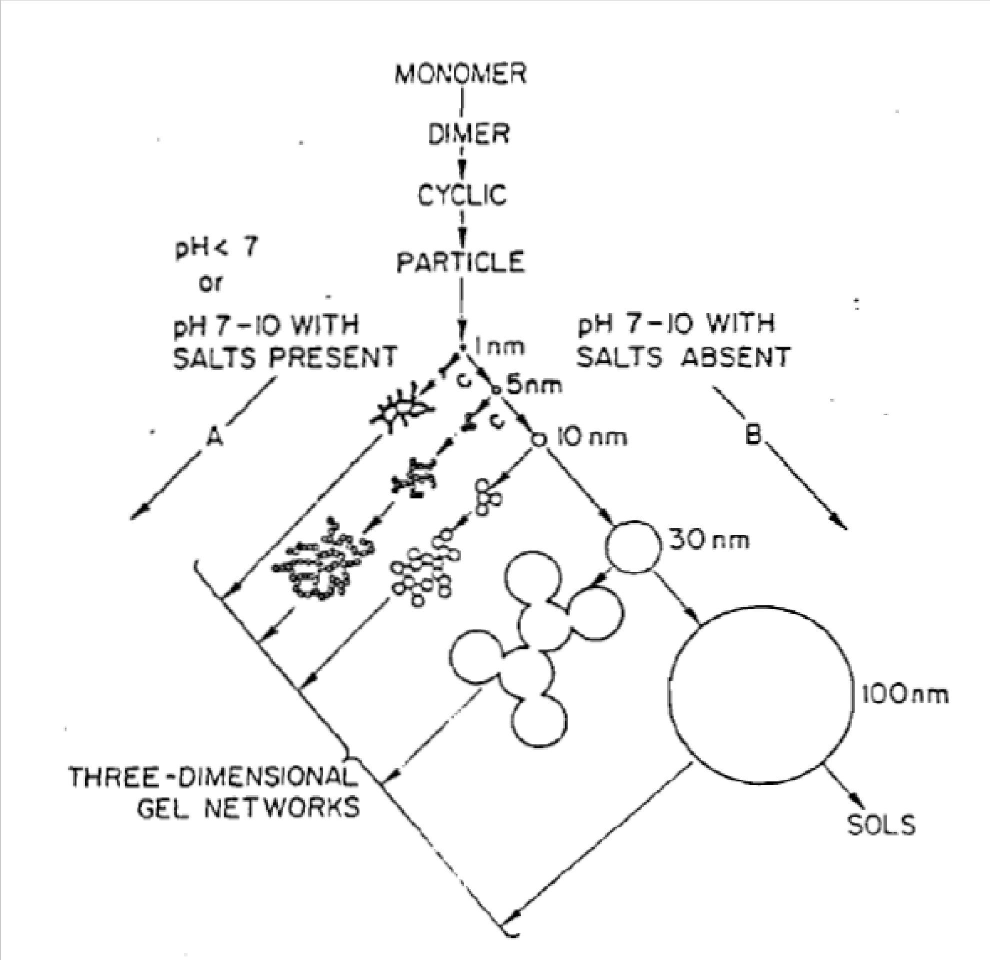

Figure 12 Polymerization and precipitation of alkaline metal silica solution (Iler, 1979).

Whereas diluted solutions (< 0,01 M Si) contain only the monosilicic acid H_4SiO_4 (aq) and its associated anions $H_3SiO_4^-$ and $H_2SiO_4^{2-}$, SAS contain a variety of oligomers $\{x \cdot H_4SiO_4\}$, with x up to 8, and their conjugated anions (Gaboriaud, 1999):

$$\{x \cdot H_4SiO_4\} \longleftrightarrow Si_xO_z(OH)^{y-}_{4x+y-2z} + y \cdot H^+ + (z - y) \cdot H_2O \quad (3)$$

A general framework for the polymerization/precipitation process is depicted in Figure 12 (Iler, 1979) but more detailed descriptions have only been available recently. The structure of oligomers can be described from ^{29}Si NMR spectroscopy (Figure 13).

Solution speciation, i.e., the distribution at equilibrium of concentrations and activities of dissolved species, can be calculated at conditions (temperature T, pressure P, concentration) for which equilibrium constants are available. Provided that relevant data are known, it is the most straightforward and rigorous way to predict pH and composition evolution when mixing the SAS with other

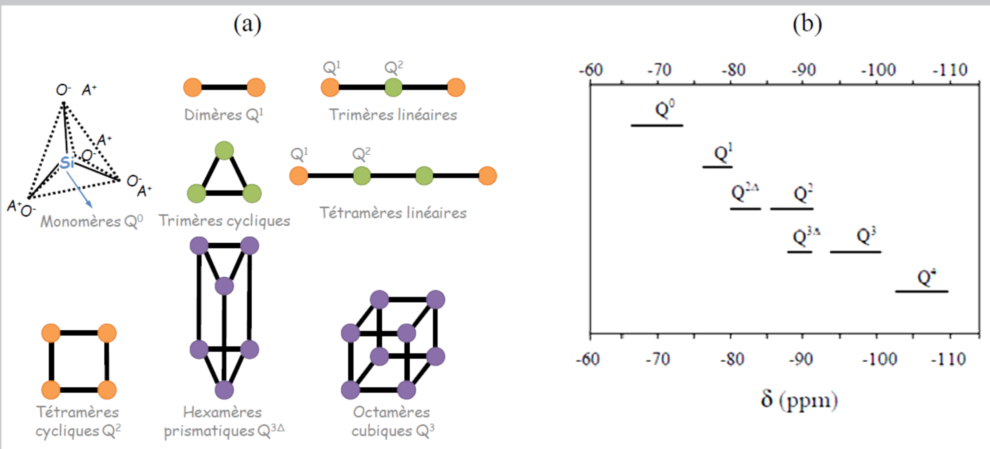

Figure 13 Silicic oligomer structures revealed by ^{29}Si NMR spectroscopy, where Q represents the SiO4 tetrahedron (coloured points), Q^n denotes the structure type (n is the number of bonding O, $n < 4$), and δ is the observed « chemical shift » measured in ^{29}Si NMR spectroscopy (Prud'homme, 2011).

solution, and to calculate saturation with respect to solid phases, e.g., a silica phase likely to precipitate when the SAS is acidified, or a mineral phase with which the SAS is in contact in a reservoir. An example of common species distribution is represented in Figure 14. A relatively sophisticated model was given by Lagerström (1959) (see Table 5 in the paper). Much more recently, Felmy et al. (2001) elaborated a thermodynamic model, based on Pitzer's formalism for activity correction in solutions of high ionic strength (see their Table II for Keq and Table III for Pitzer parameters). The same kind of approach was followed by Provis et al. (2005) (resp. their Tab.1 and Tab.2).

Gaboriaud (1999) called $K_{x,y}$ the constant associated to equilibrium (3), that means:

$$K_{x,y} = ((Si_xO_z(OH)^{y-}_{4x+y-2z}) \cdot (H^+)^y) / (H_4SiO_4)^x \tag{4}$$

where (E) denotes the activity of a species E, and if water activity (H_2O) is assumed to be 1. He showed that :

$$logK_{x,y} = y \cdot logK_{1,1} + (1 - x) \cdot logK_s \tag{5}$$

where $K_s = (H_4SiO_4)$ is the solubility of silica :

$$SiO_2 + 2H_2O \longleftrightarrow H_4SiO_4 \tag{6}$$

Appropriate values for $K_{x,y}$ must be adjusted to take into account the high concentration character (high ionic strength), and a convenient activity model (Pitzer). Therefore Gaboriaud (1999) proposes the values tabulated in Table 2 for SAS at $R_m = 2$, and in Table 3 for SAS at $R_m = 3$. The use of these $K_{x,y}$ values is subordinated to the use of the Pitzer's activity model with parameters given in the same document.

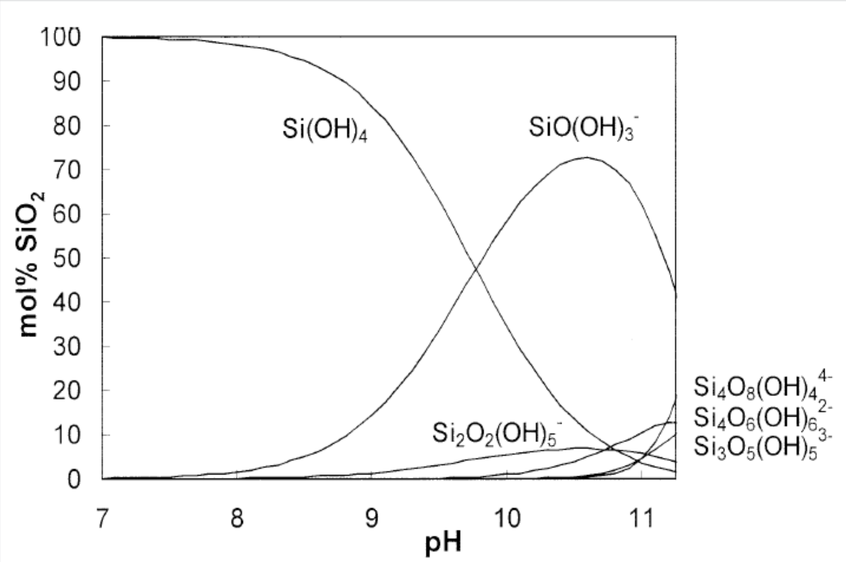

Figure 14 Distribution of the most abundant silicic species, at 25°C and at equilibrium with amorphous silica (Dietzel, 2000).

Table 2 Value of log $K_{x,y}$ for $R_m = 2$ (Gaboriaud, 1999). Values indicated in bold character were modified with respect to eqn (5).

Charge Espèce y	Log ($K_{x,y}$)					
	monomère x=1	dimère x=2	trimère x=3	tétramère x=4	hexamère x=6	octamère x=8
0	0	2,7	5.4	8,1	13.5	18.9
1	-9,8	-7,1	-4,4	-1.7	3.7	9.1
2	**-24,0**	**-19,8**	**-15,3**	-11.5	-6.1	-0.7
3		**-33,7**	**-28,6**	**-24,0**	-15.9	-10.5
4			**-44,6**	**-37,7**	**-30,3**	-20.3
5					**-44,3**	**-35,7**

Table 3 Value of log $K_{x,y}$ for R_m = 3 (Gaboriaud, 1999). Underlined values were modified, additionally to those already indicated in the previous table.

Charge Espèce y	Log (Kx,y) monomère x=1	dimère x=2	trimère x=3	tétramère x=4	hexamère x=6	octamère x=8
0	0	2,7	5.4	8,1	13.5	18.9
1	-9,8	-7,1	-4,4	<u>*0,6*</u>	3.7	9.1
2	**-24,0**	**-19,8**	**-15,3**	<u>*-12,0*</u>	-6.1	-0.7
3		**-33,7**	**-28,6**	**-24,0**	<u>*-16,5*</u>	-10.5
4			**-44,6**	**-37,7**	**-30,3**	<u>*-24,4*</u>
5					**-44,3**	**-35,7**

Table 4 Silico-alkaline solutions for which Gaboriaud (1999) experimented acidification.

SiO2 mol	SiO2/Na2O mol ratio (Rm)	Na2O (g) for 1 mol SiO2	dissolved mass g	SiO2/Na2O mass ratio
0,375	2,0	30,99	91,07	1,94
0,75	2,0	30,99	91,07	1,94
1,5	2,0	30,99	91,07	1,94
0,375	3,0	20,66	80,74	2,91
0,75	3,0	20,66	80,74	2,91
1,5	3,0	20,66	80,74	2,91

Gaboriaud (1999) used these values to simulate acidification of 6 distinct SAS (Table 4), which was also performed experimentally by incremental addition of 0,5 ml of 1 M HCl to 10 ml SAS (example Figure 15). Gelling (gélification in the figure) is a behavior observed at decreasing Si concentration (and pH) (Figure 16):

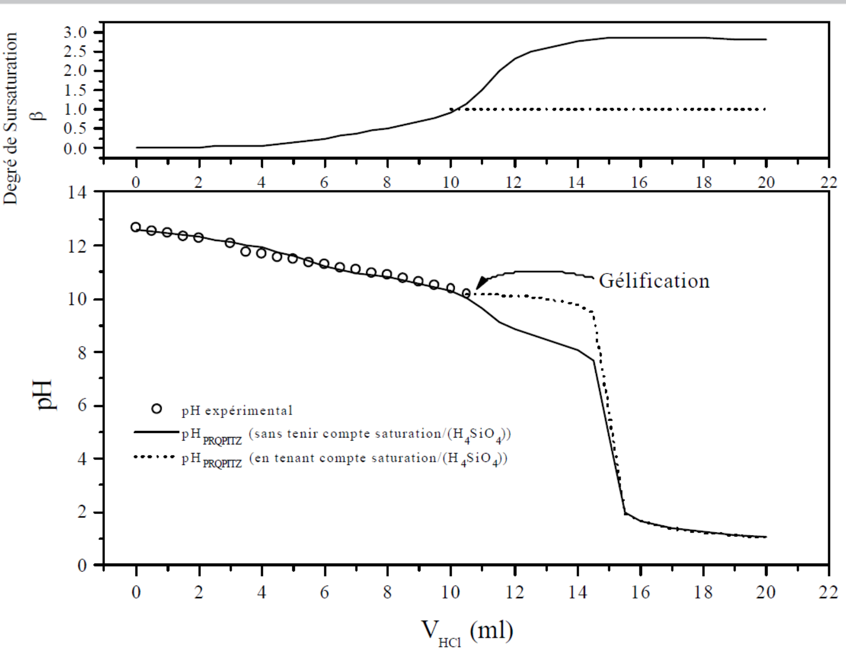

Figure 15 Acidification of a SAS containing 1,5 mol·l-1 SiO_2 and 1 mol·l-1 Na_2O (Gaboriaud, 1999). Two calculations were made, one preserves oversaturation with respect to silica (dotted line), the other respects equilibrium by silica precipitation (continuous line).

- Domain A : limpid, stable solution;
- Domain B : gelling, transparent gel, stable except if T increase, or agitation, or water dilution;
- Domain C : gelling, white gel, stable except if T increase or water dilution, ripening with time to form white grains that settle down;
- Domain D : gelling, ripening irreversibly to solid.

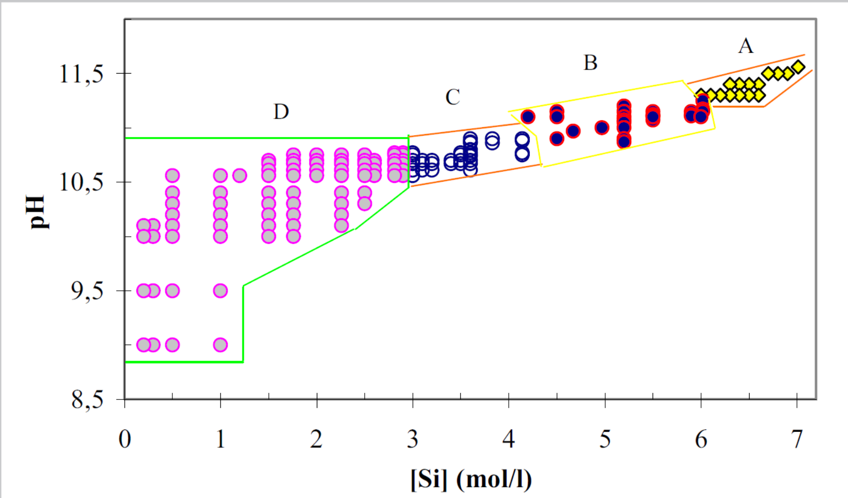

Figure 16 Various behavior of SAS observed at varying Si concentration and pH (Tognonvi, 2009). Domain A : limpid, stable solution ; Domain B : gelling, transparent gel, stable except if T increases, or agitation, or water dilution ; Domain C : gelling, white gel, stable except if T increases or water dilution, ripening with time to form white grains that settle down ; Domain D : gelling, ripening irreversibly to solid.

Oligomers are described as purely Si-O-H structures in all the publications we could refer to, except Tognonvi (2009) and (Tognonvi et al., 2010) who introduced Na-Si-O-H structures to account for the observed gels that appear from Na-Si waterglass (Figure 17). Their approach combined small-angle X-ray scattering (SAXS) to ^{29}Si NMR spectroscopy. The concentrated sodium solution had the following characteristic: pH=11.56, [Si]=7mol/l, Si/Na atomic ratio=1.71. Initially at the highest pH (11.56), the identified species is a $Si_7O_{18}H_4Na_4$ neutral complex (Figure 17). As the pH decreases with water dilution, the above neutral complex is dissociated progressively into $(Si_7O_{18}H_4\text{-}Na_{4-n})^{n-}$ and Na^+ ions. The same authors also studied the complexes formed during dilution with hydrochloric acid (Tognonvi et al., 2011a). In particular, in the pH range 9-10.75 and Si concentration between 0.2-2.9 mol/l, irreversible gels are formed and solids are generated. According to this interpretation, the $Si_7O_{18}H_4Na_4$ complex and its associated anions (equilibria [5] to [8] in Tognonvi et al., 2010) contain the major part of the dissolved silica in concentrated SAS at high pH. Unfortunately, they did not provide the K_{eq} constants attached to these equilibria.

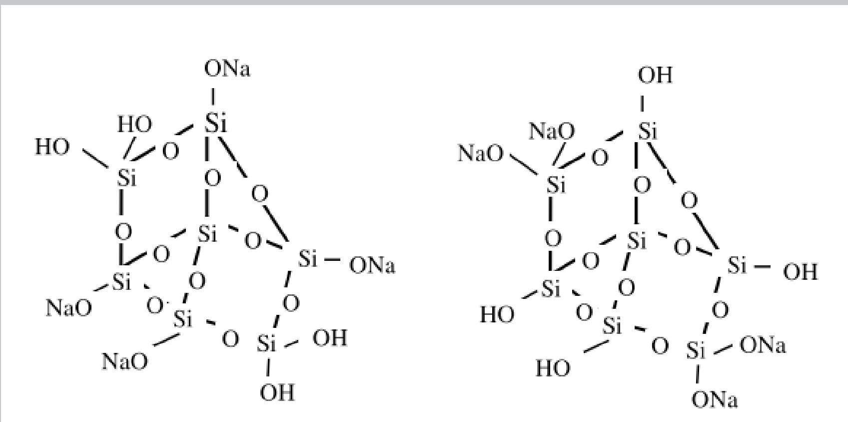

Figure 17 Structure of two possible $Si_7O_{18}H_4Na_4$ complexes compatible with the NMR and SAXS measurements (Tognonvi et al., 2010).

2.4 Physical properties of sodium silicate alkaline solution

Viscosity and density can be found in individual studies. Charts showing general trends are available since 1952 (Vail, 1952). For viscosity (Figure 18), we observe a sharp decrease in a narrow range of Na_2O content for Na silicate alkaline solution diluted in water. Similarly, the pH is not sensitive to water dilution (Figure 19) unless one uses very large dilution ratios. Note however that the pH may reach a maximum for high SiO_2/Na_2O ratio (e.g. 3 in Figure 19).

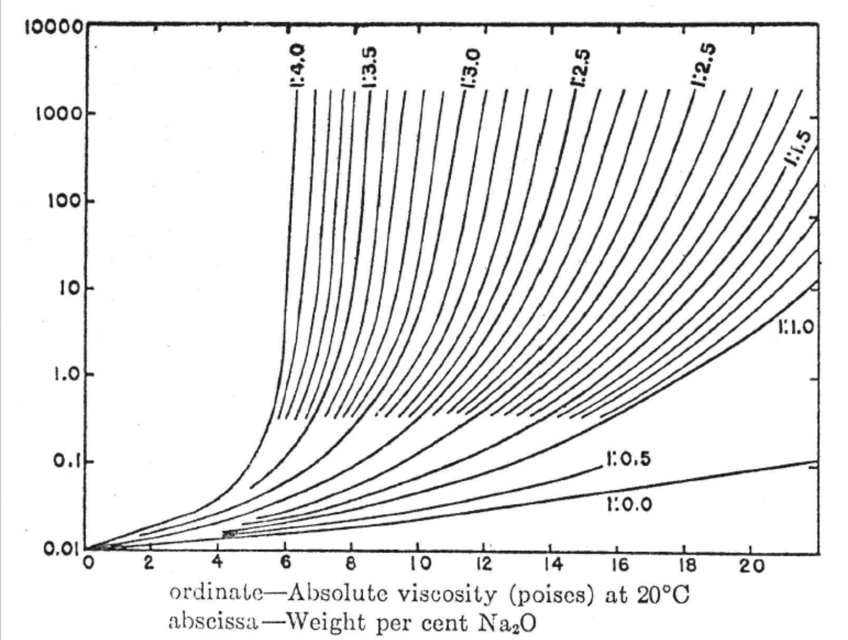

Figure 18 Viscosity chart (Vail, 1952) at 20°C for constant Na_2O /SiO_2 ratio (by weight) as a function of Na_2O content; the solution is diluted with water (Vail, 1952).

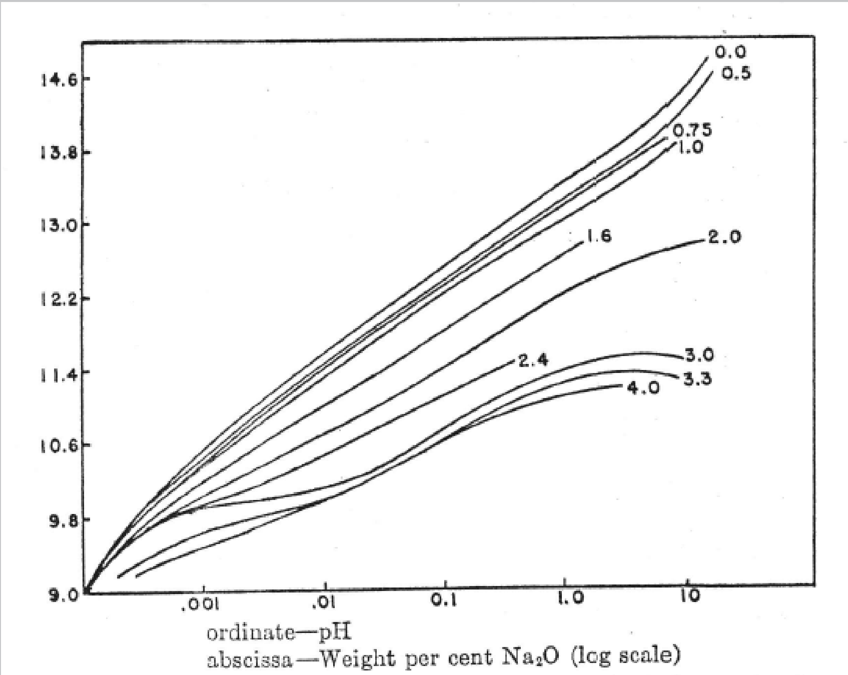

Figure 19 pH for constant SiO_2/Na_2O ratio (by weight) as a function of Na_2O content; the solution is diluted with water (Vail, 1952).

3 EXPERIMENTAL RESULTS

3.1 Solution characterization

Sigma-Aldrich solutions

The first tests were performed using a solution provided by Sigma-Aldrich (ref. 33844, main characteristics listed in Table 5). Although it is not planned to be used in field tests, CO_2 experiments have been performed with this solution. Viscosity and specific gravity for different water dilutions are plotted in Figure 20 and Figure 21. Excluding the points for the pure solution (100%), the viscosity variations can be modeled using exponential functions for viscosity at each temperature (20 and 40°C). This is in agreement with the general trends discussed above (Vail, 1952): at large dilution, the viscosity is described by an exponential law up to a certain limit at which it increases sharply. For density, a linear relationship can be used for both temperature (20 and 40°C). We chose to work with a solution diluted at 50 wt% in order to have a reasonable viscosity. This dilution does not significantly decrease the pH, as expected.

Table 5 Characterization of the Sigma-Aldrich solution (SA solution).

Sigma-Aldrich solution		Source
SiO2 content	26.7 wt%	Manufacturer
SiO2 content	26.1 wt% 6.04 mol/l	Measured
SiO2/Na2O	2.2	Measured
Na2O	11.8 wt% 2.645 mol/L	Measured
pH	11.9	Measured
Specific density	1.39 g/cm^3 1.47 g/cm^3 at 20°C	Manufacturer Measured
Viscosity	233.5 mPa.s at 20°C 78.6 mPa.s at 40°C	Measured Measured

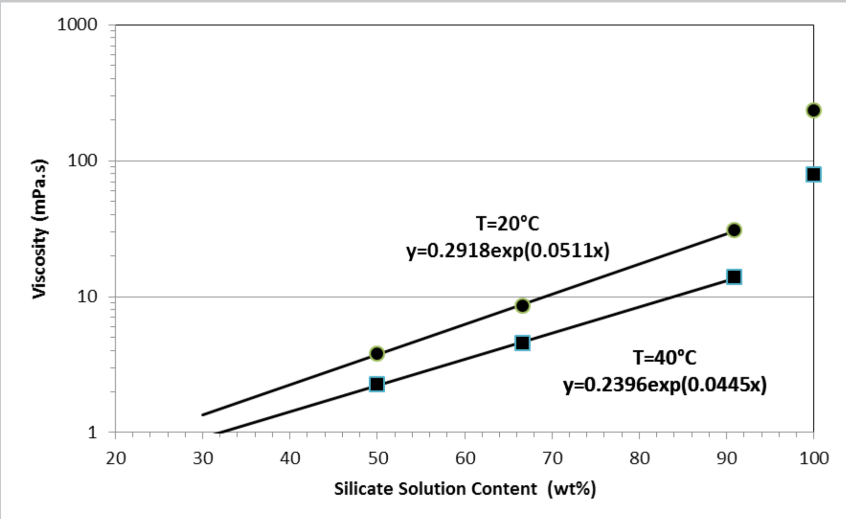

Figure 20 Viscosity of water diluted solution for two temperatures. The solution considered here is the SA solution.

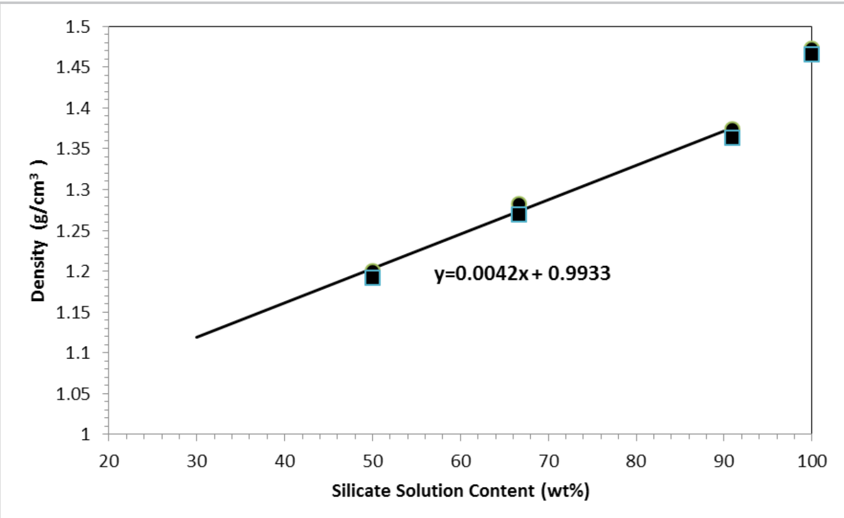

Figure 21 Density of water diluted silica solution at 20°C and 40°C. The solution considered here is the SA solution.

Woellner solutions

The solutions planned for field tests are provided by Woellner, a leading manufacturer of silicates (Table 6). Among the 4 products available, we chose a potassium silicate with the lowest viscosity, BetolK28T. Diluted at 50wt%, the viscosity is reduced to 1.1 cP at 40°C, with a density of 1.11 g/cm^3.

Table 6 Characterization of Woellner solutions (SA solution).

Product Name	SiO_2 %	Na_2O %	K_2O	Molar ratio	Viscosity (cP)	Density	pH
Ligasil 39	27.5	8.3	0	3.47	100	1.37	11.3
NaSil HK35	26.1	7	0	3.85	150	1.32	11.3
Betol K35T	23.9	0	10.9	3.43	55	1.32	11.0
Betol K28T	20.5	0	8.2	3.92	28	1.25	10.8

3.2 Batch experiments: precipitation using CO_2

Several batch experiments were performed with the SA solution to see if precipitates are generated. In a reactor maintained at 40°C, different diluted solutions were placed in contact with CO_2; the reactor is then closed and the pressure recorded (Figure 22).

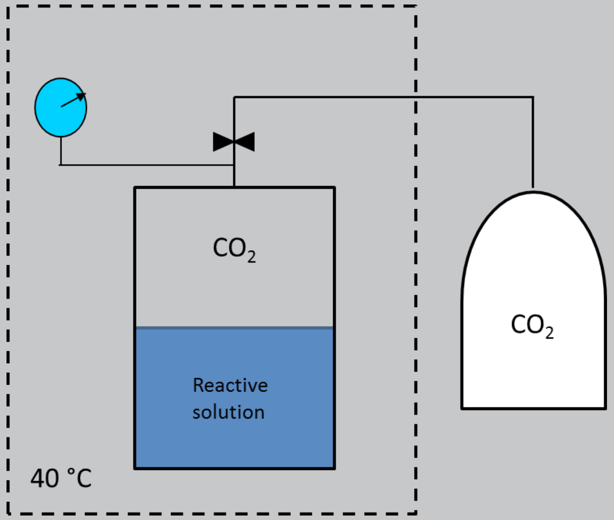

Figure 22 Schematic of batch experiments with CO_2. The reactor is maintained at a constant temperature and the gas pressure recorded.

Table 7 Parameters of batch experiments. The solution is the SA solution described in Table 5.

Batch exp. #	Dilution	Volume ratio, gas to total liquid (%)	Pressure (bar)	Final pH	Observation
1	Sol 100 g Water 10g	40	50	Not measurable	Reactor totally filled with solids
2	Sol 100g Water 10g	40	10	11.9	Thick solid film at the surface 3.82% heavier
3	Sol 100g Water 10g	40	10 bar CO2 40 bar Argon	11.8	Thick solid film at the surface 3.82% heavier
4	Sol 50g Water 50g		50 bar CO2	Not measurable	Reactor totally filled with solids

The run products for experiments 1-3 (10% water, 90% water glass solution) are about 4 wt% heavier than the initial solution introduced in the reactor, which indicates that CO_2 has been trapped in the solid run products. It indeed appears that solid carbonate phases are formed as well as amorphous silica gel, as it is indicated by the presence of a solid white precipitated product surrounded by the transparent silica gel. This observation is confirmed by XRD data (Figure 25), which indicates the presence of two different sodium carbonates, one being hydrated and having thus a higher molar volume.

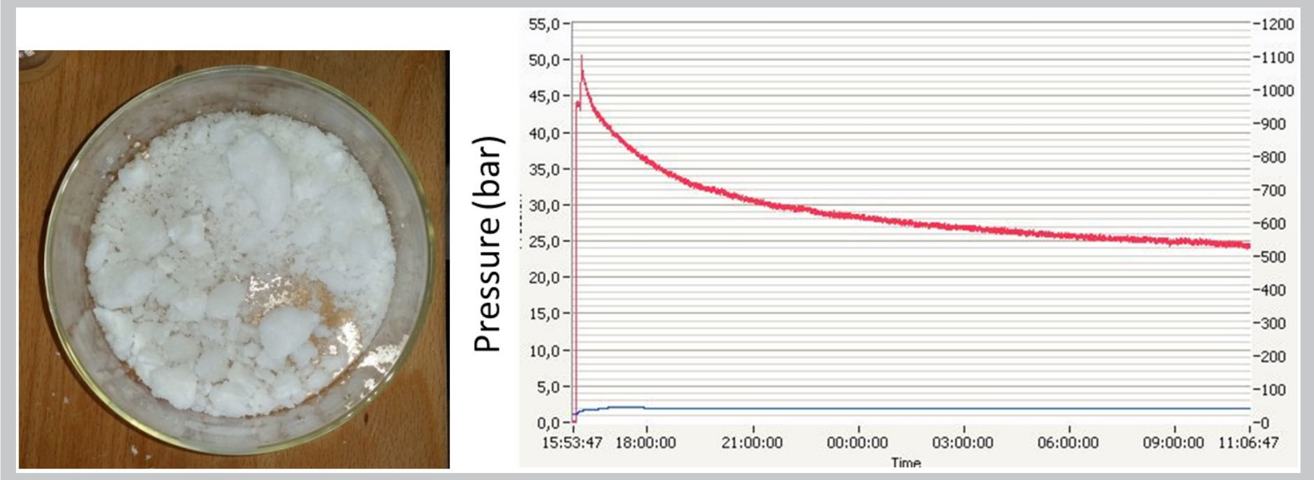

Figure 23 Batch experiment 1; after 19 hours, the reactor was full of solids, and no water was left; the solid contains trapped water that was measured with NMR. 25 bar of CO_2 remains in excess.

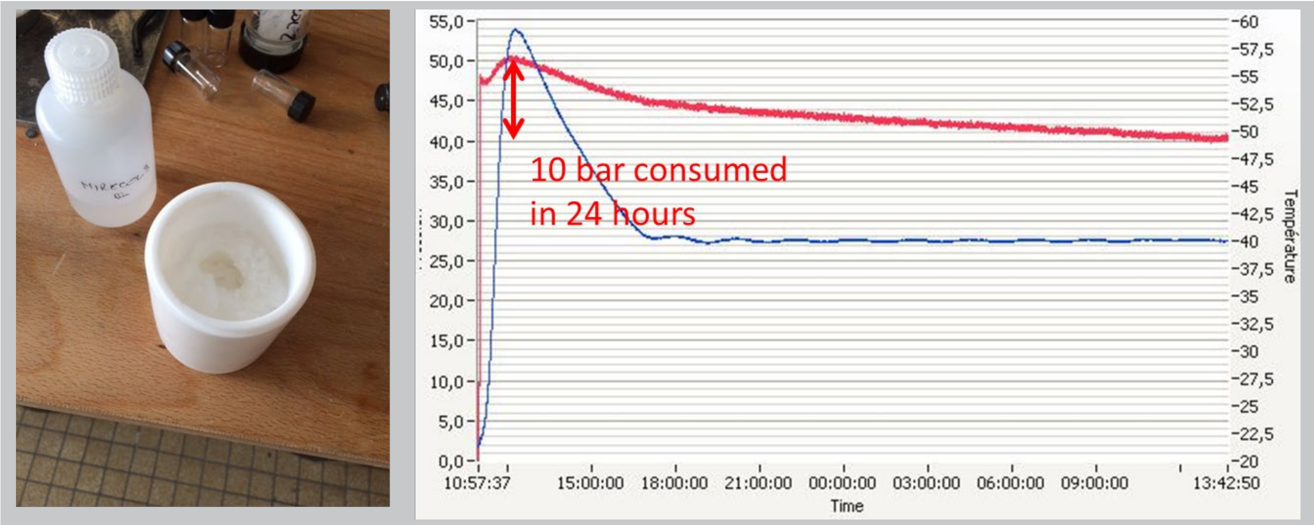

Figure 24 Batch experiment 3; after 24 hours, the 10 bar of CO_2 have been completely consumed, and a solid carbonate phase surrounded by silica gel has formed on top of the remaining water glass solution.

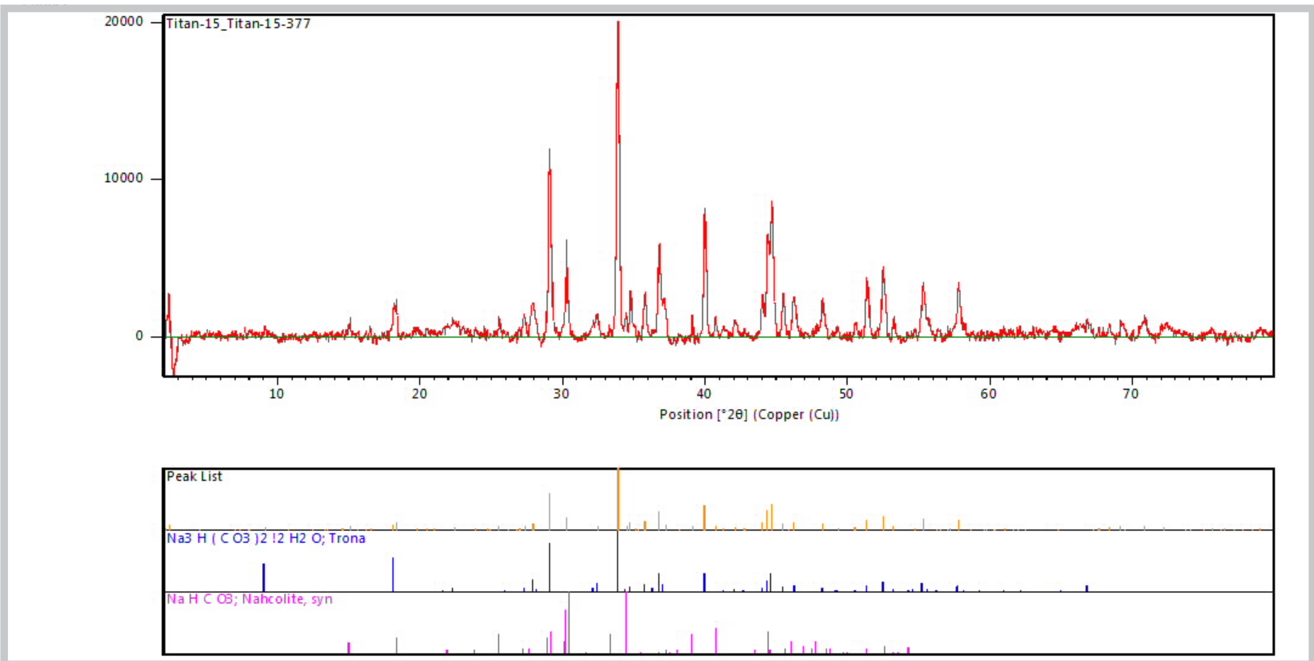

Figure 25 XRD spectrum of experiment 3 : anhydrous (nahcolite), but mostly hydrous sodium carbonates (trona) have formed within the run products, trapping the CO_2 and potentially increasing the molar volume of the amorphous silica gel.

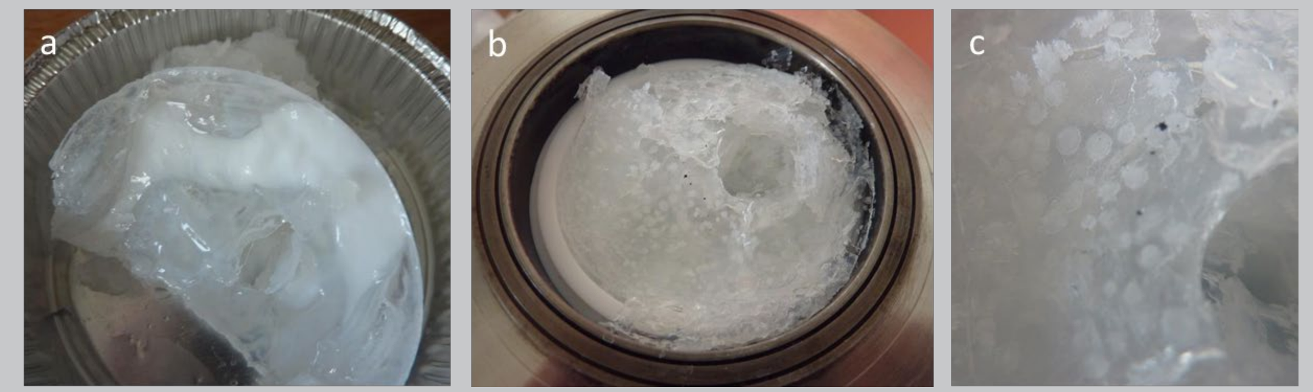

Figure 26 (a) Run products of experiment 2; silica gel is observed around a more solid white phase, formed of carbonates. (b)-(c) Run products of experiment 4. White centimeter-sized phases, which we identify as carbonates, can be observed in the silica gel.

It should be noted that the silica gel is extremely hydrated, and the water linked to the silica can apparently trap dissolved CO_2 within its matrix. Indeed, under 50 bar of CO_2, experiment 1 (90% water glass solution, 10% water) showed an increase of mass of 4 wt% in the run products. Under the same pressure of CO_2, experiment 4, which had more water in the reactive solution (50%/50%) showed an increase of mass of 10%. Since experiment 4 had less Na available to form Na-carbonates than experiment 1-3, the excess amount of trapped CO_2 must have been dissolved in the gelified water of the solid silica phase.

To quantify the degree of hydration of the solid phase with a rudimentary method, 26.4 g of solid was placed over 24h at 60°C in an anhydrous environment. Only 6.75 g remained after 24h. After 48h, 6.67 g. After a week, 6.52 g. In other words, it appears that around 75 wt% of the formed phase was composed of water. Since water actually represented around 83.5 wt% of the initial mixture (50% water glass solution, 50% pure water), it represents around 75.9 wt% of the run product incorporating trapped CO_2. This suggests that the residue remained feebly hydrated (0.9 wt%) and that the carbonates formed remain stable.

Hydration can also be quantified using low field NMR techniques. This was performed for the solids of experiment 1, using a solution containing less water. From the T_1-T_2 maps, we see that the T_2 relaxation times of the water is small (about 20 ms, main peak), indicating a high degree of confinement. This is also confirmed by a T_1/T_2 ratio of 2, a clear signature of water confined in a porous media and in interaction with a solid. The secondary tail at larger relaxation values ($T_2 \sim 300$ ms) may be due to water at the external surface of the solids. Quantitatively, the total mass of the sample was 3141.2 mg, and the measured mass of water by NMR was 192.8 mg, thus representing only 6% of the total mass. However, uncontrolled drying occurred for this sample.

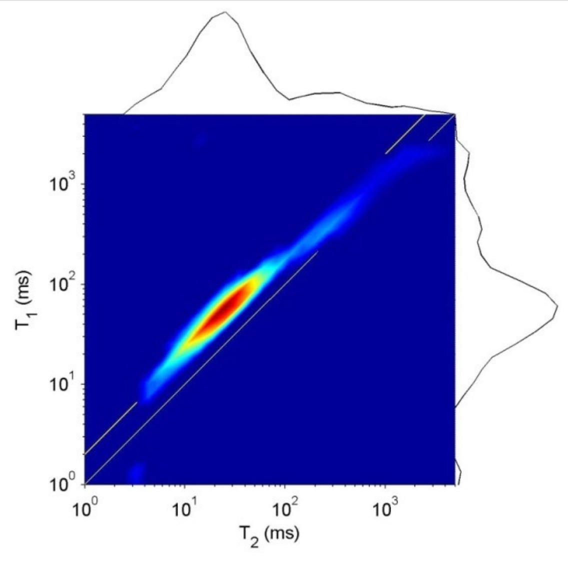

Figure 27 Low field NMR relaxation time T_1-T_2 maps for the water present in the precipitated "solids". Lines indicate a T_1/T_2 ratio of 1 and 2.

3.3 Experiments in porous media with CO_2

An experiment was performed on a sand pack made of natural quartz grains (100-160 µm size). The protocol was the following:

- After saturation with 20 gr/l NaCl brine, measure permeability
- Inject the reactive solution in the column and monitor the pH at the outlet; stop when the pH has reached the value of the solution,

- Flush all tubing and end-pieces with brine,
- Flush all tubing and end-pieces with CO_2,
- Inject CO_2 through the column (24 hours) and measure the amount of solution left in the column,
- Inject brine to remove the reactive solution and CO_2 left,
- Measure the brine permeability.

It is designed to observe the change of permeability to water due the precipitation/adsorption of the reactive solution in the column. Potential artifacts due to plugging the inlet/outlet tubing are avoided when following the above protocol, and the design of the end-pieces of the cell has two entries available to allow flushing of the inlet/outlet faces of the sample (Figure 28). The pore pressure can be set by a back-pressure regulator. X-ray CT scanning has also been performed to observe the change of porosity along the column.

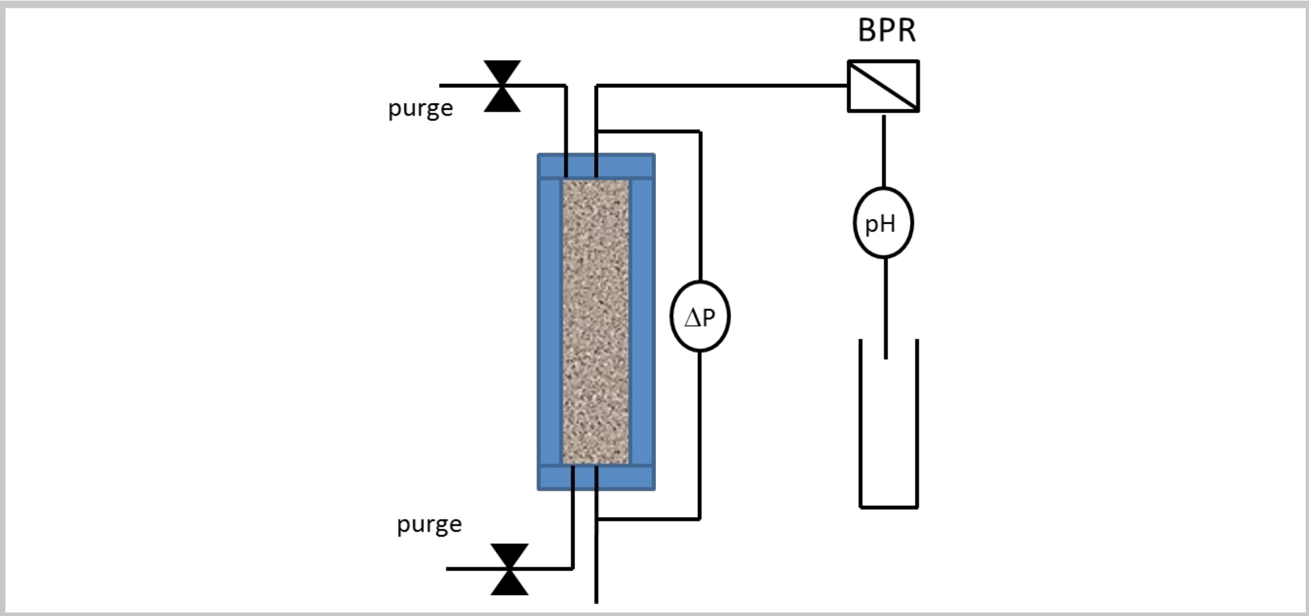

Figure 28 Schematic of the experimental set-up for testing reactive solutions in porous media. The column has an inner diameter of 28.4 mm and the sand-pack has a length of 140 mm (maximum).

Using the SA solution diluted with water (50wt%), the permeability decreased from 3220 mD down to 565 mD with little change of porosity (47%).

Using the SA solution diluted with water (50wt%), the CO_2 was continuously injected at a flow rate of 100ml/hr (at 10 bar). After CO_2 breakthrough, the liquid saturation was 67% and no further liquid production was observed. After flushing with brine and returning to 100% brine saturation, the permeability decreased from 3220 mD down to 565 mD with little change of porosity (47%), not detectable by CT scan (not shown). The continuous flow of CO_2 along the sand-pack corresponds to a situation in which the gas is in excess. For this solution, CO_2 at 10 bar does not allow strong precipitation (presumably), as observed in batch experiments.

A similar experiment was performed again using BetolHK35 solution diluted at 50wt% (same sandpack). However, the pore pressure was set at 50 bar (40°C). In this case, the CO_2 injection was impossible after 10 min of flushing (and after breakthrough). The sand-pack was totally plugged and no water permeability could be measured.

3.4 Precipitation using CO_2: conclusions

Using CO_2 to precipitate silica is an efficient means to form various solids at high CO_2 pressure. However, the reaction kinetics are fast and difficult to control. In addition, there is no theoretical basis to predict the run products. In a porous media (sand-pack), the decrease of permeability is moderate (a factor of 6) at low pressure (10 bar). At higher pressure (50 bar), the porous media is plugged and the permeability is not measurable (with a standard device; the permeability could be reduced to extremely low values smaller than 1 µD, but this not known).

Based on these observations and especially in view of the lack of possible control of the kinetics of precipitation, it was decided to explore a different option: use of a weak acid to initiate a precipitation the kinetics of which are compatible with field operations.

3.5 Batch experiments: precipitation using acetic acid

The solution used in these experiments is Betol K28T diluted with water (50wt%). Following the methodology of Tognonvi (2009), we tested several mixtures of diluted Betol and acetic acid (1M), similar to vinegar. Precipitation was qualitatively observed for various fractions of diluted solution and acid at 40°C (Figure 29). When enough acid is present, solid precipitates are observed after a variable time and these solids cannot be dissolved again back into water. If the acid content is too low (not shown), the gel is weaker and reversible. These tests allowed 3 acid concentrations to be tested in more detail using rheological and NMR measurements, as described in the next section.

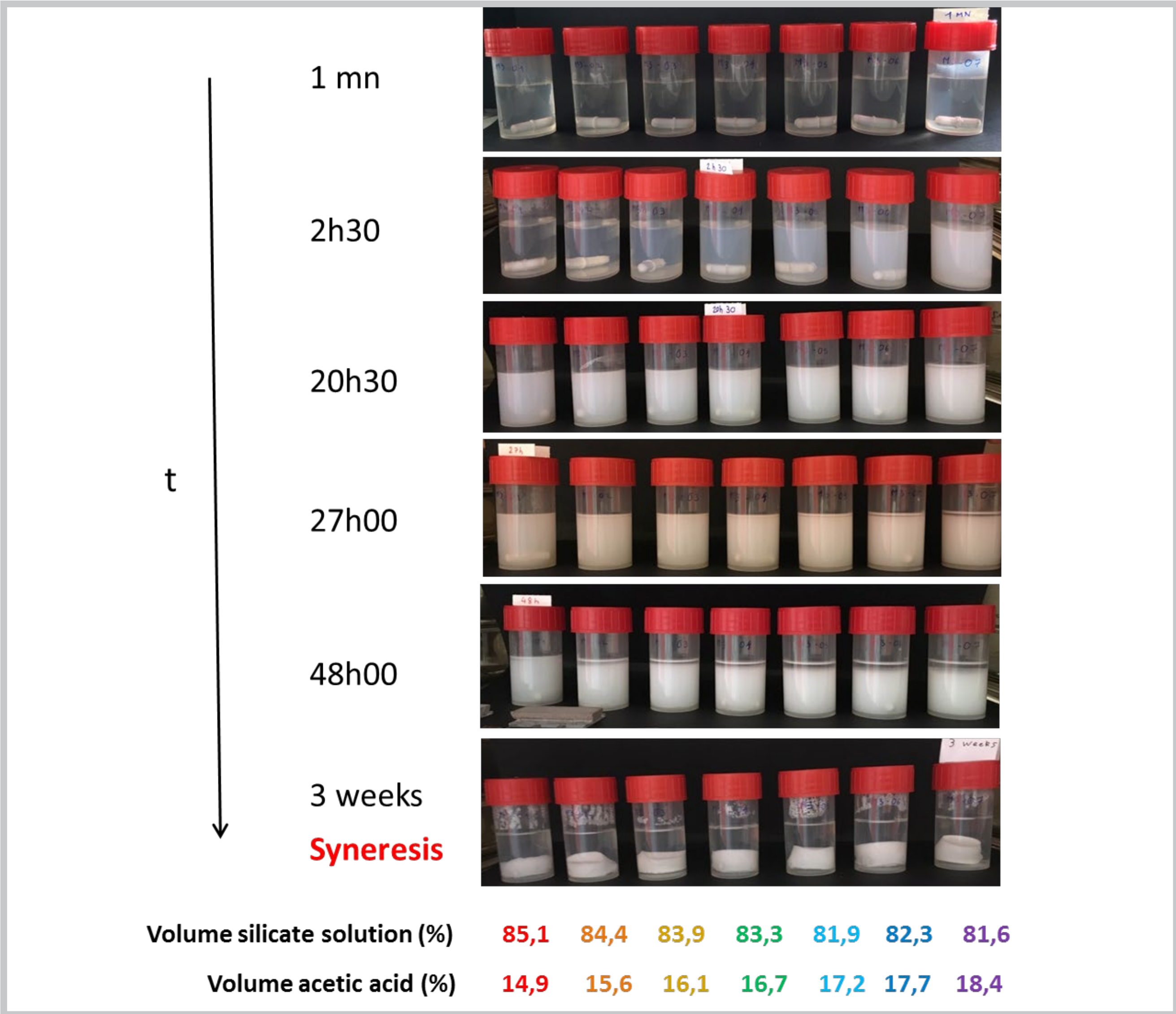

Figure 29 Precipitation experiments with acetic acid (1M) at different times. Solution: BetolK28T diluted with water (50wt%).

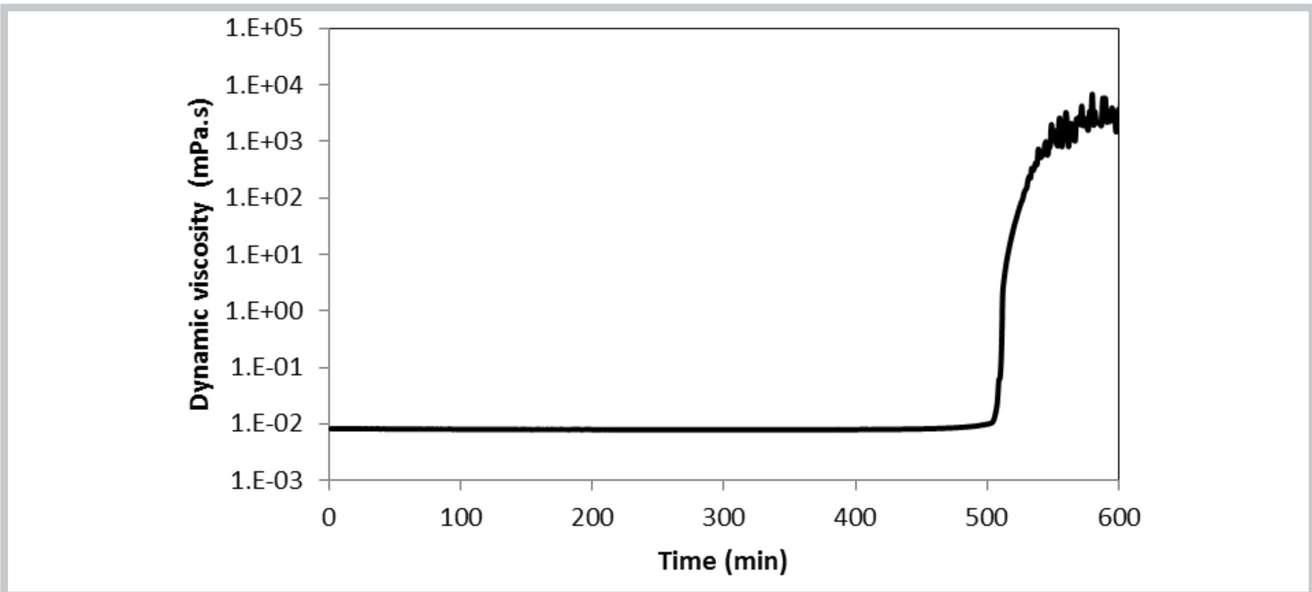

Figure 30 Evolution of the viscosity of a mixture diluted Betol K28T with 15.7wt% of acetic acid 1M. Temperature: 40 °C.

3.6 Measurements of gelling times

The gelling times can be obtained very precisely from rheological measurements. The instrument used is a MCR300 from Physica. The geometry is a cone-plate maintained at 40°C using a Peltier set-up, together with a system minimizing evaporation and contact with air. The rheometer was operated in an oscillating mode at low frequency (1Hz) and small oscillating angle (<10°), yielding a shear rate as small as possible. Such protocol are common when studying polymers.

A typical result is shown in Figure 30. The purpose of the graph is to show the sudden increase in viscosity after 500 minutes, defining precisely the gelling time t_g (in this case 510 min); note that the viscosity value before gelling may not be accurate and it has been measured using another geometry.

The viscosity measurements tend to indicate that no change in the mixture occurs before t_g but this is not true. Another useful method is to study the evolution of the water interactions within the mixture, and this is given by the NMR relaxation measurements as a function of time (Figure 31, performed with a 23 MHz apparatus from Oxford instrument); the T_2 relaxation time characterizing the mixture decreases progressively from the initial and maximum T_{2m} down to a plateau value T_{2p}. By comparing several viscosity and NMR measurements, we established that the abrupt change of viscosity corresponds to the time at which the relaxation time T_2 $(t = t_g)$ is such that the relative variation of relaxation times is 0.235, i.e.,

$$(T_2 (t = t_g) - T_{2p}) / (T_{2m} - T_{2p}) = 0.235$$

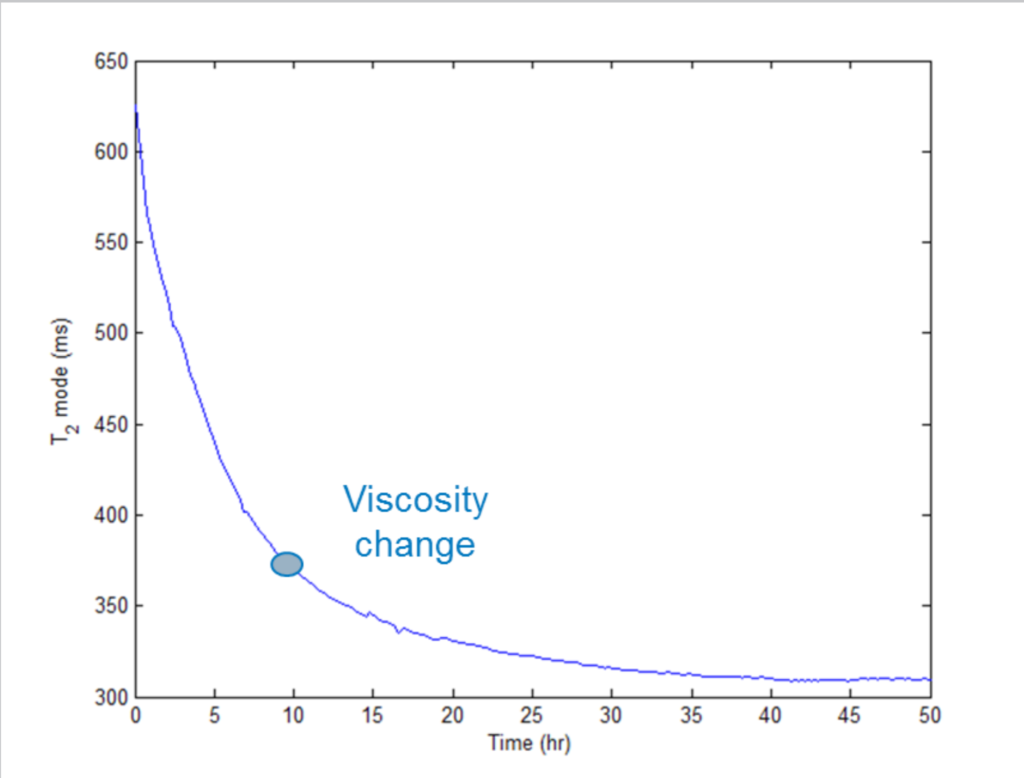

Figure 31 Evolution of the T_2 relaxation time for the same mixture as in Figure 30 The circle indicate the gelling time tg (abrupt change of viscosity).

3.7 Effect of temperature and acid concentration

To study the effect of temperature on gelling times t_g, we use NMR measurements and the relationship between rheological and NMR relaxation measurements described above. NMR measurements are more convenient to use at high temperature and provide more information. The sensitivity can be described using an Arrhenius law (Figure 32):

$$t_g \propto \exp\left(-\frac{E_a}{RT}\right)$$

where E_a is an activation energy (J/mol), R is the gas constant (8. 314 J/mol/K) and T is the temperature in Kelvin. From the data, we found E_a = 80kJ/mol (Figure 32). Such a value is in agreement with literature as discussed earlier. Expressed in more practical units, such an activation energy means a strong dependence with temperature. For example, at 40°C, we have a gelling time of 510 min (8.5 h), at 50°C, 193 min (3.2 h) and at 60°C , 77 min (1.3 h).

Increasing the acid fraction above 15.7% decreases the gelling time by a factor of about 4.5 (Figure 33) but it is not possible to increase the gelling time by lowering further the acid fraction. Hence, it appears that, using acetic acid, a maximum and ideal value is reached (about 15.7%).

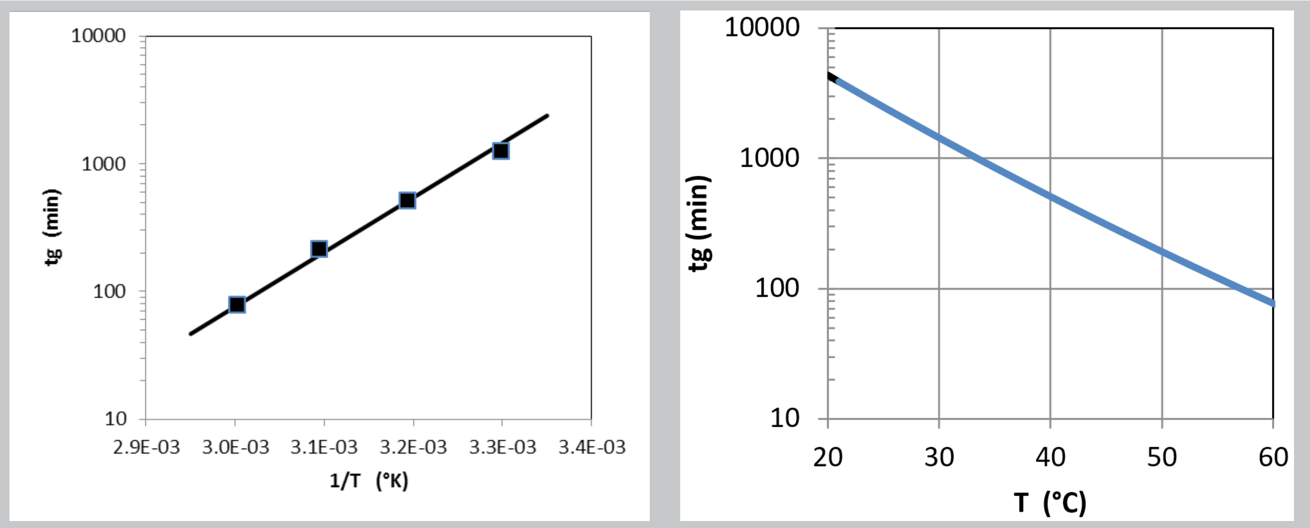

Figure 32 Gelling times determined by NMR as a function of temperature (data points at 30, 40, 50 and 60°C). BT28 solution diluted with 50wt% water. Acetic acid content: 15.7wt%.

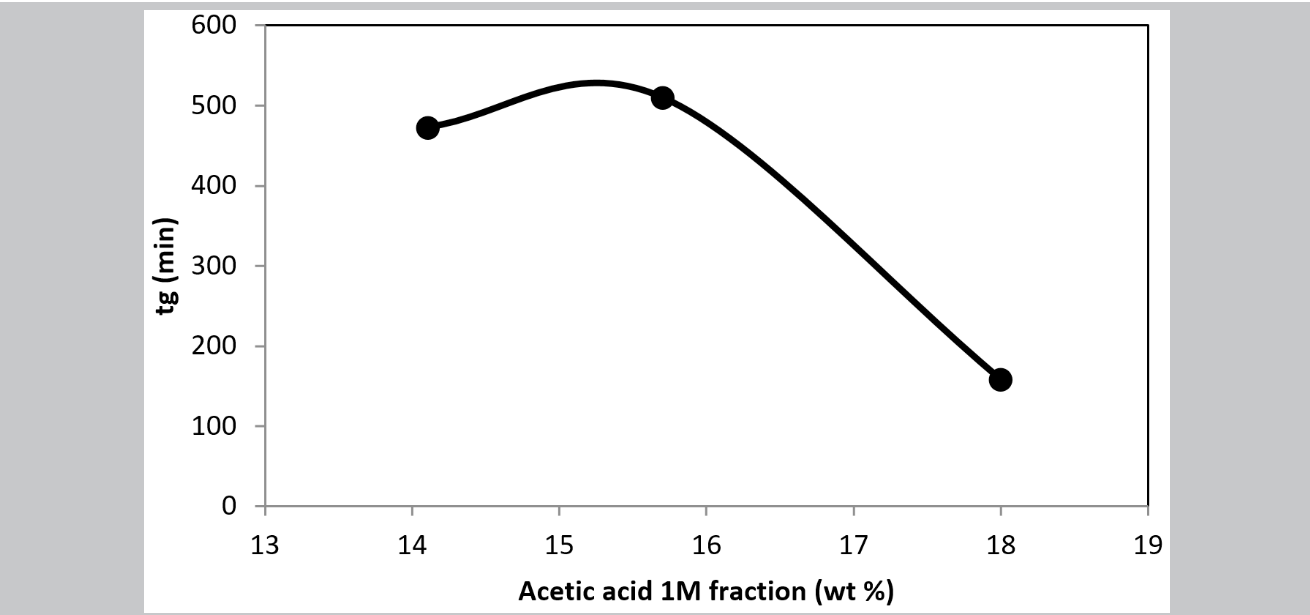

Figure 33 Gelling times as a function of acetic acid fraction at 40°C. Lowering the amount of acid in the solution does not increase the gelling times.

3.8 Experiments in porous media with acetic acid

The strength of the gel was tested in a porous media in a flooding cell (Figure 34). In a similar way to CO_2 injection experiments, we injected the mixture in different porous media. The samples are small plugs 2 cm in diameter and 3 cm long. The applied confining pressure was 80 bar, and the pore pressure was 20 bar. The protocol was the following:

- After saturation with 20 gr/l NaCl brine, measure the permeability to brine,
- Inject the reactive solution into the plug and monitor the pH at the outlet; stop when the pH has reached the value of the injected solution,
- Flush all tubing and end-pieces with brine,
- Wait for 24 hours or more,
- Inject brine through the tubing and end-pieces to verify that they are not plugged,
- Try to inject brine through the porous media.

This protocol was performed at 40°C. Several experiments of this type were performed and they all indicate that the porous media was severely plugged. For example, a pressure differential of about 20 bar could be applied to the plug before measuring a significant flow rate. Since the plug length was 3 cm, these tests give therefore a gel strength of the order 600 bar/m. This test was also performed with several differential pressure steps applied for longer period of times and it gave similar results. The tests were performed on a Vosges sandstone (50 mD) and a sample from the Bečej field (5mD).

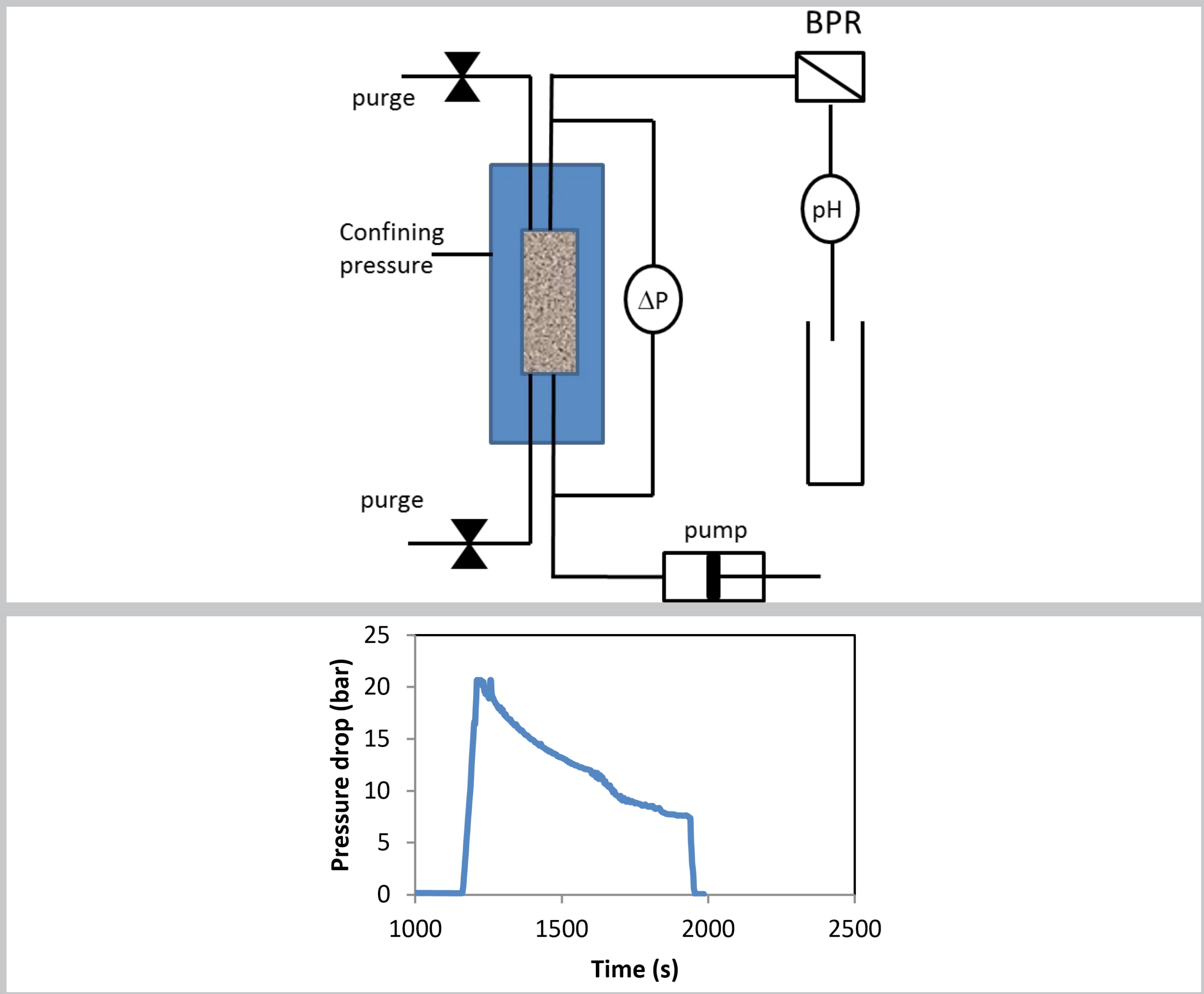

Figure 34 Simplified schematic of the experimental set-up for testing reactive solutions in porous media (left). The cell allows flushing all the tubing and end pieces to remove the reactive solution after flooding the porous media. The graph shows that a pressure differential of 20 bar could be applied before the gel breaks and allows brine to flow through the porous media.

4 SUMMARY AND CONCLUSION

In the framework of the MiReCOL three-year European project [1], a method for treating the surroundings of a well using a reactive suspension is studied. Among many possible choices, silicate based solutions were selected due to the following key qualities: high performance, long term chemical stability (w.r.t. acid), good injectivity (low viscosity and no particles) and no or little environmental impact.

Silica-alkaline solutions are aqueous solutions containing high concentrations of SiO_2 and A_2O, where the alkaline element A is generally sodium (Na) or potassium (K). Commercial stable solutions exist with a high molar ratio SiO_2/A_2O, spanning from 1.6 up to 3.9 with pH values above 11.5. When the pH is lowered either in contact with CO_2 or using an acid, silica precipitates to form particles. Below a pH of approximately 9 according to the solubility curve, the particles formed are stable and no back-dissolution is possible unless the pH is increased again. Hence, one expects a long-term stable chemical stability. Under certain circumstances, when induced in a porous media, this process has the potential to plug the formation around a well, to prevent gas or liquid flow through the treated formation.

An experimental investigation of the precipitation of commercial low cost sodium and potassium silicate solutions using a weak acid to lower the pH has been performed. Preliminary results using CO_2 indicate that the reaction kinetics are too fast and the plugging too strong to permit practical field implementation. Hence, laboratory experiments were performed testing various concentrations of acetic acid added to the commercial silica based solution, and estimating the bulk gelation times before the mixture became too viscous for injection. The impact of temperature was determined by performing experiments at 20, 40 and 60°C, with gelation times estimated between a few minutes up to 4 days. Multiple characterizations of the run products were performed using high resolution physico-chemical techniques. To follow the kinetics, several complementary techniques were used: rheological visco-elastic properties to observe the gel onset and NMR relaxation time measurements to follow the gradual increase of water interactions within the gel.

The ability of the precipitates to plug a porous media was tested on analog sandstone samples representative of CO_2 storage formations, as well as a sample from the Bečej field (Serbia). With a viscosity close to water and no particles present in the liquid, injection of such products is possible in almost any permeable media. Using an optimum mixture tuned as described above, the solution is simply injected through the porous media and then left at constant temperature (e.g. 40°C) for precipitation. After a few days, a breakthrough experiment is performed by increasing gradually the differential pressure across the sample. The results obtained so far indicate a very large strength of the order of 600 bar/m.

5 ACKNOWLEDGEMENTS

We thank Jorg Lind (Woellner company) for providing the various alkaline silicate solutions used during this project. Discussions with Sylvie Rossignol (University of Limoges) were also of great help for better understanding the chemical structure of the solutions.

References

Azeiteiro, L.C., Velosa, A., Paiva, H., Mantas, P.Q., Ferreira, V.M., and Veiga, R. (2014) Development of grouts for consolidation of old renders. Construction and Building Materials, 50, 352–360. Elsevier Ltd.

Bergna, H.E. and Roberts, W.O. (2006) Colloidal Silica: Fundamentals and Applications. Taylor & Francis, 895 pp.

Dietzel, M. (2000) Dissolution of silicates and the stability of polysilicic acid. Geoch. Cosmoch. Acta 64 (19), 3275-3281.

Felmy, A.R., Cho, H., Rustad, J.R., Mason, M.J. (2001) An Aqueous Thermodynamic Model for Polymerized Silica Species to High Ionic Strength. Journal of Solution Chemistry 30 (6), 509-525.

Gaboriaud, F. (1999) Étude du rôle de l'ion alcalin au cours de la gélification des solutions silico-alcalines déstabilisées par addition d'ions calcium. Ph.D Univ. de Bourgogne, 175 p.

Hamouda, A.A. and Amiri, H.A.A. (2014) Factors Affecting Alkaline Sodium Silicate Gelation for In-Depth Reservoir Profile Modification. Energies, 7, 568–590.

Iler, R.K. (1979) The Chemistry of Silica. Solubility, Polymerization, Colloid and Surface Properties, and Biochemistry. JOHN WILEY & SONS, 868 pp.

Ito, T., Xu, T., Tanaka, H., Taniuchi, Y., and Okamoto, A. (2014) Possibility to remedy CO_2 leakage from geological reservoir using CO 2 reactive grout. International Journal of Greenhouse Gas Control, 20, 310–323. Elsevier Ltd.

Jung, C.Y., Kim, J.S., Chang, T.S., Kim, S.T., Lim, H.J., and Koo, S.M. (2010) One-Step Synthesis of Structurally Controlled Silicate Particles from Sodium Silicates using a Simple Precipitation Process. Langmuir, 26, 5456–5461.

Kouassi, S.S., Tognonvi, M.T., Soro, J., and Rossignol, S. (2011) Consolidation mechanism of materials obtained from sodium silicate solution and silica-based aggregates. Journal of Non-Crystalline Solids, 357, 3013–3021. Elsevier B.V.

Lagerström, G. (1959) Equilibrium studies of polyanions. III. Silicate ions in NaClO4 medium. Acta Chimica Scandinavica 13, 722-736.

Lakatos, I., Lakatos-Szabo, J., Tiszai, G., Palásthy, G., Kosztin, B., and Trömböczky, S. (1999) Application of Silicate-Based Well Treatment Techniques at the Hungarian Oil Fields. in: Proceeding of the Society of Petroleum Engineers SPE 56739.

Lakatos, I., Lakatos-szabó, J., and Sciences, E. (2012) Reservoir Conformance Control in Oilfields Using Silicates : State-of-the-Arts and Perspectives. in: Proceeding of the Society of Petroleum Engineers SPE 159640.

Lakatos, I., Medic, B., Jovicic, D., Basic, I., Lakatos-Szabo, J., and Tiszai, G. (2014) Restriction of gas losses in a overpressurised CO_2 reservoir using gel technology. International journal of Oil , Gas and Coal Technology, 8, 135–152.

Manceau, J., Hatzignatiou, D.G., Lary, L. De, Jensen, N.B., and Réveillère, A. (2014) Mitigation and remediation technologies and practices in case of undesired migration of CO_2 from a geological storage unit — Current status. International Journal of Greenhouse Gas Control, 22, 272–290. Elsevier Ltd.

Metin, C.O., Rankin, K.M., and Nguyen, Q.P. (2014) Phase behavior and rheological characterization of silica nanoparticle gel. 93–101.

Provis, J.L., Duxson, P., Lukey, G.C., Separovic, F., Kriven, W.M., Deventer, J.S.J. van (2005) Modeling Speciation in Highly Concentrated Alkaline Silicate Solutions. Ind. Eng. Chem. Res. 44, 8899-8908.

Prud'homme, E. (2011) Rôles du cation alcalin et des renforts minéraux et végétaux sur les mécanismes de formation de géopolymères poreux ou denses. Ph.D. Univ. Limoges, 150 p.

Stavland, A., Jonsbråten, H.C., Vikane, O., Skrettingland, K., and Fischer, H. (2011) In-Depth Water Diversion Using Sodium Silicate on Snorre - Factors Controlling In-Depth Placement. in: Proceeding of the Society of Petroleum Engineers SPE 143836.

Tognonvi, M., Massiot, D., Lecomte, A., Rossignol, S., and Bonnet, J.P. (2010) Identification of solvated species present in concentrated and dilute sodium silicate solutions by combined 29 Si NMR and SAXS studies. Journal of Colloid and Interface Science, 352, 309–315.

Tognonvi, M., Rosignol, S., and Bonnet, J.P. (2011a) Physical-chemistry of sodium silicate gelation in an alkaline medium. Journal of Sol-Gel Science and Technology, 58, 625–635.

Tognonvi, M.T., Rossignol, S., and Bonnet, J. (2011b) Effect of alkali cation on irreversible gel formation in basic medium. Journal of Non-Crystalline Solids, 357, 43–49. Elsevier B.V.

Tognonvi, M.T. (2009) Physico-chimie de la gélification du silicate de sodium en milieu basique. Ph.D Univ. Limoges, 166 p.

Vail, J.G. (1952) Soluble Silicates: their Properties and Uses. Reinhold Publishing Corporation New York, 354 pp.

APPENDIX: BETOL K28 T SOLUTION

Table 8 Characteristics of the silicate solution provided by the manufacturer (Woellner).

Betol K28 T solution		Source
SiO2 content SiO2/K2O K2O	20.5 wt% 2.645 mol/L 3.92 8.2 wt%	Manufacturer
pH	10.8 (*) 11.62	Manufacturer Measured
Specific density	1.25 g/cm^3	Manufacturer
Viscosity	28 mPa.s at 20°C	Manufacturer
(*) at a dilution of 10% in water		

Table 9 Characteristics of the diluted solution

Betol K28 T / Water solution 50 : 50 by weight		Source
SiO2 content	1.90 mol/L	Manufacturer
pH	11.41	Measured
Specific density	1.11 g/cm^3 at 20°C	Measured
Viscosity	1.20 mPa.s at 29.7°C 1.08 mPa.s at 41.9°C 0.99 mPa.s at 63.6°C	Measured

woellner

Betol® K 28 T

Binder and Adhesive for Silicate based Coatings and Glues

Chemical description

Betol K 28 T is an inorganic binder based on an aqueous solution of potassium silicate.

Mode of action

Betol K 28 T reacts with and adheres to mineral surfaces by silicification. Due to the good bonding capacity and high temperature stability, fire and acid proof glues and sealants can easily be formulated.

Specification (average values)

Dry content:	approx. 28,0 %	007 *)
Density (20°C):	approx. 1,25 g/cm³	042 *)
pH: (10 % in water)	approx. 10,8	008 *)
Viscosity (20°C):	approx. 28 mPas	053 *)
Solubility:	soluble in water in any proportion	

*) *Internal method code – description available on request*

Properties

- good bonding power and effect,
- excellent adhesion to mineral surfaces,
- heat and acid resistant,
- stable even under extreme climatic conditions,
- anticorrosive, antistatic, stable against UV radiation,
- alkaline liquid.

Application

- construction industry,
- construction chemicals,
- acid proof and refractories,
- mineral coatings,
- hardener for mineral (e.g. cement) based mortars or plasters,
- sealing of brick walls against rising humidity.

Note

Keep Betol K 28 T in closed receptacles. Before application a thorough hiding of glass, ceramics, light metals and natural stones is necessary. In case of spilling or splashing wash immediately with water. At the end of the work clean tools immediately with (warm) water.

Storage

Protect Betol K 28 T from frost. Storage stability in closed containers at least 12 months. Do not store Betol K 28 T in aluminium or galvanized receptacles.

Chapter XXV

Sealing CO_2 wells – Bečej field test

Jafar Abdollahi[1], Ivan Basic[2], Inge M. Carlsen[1], Marc Fleury[3], Cor Hofstee[4], Dusan Karas[2], Aleksandar Patrnogic[2], Bernd Wiese[5], Jens Wollenweber[4]
[1] PRORES AS, Norway
[2] NIS, Serbia
[3] IFPEN, France
[4] TNO, The Netherlands
[5] GFZ, Germany

SUMMARY

The test of a novel sealant material has been performed in a shaly sandstone reservoir part of the Bečej field, at a depth of 600m. An interval of 3.5m was perforated and 2 m^3 of sealant injected in the presence of CO_2. The sealant prepared at the surface was designed to form a gel after 8.5 h at the formation temperature (40 °C), without the need for CO_2.

The success of this field test is evaluated through different goals: Upscaling and mixing fluid in the field, Avoid gelation in open borehole, Place sealant in formation, Seal formation, and Evaluate long term sealing performance. All goals were reached, except that only short term sealing capacity was observed. The reasons for the break of the gel were analyzed and some key lessons learned. Among the most important are the lower than expected temperature of the formation, and gravity segregation effects producing non homogenous sealant placement.

Note: this report has not been made publicly available, thus only the title and public abstract are provided.

Chapter XXVI

Polymer-based gels for remediation of well leakage

Mojgan H. Mosleh[1], Rajesh Govindan[1], Ji-Quan Shi[1], Guangyao Si[1], Anna Korre[1], Sevket Durucan[1]
[1] Imperial College, UK

SUMMARY

This report, as part of the MiReCOL project, presents the outcome of the research conducted at Imperial College to assess the application of the polymer-gel solutions in remediation of CO_2 leakage through wellbore cement under deep reservoir conditions. The main objective of this research was to investigate the sealing behaviour of polymer-gel solutions at the rock-cement-casing interfaces as well as induced fractures through cement under simulated down-hole conditions. The results are presented and discussed in this report. Imperial College's wellbore cell has been used to characterise the permeability of the wellbore cement, before and after polymer-gel injection. The permeability results are implemented in reservoir models to simulate the effect of polymer-gel on remediation of CO_2 leakage in a deep reservoir.

The experiments presented here have also formed the baseline for comparison with latex-based smart cement development in MiReCOL, which is presented in another report. These results are used to calibrate numerical models of wellbore leakage. The application of other novel materials as sealants is described in a further report prepared by Imperial College.

Note: this report has not been made publicly available, thus only the title and public abstract are provided.

Chapter XXVII

Smart cement with a latex-based component for remediation of well leakage

Mojgan H. Mosleh[1], Rajesh Govindan[1], Ji-Quan Shi[1], Anna Korre[1], Sevket Durucan[1]
[1] Imperial College, UK

SUMMARY

This report, as part of the MiReCOL project, presents the outcome of the research conducted at Imperial College to assess the development and application of a smart cement with latex-based component for remediation of CO_2 leakage through wellbore cement under deep reservoir conditions. The main objective of this research was to investigate the sealing behaviour of latex-based cement at the rock-cement-casing interfaces, as well as induced fractures through the cement under simulated down-hole conditions.

Imperial's wellbore cell has been used to characterise the permeability of the wellbore cement, before and after CO_2 injection. The experiments carried out with the latex cement have formed the baseline for comparison with polymer-gel solution based wellbore remediation techniques reported under a different report in MiReCOL. These results were used to calibrate numerical models of wellbore leakage, which were implemented in simulating the use of latex-cement in remediating CO_2 leakage in a deep reservoir.

The results are presented and discussed in this report.

Note: this report has not been made publicly available, thus only the title and public abstract are provided.

Chapter XXVIII

Polymer resin for squeezing

Jelena Todorovic[1], Martin Raphaug[1], Erik Lindeberg[1], Torbjørn Vrålstad[1], Maike Buddensiek[1]
[1] SINTEF PR, Norway

SUMMARY

The objective of this work was to test the sealing ability of a commercially available temperature-activated polymer resin with respect to cement failure at laboratory scale. Two different well leakage scenarios were considered: (a) failure of the cement sheath (via micro-annuli, cracks, voids) and (b) debonding at the cement-casing interface. Cement core samples with artificially created leak paths were prepared: (1) a cement core cut in half axially and reassembled with a thin steel plate, (2) a cement core in two halves with moulded vertical leak paths in the centre. Permeability of the samples and average fracture thickness of the leak paths were measured before and after the squeeze procedure. The polymer resin was then squeezed into the core samples along the leak paths, and left to cure. After repeated permeability measurements, the samples were disassembled and the affected surfaces were studied by optical microscopy. The polymer resin proved to be fairly successful in plugging the designed leak paths: permeability and the average fracture thickness were significantly reduced after the treatment for both samples.

1 INTRODUCTION

This report is part of the research project MiReCOL (Mitigation and Remediation of CO_2 leakage) funded by the EU FP7 programme. Research activities aim at developing a handbook of corrective measures that can be considered in the event of undesired migration of CO_2 in the deep subsurface reservoirs. MiReCOL results support CO_2 storage project operators in assessing the value of specific corrective measures if the CO_2 in the storage reservoir does not behave as expected. MiReCOL focuses on corrective measures that can be taken while the CO_2 is in the deep subsurface. The general scenarios considered in MiReCOL are 1) loss of conformance in the reservoir (undesired migration of CO_2 within the reservoir), 2) natural barrier breach (CO_2 migration through faults or fractures), and 3) well barrier breach (CO_2 migration along the well bore).

Long term success of CO_2 storage is heavily dependent on maintaining well integrity. Wells have been identified as the most important potential leakage pathways in a CO_2 storage project [1-3]. Complex well construction, in general consisting of casings/liners of different diameters, cement in the A, B and C annuli between the casings, packers, and other well barrier elements, creates numerous possibilities for leakage pathways. Well leakage scenarios have been thoroughly examined in MiReCOL report D8.1 "Description of CO_2 well failure modes, causes and consequences", 2015. Specifically, if we consider cement failure as the cause of CO_2 leakage, possible leakage pathways can occur at the casing-cement or cement-formation interfaces, or through fractures or mud channels in the bulk cement [2].

Decades of CO_2-flooding operations in enhanced oil recovery provide a valuable insight into the medium-term consequences of CO_2 leakage through the wellbore system [4]. Cement zones that have reacted heavily with CO_2 observed at casing-cement and cement-shale interfaces gave clear evidence of CO_2 migration along both of these interfaces. The extensive study by Carey et al. [4] inspired a number of laboratory-scale studies of the cement and casing integrity in contact with carbonated brine, where references [5-8] are examples of more recent studies. These studies [4-8] have consistently proven the effects of prolonged reaction of cement with CO_2-brine, i.e. calcium migration, dissolution and formation of distinct zones in the cement matrix – such as depleted portlandite, $CaCO_3$ precipitation and a silica-rich amorphous zone. Although partial plugging and permeability reduction of the leak paths at the casing-cement or cement-formation interfaces, or of the cement bulk may be achieved by carbonate deposition [4,5,7], in case of larger initial leak paths degradation of the cement after prolonged CO_2-brine flow becomes a prominent process [7,8].

Thus prevention and remediation options for any potential leakage through the wellbore system play a crucial role in the implementation of large scale CO_2 storage. A remediation operation can be described as an attempt to repair a leak in a well barrier element, such as the annular cement, tubing or casing. Squeeze cementing is the most common remediation practice in oil and gas industry used for various well leakage scenarios [9,10]. Squeeze cementing is typically used to solve lost circulation during drilling or to repair poorly cemented sections or leaks in the casing/liner, or to prevent migration of fluids within the wellbore system. This operation is usually performed at the time of running the casing, i.e. during well construction if the primary cement job failed. However, it can also be used for remediation of leakage later in the life-cycle of a well.

Squeeze cementing is generally performed by perforating the casing and squeezing a sealant behind the casing. The sealant is most commonly Portland G cement slurry with appropriate additives, but a temperature-activated or pressure-activated polymer resin may be used instead. An important disadvantage of the cement slurry is that the relatively large particle size limits placement efficiency into micro-cracks and small void spaces [9]. On the other hand, polymer resin materials can be designed to have viscosity close to water prior to curing, which makes them very suitable for squeezing into micro-cracks.

Temperature-activated sealants can be in principle used for squeeze cementing operations, yet this is not a common practice in the oil and gas industry. Temperature-activated sealants are polymer resin systems designed to cure at a specific temperature. This allows placement, pumping or squeezing of the resin while in the liquid state into the desired interval, and subsequent curing when the resin reaches the appropriate temperature. Curing temperature, density, viscosity and curing time can be accurately designed for a particular application. In general polymer resins tolerate some degree of contamination and are compatible with most wellbore fluids and cements. In addition, treatments with polymer resin systems can be reversible (via milling or acid treatment). There have been some reports of successful field application of temperature activated sealants, for example in the Middle East as a lost circulation material while drilling gas wells offshore [11], and for plugging and abandonment operations [12]. Temperature activated sealants can be in principle used in squeeze cementing operations for remediation of casing/liner and annular cement integrity loss.

The objective of this work was to test the sealing ability of a commercially available temperature-activated polymer resin with respect to cement failure at laboratory scale. Two different well leakage scenarios were considered: (a) failure of the cement sheath (via micro-annuli, cracks, voids) and (b) debonding at the cement-casing interface. For simplicity casing perforation was avoided in our experimental setup and we started with cement core samples with artificially created leak paths at the cement-cement and cement-steel interfaces. The samples were: (1) a cement core cut in half axially and reassembled with a thin steel plate in between, (2) a cement core in two halves with moulded vertical leak paths in the centre. A standard core-flooding setup with addition of an injection coil was used in this work. Permeability of the samples and average fracture thickness of the leak paths were measured before and after the squeeze procedure. The polymer resin was then squeezed into the core samples along the leak paths, and left to cure. After repeated permeability measurements, the samples were disassembled and the affected surfaces were studied by optical microscopy.

2 ENERGY PROCEDIA PUBLICATION: REMEDIATION OF LEAKAGE THROUGH ANNULAR CEMENT USING A POLYMER RESIN: A LABORATORY STUDY

The results of this work were presented at the 8th Trondheim Conference on CO_2 Capture, Transport and Storage (TCCS-8), Trondheim, Norway, June 16-18, 2015. The following manuscript will be published in Energy Procedia.

REMEDIATION OF LEAKAGE THROUGH ANNULAR CEMENT USING A POLYMER RESIN: A LABORATORY STUDY

Jelena Todorovic[a], Martin Raphaug[b], Erik Lindeberg[b], Torbjørn Vrålstad[a], Maike-Liselotte Buddensiek[b]

[a]SINTEF Petroleum Research, Department of Drilling and Well, S.P. Andersens vei 15B, Trondheim 7031, Norway

[b]SINTEF Petroleum Research, Department of Exploration and Reservoir Technology, S.P. Andersens vei 15B, Trondheim 7031, Norway

Abstract

Long term success of CO_2 storage is heavily dependent on maintaining well integrity. Prevention and remediation of leakage through wells plays a crucial role in large scale implementation of CO_2 storage. Squeeze cementing is the most common remediation practice in the oil and gas industry used for various well leakage scenarios. The objective of this work was to test the sealing ability of a commercially available temperature-activated polymer resin in a laboratory-scale squeeze cementing operation. Two well leakage scenarios were selected: micro-annuli or cracks in cement and debonding at cement-casing interface. Cement (with or without steel) core samples with designed vertical leak paths were prepared. Permeability of the samples was measured both before and after the squeeze procedure. Then the samples were disassembled and studied by optical microscopy. The squeeze procedure proved to be successful for plugging the designed leak paths.

Peer-review under responsibility of the Programme Chair of The 8th Trondheim Conference on CO_2 Capture, Transport and Storage.

Keywords: "micro-anulli; CO_2 leakage; squeeze cementing; temperature-activated polymer resin; permeability"

Introduction

Long term success of CO_2 storage is heavily dependent on maintaining well integrity. Wells have been identified as the most important potential leakage pathways in a CO_2 storage project [1-3]. Complex well construction, in general consisting of casings/liners of different diameters, cement in the annuli A, B and C between the casings, packers, and other well barrier elements, creates numerous possibilities for leakage pathways. Specifically, if we consider cement failure as the cause of CO_2 leakage, possible leakage pathways can be at casing-cement or cement-formation interfaces, or through fractures or mud channels in the cement bulk [2]. Decades of CO_2-flooding operations in enhanced oil recovery provide a valuable insight into medium-term consequences of CO_2 leakage through the wellbore system [4]. Cement zones heavily reacted with CO_2 observed at casing-cement and cement-shale interfaces were a clear evidence of CO_2 migration along both of these interfaces. The extensive study by Carey et al. [4] inspired a number of laboratory-scale studies of the cement (and casing) integrity in contact with carbonated brine, where references [5-8] are examples of more recent studies. These studies [4-8] have consistently proved effects of prolonged reaction of cement with CO_2-brine: calcium migration, dissolution and formation of distinct zones in the cement matrix – such as depleted portlandite, carbonated ($CaCO_3$ precipitation) and amorphous zone (silica rich). Although partial plugging and reduction of permeability of the leak paths at casing-cement or cement-formation interfaces, or through cement bulk, may be achieved by carbonate deposition [4,5,7], in case of larger initial leak paths dissolution and degradation of the cement upon prolonged CO_2-brine flow become prominent processes [7,8].

Thus prevention and remediation options for any potential leakage through the wellbore system play a crucial role in implementation of large scale CO_2 storage. Remediation operation can be described as an attempt to repair a leak in a well barrier element, such as the annular cement, tubing or casing. Squeeze cementing is the most common remediation practice in oil and gas industry used for various well leakage scenarios [9,10]. Squeeze cementing is generally performed by perforating the casing and squeezing a sealant behind the casing. The sealant is most commonly Portland G cement slurry with appropriate additives, but a temperature-activated or pressure-activated polymer resin may be used instead. Squeeze cementing is typically used to solve lost circulation during drilling, or to repair poorly cemented sections, or leaks in the casing or liner or to prevent migration of fluids within the wellbore system. This operation is usually performed at the time of running the casing, i.e. during well construction if the primary cement job failed. However, it can be used for remediation of leakage later on in the life-cycle of a well.

Temperature-activated sealants can be in principle used for squeeze cementing and repair of casing leaks and annular cement failure. Temperature-activated sealants are polymer resin systems designed to cure at a specific temperature. This allows placement, pumping or squeezing of the cement slurry while in the liquid state into the desired interval, and subsequent curing when the resin reaches the appropriate temperature. Curing temperature, density, viscosity and curing time can be accurately designed for a particular application. In general polymer resins tolerate some degree of contamination and are compatible with most wellbore fluids and cements. In addition, treatments with polymer resin systems can be reversible (via milling, acid treatment). There have been some reports of successful field applications of temperature-activated sealants, for example as lost circulation material [11] or for plugging and abandonment operations [12].

The objective of this work was to test the sealing ability of a commercially available polymer resin with respect to cement failure at laboratory scale. Two different well leakage scenarios were considered: (a) failure of the cement sheath (via micro-annuli, cracks, voids) and (b) debonding at the cement-casing interface. For simplicity casing perforation was avoided in our experimental setup and the starting points were cement core samples with artificially created leak paths at the cement-cement and cement-steel interfaces. Permeability of the samples and average fracture thickness of the leak paths were measured before and after the squeeze procedure. Temperature-activated polymer resin was then squeezed into tempered core samples along the leak paths, and left to cure. After repeated permeability measurements, the samples were disassembled and affected surfaces were studied by optical microscopy.

Experimental

Sample Preparation

Two core samples were prepared as shown in Figs.1 and 2. In both cases, Portland G cement slurry was prepared according to API specification 10A. Cement slurry was poured into a rubber sleeve for core flooding (1.5″ inner diameter, about 25 cm in length) plugged at the bottom side, to obtain the correct sample dimensions. The cement cores were initially curing in an oven at 66 C° at atmospheric pressure for several days and afterwards taken out to cure further at room temperature.

In case of sample 1, shown in Fig. 1, the cement core was pulled out of the rubber sleeve and vertically sliced in halves. The core was further cut to 14.7 cm in length and the end faces were grinded. Cement halves were then assembled with 0.5 mm thick stainless steel plate, as shown in Fig. 1(a). Rough edges were filled with plaster and the surface was polished, see Fig. 1(b). Such an assembled sample was mounted back into a rubber sleeve.

Figure 1 Sample 1 - cement sample with a steel plate: (a) Half-cylinders reassembled with a steel plate; (b) Rough edges of the cement halves were filled with plaster and surface was polished.

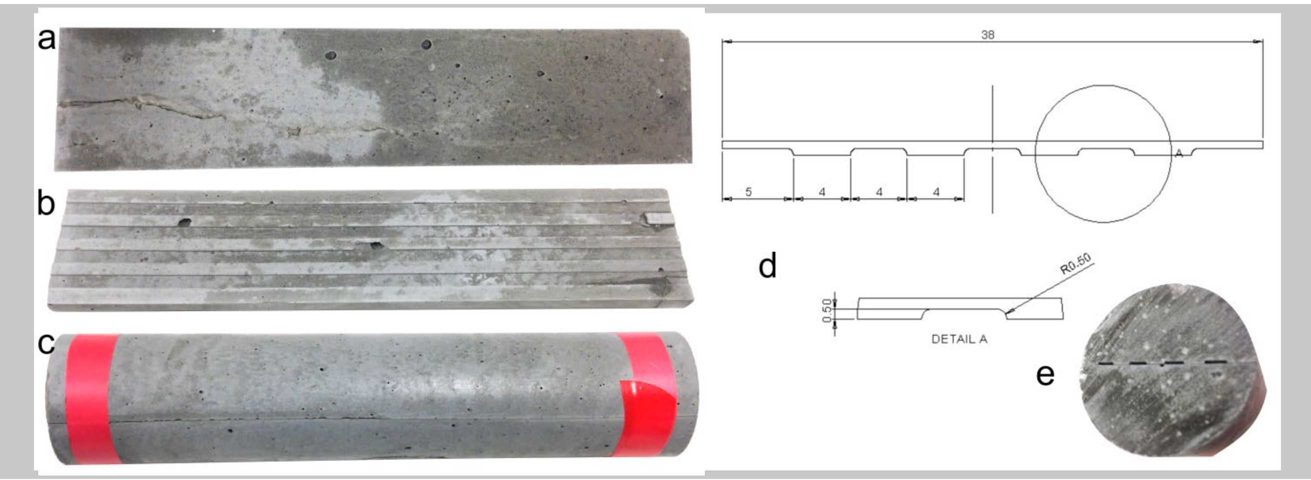

Figure 2 Sample 2 - cement sample with designed vertical leak paths: (a) Half-cylinder with a smooth surface; (b) Half-cylinder with a patterned surface; (c) Cement halves reassembled; (d) Technical drawing of the cross section of the PEEK mould, numbers are in mm. (e) Side view of the leak paths.

In case of sample 2, shown in Fig. 2, a plastic (PEEK) plate mould was designed to create vertical leak paths. Drawing of the cross section of the mould is shown in Fig. 2(d). The cement slurry cured against the plastic mould which was set in the center of a rubber sleeve. The excess cement at the ends of the core was cut off together with the rubber sleeve, giving the final core length of 17.2 cm. The final cement core with the plastic mould was then removed from the sleeve and easily disassembled, as shown in Figs. 2(a,b). Both cement interfaces were rather smooth, apart from some voids and one fracture running along the interface with the mould, as seen in Fig. 2(a). In this case, the edges of the cement halves remained smooth, which made reassembling of the sample straightforward as seen in Figs. 2(c,e).

Injection Setup and Procedure

The setup used for these experiments is based on a general core flooding scheme, as shown in Fig. 3(a). It contains most of the common equipment to perform a core flooding, such as a pump, back pressure valve and a differential pressure gauge. The core holder is illustrated in Fig. 3(b). As an addition to this setup we have added an injection coil, made out of 1/8 inch Teflon tubing, illustrated in more detail in Fig. 3(c). The injection coil is filled with polymer resin by using a syringe. The polymer resin was injected into the core sample by flooding brine as a displacing fluid into the bottom of the coil. By using the injection coil, only a small volume of the polymer resin was injected into the core flooding system and unnecessary contamination was avoided. The polymer resin was designed to cure at 60°C, well above ambient temperature, in order to avoid plugging of the core flooding system.

The following core-flooding procedure was used for both samples. The confining pressure was 50 bars throughout the whole experiment. The initial fracture permeability was measured with 1% NaCl solution at ambient temperature and with a back pressure of 20 bars. Next, the core holder and core sample were heated to 60°C. The polymer resin mixing method was the same for both samples, to achieve the same gelling and curing time. The injection time was the same (8 min) for both samples, but the injection rate was increased for sample 2 since the fracture volume was larger, see Table 1. The injection into sample 1 was performed from the top, whereas for sample 2, the bottom-up direction was chosen to ensure better filling of the large leak paths. In both cases, the injected volume was a sum of the system (dead) volume and 80% of the calculated fracture volume. The shut in period was about 200 min during which the core holder was closed. After the setting period, the core holder was dismounted and the injection and outlet ports were cleaned from the residual polymer resin. Then the permeability measurement was repeated. The apparent average fracture thickness was calculated before and after the treatment.

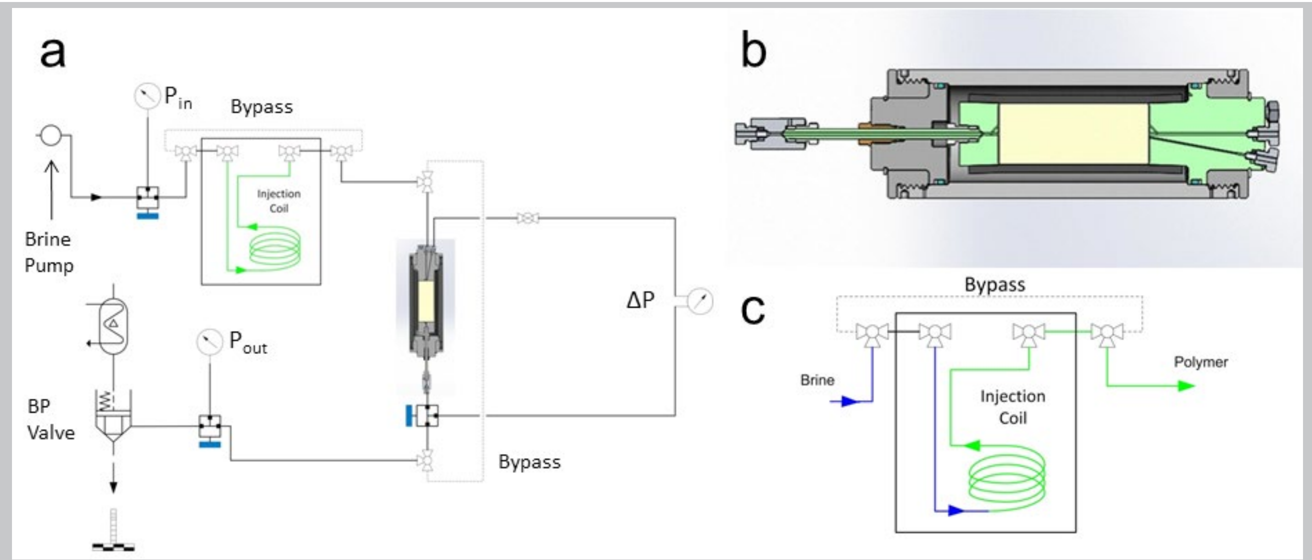

Figure 3 Illustration of the injection setup: (a) Flow setup scheme; (b) Core holder; (c) Illustration of polymer resin injection procedure.

Results and Discussion

The permeability measured before and after the injection test, plus measured and calculated average fracture thickness for both samples are summarized in Table 1. The apparent average fracture thickness was determined using Darcy's law and verified by volumetric and geometrical measurements of the leak path. The initial fracture thickness values determined by these two methods are in agreement. The measured fracture thickness (column 4 in Table 1) was slightly larger than fracture thickness calculated using Darcy's law (column 5 in Table 1) for sample 1. For sample 2, the initially measured fracture thickness was a nominal value of 0.5 mm according to the design of the leak paths, see Fig. 2(d).

Despite being assembled from loose pieces of cement and steel, and filled with plaster on the edges, sample 1 had a rather small volume of void space between the cement, steel and plaster, resulting in average fracture thickness of 17 µm. After the treatment with the polymer resin, the fracture permeability dropped to nearly 0 Darcy indicating complete plugging of the leak path. In the case of sample 2, the initial leak path volume was much larger, resulting in much higher initial permeability (1717 Darcy) and an average fracture thickness of 467 µm. After the treatment, the permeability of sample 2 reduced to about the same value as the initial permeability of sample 1, still resulting in measurable flow through the sample. Nevertheless, the reduction of permeability by a factor of 42 was significant and the average fracture thickness dropped to 25 µm.

Table 1 Permeability values and average fracture thickness before and after polymer resin injection for samples 1 and 2.

Sample	Fracture Permeability before (Darcy)	Fracture Permeability after (Darcy)	Measured Fracture Thickness before (µm)	Calculated Fracture Thickness before (µm)	Calculated Fracture Thickness after (µm)	Injection rate (ml/min)
1	47	~ 0	20	17	0	0.1
2	1717	41	500	467	25	0.3

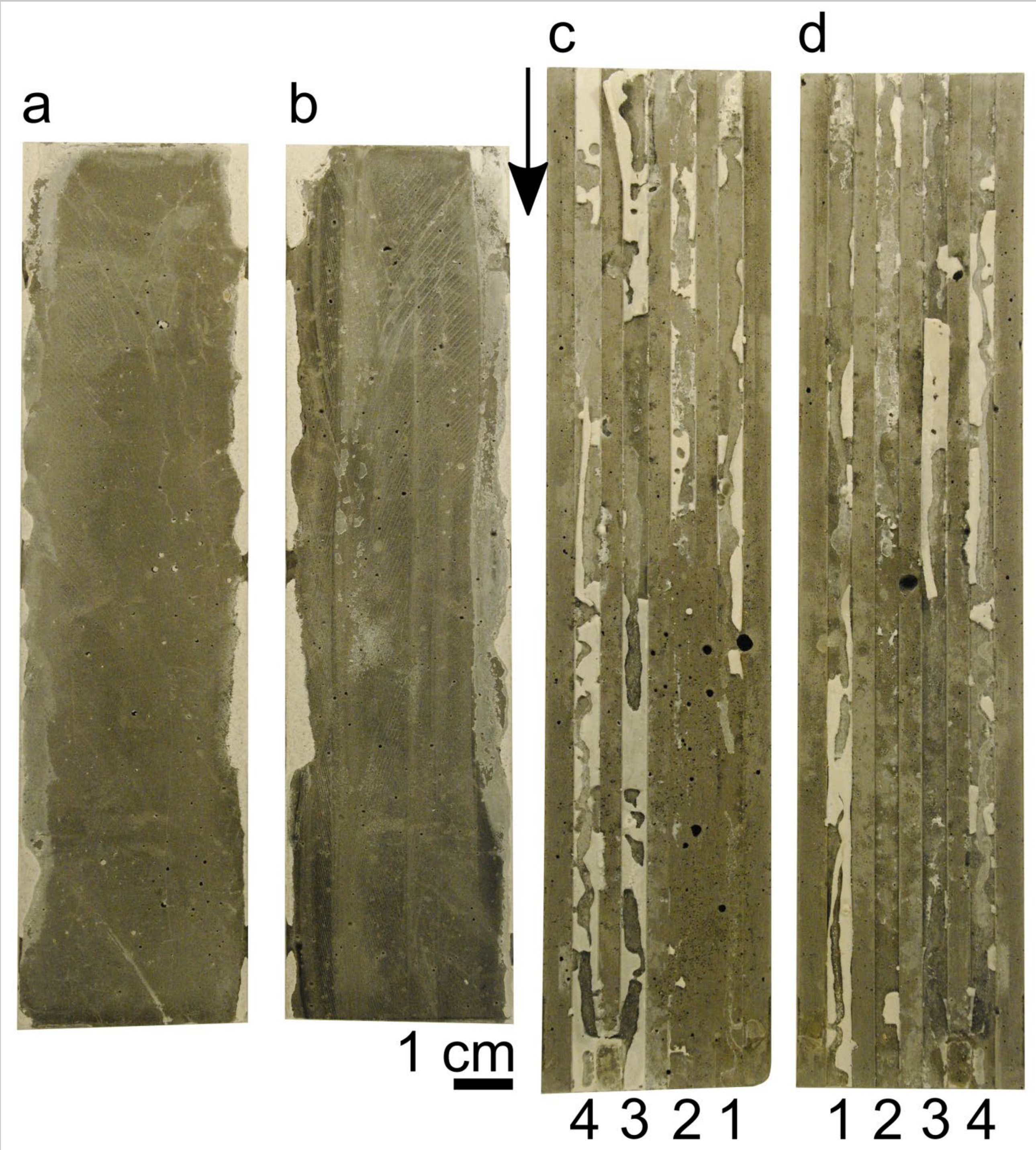

Figure 4 Overview images of the cement surfaces exposed to polymer resin, injection direction is indicated by the arrow: (a,b) Sample 1 - surfaces against the steel plate; (c) Sample 2 – smooth surface; (d) Sample 2 – patterned surface. Numbers in (d) mark the grooves in the patterned surface, and in (c) polymer resin remaining attached to the smooth surface from the respective groove.

After the treatment with the polymer resin, the samples were opened and the cement surfaces exposed to the resin were studied. Overview photos of both cement surfaces for samples 1 and 2 are shown in Fig. 4. The injection direction for both samples is indicated by the arrow, and the designed leak paths in sample 2 are numbered. The smooth surface of sample 2 is shown in Fig. 4(c), whereas the patterned surface appears in Fig. 4(d).

For the sample 1, a thin layer of polymer resin remained unevenly spread across both cement surfaces, and also on the steel plate (not shown). The polymer resin is the light grey layer in Fig. 4(a,b). The resin was mostly concentrated at the top part of the sample where the injection was initiated. The resin penetrated to a great extent through the gap between the cement and plaster (white material on the edges of the sample 1). On the cement-plaster interface to the left in Fig. 4(a) and to the right in Fig. 4(b), the resin reached all the way to the bottom surface, whereas on the other sides the resin has not reached all the way to the bottom.

In the case of sample 2, the polymer resin acted as a binding agent between the cement halves. When the halves were detached, some resin remained glued onto both surfaces. The polymer resin reached the bottom surface of sample 2 as well, and cured within the leak paths. However, none of the leak paths was completely filled with the cured polymer resin. Comparing Figs. 4(a) and (b), it can be seen that leak paths 1, 3 and 4 were filled to a large extent, whereas leak path 2 was partly filled mostly in the upper half of the sample.

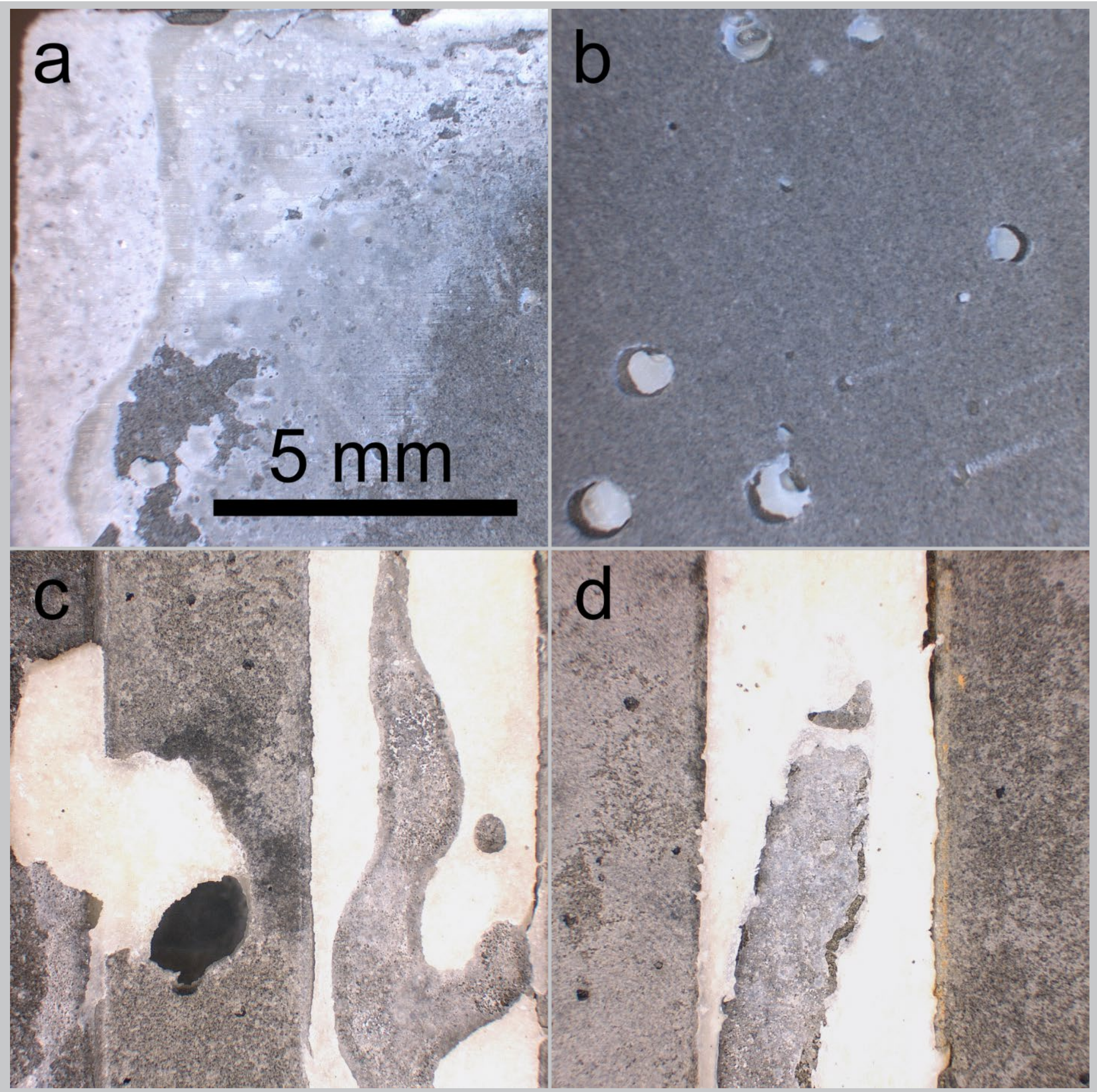

Figure 5 Cement surface exposed to polymer resin: (a) Sample 1 - top left corner of the cement half in Fig. 4(a); (b) Sample 1: partially filled interface voids in the central region of the same cement half-piece; (c) Sample 2 - polymer resin partially filling the grooves and an interface void in between the grooves 3 and 4; (d) Sample 2 - polymer resin partially filling one of the grooves.

More detailed optical images of the cement surfaces exposed to the polymer resin treatment in samples 1 and 2 are presented in Fig. 5. The bright region towards the edge of sample 1 in Fig. 5(a) is plaster also seen in Figs. 4(a,b). The cured polymer resin has light grey colour and is filling the gap between the plaster and the cement, and a thin layer is covering the cement surface. Fig. 5(b) shows some partially filled interface voids, which can be also noticed in the overview images in Fig. 4(a). Some of the interface voids appeared to be completely filled, while others were empty or the resin remained attached to the steel. In sample 2, the polymer resin partially filled some of the interface voids as shown in Fig. 5(c), but the most of the resin neatly cured within the grooves as seen Fig. 5(d).

The use of the same injection procedure as for sample 1, was not the most efficient approach for a large leak path volume in sample 2. To improve filling of such large designed leak paths, the injection procedure needs to be modified. Injecting only 80 % of the fracture volume was a safety measure, but it did not prevent plugging of the injection and outlet ports in either of the tests. Hence, the injected polymer resin volume and injection pressure and rate can be increased, but with expectation that the injection and outlet ports will be plugged upon curing. In addition, back pressure should be introduced during curing in order to contain the injected polymer resin more efficiently within the leak paths. Another option is to prolong the shut in period to ensure better curing of the injected polymer resin.

Conclusions

The injection setup was adequate for a laboratory scale squeeze operation into cement(-steel) core samples. The polymer resin properties such as viscosity, gelling and curing time were adjusted with respect to the leak path size and shape. The polymer resin proved to be fairly successful in plugging the designed leak paths for the two selected leakage scenarios: cement-casing debonding and fractures in annular cement. The polymer resin penetrated through the whole sample length in both cases.

The permeability and the average fracture thickness were significantly reduced after the treatment. In case of cement-steel sample, which had a small initial leak path (17 µm thick on average), the average fracture thickness dropped to nearly zero after the treatment and no flow was established. In a practical situation however, such small fractures (17 µm) pose a smaller problem with respect to the long term CO_2 escape. The performance in the large fracture (nominal thickness 0.5 mm) is however, even more important because a fracture of this size can cause severe leakage [13] if it extends through the entire cemented interval. A reduction in permeability in the large fractures by a factor of 42 corresponding to a reduction in apparent fracture thickness from 467 µm to 25 µm is remarkable. A recommendation for future work would be improving the plugging performance of the polymer resin by optimizing the injection and curing procedure.

Acknowledgements

This research was funded by the European Union Seventh Framework Programme (FP7/2007-2013), sub-programme ENERGY.2013.5.2.1 “Mitigation and remediation of leakage from geological storage”, under grant agreement No. 608608 “Mitigation and remediation of CO_2 leakage” (MiReCOL). The project receives additional funding from Statoil, GDF SUEZ and Shell. We thank WellCem AS for providing a temperature-activated polymer resin and for their collaboration during the injection tests.

References

[1] Metz B, Davidson O, de Coninck H, Loos M, Meyer L. IPCC Special Report on Carbon Dioxide Capture and Storage. Cambridge University Press: Intergovernmental Panel on Climate Change, 2005.
[2] Celia MA, Bachu S, Nordbotten JM, Gasda SE, Dahle HK. Quantitative Estimation of CO_2 Leakage from Geological Storage: Analytical Models, Numerical Models, and Data Needs. 2006.
[3] Bachu S, Celia MA. Assessing the Potential for CO_2 Leakage, Particularly Through Wells, From Geological Storage Sites. Carbon Sequestration and Its Role in the Global Carbon Cycle, Geophysical Monograph Series. 2009;183:203-16.
[4] Carey JW, Wigand M, Chipera SJ, WoldeGabriel G, Pawar R, Lichtner PC, et al. Analysis and performance of oil well cement with 30 years of CO_2 exposure from the SACROC Unit, West Texas, USA. International Journal of Greenhouse Gas Control. 2007;1(1):75-85.
[5] Carey JW, Svec R, Grigg R, Zhang J, Crow W. Experimental investigation of wellbore integrity and CO_2-brine flow along the casing-cement microannulus. International Journal of Greenhouse Gas Control. 2010;4(2):272-82.
[6] Duguid A, Scherer GW. Degradation of oilwell cement due to exposure to carbonated brine. International Journal of Greenhouse Gas Control. 2010;4(3):546-60.
[7] Walsh SDC, Du Frane WL, Mason HE, Carroll SA. Permeability of wellbore-cement fractures following degradation by carbonated brine. Rock Mechanics and Rock Engineering. 2013;46(3):455-64.
[8] Ozyurtkan MH, Radonjic M. An experimental study of the effect of CO_2 rich brine on artificially fractured well-cement. Cement and Concrete Composites. 2014;45:201-8.
[9] Nelson EB, Guillot D. Well Cementing: Schlumberger; 2006.
[10] Manceau J-C, Hatzignatiou DG, de Lary L, Jensen NB, Reveillere A. Mitigation and remediation technologies and practices in case of undesired migration of CO_2 from a geological storage unit – Current status. International Journal of Greenhouse Gas Control. 2014;22:272-90.
[11] Knudsen K, Leon GA, Sanabria AE, Ansari A, Pino RM. First Application Of Thermal Activated Resin As Unconventional LCM In The Middle East. IPTC-18151-MS. 2014.
[12] Beharie C, Francis S, Øvestad KH. Resin: An Alternative Barrier Solution Material. SPE-173852-MS. 2015.
[13] Lindeberg E. The Quality of a CO_2 Repository: What is the sufficient retention time of CO_2 stored underground. Proceeding of the 6th International Greenhouse Gas Control Technologies, Kyoto, J Gale and Y Kaya (Eds) Elsevier Science Ltd. 2003;Vol. I:255-60.

Chapter XXIX

Novel materials and technologies for remediation of well leakage

Mojgan H. Mosleh[1], Rajesh Govindan[1], Ji-Quan Shi[1], Anna Korre[1], Sevket Durucan[1]
[1] Imperial College, UK

SUMMARY

This element of the MiReCOL project aims to provide a state-of-the-art review on potential suitability of novel materials such as biofilms and bacteria in remediation of CO_2 leakage from storage reservoirs.

Various microorganisms and bacteria have been used and investigated by researchers for their ability in blocking CO_2 leakage pathways. Laboratory scale investigations including several core flooding experiments have been reviewed to assess the effectiveness of biofilms and biomineralisation in permeability reduction of porous medium.

The growth and performance of biofilm under supercritical conditions has also been studied by several researchers and the results of their investigation are summarised in this report.

Note: this report has not been made publicly available, thus only the title and public abstract are provided.

Chapter XXX

Overview of current knowledge and technology gaps for novel remediation technologies

Jafar Abdollahi[1], Inge Manfred Carlsen[1], Jens Wollenweber[2]
[1] PRORES AS, Norway
[2] TNO, The Netherlands

SUMMARY

This report provides an overview of current knowledge gaps and novel remediation technologies for CO_2 well leakages. Data is always crucial to build a knowledge based approach for identify gaps for corrective measures of a problem.

Well integrity experience from the oil and gas industry has been the major source of information for this study as there are still very limited data available from leaking CO_2 wells. The corrosive environment of CO_2 wells give specific challenges to the well infrastructure including tubular annular cement.

Typical well lifecycle issues for a leaking CO_2 well are given together with an overview of knowledge gaps and technology status for remediation. Well diagnostics, novel materials, re-installation techniques are among the key gaps. Lack of relevant CO_2 well integrity data is a major area of concern for further assessment of knowledge and technology gaps. Full scale well experiments of new formation sealing materials, as the ongoing MIRECOL field test in a NIS well, are a crucial source of information in this matter.

For the future, R&D focus should be on establishing a CO_2 well database consisting of both research experience and real field cases. Further work is also required on finding efficient formation sealing materials and squeezing techniques.

ABBREVIATIONS

EOR Enhanced oil recovery
NIS Serbian multinational oil and gas company
NORSOK Norwegian standard
O&G UK Oil and gas UK
PWC Perforate, wash & cement
P&A Plug and abandonment
TRL technology readiness level
WBE Well barrier element
WP Work Package

1 INTRODUCTION

This report is part of the research project MiReCOL (Mitigation and Remediation of CO_2 Leakage) funded by the EU FP7 programme. The research activities aim at developing a handbook of corrective measures that can be considered in the event of undesired migration of CO_2 in subsurface reservoirs both through geology formations and along wells. Sub project 3 (SP3) is covering leakages along the well with two work packages (WP), WP8 and WP9, covering oil and gas best practices and novel materials and technologies.

This report belongs to WP9 with task 9.7. The objective of this task is to give an overview of current knowledge and technology gaps as a basis for further development of novel remediation solutions. While focus is on active CO_2 wells, also subjects related to the drilling and abandonment phases are discussed briefly.

Data are always crucial to build a knowledge based approach for identify gaps for corrective measures of a problem. The amount of relevant CO_2 well integrity data is still very limited, therefore well integrity experience from the oil and gas industry with expert judgement of additional CO_2 impact are used in this report.

2 ASSESSMENT OF CURRENT KNOWLEDGE AND TECHNOLOGY GAPS

To be able to define knowledge and technology gaps of leaking CO_2 wells one needs to understand the entire well lifecycle with well processes and well barrier element functions. CO_2 wells differ from traditional oil and gas wells as creating a potentially more corrosive well environment with a perceived higher risk for well leakages.

Focus of this report is on active wells including well intervention and workover phases. This chapter consists of two sub-chapters discussing issues for consideration related to CO_2 lifecycle well operations with current remediation gaps of leaking wells.

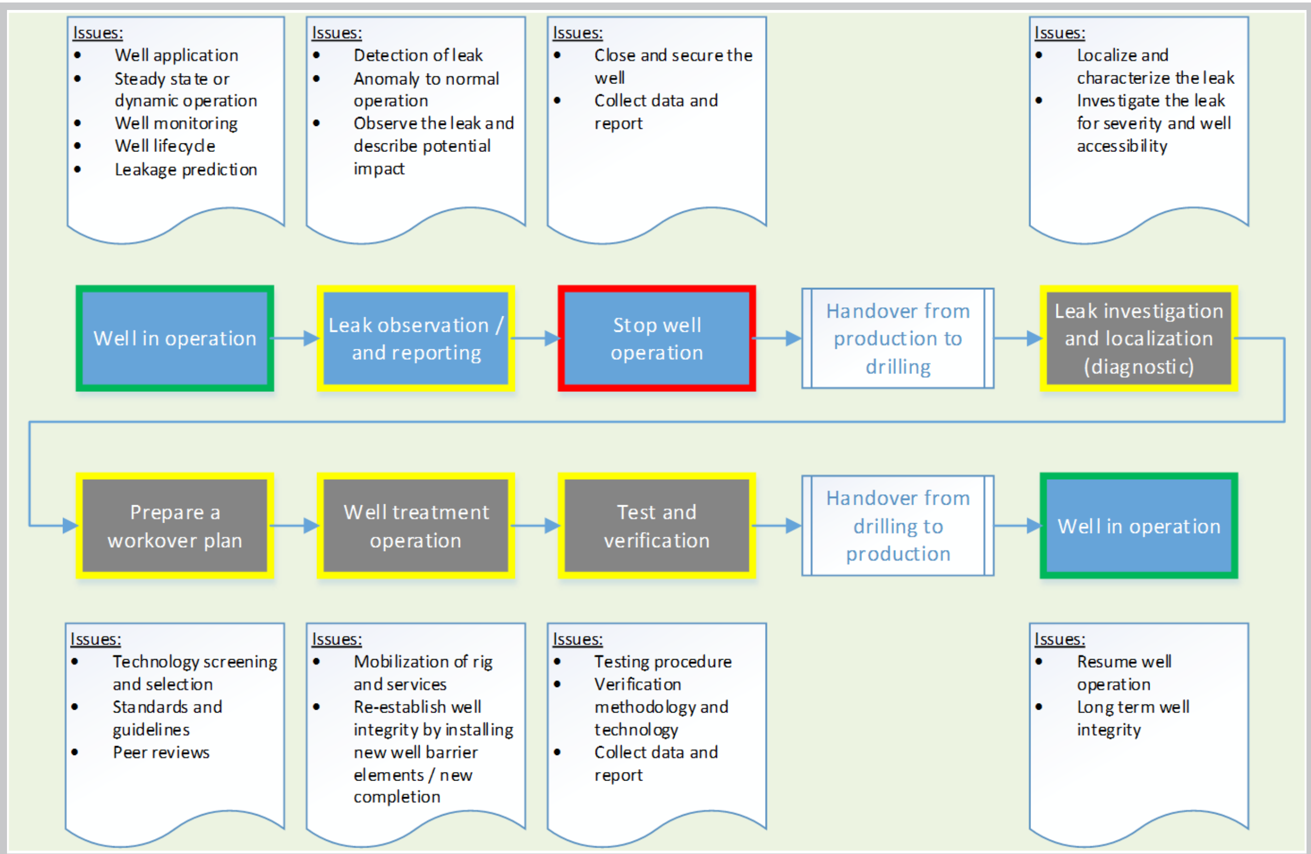

Figure 1 Well lifecycle and issues related to a leaking CO_2 well.

The drilling phase is excluded and needs to be treated separately as for example blow-outs are not considered as a traditional well leak. It should however be mentioned that uncontrolled leaks from wells using CO_2 for EOR purposes have been experienced during well intervention and lost well integrity due to corroded well tubular. Such leaks containing CO_2 have been seen to escalate into an uncontrolled well as a blow-out. Those blow-outs can be violent with uncommon consequences as destroyed BOPs due to hydrate particles in the well stream and frozen surface equipment.

2.1 Well Integrity Issues

Figure 1 illustrates a lifecycle flowchart for a CO_2 operating well. The blue and dark grey boxes refer to disciplinary responsibilities and issues for consideration for the production and drilling departments of the well operator respectively.

The "traffic light" colored lining of the boxes indicates the operability of the well. Green indicates normal operation, yellow indicates investigation and treatment while red indicates suspension of well operations.

2.2 Synergy with Oil and Gas Wells

There are several knowledge gaps related to CO_2 well integrity and some of them are discussed in this chapter. As mentioned earlier, integrity data on such wells are crucial to identify gaps and as input to R&D for corrective measures. At this stage, general oil and gas well integrity experience and expert judgment need to be used.

Conducting studies with laboratory and field scale experiments are essential to reduce gaps that are unknown to the CO_2 society. The MiReCOL (Task 9.2) field testing of a CO_2 formation sealing material at the NIS facilities in Serbia is an important event in this respect.

Major incidents and accidents in the oil and gas industry like the Macondo blow-out have led to more attention on life cycle well integrity issues. Professional societies and organizations like the Society of Petroleum Engineers (www.spe.org), Norwegian Oil and Gas Association (www.norskoljeoggass.no/en/) and Oil & Gas UK (www.oilandgas.co.uk) are important arenas for knowledge sharing of this subject. Standards and guidelines are being published through NORSOK (www.standard.no/en) and Oil & Gas UK.

One challenge with public information, as also seen in the oil and gas industry, is that what is being reported and shared have a focus on success histories. There is much to be learned from failures that needs to be captured and discussed controversially. Case based and dedicated studies are therefore needed to avoid filtered data. Still, the experience from the oil and gas industry is necessary and is being used as a basis for this study.

Lifecycle well integrity is a complex issue involving well construction, production, intervention and plugging and abandonment (P&A). Well intervention techniques and retrofit systems are important measures to the industry for increased and continued well productivity. Moreover, P&A is currently an important well technology driver due to new and stricter regulations and the volume of wells to be plugged in the near future. As an example, in Norway, the Norwegian Oil and Gas Association has been arranging a yearly P&A seminar since 2011 for experience sharing and discussing novel technologies.

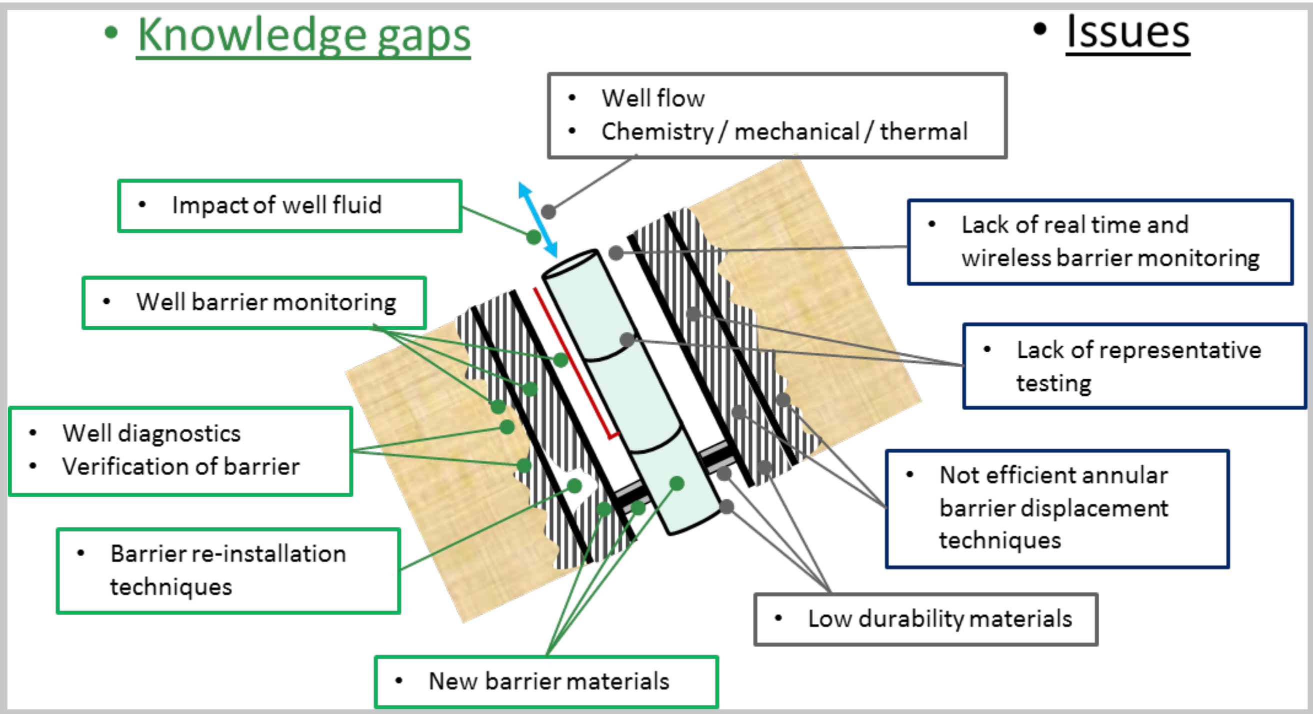

Figure 2 Schematics of a CO_2 operating well showing knowledge gaps and issues.

Important issues being focused for oil and gas P&A relevant also for CO_2 well integrity are listed below:

- Well integrity in a long life (eternal) perspective
- Well diagnostics to investigate multiple well tubulars
- Special challenges related to annular cement quality and re-installation
- Qualification of new materials as an alternative to cement
- Testing and verification of new and re-installed well barriers

2.3 Knowledge and Technology Gaps

Figure 2 illustrates a part of a well infrastructure including basic well barrier elements for a typical CO_2 well in operation. Current knowledge gaps are shown in green boxes with connected issues in black boxes.

2.3.1 Technology Categories and Readiness Level

Important technology categories for treatment of well leakages are given below with few examples together with a high level judgement of readiness:

- Well diagnostics
  - Logging of annular cement through multiple tubulars (technology gap with ongoing R&D)
  - Characterization of creeping shale as an alternative annular well barrier and/or plugging method (case specific studies and ongoing research)
  - Downhole and surface well monitoring (ongoing engineering)
- New materials
  - Resins (existing and ongoing engineering)
  - Non-consolidating and gas tight grouts (existing and ongoing engineering)
  - Internal tubular patch (existing and ongoing engineering)
  - Platelet technology (developed for pipeline leaks, R&D for downhole applications)
- Installation techniques
  - Perforate, wash and cement run on coiled tubing (existing and ongoing engineering)
  - Rigless solutions for platform and subsea well intervention (partly existing and under development)
  - Hydraulic and control lines present at barrier depth (regulation requirement and technology gap)
  - Long and highly deviated wells with eccentric casing (regulation requirement and technology gap)
  - High energy solutions for melting tubular (R&D)
- Verification of new well barriers
  - Representative pressure testing (technology gap and R&D)
- CO_2 well integrity and reliability management system
  - Well completion database with operational history
  - Well equipment reliability database
  - System for capturing, reasoning and re-use of experience (CBR)

Table 1 Overview of well integrity issues and related gaps.

Well topic	Issue	Knowledge gap	Technology gap	TRL status	Example
Diagnostics	Annular cement	Presence and quality	Reliable measurements	TRL 0 - 2	Acoustics, electric and nuclear magnetic
New materials	Alternatives to metal and cement	Sealing capability and long life durability	Material technology	TRL 1-4	Resins
Installation	Well access and barrier placement	How and where to install barriers	Conveyance and placement techniques	TRL 2 - 7	Perforate, wash and cement (PWC)
Verification	Testing of cement bond and tubular connections	Methodology	Representative fluids and joint less tubular	TRL0	Gas instead of mud,
Monitoring	Detect leakages over individual well barriers	Methodology	Real time monitoring of barriers behind another barrier	TRL 0 - 2	Wireless technology, acoustics and electromagnetic
Database and reasoning	CO_2 well integrity database	Mindset as such databases exist for O&G	Database does not exist	TRL 1 - 7	Well integrity and reliability management systems

2.3.2 Overview of Well Integrity Issues and Related Gaps

Table 1 gives an overview of well integrity issues with related knowledge and technology gaps. Examples are also given with status and technology readiness level (TRL) as much used for R&D projects within O&G and space industry (see also Appendix A).

3 CONCLUSIONS

Current knowledge and technology gaps for remediation of leaking CO_2 wells have been addressed and mapped in this report. Well integrity experience from the oil and gas industry has been the major source of information for this study as there are still very limited data available from leaking CO_2 wells. The corrosive environment of CO_2 wells give specific challenges to the well infrastructure including tubular annular cement.

Typical well lifecycle issues for a leaking CO_2 well are given together with an overview of knowledge gaps and technology status for remediation. Well diagnostics, novel materials, re-installation techniques are among the key gaps. Lack of relevant CO_2 well integrity data is a major area of concern for further assessment of knowledge and technology gaps. Full scale well experiments as the ongoing NIS field test of new formation sealing materials are crucial source of information in this matter. Also, worldwide sharing of CO_2 well data can be useful to develop knowledge gaps, and implement best practices and trends for remediation techniques and methodologies of leaking wells.

For the future, R&D focus should be on establishing a CO_2 well database consisting of both research experience and real field cases. Further work is also required on finding efficient formation sealing materials and squeezing techniques.

References

NORSOK Standard D-010, Rev.4, June 2013.
Oil & Gas UK, guidelines on qualification of materials for the suspension and abandonment of wells, issue 1, July 2012.
Vrålstad L. and et. al. 2014-2016. "MiReCOL report D8.1".
Todorovic J. and et. al. 2014 – 2016. "MiReCOL report D8.2".
Abdollahi J. 2007. "Analyzing Complex Oil Well Problems through Cased-Based Reasoning", PhD thesis, Trondheim, November 2007.
The Norwegian Oil & Gas Association, P&A Forum (PAF), Seminars 2011 – 2015.
Skinner L. 2003. "CO_2 Well Blowouts: An Emerging problem." World Oil 224 (1).
Stephen Jewell, Bill Senior 2012, "CO_2 storage liabilities in the North Sea an assessment of risks and financial consequences".
Porse S., Wade S. and Hovorka S. 2014, "Can we Treat CO_2 Well Blowouts like Routine Plumbing Problems? A Study of the Incidence, Impact, and Perception of Loss of Well Control", Elsevier 2014.
International Energy Agency (IEA) Greenhouse Gas R&D Programme, 2009. "Long term Integrity of CO_2 Storage – Well Abandonment".
S. Taku Ide, S. Julio Freidmann, and Howard J. Herzog. "CO_2 Leakage Through Existing Wells: Current technology and Regulations".

APPENDIX A: TECHNOLOGY READINESS LEVEL (TRL)

Technology readiness levels (TRLs) is a road map of estimating technology maturity of a project. There are different definitions are used for different applications such as military, space, oil & gas, etc. The following definition is based on API recommended practices used in the oil and gas industry. An important milestone in R&D is TRL 4 when a new technology is qualified for first use.

Level	Development stage	Hardware development
TRL 0	Unproven idea/proposal	Paper concept. No analysis or testing has been performed
TRL 1	Concept demonstrated.	Basic functionality demonstrated by analysis, reference to features shared with existing technology or through testing on individual subcomponents/subsystems. Shall show that the technology is likely to meet specified objectives with additional testing
TRL 2	Concept validated.	Concept design or novel features of design validated through model or small scale testing in laboratory environment. Shall show that the technology can meet specified acceptance criteria with additional testing
TRL 3	New technology tested	Prototype built and functionality demonstrated through testing over a limited range of operating conditions. These tests can be done on a scaled version if scalable
TRL 4	Technology qualified for first use	Full-scale prototype built and technology qualified through testing in intended environment, simulated or actual. The new hardware is now ready for first use
TRL 5	Technology integration tested	Full-scale prototype built and integrated into intended operating system with full interface and functionality tests
TRL 6	Technology installed	Full-scale prototype built and integrated into intended operating system with full interface and functionality test program in intended environment. The technology has shown acceptable performance and reliability over a period of time
TRL 7	Proven technology	Technology integrated into intended operating system. The technology has successfully operated with acceptable performance and reliability within the predefined criteria

Section VIII

NEAR-SURFACE ENVIRONMENTAL REMEDIATION METHODS AND PLANS

Chapter XXXI

Near-surface CO_2 leakage remediation methods, including effectiveness and costs

Mark Wilkinson[1], Katriona Edlmann[1], Ivana Demic[2], Anna Korre[3]
[1] Univeristy of Edinburgh, UK
[2] NIS, Serbia
[3] Imperial College, UK

SUMMARY

While strenuous efforts will be made to minimise the risk of the leakage of CO_2 from engineered storage sites, there will always remain a residual risk that CO_2 could migrate from the storage site into the shallow subsurface along permeable pathways such as faults or wells. This report provides a comprehensive review of the available techniques for CO_2 leakage remediation in the near surface environment considering relevant experience and expertise from pilot scale CCS projects and natural analogues, as well as CO_2-EOR operations, natural gas storage, the geothermal industry, groundwater pollution remediation, industrial waste remediation and dam construction. The applicability of each method to remediate CO_2 leakage in the near surface environment, the ease of implementation of the method and the associated costs were compiled to produce a summary table of the probable roles of the available remediation techniques, to assess the relative merits of near-surface CO_2 leakage remediation methods. The review carried out and summarised in this report suggests that a wide range of techniques are available for near surface CO_2 remediation, and that any remediation strategy will need to be site specific to be effective.

1 INTRODUCTION

The objective of this report is to provide a comprehensive review of the available approaches to remediation of CO_2 leakage in the near surface environment, and of the plans implemented to remediate any leakage from engineered CO_2 storage sites, including criteria used to assess the effectiveness of the methods and the costs of mitigation.

While strenuous efforts will be made to minimise the risk of the leakage of CO_2 from engineered storage sites, there will always remain a residual risk that CO_2 could migrate outside the storage site into the shallow subsurface along permeable pathways such as faults or wells. CO_2 leakage from geological storage will not necessarily negate the net reduction in CO_2 emissions as it is physically impossible that all of the injected CO_2 would be returned to the atmosphere during leakage due to the various trapping mechanisms operating within the subsurface. However, the leakage must be controlled as it could ultimately result in the closure of the storage project; fining of the operator by the relevant authorities; the return of credits for carbon storage; and damage to the reputation of the site operator. Regardless of the style of leakage there may be adverse health, safety and environmental risks associated with elevated levels of CO_2 in the near surface. The impact of CO_2 leakage will vary on a site by site basis; in some cases the effect may be negligible, where as in other cases it may cause serious human, agricultural, environmental or economic impacts. Recently completed projects such as QICS (Quantifying and monitoring potential ecosystem impacts of geological carbon storage; http://www.bgs.ac.uk/qics/home.html) and the EU funded ECO$_2$ project (Sub-seabed CO_2 Storage: Impact on Marine Ecosystems; http://www.eCO$_2$-project.eu/) helped to define the changes in selected environments, in this case the marine realm, through experimental and modelling work.

In May 2009, the EU directive on the geological storage of CO_2 included the requirement for a corrective measures plan to be submitted with any storage permit application (EU Directive, 2009). The directive defines leakage as any release of CO_2 from the 'storage complex' and states that measures must be taken to protect human health, along with other measures deemed necessary by the national authority, as a remediation plan.

Examples of CO_2 and other leakage into the near surface from natural sources, groundwater remediation, industrial waste, geothermal, CO_2-EOR and oil and gas operations provide analogues for the CO_2 storage industry and facilitate the evaluation of mitigation and remediation procedures. They provide valuable insights into the nature of the leakage and the impact of elevated CO_2 levels on human health, biodiversity, ecology, agriculture, surface water, and ground water quality in the near surface. They also allow to assess the effectiveness and suitability of the remedial measures.

The next section defines what is considered near surface environment in the context of this work and discusses the potential CO_2 leakage routes. The remediation techniques considered suitable for CO_2 leakage remediation originate in other relevant fields, as there is relatively little experience of remediation of shallow CO_2 leaks. Such fields are:

1. The control of groundwater pollution, especially potable water – in near surface environments. CO_2 in the gas phase has a similar density to some volatile organic compound (VOC) vapours, which are a common pollutant that is considered in remediation. However, it should be noted that CO_2 is non- toxic at low concentrations and is generally sourced from below the rock / soil matrix that requires remediation (Zhang et al., 2004);
2. Oil / gas operations (including EOR / CO_2 EOR) including both routine and acute incident scenarios – there are no recorded instances of leakage to the surface that did not involve boreholes;
3. Natural gas storage projects (review in Benson and Hepple, 2005);
4. CO_2 production for EOR (e.g. the blow-out at Sheep mountain, Colorado, USA; IEA GHG, 2007 p. 38);
5. Natural analogues for surface leakage (e.g. Crystal Geyser, Utah, USA);
6. Geothermal power in high-CO_2 regions (e.g. Torre Alfina, Italy);
7. The grouting of the foundations of dams (for water storage);
8. Pilot-scale and proposed industrial-scale carbon capture and storage (CCS).

1.1 Definition of near surface

The primary focus of this report is leakage that is 'near surface', which is a term that should be clearly defined in the context of this report. Near surface could be defined in relation to the following criteria:

1. The top of the storage complex (Figure. 1; i.e. everything above the storage complex is deemed to be near surface);
2. The phase change boundary for CO_2, so that the CO_2 is in the gas phase, usually cited to be at c. 800m for a 'normal' geothermal gradient;
3. The maximum depth for meteoric / potable water zone which is at c. 500 m depth, but may not exist at all in an offshore setting;
4. The depth of the shallowest aquifer, though this could be the storage reservoir in some cases;
5. The top of the sediment consolidation zone (>c. 60 – 70° C for the onset of significant cementation by quartz overgrowth; the cementation of limestones begins at much shallower depths, effectively at the sea floor; mudrocks are cohesive so this definition is difficult to apply);
6. The lower limit of the biological zone (c. 60 – 70° C);

7. An arbitrary depth below the ground surface, seafloor or sea surface;
8. The depth range of typical remediation techniques used by the pollution clean-up industry rather than by the hydrocarbon industry.

Here we adopt the last of the above approaches. This is partly to avoid overlap with the other work packages of the MiReCOL project, which will consider the remediation of leakage using many of the techniques developed and implemented in the field by the hydrocarbon industry. The techniques considered here will not be examined by any other part of the project, and are (at least sometimes) not covered in detail by recent reviews of techniques for the remediation of CO_2 leakage.

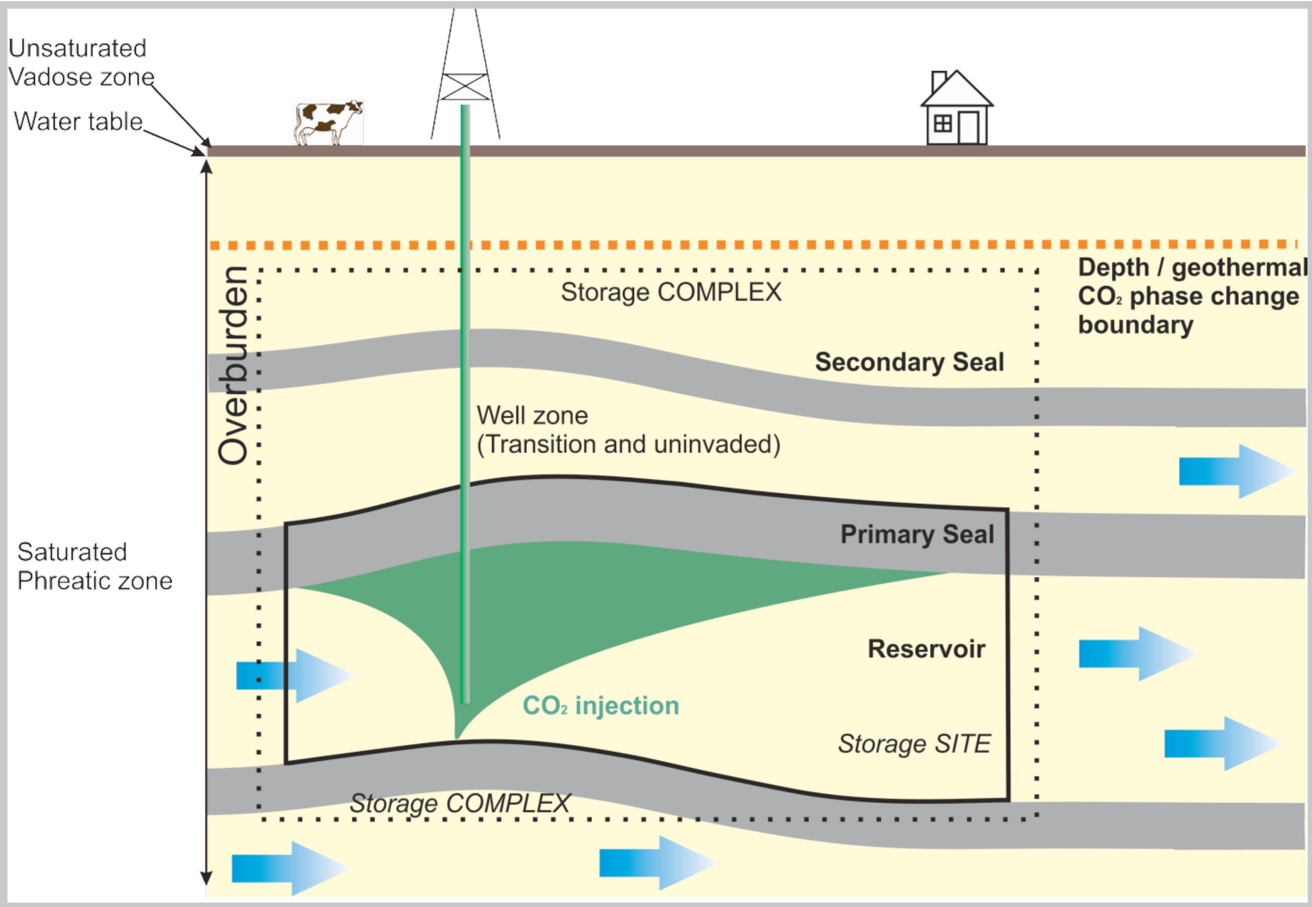

Figure 1 The CO_2 storage complex.

Given that the focus of this review is the near surface environment, then there are a number of factors which make this environment different from that being considered for the deeper subsurface, which is the realm of the hydrocarbon industry:

1. Low to very low water salinity (typically << 35 ppt NaCl, i.e. seawater equivalent);
2. Higher water flow rates;
3. CO_2 in gas phase, possibly present as hydrates;
4. Natural fractures may be open due to low confining pressure (e.g. Becker and Lynds, 2012);
5. In an active sedimentary basin:
    a. unconsolidated, uncemented sediments;
    b. very high porosity and permeability (> 20 % and Darcy scale permeability);
    c. low capillary entry pressure;
    d. biological activity including:
        - biodegradation of hydrocarbons;
        - formation of kerogen and biogenic methane;
    e. lack of structures (traps) to collect leaked CO_2;
    f. lack of (active) faults as pathways for leakage;
    g. presence of polygonal clay shrinkage cracks (Cartwright et al., 2003).

The possible pathways for the leakage of CO_2 in the near surface are similar to those associated with leakage at typical hydrocarbon depths:

1. Boreholes – both abandoned and active;
2. Faults and fractures, including both those sufficiently large for resolution using seismic imaging, and those too small for seismic resolution;
3. Matrix rock porosity within lithologies such as sandstones and limestones.

1.2 Trade names and proprietary products

No proprietary products are identified in this report, and consequently no recommendations or endorsements (or otherwise) of commercial products are made. The remediation techniques described in this report require the use of many products and services that are available commercially, many of which have been developed by the pollution remediation industry. It is the responsibility of the user of this report to identify suitable products and service providers for the techniques described herein.

1.3 Near surface impacts that are considered as requiring mitigation intervention

Elevated CO_2 concentrations in the near surface environment can impact upon resources both within the subsurface, and above. Onshore, the major resource located within the near surface environment is potable water. In the USA, a volume of the subsurface surrounding an area from which ground water is abstracted is defined as a wellhead protection area, which is "the surface and subsurface area surrounding a water well or well field, supplying a public water system, through which contaminants are reasonably likely to move toward and reach such water well or well field" (US EPA, 1987). Many States within the USA have defined wellhead protection areas on the basis of the time taken for contaminants to flow from the boundary of the area to the point of abstraction of the groundwater (Bai et al., 2000, p.42). As such, any contamination of groundwater within such a wellhead protection area would require remediation, or at least an assessment of the likely consequences of the contamination.

It should be noted that the addition of CO_2 to subsurface groundwater resources is not, in itself, necessarily a problem – ironically, carbonated water is sold for a premium price on Western World markets, and water carbonated from subsurface sources has the highest premium of all. However, as has been well documented, CO_2 dissolves in water to form a weak acid. This can then mobilise toxic metals e.g. Li, Mg, Ca, Rb, Sr, Mn, Fe, Co, Ni, Zn (Little and Jackson, 2010) including arsenic (As) and lead (Pb) (Benson and Hepple, 2005). Standards for groundwater and drinking water composition, in this case maximum allowable concentrations of metals, for the EU, UK and USA are listed in Table 1.

Table 1 Standards for groundwater and drinking water composition, in this case maximum allowable concentrations of metals, for the EU, UK and USA. References: (1) SEPA (2010); (2) Scottish Government (2010); (3) US EPA (2009); (4) European Council (1998) (Based on table compiled by Kit Carruthers of the University of Edinburgh).

Metal	Water Quality Standards				
	Marine	Fresh	Drinking Water		
	SEPA EQS (µg/l) (1)	SEPA EQS (µg/l) (1)	Scottish Water (µg/l) (2)	US EPA (µg/l) (3)	EU (4) (µg/l)
Aluminium	15	15	200	200	200
Antimony	-	-	5	6	5
Arsenic	25	50	10	10	10
Barium	-	-	-	2000	
Boron (5)	7	2	1	-	1
Cadmium	0.20	0.25	5	5	5
Calcium	-	-	-	-	
Cobalt	3	3	-	-	
Copper	5,000	28	2000	1,300	2000
Chromium	0.6	3.4	50	100	50
Iron	1,000	1,000	200	300 (4)	200
Lead	7.2	7.2	25	15	10
Magnesium	-	-	-	-	
Manganese	-	30	50	50 (4)	50
Mercury	0.05	0.05	1	2	1
Nickel	20	20	20	-	20
Potassium	-	-	-	-	
Selenium	-	-	10	50	10
Sodium	-	-	-	-	200
Titanium	-	-	-	-	
Uranium	-	-	-	30	
Vanadium	100	60	-	-	
Zinc	40	125	-	5,000 (4)	

The ground surface itself is also a valuable resource, used for virtually every activity in which humans are involved. The monetary value of the land surface is highly variable – land in a city centre may be worth literally millions of dollars per square metre, whereas desert or other 'waste' land has little or no monetary value.

High levels of CO_2 contamination can reduce crop yields; impair/kill vegetation entirely as at Mammoth Lake, USA (Lewicki et al, 2008); or render buildings unsafe for human habitation. The ingress of CO_2-rich ground gas into buildings within Arkwright Town in Derbyshire, UK, caused the demolition of the entire village, and its relocation to a safe location at a reported cost of 15 M GBP (value in 1990's; Independent, 1994). The leakage of CO_2 to the surface in any inhabited area is likely to require some form of remediation, which could be as varied as subsurface intervention or the education of the local inhabitants to avoid highly contaminated areas. Potentially, leakage to an agricultural area may have to be remediated also, though with relatively low value agricultural land the cost of remediation may well exceed the value of any lost productivity of the land.

Table 1 Standards for groundwater and drinking water composition, in this case maximum allowable concentrations of metals, for the EU, UK and USA. References: (1) SEPA (2010); (2) Scottish Government (2010); (3) US EPA (2009); (4) European Council (1998) (Based on table compiled by Kit Carruthers of the University of Edinburgh).

Metal	Water Quality Standards				
	Marine	Fresh	Drinking Water		
	SEPA EQS (µg/l) (1)	SEPA EQS (µg/l) (1)	Scottish Water (µg/l) (2)	US EPA (µg/l) (3)	EU (4) (µg/l)
Aluminium	15	15	200	200	200
Antimony	-	-	5	6	5
Arsenic	25	50	10	10	10
Barium	-	-	-	2000	
Boron (5)	7	2	1	-	1
Cadmium	0.20	0.25	5	5	5
Calcium	-	-	-	-	
Cobalt	3	3	-	-	
Copper	5,000	28	2000	1,300	2000
Chromium	0.6	3.4	50	100	50
Iron	1,000	1,000	200	300 (4)	200
Lead	7.2	7.2	25	15	10
Magnesium	-	-	-	-	
Manganese	-	30	50	50 (4)	50
Mercury	0.05	0.05	1	2	1
Nickel	20	20	20	-	20
Potassium	-	-	-	-	
Selenium	-	-	10	50	10
Sodium	-	-	-	-	200
Titanium	-	-	-	-	
Uranium	-	-	-	30	
Vanadium	100	60	-	-	
Zinc	40	125	-	5,000 (4)	

The leakage of CO_2 to the seafloor is a possible consequence of migration from an offshore storage site (e.g. Kirk, 2011). While the seafloor may not have monetary value as such (in the sense that it cannot be bought or sold), it is extensively used for many activities, including the siting of facilities for the production of oil and gas; the siting of wind farms; the anchorage of aquiculture facilities such as fish farms; and the harvesting of naturally growing marine food sources such as fish and sand eels. Some areas benefit from legal protection, such as Special Areas of Conservation (SAC) within the UK territorial waters, as defined under the UK Habitats Directive. They are areas of international importance for either or both threatened habitats and species. The leakage of CO_2 to the seabed and the overlying water column would possibly require remediation if the area were protected, or was utilised in one of the ways described below. The consequences of leakage will depend upon the nature of the leakage site – a site with strong tidal currents, for example, may have little impact compared to an area with little water flow or exchange. Consequently, the need for remediation will have to be assessed on a site-by-site basis.

An impact of leakage which is not related to the site of leakage as such is that of return of the stored CO_2 back to the atmosphere. Since the aim of CCS is to prevent the addition of CO_2 to the atmosphere and oceans, migration outside the storage complex into the near surface environment (and hence through time possibly into the oceans and atmosphere) should be prevented where possible. Equally, if financial reward has been accepted for the avoidance of CO_2 emissions to the atmosphere, for example through the European Emissions Trading Scheme (EU ETS), then emitting CO_2 into the atmosphere will engender a financial penalty and hence encourage remediation. However, it should be noted that the cure can be worse than the disease, in that the carbon footprint of remediation schemes can be very high (Ellis and Hadley, 2009). These authors cite a proposed scheme from the USA in which it was estimated that the difference between two proposed remedies could be as high as 2 percent of the annual greenhouse gas emissions of the state of New Jersey. Care should be taken that the remediation of a leak does not actually increase net CO_2 emissions compared to allowing the leak to continue unabated.

1.4 Natural analogues for surface leakage

Natural analogues for the remediation of CO_2 leakage are locations where naturally-occurring CO_2 is leaking into the near surface, many of which have been studied either because of environmental effects such as vegetation die-off, or because of interest in geological carbon storage. It is unusual to attempt to remediate a natural leak, as they are either simply avoided or, in some cases, are exploited for naturally-carbonated water, which is sold for a premium price as in the Eifel region of Germany (Ulrich, 1958). In some countries with large areas of land that are affected by high fluxes of natural CO_2, then avoiding such areas for building has not proved to be practical, and in Italy for example, significant numbers of people live in areas of high natural emissions (e.g. Carapezza et al., 2003). A recent review of leakage rates for the EU-funded QICS project (Kirk, 2011) covered both onshore and offshore sites, but is not comprehensive. As an example, there only 2 Italian sites in the Kirk (2011) review, but 286 natural CO_2 seeps in Italy and Sicily listed in a database of such sites (Googas Catalogue, 2009). A further compilation of non-volcanic CO_2 leakage sites is in Mörner and Etiope (2002), with c. 25 diffuse sites, and c. 30 vents listed worldwide. A comprehensive compilation of natural CO_2 leakage sites is beyond the scope of this project, and in any case sites of leakage directly from volcanoes is here considered to be less valuable as analogues than leakage from natural accumulations of CO_2 from sedimentary basins which mimic the likely conditions of engineered CO_2 storage more closely. Tables 2 and 3 summarise the sites from Kirk (2011) and others. Sub-sea sites are included, although the present authors consider that the difficulty of implementing most of the remediation techniques described in this report make shallow intervention in an offshore setting an unlikely option.

An important caveat to this review is that, as the topic is near surface leakage, then inevitably all the cases described involve the leakage of CO_2 into the near surface environment. It would be misleading to give the impression that all, or even many, sites of natural subsurface CO_2 accumulation are leaking – many do not have any surface expression. Sites such as the high-CO_2 province in the Northern North Sea that includes the well-known Sleipner and Miller fields (Lu et al., 2009; 2010), and the less well-known CO_2 province in the Southern North Sea that includes the Fizzy prospect (Wilkinson et al., 2009) have no known surface expression and give confidence that carefully chosen storage sites will hold CO_2 for geological periods of time. The above indicate that the majority of known sub-sea leakage sites are from vents, which may occur either singly or in clusters.

Table 2 Offshore natural analogue sites.

Site	Flux rate	Surface expression	Water depth (m)	References
Panarea Southern Tyrrhenian Sea (Italy)	1670 – 8500 $t/m^2/year$	Linear faults and vents aligned on faults	up to 30m	Tassi et al. (2009); Caramanna (2010); Lombardi (2010); Etiope et al. (2007)
Ischia, Italy	12.8 $t/m^2/year$	Vents, <5 per m^2	<5	Lombardi (2010); Hall-spencer et al. (2008);
Champagne area, Mariana arc	35000 t/year as liquid drops	Vents	1600	Lupton et al., 2006
Hatoma Knoll, Okinawa Trough	-	Vents	700 - 1400	Shitashima et al., 2008
Salt Dome Juist, German North Sea	1 – 10 t/day	Point source above dome	-	McGinnis et al. (2011)

The nature of natural CO_2 seeps is very variable (bubbling water, diffuse, vent, spring, well, fumarole; Roberts et al. 2011), and the area over which leakage occurs is also variable. Some implications for the remediation of engineered CO_2 storage sites can be made.

Table 3 Onshore natural analogue sites.

Site	Flux rate (t/m²/year)	Surface expression and area	References
Laacher See caldera, Germany	variable, 0.0084 – 0.020 diffuse; 500 – 1200 close to vent; background 0.011	2 vents; diffuse; bubbles in the lake water; area c. 2 by 1 km	Jones et al. (2009); Krüger et al. (2009); Aeschbach-Hertig et al. (1996); Gal et al. (2011)
Ukinrek Maars, Alaska	0.25 – 0.43	diffuse with 4 zones of plant kill, 30,000 – 50,000 m²; 2 vents 3 km away	Evans et al. (2009)
Furnas and Fogo volcanoes, Azores	0 – 1.7	diffuse near fumarole fields	Viveiros et al. (2008)
Horseshoe Lake, Mammoth Mountain, California USA	0.08 – 1.3	diffuse, 6 tree-kill areas, largest 120,000 m²	Lewicki et al. (2008)
Pululhua caldera, Ecuador	detection limit – 0.052	linear trend	Padrón et al. (2008)
Rekjanes geothermal field, Iceland	2.5	diffuse (soil gas), steam vents, mud pools	Fridriksson et al. (2006)
Rapolano fault	52560	vents, production wells	Mörner and Etiope (2002); Rogie et al. (2000)
Little Grand Wash Fault, Utah, USA	0.3 – 1.0	carbonates springs; abandoned exploration well	Burnside (2010); Han et al. (2013)
Northern Fault, Salt Wash Graben, Utah, USA	0.04 – 0.12; 12,000 t/year from Crystal Geyser	springs and abandoned exploration well	Burnside (2010); Gouveia et al., 2005
Pannonian Basin, Hungary	1100 – 3670 (total)	bubbling wells, streams, springs	Pearce et al (2010); Sherwood Lollar et al (1997)
Mefite d'Ansanto, Italy	338,000 – 730,000 (estimates vary)	numerous gas vents	Chiodini et al. (2010); Rogie et al. (2000); Italiano et al. (2000)
Latera Caldera, Italy	0.0012 – 1.3, background <0.008	4 vents on faults	Annunziatellis et al. (2008)
Italy (other)	< 1 to > 100 ton / day	Bubbling water; diffuse; vent; spring; well; fumarole	Roberts et al (2011); Googas Catalogue (2009)
Springerville, Arizona, USA	~63 kTon/year	high CO_2 groundwater, travertine	Keating et al. (2014); Allis et al. (2005)

Firstly, the total area over which CO_2 can leak at a single site can be substantial. For example both the modern and the paleo-leakage zone along the Little Grand Wash Fault, Utah, USA are approximately 3 km long (Shipton et al., 2004, 2005; Burnside, 2010; Jung et al, 2014; Figure 2), though leakage is apparently restricted to the fault trace. In contrast, in the nearby Salt Wash Graben there is evidence of paleo-leakage (travertine mounds) at least 500m into the footwall of the fault (Burnside, 2010).

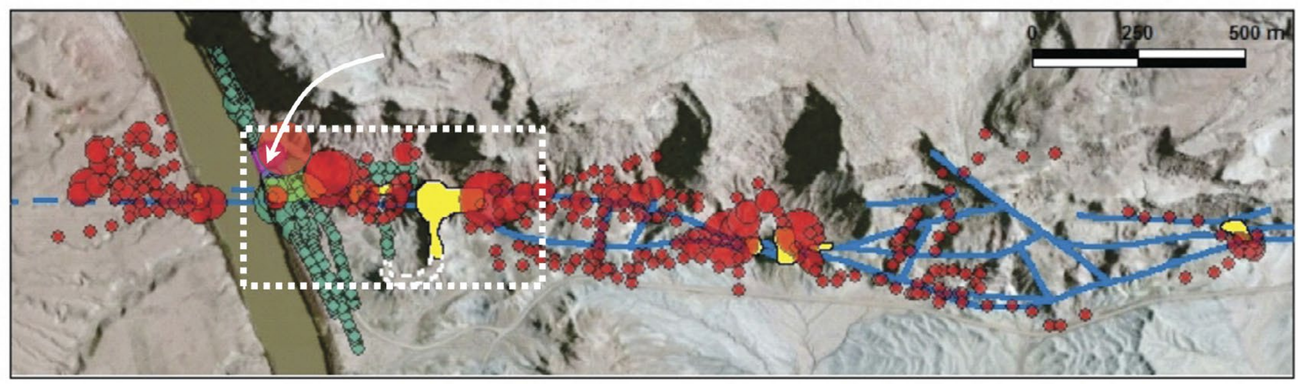

Figure 2 The distribution of modern CO_2 leakage along the Little Grand Wash Fault, Utah, USA (Jung et al., 2014). Small circles 0 – 20 g/m²/day, largest circles are >1500 g/m²/day. Note detectable leakage over c. 3km of the fault.

At Laacher See, Germany, high CO_2 concentrations have been recorded over an area of approximately 2 by 1 km (Gal et al., 2011), some of which are easily visible such as bubbles in the lake and surface vents, but others have been detected only by gas monitoring (Figure 3). At Mammoth Mountain, California, there are 6 distinct areas of tree-kill due to high CO_2 concentrations, the largest is c. 120,000 m² (Lewicki et al., 2008).

At Springerville, Arizona, USA, 49 individual travertine mounds associated with a natural deep CO_2 reservoir are found over approximately 20km², they are spatially associated with fold axes and faults (Embid et al., 2006; Figure 4).

The travertines at the both the Little Grand Wash Fault, and Springerville, both suggest leakage from a large number (49 in the case of Springerville; Embid et al., 2006) of distinct leakage sites. It is not known for certain why an individual leakage point is abandoned in favour of another, but a reasonable assumption is that the sub-surface fractures that are carrying the fluids (both CO_2 and water) to the surface become cemented up. In the case of the Little Grand Wash Fault, then modern-day erosion has dissected some of the older travertines, showing extensive veins of calcite and aragonite (Shipton et al., 2004, 2005; Burnside, 2010) which are presumably the paleo-fluid conduits. Once an individual leakage point (travertine mound) becomes sealed, then leakage moves to a nearby alternative site.

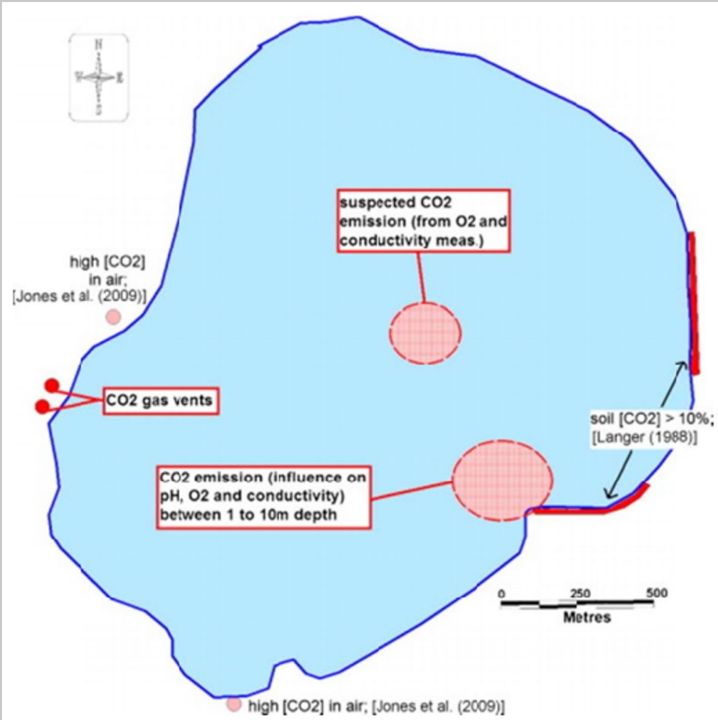

Figure 3 At Lacher See, Germany, high CO_2 concentrations have been recorded over an area of approximately 2 by1 km (Gal et al., 2011, their Fig. 11).

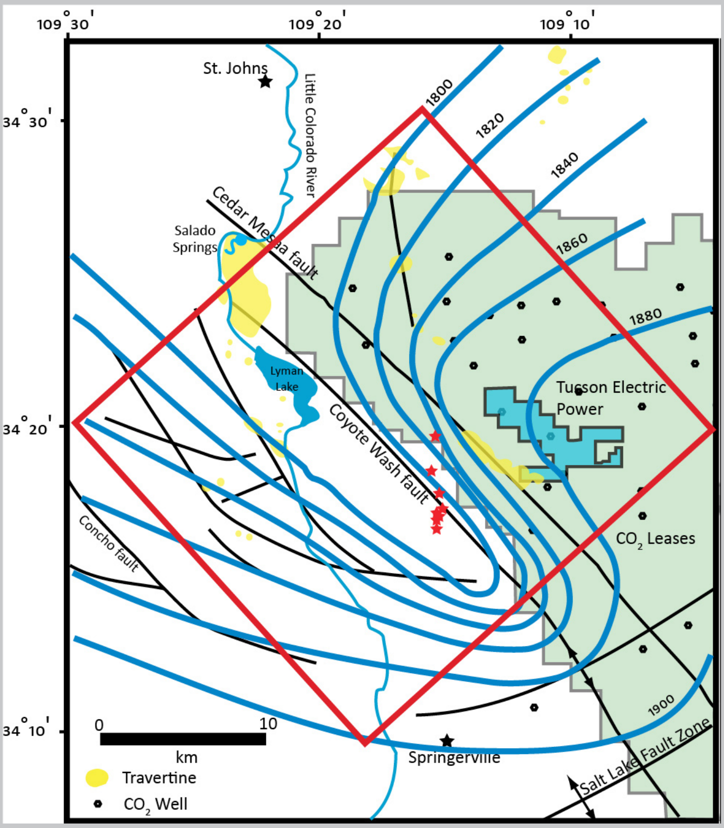

Figure 4 Travertine (yellow) as an indicator of paleo-leakage of CO_2 around Springerville, Arizona, USA. From Keating et al., 2014).

The volcanic craters of Ukinrek Maars, Alaska date from only 1977. Between 30,000 and 50,000 m^2 of ground area has conspicuous plant damage or death (Evans et al., 2009). Geographically separate gas vents, linked geochemically to the same source, lie some 3 km from the damaged vegetation (Evans et al., 2009).

On the assumption that leakage from an engineered storage site followed similar patterns, then it might be deduced that leakage, if prevented at a localised high flux site (for example by grouting the fluid-conduit fractures), will move to another site nearby. Furthermore, a single underground source can supply CO_2 to a large area – certainly measured in square kilometres, or kilometres in length if following a fault trace. Larger areas can be affected by CO_2 emissions, e.g. 25 km^2 in the case of a 1995 event in the Alban Hills of Rome, Italy (Quattrocchi et al., 1998, cited in Pizzino et al., 2002) though whether this comes from a single underground source, as would be the case with a leaking storage reservoir, is uncertain.

The rate at which CO_2 concentrations build up during natural release events can be very rapid, though release events can be short (days). Annunziatelli et al. (2003) describe a sudden release of CO_2 from the ground in the Italian town of Cava dei Selci. Groundwater pH decreased from 6.0 to 5.5, and pCO_2 increased from 0.7 to 2.5 bars. The affected area was about 10,000 m^2. In separate events in October 1999 and in March 2000, 30 cows and some sheep died due to asphyxiation by CO_2 (Annunziatelli et al., 2003). Faulting has been implicated in at least some release events (Quattrocchi and Venanzi, 1989; Quattrocchi and Calcara, 1994; Calcara et al., 1995; Quattrocchi and Calcara, 1998). Another control of release events is the weather – monitoring of CO_2 levels on São Miguel Island in the Azores shows that soil water content, barometric pressure, wind speed and rainfall explain much of the observed variation in soil gas concentrations (Viveiros et al., 2008). Rapid decreases in barometric pressure are especially associated with sudden increases in CO_2 concentration in residential buildings, with detected levels in the Azores exceeding 20 % - though the studied house lies within a volcanic caldera! (Viveiros et al.,2008). Similar results were obtained at Mammoth Mountain, California, where average daily CO_2 fluxes were correlated with both average daily wind speed and atmospheric pressure, the degree of correlation depended on the magnitude of the fluctuations in the atmospheric parameters (Lewicki et al., 2008). The authors noted that any genuine change in the CO_2 supply from depth would be at least partly obscured by the meteorological effects.

A further lesson from natural analogues is that CO_2 can lie undetected at shallow depths within the crust, both within unconsolidated high porosity sediments but also within consolidated bedrock (Carapezza and Tarchini, 2007) The CO_2 can then be released to the surface by routine engineering activities such as the drilling of shallow groundwater boreholes, or the removal of low permeability cover during excavation (Carapezza and Tarchini, 2007; Barberi et al., 2007). The remediation of such a case is described below.

Natural analogues also enable study of the effects of the CO_2 on the flora and fauna of the leakage site. At Laacher See, Germany, an investigation of microbial communities in the soil showed significant differences between CO_2-rich (>90 % soil gas), medium CO_2 (20%), and a control site with background CO_2 concentrations (Krüger et al., 2009). The ecosystem was interpreted to have adapted to the different conditions through species substitution or adaptation, with a shift towards anaerobic and acidophilic species under elevated CO_2 concentrations. Krüger et al. (2009) suggested that it might be possible to identify botanical and microbial species whose presence or absence provide easily detectable indicators for the leakage of CO_2.

The infamous lethal release of CO_2-rich gas from Lake Nyos, Cameroon, in 1986 is cited as an example of the potential dangers of CCS. Studies of other naturally-CO_2 rich lakes enable a more balanced view to be taken. The Laacher See in Germany has a flux of CO_2-rich gases into the deep water, but seasonal overturning allows the release of the CO_2 without concentrations building to dangerous levels (Aeschbach-Hertig et al., 1996). The Cuicocha caldera lake in Ecudor also has an overturn period from June to August, again allowing volcanically-derived CO_2 to escape (Padrón et al., 2008). The physical and climatic conditions of a lake are hence crucial in determining the extent to which a CO_2 leak might be dangerous to life, and seasonal overturning (or stable stratification) is the most important factor. Natural analogues can also be used to assess the risks to life associated with natural (and presumably engineered) CO_2 leakage. Roberts et al. (2011) calculated that the risk of accidental human death from CO_2 seeps in Italy to be 10-8 year-1 to the exposed population, note not to the population at large. Roberts et al. (2011) pointed out that the CO_2 risk is significantly lower than that of many socially accepted activities, such as driving a car for which the risk of death is reported as 1.8x10-4 per year.

In summary, natural leakage from known single reservoirs can cover large areas at the surface (> 10 km^2), and commonly follows the traces of faults. Gas release can be either steady state or episodic, sometimes with an obvious control by tectonic activity. Undetected CO_2 can exist in high concentrations at shallow depths, and be released by the drilling of boreholes, or by excavation though a low permeability caprock.

2 MONITORING AND REPORTING PROTOCOLS

Emphasis should be on achieving the earliest possible detection of CO_2 migration from the reservoir, to maximise the time available for suitable mitigation actions to be implemented before leakage (migration of CO_2 out of the storage complex) occurs, and also to provide sufficient time for full remediation prior to any planned transfer of liability from the operator to the competent authority (CO_2CARE, 2013). This review of industry best practises concluded that the design of a risk-based remediation plan would be an essential step in abandoning a storage site. Bai et al. (2000) describe a network of 'sentinel' wells that surround a sensitive resource, in this case a drinking water supply, that allow sufficient time after the detection of contaminants in one of the wells to plan and implement remediation methods.

The adoption of an incident response protocol in advance of a CCS project is vitally important (IEA GHG, 2007). Lack of a protocol for responding to CO_2 leakage allegations can lead to years of complaints to government and industry from landowners, with landowners eventually seeking answers from unqualified sources. Wrong conclusions and inaccurate information will then distribute in the international press, affecting public perception of CCS.

An example of this is the Weyburn-Midale CO_2 monitoring and storage project (LaFleur, 2010; 2011). In January 2011, farmers living near the IEAGHG Weyburn-Midale CO_2 Monitoring and Storage Project (Saskatchewan Canada) announced to the press that leaking CO_2 from the storage reservoir was reaching ground surface and impacting their land. The story of leakage originated from an independent study commissioned by the landowners after years of complaints that government and industry officials had not addressed to their satisfaction (LaFleur, 2010; 2011). CCS experts questioned the technical merit of the independent study. To address the uncertainty in the source of the CO_2 on the Kerr farm, and in keeping with its mission to advance best practices and performance verification for geologic carbon storage, the International Performance Assessment Centre for Geologic Storage of Carbon Dioxide (IPAC-CO_2) commissioned a scientific study at the Kerr farm, with the Bureau of Economic Geology's Gulf Coast Carbon Center as the technical lead. One important finding of the study was that soil CO_2 on the land was natural and not the result of a CO_2 storage leak (Sherk et al., 2011; Romanak et. al, 2014).

Guidelines from the IEAGHG state that "Under EU regulations, requirements for leaked emissions falls under the EU Emissions Trading Scheme (EU ETS) (Directive 2003/87/EC)" which, operating since 2005, builds upon the Kyoto Protocol, the Clean Development Mechanism (CDM) and Joint Implementation (JI) (EC, 2008); and for geological storage of CO_2 would now be triggered by the EU CCS Directive which entered into force in 2009. Article 16 of the EU CCS Directive 2009/31/EC lays out requirements in the event of leakages or significant irregularities, dictating that should any leakage occur then there would be a surrender of allowances under the EU ETS. In June 2010, Decision 2007/589/EC (establishing guidelines for the monitoring and reporting of greenhouse gas emissions pursuant to Directive 2003/87/EC) was amended to say leakage 'may be excluded as an emission source subject to the approval of the competent authority, when corrective measures pursuant to Article 16 of Directive 2009/31/EC have been taken and emissions or release into the water column from that leakage can no longer be detected.' A further amendment to Decision 2007/589/EC under Annex XVIII adds 'Monitoring shall start in the case that any leakage results in emissions or release to the water column. Emissions resulting from a release of CO_2 into the water column shall be deemed equal to the amount released to the water column' and defines an approach for quantification, stating 'The amount of emissions leaked from the storage complex shall be quantified for each of the leakage events with a maximum overall uncertainty over the reporting period of ± 7.5%. In case the overall uncertainty of the applied quantification approach exceeds ± 7.5%, an adjustment shall be applied'

2.1 Existing monitoring and reporting protocols

The principles of the existing CO_2 surface leakage monitoring and reporting protocols are drawn from authoritative international guidance produced by the Intergovernmental Panel on Climate Change (IPCC) in its Revised 1996 IPCC Guidelines for National Greenhouse Gas Inventories (IPCC Guidelines) and related Good Practice Guidance and Uncertainty Management in National Greenhouse Gas Inventories (Good Practice Guidance). These documents can be accessed from the web at:

- http://www.ipcc-nggip.iges.or.jp/public/gl/invs1.htm and,
- http://www.ipcc-nggip.iges.or.jp/public/gp/gpgaum.htm respectively.

The current CO_2 monitoring and reporting protocols are discussed briefly in the following paragraphs:

1. EU Environmental Liabilities Directive;
2. London Convention and protocol;
3. EU Emissions Trading System;
4. IPCC Guidelines and good practice reports;
5. UNFCCC Kyoto protocol committee for developed countries;
6. UNFCCC Kyoto protocol CDM for developing countries;
7. US EPA GHG Emissions.

<u>EU Environmental Liabilities Directive</u>

Any damage to the environment - such as groundwater pollution caused by CO_2 leakage could be covered by the EU Environmental Liabilities Directive (which focuses on habitats, water and land pollution). Under this directive an operator is liable for damage up to 30 years after an incident takes place, irrespective of the time the facility closes. In the UK, the Environment Agency is able to order companies to restore polluted environments through this directive, although it is unclear how this would apply to the sea, (EU Directive, 2004).

The London Protocol to the London Convention

An international framework governing the disposal (dumping) of industrial waste at sea which was amended in 2006 to allow "CO_2 from capture processes" to be stored under the seabed. This amendment came into force in 2007, but a further amendment is necessary to allow for the storage of CO_2 that has crossed an international border (trans- border CO_2). In 2007, the Convention for the Protection of the Marine Environment of the North-East Atlantic ("OSPAR Convention") was also amended to allow CO_2 storage in geological formations under the seabed. This amendment has yet to be ratified, and so is not in force.

EU Emissions Trading System (ETS)

An EU ETS operator must propose a monitoring plan when applying for a greenhouse gas emissions permit (or emissions plan for aviation operators). The monitoring plan provides information on how the EU ETS operator's emissions will be measured and reported. A monitoring plan must be developed in accordance with the European Commission's Monitoring and Reporting Regulation and be approved by an EU ETS Regulator. The reporting year runs from 1 January to 31 December each year.

http://ec.europa.eu/clima/policies/ets/monitoring/index_en.htm

The EU ETS requires all annual emissions reports and monitoring to be verified by an independent verifier in accordance with the Accreditation and Verification Regulation. A verifier will check for inconsistencies in monitoring with the approved plan and whether the data in the emissions report is complete and reliable. Annual emissions are reported in accordance with two Commission Regulations: the Monitoring and Reporting Regulation (MRR); and the Accreditation and Verification Regulation (AVR).

IPCC permit

The IPCC Guidelines and good practice reports give guidance on monitoring, verification and estimation of uncertainties, as well as on quality assurance and quality control measures (IPCC, 2006, v.2 Chapter 5). General guidance is given on how to plan a monitoring programme; what to monitor; and how to report on results. The purpose of verifying national inventories is to establish their reliability and to check the accuracy of the reported numbers by independent means. The guidelines work on the principle that with good site characterisation, risk assessment of leakage, monitoring and reporting, then zero leakage can be assumed unless monitoring indicates otherwise.

Monitoring includes: measurement of background CO_2 flux; continuous measurement of CO_2 injected; monitoring of injection emissions; periodic monitoring of CO_2; and monitoring of CO_2 fluxes to surface.

Kyoto Protocols

A series of ratifications from 2008 - 2012 (Kyoto 1st Period) for:

- Developed country emission commitments;
- CCS included in KP Art 2.1;
- IPCC GHG Guidelines (2006) allows CCS to be included;
- CDM – Policy mechanism for rewarding CO_2 reduction in developing countries. Project-based carbon credits.

US EPA - GHG Emissions

The US Environmental Protection Agency (EPA) mandates for the reporting of the injection of greenhouse gasses and the geological sequestration of CO_2 (Final rule federal register Vol 75 p75060 Dec 1 2010 http://www.epa.gov/ghgreporting/reporters/subpart/rr.html).

The requirement is to report GHG data to the EPA annually, including:

- EPA approved site specific monitoring reporting and verification plan;
- Quantify and report amount of CO_2 stored;
- Detect and quantify emissions to surface;
- Verify whether leakage and distinguish from baseline.

2.2 Reporting protocols

Under the Clean Air Act, the US EPA Office of Air specified rules for the mandatory reporting of greenhouse gases (MRR) from upstream suppliers of fossil fuels and industrial gasses as well as downstream emitters of GHG's. The rule covers many activities associated with CCS and EOR. It requires the monitoring, measurement and reporting of GHG emissions. The EPA estimate that facility level GHG emission reporting will cover 90% of emissions from electricity generation, 85% of total oil and gas industry emissions and 60% of emissions from ethanol production (Granger Morgan, 2012). Any facility that captures and exports CO_2 must report the mass of CO_2 so captured and exported. The reporting protocol also requires the development of a site specific monitoring, reporting and verification plan (MRV) that must include, Figure 5:

1. Leakage risk assessment – the identification of all potential leakage pathways;
2. Monitoring strategy – a site specific plan that may include a combination of subsurface, vadose, surface water and / or atmospheric monitoring – leakage must be quantified if CO_2 is detected at the surface;
3. Pre-injection environmental baselines – site specific establishment of pre-injection CO_2 levels;
4. Site specific mass balance equations to calculate the net amount of CO_2 sequestered.

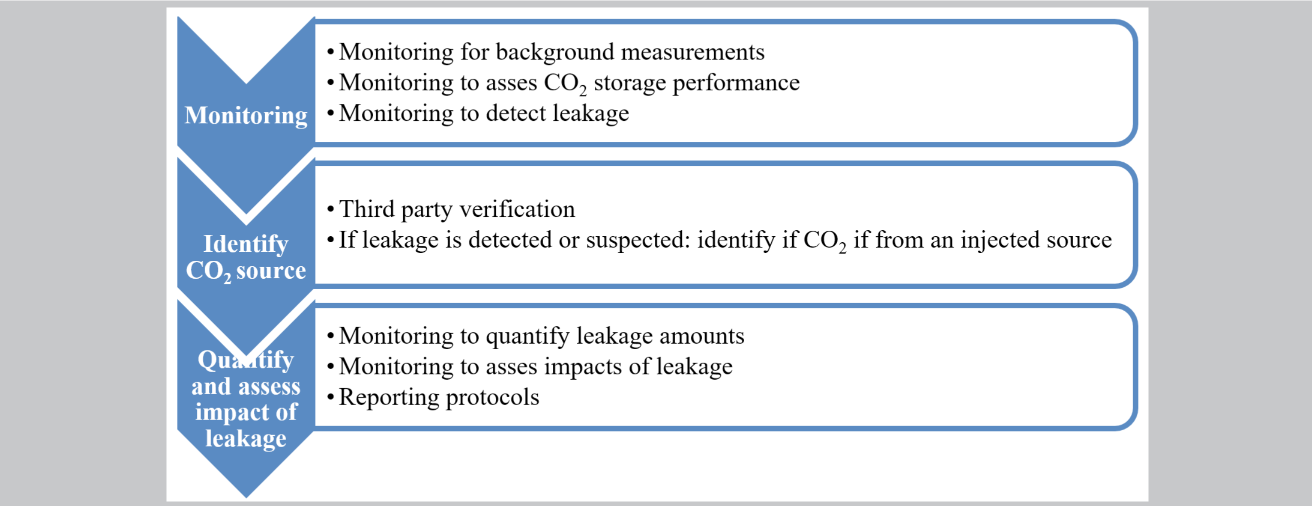

Figure 5 Shallow surface monitoring and reporting (Figueiredo el al. 2012).

2.3 CO_2 leakage monitoring

The crucial factor for monitoring and reporting protocols is that: the leakage of CO_2 must be distinguished from variable natural background CO_2 levels.

Benson (2004) stated that a site with a storage rate of ~4 MT /year, with a homogenous (i.e. diffusive) leakage of 0.1 % per year of the stored CO_2 within an area of 10 km × 10 km, would produce a CO_2 flux two to three orders of magnitude less than that of a typical ecosystem, and four to five orders less than fluxes found in some geothermal areas. However, if the same flux is localised in a restricted area, (small surface site, well bore, fault etc.) the CO_2 flux will locally far exceed the background level and will be easy to detect through monitoring to produce an early warning.

There are a number of considerations that must be taken into account when undertaking the monitoring of potential leakage, including:

1. variation in background levels;
2. the risk of false positives;
3. the need for wide spatial coverage – hence low resolution;
4. the need for high sensitivity and low uncertainty;
5. the definition of the area to be monitored;
6. the uncertainty in measurements may exceed accuracy requirements;
7. cost.

In particular, it is crucial to quantify the background CO_2 fluxes and concentrations which are dependent on CO_2 production in the soil; the movement of CO_2 from sub-soil sources into the soil; and the exchange of CO_2 with the atmosphere as controlled by concentration (diffusion) and pressure (advection) gradients.

Biologically produced CO_2 in soils (i.e., soil respiration) is derived from root respiration and the decay of organic matter. While many factors may influence soil respiration rates, changes in atmospheric and soil temperature and soil moisture have been shown to strongly affect these rates and related concentrations and fluxes (Lewicki and Oldenburg, 2004). CO_2 that enters soil from sub-soil sources can be derived from groundwater degassing of CO_2 derived from respiration, atmospheric, and carbonate mineral sources. Also, production of CO_2 at sub-soil depths can occur by oxidative decay of relatively young or ancient (e.g., peat, lignite, kerogen) organic matter in the vadose zone (Lewicki and Oldenburg, 2004). Exchange of soil CO_2 from subsurface sources with the atmosphere can occur by diffusion and/or advection, (Baldocchi et al 2001). Diffusive flux depends on the gas production rate and soil temperature, moisture and properties such as porosity, with each of these factors varying in both space and time. Advective flow can be driven by fluctuations in atmospheric pressure, wind, temperature, and rainfall (Lewicki and Oldenburg, 2004).

There are a variety of methods available to detect and monitor shallow surface CO_2 leakage including (for sources see below):

1. Surface gas laser monitoring;
2. Remote sensing;
3. Ecosystem monitoring;
4. Soil gas flux;
5. Gas concentration / geochemistry / isotopes;
6. Soil geochemistry;
7. Fluid chemistry of shallow groundwater.

Surface gas laser monitoring
Surface gas monitoring was carried out at the In Salah Gas project in 2009 using a Boreal Laser open path laser CO_2 detector, linked to a gasFinder FC analyser and mounted at a height of 38 cm above ground on a Toyota Landcruiser (Jones et al., 2011). The detector used a wavelength of 2 μm and had a sensitivity of around 5-10 ppm for CO_2.

Remote Sensing
Direct detection of CO_2 can be undertaken using high resolution hyperspectral imagery to detect and map the effects of elevated CO_2 soil concentrations on the roots of plants. It can also detect hidden faults which may localize CO_2 leakage. Elevated CO_2 levels deprive the plant root system of oxygen, which will degrade plant health and species distribution (Pickles and Cover, 2005).

Ecosystem monitoring
Ecosystem monitoring is based upon a detailed analysis of the non-mobile organisms, i.e. plants, meiofauna and the microbial populations inhabiting the soil at a suspected leak. These are then compared with control sites representing the background ecosystem to be expected without disturbances.

Soil gas flux monitoring
Recent advances in cone penetrometer and sensor technology have enabled contaminated sites to be rapidly characterised using vehicle-mounted direct push probes. Probes are available for directly measuring contaminant concentrations in-situ, in addition to measuring standard stratigraphic data, to provide flexible, real-time analysis. The probes can also be reconfigured to expedite the collection of soil, groundwater, and soil gas samples for subsequent laboratory analysis (Sara, 2003).

A range of technologies exists to measure CO_2 concentrations and fluxes in the shallow subsurface and the atmospheric surface layer (Lewicki and Oldenburg 2004; IEA GHG, 2012). These technologies include:

1. The infrared gas analyser (IRGA) for measurement of point CO_2 concentrations;
2. The accumulation chamber (AC) technique to measure point soil CO_2 fluxes;
3. The eddy covariance (EC) method to measure net CO_2 flux over a given area;
4. Light distancing and ranging (LIDAR) to measure CO_2 concentrations over an integrated path.

Gas concentrations / geochemistry / isotopes
A combination of concentrations and isotopic ratios of gases is frequently combined with soil gas flux measurements. Soil gas samples are most typically collected using small, lightweight soil probes. The method involves driving a hollow steel tube into the ground, typically to a depth of 0.5 - 1.0 m, and drawing soil air to the surface for analysis. Analysis can be conducted in the field using portable equipment or the samples stored in pre-evacuated airtight containers for laboratory analysis. In addition to CO_2, other gas species can be targeted: due to their association with the reservoir (e.g. CH_4 or H_2S in CO_2-EOR projects); man-made tracers that are added to the injected stream (e.g. fluorocarbons); or natural tracer gases (e.g. helium or radon). Isotopic analyses can also be conducted such as carbon in CO_2 ($^{\delta 13}C$ to determine origin and ^{14}C to determine age).

Soil geochemistry
Mineralogical studies of the clay-rich soils of the natural CO_2 leakage site at Latera, Italy, have indicated variations in soil geochemistry associated with increased acidity and anoxic conditions (Beaubien et al., 2008; Pettinelli et al., 2008). In particular, the results showed an increase in the concentration of K-feldspar with an associated decrease in albite, and a decline in the occurrence of oxides such as MgO, CaO, Fe_2O_3 and Mn_3O_4 in the region of the gas vent compared with the surrounding soils. However, soil geochemistry analyses related to mineralogy may be unsuitable for CO_2 leakage monitoring due to the slow reaction rates involved.

Fluid chemistry of shallow groundwater
CO_2 is a natural constituent of groundwater. Depending on the pH and chemical composition of the groundwater, CO_2 will form various chemical species. The concentrations of these species can be measured with established hydrochemical methods reasonably accurately. The quantification of leakage requires the integration of groundwater volumes and fluxes multiplied by the concentrations of carbon species that originate from the CO_2 ascending from the storage reservoir (IEA GHG 2007).

2.4 CO_2 leakage characterisation

Quantification of CO_2 leakage

Four steps are necessary to quantify leakage (IEAGHG, 2012):

1. Detection of leakage through implementation of an appropriate monitoring strategy;
2. Sampling of phases and analysing concentrations of carbon species – i.e. whether the CO_2 represents leakage from storage or a natural background flux;
3. Volume or flux measurements – although, it may be difficult to measure all the leakage mechanisms, such as free phase gas or dissolved gas;
4. Calculation of leakage mass or flux – however, along with measurement accuracy, flux calculations are further complicated by the natural variability in background values.

Measurement uncertainties

Given the specific requirement in the EU for defining the level of uncertainty in quantification of leakage, it is important to consider the current knowledge of the uncertainties associated with measurement instrumentation and techniques. The level of uncertainty will decrease with further refinement through increased application; however, the natural system will always impose some level of uncertainty. For example, in surface water chemistry techniques, Mau et al. (2006) estimated 10 to 20% of their uncertainty was due to variations in the local background with over 50% due to variations in flow velocity. From reported research there is evidence to suggest some technologies in their current level of development may have uncertainty ranges exceeding the required range of ±7.5%, i.e. Trotta et al. (2010) estimated the largest uncertainties can range from 10 to 40% for different set-ups of eddy-covariance-based estimates of net ecosystem exchange; and uncertainty of CO_2 flux increases with increasing absolute magnitude of the flux (Hollinger & Richardson, 2005).

Attribution of CO_2 source

Techniques to attribute the origin of potential leakage of CO_2 include:

1. Stable carbon isotopic ratio – not always definitive;
2. Noble gas abundance and isotopic ratios;
3. Tracer gas signature – may give false positives;
4. Process based soil gas – using simple gas ratios (CO_2, CH_4, N_2 and O_2).

2.5 Monitoring costs

IEA GHG (2007, p.140) give a table of costs associated with monitoring and leak detection for 3 scenarios:

- A CO_2-EOR scheme with additional CO_2 storage;
- A saline aquifer with high residual gas saturation as the CO_2 plume is fairly static after injection;
- A saline aquifer with low residual gas saturation as the CO_2 plume is mobile after injection.

In both cases a 'basic' and 'enhanced' cost was calculated, which ranged from c. 1 – 40 M USD (2007 prices). Additional costs were estimated for well integrity logging, of 12 – 18 M USD for 10 CO_2 injection wells over 50 years.

3 CLASSIFICATION OF SITES REQUIRING MITIGATION

Mitigation planning involves an iterative process where the site characterisation / baseline data and the ongoing monitoring of the site feed into the risk assessment, which in turn informs the remediation action which then required further monitoring and risk analysis (Oldenburg, 2008; Figure 6).

3.1 Site Characterisation – Baseline data

Baseline data of the storage site should be acquired during the initial appraisal phase of a project. Relevant data should be collected in an efficient and cost-effective manner. This provides a baseline from which monitoring can identify any changes in the shallow subsurface.

The best case remediation plans are implemented at initial site characterisation (IEA GHG, 2007), where:

1. favourable storage sites with low risks of CO_2 leakage are selected during site characterisation;
2. emphasis is placed on well integrity, both active and abandoned;
3. comprehensive monitoring systems for the CO_2 storage site are installed and maintained;
4. a phased series of reservoir simulation-based modelling is undertaken to track and predict the location of the CO_2 plume;
5. a "Ready-to-Use" contingency plan/strategy for remediation is established.

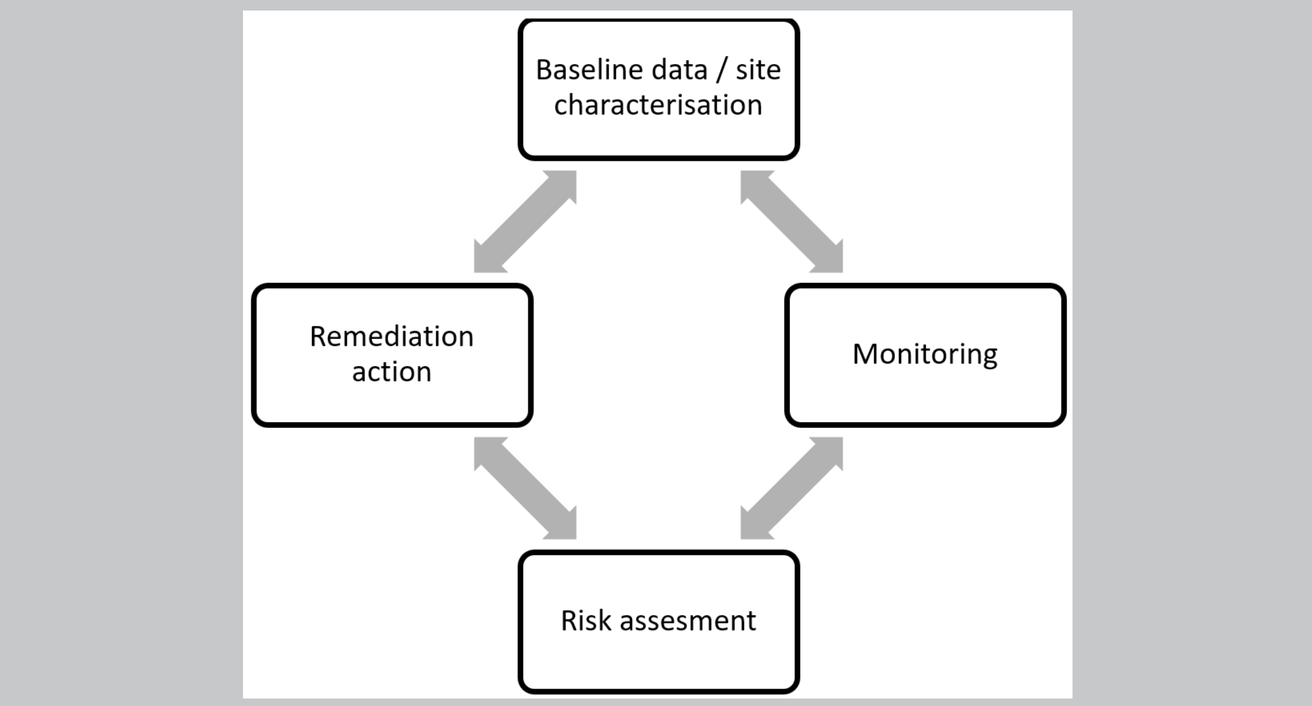

Figure 6 Classification of sites requiring remediation (Oldenburg, 2008).

Recent advances in cone penetrometer and sensor technology have enabled contaminated sites to be rapidly characterised using vehicle-mounted direct push probes. Probes are available for directly measuring contaminant concentrations in-situ, in addition to measuring standard stratigraphic data, to provide flexible, real-time analysis. The probes can also be reconfigured to expedite the collection of soil, groundwater, and soil gas samples for subsequent laboratory analysis (Sara, 2003)

Non-invasive geophysical techniques such as ground-penetrating radar; cross-well radar; electrical resistance tomography; vertical induction profiling; and high resolution seismic reflection produce computer-generated images of subsurface geological conditions and are qualitative at best. Other approaches, such as chemical tracers, are used to identify and quantify contaminated zones, based on their affinity for a particular contaminant and the measured change in tracer concentration between wells employing a combination of conservative and partitioning tracers (Darnault, 2008).

3.2 Risk Assessment

Once site contamination has been confirmed by a programme of thorough site characterisation and monitoring, a risk assessment is performed. A risk assessment is a systematic evaluation used to determine the potential risk posed by the detected contamination to human health and the environment under present and possible future conditions (Darnault, 2008). If the risk assessment reveals that an unacceptable risk exists due to the contamination, a remediation strategy must be developed to assess the problem. If corrective action is deemed necessary, the risk assessment will assist in the development of remedial strategies necessary to reduce the potential risks posed by CO_2 contamination of the shallow subsurface (Sara, 2003).

The USEPA and the American Society for Testing and Materials (ASTM) have developed comprehensive risk assessment procedures. The USEPA procedure was originally developed by the United States Academy of Sciences in 1983. It was adopted with modifications by the USEPA for use in Superfund feasibility studies and RCRA corrective measure studies (USEPA, 1989). This procedure provides a general, comprehensive approach for performing risk assessments at contaminated sites. It consists of four steps:

1. hazard identification;
2. exposure assessment;
3. toxicity assessment;
4. risk characterisation.

The ASTM Standard E 1739-95, known as the Guide for Risk-Based Corrective Action (RBCA), is a tiered assessment originally developed to help assess sites that contained leaking underground storage tanks containing petroleum (ASTM, 2002).

A flow chart of severity / risk is based on:

1. depth (minimum);
2. onshore / offshore setting;

3. well description, completion, age, cement character;
4. matrix (soil vadose, soil phreatic, alluvium, 'solid' rock);
5. leakage rate;
6. quantity already leaked;
7. existing impacts including human impact;
8. land use (urban, agriculture, undeveloped);
9. geometry of the leak (diffuse, focussed, along a well);
10. hydrology (regional water flow rate / direction).

3.3 Remediation action

When the results of the risk assessment reveal that a site does not pose risks to human health or the environment, then no remedial action is required, but often further monitoring of a site may be required to validate the results of the risk assessment. Corrective action is required when risks posed are deemed unacceptable in the risk assessment. When action is required, a remediation plan must be developed to ensure that the intended remedial method complies with all technological, economic, and regulatory considerations.

The costs and benefits of various remedial alternatives are often weighed by comparing the flexibility, compatibility, speed, and cost of each method (Reddy, 1999). A remedial method must be flexible in its application to ensure that it is adaptable to site-specific soil and groundwater characteristics. The selected method must be able to address site contamination while offering compatibility with the geology and hydrogeology of the site.

The remediation objectives are to:

1. Bring contaminant levels to below environmental standard limits ;
2. Reduce mobile separate phase CO_2 to limit growth of the leakage plume;
3. Remove CO_2 from the aquifer in both gas and liquid phase;
4. Reduce the aqueous phase concentration of CO_2 – minimising decrease in pH.

The efficacy of the remediation technique will depend on (Hamby, 1996):

1. The size of the aquifer;
2. The size, shape and distribution of the CO_2 plume;
3. The leakage rate (possibly by multiple flow processes);
4. Whether there is two zone saturation gradient within the leak, i.e. a cone shaped plume with high gas saturation at top and a gravity tongue at bottom;
5. The total leakage amount;
6. Well orientation, horizontal or vertical;
7. Well depth in relation to aquifer;
8. Well spacing.

Generally, remediation methods are divided into two categories: in-situ remediation methods and ex-situ remediation methods. In-situ methods treat contaminated groundwater in-place, eliminating the need to extract groundwater. In-situ methods are advantageous because they often provide economic treatment, little site disruption, and increased safety due to lessened risk of accidental contamination exposure to both on-site workers and the general public within the vicinity of the remedial project (Darnault, 2008). Successful implementation of in-situ methods, however, requires a thorough understanding of subsurface conditions. Ex-situ methods are used to treat extracted groundwater. Surface treatment may be performed either on-site or off-site, depending on site-specific conditions. Ex-situ treatment methods are attractive because consideration does not need to be given to subsurface conditions. Ex-situ treatment also offers easier control and monitoring during remedial activity implementation (Reddy, 1999).

4 REMEDIATION AIMS AND IMPLEMENTATION

4.1 The aims and objectives of remediation

The aims and objectives of remediation of leaked CO_2 will vary from site to site, according to the likely impacts and consequences. Generally, the aims will include:

1. To stop the source of the leakage – in the context of the near surface, the leak is almost certainly sourced from a much a deeper storage reservoir, and mitigation at depth is probably more appropriate;
2. To reduce the mobile free phase CO_2, to limit the continued growth of the leakage plume, i.e. to prevent the spread of the contamination (Esposito and Benson, 2012);
3. To delay the spread of a plume or dissolved CO_2, either while plans are drawn up for permanent remediation, or while legal action takes place to determine who is going to pay for remediation;

4. To remove CO_2 from the aquifer in both gas and aqueous phase, both to recover the CO_2 for disposal and to restore the aquifer back to pre-contamination conditions (Esposito and Benson, 2012);
5. To minimise the decrease in pH from the formation of carbonic acid. Minimising the drop in pH may indirectly decrease the amount of secondary contamination from the CO_2 leakage caused by the mobilisation of heavy metal ions (e.g. Esposito and Benson, 2012; Keating et al., 2014);
6. To directly reduce the concentration of mobilised toxic metals to either background levels, or to levels acceptable to relevant legislation.
7. To reduce the concentration of hydrocarbons that may be mixed with, or dissolved in, the leaking CO_2, especially if the primary storage reservoir is a depleted gas or field, or a depleted oil field with a high proportion of light oil that can volatilise into the free CO_2 phase;
8. Prevent the CO_2 from reaching the surface, to avoid payment of fines or the return of credits for the avoidance of CO_2 emissions;
9. Prevent the CO_2 from reaching habitations or other sensitive locations ('receptor' in pollution control terminology).

4.2 Published remediation or leakage plans

For CO_2 storage schemes, a small number of emergency plans have been published worldwide, that describe the actions to be taken in the event of an unplanned release or irregularity in the movement of the CO_2.

4.2.1 Decatur CO_2 injection project emergency plan

For the Decatur CO_2 injection project, Illinois, USA, the Emergency and Remedial Response Plan (ERRP) describes actions that the owner / operator (Archer Daniels Midland; ADM) shall take to address movement of the injection fluid or formation fluid in a manner that may endanger an underground source of drinking water (USDW) during the construction, operation, or post-injection periods. The ERRP includes the effects of both the direct movement of the injected CO_2, and also the associated pressure front. The plan summary has the following actions (Decatur, unknown date):

1. Initiate shutdown plan for the injection well, i.e. cease the injection of CO_2;
2. Take all steps reasonably necessary to identify and characterise any release;
3. Notify the permitting agency (UIC Program Director) of the emergency event within 24 hours;
4. Implement applicable portions of the approved ERRP.

In the event of evidence of contamination of groundwater by the CO_2, directly or indirectly, then the following remediation is planned (Decatur, unknown date):

1. Arrange for an alternate potable water supply, if the USDW was being utilised and has been caused to exceed drinking water standards;
2. Proceed with efforts to remediate USDW to mitigate any unsafe conditions (e.g., install system to intercept/extract brine or CO_2 or "pump and treat" to aerate CO_2-laden water);
3. Continue groundwater remediation and monitoring on a frequent basis (frequency to be determined by ADM and the UIC Program Director) until unacceptable adverse USDW impact has been fully addressed.

4.2.2 FEED study for Shell Goldeneye (UK) project

The Shell Goldeneye project, a component part of the Scottish Power CCS Consortium, involves the storage of CO_2 in the Goldeneye field, a soon-to-be depleted gas field approximately 100 km offshore in the UK North Sea. Although the original project was abandoned in October 2011, the product of a Government-funded FEED (Front-end engineering design) study is published in the UK National Archives (http://webarchive.nationalarchives.gov.uk/). The Goldeneye field is the storage site for the Peterhead CCS Project which in March 2013 was chosen as one of two CCS demonstration projects to progress to the next stage of the UK Government's CCS Commercialisation Competition funding.

The 'Corrective Measures Plan' is described in Scottish Power CCS Consortium (2011). Section 7.5 covers the scenario that 'CO_2 Flows Up To Near Seabed / At Seabed', which is considered to be 'not possible' without the CO_2 following a problematic well, so that remediation interventions would be focussed on that well (p. 38). Moreover, the flow of CO_2 to the seabed would inevitably involve the flow through, or the bypassing of, the primary seal. Hence, the mitigation measures considered for this scenario would be deployed. However, 'No remedial actions can remove CO_2 that has already migrated above the primary seal and therefore following consultations with the regulator, an additional storage license will be sought.' (p. 28). The principal remediation method considered for failure of the primary seal (away from a borehole) appears to be the reduction in pressure close to the leak by changing the pattern of CO_2 injection, in the expectation that the seal has failed by stress fracturing or the opening of existing fractures by excessive fluid pressure within the reservoir. The possibility of drilling a relief well is discussed, though whether this is to reduce pressures close to the primary seal; to inject sealants; or for some other purpose is not specified. The problems of locating a leak with sufficient precision to make remediation a realistic possibility, and the questionable likelihood of successful remediation are highlighted.

Under certain circumstances (e.g. migration through the primary seal via a diffuse fracture network), it was considered that may have been be easier to fix a leak path where this passes through the secondary seal. Again, this was considered to be most likely along a borehole. In the event that migration occurred through both the primary and secondary seals, and none of this migration path was related to boreholes, then it was considered that remedial interventions were unlikely to be successful. It was suggested that, in consultation with the regulator, the decision to intervene or not would be considered taking into account the likely effectiveness of intervention alternatives (relief wells).

In the event of leakage from an abandoned well, then re-entry directly from the surface is impossible (p.65) as the wells are severed below the surface of the seabed sediment. Therefore, a relief well must be drilled, with the advantage that casing can be set and cemented prior to entry into the leaking well. This re-entry has to be performed at a depth such that there is sufficient integrity (strength) in the formation (i.e. the formation will not fracture as the leaking well is entered) to withstand the pressure within the affected borehole, as the casing is milled away to gain entry (p.65). It is noted that milling through casing is not without its hazards; it is entirely possible to mill into the well, and back out the other side, leaving the well casing badly damaged.

It is considered very difficult or near impossible to enter an uncased section of a borehole, as it is conventional to use the magnetic or / conductive nature of casing to locate the borehole – this is not a problem at shallow depths where casing will be present. If there is magnetic material in the uncased section (e.g. a jammed drill string or production tubing) then it is possible to locate that instead. Past attempts at re-entry via a relief well show that 10+ attempts may be needed to locate the well, using successive sidetracks. The detection technique used to locate the leaking well, magnetic ranging, works at c. 60m distance. The time estimated for drilling a relief well into a cased hole target is around 55 days. Sourcing and mobilising a rig would be additional to this.

In the event of a CO_2 blow-out (p.74), the suggested remediation consists of:

1. injecting kill fluid (hazards are toxic gases and low temperatures) – this may not be possible;
2. drilling a relief well, sufficiently deviated to place the drill rig a safe distance from the affected platform (i.e. several km).

In the event of a blow out that is not at a well – the only suggested mitigation technique is to expect that the leakage path self-seals (!) as the pressure drops and the fractures close.

4.2.3 FEED study for EON Kingsnorth (UK) project:

The FEED study for the EON Kingsnorth project appears not to include a plan for the remediation of any CO_2 leakage. In EON (2010) there are numerous references to FEED2, which was presumably a planned follow-on to the published FEED study. However, this is not available. Regarding the effect of "Generation of potential migration/leak paths along well bores", 'Further Action' is described as "Further review and remedial actions to be addressed in the final design and procedures in FEED2" (EON, 2010, section 2.3, p. 6).

4.2.4 Rotterdam Capture and Storage Demonstration Project (ROAD), Netherlands

The ROAD project aims to capture 1.1 Mt of CO_2 per year from the Rotterdam area, and store it in a depleted offshore gas field. The corrective measures plan is available (http://www.rvo.nl/sites/default/files/sn_bijlagen/bep/70-Opslagprojecten/ROAD-project/Fase1/4_Aanvragen/A-06-2-Aanvulling-opslagvergunning-kl-354540.pdf; from p.437) in the Dutch language but is summarised by Steeghs et al. (2014). The plan is based on three principles:

- Corrective measures are site and risk specific, and linked to the risk management plan;
- The implementation of corrective measures is triggered by pre-defined monitoring outcomes;
- Corrective measures will take place in the event of a leak which is considered a significant irregularity.

The plan is structured as: the contingency scenario; consequences; and the corresponding corrective measures. A traffic light system is used to describe the conformance of the site, with 'red' triggering the implementation of the corrective measures. The part of the corrective measures plan which is most relevant to the shallow leakage described in this report is the scenario of CO_2 leakage from the reservoir into the biosphere. The suggested measures are: additional monitoring, and the cessation of injection, either temporarily or permanently. Communication, for example with the competent authority, and information sharing are also considered to be important, regardless of the nature of the irregularity or leakage. Back production of injected CO_2, followed by alternative storage or controlled release into the atmosphere would take place after the cessation of injection, with the aim of returning the storage complex back into a stable state.

4.2.5 Sleipner, North Sea, monitoring and remediation plans

Sleipner is an off shore storage site and as such a series of 3D seismic surveys have been carried out over the storage area to monitor the evolution of the site in relation to the baseline survey taken before injection started and to feed into the reservoir modelling. As such, the monitoring data generated are also used in long term simulations (IEA 2005). No published remediation plan have been located found by the present study.

4.2.6 In-Salah, Algeria, monitoring and remediation plans

A 5-6 year $30 million "In Salah Gas CO_2 storage Assurance Joint Industry Project" has been proposed and taken place in the Algerian Sahara. For both commercial and technical reasons, the CO_2 gas is separated from the natural gas in the same manner as on Sleipner. In Salah is the first geological CO_2 storage site in the deep saline formation of an active gas reservoir. Since the start-up in 2004, more than three million tonnes of CO_2 have been stored below ground. Near surface environmental monitoring was designed to monitor the CO_2 levels in the soils, at ground surface and in the atmosphere just above ground surface. Extensive field investigations, carried out in 2009–2010, consisted of near-ground atmospheric CO_2 measurements with a mobile open-path laser system; soil gas pressure and flux measurements; botanical and microbiological surveys; initiation of longer-term subsurface monitoring of radon and other gases (Jones et al., 2011). Independent of these studies, due to preliminary conclusions regarding the reservoir properties (mainly related to capacity), the injection of CO_2 was reduced in mid-2010 and stopped in June of 2011 as a safety measure (http://www.statoil.com/en/ TechnologyInnovation/NewEnergy/CO_2CaptureStorage/Pages/InSalah.aspx, updated 17 Dec 2013). No published remediation plan has been located in the present study.

4.2.7 Weyburn, Canada monitoring and remediation plans

Soil gas studies were undertaken to establish background concentrations of CO_2 and other gasses. Three periods of sampling occurred over a 360 point grid, there is also continued comparison with a control site 10km away. An alleged surface leakage at the Weyburn project was reported by Petro-Find Geochem, a company commissioned by local landowners to investigate surface emissions at their property, who undertook geochemical soil gas surveys and concluded that the anomalous levels of CO_2 were the result of leakage of CO_2 injected at Weyburn (LaFleur, 2010). This conclusion sparked contrasting perceptions between the experts and public (and the media) regarding the risks of CO_2 storage (Boyd et al., 2013). Subsequently, three separate studies for the Weyburn-Midale project, the International Performance Assessment Centre for Geological Storage of CO_2 (IPAC-CO_2) and Cenovus Energy, who operated the Weyburn project, independently monitored, investigated, and reassured that it was a false positive detection (Sherk et al., 2011; Trium and Chemistry Matters, 2011; Beaubien et al., 2013; Romanak et al, 2014). No published remediation plan has been located in the present study.

4.2.8 Rangely, Colorado, US, monitoring and remediation plans

CO_2 has been stored as a by-product of EOR, and soil gas and soil atmosphere flux measurements have been made at the site along with a hyperspectral survey. Seasonal variations in the desert location means there are strong fluctuations in natural CO_2 flux, and leakage CO_2 is easier to detect in the winter (IEA, 2005). No published remediation plan has been located in the present study.

5 REMEDIATION TECHNOLOGIES

5.1 Previous reviews of remediation technologies and methodologies

The most recent review of the remediation of the leakage of CO_2 from a CO_2 storage site is that of Manceau et al. (2014). It is broad in scope, but includes the remediation of near surface leakage as part of a wider review. Other relevant reviews include:

- Zhang et al. (2004) – vadose zone remediation;
- Benson and Hepple (2005): early detection of CO_2 leakage and remediation;
- IPCC (2005);
- Oldenburg and Unger (2005) present a model of CO_2 leakage specifically designed for the near-surface;
- IEA GHG (2007), very comprehensive review;
- Kirk (2011), a very useful review of natural CO_2 emissions sites, as a part of the UK QICS project;
- Rütters et al. (2013), from CGS Europe, State of the art monitoring methods to evaluate CO_2 storage site performance.

Outside the fledgling CCS literature, there is little or nothing published concerning the remediation of CO_2 leakage. The journal 'Remediation' which, as the title suggests, is dedicated to environmental clean-up technologies, techniques and costs, appears to have no papers specifically concerning the remediation of leaks of CO_2. No textbook appears to consider the problem. Given that textbooks are generally considered to be some 10 years behind journals this is unsurprising.

5.2 Classification of remediation techniques

There are a number of different remediation technologies suitable for the near surface remediation of CO_2 leakage, which can be classified by:

1. Objective of the technology (containment or treatment);
2. Process involved in the remediation (physical, chemical, biological or thermal);
3. Location of the remediation process (in situ or ex-situ).

<u>Containment versus treatment</u>

Containment prevents the spread of the CO_2 without necessarily removing or degrading the contamination. Treatment transforms the CO_2 into less toxic, or non-toxic concentrations. Containment is typically cheaper, can be used until a more efficient clean up technology becomes available, can provide a means of evaluating the potential for natural attenuation processes to degrade the

CO_2 and can present a lower overall risk as CO_2 exposure can be minimised (Oldenburg; 2008). Many remediation technologies will involve both containment and treatment.

In-situ or ex-situ remediation

Here it is important to highlight the distinction between the application of the remediation technology versus the location of the remediation treatment, for example in pump and treat the pumping is in-situ but the treatment of the CO_2 contamination is ex-situ (Sara, 2003).

Table 4 Summary of the shallow surface CO2 remediation technologies available.

Remediation	Remediation Technique	Containment or treatment	in-situ or ex-situ	Active or passive
Fluid control measures	Pump and treat	Treatment	In-situ technology, ex-situ treatment	Active
	Pump and treat with cap	Containment and treatment	In-situ technology, ex-situ treatment	Active
	Water injection	Treatment	In-situ technology, ex-situ treatment	Active
	Hydrodynamic isolation	Treatment	In-situ	Active
	Air stripping	Treatment		Active
	Hydraulic barrier	Containment and treatment	In-situ	Active
Cut off wall (unconfined aquifer)	Cut-off wall / slurry wall	Containment	In-situ	Passive
	Two-phase diaphragm wall	Containment	In-situ	Passive
	Composite diaphragm wall	Containment	In-situ	Passive
	Interlocking bored-pile diaphragm wall	Containment	In-situ	Passive
	Installation of thin wall and sheet pile into the soil	Containment	In-situ	Passive
	Injection permeation grouting	Containment	In-situ	Passive
	Jet grouting	Containment	In-situ	Passive
	Frozen wall	Containment	In-situ	Passive
	Bio barrier	Containment	In-situ	Passive
	Water control agent	Containment	In-situ	Passive
	High strength rigid set material	Containment	In-situ	Passive
	Organic polymer sealant	Containment	In-situ	Passive
	Super absorbent crystals	Containment	In-situ	Passive
	Granular activated carbon	Treatment	In-situ technology, ex-situ treatment	Active
Cut off wall - Fractured aquifer	Grout curtain	Containment	In-situ	Passive
Permeable reactive barriers (treatment walls)	Sorption barriers	Treatment	In-situ	Passive
	Ionic species removal	Treatment	In-situ	Passive
	Microbes	Treatment	In-situ	Passive
	Carbonation stabilisation	Treatment	In-situ	Passive
	De-acidisation	Treatment	In-situ	Passive
Soil Zone remediation	Soil vapour extraction	Treatment	In-situ technology, ex-situ treatment	Active
	Air sparging	Treatment	In-situ technology, ex-situ treatment	Active
	Bioslurping	Treatment	In-situ technology, ex-situ treatment	Active
	De-acidise soil	Treatment	In-situ	Passive
	Thermal treatment	In-situ technology, ex-situ treatment	In-situ technology, ex-situ treatment	Active
	Capping	Containment	In-situ	Passive
	Gas collection trench	Treatment	In-situ	Passive
	Ecosystem restoration	Treatment	In-situ	Active
Bioremediation	Bioremediation of low pH groundwaters	Treatment	In-situ	Passive
	Bioremediation of CO_2	Treatment	In-situ	Passive
	Bioremediation of toxic metals	Treatment	In-situ	Passive
	Bioremediation of hydrocarbons	Treatment	In-situ	Passive
	Natural attenuation	Containment	In-situ	Passive
Buildings	Passive vapour intrusion mitigation	Treatment	In-situ	Passive
	Passive / active sub slab venting	Treatment	In-situ	Passive
	Active vapour intrusion mitigation – subsurface pressurisation	Treatment	In-situ	Active
	Block wall depressurisation	Treatment	In-situ	Passive
	Active ventilation	Treatment	In-situ	Active
	Passive ventilation	Treatment	In-situ	Passive
	Demolish and rebuild to suitable standards.	Treatment	In-situ	Active

Active or passive technologies

Passive containment refers to treatment systems that clean up the CO_2 contamination without the need for energy input for the treatment process to be effective. In contrast, active technologies require further enhancements or energy inputs to achieve the required level of clean up (Reddy, 1997). Active systems are generally more expensive than passive systems.

These are a number of remediation techniques available for the shallow surface clean-up of CO_2 which are now presented and a summary of their remediation technologies are given in Table 4.

5.3 Remediation techniques (1): Fluid control measures

5.3.1 Pump-and-treat

Pump and treat is probably the most common technique used in pollution control. The idea is simple – the contaminated groundwater is brought to the surface through a number of purpose-drilled boreholes, and is treated at the surface. After treatment, it may be re-injected into the aquifer, or used for other purposes. IEA GHG (2007) suggest that horizontal pinnate (leaf-vein pattern) drilling described by von Shoenfeeldt et al. (2004) could access and extract near-surface accumulations of CO_2. Esposito and Benson (2012) model both vertical and horizontal extraction wells to remove the CO_2 in both the gas and aqueous phase. They conclude that small plumes of CO_2 with no gravity tongue can be remediated effectively through a single vertical well located in the middle, with a time span of several years. Large plumes of free-phase CO_2 where a gravity tongue has formed will require horizontal wells, and in excess of 10 years for effective remediation. In this scenario, Esposito and Benson (2012) suggest that injecting water to quickly immobilize and dissolve the CO_2 may be as effective in the short term. For larger plumes, a combination of sequential and/or simultaneous injection and extraction from multiple wells is likely to be required. However, Esposito and Benson (2012) conclude overall, that even a large plume of CO_2 can be contained and remediated effectively using the methods described.

If CO_2-rich water is brought to the surface, then it must be treated to remove the CO_2 before it can be re-injected. Both Benson and Hepple (2005) and IEA GHG (2007) suggest aerating the water to remove the CO_2. Given the low solubility of CO_2 in water at atmospheric pressure, and the likely resulting low concentrations of CO_2 in the air that is used in the aeration process, it seems highly unlikely that the CO_2 removed from the water could be collected for re-injection, and certainly not within any probable budgetary constraints. It is, therefore, highly likely that the CO_2 will be vented to the atmosphere.

If toxic metals are present within the CO_2-rich water at concentrations above background levels, or above statutory levels for potable water, then these must be removed before the water can be re-injected.

Pump-and-treat can be done is conjunction with a treatment wall, or PRD (Figure 7; Fetter, 1990). The contaminated groundwater is extracted from one side of the wall, treated and injected back into the aquifer on the uncontaminated side.

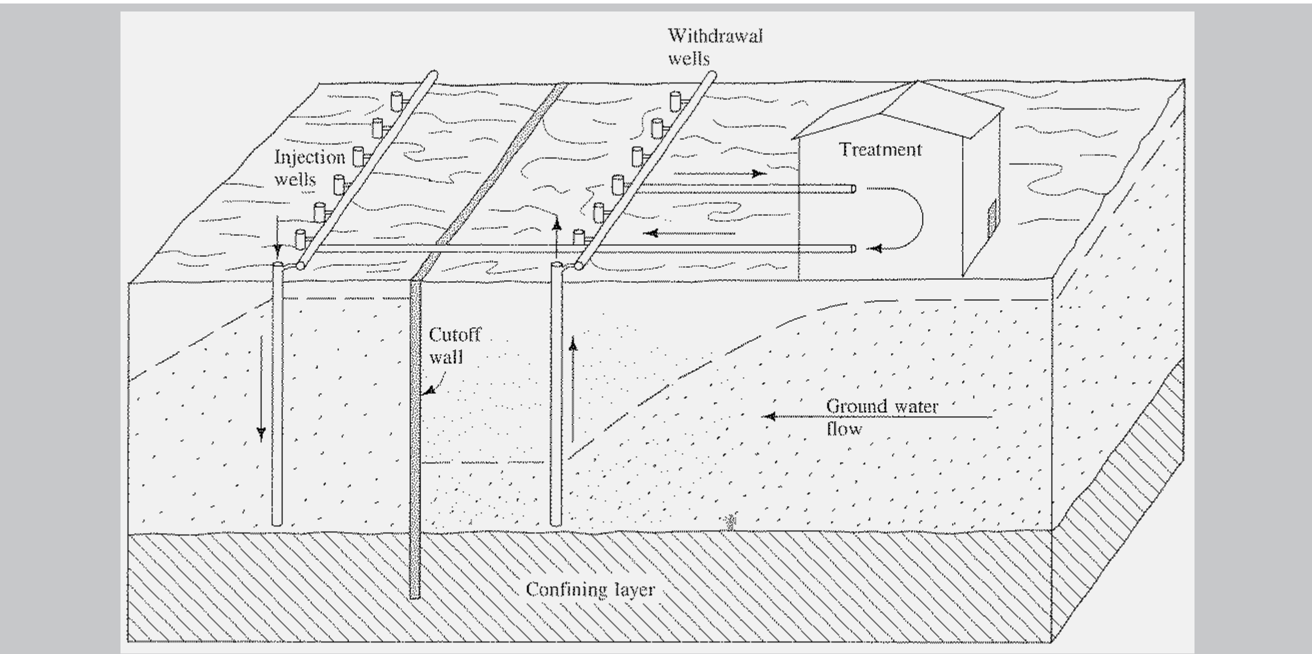

Figure 7 Pump-and-treat in association with a treatment wall (Fetter, 1999).

5.3.1.1 Pump and treat with a cap or vapour barrier

IEAGHG (2007, p.132) after Benson and Hepple (2005) suggested that the flux of CO_2 from a subsurface leak to the atmosphere could be halted, or at least slowed, by an impermeable cap or vapour barrier. The CO_2 could be pumped from below the barrier to reduce the concentration, or presumably for recovery and re-injection. Similar technology is used in land-fill sites, to prevent rain water for seeping into the landfill, and hence to prevent the contaminants from leaching from the site (CPEO, 2014). This is not especially similar to the case of a CO_2 leak, where the aim is (presumably) to prevent the CO_2 from reaching the atmosphere. The USA Resource Conservation and Recovery Act (RCRA) established standards for landfill caps. For non-hazardous waste landfills a cap consists of three layers:

1. An upper vegetative (topsoil) layer;
2. A drainage layer; and
3. A low permeability layer made of a synthetic material (geomembrane, synonym: flexible membrane liner or FML; Daniel and Koerner, 2007) covering c. 0.6 m of compacted clay.

For hazardous waste landfills the standard is more onerous (Daniel and Koerner, 2007). The performance of the caps varies, for example drying of the clay layer can lead to cracking and loss of integrity (CPEO, 2014). The caps function most effectively where most of the waste is above the water table, and only have a design life of 50 – 100 years. They require monitoring to ensure that parameters such as soil moisture are not changing, and that earthquakes or subsidence have not compromised the cap (CPEO, 2014). Caps have been built for radon gas and may provide a better analogue for CO_2 leakage than do non-radioactive waste repositories, unfortunately there seems to be very little description of such systems in the literature. Costs for barrier components are given in Daniel and Koerner (2007), but are taken from Shepherd et al. (1993) and so are substantially out of date.

5.3.1.2 Hydrodynamic isolation

This is a variant of pump-and-treat, whereby one or more boreholes are used to extract porewater from an aquifer, and the boreholes are so placed that all the porewater which flows through the contaminated zone is extracted to the surface (Fetter, 1999; Figure 7). The advantage of this approach is that the contaminant plume is stabilised, preventing the plume from reaching the uncontaminated parts of the aquifer. The contaminated water may require to be treated, after which it can be re-injected into the subsurface if desired, usually down-flow from the contaminated zone.

The technique has been developed for sparingly soluble pollutants, which remain in largely in place while a portion dissolves and is removed by groundwater flow. As such, this technique could be applicable to the remediation of CO_2 leakage. For example, if free phase CO_2 had accumulated in a shallow pericline (dome) within an aquifer (so that the CO_2 was trapped by buoyancy within

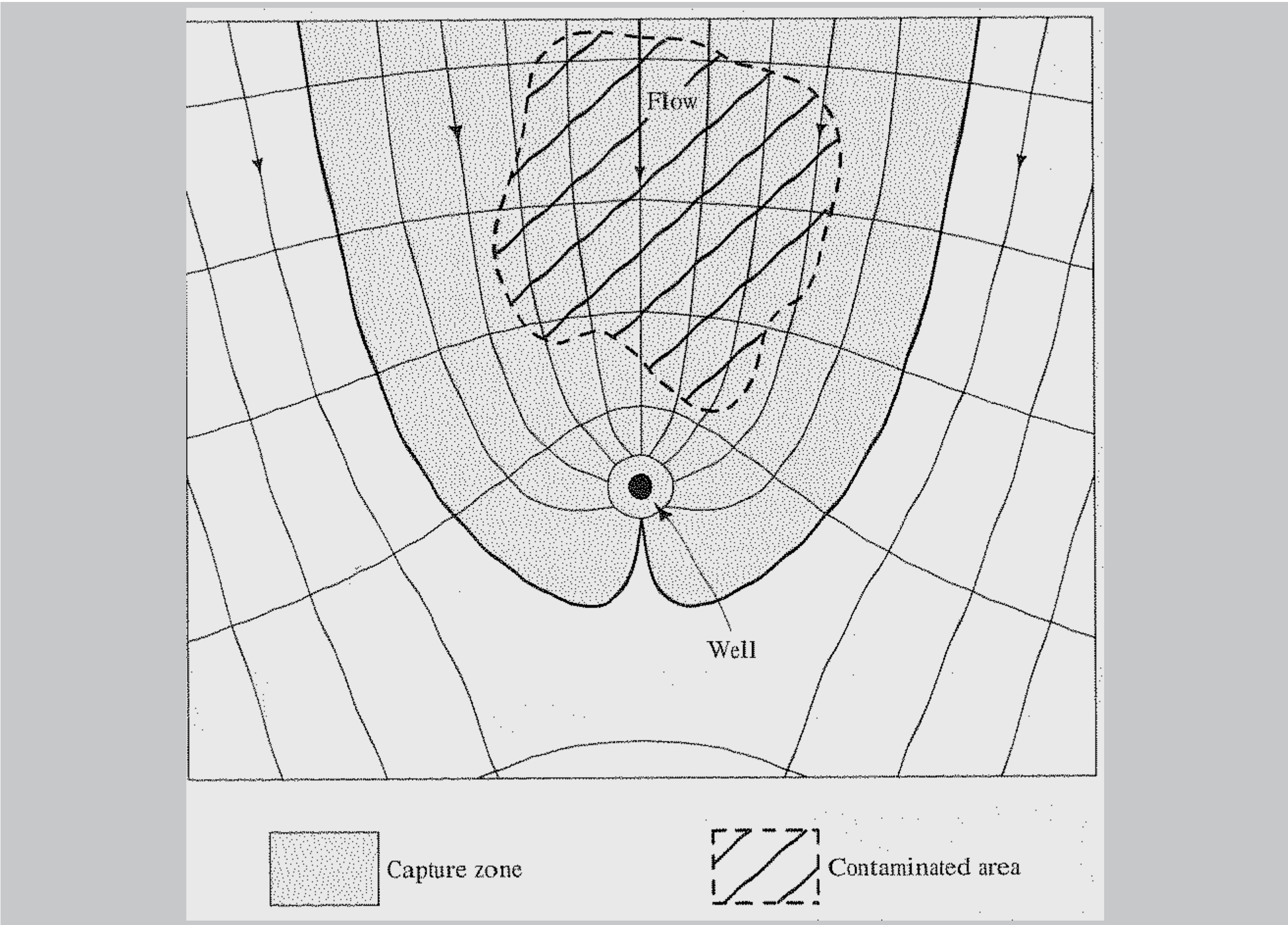

Figure 8 Hydrodynamic isolation of the contaminated portion of an aquifer, plan view. From Fetter (1999)

the dome) but the flow of ground water was taking dissolved CO_2 from the free-phase accumulation, and transporting it along the aquifer, then hydraulic isolation would prevent the spread of the dissolved CO_2. The isolation technique is especially useful if a delay is anticipated in implementing a more permanent remediation solution, either while a study is undertaken, or because legal action over the costs of remediation is anticipated to delay the implementation of any more costly techniques.

In the event that the surface treatment plant must shut down temporarily, perhaps for routine maintenance, then Fetter (1999) suggests that the pumping and re-injection of untreated water may be preferable to the cessation of pumping, as the latter option may allow the plume to spread beyond the limits of the stabilised zone. With multiple well systems, there is the possibility of shutting one well periodically for maintenance, while maintaining effective isolation.

5.3.1.3 Air stripping

A pump and treat method. The contaminated water is pumped for surface treatment, where air is pumped through CO_2 saturated water and the CO_2 is removed through evaporation. The contaminated water is sprayed into a packing material designed to increase surface area, air is blown over the water at the base of the tank, the CO_2 vapours collected by accumulation and the separated clean water collected. The process is relatively quick and cheap but will depend on CO_2 concentration or volume (Khan et al., 2004). The method does not remove the residually trapped CO_2 in the formation so this may need additional treatment.

5.3.2 Water injection

The purpose of water injection is to dissolve the gaseous CO_2 and increase capillary trapping (Esposito and Benson, 2012). The treatment differs from a pump and treat method in that it does not involve bringing either water or CO_2 to the surface. Instead the free-phase CO_2 is immobilized as residual saturation falls below the critical saturation, isolating 'bubbles' of CO_2 within the pore spaces with an relative (effective) permeability of zero.

5.3.3 Hydraulic barrier

A hydraulic (or pressure) barrier is a remediation technique that can be used for the scenario that a storage reservoir is leaking into an overlying aquifer via a previously undetected leak path, such as a fault or borehole. Water is injected into the aquifer, with the objective of raising the pore fluid pressure of the aquifer sufficiently to counter the buoyancy force that is driving the vertical migration of the CO_2.

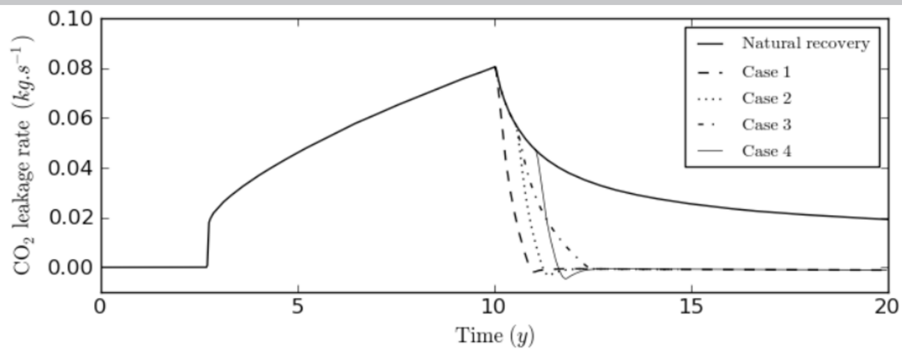

Case	Brine injection design			CO2 in the shallower aquifer after 1000 years	
	Delay (month)	Flow-rate (m3/h)	Duration (month)	in tons	Part having leaked after 10 years
Natural recovery	0	0	0	166250	96%
1	0	30	12	6640	4%
2	6	30	10	7141	11%
3	6	15	18	7359	14%
4	12	30	8	7351	14%

Figure 9 Remediation using the hydraulic barrier method after CO_2 injection stops at 10 years and at a time when 6342 tons of CO_2 were in the shallower aquifer. From Réveillère and Rohmer (2011).

Similar results are presented in Réveillère et al. (2012; Figure 9). Both papers conclude that the pressure barrier method is very successful where leakage is into an overlying aquifer, and where intervention begins fairly quickly. Highly permeable aquifers can present problems where water injection rates would have to be unrealistically high. Correctly locating the point of leakage is also important, as an injection well even 1 km from the leak point is significantly less effective, taking almost 3 years to prevent flow in the modelled case, as opposed to less than 6 months for a well within a few metres of the leak.

5.3.4 Summary of fluid control remediation measures

Table 5 presents a summary of the fluid control remediation methods. The table presents a short summary of the principals of each technique, additional information, CO_2 applicability considerations and the technical pros and cons.

Table 5 Summary of the fluid control remediation methods

Remediation technique	Principles	Information	CO_2 applicability considerations	Pros / cons
Pump and Treat	Ground water is pumped from wells to an above ground treatment system that removes the CO_2. Pump and treat can also be used to contain the contaminant plume to stop it spreading by pumping the contaminated water towards the wells.	CO_2-rich water is brought to the surface, and then it must be treated to remove the CO_2 before it can be re-injected. Toxic metals must also be removed before re-injection.	IEA GHG (2007) suggests aerating the water to remove the CO_2. Given the low solubility of CO_2 in water and the likely low concentrations of CO_2 in the air that is used in the aeration process. It is therefore highly likely that the CO_2 will be vented to the atmosphere.	Esposito and Benson (2012) conclude that small plumes of CO_2 can be remediated effectively through a single vertical well located in the middle of the contaminated zone over a time scale of a few years. Larger plumes require horizontal wells and timescales in excess of 10 years.
Pump and treat with cap or vapour barrier - Impermeable barrier	The flux of CO_2 from a subsurface leak could be halted by an impermeable cap or vapour barrier. CO_2 would be pumped from below the barrier and treated using pump and treat.	Caps are useful to prevent rain leaching from the surface. The caps work best where most of the CO_2 is above the water table and tend to have a design life of 50-100 years.	Caps have been built for Radon gas capping so indicate that they may be suitable for CO_2 applications. If caps are combined with pump and treat it should be an effective technology.	Caps require monitoring as they may be compromised by earthquakes or subsidence. Cost will depend on extent of barrier and barrier material.
Water injection to dissolve the CO_2	Residually trapped as immobile gas phase CO_2 can be removed by dissolving it in injected water and extracting it as dissolved phase for surface treatment and possible re-injection.	A pump and treat method.	Does not remove CO_2 from the aquifer, so if remediation goal is to remove CO_2 additional measures required	May be a useful short term method to reduce the concentration of CO_2; however it will not remove all the residually trapped CO_2.
Hydrodynamic isolation	This is a variant of pump-and-treat, whereby one or more boreholes are used to extract porewater from an aquifer, and the boreholes are so placed that all the porewater which flows through the contaminated zone is extracted to the surface for treatment and possible re-injection.	The CO_2 contaminated water may require to be treated, after which it can be re-injected into the subsurface if desired, usually down-flow from the contaminated zone.	If the flow of ground water was taking dissolved CO_2 from the free-phase co2 accumulation, and transporting it along the aquifer, then hydraulic isolation would prevent the spread of the dissolved CO_2.	It stabilises the CO_2 plume, preventing its spread into the uncontaminated reservoir.
Air stripping	Air is pumped through CO_2 saturated water and the CO_2 is removed through evaporation	A pump and treat method – contaminated water is sprayed into a packing material designed to increase surface are, air is blown over the water at the base of the tank, the CO_2 vapours collected by accumulation and the separated clean water collected.	Does not remove the residually trapped CO_2 in the formation so may still need additional treatment	Process is relatively quick and cheap but will depend on CO_2 concentration or volume.
Hydraulic barrier	Water is injected into the aquifer, with the objective of raising the pore fluid pressure of the aquifer sufficiently to counter the buoyancy force that is driving the vertical migration of the CO_2.	Effective when a storage reservoir is leaking into an overlying aquifer via a previously undetected leak path, such as a fault or borehole.	Réveillère et al. (2012) conclude that the pressure barrier method is effective if there is quick intervention, the aquifer is not very highly permeable and the source of leakage is accurately located.	Effective if there is quick intervention, the aquifer is not very highly permeable and the source of leakage is accurately located.

5.4 Remediation techniques (2) – Cut-off Wall in an unconfined (surface) aquifer

The aim of a cut-off wall is to isolate one portion of an aquifer from another portion, for example to isolate the contaminated portion of an aquifer from an uncontaminated portion, or to interrupt a flow path that would carry CO_2 or mobilised toxic metals towards, for example, a residential area. Experience in this field is from the landfill industry; the remediation of contaminated land; and hydraulic and foundation engineering particularly for dams (e.g. Weaver and Bruce, 2007). Imperfections in the wall can reduce effectiveness considerably: a 1 m^2 hole can allow as much water bypass as 100,000 m^2 of good quality wall (Düllmann, 1999 in Meggyes, 2005). Walls can be either single, or a chamber geometry can be adopted, where by 2 parallel walls are linked at c. 50 m intervals by cross walls. The porewaters within the chambers can be individually pumped, and monitored for leakage. The scale of cut-off walls can be large – a 3.7 km long cut-off wall chamber system was constructed to contain the landfill in Vorketzin, near Berlin, where waste from the former West Berlin had been deposited (Kellner and Scheibel, 2004, cited in Meggyes, 2005). Costs are substantial too, specimen outline economic estimates by Hiebert (1998, in Meggyes, 2005) are a cost range of US$ 6.5 - 10.7 million for a biobarrier and US$ 9.8-13.5 million for a grout curtain 3200 m long and 30 m deep. A sheet-pile wall only 12 m depth but of the same length would cost US$15-17 million (2005 prices).

Meggyes (2005) summarises the available construction methods for cut-off walls, including a summary table from Jessberger (1992, translated from German) and an example cost calculation. The techniques described in Meggyes (2005) allow the construction of cut-off walls to more than 100 m below the ground surface:

5.4.1 Excavation and replacement, the traditional method:

For a single phase diaphragm wall, individual panels 0.4 – 1.0 m thick are constructed in a trench which is typically 0.6 – 1 m wide and up to 18 m deep if dug with backhoe, or up to 36 m deep, if dug with clam-shell shovel (Need and Costello, 1984). A self-hardening slurry is pumped into the trench, e.g. bentonite-cement mix. In the 'Pilgrim's Pace' method (Meggyes, 2005), the wall in made of panels, of which alternating ones are formed in the first phase (i.e. panels 1, 3, 5 etc). When the filler has hardened after 36 – 48 hours, the intermediate panels (2, 4, 6 etc) are dug out, removing 0.3 – 0.6 m of the ends of the primary panels leaving clean surfaces. As the primary panels are not yet hardened, infilling the gaps results in a seamless wall.

5.4.2 Two-phase diaphragm wall (> 50 m depth).

In this construction method, the trench is held open during digging by a slurry of bentonite and water, which acts in a similar way to drilling mud during the drilling of a borehole. The fluid in the slurry penetrates the permeable formation of the trench walls leaving a filter cake (Fetter, 1999, p.434). In the second phase, the bentonite slurry is replaced by the final barrier material using tremie pipes. The wall is constructed in panels bounded by stop-end tubes, which can cause imperfections in the final wall once removed. To ensure efficient replacement of the initial bentonite slurry, the density of the cut-off slurry must exceed that of the bentonite slurry by at least 500 kg/m^3.

5.4.3 Composite diaphragm wall (c. 30 m depth)

In both the above methods, additional elements can be inserted into the wall, such as sheet plies, glass walls or tiles, and geomembranes (the most common). The aim is to improve strength and / or water tightness.

5.4.4 Interlocking bored-pile diaphragm wall (c. 20 m depth)

An interlocking bored-pile diaphragm wall is constructed with secant piles, which are overlapping holes filled with concrete. One pile cuts into the next so that they are in direct contact, along an arc of the intact pile. The piles are constructed in a sequence of 1,3, 5 followed by the overlapping 2, 4, 6 etc.

5.4.5 Displacement of soil and installation of sealing material

Thin wall (18 – 23 m depth) - firstly sheet piles, then heavier steel beams are vibrated into the ground and a clay-cement-water mix is injected into the void as the beams are retracted. The panels are cut into the adjacent ones, so ensuring that there is an overlap and water-tightness. A high density slurry of c. 16000 kg/m^3 is required to prevent closure of the hole while the pile is being retracted. A well-proven mixture is 25 kg bentonite; 175 kg Portland cement; 800 kg rock flour and 640L water (Arz, 1988).

For a sheet-pile wall, sheet plies are manufactured from steel, or less commonly aluminium, concrete or wood. These are driven into the ground. There is minimal disposal of soil or other contaminated material, and with modern 'labyrinth' joints or sealing pastes and plastic sealants there is little leakage.

5.4.6 In-situ permeability reduction

5.4.6.1 Injection

A cement-suspension, artificial resin or water glass-based material is injected through boreholes. The separation between boreholes depends upon the rock permeability, the viscosity of the injected fluid, and the maximum pressure of injection.

5.4.6.2 Jet grouting

Soilcrete columns are constructed using a rotary drilling technique, with a high density mud for both cutting medium and sealant.

5.4.6.3 Frozen wall

Pore water is converted into ice by the continuous circulation of a cryogenic fluid within a system of small diameter closed ended pipes installed in a pattern to match the contaminated area. The frozen water acts as a bonding agent fusing together particles of soil or rock to significantly increase strength and decrease permeability. The technique is most probably of no value over geological timescales as it requires the active (powered) circulation of refrigerant or liquid nitrogen. However, the technique could be of use in the short term (e.g. for temporary containment) for example if the source of the CO_2 contamination was sealed, leaving only shallow contamination to be remediated.

5.4.6.4 Bio-barrier.

The injection of bacteria to form biofilm barriers or bio-barriers in permeable formations which plug, clog or foul the pore network to contain or reduce the migration of the CO_2. Reductions in the hydraulic conductivity of one to three orders of magnitude have been

Table 6 Summary of the cut-off wall in unconfined surface aquifer remediation methods

Remediation technique	Principles	Information	CO_2 applicability considerations	Pros / cons
Cut-off wall / Slurry wall: Excavation and replacement	The aim of a cut-off wall is to isolate one portion of an aquifer from another portion, for example to isolate the contaminated portion of an aquifer from an uncontaminated portion, or to interrupt a flow path that would carry CO_2 or mobilised toxic metals towards, for example, a residential area	Single phase diaphragm wall (up to 35 m depth). A trench is excavated and filled with stabilising slurry typically bentonite cement and water. The slurry forms a filter cake with low hydraulic conductivity on the side walls of the trench and the remaining cement slurry then sets.	Important considerations in the slurry are solid content, type of bentonite and type of cement and care should be taken to ensure these materials are CO_2 resistant.	Requires a full excavation trench over what could be considerable distances and depths. Imperfections in the wall can reduce effectiveness considerably. Although cut-off walls are not used extensively for long-term containment, they may be used in conjunction with other remediation technologies to aid in temporary, partial containment
Excavation and replacement: Two-phase diaphragm wall	The first phase is the same as a single phase wall described above. In addition the bentonite slurry is replaced with a different final barrier material that has a higher density than the bentonite slurry	Two-phase diaphragm wall facilitates walls >50m depth.	The inner core material can be of a material with enhanced CO_2 resistant properties.	As above
Excavation and replacement: Composite diaphragm wall	In addition to the two phases of slurry and final barrier material further elements can be inserted into the wall such as sheet piles or geo-membranes.	The aim of the additions to the wall structure is to enhance strength and / or water tightness.	The addition of a geo-membrane can enhance the CO_2 resistant properties of the cut-off wall.	As above
Excavation and replacement: Interlocking bored-pile diaphragm wall	In addition to the two phases of slurry and final barrier material interlocking piles are inserted.	The aim of the addition of interlocking piles into the wall structure is to enhance strength and / or water tightness.	The addition of interlocking piles into the wall structure can enhance the CO_2 resistant properties of the cut-off wall.	As above
Installation of thin wall and sheet pile into the soil	Piles are vibrated into the ground and a clay-cement-water mix is injected. The piles are cut into the adjacent ones, so ensuring that there is an overlap and water-tightness	There is minimal disposal of soil or other contaminated material, and with modern 'labyrinth' joints or sealing pastes and plastic sealants there is little leakage	Impermeable CO_2 resistant materials can be used.	There is a significant reduction in amount of soil excavated. However corrosion is a problem with respect to the use of sheet-pile walls.
In-situ permeability reduction: injection permeation grouting	Permeation grouting is the injection of a liquid grout that fills the natural porosity and then gels to form a solid void-filling material A cement-suspension, artificial resin or water glass-based material is injected through boreholes into the porous soil.	There is concern over the integrity of the containment system and potential leakage of CO_2 through gaps in the barriers, such as high permeability zones between the grout. The separation between boreholes depends upon the rock permeability, the viscosity of the injected fluid, and the maximum pressure of injection.	Care should be taken to ensure that the cement-suspension, artificial resin or water glass-based material is CO_2 resistant.	Concern over the integrity of the containment system and potential leakage of CO_2 through gaps in the barriers, such as high permeability zones between the grout. Although jet grouting barriers do not provide long-term containment, they could be used in conjunction with other remediation technologies to aid in temporary, partial containment.
In-situ permeability reduction: jet grouting (deep soil mixing)	Jet grouting uses high-energy emplacement of cement or chemical grout materials whereby the sediment is displaced and mixed with the grouting material.	There is concern over the integrity of the containment system and potential leakage of CO_2 through gaps in the barriers, such as high permeability zones between the grout.	Jet grouting cement, biofilms, foam, gels must be CO_2 resistant	Although jet grouting barriers do not provide long-term containment, they could be used in conjunction with other remediation technologies to aid in temporary, partial containment.

Remediation technique	Principles	Information	CO_2 applicability considerations	Pros / cons
In-situ permeability reduction: frozen wall	A coolant is continuously circulated through refrigeration pipes which are embedded in the ground. The coolant will be at around -20ºC which will freeze the surrounding soil and create the wall.	The entire system is closed; no materials are injected into the ground	Requires the active (powered) circulation of refrigerant coolant or liquid nitrogen.	Most probably of no value over geological timescales as requires the active (powered) circulation of refrigerant or liquid nitrogen. Though could be of use in the short term (e.g. for temporary containment) for example if the source of the CO_2 contamination was sealed, leaving only shallow contamination to be remediated
Bio-barrier	The injection of bacteria to form biofilm barriers or bio-barriers in permeable formations which plug, clog or foul the pore network to contain or reduce the migration of the CO_2	Reductions in the hydraulic conductivity from one to three orders of magnitude have been reported using many types of bacteria including stimulation of indigenous bacteria (biostimulation), and injection of full-sized living and dead bacteria (Dennis and Turner 1998).	For bio-barriers to be effective the right temperature, nutrients and food must be present, if conditions are not ideal it won't work. The resulting biofilm must also be resistant to CO_2	Possibly unlikely to be suitable for CO_2 remediation as to get ideal concentrations for biofilm generation require very specific conditions, the biofilm must be CO_2 resistant of the bacteria use the CO_2 as food plus the timescales will be long.
Water control agent	Utilises the injection of very capable water control agents into the pore network to block the flow of CO_2 contaminated water.	Utilises technology developed in the hydrocarbon industry to plug high permeability thief zones.	Work needed into resistance of proprietary water control agents to CO_2.	Technology available and low cost. Resistance to CO_2 untested.
High strength rigid set material	Utilises the injection of rigid set polymer to block matrix to flow	Utilises technology developed in the hydrocarbon industry.	Work needed into resistance of proprietary rigid set polymer to CO_2.	Technology available and low cost. Resistance to CO_2 untested.
Organic polymer sealant	Utilises the injection of Organic cross-linked polymer blocks matrix to flow	Utilises technology developed in the hydrocarbon industry.	Work needed into resistance of proprietary Organic cross-linked polymer to CO_2.	Technology available and low cost. Resistance to CO_2 untested.
Super absorbent crystals	Utilises the injection of Cross-linked polyacrylamide superabsorbent crystals for flow barrier	Utilises technology developed in the hydrocarbon industry.	Work needed into resistance of proprietary Cross-linked polyacrylamide superabsorbent crystals to CO_2. Works Best in fractures	Technology available and low cost. Resistance to CO_2 untested.

reported (Denis and Turner, 1998). For bio-barriers to be effective the temperature must be suitable, and nutrients and food must be present; if conditions are not ideal the technique will not work. The resulting biofilm must also be resistant to CO_2.

5.4.6.5 Water control agent.

This technique utilises the injection of water control agents into the pore network to block the flow of CO_2 contaminated water. Utilises technology developed in the hydrocarbon industry to plug high permeability thief zones (Halliburton, 2014). Work is needed into the resistance of proprietary water control agents to CO_2.

5.4.6.6 High strength rigid set material

This technique utilises the injection of a rigid setting polymer into the pore network to block the flow of CO_2 contaminated water. Utilises technology developed in the hydrocarbon industry (Halliburton, 2014). Work is needed into resistance of proprietary high strength rigid set materials to CO_2.

5.4.6.7 Organic polymer sealant

This technique utilises the injection of an organic cross-linked polymer into the pore network to block the flow of CO_2 contaminated water. Utilises technology developed in the hydrocarbon industry (Halliburton, 2014). Work is needed into resistance of proprietary organic polymer sealant materials to CO_2 on the timescale relevant to CO_2 storage.

5.4.6.8 Super absorbent crystals

This technique utilises the injection of super absordant crystals into the pore network to block the flow of CO_2 contaminated water. It utilises technology developed in the hydrocarbon industry, Halliburton (2014). Work is needed into resistance of proprietary super absorbent crystals to CO_2.

5.4.7 Summary of cut-off wall in unconfined surface aquifer remediation measures

Table 6 presents a summary of the cut-off wall in unconfined surface aquifer remediation methods. The table presents a short summary of the principles of each technique, additional information, CO_2 applicability considerations and the technical pros and cons.

5.5 Remediation techniques (3) – Cut-off walls in fractured rock (Grout curtains)

The migration of naturally occurring CO_2 along faults and fractures has been documented at several sites worldwide, e.g. Keating et al. (2014); Wilkinson et al. (2009). In any inverted sedimentary basin, which will include many basins that are currently onshore, there is the possibility that the surficial rock will have been buried to substantial depths prior to uplift and erosion. This burial causes compaction of the rock, lithification or induration, and the reduction in porosity and permeability. Many such rocks have been subjected to tectonic forces, for example during basin inversion and uplift, and are now fractured. The resulting bulk properties of the rock, with respect to fluid flow, may be dominated by the fractures if the rock matrix is effectively impermeable, or a by the dual-porosity network of fractures plus matrix porosity if the latter is significant. In either case, a substantial body of expertise exists that has been developed associated with the engineering of the foundations of dams, which must be made effectively impermeable to water flow (e.g. Weaver and Bruce, 2007).

The technologies used for remediation in fractured rock may be the same as those used in the remediation of pollution in porous media (Bruell and Inyang, 2000), or these techniques may not be appropriate. However, the engineering properties of highly indurated but fractured rock are not the same as less indurated but porous rock, so that there are important differences. Natural fracture systems are extremely heterogeneous, with highly variable number, density, size, and direction of fractures. A potential problem is that of very low bulk permeability, so that a pollutant may be very difficult to extract from the fracture system using the standard shallow remediation techniques (soil vapour extraction; air sparging; bioremediation). In the case of contamination by highly toxic organic chemicals, standard practise has involves fracturing the low permeability rock, to increase bulk permeability (Bruell and Inyang, 2000). Both hydrofracturing and pneumatic fracturing are used, the latter is identical in principle to the procedure used for 'fracking' in shales associated with the production of shale oil and gas. In this case, the 'fracking' fluid needs to be sufficiently viscous so that it will not flow into the formation, so that a biodegradable gel (e.g. cross-linked food grade guar gum) and sand are used. An enzyme is also added, which later degrades the biodegradable gel, leaving the fractures open to fluid flow. The sand acts as a 'proppant', preventing the fractures from closing when the pressure is reduced. Pneumatic fracturing relies upon self- propping as a proppant cannot be added to the injected air, an example of self-propping mechanisms include block shift. While fracturing is a rapidly moving field, the reported spatial extents of fracture propagation for remediation are rather limited, only mm-scale fractures extending less than 10 m for pneumatic fracturing and up to 1.0 cm fractures extending only 10 m for fluid fracturing (Suthersan 1997; Nyer et al. 1996).

The following investigative techniques are used to characterise fractured rock sites (Paillet 1991; Shapiro and Hsieh, 1991; Bruell and Inyang, 2000; Weaver and Bruce, 2007):

1. Surface and regional geology including mapping if not available at a suitable resolution or if fractures are not well mapped;
2. Trenching for enhanced geological mapping;
3. Photointerpretation (for regional fracture patterns);
4. Exploratory drilling;
5. Surface geophysics including refraction seismic surveys;
6. Borehole geophysics;
7. Cross-hole tomographic imaging using seismic or electromagnetic sources;
8. Geochemical analysis,
9. Tracer testing;
10. Acoustic televiewers to produce a photo-like image of borehole walls (using a scanning ultrasonic beam) for characterising fractures with respect to position, strike, dip, and relative aperture (Paillet 1991);
11. Cross-hole flow logging utilising packers to isolate individual fractures intersecting boreholes, by positioning packers above and below the fracture of interest. Pumping of individual fractures can be used to reveal interconnectivity and hydraulic properties of selected fracture groups.

The aim is to predict the fluid and chemical movement at a site. Bruell and Inyang (2000) note that, in fractured rock, site characterization can be expensive due to the cost of boreholes and the often complex and lengthy field testing. Weaver and Bruce (2007) emphasise that the site geology and hydrogeology must be understood before any plan of remediation can be drawn up. Important aspects of the hydrogeology include (Weaver and Bruce, 2007):

1. Any surface streams feeding the groundwater table;
2. Any shallow perched groundwater;
3. The relationship between the piezometric surface and the ground surface;
4. The lowest pietzometric level;
5. Seasonal variations in the pietzometric level;
6. The direction and flow of the groundwater.

The bedrock type influences grouting procedures and the likelihood of success (Weaver and Bruce, 2007), with the following common rock types:

1. Shales and mudrocks – very variable in character, and often with poor bonding vertically, so that grout separates and penetrates bedding planes, but achieves little penetration into either pre-existing fractures or matrix porosity;
2. Interbedded sands and mudstones – the more brittle sandstones are commonly jointed due to unloading, and may require elaborate curtain grouting;
3. Weakly cemented sandstones – joints and fractures filled with weakly consolidated sand may be impossible to grout successfully;
4. Conglomerate – performance depends on the degree of cementation of the matrix;
5. Limestones – solution caverns present obvious problems;
6. Gypsum and anhydrite – may be impossible to grout;
7. Volcanic and pyroclastic rocks – lava tubes and cooling joints are challenging;
8. Granite and metamorphic rocks – it is unlikely that the remediation of a CO_2 leak would involve these rock types.

The permeability of the fractured rock is crucial to the design of a grouting programme as conventional grouting materials will not penetrate the very fine fractures associated with low permeabilities (Weaver and Bruce, 2007). In-situ bulk rock permeability is conventionally measured using flow tests in boreholes, on 3 – 5 m length sections of the borehole. Longer test intervals are not recommended, on grounds that the results cannot be adequately tied to the subsurface geology. If high permeabilities are detected at low test pressures (10-3 cm/s; Waever and Bruce, 2007) then tests at higher pressures are not required. With lower permeabilities (1 – 5 × 10-4 cm/s) then flow tests at higher pressures (500 – 1500 kPa) should be run for 5 or 10 minute intervals. The Lugeon unit, which is defined as a water pumping rate of 1 L/m of hole per minute of test at a pressure of 10 atmospheres, is the permeability unit most commonly used in connection with grouting. Because application of water at a pressure of 10 atm at shallow depth would be potentially damaging to many foundations, testing of permeability is commonly conducted at a lower pressure, and the permeability under 10 atmospheres is calculated. This is referred to as the modified Lugeon test (Weaver and Bruce, 2007, p.382).

Unless very high quality data is available from an analogue site, it is considered to be prudent to conduct a test grouting programme (Weaver and Bruce, 2007, p. 67). This will determine:

1. The residual permeability after grouting (otherwise expressed as the coefficient of permeability reduction), a parameter that cannot be determined by any other method;
2. The average grout consumption for each step;
3. The maximum allowable spacing between the centres of the boreholes for the final grouting stage.

Grout curtains are constructed by injecting grout into one or more rows of boreholes drilled for that purpose. The initial (primary) holes are relatively widely spaced (6 – 12 m apart; Weaver and Bruce, 2007, p. 72), so that the grout is unlikely to flow from one hole to another. The spacing between these holes is then split midway by secondary holes. This split-spacing sequence is repeated with tertiary holes, quaternary holes, and so on until the progressive reduction in the volume of grout injected into the holes or, more significantly, the results of permeability tests made in the final holes indicate that the design criterion for permeability reduction has been achieved. Note that Weaver and Bruce (2007, p.72) recommend that the predicted number of boreholes should be deliberately over-estimated, and suggest that 50 % is a suitable safety margin. In the event that the initial estimate is too low, then both time and cost over-runs are unavoidable, with predictable consequences.

Boreholes for grouting are traditionally drilled perpendicular to the landscape, with the aim of building as curtain of constant thickness, or to drill vertically for a constant length. Ideally, boreholes would be oriented so that all likely orientations of fractures are intercepted and sealed, with the specific aim of avoiding drilling parallel to the orientation of any significant fracture set (Weaver and Bruce, 2007, p. 72). Although single-row configurations of boreholes has been used, because of the possibility of incomplete grout penetration, then Weaver and Bruce (2007, p. 73) recommend the multiple-row curtains. In the USA, a three row configuration (for dam foundations) is commonly adopted, though the outer rows are not grouted to be independently sealing. If two rows are used, they can be drilled at opposing angles rather than parallel to each other.

Injection of grout into each hole is done in a series of stages of selected length that may vary with the depth of the stage and the geological conditions encountered. Depending principally on the condition of the rock related to its mechanical competence, either descending stage grouting (downward stages) as the hole is being drilled may be required, or grouting may take place as a series of ascending stages (ascending stage grouting) temporarily sealed off with a packer after the hole has been drilled and remains open and stable to the final planned depth.

Grouting materials can be classified as follows (Weaver and Bruce, 2007; p. 87):

1. Particulate (suspension or cementitious) grouts. Mixtures of water and cement plus other particulate solids such as fly ash, clays, or sand, and chemical additives. They may be stable (i.e., have minimal bleeding) or unstable when left at rest;
2. Colloidal solutions, in which viscosity progressively increases with time. Often sodium silicate-based;
3. Pure solutions, in which viscosity is essentially constant until setting. Often resin-based;
4. Others, used relatively infrequently and only in certain applications requiring special performance characteristics.

The composition water used in the grout mix can have significant effects upon grout performance, for example suspended solids or dissolved sulphates are to be generally avoided (Weaver and Bruce, 2007). This may be a significant consideration for the construction of grout curtains in areas with an arid or semi-arid climate. The composition of cements (both Portland and otherwise) and other components of grout is considered in great detail by Weaver and Bruce (2007). Important factors of the final grout mix are the rheology; viscosity; cohesion; specific gravity; settlement (i.e. the tendency for water to escape from the grout while at rest); filtration pressure (i.e. the ease with which filter cake builds up on the walls of the boreholes); grain size and water-repellence (and hence resistance to washing out when injected below the water table; Weaver and Bruce, 2007).

The penetration of the grout is controlled by the following properties of the rock fractures: aperture dimensions; surface roughness; hydraulic routing (hydraulic percolation pathways within the fracture network); tortuosity; porosity; and permeability (Weaver and Bruce, 2007). The effectiveness of the grouting is affected by procedural factors including: drilling methods and procedures; borehole deviation; the choice of circulating medium within the borehole (the drilling mud in oil industry terminology); the staging of the drilling and the protection of the open boreholes from the ingress of contaminants and detritus (Weaver and Bruce, 2007). Factors which influence the durability of the grout curtain, which may be crucial in the case of a long-term leak of CO_2, include:

Table 7 Summary of the cut-off wall in fractured rock remediation methods.

Remediation technique	Principles	Information	CO_2 applicability considerations	Pros / cons
Hydrofracking	Natural fracture systems are extremely heterogeneous and a potential problem is that of very low bulk permeability. Fracturing the low permeability rock, to increase bulk permeability. Both hydro-fracturing and pneumatic fracturing are used. This facilitates and more thorough deployment of the grout material.	The 'fracking' fluid needs to be sufficiently viscous so that is will not flow into the formation, so that a biodegradable gel (e.g. cross-linked good grade guar gum) and sand are used. An enzyme is also added, which later degrades the biodegradable gel, leaving the fractures open to fluid flow. The sand acts as a 'propant', preventing the fractures from closing when the pressure is reduced.	The hydrofracking simply facilitates the application of the sealing material into the fractured rock more effectively and must be used in conjunction with a filling and clogging grout material.	Facilitates greater dispersion of the clogging grout material, but risks increasing the CO_2 leakage.
Grout curtain	Grout curtains are constructed by injecting grout into one or more rows of boreholes. Ideally, boreholes would be oriented so that all likely orientations of fractures are intercepted and sealed. Injection of grout into each hole is done in a series of stages of selected length that may vary with the depth of the stage and the geological conditions encountered. Depending principally on the condition of the rock related to its mechanical competence	The permeability of the fractured rock is crucial to the design of a grouting programme as conventional grouting materials will not penetrate the very fine fractures associated with low permeabilities. Bedrock type influences grouting procedures and the likelihood of success. The penetration of the grout is controlled by the following properties of the rock fractures: aperture dimensions; surface roughness; hydraulic routing (hydraulic percolation pathways within the fracture network); tortuosity; porosity; and permeability	Important factors of the final grout mix are the rheology; viscosity; cohesion; specific gravity; settlement (i.e. the tendency for water to escape from the grout while at rest); filtration pressure (i.e. the ease with which filter cake builds up on the walls of the boreholes); grain size and water-repellence. In the specific case of the remediation of a leak of CO_2, then a grout that is reactive to CO_2 could be used. Reaction between the silicate solution and CO_2 causes the precipitation of amorphous silica.	Boreholes ideally orientated to intersect as many fractures as possible, fracture permeability important and can be enhanced through hydrofracking. Grout material must be compatible with CO_2.

1. The geochemical environment, i.e. presence or absence of deleterious minerals in the host rock (Osende, 1985, and Mielenz, 1962, present a list which includes minerals abundant in virtually every common rock type!);
2. The nature of the groundwater, whether aggressive or not to the grout;
3. The hydraulic gradient, a high gradient may shear the grout; will exacerbate dissolution; and will enhance mechanical erosion rates;
4. The erodability or solubility of the host rock, especially if minerals such as gypsum or anhydrite are present.

In the specific case of the remediation of a leak of CO_2, then a grout that is reactive to CO_2 could be used (Ito et al., 2014). Reaction between the silicate solution and CO_2 causes the precipitation of amorphous silica. Laboratory experiments show a 99% reduction in permeability in a glass-bead artificial rock with an initially high permeability of several Darcy's.

5.5.1 Summary of cut-off wall in fractured rock remediation measures

Table 7 presents a summary of the cut-off wall in fractured rock remediation methods. The table presents a short summary of the principles of each technique, additional information, CO_2 applicability considerations and the technical pros and cons.

5.6 Remediation techniques (4) - Treatment walls (or Permeable Reactive Barriers, PRB's)

Treatment walls (or permeable reactive barriers, PRB's) are structures installed in the shallow subsurface that trap or alter pollutants that are carried though the wall by natural groundwater flow (EPA, 1996), Figure 10. Treatment walls work best with a porous and permeable aquifer with a 'high' rate of water flow (EPA, 1996). The pollutants are either:

1. Adsorbed onto the porous and permeable fill of the wall, involving some or all of chemical adsorption; ion exchange, co-precipitation, solid-solution formation (Roehl et al., 2005). Usually there is no change in the oxidation state of the contaminant metal. The specific surface area of the absorbant is critical;
2. Precipitated as an insoluble salt by reacting with the fill of the wall;
3. Degraded into harmless by-products by biologically mediated reactions.

Barrier fills typically include activated charcoal and iron fillings, numerous examples of experiences with both fill types are described by Roehl et al. (2005). The flow of water can be directed towards the wall by impermeable barriers installed within the aquifer, the so-called 'funnel and gate' system, (Figure 11), see sections on grouting and cutoff walls for the construction and other details of impermeable barriers within aquifers. The cost of the barrier will be an important factor in determining whether a continuous or funnel-and-gate configuration is used – a cheap fill material favours the continuous geometry. The cost of replacing spent reactive material is one of the factors that limit the utility of treatment walls (Freethey et al., 2005). Treatment walls can be permanent, semi-permanent or replaceable (Roehl et al., 2005, p.2).

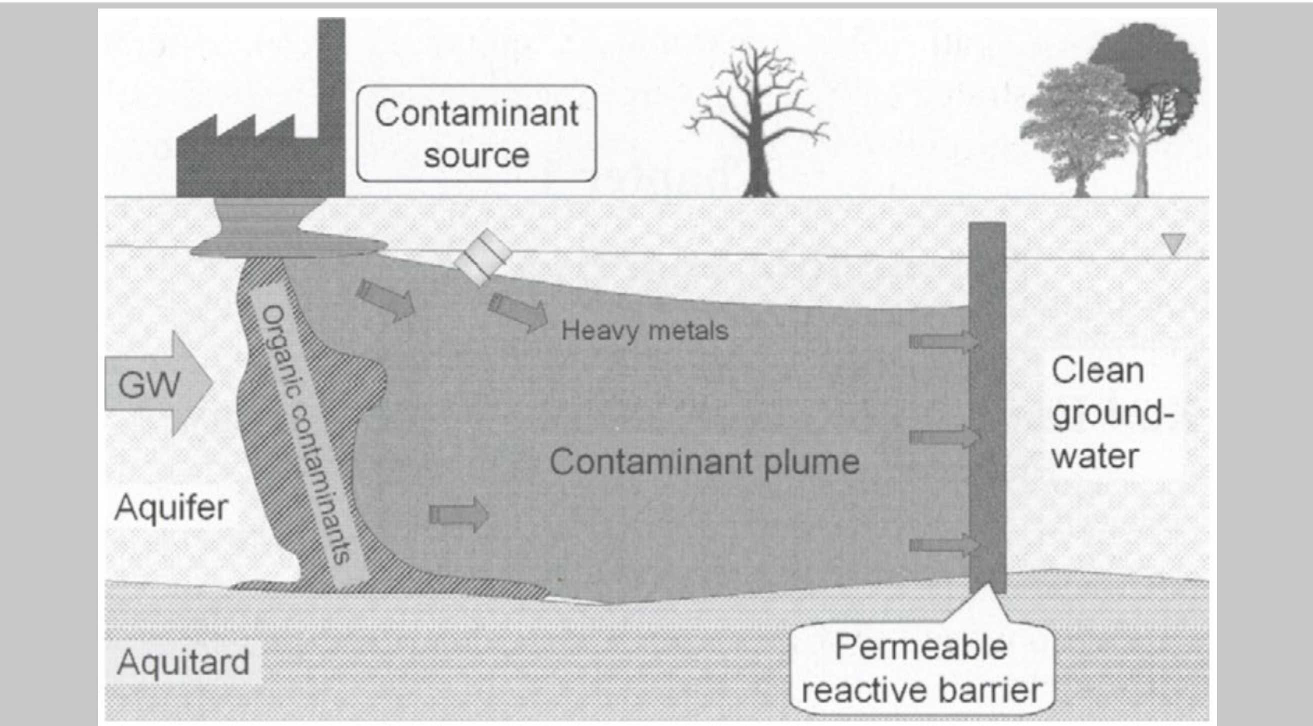

Figure 10 The treatment wall, or permeable-reactive barrier (PRB) concept as applied to conventional surface pollution. From Roehl et al. (2005)

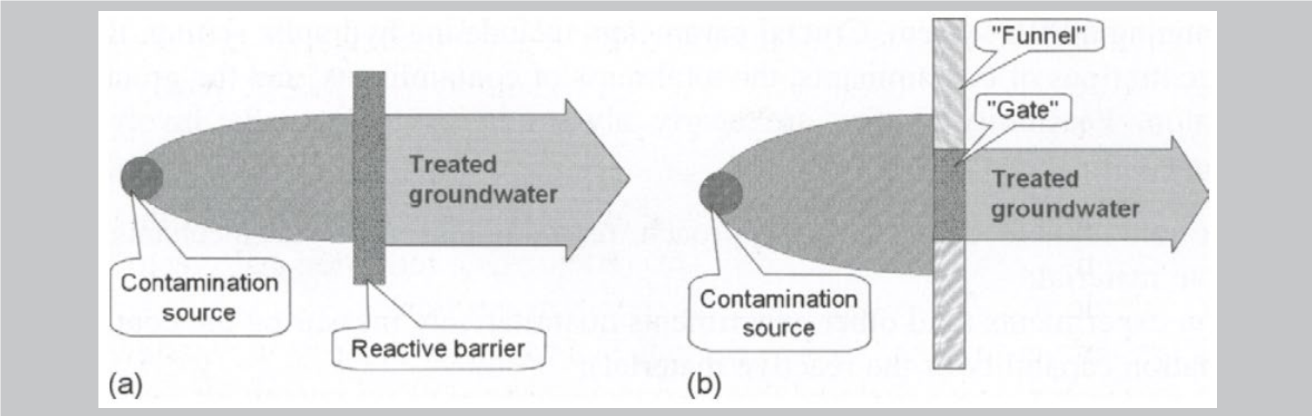

Figure 11 A continuous treatment wall (left) and the 'funnel and gate' configuration. From Roehl et al. (2005).

Because treatment walls are low maintenance and have no ancillary equipment such as tanks, pumps or containers, they can be used not only in industrial settings, but at least in principle in urban areas. Treatment walls offer several advantages over other remediation technologies (Carey et al., 2001):

1. Demonstrated as effective, but mostly for e.g. chlorinated solvents;
2. Below ground, so unobtrusive;
3. Passive, low environmental impact;
4. Retain the groundwater resource;
5. Minimal volume of soil and water to be handled;
6. Potentially low cost, with possible exception of monitoring operations;
7. Potential design lives of decades.

There are also disadvantages (Carey et al., 2001):

1. Decades may be needed to deal with a persistent source of pollution;
2. Long-term monitoring is required;
3. Site characterisation is often complex and costly;
4. Sub-surface structures can be problematic;
5. Deeper plumes (i.e. anything not in the top m or at most 10's m) problematic for construction and design;
6. Possible need to remove after use, or to renew reactive material;
7. Use is constrained by geological conditions, including fractured rocks.

Factors to be considered when planning and installing a treatment wall include (Roehl et al., 2005):

1. Property boundaries;
2. The position of underground utilities e.g. pipes, gas lines;
3. The disruption to existing site activities during the construction phase;
4. The need to dewater the construction pit, and the disposal of the water;
5. Logistics and management of material placement (e.g. quality control; homogeneous filing of the reactors; dust prevention etc.);
6. H&S issues;
7. Unforeseen ground conditions such as undetected subsurface structures such as old foundation walls.

Planning of the treatment wall should take into account at least the following factors (Roehl et al., 2005):

1. Choice of removal mechanism and the material itself;
2. Relevant experiments to determine the attenuation properties of the reactive material (column experiments, e.g. Banasiak and Indraratna, 2012);
3. The likely time the treatment wall will be required for;
4. The thickness of the barrier which must be sufficiently thick so that the pore water is in contact with the reactive material for sufficiently long to reduce contamination to acceptable levels.

The performance requirements for a treatment wall are (Meggyes, 2005):

1. Replaceability of the reactive materials;
2. Higher permeability than the surrounding reservoir (50 – 200 times higher);

3. Resistance to fines washed in from the reservoir;
4. Long life span.

The selection of a construction technique mainly depends on the character of the site (Gavaskar, 1999 in Meggyes, 2005):

1. Most importantly: depth. The deeper the target reservoir, the more specialist are the methods of construction re required, and the higher the costs;
2. Geotechnical character of the site: soil or rock strength; any subsurface obstacles;
3. Soil excavation, disposal of contaminated soil;
4. H&S during construction, e.g. entry of personnel into the excavation.

Although very shallow barriers (< 8 m, Meggyes, 2005) may consist only of the reactive fill, deeper barriers typically have a layered construction with a layer of gravel to filter fines from the inflowing pore water, to prevent entry to the reactive core. The top of the barrier is usually covered by a low permeability material, i.e. clay, to prevent contact with oxygen in the overlying air. Pumping and 'treatability' tests may have to be conducted prior to the onset of construction. Column tests are the standard technique used to assess the reactive material to be used for a given site (Meggyes, 2005).

The techniques used for the construction of treatment walls are similar to those described above for cut-off walls (Maggyes, 2005). To date, the majority of treatment walls have been installed by conventional excavation techniques – i.e. a trench is dug with an excavator, and simply filled from the surface with the reactive material (Freethey et al., 2005). The relatively shallow depth of operation (15 m) lead Manceau et al., (2014), in a review of techniques for the remediation of CO_2 leakage, to reject treatment walls as a viable technique. However, in a situation with CO_2 contamination in a thin surficial aquifer, perhaps fluvial or alluvial sediments resting on relatively impermeable basement, then the technique might have potential. Note that Freethey et al. (2005) suggest that 21 m is a more realistic depth limit assuming the availability of 'modified' excavators. Techniques for deeper installation include (Freethey et al., 2005 and refs therein):

1. Tremie tube (http://www.tremiepipe.com/) / mandrel;
2. Deep soil mixing within individual circular casings (caisson) using multiple augers with the reactive material injected through the hollow kelly bar of the mixing tools (Meggyes, 2005);
3. High-pressure jetting and milling – in low strength rocks, a slurry jet excavates the aquifer between vertical stop end tubes, while in stronger rocks, a milling head is driven by a hydraulic motor;
4. Vertical hydraulic fracturing - similar to the techniques developed for 'fracking' shale for oil and gas. A fluid with a 'proppant' such as sand is injected at high pressure. Can be used to place reactive material into an aquifer, or to generate zones of high permeability to direct fluids towards reactive gates (Meggyes, 2005). The reactive material cannot be recovered, placing limitations upon the nature of the material;
5. Deep well injection – reactive material is injected into a series of closely-spaced boreholes with no geometrical boundaries, merging to form a continuous wall. Ensuring that there are no significant gaps within the wall, allowing flow to bypass the wall, is a problem. Injection can be into either induced fractures (as above) or into the natural porosity of the reservoir (Meggyes, 2005). With low permeability reservoirs, the injected material may be limited to liquids (i.e. not suspensions or slurries);
6. Deep aquifer remediation tools (DARTs): Freethey et al. (2005) and Maggyes (2005) describe this method for installing treatment walls in so-called 'deep' aquifers (deep in the context of groundwater treatment means that the aquifer is confined, i.e. is not immediately at the surface, and / or that the depth to the base of the aquifer exceeds c. 21 m). DARTs consist of a series of closely-spaced boreholes with rigid polyvinyl chloride shells, each with high-capacity flow channels that contains the permeable reactive material and flexible wings to direct the flow of groundwater into the reactive material. The reactive material used in a DART should be chosen to have a hydraulic conductivity 50 to 200 times greater than the hydraulic conductivity of the host aquifer material (Freethey et al., 2005). Configurations of DARTs are shown in Figures 12 and 13.

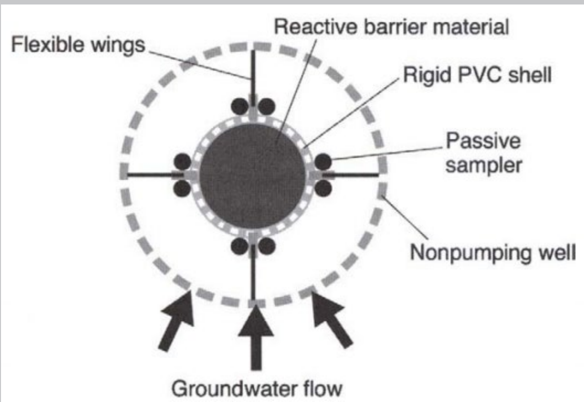

Figure 12 Schematic diagram of a deep aquifer remediation tool (DART), plan view. From Freethey et al. (2005).

Indicative cost estimates for treatment walls are given in Meggyes (2005, his Table 2.5). Regulatory and economic aspects of the use and construction of treatment walls are discussed in detail by Simon et al. (2005). The UK situation for regulation is summarised by the Environment Agency (Carey et al., 2002), who include screening criteria for the feasibility of a project.

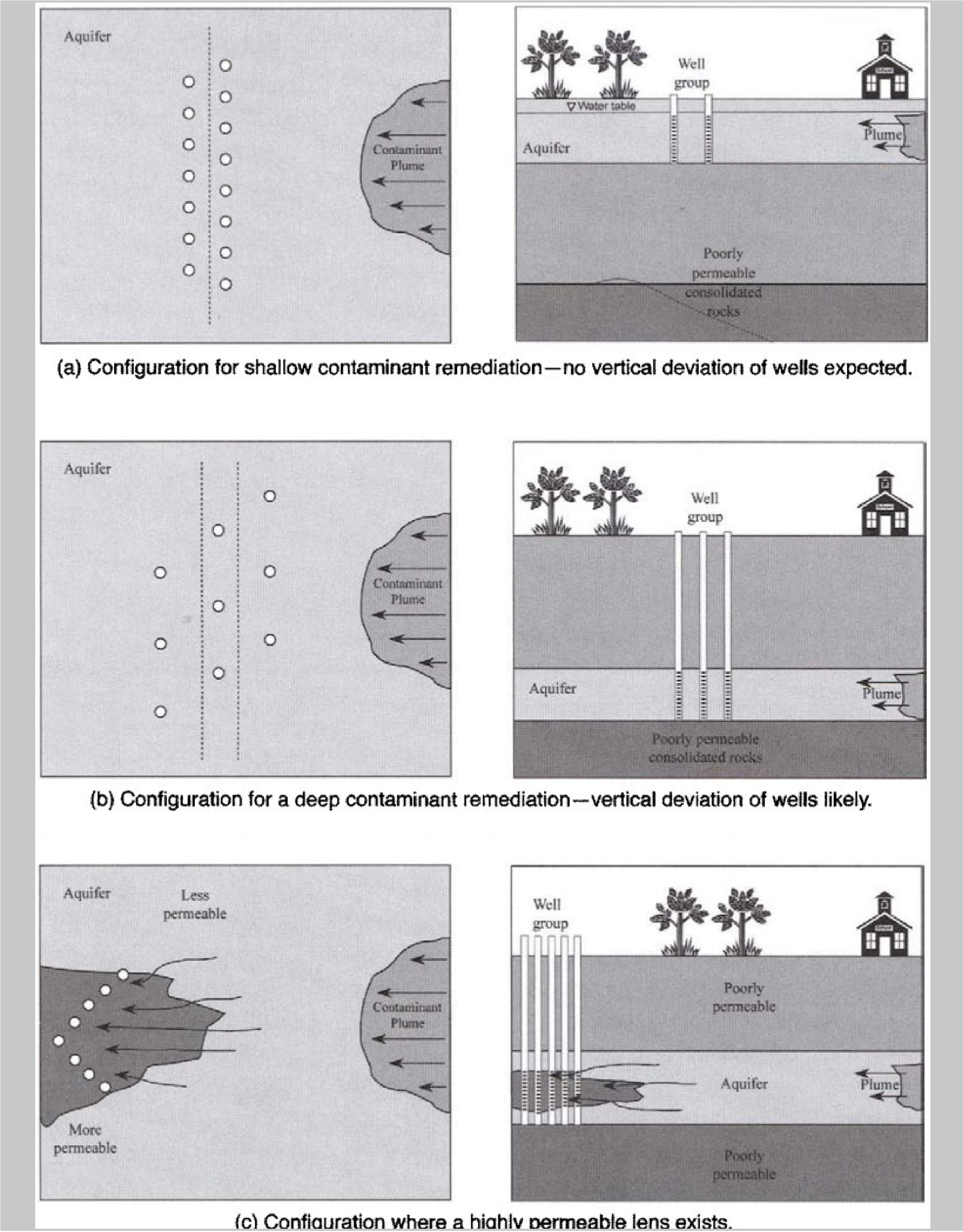

Figure 13 Three configurations for 'deep' aquifer remediation tools (DARTs). Plan on left, and cross-section on the right. From Freethey et al. (2005).

5.6.1 Ionic species removal

Some ionic species can be removed by reductive immobilisation, such as chromium, nickel, lead, uranium, sulphate, nitrate, phosphate, arsenic and molybdenum (Roehl et al, 2005). For example, chromate - a carcinogen - can be removed from groundwater using elemental iron as the reactive material, through a coupled reduction/precipitation mechanism (Blowes et al., 2000):

$$Fe^{0}_{(solid)} + CrO_4^{2-} + 8H^+ \rightarrow Fe^{3+} + Cr^{3+} + 4H_2O$$
$$(1 - x)Fe^{3+} + xCr^{3+} + 4H_20 \rightarrow Fe_{(1\_x)}\,Cr_xOOH_{(solid)} + 3H^+$$

Reohl et al. (2005) list a series of possible reactions that can be employed, including the use of bacterial sulphate reduction fed by compost or wood chips, to produce alkalinity and raise pH. Dissolved metals precipitate as hydroxides as a consequence. Mercury can be removed by reaction with elemental copper shavings derived from scrap, though the released copper must then be removed from the pore water through the use of a zeolite filter.

5.6.2 Sorption barriers

For sorption barriers, a wide range of reactive materials have been utilised. These include (Roehl et al., 2005):

1. Activated carbon in granular form derived from coal, wood, nutshells and other carbon rich materials for a wide range of both organic and inorganic contaminants (the most common material used to date);
2. Phosphate minerals such as hydroxyapatite and biogenic apatite such as fishbones (for the removal of Pb, Sb, U);
3. Others tailored for specific applications e.g. diatomite with silane surfaces.

Factors that must be taken into account when selecting a reactive material include (Roehl et al., 2005):

1. Reactivity - high reactivity enables a barrier to achieve the desired reaction with minimal thickness;
2. Stability – as replacement may be difficult, the material should remain reactive for long periods of time. Stability to changes in pH, temperature and pressure are also desirable;
3. Availability and cost – low bulk cost is desirable as the volume of reactant required may be large;
4. Hydraulic performance – the bulk permeability must exceed that of the surrounding soil or aquifer;
5. Environmental compatibility – there should be no unwanted by-products;
6. Safety – the material should be safe to handle during installation, and during any replacement operations.

5.6.3 Treatment walls – de-acidisation

For the remediation of aquifer water that is contaminated with CO_2, there are two remediation tasks:

1. Remove the CO_2 and raise the pH of the water;
2. Remove any toxic metals that have been mobilised by the reduced pH of the water – clearly the suite of metals that have been mobilised is crucial here in the design of the reactive material.

In the case of contamination of an aquifer by CO_2, then the material within the barrier must react with, or otherwise immobilise the CO_2, and must be sufficiently abundant and cheap to make deployment practical. It is not clear if a treatment wall has ever been used for the remediation of a CO_2-contaminated aquifer. A relatively recent book on the subject of treatment walls (Roehl et al., 2005) does not explicitly discuss CO_2 amongst the pollutants covered. However, treatment walls have been used to remediate acid mine drainage, which is a common pollution problem worldwide and which can be considered to be a useable analogue for the remediation of groundwater acidified by the addition CO_2. In Australia, Banasiak and Indraratna (2012) describe the construction of a treatment wall successfully neutralised the acidic groundwater from c. pH 3 to c. pH 7.3 and removed around 95 % of dissolved Al and Fe. Twenty five alkaline materials were tested (as batch experiments) as candidates for the reactive core of the treatment wall, including recycled concretes, limestone, oyster shells, calcite-bearing zeolitic breccias, air-cooled blast furnace slag (ACBFS), lime and fly ash. Drain water collected from the remediation site was used for the tests. Column tests were conducted on the best performing materials (recycled concrete and oyster shells) and the recycled concrete was selected as having the longest life times and resistance to clogging by precipitates. The dimensions of the barrier are not analogous to probable remediation of a CO_2 leak – the barrier was only 18 m by 3 m. Any CO_2 leak might be expected to be rather larger unless the leak is highly constrained laterally.

Calcite has been used as a reactive barrier (along with CO_2 injection to improve the removal efficiency of fluoride – hardly applicable here; Turner et al., 2008) and could perhaps be used, if not to remove the CO_2, then to moderate the pH of the acidified CO_2-rich groundwater (Naftz et al., 2003) as has been used for the treatment of acid mine drainage. Limestone is a cheap and readily available source of calcite, however problems encountered are the low solubility of calcite (Morel and Hering, 1993), and armouring. The latter occurs when iron is dissolved in oxic groundwater, as is common with acid mine drainage for example, and the iron reacts with bicarbonate in solution to produce iron (III) oxyhydroxides which precipitate on the surface of the limestone particles, effectively isolating the reactive calcite from the groundwater (Sun et al., 2000; Waite et al., 2002). A high slope of the ground (> 20 %) prevents armouring (Ziemkiewicz et al., 1997), as does periodic disturbance (Rose and Laurenso, 2000 in Waite et al., 2002). Neither of these conditions is likely to be appropriate for the remediation of a significant CO_2 leak.

5.6.4 Carbonation stabilisation

In this technique, contaminated groundwater and soil is mixed with binding agents that cause a chemical reaction with the CO_2 to trap it and reduce environmental release. Carbonation is a strongly exothermic reaction and calcium carbonate ($CaCO_3$) is formed by the reaction between cementitious materials and CO_2. Mineral carbonation is one of technologies utilising CO_2, and is used to form carbonated materials by the reaction between CO_2 and Ca or Mg-bound compounds such as wollastonite ($CaSiO_3$), olivine (Mg_2SiO_4), and serpentine.

5.6.5 Microbes

Microbes are used to clean up CO_2 contaminated soil and groundwater. Bioremediation uses microbes that use the CO_2 for food and energy. Work is undergoing with Chlorella Microalgaen. Also coccolithophorid algae can sequester carbon by photosynthesis as well as in calcium carbonate scales known as coccoliths. There are a number of high CO_2 tolerant micro algae:

- Cyanidium caldarium - Seckbach et al. (1970);
- Scenedesmus sp. - Hanagata et al. (1992);
- Chlorococcum littorale - Kodama et al. (1993);
- Synechococcus elongatus - Miyairi (1995);

Table 8 Summary of the permeable reactive barriers (treatment walls) remediation methods.

Remediation technique	**Principles**	**Information**	**CO_2 applicability considerations**	**Pros / cons**
Treatment walls (permeable reactive barriers PRB)	Treatment walls (or permeable reactive barriers, PRB's) are structures installed in the shallow subsurface that trap or alter pollutants that are carried though the wall by natural groundwater flow. Treatment walls work best with a porous and permeable aquifer with a 'high' rate of water flow. There are numerous methods to install treatment walls which are covered in the full report.	The CO_2 pollutants are adsorbed, precipitated, react to form less harmful material or are degraded.	There are many applications that will be suitable for CO_2 application and they are presented below.	They are effective, unobtrusive, passive, retain groundwater resources, minimal soil volumes handled, lower cost and long design lives. But long term monitoring required, site characterisation is complex and costly, deeper plumes difficult to handle and use is geologically constrained to porous media. Over time reactive materials become less effective at removing CO_2 and the contaminated reactive material needs to be removed and replaced with fresh material.
PRB – sorption barriers	The CO_2 pollutants are adsorbed by the core material within the permeable barrier.	Suitable materials for sorption barriers include activated carbon, phosphate minerals and other site specific materials such as diatomite with silane surfaces.	CO_2 is readily sorbed onto coal so the technology should be applicable to CO_2 remediation.	Factors to consider are: reactivity, stability, availability, cost, environmental compatibility, safety and hydraulic performance.
PRB – Ionic species removal	Ionic removal can be achieved by electrical currents through inert electrodes, reactive materials and ion exchange resin.	Some ionic species can be removed by reductive immobilisation, such as chromium, nickel, lead, uranium, sulphate, nitrate, phosphate, arsenic and molybdenum	Will remove trace elements mobilised by the CO_2 – rather than the CO_2 itself.	Cost and effectiveness will be important factors and cleans up trace elements rather than the CO_2.
PRB - Microbes	Microbes are used to clean up CO_2 contaminated soil and groundwater. Bioremediation uses microbes that use the CO_2 for food and energy.	Work is undergoing with Chlorella Microalgaen. Also coccolithophorid algae can carbon by photosynthesis as well as in calcium carbonate scales known as coccoliths.	There are a number of high CO_2 tolerant micro algae. Cyanidium caldarium - Seckbach et al. (1970); Scenedesmus sp. - Hanagata et al. (1992); Chlorococcum littorale -Kodama et al. (1993); Synechococcus elongatus -Miyairi (1995); Euglena gracilis - Nakano et al. (1996); Chlorella sp. -Hanagata et al. (1992); Eudorina spp. -Hanagata et al. (1992)	For bioremediation to be effective the right temperature, nutrients and food must be present, if conditions are not ideal it won't work

Remediation technique	Principles	Information	CO_2 applicability considerations	Pros / cons
PRB - Carbonation stabilisation	Contaminated groundwater and soil is mixed with binding agents that cause a chemical reaction with the CO_2 to trap it and reduce environmental release.	Carbonation is a strongly exothermic reaction and calcium carbonate ($CaCO_3$) is formed by the reaction between cementitious materials and CO_2	Mineral carbonation is one of technologies utilizing CO_2, and is used to form carbonated materials by the reaction between CO_2 and Ca or Mg-bound compounds such as wollastonite ($CaSiO_3$), olivine (Mg_2SiO_4), and serpentine	Reaction rates will determine effectiveness.
PRB – de-acidisation	Alkali materials are used as the reactive core in the permeable barrier such as; recycled concretes, limestone, oyster shells, calcite-bearing zeolitic breccias.	Banasiak and Indraratna (2012) describe the construction of a treatment wall which successfully neutralized the acidic groundwater from c. pH 3 to c. pH 7.3.	Treatment walls have been used to remediate acid mine drainage. and which can be considered to be a useable analogue for the remediation of groundwater acidified by the addition CO_2	Choice of reactive material will be site specific. Technology is established but needs further investigation for CO_2 remediation.

- Euglena gracilis - Nakano et al. (1996);
- Chlorella sp. - Hanagata et al. (1992);
- Eudorina spp. - Hanagata et al. (1992).

For bioremediation to be effective the temperature must be appropriate, and nutrients and food must be present; if conditions are not suitable then the technique will not work.

5.6.6 Summary of permeable reactive barriers (treatment walls) remediation measures

1. Treatment walls (PRB's) offer the potential to remediate both low pH and toxic metal mobilisation as a consequence of a shallow CO_2 leak;
2. The technology is well established from remediating other types of pollution, but has probably never been applied to the contamination of an aquifer by CO_2;
3. Costs may be substantial (millions of pounds) assuming that a barrier of km length needs to be constructed;
4. The choice of reactive material depends upon the toxic metals that have been mobilised, and is site-specific. The most suitable reactive material can be determined by experiment.

Table 8 presents a summary of the Permeable Reactive Barriers (treatment walls) remediation methods. The table presents a short summary of the principles of each technique, additional information, CO_2 applicability considerations and the technical pros and cons.

5.7 Remediation techniques (5) – Soil zone contamination

A number of techniques have been developed to treat contamination in the vadose or soil zone, and technologies can be considered to be mature with a 35 year history (Benson and Hepple, 2005; Zhang et al., 2004). Soil-vapour extraction and air sparging are the most common. IEA GHG (2007) suggest that large amounts of CO_2 could be removed with these technologies.

5.7.1 Soil-vapour extraction

Published models of soil-vapour extraction (SVE) with both analytical and numerical results enable good use of resources (Zhang et al., 2004 and refs. therein). Both active and passive methods (i.e. with and without powered pumping of the air, respectively) have been modelled (Zhang et al., 2004). Factors determining the effectiveness are (Zhang et al., 2004):

1. The intrinsic permeability of the porous medium – a high permeability is required to allow for a reasonable flow of air;
2. Soil water content – water saturation must be sufficiently low to allow the flow of air;
3. Henry's Law coefficient of the target compound – high solubility and low vapour pressure require higher (or longer duration) flow of air;
4. The ratio of horizontal to vertical permeability (kv/kh). A high ratio enhances the effective horizontal radius of a single well (Shan et al., 1992);
5. The anisotropy of the porous medium (Shan et al., 1992).

Where the water table is more than 3 m deep, then shallow boreholes are drilled into the very shallow subsurface (Fetter, 1999). The wells are completed with a slotted plastic well screen, but with a solid plastic casing for the top 1.5 m or so. The completed sections of the borehole are filled with course gravel backfill, to maximise air flow. The top portion of the borehole must be cemented with grout, so that the annular space is filled and air cannot be sucked down directly from the surface. Ground gas is pumped from the boreholes, and in the case of CO_2 would be vented to air as CO_2 capture would be prohibitively expensive. If very high concentrations of CO_2 were being remediated, then the CO_2-contaminated ground gas could be mixed with clean air, to reduce the CO_2 concentration, before the air is vented. Passive boreholes are also drilled, to enable the inflow of air from the atmosphere; these are also completed (perforated) only below c. 1.5 m depth (Figure 14).

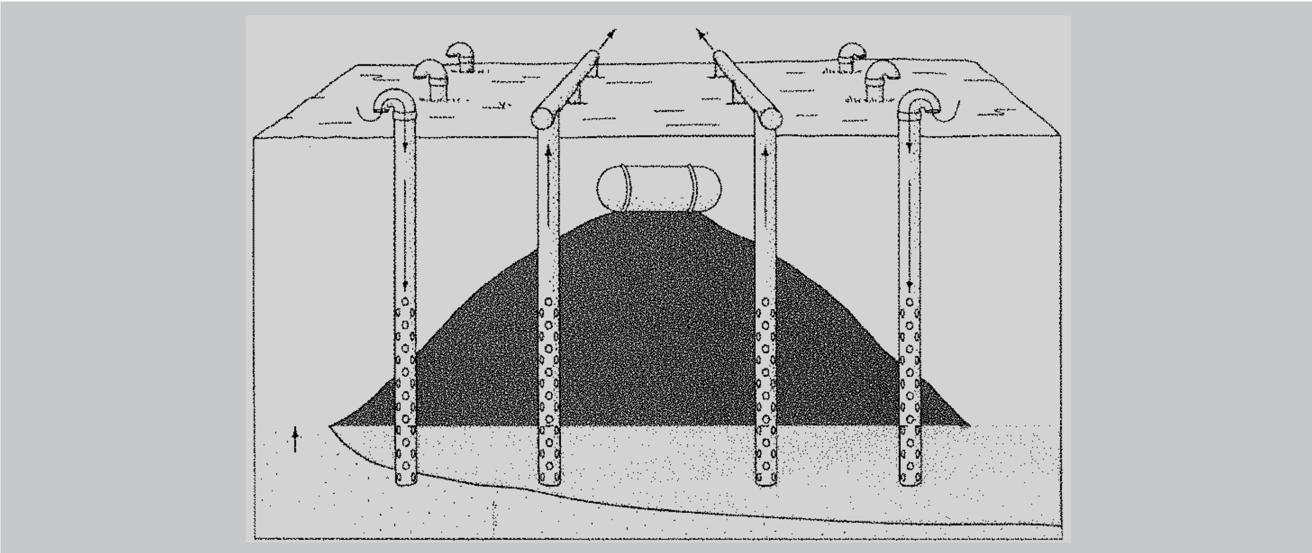

Figure 14 Soil-vapour extraction by boreholes for a groundwater table more than 3 m below the surface. From Fetter (1999).

If the water table is less than c. 3 m below the ground surface, then the borehole technique is not practical, and trenches can be used instead (Fetter, 1999). The trenches are excavated to just above the highest point that the ground water table is expected to reach, allowing for seasonal variation. A layer of gravel is laid in the excavated trench, followed by a perforated plastic pipe which is covered with gravel. The remainder of the trench is filled with a low permeability material, such as clay, to prevent air ingress direct from the atmosphere. Ground gas is actively pumped from the pipes. Passive trenches are also constructed, with a surface connection but no active pumping (see Figure 15), these allow the ingress of atmospheric air. If the CO_2 is contaminated with hydrocarbons (for example if the storage is in a depleted gas field) then the extracted vapours could be explosive when mixed with air. Suitable precautions must be taken in this circumstance.

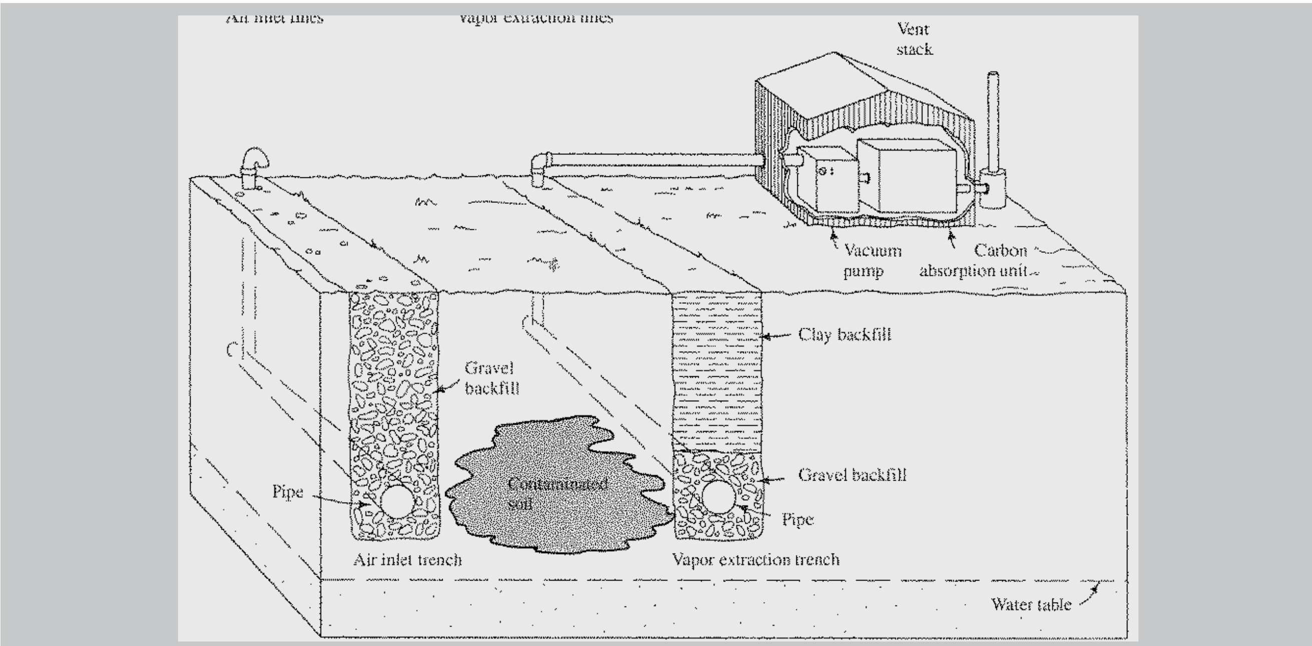

Figure 15 Trenches for the extraction of ground gas for shallow water tables. From Fetter (1999).

Zhang et al. (2004) concluded, from modelling CO_2 leakage scenarios, that standard passive and active soil vapour extraction will be effective for remediating potential CO_2 leakage plumes in the vadose zone. They found that:

1. In the scenarios modelled (Figure 16) the time required to half the concentration of CO_2 in the ground gas was from 0.27 – 2.5 years;
2. Movements of ground gas induced by natural variations in air pressure (barometric pumping) enhanced the modelled rate of removal compared to models with no barometric pumping;
3. Passive removal of CO_2 from high water saturation regions near the water table is limited by low gas saturation and high solubility in groundwater;
4. For vertical wells, the screen should not be too close to the water table;
5. An impermeable cover improves the removal rate;
6. A combination of both vertical and horizontal wells is more effective than either type alone;
7. High kv/kh results in a high rate of removal early on, but a lower rate in the letter stages.

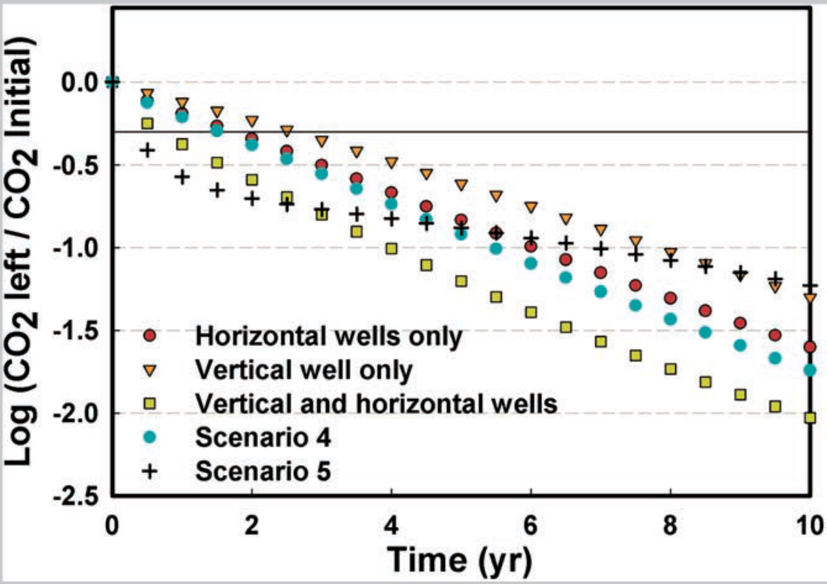

Figure 16 Remaining CO_2 vs. time, for soil-vapour extraction scenarios modelled scenarios by Zhang et al. (2004). Scenario 4 = longer horizontal well length; scenario 5 = higher kv/kh than scenarios 1 – 4.

5.7.2 Air sparging and bioslurping

Air sparging consists of injecting air below the water table. CO_2 dissolves in rising bubbles of air, as the two gases (mixtures) are fully miscible at the pressures and temperatures of interest. The volumes of air injected are 'small', and 2.5 cm diameter wells are sufficient. The system must be designed to avoid the air rising up the borehole casing (Fetter, 1999), instead an inverted cone of bubbles should be produced. In practise, the air bubbles follow pathways of high permeability, so that initial recovery rates are high, and quickly fall as the recovery becomes limited to diffusion. Air sparging can be used in conjunction with a vadose zone extraction system.

Vacuum-enhanced recovery, or bioslurping, uses both air and water to remove the CO_2. The well is designed so that the level of the water table can be depressed to close to the bottom of the well by groundwater removal, followed by pumping of the ground gas. The aquifer below the level of the depressed water table is remediated only by the extraction of the porewater (Fetter, 1999).

5.7.3 Addition of alkali to soil

If soil has become acidified from contact with leaked CO_2, then IEA GHG (2007, p. 132) suggest remediation by irrigation and drainage, or the addition of agricultural supplements such as lime.

5.7.4 In-situ thermal treatments

Thermal treatments mobilise CO_2 through heat towards wells where it is collected, (EPA 2012). There are three methods to generate heat:

1. Electrical resistance heating, where an electrical current passes between electrodes generating heat as the current meets resistance from the soil, converting groundwater into steam;
2. Steam enhanced extraction, where steam is injected underground by pumping;
3. Thermal conduction heating, where heaters in underground pipes heat the contaminated area.

CO_2-rich vapour is brought to the surface, and then it must be treated to remove the CO_2 before it can be re-injected. Toxic metals must also be removed before re-injection. Thermal treatments can take a few months to a few years to clean up a site. The clean-up time depends on the CO_2 concentration, area of contamination, depth of contamination variety of soil causing uneven heating and organic content of the soil which can cause the CO_2 to sorb rather than evaporate.

Table 9 Summary of the soil zone remediation methods.

Remediation technique	Principals	Information	CO_2 applicability considerations	Pros / cons
Gas collection trench	As CO_2 is a dense gas, a gas collection trench could collect the CO_2	Trench is filled with crushed rock and lined with a vapour barrier.	Widely used in landfill sites for methane gas collection, and should be applicable to CO_2.	Cheap and basic method to collect soil CO_2.
Ecosystem restoration	The process of returning a contaminated site to a natural environment, similar to that that existed before the leakage.	Done through fertilisers, nutrients and other soil amendments, restoring watercourses, planting native trees, shrubs etc and re-establishing wildlife.	Standard practise in mining remediation.	The final step in the remediation process.
Soil vapour extraction (SVE)	Contaminated vapours are removed from soil above the water table for treatment above ground by applying a vacuum to pull the vapours out. Vapours can be collected in boreholes if the water table is more than 3m deep and trenches if the water table is less than 3m deep.	One or more extraction wells are drilled above the water table which must be deeper than 3 feet below the ground surface. A vacuum pump creates a vacuum which pulls the air and vapours through the soil and up the well for surface treatment. Effectiveness is determined by permeability, soil water content and anisotropy of the porous medium.	Process is relatively quick and cheap but will depend on CO_2 concentration or volume. Does not trap the CO_2 as it is captured as a gas so will still need additional treatment.	Zhang et al. (2004) concluded, from modelling CO_2 leakage scenarios, that standard passive and active soil vapour extraction will be effective for remediating potential CO_2 leakage plumes in the vadose zone
Air sparging	Contaminated vapours are removed from below ground for treatment above ground. Air is pumped underground to help extract the CO_2 from groundwater and wet soil beneath the water table. Air facilitates the evaporation of CO_2.	Needs one or more injection well into the groundwater soil as air bubbles through the soil it carries the CO_2 vapour upwards into the soil above the water table – this mixture of air and vapour can be extracted for treatment using soil vapour extraction (SVE)	Process is relatively quick and cheap but will depend on CO_2 concentration or volume. Does not trap the CO_2 as it is captured as a gas so will still need additional treatment.	In practise, the CO_2 and air bubbles follow pathways of high permeability, so that initial recovery rates are high, and quickly fall as the recovery becomes limited to diffusion. Air sparging can be used in conjunction with a vadose zone extraction system.
Bioslurping / vacuum enhanced recovery	Uses similar techniques to air sparging, except it uses both air and water to remove the CO_2.	The well is designed so that the level of the water table can be depressed to close to the bottom of the well by groundwater removal, followed by pumping of the ground gas.	The aquifer below the level of the depressed water table is remediated only by the extraction of the porewater	In practise, the CO_2 and air bubbles follow pathways of high permeability, so that initial recovery rates are high, and quickly fall as the recovery becomes limited to diffusion. Bioslurping can be used in conjunction with a vadose zone extraction system.
Alkali to de-acidise soil / pH buffering	Soil that have been acidized by CO_2 could be remediated with irrigation, drainage and an alkali such as lime.	Irrigation, drainage and agricultural methods can deliver the alkali materials	IEA GHG (2007, p. 132) suggest remediation by irrigation and drainage, or the addition of agricultural supplements such as lime.	Including lime into the soil is a cheap and effective well tested method to de-acidise the soil.
In situ thermal treatment (steam)	Thermal treatments mobilise CO_2 through heat towards wells where it is collected. There are three methods to generate heat: Electrical resistance heating, steam enhanced extraction and thermal conduction heating.	Contaminated soil is heated to vaporise the CO_2 and water which means the gas CO_2 can move easily through the soil. Heat is generated by electrical resistance heating (electrical currents), steam enhanced extraction or thermal conduction heating (heaters)	CO_2-rich vapour is brought to the surface, and then it must be treated to remove the CO_2 before it can be re-injected. Toxic metals must also be removed before re-injection.	Thermal treatments can take a few months to a few years to clean up a site. The clean up time depends on CO_2 concentrations, area of contamination, depth of contamination variety of soil causing uneven heating and organic content of the soil which can cause the CO_2 to sorb rather than evaporate.
Capping	A cover is placed over the CO_2 contaminated soil	Concrete, vegetation, drainage layers, geomembranes or clay can be used as a cap material.	Capping does not remove or destroy the CO_2 but isolates it and keeps it in place to avoid or minimise contamination effects on the surface	A short term solution to prevent surface leakage.

5.7.5 Gas collection trench

As CO_2 is a dense gas, a gas collection trench could collect the CO_2 if the trench is filled with crushed rock and lined with a vapour barrier. The method is widely used in landfill sites for methane gas collection, and should be applicable to CO_2, Darnault (2008).

5.7.6 Capping

A cover is placed over the CO_2 contaminated soil. Concrete, vegetation, drainage layers, geomembranes or clay can be used as a cap material. Capping does not remove or destroy the CO_2 but isolates it and keeps it in place to avoid or minimise contamination effects on the surface (Oldenburg, 2008).

5.7.7 Ecosystem restoration

The process of returning a contaminated site to a natural environment, similar to that that existed before the leakage. Done through fertilisers, nutrients and other soil amendments, restoring watercourses, planting native trees, shrubs etc and re-establishing wildlife. The final step in the remediation process.

5.7.8 Summary of soil zone remediation measures

Table 9 presents a summary of the soil zone remediation methods. The table presents a short summary of the principles of each technique, additional information, CO_2 applicability considerations and the technical pros and cons.

5.8 Remediation techniques (6) – Bioremediation

Bioremediation is the process where a biological agent (bacteria, fungi, plant, enzyme) is used to reduce contamination mass and toxicity in the soil, groundwater and air. It is typically low cost, but bioremediation of CO_2 is yet to be fully tested. The factors affecting bio-remediation are (Shackelford and Jefferis 2000):

1. Microorganisms: Natural organisms are best as introduced organism may need acclimatised and suitable environmental conditions may need to be provided;
2. Toxicity: need non-toxic conditions;
3. Water: 25-85% water holding capacity desirable in the soil;
4. Oxygen: Aerobic conditions required, which may be a problem if CO_2 concentrations are too high and oxygen may need to be added;
5. Electron acceptors: O_2 (aerobic conditions); NO^{3-}, Fe^{3+}, Mn^{2+}, and SO_4^{2-} otherwise;
6. pH: 5.5 – 8.5 is optimum;
7. Nutrients: N, P and other nutrients required for microbial growth;
8. Temperature: affects degradation rates.

5.8.1 Bioremediation of hydrocarbon contamination

If the leaking CO_2 has encountered high concentrations of hydrocarbons, then these may have mixed or evaporated into the CO_2 phase. This is perhaps most likely where the primary storage reservoir of a CCS scheme is a depleted hydrocarbon field, especially a gas field or an oil field with a light (volatile) oil. Bioremediation generally uses in-situ microbes, the majority of which are bacteria that are absorbed onto the surfaces of rock and soil particles (Fetter, 1999). Bacteria that can degrade hydrocarbons are thought to be ubiquitous in the subsurface (Atlas, 1975). The principle is to add 'food' i.e. nutrients for the bacteria, to speed up what are otherwise natural biodegradation processes. The nutrient requirements of the native bacteria must be determined by culturing in a laboratory, and the experiments should attempt to reproduce the conditions of the subsurface as accurately as possible. Nutrients are added in varying proportions and concentrations to different cultures, and the rate of degradation of the contaminant is measured. Carbon can be added as methanol or molasses for example (Fetter, 1999).

If the hydrocarbons are in the soil zone, then the nutrients must be injected below the root zone of any plants growing on the site, otherwise the main effect will be to fertilise the plants! An infiltration gallery (a structure to contain water and direct it into the soil) is built above the contaminated zone, and periodically filled with water in which the optimum nutrients are dissolved, along with oxygen. Additional oxygen is allowed to diffuse into the soil when the infiltration gallery dries out between flooding events; or can be added by sparging with air or pure oxygen; or through the use of hydrogen peroxide. The latter can be toxic to micro-organisms so cannot always be utilised. Active recovery of ground water from shallow boreholes can be used to encourage the circulation of pore water in the remediation zone. In many cases, the only nutrient that need be added is oxygen, which can be circulated by soil-vapour extraction. If the soil is dry, then humid air may be used (Fetter, 1999).

5.8.2 Bioremediation of low pH groundwaters

Bacterial activity within groundwater could be artificially increased by the injection of urea, which can increase pH (Dupraz et al. (2009) and potentially remediate the effects of dissolved CO_2. Calcite may be precipitated as a by-product, though in a real aquifer the supply of calcium ions would presumably limit this process. It is unknown whether this technique has ever been tested outside of a laboratory. Ménez et al. (2007) list several mechanisms by which bacteria may alter pH:

1. Remove CO_2 by e.g. photosynthesis, clearly restricted to the very shallow subsurface and is involved in the precipitation of travertine and tufa;
2. Generate CO_2 by aerobic or anaerobic oxidation of organic matter, allegedly resulting in the precipitation of calcite;
3. Generate CO_2 and ammonia by aerobic or anaerobic oxidation of nitrogen compounds, increasing pH and triggering the precipitation of calcite;
4. Generate CH_4 or acetate from CO_2, an important process in the subsurface;
5. Reduce sulphate anaerobically, promoting calcite precipitation.

5.8.3 Bioremediation of dissolved toxic metals

Several studies have suggested that it may be possible to remove toxic metals that are in solution in porewaters by incorporating the metals into calcite precipitated through bacterial action (Fujita et al., 2000; Warren et al., 2001; Mitchell and Ferris, 2005). The technique is likely to be effective only for divalent ions (e.g. Pb, Zn, Ba, and Cd) and radionuclides (e.g., ^{90}Sr and ^{60}Co). The technique may be

Table 10 Summary of the bioremediation methods.

Remediation technique	Principles	Information	CO_2 applicability considerations	Pros / cons
Bioremediation of low pH groundwaters	CO_2 acidises the soil and bacteria activity can be used to remediate this acidisation.	Bacterial activity within groundwater could be artificially increased by the injection of urea, which can increase pH (Dupraz et al. (2009) and potentially remediate the effects of dissolved $_{CO2}$	Bacteria may alter pH by removal of CO_2 by photosynthesis, generate CO_2 by aerobic oxidation of organic matter, generate CO_2 and ammonia by aerobic oxidation of nitrogen compounds, generate CH_4 from CO_2, reduce sulphate anaerobically promoting calcite precipitation.	Small area of effect and long time scale inhibits effectiveness.
Bioremediation of CO_2	Microbes are used to clean up CO_2 contaminated soil and groundwater. Bioremediation uses microbes that use the CO_2 for food and energy.	Work is undergoing with Chlorella Microalgaen. Also coccolithophorid algae can carbon by photosynthesis as well as in calcium carbonate scales known as coccoliths.	There are a number of high CO_2 tolerant micro algae. Cyanidium caldarium - Seckbach et al. (1970); Scenedesmus sp. - Hanagata et al. (1992); Chlorococcum littorale - Kodama et al. (1993); Synechococcus elongatus -Miyairi (1995); Euglena gracilis - Nakano et al. (1996); Chlorella sp. -Hanagata et al. (1992); Eudorina spp. -Hanagata et al. (1992)	For bioremediation to be effective the right temperature, nutrients and food must be present, if conditions are not ideal it won't work.
Bioremediation of toxic metals	Studies have suggested that it may be possible to remove toxic metals that are in solution in pore waters by incorporating the metals into calcite precipitated through bacterial action.	The technique is likely to be effective only for divalent ions (e.g. Pb, Zn, Ba, and Cd) and radionuclides (e.g., ^{90}Sr and ^{60}Co).	The technique is likely to be effective only for divalent ions (e.g. Pb, Zn, Ba, and Cd) and radionuclides (e.g., ^{90}Sr and ^{60}Co).	Small area of effect and long time scale inhibits effectiveness.
Bioremediation of hydrocarbons	If the leaking CO_2 has encountered high concentrations of hydrocarbons, then these may have mixed or evaporated into the CO_2 phase.	Bacteria that can degrade hydrocarbons are thought to be ubiquitous in the subsurface. Bacteria that can degrade hydrocarbons are thought to be ubiquitous in the subsurface.	The nutrient requirements of the native bacteria must be determined by culturing in a laboratory, and the experiments should attempt to reproduce the conditions of the subsurface as accurately as possible. If the hydrocarbons are in the soil zone, then the nutrients must be injected below the root. In many cases, the only nutrient that need be added is oxygen, which can be circulated by soil-vapour extraction. If the soil is dry, then humid air may be used	Tested method within hydrocarbon clean-up.
Natural attenuation	The process of immobilizing, retarding, or degrading the CO_2 contaminants in the soil or ground water that results from geochemical interactions between the natural geological material and chemical constituents in the ground water.	Natural geochemical attenuation mechanisms can include cation and anion exchange with clays, adsorption of cations and anions on hydrous metal oxides (e.g., iron and manganese oxides), sorption on organic matter or organic carbon, precipitation of metals from solution, and co-precipitation by adsorption.	CO_2 has a high propensity to adsorb onto organic carbon.	Natural attenuation has high costs associated with monitoring as the site needs to be monitored to determine whether or not natural attenuation processes will remediate the site, or whether enhanced remediation steps need to be taken.

more effective than precipitation by redox reactions, whereby previously co-precipitated species may be inadvertently liberated into pore waters (Mitchell and Ferris, 2005). Bacterial precipitation of calcite through ureolysis (the hydrolysis of urea to ammonium and carbon dioxide) has also been proposed as a method of selectively reducing porosity and permeability in the subsurface (Ferris et al., 1996; Stocks-Fischer et al., 1999) and for the removal of calcium from industrial wastewater (Hammes et al., 2003).

5.8.4 Natural attenuation

Natural attenuation can be defined as the process of immobilizing, retarding, or degrading the CO_2 contaminants in the soil or ground water that results from geochemical interactions between the natural geological material and chemical constituents in the ground water (Rouse and Pyrith 1993). Natural geochemical attenuation mechanisms can include cation and anion exchange with clays, adsorption of cations and anions on hydrous metal oxides (e.g., iron and manganese oxides), sorption on organic matter or organic carbon, precipitation of metals from solution, and co-precipitation by adsorption. With regards to CO_2, it has a high propensity to adsorb onto organic carbon.

An assessment of the extent to which geological materials will attenuate the migration of CO_2 in the soil or ground water requires knowledge of:

1. The properties and mineralogy of the geological material (porous medium);
2. The properties of the contaminated ground water; and
3. The chemical conditions (e.g., pH and Eh) that are established during contact of the contaminated groundwater with the geological material.

Natural attenuation has high costs associated with monitoring as the site needs to be monitored to determine whether or not natural attenuation processes will remediate the site, or whether enhanced remediation steps need to be taken.

5.8.5 Summary of bioremediation measures

Table 10 presents a summary of the bio-remediation methods. The table presents a short summary of the principles of each technique, additional information, CO_2 applicability considerations and the technical pros and cons.

5.9 Remediation techniques (7) - Residential buildings

The problem of ground gas entering residential and other buildings has a long history, which has in extreme cases caused entire settlements to be demolished and rebuilt in safer areas at high cost, e.g. Arkwright Town in Derbyshire, UK, at a reported cost of 15 M GBP (value in 1990's; Independent, 1994) . The main gases of concern are methane, radon and CO_2, all of which can be ultimately fatal to humans. It is the case that the majority of experience of ground gas remediation (at least in the UK) concerns radon gas, and to a lesser extent, methane. There seems to be no accessible literature (at least in English) concerning CO_2 ingress into buildings in Italy for example, which is well known as the location of numerous natural CO_2 leakage sites. In the UK, the remediation of ground gas penetration into buildings is covered by British Standard BS 8485:2007 (BSI, 2007), though it is clear that the code is designed for gas generated at shallow depths of burial such as methane from landfill, rather than CO_2 escaping from a deep source. Ground gas enters a house or other building by a variety of pathways, Figure 17.

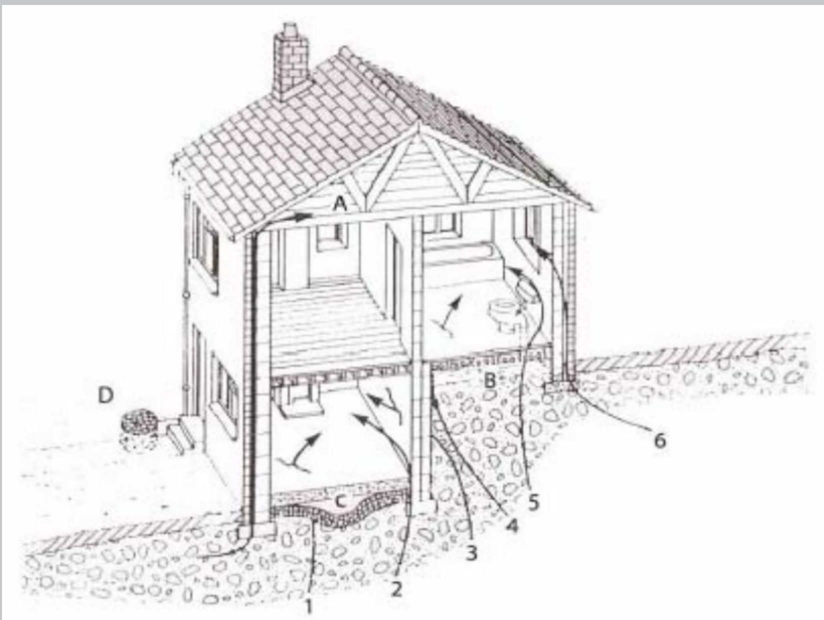

Figure 17 Typical pathways for ground gas to enter a house or other building. From CIRIA 149 (1995) in NHBC (2007).

The process of characterisation and remediation is summarised as follows, with comments regarding the applicability to CO_2 remediation from a leaking deep storage site (BSI, 2007):

1. Desk study to construct a conceptual model of the gas sources and likely migration pathways. This should include the history and current use of the site; the geology and hydrogeology of the site; and the buildings (receptors) that are or could be affected;
2. A site walk-over study or reconnaissance;
3. Site investigation;
4. Geology and hydrogeology; made-ground; contamination; source of gas. Boreholes and trial pits are suggested though these may be more appropriate to shallow gas sources than to a leaking deep CO_2 source;
5. Install monitoring installations adequate to determine gas source and migration pathways, and likely receptors. Frequency and duration of monitoring must be sufficient to characterise changes in the gas regime due to changes in ambient conditions;
6. Gas flow rate and concentration must be assessed adequately, including measurements when atmospheric pressure is falling;
7. Estimation of an indicative gas flow rate for the entire site, or rates for each section of the site if division if required (known as 'site characteristic hazardous gas flow rate' or 'gas screening value'). This is ranked on a scale of 1 – 7 which implies a level of assessed hazard.
8. Choice of remediation solution. The factors involved are:
   a. Characteristic gas situation;
   b. Construction of foundations and ground slab (if any);
   c. Size (especially width) of building;
   d. Use of building (e.g. domestic or industrial, room size and degree of control over utilisation);
   e. Management of gas control facilities and service provision;
   f. Views of client or building owner.

The process of selection should be transparent. BS8485:2007 recognises that off-site remediation may be the most appropriate, i.e. it may be possible to intercept the leaking gas between the source and the affected buildings (see remainder of this report for appropriate technologies) rather than intervene at the buildings themselves.

Robinson (2010) reports on attempts to prevent CO_2 ingress into a home from subsurface sources, in this case from the reclaimed coal-mine spoil upon which the house was built. The CO_2 concentrations within the building were found to correlate with external weather-related conditions, with the first two being the strongest predictors:

1. Rapid drops in barometric pressure;
2. Rainfall;
3. Windy conditions;
4. Cold weather.

There are at least ten different systems that might be adopted to prevent the build-up of CO_2 in a basement or other parts of a building, at least some of which consist of simply increasing the amount of ventilation within the utilised space of the building (as opposed to non-utilised space e.g. crawl ways, wall cavities). Some of these are taken from the literature concerning the ingress of radon into houses as experience with CO_2 ingress is relatively limited. These remediation techniques must all be used in conjunction

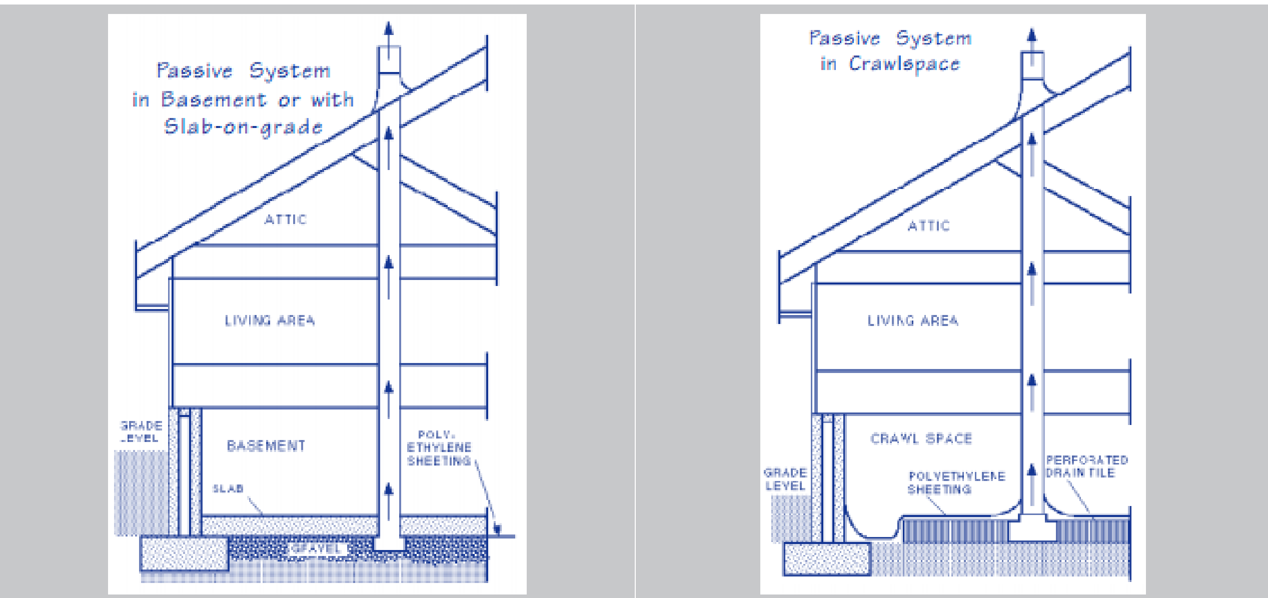

Figure 18 Passive sub-slab (left diagram) or sub-membrane (right diagram) depressurization system (Hodgson, 2011).

with a programme of sealing of all likely joints, cracks and surfaces whereby CO_2 might enter a building; the installation of gas-proof floor drains and sump-pit covers (Robinson, 2010) and, at least in some cases, the sealing of the loft hatch to reduce the upward flow of air within the house (Hodgson et al., 2011). Note that, in the case described by Robinson (2010), none of the techniques successfully prevented the ingress of CO_2 during adverse weather conditions, and that the analysis of Hodgson et al. (2011) gave success rates for radon remediation of 35 – 74 % (to below the legal safety limit). Indicative costs vary from 200 – 800 GBP per installation guideline (excluding the demolition option 8, below), with a maximum of 2,000 GBP for an actively pumped radon sump (UKRadon, 2014). The size of the building, the complexity of the floor construction, and the surface upon which the building is cited are presumably factors determining cost. The techniques are briefly described:

5.9.1 Passive sub-slab or sub-membrane depressurization system

Passive sub-slab (Figure 18 left) or sub-membrane (Figure 18 right) depressurization system (EPA, 2001) are also known as a 'passive sump' (Hodgson, 2011). This should reduce the gas concentration below the floor slab to acceptable levels, i.e. not just in the occupied volume of the building (BSI, 2007). The vented layer can be open void, or constructed from gravel, geocomposites, polystyrene or other materials (BSI, 2007).

5.9.2 Active sub-slab or sub-membrane depressurisation system

This method is also known as an 'active sump' Figure 19 ((EPA, 2001; Hodgson, 2011). This should reduce the gas concentration below the floor slab to acceptable levels, i.e. not just in the occupied volume of the building (BSI, 2007). The effectiveness of membranes is crucially dependant on the design of the installation, the resistance to damage after installation, and the quality of any seals (BSI, 2007):

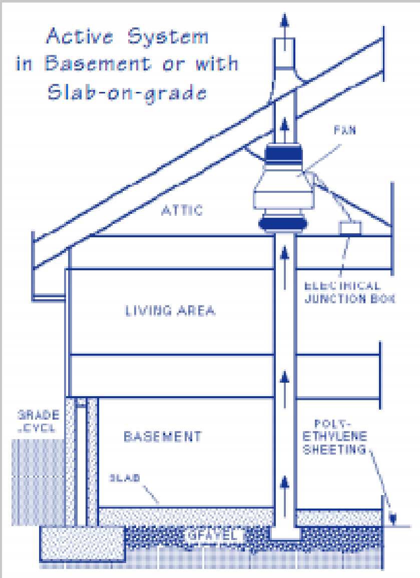

Figure 19 Active sub-slab or sub-membrane depressurisation system (Hodgson, 2011).

5.9.3 Block-wall depressurisation

A hole is drilled into the wall surrounding the basement (which must be of the cavity type), and a pipe and fan attached, venting the air at a safe height above the basement (Robinson, 2010).

5.9.4 Block-wall and sub-slab pressurisation

Similar to the above (3) but with the air flow reversed, and with a further pipe allowing the air access to below the basement slab (Robinson, 2010).

5.9.5 Positive ventilation

A fan in the roof space blows air into the living space, increasing ventilation, and presumably slightly increases the air pressure within the house so reducing the flow of CO_2 into the dwelling (Hodgson et al., 2011).

5.9.6 Natural under-floor ventilation

Under-floor ventilation is increased by clearing or replacing airbricks with modern vents and / or increasing the number of vents (Hodgson et al., 2011).

5.9.7 Passive ventilation

Trickle vents in windows increase ventilation (Hodgson et al., 2011).

5.9.8 Positive pressure

A fan blows air into the basement, increasing the air pressure and preventing the ingress of external CO_2 (Fetter, 1999). Not suitable for climates where the outside air is below freezing in winter, otherwise the cold air can cause water pipes within the basement to freeze. Probably for this reason the technique is absent from current USA and UK sources of information. Ventilation installed in a car park located in a basement or undercroft is likely to be both adequate and highly effective (BSI, 2007).

5.9.9 Demolish the buildings and rebuild

If all other options fail, then the only option may be to demolish the buildings and rebuild to a standard to prevent CO_2 ingress following standards set by for example Scivyer (2007) and other reports by the UK's Building Research Establishment (BRE, http://www.bre.co.uk/), or by the National House-Building Council (NHBC, 2007). This option has recently been adopted for a group of houses affected by CO_2 ingress in Gorebridge, Scotland (BBC News, 2014). The cost of rebuilding the houses has been reported as being 12 M GBP (June 2014). The removal of the village of Arkwright town (UK), in the 1990's was of comparable cost as described above. The inflation-adjusted cost would presumable be substantially higher than the Gorebridge case.

For many of the techniques described above, as with some other domestic building work, it is possible to 'Do It Yourself' to some extent, and that the work could potentially be conducted by contractors with varying levels of relevant experience. The Radon Council (UK) note that 'Some techniques, such as the use of extract fans to increase ventilation can in fact exacerbate the problem and cause greater volumes of the gas to be drawn into the property. It would therefore be unwise to place such responsibility in the hands of an unskilled contractor.' (http://www.radoncouncil.org/ testing.html). An analysis of the effectiveness of a variety of

Table 11 Summary of the building remediation methods

Technique	Principles	Information	CO_2 applicability considerations	Pros / cons
Passive vapour intrusion mitigation	Prevents the entry of CO_2 vapours into buildings.	Sealing of all openings or vapour entry points. Installing vapour barriers of geomembrane or plastic beneath buildings to prevent vapour entry.	Applicable to CO_2 vapour intrusion. Permanent monitoring and alarm systems should be installed in the building	Cheap
Passive / active sub slab venting	A venting layer is built beneath a building so vapours move through the venting layer towards the sides and vented outside.	Passive venting can be by passive sub slab or sub membrane with porous sub base vented to the outside. Active sub slab or sub membrane with fan extraction venting from below the sub slab	Applicable to CO_2 vapour intrusion. Permanent monitoring and alarm systems should be installed in the building	Cheap
Active vapour intrusion mitigation - Subsurface pressurisation	The pressure difference between the subsurface and inside of the building keeps the CO_2 vapours out.	Subslab depressurisation involves linking a fan to a small pit dug into the basement to vent the vapours outside. Building overpressurisation involves adjusting the heating, ventilation and air conditioning to increase the pressure indoors relative to that of the basement area.	Applicable to CO_2 vapour intrusion. Permanent monitoring and alarm systems should be installed in the building	Effective
Block wall depressurisation	A hole is drilled into the wall surrounding the basement (which must be of the cavity type), and a pipe and fan attached, venting the air at a safe height above the basement	This can be combined with sub slab pressurisation but with air flow reversed and a further pipe allowing the air access to below the sub slab.	Applicable to CO_2 vapour intrusion. Permanent monitoring and alarm systems should be installed in the building	Effective
Positive ventilation / pressure	Air is blown into the living space increasing ventilation and air pressure in the house, reducing the flow of CO_2 into the house.	Ventilation and air pressure is increased, reducing CO_2 ingress.	Applicable to CO_2 vapour intrusion. Permanent monitoring and alarm systems should be installed in the building	Effective
Natural underfloor ventilation / passive ventilation	Trickle vents in windows and air vents in the building base walls increase ventilation	Ventilation is increased, reducing CO_2 ingress.	Applicable to CO_2 vapour intrusion. Permanent monitoring and alarm systems should be installed in the building	Effective
Demolish building and rebuild to a standard preventing CO_2 ingress.	This option has recently been adopted for a group of houses affected by CO_2 ingress in Gorebridge, Scotland (BBC News, 2014). The cost of rebuilding the houses has been reported as being 12 M GBP (June 2014).	Re-build to standards set by UK's building research Establishment or National House Building Council.	Prevents future CO_2 intrusion.	Expensive

techniques, in the context of radon, did not attempt to distinguish between DIY or professional installation, or of the competence of the professional contractors (Hodgson et al., 2011). In the context of CO_2 remediation, the DIY issue is probably not relevant. However, the experience of any contractors, most probably gained in the field of radon or methane gas remediation rather than CO_2, might be a factor in deciding effectiveness and ultimately, costs. It is here assumed that ineffective remediation will require further work, and ultimately, further costs.

Monitoring of CO_2 levels after remediation can be achieved using hand-held equipment at suitable intervals, though BSI (2007) regards this as a low-effectiveness strategy. They suggest permanent monitoring and alarm systems should be installed in the building, and preferably in the venting or diluting system itself (BSI, 2007).

5.9.10 Summary of building remediation measures

1. The cost of remediation for a home is small on the scale of the other costs in a CCS scheme, unless demolition and rebuilding is the only effective option;
2. Based on very limited experience with CO_2, and much more experience with radon gas, the success rate of remediation is only around 50 %;
3. Monitoring of CO_2 levels must be over a protracted period of time (weeks or months), as concentration depends upon external factors such as temperature and rainfall;
4. Remediation can be a lengthy process, as different (and progressively more expensive) techniques are employed;
5. Contractors with relevant experience are preferred.

Table 11 presents a summary of the building remediation methods. The table presents a short summary of the principles of each technique, additional information, CO_2 applicability considerations and the technical pros and cons.

5.10 Principles for remediation technologies screening and costs analysis

In order to propose a realistic approach for the selection of appropriate CO_2 leakage remediation technologies, analogue approaches from the contaminated land remediation field have been reviewed. The most comprehensive approach is the Remediation Technologies Screening Matrix and Reference Guide, 4th Edition which has been developed by the Federal Remediation Technologies Roundtable (FRTR) in the USA (http://www.frtr.gov/matrix2/top_page.html).

This concept will be further investigated and refined for CO_2 leakage remediation during the Mirecol project using the treatment technologies screening matrix proposed by the FRTR and the Remedial Action Cost Engineering and Requirements (RACER) software as a starting point. RACER was developed under the direction of the U.S. Air Force for estimating environmental investigation and cleanup costs. The most recent version 11.2 was released in October 2014 by AECOM (the company maintaining the software, http://www.aecomassetmanagement.com/index.php/racer/) and is available for download.

Similar to contaminated land remediation, the characteristics of the CO_2 leakage remediation site and the specific operating conditions are expected to affect significantly the performance of each technology as well as the costs of implementation. In addition, the relevant factors to each remediation technology-are specific to the technique. Therefore, it is difficult to estimate the costs accurately.

For this reason, it is proposed that technology costs to be estimated in Mirecol may be classified in coarse relative cost categories (above average, average and below average) using the expected technology specific capital costs and the operating/maintenance costs. Technology performance will likely be evaluated in terms of remediation reliability and maintainability, time to implementation, availability and the technology development status (maturity).

6 REMEDIATION AND MONITORING OF CO_2 LEAKAGE FROM THE BEČEJ FIELD, SERBIA

The Bečej field is located in the northern part of Serbia, about 130 km north of Belgrade. The field was discovered in 1951 and named after Bečej, a city located nearby. The field is located in the southeastern part of the Pannonian basin and its geologic structure is complex. The reservoir fluid consists of CO_2 (87-94 mol %), hydrocarbons C1-C7 (3.80 - 7.54 mol %) and nitrogen (1.83 - 5.31 mol %). At the surface, the total dissolved salt content of the formation water is 4.4 g/l; the water is slightly acidic (pH=6.6) because of the residual dissolved carbon dioxide. Under reservoir conditions, the CO_2-saturated water is much more acidic; chemical analysis of those samples indicated 58.2 g/l TDS and presence of high amount of free and dissolved CO_2. The CO_2 pool of the Bečej field is in the heterogeneous massive reservoir of Upper Cretaceous flysch and Badennian sedimentary deposits. The reservoir is located along a regional fault zone, along which felsic igneous rock was intruded, which generated carbon dioxide during metamorphism of the country rock. The lower part of the reservoir is formed of Upper Cretaceous siltstones, marlstones and very fine grained sandstones which lay transgressively over Paleozoic basement of metamorphic and igneous rocks. The upper part of the reservoir consists of shallow marine Badennian (middle Miocene) facies such as fine to medium grained sandstones composed of mineral, rarely rock or organic detritus with calcite cement and organic limestones.

The Badennian rocks are overlain unconformably boundary by the Lower Pontian (uppermost Miocene) marlstones, clayey and marly sandstones and clays deposited in caspi-brackish condition. Sedimentation continued throughout the Upper Pontian and during that period the caspi-brackish depositional environment gradually altered to lacustrine. The sediments are alternating poorly cemented sandstones and clayey sandstones and marlstones in the lower part of the unit, while sands and clays dominate in upper part. Laminae of coal and coaly clays are very frequent. Over the course of the Pliocene and Quaternary the depositional environment changed from lacustrine to fluvio-lacustrine, fluvial and aeolian environment. During these periods layers of alternating sands and clays and their varieties were deposited. Geological cross sections of the Bečej area are shown in Figure 20.

The Upper Pontian and Pliocene sandstones and sands have great significance as very porous and permeable rocks saturated with hydrocarbon gasses and geothermal groundwater. Small reservoirs of methane were also explored through the drilling of several wells, these gave positive results but all the wells were abandoned after the CO_2 of the gas increased. On the basis of seismic surveying, a total of eight small hydrocarbon reservoirs are defined with a depth range from 450 to 900 m.

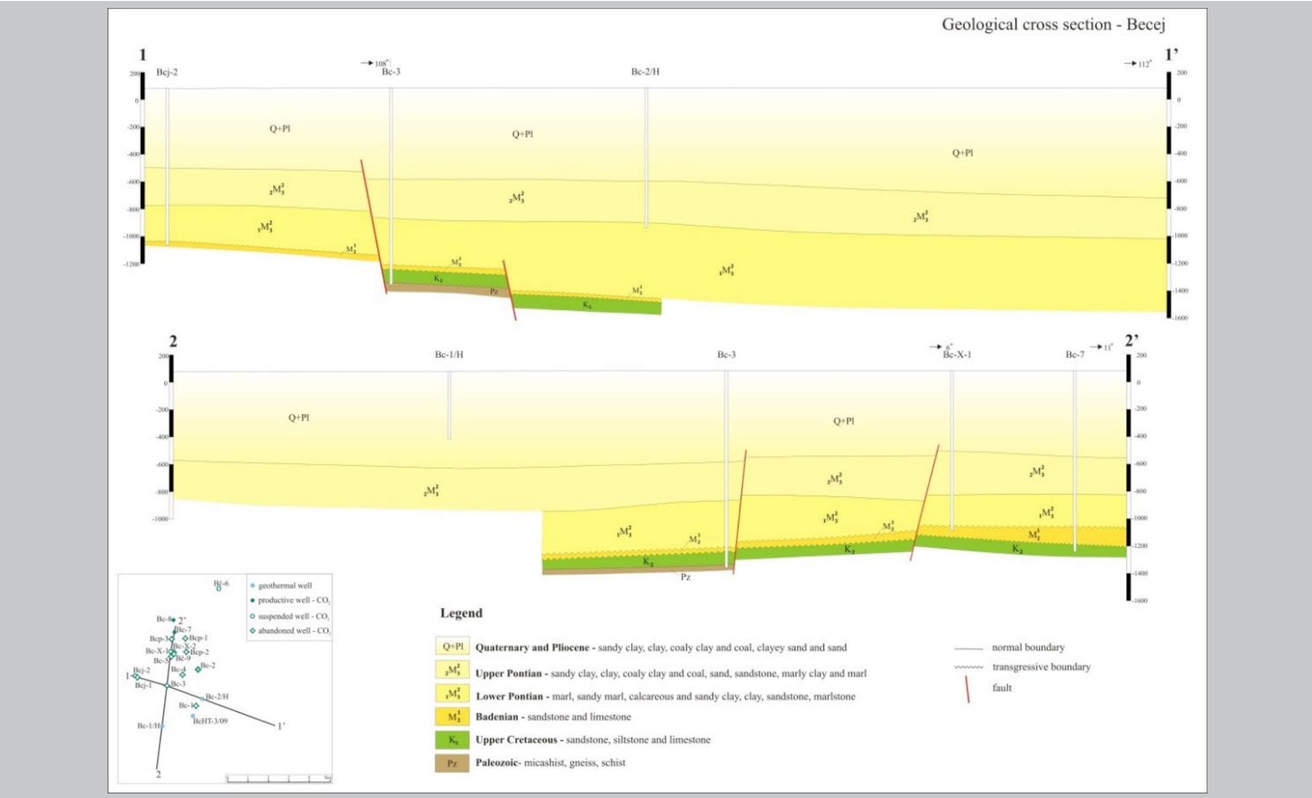

Figure 20 Geological cross-sections of the Bečej field.

Beside the hydrocarbon reservoirs, geothermal groundwater is an important mineral resource, with a long history of exploitation. All the geothermal wells are artesian flowing wells because they are tapping confined aquifers saturated with water and gas, dominantly methane. Water from aquifers at 400 m depth has a temperature of 35 °C and it has been used for drinking and bathing in Bečej spa more than hundred years. The deep wells provide waters of 60 to 65 °C used for space heating of the hotel and sport center in Bečej.

A blowout of CO_2 in the Bečej field happened during the drilling of well Bč-5 at a depth of 1093.25 m and uncontrolled leakage lasted from 10.11.1968 until 06.06.1969. Carbon dioxide leaked to the surface; however, the total amount of gas leaked from the reservoir was estimated to be tens of times larger than the surface emissions. The borehole collapse, which caused the self-killing of the well and the cessation of leakage to the atmosphere, but the process of gas migration from the reservoir was not stopped. The seepage of CO_2 gas continued into the shallower aquifers above the CO_2 reservoir.

The impact was closely monitored because of the vicinity of a populated area and with special attention to gas migration in groundwater reservoirs, especially in an unconfined aquifer. The monitoring objectives involved more than 30 wells with depths in the range from 10 to 300 with a radius of 1000 m around well Bč-5. The new remediation wells Bč-X-1 and Bč-X-2 were drilled in 1969 for pressure measurements in the reservoirs at depths from 740-850 m.

6.1 Blowout of CO_2 from well Bč-5 and applied methods of remediation and monitoring

Based on the analysis of collected data, the event was divided into seven phases:

1. Phase I - 10.11.1968 up to 17.05.1969

A concentration of 10 % CO_2 in gas was measured in an unconfined aquifer with decreasing concentrations as the distance from the source of leakage increased. The cause of the high concentration was spilling of gas on the surface covering an area of 3 km × 0.3 km toward the channel Mrtva Tise. In this area the CO_2 concentration in the air was up to 50 %. The leakage of gas was primarily through a surface crater formed at the location of well Bč-5 (Figure 21). The impact on the confined aquifers, subartesian or artesian, was not known at this stage.

Figure 21The blowout of CO_2 on well Bč-5.

2. Phase II - 17.05.1969 to 06.06.1969

The process of the seepage of CO_2 into the shallow aquifers resulted in the bubbling and raising of water levels in monitored water wells, while the intensity of leakage to the atmosphere reduced. Higher concentrations of CO_2 caused the formation of small ponds on the surface around the crater during this stage.

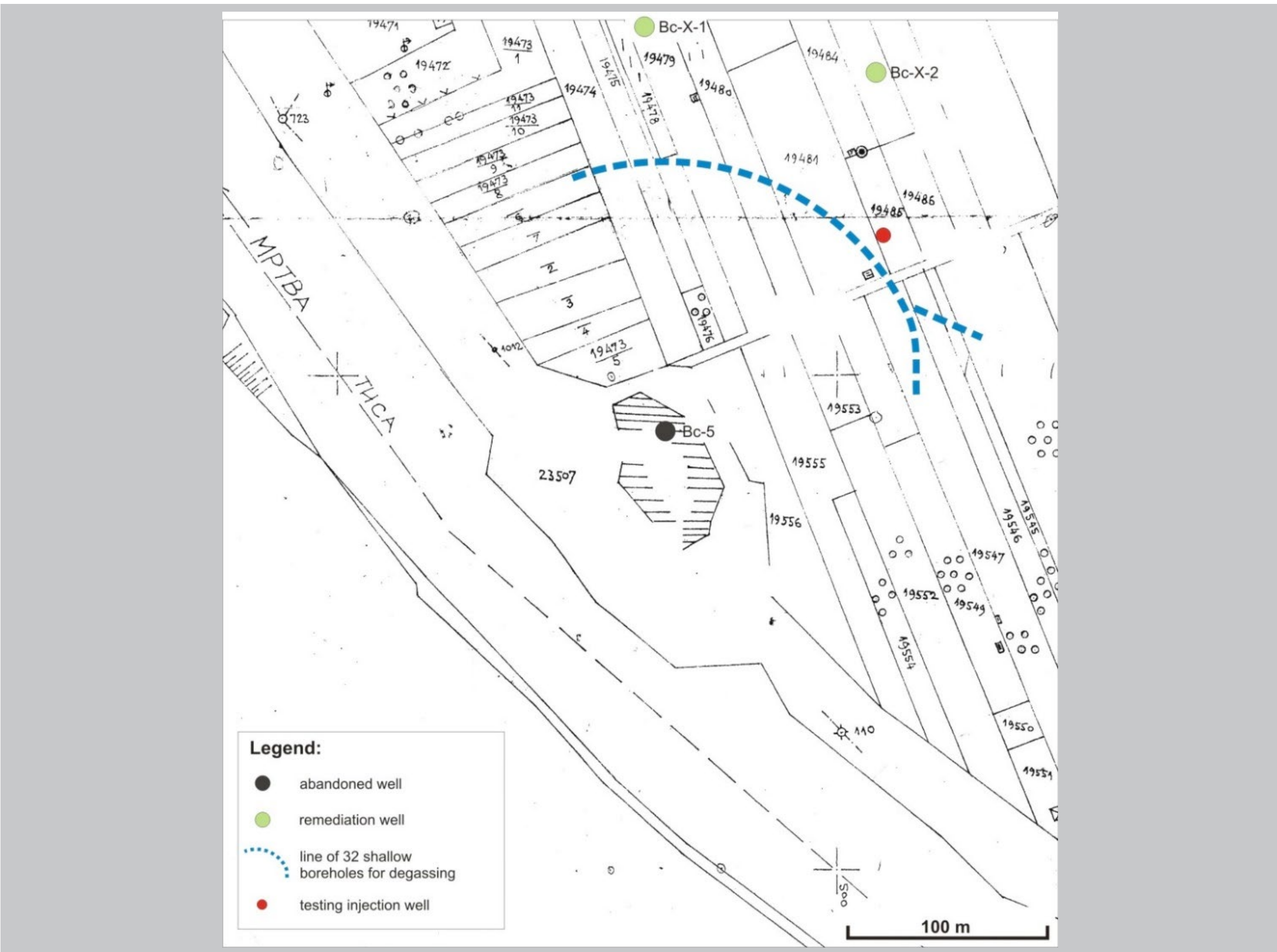

Figure 22 The position of boreholes for degassing of groundwater and soil.

This period can be divided into four stages:

- Stage 1. – The main characteristics of this stage are bridging of the borehole by produced formation solids, the suppression of eruptions within the crater and the highest rate of gas seepage into the unconfined aquifer. The gas intrusion was progressing toward the drilling sites of two new remediation wells Bč-X-1 and Bč-X-2. To prevent further advancement of the gas a line consisting of 32 shallow boreholes for the degassing of groundwater and vadose zone was installed. The boreholes were at a distance of 135 m in the north and east direction from the damaged well Bč-5 (depth of boreholes range from 10 to 15 m). The degassing processes manifested in intensive venting and eruptions of gasified water. Since the method of degassing through shallow wells was successful and enough to stop the flow path that carried the CO_2, additional measures such as the idea of creating a grout curtain was abandoned (Figure 21). The end of the seepage into the unconfined aquifer was registered on 02-03.06.1969.
- Stage 2. – The bridging in the wellbore happened at a depth of 50 m that had influence on the confined aquifers laying between 50 and 130 m. The frequency of great eruptions reduced and was gradually replaced with bubbles that often occurred on the surface of the pond formed on the site of the well.
- Stage 3. – The bridging in the wellbore happened at a depth below 150 m that caused a sudden decrease of water level in subartesian water wells on 04-05.06.1969.
- Stage 4. – The wellbore collapse stopped the eruption on 06.06.1969. Since there was no record of increase of the capacity of the monitored artesian water wells up to 300 m depth the conclusion was that collapse probably occurred in wellbore at depths between 320 and 825 m.

3. Phase III - period from 06.06.1969 to 03.08.1969

During this period no influences on aquifers up to 300 m were recorded.

4. Phase IV - period from 03.08.1969 to 08.05.1970

Pressure monitoring started at the newly drilled wells Bč-X-2 and Bčp-2 and a significant increase of pressure was measured in the "hydrocarbon reservoir I" at 825-832 m in well Bč-X-2. The well produced periodically at different production rates during the beginning stage of monitoring period and the CO_2 content in the gas composition increased from 1.2 to 22 mole% in three weeks.

5. Phase V - period from 08.05.1970 to 08.12.1970

The monitoring of CO_2 migration from the reservoir into the hydrocarbon reservoir I and hydrocarbon reservoir II above it continued and included a new well Bčp-3 (Table 12). The pressure data from this period indicated that the migration processes from the CO_2 reservoir into the hydrocarbon reservoir I had almost finished along with a stop in migration from reservoir I into reservoir II (Figure 23). The gathered data of static pressures led to conclusion that the wellbore collapsed at depths between the reservoir of carbon-dioxide and the hydrocarbon reservoirs.

Table 12 Basic data of static pressure measurements at wells Bč-X-2, Bčp-2 and Bčp-3.

Well	Interval (m)	Hydrocarbon reservoir	Start of measurement	End of measurement
Bc-X-2	825 - 832	I reservoir	26.08.1969	28.02.1973
Bcp-2	746.5 - 750.5	II reservoir	02.04.1970	28.02.1973
Bcp-3	838 - 842 846.5 - 849	I reservoir	01.09.1970	28.02.1973

6. Phase VI - period from the 08.12.1970 to 04.05.1971

The monitoring of CO_2 continued. The gas migrations were evaluated as processes in stagnation, because no indications of gas migration was evidenced either between reservoirs I and II or from reservoir II into shallower confined layers saturated with hydrocarbons and groundwater.

7. Phase VII - period from 04.05.1971 to 28.02.1973

At the end of the monitoring period the final conclusion was that leakage of CO_2 stopped.

6.2 Monitoring and remediation of CO_2 leakage

During 1980's NIS conducted the periodical control of water quality and no evidence of any increase of CO_2 concentration was detected in groundwater samples from aquifers up to 400 m depth.

At the same time the continuing decline of pressure in the CO_2 reservoir indicated that the collapsed wellbore, Bč-5 represented the flow path to leakage in above layers of the Pontian and Pliocene age. This assumption was confirmed by the results of geophysical

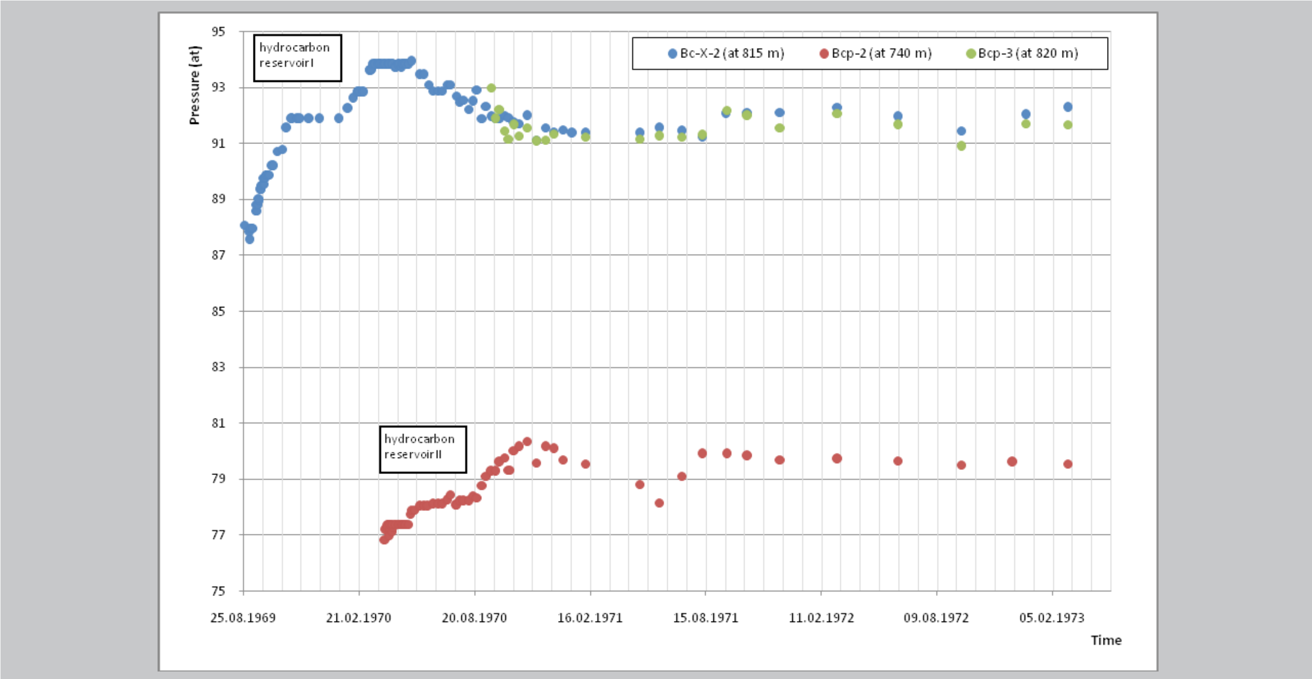

Figure 23 The static pressure measured at wells Bč-X-2, Bčp-2 and Bčp-3 from 1969-1973.

well logging conducted in Bč-X-1 in 1982, 1986 and 1991 and by drilling of Bcj-1 in 1996 (gas sample from layer at 893-911 m - 15.19 mole % CH_4, 79.8 mole % CO_2) and Bčj-2 in 2002 (gas sample from layer at 658.43-672 m - 44.41 mole % CH_4, 51.33 mole % CO_2, gas sample from layer at 428-440 m – gas composition not analysed, test on field gas did not support burning). All these layers have increased static pressures 27.6 to 34.3 % higher than hydrostatic pressure.

The accumulations of carbon-dioxide in layers above the CO_2 reservoir were registered by earlier explorations in the Bečej area (e.g. reservoirs of the Lower Pontian age on well Bč-2 tested in 1952) but the blowout in 1968 and linked processes that followed afterward caused intensive migration and leakage of CO_2. The leaked gas was trapped in the layers represented by sandstones of the Pontian and Pliocene age and the collapsed wellbore was identified as a prime source of leakage. This knowledge led to conclusion that some further measures of remediation should be conducted to seal wellbore Bč-5. The method of injecting of silica solution was chosen and the operation carried out in 2007.

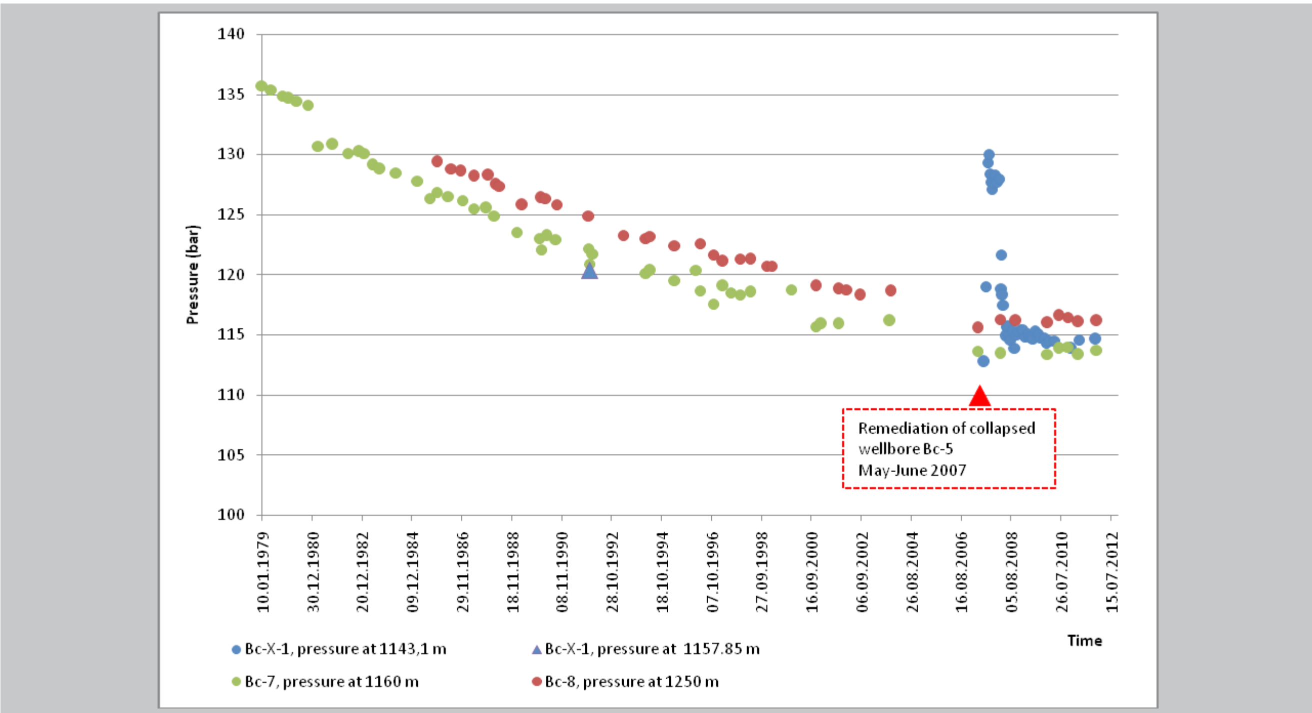

Figure 24 Monitoring pressure of CO_2 reservoir in well Bč-X-1 (1979-2011).

The monitoring plan of effects of injection included:

- Monitoring of the pressure of CO_2 reservoir in well Bč-X-1;
- Monitoring of CO_2 flux in soil;
- Monitoring of the quality of water from pond formed on the site of destroyed well Bč-5; and
- Monitoring of the quality and gas composition of groundwater from shallow aquifers up to 70 m depth.

The monitoring started a year before the remediation method was applied so it was not possible to determine exact natural concentrations of CO_2 in soil and water and the frequency of measuring was once a month. The effects of blowout had disturbed the natural conditions on site so the data were gathered to establish the reference values for the analyses of deviation during the monitoring of remediation in the period July 2006-May 2007. The samples of groundwater taken from 4 observation wells that had been drilled in the period June-July 2006 enabled the monitoring of the water quality and CO_2 flux in soil to start a year before the injection of sealant was performed. The drilling of the injection well Bč-9 and subsequently the sealing of wellbore of Bč-5 was conducted in 2007 after which the monitoring was carried on for 5 years after finishing the remediation.

6.2.1 Monitoring of the pressure of CO_2 reservoir in well Bč-X-1

The static pressure was monitored within the CO_2 reservoir in production interval 1135.7-1150.5 m. Given the results of the pressure measurements when compared with previous measurements (including those from the other production wells) it indicated that the repair of the collapsed wellbore resulted in ceasing the constant pressure decline (Figure 23). This indicates that the leakage of CO_2 was significantly reduced if not completely stopped and remediation had been successful.

6.2.2 Monitoring of CO_2 flux in soil

CO_2 flux in soil was measured at 22 points by apparatus LI-6400 Portable Photosynthesis System (LICOR Inc., Lincoln, Nebraska). Along with the flux measurements, values of pH and soil moisture were also collected as well as the meteorological parameters that lasted during measuring (air temperature and pressure, humidity, wind, insolation).

6.2.3 Monitoring of the quality of water in the pond formed on the site of destroyed well Bč-5

During monitoring the signs of degassing on the pond surface were constantly visible on several locations, CO_2 content was in the range of 4.62 to 66.8 g/l with pH values from 6.99 up to 9.31 (in some samples no CO_2 were measured).

6.2.4 Monitoring of the quality and gas composition of groundwater from shallow aquifers up to 70 m depth

The positions and technical characteristics of the monitoring wells are given in Figure 24 and Table 13.

Table 13 The technical characteristics of monitoring wells.

Well	Screen (m)	Distance from Bc-5 (m)	Construction
Bc-5-1/P	13-19	21.08	PVC d 75 mm
Bc-5-2/P	61-67	42.40	PVC d 125/75 mm
Bc-5-3/P	55.5-61.5	84.54	PVC d 125/75 mm
Bc-5-4/P	13-19	59.90	PVC d 125/75 mm

The following set of parameters were analysed: sample temperature, groundwater level, pH value, alkalinity, hardness, CO_2 content, consumption $KMnO_4$, dry residue, major cations (Na, K, Ca, Mg) and anions (bicarbonates, carbonates, sulphates, chlorides and nitrates).

After five years of monitoring of groundwater quality it was concluded that the measured concentrations of CO_2 did not exceed usual values for groundwater in shallow confined and unconfined aquifers except in samples taken from well Bč-5-1/P. This monitoring well is the closest to the former location of well Bč-5 and remarkable deviations are recorded especially in comparison to results of water samples from well Bč-5-4/P since both screened the unconfined aquifer at the same depth (the concentration of CO_2 in Bč-5-1/P is several times higher than in well Bč-5-4/P). Beside CO_2, the other measured parameters that deviated are pH, content of carbonates and bicarbonates, hardness, dry residue and consumption $KMnO_4$.

Figure 26 shows the graph of average annual concentrations that content of CO_2 reaches its maximum value in the fourth year of monitoring and then has a trend of decline in all monitored wells. During monitoring the smallest values were registered in the last year and these results pointed out that remediation of well Bč-5 had been carried out successfully.

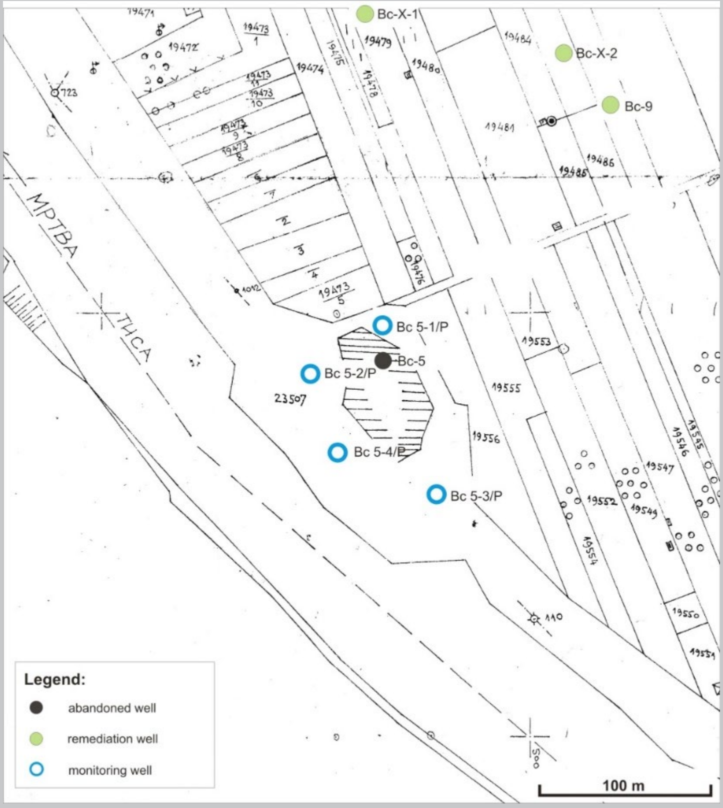

Figure 25 The positions of the monitoring wells in shallow aquifers up to 70 m depth.

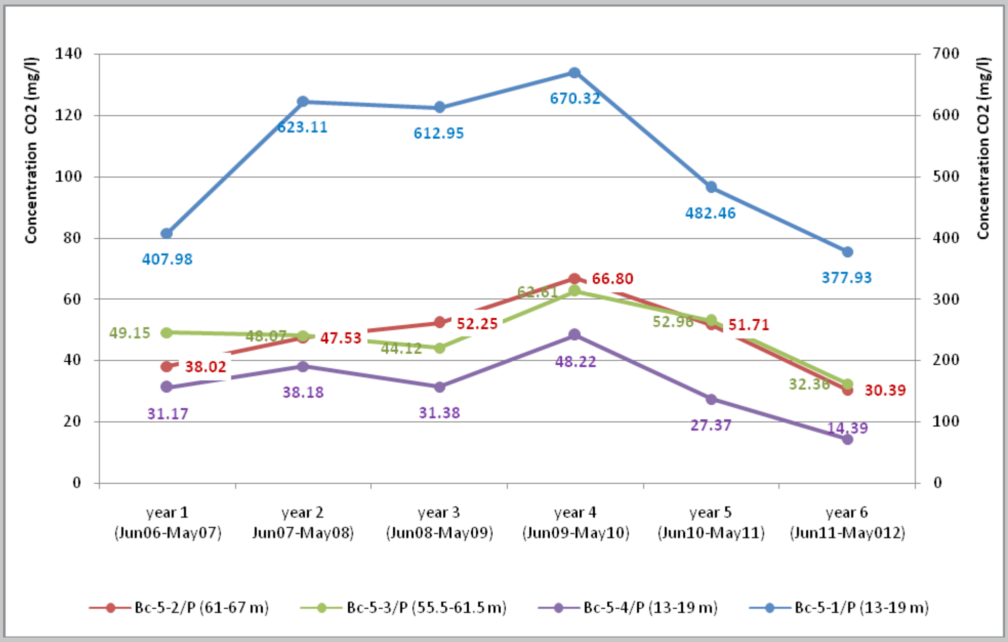

Figure 26 The average annual concentration of CO_2 in groundwater on site of Bč-5 (2006-2012).

6.3 Cost summaries

6.3.1 Costs of remediation and monitoring operations at the Bečej field

The costs of remediation and monitoring operations are calculated on the base of 2014 prices in NIS and given in Table 14.

6.3.2 Costs of remediation and monitoring operations in the literature

IEA GHG (2007, p.140) give a table of costs associated with remediation. Shackelford and Jefferis (2000) indicate the following two cost comparisons of remediation technologies in the US. Tables 15 are costs in the context of remediation of dense non aqueous phase liquids and Table 16 are costs in respect to Brownfields remediation, regardless of type of contaminant with only treatment technologies included. Neither is specifically to CO_2 contamination.

Table 14 Costs of remediation and monitoring operations in Bečej field.

Stage	Scope of work	Estimated costs (million EUR)
Blowout and monitoring the effects (1968-1972)		**2.50**
Monitoring of the quality of groundwater	Wells - depth from 10 to 400 m, approximately 300 analyses, mainly analyses of gas composition	0.02
Drilling of shallow boreholes	32 shallow boreholes for degassing of groundwater and vadose zone	0.05
Drilling of injecting boreholes	3 shallow boreholes and testing for forming an injection curtain	0.02
Drilling of remediation well Bc-X-1	Drilling and completion of well - 1150 m	1.15
Drilling of remediation well Bc-X-2	Drilling and completion of well - 860 m	0.86
Pressure measurement	Conducting measurement on three wells (1969-1972)	0.18
Consulting services	Design of project, interpretation of collected data, etc.	0.23
Monitoring of the quality of groundwater (1979 and 1988)		**0.01**
Monitoring of the quality of groundwater	Wells - depth from 80 to 400 m, approximately 100 analyses, mainly analyses of gas composition	0.01
Monitoring the effects of CO_2 leakage (1982, 1986 and 1991)		**0.25**
Workover on well Bc-X-1	Geophysical well logging, well cementing (1982, 1986, 1991), hydrodynamic measurements, test of injection (1991)	0.25
Monitoring of CO_2 leakage and remediation of well Bc-5 (2006-2012)		**2.00**
Drilling and injection on well Bc-9	Drilling and completion of well - 1150 m, injection operation	1.65
Workover on well Bc-X-1	Preparation for pressure measurement	0.01
Pressure measurement	Conducting measurement (2007-2011)	0.08
Drilling of monitoring wells	Drilling of 4 wells	0.04
Monitoring the effects of remediation	Monitoring of CO_2 flux in soil, monitoring of the quality of water from pond formed on site of destroyed well Bc-5, monitoring of the quality and gas composition of groundwater from shallow aquifers up to 70 m depth	0.04
Consulting services	Design of project, interpretation of collected data, etc.	0.18
	Total	**4.76**

Table 15 Cost comparison of selected in situ technologies (modified after Grubb and Sitar 1995).

Technology **(C = containment; T = treatment)**	**Approx. Cost ($US/m^3) (from 2000)**
Bioremediation (T)	20–80
Shallow Soil Mixing (T)	35- 85
Permeable Reactive Walls (T)	65-130
Water Flooding (T)	65-130
Soil Vapour Extraction (T)	65-130
Steam Injection (T)	65-160
Slurry Walls (C)	75-140/m^2
Grouting (C)	80-130
Radio Frequency Heating (T)	85-210
Soil Flushing (T)	100-160
Air Sparging (T)	100-160
Electro-osmosis (T)	100-200
Electrokinetics (T)	> $17/Mg
Deep Soil Mixing (T)	170-340

Table 16 Cost comparison of in situ treatment technologies (after Reddy et al. 1999).

Technology	Approx. Cost ($US/m^3)
Bioremediation	30-340
Soil Heating	55-110
Electrokinetics	100-140
Soil Vapor Extraction	< 110
Phytoremediation	< 110
Soil Flushing	105-215/m^2
Stabilization/Solidification	130-200/m^2

The costs estimated will always be a ball park figure as each costing will be site specific, but for comparative purposes the Bečej costs and the quoted costs from sections 19.1 and 19.2 indicate that:

1. Bioremediation tends to be the cheapest technology;
2. Stabilisation/solidification, especially with respect to deep soil mixing, is relatively expensive;
3. Slurry walls are expensive and depend on the length of the wall required;
4. Active soil zone remediation techniques are relatively equal in cost;
5. Containment is the cheapest technology for metals remediation; and
6. The costs associated with most of the in situ enhanced removal technologies vary by only a factor of ~ 2;
7. Drilling a new well is expensive, workover of existing wells is much cheaper (approximately one sixth of the cost of a new well);
8. Monitoring costs are very small in comparison with treatment costs (approximately one tenth).

7 CONCLUSIONS

7.1 Remediation techniques summary

An assessment by one of the authors, Edlmann, of the probable role each of the remediation techniques with regards to CO_2 remediation was undertaken. The assessment is based upon the information presented in this report and is the opinion of the investigator.

The probable role was assessed in terms of:

1. Practicality of application to CO_2 contamination. Is there an established CO_2 remediation application (or at least a reasonable expectation that the application would successfully remediate CO_2) or is it a potential but untested possibility;
2. Ease of implementation of the remediation technology – is it an easy deployed in-situ technology with passive maintenance or a technology that requires significant ground works and implementation infrastructure and active maintenance;
3. Cost – reasonable or so expensive it prohibits the use of the technology.

A summary of the probable role grading process can be seen in Table 17.

The results are presented in Table 18. The table also includes information on what improvements or further research is required to increase its likelihood of applicability of CO_2 contamination remediation.

The results from Table 18 indicate that there are a wide range of remediation techniques available for near surface CO_2 remediation and that any remediation strategy will be site specific.

Table 17 Summary of the probable role grading

Probable role	CO_2 applicability	Ease of technology implementation	Costs
Likely	Proven / established CO_2 applicability	Relatively straightforward technology application	Reasonable
High intermediate	Potentially applicable to CO_2 contamination	Relatively straightforward technology application	Reasonable
Intermediate	Potentially applicable to CO_2 contamination	Complex technology application	High
Minor	Potentially applicable to CO_2 contamination	Complex technology application	Very high
Unlikely	not directly applicable to CO_2 contaminations	Complex technology application	Very high

Table 18 Summary assessment of the probable role each of the remediation techniques with regards to CO_2 remediation.

Remediation	Remediation Technique	Probable role	Improvements / comments
Fluid control measures	Pump and treat	**Likely**	Larger plumes may require horizontal wells and longer remediation times.
	Pump and treat with cap	**Likely**	Cost will depend on extent of cap
	Water injection	**High Intermediate**	Useful short term to reduce concentration of CO_2, but residually trapped CO_2 remains.
	Hydrodynamic isolation	**Likely**	Stabilises CO_2 plume
	Air stripping	**Likely**	Process is quick and relatively cheap
	Hydraulic barrier	**High Intermediate**	Works if aquifer is not very permeable and location of leak is known
Cut off wall (unconfined aquifer)	Cut-off wall / slurry wall	**Intermediate**	High costs depending on length of wall, risk of wall leakage and degradation. Only provide partial containment and further clean up technologies needed
	Two-phase diaphragm wall	**Intermediate**	High costs depending on length of wall, risk of wall leakage and degradation. Only provide partial containment and further clean up technologies needed
	Composite diaphragm wall	**Intermediate**	High costs depending on length of wall, risk of wall leakage and degradation. Only provide partial containment and further clean up technologies needed
	Interlocking bored-pile diaphragm wall	**Intermediate**	High costs depending on length of wall, risk of wall leakage and degradation. Only provide partial containment and further clean up technologies needed
	Installation of thin wall and sheet pile into the soil	**Intermediate**	High costs depending on length of wall and risk of sheet material corrosion
	Injection permeation grouting	**Intermediate**	Leakage risk through permeability gaps. Only provide partial containment and further clean up technologies needed
	Jet grouting	**Intermediate**	Leakage risk through permeability gaps. Only provide partial containment and further clean up technologies needed
	Frozen wall	**Unlikely**	Requires the active (powered) circulation of refrigerant coolant or liquid nitrogen
	Bio barrier	**Intermediate**	Technology untested in situ for CO_2, costs and application low.
	Water control agent	**High intermediate**	Technology available and low cost. Resistance to CO_2 untested.
	High strength rigid set material	**High intermediate**	Technology available and low cost. Resistance to CO_2 untested.
	Organic polymer sealant	**High intermediate**	Technology available and low cost. Resistance to CO_2 untested.
	Super absorbent crystals	**High intermediate**	Technology available and low cost. Resistance to CO_2 untested.
	Granular activated carbon	**Likely**	Process is relatively quick and cheap but will depend on CO_2 concentration or volume
Cut off wall - Fractured aquifer	Grout curtain	**Likely**	Boreholes ideally orientated to intersect as many fractures as possible, fracture permeability important and can be enhanced through hydrofracking. Grouting materials need to be CO_2 resistant

Remediation	Remediation Technique	Probable role	Improvements / comments
Permeable reactive barriers (treatment walls)	Sorption barriers	**Likely**	Sorption materials need to be CO_2 specific. Over time reactive materials become less effective at removing CO_2 and the contaminated reactive material needs to be removed and replaced with fresh material.
	Ionic species removal	**High Intermediate**	Established procedure to clean up the trace elements potentially mobilised by the CO_2 contamination
	Microbes	**Intermediate / minor**	A cheap option but CO_2 specific microbes that will be in optimum conditions are hard to establish
	Carbonation stabilisation	**Intermediate / minor**	A cheap option but carbonation rates are hard to establish
	De-acidisation	**Likely**	Established cheap technology
Soil Zone remediation	Soil vapour extraction	**Likely**	Potential to be used in conjunction with containment treatments.
	Air sparging	**High Intermediate**	CO_2 will follow high permeability pathways so initial recovery rates high but will fall off as recovery is limited to diffusion. Potential to be used in conjunction with containment treatments
	Bioslurping	**High Intermediate**	CO_2 will follow high permeability pathways so initial recovery rates high but will fall off as recovery is limited to diffusion. Potential to be used in conjunction with containment treatments
	De-acidise soil	**Likely**	Established cheap technology
	Thermal treatment	**Intermediate**	Costs high and not for CO_2 plume but clean-up of the trace elements potentially mobilised by the CO_2 contamination
	Capping	**Likely**	Cost will depend on extent of cap and most likely to be used in conjunction with a treatment.
	Gas collection trench	**Likely**	Cheap and established method to collect soil gas.
	Ecosystem restoration	**Likely**	Final result of any contamination clean up.
Bioremediation	Bioremediation of low pH groundwaters	**Intermediate**	Cheap established option, but extent controlled by ideal biological condition.
	Bioremediation of CO_2	**Minor**	Cheap, extent controlled by ideal biological condition. But CO_2 specific microbes sill to be field tested.
	Bioremediation of toxic metals	**Intermediate**	Cheap established option, but extent controlled by ideal biological condition.
	Bioremediation of hydrocarbons	**Intermediate**	Cheap established option, but extent controlled by ideal biological condition.
	Natural attenuation	**Likely / Intermediate**	May be first step in the risk assessment procedure, however high costs associated with monitoring.
Buildings	Passive vapour intrusion mitigation	**Likely**	Established cheap technology
	Passive / active sub slab venting	**Likely**	Established cheap technology
	Active vapour intrusion mitigation – subsurface pressurisation	**Likely**	Established cheap technology
	Block wall depressurisation	**Likely**	Established cheap technology
	Active ventilation	**Likely**	Established cheap technology
	Passive ventilation	**Likely**	Established cheap technology
	Demolish and rebuild to suitable standards.	**Minor**	Final resort if other building remediation technologies are unsatisfactory.

8 ACKNOWLEDGEMENTS

The MiReCOL project is funded by the European Community's Seventh Framework programme (ENERGY.2013.5.2.1) under grant agreement no. 608608. The project partners acknowledge the following funding partners for their contributions: Statoil and Shell.

References

Aeschbach-Hertig, W., Kipfer, R., Hofer, M., Imboden, D.M., Wieler, R. and Signer, P., 1996, Quantification of gas fluxes from the subcontinental mantle: the example of Laacher See, a maar lake in Germany. Grochimica et Cosmochlmica Acta, 60, 33-41.

Annunziatellis, A., Beaubien, S E., Bigi, S., Ciotoli, G., Coltella, M., And Lombardi, S., 2008, Gas migration along fault systems and through the vadose zone in the Latera caldera (central Italy): Implications for CO_2 geological storage. International Journal of Greenhouse Gas Control, Vol. 2, p. 353–372.

Annunziatellisa, A., Ciotolia, G., Lombardi, S., and Nolasco, F., 2003, Short- and long-term gas hazard: the release of toxic gases in the Alban Hills volcanic area (central Italy). Journal of Geochemical Exploration, 77, 93–108.

Arz, P., 1988. Dichtwandtechnik ftir seitliche Umschliegungen. Bauwirtschaft 110 (B42), 831-835, in German.

Atlas, R.M.,1975, Effects of temperature and crude oil composition on petroleum biodegradation. Applied and Environmental Microbiology, v. 30, p. 396 – 403.

Bai, M., Abousleiman, Y., Inyang, H.I., Mo, H, and Roegiers, J-C., 2000, Analysis of capture zone and pump-and-treat methods in fractured rocks. In: Inyang, H.I. and Bruell, C.J. (Eds..) Remediation of Rock Masses, American Society of Civil Engineers Press, Virginia, USA, pp. 42 – 55.

Banasiak, L. and Indraratna, B., 2012, Permeable reactive barrier (PRB) technology: An innovative solution for the remediation of acidic groundwater from acid sulphate soil (ASS) terrain. In R. Hryciw, A. Athanasopoulos-Zekkos N. Yesiller (Eds.), GeoCongress 2012(pp. 3523-3432). American Society of Civil Engineering. http://ro.uow.edu.au/cgi/viewcontent.cgi?article=7522&context=engpapers Accessed 1 July 2014.

Barberi, F., Carapezza, M.L., Ranaldi, M., and Tarchini, L., 2007, Gas blowout from shallow boreholes at Fiumicino (Rome): Induced hazard and evidence of deep CO_2 degassing on the Tyrrhenian margin of Central Italy. Journal of Volcanology and Geothermal Research, 165, 17–31.

Baldocchi, D., Falge, E., Gu, L. et al. 2001: FLUXNET: A new tool to study the temporal and spatial variability of eco-system scale carbon dioxide, water vapour, and energy flux densities. American Meteorological Society, 82, 2435-2455

BBC News, 2014, Plan to demolish Gorebridge homes after carbon dioxide gas leak. http://www.bbc.co.uk/news/uk-scotland-edinburgh-east-fife-27812488, accessed 24 June 2014.

Beaubien, S. E., Ciotoli, G., Coombs, P., Dictor, M. C., Kruger, M., Lombardi, S., Pearce, J. M. and West, J. M., 2008. The impact of a naturally-occurring CO_2 gas vent on the shallow ecosystem and soil chemistry of a Mediterranean pasture (Latera, Italy). International Journal of Greenhouse Gas Control, 2, 373-387.

Beaubien, S. E., Jones, D. G., Gal, F., Barkwith, A. K. A. P., Braibant, G., Baubron, J. C., Ciotoli, G., Graziani, S., Lister, T. R., Lombardi, S., Michel, K., Quattrocchi, F., Strutt, M. H., 2013. Monitoring of near-surface gas geochemistry at the Weyburn, Canada, CO_2-EOR site, 2001–2011. International Journal of Greenhouse Gas Control, 16(1), pp. 236-262.

Becker, T.P., and Lynds, R., 2012, A geologic deconstruction of one of the world's largest natural accumulations of CO_2, Moxa arch, southwestern Wyoming: Aapg Bulletin, v. 96, p. 1643-1664.

Benson, S. and Hepple, R, 2005, Prospects for early detection and options for remediation of leakage from CO_2 storage projects. In: Thomas, D.C. and Benson, S.M. (Eds.) Carbon Dioxide Capture for Storage in Deep Geologic Formations, Volume 2. Elsevier.

Blowes, D.W., Ptacek, C.J., Jambor, J.L., 1997. In-situ remediation of Cr(VI)-contaminated groundwater using permeable reactive walls: laboratory studies. Environ. Sci. Technol. V. 31, p. 3348 - 3357.

Boyd, A.D., Liu, Y., Stephens, J.C., Wilson, E.J., Pollak, M., Peterson, T.R., Einsiedel, E., Meadowcroft, J., 2013. Controversy in technology innovation: Contrasting media and expert risk perceptions of the alleged leakage at the Weyburn carbon dioxide storage demonstration project, Vol. 14, pp. 259 - 269.

Bruell, C.J. and Inyang, H.I., 2000, The Fundamentals of Remediation in Rock Masses. In: Inyang, H.I. and Bruell, C.J. (eds), Remediation in Rock Masses. American Society of Civil Engineers Press, Virginia, USA. pp. 1 – 11.

BSI, 2007, Code of practise for the characterisation and remediation from ground gas in affected developments. British Standard BS8485:2007.

Burnside, N.M., 2010, U-Th dating of travertine on the Colorado Plateau: Implications for the leakage of geologically stored CO_2. PhD thesis, The University of Glasgow, pp306. http://theses.gla.ac.uk/1988/, accessed Sept 2014.

Calcara, M., Lombardi, S., and Quattrocchi, F., 1995, Geochemical Monitoring for seismic surveillance in the Alban Hills region, In R. Rigila (ed.), Special Volume: "The Volcano of Alban Hills", 283 pp. 243–265.

Caramanna, G., 2010, Study of a submarine CO_2 natural analogue by means of Scientific Diving techniques. Presentation at IEAGHG Natural releases of CO_2 workshop.

Carapezza, M.L., Badalamenti, B., Cavarra, L. and Scalzo, A., 2003, Gas hazard assessment in a densely inhabited area of Colli Albani Volcano (Cava dei Selci, Roma). Journal of Volcanology and Geothermal Research, 123, 81-94.

Carapezza, M.L. and Tarchini, L., 2007, Accidental gas emission from shallow pressurized aquifers at Alban Hills volcano (Rome, Italy): Geochemical evidence of magmatic degassing? Journal of Volcanology and Geothermal Research, 165, 5–16.

Carey, M. A., Fretwell, B. A., Mosley, N. G. & Smith, J. W. N., 2001, Guidance on the use of permeable reactive barriers for remediating contaminated groundwater. National Groundwater & Contaminated Land Centre report NC/01/51, UK Environment Agency. https://www.gov.uk/government/uploads/system/uploads/attachment_data/file/290423/scho0902bitm-e-e.pdf Accessed 1 July 2014.

Cartwright, J., James, D., and Bolton, A., 2003, The genesis of polygonal fault systems: A review. In: van Rensbergen, P., Hillis, R.R., Maltman, A.J., and Morley, C.K., eds., Subsurface Sediment Mobilization: Geological Society of London Special Publication 216, p. 223–243.

Chiodini, G., Granieri, D., Avino, R., Caliro, S., Costa, A., Minopoli, C. and Vilardo G., 2010, Non-volcanic CO_2 Earth degassing: The case of Mefite d'Ansanto (Southern Apennines), Italy. Geophysical Research letters, 37, L11303, doi:10.1029/2010GL042858.

CO_2CARE, 2013, CO_2 Site Closure Assessment Research D5.4 Best Practice Guidelines. British Geological Survey.

CPEO, 2014, Landfill Caps and Enhancements. Centre for Public Environmental Oversite (USA). http://www.cpeo.org/techtree/ttdescript/lancap.htm Accessed 7 July 2014.

Daniel, D and Koerner, R., 2007, Waste Containment Facilities: Guidance for Construction Quality Assurance and Construction Quality Control of Liner and Cover Systems (2nd Ed.) American Society of Civil Engineers Press, Virginia, USA. pp. 133-206.

Darnault, Christophe J. G, 2008. Overexploitation and Contamination of Shared Groundwater Resources. Springer Science & Business Media, 1 Jan 2008

Decatur, unknown date, Attachment F: emergency and remedial response plan for ADM CCS#2 http://www.epa.gov/region5/water/uic/adm/pdfs/adm-ccs2-attachment-f-emergency-and-remedial-response-plan-201404.pdf, accessed Nov 2014

Dillman, H., 1999. Geotechnical Bureau Prof. Dr.-Ing. H. Dtillmann, Aachen, Germany, statement on cut-off walls. Sardinia 99, Seventh International Waste Management and Landfill Symposium. Margherita di Pula, Sardinia, Italy.

Dupraz, S., Parmentier, M., Méneza, B, and Guyot, F., 2009, Experimental and numerical modeling of bacterially induced pH increase and calcite precipitation in saline aquifers. Chemical Geology, v. 265, p. 44 – 53.

Dennis, M. L. and Turner, J. P. 1998. "Hydraulic conductivity of compacted soil treated with biofilm". J. Geotech. and Geoenviron.. Engrg., ASCE, Reston, Virginia, USA, 124(2):120-127.

Ellis, D.E. and Hadley, P.W., 2009, Sustainable Remediation White Paper—Integrating Sustainable Principles, Practices, and Metrics Into Remediation Projects. Remediation, v. 19, p. 5 – 114.

Embid, E.H., Crossey, L.J, Karlstrom, K.E., Eagar, K.C., Fouch, M.J., Crumpler, L.S., and Aubele, J.C., 2006, "Chemical volcanoes" in the Springerville area, Arizona: using travertines, springs, and microseismicity to link water quality, paleohydrology and neotectonics. Geological Society of America, paper 7-1. Rocky Mountain Section–58th Annual Meeting (17–19 May 2006). https://gsa.confex.com/gsa/2006RM/finalprogram/abstract_104992.htm Accessed October 2014.

EON, 2010, Kingsnorth Carbon Capture & Storage Project: Risk Assessment and Mitigation. KCP-RDS-CRE-REP-1009. http://webarchive.nationalarchives.gov.uk/20111209170139/https://www.decc.gov.uk/Media/viewfile.ashx?FilePath=11/ccs/chapter7/7.27-risk-assessment-and-mitigation.pdf&filetype=4 Accessed 27 July 2014.

EPA, 1996, A Citizen's Guide to Treatment Walls, USA Environmental Protection Agency EPA 542-F-96-016. http://www.clu-in.org/download/remed/walls.pdf accessed 27 Jun 2014.

EPA, 2001, Building radon out, a step-by-step guide on how to build radon-resistant homes. USA Environmental Protection Agency, EPA/402-K-01_002. http://www.epa.gov/radon/pdfs/buildradonout.pdf accessed Nov 2014

EPA, 2012 Citizen's Guide to In Situ Thermal Treatment. EPA 542-F-12-013. http://www.epa.gov/tio/download/citizens/a_citizens_guide_to_in_situ_thermal_treatment.pdf accessed Nov 2014

EPA, 2008, Geologic CO_2 Sequestration Technology and Cost Analysis - Technical Support Document, 61p. http://nepis.epa.gov/Exe/ZyPURL.cgi?Dockey=P1002SKS.txt accessed 23 March 2015.

Esposito, A. and Benson, S.M., 2012, Evaluation and development of options for remediation of CO_2 leakage into groundwater aquifers from geologic carbon storage. International Journal of Greenhouse Gas Control, 7, 62 – 73.

Etiope, G., Fridriksson, T., Italiano, F., Winiwarter, W. And Theloke, J., 2007, Natural emissions of methane from geothermal and volcanic sources in Europe. Journal of Volcanology and Geothermal Research 165, p. 76–86.

European Council, 1998, The quality of water intended for human consumption. Official Journal of the European Communities, COUNCIL DIRECTIVE 98/83/EC.

EU Directive 2004/35/EC European Parliament on environmental liability with regard to the prevention and remedying of environmental damage (ELD). 2004 http://ec.europa.eu/environment/legal/liability/ accessed Nov 2014

EU-ETS 2014. Consolidated version of Directive 2003/87/EC of the European Parliament and of the Council establishing a scheme for greenhouse gas emission allowance trading within the Community and amending Council Directive 96/61/EC. http://eur-lex.europa.eu/legal-content/EN/TXT/?uri=CELEX:02003L0087-20140430, accessed Nov 2014

Evans, W C., Bergfeld, D., McGimsey, R.G., and Hunt, A.G., 2009, Diffuse gas emissions at the Ukinrek Maars, Alaska: Implications for magmatic degassing and volcanic monitoring. Applied Geochemistry, 24, 527–535.

Ferris, F.G., Stehmeier, L.G., Kantzas, A., and Mourits, F.M. (1996) Bacteriogenic mineral plugging. Journal of Canadian Petroleum Technology, v. 35, p. 56–61.

Fetter, C.W., 1999, Contaminant Hydrogeology. 2nd Edition. Prentice Hall, New Jersey, USA. 500p. ISBN 0-13-751215-5.

Fridriksson T., Kristjánsson B. R., Ármannsson H., Margrétardóttir E., Ólafsdóttir S. and Chiodini G., 2006, CO_2 emissions and heat flow through soil, fumaroles, and steam heated mud pools at the Rekjanes geothermal area, SW Iceland. Applied Geochemistry 21,

1551-1569.
Freethey, G.W., Naftz, D.L., Rowland, R.C. and Davis, J.A.,2005, Deep Aquifer Remediation Tools: Theory, Design, and Performance Modeling. In: Naftz, D.l., Morrison, S.J., Fuller, C.C., and Davis, J.A., 2003, Handbook of Groundwater Remediation using Permeable Reactive Barriers. Elsevier, pp. 133 – 161.
Figueiredo M, Bacanskas L, and Kolian M. 2012. Greenhouse gas reporting for geological sequestration of Carbon Dioxide. Carbon Management and Tech. Conf. Orlando, Florida USA, 7-9 February 2012, CMTC 151426.
Fujita Y., Ferris F. G., Lawson R. D., Colwell F. S., and Smith R. W., 2000, Calcium carbonate precipitation by ureolytic subsurface bacteria. Geomicrobiology J. 17, 305–318.
Gal, F., Brach, M., Braibant, G., Jouin, F., and Michel, K., 2011, CO_2 escapes in the Laacher See region, East Eifel, Germany: application of natural analogue onshore and offshore geochemical monitoring. International Journal of Greenhouse Gas Control, 5, 1099-1118.
Gavaskar, A.R., 1999. Design and construction techniques for permeable reactive barriers. Journal of Hazardous Materials v. 68, p. 41-71.
Granger Morgan 2012 Carbon Capture and Sequestration: Removing the Legal and Regulatory Barriers. RFF Press. ISBM 978-1-61726-101-5
Googas Catalogue (2009) Results of the INGV-DPCV5 project: the catalogue of italian gas emissions, Coordinated by Chiodini, G, Valenza M. http://googas.ov.ingv.it/ [Accessed August 2014].
Gouveia, F. J., Johnson, M. R., Leif, R. N., and Friedmann, S. J., 2005, Aerometric measurement and modeling of the mass of CO_2 emissions from Crystal geyser, Utah: Lawrence Livermore National Lab Report UCRL-TR-211870: http://www.llnl.gov/tid/lof/documents/pdf/316304.pdf (accessed Sept 2014).
Grubb, D. G. and Sitar, N. 1995. "Review of technologies for in-situ cleanup of DNAPLs". Geoenvironment 2000, Y. B. Acar and D. E. Daniel, eds., ASCE, Reston, Virginia, USA, 1646-1662.
Hall-Spencer, J.M., Rodolfo-Metalpa, R., Martin, S., Ransome, E., Fine, M., Turner, S.M., Rowley, S.J., Tedesco, D. & Buia, M-C., 2008, Volcanic carbon dioxide vents show ecosystem effects of ocean acidification. Nature, 454, 96-99.
Halliburton cementing brochure, 2014. http://www.halliburton.com/en-US/ps/cementing/cementing-solutions/default.page?node-id=hdhdvbxc, accessed Nov 2014
Hamby D.M. 1996, Site remediation techniques supporting environmental restoration activities: a review. The Science of the Total Environment, Volume 191, Number 3, 22 November 1996, pp. 203-224 (22)
Hammes, F., Seka, A, de Kniff, S., and Verstraete, W., 2003, A novel approach to calcium removal from calcium-rich industrial waste water. Water Research, v. 37, p. 699 – 704.
Hanagata N, Takeuchi T, Fukuju Y, Barnes DJ, Karube I 1992 Tolerance of microalgae to high CO_2 and high temperature. Phytochemistry 31:3345–3348
Hiebert, R., 1998. Using biological barriers to control movement of contaminated groundwater, Subsurface Barrier Technologies Conference, Tucson, AZ, USA, International Business Communications. Hodgson, S.A., Zhang, W., Bradley, E.J., Green, B.M.R. and McColl, N.P., 2011, An analysis of radon remediation methods. Public Health England, HPA-CRCE-019. http://www.hpa.org.uk/Publications/Radiation/CRCEScientificAndTechnicalReportSeries/HPACRCE019/ Accessed 23 Jun 2014.
Hollinger, D. Y. and Richardson, A. D., 2005. Uncertainty in eddy covariance measurements and its application to physiological models. Tree Physiology, 25, 873– 885.
IEA GHG, 2007, Remediation of leakage from CO_2 storage reservoirs. International Energy Agency Greenhouse Gas Technical Study 2007/11.
IEA GHG, 2005 A review of natural CO_2 occurrences and releases and their relevance to CO_2 storage. http://ieaghg.org/docs/General_Docs/Reports/2005-8.pdf, accessed Nov 2014
IEA GHG, 2012 Quantification techniques for CO_2 leakage, http://ieaghg.org/docs/General_Docs/Reports/2012-02.pdf, accessed Nov 2014
Independent (Newspaper), 1994, Why will the village cross the road? http://www.independent.co.uk/arts-entertainment/why-will-the-village-cross-the-road-school-chipshop-postoffice-pub-arkwright-town-is-a-small-derbyshire-mining-community-typical-of-those-that-once-dotted-the-coal-regions-now-british-coal-wants-to-start-opencast-mining-which-means-destroying-the-old-village-and-building-a-new-one-right-next-door-1370668.html Accessed 27 June 2014.
Inyang, H.I. and Bruell, C.J., 2000, Remediation in Rock Masses. American Society of Civil Engineers Press, Virginia, USA.
IPCC, 2005. Underground geological storage. In: Intergovernmental Panel on Climate Change Special Report on Carbon Dioxide Capture and Storage. Prepared by Working Group III of the IPCC. Cambridge University Press, New York, pp.195–276.
IPCC, 2006, Guidelines for National Greenhouse Gas Inventories http://www.ipcc-nggip.iges.or.jp/public/2006gl/index.html, accessed Nov 2014
Italiano, F., Martelli, M., Martinelli, G., and Nuccio, P.M., 2000, Geochemical evidence of melt intrusions along lithospheric faults of the Southern Apennines, Italy: geodynamic and seismogenic implications. Journal of Geophysical Research, 105 (B6), 13569–13578.
Jessberger, H.L., 1992. ITVA Arbeitspapier Dichtwände (in German). Jones, D G., Barlow, T., Beaubien, S.E., Ciotoli, G., Lister, T R., Lombardi, S., May, F., Möller, I., Pearce, J.M., and Shaw, R.A. 2009. New and established techniques for surface gas monitoring at onshore CO_2 storage sites. Energy Procedia, 1, 2127–2134.
Jones, D. G., Lister, T. R., Smith, D. J., West, J. M., Coombs, P., Gadalia, A., Brach, M., Annunziatellis, A. and Lombardi, S. 2011. In Salah Gas CO_2 Storage JIP: Surface gas and biological monitoring. Energy Procedia, 4:3566-3573.
Jung, N.-H., Hana W.S., Watson, Z.T., Graham, J.P., and Kim, K.-Y., 2014, Fault-controlled CO_2 leakage from natural reservoirs in the Colorado Plateau, East-Central Utah. Earth and Planetary Science Letters, 403, 358–367.

Keating, E., Newell, D., Dempsey, D., and Pawar, R., 2014, Insights into interconnections between the shallow and deep systems from a natural CO_2 reservoir near Springerville, Arizona. International journal of Greenhouse Gas Control, v. 25, p. 162 – 172.

Kellner, C., Scheibel, B., 2004, Innovative SicherungsmaBnahmen ftir Deponien-Ausftihrung der Kammerdichtwand Vorketzin. 11. Braunschweiger Deponie- und Dichtwandseminar 2004. Mitteilung des Instituts ftir Grundbau und Bodenmechanik, Vol. 74. Technische Universit/it Braunschweig, pp. 363-380, in German. Kirk, K., 2011, Natural CO_2 flux literature review for the QICS project. British Geological Survey Commissioned Report, CR/11/005. 38pp. http://www.bgs.ac.uk/qics/reports/Natural%20Flux%20literature%20reviewFINAL.pdf Accessed 4 July 2014.

Krüger, M., West, J., Frerichs, J., Oppermann, B., Dictor, M.-C., Joulian, C., Jones, D., Coombs, P., Green, K., Pearce, J., May, F. and Möller, I., 2009, Ecosystem effects of elevated CO_2 concentrations on microbial populations at a terrestrial CO_2 vent at Laacher See, Germany. Energy Procedia, 1, 1933–1939.

Lewicki J. L. and Oldenburg C.M. 2004. Integrated near-surface monitoring and analysis for CO_2 storage verification. Am. Chem. Soc., Div. Fuel Chem. 2004, 49 (1), 427

Little, M. G.; Jackson, R. B., 2010, Potential Impacts of Leakage from deep CO_2 Geosequestration on Overlying Freshwater Aquifers. Environ. Sci. Technol., 44, 9225 – 9232.

Lombardi, S., 2010, A resource for studying potential impacts, examining gas migration processes and testing monitoring techniques. IEAGHG workshop: Natural releases of CO_2: Building knowledge for CO_2 storage Environmental Impact Assessments. Maria Laach, Germany, 2nd – 4th November 2010.

Keating, E., Newell, D., Dempsey, D., and Pawar, R, 2014, Insights into interconnections between the shallow and deep systems from a natural CO_2 reservoir near Springerville, Arizona. International Journal of Greenhouse Gas Control, v. 25, p. 162 – 172.

Khan F.I., Husain T., Hejazi R. 2004. An overview and analysis of site remediation technologies. Journal of Environmental Management 71 (2004) 95–122

Kodama M, Ikemoto H, Miyachi S 1993. A new species of highly CO_2- tolerant fast-growing marine microalga suitable for high-density culture. J Mar Biotechnol 1:21–25

LaFleur, 2010, Geochemical Soil Gas Survey: A Site Investigation of SW30-5-13-W2M Weyburn Field, Saskatchewan. Saskatoon, SK: Petro-Find Geochem Ltd.

LaFleur, 2011, Geochemical Soil Gas Survey: A Site Investigation of SW30-5-13-W2M, Weyburn Field, Saskatchewan, Monitoring Project Number 2. Saskatoon, SK: Petro-Find Geochem Ltd.

Lewicki, J. L., Fischer, M.L. and Hilley, G.E., 2008, Six-week time series of eddy covariance CO_2 flux at Mammoth Mountain, California: performance evaluation and role of meteorological forcing. Journal of Volcanology and Geothermal Research, 171, p. 178-190.

Lewicki J.L and Oldenburg, C.M. 2004 Intergrated near surface monitoring and analysis for CO_2 storage verification. Am Chem./ Soc., Div Fuel Chem. 2004, 49 (1), 427.

Lu, J., Wilkinson, M., Haszeldine, R.S., & Boyce, A,J., 2010, Carbonate cements in Miller field of the UK North Sea: a natural analog for mineral trapping in CO_2 geological storage, Environmental Earth Sciences, 62, 507-517.

Lu, J., Wilkinson, M. , Haszeldine, R.S., & Fallick, A.E., 2009, Long-term performance of a mudrock seal in natural CO_2 storage. Geology, 37, 35 – 38.

Lupton, J., Butterfield, D., Lilley, M., Evans, L., Nakamura, K., Chadwick Jr., W., Resing, J., Embley, R., Olson, E., Proskurowski, G., Baker, E., De Ronde, C., Roe, K., Greene, R., Lebon, G. And Young, C. 2006. Submarine venting of liquid carbon dioxide on a Mariana Arc volcano. Geochem. Geophys. Geosyst., 7, Q08007, doi: 10.1029/2005GC001152.

Manceau J.-C., Hatzignatiou, D.G., Lary L. de, Jensen, N.B. Réveillère, A., 2014, Mitigation and remediation technologies and practices in case of undesired migration of CO_2 from a geological storage unit—Current status. International Journal of Greenhouse Gas Control, v. 22, 272 – 290.

Mau, S., Sahling, H., Rehder, G., Suess, E., Linke, P. and Soeding, E., 2006. Estimates of methane output from mud extrusions at the erosive convergent margin off Costa Rica. Marine Geology, 225(1-4), 129-144.

McGinnis, D.F., Schmidt, M., DelSontro, T., Themann, S., Rovelli, L., Reitz, A. and Linke, P., 2011, Discovery of a natural CO_2 seep in the German North Sea: Implications for shallow dissolved gas and seep detection. Journal of Geophysical Research: Oceans, 116, C03013.

Meggyes, T., 2005, Construction methods of permeable reactive barriers. In: Roehl, K.E., Meggyes, T., Simon, F.-G., and Stewart, D.I. (Eds.) Long-term performance of permeable reactive barriers. Elsevier, Netherlands, p. 27-52.

Ménez, B., Dupraz, S., Gérard, E., et al., 2007. Impact of the deep biosphere on CO_2 storage performance. Geotechnologien Science Report 9, 150–163. http://issuu.com/geotechnologien/docs/sr09, accessed Nov 2014

Mielenz, R. C., 1962, Petrography applied to Portland cement concrete. In: Reviews in Engineering Geology, Edited by T. Fluhr and R. F. Legget, Vol. 1, The Geological Society of America., New York, 1–30.

Mitchell, A.C., Ferris, F.G., 2005. The coprecipitation of Sr into calcite precipitates induced by bacterial ureolysis in artificial groundwater: temperature and kinetic dependence. Geochimica et Cosmochimica Acta, v. 69, p. 4199–4210.

Miyairi S. 1995 CO_2 assimilation in a thermophilic cyanobacterium. Energy Convers Manage 36:763–766

Morel, F. M. M., and Hering, J. G., 1993, Principles and Applications of Aquatic Chemistry. Wiley, New York.

Mörner, N.-A. and Etiope, G. 2002. Carbon degassing from the lithosphere. Global and Planetary Change, 33,185-203.

Naftz, D.I., Morrison, S.J., Fuller, C.C., and Davis, J.A., 2003, Handbook of Groundwater Remediation using Permeable Reactive Barriers. Elsevier, ISBN: 978-0-12-513563-4.

Nakano Y, Miyatake K, Okuno H, Hamazaki K, Takenaka S,Honami N, Kiyota M, Aiga I, Kondo J. 1996 Growth ofphotosynthetic algae Euglena in high CO_2 conditions and its photosynthetic characteristics. In: International Symposiumon Plant Production in Closed

Ecosystems 440,pp 49–54
Need, E.A., and Costello, M.J., 1984, Hydrogeologic aspect s of slurry wall isolation systems in areas of high downward gradients. In: Proceedings of the forth National Symposium and Exposition on Aquifer Restoration and Ground Water monitoring, Dublin, Ohio. National water well Association, 18 – 26.

NHBC, 2007, Guidance on evaluation of development proposals on sites where methane and carbon dioxide are present. National House-Building Council (UK). http://www.nhbc.co.uk/NHBCpublications/LiteratureLibrary/Technical/filedownload,29440,en.pdf Accessed 27 June 2014.

Nyer, E. K. et al. 1996. In Situ Treatment Technology, Boca Raton, FL. CRC Press.

Oldenburg, C.M., 2008. Screening and ranking framework for geologic CO_2 storage site selection on the basis of health, safety and environmental risk: Environmental Geology v.54, no.8, p1687-1694.

Oldenburg, C.M. and Unger, A.A.J., 2005, Modeling of near-surface leakage and seepage of CO_2 for risk characterization. In: Thomas, D.C. and Benson, S.M. (Eds.) Carbon Dioxide Capture for Storage in Deep Geologic Formations, Volume 2. Elsevier, pp. 1205 – 1215.

Osende, J., 1985, The Durability of Cement Grouts. Fifteenth Congress on Large Dams Transactions. pp.759-766, Q. 58, R. 43, Volume 3, , Lausanne, Switzerland, International Commission on Large Dams, Paris, June 1985.

Padrón, E., Hernández, P.A., Toulkeridis, T., Pérez, N.M., Marrero, R., Melián, Virgili, G., and Notsu, K., 2008, Diffuse CO_2 emission rate from Pululahua and the lake–filled Cuicocha calderas, Ecuador. Journal of Volcanology and Geothermal Research, 176, 163–169.

Paillet, F. L. 1991. "Comparing Geophysical Logs to Core and Cross-Hole Flow Logging in the Mirror Lake Drainage Basin." U.S. Geological Survey Toxic Substances Hydrology Program-Proceedings of the Technical Meeting, Monterey, CA, 162-171.

Pearce, J., Czernichowski-Lauriol, I., Lombardi, S., Brune, S., Nador, A., Baker, J., Pauwels, H., Hatziyannis, G., Beaubien, S. and Faber, E., 2004, A review of natural CO_2 accumulations in Europe as analogues for geological sequestration. Geological Society, London, Special Publications 2004, v. 233, p. 29-41.

Pettinelli, E., Beaubien, S. E., Lombardi, S. and Annan, P., 2008. GPR, TDR, and geochemistry measurements above an active gas vent to study near-surface gas-migration pathways. Geophysics, 73, A11-A15.

Pickles W. L. and Cover W.A. (2005) Vol 2 Chapter 22: Hyperspectral Geobotanical Remote Sensing for CO_2 Storage Monitoring in Carbon Dioxide Capture for Storage in Deep Geologic Formations – Results from the CO_2 Capture Project Geologic Storage of Carbon Dioxide with Monitoring and Verification - Volume 2 Edited by: Sally M. Benson, Lawrence Berkeley Laboratory, Berkeley, CA, USA

Pizzino, L., Galli, G., Mancini, C., Quattrocchi, F., and Scarlato, P., 2002, Natural Gas Hazard (CO_2, 222Rn) within a Quiescent Volcanic Region and its relations with tectonics: the case of the Ciampino-Marino Area, Alban Hills Volcano, Italy

Quattrocchi, F. and Venanzi, V., 1989, Sulla scelta di un sito per il monitoraggio di parametri idrogeochimici per lo studio di premonitori sismici nell' area dei Colli Albani, Proc. VIII Convegno GNGTS 1989, CNR - - Roma, pp. 259–266.

Quattrocchi, F. and Calcara, M., 1994, Groundwater chemistry in some Italian seismic areas: space and time correlations with tectonic features and seismic activity, Mineralogical Magazine, 58, 750 751.

Quattrocchi, F. and Calcara, M., 1998, Test-sites for earthquake prediction experiments within the Colli Albani region, Physics and Chemistry of the Earth, 23, 915–920.

Quattrocchi, F., Pizzino, L., Guerra, M., and Scarlato, P.: 1998, Geochemical Hazard of the Colli Albani quiescent volcano: CO_2 and 222Rn surveillance in Ciampino-Marino-Rocca di Papa area, Proceedings of the International Symposium "Cities on Volcanoes", Rome-Naples, 28/6-4/7/98, p. 114. (In Italian).

Randhol, P., Valencia, K., Taghipour, A., Akervoll, I., Carlsen, I.M., 2007. Ensuring well integrity in connection with CO_2 injection. SINTEF Petroleum Research, Report no. 31.6920.00/02/07, 27 December, 2007

Reddy, K. R., Adams, J. A., and Richardson, C. 1999. "Potential technologies for remediation of Brownfields". Practice Period. of Haz., Toxic, and Rad. Waste Mngmt. , ASCE, Reston, Virginia, USA, 3(2):61-68.

Réveillère, A. and Rohmer, J., 2011, Managing the risk of CO_2 leakage from deep saline aquifer reservoirs through the creation of a hydraulic barrier. Energy Procedia 4 (2011) 3187–3194.

Réveillère, A.,Rohmer, J., and Manceau, J.-C., 2012, Hydraulic barrier design and applicability for managing the risk of CO_2 leakage from deep saline aquifers. International Journal of Greenhouse Gas Control, 9, 62 – 71.

Roberts, J.J., Wood, R.A., and Haszeldine, R.S., 2011, Assessing the health risks of natural CO_2 seeps in Italy. Proceedings of the National Academy of Science, 108, 16545–16548.

Roehl, K.E., Meggyes, T., Simon, F.-G., and Stewart, D.I., 2005, Long-term performance of permeable reactive barriers. Elsevier, Netherlands.

Roehl, K.E., Czurda, K., ., Meggyes, T., Simon, F.-G., and Stewart, D.I., 2005, Permeable reactive barriers. In: Roehl, K.E., Meggyes, T., Simon, F.-G., and Stewart, D.I. (Eds.) Long-term performance of permeable reactive barriers. Elsevier, Netherlands, p. 1 – 25.

Rogie, J.D., Kerrick, D.M., Chiodini, G. and Frondini, F., 2000, Flux measurements of non-volcanic CO_2 emission from some vents in central Italy. Journal of Geophysical Research, 105 (B4), 8435-8445.

Romanak, K, Sherk, GW, Hovorka, SD, Yang, C., 2013, Assessment of alleged CO_2 leakage at the Kerr farm using a simple process-based soil gas technique: Implications for carbon capture, utilization, and storage (CCUS) monitoring, Energy Procedia; 37: 4242-4248.

Romanak, K. D., Wolaver, B., Yang, C., Sherk, G. W., Dale, J., Dobeck, L. M., Spangler, L. H., 2014. Process-based soil gas leakage assessment at the Kerr Farm: Comparison of results to leakage proxies at ZERT and Mt. Etna. International Journal of Greenhouse Gas Control, 30, pp. 42-57.

Rose, A. W., and Laurenso, F. J., 2000, Evaluation of two open limestone channels for treating acid mine drainage. In "Proceedings 2000 National Meeting of the American Society for Surface Mining and Reclamation," pp. 236-247. American Society for Surface

Mining and Reclamation, Tampa, FL.

Rouse, J. V. and Pyrith, R. Z. 1993. "Geochemistry". Chapter 2, Geotechnical Practice for Waste Disposal, D. E. Daniel, ed., Chapman and Hall, London, 15-32.

Rutters, H., Möller I., May, F., Flornes, K., Hladik, V., Arvanitis, A., Gulec, N., Bakiler, C., Dudu, A., Kucharic, L., Juhojuntti, N., Shogenova, A., Georgiev, G., 2013, State-of-the-art monitoring methods to evaluate CO_2 storage site performance. CGS Europe report D3.3, Korre A., Stead, R., and Jensen, N.B. (eds), 109p. http://repository.cgseurope.net/eng/cgseurope/knowledge-repository/key-reports/Monitoring.aspx, accessed Nov 2014

Sara M.N. 2003. Site Assessment and remediation handbook, second ed. CRC Press, 27 Jun 2003

SEPA, 2010, Environmental Standards for Discharges to Surface Waters: Supporting Guidance (WAT-SG-53). v.3.1. http://www.sepa.org.uk/water/regulations/guidance/idoc.ashx?docid=60ab10e9-2537-4530-be17-d6e39b0c8158&version=-1, accessed Nov 2014

Scivyer, C., 2007, Radon, guidance on protective measures for new buildings. Building Research Establishment, UK.

Scottish Parliament, 2010, Water Supply, The Water Quality (Scotland) Regulations 2010. http://www.legislation.gov.uk/ssi/2010/95/pdfs/ssi_20100095_en.pdf, accessed Nov 2014

ScottishPower CCS Consortium, 2011, Corrective Measures Plan UK Carbon Capture and Storage Demonstration Competition UKCCS - KT - S7.20 - Shell - 001 http://webarchive.nationalarchives.gov.uk/20130109092117/http://www.decc.gov.uk/en/content/cms/emissions/ccs/innovation/ccsfunding/ccsfunding.aspx , accessed Nov 2014

Shackelford, C. D., & Jefferis, S. A. 2000,. Geoenvironmental Engineering For In Situ Remediation. International Society for Rock Mechanics, November 19

Shapiro, A. M., and P.A. Hsieh, 1991. Research in Fractured-Rock Hydrogeology: Characterizing Fluid Movement and Chemical Transport in Fractured Rock at the Mirror Lake Drainage Basin, New Hampshire. Geological Survey Toxic Substances Hydrology Program - Proceedings of the Technical Meeting, Monterey, CA, 155-161.

Shepherd, J., Rivette, C. A., and Nava, R. C., 1993, Landfill liner CQA: A summary of real costs and a question of true value. In; Proceedings of the 6th GRI Seminar, MQC/MQA and CQC/CQA of Geosynthetics, Geosynthetic Research Institute, Philadelphia, 29–35.

Seckbach J, Baker FA, Shugarman PM. 1970. Algae thrive under pure CO_2. Nature 227:744–745

Sherwood Lollar, B., Ballentine, C.J. And O'Nions, R.K., 1997, The fate of mantle-derived carbon in a continental sedimentary basin: Integration of C/He relationships and stable isotope signatures. Geochimica et Cosmochimica Acta, 61, 2295-2307.

Shipton, Z.K., Evans, J. P., Dockrill B., Heath J., Williams A., Kirchner D. and Kolesar P. T., 2005, Natural leaking CO_2-charged systems as analogs for failed geologic sequestration reservoirs. In: Thomas D. and Benson S.M. (Eds). Carbon Dioxide Capture for Storage in Deep Geologic Formations; Results from the CO_2 Capture Project, Volume 2. Elsevier Science. p. 699-712.

Shipton, Z.K. and Evans, J.P. and Kirchner, D. and Kolesar, P.T. and Williams, A.P. and Heath, J., 2004, Analysis of CO_2 leakage through "low-permeability" faults from natural reservoirs in the Colorado Plateau, southern Utah. In Baines, S.J. and Worden, R.H. (Eds) Geological storage of carbon dioxide. Geological Society, London, Special Publications, no.233, p.43-58.

Shitashima, K, Maeda, Y, Koike, Y and Ohsumi, T., 2008, Natural analogue of the rise and dissolution of liquid CO_2 in the ocean. International journal of greenhouse gas control, 2, 95-104.

Simon, F.-G., Ludwig, S., Meggyes, T., Stewart, D.I. and Roehl, K.E., 2005, Regulatory and economic aspects. In: Roehl, K.E., Meggyes, T., Simon, F.-G., and Stewart, D.I. (Eds.) Long-term performance of permeable reactive barriers. Elsevier, Netherlands, p. 311 – 321.

Shan, C., R.W. Falta, and I. Javandel. 1992. Analytical solutions for steady state gas flow to a soil vapor extraction well. Water Resources Research, v. 28, p. 1105–1120.

Sherk, G. W., Romanak, K. D., Dale, J., Gilfillan, S. M. V., Haszeldine, R. S., Ringler, E. S., Wolaver, B. D., and Yang, C., 2011, The Kerr investigation: findings of the investigation into the impact of CO_2 on the Kerr property: IPAC Research Inc., final report prepared for property owners Cameron and Jane Kerr, 181 p.

Steeghs, P., Neele, F., Gittins, C., Ros, M., 2014, Drafting a monitoring plan for the ROAD project under the EU CCS Directive. Energy Procedia, v. 63, p. 6680 – 6687.

Stocks-Fischer, S., Galinat, J.K., and Bang, S.S., 1999, Microbiological precipitation of $CaCO_3$. Soil Biology and Biochemistry, v. 31, p. 1563–1571.

Sun, Q., McDonald, L. M., Jr., and Skousen, J. G., 2000, Effects of armouring on limestone neutralization of AMD. In: West Virginia Surface Mine Drainage Task Force Symposium. Morgantown, WV.

Suthersan S. S. 1997. Remediation Engineering: Design Concepts, Boca Raton, FL. CRC Press.

Tassi, F, Capaccioni, B, Caramanna, G, Cinti, D, Montegrossi, G, Pizzino, L, Quattrocchi, F, Vaselli, O., 2009, Low-pH waters discharging from submarine vents at Panarea Island (Aeolian Islands, southern Italy) after the 2002 gas blast: Origin of hydrothermal fluids. Applied Geochemistry, 24, 246-254.

Trium Inc. and Chemistry Matters, 2011. Site Assessment (SW-30-05-13-W2M), near Weyburn, Saskatchewan, report prepared for Cenovus Energy Inc., p. 39.

Trotta, C.,Fratini, G. And Papale, D., 2010. Quantification of uncertainty in eddy-covariance flux estimates of CO_2 and energy due to raw data processing. American Geophysical Union, Fall Meeting 2010, abstract #B11D-0399.

Turner, B.D., Binning, P.J., and Sloan, S.W., 2008, A calcite permeable reactive barrier for the remediation of Fluoride from spent potliner (SPL) contaminated groundwater. Journal of Contaminant Hydrogeology, v. 95, p. 110 – 120.

Ulrich, J., 1958, Die mineralquellen der Vulkaneifel und ihre wirtschaftliche auswertung. Gewiiss. Abwiiss., 19, 66-80.

UKRadon, 2014, How to reduce radon levels, by Public Health England. http://www.ukradon.org/information/reducelevels, accessed 23 June 2014.

US EPA, 1987, Guidance for Delineation of Wellhead-protection Areas U.S. Environmental Protection Agency, Office of Groundwater

Protection, Washington, DC. http://nepis.epa.gov/Exe/ZyPURL.cgi?Dockey=2000LO01.txt Accessed 4 July 2014.

US EPA, 2009, National primary drinking water regulations. United States Environmental Protection Agency. http://water.epa.gov/drink/contaminants/upload/mcl-2.pdf

Viveiros, F., Ferreira, T., Cabral Vieira, J., Silva, C., and Gaspar, J L., 2008, Environmental influences on soil CO_2 degassing at Furnas and Fogo volcanoes (São Miguel Island, Azores archipelago). Journal of Volcanology and Geothermal Research, 177, 883–893.

von Shoenfeeldt, H., Zupanik, J., Wight, D., and Stevens, S.H, 2004, Unconventional drilling methods for unconventional reservoirs in the US and overseas. International Coalbed Methane Symposium, University of Alabama, Tuscaloosa, Alabama, May 2004.

Waite, T.D., Desmier, R., Melville, M., and Macdonald, B, 2002, Preliminary investigation into the suitability of permeable reactive barriers for the treatment of acid sulfate soils discharge. In: Naftz, D.L., Morrison, S.J., Fuller, C.C. and Davis, J.A. (Eds.) Handbook of Groundwater Remediation using Permeable Reactive Barriers, Applications to Radionuclides, Trace Metals, and Nutrients. Elsevier. ISBN: 978-0-12-513563-4

Warren L. A., Maurice P. A., Parmar N., and Ferris F. G., 2001, Microbially mediated calcium carbonate precipitation: Implications for interpreting calcite precipitation and for solid-phase capture of inorganic contaminants. Geomicrobiology Journal, v.18, p. 93–115.

Weaver, K.D., and Bruce, D.A., 2007, Dam foundation grouting. American Society of Civil Engineers, Virginia USA. 473 pp.

Wilkinson, M., Gilfillan, S.M.V., Haszeldine, R.S. & Ballentine, C.J., 2009, Plumbing the depths – testing natural tracers of subsurface CO_2 origin and migration, Utah, USA. In: M. Grobe, J.C. Pashin, and R.L. Dodge (editors) Carbon dioxide sequestration in geological media — State of the science: AAPG Studies 59, p.619 - 634.

Wilkinson, M., Haszeldine, R.S., Fallick, A.E., Odling, N., Stoker, S. & Gatliff, R., 2009, CO_2 - Mineral reaction in a natural analogue for CO_2 storage: implications for modelling. Journal of Sedimentary Research, 79, 486 - 494.

Zhang,Y., Oldenburg, C.M., and Benson, S.M., 2004, Vadose zone remediation of carbon dioxide leakage from geologic carbon dioxide sequestration sites. Vadose Zone Journal, v. 3, p.858–866.

Ziemkiewicz, P. F., Skousen, J. G., Brant, D. L., Sterner, P. L., and Lovett, R. J., 1997, Acid mine drainage treatment with armored limestone in open limestone channel. J. Environ. Qual. v. 26, p. 1017-1024.

Section IX

ASSESSMENT OF REMEDIATION CONSEQUENCES AND CORRECTIVE MEASURES HANDBOOK

Chapter XXXII

Report on individual remediation techniques scoring method and classification/ranking results

Rajesh Govindan[1], Mojgan Hadi Mosleh[1], Anna Korre[1], Sevket Durucan[1],
Niklas Heinemann[2], Mark Wilkinson[2]
[1] Imperial College, UK
[2] University of Edinburgh, UK

SUMMARY

The objective of the task presented in this deliverable report is to synthesise the results of the modelling studies carried out in the MiReCOL project, focusing on various mitigation and remediation techniques, and carrying out an evaluation of their performance as either threat barriers (for risk reduction) or recovery and preparedness measures (for consequence benefits) that can be achieved. The issues considered were relating to technology specific issues of the techniques, including their implementation costs.

A methodology was proposed to quantify the effectiveness of the techniques in a manner which allows for a comparison of the indicative performance metrics, based on the results of the scenarios that were investigated. The overall performance characterisation was based on five dimensions, as agreed during the course of the project, namely:

- likelihood of success
- spatial extent
- longevity
- response speed
- cost efficiency

The overarching goal is to subsequently feed the outcomes of this report into the on-line remediation selection tool which was developed in parallel.

1 INTRODUCTION

1.1 Objective

The overall objective of WP11 is to synthesise the results of CO_2 leakage mitigation/remediation modelling studies carried out during the MiReCOL project and to evaluate their performance as either threat barriers for potential leakage risk reduction, or recovery and preparedness measures for leakage consequence reduction. The technology specific issues of relevant techniques, including their implementation costs, were considered in this deliverable report.

1.2 Bow-tie analysis

A number of projects have adopted the bow-tie analysis for risk management across a variety of business sectors world-wide, and the method has been in widespread use since the mid-1990s. In the bow-tie analysis, a 'top event' is initially identified. In the case of CO_2 storage, this is often an event of leakage from the storage reservoir. The threats such as a leaky fault or injection induced overpressure, which might trigger the top event, are then identified. The threat barriers, referred to as risk mitigation techniques, are subsequently assessed in order to reduce or eliminate the threat. If the top event is already occurring at the time of analysis, e.g. an identified leakage of CO_2 from the storage reservoir, the method considers consequences, such as loss of CO_2 storage permanence or environmental impacts and, using consequence barriers, aims to limit such adverse impacts. Thus, the bow-tie diagram also facilitates the assessment of recovery and preparedness measures, referred to as remediation techniques, in order to reduce the severity of the consequences. Figure 1 illustrates the bow-tie diagram for WP11, indicating all the techniques that were investigated under the scope of the MiReCOL project.

1.3 Assessment methodology

In order to evaluate the mitigation and remediation techniques, the results that were presented previously in the MiReCOL project SP1 to SP3 deliverable reports were analysed. In particular, the quantification of effectiveness of a technique is generally based on either: (a) the delay achieved in the arrival time of the CO_2 plume at the location of a potential threat, e.g. leaky faults or fractures; (b) the reduction in amount of CO_2 that could migrate beyond the reservoir spill point; (c) the reduction in amount of CO_2 that may leak through sub-seismic fractures in the caprock into a shallower formation; (d) the reduction in the reservoir pressure which could potentially induce or exacerbate leakage; or (e) the enhancement of the dissolution of injected CO_2 in the reservoir brine to either reduce the local pressure or the amount of CO_2 that may leak.

1.3.1 Success probability estimation

The results obtained for the effectiveness were pooled to generate cumulative probability plots that allow for the quantification of the expected values of success of the implementation of the techniques, however, conditioned only on the mitigation and remediation scenarios that were detailed in the different SP1 – SP3 work packages. It is also important to note that in the mitigation case, the implementation could either improve, or unexpectedly make matters worse, and hence the mitigation effectiveness could range between negative (not effective) and positive (effective) values, whereas for the remediation case, effectiveness values were assumed to be strictly non-negative.

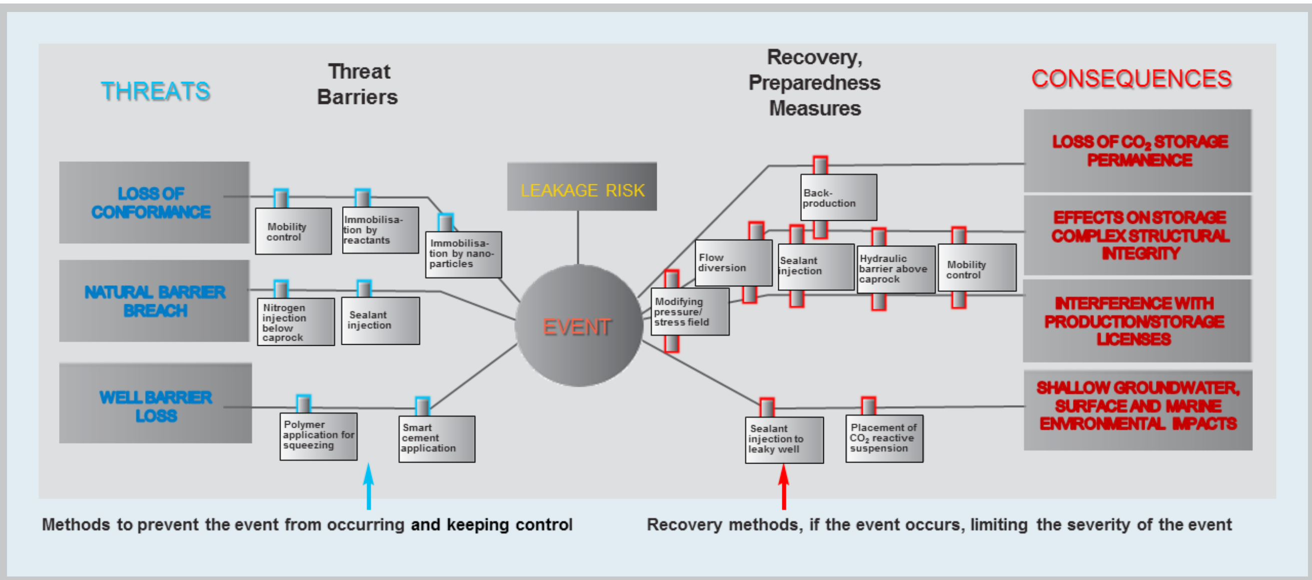

Figure 1 The bow-tie diagram for the MiReCOL project.

1.3.2 Overall performance characterisation

Furthermore, the scoring/ranking of individual techniques was implemented using an ordinal classification (low, medium and high) in five dimensions, namely: (a) likelihood of success (see Table 1); (b) spatial extent (see Table 2); (c) longevity (see Table 3); (d) response speed (see Table 4); and (e) cost efficiency (see Table 5), based on the results that were obtained for different scenarios.

Table 1 Classification of the likelihood of success dimension.

Rank	Likelihood of Success (%)
Low	0 - 33
Medium	34 - 66
High	67 - 100

Table 2 Classification of the spatial extent dimension.

Rank	Spatial Extent (km^2)
Low	0 - 1
Medium	1 - 5
High	> 5

Table 3 Classification of the longevity dimension.

Rank	Longevity (years)
Low	0 - 1
Medium	1 - 10
High	>10

Table 4 Classification of the response speed dimension.

Rank	Response Speed (years)
Low	>1
Medium	0.1 - 1
High	0 - 0.1

Table 5 Classification of the cost efficiency dimension.

Rank	Cost Efficiency (M€)
Low	> 10
Medium	1 - 10
High	0 - 1

Despite being a qualitative output, the resulting spider chart outputs represent the best efforts that could possibly be made to standardise the scales in different dimensions in order to ensure that it is indicative of the overall merit of a given technique, and also allowing for making a comparison between techniques.

2 ASSESSMENT OF THE CONSEQUENCES RELATED TO MITIGATION TECHNIQUES

2.1 Adaption of injection strategy to control the migration of CO_2 plume in the reservoir

The selection of an appropriate CO_2 injection strategy offers the potential for increasing both the safety and longevity of containment in the storage reservoir. It can potentially prevent, or at least retard, CO_2 from arriving at and passing through (pre-defined) undesired migration paths, such as faults, fracture zones or spill points. By doing this, it may also decrease the necessity for active remediation, such as gel and foam injection, brine injection or chemical immobilisation of CO_2, at a later stage of the storage cycle. Therefore, selection of an injection strategy as a proactive measure would be cost efficient when compared to the implementation of an active remediation technique.

The impact of threat mitigation through the variation of injection location and rate, taking into account of the geological conditions, were investigated by GFZ at the Ketzin site, Germany. The results were discussed in detail in deliverable D3.2.

In order to quantify the success of the adaptation of injection strategy in threat mitigation, i.e. the percentage of delay achieved in the simulated time taken for the plume to arrive at undesired migration pathways that potentially result in CO_2 leakage, a cumulative probability plot was generated by pooling the results obtained for all the scenarios that were considered. Figure 2a illustrates that if the desirable mitigation level is assumed to be 20% or greater, then the probability of success for threat mitigation is only 10%. Moreover, the probability of occurrence of a situation worse than the baseline scenario (when no mitigation is implemented, corresponding to 0% threat mitigation level) is approximately 75%, which additionally undermines the applicability of the technique in the given context. Figure 2b illustrates a summary of the outcomes of the technique considering all the dimensions.

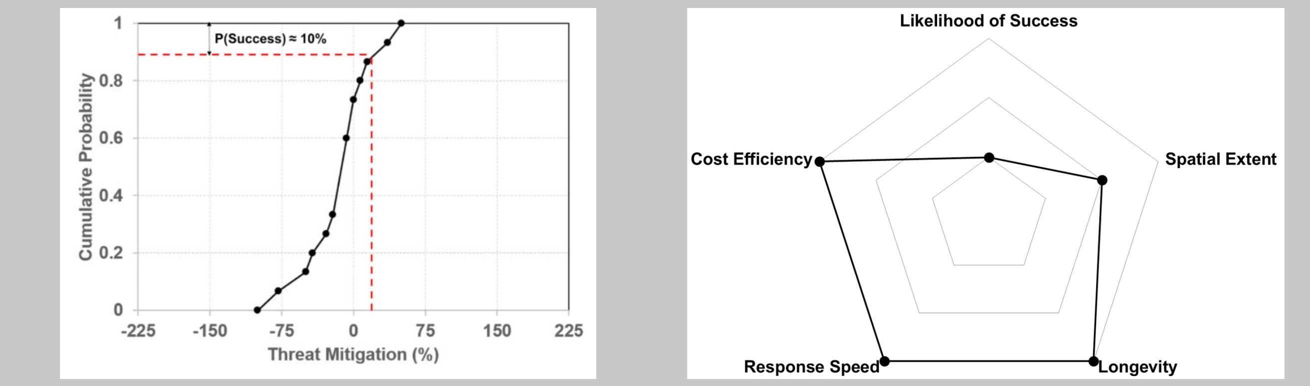

Figure 2 Adaptation of injection strategy technique: (a) success probability; (b) spider chart.

2.2 Novel approaches to lower reservoir pressure by accelerating convective mixing between brine and CO_2

The possibility for enhancing the dissolution of CO_2 in brine was investigated with a view that it: (a) potentially lowers the pressure of the reservoir during CO_2 injection; and (b) ensures that CO_2 would no longer migrate as a separate phase, and thus restricted to the migration of reservoir brine which is relatively much slower owing to its higher density. In order to enhance CO_2 dissolution during the injection phase, the co-injection of CO_2 with nanoparticles (NPs) to enhance convective mixing was considered. The proposed method enhances the natural process of convective mixing by increasing the density of the CO_2-saturated brine by using NPs. Heavy NPs (e.g. metals and/or metal oxides, which are in the order of 1-50 nm in size) move into the brine together with the CO_2, which increases the density of the CO_2-saturated brine which results in an increased rate of convective mixing.

To evaluate the feasibility of using NPs for remediation and/or mitigation, TNO evaluated to two aspects, namely: (a) the placement of NPs; (b) the quantification of enhancement of convective mixing, thereby increasing the dissolution of CO_2 into the brine. For the first aspect, investigations included the simulation of the injection of a mixture containing NPs at the interface between the CO_2 and brine in the reservoir. The main question addressed by the NPs placement simulation was relating to the acceptable density of the NP-CO_2 mixture for injection. It was concluded that a homogeneous mixture would be heavier than CO_2, but lighter than brine. If the mixture is too heavy, then it would move into the brine and not spread on the interface. On the other hand, if the mixture is too light (i.e. density difference with the CO_2 is small), the spreading would not be efficient. Furthermore, for the second aspect, a situation was assumed wherein a mixture of free CO_2 and NPs layer is present on top of brine (both are assumed stationary). Equations from the literature for the estimation of CO_2 dissolution resulting from convective mixing were implemented. The results obtained were discussed in detail in deliverable D4.5.

In order to quantify the success of the NP injection in threat mitigation, i.e. the percentage increased CO_2 dissolution into reservoir brine for the simulated time, a cumulative probability plot was generated by pooling the results obtained for all the scenarios that were considered. Figure 3a illustrates that if the desirable mitigation level is assumed to be 20% or greater, then the probability of success for threat mitigation is 85%. In addition, it is observed that the minimum threat mitigation level is 10%, suggesting that there is a noticeable improvement from the baseline scenario. Figure 3b illustrates a summary of the outcomes of the technique considering all the dimensions.

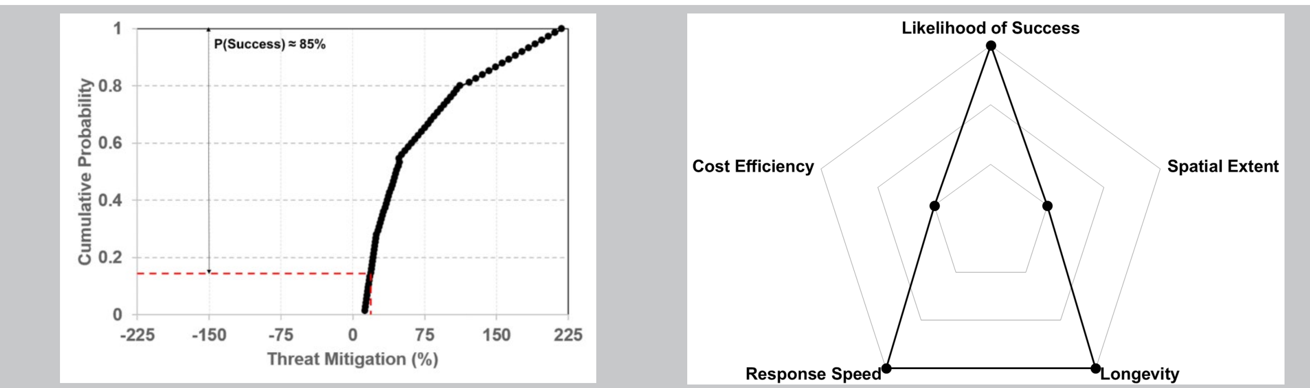

Figure 3 Acceleration of convective mixing technique: (a) success probability; (b) spider chart.

2.3 Smart cement with a latex-based component for mitigation of potential well leakage

Although the capacity and injectivity of a geological formation plays an important role in its consideration for CO_2 storage, the prevailing confinement conditions are also necessary. If, however, the formation meets all the required conditions, the only potential means of CO_2 leakage should theoretically be via the wellbore. Wellbores have been identified as the most likely pathways of leakage at a CO_2 storage site. Multiple leakage pathways could be associated with the wellbore that are often formed due to inadequate well completion, or the use of unstable wellbore materials in a CO_2-rich setting. The proposed method using smart cement presents a novelty in the mitigation of the risk of CO_2 leakages from deep reservoirs via wellbores. Imperial College investigated the use of latex-based smart cement for the purpose of CO_2 leakage mitigation at the wellbore. The main objectives were: (a) to investigate the effectiveness of smart cement in the mitigation of leakage either through the casing-cement or casing-rock interfaces, or through the fractures within the cement itself; (b) to characterise the latex-cement mixture for its permeability, mechanical behaviour and strength using core samples; (c) to characterise the permeability of latex-cement under deep reservoir conditions by subjecting samples of the latex-cement to CO_2 flow using Imperial College's wellbore cell; (d) to compare stress-permeability behaviour of the microannulus of the latex-cement with that of Class G Portland cement. The experimental observations of permeability, mechanical properties and sealing characteristics of the latex-cement cement was subsequently used as an input to a wellbore numerical model to study the effectiveness of remediation through the use of latex-cement for overall integrity of CO_2 storage. The results obtained were discussed in detail in deliverable D9.4.

In order to quantify the success of smart cement implementation in threat mitigation, i.e. the percentage of the amount of leakage reduction achieved, should leakage unexpectedly occur within the simulated time periods, a cumulative probability plot was generated by pooling the results obtained for all the scenarios that were considered. Figure 4a illustrates that if the desirable mitigation level is assumed to be 20% or greater, then the probability of success for threat mitigation is 70%. In addition, it is estimated that the probability of occurrence of a situation worse than the baseline scenario is approximately 20%. Figure 4b illustrates a summary of the outcomes of the technique considering all the dimensions.

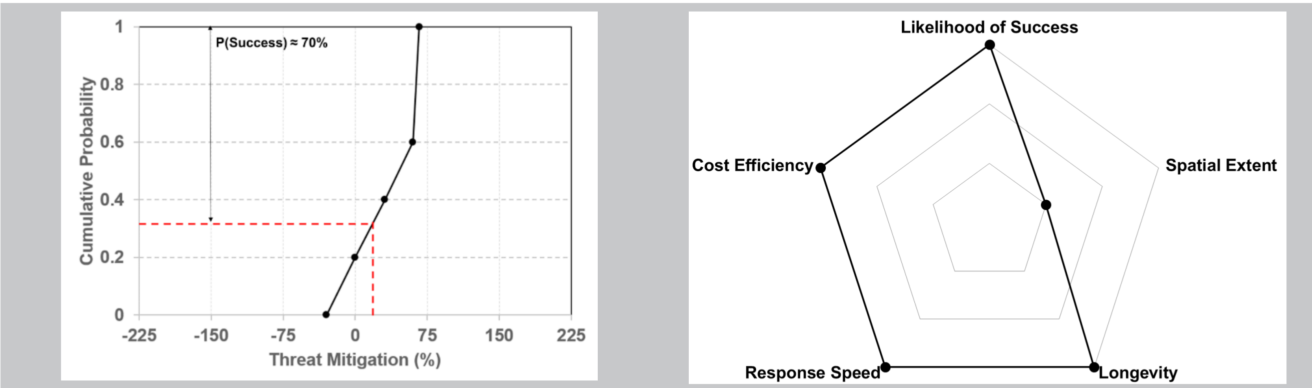

Figure 4 Smart cement wellbore technique: (a) success probability; (b) spider chart.

3 ASSESSMENT OF THE CONSEQUENCES RELATED TO REMEDIATION TECHNIQUES

3.1 Options to enable the flow diversion of CO_2 plume

3.1.1 Foam injection

Foam is used in the oil and gas industry for mobility control of gas sweep during enhanced oil recovery. The desired effect is to reduce the mobility of the gas, forcing the injected gas to take alternative paths thus contacting more oil as well as delaying gas breakthrough in the production wells. Foam is also used to reduce gas coning/cresting at production wells. In the current context, foam injection was investigated by SINTEF as a technique to remediate CO_2 leakage, in the event of an unexpected migration of the plume in the reservoir. It primarily involves the injection of a solution comprising of surfactant and brine in the reservoir. The solution reacts with the CO_2 in-place leading to the generation of foam, which causes the reduction in the mobility of the CO_2, thereby minimising potential leakage. The plugging effect of foam treatment depends on several factors, including the reservoir geology, position and type of leakage, injected surfactant volumes, surfactant concentration, adsorption, foam strength and foam stability. The main purpose of the study was to explore the ranges of some of these factors and to quantify their impact on a leakage event. The results obtained were discussed in detail in deliverable D3.3.

In order to quantify the success of foam injection for leakage remediation, i.e. the percentage of the amount of leakage reduction achieved after the detection of occurrence of an unexpected leakage within the simulated time periods, a cumulative probability plot was generated by pooling the results obtained for all the scenarios that were considered. Figure 5a illustrates that if the desirable remediation level is assumed to be 20% or greater, there is a nil probability of success for leakage remediation. The threshold remediation level to measure success, however, is dependent on the cumulative amount of CO_2 that is injected prior to leakage detection. In other words, a higher threshold is desirable if a large amount is injected into the reservoir, representing a conservative measure of success. More specifically, in the scenarios considered, the cumulative amount of CO_2 injected is 7.5Mt and the amount leaked beyond the spill point is approximately 4Mt. Hence, a higher threshold remediation level (>20%) would be desirable. Figure 5b illustrates a summary of the outcomes of the technique considering all the dimensions.

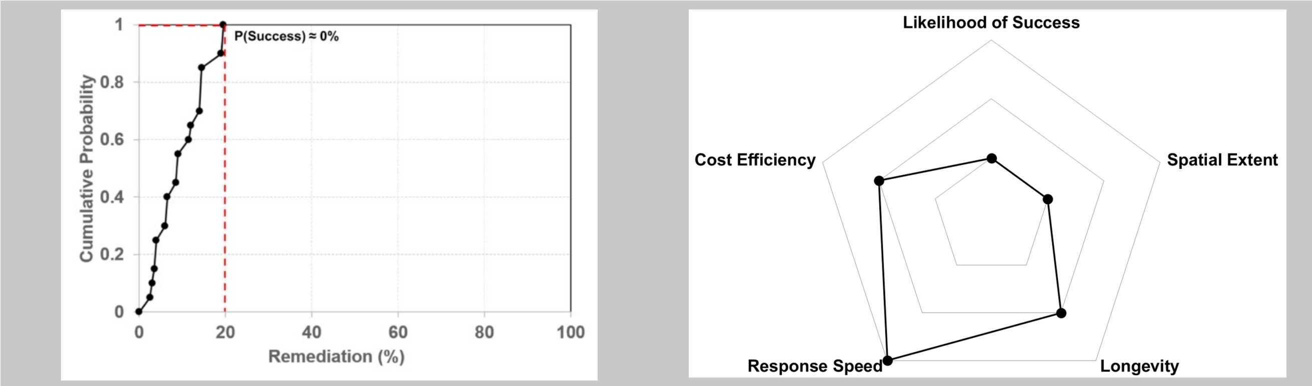

Figure 5 Foam injection technique: (a) success probability; (b) spider chart.

3.1.2 Polymer-based gel injection

Cross-linked hydrolysed polymer-gel injection is used in petroleum industry to improve conformity of fluid flow in the reservoir, remediate leakage around wells, and also used in conjunction with enhanced oil recovery at various temperature and pressure conditions. Water-based gels are highly elastic semi-solids with high water content, trapped in the three-dimensional polymer structure of the gel. Polyacrylamide (PAM) is the main cross-linked polymer used mostly by the industry. The use of biopolymers is more challenging as compared to the synthetic polymers due to chemical degradation at higher temperatures, causing the loss of mechanical strength. Most of polymer-gel systems are based on crosslinking of polymers with a heavy metal ion. The most commonly used heavy metal ion is chromium III. However, in view of its toxicity and related environmental concerns, its application in reservoir conformance and CO_2 leakage remediation is considered to be limited. Therefore, more environmental friendly crosslinkers such as boron, aluminium and zirconium have been proposed and used in recent years.

Imperial College used numerical simulators to implement the known interaction properties of polymer solution and crosslinkers using data from the literature and laboratory tests. The effect of reservoir permeability, polymer and crosslinker concentrations, pH and gelation kinetics were investigated. The property-based results were further translated into the simulation of scenarios for CO_2 leakage remediation using polymer-gel injection in the reservoir. The results obtained were discussed in detail in deliverable D6.3.

In order to quantify the success of polymer-gel injection for leakage remediation, i.e. the percentage of the amount of leakage reduction achieved after the detection of occurrence of an unexpected leakage within the simulated time periods, a cumulative probability plot was generated by pooling the results obtained for all the scenarios that were considered. Figure 6a illustrates that if the desirable remediation level is assumed to be 20% or greater, there is a 100% probability of success for leakage remediation. The high success probability in this case is only indicative and, as highlighted for foam injection in the previous section, is dependent on the cumulative amount of CO_2 that is injected prior to leakage detection. Figure 6b illustrates a summary of the outcomes of the technique considering all the dimensions.

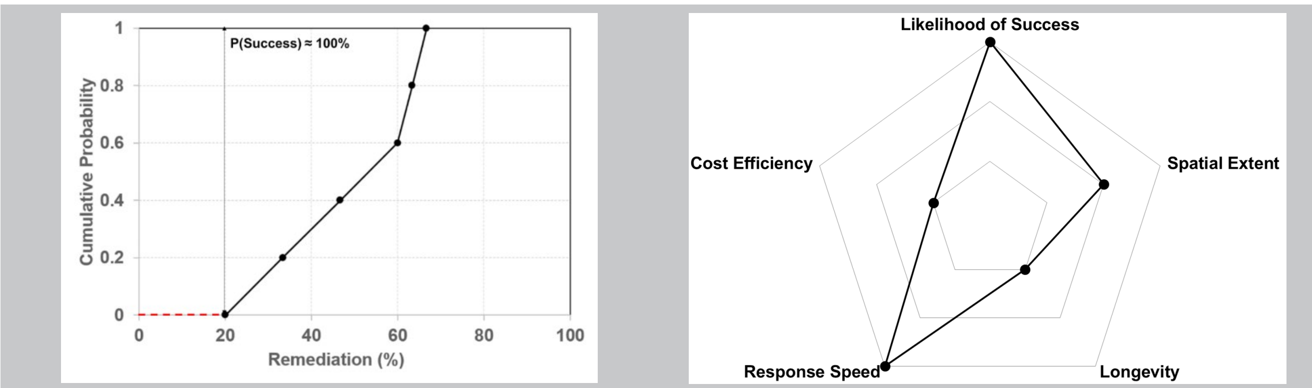

Figure 6 Polymer-gel injection technique: (a) success probability; (b) spider chart.

3.1.3 Brine/Water injection

In secondary oil recovery, brine or water injection has a long history either to support reservoir pressure or to displace oil towards producing wells. There is a range of techniques and theories (e.g. Buckley Leverett analysis) about how water injection can be used to increase oil recovery. Volumetric sweep management and realignment of production in contiguous layers are the nearest analogues in the oil industry to the use water injection in order to stop the migration of CO_2. Industry has studied several mechanisms by which water injection can be used to reduce CO_2 migration, such as: (1) creating a high pressure barrier in front of the migrating CO_2 plume; (2) chasing CO_2 with brine ensuring storage security; and (3) injecting water directly into the advancing CO_2 plume.

Three different examples of water injection remediation have been investigated by the project partners, listed as follows:

- SINTEF used a portion of the Johansen formation as the basic model with water injection in front of the CO_2 migration plume. The model was modified to represent the key characteristics of twenty other possible CO_2 storage aquifers.
- Using a generic model, Imperial College studied the reduction of CO_2 leakage through a sub-seismic fault by means of water injection via the well previously used for CO_2 injection.
- TNO also used the Johansen model to simulate ten alternative scenarios using a combined approach of water injection and CO_2 back-production as remediation measures.

The results obtained were discussed in detail in deliverable D3.4.

In order to quantify the success of brine/water injection for leakage remediation, i.e. the percentage of the amount of leakage reduction achieved after the detection of occurrence of an unexpected leakage within the simulated time periods, a cumulative probability plot was generated by pooling the results obtained for all the scenarios that were considered. Figure 7a illustrates that if the desirable remediation level is assumed to be 20% or greater, the estimated probability of success for leakage remediation is 35%. A summary of the outcomes of the technique considering all the dimensions is illustrated in Figure 7b.

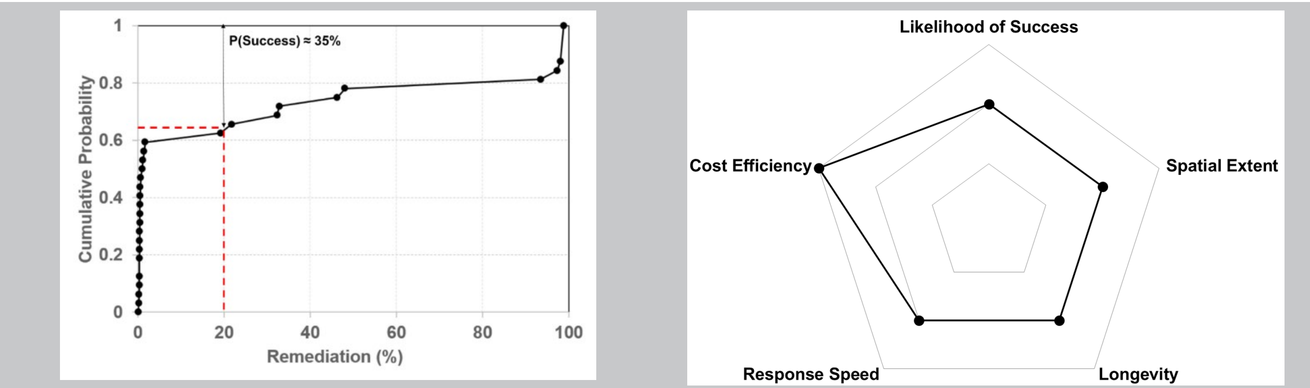

Figure 7 Brine/water injection technique: (a) success probability; (b) spider chart.

3.1.4 Brine/Water withdrawal

The over-pressurisation of the reservoir during CO_2 injection is of concern because it could have a large-scale impact, namely interference with the operations in neighbouring oil and gas fields, or CO_2 storage sites that could co-exist in the same formation. Such interference also has regulatory implications since issuing permits to operators would then be based on the outcome of a multi-site process evaluation, which can be quite involved, and rather unnecessary. In the literature, it was demonstrated that by producing brine from the reservoir, the pressure-driven leakage was minimised and consequently the net of amount of leakage is largely buoyancy-driven, thus reducing the rate of leakage. While pressure management via brine extraction is not be considered a mandatory component for large-scale CO_2 storage projects, it could also potentially provide many other benefits, such as increased storage capacity utilisation, simplified permitting, smaller area of review for site monitoring, and the manipulation of CO_2 plume in order to increase its sweep efficiency.

Imperial College investigated the technique using numerical simulations of CO_2 storage and leakage remediation for an offshore and compartmentalised depleted gas reservoir, called the P18-A block (in the Dutch offshore region). The scenarios considered the study of a cluster of gas fields in the reservoir in order to understand the plume migration and reservoir pressure response during CO_2 injection, and the remediation achieved using brine withdrawal in terms of flow diversion and pressure relief. The results obtained were discussed in detail in deliverable D4.4 (Chapter IX).

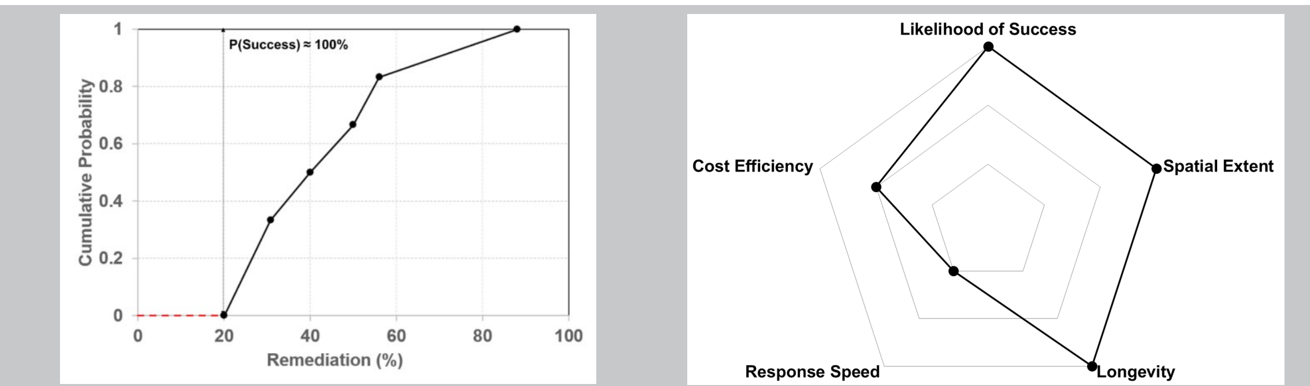

Figure 8 Brine/water withdrawal technique: (a) success probability; (b) spider chart.

In order to quantify the success of brine/water withdrawal for leakage remediation, i.e. the percentage of the amount of leakage reduction achieved after the detection of occurrence of an unexpected leakage within the simulated time periods, a cumulative probability plot was generated by pooling the results obtained for all the scenarios that were considered. Figure 8a illustrates that if the desirable remediation level is assumed to be 20% or greater, the estimated probability of success for leakage remediation is 100% (indicative). A summary of the outcomes of the technique considering all the dimensions is illustrated in Figure 8b.

3.2 Blocking of CO_2 movement by immobilisation of CO_2 in solid reaction products

Experience with unintentional precipitation or scaling and formation damage, as commonly encountered in the oil and gas or geothermal industries, sheds some light onto the possibilities for forming solid reactants. Minerals observed to form 'naturally' within the reservoir may all be potential candidates for controlled precipitation. Frequently occurring scales associated with oil and gas production are calcite, anhydrite, barite, celestite, gypsum, iron sulphide and halite. Re-injection of production water is prone to scaling of calcium carbonate, while strontium, barium and calcium sulphates are more relevant for seawater injection. In addition to fluid-fluid reactions, fluid-gas interaction could promote mineralisation. Controlled intentional clogging due to salt precipitation, which occurs when the solubility is exceeded by the evaporation into injected dry gas, could potentially prevent the leakage of CO_2. This process is similar to salt scaling in natural gas and oil production, and CO_2 injection in saline aquifers and depleted gas fields.

TNO investigated scenarios to study the feasibility of injecting a lime-saturated solution as a CO_2-reactive solution above the caprock, at the location where the leakage has been detected. The solution has a low viscosity which simplifies the injection process. The results derived for the injection of the lime-saturated solution provided a general insight in leakage remediation using non-swelling CO_2 reactive substances. However, the production and practical use of such a fluid was beyond the scope of the study. The results obtained were discussed in detail in deliverable D3.5 (Chapter V).

In order to quantify the success of the injection of CO_2-reactive lime-saturated water investigated in this project, i.e. the percentage of the amount of leakage rate reduction achieved after the detection of occurrence of an unexpected leakage within the simulated time periods, a cumulative probability plot was generated by pooling the results obtained for all the scenarios that were considered. Figure 9a illustrates that if the desirable remediation level is assumed to be 20% or greater, the estimated probability of success for leakage remediation is 90%. A summary of the outcomes of the technique considering all the dimensions is illustrated in Figure 9b.

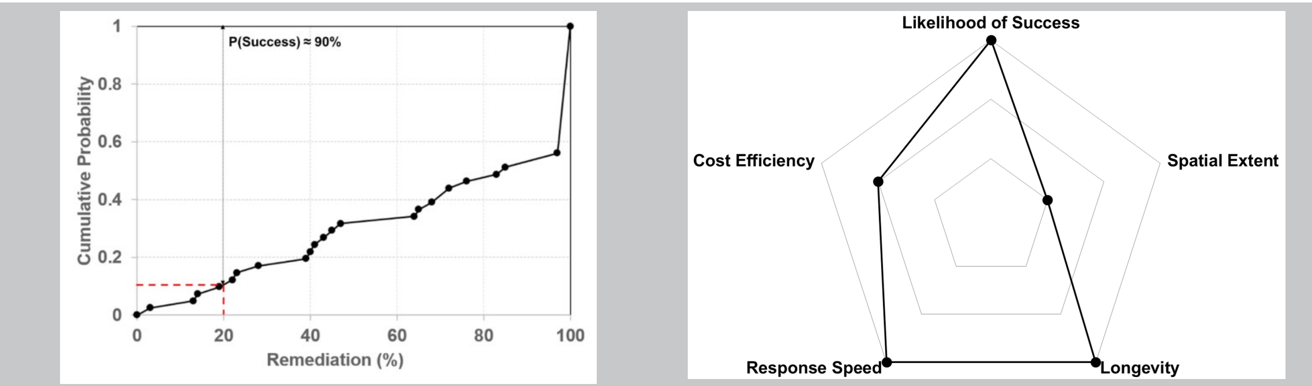

Figure 9 Polymer-gel injection technique: (a) success probability; (b) spider chart

3.3 CO_2 back-production

The back-production of formerly injected CO_2 may provide a suitable technique to: (1) mitigate undesired migration of CO_2 in the reservoir by inducing a pressure-gradient driven directed flow of CO_2; and (2) manage the reservoir pressure. Furthermore, the production of CO_2 will also form an integral part of any temporary storage of CO_2 in the frame of a different carbon capture storage and utilisation and/or power-to-gas concepts. In CO_2 storage combined with enhanced hydrocarbon recovery, CO_2 will be co-produced with the recovered hydrocarbons. The production ratio of gas to reservoir fluid is an important design parameter in all contexts. Below a minimum flow velocity in a well, the critical Turner velocity, no fluid is produced, and hence well load up (cone shaped brine accumulation) occurs.

The CO_2 back-production technique was investigated in this project using case studies based on two examples, each an offshore and onshore site, listed as follows:

- GFZ and Imperial College jointly carried out numerical studies prior to and after the Ketzin pilot field test to support its design and demonstrate the performance of the history-matched backproduction model, and thereby estimate the expected reduction in reservoir pressure achieved.
- TNO carried out a case study for the K12-B gas field in the North Sea to investigate the back-production technique. Numerical analyses focused on key factors such as recovery rate, CO_2 ratio, well pressure and water co-production.

The results obtained were discussed in detail in deliverable D4.3 (Chapter VIII).

In order to quantify the success of CO_2 production technique, i.e. the percentage of the reduction in reservoir pressure achieved within the simulated time periods as an indirect indicator for potential leakage reduction, a cumulative probability plot was generated by pooling the results obtained for all the scenarios that were considered. Figure 10a illustrates that if the desirable remediation level is assumed to be 20% or greater, the estimated probability of success for potential leakage remediation is 80%. A summary of the outcomes of the technique considering all the dimensions is illustrated in Figure 10b.

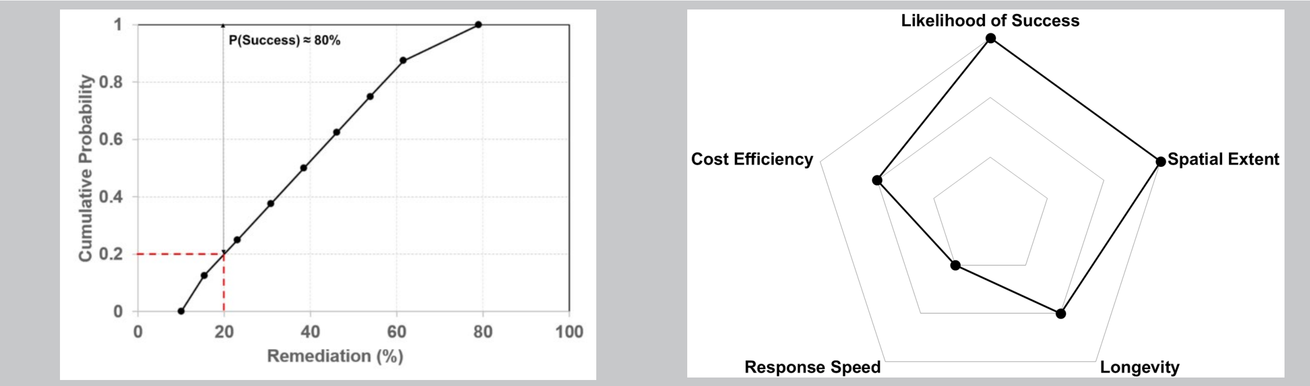

Figure 10 CO_2 backproduction technique: (a) success probability; (b) spider chart.

3.4 Hydraulic barrier

It has been suggested that injection of brine above the caprock, at a higher pressure than the CO_2 pressure in the reservoir, would create an inverse pressure gradient to reverse the flow direction and increase the solubility of CO_2 in the saline water barrier formed, and prevent or limit leakage. Furthermore, coupled with fluid management procedures during aquifer storage (saline water extraction and re-injection above the caprock), this can also be used to minimise displacement and migration of native brine, and avoid pressure build up in closed or semi-closed structures.

Imperial College investigated the effectiveness of pressure gradient reversal (PGR), a hydraulic barrier technique, as a potential remediation technique for CO_2 leakage from deep saline aquifers using a generic and geologically realistic model, comprising of the reservoir, caprock and an overlying shallow aquifer. The focus was on the role of controlling parameters which may affect the success or failure of the hydraulic barrier technology considered. The results obtained were discussed in detail in deliverable D7.3 (Chapter XX).

In order to quantify the success of the hydraulic barrier technique, i.e. the percentage of the amount of leakage rate reduction achieved after the detection of occurrence of an unexpected leakage within the simulated time periods, a cumulative probability plot was generated by pooling the results obtained for all the scenarios that were considered. Figure 11a illustrates that if the desirable remediation level is assumed to be 20% or greater, the estimated probability of success for leakage remediation is 95%. A summary of the outcomes of the technique considering all the dimensions is illustrated in Figure 11b.

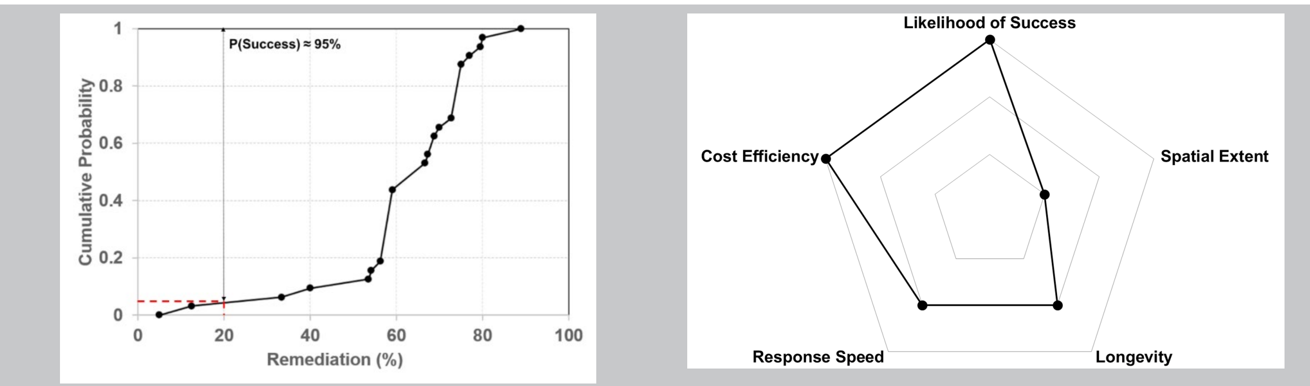

Figure 11 Hydraulic barrier technique: (a) success probability; (b) spider chart.

3.5 Polymer-gel-based sealant injection

3.5.1 Well leakage remediation

The use of synthetic and biopolymer solutions by the petroleum industry has been mostly associated with enhanced oil recovery and widely used around the world. For polymer-gel compounds (usually crosslinked with a heavy metal), the application is considered for water-cut and flow conformance control within the reservoir as well as leakage remediation in the near wellbore area. The polymer solution is composed of molecular chains of the chosen polymer, a carrier fluid such as water or brine, and a crosslinker such as chromium III, zirconium, and aluminium. Polymers are made of coiled chains, especially of high molecular weight polymers. Once they are added into solution, the charged areas on the chain repel each other and force the chain to uncoil. As a result, the viscosity of the solution increases. Generally, the charge also affects the speed at which the chain uncoils. The higher charged polymers will uncoil faster, whereas, non-ionic polymers may never fully uncoil since they carry no charge.

Imperial College carried out both laboratory tests and numerical simulations in order to understand the effectiveness of polymer-gel treatment on the permeability reduction of wellbore cement, thereby effectively minimising CO_2 leakage through a microannulus between cement and casing interface, and in near wellbore region of the host/caprock. In particular, deep, high temperature and high pressure reservoir conditions were considered for the simulations. The results obtained were discussed in detail in deliverable D9.3 (Chapter XXVI).

In order to quantify the success of the use of polymer-gel based sealant injection for wellbore leakage remediation, i.e. the percentage of the amount of leakage reduction achieved after the detection of occurrence of an unexpected leakage within the simulated time periods, a cumulative probability plot was generated by pooling the results obtained for all the scenarios that were considered. Figure 11a illustrates that if the desirable remediation level is assumed to be 20% or greater, the estimated probability of success for leakage remediation is 100% (indicative). A summary of the outcomes of the technique considering all the dimensions is illustrated in Figure 11b.

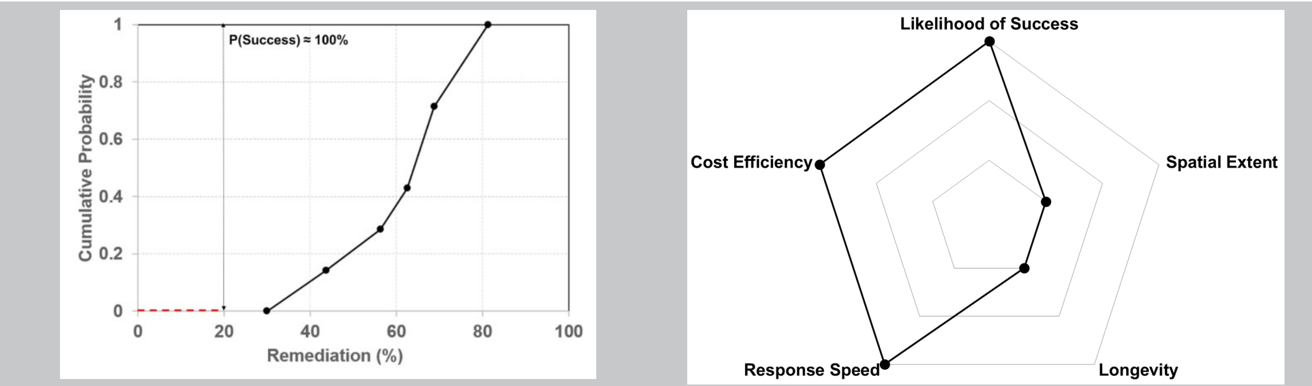

Figure 12 Polymer-gel sealant injection technique: (a) success probability; (b) spider chart.

3.5.2 Caprock leakage remediation

Additionally, polymer-gel injection above the caprock (in an assumed shallow aquifer) to seal fractures was investigated by Imperial College in deliverable D6.3 (Chapter XVI). The results obtained suggest that the performance outcomes of the technique are similar to those presented previously in section 3.1.2.

4 CONCLUSION

In this deliverable report, a methodology for assessing the overall performance of various techniques that were investigated under the scope of the MiReCOL project was discussed. Based on the bow-tie analysis approach, the techniques were broadly placed under two groups. The techniques that deal with a potential threat (or risk), such as a leaky fault or injection induced over-pressure, were referred to as mitigation techniques that reduce or eliminate the threat. On the other hand, those that deal with the consequences of leakage, such as loss of CO_2 storage performance or environmental impacts, were referred to as remediation techniques that reduce the severity of the consequences.

In order to standardise the assessment for the two groups of techniques, five performance metrics (dimensions) were considered, namely: (a) likelihood of success; (b) spatial extent; (c) longevity; (d) response speed; and (e) cost efficiency. The results obtained from the scenarios analysed for each technique in the MiReCOL project were used to classify (or rank) the performance of the technique based on these dimensions, leading to overall performance outcomes in the form of probability plots and spider chart visualisations.

Such visualisation tools are considered to be particularly useful in facilitating the general comparison between techniques, or choosing a portfolio of techniques, for operators dealing with a situation where CO_2 storage security may be compromised in the field. In view of this, the project aimed to use the results presented in this report to design a portfolio optimisation protocol to enable the selection of a subset of techniques for a given leakage scenario. Moreover, the purpose is also to subsequently feed the outcomes of this report into an on-line remediation selection tool which has been developed in parallel under SP5 (Section 3).

Chapter XXXIII

Report on methodology for the CO_2 storage remediation portfolio optimisation and the results of the scenario analysis

Rajesh Govindan[1], Zhenggang Nie[1], Anna Korre[1]
[1] Imperial College, UK

SUMMARY

A methodology is proposed to develop an effective framework which allows for the optimal allocation of resources for remediation technology implementation, considering the uncertainty with regards to their outcome, i.e. success or failure. It benefits from the assessment of the remediation techniques that was previously carried out based on five performance metrics, namely: (a) likelihood of success; (b) spatial extent; (c) longevity; (d) response speed; and (e) cost efficiency. Thus, the specific objective of the work presented in this deliverable report is to assimilate these metrics in the design of a protocol for optimising the selection of a subset of remediation techniques, representing the desirable remediation portfolio under uncertainty, in terms of the expected values of their implementation costs.

1 INTRODUCTION

1.1 Objective

The overall objective of WP11 is to synthesise the results of modelling studies carried out under the scope of the MiReCOL project. The bow-tie analysis was used to facilitate the assessment of broadly two groups of techniques that were investigated in the project (see Figure 1):

- threat barriers, referred to as risk mitigation techniques, for recovery and preparedness; and
- consequence barriers, referred to as remediation techniques, in order to reduce the severity of the consequences.

The assessment involved the performance characterisation of remediation techniques that address a broad range of consequences owing to CO_2 leakage, including the loss of storage permanence, effects on the complex structural integrity, and possible interference with production or other storage licenses. A standardised ranking system based on technology-specific performance metrics, viz. the likelihood of success, spatial extent, longevity, response speed, and cost efficiency, was implemented.

However, it is recognised that the assessment lacks value for consequence reduction, unless it is complemented with an effective framework which allows for the optimal allocation of resources for remediation technology implementation, considering the uncertainty with regards to their outcome, i.e. success or failure. Thus, the specific objective of the work presented in this deliverable report is to design a protocol for optimising the selection of a subset of remediation techniques, representing the desirable remediation portfolio under uncertainty, in terms of the expected values of their implementation costs.

1.2 Optimal remediation portfolio

In order to achieve the aforementioned objective of remediation portfolio optimisation, a methodology was developed based on the concept of decision trees, which are probabilistic models for structured decision making comprising of a sequence of one or more decisions and their respective possible outcomes, characterised by probability distributions, with the aim of maximising/minimising the expected value of a user-defined utility/cost function (Fraser and Jewkes, 2013).

Thus, it provides a mechanism to decompose the large and complex problem of defining a remediation portfolio into smaller decision making steps by selecting from a range of techniques with variable success likelihoods, as presented previously in MiReCOL deliverable D11.2 and briefly discussed in the following section. In addition, the decision tree was designed in a manner which allows user customisation. In other words, depending on the circumstances, such as the site-specific conditions and leakage severity, users have the flexibility to prioritise amongst the performance metrics over time. Thus, the expected value of the implementation costs incurred in a given portfolio was determined, and the one which minimises the cost function for consequence reduction, considering the uncertainty in the success of its implementation, was flagged as the optimal portfolio.

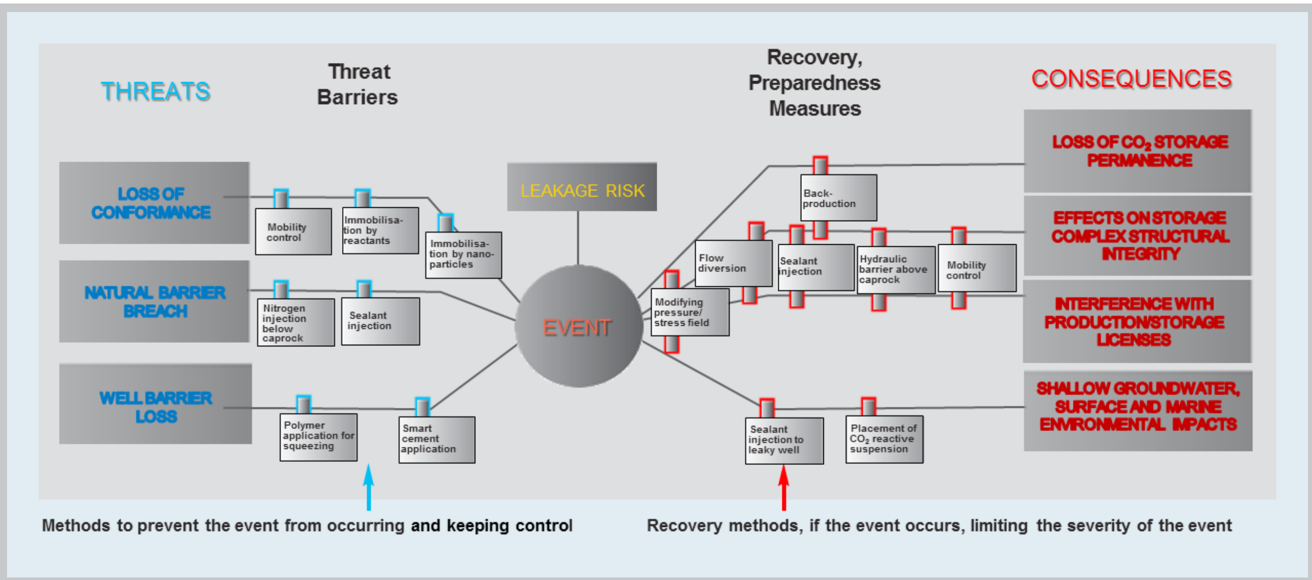

Figure 1 The bow-tie diagram for the MiReCOL project.

2 CO_2 LEAKAGE REMEDIATION TECHNIQUES AND PERFORMANCE ASSESSMENT

2.1 Remediation techniques investigated in the project

2.1.1 Flow diversion of CO_2 plume using foam injection

Foam is used in the oil and gas industry for mobility control of gas sweep during enhanced oil recovery. The desired effect is to reduce the mobility of the gas, forcing the injected gas to take alternative paths thus contacting more oil as well as delaying gas breakthrough in the production wells. Foam is also used to reduce gas coning/cresting at production wells.

In the current context, foam injection was investigated by SINTEF as a technique to remediate CO_2 leakage, in the event of an unexpected migration of the plume in the reservoir. It primarily involves the injection of a solution comprising of surfactant and brine in the reservoir. The solution reacts with the CO_2 in-place leading to the generation of foam, which causes the reduction in the mobility of the CO_2, thereby minimising potential leakage. The plugging effect of foam treatment depends on several factors, including the reservoir geology, position and type of leakage, injected surfactant volumes, surfactant concentration, adsorption, foam strength and foam stability. The main purpose of the study was to explore the ranges of some of these factors and to quantify their impact on a leakage event. The results obtained were discussed in detail in deliverable D3.3.

2.1.2 Flow diversion of CO_2 using polymer-based gel injection

Cross-linked hydrolysed polymer-gel injection is used in petroleum industry to improve conformity of fluid flow in the reservoir, remediate leakage around wells, and also used in conjunction with enhanced oil recovery at various temperature and pressure conditions. Water-based gels are highly elastic semi-solids with high water content, trapped in the three-dimensional polymer structure of the gel. Polyacrylamide (PAM) is the main cross-linked polymer used mostly by the industry. The use of biopolymers is more challenging as compared to the synthetic polymers due to chemical degradation at higher temperatures, causing the loss of mechanical strength. Most of polymer-gel systems are based on crosslinking of polymers with a heavy metal ion. The most commonly used heavy metal ion is chromium III. However, in view of its toxicity and related environmental concerns, its application in reservoir conformance and CO_2 leakage remediation is considered to be limited. Therefore, more environmental friendly crosslinkers such as boron, aluminium and zirconium have been proposed and used in recent years.

Imperial College used numerical simulators to implement the known interaction properties of polymer solution and crosslinkers using data from the literature and laboratory tests. The effect of reservoir permeability, polymer and crosslinker concentrations, pH and gelation kinetics were investigated. The property-based results were further translated into the simulation of scenarios for CO_2 leakage remediation using polymer-gel injection in the reservoir. The results obtained were discussed in detail in deliverable D6.3 (Chapter XVI)

2.1.3 Flow diversion of CO_2 using brine/water injection

In secondary oil recovery, brine or water injection has a long history either to support reservoir pressure or to displace oil towards producing wells. There is a range of techniques and theories (e.g. Buckley Leverett analysis) about how water injection can be used to increase oil recovery. Volumetric sweep management and realignment of production in contiguous layers are the nearest analogues in the oil industry to the use water injection in order to stop the migration of CO_2. Industry has studied several mechanisms by which water injection can be used to reduce CO_2 migration, such as: (1) creating a high-pressure barrier in front of the migrating CO_2 plume; (2) chasing CO_2 with brine ensuring storage security; and (3) injecting water directly into the advancing CO_2 plume.

Three different examples of water injection remediation have been investigated by the project partners, listed as follows:

- SINTEF used a portion of the Johansen formation as the basic model with water injection in front of the CO_2 migration plume. The model was modified to represent the key characteristics of twenty other possible CO_2 storage aquifers.
- Using a generic model, Imperial College studied the reduction of CO_2 leakage through a sub-seismic fault by means of water injection via the well previously used for CO_2 injection.
- TNO also used the Johansen model to simulate ten alternative scenarios using a combined approach of water injection and CO_2 back-production as remediation measures.

The results obtained were discussed in detail in deliverable D3.4 (Chapter IV).

2.1.4 Flow diversion of CO_2 using brine/water withdrawal

The over-pressurisation of the reservoir during CO_2 injection is of concern because it could have a large-scale impact, namely interference with the operations in neighbouring oil and gas fields, or CO_2 storage sites that could co-exist in the same formation. Such interference also has regulatory implications since issuing permits to operators would then be based on the outcome of a multi-site process evaluation, which can be quite involved, and rather unnecessary. In the literature, it was demonstrated that by producing brine from the reservoir, the pressure-driven leakage was minimised and consequently the net of amount of leakage is largely buoyancy-driven, thus reducing the rate of leakage. While pressure management via brine extraction is not be considered a mandatory component for large-scale CO_2 storage projects, it could also potentially provide many other benefits, such as increased storage capacity utilisation, simplified permitting, smaller area of review for site monitoring, and the manipulation of CO_2 plume in order to increase its sweep efficiency.

Imperial College investigated the technique using numerical simulations of CO_2 storage and leakage remediation for an offshore and compartmentalised depleted gas reservoir, called the P18-A block (in the Dutch offshore region). The scenarios considered the study of a cluster of gas fields in the reservoir to understand the plume migration and reservoir pressure response during CO_2 injection, and the remediation achieved using brine withdrawal in terms of flow diversion and pressure relief. The results obtained were discussed in detail in deliverable D4.4 (Chapter IX).

2.1.5 Blocking of CO_2 movement by immobilisation of CO_2 in solid reaction products

Experience with unintentional precipitation or scaling and formation damage, as commonly encountered in the oil and gas or geothermal industries, sheds some light onto the possibilities for forming solid reactants. Minerals observed to form 'naturally' within the reservoir may all be potential candidates for controlled precipitation. Frequently occurring scales associated with oil and gas production are calcite, anhydrite, barite, celestite, gypsum, iron sulphide and halite. Re-injection of production water is prone to scaling of calcium carbonate, while strontium, barium and calcium sulphates are more relevant for seawater injection. In addition to fluid-fluid reactions, fluid-gas interaction could promote mineralisation. Controlled intentional clogging due to salt precipitation, which occurs when the solubility is exceeded by the evaporation into injected dry gas, could potentially prevent the leakage of CO_2. This process is similar to salt scaling in natural gas and oil production, and CO_2 injection in saline aquifers and depleted gas fields.

TNO investigated scenarios to study the feasibility of injecting a lime-saturated solution as a CO_2-reactive solution above the caprock, at the location where the leakage has been detected. The solution has a low viscosity which simplifies the injection process. The results derived for the injection of the lime-saturated solution provided a general insight in leakage remediation using non-swelling CO_2 reactive substances. However, the production and practical use of such a fluid was beyond the scope of the study. The results obtained were discussed in detail in deliverable D3.5 (Chapter V).

2.1.6 CO_2 back-production

The back-production of formerly injected CO_2 may provide a suitable technique to: (1) mitigate undesired migration of CO_2 in the reservoir by inducing a pressure-gradient driven directed flow of CO_2; and (2) manage the reservoir pressure. Furthermore, the production of CO_2 will also form an integral part of any temporary storage of CO_2 in the frame of a different carbon capture storage and utilisation and/or power-to-gas concepts. In CO_2 storage combined with enhanced hydrocarbon recovery, CO_2 will be co-produced with the recovered hydrocarbons. The production ratio of gas to reservoir fluid is an important design parameter in all contexts. Below a minimum flow velocity in a well, the critical Turner velocity, no fluid is produced, and hence well load up (cone shaped brine accumulation) occurs.

The CO_2 back-production technique was investigated in this project using case studies based on two examples, each an offshore and onshore site, listed as follows:

- GFZ and Imperial College jointly carried out numerical studies prior to and after the Ketzin pilot field test to support its design and demonstrate the performance of the history-matched backproduction model, and thereby estimate the expected reduction in reservoir pressure achieved.
- TNO carried out a case study for the K12-B gas field in the North Sea to investigate the back-production technique. Numerical analyses focused on key factors such as recovery rate, CO_2 ratio, well pressure and water co-production.

The results obtained were discussed in detail in deliverable D4.3 (Chapter VIII).

2.1.7 Hydraulic barrier

It has been suggested that injection of brine above the caprock, at a higher pressure than the CO_2 pressure in the reservoir, would create an inverse pressure gradient to reverse the flow direction and increase the solubility of CO_2 in the saline water barrier formed, and prevent or limit leakage. Furthermore, coupled with fluid management procedures during aquifer storage (saline water extraction and re-injection above the caprock), this can also be used to minimise displacement and migration of native brine, and avoid pressure build up in closed or semi-closed structures.

Imperial College investigated the effectiveness of pressure gradient reversal (PGR), a hydraulic barrier technique, as a potential remediation technique for CO_2 leakage from deep saline aquifers using a generic and geologically realistic model, comprising of the reservoir, caprock and an overlying shallow aquifer. The focus was on the role of controlling parameters which may affect the success or failure of the hydraulic barrier technology considered. The results obtained were discussed in detail in deliverable D7.3 (Chapter XX).

2.1.8 Polymer-gel-based sealant injection for well leakage remediation

The use of synthetic and biopolymer solutions by the petroleum industry has been mostly associated with enhanced oil recovery and widely used around the world. For polymer-gel compounds (usually crosslinked with a heavy metal), the application is considered for water-cut and flow conformance control within the reservoir as well as leakage remediation in the near wellbore area. The polymer solution is composed of molecular chains of the chosen polymer, a carrier fluid such as water or brine, and a crosslinker such as chromium III, zirconium, and aluminium. Polymers are made of coiled chains, especially of high molecular weight polymers. Once they are added into solution, the charged areas on the chain repel each other and force the chain to uncoil. As a result, the viscosity of the solution increases. Generally, the charge also affects the speed at which the chain uncoils. The higher charged polymers will uncoil faster, whereas, non-ionic polymers may never fully uncoil since they carry no charge.

Imperial College carried out both laboratory tests and numerical simulations to understand the effectiveness of polymer-gel treatment on the permeability reduction of wellbore cement, thereby effectively minimising CO_2 leakage through a microannulus between cement and casing interface, and in near wellbore region of the host/caprock. Specifically, deep, high temperature and high pressure reservoir conditions were considered for the simulations. The results obtained were discussed in detail in deliverable D9.3 (Chapter XXVI).

2.1.9 Polymer-gel-based sealant injection for caprock leakage remediation

Additionally, numerical simulations for polymer-gel injection above the caprock (in an assumed shallow aquifer) to seal fractures was also carried out by Imperial College. The results obtained were discussed in detail in deliverable D6.3 (Chapter XVI).

2.2 Ranking of remediation techniques

The ranking of the remediation techniques was implemented using an ordinal classification - Low (L), Medium (M), and High (H) - based on the five performance metrics after pooling the results obtained from the leakage remediation simulation studies for each of the techniques (see Tables 1 - 5).

Despite being a qualitative ranking procedure, it represents the best efforts that could possibly be made to standardise the scales for the different metrics in order to ensure that the ranking is indicative of the overall merit of a given technique, and also allows for making a useful comparison between techniques. The rankings obtained were previously presented as success probability plots and spider chart visualisations in deliverable D11.2 (Chapter XXXII), and are summarised here in Table 6.

Table 1 Classification of the likelihood of success.

Rank	Likelihood of Success (%)
Low	0 - 33
Medium	34 - 66
High	67 - 100

Table 2 Classification of the spatial extent.

Rank	Spatial Extent (km^2)
Low	0 - 1
Medium	1 - 5
High	> 5

Table 3 Classification of the longevity.

Rank	Longevity (years)
Low	0 - 1
Medium	1 - 10
High	>10

Table 4 Classification of the response speed.

Rank	Response Speed (years)
Low	>1
Medium	0.1 - 1
High	0 - 0.1

Table 5 Classification of the cost efficiency.

Rank	Cost Efficiency (M€)
Low	> 10
Medium	1 - 10
High	0 - 1

Table 6 Qualitative ranking of remediation techniques.

#	Technique	Performance Characterisation Metrics				
		Likelihood of Success	Spatial Extent	Longevity	Response Speed	Cost Effectiveness
1	Foam injection	L	L	M	H	M
2	Polymer-based gel injection	H	M	L	H	L
3	Brine/water injection	M	M	M	M	H
4	Brine/water withdrawal	H	H	H	L	M
5	Solid reaction products	H	L	H	H	M
6	CO_2 backproduction	H	H	M	L	M
7	Hydraulic barrier	H	L	M	M	H
8	Polymer-based sealant for well leakage	H	L	L	H	H
9	Polymer-based sealant for caprock leakage	H	L	L	H	H

3 METHODOLOGY FOR REMEDIATION PORTFOLIO OPTIMISATION

3.1 Remediation portfolio design and development

The design of the remediation portfolio was carried out inline with the principles of modelling and evaluation of decision trees. Three types of nodes were initially identified to model the portfolio, viz. (a) the decision node (D), which represents a point in time when the CO_2 storage site operator is obliged to make a choice from a given set of remediation techniques on the basis of his/her preferences (weights) for the performance metrics; (b) the chance node (S), associated with a random outcome which is anticipated by the operator as being either 'success' or 'failure' of implementation, and typically characterised by a Bernoulli distribution; and (c) the leaf node/endpoint (C), which represents a point where the cost function for an outcome of the terminal decision taken is indicated.

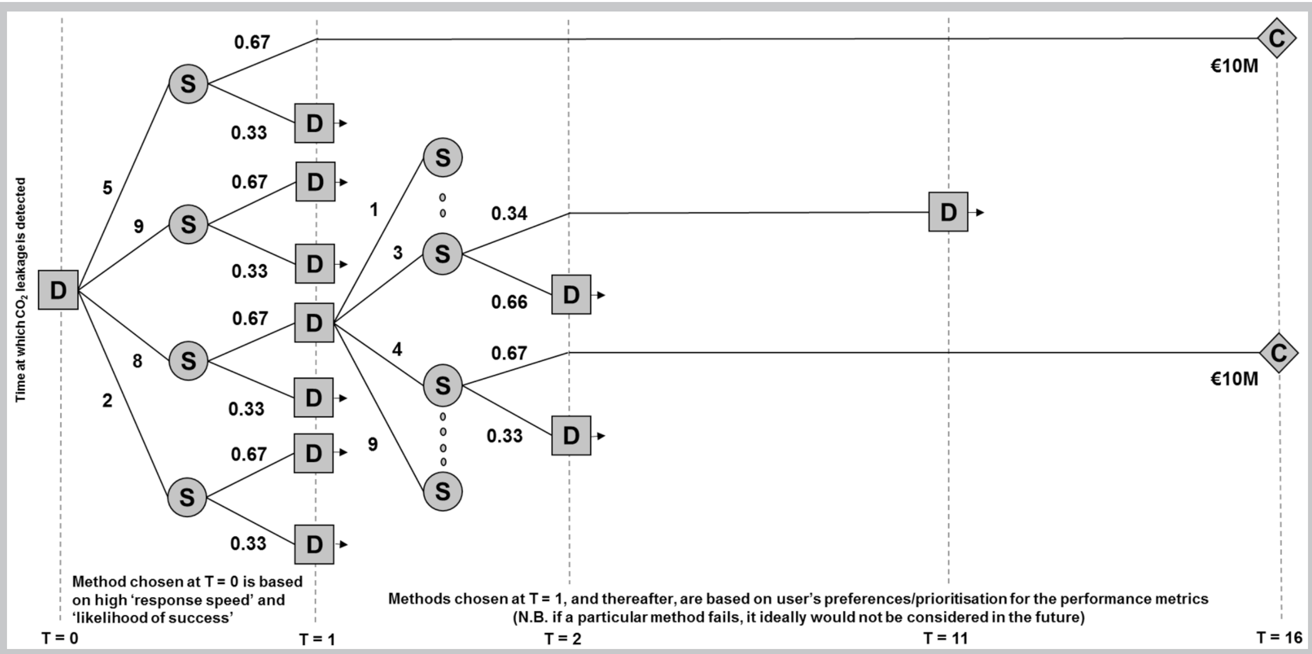

Figure 2 The decision tree structure for remediation portfolio optimisation.

Figure 2 illustrates the basic structure of the decision tree developed for the purpose of remediation portfolio optimisation. The timeline for decision-making begins when leakage from the storage complex is detected (at T=0). The length of an individual decision time-step ideally depends on the outcome of the operator's choice, i.e. if the selected technique is successful, its longevity would define the length of the time-step. It is also assumed that, in practise, a failed outcome would require the operator to take a new decision within one year since the last choice was made.

The methodology for remediation portfolio optimisation broadly comprises two steps:

- *Enumeration*: The exhaustive listing of alternatives in the decision tree is based on the preference/weighting for the five performance metrics over time. It is envisaged that at the time when leakage is detected, emphasis would be aptly placed on those techniques that have a relatively higher likelihood of success and a response speed, in order to enable the operator to take control of the situation. As time progresses, the weightings are allowed to become flexible and adaptive, depending on the site-specific conditions and leakage severity. However, the dynamic enumeration often leads to a complex decision tree and would need to be executed programmatically.

- *Backward Induction*: Following the enumeration of the decision tree, the computational task of remediation portfolio optimisation, i.e. the minimisation of the cost function for consequence reduction, was solved using a straightforward tree-traversal algorithm, which is an instance of an approach called backward induction in the game-theoretic and economic literature (Koller and Friedman, 2009). The algorithm proceeds backwards from the leaf nodes to the root node (the decision node at T=0) of the decision tree. The expected value of the cost function was computed at the beginning of every time-step when multiple choices are available for decision-making, subject to the operator's weightings, as described previously. Thus, the decision node takes on the choice which corresponds to the minimum expected value of the cost function, thereby indicating the optimal remediation portfolio.

3.2 Examples of remediation portfolio scenario optimisation

Two distinct scenarios were analysed in order to reflect the different operational constraints that apply to remediation options when leakage is detected during the injection period, or otherwise during the period after CO_2 injection has ceased.

3.2.1 Remediation of leakage detected during the injection period

One of the scenarios assumed in the study is the remediation of CO_2 leakage from the storage complex during the injection period. In this case, the operator would initially prioritise the implementation of those techniques that have a relatively higher likelihood of success and response speed, corresponding to decision node D1, by assigning an equal weightage to these performance metrics. As a result, either of the techniques labelled 2, 5 or 9 (see Table 6) would be selected. Once the leakage situation is brought under control, it was assumed that the subsequent decision node D2 would be based on the preference for techniques, labelled 4 and 6 (see Table 6), that have a relatively higher likelihood of success, spatial extent and longevity. The additional rules that were followed for the purpose of enumeration of the decision tree are as follows:

- If a particular method fails at either of the decision nodes, D1 or D2, other equally performing options would be tested; the failed method, however, will not be re-used for subsequent decision-making;
- For the purpose of visualisation, all the nodes in the decision tree and the connecting edges are colour-coded - green if it indicates a successful pathway, and red otherwise;
- The costs indicated at the leaf nodes would include an assumed penalty of €5M, in addition to the cost of the technique implemented, if it corresponds to a pathway which is colour-coded as red; the red leaf nodes represent the stopping condition where all the preferred options have been exhausted, and hence the attempt for remediation has failed;
- The remediation portfolios would span up to a maximum of 20 years.

Figures 3 and 4 illustrate two possible examples of remediation portfolios, starting with the injection of polymer-gel for flow diversion in the reservoir and solid reaction products respectively. Using backward induction, the expected value of aggregate costs incurred by the operator are €34.2M and €20.9M.

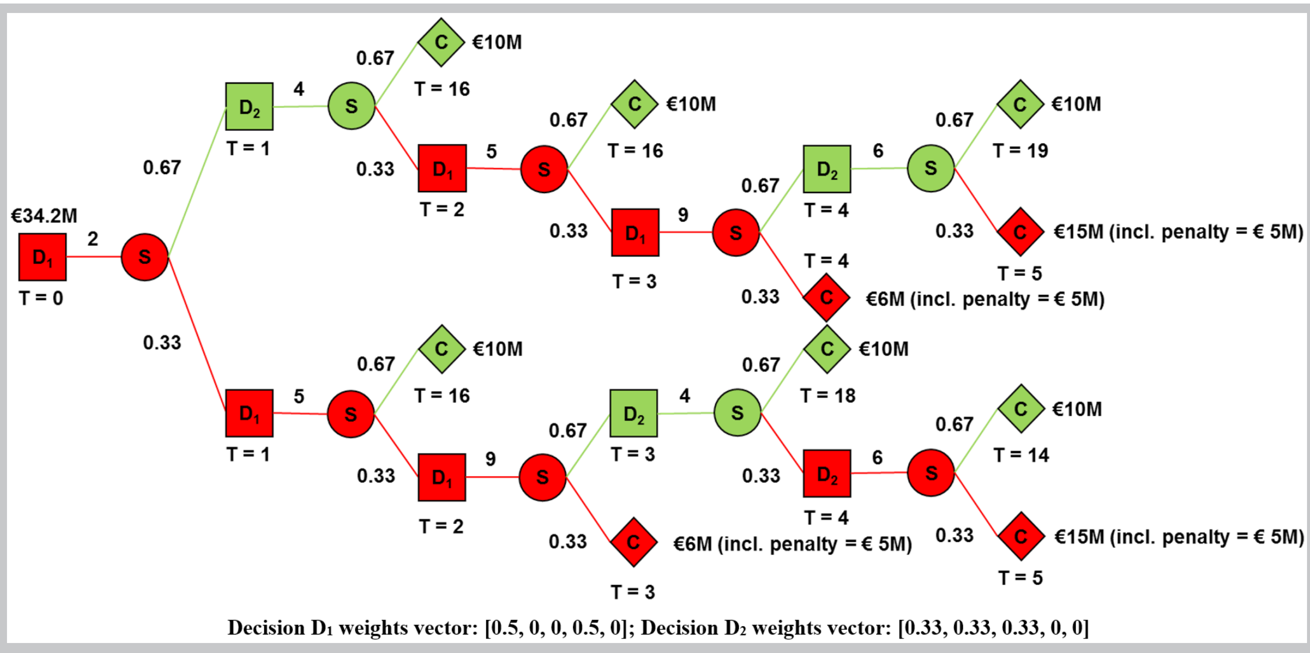

Figure 3 An example of decision tree enumeration for the remediation of leakage detected during the injection period.

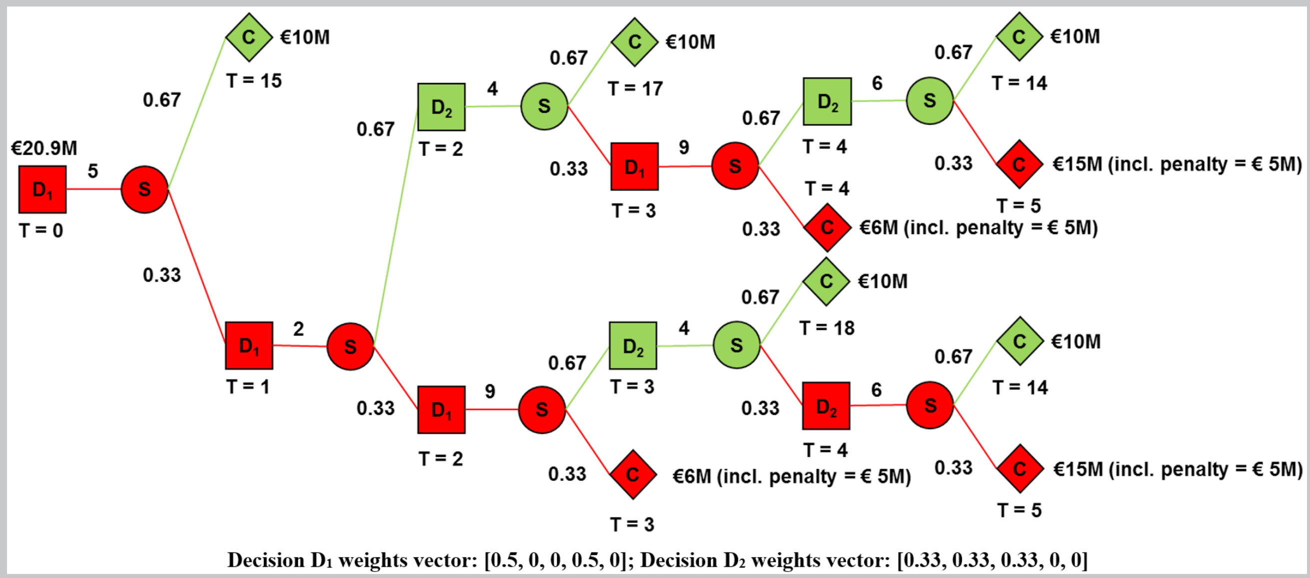

Figure 4 Another example of decision tree enumeration for the remediation of leakage detected during the injection period.

3.2.2 Remediation of leakage detected during the post-injection period

The other scenario assumed is the remediation of CO_2 leakage from the storage complex during the post-injection period. In this case, the operator would initially prioritise the implementation of those techniques that have a relatively higher likelihood of success, spatial extent and response speed, corresponding to decision node D1, by assigning an equal weight to each of these performance metrics. As a result, only one of the remediation techniques, labelled 2 (see Table 6), would be selected. Once the leakage situation is brought under control, it was assumed that the subsequent decision node D2 would be based on the preference for techniques, labelled 4 and 6 (see Table 6), that have a relatively higher likelihood of success, spatial extent and longevity. All the rules that were followed previously, for the purpose of enumeration of the decision tree, were also assumed to hold good in this scenario. Figures 5 illustrates an example of a possible remediation portfolio, starting with the injection of polymer-gel for flow diversion in the reservoir. Using backward induction, the expected value of aggregate costs incurred by the operator is €31.4M.

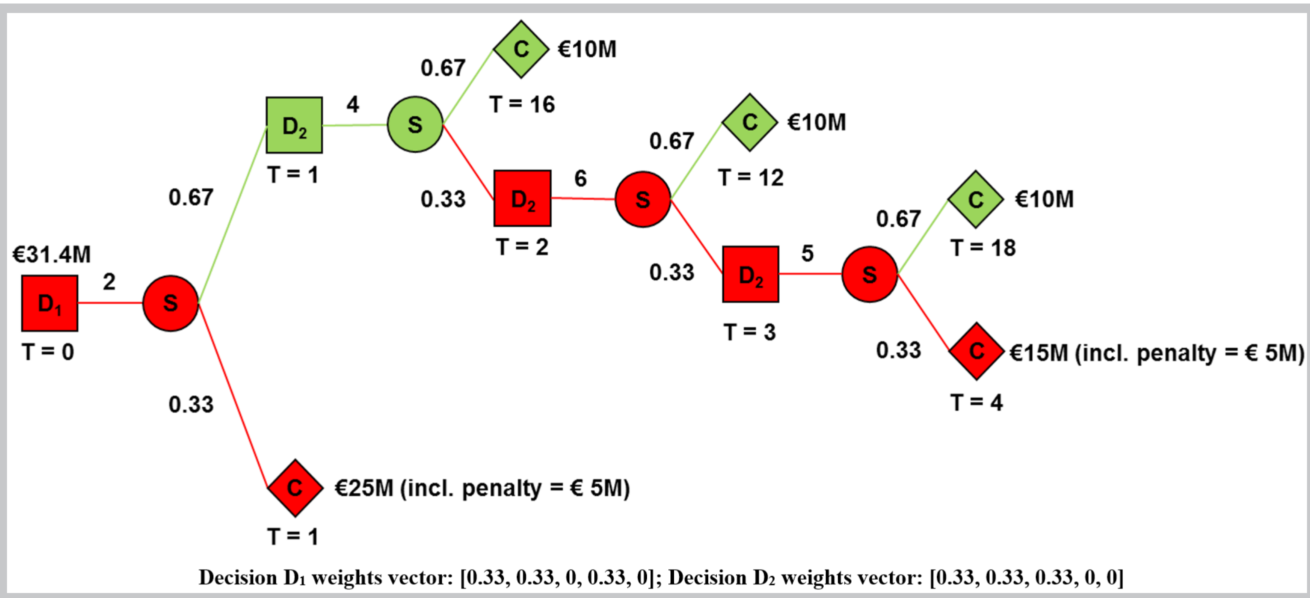

Figure 5 An example of decision tree enumeration for the remediation of leakage detected during the post-injection period.

4 CONCLUSIONS

In this deliverable report, a methodology was presented for designing a protocol to optimise the selection of a subset of leakage remediation techniques, representing the desirable remediation portfolio, in terms of the expected values of their implementation costs. It benefits from the performance characterisation/ranking of techniques that was previously investigated under the scope of the MiReCOL project based on five performance metrics, namely: (a) likelihood of success; (b) spatial extent; (c) longevity; (d) response speed; and (e) cost efficiency.

The remediation portfolio optimisation approach is based on the principle of structured decision-making under uncertainty. Examples of decision trees were developed based on remediation of leakage detected during the injection and post-injection periods. The enumeration step was used to construct the exhaustive listing of alternatives in the decision tree based on the operator's preference for the performance metrics. In particular, at the time when leakage is detected, emphasis would be aptly placed on those techniques that have a relatively higher likelihood of success and a response speed in both scenarios. As time progresses, the preferences are expected to change depending on the site-specific conditions and leakage severity, which could lead to a complex decision tree, and hence the approach would require software development using efficient data structures and algorithms, in terms of computational speed, in order to cope with the combinatorial requirements of dynamic decision-making.

Furthermore, the backward induction algorithm was implemented to estimate the projections for the aggregate costs of the example remediation portfolios that were developed. For the case where leakage detection occurs during injection, a comparison was made between two possible portfolios. In particular, the portfolio where remediation starts-off with the injection of solid reaction products into the reservoir is more cost efficient than the one which implements polymer-gel injection for flow diversion in the reservoir. However, a full enumeration was not possible, and hence there is scope to further improve on this optimal solution. On the other hand, for the case where leakage detection occurs in the post-injection period, for the assumed set of initial preferences that were chosen, polymer-gel injection for flow diversion in the reservoir appears to be the best technique in order to take speedy control of the situation, based on the performance assessment that was carried out previously.

Thus, the approach for the identification of optimal remediation portfolios presented in this report demonstrates promise for its real world application in the field, if the dynamic scaling of the decision trees is implemented through a dedicated software development activity, which is currently beyond the scope of the MiReCOL project. Nevertheless, the methodology developed is proven and results from this work provide an important input for the handbook of corrective measures that is separately prepared in the project.

References

Fraser, N.M. and Jewkes, E.M., 2012. Engineering Economics: Financial Decision Making for Engineers. Pearson Education Canada.
Koller, D. and Friedman, N., 2009. Probabilistic graphical models: principles and techniques. MIT press.

Chapter XXXIV

Web-based tool of corrective measures – summary report

Logan Brunner[1]
[1] TNO, The Netherlands

SUMMARY
The work conducted throughout the MiReCOL project consisted of studying and simulating many remediation techniques for CO_2 storage. The final aspect was developing an online web app to host a web tool and online handbook to present the findings from the project, for the use of CO_2 operators, regulators, decision makers, and the public. This deliverable details the work done to create the MiReCOL web app, as well as presents a reading guide, or manual, to use the web tool and handbook. Within the web tool, the guide explains the source of information and the functionality of the site analysis, the well remediation analysis, and the technique analysis. Regarding the handbook, the guide explains the organization and sources of information.

1 INTRODUCTION

Carbon dioxide capture and storage [CCS] is a technology that has promising capabilities for emission reduction in the energy generation fields, as well as the materials industry (IEA, 2013) (IPCC, 2014). Already, there are projects underway that exhibit the functionality of this technology (Global CCS Institute, 2015). To support the growth of this field, stakeholders must be informed of the process itself as well as the risks and implications involved.

Several tools have been developed to help promote this knowledge sharing, including GERICO: management of risks for CO_2 storage (Le Guénan et al., 2011)[1]; the monitoring selection tool on the IEAGHG website (BGS, 2010)[2]; and the National Risk Assessment Partnership's tool on quantifying risks of CO_2 storage (Pawar et al., 2016). To accompany these existing tools and fill in the gap of knowledge about remediation techniques, MiReCOL provides studies and information on new and existing methodologies to mitigate and remediation a CO_2 storage site. The result of this project is a web app[3] which hosts a web tool to assess the various remediation techniques, as well as a handbook which offers literature on these techniques

This web app is meant to serve as a reference for CO_2 storage operators, regulators, authorities, decision makers, and the public to learn more about remediation measures available in the case of undesired CO_2 migration. The tool is intended to aid the research process and does not replace creating a remediation or contingency plan. Within the project, some practices are quite well established, while many are still in the beginning phases, which has been noted by using technology readiness levels [TRL] (TRLs, 2014). This is to give a perspective of how practical the remediation techniques are.

The following section details how to use the web app, regarding both the web tool and the handbook, while the sections thereafter explain more of the background knowledge used to formulate the web tool and handbook. The way the tool was developed is described in Section 3, including the calculations behind the tool. Section 4 contains the source of the data and information used in the web app and the conclusion wraps up the deliverable and concerns the applications where this web app can be used.

2 WEB APP MANUAL

This section is meant to serve as a reading guide for the use of the web app, which includes two main sections: the web tool and the handbook. Both of these features are intended to offer guidance and information for CO_2 storage operators, CO_2 storage regulators, competent authorities, and the public on different remediation techniques and their impacts.

The MiReCOL web app is located online at http://tool.mirecol-CO_2.eu. This web app is best viewed using the web browser Mozilla Firefox or Google Chrome. It functions using Internet Explorer and Microsoft Edge, except some features are limited. Once on the site, there are options to view the two parts of the web app (the web tool and the handbook), as well as an option to learn more about the web app and MiReCOL project (Figure 1).

Figure 1 Screenshot of the MiReCOL web app home page.

On the "About" page, you will find a brief description of the MiReCOL web app, information about the project in general, partners involved, and contact information. There is a link to the MiReCOL website as well (http://mirecol-CO_2.eu), which provides more

1 http://gerico.brgm.fr/
2 http://ieaghg.org/ccs-resources/monitoring-selection-tool1
3 http://tool.mirecol-CO_2.eu

information about the project, the scientific blog, events and relevant sites, publications, and a listing of the partners (Figure 2).

Figure 2 The original MiReCOL project website.

2.1 USING THE WEB TOOL

Once selecting the web tool option, two selections are provided: “Site Remediation” and “Well Remediation”. The former offers two functions (explained in Section 2.1.1):

1. Compare the leakage reduction potential from all the investigated remediation techniques based on their overall performance (Technique analysis).
2. Enter your site details, and find the closest scientific simulations for each remediation technique to determine their effectiveness (Site analysis).

The “Well Remediation” selection will take you to the assessment of a leakage via a well barrier failure, described in Section 2.1.2.

Important to note is that the web tool assumes the user has already detected an irregularity in monitoring, suggesting migration of the CO_2 plume.

2.1.1 Site Remediation

The following sub-sections describe the options once navigating to the “Site Remediation” page. At the bottom of the page is a button that reads “Back to remediation selection”, which will take you back to the page which displays the options of site remediation or well remediation.

2.1.1.1 Technique analysis

This part of the tool displays several dropdown options, as well as a graph titled “Probability of success for remediation techniques”. Upon loading the webpage, each remediation technique investigated in the MiReCOL “Report on individual remediation techniques scoring method and classification/ranking results” (Korre, 2017, link) is depicted in the plot. The name of the remediation technique is on the x-axis, and the probability of success (in percent) is on the y-axis.

To narrow down the options shown, you can select values for each of the dropdown menus (which are spatial extent, cost efficiency, response time, longevity, and TRL), and the plot will be dynamically updated with the remediation techniques that fit that selection (see Figure 3). For example, if you would only like to view remediation options that are low cost, then you would go to the “Cost efficiency” dropdown, and select “High (0-1 M€)”. If you selected “Medium (1-10 M€)”, then remediation techniques with both medium and high cost efficiencies would be displayed. To reset the choices you have made, click the “Reset selections” to see all the remediation techniques again.

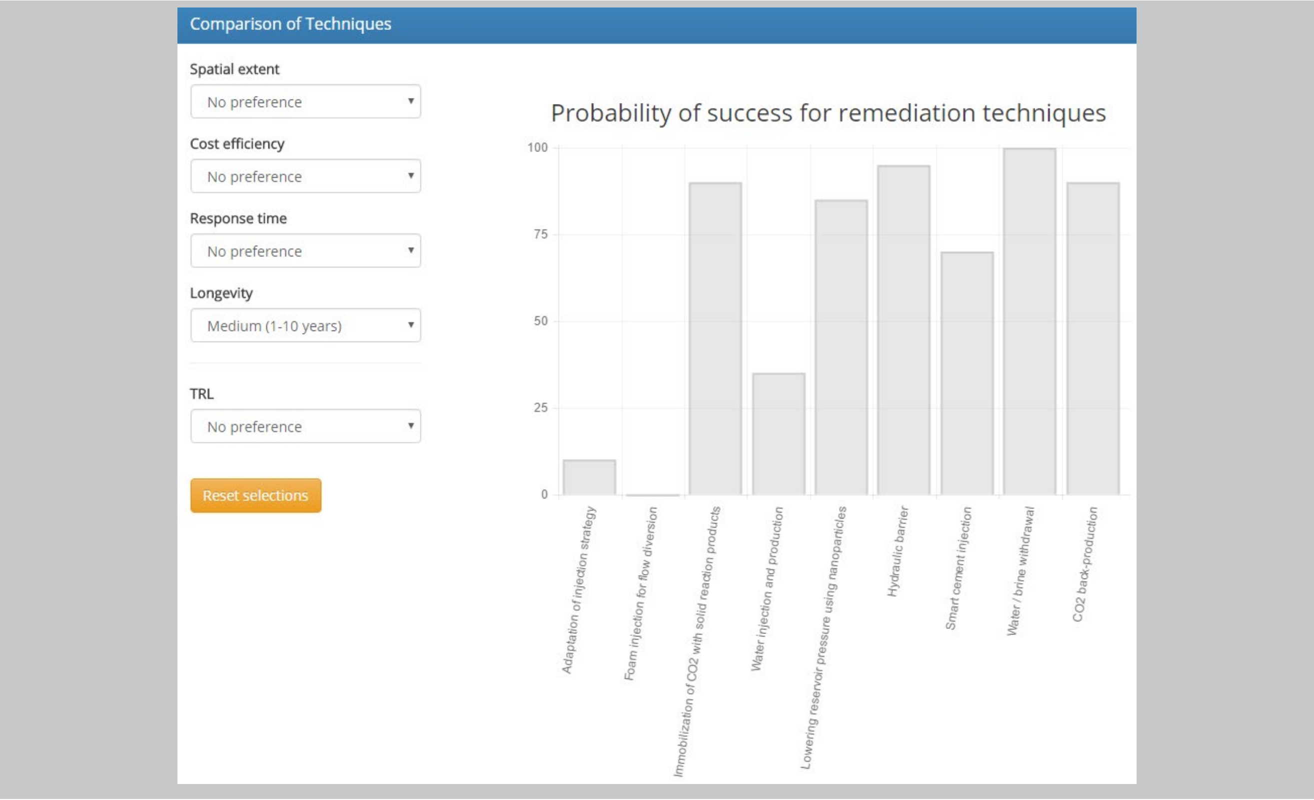

Figure 3 Selection options and output bar chart from the "Technique analysis" page, displaying probability of success for those techniques that meet the selected criteria.

Below the bar chart is a list of the remediation techniques that meet the user's selected criteria. Clicking one of the techniques displays the TRL and a radar chart, which illustrates how the technique performs on a 3-point scale in regards to likelihood of success, spatial extent, longevity, response time, and cost efficiency. The farther from the centre of the chart, the better the metric is. An overview of the technique and associated MiReCOL deliverables are listed (Figure 4), as well as a description of the ranking of the radar chart (Figure 5). At the bottom of the page are links to the two MiReCOL studies from which this information is pulled, "Report on individual remediation techniques scoring method and classification/ranking results" (Korre, 2017, link) and "Report on methodology for the CO_2 storage remediation portfolio optimisation and the results of the scenario analysis" (Govindan et al., 2017, link).

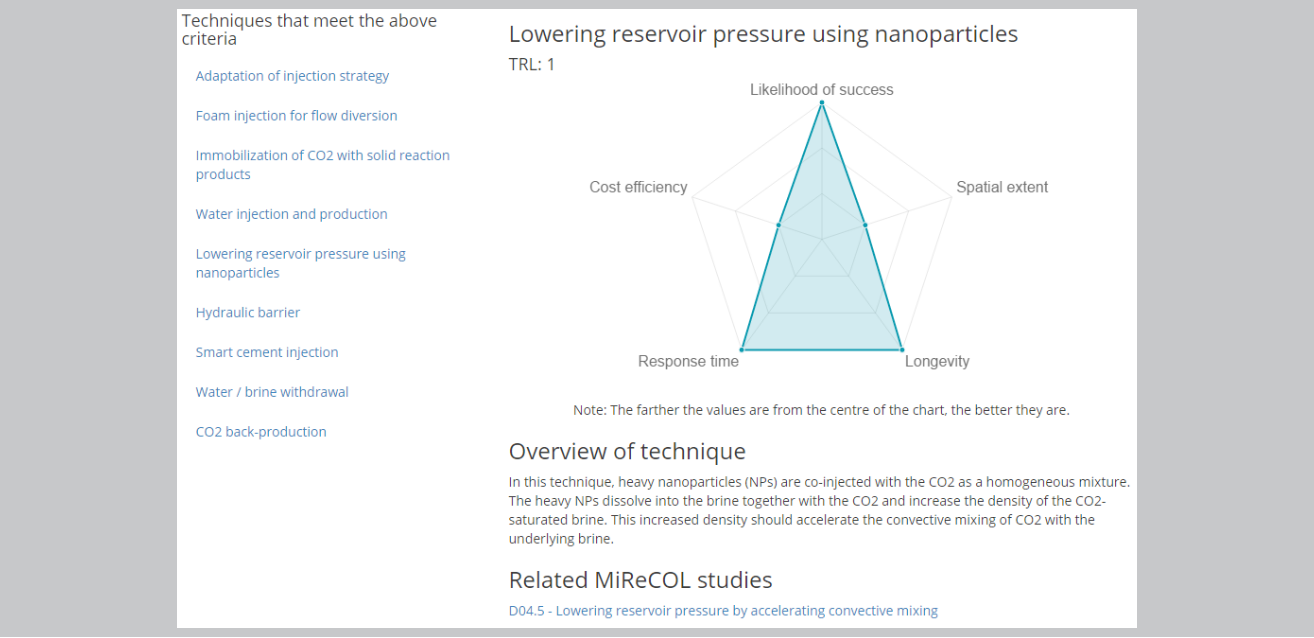

Figure 4 Output techniques listed on the "Technique analysis" page based on user selection, along with the selected technique TRL, radar chart, overview of the technique, and related deliverables.

Description of ranking for the radar chart

The following table details what each rank means for each of the five criteria displayed on the chart. Despite being a qualitative output, the resulting spider chart outputs represent the best efforts that were made to standardise the scales in different dimensions in order to ensure that it is indicative of the overall merit of a given technique, and also facilitate comparison between techniques.

Rank	Likelihood of success (%)	Spatial extent (km2)	Longevity (years)	Response time (years)	Cost efficiency (M€)
Low [1]	0 - 33	0 - 1	0 - 1	> 1	> 10
Medium [2]	34 - 66	1 - 5	1 - 10	0.1 - 1	1 - 10
High [3]	67 - 100	> 5	> 10	0 - 0.1	0 - 1

Figure 5 Table clarifying the ranking system of the radar chart found on the “Technique analysis” page.

Site analysis

This aspect is intended to learn more about the user’s site and provide an idea of how different remediation techniques would work. Though this tool does not assess the user’s actual site, it attempts to find the closest scenario that was simulated for each remediation technique. This allows reuse of the simulations run during the MiReCOL project, without requiring intensive calculation and modelling while using the web tool.

Upon loading the page, the user is to answer the questions (to the best of their knowledge) about the site they would like to investigate, as shown in Figure 6. For the tool to function, all the questions must be submitted. Once answering the questions on the first screen, press “Next” to go to the following questions. The questions deal with the user’s reservoir, the CO_2 stored in the reservoir, the user’s idea of the CO_2 migration, and questions on mitigation options. Once answering the questions, select the “Submit” button to go to the “Output” page and see the results of your site input.

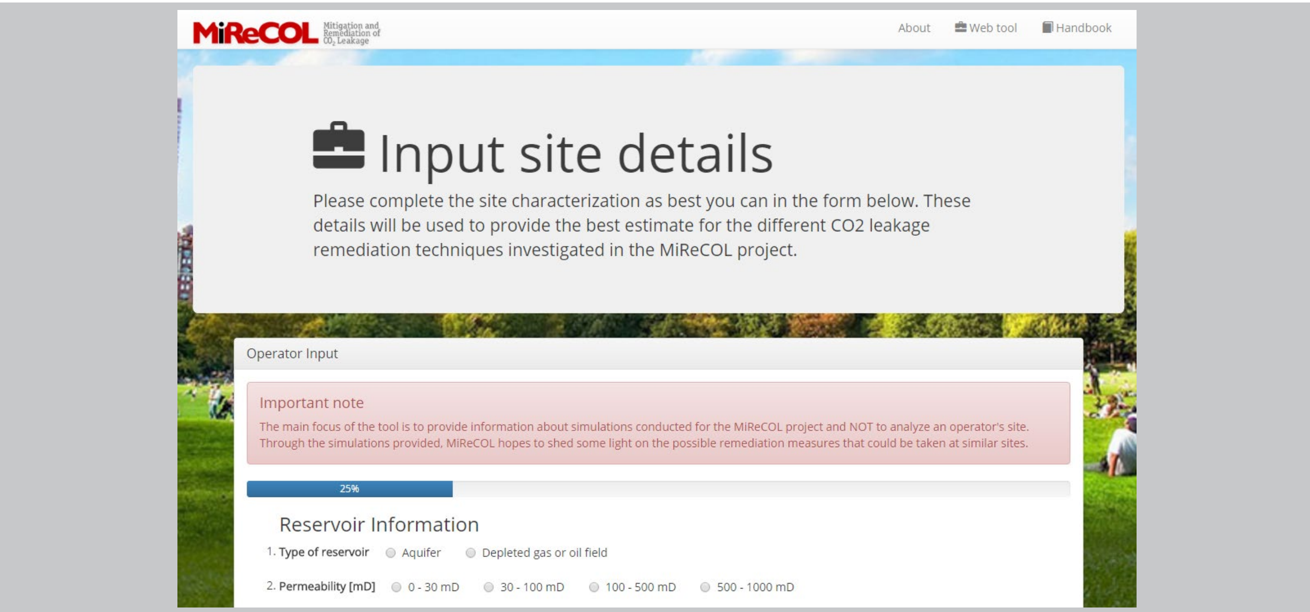

Figure 6 Screenshot of the “Site analysis” page in the MiReCOL web tool.

On the “Output” page, there is a radar chart next to two dropdown menus (see Figure 7). This section allows you to visually compare output criteria of the closest scenario (to the user’s input) from two remediation techniques. Selecting a technique under “First Technique” will display one set of data on the radar chart in orange, the overall score for that technique, and the technology readiness level of that technique. Selecting a technique under “Second Technique” will display the same type of data for another technique, this time in blue. The radar chart shows five output criteria, likelihood of success, spatial extent, materials/cost, response time, and longevity.

- The likelihood of success is the interpretation of the scientist who ran the simulations, but the main idea is the likelihood that this technique halts CO_2 migrations. Below the radar chart, in the list of the remediation techniques under the heading “Other Notes”, some scientists have further specified their definition of this criterion.
- The spatial extent relates to the distance over which this remediation technique will function. As a base notion, this value is the distance simulated in the experiments.

- The materials and cost values are to give an idea of what is required for this remediation technique. As it can be difficult to know costs of a remediation without performing a full-site analysis, the ranking in the radar chart serves as an estimation. This value is different from the "Technique analysis" section, in that it is simply cost and not cost efficiency.
- The response time can be thought of as the time it takes for the remediation to be set up and to start preventing CO_2 migration.
- Longevity is the time that the remediation will stay in place. Similar to spatial extent, this criterion is based on the simulations that the scientists ran, while some include the point that once in place, these remediation techniques would be permanent.

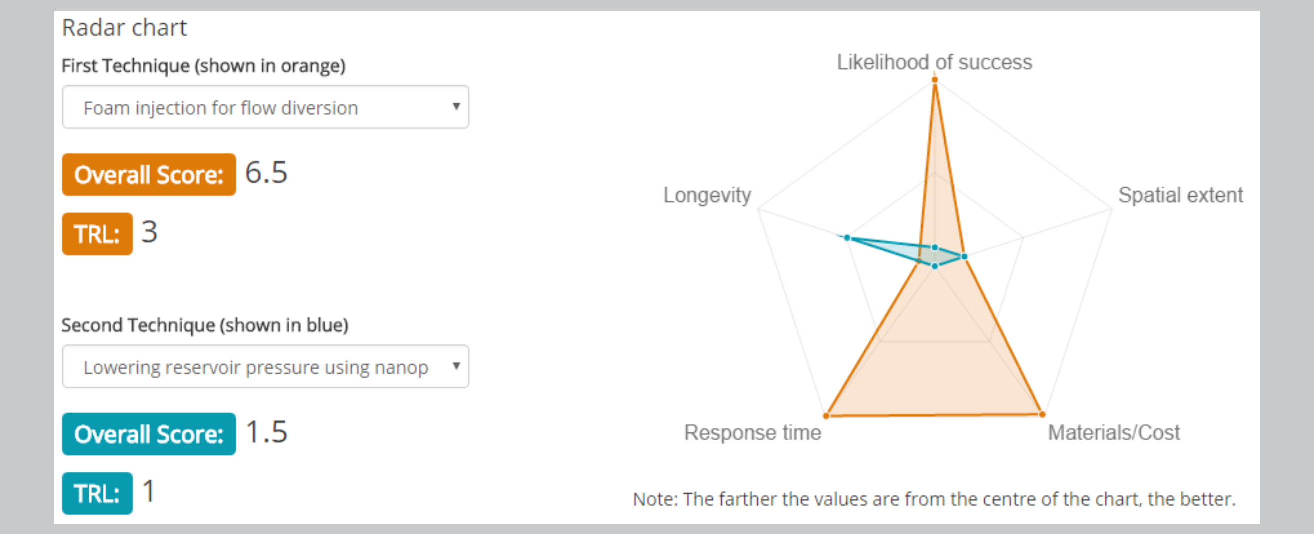

Figure 7 Screenshot of the radar chart on the site analysis output page.

Directly below the radar chart is a table with user input and the closest scientific scenarios. What this contains in the second column is a list of the input parameters from the user. The following columns are the scientific simulations that are closest to the user's input values. For example, the third column shows the technique of "foam injection for flow diversion" (Wessel-Berg et al., 2015, link), which had several simulations run. The user's input is compared to each scenario, and the closest one is selected and displayed in this table.

Further down on the page are the outputs of each remediation technique. They are divided into two categories: appropriate and inappropriate. A method would be deemed inappropriate if the user input a feature that is not compatible with the remediation technique. To demonstrate, if the user had noted that his site had no neighbouring reservoir, then the remediation technique "flow diversion to nearby compartment" (Orlic et al., 2016, link) would be placed under the "Inappropriate methods" section. Within

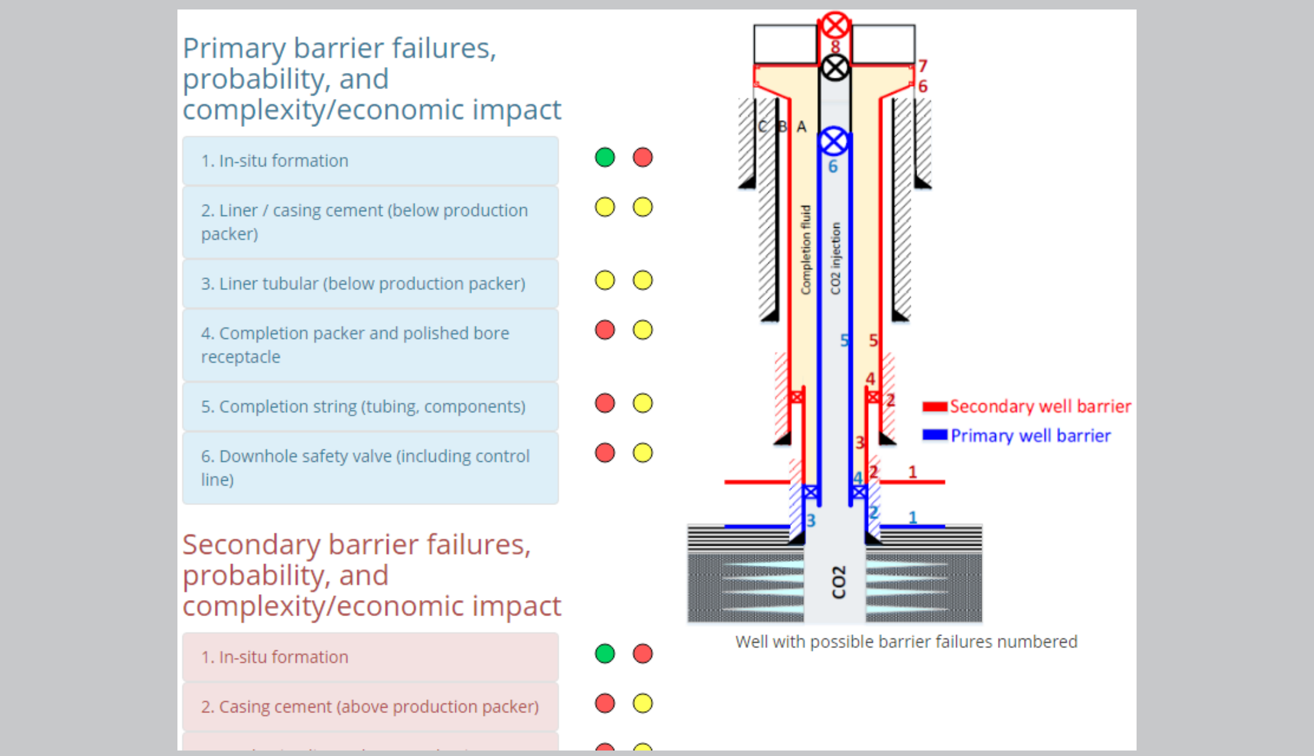

Figure 8 Screenshot of the initial page of the well remediation tool.

each remediation technique are displayed the output criteria, as described above for the radar chart, as well as other notes which are further comments about the terminology from the scientists who performed the simulations. Finally, associated risks to the remediation technique and associated MiReCOL deliverables are listed.

2.1.2 Well remediation

If the well remediation option is selected, the initial screen shows a list of primary (in blue) and secondary (in red) barriers found in a typical well (Figure 8). These barriers are possible failure locations if a leak is in the well. To better illustrate this, the image to the right of the barrier list has colour-coded lines and numbers which correspond to the numbers in the barrier list. Thus, if the failure location is at the blue number 4, then the user can see in the list that the blue number 4 is the “completion packer and polished bore receptacle”.

The two dots next to each barrier display the “probability” and “complexity/economic impact” of that barrier. Hovering over each dot will show these labels. The first dot, represents the probability of that barrier failing, while the second dot represents the difficulty or cost of replacing that barrier. The colour key lower on the page explains what these traffic light colours mean in the context of well barriers, as shown in Figure 9.

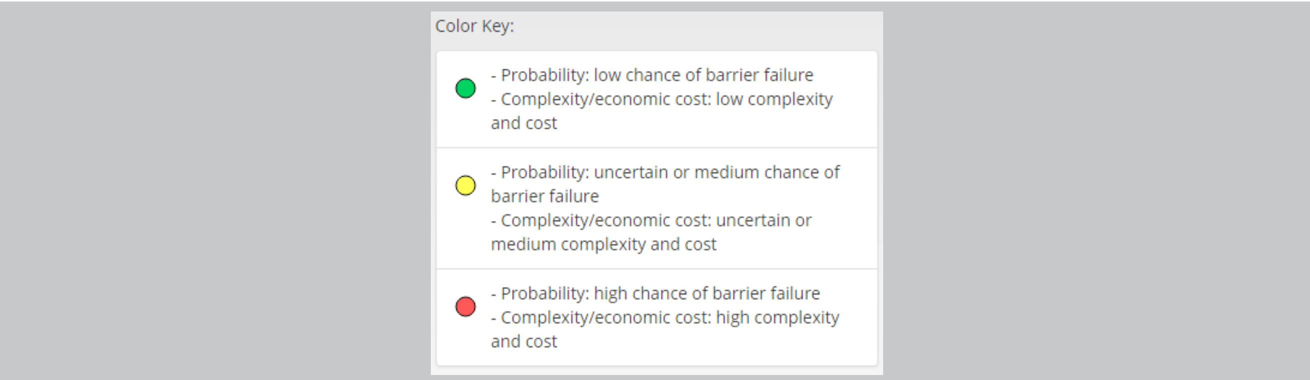

Figure 9 The colour key for the two dots next to each well barrier on the well remediation page.

Once deciding on a barrier to investigate, clicking on that option will display a window within the page that describes the well barrier further (Figure 10). This window displays a short description of the barrier, the probability and complexity/economic cost dots again, possible causes of the barrier failing, and an image to show the barrier.

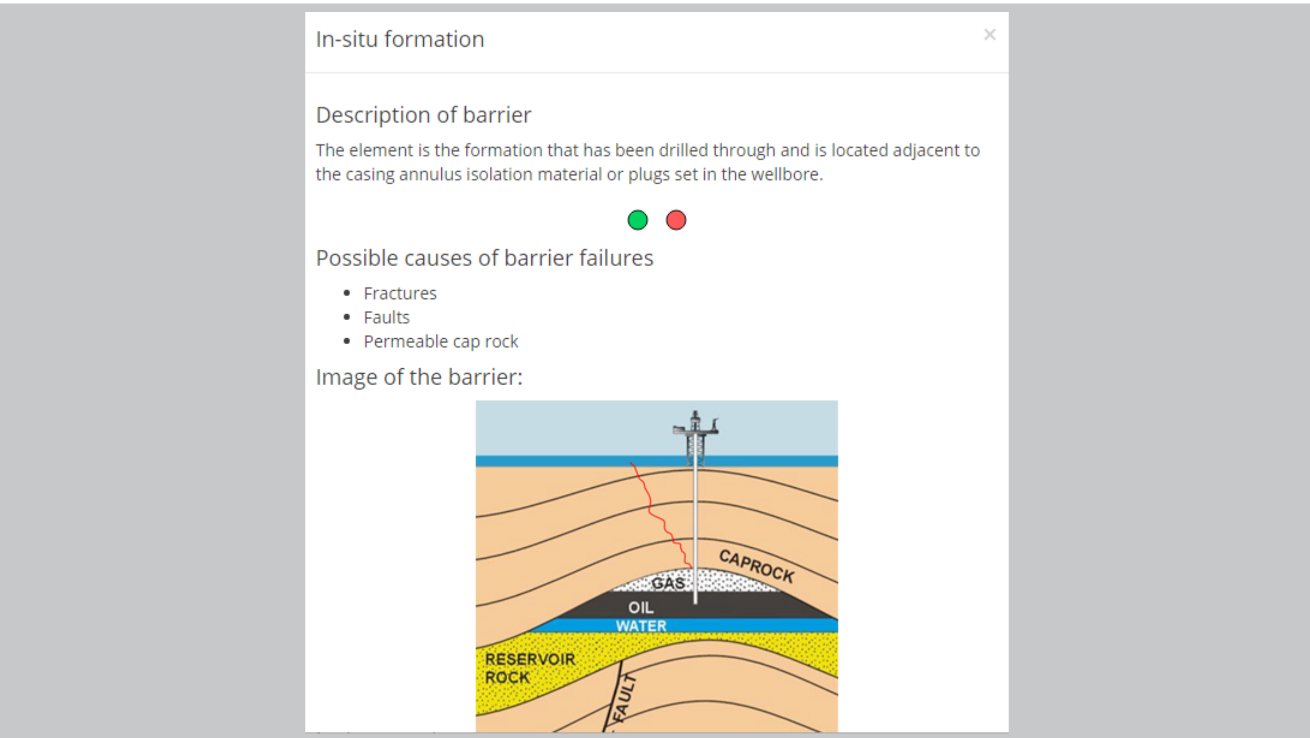

Figure 10 Description shown once clicking on a well barrier on the well remediation page.

If this is the barrier you desire to remediate, then you can click on the button "Select this barrier" to continue onto the next page. If you would like to go back to select a different barrier from the lists, then you can either click outside of the popup window or select "Close". After selecting a barrier, suggested remediation practices are listed first on the page (see Figure 11). Below this are listed technical and economic risks, which are colour-coded with a traffic light colour to display the overall risk for these two risk categories. Green signifies low risk, yellow signifies medium risk, and red signifies high risk. Once finished with this page, you are able to either investigate more well barrier failures, by clicking on the "Back to all barriers" button, or go back to the menu with the options of site or well remediation, by clicking on the "Back to remediation selection" button.

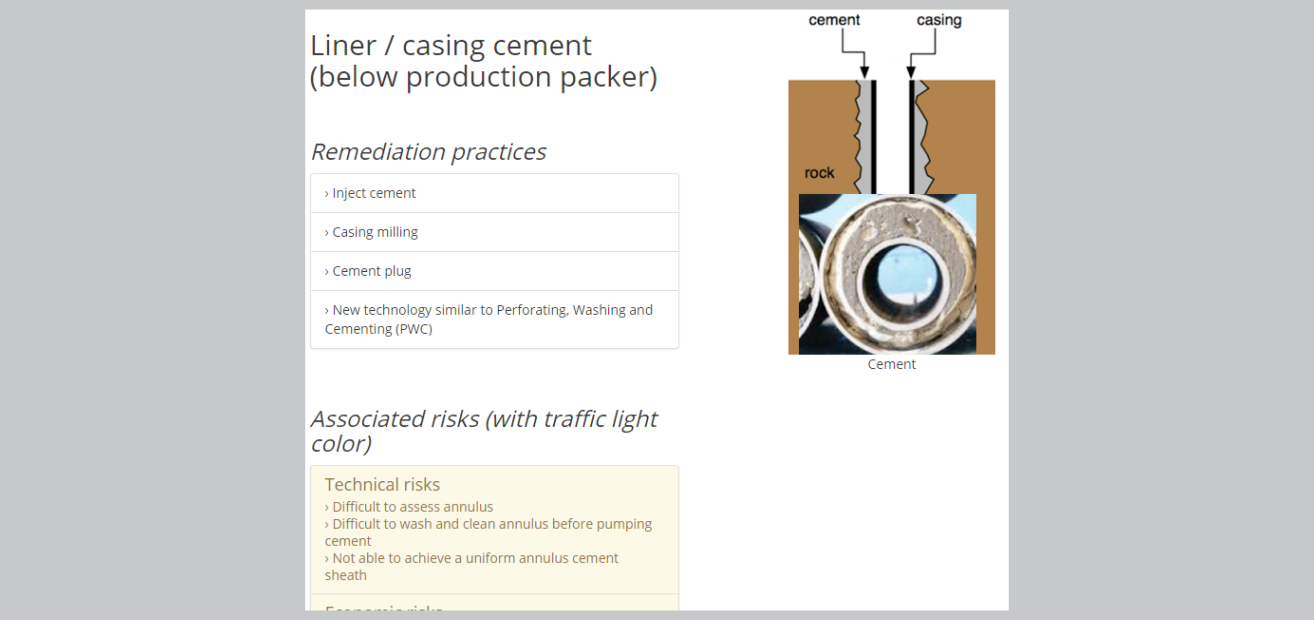

Figure 11 Screenshot of the well remediation page, once a barrier has been selected as that which needs to be remediated.

2.2 Using the handbook

The MiReCOL online handbook groups together the remediation techniques, deliverables, publications and other literature from the project. This is organized in three tabs (Figure 12):

- Remediation techniques
- MiReCOL reports
- Downloadable literature

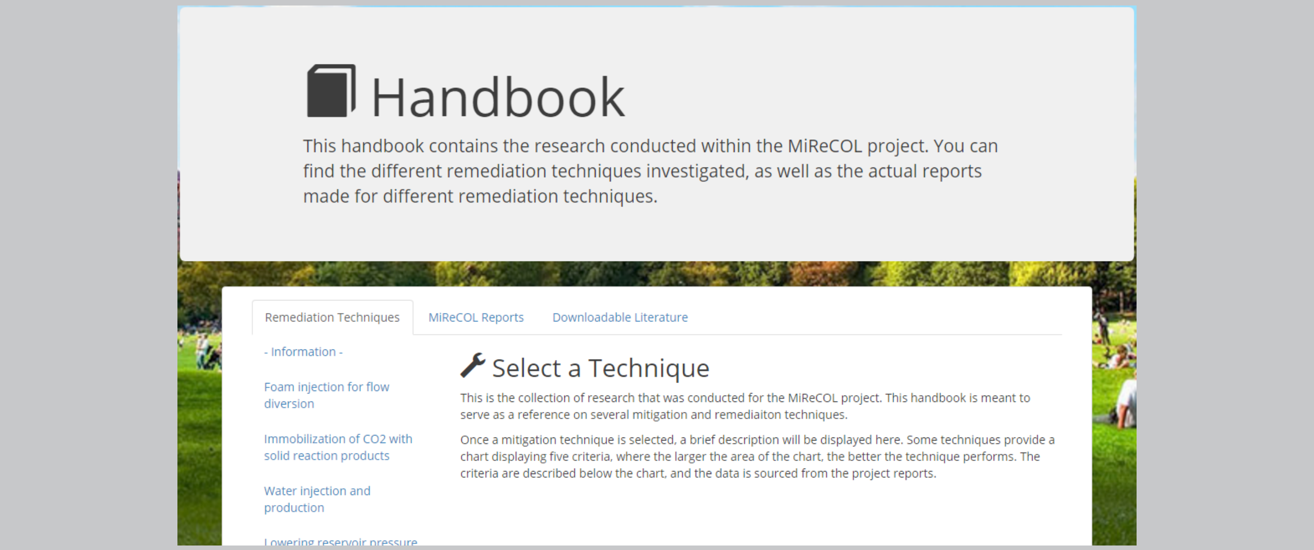

Figure 12 Screenshot of the initial page of the online handbook, showing the three tab options: remediation techniques, MiReCOL reports, and downloadable literature.

2.2.1 Remediation techniques

The default screen shows this tab. In the column to the left, you can see listed the different remediation techniques that were investigated in MiReCOL. Upon clicking one of the techniques, the middle content of the page changes to display that technique name along with the TRL and a brief overview of the technique. If the technique was analysed in Deliverable 11.2 (Korre, 2017, link), then a radar chart (and table explaining the chart ranking) is displayed along with the TRL and overview (Figure 13).

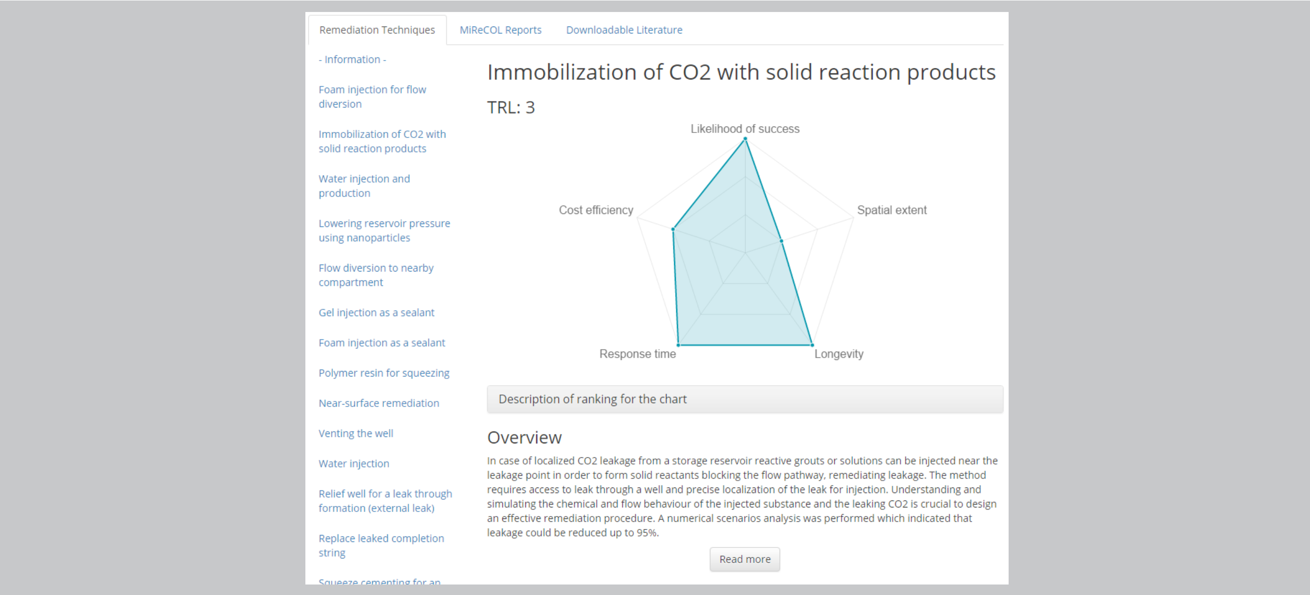

Figure 13 The remediation techniques tab in the online handbook, showing the TRL, a radar chart, and an overview of the selected technique.

You can click on the "Read more" button to view more about the technique, including the methodology of either the remediation technique or the modelling of the technique, the materials related to implementing the technique, associated risks and impacts, application areas, case studies of this technique, the MiReCOL reports that deal with the technique, and finally references to information about the technique.

2.2.2 MiReCOL reports

Clicking on the second tab takes you to the "MiReCOL reports" section of the handbook. In the column on the left, you see the list of remediation categories, which split up the remediation techniques into groups. By clicking on one of these, you will see a list of MiReCOL reports at the top of the main content area. Then, you select one of those deliverables, which will then display the abstract of the report, as well as a link to download the deliverable.

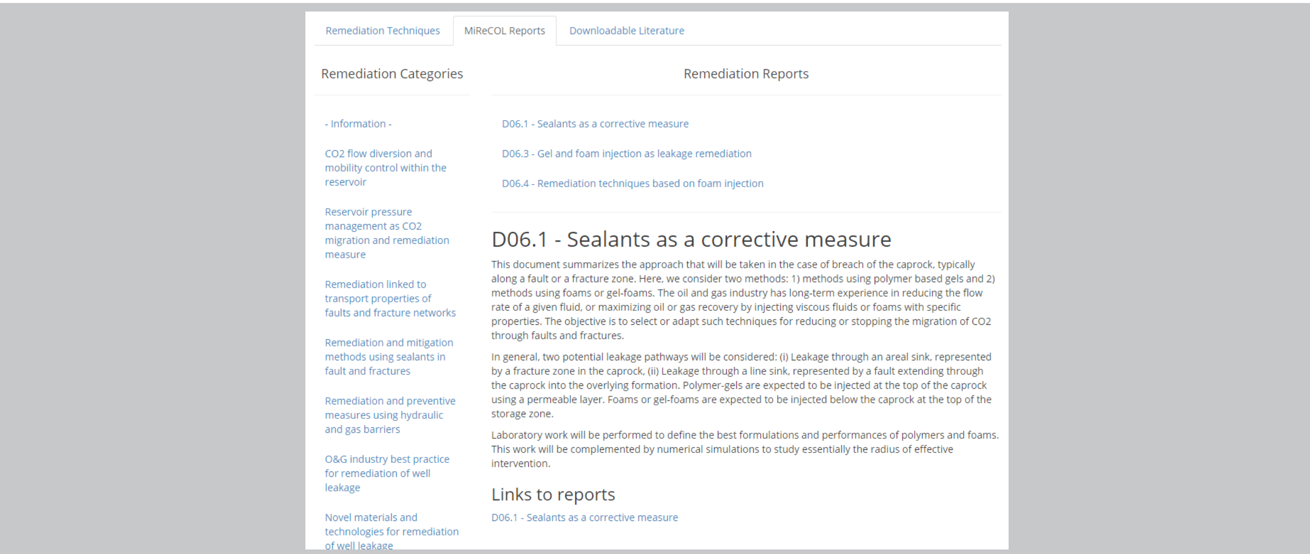

Figure 14 Screenshot of the MiReCOL Reports section of the online handbook. Remediation categories are listed on the left, and once a category is chosen, the remediation reports are shown in the middle, followed by the abstract and link to the selected report.

2.2.3 Downloadable literature

The final tab of the online handbook is a large listing of the different literature that has come out of the MiReCOL project. This information is grouped into three categories: scientific publications, conference presentations, and MiReCOL deliverables. The scientific publications are articles written during the project, while conference presentations are the slides from MiReCOL presentations. You can select each listed item to download the piece of literature.

3 TOOL DEVELOPMENT

The web tool has been developed in the latter half of the MiReCOL project. The appearance of the tool has not been changed drastically, but the inner workings of the tool has been. The website is written in JavaScript, with the front-end framework being developed using React Bootstrap and the back-end using Node.js and Express. The site uses a MySQL database to store some information displayed on the website. The three main interactive functionalities of the web tool are the technique analysis (Section 2.1.1.1), the site analysis (Section 2.1.1.2), and the well remediation (Section 2.1.2). While the technique analysis and the well remediation information is rather static (developed primarily from MiReCOL deliverables), the site analysis information is sourced from many scientists within the project. Thus, this section will focus on the development of the site analysis feature.

What the tool is founded on are the simulated results from the remediation techniques within the project. The difficult task was to translate those results into this tool, so that intensive calculations would not have to be performed within the web tool. The idea that was developed was to use a lookup of the scientists' simulations to provide the user with similar sites to his own.

3.1 Final version

The final version of the tool relies on a lookup table to present information to the web tool user. The scientists in the project were asked to make a list of the important input parameters into their simulations of their remediation technique. What was determined important were input parameters that changed the outputs when they ran simulations of their remediation technique. These are similar to the input questions in the aforementioned iteration, such as permeability or amount of CO_2 stored. The scientists themselves then selected a range of scenarios to run, by varying the different input parameters. For each of the simulations, they were asked to provide output values for the five output criteria: 1) likelihood of success, 2) spatial extent of remediation, 3) cost of remediation, 4) response time of the remediation, and 5) the longevity of the remediation. Along with these output criteria, the scientist was asked for a list of the materials required (to primarily show to the user to aid with the estimation of cost), as well as any extra comments they wanted to note about the technique.

Having this as the base of the information, the tool was then developed to read in user input about his site and compare that input to the scientists' scenarios. By comparing all the scenarios from each technique to the user's input parameters, then the closest scientist scenario for each technique could be displayed to the user to help him evaluate his own site. The manner in which the tool selects the closest scenario is via Gower's similarity coefficient (Gower, 1971), further detailed in the calculations in Section 3.2. The selected scenario for each remediation technique is then displayed on the output page after the user submits his site details.

These output criteria were then incorporated into the radar chart displayed on the output page. Each criterion is normalized on a 10-point scale so as to be able to compare the different techniques. After having these scenarios to display, an overall score and the TRL for each technique was thought to be useful. The overall score is the summation of the five output criteria normalized on a 10-point scale. Note that since low cost and fast response time are desired, these values were appropriately valued so that higher values of these would result in a lower overall score than lower values. The TRL values were estimated by scientists in the project, so that the web tool user could determine how developed the techniques are.

To touch on the remaining two aspects of the tool, the technique analysis and the well remediation are based on more static data relating to the remediation technique in general, as opposed to the scenario-based methodology of the site analysis. The technique analysis was developed having the MiReCOL deliverable dealing with the classification and ranking of the various remediation methods (Korre, 2017, link). This data could easily be displayed in graphical form, along with criteria that specify the user's preferences. The well remediation part of the web tool is based on the material from assessing the best practices from the oil and gas industry (Abdollahi et al., 2017, link). These resulted in several barriers that could fail, along with their typical remediation. The three aspects of the tool try to interactively engage the user to best describe the various techniques of remediating a CO_2 storage site.

3.2 Calculations within the tool

Despite the tool mostly displaying static information, the scenario aspect of the site analysis provides opportunity for calculations in the background of the tool. The main one is encountered after the user inputs the parameters to his site in the site analysis tool. What the tool then does is searches the scenarios simulated by the scientists to find the most similar scenario to that of the user. The tool then uses Gower's similarity coefficient to come up with a single value related to how similar the user's input is to each scientist scenario.

The way this method works is that there are two sets of data (in our case, the user's input and one scientist scenario). Then, this algorithm goes through each data entry, comparing that of the two sets of data. The way that it compares the data depends on the type of data it is. If the data point is categorical, then the algorithm compares whether the text is the same or not. If the data point is binary, then the algorithm compares whether they agree positively or not. Finally, if the data point is numerical, then the algorithm finds the relative proximity of the data points (relative to the range of the numerical data). These each generate a "score" that can then be multiplied by a weight, and summed to form the numerator of the similarity equation. The denominator is made up of the applicability of comparing the data point from the two data sets multiplied by the weight, and summing that value. The numerator is divided by the denominator to result in the overall similarity coefficient between the two data sets.

To further explain, this is the equation used to calculate Gower's similarity coefficient:

$$S_{ij} = \frac{\sum_{k=1}^{v} s_{ijk} w_k}{\sum_{k=1}^{v} \delta_{ijk} w_k} \tag{1}$$

Where S_{ij} is the total similarity between data sets i and j; v is the total number of data points in data sets i and j; k is the single data point; s_{ijk} is the "score" of data sets i and j with regard to data point k; w_k is the weight of data point k; and δ_{ijk} represents the ability to compare data point k between data sets i and j (this value is a 0 if they cannot be compared, and a 1 if they can be compared).

The "scores" depend on the type of data. For categorical data, the score is either a 1 if the two entries match, or a 0 if the two entries mismatch. For binary data, the "score" and the applicability are determined by the following Table 1 from Gower (1971).

Table 1 Table from Gower (1971) showing scores and applicability value used for binary data.

	Values of character k			
Individual i	+	+	-	-
j	+	-	+	-
s_{ijk}	1	0	0	0
δ_{ijk}	1	1	1	0

Lastly, for numerical data, the score is calculated using the equation

$$s_{ijk} = 1 - \frac{|x_i - x_j|}{R_k} \tag{2}$$

Where x_i and x_j are the numerical data points of data sets i and j, and R_k is the total range of the data point k. Thus, s_{ijk} can range between 0 and 1 for numerical data.

In this way are all the similarity values for each scenario and the user's input generated. Once that is calculated, then the scenario with the highest similarity coefficient within each remediation technique is selected to display to the user.

The next calculation are the normalized data to show on the radar chart on the output page. For each of the remediation techniques, there is one set of normalized data for each of the 5 output criteria, given by each scientist for each scenario. These normalized values are calculated by using the minimum output criteria and the range of each output criteria across all the remediation techniques. For each output criteria for each technique, a value from 0 to 1 is generated by using the following equation, and then multiplied to create a normalized value from 0 to 10.

$$x_{ij} = \frac{c_{ij} - m_i}{r_i} \tag{3}$$

Where x_{ij} is the normalized value of output criteria i for remediation technique j; c_{ij} is the value for output criteria i for remediation technique j; m_i is the minimum value for output criteria i, across all remediation techniques; and r_i is the range of output criteria i, across all remediation techniques.

The final calculation is the overall score, also shown on the output page. This score is based on the five normalized values previously calculated. These five values are summed, and then normalized to a 10-point scale (similar to the normalized calculation in equation [3]).

4 SOURCE OF INFORMATION IN THE WEB APP

The information found in the online web app is based on the MiReCOL deliverables, as well as from the scientists who participated in this project. When material outside of the deliverables was required, the scientists or experts were asked to provide additional knowledge, simulations, or text for the web app.

4.1 Tool

4.1.1 Site Remediation

4.1.1.1 Technique analysis

The data behind this section of the tool come from results from Deliverable 11.2, Report on the individual remediation techniques scoring method and classification/ranking results, as well as values from scientists within the project (Korre, 2017, link). The values for the bar graph are a result of D11.2, which was sourced from deliverables in the MiReCOL project, while the overview paragraph and TRL value estimations come from the scientists within the project, based on the EU Horizon 2020 definition of TRL (TRLs, 2014). The probability of success was found by plotting every scenario run for each remediation technique on a cumulative probability vs. percent remediation graph. Then, the probability of success displayed in the bar graph is when the percent remediation reaches a value of 20%. To provide an example, Figure 15 shows the data points from the scenarios of the brine/water injection remediation technique (Drysdale et al., 2017, link), the line where the percent remediation is at 20%, and an orthogonal line pointing at 65% cumulative remediation. The value of 35% (calculated from 100% - 65%) is then the displayed probability of success in the bar charts on the "Technique analysis" page.

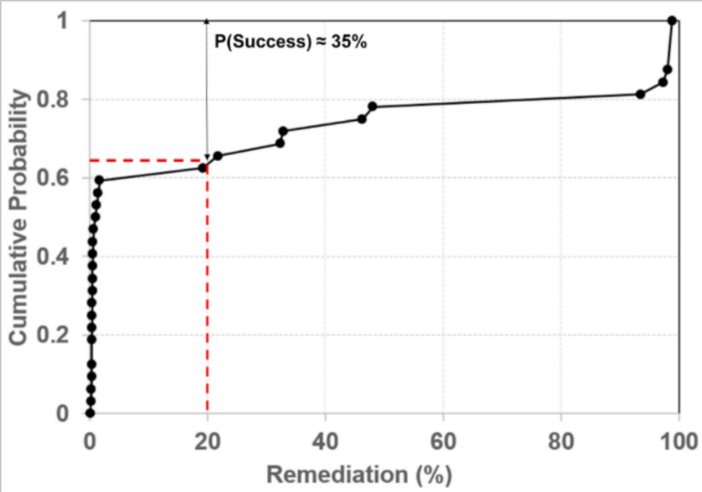

Figure 15 Example plot of cumulative probability vs. percent remediation for the remediation technique of brine/water injection, taken from MiReCOL Deliverable 11.2 (Chapter XXXII).

4.1.1.2 Site analysis

The site analysis is based on material requested specifically from the scientists within the MiReCOL project. The development of this aspect of the web tool was influenced by the type of scientific simulations performed for each of the techniques. The use of some of these are explained in Section 3.2, which details the calculations behind the tool.

Input variables: Initially, a list of the input variables used in the simulations was requested from each remediation technique scientist. This was not intended to include all input variables which influence the simulations, but rather the most important variables which affect the results of the simulations.

Weight of input variables: For each input variable, their estimated weight of influence was asked of the scientists, summing up to a value of 100. Thus, if an input variable #1 had little influence on the output simulations and input variable #2 had a high influence, then input variable #1 would have a low weight, while input variable #2 would have a large weight.

Range of input variables: Then, the range of these input variables used in their scientific simulations was requested, as well as logical sub-ranges which divided the ranges up into different groupings. To take the input variable of permeability as an example, the suggested range for all simulations was between 0 and 1000 mD, and the corresponding sub-ranges were 0-30 mD, 30-100 mD, 100-500 mD, and 500-1000 mD. These ranges are the selections shown on the "Site analysis" page of the web tool.

Scenarios (list of simulations run): The scientists listed the simulations they ran, which appeared as a list of the input variables they used accompanied by the values they used for each input variable. Each simulation they ran was considered a "scenario". This resulted in a set of scenarios for each remediation technique.

Output criteria: After establishing the scenarios for each remediation technique, each scientist was asked to provide an estimation/calculation of the five output criteria used throughout this project: likelihood of success, spatial extent of remediation, cost of remediation, response time of the remediation, and the longevity of the remediation. This was asked for each scenario. Because cost heavily depends on site location and situation, they were placed in ranges, and the scientists provided a list of materials required to accompany this output criterion.

Overall score and TRL: The values for the overall score provided are calculated from the aforementioned output criteria and explained in Section 3.2. The TRLs were provided by project scientists involved in the remediation technique studies, based on the EU Horizon 2020 guidelines for TRLs (TRLs, 2014).

Other Notes and Associated Risks: These two parts were provided by the scientists performing the simulations to explain any additional meanings of the output criteria, as well as any risks that should be noted to better assess the remediation technique.

4.1.2 Well remediation

The information for the well remediation came from the deliverables in Work Package 8, O&G industry best practice for remediation of well leakage, and Work Package 9, Novel materials and technologies for remediation of well leakage. More specifically, the knowledge comes from Deliverable 8.3, Assessment of Oil & Gas Remediation Technologies for CO_2 Wells (Abdollahi et al., 2017, link), as well as analysis from the well experts involved in the project. The knowledge the experts shared was the risks associated with the remediation practices, as well as images of the various well remediation techniques.

4.2 Handbook

The first tab on the handbook page contains most of the remediation techniques covered in the MiReCOL project. The sections of text were written by the scientists in the project who performed the modelling of the techniques.

The second tab simply lists the work packages within the projects and the corresponding deliverables from each work package. The abstract shown comes from the associated deliverable.

The final tab, Downloadable Literature, comes from literature published or presented about studies in the MiReCOL project. The majority comes from the Greenhouse Gas Control Technologies, CO_2GeoNet, and the Trondheim CCS conferences.

The following two sections contain the reports and publications from the MiReCOL project that can also be found on the MiReCOL website.

4.2.1 Public reports from the MiReCOL project

- Current flow diversion techniques relevant to CO_2 leakage remediation (D3.1 – link)
- Adaption of injection strategy as flow diversion option (D3.2 – link)
- Gel and foam injection as flow diversion option in CO_2 storage (D3.3 – link)
- Brine-water injection as flow diversion option in CO_2 storage operations (D3.4 – link)
- Blocking of CO_2 movement by immobilization of CO_2 in solid reaction products (D3.5 – link)
- Reservoir pressure management (D4.1 – link)
- The impact of hysteresis effects as remediation measure (D4.2 – link)
- CO_2 back production at the Ketzin and K12-B sites (D4.3 – link)
- Brine/water withdrawal as pressure management and flow diversion option (D4.4 – link)
- Lowering reservoir pressure by accelerating convective mixing (D4.5 – link)
- Remediation linked to faults and fractures (D5.1 – link)
- The effects of stress on leakage through faults (D5.2 – link)
- Remediation of leakage by diversion to nearby compartment (D5.3 – link)
- Sealants as a corrective measure (D6.1 – link)
- Gel and foam injection as leakage remediation (D6.3 – link)
- Remediation techniques based on foam injection (D6.4 – link)
- Hydraulic and gas barriers as a corrective measure (D7.1 – link)
- Study of N_2 as a mean to improve CO_2 storage safety (D7.2 – link)
- Remediation and preventive measures using hydraulic barrier method (D7.3 – link)
- Description of leakage scenarios (D8.1 – link)
- Overview of available well leakage remediation technologies (D8.2 – link)
- Assessment of OG Remediation Technologies for CO_2 wells (D8.3 – link)
- CO_2 reactive suspensions (D9.1 – link)
- Polymer resin for squeezing (D9.5 – link)
- Novel materials and technologies for remediation of well leakage (D9.7 – link)
- Near-surface CO_2 leakage remediation methods (D10.1 – link)
- Report on individual remediation techniques (D11.2 – link)
- Methodology for the CO_2 storage remediation portfolio optimisation (D11.3 – link)
- Handbook of corrective measures (D13.1 – link)
- Web-based tool of corrective measures - summary report (D13.2, this report – link)

4.2.2 Publications from the MiReCOL Project

- Antropov, A. et al., 2017. Effect of in-situ stress alterations on flow through faults and fractures in the cap rock. Energy Procedia, in press.
- Batôt, G., Fleury, M. and Nabzar, L., 2016. Study of CO_2 foam performance in a CCS context. In The 30th International Symposium of the Society of Core Analysts-Snowmass. (link)
- Batôt, G. et al., 2017. Reducing CO_2 flow using foams. Energy Procedia, in press.
- Bossie-Codreanu, D. et al., 2017. Study of N_2 injection as a mean to improve storage safety. Energy Procedia, in press.
- Bossie-Codreanu, D., 2017. Remediation processes using a dimensionless classification of potential storage sites. Energy Procedia, in press.

- Brunner, L. et al., 2017. MiReCOL – a handbook and web tool of remediation and corrective actions for CO_2 storage sites. Energy Procedia, in press.
- Durucan, S., Korre, A., Shi, J.Q., Govindan, R., Mosleh, M.H. and Syed, A., 2016. The Use of Polymer-gel Solutions for CO_2 Flow Diversion and Mobility Control within Storage Sites. Energy Procedia, 86, pp.450-459. (link)
- Fleury, M. et al., 2017. A silicate based process for plugging the near well bore formation. Energy Procedia, in press.
- Govindan, R. et al., 2017. The assessment of CO_2 backproduction as a technique for potential leakage remediation at the Ketzin pilot site in Germany. Energy Procedia, in press.
- Karas, D., Demic, I., Kultysheva, K., Antropov, A., Blagojevic, M., Neele, F., Pluymaekers, M. and Orlic, B., 2016. First field example of remediation of unwanted migration from a natural CO_2 reservoir: the Bečej field, Serbia. Energy Procedia, 86, pp.69-78. (link)
- Korre, A. et al., 2017. Assessment of the effectiveness of corrective measures for CO_2 storage risk mitigation and remediation. Energy Procedia, in press.
- Lavrov, A., 2016. Dynamics of stresses and fractures in reservoir and cap rock under production and injection. Energy Procedia, 86, pp.381-390. (link)
- Lavrov, A., 2016. Fracture permeability under normal stress: a fully computational approach. Journal of Petroleum Exploration and Production Technology, pp.1-14. (link)
- Loeve, D. et al., 2017. Diversion of CO_2 to nearby reservoir compartments for remediation of unwanted CO_2 migration. Energy Procedia, in press.
- Mosleh, M.H., Govindan, R., Shi, J.Q., Durucan, S. and Korre, A., 2016, May. Application of Polymer-Gel Solutions in Remediating Leakage in CO_2 Storage Reservoirs. In SPE Europec featured at 78th EAGE Conference and Exhibition. Society of Petroleum Engineers. (link)
- Mosleh, M.H. et al., 2017. Development and characterisation of a smart cement for CO_2 leakage remediation at wellbores. Energy Procedia, in press.
- Mosleh, M.H. et al., 2017. The use of polymer-gel remediation for CO_2 leakage through faults and fractures in the caprock. Energy Procedia, in press.
- Neele, F., Grimstad, A.A., Fleury, M., Liebscher, A., Korre, A. and Wilkinson, M., 2014. MiReCOL: developing corrective measures for CO_2 storage. Energy Procedia, 63, pp.4658-4665. (link)
- Peters, E. et al., 2017. Accelerating dissolution of CO_2 in brine by enhancing convective mixing as a potential remediation option. Energy Procedia, in press.
- Pizzocolo, F., Hewson, C.W. and ter Heege, J.H., 2016, June. Polymer-Gel Remediation of CO_2 Migration through Faults and Caprock: Numerical Simulations Addressing Feasibility of Novel Approaches. In 50th US Rock Mechanics/Geomechanics Symposium. American Rock Mechanics Association. (link)
- Todorovic, J., Raphaug, M., Lindeberg, E., Vrålstad, T. and Buddensiek, M.L., 2016. Remediation of Leakage through Annular Cement Using a Polymer Resin: a Laboratory Study. Energy Procedia, 86, pp.442-449. (link)
- Wagner, F.M., Wiese, B., Schmidt-Hattenberger, C. and Maurer, H., 2016, May. Insights on CO_2 Migration Based on a Multi-physical Inverse Reservoir Modeling Framework. In 78th EAGE Conference and Exhibition 2016-Workshops. (link)
- Wasch, L. et al., 2017. Mitigating CO_2 leakage by immobilizing CO_2 into solid reaction products. Energy Procedia, in press.
- Wilkinson, M. et al., 2017. MiReCOL: Remediation of shallow leakage from a CO_2 storage site. Energy Procedia, in press.

5 CONCLUSION

The web app is intended to cater to several stakeholders in the carbon storage field: storage operators, storage authorities and regulators, decision makers, and the public. The website is a platform to inform these stakeholders and make them aware of the practices performed and risks that are evaluated when dealing with such technologies.

The web tool portion of this website is an interactive manner in which users evaluate the different options and then make an informed decision as to what they should do in the case of unwanted CO_2 migration. This can either be performed based on a user's input site, or simply by viewing the general functionality of all the techniques. For storage operators, this is practical to know what remediation techniques are available and how far developed they are. This tool can also help operators create their contingency plan, something required before operating a CO_2 storage site, by having a single place to learn about and assess several different remediation techniques.

As for regulators, decision makers, and the public, the web tool can also aid them in knowing what actions are available to storage operators. It is possible that these stakeholders are not aware of the choices and trade-offs that an operator has to consider, so this tool also serves as a resource to inform them about various remediation techniques.

The handbook shares many of the same applications as the tool, but also offers the ability to view the journal articles, reports, and presentations conducted within the MiReCOL project. This can be useful for those who would like to go more in-depth into a remediation technique.

This web app is a contemporary way of presenting and summarizing information for a large carbon storage remediation project. This is an important step in disseminating information to stakeholders and interested parties.

References

Abdollahi, J., Carlsen, I.M., and Wollenweber, J., 2016. Assessment of Oil & Gas Remediation Technologies for CO_2 Wells. MiReCOL, Mitigation and remediation of leakage from geological storage, Deliverable 8.3, link.

British Geological Survey (BGS), 2010. Monitoring selection tool. IEA Greenhouse Gas R&D Programme. Available at: http://ieaghg.org/ccs-resources/monitoring-selection-tool.

Drysdale, R., Durucan, S., Korre, A., Wiese, B., and Loeve, D., 2017. Brine/water injection as flow diversion option in CO_2 storage operations. MiReCOL, Mitigation and remediation of leakage from geological storage, Deliverable 3.4, link.

Global CCS Institute, 2015. Global Status of CCS: 2015, Summary Report. Melbourne, Australia: Global Carbon Capture and Storage Institute.

Gower, J.C., 1971. A general coefficient of similarity and some of its properties. Biometrics, pp.857-871.

IEA, 2013. Technology Roadmap: Carbon capture and storage. IEA.

Intergovernmental Panel on Climate Change (IPCC), 2014. Climate Change 2014: Synthesis Report. Cambridge University Press.

Govindan, R., Nie, Z., Korre, A. and Durucan, S., 2017. Report on methodology for the CO_2 storage remediation portfolio optimisation and the results of the scenario analysis. MiReCOL, Mitigation and remediation of leakage from geological storage, Deliverable 11.3, link.

Korre, A., 2017. Report on individual remediation techniques scoring method and classification/ranking results. MiReCOL, Mitigation and remediation of leakage from geological storage, Deliverable 11.2, link.

Le Guénan, T., Manceau, J.C., Bouc, O., Rohmer, J. and Ledoux, A., 2011. GERICO: A database for CO_2 geological storage risk management. Energy Procedia, 4, pp.4124-4131.

Orlic, B., Loeve, D. and Peters, E., 2016. Remediation of leakage by diversion of CO_2 to nearby reservoir compartments. MiReCOL, Mitigation and remediation of leakage from geological storage, Deliverable 5.3, link.

Pawar, R.J., Bromhal, G.S., Chu, S., Dilmore, R.M., Oldenburg, C.M., Stauffer, P.H., Zhang, Y. and Guthrie, G.D., 2016. The National Risk Assessment Partnership's integrated assessment model for carbon storage: A tool to support decision making amidst uncertainty. International Journal of Greenhouse Gas Control, 52, pp.175-189.

Technology readiness levels (TRLs), 2014. Horizon 2020 – Work Programme 2014-2015, General Annexes. Available at: https://ec.europa.eu/research/participants/data/ref/h2020/wp/2014_2015/annexes/h2020-wp1415-annex-g-trl_en.pdf.

Wessel-Berg, D., Korre, A., Durucan, S. and Drysdale, R., 2015. Gel and foam injection as flow diversion option in CO_2 storage. MiReCOL, Mitigation and remediation of leakage from geological storage, Deliverable 3.3, link.

End of Document